

Lecture Notes in Civil Engineering

Chintalacheruvu Madhusudana Rao  
K. C. Patra  
D. Jhajharia  
Sangeeta Kumari *Editors*

# Advanced Modelling and Innovations in Water Resources Engineering

Select Proceedings of AMIWRE 2021

 Springer

# Lecture Notes in Civil Engineering

Volume 176

## Series Editors

Marco di Prisco, Politecnico di Milano, Milano, Italy

Sheng-Hong Chen, School of Water Resources and Hydropower Engineering,  
Wuhan University, Wuhan, China

Ioannis Vayas, Institute of Steel Structures, National Technical University of  
Athens, Athens, Greece

Sanjay Kumar Shukla, School of Engineering, Edith Cowan University, Joondalup,  
WA, Australia

Anuj Sharma, Iowa State University, Ames, IA, USA

Nagesh Kumar, Department of Civil Engineering, Indian Institute of Science  
Bangalore, Bengaluru, Karnataka, India

Chien Ming Wang, School of Civil Engineering, The University of Queensland,  
Brisbane, QLD, Australia

**Lecture Notes in Civil Engineering (LNCE)** publishes the latest developments in Civil Engineering—quickly, informally and in top quality. Though original research reported in proceedings and post-proceedings represents the core of LNCE, edited volumes of exceptionally high quality and interest may also be considered for publication. Volumes published in LNCE embrace all aspects and subfields of, as well as new challenges in, Civil Engineering. Topics in the series include:

- Construction and Structural Mechanics
- Building Materials
- Concrete, Steel and Timber Structures
- Geotechnical Engineering
- Earthquake Engineering
- Coastal Engineering
- Ocean and Offshore Engineering; Ships and Floating Structures
- Hydraulics, Hydrology and Water Resources Engineering
- Environmental Engineering and Sustainability
- Structural Health and Monitoring
- Surveying and Geographical Information Systems
- Indoor Environments
- Transportation and Traffic
- Risk Analysis
- Safety and Security

To submit a proposal or request further information, please contact the appropriate Springer Editor:

- Pierpaolo Riva at [pierpaolo.riva@springer.com](mailto:pierpaolo.riva@springer.com) (Europe and Americas);
- Swati Meherishi at [swati.meherishi@springer.com](mailto:swati.meherishi@springer.com) (Asia - except China, and Australia, New Zealand);
- Wayne Hu at [wayne.hu@springer.com](mailto:wayne.hu@springer.com) (China).

**All books in the series now indexed by Scopus and EI Compendex database!**

More information about this series at <https://link.springer.com/bookseries/15087>

Chintalacheruvu Madhusudana Rao · K. C. Patra ·  
D. Jhajharia · Sangeeta Kumari  
Editors

# Advanced Modelling and Innovations in Water Resources Engineering

Select Proceedings of AMIWRE 2021

 Springer



*Editors*

Chintalacheruvu Madhusudana Rao  
Department of Civil Engineering  
National Institute of Technology  
Jamshedpur  
Jamshedpur, Jharkhand, India

D. Jhajharia  
Department of Soil and Water Conservation  
Engineering  
College of Agricultural Engineering  
and Post Harvest Technology  
Central Agricultural University  
Gangtok, Sikkim, India

K. C. Patra  
Department of Civil Engineering  
National Institute of Technology Rourkela  
Rourkela, Odisha, India

Sangeeta Kumari  
Department of Civil Engineering  
National Institute of Technology  
Jamshedpur  
Jamshedpur, Jharkhand, India

ISSN 2366-2557

ISSN 2366-2565 (electronic)

Lecture Notes in Civil Engineering

ISBN 978-981-16-4628-7

ISBN 978-981-16-4629-4 (eBook)

<https://doi.org/10.1007/978-981-16-4629-4>

© The Editor(s) (if applicable) and The Author(s), under exclusive license to Springer Nature Singapore Pte Ltd. 2022

This work is subject to copyright. All rights are solely and exclusively licensed by the Publisher, whether the whole or part of the material is concerned, specifically the rights of translation, reprinting, reuse of illustrations, recitation, broadcasting, reproduction on microfilms or in any other physical way, and transmission or information storage and retrieval, electronic adaptation, computer software, or by similar or dissimilar methodology now known or hereafter developed.

The use of general descriptive names, registered names, trademarks, service marks, etc. in this publication does not imply, even in the absence of a specific statement, that such names are exempt from the relevant protective laws and regulations and therefore free for general use.

The publisher, the authors and the editors are safe to assume that the advice and information in this book are believed to be true and accurate at the date of publication. Neither the publisher nor the authors or the editors give a warranty, expressed or implied, with respect to the material contained herein or for any errors or omissions that may have been made. The publisher remains neutral with regard to jurisdictional claims in published maps and institutional affiliations.

This Springer imprint is published by the registered company Springer Nature Singapore Pte Ltd.

The registered company address is: 152 Beach Road, #21-01/04 Gateway East, Singapore 189721, Singapore

# Contents

## Hydrological Modelling

|   |    |
|---|----|
| <b>Trends of Rainfall and Temperature over Chhattisgarh During 1901–2010</b> .....  | 3  |
| Shashikant Verma, A. D. Prasad, and Mani Kant Verma   |    |
| <b>Estimation and Simulation of Flows into an off-Taking Canal Using ANSYS</b> .....  | 21 |
| V. Chakravarthy, S. V. S. N. D. L. Prasanna, and N. Suresh Kumar  |    |
| <b>Drought Evaluation of Tiruchirapalli City, India, Using Three Meteorological Indices</b> .....   | 31 |
| K. Sasireka and C. R. Suribabu  |    |
| <b>Forecasting of Meteorological Drought Using Machine Learning Algorithm</b> .....   | 43 |
| Ayilobeni Kikon and Paresh Chandra Deka   |    |
| <b>Assessment of Economic Value of Doddabommasandra Lake Using Contingent Valuation Method and Travel Cost Method</b> .....                                       | 53 |
| D. N. Shilpa, K. Nruthya, L. G. Santhosh, Simran Sanu, and Anukul Nidhi   |    |
| <b>Meteorological Drought Analysis Using SPI-6 for Marathwada Region, Maharashtra State, India</b> .....  | 71 |
| A. B. Pachore and D. G. Regulwar  |    |
| <b>Analysis and Comparison of Fuzzy Logic and Neural Network Based Study for Rainfall Predictions and Hydrological Modelling: A Case Study of Ahmedabad</b> ..... | 83 |
| Utkarsh Nigam, Vinod Kumar M. Patel, and Sanjay Kumar M. Yadav  |    |

|   |     |
|---|-----|
| <b>A Synoptic-Scale Assessment of Flood Events and ENSO—Streamflow Variability in Sheonath River Basin, India</b> .....                             | 93  |
| Mohammed Azharuddin, Shashikant Verma, Mani Kant Verma, and A. D. Prasad  |     |
| <b>Effect of Climate Change on Spring Discharge Management System of the Himalayan Region in India</b> .....  | 105 |
| Kunal Sharma and Nirban Laskar  |     |
| <b>Assessment of Digital Elevation Models Based on the Drainage Morphometric Parameters for the Tawi River Basin</b> .....                          | 119 |
| Ravindra V. Kale, P. G. Jose, A. K. Taloor, and Rajat Kumar   |     |
| <b>Comparison of HEC-HMS and SWAT Hydrological Models in Simulating Runoff at Machhu River Catchment, Gujarat, India</b> .....                      | 141 |
| Kishanlal Darji, Dhruvesh Patel, and Indra Prakash  |     |
| <b>Flood Hazard Assessment of Baitarani River Basin Using One-Dimensional Hydrodynamic Model</b> .....  | 157 |
| Aman Kumar and K. C. Patra  |     |
| <b>River Geometry Extraction from Cartosat-1 DEM for 1D Hydrodynamic Flood Modeling Using HEC-RAS—A Case of Navsari City, Gujarat, India</b> .....  | 173 |
| Azazkhan Ibrahimkhan Pathan, Prasit Girish Agnihotri, and Dhruvesh Patel  |     |
| <b>Impact Assessment of Environmental Flows Using CORDEX Regional Climate Models: Case Study of Nagarjuna Sagar Dam, Krishna River, India</b> ..... | 187 |
| Rajesh Maddu, Krishna Mohan Ganta, Rehana Shaik, and C. T. Dhanya   |     |
| <b>Trend Analysis of Annual, Seasonal, and Monthly Streamflow in Naula Watershed, Uttarakhand (India)</b> .....                                     | 205 |
| Anurag Malik and Anil Kumar   |     |
| <b>Hydrologic Response Estimation Using Different Descriptors for Upper Baitarani River Basin</b> .....   | 219 |
| Avijit Bardhan and Chintalacheruvu Madhusudana Rao  |     |
| <b>Temperature and Precipitation Towards the End of the 21st Century in Pecan Producing Areas of Mexico</b> .....                                   | 235 |
| Arturo Corrales-Suastegui, Gerardo Martinez-Diaz, Osias Ruiz-Alvarez, Miguel Angel Gonzalez-Gonzalez, and Edgar G. Pavia                            |     |

**Water Resources System Planning and Management**

**Effect of Water Distribution Network Pipes Size on Flow Rate of a House Connection and Its Hydraulic Analysis** ..... 257

C. R. Suribabu and P. Sivakumar

**Leakage Optimization of Water Distribution Network Using Artificial Intelligence** ..... 265

Sejal Desai and Gargi Rajapara

**The Effect of Pipe Age and Piping Materials on Chlorine Decay in a Pilot Loop Water Distribution Network** ..... 285

C. Ramprasad and C. R. Suribabu

**Hydraulic Analysis of Drinking Water Distribution Network Using WaterCAD Simulation: Case of Purba Medinipur in West Bengal** ..... 301

Koushik Debnath, Subhasish Das, and Biprodip Mukherjee

**Comparison Model Study Using WaterGEMS and EPANET Software Programs for Clearwater Rising Main at Bhangar in West Bengal** ..... 315

Biprodip Mukherjee, Prasun Das, and Subhasish Das

**A Conceptual Approach toward Water Management with Aquaponics** ..... 329

Sana Kaja, Rajasekar Veeramani, and Mohammad Tanveer

**Water Distribution Network Analysis Using EPANET: A Case Study of Surat City** ..... 339

Nitin Singh Kachhawa and Surendra Borana

**Impact of Different Parameters in the Development of Operating Policies of a Reservoir Using Stochastic Dynamic Modelling Technique** ..... 353

Ashrumochan Mohanty, Satish Chandra Bhuyan, and Sangeeta Kumari

**Feasibility Analysis and Design of Water Distribution System for Ghadara (East Singhbhum District) Using Water Gems** ..... 371

Abu Rashid and Sangeeta Kumari

**Remote Sensing/Geospatial Techniques in Water Resources**

**Identification of Flood Vulnerable Area for Kharun River Basin by GIS Techniques** ..... 385

Bhupendra Kumar Dhiwar, Shashikant Verma, and A. D. Prasad

**Seepage of Water Quality Analysis of a Concrete Gravity Dam Using Langlier and Aggressive Index** ..... 409

Satish Chandra Bhuyan, Jyotirmaya Behera, Jyoti Kar, and Prakash Kumar Barik

|  |     |
|--|-----|
| <b>Application of GIS and Geostatistical Interpolation Method for Groundwater Mapping</b> .....  | 419 |
| Ashesh Chakma, Tridip Bhowmik, Santanu Mallik, and Umesh Mishra  |     |
| <b>Estimation of Glacier Ice Velocity and Thickness Using Optical Remote Sensing</b> .....   | 429 |
| Sunita and Amanpreet   |     |
| <b>Groundwater Quality Indexing Using Weight Overlay Analysis and GIS—A Case of Rel River Catchment</b> .....  | 447 |
| Tulansi Patel, Heli Patel, Meet Trada, Jay Hirpara, Prateek Bhura, Akshesh Prajapati, Dhruv Tavethia, Dhruvesh Patel, and Naimish Bhatt                                      |     |
| <b>Flood Damages Assessment Using Remote Sensing and GIS: A Case Study of 2018 Kodagu Floods</b> .....   | 463 |
| Jagadish Vengala, Manish S. Dharek, Prashant Sunagar, K. S. Sreekesava, Kilabanur Pramod, Darshan Baliga, P. S. Haripriya, and Poornachandra Thejaswi                        |     |
| <b>Groundwater Heavy Metal Contamination Mapping Using Geographic Information System (GIS): A Case of Nashik Thermal Power Station, Eklahare, Nashik (M.S.), India</b> ..... | 477 |
| Vrushali V. Sasane and Alka S. Kote  |     |
| <b>Using Earth Observations and GLDAS Model to Monitor Water Budgets for River Basin Management</b> .....  | 493 |
| Chiranjit Singha and Kishore C. Swain  |     |
| <b>Utility of Geomatics in Land Use Land Cover Change Detection and Accuracy Analysis</b> .....  | 517 |
| G. Padmaja and M. V. S. S. Giridhar  |     |
| <b>Ground Water and Water Quality Models</b>   |     |
| <b>Urbanization Implications on Local Climate and Groundwater Levels Using Index-Based Techniques</b> .....  | 531 |
| V. Shiva Chandra and T. Reshma   |     |
| <b>Seasonal Groundwater Table Depth Prediction Using Fuzzy Logic and Artificial Neural Network in Gangetic Plain, India</b> .....  | 549 |
| Kusum Pandey and Anurag Malik  |     |
| <b>An Identification of Suitable Location to Construct Underground Sump for Rooftop Rainwater Harvesting in the Campus of Debre Tabor University</b> .....                   | 565 |
| G. Venkata Ramana, Ch.V. S. S. Sudheer, and R. Suresh Kumar  |     |
| <b>A Novel Statistical Approach for Infiltration Model Analysis</b> .....  | 577 |
| Sunith John David, K. U. Abdu Rahiman, and V. Subha  |     |

|   |     |
|---|-----|
| <b>Assessment of Groundwater and Lake Water Quality at S. Bingipura Dumpsite</b> .....  | 585 |
| R. Manjunath, B. Umadevi, and E. T. Arasu   |     |
| <b>Assessment of Contaminant Migration Using MT3DMS Model</b> .....   | 599 |
| P. Anil Kumar, G. N. Pradeep Kumar, and M. J. Nandan  |     |
| <b>Water Quality Analysis at Mancherial, Jagdalpur and Konta Using Non-parametric Methods</b> .....   | 609 |
| Chintalacheruvu Madhusudana Rao, Prakhar Modi, and D. Jhajharia   |     |
| <b>Assessment of Water Quality of River Mutha for Onsite Treatment of Polluted River Water</b> .....  | 621 |
| Rohini More and Sameer Shastri  |     |
| <b>Comparative Study of Physical and Chemical Parameters of Lakes in Medchal District</b> .....   | 635 |
| R. Suresh Kumar, Ch.V. S. S. Sudheer, G. Venkata Ramana, and N. Sri Ramya   |     |
| <b>Environmental Modelling</b>  |     |
| <b>An Experimental Study on Removal of Cadmium Using <i>Annona Squamosa</i> Seed Powder and <i>Phyllanthus Acidus</i> Seed Powder</b> .....                         | 647 |
| T. Aruna Devi, R. Jeykumar, and R. Ilangovan  |     |
| <b>A Comparative Study on Environmental Impact Assessment of Recirculating Aquaculture System and Raceway System</b> .....  | 667 |
| Pradeep Ramesh, Mohammad Tanveer, R. S. Dharani Shree, and R. Gokul   |     |
| <b>Exploring the Efficacy of Anammox Hybrid Reactor Technology Towards Nitrogen Removal: A Promising Alternative to Conventional Nitrogen Removal Systems</b> ..... | 679 |
| Swati Tomar, S. K. Gupta, and R. K. Verma   |     |
| <b>Smart and Water-Efficient Automatic Drip Irrigation System</b> .....   | 693 |
| Sanmit P. Nalawade and Pravin A. Manatkar   |     |
| <b>Analytical Study of Scour Mechanism Around Immersed Rectangular Vane Structures</b> .....  | 703 |
| Priyanka Roy, Subhasish Das, Anupama Dey, and Rajib Das   |     |
| <b>Riverbank Erosion for Different Levels of Impurity of Water—A Micro-analysis</b> .....   | 719 |
| Debasish Biswas, Arijit Dutta, Sanchayan Mukherjee, and Asis Mazumdar   |     |

|   |     |
|---|-----|
| <b>Optimizing Irrigation Requirement of Soil Test-Based Fertilizer Recommendation Models for Targeted Yields of Cabbage and Broccoli in a Typic Fluvaquept Soil</b> ..... | 729 |
| Kallol Bhattacharyya, Agnibha Sinha, Sudip Sengupta, Shubhadip Dasgupta, Sanmay Kumar Patra, Pradip Dey, and Debasis Mazumdar   |     |
| <b>Drip Fertigation with Fertilizer Prescription Through STCR—IPNS—A Way Forward Towards Climate Change Mitigation</b> .....  | 749 |
| Santhi Rangasamy, Maragatham Subramaniam, Praveena Katharine Stephen, and Pradip Dey  |     |
| <b>Effective Utilization of Water Resources Through Floating Solar Photovoltaic (FSPV) Technology: An Emerging Idea of Sustainable Development</b> .....                  | 759 |
| Mehebab Alam  |     |
| <b>Pumped Hydrostorage (PHS) Plant: A Scheme for Overall Efficiency Improvement by Recycling the Water</b> .....  | 769 |
| Mehebab Alam  |     |
| <b>Identification of New Sites for Micro-Compost Centers: A Predictive Study for Erode Urban Region</b> .....   | 779 |
| S. Anandakumar, M. Kowsalya, K. Santhosh Kumar, M. Rama Krishnan, S. Praveenkumar, G. Mini Karthi, G. S. Rampradheep, and S. Jeeva Chithambaram                           |     |

## About the Editors

**Dr. Chintalacheruvu Madhusudana Rao** is an Associate Professor of the Department of Civil Engineering of NIT Jamshedpur. He holds Ph.D. degree in Hydrology from the Department of Hydrology, IIT Roorkee; an M.E. degree in Irrigation Water Management from Centre for Water Resources and Ocean Management of Anna University, Guindy, Chennai; and a B.Tech. degree in Civil Engineering from V. R. Siddhartha Engineering College, Vijayawada affiliated to Nagarjuna University, Guntur. His research interest includes surface water and groundwater hydrology, Geospatial technology applications for water resources engineering, rainfall-runoff modelling, climate change impact assessment, watershed modelling, river flood modelling, flood forecasting, river water quality modelling, open channel hydraulics and applications of optimization tools for water resources planning and management. He has 22 years of academic experience. He has published more than 30 research papers in peer-reviewed journals and national and international conferences. Presently he is the Co-principal Investigator of Department of Atomic Energy (DAE), Board of Research in Nuclear Sciences (BRNS), Government of India sponsored project titled “Spatial Distribution of Uranium and Associated Water Quality Parameters in groundwater/drinking water of seven districts (East Singhbhum, Saraikela Kharsawan, West Singhbhum, Khunti, Simdega, Gumla, Latehar) of Jharkhand”. He is the reviewer for *Journal of Climate Change* (Springer Series), *Journal of Hydrologic Engineering* and Book Projects (ASCE Publications), *International Journal of Environmental Studies* (Taylor & Francis Group), *Current Science Journal* (Indian Academy of Sciences) and *Applied Water Science journal* (Springer).

**Prof. K. C. Patra** is a Civil Engineer of international repute who is currently working as professor (HAG) in the Civil Engineering Department at the National Institute of Technology, Rourkela, Odisha. He has worked as the Head of Civil Engineering Department and DEAN (Alumni Relations and Resources Generation) at the Institute. Prof. Patra graduated with a Bachelor’s degree in Civil Engineering from NIT Rourkela, in 1981. He obtained his M.Tech. and PG (Diploma) from the University of (IIT) Roorkee, where he stood first amongst first class in the entire University in 1987 and received the Prestigious Chancellors Gold Medal. He obtained Ph.D.



degree from IIT Kharagpur. Prof. Patra has vast teaching, research and administrative experience spanning over the last 39 years. He has published several books on water resources and hydraulic engineering. Prof. Patra has published more than 232 papers in water resources and hydraulic engineering. He is a member of the editorial board of *Advances of Fluid Mechanics* and reviewer of many international journals.

**Prof. D. Jhajharia**, Ph.D., is currently working as Professor in Department of Soil and Water Conservation Engineering, College of Agricultural Engineering and Post Harvest Technology (Central Agricultural University), Ranipool, Gangtok, Sikkim, India. He is also acting as principal investigator of All India Coordinated Research Project on Plasticulture Engineering Technology CAEPHT (Gangtok) centre, which is funded entirely by ICAR (Indian Council of Agricultural Research) Central Institute of Post Harvest Engineering and Technology, Ludhiana, India, since 2016. He did graduation from College of Technology and Engineering (MPUAT), Udaipur, Rajasthan, India, in Agricultural Engineering in 1998, and post-graduation from Indian Institute of Technology Delhi, India, in Water Resources Engineering from Department of Civil Engineering. He obtained his Ph.D. degree from Department of Hydrology, Indian Institute of Technology Roorkee, Uttarakhand, India. He is one of the co-authors of *Handbook of Conservation Agriculture* published by CRC Press, Taylor and Francis Group, Boca Raton, USA. He along with Prof. Kumar, Prof. V. P. Singh, Prof. Mirabbasi published *Agricultural Impacts of Climate Change* and *Applied Agricultural Practices for Mitigating Climate Change* published by CRC Press, Taylor and Francis Group, Boca Raton, USA. He was elected as the Fellow of Indian Association of Hydrologists, Roorkee (in 2015), Society of Extension Education, Agra (in 2018) and Indian Water Resources Society, Roorkee (2019). He is recipient of Distinguished Alumni Award (in 2016) by College of Technology and Engineering Alumni Society, CTAE (MPUAT), Udaipur. He is the recipient of the prestigious Science Without Border scholarship—Young Talent of CNPq, Brazil and has spent about 6 months as Research Collaborator at Department of Agronomy, Universidade Federal Rural De Pernambuco (UFRPE), Ministry of Education, Brazil.

**Dr. Sangeeta Kumari** is currently working as an assistant professor at National Institute of Technology Jamshedpur, Jharkhand, India. She holds Ph.D. degree in water resources engineering from Indian Institute of Science, Bangalore; M.S. (by research) in water resources engineering from Indian Institute of Technology Madras, Chennai; and B.Sc. Engineering in Civil Engineering from Muzaffarpur Institute of Technology, Bihar, India. Her research area includes water resources systems, applied hydrology, hydraulic engineering, reservoir operation, fuzzy set theory, uncertainty analysis, genetic algorithm, irrigation and drainage engineering, infiltration models, ground water and stochastic hydrology. She has published research papers in *ASCE Journal of Irrigation and Drainage Engineering* and *ISH Journal of Hydraulic Engineering*. She has recently authored one book chapter in the book *An Introduction to Fuzzy Sets, Series: Mathematics Research Developments*, Nova Science Publishers. She has participated in international conferences such as American Geophysical Union (AGU) Fall Meeting, and International Conference on Hydraulics, Water

resources and Environmental Engineering, (ISH—HYDRO). She is reviewer of journals such as *ASCE Journal of Irrigation and Drainage Engineering*, *ISH Journal of Hydraulic Engineering*, *Journal of Hydrology and Water Supply*. She is associate member of American Society of Civil Engineering (ASCE) and life members of Indian Society for Hydraulics (ISH) and Indian Water Works Association (IWWA). She has industrial experience of 4.5 years in consultancy firms.

# Hydrological Modelling

# Trends of Rainfall and Temperature over Chhattisgarh During 1901–2010



Shashikant Verma, A. D. Prasad, and Mani Kant Verma

**Abstract** Concerning climate change, it is necessary to examine the statistical behavior of meteorological variables particularly in a country where rain-fed agriculture is predominant, it is crucial to assess the climate-induced changes and suggest the appropriate adaptation strategies. The main objectives of the present study are as follows: (i) to analyze trends in rainfall and temperatures over Chhattisgarh during 1901–2010. (ii) to detect the monotonic trends in seasonal, and annual rainfall and temperature using Mann–Kendall (MK) technique. In this paper, the results reveal that the very comparable trends were observed after the change point (1962–2010), whereas before the change point (1901–1961) converse trends have been observed, i.e., pre-change points showing growing patterns of rainfall, although post-change precipitation showed a decreasing trend. The greatest decrease in the Jashpur district is found at  $-2.23$  mm per year. The rate of decrease in annual rainfall over the 110 years is  $-0.443$  mm per year for the entire state. The results indicated that the complete study area is having a downward trend of rainfall. Some districts like Dhamtari, Kanker, Mahasamund, Sarguja, and Raipur are showing a drastic downfall in rainfall. Thus, the study of rainfall and temperature trend analysis may help to forecast the future climate change scenario and allow effective and sustainable regional water resource management.

**Keywords** Mann Kendall · Sen slope · Change point · Spatio-temporal trend · Climate change · Variability · Meteorological data

---

S. Verma (✉) · A. D. Prasad · M. K. Verma  
Civil Engineering Department, National Institute of Technology, Raipur, Raipur 492001, India  
e-mail: [sverma.phd2018.ce@nitrr.ac.in](mailto:sverma.phd2018.ce@nitrr.ac.in)

A. D. Prasad  
e-mail: [adprasad.ce@nitrr.ac.in](mailto:adprasad.ce@nitrr.ac.in)

M. K. Verma  
e-mail: [manikverma.ce@nitrr.ac.in](mailto:manikverma.ce@nitrr.ac.in)

## 1 Introduction

Water is a natural resource and is designed for all projects, created and managed, its accessibility is a significant issue. Indian farming mainly focuses on the distribution and allocation of rainfall. The main variable in the preparing and management of water resources operations such as agricultural manufacturing, changes in water requirements, irrigation, and reservoirs is the distribution of rainfall [1]. Climate change is associated with different hydro-meteorological behavior parameters relative to two separate stages. Climate variability is not a technique of very short duration. It requires years or decades for a noticeable climate change [2]. The differences in temperature and the uneven rainfall first appear in the image when the word changes in climate are coined. This can lead from India's view of severe harmful circumstances due to bad adjustment policies and a very big population [3]. Intensive flooding and serious drought may simultaneously prevail in different areas of the nation [4]. Comprehensive human initiatives would further intensify this. However, the question to be researched is whether it is a drought or a flood, and the variability in Rainfall will be a significant impact on these components [5]. In India, it counts for rainfall due to the South-West monsoon, which is June–September Rainfall. In the perspective of the increase in temperature, rainfall is also anticipated to increase in favor of such climate change in certain areas of the globe. In various geographical places in India, several researchers worked on trend analysis of rainfall. Most of the studies were used to define trends using non-parametric and linear regression test methods. We used non-parametric methods in this stud because the World Meteorological Organization (WMO) indicates that it is a free distribution and robust against outliers to identify significant monotonous upward and downward trends for specific climatic and hydrological time scales [4].

Spatio-temporal changes in Rainfall information that can occur gradually, rapidly, and suddenly (following a steady trend), (phase change), or in a more complicated way can be differentiated over time based on shifts in the features of data distribution (mean, center, variance, kurtosis, skewness, autocorrelation, etc.) [6]. Sudden or permanent changes in climate variables may occur through typical climatic patterns or through changes or errors in how measurements are made.

Having analyzed 30 monthly, seasonal, and annual rainfall trends over 135 years (1871–2005) in Indian subdivisions, rising annual rainfall was observed in a single subdivision. (Chhattisgarh) for half of the districts and decreasing Rainfall. Rainfall decreased here on an annual and storm case, although pre-and post-storm rainfall and winter rainfall [7].

## 2 Study Area

In the eastern central part of India, Chhattisgarh is located with a total population of 25.5 million and a total area of 135,191 km<sup>2</sup>, it is the 10th largest state of India

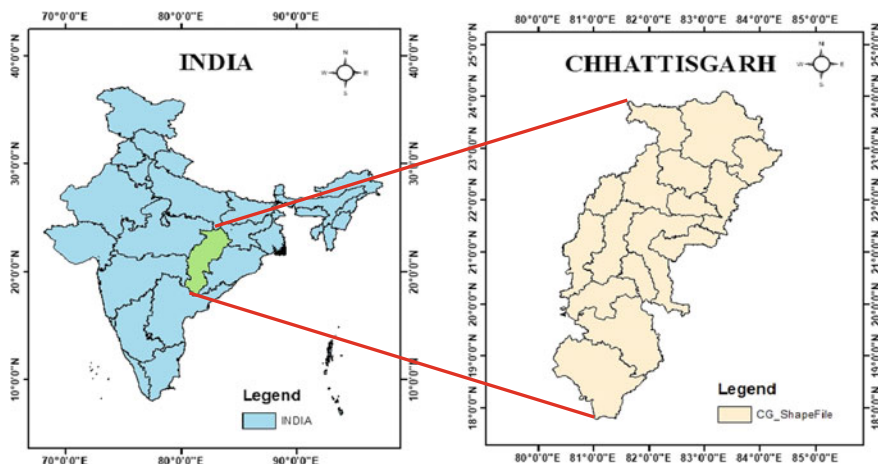


**Fig. 1** Index map of Chhattisgarh state

and 16th most populated state of the country as shown in Fig. 1. Chhattisgarh is a resource-rich state, power surplus state, and also produces 15% of the total steel for the country. Agriculture is considered to be the chief economic occupation of the state. In India, it is one of the fastest-developing states. Chhattisgarh is having a tropical climate. Due to its proximity to the Cancer Tropic and its dependency on the monsoons for rainfall, the climate is warm and humid. Summer temperatures exceed 45 °C in this area. The monsoon season begins at the end of June to October and is a welcome heat respite. Chhattisgarh receives 1292 mm of rainfall on average. The Winter season stretches from November to January; winters have low temperatures and less humidity and are pleasant.

## 2.1 Climate of Chhattisgarh

The climate of Chhattisgarh is tropical. Due to its proximity to the Cancer Tropic and its dependency on the rainstorm of the downpour, it is warm and humid. An assortment of three periods of Chhattisgarh can be seen.

- Summer is from April to June in Chhattisgarh and temperatures can reach 46 °C. The highest temperature was found in Champa. Champa is the most sweltering spot in the area, where the normal temperature is 36 °C.
- The rainstorm or the monsoon season is from late June to October and is an appreciated break structure the warmth. On a normal Chhattisgarh gets a normal of 1292 mm of a downpour. January is the coldest month with a daily average temperature of 30 °C and a daytime average temperature of 10.2 °C.

- November to January is the time for the winter season in Chhattisgarh. The ‘Pat’ region of Chhattisgarh is colder. The average lowest temperature is found at 16.1 °C at Ambikapur.

## 2.2 Data Used

The various sets of data have been used where the study course of Chhattisgarh state. The basic data, which were collected and used during the entire works, are rainfall & temperature. Among all the data were collected by visiting respective areas concerned with the state. The most important parameters such as rainfall, temperature collected from different meteorological stations of Chhattisgarh.

## 3 Methodology

To examine spatio-temporal rainfall shifts, monthly rainfall data were used to generate annual time series, pre-monsoon, monsoon, post monsoon, and winter. Ideally, Rainfall data used to investigate Rainfall patterns should be affected only by climatic and atmospheric circumstances; however, the homogeneity of Rainfall records over time may be affected by distinct components such as station place, station maintenance, monitoring methods, and tools [8]. Therefore, further pattern investigation was performed on the pre and post-change point information sequences after the most likely change point was identified. The following experiments have been used to investigate trends in rainfall.

- The Pettitt Mann–Whitney test described the most likely shift year in the annual Rainfall ‘Pettitt [9]’ sequence. Below are the PMW test details given:

Assume a time series with a length of  $n(x_1, x_2, \dots, x_n)$  and with  $t$  being the most likely time point of transition. It is then possible to derive two samples,  $(x_1, x_2, \dots, x_t)$  and  $(x_{t+1}, x_{t+2}, \dots, x_n)$  by splitting the time series at time  $t$ . The following steps are used to derive an index,  $U_t$ :

$$K_T = \max |U_{t,T}|, \quad (1)$$

where,

$$U_{t,T} = \sum_{i=1}^t \sum_{j=i+1}^T \text{sgn}(x_j - x_i) \quad (2)$$

$$\text{sgn}(x_j - x_i) = \begin{cases} 1 & \text{if } (x_j - x_i) > 0 \\ 0 & \text{if } (x_j - x_i) = 0 \\ -1 & \text{if } (x_j - x_i) < 0 \end{cases} \quad (3)$$

A  $Ut$  plot against  $t$  for a time series with no change point, will result in  $ut$ 's continuously rising value. However, if there is a point of change (even a local point of change) then  $U_t$  would increase to the point of change and then start to decrease. In a time series followed by a decrease, this increase can occur several times, indicating several local change points. As such, the issue remains to determine the most important point of change.

$$Kt = \max_{1 \leq t \leq T} |Ut| \quad (4)$$

$$P = 1 - \exp \frac{-6K_T^2}{T^3 + T^2} \quad (5)$$

- In the data series, the proximity of serial correlation was distinguished by the autocorrelation coefficient.
- Using the autocorrelation function, the non-auto-correlated/auto-correlated sequences are verified and the presence of patterns in annual and seasonal rainfall is distinguished.
- The variance coefficient (CV) means how the various sub-datasets differed from the mean of the corresponding dataset [10].

### 3.1 Study of Time Series

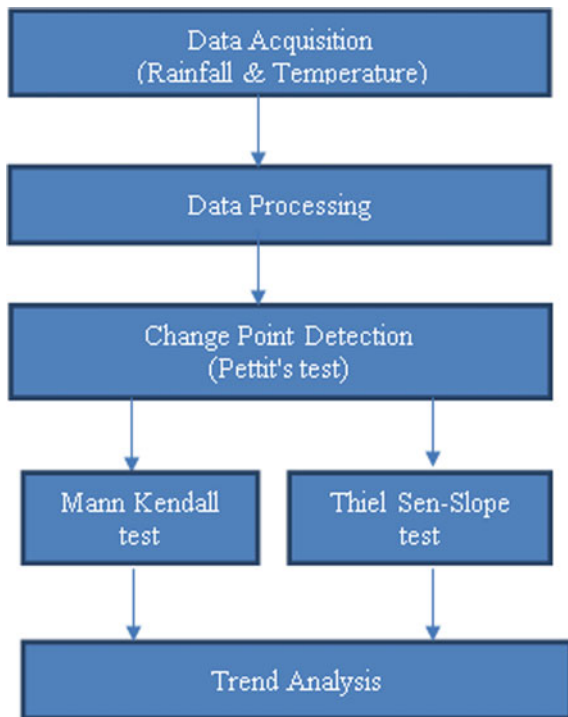
A time series is a series of random variable statistics usually collected over time and time series analysis is a method to fit time series to a proper model. Occurs in many applications (such as temperature, rainfall, Rainfall) [11, 12]. Time series method analysis predates those for specific stochastic processes and chains of Markov. The purpose of the study of time series is to describe and summarize data and conferences from time series to the low-dimensional model and to forecast future projections. This study comprises the various steps involved in the methodology of the work carried out and the proposed methodology flow chart as shown in Fig. 2. Trend Analysis applied separately for monthly time series data by using two frequently used non-parametric methods, Mann–Kendall [13] and Sen's Slope [14] are used.

### 3.2 An Analytical Method for Analyzing Trends

The Mann–Kendall (MK) test aims to assess statistically whether the interest variable has a monotonous upward or downward tendency over time series “Hirsch and Slack [15]” A monotonous upward (downward) trend includes overtime constantly increasing (declining) variables, but the trend may or may not be linear at times. No hypothesis is required for this technique (i.e., distribution). And often referred to as the Kendall tau stats, it was commonly used in climate time series testing for trend



**Fig. 2** Methodology flow chart



randomness “Zhang et al. [16]” The sample size in the MK test statistics should not be less than 30. To detect a trend, it is the most commonly used to analyze climate and hydrological time series “Zhang et al. [17]” whereas the statistical parameters of rainfall series shown in Tables 1 and 2.

The test is based on statistical  $S$  as described below in Eq. (6),

$$S = \sum_{i=1}^{N-1} \sum_{j=i+1}^N \text{sgn}(x_j - x_i) \quad (6)$$

where  $N$  is the data point number in the specified time sequence,  $x_i$  and  $x_j$  are the time scale  $i$  and  $j$  data values shown in Eq. (7) respectively.

$$\delta = (x_j - x_i) \quad (7)$$

$$\text{sgn}(x_j - x_i) = \begin{cases} 1 & \text{if}(x_j - x_i) > 0 \\ 0 & \text{if}(x_j - x_i) = 0 \\ -1 & \text{if}(x_j - x_i) < 0 \end{cases} \quad (8)$$

**Table 1** Statistical parameter of rainfall data

| Districts   | Annual    |         |        | Winter    |         |        | Monsoon  |           |         |        |       |
|-------------|-----------|---------|--------|-----------|---------|--------|----------|-----------|---------|--------|-------|
|             | Mean (mm) | SD (mm) | CV (%) | Mean (mm) | SD (mm) | CV (%) | % Annual | Mean (mm) | SD (mm) | CV (%) |       |
| Bastar      | 1284.64   | 201.14  | 16.10  | 17.24     | 15.21   | 88.20  | 1.38     | 1040.66   | 38.84   | 17.16  | 83.34 |
| Bilaspur    | 736.39    | 176.77  | 24.00  | 65.62     | 30.46   | 46.42  | 8.91     | 604.01    | 169.20  | 28.01  | 82.02 |
| Raigarh     | 1375.44   | 212.73  | 15.46  | 29.17     | 19.90   | 68.22  | 2.12     | 1237.58   | 197.89  | 15.99  | 89.97 |
| Raipur      | 1264.60   | 185.47  | 14.66  | 22.68     | 17.16   | 75.68  | 1.79     | 1115.36   | 170.00  | 15.24  | 88.19 |
| Rajnandgoan | 1273.18   | 196.22  | 15.41  | 28.25     | 21.62   | 76.52  | 2.21     | 1134.15   | 175.51  | 15.47  | 89.08 |
| Dantewada   | 1084.61   | 173.36  | 15.98  | 14.77     | 12.87   | 87.18  | 1.36     | 870.58    | 147.53  | 16.94  | 80.26 |
| Dhamtari    | 1256.27   | 199.33  | 15.86  | 17.78     | 14.68   | 82.56  | 1.41     | 1107.75   | 184.10  | 16.61  | 88.17 |
| Durg        | 1216.25   | 179.52  | 14.76  | 23.28     | 17.38   | 74.64  | 1.91     | 1083.27   | 161.25  | 14.88  | 89.06 |
| Janjgir     | 1306.26   | 188.47  | 14.42  | 28.86     | 19.89   | 68.93  | 2.20     | 1165.53   | 172.93  | 14.83  | 89.22 |
| Jashpur     | 1418.29   | 244.89  | 17.26  | 38.35     | 24.97   | 65.11  | 2.70     | 1266.76   | 227.09  | 17.92  | 89.31 |
| Mahasamund  | 1275.53   | 189.28  | 14.83  | 23.68     | 17.96   | 75.83  | 1.85     | 1131.10   | 175.51  | 15.51  | 88.67 |
| Kanker      | 1234.23   | 200.00  | 16.21  | 26.66     | 18.89   | 65.46  | 2.10     | 885.18    | 157.63  | 17.80  | 71.71 |
| Kawardha    | 1329.57   | 189.84  | 14.27  | 42.00     | 29.46   | 70.16  | 3.15     | 1187.24   | 168.10  | 14.15  | 89.29 |
| Korba       | 1267.25   | 178.76  | 14.10  | 35.94     | 23.99   | 66.75  | 2.83     | 1125.95   | 159.89  | 14.20  | 88.84 |
| Koriya      | 1143.3    | 181.78  | 15.90  | 52.90     | 33.28   | 62.90  | 87.29    | 998.05    | 159.76  | 16.00  | 87.29 |
| Surguja     | 1286.92   | 221.54  | 17.21  | 44.81     | 28.13   | 62.76  | 3.48     | 1134.14   | 202.13  | 17.82  | 88.12 |

**Table 2** Statistical parameter of rainfall data (Contd.)

| Districts   | Summer    |         |        |          | Post monsoon |         |        |          |
|-------------|-----------|---------|--------|----------|--------------|---------|--------|----------|
|             | Mean (mm) | SD (mm) | CV (%) | % Annual | Mean (mm)    | SD (mm) | CV (%) | % Annual |
| Bastar      | 84.44     | 38.84   | 46.00  | 6.76     | 106.29       | 67.44   | 63.45  | 8.51     |
| Bilaspur    | 52.30     | 24.83   | 47.48  | 7.10     | 14.45        | 11.57   | 80.09  | 1.96     |
| Raigarh     | 55.05     | 29.57   | 53.72  | 4.00     | 53.63        | 34.33   | 64.01  | 3.89     |
| Raipur      | 62.26     | 29.16   | 46.83  | 4.92     | 64.28        | 41.53   | 64.60  | 5.08     |
| Rajnandgoan | 46.27     | 25.85   | 55.87  | 3.63     | 64.49        | 48.64   | 75.41  | 5.06     |
| Dantewada   | 74.20     | 33.80   | 45.55  | 6.84     | 125.04       | 70.97   | 56.75  | 11.52    |
| Dhamtari    | 62.42     | 30.84   | 49.41  | 4.96     | 68.29        | 46.41   | 67.96  | 5.43     |
| Durg        | 47.19     | 24.41   | 51.72  | 3.88     | 62.50        | 44.76   | 71.62  | 5.13     |
| Janjgir     | 56.76     | 28.54   | 50.27  | 4.34     | 55.10        | 34.82   | 63.19  | 4.21     |
| Jashpur     | 52.57     | 31.86   | 60.62  | 3.70     | 60.60        | 40.86   | 67.43  | 4.27     |
| Mahasamund  | 62.88     | 30.11   | 47.89  | 4.90     | 57.86        | 36.67   | 63.38  | 4.53     |
| Kanker      | 80.24     | 52.90   | 65.93  | 6.50     | 242.25       | 79.99   | 33.02  | 19.62    |
| Kawardha    | 40.45     | 22.67   | 56.04  | 3.04     | 59.87        | 44.31   | 74.01  | 4.50     |
| Korba       | 45.78     | 24.13   | 52.72  | 3.61     | 59.57        | 39.61   | 66.49  | 4.70     |
| Koriya      | 42.83     | 25.27   | 58.99  | 3.74     | 49.50        | 34.59   | 69.89  | 4.32     |
| Surguja     | 43.41     | 25.78   | 59.39  | 3.37     | 64.53        | 44.58   | 69.09  | 5.01     |

In Eq. (8), the mean and variance of the  $S$  statistics are assumed to be independent and identically distributed [18] and  $E(S) = 0$  therefore,

$$\text{Var}(S) = \frac{N * (N - 1) * (2N + 5) - \sum_{k=1}^n tk * (tk - 1) * (2tk + 5)}{18} \tag{9}$$

where  $N$  is the number of the group (the difference between the results compared is null) and  $tk$  is the number of data points connected in the  $k$ th cluster. Using Eq. (10), to calculate the  $Z$  statistics or standard normal deviation:

$$Z = \left\{ \begin{array}{l} \frac{s - 1}{\sqrt{\text{var}(s)}} \text{ if } S > 0, \\ 0 \text{ if } S = 0, \\ \frac{s + 1}{\sqrt{\text{var}(s)}} \text{ if } S < 0 \end{array} \right\} \tag{10}$$

Here, if the value of  $|Z| > Z^*$  then in a two-tailed test, it rejects the null hypothesis of no trend at 5% of the significance level. (the trend is significant) [18].

### 3.3 Thiel Sen's Slope

The slope of Thiel Sen helps estimate the shift in the magnitude of a linear trend and was most frequently used to define the magnitude of the time series hydro-meteorological. If there is a linear trend, Sen [14] will develop a simple non-parametric method.

Here, the full information group's Slope ( $T_i$ ) is calculated are as given below in Eq. (11) [19].

$$T_i = \frac{x_j - x_k}{j - k} \text{ for } i = 1, 2, 3, 4, \dots, N \tag{11}$$

where, at time  $j$  and  $k$  ( $j > k$ ) respectively, the data sizes are  $x_j$  and  $x_k$ . The slope estimator's median  $Q_i$  is depicted in Eq. (12), as,

$$Q_i = \left\{ \frac{TN + 1}{2}, N \text{ is odd}, \frac{1}{2} \left( \frac{TN}{2} + \frac{TN + 2}{2} \right), N \text{ is even} \right\} \tag{12}$$

A positive  $Q_i$  value is shown by the increasing trend, and an adverse valuation in the defined time series is a downward trend.

### 3.4 Monthly Trend Analyzes

At a 5 percent significance stage, the MWPT-based rainfall time series homogeneity experiments were performed.  $H_0$  represented a homogeneous structure and  $H_a$  represented a heterogeneous system in the rainfall time series, i.e., the prospective presence of a change point. Alexandersson [20], Roy [21] as shown in Table 3. Each changing point in rainfall data (monthly, seasonally, or annually) was recognized by the MWP experiments. Both studies suggested that 1961. Across the Chhattisgarh state, the most probable shift point in the rainfall series was shown in Table 4 which summarizes the change points of the various district.

## 4 Results and Discussion

Statistical Characteristics of Annual and Seasonal Rainfall:

The 110-year average  $\pm$  standard deviation rainfall of the state was  $1234.45 \pm 194.94$  mm and ranged from a minimum of 736.39 mm per year (Pmin) to a peak of 1418.19 mm (Pmax) respectively. For the pre-monsoon period (Pmin = 40.45 mm, Pmax = 84.44 mm,  $\sigma_p = 29.91$  mm), Rainfall statistics were also created. Monsoon time (Pmin = 604.01 mm, Pmax = 1266.76 mm,  $\sigma_p = 166.71$  mm), post monsoon time (Pmin = 14.45 mm, Pmax = 242.25 mm,  $\sigma_p = 45.06$  mm), and wintertime

**Table 3** Categories of Mann–Kendall Z statistics “Roy [21]”

| Z Statistics   | The Significance Level of the Trend                        |
|----------------|--|
| >1.96          | An increasing trend with >95% of the significance level    |
| >1.65          | An increasing trend with >90% of the significance level    |
| 1.64 to 0.84   | An increasing trend with >90–80% of the significance level |
| 0.83 to 0.52   | An increasing trend with >80–70% of the significance level |
| 0.52 to 0.00   | Increasing trend but Insignificance                        |
| 0.00 to –0.52  | Decreasing trend but Insignificance                        |
| –0.52 to –0.83 | Decreasing trend with >80–70% of the significance level    |
| –0.83 to –1.64 | Decreasing trend with >90–80% of the significance level    |
| <–1.65         | Decreasing trend with >90% of the significance level       |
| <–1.96         | Decreasing trend with >95% of the significance level       |

**Table 4** Results of Mann–Whitney Pettit’s test from 1901–2010

| Stations    | Location                 | Pettit’s Test |                |
|-------------|--------------------------|---------------|----------------|
|             |                          | t (Year)      | Trend          |
| Bastar      | (19.10° N to 81.95° E)   | 1963          | H <sub>a</sub> |
| Bilaspur    | (22.07° N to 82.13° E)   | 1974          | H <sub>a</sub> |
| Raigarh     | (21.89° N to 83.39° E)   | 1949          | H <sub>a</sub> |
| Raipur      | (21.25° N to 81.62° E)   | 1961          | H <sub>a</sub> |
| Rajnandgoan | (21.09° N to 81.03° E)   | 1961          | H <sub>a</sub> |
| Dantewada   | (18.84° N to 81.38° E)   | 1923          | H <sub>a</sub> |
| Dhamtari    | (20.70° N to 81.55° E)   | 1961          | H <sub>a</sub> |
| Durg        | (21.19° N to 81.28° E)   | 1961          | H <sub>a</sub> |
| Janjgir     | (21.97° N to 82.47° E)   | 1961          | H <sub>a</sub> |
| Jashpur     | (22° 53’ N to 84° 12’ E) | 1949          | H <sub>a</sub> |
| Mahasamund  | (21.10° N to 82.09° E)   | 1961          | H <sub>a</sub> |
| Kanker      | (20.19° N to 81.07° E)   | 1961          | H <sub>a</sub> |
| Kawardha    | (22.00° N to 81.22° E)   | 1949          | H <sub>a</sub> |
| Korba       | (22.35° N to 82.75° E)   | 1949          | H <sub>a</sub> |
| Koriya      | (23° 38’ N to 82°38 E)   | 1978          | H <sub>a</sub> |
| Surguja     | (23° 10’ N to 83° 15’ E) | 1949          | H <sub>a</sub> |

Where H<sub>a</sub> year at which change occurred in time series

( $P_{min} = 14.77$  mm,  $P_{max} = 65.62$  mm,  $\sigma_p = 21.61$  mm). During the study period, these statistics demonstrate the limitations of rainfall variability to better comprehend rainfall behavior.

The MK and Theil-Sen shift estimator test(s) were applied to every district(s) at all times. Test statistics for MK test ( $\alpha = 5\%$  significance level shown in Table 4) this means that the three-time scale increases ( $Z > 0$ ) and decreases ( $Z < 0$ ). (1901–2010), pre- (1901–1961) and post-change (1962–2010) comprehensive series. Out of 192 cases, 4 and 13 cases are major positive and negative trends based on the Mann Kendall test, respectively, for all 16 districts' monthly trends ( $16 * 12 = 192$  cases). Most of the major negative trends emerged in September, similarly, for annual and seasonal trends ( $16 * 5 = 80$  cases) out of 80 cases, 1 and 20 cases are significantly positive and negative patterns for the rainfall and temperature time series as shown in Table 5 and Table 6 respectively.

**Table 5** Mann Kendall Z statistics for annual and seasonal rainfall

| Districts   | Mann Kendall Z statistics |         |             |              |        |
|-------------|---------------------------|---------|-------------|--------------|--------|
|             | 1901–2010                 |         |             |              |        |
|             | Annual                    | Monsoon | Pre-monsoon | Post monsoon | Winter |
| Bastar      | -0.170                    | -0.328  | 0.974       | 0.979        | 0.586  |
| Bilaspur    | 1.825                     | 2.064*  | 1.824*      | 1.553        | -0.927 |
| Raigarh     | -2.81*                    | -2.29   | -1.54       | 0.21         | -0.71  |
| Raipur      | -2.70*                    | -1.64   | -1.69       | 0.10         | -0.30  |
| Rajnandgoan | -2.39*                    | -1.75   | -0.84       | -0.06        | 0.19   |
| Dantewada   | 1.705                     | 1.576   | 1.348       | 1.263        | -1.764 |
| Dhamtari    | -2.236*                   | -2.107  | -0.269      | 0.093        | -0.984 |
| Durg        | -2.761*                   | -2.568* | -1.126      | 0.245        | 1.390  |
| Janjgir     | -2.94*                    | -2.33*  | -1.61       | -0.005       | -0.49  |
| Jashpur     | -2.50*                    | -2.13*  | -1.15       | 0.06         | -0.72  |
| Mahasamund  | -2.77*                    | -2.01*  | -2.01*      | 0.10         | -0.54  |
| Kanker      | -2.13*                    | -0.77   | -1.49       | -0.03        | -0.35  |
| Kawardha    | -2.49*                    | -2.30*  | -0.55       | -0.24        | 0.28   |
| Korba       | -2.64*                    | -2.65*  | -0.94       | -0.16        | -0.09  |
| Koriya      | -1.93                     | -2.30*  | -0.25       | -0.23        | 0.09   |
| Surguja     | -2.44*                    | -2.46*  | -0.83       | -0.27        | -0.23  |

Where +ive sign represents an increasing trend, the -ive sign represents the decreasing trend and the \*mark represents trend at a 5% significant level

**Table 6** Mann Kendall Z statistics for annual and seasonal temperature

| Districts   | Mann Kendall Z Statistics |         |             |              |        |
|-------------|---------------------------|---------|-------------|--------------|--------|
|             | 1901–2010                 |         |             |              |        |
|             | Annual                    | Monsoon | Pre-Monsoon | Post Monsoon | Winter |
| Bastar      | 6.63*                     | 3.00*   | 4.03*       | 4.08*        | 5.31*  |
| Bilaspur    | 191                       | −3.24*  | 2.81*       | 1.05         | 3.61*  |
| Raigarh     | 4.45*                     | −2.29*  | 1.00        | 4.34*        | 5.37*  |
| Raipur      | 5.32*                     | 1.07    | 1.97*       | 4.35*        | 5.46*  |
| Rajnandgoan | 5.22*                     | 1.17    | 2.28*       | 4.22*        | 5.22*  |
| Dantewada   | 7.06*                     | 3.94*   | 4.70*       | 4.32*        | 5.41*  |
| Dhamtari    | 5.73*                     | 1.64    | 2.67*       | 4.30*        | 5.48*  |
| Durg        | 5.21*                     | 1.12    | 2.16*       | 4.31*        | 5.37*  |
| Janjgir     | 4.69*                     | 0.21    | 1.19        | 4.51*        | 5.48*  |
| Jashpur     | 4.33*                     | −0.27   | 0.83        | 4.71*        | 5.13*  |
| Mahasamund  | 4.78*                     | 0.67    | 1.57        | 4.35*        | 5.32*  |
| Kanker      | 6.10*                     | 2.20*   | 3.32*       | 4.30*        | 5.41*  |
| Kawardha    | 4.98*                     | 0.68    | 1.48        | 4.90*        | 5.26*  |
| Korba       | 4.70*                     | 0.19    | 1.16        | 4.92*        | 5.42*  |
| Koriya      | 4.76*                     | −0.40   | 0.98        | 5.33*        | 5.32*  |
| Surguja     | 4.60*                     | −0.27   | 0.83        | 5.10*        | 5.20*  |

Where +ive sign represents an increasing trend, the −ve sign represents the decreasing trend and the \* mark represents trend at a 5% significant level

#### 4.1 Magnitude of Trend:

When evaluating, the rate of rainfall changes over time (mm per year) for annual and seasonal series throughout a significant number of districts. The greatest decrease in the Jashpur district was found (−2.23 mm per year). The rate of decrease in annual rainfall over the 110 years was −0.443 mm per year for the whole state. This is represented in Tables 7 and 8 for rainfall and temperature time series respectively.

## 5 Conclusion

In Chhattisgarh State, the trends and variability in annual and seasonal rainfall and temperature time series were studied. For exploring these trends, the Mann–Kendall, and Sen slope test were used. The incline assessment experiments of the Sen were used for pattern recognition to locate possible changes in patterns of rainfall, the Mann–Whitney–Pettitt test was used to evaluate the breakpoint. The incline assessment experiments of the Sen were used for pattern recognition to locate possible

**Table 7** The magnitude of trend for annual and seasonal rainfall series

| Districts   | 1901–2010 |         |             |              |        |
|-------------|-----------|---------|-------------|--------------|--------|
|             | Annual    | Monsoon | Pre-Monsoon | Post Monsoon | Winter |
| Bastar      | -0.83     | -0.14   | 0.65        | 0.04         | 0.03   |
| Bilaspur    | 0.68      | 0.24    | 0.12        | 0.16         | -0.03  |
| Raigarh     | -2.08*    | -1.42   | -0.51       | 0.01         | -0.04  |
| Raipur      | -1.68     | -0.81   | -0.51       | 0.01         | -0.01  |
| Rajnandgoan | -1.78     | -0.98   | -0.33       | -0.009       | 0.01   |
| Dantewada   | 0.71      | 0.81    | 0.03        | 0.02         | -0.03  |
| Dhamtari    | -1.63     | -0.46   | -0.66       | 0.02         | -0.009 |
| Durg        | -1.61     | -0.71   | -0.40       | 0.001        | 0.007  |
| Janjgir     | -1.81     | -1.31   | -0.46       | -0.002       | -0.03  |
| Jashpur     | -2.23*    | -1.72   | -0.38       | 0.004        | -0.06  |
| Mahasamund  | -1.80     | -1.01   | -0.57       | 0.01         | -0.02  |
| Kanker      | -1.59     | -0.48   | -0.54       | -0.005       | -0.01  |
| Kawardha    | -1.59     | -1.15   | -0.20       | -0.02        | 0.02   |
| Korba       | -1.71     | -1.44   | -0.25       | -0.01        | -0.009 |
| Koriya      | -1.22     | -1.24   | -0.07       | -0.02        | 0.01   |
| Surguja     | -1.85     | -1.75   | -0.29       | -0.02        | -0.02  |

Where +ve sign represents an increasing trend, the -ve sign represents the decreasing trend and the \* mark represents trend at a 5% significant level

changes in patterns of rainfall, Positive and negative Z statistics from the Mann-Kendall, and Sen slope test studies showed positive and negative trends in Chhattisgarh State. The whole assessment was conducted at the 5% significance level. The complete series (1901–2010) showed a decreasing trend in rainfall with the annual and pre-monsoon rainfall series, but post monsoon rainfall showed no trend. After the change point (1962–2010), very comparable trends were observed, while converse trends were observed before the change point (1901–1961), i.e., pre-change points showed rising rainfall patterns, while post-change rainfall showed a decreasing trend. The highest decline was noticed in the Jashpur district (-2.23 mm per year). For the entire state, the rate of decrease in annual precipitation over 110 years was -0.443 mm per year. Spatio-temporal variation within the Chhattisgarh state showed a coefficient of variation (CV) of 16.02%. The results indicated that the complete study area is having a downward trend of rainfall. Some districts like Dhamtari, Kanker, Mahasamund, Surguja, Raipur are showing the drastic downfall of rainfall and this study also depicts the annual rainfall and monthly temperature of the entire state is increases excluding monsoon and pre-monsoon seasons of Baster, Koriya, and Dantewada respectively. Other districts like Jashpur, Dantewada, Bilaspur, Surguja are changing drastically.



**Table 8** The magnitude of trend for annual and seasonal temperature

| Districts   | 1901–2010 |               |              |              |        |
|-------------|-----------|---------------|--------------|--------------|--------|
|             | Annual    | Monsoon       | Pre-Monsoon  | Post Monsoon | Winter |
| Bastar      | 0.10      | <b>-0.02</b>  | 0.032        | 0.02         | 0.033  |
| Bilaspur    | 0.037     | 0.24          | 0.12         | 0.004        | 0.02   |
| Raigarh     | 0.06      | 0.0003        | 0.008        | 0.02         | 0.03   |
| Raipur      | 0.07      | 0.008         | 0.01         | 0.02         | 0.03   |
| Rajnandgoan | 0.08      | 0.01          | 0.01         | 0.02         | 0.03   |
| Dantewada   | 0.11      | 0.02          | <b>-0.11</b> | 0.03         | 0.03   |
| Dhamtari    | 0.08      | 0.01          | 0.02         | 0.02         | 0.03   |
| Durg        | 0.085     | 0.008         | 0.01         | 0.02         | 0.03   |
| Janjgir     | 0.06      | 0.001         | 0.009        | 0.02         | 0.03   |
| Jashpur     | 0.06      | <b>-0.002</b> | 0.006        | 0.02         | 0.03   |
| Mahasamund  | 0.07      | 0.005         | 0.01         | 0.02         | 0.03   |
| Kanker      | 0.09      | 0.01          | 0.02         | 0.02         | 0.03   |
| Kawardha    | 0.07      | 0.004         | 0.01         | 0.02         | 0.03   |
| Korba       | 0.07      | 0.001         | 0.008        | 0.02         | 0.03   |
| Koriya      | 0.06      | <b>-0.03</b>  | 0.008        | 0.02         | 0.03   |
| Surguja     | 0.06      | <b>-0.002</b> | 0.006        | 0.02         | 0.03   |

Where +ve sign represents an increasing trend, the -ve sign represents the decreasing trend and the bold value represents trend at a 5% significant level

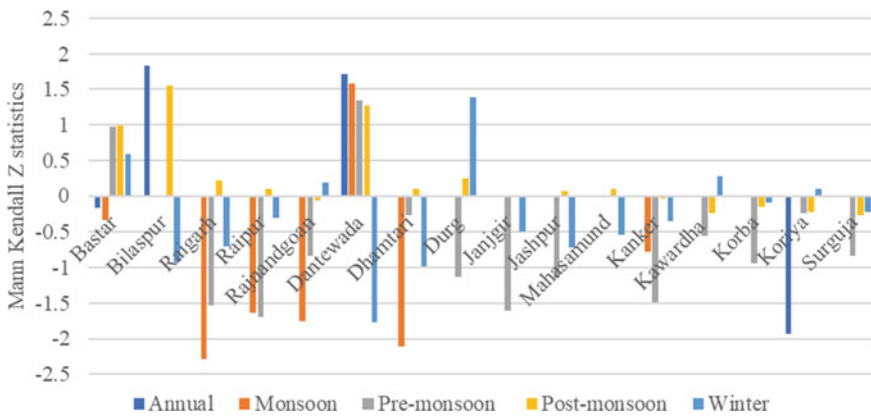


**Fig. 3** Mann Kendall test statistics for rainfall data over Chhattisgarh state during 1901–2010

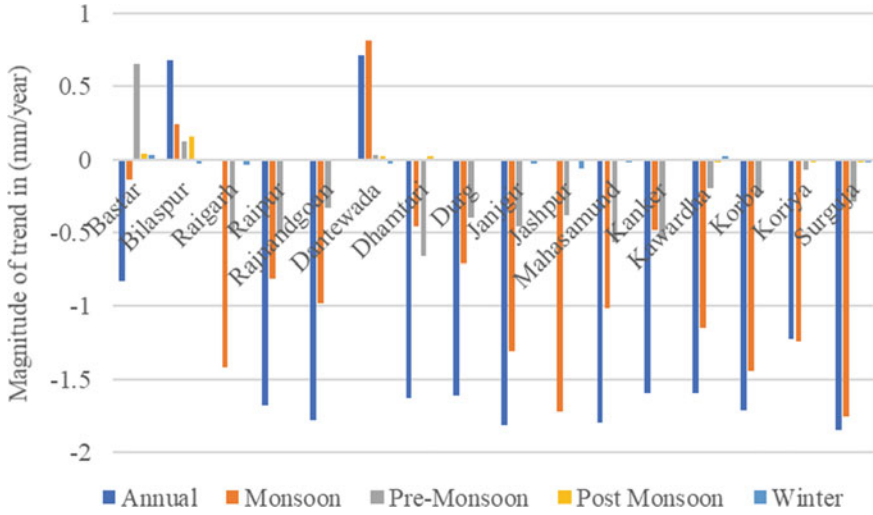


Fig. 4 Magnitude of trend for rainfall data over Chhattisgarh state during 1901–2010

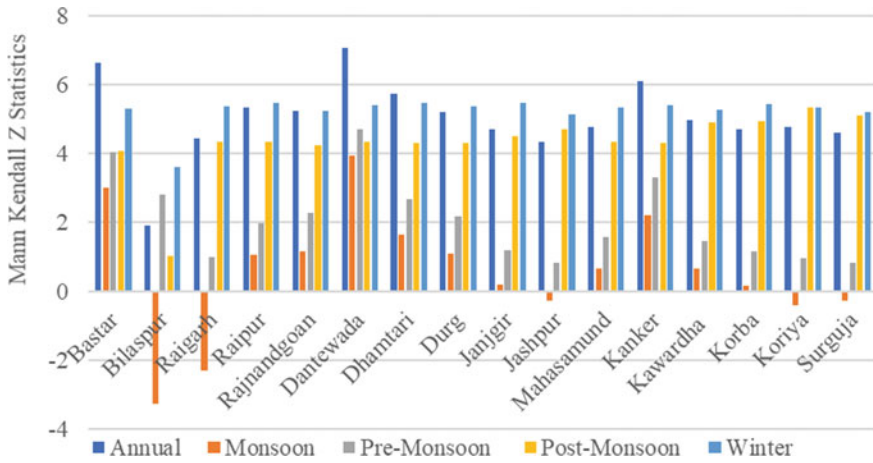
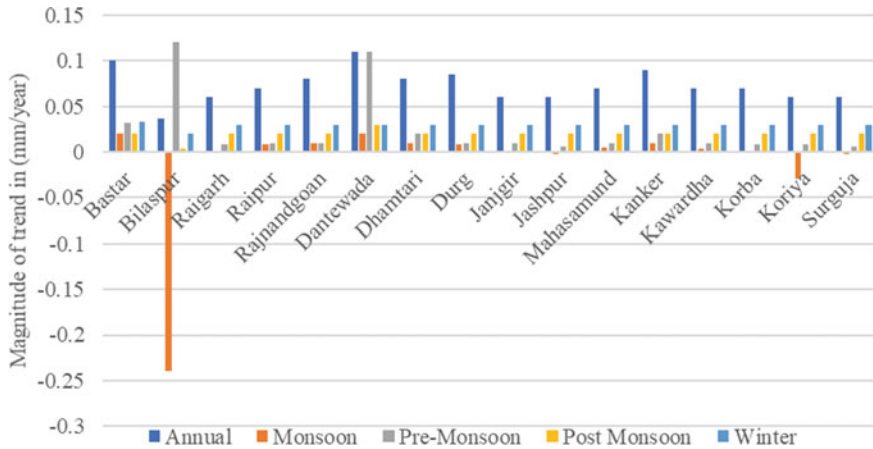


Fig. 5 Mann Kendall test statistics for temperature over Chhattisgarh state during 1901–2010



**Fig. 6** Magnitude of trend for temperature over Chhattisgarh State during 1901–2010

**Acknowledgments** The author would like to thank the Raipur (C.G.) State Data Center and the Indian Meteorological Department (IMD) of Pune, Govt. India for the provision of information on rainfall and temperature, which helped to complete this research work. The comments and feedback received from numerous reviewers have helped to develop the work.

## References

1. Chakraborty S, Pandey RP, Chaube UC, Mishra SK (2013) Trend and variability analysis of rainfall series at Seonath River Basin, Chhattisgarh (India). *J Appl Sci Eng Res* 2(4):425–434. <https://doi.org/10.6088/ijaser.020400005>
2. Swain DL, Horton DE, Singh D, Diffenbaugh NS (2016) Trends in atmospheric patterns conducive to seasonal precipitation and temperature extremes in California. *Sci Adv* 2(4):e1501344
3. Mudelsee M (2018) Trend analysis of climate time series: A review of methods. *Earth Sci Rev.* <https://doi.org/10.1016/j.earscirev.2018.12.005>
4. Gosain AK, Rao S, Basuray D (2006) Climate change impact assessment on hydrology of Indian river basins. *Current Sci* 346–353
5. Katz RW, Brown BG (1992) Extreme events in a changing climate: variability is more important than averages. *Clim Change* 21(3):289–302. <https://doi.org/10.1007/BF00139728>
6. Kundzewicz ZW, Robson AJ (2004) Change detection in hydrological records—a review of the methodology/revue méthodologique de la détection de changements dans les chroniques hydrologiques. *Hydrol Sci J* 49(1):7–19. <https://doi.org/10.1623/hysj.49.1.7.53993>
7. Kumar V, Jain SK, Singh Y (2010) Analysis of long-term rainfall trends in India. *Hydrol Sci J* 55(4):484–496. <https://doi.org/10.1080/02626667.2010.481373>
8. Wang X, Huang G, Lin Q, Nie X, Liu J (2015) High-resolution temperature and Rainfall projections over Ontario, Canada: a coupled dynamical-statistical approach. *Q J R Meteorol Soc* 141(689):1137–1146. <https://doi.org/10.1002/qj.2421>
9. Pettit AN (1979) A non-parametric approach to the change-point problem. *Appl Stat* 28(2):126–135. <https://doi.org/10.2307/2346729>

10. Landsea CW, Gray WM (1992) The strong association between western Sahelian monsoon rainfall and intense Atlantic hurricanes. *J Clim* 5(5):435–453
11. Adhikari R, Agrawal RK (2013) An introductory study on time series modeling and forecasting. arXiv preprint [arXiv:1302.6613](https://arxiv.org/abs/1302.6613)
12. Longobardi A, Villani P (2010) Trend analysis of annual and seasonal rainfall time series in the Mediterranean area. *Int J Climatol* 30(10):1538–1546. <https://doi.org/10.1002/joc.2001>
13. Kendall, M., 1975. *Multivariate analysis* (No. BOOK). Charles Griffin.
14. Sen PK (1968) Estimates of the regression coefficient based on Kendall's tau. *J Am Stat Assoc* 63(324):1379–1389. <https://doi.org/10.2307/2285891>
15. Hirsch RM, Slack JR (1984) A nonparametric trend test for seasonal data with serial dependence. *Water Resour Res* 20(6):716–732. <https://doi.org/10.1029/WR020i006p00727>
16. Zhang X, Harvey KD, Hogg WD, Yuzuk TR (2001) Trends in Canadian streamflow. *Water Resour Res* 37(4):987–998. <https://doi.org/10.1029/2000WR900357>
17. Zhang Q, Liu C, Xu CY, Xu Y, Jiang T (2006) Observed trends of annual maximum water level and streamflow during past 130 years in the Yangtze River basin, China. *J Hydrol* 324(1–4):255–265. <https://doi.org/10.1016/j.jhydrol.2005.09.023>
18. Potvin C, Roff DA (1993) Distribution-free and robust statistical methods: viable alternatives to parametric statistics. *Ecology* 74(6):1617–1628. <https://doi.org/10.2307/1939920>
19. Parthasarathy B, Dhar ON (1975) Trend analysis of annual Indian rainfall. *Hydrol Sci Bull* 20(2):257–260
20. Alexandersson H (1986) A homogeneity test applied to Rainfall data. *J Climatol* 6(6):661–675. <https://doi.org/10.1002/joc.3370060607>
21. Roy AD (2015) Trend detection in temperature and rainfall over Rajasthan during the last century. *Asian J Res Soc Sci Hum* 5(2):12–26. <https://doi.org/10.5958/2249-7315.2015.00022.2>
22. Jebb AT, Tay L, Wang W, Huang Q (2015) Time series analysis for psychological research: examining and forecasting change. *Front Psychol* 6:727
23. Li J, Jiang Y, Fan R (2007) Recognition of biological signal mixed based on wavelet analysis. In: Jiang Y et al (eds) *Proceedings of UK-China sports engineering workshop*. World Academic Union, Liverpool, pp 1–8 (Use “References” Style)
24. Dewri R, Chakraborti N (2005) Simulating recrystallization through cellular automata and genetic algorithms. *Modelling Simul Mater Sci Eng* 13(3):173–183

# Estimation and Simulation of Flows into an off-Taking Canal Using ANSYS



V. Chakravarthy, S. V. S. N. D. L. Prasanna, and N. Suresh Kumar

**Abstract** The modern technologies in the area of water resources engineering are gaining lot of importance in the present days. These technologies play a vital role in advancement toward the intricate approach for solving various real-life problems. One such initiation is the simulation analysis. The major advantage of this approach is the reduction in the utilization of natural resources for physical modeling. The present investigation is aimed at application of this methodology for analyzing the flows into an off-taking canal. The flow rate in a natural stream may vary significantly during different periods of the year. A canal head regulator is needed not only for diverting water but also for regulating the water supplies into an off-taking canal whenever required. The primary goal of the current examination is to simulate the water surface profile for pond level flow condition. The waterway of the head regulator should be adequate in order to pass the required discharge into the canal with considered pond level. The studies were carried out for half supply depth in the canal with pond level condition. The hydraulic calculations performed for pond level flow condition will enable the level of jump formation. Accordingly, from the simulation analysis the cistern dimensions can be arrived and the thickness of the sloping floor can be computed. Even without performing the physical modeling, it is possible to arrive at important design parameters of Canal Head Regulator. In the present investigations, the simulation methodology was carried out using two different turbulence models viz.,  $k-\varepsilon$ , and  $k-\omega$  computing height and length of jump. The simulation results were observed to have good agreement with the analytical estimations.

**Keywords** Head regulator · Pond level · Turbulence models · Volume fraction

## 1 Introduction

The structure constructed at the head of canal taking-off from a reservoir behind a weir is termed as head regulator. It comprises of a number of spans separated by piers

---

V. Chakravarthy · S. V. S. N. D. L. Prasanna · N. Suresh Kumar (✉)  
Department of Civil Engineering College of Engineering (A), Osmania University, Hyderabad,  
Telangana 500007, India

and functioned by gates similar to that in the case of a barrage. The various regulation works of canal head regulator can be categorized as Canal Fall, Head Regulator or head sluice; Cross regulator; Canal Escape and Canal Outlet.

Of various regulation works, the head regulator and cross regulator regulate the flow into the off-taking and the parent channel respectively. The distributary head regulator controls the supply entering the distributary and is available at the head of the distributary. It plays a significant role in providing a necessary link between the parent channel and the distributing channel. A distributary head is a regulator, and also acts as a meter of supply and as a silt selective structure. A cross regulator is constructed on the main canal at the downstream of the off-take to head up the water level. This enables the off-taking channel to draw the essential supply. The present study was carried out for hypothetical data to investigate the application and performance of the simulation analysis in evaluating the required results for hydraulic engineering applications.

The study focuses on the following objectives to elaborate the detailed understanding of the flow through canal head regulator.

- To analytically estimate the pre-jump, post-jump and length of the jump on the downstream side of the canal head regulator for pond level flow condition
- To estimate and compare the hydraulic jump parameters using ANSYS–CFD
- To plot the water surface profile over the canal head regulator using Simulation analysis through user-defined function (UDF).

## 2 Literature Review

The literature review revealed that not many studies were oriented toward the estimation and simulation of flow over canal head regulators. The estimation of flow profile plays a significant role in the design of further appurtenances downstream of the regulator.

Clemmens et al. [1] carried out simulation analysis adopting three commercially available unsteady-flow simulation software packages to evaluate different characteristics of the unsteady flows. The software packages adopted for automatic control operation of gates by means of an algorithm are *Canal CAD* from the Univ. of Iowa, Hydraulics Lab; *Mike 11 version 3.2* from the Danish Hydraulic Institute; and *Sobek* from Delft Hydraulics. The authors stated that Canal CAD software can be used in the analysis of simple channels and theoretical studies. They expressed that the two packages viz., Mike 11 and Sobek can handle a wide variety of complexities in fixing canals, running simulations and in results interpretation. Further, they concluded from their investigations that the codes adopted, had great difficulty in establishing steady-state conditions.

Fang et al. [2] carried out investigations to simulate the flow transition. The authors adopted method of characteristics approach to solve de Saint Venant equations for arriving at simple channel model. The studies were carried out on ninth and tenth branches of north trunk channel in Yin Tang irrigation district, Tangyuan County,

Heilongjiang province. The channels were of trapezoidal cross-section and lined using concrete. The variations in the upstream water level were simulated along with the changes in the flow on the downstream part. The consistency of the model was verified by comparing the numerical results and the simulation results obtained from MIKE11 software. The authors stated that the MIKE11 software is not efficient in simulating the regulation of gate opening and further stated that it is very costly. The authors also expressed that the present study results could be more authenticated by comparing them with the measured data.

From the present review, it was observed that none of the studies were concentrated toward the simulation of flow through canal head regulator. It was evident that extensive studies are required toward the understanding the behavior of flow and its characteristics. As physical modeling is very expensive involving lot of resources, there is an utmost requirement for an alternative methodology. The exact goal of the present investigation is to estimate the flow characteristics by means of simulation analysis.

### 3 Methodology

The present work was carried out in two different phases viz., analytical and simulation analysis, in order to estimate various characteristics of hydraulic jump as mentioned below.

#### 3.1 Analytical Analysis

The analytical computations were performed based on the following equations for the definition sketch of the hypothetical data as shown in Fig. 1. The normal depth was calculated by trial and error from Manning’s equation.

$$Q = \left( \frac{By_n}{n} \right) \left( \frac{By_n}{B + 2y_n} \right)^{2/3} (S)^{1/2} \tag{1}$$

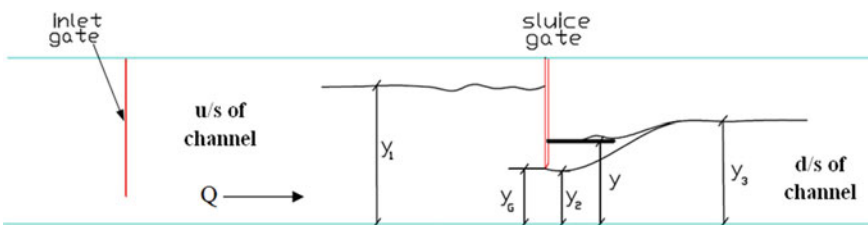


Fig. 1 Definition sketch

**Table 1** Energy loss values—analytical results

| Gate opening (m) | Flow condition | Discharge (cumec) | Flow velocity through the gate $V_2$ (m/s) | Normal depth, $y_n$ (m) | Pre-jump depth (m) | Sequent depth, $y_3$ (m) | Energy loss, $\Delta E$ (m) | Length of the jump (m) |
|------------------|----------------|-------------------|--|-------------------------|--------------------|--------------------------|-----------------------------|------------------------|
| 0.40             | Pond level     | 90.0              | 8.064                                      | 1.7421                  | 0.248              | 1.694                    | 0.1861                      | 7.230                  |

The conjugate depth is calculated from the following relation.

$$\frac{y_3}{y_2} = \frac{1}{2} \left( -1 + \sqrt{1 + 8Fr_2^2} \right) \quad (2)$$

From the momentum equation, between Eqs. (2) and (3), the energy terms are satisfied on both the sides of the equation confirming the value of the gate opening. At Eq. (2), the hydrostatic thrust term is based on ‘y’ not ‘ $y_2$ ’ [3].

$$\frac{y^2}{2} + \frac{Q^2}{gB^2y_2} = \frac{y_3^2}{2} + \frac{Q^2}{gB^2y_3} \quad (3)$$

The nomenclature adopted is appended herewith.  $B$  = width of the channel,  $y_n$  = normal depth,  $n$  = manning’s coefficient,  $V_2$  = velocity at depth  $y_2$ ,  $Fr_2$  = Froude’s number at section-2,  $y_1$  = approach flow depth,  $y_G$  = gate opening,  $y$  = depth of flow just  $d/s$  of gate;  $y_2$  = flow depth before formation of hydraulic jump (initial depth),  $y_3$  = flow depth after the formation of hydraulic jump (sequent depth). The analytical results for the pond level flow condition from basic governing equations are presented in Table 1.

### 3.2 Simulation Analysis

In the current investigation, a numerical modeling method via ANSYS–CFD (Fluent) was adopted. The finite volume approach was adopted for solving Reynolds-Averaged Navier-Stokes equations for evaluating the results. This approach was implemented in the existing study to estimate the height and length of the jump. The simulation methodology was carried out in three phases viz., Pre-processing, Processing and Post-processing. The geometry generated is detailed in Fig. 2. The discredited mesh of present study was generated in design modeler of ANSYS with the minimum orthogonal quality of 0.75 and with the maximum aspect ratio as 2.83.

To solve the equation system, boundary conditions are the next important criteria that help the system to understand the flow pattern. The typical boundary conditions very widely adopted in CFD are as follows. The boundary conditions adopted for



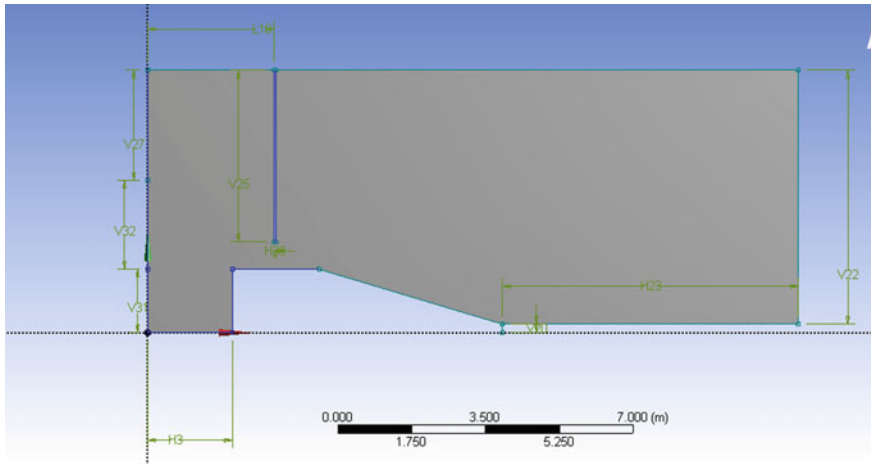


**Fig. 2** Geometry of pond level canal head regulator

the present investigations are velocity inlet, pressure outlet and wall. The analysis for convergence was carried out with 1/1000 as time step size and extended the study for more than 1000-time steps. The maximum iterations for each run were taken as 30. The flow was spotted to hit the downstream side and was observed to develop hydraulic jump. The required flow pattern was observed to arrive after 15,000 iterations. The Reynolds-Averaged Navier–Stokes equations for 2-D steady-state incompressible flows, are presented as

$$\frac{\partial \bar{u}}{\partial x} + \frac{\partial \bar{v}}{\partial y} = 0 \tag{4}$$

$$\rho \left( \bar{u} \frac{\partial \bar{u}}{\partial x} + \bar{v} \frac{\partial \bar{u}}{\partial y} \right) = -\frac{\partial \bar{p}}{\partial x} + \frac{\partial}{\partial x} \left( \mu \frac{\partial \bar{u}}{\partial x} - \rho u' u' \right) + \frac{\partial}{\partial y} \left( \mu \frac{\partial \bar{u}}{\partial y} - \rho u' v' \right) \tag{5}$$

$$\rho \left( \bar{u} \frac{\partial \bar{v}}{\partial x} + \bar{v} \frac{\partial \bar{v}}{\partial y} \right) = -\frac{\partial \bar{p}}{\partial y} + \frac{\partial}{\partial x} \left( \mu \frac{\partial \bar{v}}{\partial x} - \rho u' v' \right) + \frac{\partial}{\partial y} \left( \mu \frac{\partial \bar{v}}{\partial y} - \rho v' v' \right) \tag{6}$$

In the above momentum equations, the stress terms are  $-\rho u' u'$ ,  $-\rho v' v'$  and  $-\rho u' v'$ , defining the first two terms as normal stresses and the last term as shear stress [4]. The present investigations were carried out using

$$\frac{\partial k}{\partial t} + U_j \frac{\partial k}{\partial x_j} = \tau_{ij} \frac{\partial U_i}{\partial x_j} - \varepsilon + \frac{\partial}{\partial x_j} \left[ (v + v_T / \sigma_k) \frac{\partial k}{\partial x_j} \right] \tag{7}$$

The first term on the RHS in the above equation symbolizes the rate of production of  $k$  or  $\varepsilon$ , the second term demonstrates the rate of destruction of  $k$  or  $\varepsilon$  and the third term illustrates the transport of  $k$  or  $\varepsilon$  by diffusion. Further, the first term on the LHS

represents the rate of change of  $k$  or  $\varepsilon$  and the second term explains the transport of  $k$  or  $\varepsilon$  by convection.

Dissipation Rate:

$$\frac{\partial \varepsilon}{\partial t} + U_j \frac{\partial \varepsilon}{\partial x_j} = C_{e1} \frac{\varepsilon}{k} \tau_{il} \frac{\partial U_i}{\partial x_j} - C_{e2} \frac{\varepsilon^2}{k} + \frac{\partial}{\partial x_j} \left[ (v + v_T / \sigma_\varepsilon) \frac{\partial k}{\partial x_j} \right] \quad (8)$$

The production and the dissipation terms of Eq. (8) are formed from the production and dissipation terms of the turbulent kinetic energy ascended by  $\varepsilon/k$  and multiplied by empirical constants and wall damping functions ( $C_{e1}$  and  $C_{e2}$ ). An extra damping function shall be included for eddy viscosity term in  $k$ - $\varepsilon$  equation by near walls so that turbulent kinetic energy and epsilon shall have proper behavior in the near region. The Closure coefficients and auxiliary relations adopted are  $C_{e1} = 1.44$ ,  $C_{e2} = 1.92$ ,  $\sigma_k = 1.0$ ,  $\sigma_\varepsilon = 1.3$ ,  $\omega = \varepsilon / (C_\mu k)$  [4, 5].

In the current investigation,  $k$ - $\varepsilon$  turbulence model was used to pretend the flow by Volume of Fluid (VOF) approach. The filled cells between the upstream and downstream of the canal head regulator we retargeted to evaluate the volume fraction of water. The Graphics and Animations option in Fluent solver enables to plot the contours of multiphases viz., water and air, velocity profiles, etc. From the simulations, two different phases via. water (Red color) with a value of 1.0 and air (Blue color) with the zero value clearly elaborates the understanding of variations in multiphase analysis. The contours of volume fraction for HFL condition obtained for  $k$ - $\varepsilon$  and  $k$ - $\omega$  turbulence models are highlighted in Fig. 3. It is clear from Fig. 3 that the length of the jump computed from the simulation results is in corroboration with 5–7 times the height of the jump. Hence, it is observed that the length of the jump and cistern dimensions will be adequate to dissipate the energy of the jump.

It is evident from the contours that the value of height and length of the jump cannot be read from the contour plots. So, the quantitative results of length and height of the jump were estimated by user-defined function. The macros featuring the volume fractions at various cell points beginning from the entrance of the gate were programmed and executed in the Fluent solver. This code enabled to evaluate

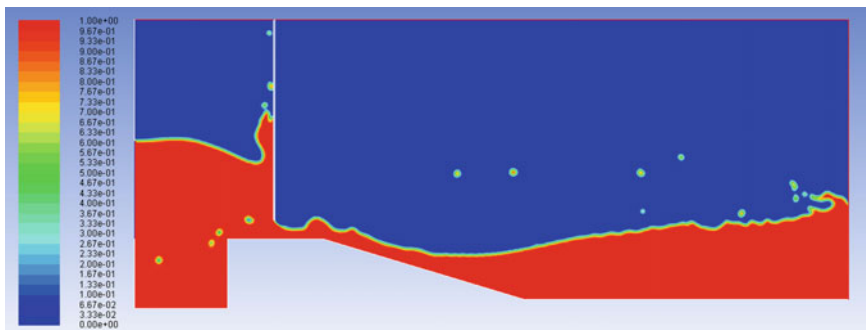


Fig. 3 Contours of volume fraction of pond level (90 cumec)  $k$ -epsilon model

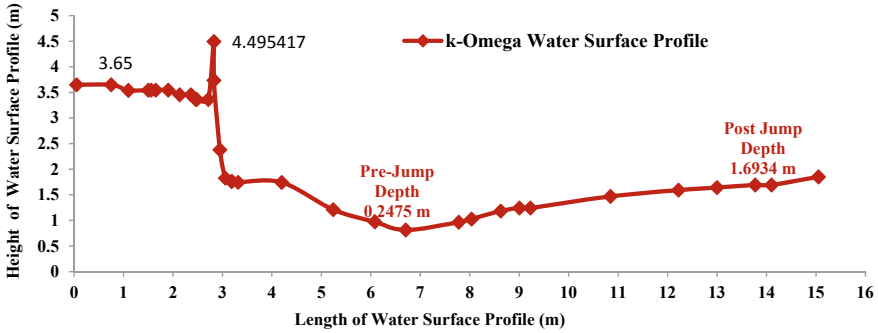


Fig. 4 Water surface profile from UDF results *k-omega* turbulence model

Table 2 UDF analysis results of *k-ε* and *k-ω* turbulence model

| Gate opening (m) | Flow condition | Discharge (cumec) | Pre-jump height (m) |            | Post-jump height (m) |            | Length of the Jump (m) |            |
|------------------|----------------|-------------------|---------------------|------------|----------------------|------------|------------------------|------------|
|                  |                |                   | <i>k-ε</i>          | <i>k-ω</i> | <i>k-ε</i>           | <i>k-ω</i> | <i>k-ε</i>             | <i>k-ω</i> |
| 0.40             | Pond level     | 90.0              | 0.2477              | 0.2475     | 1.6935               | 1.6934     | 7.229                  | 7.2295     |

the coordinates and volume fraction values at the required cells in the control domain of the geometry. These quantitative values correspond to the required parameters, viz. pre-jump, post-jump depths as well as the length of the jump. The water surface profile was also extracted from the UDF program for *k-Epsilon* and *k-Omega* turbulence models. The plot obtained from *k-Omega* model is highlighted in Fig. 4. In addition, the results of jump height and length obtained from the simulation analysis are detailed in Table 2.

It is clearly seen from Fig. 4 that water is impinging against the breast wall. Hence, in the absence of breast wall water might have splashed to the *d/s* side of the structure.

### 4 Results and Discussions

Based on the present investigations carried out in two different phases, the following results were deduced.

- The pre-jump height, post-jump height and the length of the jump were analytically estimated for PL at 90 cumec.
- The height of the pre-jump, post-jump and the length of the jump for pond level flow condition were analyzed in Fluent with *k-Epsilon* and *k-Omega* turbulence models.
- The pre-jump, post-jump height and the length of the jump values evaluated by the interpretation and execution of the macro generated using a user-defined function

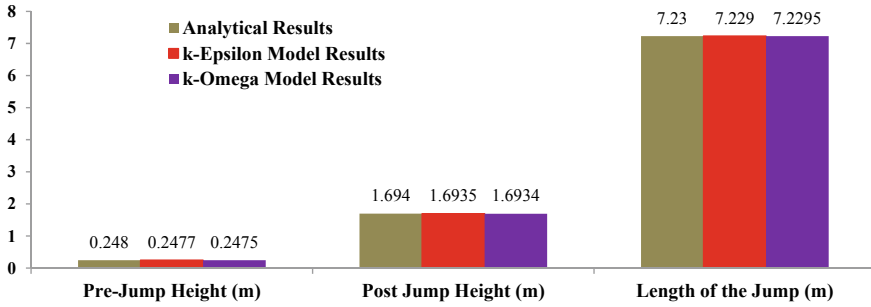


Fig. 5 Comparative results

Table 3 Comparative results

| Gate opening (m) | Flow condition and discharge | Pre-jump height % error     |                           | Post-jump height % error    |                           | Length of jump % error      |                           |
|------------------|------------------------------|-----------------------------|---------------------------|-----------------------------|---------------------------|-----------------------------|---------------------------|
|                  |                              | Analytical and $k-\epsilon$ | Analytical and $k-\omega$ | Analytical and $k-\epsilon$ | Analytical and $k-\omega$ | Analytical and $k-\epsilon$ | Analytical and $k-\omega$ |
| 0.40             | Pond level (90 cumec)        | 0.12                        | -0.20                     | 0.03                        | 0.04                      | 0.01                        | -0.01                     |

programmed for multiphase analysis were observed to have fair agreement with the analytical results as highlighted in Fig. 5.

- The comparative results of pre-jump, post-jump and length of the jump are observed to have less than 1% error between the analytical and simulated results as shown in Table 3.
- The water surface profile was observed to have same orientation by k-Epsilon and k-Omega turbulence models as detailed in Fig. 6.

## 5 Conclusions

Most of the hydraulic engineering applications involve turbulence flows. Turbulence flows comprise of nonlinear partial differential equations that are time-consuming and difficult for solving using traditional methods. The Hydraulic Engineering applications are largely evaluated by physical modeling for their detailed understanding before construction. This traditional process requires large resources and will enable to evaluate only few important parameters. The study of turbulence in Hydraulic Engineering problems involves thorough understanding of the physical concepts of the applications. Further, the results obtained from turbulence modeling needs to be compared, either the experimental and/or analytical solutions. The ANSYS-CFD modeling method adopted in the present study is user-friendly and facilitates to solve nonlinear partial differential equations within less time depending upon the size of

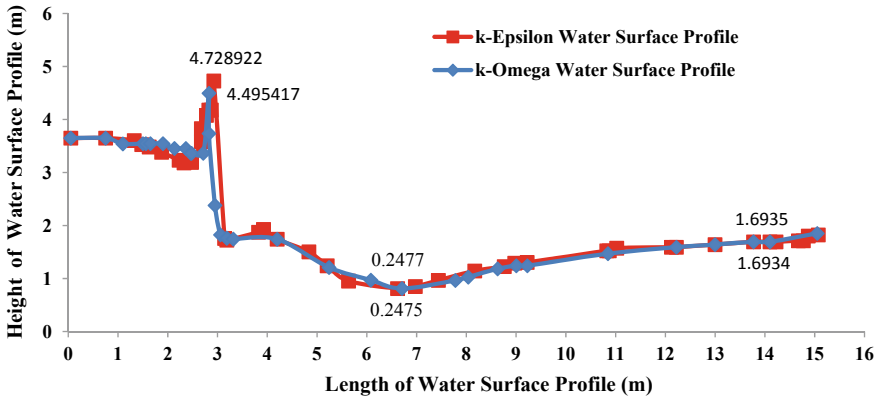


Fig. 6 Comparative graph of water surface profile

the control domain. This technique also enables to reduce the resource utilization and can be largely adopted to evaluate various turbulence parameters accurately.

## References

1. Clemmens AJ, Bautista ME, Wahlin BT, Strand RJ (2005) Simulation of automatic canal control systems. *J Irrig Drain Eng* 4(324):324–335. [https://doi.org/10.1061/\(ASCE\)0733-9437\(2005\)131](https://doi.org/10.1061/(ASCE)0733-9437(2005)131)
2. Fang T, Gu Y, He X, Liu X, Han Y, Chen J (2018) Numerical simulation of gate control for unsteady irrigation flow to improve water use efficiency in farming. *Water* 10:1196. <https://doi.org/10.3390/w10091196>
3. Suresh Kumar N, Prasanna SVSNDL (2018) Turbulence modelling for estimation of hydraulic jump height. *Recent Trends Fluid Mech* 5(3):1
4. Sayma A (2009) *Computational fluid dynamics*. Venus Publishing, ApS, pp 25–31 ([www.bookey.com](http://www.bookey.com))
5. Prasanna SVSNDL, Suresh KN (2019) Simulation and analytical estimation of spillway flip bucket parameters. *Int J Innov Technol Explor Eng* 8(12):4062–4066. <https://doi.org/10.35940/ijitee.L3632.1081219>

# Drought Evaluation of Tiruchirapalli City, India, Using Three Meteorological Indices



K. Sasireka and C. R. Suribabu

**Abstract** Large communities of people worldwide are affected by droughts, causing major economic losses, environmental harm, and social deprivation. The characteristics of the drought are hard to define, detect and monitor. Drought events are quantified by several indices when there is no real ground-level assessment system available. The drought indexes such as Standardized Precipitation Index (SPI), Statistical Z score (SZs) and China-Z Index (CZI) that can provide a direct, simple and quantitative evaluation of the key characteristics of intensity, duration of drought, and spatial extent. This article analyzes the SPI, statistical Z score and CZI on different time scales such as annual and seasonal (North–East, South–West Winter and Summer) by taking Tiruchirapalli as a study area using 25 years (1981–2005) of monthly rainfall data. In this analysis, the implementation of each index is compared and the study results suggest that the CZI and SZs can provide similar results and shows the minor deviation to the SPI for all time scales, and that the CZI and SZs computations are comparatively easy compared to the SPI.

**Keywords** Rainfall · Drought · SPI · China-Z index · Statistical Z score

## 1 Introduction

The main disasters namely floods and drought have been taken into account while formulating any development plans in any region. The execution of any development plan mainly depends upon the occurrence, intensity and distribution of these two extreme events. Among the different types of drought the most important drought is Meteorological drought. It identifies stages of drought on the basis of the number of days with precipitation below certain specified threshold [3]. The length of prolonged

---

K. Sasireka (✉) · C. R. Suribabu  
School of Civil Engineering, SASTRA Deemed University, Thanjavur, India  
e-mail: [sasireka@civil.sastra.edu](mailto:sasireka@civil.sastra.edu)

C. R. Suribabu  
e-mail: [suribabu@civil.sastra.edu](mailto:suribabu@civil.sastra.edu)

and severe drought cycles can have important consequences for conditions in agriculture, socio-economic and the climate. Comprehensive and adequate knowledge on past drought variations will allow adequate management of future drought risks [13]. Appropriate assessment of the drought characteristics is therefore critical for ensuring the effective use of water resources, agricultural and power productions. Many of the indices considered in the existing literature when evaluating meteorological drought use rainfall as the only input parameter or in conjunction with other meteorological elements.

Among the different type of drought indices, such as Palmer [8], Deciles, the China-Z index (CZI; Wu et al. [12]), and the Reconnaissance Drought Index [11] the choice of selection of the indices are based on its quality and availability of the data. Many of these indices are determined based on meteorological factors such as temperature and rainfall. In this paper CZI developed in China, the Z score Index and SPI were chosen due to their applicability to different time scales and climatic conditions. The SPI developed by McKee et al. [7] is based solely on rainfall data and is generally used for assessing and quantifying drought [6]. Suribabu and Evangelin Ramani [10] used SPI, CZI and SZs indices to find the landslide triggering factor based on the moisture level in Coonoor Hill Station. SPI's popularity is based primarily on its suitability for various time scales and its ease in testing without needing any statistical constraints.

## 2 Study Area

Tiruchirapalli district covers 4404 km<sup>2</sup> of which 1852 km<sup>2</sup> (about 42%) is agricultural land. Figure 1 shows the study area and it is situated in central Tamil Nadu and lies in the state's most fertile area of the Kaveri delta zone. Despite receiving most of its rainfall from the North-East (NE) Monsoon, Tamil Nadu receives adequate rainfall from both Monsoon seasons, making it predominant for agriculture. The annual Normal 760 mm rainfall is slightly less than the 945.00 mm state average. The 25-year daily Rainfall data from the IMD for the period 1981 to 2005 is used in this paper. Even though Meteorological department is able to consistently provide forecasts with good accuracy for a short span of time, the daily rainfall data is utilized to forecast for a long term, to plan cultivation of long-term crops by stochastic methods.

Rainfall time series of Tiruchirapalli city for various time scales is shown in Fig. 2. Figure 2 shows the maximum annual rainfall of about 1200 mm has occurred in the year 1983 and 2005 at a time interval of 22 years. From Fig. 2, it has been concluded that the NE rainfall time series pattern is similar to the annual rainfall pattern and it depicts that more contribution of NE rainfall than SW rainfall. The Tiruchirapalli city gains very meager quantity of rainfall from winter season compared to summer rainfall. Table 1 shows the average rainfall, standard deviation of different time scale as well as skewness of rainfall data. The winter rainfall shows the lowest standard deviation of 45.29 mm and it depicts that the rainfall distribution is very close to the mean rainfall and the annual rainfall shows the highest standard deviation of

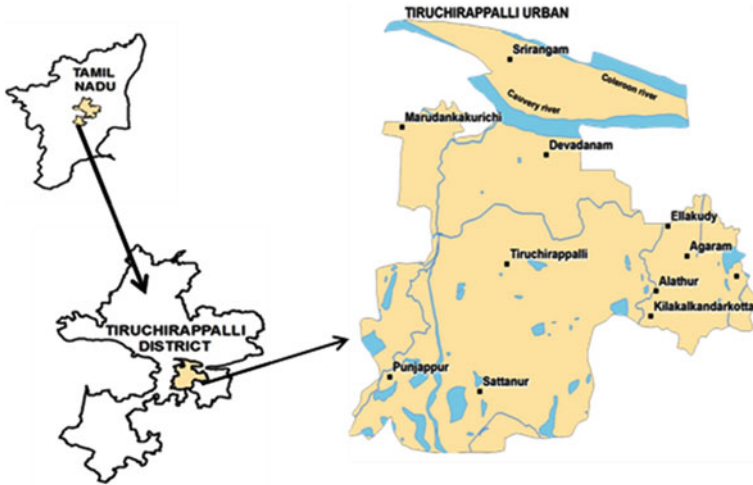


Fig. 1 Study area

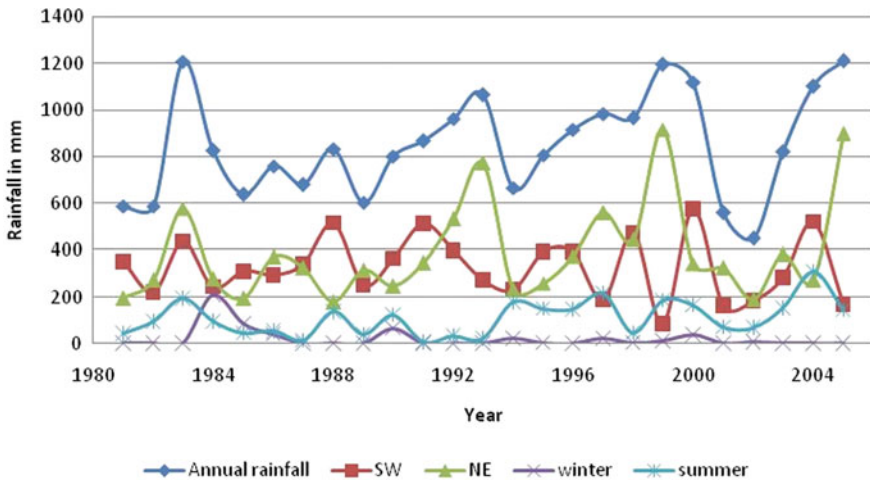


Fig. 2 Rainfall time series of Trichy city in different time scale

Table 1 Rainfall statistics of the study area

| Rainfall time scale | Mean (mm) | Standard deviation | Skewness |
|---------------------|-----------|--------------------|----------|
| Annual              | 849.29    | 221.46             | 0.1209   |
| SW                  | 326.80    | 130.27             | 0.1908   |
| NE                  | 392.02    | 209.40             | 1.4502   |
| Winter              | 20.54     | 45.29              | 3.3985   |
| Summer              | 109.92    | 75.56              | 0.6722   |



221.46 mm and this reflects the rainfall values being distributed far away from the mean annual rainfall. The positive value of the skewness represents the rainfall data are skewed right, and if the skewness value is greater than one it represents the data are highly skewed. It can be shown from Table 1 that the winter rainfall data is highly skewed than the other time scale data.

### 3 Methodology

Three Drought indices have been used to classify the historic data into seven categories moisture condition of the city ranging from Extremely Wet (EW) to Extremely Dry (ED). Twenty-five years of daily rainfall collected from IMD for the years 1981–2005 has been used to assess severity of drought occurrence in those periods. To assess the drought characteristics of the city, three indices namely SPI, CZI and SZs are selected as these three indices has a common classification and range of values for each classification. For example, if any the index value for a particular month falls between  $-0.99$  and  $0.99$  it is classified as Normal.

#### 3.1 Statistical Z score (SZs)

It has been used in many researches because of a simple calculation [1, 2]. The SZs index is a dimensionless quantity widely used in statistics. It is given by

$$Z = ((x - \mu))/\sigma \quad (1)$$

where  $x$  = individual rainfall value,  $\mu$  = long-term mean,  $\sigma$  = standard deviation.

#### 3.2 China-Z Index (CZI)

The CZI is related to cube-root transformation of Wilson–Hilferty [5]. Assuming the precipitation data are in line with Pearson Type III distribution.

$$CZI = \frac{6}{C} \left( \frac{C}{2} Z + 1 \right)^{\frac{1}{3}} - \left( \frac{6}{C} \right) + \left( \frac{C}{6} \right) \quad (2)$$

$$C = \frac{\sum_{i=1}^n (x_i - \mu)^3}{n\sigma^3} \quad (3)$$

where  $C$  = coefficient of skewness,  $x$  = precipitation for period  $i$ , and  $Z$  = Statistical Z index.

### 3.3 Standard Precipitation Index (SPI)

SPI is used in this study due to its advantages discussed below by [4].

1. Rainfall data alone sufficient for the assessment of drought using SPI.
2. The topography also doesn't significantly affect the SPI.
3. The various time scales described by the SPI help to characterize the drought conditions that are useful for hydrological and agricultural applications.
4. Another advantage lies in its standardization, which guarantees consistent frequencies of extreme events irrespective of the place and time.

In essence, computation of SPI starts with constructing a frequency distribution for a given time span from precipitation data at a site. In this method, the data is fitted with gamma probability and then fitted to normal distribution such that the SPI of a location has a zero mean [7].

The cumulative likelihood using the Gamma distribution is as follows:

$$G(x) = \frac{1}{\beta^\alpha \tau(\alpha)} \int_0^x x^{\alpha-1} e^{-x/\beta} dx \text{ for } x > 0 \tag{4}$$

where  $x$  = the precipitation value,  $\alpha$  = the shape parameter,  $\beta$  = the scale parameter, and  $\tau(\alpha)$  = Gamma function.

It can be easily calculated using built in function available in MS-Excel function as given below:

$$SPI = NORMSINV(GAMMADIST(\mu, \alpha, \beta, TRUE)) \tag{5}$$

The  $\alpha$  and  $\beta$  value can be determined using maximum likelihood method as follows:

$$\alpha = \frac{1}{4A} \left( 1 + \sqrt{1 + \frac{4A}{3}} \right) \tag{6}$$

$$\beta = \frac{\mu}{\alpha} \tag{7}$$

$$A = \ln(\mu) - \frac{\sum \ln(x)}{n} \tag{8}$$

where  $\mu$  = mean value of precipitation,  $x$  = precipitation and  $n$  = rainfall observations in numbers.

### 4 Results and Discussion

The given period was classified into seven types based on the indices calculated. Table 2 shows the range of drought indices for SPI, CZI and statistical Z score. All three indices gave coherent results with regard to the classification.

The 25 years of daily rainfall data had been used in this analysis to compute the value of drought indices for various time scales such as monthly, annual, seasonal (NE, SW, and Winter) to evaluate the wet and dry periods of the Trichirapalli city. The calculation of three drought indices was carried out using Ms-Excel software. Zero monthly rainfall is considered to be 0.01 mm in order to calculate the SPI value as it is obtained by Gamma distribution. It should be noted that the distribution of Gamma is not defined for zero value. Considering zero precipitation months as 0.01 mm, the calculation of standard deviation and long-term mean value is not affected. The  $\alpha$  and  $\beta$  values are calculated on the basis of Eqs. 6, 7 and 8. The built-up function represented by Eq. 5 is employed to determine the SPI value for each month, annual and seasonal value directly. Monthly drought indices are initially computed for each year. The rainfall values for the NE monsoon period (October, November and December), SW monsoon period (June–September), Winter (January and February) and Summer (March–May) are aggregated for each year to assess indices for different time scale. The deviation of SPI values was analyzed by comparing its value with SZs and CZI value.

**Table 2** Different types of drought indices based on index value

| SPI, CZI and Z score | Class          | Symbol |
|----------------------|----------------|--------|
| $\geq 2$             | Extremely wet  | EW     |
| 1.5 to 1.99          | Severely wet   | SW     |
| 1 to 1.49            | Moderately wet | MW     |
| -0.99 to 0.99        | Normal         | N      |
| -1 to -1.49          | Moderately dry | MD     |
| -1.5 to -1.99        | Very dry       | VD     |
| $\leq -2$            | Extremely dry  | ED     |

**Table 3** Status of moisture level in recent 20 years (1991–2010)

| Rainfall time scale | EW  |     |     | VW  |     |     | MW  |     |     | N   |     |     |
|---------------------|-----|-----|-----|-----|-----|-----|-----|-----|-----|-----|-----|-----|
|                     | SPI | SZs | CZI | SPI | SZs | CZI | SPI | SZs | CZI | SPI | SZs | CZI |
| Annual              | 0   | 0   | 0   | 2   | 3   | 3   | 4   | 2   | 2   | 14  | 15  | 15  |
| SW                  | 0   | 0   | 0   | 1   | 1   | 1   | 4   | 4   | 4   | 15  | 15  | 15  |
| NE                  | 2   | 2   | 0   | 1   | 1   | 3   | 1   | 0   | 0   | 17  | 21  | 18  |
| Winter              | 1   | 1   | 1   | 1   | 0   | 0   | 2   | 2   | 2   | 9   | 22  | 22  |
| Summer              | 0   | 1   | 1   | 1   | 0   | 0   | 3   | 3   | 3   | 17  | 17  | 17  |

**Table 4** Status of moisture level in recent 20 years (1991–2010)

| Rainfall time scale | MD  |     |     | VD  |     |     | ED  |     |     |
|---------------------|-----|-----|-----|-----|-----|-----|-----|-----|-----|
|                     | SPI | SZs | CZI | SPI | SZs | CZI | SPI | SZs | CZI |
| Annual              | 4   | 4   | 4   | 0   | 1   | 1   | 1   | 0   | 0   |
| SW                  | 4   | 4   | 4   | 0   | 1   | 1   | 1   | 0   | 0   |
| NE                  | 4   | 1   | 4   | 0   | 0   | 0   | 0   | 0   | 0   |
| Winter              | 12  | 0   | 0   | 0   | 0   | 0   | 0   | 0   | 0   |
| Summer              | 2   | 4   | 3   | 1   | 0   | 1   | 1   | 0   | 0   |

Tables 3 and 4 give moisture category based on SPI, CZI and SZs for various time scales. It can be seen from Table 3 that EW moisture categorization for NE and winter season is similar for both SPI and SZs method and for same moisture category all three indices shows the similar result for annual and SW season. For ED moisture category, the similar results are observed for both SZs and CZI for all the time scale. For normal moisture category, there is no deviation between CZI and SZs for all time scale except NE season. For MW category, both the method CZI and SZs show similar results for all time scale. By considering all the moisture category and different time scale, the CZI and SZs provided a similar result and it shows only minor deviation from results of SPI.

Table 5 shows the values of regression coefficient and corresponding equation between the (i) SPI and SZs, (ii) SPI and CZI, and (iii) SZs and CZI, for annual and seasonal rainfall. By considering above all three cases the range of regression coefficient varies from maximum of 0.999 to 0.643. The regression coefficient results show that for annual and SW season SZs versus CZI gives best fit than SPI. The lowest value of  $R^2$  values such as 0.643, 0.853 and 0.904 identified for winter season for all three cases respectively.

From Table 5, it has been concluded that the  $R^2$  value obtained between SZs versus CZI is maximum for all time scale compared to other two cases.

Figure 3a–d shows the linear regression plot between the values of SPI and SZs for historical year 1981–2005. This means that for all the time period, except for the winter season, the SPI normally has a strong relationship. This is because that SZs shows the moderate dry condition and at the same year SPI shows the normal conditions, so that most of the points are far away from the regression line. The above said trend but better relationship is observed in the case of regression plot between SPI and CZI which is shown in Fig. 4a–e. Figure 5a–e shows the regression plot between SZs vs. China-Z Index shows the better relationship between these drought indices which is concluded from the regression coefficient is above 0.9 for all the time scale. By considering all the regression plots, SZs vs CZI shows better relationships for all the time scale except NE values. But regression plot between SPI versus SZs and SPI versus CZI Fig. 3b and Fig. 4b respectively show high relationship in NE season.

**Table 5** Regression equation and its coefficient for different indices

| Rainfall time scale | Linear equation      |                      |                      | Regression coefficient ( $R^2$ ) |                |                |
|---------------------|----------------------|----------------------|----------------------|----------------------------------|----------------|----------------|
|                     | SPI versus SZs       | SPI versus CZI       | SZs versus CZI       | SPI versus SZs                   | SPI versus CZI | SZs versus CZI |
| Annual              | $y = 0.975x$         | $y = 0.976x$         | $y = 0.999x$         | 0.991                            | 0.994          | 0.999          |
| SW                  | $y = 0.964x - 0.001$ | $y = 0.967x$         | $y = 0.997x + 0.001$ | 0.969                            | 0.978          | 0.999          |
| NE                  | $y = 0.968x + 0.005$ | $y = 0.877x + 0.045$ | $y = 0.879x + 0.041$ | 0.975                            | 0.998          | 0.964          |
| Winter              | $y = 0.773x + 0.115$ | $y = 0.568x + 0.348$ | $y = 0.606x + 0.263$ | 0.643                            | 0.853          | 0.904          |
| Summer              | $y = 0.935x - 0.004$ | $y = 0.939x + 0.002$ | $y = 0.975y + 0.006$ | 0.916                            | 0.959          | 0.989          |

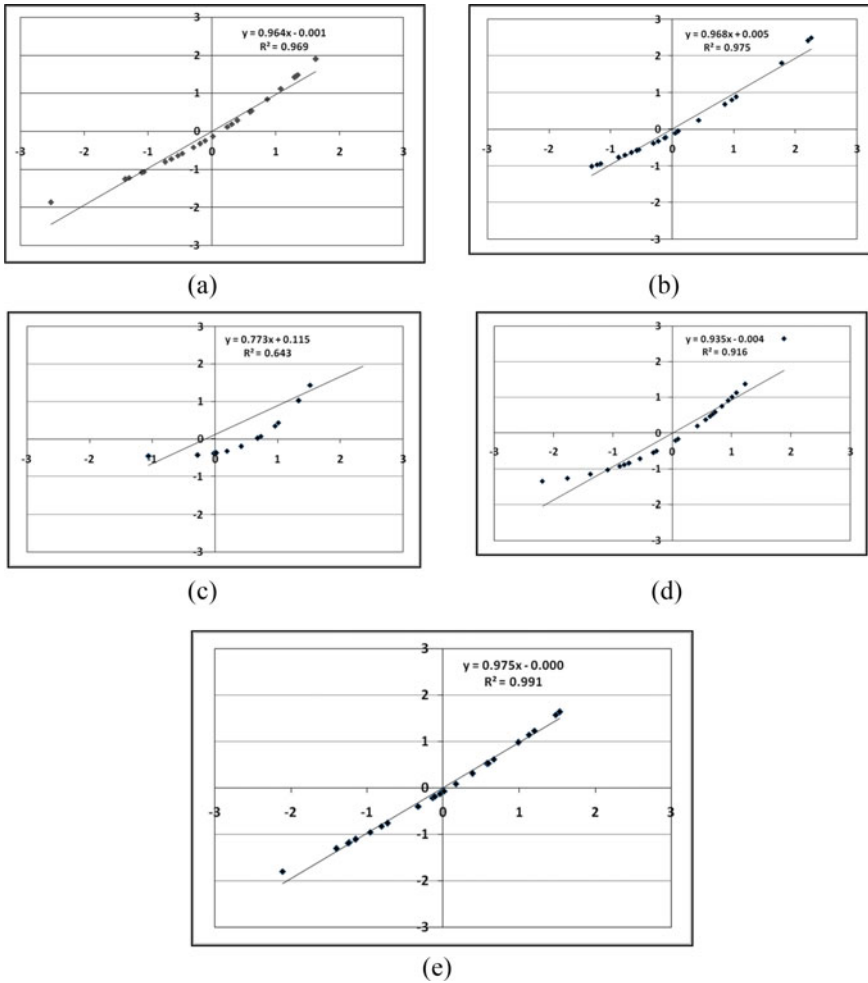


**Fig. 3** Linear regression plot of SPI versus SZs for different times scale. **a** SW, **b** NE, **c** winter, **d** summer and **e** annual rainfall

## 5 Conclusion

Based on the findings on the Trichirapalli city using monthly precipitation from the current drought analysis, the following conclusions can be drawn. This paper shows that SPI, CZI and SZs are effective tools for identifying, detecting and tracking flood and drought. The flexibility of the above methods enables checking of water supplies or fluctuations in precipitation at various timescales. In contrast, since it is derived solely from rainfall data, they are simpler than PDSI. With various time scales the CZI and SZs are very similar to the SPI. Suribabu and Neelakantan [9] concluded that there is fair agreement between three indicators for the annual moisture classification

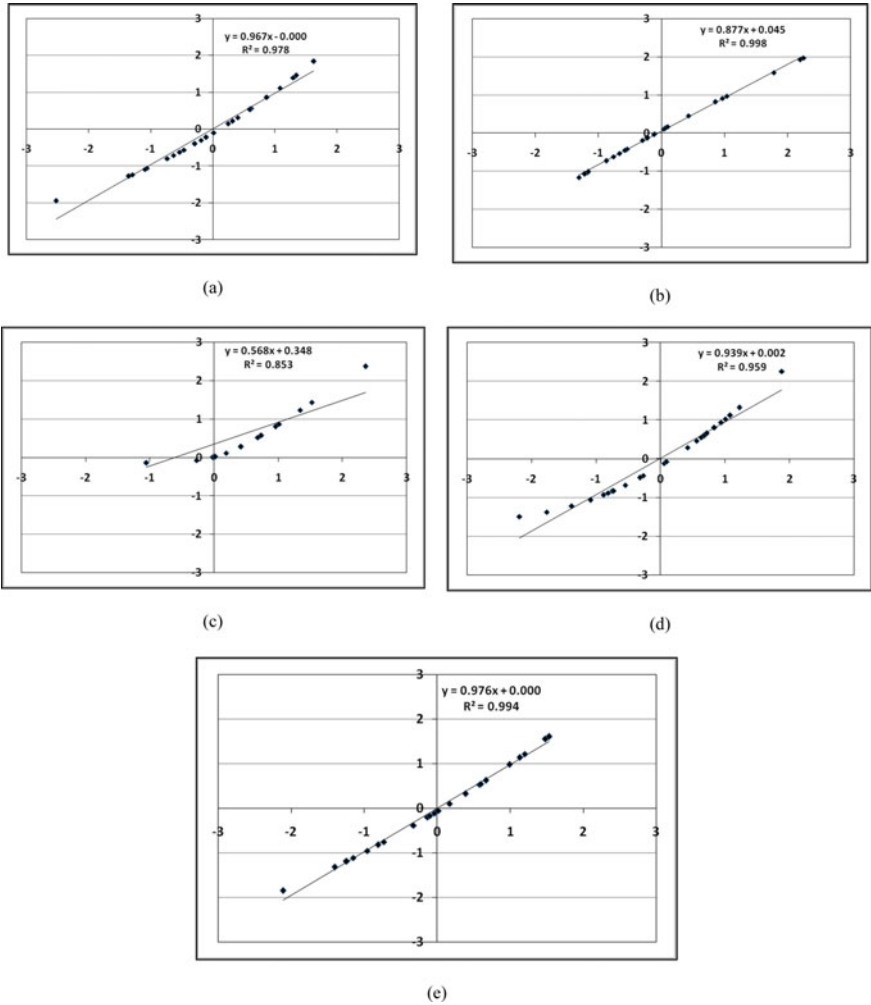


**Fig. 4** Linear regression plot of SPI versus CZI for different times scale. **a** SW, **b** NE, **c** winter, **d** summer and **e** annual rainfall

and disagreement for the monthly moisture classification. In this paper, the findings show that the results of three indices for annual and monthly time series are identical for Normal moisture category. The main advantages of the CZI and SZs indices are that the computations of these two indices are simpler, and both indices allow missing data. This versatility is especially important for the areas where weather information is frequently incomplete. The study results using 25 years of rainfall data reveals that there is no extreme climatic conditions either severe dry or wet. Most of the year rainfall was close to be normal. This shows a favorable trend for farmers as the

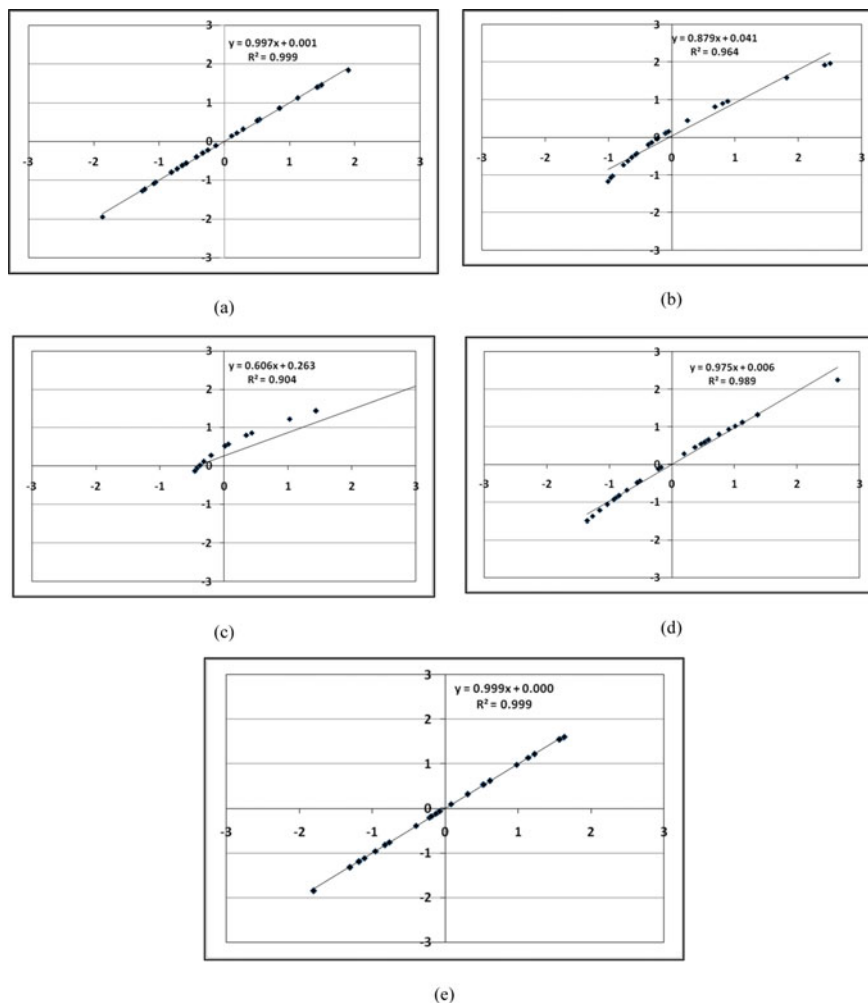


**Fig. 5** Linear regression plot of SZs versus CZI for different times scale. **a** SW, **b** NE, **c** winter, **d** summer and **e** annual rainfall

chances of normal rainfall are fairly stable across different methods corresponding to the selected years for analysis.

## References

1. Akhtari R, Morid S, Mahdian MH, Smakhtin V (2009) Assessment of areal interpolation methods for spatial analysis of SPI and EDI drought indices. *Int J Climatol* 29:135–145



2. Dogan S, Berktaş A, Singh VP (2012) Comparison of multi-monthly rainfall-based drought severity indices, with application to semi-arid Konya closed basin, Turkey. *J Hydrol* 470:255–268. <https://doi.org/10.1016/j.jhydrol.2012.09.003>
3. Fiorillo F, Guadagno FM (2010) Karst spring discharges analysis in relation to drought periods, using the SPI. *Water Resour Manage* 24:1867–1884
4. Hayes M, Wilhite DA, Svoboda M, Vanyarkho O (1999) Monitoring the 1996 drought using the standardized precipitation index. *Bull Am Meteor Soc* 80(3):429–438
5. Kendall MG, Stuart A (1977) *The advanced theory of statistics, vol 1. Distribution Theory* Charles Griffin Company, London, pp 400–401
6. Livada I, Assimakopoulos VD (2006) Spatial and temporal analysis of drought in Greece using the standardized precipitation index (SPI). *Theor Appl Climatol* 89:143–153
7. Mckee TB, Doesken NJ, Kleist J (1993) The relationship of drought frequency and duration to time scales. In: *Proceedings of the 8th conference on applied climatology*. Anaheim, CA, USA, pp 179–184
8. Palmer WC (1965) *Meteorological drought*. US Department of Commerce Weather Bureau Research Paper No. 45
9. Suribabu CR, Neelakantan TR (2018) Assessment of dry and wet periods using selected rainfall-based drought indicators—a case study. *ISH J Hydraul Eng*. <https://doi.org/10.1080/09715010.2018.1542635>
10. Suribabu CR, Ramani Sujatha E (2019) Evaluation of moisture level using precipitation indices as a landslide triggering factor—a study of Coonoor hill station. *Climate* 7:111. <https://doi.org/10.3390/cli7090111>
11. Tsakiris G, Pangalou D, Vangelis H (2007) Regional drought assessment based on reconnaissance drought index (RDI). *J Water Resour Manage* 21:821–833
12. Wu H, Hayes MJ, Weiss A, Hu QI (2001) An evaluation of the standardized precipitation index, the China Z-index and the statistical Z- score. *Int J Climatol* 21:745–758
13. Xu K, Yang D, Yang H, Li Z, Qin Y, Shen Y (2015) Spatio-temporal variation of drought in China during 1961–2012: a climatic perspective. *J Hydrol* 526:253–264

# Forecasting of Meteorological Drought Using Machine Learning Algorithm



Ayilobeni Kikon and Paresh Chandra Deka

**Abstract** Drought forecasting is one of the crucial tools for the water management system, and understanding the different climatic variables affecting the occurrences of drought is a major scientific challenge. In this study, drought forecasting is done for the Peninsular region of India using different machine learning algorithms. A meteorological drought index known as Standardized Precipitation Index (SPI) which is dependent on the precipitation is taken into account for analysis. The SPI with a different timescale for 3-, 6-, 9-, 12-month were calculated from 1958–2017 for 60 years. SPI is a function of precipitation and the trend of rainfall followed may be found to be similar in some regions. Two different models, GA-ANFIS and GRNN were compared in this study. The results obtained from the statistical performance assessment of the models were compared with each other. For different timescale, there is a variation in its evaluation metrics. Comparing the performance assessment of the two different models, it is noticeable that the performance assessment of the statistics of the GA-ANFIS model outperformed GRNN model.

**Keywords** Drought forecasting · SPI · Machine learning algorithm

## 1 Introduction

Drought is a condition occurring in a region due to the deficit of precipitation. The occurrence of drought in a region may not have an immediate effect like that of floods, but in the long run, it causes a huge impact on the economy as well as the environment. Drought is one of the complicated hydrologic features of arid and semi-arid regions with firm reasoning on the sustainability of water resources, agriculture and environmental management [2, 12]. Drought, even for a very short period causes significant damage to the local economy of a region. Drought mostly causes due to the lack of precipitation, human activities such as over farming, deforestation, and excessive irrigation. Drought forecasting has a great impact on agricultural activity

---

A. Kikon (✉) · P. C. Deka

Department of Water Resources and Ocean Engineering, National Institute of Technology, Surathkal, Karnataka 575025, India

and water availability and is therefore particularly important for ensuring the water management system.

Globally, drought is becoming one of the major challenges in many places. Climate changes and alteration of rainfall patterns indices [6] are one of the major reasons leading to drought conditions in many places. Drought indices are the parameters which help in detecting the change in rainfall patterns. Literature study shows that there are multiple approaches for analyzing drought forecasting which has their pros and cons in their approaches [4]. Autoregressive moving average (ARIMA) model is the most broadly utilized models for time series models. ARIMA model being used with the vegetation temperature condition index (VTCI) for forecasting the future changes and the Autoregressive (AR) models were found to be suitable for VTCI series [5]. A stochastic model (ARIMA) has been developed to fit and predict the Standardized Precipitation Evapotranspiration Index (SPEI) where ARIMA models prove to be advantageous for forecasting drought and assist in water resources management and designers to prioritize safeguard in advance considering the severity of the drought [11]. Recently, there has been an increase in forecasting drought using different indices and models.

Drought study has extended huge importance owing to global warming and climate change. The probability of occurrence of taking into consideration of different time scales in semi-arid regions causes hydrologic and agricultural drought [1]. A wavelet-based model wavelet-Extreme Learning Machine (w-ELM) developed shows improvement in the operation of forecasting drought models and mitigation plan, sustainable water-use policies and water management systems [3].

An ample number of drought indices have been established. The drought indices with intermediate time steps ranging from 7 to 18 months have the maximum predictive values for finding droughts conditions and the SPI drought index was observed to be more sensitive to multi-monthly cumulative precipitation changes [8]. Interaction with topo-climatic factors such as solar radiation, soil dampness and slope, together with drought duration, plays a significant role in withstanding drought phenomenon [7]. Variations in the meteorological drought are caused due to the spatial and temporal variability of precipitation occurrences [10].

This paper focuses on the meteorological drought forecasting with different machine learning technique. Section 2 describes materials and the data use, the method implemented in the study. Section 3 describes the results and discussion followed by a conclusion.

## 2 Materials and Methodology

### 2.1 Study Area

According to the India Meteorological Department (IMD), Pune, the study area, the South Peninsular India region includes Coastal Andhra, Coastal Karnataka, Kerala,

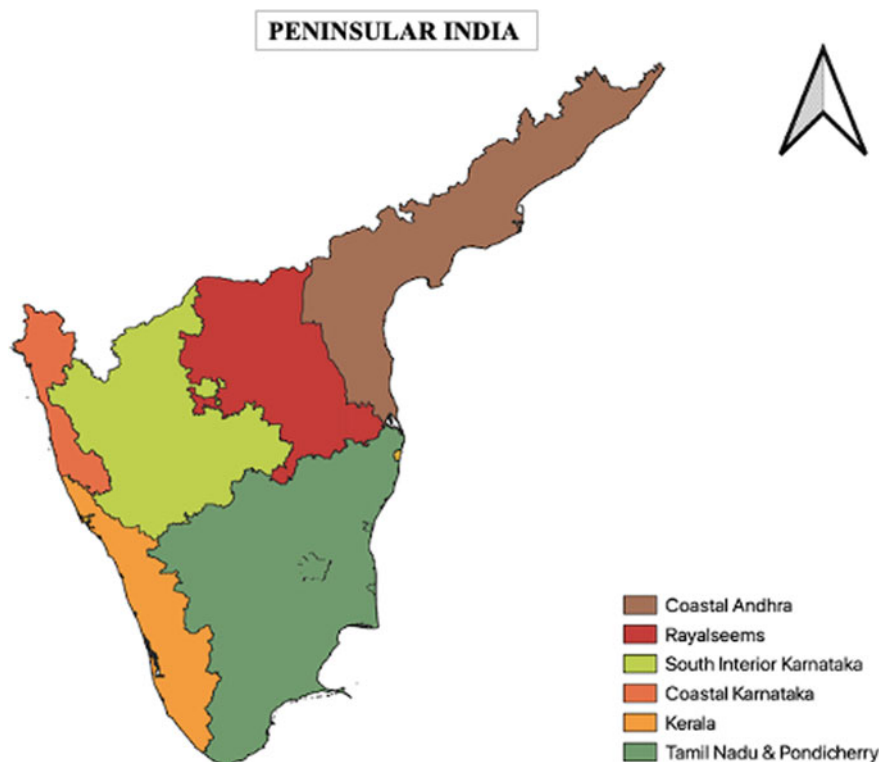


**Fig. 1** The study area: Peninsular India

Rayalseema, South Interior Karnataka, Tamil Nadu and Pondicherry. The data used for the study was from 1958–2017 for 60 years. Monthly rainfall data for Peninsular India were acquired from the India Meteorological Department, Pune. Figure 1 shows the Study Area-Peninsular India. In Peninsular India, Pre-monsoon occurs from March to May, Monsoon from June to September, Post-monsoon from October to November and Winter from December to February. The hottest month in this region occurs in April and May.

## 2.2 Methodology

### 2.2.1 Standardized Precipitation Index (SPI)

SPI is one of the widely used drought indexes on a range of timescale. The SPI with different climates can be computed and compared for all places. It uses precipitation

**Table 1** SPI values

|               |                |
|---------------|----------------|
| >2            | Extremely wet  |
| 1.5 to 1.99   | Very wet       |
| 1.0 to 1.49   | Moderately wet |
| -0.99 to 0.99 | Near normal    |
| -1.0 to -1.49 | Moderately dry |
| -1.5 to -1.99 | Severely dry   |
| < -2          | Extremely dry  |

data and categorizes dryness or abnormal wetness with different timescales corresponding with the availability of time. The SPI can be created with various timescales ranging from 1 to 36 months using monthly precipitation data as input. McKee et al. [9] classified SPI to define drought intensities resulting from the SPI. The computation of SPI for any place is dependent on the long-term precipitation record. The positive values indicate more than mean precipitation, and negative values indicate less than mean precipitation. According to the SPI values from Table 1, the onset of drought begins when the SPI values are equal or less than  $-1.0$  and ends when the value becomes more than zero.

The SPI evaluation requires fitting a probability distribution to cumulative monthly precipitation series (3, 6, 9, 12-month). The SPI is calculated to build a frequency distribution from the historical precipitation data at a region for a specific time. Then, a theoretical probability density function of the gamma distribution is fitted to the empirical distribution of precipitation frequency for the particular time scale.

### 2.2.2 Generalized Regression Neural Network (GRNN)

Specht [13] introduced GRNN and it is categorized as a probabilistic neural network. It represents an improved technique based on non-parametric regression in the neural networks. It can be used for regression, prediction and classification. It requires only a fraction of the training samples needed for backpropagation neural networks. Hence, the probabilistic neural network uses are beneficial to converge the underlying function of the data with only a few training samples available.

### 2.2.3 Genetic Algorithm-Adaptive Neuro-Fuzzy Inference System (GA-ANFIS)

GA-ANFIS system performs optimization in MATLAB environment by using testing datasets. The main modeling procedure is an optimization task executed by GA-ANFIS, where the precision and compactness of fuzzy models are subjects of optimization. Testing of different datasets is done to find the optimized value.

Figure 2 describes the flowchart of the methodology adopted in this study. The input variable used in the study is precipitation data. Computation of SPI for 3, 6, 9

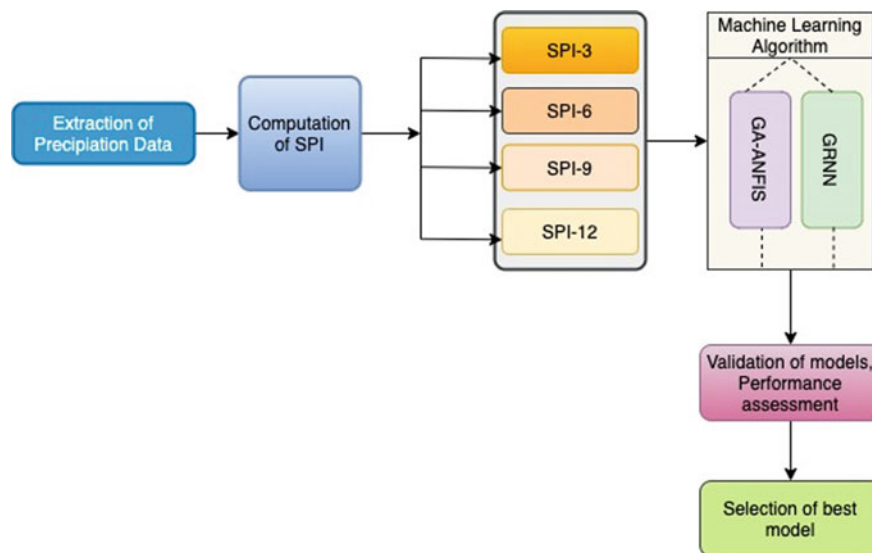


**Fig. 2** Flowchart of methodology

and 12-month were evaluated. Then the model was trained to utilize 70% of the data and the rest 30% of the data was used for testing. The testing data forecasted values are then compared with the known observed values of different timescale SPI. The performance of the various models for forecasting SPI was done.

### 3 Results and Discussion

In the Peninsular region, there are six regions; Coastal Andhra, Coastal Karnataka, Kerala, Rayalseema, South Interior Karnataka and Tamil Nadu and Pondicherry. Table 2 summarizes the performance assessment of different models in drought forecasting having different timescale, SPI3, SPI6, SPI9 and SPI12. The comparative statistics of GA-ANFIS and GRNN models for different timescale used are shown in Table 2. The performance assessment statistics was done for Mean Absolute Error (MAE), Normalized Nash–Sutcliffe Efficiency (NNSE), Root Mean Square Error (RMSE) and Coefficient of determination ( $R^2$ ).

In this study, the objective was to evaluate the meteorological drought index, SPI and compare the performance using a different machine learning algorithm. It is noticeable that the performance assessment of the statistics of the GA-ANFIS model outperformed the GRNN model. As the timescale increases, there are small abnormalities observed in the performance measures of the model. For the best model, the value of  $R^2$  which is obtained from the scatterplot of observed and forecasted SPI of different timescale is estimated to be close to unity. The higher timescale, the

**Table 2** Performance assessment of GA-ANFIS and GRNN models

| Region                   | Statistics     |        | GA-ANFIS |                |        |        |        |                | GRNN   |        |        |        |       |        |        |        |        |        |        |        |        |        |        |        |        |        |        |        |        |        |        |
|--------------------------|----------------|--------|----------|----------------|--------|--------|--------|----------------|--------|--------|--------|--------|-------|--------|--------|--------|--------|--------|--------|--------|--------|--------|--------|--------|--------|--------|--------|--------|--------|--------|--------|
|                          | MAE            | NNSE   | RMSE     | R <sup>2</sup> | MAE    | NNSE   | RMSE   | R <sup>2</sup> | SPI3   | SPI6   | SPI9   | SPI12  | SPI3  | SPI6   | SPI9   | SPI12  |        |        |        |        |        |        |        |        |        |        |        |        |        |        |        |
| Coastal Andhra           | MAE            | 0.596  | 0.6223   | 0.7668         | 0.39   | 0.436  | 0.7524 | 0.5966         | 0.67   | 0.49   | 0.8295 | 0.4918 | 0.79  | 0.3626 | 0.882  | 0.397  | 0.86   | 0.6156 | 0.4821 | 0.7259 | 0.639  | 0.7815 | 0.37   | 0.64   | 0.5005 | 0.7318 | 0.5941 | 0.6559 | 0.7318 | 0.8283 |        |
|                          | NNSE           | 0.6036 | 0.7723   | 0.34           | 0.48   | 0.661  | 0.6549 | 0.5421         | 0.63   | 0.80   | 0.7262 | 0.5421 | 0.63  | 0.7788 | 0.353  | 0.7876 | 0.6624 | 0.5344 | 0.32   | 0.47   | 0.63   | 0.79   | 0.6285 | 0.5941 | 0.6559 | 0.7318 | 0.5941 | 0.6559 | 0.7318 | 0.8283 |        |
|                          | RMSE           | 0.5933 | 0.6336   | 0.7395         | 0.42   | 0.4364 | 0.7208 | 0.6031         | 0.4837 | 0.71   | 0.7788 | 0.4837 | 0.71  | 0.7788 | 0.353  | 0.7876 | 0.6624 | 0.5344 | 0.32   | 0.47   | 0.63   | 0.79   | 0.6285 | 0.5941 | 0.6559 | 0.7318 | 0.5941 | 0.6559 | 0.7318 | 0.8283 |        |
|                          | R <sup>2</sup> | 0.5815 | 0.6523   | 0.7654         | 0.47   | 0.4815 | 0.7169 | 0.6478         | 0.6    | 0.77   | 0.7807 | 0.5334 | 0.71  | 0.77   | 0.462  | 0.8027 | 0.6903 | 0.5567 | 0.42   | 0.57   | 0.70   | 0.76   | 0.6088 | 0.6304 | 0.6904 | 0.6903 | 0.5567 | 0.4773 | 0.4773 | 0.4773 | 0.4773 |
| Coastal Karnataka        | MAE            | 0.6096 | 0.6036   | 0.7723         | 0.34   | 0.4364 | 0.7208 | 0.6031         | 0.4837 | 0.71   | 0.7788 | 0.4837 | 0.71  | 0.7788 | 0.353  | 0.7876 | 0.6624 | 0.5344 | 0.32   | 0.47   | 0.63   | 0.79   | 0.6285 | 0.5941 | 0.6559 | 0.7318 | 0.5941 | 0.6559 | 0.7318 | 0.8283 |        |
|                          | NNSE           | 0.5933 | 0.6336   | 0.7395         | 0.42   | 0.4364 | 0.7208 | 0.6031         | 0.4837 | 0.71   | 0.7788 | 0.4837 | 0.71  | 0.7788 | 0.353  | 0.7876 | 0.6624 | 0.5344 | 0.32   | 0.47   | 0.63   | 0.79   | 0.6285 | 0.5941 | 0.6559 | 0.7318 | 0.5941 | 0.6559 | 0.7318 | 0.8283 |        |
|                          | RMSE           | 0.5815 | 0.6523   | 0.7654         | 0.47   | 0.4364 | 0.7208 | 0.6031         | 0.4837 | 0.71   | 0.7788 | 0.4837 | 0.71  | 0.7788 | 0.353  | 0.7876 | 0.6624 | 0.5344 | 0.32   | 0.47   | 0.63   | 0.79   | 0.6285 | 0.5941 | 0.6559 | 0.7318 | 0.5941 | 0.6559 | 0.7318 | 0.8283 |        |
|                          | R <sup>2</sup> | 0.5815 | 0.6523   | 0.7654         | 0.47   | 0.4364 | 0.7208 | 0.6031         | 0.4837 | 0.71   | 0.7788 | 0.4837 | 0.71  | 0.7788 | 0.353  | 0.7876 | 0.6624 | 0.5344 | 0.32   | 0.47   | 0.63   | 0.79   | 0.6285 | 0.5941 | 0.6559 | 0.7318 | 0.5941 | 0.6559 | 0.7318 | 0.8283 |        |
| Kerala                   | MAE            | 0.5933 | 0.6336   | 0.7395         | 0.42   | 0.4364 | 0.7208 | 0.6031         | 0.4837 | 0.71   | 0.7788 | 0.4837 | 0.71  | 0.7788 | 0.353  | 0.7876 | 0.6624 | 0.5344 | 0.32   | 0.47   | 0.63   | 0.79   | 0.6285 | 0.5941 | 0.6559 | 0.7318 | 0.5941 | 0.6559 | 0.7318 | 0.8283 |        |
|                          | NNSE           | 0.5933 | 0.6336   | 0.7395         | 0.42   | 0.4364 | 0.7208 | 0.6031         | 0.4837 | 0.71   | 0.7788 | 0.4837 | 0.71  | 0.7788 | 0.353  | 0.7876 | 0.6624 | 0.5344 | 0.32   | 0.47   | 0.63   | 0.79   | 0.6285 | 0.5941 | 0.6559 | 0.7318 | 0.5941 | 0.6559 | 0.7318 | 0.8283 |        |
|                          | RMSE           | 0.5815 | 0.6523   | 0.7654         | 0.47   | 0.4364 | 0.7208 | 0.6031         | 0.4837 | 0.71   | 0.7788 | 0.4837 | 0.71  | 0.7788 | 0.353  | 0.7876 | 0.6624 | 0.5344 | 0.32   | 0.47   | 0.63   | 0.79   | 0.6285 | 0.5941 | 0.6559 | 0.7318 | 0.5941 | 0.6559 | 0.7318 | 0.8283 |        |
|                          | R <sup>2</sup> | 0.5815 | 0.6523   | 0.7654         | 0.47   | 0.4364 | 0.7208 | 0.6031         | 0.4837 | 0.71   | 0.7788 | 0.4837 | 0.71  | 0.7788 | 0.353  | 0.7876 | 0.6624 | 0.5344 | 0.32   | 0.47   | 0.63   | 0.79   | 0.6285 | 0.5941 | 0.6559 | 0.7318 | 0.5941 | 0.6559 | 0.7318 | 0.8283 |        |
| Rayalseema               | MAE            | 0.5815 | 0.6523   | 0.7654         | 0.47   | 0.4364 | 0.7208 | 0.6031         | 0.4837 | 0.71   | 0.7788 | 0.4837 | 0.71  | 0.7788 | 0.353  | 0.7876 | 0.6624 | 0.5344 | 0.32   | 0.47   | 0.63   | 0.79   | 0.6285 | 0.5941 | 0.6559 | 0.7318 | 0.5941 | 0.6559 | 0.7318 | 0.8283 |        |
|                          | NNSE           | 0.5815 | 0.6523   | 0.7654         | 0.47   | 0.4364 | 0.7208 | 0.6031         | 0.4837 | 0.71   | 0.7788 | 0.4837 | 0.71  | 0.7788 | 0.353  | 0.7876 | 0.6624 | 0.5344 | 0.32   | 0.47   | 0.63   | 0.79   | 0.6285 | 0.5941 | 0.6559 | 0.7318 | 0.5941 | 0.6559 | 0.7318 | 0.8283 |        |
|                          | RMSE           | 0.5815 | 0.6523   | 0.7654         | 0.47   | 0.4364 | 0.7208 | 0.6031         | 0.4837 | 0.71   | 0.7788 | 0.4837 | 0.71  | 0.7788 | 0.353  | 0.7876 | 0.6624 | 0.5344 | 0.32   | 0.47   | 0.63   | 0.79   | 0.6285 | 0.5941 | 0.6559 | 0.7318 | 0.5941 | 0.6559 | 0.7318 | 0.8283 |        |
|                          | R <sup>2</sup> | 0.5815 | 0.6523   | 0.7654         | 0.47   | 0.4364 | 0.7208 | 0.6031         | 0.4837 | 0.71   | 0.7788 | 0.4837 | 0.71  | 0.7788 | 0.353  | 0.7876 | 0.6624 | 0.5344 | 0.32   | 0.47   | 0.63   | 0.79   | 0.6285 | 0.5941 | 0.6559 | 0.7318 | 0.5941 | 0.6559 | 0.7318 | 0.8283 |        |
| South Interior Karnataka | MAE            | 0.6492 | 0.6444   | 0.8135         | 0.47   | 0.4758 | 0.7341 | 0.6116         | 0.64   | 0.77   | 0.3777 | 0.5076 | 0.77  | 0.288  | 0.6332 | 0.52   | 0.4066 | 0.8324 | 0.6332 | 0.52   | 0.4066 | 0.3696 | 0.6332 | 0.6528 | 0.7024 | 0.8038 | 0.8324 | 0.8324 | 0.8324 | 0.8324 |        |
|                          | NNSE           | 0.6444 | 0.8135   | 0.47           | 0.4758 | 0.7341 | 0.6116 | 0.64           | 0.77   | 0.3777 | 0.5076 | 0.77   | 0.288 | 0.6332 | 0.52   | 0.4066 | 0.8324 | 0.6332 | 0.52   | 0.4066 | 0.3696 | 0.3696 | 0.6332 | 0.6528 | 0.7024 | 0.8038 | 0.8324 | 0.8324 | 0.8324 | 0.8324 |        |
|                          | RMSE           | 0.6492 | 0.6444   | 0.8135         | 0.47   | 0.4758 | 0.7341 | 0.6116         | 0.64   | 0.77   | 0.3777 | 0.5076 | 0.77  | 0.288  | 0.6332 | 0.52   | 0.4066 | 0.8324 | 0.6332 | 0.52   | 0.4066 | 0.3696 | 0.6332 | 0.6528 | 0.7024 | 0.8038 | 0.8324 | 0.8324 | 0.8324 | 0.8324 | 0.8324 |
|                          | R <sup>2</sup> | 0.6492 | 0.6444   | 0.8135         | 0.47   | 0.4758 | 0.7341 | 0.6116         | 0.64   | 0.77   | 0.3777 | 0.5076 | 0.77  | 0.288  | 0.6332 | 0.52   | 0.4066 | 0.8324 | 0.6332 | 0.52   | 0.4066 | 0.3696 | 0.3696 | 0.6332 | 0.6528 | 0.7024 | 0.8038 | 0.8324 | 0.8324 | 0.8324 | 0.8324 |

(continued)

**Table 2** (continued)

| Region                     | Statistics     | GA-ANFIS |        |        |       | GRNN   |        |        |        |
|----------------------------|----------------|----------|--------|--------|-------|--------|--------|--------|--------|
|                            |                | SPI3     | SPI6   | SPI9   | SPI12 | SPI3   | SPI6   | SPI9   | SPI12  |
| Tamil Nadu and Pondicherry | MAE            | 0.6668   | 0.4388 | 0.4045 | 0.323 | 0.8385 | 0.7572 | 0.8215 | 0.8959 |
|                            | NNSE           | 0.7308   | 0.4719 | 0.9143 | 0.94  | 0.5965 | 0.3225 | 0.6597 | 0.6289 |
|                            | RMSE           | 0.8386   | 0.8056 | 0.5192 | 0.464 | 1.1363 | 1.1038 | 1.2179 | 1.4072 |
|                            | R <sup>2</sup> | 0.65     | 0.62   | 0.92   | 0.93  | 0.42   | 0.57   | 0.83   | 0.77   |



better performance is obtained. Comparing with the other region of the study area, it shows that the region of Tamil Nadu and Pondicherry shows a higher meteorological drought. Out of the two models, GA-ANFIS outperformed GRNN in all the Peninsular region. The representation of the scatter plot diagrams for SPI3, SPI6, SPI9 and SPI12 for all the Peninsular region are presented in Fig. 3a–f. From the scatterplot diagram of GA-ANFIS with the different timescale of SPI3, SPI6, SPI9 and SPI12, it shows that higher the timescale range, better efficiency it performs. Comparing the  $R^2$  from the scatterplot diagram of GA-ANFIS from Fig. 3a–f, Tamil Nadu and Pondicherry region gives a better performance output than the rest of the other five regions for the different timescale SPI.

Figure 4a–f shows the scatterplot for GRNN. In the GRNN model, Coastal Andhra has a better efficiency performance as illustrated in the scatterplot diagram from Fig. 4a–f. Since each region of Peninsular region has different rainfall distribution, there is a variation in the performance assessment for the statistical indices like MAE, NNSE and RMSE.

From the scatterplot, comparing the two models, it illustrates that GA-ANFIS has a better performance efficacy for all the different timescale. The goodness of fit for the different models for assessing the drought was verified using a scatterplot diagram between the observed and the forecasted SPI using linear regression statistics.

Figure 5a–f represents the time series of the observed and forecasted SPI generated by GA-ANFIS and GRNN models. From the time series plot, only testing data was taken into consideration for the analysis. From the results obtained, it indicates that GA-ANFIS model outperformed GRNN model in the study region for all the different timescale SPI (3-, 6-, 9-, 12-month). The onset and the occurrence of rainfall are not

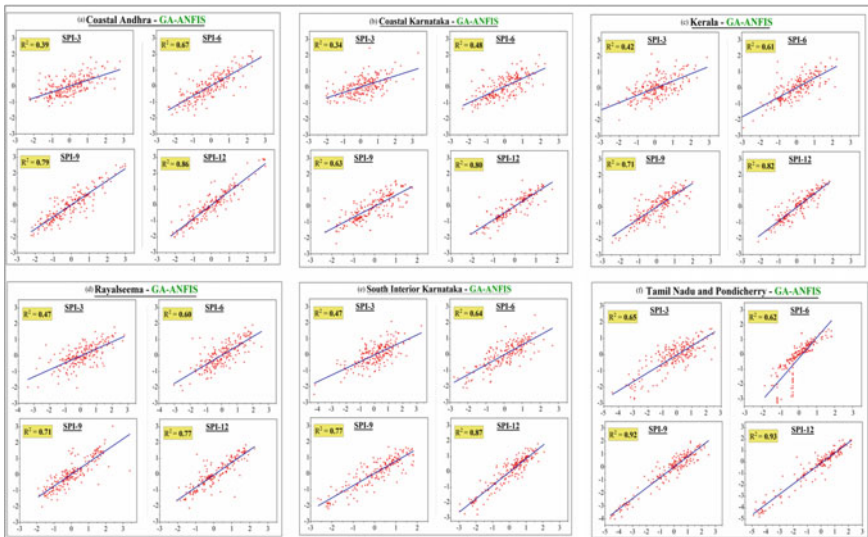


Fig. 3 a–f: Scatterplot for GA-ANFIS

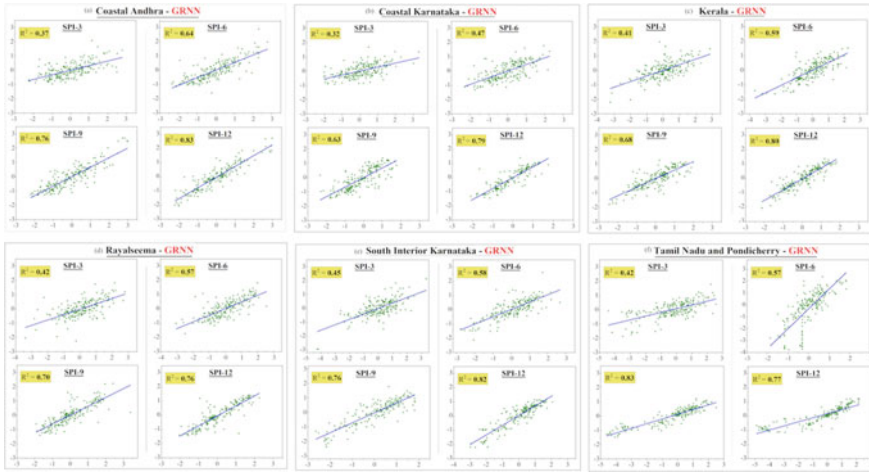


Fig. 4 a-f: Scatterplot for GRNN

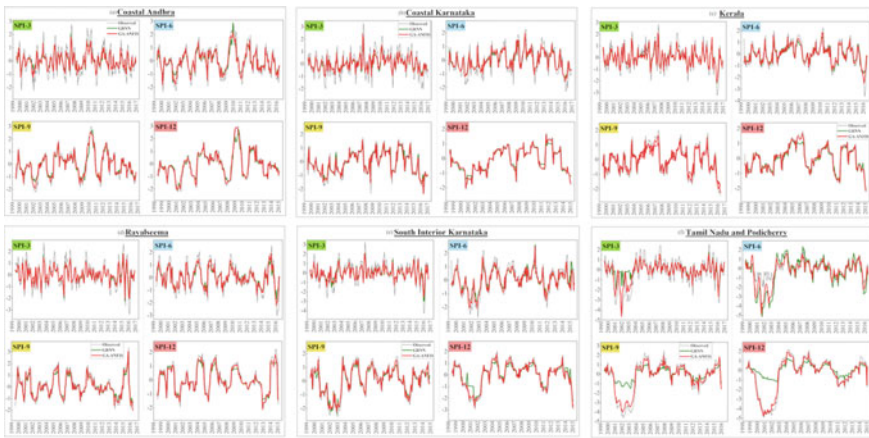


Fig. 5 a-f: Time series of Peninsular India for SPI3, SPI6, SPI9 and SPI12

constant for all the Peninsular region. Due to its temporal and spatial variability, there is a variation in the distribution of rainfall leading to variations in its meteorological drought.

## 4 Conclusion

The study was done for 60 years from 1958–2017. In this study meteorological drought index, SPI having different timescale was used for the analysis. The performance of the different timescale SPI was determined. A hybrid model of GA-ANFIS and GRNN has been developed to predict the drought in Peninsular India. Based on the performance, best model has been selected for forecasting drought in this study. SPI for 3, 6, 9 and 12-month were evaluated and then forecasted using GA-ANFIS and GRNN model. In this study, the two models GA-ANFIS and GRNN were compared and its results show that GA-ANFIS model gives a better performance in forecasting drought as compared with GRNN model.

**Acknowledgements** The authors would like to express gratitude to Mr. Akash Gupta, Student Department of Materials & Metallurgical Engineering, NITK for helping out in this paper.

## References

1. Adib A, Marashi SS (2019) Meteorological drought monitoring and preparation of long-term and short-term drought zoning maps using regional frequency analysis and L-moment in the Khuzestan province of Iran. *Theor Appl Climatol* 137(1–2):77–87
2. Belayneh A, Adamowski J, Khalil B, Ozga-Zielinski B (2014) Long-term SPI drought forecasting in the Awash River Basin in Ethiopia using wavelet neural networks and wavelet support vector regression models. *J Hydrol* 508:418–429
3. Deo RC, Tiwari MK, Adamowski JF, Quilty JM (2017) Forecasting effective drought index using a wavelet extreme learning machine (W-ELM) model. *Stoch. Environ. Res. Risk Assess.* 31(5):1211–1240
4. Fung KF, Huang YF, Koo CH, Soh YW (2020) Drought forecasting: a review of modelling approaches 2007–2017. *J Water Clim Change* 11(3):771–799
5. Han P, Wang PX, Zhang SY, Zhu DH (2010) Drought forecasting based on the remote sensing data using ARIMA models. *Math Comput Model* 51(11–12):1398–1403
6. Huang YF, Ang JT, Tiong YJ, Mirzaei M, Amin MZM (2016) Drought forecasting using SPI and EDI under RCP-8.5 climate change scenarios for Langat River Basin, Malaysia. *Procedia Eng* 154:710–717
7. José Vidal-Macua J, Ninyerola M, Zabala A, Domingo-Marimon C, Pons X (2017) Factors affecting forest dynamics in the Iberian Peninsula from 1987 to 2012. The role of topography and drought. *For Ecol Manage* 406(October):290–306
8. Li F, Li H, Lu W, Zhang G, Kim JC (2019) Meteorological drought monitoring in Northeastern China using multiple indices. *Water (Switzerland)* 11(1):1–17
9. McKee TB, Doesken JK, Kleist J (1993) The relationship of drought frequency and duration to time scales. In: *Proceedings of the 8th conference of applied climatology*, 17–22 January. Anaheim, CA
10. Mondol MAH, Ara I, Das SC (2017) Meteorological drought index mapping in Bangladesh using standardized precipitation index during 1981–2010. *Adv Meteorol* 2017
11. Mossad A, Alazba AA (2015) Drought forecasting using stochastic models in a hyper-arid climate. *Atmosphere (Basel)* 6(4):410–430
12. Saadat H, Adamowski J, Bonnell R, Sharifi F, Namdar M, Ale-Ebrahim S (2011) Land use and land cover classification over a large area in Iran based on single date analysis of satellite imagery. *ISPRS J Photogramm Remote Sens* 66(5):608–619
13. Specht DF (1991) Probabilistic neural networks and general regression neural networks. *Tetrahedron Lett* 296–300

# Assessment of Economic Value of Doddabommasandra Lake Using Contingent Valuation Method and Travel Cost Method



D. N. Shilpa, K. Nruthya, L. G. Santhosh, Simran Sanu, and Anukul Nidhi

**Abstract** Lakes are a common example of water ecosystems. A plethora of benefits can be associated to water ecosystems that cater to human consumption and environmental needs alike. The water ecosystem services must be quantified so as to know how much these water services actually cost and what would be the best way to allocate them. The services and benefits from a water ecosystem are clearly of non-market type and it would only be logical to employ non-market valuation techniques to obtain the Total Economic Value. Here, the Willingness to Pay (WTP) for the ecosystem benefits is calculated which reflects the value of the ecosystem. The study aimed at evaluating ecosystem benefits at Doddabommasandra Lake, Bengaluru, India by incorporating Contingent Value Method (CVM) and Travel Cost Method (TCM). The objective of the study was to obtain visitors' WTP for the ecosystem and available or proposed recreational services at the lake. Survey was carried out on the target demography including regular and occasional visitors. Questionnaire with open-ended questions was used for CVM. Based on the responses, Willingness to Pay for various categories such as Entrance Fees, Offshore Recreational Services, Gymnastics, Vegetation Cover, and Infrastructure was estimated using CVM and averaged. For TCM, a zonal approach was incorporated to develop Demand Curve relating Travel costs with a number of visits. Regression Analysis was conducted to establish a relation between variables such as Travel distance, Travel time, Number of visits per week, and Travel cost.

**Keywords** Economic value of water · Contingent valuation method · Travel cost method · Ecosystem valuation · Willingness to pay · Doddabommasandra Lake

---

D. N. Shilpa (✉) · K. Nruthya · L. G. Santhosh · S. Sanu · A. Nidhi  
Department of Civil Engineering, M. S. Ramaiah Institute of Technology, Bengaluru 560054,  
India

© The Author(s), under exclusive license to Springer Nature Singapore Pte Ltd. 2022  
C. M. Rao et al. (eds.), *Advanced Modelling and Innovations in Water Resources Engineering*, Lecture Notes in Civil Engineering 176,  
[https://doi.org/10.1007/978-981-16-4629-4\\_5](https://doi.org/10.1007/978-981-16-4629-4_5)

## 1 Introduction

Lakes can be considered an essential part of the ecosystem. Considering, the global water resource, natural and artificial lakes account for 90% of the fresh water available to mankind. Hence, serve as an essential component of human environment. It provides varieties of environmental benefits like replenishing groundwater, modulating the floods and drought effects, hosts the ecosystem, etc. Along with this lake also provides ample opportunities for agricultural activities, recreational activities, etc.

It is difficult to express all the benefits derived from lake water in terms of tangible monetary market value, as is the case with other environmental or ecological commodities because they are not traded, generally termed as 'missing markets'. However, such goods and services do possess economic value by the virtue of their mere existence and services offered in hosting the ecosystem. It is difficult to assess economic value of lake water by traditional measures as the quality of water, aesthetics, and other such amenities are not normally tangible in terms of monetary value priced in the market. Absence of such system has led to precise non-market evaluation techniques. The Travel Cost Method (TCM or TC here onwards) and Contingent Valuation Method (CVM or CV here onwards) are the most widely used non-market evaluation techniques.

Doddabommasandra Lake located near Vidyaranyapura of Bangalore Urban, Karnataka, India is considered for economic value assessment. Lake has the water spread area of 124.35 acres (0.5058 km<sup>2</sup>). It is a seasonal lake, generally replenished by rainfall. The average elevation around the area is 902.56 m. It is located at 13°03'55"N 77°33'45.57"E. The site was selected considering the fact that Bharat Electronics Ltd. (BEL) has been working towards the rejuvenation of the lake as a part of Vidyaranyapura Smart Ward Program. The organization has also set up a 10 MLD Sewage Treatment Plant (STP) worth Rupees 135 Million. The vicinity of the lake comprises people belonging to different socio-economic strata and income groups. This aspect needed to be invariably considered in the data collection and analysis of the study.

## 2 Review of Literature

Literature towards assessment of economic value using non-market evaluation techniques such as Travel Cost Method and Contingent Valuation Method were reviewed. For the thorough understanding and efficient review of literature, this section has been presented under various categories.

## **2.1 Willingness to Pay**

Willingness to Pay (WTP here onwards) is the price (or range thereof) which a visitor (in context to Doddabammasandra Lake) is willing to spend in order to benefit from the services offered. Cangelosi [1] proposed a structure for quantifying non-market parameters in a financial perspective; costs and benefits associated are employed in computing the WTP value.

Verma [2] demonstrated the calculation of mean WTP voluntarily and as tax (WTP based on income, WTP based on distance of residence, etc.) of Bhoj Wetlands. A similar approach was incorporated for calculating the WTP through Contingent Value Method as well as Travel Cost Method in this study.

Leinhoop et al. [3] established that future benefits or potential developments to the provincial economy influenced WTP values significantly, and significant variations were observed in WTP value quoted by responders when interviewed on site and at home in post mining lakes in Germany. The economic and opinion disparity of the communities around Doddabommasandra Lake was taken into consideration by studying this model. It was necessary to anticipate the variation in residents' and visitors' Willingness to Pay for the ecosystem services offered by Doddabommasandra Lake.

As suggested by Desta Smegnew [4], different socio-economic variables comprising of the residents' place on the economic spectrum and their line of work affect the households' WTP. This further necessitated the consideration of socio-economic disparity and income levels for the purpose of the study.

## **2.2 Non-Market Valuation Techniques**

As expressed earlier, the ecosystem services offered by the lake are non-market-like services and cannot be monetized. Hence such ecosystem benefits must be evaluated using Non-Market Valuation Techniques.

Ward et al. [5] explained the accounts for opportunity travel cost time which emphasizes on the matter that according to some respondents' travel time might not be cost but is a part of the recreation process. This was considered in zonal travel cost method. Sagoff [6] demonstrated in detail, the estimation of the average value of WTP for an individual or household and extrapolation of results to the population under consideration which was resourceful in preparing the model for Contingent Value Method used in this study.

Früh et al. [7] presented the rapid assessment of land use plans, zoning regulations, and environmental restoration based on changes over time emphasizing the practical use of zoning methods in study of ecosystems through Travel Cost Method. Hence, Früh's model of zoning was a resourceful reference in forming such zones in our study.

Alora et al. [8] and Pan et al. [9] estimated the economic value of Pilikula lake by considering both TCM and CVM average WTP stated by visitors for the economical services provided by Pilikula Lake water. This rendered to be the most relevant study as both the lakes demonstrate similarities and the objectives of these studies have large common grounds.

### ***2.3 Ecology and Economy***

Open-ended questioning of the visitors at Doddabommasandra Lake showed that good fraction of them wish to have better quality of water in the lake and a cleaner shore. Michael et al. [10] and Schuetz et al. [11] emphasized the importance of water clarity, quality of swimming services, and scenic beauty to the consumers looking to choose which lake they wish to visit and their trends in buying property around the vicinity of that lake. Further, Yirang et al. [12] assessed the value of ecological services rendered by lakes and marshy wetlands in China considering quality of water, biodiversity, and various economic indices. This validates the fact that, by human nature, visitors show better affinity towards lakes with superior water quality, and the Willingness to Pay is subject to the water quality and the community's collective attitude towards the water quality of the lake concerned.

### ***2.4 Regression Analysis***

Data collected from the online questionnaire survey was to be analyzed as a part of Travel Cost Method to assess WTP. This analysis required Regression Analysis of multiple variables that surfaced from the data collection to establish a relation between them using least square method. Gharmandi et al. [13] studied the comparative significance of characteristics of valuation study, of wetland site, and of socio-economic and geographical context in the form of a meta-regression analysis of values. The meta-regression analysis carried out by Gharmandi was fruitful in carrying out the same in the context of Doddabommasandra Lake's economic evaluation in this study.

### ***2.5 Findings from the Literature***

- Travel time can also be a part of recreational process for visitors when it comes to visiting an ecosystem.
- Non-market benefits offered by ecosystems must be evaluated through suitable non-market evaluation techniques such as Contingent Valuation Method and Travel Cost Method.

- WTP is subject to socio-economic disparity and income groups of the population present at and around the study area which by extension is, directly and indirectly, dependent on the land use, population distribution, and distance from the study area.
- Quality of water holds a significant footing over the economic value and economic impacts on the recreational uses of a water body.
- Regression analysis is suitable for evaluating the economic value of an ecosystem as the non-market valuation of an ecosystem involves the influence of many independent variables on a dependent variable.

## 2.6 Objectives

The objectives of this study were identified as follows:

- To calculate Average Mean Willingness to Pay and Total Economic Benefits of Doddabommasandra Lake using Contingent Value Method.
- To carry out Zonal Travel Cost Method to calculate Travel Cost as Willingness to Pay for every zone in the Doddabommasandra ward and then assess Average Willingness to Pay.
- Draw an inference regarding the feasibility of making investments on Doddabommasandra Lake based on the WTP values arrived at from Contingent Value Method and Zonal Travel Cost Method.

## 3 Methodology

The first step of methodology adopted to arrive at the objectives includes rigorous literature survey. Glimpse of the review along with findings from literature has been mentioned in the earlier sections which lead to the above-mentioned objectives of the study. Preliminary studies were carried out at the site to gather first-hand information about the existing scenario and activities. This also leads to identification of stakeholders.

Meteorological and topographical data constituting secondary information along with the revenue and expenditure was collected from the lake authorities and literature survey. A pilot study was carried out to build up the questionnaire suitable to Doddabommasandra Lake to collect information from the stakeholders. Survey was carried out to assess the willingness of people to pay for the quoted improved recreational benefits from lake based on CVM and TCM.

Google forms were generated to collect responses. Trained interviewers also helped the visitors to fill the Google forms. Responses were analyzed in Microsoft Excel® using various economic and statistical tests. WTP values for various considerations were calculated and average WTP was assessed. Statistical tests were run on the responses from stakeholders as a part of regression analysis. Conclusions were



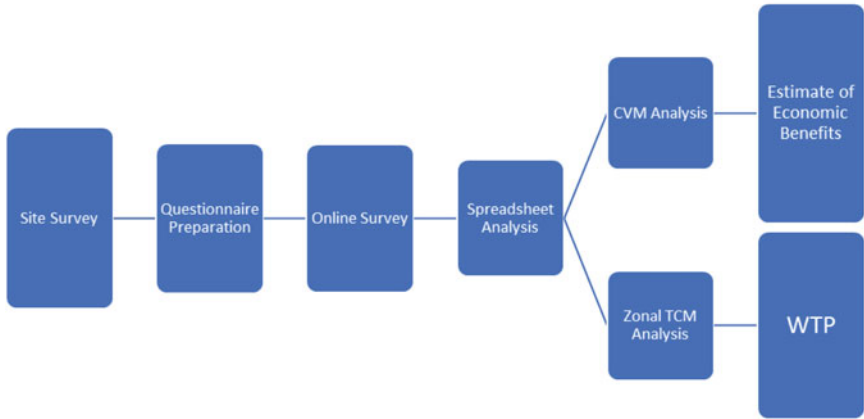


**Fig. 1** Methodology flow diagram

drawn based on the result reflected in context to regional economy, quality of life, and tourism. Refer Fig. 1 for the methodology.

### ***3.1 Evaluation of Lake Water***

The Lake can be evaluated based on the various uses offered by lake water ecosystem. This can be categorized as Direct Valuation and Contingent Valuation Method.

In Direct Valuation, various direct benefits that the lake offers like source of water, supporting aquatic life, recreational activities, etc. are considered. This includes monetary value assessment of the major benefits and the activities with income generation. Income generation from these activities can be calculated by considering the number of dependents on such activities therein as well as the revenue generated on an average yearly considering seasonality.

In Contingent Valuation Method if relevant market behavior is not observable/tangible, the CVM adopts direct questionnaire to individuals to assess WTP for an environmental resource, or the compensation that they would be willing to accept when the same resource they were deprived off for the assessment. CVM is more effective if the environmental good or service rendered by the site is familiar to the respondents.

### ***3.2 Sampling Plan***

Sample survey was carried out considering a representative sample population. Sample population included representations corresponding to various zones around

the lake considered for Zonal TCM and socio-economic background important for reliable CVM analysis.

### ***3.3 Questionnaire and Response Collection***

In this study, CVM has been adapted to mainly capture the recreational services offered by Doddabommasandra Lake to the visitors. CVM is generally used only for assessing recreational and aesthetic benefits since the entire city is not benefitted from other services. Also, the site does not inhibit any rare species because of which biodiversity conservation is no longer an important criterion. An exclusive questionnaire was adapted to elicit WTP of the visitors for better scenic and recreational benefits from the lakes.

Scenario illustrating benefits from Doddabommasandra Lake and the possible recreational developments was presented before responders through elicitations and photographs. Responders were to quote their WTP to enjoy the improved benefits from the lake. Responses regarding their proposed contribution in the form of tax whereby entire revenue generated made thereof would be directed towards the recreational benefits and maintenance of the lake.

### ***3.4 Compilation***

CVM and TCM followed in the current study considered visitation rate of the lake. These assets were analyzed later on the basis of their regional applicability and advantages in the vicinity of the lake, travel distances, their socio-economic conditions, etc. Regression analysis was then run to obtain the marginal WTP of the stakeholders for housing in locations in the vicinity of the lake.

### ***3.5 Travel Cost Method***

TCM is considered to assess value of economic use associated with ecosystem or recreational sites. In this method, values can be assigned (even for consumer surplus and not only for marginal WTP) for proposing creation of new site or elimination of a site. Travel time and travel expenses that incur to visit a site are considered as “price” of access to the site. Hence, WTP can also be derived based on the number of trips made for different travel costs.

TCM is modeled on standard economic methods and thus is relatively uncontroversial for measuring value. It is often inexpensive. TCM is built on the actual behavior of respondent than verbal responses to a hypothetical scenario. The method is developed considering the simple fact that travel cost reflects recreational value

of an ecosystem. Several ways are available to approach a problem, with variations in TCM. Simple zonal travel cost approach was adopted for the current study. It is the least expensive and simplest approach which can be used to estimate economic value for recreational services of the site.

Various steps involved in Evaluation of Lake using Zonal TCM:

- A set of zones surrounding the Doddabommasandra Lake is defined by creating concentric circles around the site at different distances.
- Information on the number of visitors from each zone is collected, and the number of visits made per year.
- Number of visits per thousand population of the zone is calculated in each zone by dividing number of visits by the zonal population in thousands.
- Travel distance and time to travel are calculated from each zone to the lake. First zone is assumed to be Zone 0 with zero travel distance and time. Each consecutive zone has increasing travel distance and time. The travel cost per trip is estimated assuming an average cost per kilometer of distance and per hour of travel time.
- Equation relating visits per capita to travel costs and other significant variables are developed for regression analysis and demand function for the average visitor is assessed.
- Demand function for visits per capita is constructed with the results of the regression analysis. First point on demand curve represents the total visitors to the lake at current access costs (assuming there is no entry fee to the lake). Then, other data points are calculated by estimating the number of visitors with various hypothetical entrance fees (assuming that an entrance fee is considered similar to or as a part of travel costs).

### ***3.6 Contingent Valuation Method***

CVM can be used to assess the economic values for all kinds of ecosystem and environmental services. This method can be used to assess both use and non-use values. It is the most widely used method for assessing non-use values. However, CVM is also the most controversial method of non-market valuation techniques. CVM is based on the fact that one would do what one would say, as opposed to what people are observed to do, this turns out to be its greatest strengths as well as greatest weaknesses. The fact that the CVM is based on the verbal response to questions, as opposed to observing their actual behavior, is the source of enormous controversy.

Various steps involved in Evaluation of Lake using CVM:

- Valuation problem is defined along with the exact services were being to be valued.
- Survey is designed for the initial focus groups interviews including questions regarding the lake.
- Further questions would further get detailed and specific and help to develop lake specific questions for the survey.

- Using standard statistical sampling techniques, sample survey is conducted for randomly selected sample of the relevant population.
- Responses is entered into a suitable format such as Google Forms and transferred into a spreadsheet.
- Data is analyzed using appropriate statistical approach for a given type of question.

## **4 Data Collection and Analysis**

### ***4.1 Data Collection***

As explained earlier CVM is based on asking people verbal questions as against observing their actual behavior. The conceptual, empirical, and practical problems associated with this assessment depend on the way respondents respond to hypothetical questions about hypothetical market scenarios. An open-ended format was adopted such that the respondents quoted their maximum WTP for a given scenario.

The Zonal TCM is applied by collecting information on the number of visits to the site from different zones. These travel and time costs increase with distance. Thus, number of visits procured at various prices considering cost of travel as a part of cost of visit is assessed. The required information was collected by conducting an online questionnaire survey using Google Forms with the near-by residents and visitors of the lake. The responses we obtained from the survey were organized and stored in the form of a spreadsheet and further analyzed on Microsoft Excel®. With this data, Demand Curve was constructed for this site and mean Willingness to Pay for the services offered by the site was estimated.

The final questionnaire was designed to assess economic value of lake water by Zonal TCM and draw information regarding, visitation rate to the lake per week, Age group, travel distance, mode of transportation, type of vehicle (if used for transportation), travel time.

Open-ended questions regarding the present services, willingness to pay any entrance fee if introduced, amount, facilities recommended including Offshore and In-Water Recreational services, Gymnastics, Vegetation cover, Infrastructure, etc., and WTP for each facility was included to assess economic value of lake water by CVM.

Along with these for socio-economic consideration, occupation, income range, and similar substitute sites were asked.

### ***4.2 Analysis Using Contingent Value Method***

CVM is used to evaluate non-market benefits of Doddabommasandra Lake which appropriates the use of Compensating Variation as a measure. Compensating Variation, in this case, was procured as Willingness to Pay.

**Table 1** Calculation of meant WTP for entrance fees

| WTP (₹) | Frequency | WTP * Frequency | Mean = $\frac{\sum(WTP*Frequency)}{\sum Frequency}$ |
|---------|-----------|-----------------|---|
| 20      | 41        | 820             |   |
| 50      | 46        | 2300            | ₹45   |
| 100     | 14        | 1400            |   |

**Table 2** Calculation of meant WTP for offshore recreational services

| WTP (₹) | Frequency | WTP * Frequency | Mean = $\frac{\sum(WTP*Frequency)}{\sum Frequency}$ |
|---------|-----------|-----------------|---|
| 20      | 35        | 700             |   |
| 50      | 52        | 2600            | ₹46.53  |
| 100     | 14        | 1400            |   |

Steps Involved in Contingent Value Method:

- Data collected from the online questionnaire survey was organized into a spreadsheet for analysis. This included the income range of the respondents.
- Average Income of all the respondents was calculated and found to be ₹ 9,57,722.77.
- Relevant values (responses) were segregated and compartmentalized into individual tables. The responses were actually the WTP amounts for each case such as WTP as Entrance Fees, WTP for Offshore Recreational Services, and many more.
- Mean WTP was calculated for each type of service.

The following Tables 1, 2, 3, 4 and 5 show the individual mean WTP for each type of service:

**Table 3** Calculation of meant WTP for gymnastics

| WTP (₹) | Frequency | WTP * Frequency | Mean = $\frac{\sum(WTP*Frequency)}{\sum Frequency}$ |
|---------|-----------|-----------------|---|
| 50      | 50        | 2500            | ₹75   |
| 100     | 51        | 5100            |   |

**Table 4** Calculation of meant WTP for vegetation cover

| WTP (₹) | Frequency | WTP * Frequency | Mean = $\frac{\sum(WTP*Frequency)}{\sum Frequency}$ |
|---------|-----------|-----------------|---|
| 15      | 43        | 645             |   |
| 25      | 35        | 875             | ₹26.44  |
| 50      | 23        | 1150            |   |

**Table 5** Calculation of meant WTP for infrastructure

| WTP (₹) | Frequency | WTP * Frequency | Mean = $\frac{\sum(WTP * Frequency)}{\sum Frequency}$ |
|---------|-----------|-----------------|---|
| 15      | 65        | 975             |   |
| 25      | 24        | 600             | ₹21.53  |
| 50      | 12        | 600             |   |

Below are the pie charts that show the distribution of WTP amounts for the various services (Fig. 2 and Table 6):

- Average of all the above calculated mean WTP amounts were found to be ₹42.9. Total Assessment of Economic Benefits from the services at the site was calculated as ₹9,46,245.30. This is the product of Average Mean WTP amounts and Population of the Doddabommasandra ward (Arithmetically Projected for 2019 as 21,640 people from 2011 census).

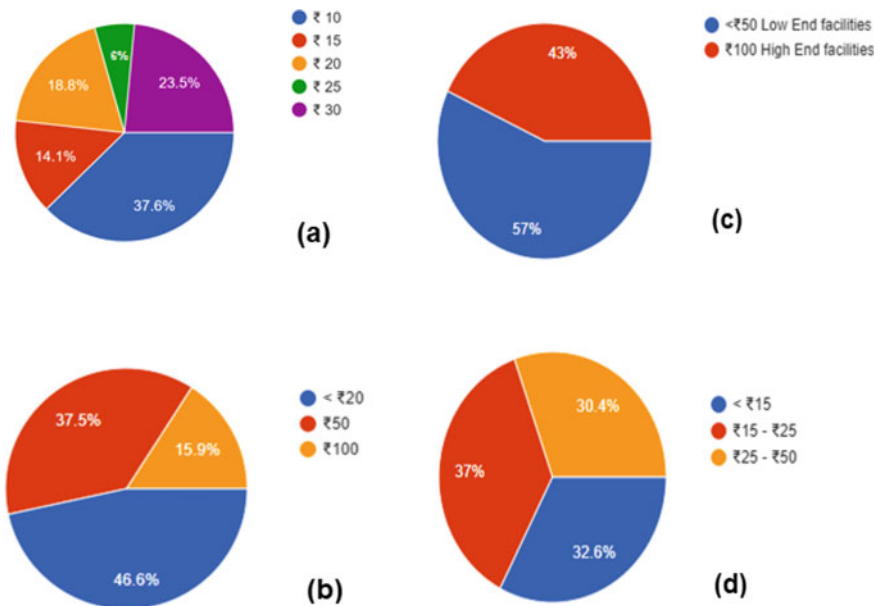


**Fig. 2** Distribution of WTP for **a** entrance fees, **b** offshore recreational services, **c** gymnastics and **d** infrastructure

**Table 6** Calculation of average mean WTP and total estimate of economic benefits

| Services                            | Average of mean willingness to pay (₹) |
|-------------------------------------|--|
| Entrance fees                       | 45                                     |
| Offshore recreation                 | 46.53                                  |
| Gymnastics                          | 75                                     |
| Vegetation cover                    | 26.44                                  |
| Infrastructure                      | 21.53                                  |
| Average                             | 42.9                                   |
| Total estimate of economic benefits | 946,245.30                             |

### 4.3 Analysis Using Zonal Travel Cost Method

Zonal TCM is based on the principle that based on the correlation between the users' behavior (i.e., the number of trips to the site) and the cost of a visit the recreational benefits at a given site can be derived from the Demand Curve.

Steps Involved in Zonal Travel Cost Method:

- Set of zones surrounding the site were defined. The zones were defined with respect to the distance traveled by the visitors in reaching the site, i.e., 2, 5, 10, and 15 kms.
- Data collected by conducting a questionnaire survey using Google Forms as explained in Contingent Value Method was used for this method as well.
- Visitation rates per 1000 population were calculated in each zone. That is the total visits per week from each zone divided by the zones' population in thousands. The total number of visits was 640.
- Average Round Trip Travel Distance and Travel Time were calculated to the site for each zone. It was assumed that people in Zone 0 have zero travel distance and zero time. However, the other zone has an increasing travel time and distance.
- A curve was plotted between Visits/1000 and Total Travel Cost per Trip which is the Demand Curve (Tables 7 and 8).

The following Eq. (1) was obtained from the Demand Curve:

**Table 7** Calculation of visits/1000

| Zone | Visits per week | Zone population | Visits/1000 |
|------|-----------------|-----------------|-------------|
| 0    | 0               | 0               | 0           |
| 1    | 213             | 1352            | 157.54      |
| 2    | 176             | 3381            | 52.06       |
| 3    | 136             | 6763            | 20.11       |
| 4    | 115             | 10,144          | 11.34       |

**Table 8** Calculation of total travel cost per trip

| Zone | Distance | Time (min) | Cost/km   | Distance * Cost/km | Cost/minute | Travel Time * Cost/min | Total travel cost per trip |
|------|----------|------------|-----------|--------------------|-------------|------------------------|----------------------------|
| 0    | 0        | 0          | 0         | 0                  | 0           | 0                      | 0                          |
| 1    | 2        | 15         | 2.68125   | 5.36               | 0.0715      | 1.0725                 | 6.44                       |
| 2    | 5        | 30         | 6.703125  | 33.52              | 0.143       | 4.29                   | 37.81                      |
| 3    | 10       | 45         | 13.40625  | 134.06             | 0.2145      | 9.6525                 | 143.72                     |
| 4    | 15       | 60         | 20.109375 | 301.64             | 0.286       | 17.16                  | 318.80                     |

$$y = -1.5866x + 220.45 \tag{1}$$

where,  $y$  = Travel (Y-axis),  $x$  = Visits per 1000 (X-axis).

In Eq. (1) if  $x$  is substituted with different values of Travel Cost, the Demand Function will be generated (Fig. 3).

- Regression Analysis was conducted to establish a linear relation between variables such as distance, travel time, visits per week, and total travel cost (Table 9).

The value of  $R^2$  here is greater than 0.5 and it represents the percentage of dependent variable variation that this linear model represents.

- From the Regression Analysis, the Regression Coefficients were calculated as shown in Table 10. The Regression Equation used is:

$$Y = \alpha + \beta_1 X_1 + \beta_2 X_2 + \beta_3 X_3 \tag{2}$$

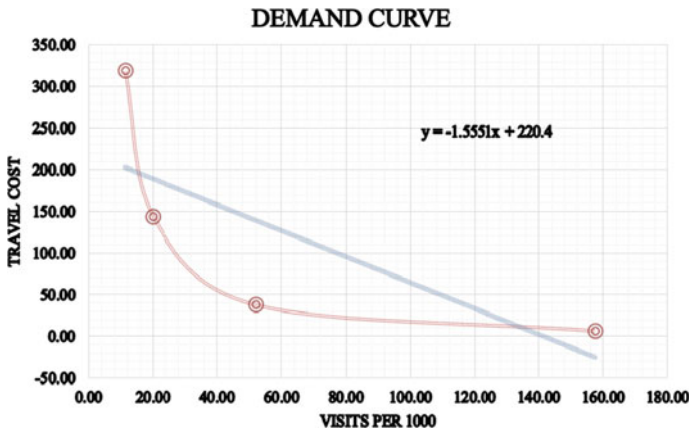


**Fig. 3** Demand curve



**Table 9** Summary output

| Regression statistics |             |
|-----------------------|-------------|
| Multiple R            | 0.995082817 |
| R Square              | 0.990189812 |
| Adjusted R Square     | 0.960759247 |
| Standard error        | 26.65031586 |
| Observations (Zones)  | 5           |

**Table 10** Regression coefficients

|                | Time (minutes) | Distance | Visits/1000 | Intercept |
|----------------|----------------|----------|-------------|-----------|
| Coefficients   | -8.528         | 45.588   | 0.1817      | 82.624    |
| Standard Error | 3.7717         | 15.194   | 0.2762      | 26.638    |
| t Stat         | -2.261         | 3.5927   | 0.658       | -0.031    |
| P-value        | 0.2651         | 0.1728   | 0.6295      | 0.9803    |
| Lower 95%      | -56.45         | -138.5   | -3.327      | -339.3    |
| Upper 95%      | 39.396         | 247.65   | 3.6909      | 337.64    |
| Lower 95.0%    | -56.45         | -138.5   | -3.327      | -339.3    |
| Upper 95.0%    | 39.396         | 247.65   | 3.6909      | 337.64    |

In equation (2):

$Y$  = Total Travel Cost.

$X_1$  = Visits/1000.

$X_2$  = Distance.

$X_3$  = Travel Time.

$\alpha$  = 82.62390973 (Regression Coefficient).

$\beta_1$  = 0.181718687 (Regression Coefficient).

$\beta_2$  = 45.58827142 (Regression Coefficient).

$\beta_3$  = -8.527861976 (Regression Coefficient).

From Eq. (2), The Travel Cost or Willingness to Pay was calculated for different zones by substituting the variables in Eq. (2) with values from Table 10. The WTP values corresponding to each zone is shown in Table 11 of Sect. 5.

**Table 11** Zonal travel costs and average willingness to pay

| Zone    | Travel cost (₹) |
|---------|-----------------|
| 0       | 0               |
| 1       | 73.95           |
| 2       | 64.19           |
| 3       | 158.41          |
| 4       | 256.84          |
| Average | 110.68          |

## 5 Results and Discussion

### 5.1 Result from Contingent Value Method

In Sect. 4, we extrapolated relevant data from the responses obtained from the online questionnaire survey and organized them into manageable tables based on the type of service in question. Then, we calculated the Mean Willingness to Pay for each service as shown from Tables 1, 2, 3, 4 and 5. From the Mean WTP amounts for each service, we calculated the Average Mean Willingness to Pay as ₹42.9 as shown in Table 6. The Total Estimate of Economic Benefits from the services at the site was calculated as ₹946,245.30 which is the product of Average of mean WTP amounts and Population of the Doddabommasandra ward. Hence, The Total Estimate of Economic Benefits calculated from Contingent Value Method is ₹946,245.30.

### 5.2 Discussion on Result from Contingent Value Method

The Total Estimate of Economic Benefits calculated is less than the Average Income Range of the target population of the ward.

$$₹946,245.30 < ₹957,722.77$$

This is in accordance with the fact that if the Average Income Range exceeds The Total Estimate of Economic Benefits, it is safe to make financial investments on the site for benefiting from the services offered and to invest in enhancement, development, and protection programs for the site. Thus, from the results of CVM analysis, we can infer that it is worthwhile to spend money in order to enjoy ecosystem benefits offered at Doddabommasandra Lake and invest in programs and actions for protection and rejuvenation of the lake.

### 5.3 Results from Zonal Travel Cost Method

In Sect. 4, we divided the Doddabommasandra ward into five zones. The zones were 0, 5, 10, and 15 km away from Doddabommasandra Lake. Then, from the responses obtained from the online questionnaire survey, we extrapolated distance, travel time, and frequency of visits required for Regression Analysis. Demand Curve was drawn from the values extrapolated from the online questionnaire survey and Demand Function was derived. Regression Analysis was conducted and then from the results thereof, Regression Coefficients were obtained. Regression Equation, i.e., Equation (2) was substituted with corresponding values of Regression Coefficients and the values from Table 10. Travel Cost or Willingness to Pay for each zone was calculated as shown below in Table 11.

Hence, The Average Willingness to Pay was calculated as ₹110.68.

### 5.4 Discussion on Results from Zonal Travel Cost Method

From Table 11, it is evident that Travel Cost is higher for zones that are further away from Doddabommasandra Lake. This does not only demonstrate the effect of distance on Travel Cost but also validates the fact Travel Time (which is a function of distance) is inclusive of the recreational process and that consumers visiting from a greater distance tend to spend more than those that stay closer to the lake.

The Average Willingness to Pay was calculated as ₹110.6766169. This value exceeds the Willingness to Pay amounts stipulated for the various lake services in the online questionnaire survey. This value also exceeds The Average Mean Willingness to Pay (₹42.9) as calculated in Contingent Value Method.

$$₹110.68 > ₹42.9$$

This suggests that financial investments to be made for restoration, development, preservation, and protection efforts shall be feasible, and return of investment can be expected.

## 6 Conclusions

The following conclusions were drawn from the current study carried out to assess economic value of Doddabommasandra Lake:

- This project established that the regional economy, quality of life, and tourism rely on quality of water of the lake.
- This project quantified the contribution of the natural amenities offered by the Lake to the regional economy.
- The average WTP by visitors towards the lake service benefits provided by Doddabommasandra Lake is assessed by both TCM and CVM.
- Offshore recreation and gymnastics are the expected extra services at the location. With extra facilities provided, there is expectation for a significant increase in visitation rate.
- The WTP by visitors for the recreation benefits is highly dependent on socio-economic and demographic variables such as age, gender, education, monthly income, and residential status.

Project findings suggest that future investments for development activities and programs that aim for restoring and protecting the lake are feasible and guarantee a substantial return of investment.

**Acknowledgments** We would hereby like to acknowledge Mr. Abhinav Kumar Piyush and Mr. Subham Kumar Agarwal for their contribution towards the work. We would also like to acknowledge the stakeholders of Doddabommasandra Lake including visitors, near-by residents, and the Authorities of the STP at lake for their kind responses and support. We would also like to thank management of M S Ramaiah Institute of Technology, Bengaluru for providing us an opportunity to carry out this work.

## References

1. Cangelosi A (2001) Revealing the economic value of protecting the great lakes. Northeast-Midwest Institute, National Oceanic & Atmospheric Administration, Washington, DC, pp 72–95
2. Verma M (2001) Economic valuation of Bhoj wetlands for sustainable use. Environmental Economics Research Committee, Indian Institute of Forest Management
3. Lienhoop N, Messner F (2009) The economic value of allocating water to post-mining lakes in East Germany. *Water Resour Manage* 23:965–980
4. Desta Y (2018) Analysis of economic value of lake Ziway: an application of contingent valuation method. *J Resour Dev Manage* 40:55–66
5. Ward FA, Beal D (2000) Valuing nature with travel cost models. A manual. Edward Elgar Publishing
6. Sagoff M (1988) *The economy of the Earth: philosophy, law, and the environment*. Cambridge University Press
7. Früh S, Gattenlöhner U, Hammerl M, Hartmann T, Hörmann S, Megerle H, Spaich F (2013) Economic value of lakes and wetlands. Global Nature Fund, University of Applied Forest Sciences Rottenburg, Lake Constance Foundation
8. Alora J, Nandagiri L (2015) Evaluation of economic value of Pilikula lake using travel cost and contingent valuation methods. *Aquat Procedia* 4:1315–1321
9. Pan W, Tang T, Deng H, Cai Q (2002) Lake ecosystem services and their ecological valuation—a case study of Baoan lake in Hubei Province. *J Appl Ecol* 13(10):1315–1318
10. Holly M, Boyle KJ, Bouchard R (2006) Water quality affects property prices: a case study of selected Maine lakes. Maine Agricultural and Forest Experiment Station
11. Schuetz JF, Boyle K, Bouchard R (2001) The effects of water clarity on economic values and economic impacts on recreational uses of ponds. Maine Agricultural and Forest Experiment Station
12. Zhang Y, Zhou D, Niu Z, Xu F (2013) Valuation of lake and Marsh wetlands ecosystem services in China. *Chin Geogr* 23(6):1–10
13. Gharmandi A, Bergh J, Brander LM, Groot H, Nunes P (2008) The economic value of wetland conservation and creation: a meta-analysis. FEEM Working Paper No. 79

# Meteorological Drought Analysis Using SPI-6 for Marathwada Region, Maharashtra State, India



A. B. Pachore and D. G. Regulwar

**Abstract** Drought is an extreme climatic event, which is recurring in nature. Drought occurs when the amount of precipitation is less than average precipitation for the region. Marathwada region of Maharashtra state, India is selected for this study. Marathwada region is facing extremely dry conditions again and again over the period. Marathwada region has 8 districts and 76 blocks. This study provides a blockwise characterization of meteorological drought from 1980 to 2014 using the Standardized Precipitation Index (SPI) at a 6-month time scale. The six-month SPI (SPI-6) is used as it characterizes the rainfall amount during the preceding half-year, and is most useful for characterizing shallow soil moisture available to crops and forage grasses. Drought duration, severity, and frequency are assessed for all 76 blocks which show considerable spatial variation. The drought condition of each block is highlighted based on drought years, duration, average SPI-6 value, and type of drought event. The most affected blocks due to droughts are Badnapur, Mukhed, Dharmabad, Khultabad, Lohara, Phulambri, Vaijapur, Ambejogai, Sengaon, Mahur, Lohara, etc. Results from this study give important information regarding blocks in which drought events occurred more frequently and are most vulnerable to it. This study is helpful for water resource planners and stakeholders to properly manage drought conditions according to their severity and location.

**Keywords** Meteorological drought · SPI-6 · Drought duration · Severity · Frequency

## 1 Introduction

Drought is generally referred to as lack of precipitation which is occurring frequently. When an amount of precipitation is below the average precipitation value of a region, it is referred to as a drought. Drought characteristics vary spatially from region to region. The development of drought is slow and it is hard to find the start and end

---

A. B. Pachore (✉) · D. G. Regulwar  
Department of Civil Engineering, Government Engineering College, Aurangabad, Maharashtra, India

© The Author(s), under exclusive license to Springer Nature Singapore Pte Ltd. 2022  
C. M. Rao et al. (eds.), *Advanced Modelling and Innovations in Water Resources Engineering*, Lecture Notes in Civil Engineering 176,  
[https://doi.org/10.1007/978-981-16-4629-4\\_6](https://doi.org/10.1007/978-981-16-4629-4_6)

71

period. The regional extent of drought is much larger as compared to other natural calamities such as flash floods and cloud bursts. Drought event often affects water supplies by the deficit in soil moisture, depletion in stream flows, and lowering of reservoir and groundwater level. The nature of drought is generally local which varies in space as well as on time scales. Therefore, the development of good management and mitigation system for drought events is necessary. 25 major drought years are recorded in India from 1871 to 2015. 1873, 1877, 1899, 1901, 1904, 1905, 1911, 1918, 1920, 1941, 1951, 1965, 1966, 1968, 1972, 1974, 1979, 1982, 1985, 1986, 1987, 2002, 2009, 2014 and 2015 were the years when drought events are recorded (Manual of Drought Management, Govt. of India). Marathwada region of Maharashtra state in India is one of the most drought-affected areas of the country. According to the Maharashtra Economic Survey of 2015–2016, 16,800 villages were affected by drought in 2014–2015, 9 million farmers were directly affected, 3225 farmers committed suicide in 2015. Aurangabad, Nanded, Latur, Parbhani, Jalna, Beed, Hingoli, and Osmanabad are eight drought-affected districts of the Marathwada region in 2014–2015. In 2014 Maharashtra's rainfall was 70.2% below normal rainfall and in 2015 it was 59.4% below the normal level. Drought analysis which is done using average data values for larger regions such as district or meteorological division does not give an accurate idea for drought conditions for that region, as precipitation deficiency can vary from one block to another within the district. SPI scale also plays a crucial role in drought studies. This study focuses on meteorological drought analysis for all 76 blocks of the Marathwada region using SPI at a 6-month time scale which is more accurate for characterizing precipitation deficiency and its consequences such as lower soil moisture, lower reservoir levels, and lower stream flows.

### ***1.1 Drought Definition***

No perfect definition of drought is available; hence defining this water scarcity is a major task in front of any researcher. An extensive review of drought is available in the literature [1]. According to the world meteorological organization [2], drought is a sustained, spatially extended deficiency of rainfall.

### ***1.2 Drought Classification***

According to Wilhite and Glantz [3], droughts are classified into four major categories which are as follows:

- Meteorological drought is a deficit of rainfall below the normal level for a sustained period. The amount of rainfall is generally considered for meteorological drought

analysis. Drought and non-drought periods are differentiated using the threshold value of the Standardized Precipitation Index.

- Hydrological drought is mainly concerned with surface and sub-surface hydrology. Within a hydrologic drought period, river flow is insufficient to fulfill the water requirement under a present water management system. PDSI (Palmer Drought Severity Index) and SWI (Standardized Water Level Index) give threshold value which is to be used as an indicator for hydrologic drought.
- Agricultural drought is triggered mainly due to meteorological drought. Deficient subsoil moisture conditions will lead to agricultural drought. The modified Palmer Drought Severity Index is used as a drought indicator. The Crop Moisture Index defines drought in terms of evapotranspiration deficit which is the difference between actual and expected weekly evapotranspiration.
- Socio-economic drought mainly considers the social and economic impacts of drought. It is concerned with the demand and supply of commercial goods.

### ***1.3 Drought Indicators/Indices***

Indicators are variables used to define drought conditions. Some of the indicators are precipitation, groundwater level, reservoir level, soil moisture, etc. [1]. Drought indicators are nothing but hydro climatological data is considered as it is and tests it with respect to threshold values without converting to index values.

Indices used to define the severity, location, duration of drought conditions. Indices are calculated numerical values used for representing drought severity. Indices are used to provide a quantitative assessment of drought severity, location, and duration.

According to WMO [2] handbook, three main approaches for assessment of drought and devising early warning systems are by making use of a single index, by making use of multiple indices, and by using combined indicators. The detailed questioner is given by WMO for selecting an index or indicator. The following key points are considered while selecting a particular index or indicator: (1) Facilitating timely identification of drought. (2) Consideration of climate, space, and time while determining drought initiation and termination. (3) Reflection of severity and impacts occurring on the ground by a particular index. (4) The need for a composite indicator. (5) Ease of using a particular index or indicator.

World Meteorological Organization [4] has given a standardized precipitation index user guide which highlights details of SPI (Standardized Precipitation Index). SPI was developed by Mckee, Doesken, and Kleist at Colorado state university in 1993. SPI is mainly used for quantification of meteorological drought. Originally SPI was calculated for 3-, 6-, 12-, 24- and 48 months' timescale.

Singh and Mishra [1] have studied various indices such as SPI for precipitation deficiency, Palmer Drought Severity Index for moisture deficiency of locality, Crop Moisture Index for evaluating moisture condition for short period such as on weekly basis for the main crop-producing region. The surface water supply index is used for representing a hydrological drought.

## 1.4 Characterization of Meteorological Drought Using SPI

Livada and Assimakopoulos [5] have used a standardized precipitation index for analysis of drought on a spatial and temporal scale. Drought events are identified and classified using drought duration and intensity data. SPI calculation is performed using monthly rainfall data for 51 years of 23 stations distributed in Greece. Wang et al. [6] studied monthly precipitation and temperature data at 633 sites in China during 1961–2012, standardized precipitation index, and standardized precipitation evapotranspiration index are calculated for drought severity investigation. Guhathakurta et al. [7] studied meteorological drought over the Indian region using a standardized precipitation index. Drought events are analyzed in connection with northeast monsoon and southwest monsoon. Gidey et al. [8] analyzed seasonal meteorological drought using SPI-3. Drought properties such as drought duration, severity, intensity, and frequency are studied both spatially and temporally. Das et al. [9] has used rainfall data from 1973 to 2016 to analyzed meteorological drought in the Linu river basin. SPI is calculated at various times scales such as 1, 3, 6, 9, 12, and 24 months. Trend analysis of drought events is done by using the Mann–Kendall test.

## 2 Methodology

6-month standardized precipitation index is used for identifying drought events. SPI can be calculated for different timescales. Timescales generally vary from 3, 6, 12, 24, and 48 months. These timescales correspond to different types of impacts due to precipitation deficit. Shorter timescales such as 1 to 2 months denote meteorological drought, 1 to 6 months SPI denotes agricultural drought and 6 to 24 months SPI denotes hydrologic drought. SPI is generally probabilistic in nature, i.e., probability distribution is fitted with rainfall record of the region and then transformed to the normal distribution, due to this normalization, SPI values above “0” shows wet conditions and below “0” shows dry conditions, where “0” correspond to long term average rainfall of the region. Based on the literature survey all SPI values below “-1” are considered for drought characterization. SPI is used because of its ease in handling and flexibility of calculation at different timescales.

Following are the detailed steps to calculate Standardized Precipitation Index for the  $i$ th year,  $j$ th month and for a time scale of  $k$  months,

- Calculation of ‘ $k$ ’ month moving average of rainfall time series  $X_{ij}^k (I = 1 \dots n)$  for month  $j$  of year  $i$ , where every ‘ $X$ ’ term is an addition of rainfall of previous  $k$  months.
- Generally, Gamma distribution is fitted for average monthly rainfall data series varying from 3-, 6- until 24 months, which is given as follows:

$$g_X(X) = \frac{1}{\beta^\xi \Gamma(\xi)} X^{\xi-1} e^{-\frac{X}{\beta}} \quad (1)$$



where, shape parameter is  $\xi$ , the scale parameter is  $\beta$ , and the gamma function at  $\xi$  is  $\Gamma(\xi)$ . Integrate Eq. (1) for getting cumulative probability distribution which is given as follows,

$$G_X(X) = \int_0^X g_X(X)dx = \frac{1}{\beta^\xi \Gamma(\xi)} \int_0^X X^{\xi-1} e^{-\frac{X}{\beta}} dx \tag{2}$$

- Two parameter gamma distribution function doesn't consider '0' values but rainfall distribution contains '0' values, therefore, mixed distribution function which will consider '0' values are taken and CDF (cumulative distribution function) is defined, which is as follows,

$$F_X(X) = q + (1 - q)G_X(x) \tag{3}$$

where,  $G(x)$ : CDF for non-zero rainfall,  $q$ : Probability of zero rainfall.

- SPI (Standardized Precipitation Index) is given by the following expression,

$$SPI = \Psi^-(F(X)) \tag{4}$$

where,  $\Psi()$ : CDF of the standard normal distribution,  $\Psi^-(F(X))$ : inverse of standard normal CDF.

SPI calculation requires only precipitation as an input variable. Temporal analysis of droughts event is done using a standardized precipitation index. 3-month SPI is used for quantification of short term drought episodes, 6-month SPI is used for quantification of the seasonal drought events, 9-month SPI is used for medium-term drought event, 12-month SPI, and 24 SPI is used for characterization of the long term drought event.

SPI has an intensity scale in which both positive and negative values are calculated, which correlates directly to wet and dry events.

### 2.1 6-Month Standardized Precipitation Index

The six-month SPI (SPI-6) characterizes the rainfall amount during the preceding half-year and is most useful for characterizing shallow soil moisture available to agricultural crops and forage grasses. The six-month SPI correlates the rainfall for that duration with the same six-month duration over the previous records. For instance, a six-month SPI at the end of September correlates the rainfall summation for April–September duration with all the previous summation for that same duration. The six-month SPI shows short to medium-term variation in rainfall and is still used as more vulnerable to situations at this scale than the Palmer Index. A six-month SPI can be highly efficient in indicating the rainfall over different seasons. For instance, a six-month SPI at the end of March would show a very good designation of the

amount of rainfall that has occurred within the very crucial wet season from October till March for definite Mediterranean locales. Data from a six-month SPI can be also correlated with stream discharge and levels of the reservoir, depending on the area and duration of a year.

## 2.2 Definition of Drought Properties

There are four main properties of drought events which are drought duration, drought severity, minimum SPI, drought inter-arrival period. These properties are discussed below:

**Drought Duration ( $D_d$ ):** Duration or period for which SPI value remains below the threshold of ‘ $-1$ ’, this consecutive time interval is taken as drought duration or also called as drought length.

**Drought Severity ( $S_d$ ):** Drought severity is defined as the summation of SPI values below “ $-1$ ” within the period of drought. Drought severity can also be stated as the summation of negative SPI values below ‘ $-1$ ’.

The severity of a drought event in the  $i$ th month is calculated by:

$$S_i = - \sum_{t=1}^D SPI_{i,t} \quad (5)$$

**Inter-arrival Time ( $L_d$ ):** Inter-arrival time of drought is defined as the period from the starting of one drought event till the beginning of the next drought event.

Depending upon the values of SPI, drought event is characterized or divided into four groups from s. no. 4 to 7 as shown in Table 1. As mention in Table 1, SPI values above 0.99 shows wet conditions, in between  $-0.99$  and  $0.99$  shows near-normal condition. All index values below  $-0.99$  are categorized into drought conditions from extremely dry to moderately dry.

**Table 1** Classification of drought event-based upon SPI values [10]

| S. No. | SPI               | Class          |
|--------|-------------------|----------------|
| 1      | +2 and above      | Extremely wet  |
| 2      | +1.5 to +1.99     | Severely wet   |
| 3      | +1 to +1.49       | Moderately wet |
| 4      | $-0.99$ to $0.99$ | Near normal    |
| 5      | $-1$ to $-1.49$   | Moderately dry |
| 6      | $-1.5$ to $-1.99$ | Severely dry   |
| 7      | $-2.0$ and less   | Extremely dry  |

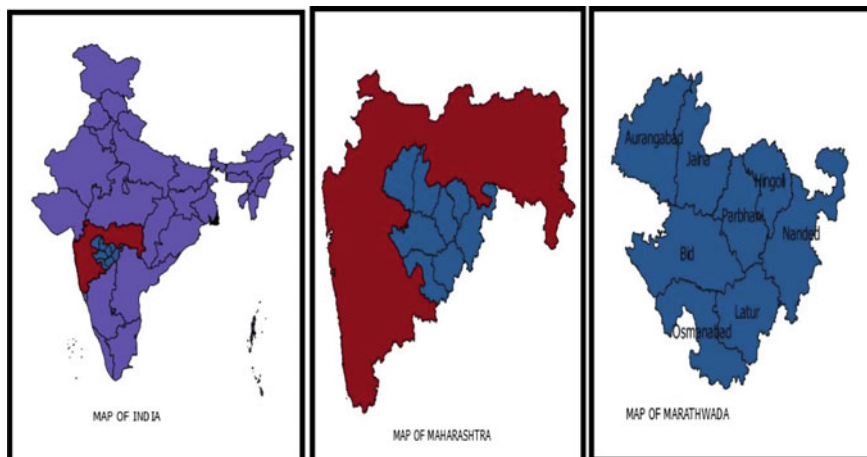


**Fig. 1** Location map of Marathwada region

### 3 Results and Discussion

#### 3.1 Study Area Details

The drought situation is faced frequently due to less rainfall in the Marathwada region. There are total eight districts in the Marathwada region which are—Hingoli, Jalna, Latur, Osmanabad, Parbhani, Aurangabad, Nanded, Beed. Marathwada region is having co-ordinates as,  $70^{\circ}5'$  East to  $78^{\circ}5'$  East in longitude whereas  $17^{\circ}5'$  North to  $20^{\circ}5'$  North in latitude. Refer Fig. 1 for a location map of the Marathwada region. The total geographic area and population of the region are  $64,590 \text{ km}^2$  and 1,87,32,785 respectively (Shodhganga). Daily precipitation data is collected from <https://globalweather.tamu.edu/> for the Marathwada region. This daily data is converted to a monthly dataset using excel. Monthly precipitation data is needed as input for SPI calculation in SPI generator software.

#### 3.2 Drought Characterization

Marathwada region of Maharashtra state has total 8 districts and is within 76 blocks. Drought characterization is done blockwise from 1980 to 2014 using SPI-6. Drought vulnerability is assessed of each block from 1980 to 2014 using drought severity/category based on SPI-6 values.

### 3.3 Blockwise Drought Vulnerability Assessment Using SPI 6

Table 2 shows, how many times a particular drought event has occurred for the Aurangabad block from 1980 till 2014, near-normal conditions have occurred 4 times, moderately dry conditions have occurred 11 times, very dry event has occurred once. Table 2 for Aurangabad block shows the start and end date of every drought event along with drought duration in month, an average of SPI-6 values for drought duration, and average monthly precipitation deficiency category. Similar drought categorization is done for all 76 blocks. Table 3 shows how many times drought of each category has occurred for the study area from 1980 to 2014. From this vulnerability assessment of each block following blocks are identified with the maximum number of near normal, moderately dry, very dry, and extremely dry events.

- The maximum number of near-normal conditions (13 times) has occurred in Badnapur, Mukhed, Dharmabad.
- The maximum number of moderately dry conditions (12 times) has occurred in Khultabad, Lohara.
- The maximum number of very dry conditions (4 times) has occurred in Phulambri, Vaijapur, Ambejogai, Sengaon, Mahur, Lohara.
- Extremely dry conditions have occurred in Gangapur, Khultabad, Bhokardan, Jafrabad, Jalna, Mantha, Kandhar, Umerga, Pathari, Gangakhed, Ahmadpur, Renapur, Chakur.

**Table 2** Drought categorization for Aurangabad block

| Start date | End date   | Drought duration | Average SPI-6 | Drought Category |
|------------|------------|------------------|---------------|------------------|
| 02/01/1981 | 04/01/1981 | 2                | -0.81         | Near normal      |
| 08/01/1981 | 02/01/1982 | 6                | -0.58         | Near normal      |
| 05/01/1983 | 08/01/1983 | 3                | -1.2          | Moderately dry   |
| 01/01/1986 | 07/01/1986 | 6                | -0.74         | Near normal      |
| 01/01/1987 | 08/01/1987 | 7                | -1.11         | Moderately dry   |
| 01/01/1992 | 06/01/1993 | 17               | -1.39         | Moderately dry   |
| 04/01/1996 | 08/01/1996 | 4                | -1.18         | Moderately dry   |
| 04/01/2000 | 05/01/2000 | 1                | -1.76         | Very dry         |
| 10/01/2000 | 06/01/2001 | 8                | -1.34         | Moderately dry   |
| 03/01/2003 | 04/01/2003 | 1                | -1.03         | Moderately dry   |
| 04/01/2004 | 05/01/2004 | 1                | -1.03         | Moderately dry   |
| 06/01/2005 | 05/01/2006 | 11               | -0.64         | Near normal      |
| 05/01/2007 | 06/01/2007 | 1                | -1.14         | Moderately dry   |
| 03/01/2008 | 02/01/2009 | 11               | -1.06         | Moderately dry   |
| 04/01/2012 | 07/01/2012 | 3                | -1.01         | Moderately dry   |
| 04/01/2013 | 06/01/2013 | 2                | -1.41         | Moderately dry   |

**Table 3** Blockwise drought vulnerability assessment

| S. No. | Name of district | Name of block | Near normal | Moderately dry | Very dry | Extremely dry |
|--------|------------------|---------------|-------------|----------------|----------|---------------|
| 1      | Aurangabad       | Aurangabad    | 4           | 11             | 1        | –             |
| 2      |                  | Gangapur      | 8           | 8              | 2        | 1             |
| 3      |                  | Kannad        | 7           | 11             | 1        | –             |
| 4      |                  | Khultabad     | 5           | 12             | 2        | 1             |
| 5      |                  | Paithan       | 11          | 10             | 2        | –             |
| 6      |                  | Phulambri     | 11          | 8              | 4        | –             |
| 7      |                  | Soygaon       | 10          | 9              | –        | –             |
| 8      |                  | Sillod        | 11          | 8              | 1        | –             |
| 9      |                  | Vaijapur      | 10          | 7              | 4        | –             |
| 10     | Bid              | Asothi        | 11          | 10             | –        | –             |
| 11     |                  | Shirurkarar   | 9           | 6              | 3        | –             |
| 12     |                  | Patoda        | 11          | 3              | 2        | –             |
| 13     |                  | Bid           | 11          | 5              | –        | –             |
| 14     |                  | Georai        | 7           | 7              | 2        | –             |
| 15     |                  | Wadwani       | 9           | 10             | 2        | –             |
| 16     |                  | Kaij          | 10          | 7              | 2        | –             |
| 17     |                  | Dharur        | 11          | 8              | 2        | –             |
| 18     |                  | Ambejogai     | 7           | 6              | 4        | –             |
| 19     |                  | Parliwainath  | 7           | 8              | 3        | –             |
| 20     | Majalgaon        | 5             | 6           | 2              | -        |               |
| 21     | Hingoli          | Sengaon       | 10          | 6              | 4        | -             |
| 22     |                  | Hingoli       | 6           | 9              | 2        | -             |
| 23     |                  | Kalamnuri     | 6           | 7              | 3        | -             |
| 24     |                  | Aundhnagnath  | 9           | 8              | 2        | -             |
| 25     |                  | Basmat        | 8           | 9              | -        | -             |
| 26     | Jalna            | Bhokardan     | 11          | 6              | 3        | 1             |
| 27     |                  | Jafrabad      | 11          | 7              | 2        | 1             |
| 28     |                  | Badnapur      | 13          | 8              | 2        | -             |
| 29     |                  | Jalna         | 6           | 4              | 1        | 2             |
| 30     |                  | Mantha        | 7           | 10             | –        | 1             |
| 31     |                  | Ambad         | 6           | 7              | 2        | –             |
| 32     |                  | Partur        | 5           | 11             | –        | –             |
| 33     |                  | Ghasavangi    | 11          | 7              | 2        | –             |
| 34     | Nanded           | Mahur         | 8           | 7              | 4        | –             |
| 35     |                  | Kinwat        | 10          | 7              | –        | –             |

(continued)

**Table 3** (continued)

| S. No. | Name of district | Name of block | Near normal | Moderately dry | Very dry | Extremely dry |   |
|--------|------------------|---------------|-------------|----------------|----------|---------------|---|
| 36     |                  | Himayatnagar  | 11          | 8              | 3        | —             |   |
| 37     |                  | Hadgaon       | 4           | 6              | 3        | —             |   |
| 38     |                  | Bhokar        | 5           | 10             | 1        | —             |   |
| 39     |                  | Ardhapur      | 10          | 9              | 3        | —             |   |
| 40     |                  | Nanded        | 7           | 9              | 1        | —             |   |
| 41     |                  | Mukhed        | 13          | 6              | 3        | —             |   |
| 42     |                  | Umri          | 9           | 9              | 3        | —             |   |
| 43     |                  | Loha          | 9           | 8              | 3        | —             |   |
| 44     |                  | Kandhar       | 10          | 6              | —        | 1             |   |
| 45     |                  | Naigaon       | 11          | 8              | 3        | —             |   |
| 46     |                  | Biloli        | 6           | 9              | 1        | —             |   |
| 47     |                  | Deglur        | 7           | 7              | 2        | —             |   |
| 48     |                  | Dharmabad     | 13          | 6              | 3        | —             |   |
| 49     |                  | Mukher        | 9           | 7              | 1        | —             |   |
| 50     |                  | Osmanabad     | Paranda     | 6              | 9        | 1             | — |
| 51     |                  |               | Bhum        | 10             | 7        | —             | — |
| 52     |                  |               | Washi       | 11             | 9        | 2             | — |
| 53     |                  |               | Kalamb      | 9              | 7        | —             | — |
| 54     |                  |               | Osmanabad   | 11             | 6        | 1             | — |
| 55     | Lohara           |               | 7           | 12             | 4        | —             |   |
| 56     | Umerga           |               | 11          | 11             | 2        | —             |   |
| 57     | Tuljapur         |               | 11          | 6              | 1        | 1             |   |
| 58     | Parbhani         | Jintur        | 6           | 8              | 2        | —             |   |
| 59     |                  | Selu          | 10          | 7              | 2        | —             |   |
| 60     |                  | Pathari       | 3           | 11             | 1        | 1             |   |
| 61     |                  | Manwat        | 7           | 8              | 4        | —             |   |
| 62     |                  | Parbhani      | 9           | 7              | 1        | —             |   |
| 63     |                  | Purna         | 9           | 9              | 3        | —             |   |
| 64     |                  | Palam         | 7           | 10             | 3        | —             |   |
| 65     |                  | Gangakhed     | 8           | 8              | —        | 1             |   |
| 66     |                  | Sonpeth       | 8           | 8              | 3        | —             |   |
| 67     | Latur            | Ahmadpur      | 9           | 6              | 1        | 1             |   |
| 68     |                  | Jalkot        | 11          | 8              | 3        | —             |   |
| 69     |                  | Renapur       | 11          | 9              | 2        | 1             |   |
| 70     |                  | Chakur        | 10          | 10             | 2        | 1             |   |

(continued)

**Table 3** (continued)

| S. No. | Name of district | Name of block  | Near normal | Moderately dry | Very dry | Extremely dry |
|--------|------------------|----------------|-------------|----------------|----------|---------------|
| 71     |                  | Udgir          | 10          | 9              | –        | –             |
| 72     |                  | Latur          | 7           | 6              | 1        | –             |
| 73     |                  | ShirurAnantpal | 11          | 12             | 2        | –             |
| 74     |                  | Deoni          | 12          | 12             | 2        | –             |
| 75     |                  | Ausa           | 9           | 8              | –        | –             |
| 76     |                  | Nilanga        | 9           | 9              | 1        | –             |

Priority should be given to above mention blocks while forming and executing a drought management plan because these are more vulnerable to drought events.

## 4 Conclusion

Meteorological drought characterization of blocks of the Marathwada region is used to assess the vulnerability of each block for a particular category of drought from 1980 till 2014. It is observed that a maximum number of near-normal conditions, i.e., 13 have occurred in Badnapur, Mukhed, Dharmabad. The maximum number of moderately dry conditions, i.e., 12 times has occurred in Khultabad, Lohara. A maximum number of very dry conditions, i.e., 4 times has occurred in Phulambri, Vaijapur, Ambejogai, Sengaon, Mahur, Lohara. Extremely dry conditions have occurred in Gangapur, Khultabad, Bhokardan, Jafrabad, Jalna, Mantha, Kandhar, Umerga, Pathari, Gangakhed, Ahmadpur, Renapur, Chakur. Drought characterization study shows how many times each category of drought occurs in a particular block. This study will help water resource planners and stakeholders to properly assess the level of risk and to manage it.

## References

1. Mishra, A.K., and Singh, V.P., 2010. A review of drought concepts. *Journal of hydrology*, 391(1–2), pp.202–216
2. WMO G (2016) Handbook of drought indicators and indices (M. Svoboda and BA Fuchs). Integrated Drought Management Programme (IDMP), Integrated Drought Management Tools and Guidelines Series, 2
3. Wilhite DA, Glantz MH (1985) Understanding: the drought phenomenon: the role of definitions. *Water Int* 10(3):111–120
4. World Meteorological Organization (2012) Standardized precipitation index user guide. World Meteorological Organization (1090)
5. Livada I, Assimakopoulos VD (2007) Spatial and temporal analysis of drought in Greece using the standardized precipitation index (SPI). *Theoret Appl Climatol* 89(3–4):143–153

6. Wang W, Zhu Y, Xu R, Liu J (2015) Drought severity change in China during 1961–2012 indicated by SPI and SPEI. *Nat Hazards* 75(3):2437–2451
7. Guhathakurta P, Menon P, Inkane PM, Krishnan U, Sable ST (2017) Trends and variability of meteorological drought over the districts of India using standardized precipitation index. *J Earth Syst Sci* 126(8):120
8. Gidey E, Dikinya O, Sebege R, Segosebe E, Zenebe A (2018) Modeling the spatio-temporal meteorological drought characteristics using the standardized precipitation index (SPI) in raya and its environs, northern Ethiopia. *Earth Syst Environ* 2(2):281–292
9. Das J, Gayen A, Saha P, Bhattacharya SK (2020) Meteorological drought analysis using standardized precipitation index over Luni river basin in Rajasthan, India. *SN Appl Sc* 2(9):1–17
10. McKee TB, Doesken NJ, Kleist J (1993) The relationship of drought frequency and duration to time scales. In: *Proceedings of the 8th conference on applied climatology*, vol 17, no 22, pp 179–183



# Analysis and Comparison of Fuzzy Logic and Neural Network Based Study for Rainfall Predictions and Hydrological Modelling: A Case Study of Ahmedabad



Utkarsh Nigam, Vinod Kumar M. Patel, and Sanjay Kumar M. Yadav

**Abstract** Rainfall based forecasting, analysis and hydrological modelling form an integral part of the study of hydrology. Now a day's many modern methods have been used for rainfall predictions. One of such tools which have been developed in recent times to promote the study of hydrological modelling and rainfall forecasting is by using fuzzy logic and ANN. The present study has been done out to analyze and compare the fuzzy logic and ANN based analysis for the rainfall predictions. Study also aims to demonstrate the use of hydrological modelling and the use of soft computing techniques for various hydrological purposes. Models developed using fuzzy logic and artificial neural network have been compared analysed and describes. Result shows that Artificial Neural Network gives suitable results over the Fuzzy Logic based model for the present study area and data taken. Analysis of the rainfall predictions and hydrological modelling for the study area has been done for fuzzy logic and the same study has been done through artificial neural network as well. The study shows that the use of Fuzzy and ANN is also suitable in Rainfall-Runoff Modelling as well. The efficiency of the model developed by Fuzzy Logic has been reflected up to 85 to 92% where is the efficiency of the model developed by artificial neural network has been reflected as 94 to 96%. Few models have been generated to compare and calibrate the analysis done on the study area.

**Keywords** Rainfall · Hydrological modelling · Fuzzy logic · ANN · Runoff · Modelling

---

U. Nigam (✉) · V. K. M. Patel  
L.D. College of Engineering, Ahmedabad, Gujarat, India

U. Nigam  
Gujarat Technical University, Ahmedabad, India

S. K. M. Yadav  
S.V. National Institute of Technology (SVNIT), Surat, India

## 1 Introduction

In this methodology, a work of dual-information-based water level prediction and results of two different data based rainfall forecasting approaches are produced: one is based on ANN framework and the second is on fuzzy logic framework. These methods are chosen since both are similar, i.e. two methods acquire qualities without depicting or justifying the conventional and theoretical reason of those works. They used to behave and initiate human perception of correlating links.

Several other researches have been done to analyze between black box models, usually emphasize simulation both in validation and calibration phase. In this paper, the work of the models are performed with great concern and precision, capacity to deal with various levels of information. Reliability and efficiency are considered since the larger amount of data of any physical constraint such as the mass conservation (typically data-driven model) can represent a potential risk of unexpected prediction, outside the calibration phase.

The capacity to work with different phases of information is considered since the fuzzy approach links and correlates inputs and outputs through a decomposition based on categories (low, high, very low, very high, etc.) while the neuron system approach links to input and output through a system of numerical weights. Mostly the two methods can work differently when executing an increasing amount of information and for this reason, two other input sets are considered in the numerical test: the Fuzzy is characterized by significant spatial and time aggregated rainfall information, while the ANN considers rainfall information more distributed in space and time.

## 2 Literature Reviews

Alvisi et al. [1] introduced three information driven degrees of water gauging models on the Reno River at Casalecchio di Reno (Bologna, Italy). One is the Neural Network approach, while the other two depend on the Mamdani and the Takagi–Sugeno fluffy rationale draws near. Alvisi reasoned that two models dependent on the fluffy rationale approach performed better when the physical wonders considered are combined by both a set number of factors and IF–THEN rationale proclamations, while the ANN approach builds its exhibition when more definite data is utilized. NFTOOL and NNTOOL. Backpropagation calculation takes 70% information for preparing, 15% for testing and 15% for approval. Ankita Sharma presumed that TRAINLM preparing capacity indicated best outcome in preparing, testing and approval of information. Additionally, LEARNNGDM is the best learning capacity with least MSE. El-Shafie et al. [2, 3] created two unique models to be specific ANN model and Multi-relapse model and executed in Alxendria, Egypt. A Feed Forward Neural Network with back engendering calculation was created to foresee precipitation on yearly and month to month premise. Measurable boundaries are

utilized to analyze both models. El-Shafie presumed that ANN model shows preferable execution over MLR model. Sharma et al. [4] anticipated precipitation in the area of Delhi (India) utilizing neural organization back spread calculation. Preparing of info information in the MATLAB is finished utilizing NFTOOL and NNTOOL. Backpropagation calculation takes 70% information for preparing, 15% for testing and 15% for approval. Ankita Sharma reasoned that TRAINLM preparing capacity demonstrated the best outcome in preparing, testing and approval of information. Additionally, LEARNGDM is the best learning capacity with least MSE. Agboola et al. [5] utilized the fluffy principles in reenacting precipitation in Nigeria. The creator made Fuzzy Logic model utilizing the following useful parts; the information base and the fluffy thinking. The essential advances associated with the model creation product fuzzification and defuzzification. To check the exactness of the model, it must be as per watched information. The mimicked information demonstrated a precision of 68%. From dissecting model yields, the creator reasoned that the model gives acceptable outcomes and a similar model can be applied to consolidate all the wrong and enormous measures of sources of info.

Srivastava et al. [6] considered the variety in soil as steady and the ecological boundaries carry on in fluffy nature. Rashi Srivastava proposed an expectation model which predicts the precipitation with boundaries as temperature and mugginess utilizing fluffy rationale. The model likewise anticipates the development of the horticulture creation dependent on fluffy rationale idea. The outcomes indicated that as temperature diminishes and stickiness expands the odds of downpour is high however as temperature increments and moistness diminishes the odds of downpour is low. Jimoh et al. [7] proposed that impact of catastrophic events, for example, flooding, dry season can be forestalled with compelling arranging. Jimoh applied fluffy rationale in the proposed model to anticipate precipitation utilizing the temperature and wind speed of the geological area. In the wake of contrasting the anticipated qualities and genuine qualities, Jimoh presumed that by knowing some climatic boundaries, one can utilize them as information factors in Fuzzy Logic show and can get precipitation as yield from the model. Jimoh suggested use of fluffy rationale as vital in other areas since two rationale levels can't take care of a large number of such issues. Kar et al. [8] recommended choice tree, bunching, K-mean and fluffy rationale as the different strategies for precipitation expectation. Different precipitation forecast strategies are looked at utilizing their points of interest, restrictions and time span. Kaveri Kar proposed that we can anticipate downpour later in the year by realizing atmosphere factors which is valuable for ranchers and farming. Just a portion of the atmosphere factors are considered yet different elements can likewise impact precipitation. Safar et al. [9] expressed that anticipating precipitation is a perplexing nature as it is particularly affected by atmosphere of Malaysia. Climate boundaries affecting precipitation and utilized in study were Atmospheric weight, temperature, mugginess, dew point and wind speed. In this investigation, the creator has attempted to discover precipitation utilizing climatic boundaries as a contribution to get precipitation as yield and inside the scope of determined yields. The model is found to have an exactness of 72%. Askilany et al. [10] utilized five climatic boundaries like relative moistness, absolute overcast spread, wind course, temperature and weight

as info factors for model. Each information variable was appointed three enrolment capacities. From all out of 243 prospects 118 fluffy IF–THEN principles are utilized. Somia A. Askliny likewise recommended that precision of the model is exceptionally reliant on the experience of the person who puts rules and the length of preparing informational collection. Mishra et al. has used the ANN in rainfall predictions [11] and Nayak et al. has also used artificial neural network in rainfall prediction [12].

### 3 Study Area and Data Collection Details

Ahmedabad in Gujarat, India, is the biggest city in the state. The Sabarmati River streams inside its middle. On the western side is the Gandhi Ashram at the waterway, which portrays the profound pioneer’s living quarters and ancient rarities. Inside the city and waterway, the Calico Museum of Textiles, when a material vendor’s chateau, has a superb assortment of collectable and present day textures. Territory: 464 km<sup>2</sup>, Elevation: 53 m, Weather: 34 °C, Wind SW at 5 km/h, 67% Humidity, Population: 55.7 lakhs (2011), Local time: Friday, 12:18 pm, Area code(s): 079, Average Rainfall: 765 mm. Normal precipitation days in May: 0.6 days, Average precipitation days in June: 3.9 days, Average precipitation days in July: 11.5 days, Average precipitation days in August: 10.7 days, Average precipitation days in September: 5 days, Average precipitation days in October: 0.8 days (Figs. 1 and 2).

To predict the rainfall and water level, data is collected from State Water Data Center (SWDC), Gandhinagar which was approached for the collection of climatic data. Following data for the 18 years have been collected: i.e. Precipitation data of 18 years for period of 1999–2017.

**Fig. 1** Study area  
Ahmedabad



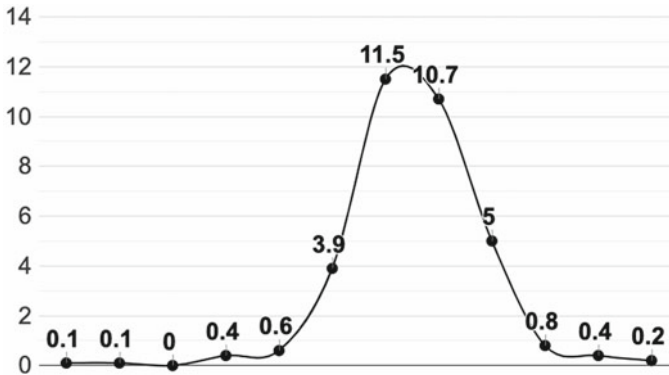


Fig. 2 Rainy days in Ahmedabad

### 4 Methodology Adopted

Precipitation gauges can be isolated into two classifications. One is by evaluating and dissecting the distinctive experimental and physical laws that oversee precipitation in a specific zone and relating stream that ascents the degree of water in the waterway. In spite of the fact that the strategy sounds reasonable enough, it has been seen that number of such boundaries that administers precipitation and water level are both spatial and worldly. In this way, the forecast utilizing the physical laws includes an excess of numerical counts and consequently, they are not computationally attainable. The subsequent strategy includes master frameworks to be fused and finding shrouded examples of how various highlights that influence precipitation and water level are really related to physical precipitation and spillover. The subsequent methodology additionally includes investigating the yields dependent on their degrees of truth utilizing fluffy rationale. It has been discovered that customary numerical models are fantastic in calculation however they are not proficient for expectation. Additionally, Empirical and numerical models can't adjust shifting examples of information and data which cannot be written in type of a capacity or equation. The advanced methodology has been discovered more reasonable. The cutting edge progressions in examination of Artificial Neural Network (ANN) and Fuzzy Logic have demonstrated that master frameworks dependent on neural organizations and fluffy rationale are precise and can be utilized in taking care of genuine issues (Figs. 3 and 4).

**ANN model:** Based on the above collected data, separate rainfall and water level prediction models are prepared using Neural Network Manager (NNTOOL) in MATLAB. 5.2.1 ANN Rainfall prediction model. The ANN Rainfall prediction model consists of input, output and in between hidden layers. The inputs used in the model are normalized data of previous 17 years of Rainfall, Temperature, Relative Humidity, Pan Evaporation and Wind speed ranging from 1999 to 2016. The number of layers is selected as 10.

Fig. 3 Flow chart ANN

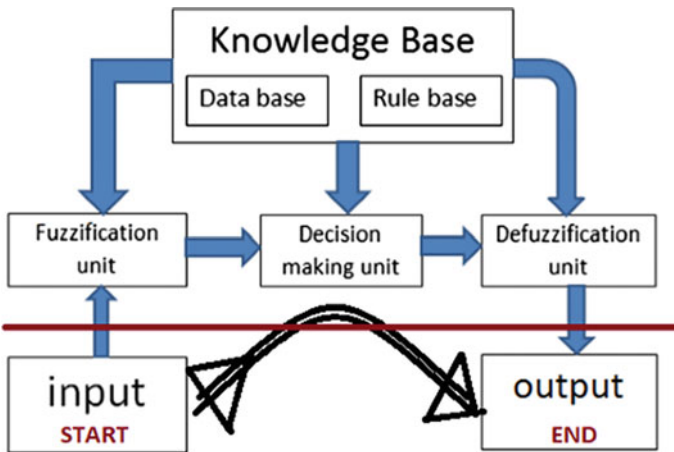
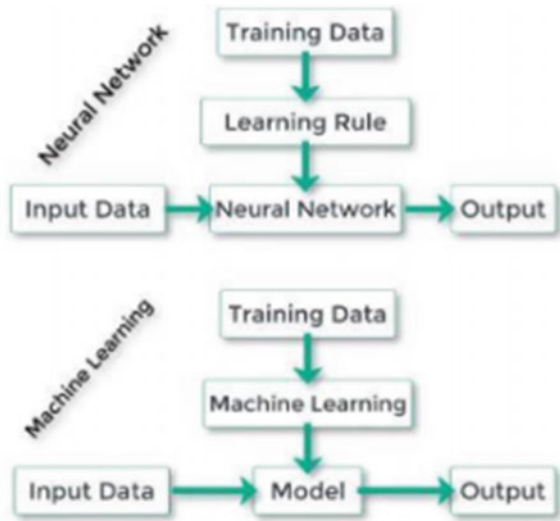


Fig. 4 Flow chart fuzzy logic

**Fuzzy Logic Model:** In Fuzzy Logic models, we use some of the climatic datasets as input and some as output. We convert crisp data into fuzzy data by fuzzification process. Then using IF-THEN rules, we find out the output. Then by using Defuzzification techniques, we convert fuzzy data into crisp data (Figs. 5 and 6).

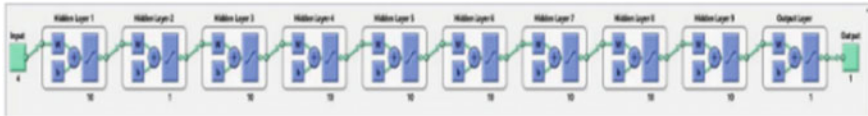


Fig. 5 Developed neural network

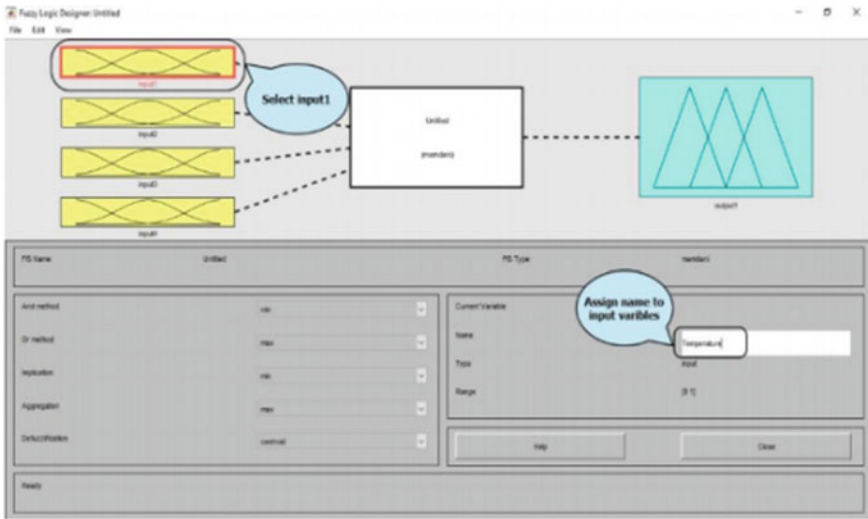


Fig. 6 Developed Fuzzy Logic Model

### 5 Comparison Analysis and Discussion of Models

Fuzzy Logic Approach: The model has been prepared using four input function and one output functions all the functions being triangular in nature. The membership gradeship of the inputs has been divided as low, medium, high and the gradeship of output function has been divided as Very Low, Low, Medium, High and Very high. The defuzzification has been done using Centroid method which is the most commonly used method and results have been obtained.

ANN Approach: The model has been used by selecting the ReLU Function as the activation function. The sigmoidal function is also used with Neuron variations as 10 to 50. The R Value for the prediction model is being obtained as more than 0.96 for all models as well. The inputs used was the climatic factors and the output obtained was the rainfall predictions.

Rainfall forecasting using artificial methods neural networks and fuzzy logic has been performed and explained in which models have been developed and analyzed. Methodology has been formulated for developing prediction based models for the rainfall predictions using ANN and Fuzzy Logic. Using ANN, 5 models have been developed for rainfall whereas 2 models of fuzzy logic have been developed and

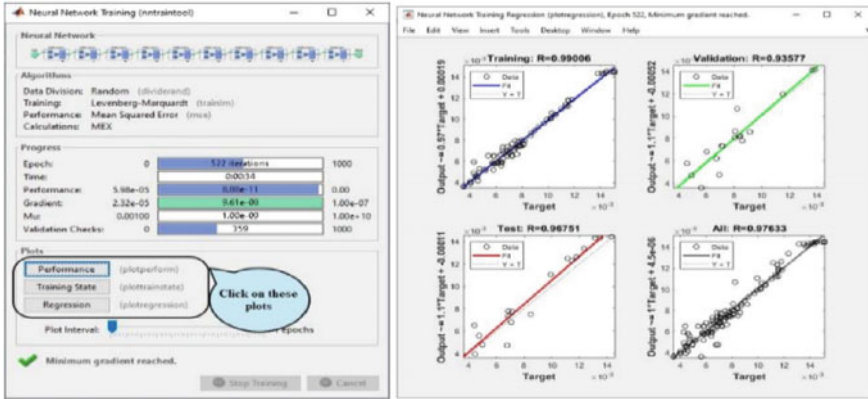


Fig. 7 Obtained results screenshot of ANN model

validated as well. Comparison of the model shows that the model formulation using the ANN or FL is a trial and error procedure which cannot avoid the epochs process. Comparison of process using both the methods shown that the model building and prediction results depend on the trial and error and epochs practices (Fig. 7).

All the models have been calibrated and validated in detail. From analysis of the results of the model, it can be predicted that accurate predictions can be done using soft computing techniques such as artificial neural networks and fuzzy logic which depends upon the weights and epochs. The results obtained using the models have been compared with actual data collected from State Water Data Center. The discrepancy ratio and errors have been rectified in the model validation and it gives betterment in results. Separate model run has been done for artificial neural networks and fuzzy logic and comparison has been done. Analysis, validation and results reflect that the models prepared using fuzzy logic is comparatively less precise than models building using artificial neural network. In ANN epochs and weight assignment plays an important role. In Fuzzy logic models, it was observed that as the number of input variables increases, accuracy of model increases (Fig. 8).

## 6 Conclusion

Rainfall forecasting Model development and building using both methods of artificial neural network and fuzzy logic has been performed and explained (Tables 1 and 2). Detailed methodology has been formulated for developing prediction based models for the rainfall predictions. Using ANN, 5 models have been prepared for rainfall whereas 2 models of fuzzy logic have been prepared and validated as well. All the models have been calibrated and validated in detail. From the analysis of results from the model, it can be said that accurate predictions can be done using modern approaches of soft computing techniques. The results obtained using the models



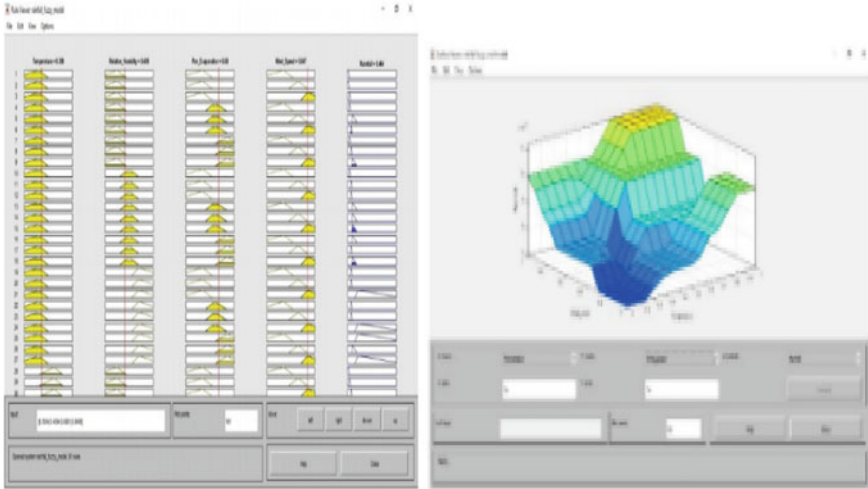


Fig. 8 Obtained result of Fuzzy logic

Table 1 Fuzzy logic model results analysis

| Model No | MSE         | RMSE        | D.R.       | % error    |
|----------|-------------|-------------|------------|------------|
| 1        | 2.44659E-05 | 0.0049463   | 1.45542714 | 0.65104749 |
| 2        | 3.03553E-05 | 0.005509568 | 1.32443664 | 0.60881328 |

Table 2 ANN model results

| Sr No. | No. of layers | No. of neurons | MSE         | RMSE        | D.R.        | % error     |
|--------|---------------|----------------|-------------|-------------|-------------|-------------|
| 1      | 10            | 2              | 0.001086229 | 0.002983876 | 1.130688299 | 32.5917798  |
| 2      | 10            | 3              | 1.27631E-06 | 0.000102282 | 1.00210639  | 0.791122567 |
| 3      | 10            | 4              | 7.13938E-07 | 7.6498E-05  | 1.000467487 | 0.598022545 |
| 4      | 10            | 5              | 0.008986904 | 0.008582724 | 1.000883258 | 0.730817447 |
| 5      | 10            | 6              | 2.40281E-06 | 0.00014034  | 1.005671819 | 1.320804897 |
| 6      | 10            | 7              | 6.21045E-07 | 7.1348E-05  | 1.003132928 | 0.59776875  |
| 7      | 10            | 8              | 3.87681E-06 | 0.000178261 | 1.005193771 | 1.664805199 |
| 8      | 10            | 9              | 2.09266E-06 | 0.000130969 | 1.003598664 | 1.08606477  |
| 9      | 10            | 10             | 5.28018E-07 | 6.57876E-05 | 0.999989028 | 0.434869612 |
| 10     | 10            | 11             | 6.35068E-07 | 7.2149E-05  | 1.001098829 | 0.54375029  |

have been compared with actual data collected from the authorized agency. The discrepancy ratio and errors have been rectified in the model validation and it gives good results. Separate model run has been done for artificial neural networks and fuzzy logic. Results reflect that the models prepared using fuzzy logic found to be less precise than models building using artificial neural network. In Fuzzy logic models, it was observed that as the number of input variables increases, accuracy of model increases.

## References

1. Alvisi S, Mascellani G et al (2006) Water level forecasting through fuzzy logic and artificial neural network approaches. *Hydrol Earth Syst Sci Discuss* 2(3):1107–1145
2. El-Shafie AH, El-Shafie A et al (2011) Artificial neural network technique for rainfall forecasting applied to Alexandria, Egypt. *Int J Phys Sci* 6(6):1306–1316
3. El-shafie A, Mukhlisin M et al (2011) Performance of artificial neural network and regression techniques for rainfall-runoff prediction. *Int J Phys Sci* 6(8):1997–2003
4. Sharma A, Nijhawan G (2015) Rainfall Prediction Using Neural Network. *Int J Comput Sci Trends Technol* 3(5) 2347-8578
5. Agboola AH et al (2013) Development of a fuzzy logic based rainfall prediction model. *Int J Eng Technol* 3(4):427–435
6. Srivastava R, Sharma P, Daniel AK (2018) Fuzzy logic based prediction model for rainfall over agriculture in northeast region. *Int J Adv Res Comput Sci* 9(Special Issue 2) 0976-5697
7. Jimoh RG et al (2013) Modeling rainfall prediction using fuzzy logic. *Int J Innov Res Comput Commun Eng* 1(4):929–936
8. Kar K, Thakur N, Sanghvi P (2019) Prediction of rainfall using fuzzy dataset. *Int J Comput Sci Mobile Comput* 8(4) 2320-088X
9. Safar NZM et al (2019) Rain prediction using fuzzy rule based system in North-West Malaysia. *Indonesian J Electr Eng Comput Sci* 14(3):1572–1581
10. Askilany SA et al (2011) Rainfall events prediction using rule-based fuzzy inference system. *Atmos Res* 101(1–2) 0169-8095
11. Mishra N, Soni HK et al (2018) Development and analysis of artificial neural network models for rainfall prediction by using time-series data. *Int J Intell Syst Appl* 10(1) 2074-9058
12. Nayak DR, Mahapatra A et al (2013) A survey on rainfall prediction using artificial neural network. *Int J Comput Appl* 72(16) 0975-8887

# A Synoptic-Scale Assessment of Flood Events and ENSO—Streamflow Variability in Sheonath River Basin, India



Mohammed Azharuddin, Shashikant Verma, Mani Kant Verma,  
and A. D. Prasad

**Abstract** The present study deals with the analysis of synoptic conditions that led to floods in the Sheonath river basin, which is the largest tributary of the Mahanadi river basin. To identify the flooding events a flood disaster database Dartmouth Flood Observatory is used and archives from this source were examined and flooding years were identified as 1994, 2005 and 2007. To verify the flood events derived from the database, data of streamflow is used, which is available at five locations in the river basin. The effect of flooding was observed in one of these five stations. The Synoptic conditions were constructed for the aforementioned flood events using geopotential height anomalies at 500 and 850 hPa pressure levels and Sea Level Pressure data. These conditions were studied three days before the flood event. It was observed that all the three flood events had a low-pressure system developing over the northwestern Bay of Bengal as the common feature. However, each synoptic system of each flood event has a different pathway of dissipation. After establishing the synoptic conditions that led to flooding, the ENSO (Sea Surface Temperature Anomalies-SSTA) and streamflow relationship are examined by the correlation approach. It was observed that the streamflow in this river basin is weakly correlated with SSTA. The Sheonath river basin doesn't experience frequent flooding, nevertheless, it is essential to study the meteorological aspects of flooding that involve the evolution of pressure patterns, change in atmospheric moisture and occurrence of precipitation that will provide a better understanding of the atmospheric drivers of floods.

---

M. Azharuddin (✉) · S. Verma · M. K. Verma · A. D. Prasad  
Department of Civil Engineering, National Institute of Technology Raipur, Raipur, Chhattisgarh  
492001, India

S. Verma  
e-mail: [sverma.phd2018.ce@nitrr.ac.in](mailto:sverma.phd2018.ce@nitrr.ac.in)

M. K. Verma  
e-mail: [manikverma.ce@nitrr.ac.in](mailto:manikverma.ce@nitrr.ac.in)

A. D. Prasad  
e-mail: [adprasad.ce@nitrr.ac.in](mailto:adprasad.ce@nitrr.ac.in)

**Keywords** Sheonath river basin · Flood · Synoptic condition · Low-pressure system · ENSO

## 1 Introduction

Floods are both a major financial and environmental hazard that affects the economy and population that gets exposed to it. Changing climate and human intervention may alter the hydro-meteorological scenario leading to increased frequency and magnitude of flooding. Examining a flood event requires addressing its meteorological, hydrological and hydraulic aspects. The meteorological aspects detail the atmospheric conditions prevalent before flooding, the hydrological aspect tells us about the amount of flow that was observed in the area of interest whereas hydraulic study details about flood characteristics such as flood extent, flow velocity and depth. Regarding meteorological conditions that cause flooding, rainfall is the most significant variable [1], a flood-like situation arises owing to the response of a catchment to extreme rainfall, unlike droughts which are the result of precipitation deficiency. These extreme rainfall events are a result of distinct synoptic-scale circulation patterns. Further, while examining floods in a river basin, it is necessary to document these circulation patterns, such that an understanding of flood producing atmospheric mechanisms can be accomplished.

El Nino Southern Oscillation (ENSO) is a large-scale coupled ocean-atmospheric phenomenon observed in the Pacific Ocean which can be associated with interannual variations in precipitation and streamflow [2]. Typically El Niño, the positive phase of ENSO, is responsible for deficit Indian Summer Monsoon (ISM) and the negative phase La Niña causes excess rainfall. As ENSO and Indian summer monsoons are strongly linked [3] it becomes essential to explore what probable effects it will have on the streamflows of Indian river basins. Moreover, there are a plethora of studies that linked ENSO to streamflow variability in a river basin using correlation-based approaches. The study conducted by Jian et al. [4] on Ganges and Brahmaputra river basin found that higher monthly discharges in the Ganges are associated with La Niña and weaker discharge with El Niño whereas for Brahmaputra river no strong relationship was observed between ENSO and monthly discharges. A study concerning the Mahanadi river basin found a significant positive correlation [5] between 5-year moving averages of ENSO index—NINO 3.4 and 5-year moving averages of streamflow at different time scales ranging from a month to season. They attributed the presence of these strong positive correlations as the key for rainfall and streamflow variability in the Mahanadi basin. Given the influence of ENSO on streamflows in the river basin, the following objectives are framed for this study: (1) To identify flood events in the Sheonath river basin using disaster database(s), (2) To understand the synoptic conditions that lead to flooding Sheonath river basin and (3) To study the relationship between ENSO and annual discharge in the river basin.

Section 2 describes the study area and Sect. 3 discusses the synoptic conditions leading to flooding followed by methodology used in examining the ENSO-discharge relationship. Section 4 concludes this study.

## 2 Study Area and Data Used

Sheonath river basin, the largest sub-basin of the Mahanadi river basin has an area of 30,761 km<sup>2</sup> which is 21.72% of the area of the Mahanadi river basin [6]. The village of Panbaras in the Rajnandgaon district is the region where the Sheonath river originates, traversing a length of 383 km from its origin [7]. The location map of the Sheonath river basin is shown in Fig. 1. To perform a synoptic-scale assessment of flood events firstly we have to identify flood events, to this end, we used a disaster database Dartmouth Flood Observatory (DFO) (described in Sect. 3.1) and peak flows during floods were identified using data on streamflow provided by Central Water Commission (CWC). APHRODITE precipitation data [8] is used in understanding the spread of rainfall over the Sheonath river basin during the period of flooding. NCEP/NCAR reanalysis-1 data [9] is used in studying the synoptic features/circulation patterns before flooding. Geopotential heights at 500 and 850 hPa and Sea level pressure (SLP) data are used here. Niño 3.4 anomalies are used to quantify ENSO.

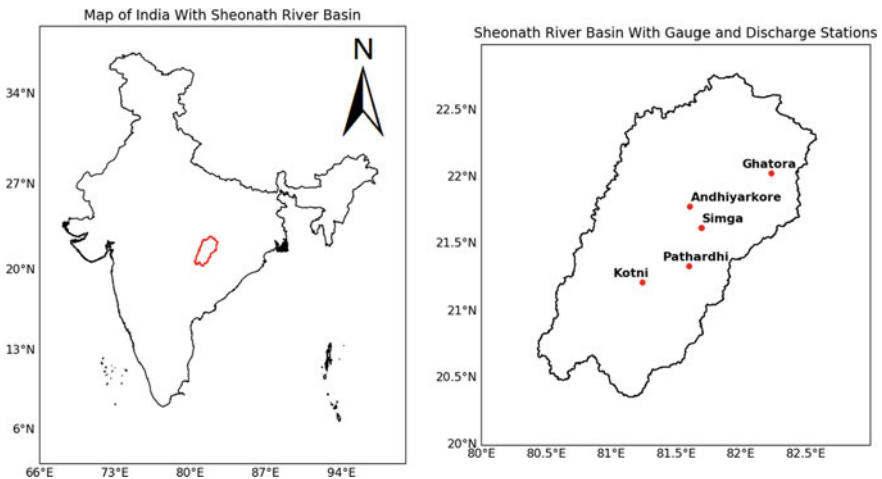


**Fig. 1** Location map of Sheonath river basin

**Table 1** Peak flows ( $\text{m}^3/\text{s}$ ) in the Sheonath river basin during flood years

| Date of peak flow (Y-m-d) | Andhiyarkore | Ghatora | Kotni   | Pathardhi | Simga      |
|---------------------------|--------------|---------|---------|-----------|------------|
| 1994-07-12                | 220.513      | 370.4   | 5269    | 1695      | 10,250     |
| 1994-07-13                | 159.829      | 290     | 4500    | 1086      | 10,821     |
| 2005-09-16                | 335          | –       | 2286    | –         | 11,000     |
| 2005-09-17                | 150          | –       | 795.98  | –         | 10,728.686 |
| 2007-07-01                | 3            | –       | 3950    | –         | 11,000     |
| 2007-07-02                | 0.99         | –       | 2550.75 | –         | 11,331     |

### 3 Methodology and Results

#### 3.1 Flood Event Identification

To identify flood events in the Sheonath river basin we used a global flood disaster database known as Dartmouth Flood Observatory (DFO) which is an active archive of flood events [10]. DFO is termed as an active archive of floods since the current flood events are added to it and this database is developed by employing news, governmental, instrumental and remote sensing sources. After going through the DFO archives beginning from 1985, we identified flood events in the years 1994, 2005 and 2007. After identifying the flood years, we looked into the discharge data for peak flows during the flood events. It was observed that of the five gauge and discharge stations in the river basin, Simga station had a profound signature of flooding and Kotni station to an extent. From Table 1 it is seen that Simga station recorded the highest peak flows during flooding. For the years of 1994, 2005 and 2007, peak flows of 10,821, 11,000 and 11,331  $\text{m}^3/\text{s}$  respectively were observed for Simga station. Figure 2 depicts the streamflow hydrograph of Simga station during the flooding period. The period of flooding is chosen as shown in Fig. 2 such that there is a rising limb, peak flow zone and falling limb which led to having 8 days as flooding duration and peak flows observed in two of these 8 days.

Given that rainfall is the chief source of flooding we looked at accumulated precipitation over the Sheonath basin during the 8 days as shown in Fig. 3 using APHRODITE precipitation data. From Fig. 3a, b and c we observe that the southern part/lower Sheonath basin received higher rainfall compared to the upper Sheonath basin.

#### 3.2 Significant Synoptic Features

To study the synoptic conditions that led to flooding, large-scale climatic variables of geopotential height at 500 and 850 hPa and sea level pressures (SLP) are used. A catchment's response (i.e. runoff) to rainfall is usually a delayed one, owing to this

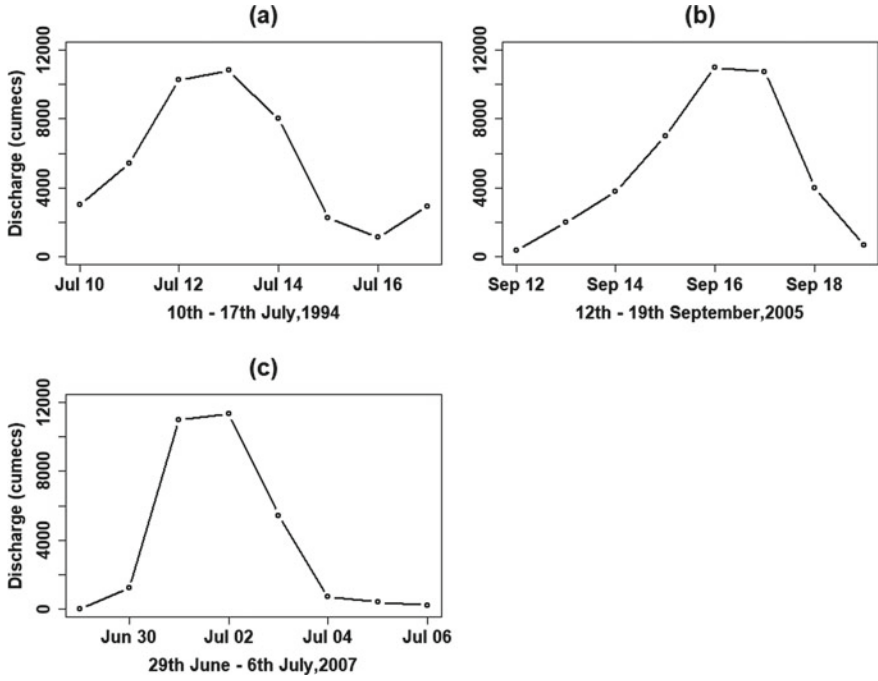


**Fig. 2** Streamflow's recorded at Simga station during flooding (**a** for the year of 1994 10–17th July 1994, **b** 12–19th September 2005 and **c** 29th June to 6th July 2007)

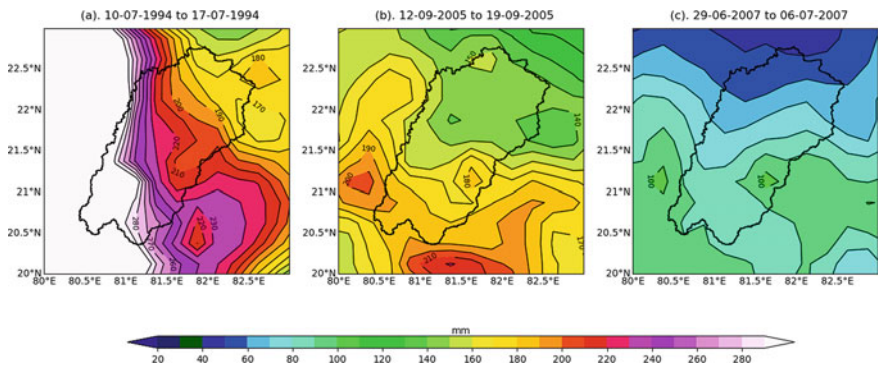


**Fig. 3** Accumulated rainfall over Sheonath basin during flood events (**a** for the year of 1994 10–17th July 1994, **b** 12–19th September 2005 and **c** 29th June to 6th July 2007)



feature one should study synoptic conditions a few days before a flooding event. For studying the synoptic conditions of summer flooding events in the Polish Sudeten Mountains [11] maps of precipitable water and mean SLP anomalies were generated 7 days before the flood event to identify the formation of negative (or) low-pressure regions. The potential atmospheric precursors of flooding are the weather mechanisms such as low-pressure regions, depressions and cyclones, etc., which brings good rainfall amounts, they form days before producing rainfall on the land surface thereby leading to flooding. Studying the formation of these weather mechanisms, along with their movement from ocean to land, helps us in characterizing the synoptic condition of a flooding event. Given the importance of these mechanisms, we studied synoptic conditions 3 days before the flooding event (i.e. 3 days before peak flows at Simga station) through geopotential height anomalies and SLP.

### 3.2.1 Flood of 1994

The flood of 1994 happened between 10 and 17th July wherein peak flows were observed during 12th and 13th July at Simga. Geopotential height anomalies were plotted for the dates of 9th, 10th and 11th July with baseline climatology of 1950 to 1990 at both 500 and 850 hPa levels. In Fig. 4a and 4d, i.e. on 09-07-1994 we see that a trough is formed over the Northwestern region in the Bay of Bengal and near the coast of Orissa. This system intensified on 10-07-1994 with its spread over Northern Orissa and Gangetic West Bengal as seen in Fig. 4b and 4e. By 11-07-1994, this system further intensified as seen in Fig. 4c and 4f. Referring to the monsoon report of 1994 [12], it is mentioned that a well-marked low-pressure region was observed between 8th and 15th July that developed over Northwest Bay and during its dissipation, it merged with monsoon trough over North Orissa and West Bengal. This Monsoon trough can be seen in Fig. 8a to 8c where a low-pressure region is

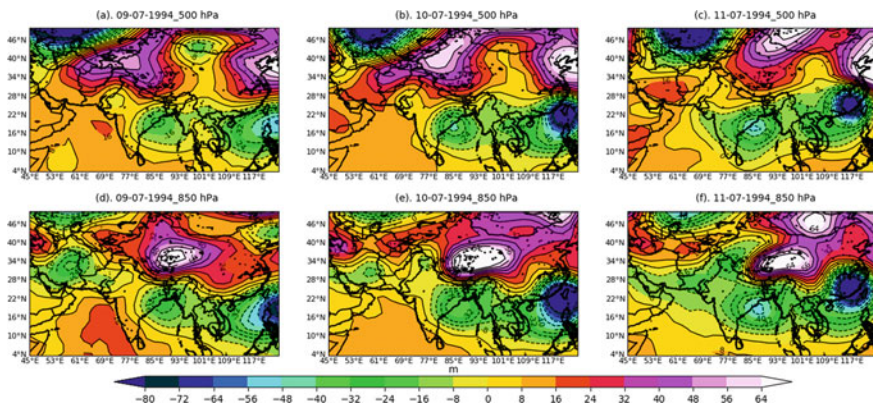


**Fig. 4** a–c Geopotential height anomalies at 500 hPa pressure level from 09 to 11th July 1994; d–f Same as a–c for 850 hPa pressure level



observed from northwestern Rajasthan towards West Bengal progressing into the Bay of Bengal.

### 3.2.2 Flood of 2005

The Sheonath river basin witnessed flooding between 12 and 19th September 2005 and peak flows were observed on 16th and 17th September. Geopotential height anomalies are plotted for 13th, 14th and 15th September with baseline climatology of 1950 to 2000 at both 500 and 850 hPa levels. As said earlier synoptic conditions were to be plotted for 3 days before peak flows, however in this case we saw that the circulation patterns in Fig. 5a to 5f are not responsible for flooding in the river basin. A low-pressure system was observed over the Arabian Sea in Fig. 5a and 5d. This system intensified into a depression on 14th [13] and by the 17th this system weakened. As the previous system was not the flood causing mechanism, we considered 3 more days before 13th September 2005 and plotted geopotential height anomalies from 10 to 12th September 2005, seen in Fig. 6a to f. In the Fig. 6a, b, d and e, i.e. on 10th and 11th September 2005, we observe the formation of a low-pressure system over the Andhra-Orissa coast which intensified into a depression by 12th which is evident from Fig. 6e and 6f. As seen from Fig. 5a to 5f this system moved in a northwest direction where it subsequently weakening after the 15th. What we did observe is that during the period between 10th and 15th September 2005, two weather systems originated, one from the Arabian Sea and the other from the Bay of Bengal and the latter system being responsible for flooding in the Sheonath river basin. SLP plots from Fig. 8d to 8f from 13 to 15th September 2005 reflect the same system as seen in Fig. 5a to 5f, however, SLP from 10 to 12th September is not shown here.

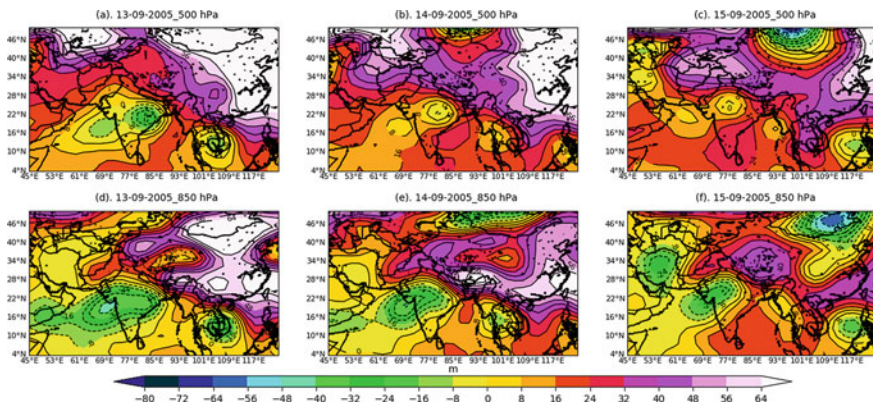


**Fig. 5** a–c Geopotential height anomalies at 500 hPa pressure level from 13 to 15th Sep 2005; d–f same as a–c for 850 hPa pressure level

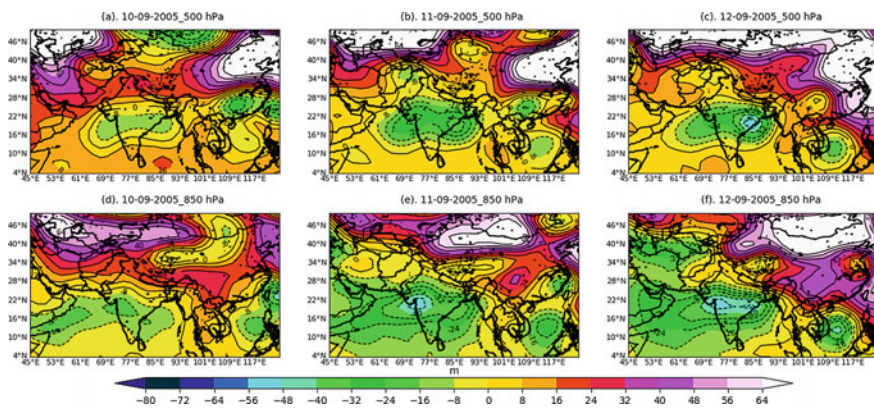


**Fig. 6** a–c Geopotential height anomalies at 500 hPa pressure level from 13 to 15th Sep 2005; d–f same as a–c for 850 hPa pressure level

### 3.2.3 Flood of 2007

In the period between 29th June and 6th July 2007, the Sheonath river basin saw another flooding event and peak flows were observed at Simga station on 1st and 2nd July. Geopotential height anomalies are plotted for 28th, 29th and 30th June with baseline climatology of 1950 to 2000 at both 500 and 850 hPa levels. Referring to the IMD report of Cyclones and Depressions [14] a deep depression was observed during the period of 28th to 30th June 2007. In Fig. 7a and 7d on 28-06-2007, we see a low-pressure system over the northwest Bay of Bengal, close to the coast of Orissa. This system progressed in the northwestern direction towards the land surface on 29-06-2007, evident from Fig. 7b and 7e. Further movement of this system into land saw

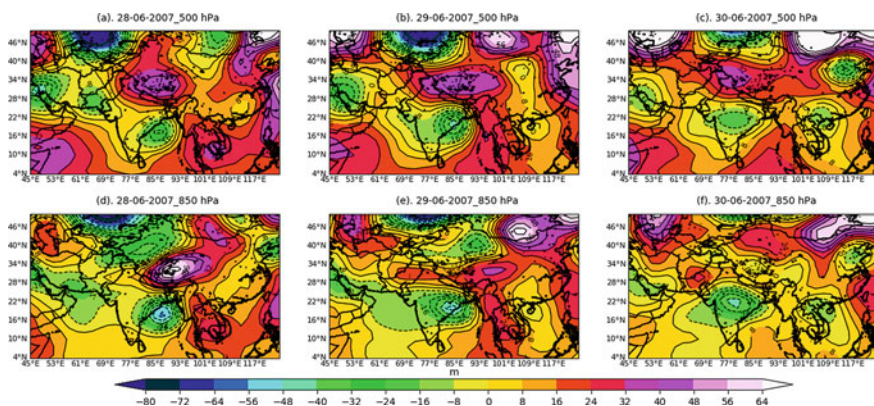


**Fig. 7** a–c Geopotential height anomalies at 500 hPa pressure level from 28 to 30th June 2007; d–f same as a–c for 850 hPa pressure level

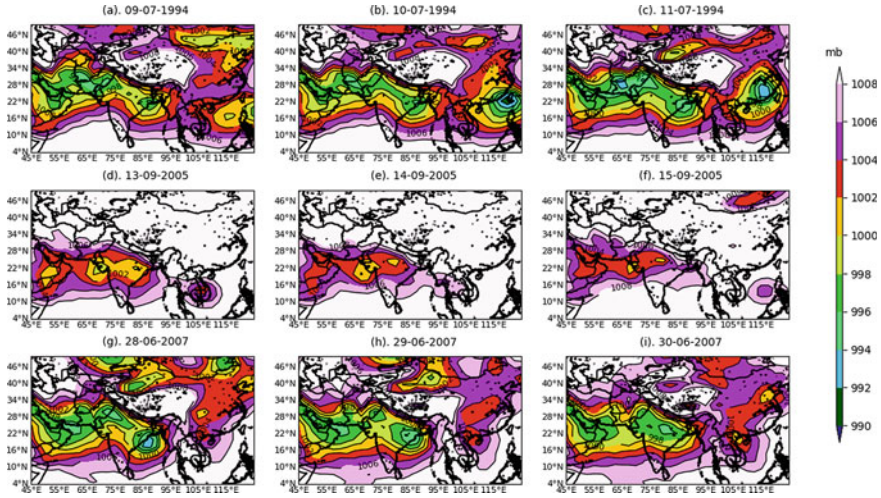


**Fig. 8** a–i Sea level pressure on given dates

it getting weakened by 30-06-2007 as seen in Fig. 7c and 7f. This aforementioned system is the causal factor for the 2007 flood in the Sheonath river basin. It is also important to note that monsoon trough is also seen during this period (Fig. 8g to 8i).

In the three flood events, one of the common features is that low-pressure systems developed over the northwestern Bay of Bengal. Further, the system of monsoon trough is also observed during the flooding years of 1994 and 2007. These low-pressure systems as said earlier are important rain producing mechanisms that form mostly during monsoon seasons (June through September) over the warm waters of Bay of Bengal. These systems brought a good amount of rain over Sheonath river basin as seen in Fig. 3, thereby leading to flooding.

### 3.3 ENSO—Streamflow Variability

The third objective of this study is to understand the relationship between annual streamflow and ENSO. This is done by examining the correlation between ENSO index and streamflow. The sea surface temperature anomaly (SSTA) from the Niño 3.4 region (120W–170W, 5S–5N) is used to quantify ENSO. The methodology developed by [2] is used to study the ENSO—discharge relationship. We choose Simga station streamflow’s to be correlated with ENSO as Simga was the only station where the effect of flooding was seen. Firstly, the annual average streamflow is determined for Simga station which spans from 1972 to 2009. The next eight quarterly averages of SSTA are calculated. These quarters include months from the previous year, coincident year and succeeding years correlated with the year of interest. The quarters considered and the correlation coefficients obtained are shown in Table 2.

**Table 2** Correlation coefficients between annual average streamflow of Simga station and mean Niño 3.4 SSTA for eight quarters (months without subscript indicate coincident years and months with the minus (plus) sign are those from the year preceding (succeeding) the coincident year or year of interest)

| Quarter   | Pearson correlation coefficient |
|---|---------------------------------|
| June <sup>-</sup> , July <sup>-</sup> , August <sup>-</sup>           | 0.223                           |
| September <sup>-</sup> , October <sup>-</sup> , November <sup>-</sup> | 0.293                           |
| December <sup>-</sup> , January, February                             | 0.273                           |
| March, April, May   | 0.077                           |
| June, July, August  | -0.1                            |
| September, October, November  | -0.1                            |
| December, January <sup>+</sup> , February <sup>+</sup>                | -0.078                          |
| March <sup>+</sup> , April <sup>+</sup> , May <sup>+</sup>            | -0.027                          |

From Table 2 we observe that the annual average streamflow of Simga is weakly correlated with 8 quarters of the ENSO index. The quarter of September<sup>-</sup>, October<sup>-</sup>, November<sup>-</sup> depicts maximum correlation which is 0.293. This indicates that nearly 8.6% of the variance in the annual flow of the Sheonath river observed at Simga station can be explained by the ENSO index for the September<sup>-</sup>, October<sup>-</sup>, November<sup>-</sup> quarter. Scatter plot in Fig. 9 depicts the relation between the annual discharge of the Sheonath river basin at Simga station and the SST index of ENSO for the quarter of September<sup>-</sup>, October<sup>-</sup>, November<sup>-</sup>.

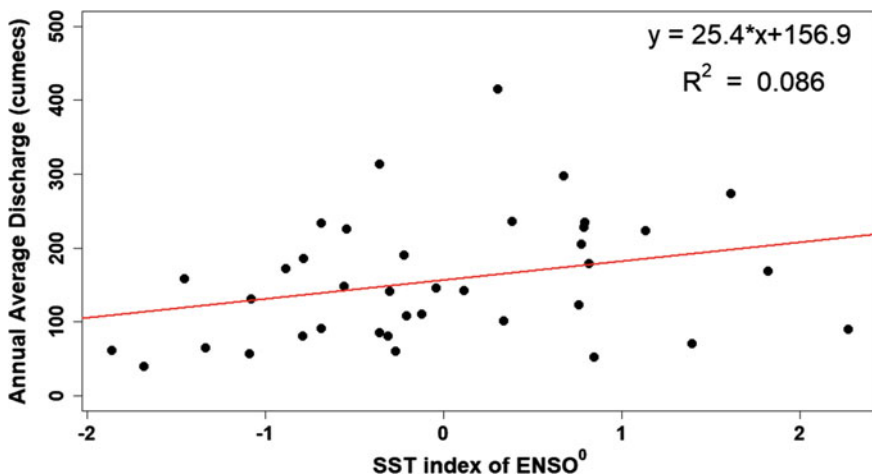


**Fig. 9** Scatter plot between annual average streamflow at Simga station and SST index Niño 3.4 for the September<sup>-</sup>, October<sup>-</sup>, November<sup>-</sup> quarter

## 4 Conclusions

This study focussed on identifying flood events and understanding the synoptic features that caused flooding in the Sheonath river basin. Flood events are identified using an active archive of global floods, i.e. DFO. Flood years identified were 1994, 2005 and 2007, these were verified with observed streamflow data of five gauging stations of the river basin. Of the five stations, only Simga station had a significant signature of flooding. Following this synoptic conditions that were responsible for flooding were studied using reanalysis data. Geopotential height anomalies at 500 and 850 hPa pressure levels and sea level pressure are considered.

The synoptic features were studied three days before the peak flows recorded at Simga station. For the three flooding events what stood as a common synoptic feature is the development of low-pressure systems over the northwestern Bay of Bengal. The final part of this study was to explore the relationship between the annual average streamflow of the river basin and ENSO. The annual average streamflow of Simga station is used as a representative of the river basin and Niño 3.4 SSTA is used to represent the ENSO phenomenon. Correlation between eight quarters of averaged SSTA and annual average streamflow are calculated and it was observed that 8.6% of the variance in the annual average streamflow can be explained by September<sup>-</sup>, October<sup>-</sup>, November<sup>-</sup> quarter. Given that the Sheonath river basin is a sub-basin of the Mahanadi river basin it will be interesting to identify flooding events over this basin to see what synoptic features exist as we will have a higher number of flood events to study.

## References

1. Doswell CA, Brooks HE, Maddox RA (1996) Flash flood forecasting: an ingredients-based methodology. *Weather Forecast* 11:560–581
2. Amarasekera KN, Lee RF, Williams ER, Eltahir EA (1997) ENSO and the natural variability in the flow of tropical rivers. *J Hydrol* 200(1–4):24–39
3. Roy I, Tedeschi RG, Collins M (2019) ENSO teleconnections to the Indian summer monsoon under changing climate. *Int J Climatol* 39(6):3031–3042
4. Jian J, Webster PJ, Hoyos CD (2009) Large-scale controls on Ganges and Brahmaputra river discharge on intraseasonal and seasonal time-scales. *Q J Royal Meteor Soc, J Atmos Sci Appl Meteor Phys Oceanogr* 135(639):353–370
5. Panda DK, Kumar A, Ghosh S, Mohanty RK (2013) Streamflow trends in the Mahanadi river basin (India): linkages to tropical climate variability. *J Hydrol* 495:135–149
6. Jain SK, Agarwal PK, Singh VP (2007) *Hydrology and water resources of India*, vol. 57. Springer Science & Business Media
7. Verma MK, Verma MK, Yadu LK, Murmu M (2017) A study of climate change impact on precipitation of Sheonath River Basin. *Indian J Sci Technol* 10:11
8. Yasutomi N, Hamada A, Yatagai A (2011) Development of a long-term daily gridded temperature dataset and its application to rain/snow discrimination of daily precipitation. *Glob Environ Res* 15(2):165–172
9. Kalnay et al (1996) The NCEP/NCAR 40-year reanalysis project. *Bull Am Meteor Soc* 77:437–470



10. Brakenridge GR Global active archive of large flood events. Dartmouth Flood Observatory, University of Colorado, <http://floodobservatory.colorado.edu/Archives/index.html>
11. Bednorz E, Wrzeński D, Tomczyk AM, Jasik D (2019) Classification of synoptic conditions of summer floods in polish Sudeten Mountains. *Water* 11(7):1450
12. De US, Desai DS, Bhandari SG (1995) Weather in India monsoon season (June to September 1994). *Mausam* 46(3):227–234
13. Jayanthi N, Lele RR, Sunitha Devi S (2006) Cyclonic storms and depressions over the North Indian Ocean during 2005. *Mausam* 57(3):379–394
14. Mazumdar AB, Khole M, Sunitha Devi S (2008) Cyclonic storms and depressions over the North Indian Ocean during 2007. *Mausam* 59(3):273–290

# Effect of Climate Change on Spring Discharge Management System of the Himalayan Region in India



Kunal Sharma and Nirban Laskar

**Abstract** Water is the world's most precious element and spring water is a strong source. The demand for clean spring water is growing because of the increased practical application of water in domestic, industrial, and irrigation applications, especially in the hilly Himalayan region of India. Lightly substantial declines in the spring flows from any source can affect the flow activity of rivers in the Himalayan regions. In the Himachal Pradesh and Ladakh area, the spring of the geothermal fields is highly common. There is definite evidence of a mixture of subsurface water with thermal water which was once present in some geothermal springs on the surface. In certain regions of Himachal Pradesh, India there is a greater water rock interface with the effect of carbonate weathering. The hallow areas of transition/fracturing also serve as a thermal spring pipeline. In the pre-and post-monsoon seasons, spring water management system release, along with hydrogeochemical, rainwater accumulation, and isotopical studies can be considered. The main challenge in India's Himalayan region is to safeguard water access, particularly in lean time. High runoff occurs during rainy seasons, and the problem is compound with urbanization, such as deforestation, the pavement of their homestay area, Mining, etc. mostly in Meghalaya, India. The restricted infiltration in the soil influences the spring's discharge. In addition, the rising temperature and precipitation variations as a result of climate change have exacerbated the mountain spring water catchment areas. A complete hydrogeological mapping of the spring shed initiative is intended to lead to a recognition of special recharging regions and interferences in the aquifer.

**Keywords** Catchment zones · Climate change · Geothermal spring · Spring recharge

---

K. Sharma  
Civil NABCONS, Guwahati, India

N. Laskar (✉)  
Department of Civil Engineering, Mizoram University, Aizawl, India

## 1 Introduction

For people living in hilly areas such as the Himalayan, the natural spring waters have an important water necessity. These supplies of water are cost-efficient, almost pollutant-free, typically directly used for consumption and for agriculture and irrigation [1]. Observation of spring discharge, which varies over time, is one of the essential variabilities of water resource management. The variabilities are directly related to change in recharge aquifer structure, and it isn't easy to observe or monitor it now [2–4]. Springs are the life rescues of people living in the Himalayas region. But massive urban expansion has led to the drying up of several springs and the lack of water. The people of the Himalayan region have relied largely on sources and small mountain rivers for their water needs, as mountain inhabitants have no need for large rivers flowing far down their routes. In the past few years, while many have already suffered deterioration, most of these springs are increasingly dry.

The hot springs' temperature varies from ambient to boiling point temperature, which depends on parameters like conductive and convective freezing, geothermal liquid, and mixing with groundwater [5]. Geothermal spring is very eco-friendly and has zero fuel consumption, and can provide power supply for heating, bathing, fish farming, etc. [6].

Springs are the primary and only source of water in the Himalayan region for rural habitats. In some areas, urban water demands were fulfilled for drinking water supply, agricultural and domestic uses [7]. The majority of spring water used in Uttarakhand, India, was found to be only for drinking purposes, though spring water used by Meghalaya was also used for both drinking and irrigation purposes. The entire Himalayan geodiversity and eco-diversity are fragile and vulnerable to natural and anthropogenic changes. Unpredictable runoff, a collision of plate tectonics activities, and environmental destruction threaten the mountainous aquifers [8]. The geological assessment of the heat cause, reservoir, and sealing rocks are the main fundamentals in the valuation of hot-rock geothermal systems [9].

## 2 Overview on Himalayan Region and Its Springs Resource

### 2.1 *Classification of Springs*

The classification of springs is generally based upon the rate of flow, seasonality of flow, temperature, water quality, and occurrence of dissolved gases. Based upon Geology features, springs may be categorized into six types: [10–12].

- **Depression springs:** Depression springs are created in unconfined aquifers where the geography overlaps the level of water, typically due to the incision of the surface stream. Because of the earth's gravitational force, these springs are created.



They are called depression or gravity springs. These are commonly located along-side cliffs and hillsides. An example is Dangala spring in Tehri of Uttarakhand and Malagiri Dhara in South Sikkim.

- **Contact springs:** The contact plane between a permeable and impermeable rock inflates water flow laterally because of high hydraulic conductivity, and the groundwater is redirected to the surface, making it a contact spring. An example is the spring flow of Umbari village Satara, Maharashtra, and Myota of Nainital, Uttarakhand.
- **Fault springs:** Fault springs are created as water flows over fault lines and discharges at the surface. Due to more significant hydraulic conductivity, faults may serve as a geographic boundary for groundwater movement and provide a preferred flow route for water due to pressure, displacement or weathering. An example is a spring at Panamik, near Siachen Glacier, Leh.
- **Sinkhole or karst springs:** The Karst spring provides a natural escape to the surface for groundwater through the hydrologically active karst mass fissures. In karst environment, the spring occurs more often in the touch areas between the carbonate masses and the impermeable rocks. Examples are Achabalnag, Andernag, and Martandnag of Anantnag, South Kashmir.
- **Joint/Fracture springs:** There may be several joints with high hydraulic conductivity in the low rock permeability. Joint springs are created as water flows through such joints. It happens because of the presence of joined or permeable rock layers in rocks of low permeability. Groundwater flow is mostly through fractures that may reach both deep and shallow aquifers. Springs are created when the earth's surface intersects with these fractures. An example is the spring of Mundani, Uttarakhand.
- **Igneous spring:** Igneous spring, also termed hot or geothermal spring, is a natural spring containing water at a temperature well above the surrounding region's air temperature. Many igneous springs discharge groundwater, which is fed by thin magma intrusions. But specific igneous springs are not synonymous with volcanic activities also. Examples are Kheerganga in Kullu, Himachal Pradesh.

## 2.2 Characteristics of Springs Are [10]

Mountain springs are the primary source of water for rural households in the Himalayan region. The essential topics related to enhancing water protection in mountain towns and cities besides reviving springs are developing accountable mountain tourist destinations, boosting trained workforce, reshaping shifting cultivation in the north-eastern hill region to ensure ecological, food, and nutritional stability, and providing the required dataset and documentation. Table 1 shows the dependency of the states of India towards spring water.

The characteristic of springs are as follows:

- (a) The discharge rate of the spring may be constant or vary.
- (b) Springs might be perennial or seasonal.

**Table 1** State depending on spring water

| Sl. No. | State                    | Approx. % of villages directly depends on Springwater |
|---------|--------------------------|---|
| 1       | Arunachal Pradesh        | 37.3  |
| 2       | Assam                    | 11.4  |
| 3       | Mizoram                  | 54.6  |
| 4       | Nagaland                 | 44.7  |
| 5       | Tripura                  | 16.1  |
| 6       | Manipur                  | 54.4  |
| 7       | Meghalaya                | 55.7  |
| 8       | Sikkim                   | 94.2  |
| 9       | West Bengal              | 32.1 (only Darjeeling)                                |
| 10      | Himachal Pradesh         | 12.6  |
| 11      | Jammu & Kashmir          | 50.6  |
| 12      | Uttarakhand              | 3.5   |
| 13      | Eastern Himalayan States | 26.7  |
| 14      | Western Himalayan States | 14.8  |
| 15      | All Himalayan States     | 20.8  |

- (c) The temperature of the spring may vary.
- (d) Seasonal variation in discharge.
- (e) Difficulty in the assessment.

### 3 Case Study on the Spring Discharge Management System

Meghalaya: Meghalaya is highly dependent on springs and groundwater with almost all villages receiving household spring water and using irrigation either completely from a spring or partially by spring or groundwater feeding streams. Through heavy rainfall, most regions in the State experience a water scarcity crisis. Water demand is increasing, and supplies may decline as a consequence of climate change, changes in land use including increased drainage, irrigation, and groundwater use, contamination of surface and groundwater, and depletion of natural recharge areas—mostly correlated with deforestation, Mining of quarry rock, gravel, coal and river sand, and tree cutting destruction of forest cover, fuelwood production, anthropogenic burning, and rotational farming. The spring shed mapping exercise yields some 2000–4000 spring data points, which helps Meghalaya plan spring shed protection actions and will establish a scaled-baseline for the program. The plan includes a comprehensive plan for water and livelihood along with Integrated Basin Development Livelihood Program; the program focuses on the study of water, type of rocks, hydrogeology features of the springs [10, <https://india.mongabay.com/2019>; <https://inrmshillong.org/publication>]. Table 2 offers data on the rainfall for Meghalaya districts for four

**Table 2** Mean and coefficient of variation rainfall statistics (2020) for the districts of Meghalaya

| District         | June   |      | July   |      | August |      | September |      | Monsoon |      | Annual |      |
|------------------|--------|------|--------|------|--------|------|-----------|------|---------|------|--------|------|
|                  | Mean   | CV   | Mean   | CV   | Mean   | CV   | Mean      | CV   | Mean    | CV   | Mean   | CV   |
| East Garo Hills  | 638.7  | 40.4 | 689.9  | 53.5 | 599.6  | 70.5 | 405.2     | 73.4 | 2343.4  | 51.8 | 3385.9 | 54.9 |
| West Garo Hills  | 796.0  | 65.0 | 729.1  | 62.6 | 556.0  | 58.9 | 472.0     | 63.2 | 2567.5  | 51.9 | 3713.7 | 48.3 |
| East Khasi Hills | 1366.5 | 39.9 | 1430.7 | 47.3 | 948.8  | 53.2 | 629.9     | 51.6 | 4375.9  | 30.2 | 6018.9 | 27.1 |
| West Khasi Hills | 617.4  | 42.8 | 775.1  | 48.9 | 536.0  | 55.4 | 387.0     | 59.2 | 2345.4  | 38.7 | 3253.7 | 42.1 |
| Jaintia Hills    | 1051.6 | 56.5 | 972.4  | 58.1 | 753.5  | 68.2 | 545.7     | 73.0 | 3307.0  | 51.9 | 4830.7 | 50.1 |
| RI-BHOI          | 347.4  | 40.9 | 390.7  | 48.0 | 366.7  | 37.0 | 324.3     | 72.6 | 1424.1  | 45.5 | 2119.3 | 50.7 |
| South Garo Hills | 437.5  | 48.0 | 446.4  | 54.1 | 355.9  | 48.8 | 302.7     | 65.2 | 1504.2  | 50.9 | 2024.1 | 46.7 |

Source Met Monograph No.: ESSO/IMD/HS/Rainfall Variability/17(2020)/41; Observed Rainfall Variability and Changes Over Meghalaya State; Pulak Guhathakurta et al. [13]; Government of India Ministry of Earth Sciences India Meteorological Department

monsoon months, southwestern monsoon season, and annually. During the southwest season, the lowest rainfall takes place over Ri-Bhoi district (1424.1 mm) with the lowest annual rainfall in the southwestern district (2024.1 mm). Figure 1 represents the map of Meghalaya and the work carried out in Meghalaya under spring water recharge has been shown in Figs. 2 and 3 respectively.

Himachal Pradesh and Ladakh: In order to understand the water quality and hydro chemical parameters of the aquifer's work mechanism, the springs of Kandela valley have been observed. It was found that there is a higher concentration of Ca<sup>2+</sup> in comparison to Mg<sup>2+</sup> followed by Na<sup>2+</sup>. The water is drinkable and safe for domestic use. The hydro chemical formation of spring can be explained by the dissolution of evaporite minerals, carbonate precipitation, and the exchange of ions [14]. Due to the linking of Northward migration of the Indian Plate and because of underplating, a large number of Geothermal fields exist in Himachal Pradesh and Ladakh region with 20 geothermal springs. The primary & trace element characteristics and stable isotopic composition ( $\delta^{13}\text{C}_{\text{DIC}}$ ,  $\delta^{18}\text{O}$  &  $\delta\text{D}$ ) of the springs were working to trace its source and procedure of metamorphic CO<sub>2</sub> degassing. The geothermal springs of the northwest Himalaya have probable to degas  $\sim 2.9 \times 10^7$  mol CO<sub>2</sub> annually in the environment [15]. The Fig. 4 represents the map of Himachal Pradesh and from Table 3, the four districts can be seen, by eg. Hamirpur, Mandi, Sirmur, and Kangra received highest rainfall compare to other districts during all the season. Kangra receives the

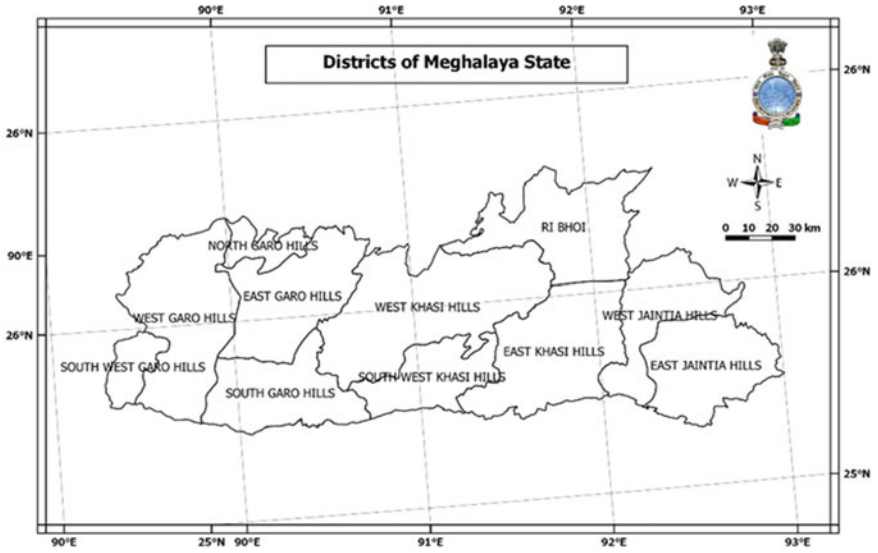


**Fig. 1** Map of Meghalaya. *Source* Government of India Ministry of Earth Sciences India Meteorological Department



**Fig. 2** Spring tap chamber is constructed to store flowing water from the Wahskur Sister spring, Village: Khelirihat, Meghalaya

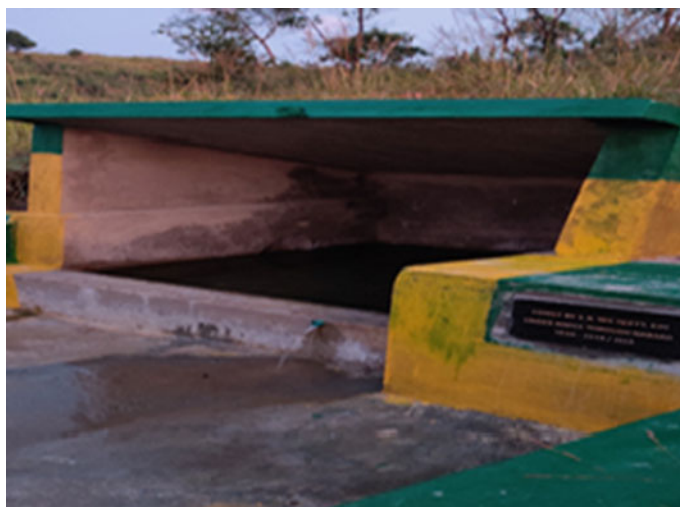


**Fig. 3** Spring tap chamber is constructed to store flowing water from the Moowalieh spring, Village: Tuber Shphrich, Meghalaya

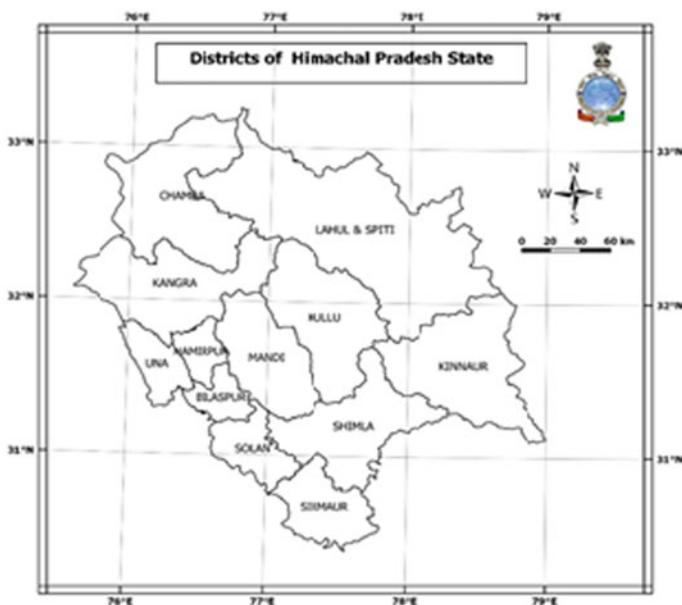


**Fig. 4** Map of Himachal Pradesh. *Source* Government of India Ministry of Earth Sciences India Meteorological Department

**Table 3** Mean and coefficient of variation rainfall statistics (2020) for the districts of Himachal Pradesh

| District        | June  |     | July  |     | August |     | September |     | Monsoon |     | Annual |    |
|-----------------|-------|-----|-------|-----|--------|-----|-----------|-----|---------|-----|--------|----|
|                 | Mean  | CV  | Mean  | CV  | Mean   | CV  | Mean      | CV  | Mean    | CV  | Mean   | CV |
| Bilaspur        | 100.5 | 287 | 257.6 | 36  | 327.8  | 88  | 147.1     | 80  | 833.0   | 74  | 1096.2 | 90 |
| Chamba          | 121.5 | 177 | 290.4 | 51  | 310.8  | 93  | 140.3     | 160 | 863.0   | 63  | 1590.8 | 66 |
| Kangra          | 177.7 | 58  | 508.2 | 28  | 589.0  | 31  | 204.8     | 47  | 1479.8  | 22  | 1860.4 | 21 |
| Kinnaur         | 35.0  | 124 | 51.1  | 65  | 52.7   | 67  | 49.8      | 74  | 188.6   | 45  | 611.3  | 41 |
| Kulu            | 85.8  | 239 | 173.5 | 44  | 167.6  | 49  | 93.5      | 75  | 520.3   | 60  | 1016.5 | 40 |
| Lahul and Spiti | 49.7  | 540 | 97.4  | 298 | 105.7  | 115 | 91.8      | 238 | 344.7   | 140 | 855.5  | 80 |
| Mandi           | 169.4 | 51  | 382.0 | 28  | 400.0  | 34  | 160.0     | 40  | 1111.3  | 21  | 1460.9 | 20 |
| Hamirpur        | 123.9 | 237 | 352.3 | 27  | 419.6  | 33  | 153.5     | 67  | 1049.3  | 52  | 1345.2 | 67 |
| Simla           | 111.5 | 190 | 211.5 | 43  | 205.6  | 37  | 122.1     | 62  | 650.8   | 51  | 1049.0 | 39 |
| Sirmur          | 167.7 | 140 | 415.2 | 37  | 383.8  | 34  | 193.4     | 64  | 1160.1  | 41  | 1446.2 | 37 |
| Solan           | 139.1 | 58  | 287.5 | 42  | 282.4  | 42  | 151.6     | 61  | 860.5   | 23  | 1156.3 | 20 |
| Una             | 110.2 | 193 | 337.2 | 92  | 373.4  | 35  | 158.0     | 146 | 978.8   | 67  | 1221.4 | 66 |

Source Met Monograph No.: ESSO/IMD/HS/Rainfall Variability/10(2020)/34; Observed Rainfall Variability and Changes over Himachal Pradesh State; Pulak Guhathakurta et al. [13]; Government of India Ministry of Earth Sciences India Meteorological Department

highest rainfall in the year. In the South West monsoon (190 mm) district of Kinnur, the lowest annual precipitation (616 mm) occurs.

- Sikkim: Under the structure of the “Mahatma Gandhi National Rural Job Guarantee Act,” daily wage village workers engaged in over 54 springs and 5 lakes, two of them permanent lakes, which provide a rejuvenation area of more than 537 hectares. Spring shed work is carried out in 30 hectares of Melli Dara reserve forest, with the support of village people and the Sumbuk development officer, and significantly improved water discharge in Khani Khola since it is the only supply for the population. The Figure 5 represents the map of Sikkim and from Table 4, it was observed that during all months and seasons, South Sikkim receives the highest rainfall in other districts. Southwestern and yearly monsoon over East Sikkim districts continues to receive lowest precipitation.

## 4 Challenges Towards Spring Shed Management

The Himalayan topography constrain poses a significant challenge for any field survey, and observations along with numerous recurrent structural instabilities with natural calamities like floods, landslides, cloud bursts, etc. hinder for studying and mapping the regions. There is no accurate data or scientific research on many springs



**Fig. 5** Map of Sikkim. *Source* Government of India Ministry of Earth Sciences India Meteorological Department

**Table 4** Mean and coefficient of variation rainfall statistics (2020) for the districts of Sikkim

| District     | June  |      | July  |      | August |      | September |      | Monsoon |      | Annual |      |
|--------------|-------|------|-------|------|--------|------|-----------|------|---------|------|--------|------|
|              | Mean  | CV   | Mean  | CV   | Mean   | CV   | Mean      | CV   | Mean    | CV   | Mean   | CV   |
| North Sikkim | 414.6 | 34.0 | 444.1 | 31.4 | 407.0  | 31.4 | 313.9     | 49.2 | 1579.6  | 27.5 | 2661.6 | 32.5 |
| West Sikkim  | 446.0 | 57.0 | 585.2 | 53.7 | 479.5  | 52.9 | 357.3     | 57.6 | 1868.0  | 52.4 | 2410.4 | 51.0 |
| East Sikkim  | 361.7 | 32.9 | 429.1 | 33.9 | 349.9  | 30.5 | 267.3     | 37.8 | 1408.0  | 22.4 | 2045.2 | 28.0 |
| South Sikkim | 479.9 | 34.4 | 595.6 | 27.3 | 513.5  | 37.3 | 382.1     | 31.3 | 1971.1  | 34.1 | 2747.9 | 38.1 |

*Source* Met Monograph No.: ESSO/IMD/HS/Rainfall Variability/23(2020)/47; Observed Rainfall Variability and Changes over Himachal Pradesh State; Pulak Guhathakurta et al. [13]; Government of India Ministry of Earth Sciences India Meteorological Department

of Himalayan regions barring a few databases like Geographical location, flow rate, and water quality parameters taken by the government and non-government agencies.

The study of rock formation, its types, and structural behavior is also an in-depth learning process to be carried out intensely in all Himalayan regions. It was also observed that most of the spring recharge regions or aquifer boundaries fall under farming, private/reserve forests or civic/private lands, etc. and which belong to the

administrative boundaries of the authorities to be taken up for the work of socio-economic development of the Himalayan region. The approach for executing the recharge actions cannot be the same in all the cases stated, and therefore it is a challenge for Government and Non-Government agencies.

Climate change, global warming, infrastructure development, hydropower generation, seismic activities are some of the factors which need to be addressed for proper implementation of spring shed management activities. In the case of agricultural and private land, community inclusion and incentives in the context of land management, horticultural or crop plants, and some infrastructure frameworks such as digging trenches, contouring, and terracing can be added. It is also a crucial move to motivating the Population to consider the complexities of hydrogeological principles and the value of site-specific regeneration steps, in contrast with the normal ridge to valley solution of numerous programs. The forest divisions manage forest lands, and so there are prohibitions on any form of activity being carried out within them [16].

## 5 Climate Impacts on the Spring System

High temperature, changes in rainfall patterns and snow cover, and a possible rise in flood and drought are the major implications for climate change associated with water resources. In general, the global hydrological cycle is exacerbated by increased temperatures. The seasonal variation in the river flow can also be greatly influenced by climate change. The changes in climate appear to increase the rainfall frequency and intensity; due to heavy rainfall events, flooding can increase [17]. Both seasonal and annual mean precipitation and evaporation effects on social and ecosystem models of water supply. The increased predicted variability in seasonal precipitation in the extremely volatile regimes already leads to a trend of “seasonally unstable regimes.” Instead, systems of low rainfall seasonality have boosted precipitation during the rainy season. In order to stop flood and increase stakeholder water sources in dry months, surplus water needs to be stored [18].

The Indus Kush Himalayas (HKW) witnessed an increase in temperatures by around 1.3 degrees from 1951 to 2014, measured by the Pune-based Indian Tropical Meteorological Institute (ITM). In recent decades, most regions of HKH have seen a declining pattern in snowfall and decline in glaciers, while several glaciers in the Karakoram range have avoided this retreat due to further winter snowfall. By the end of the twenty-first century, the average annual surface temperature over HKH is predicted to rise by approximately 5.2 degrees Celsius under the scenario of RCP8.5. People living in the Himalayas struggle already when springs dry up, and the average temperature will accelerate as well. Global climate forecasts project a rise in rainfall, but the summer monsoon precipitation over India has decreased by around 6% from 1951 to 2015 and substantially decreased over the Indo-Gangetic Plains and the Western Ghats. One of the major factors is air pollution, there has been a transition to more dry spells (27% higher in 1981–2011 compared to 1951–1980) and more



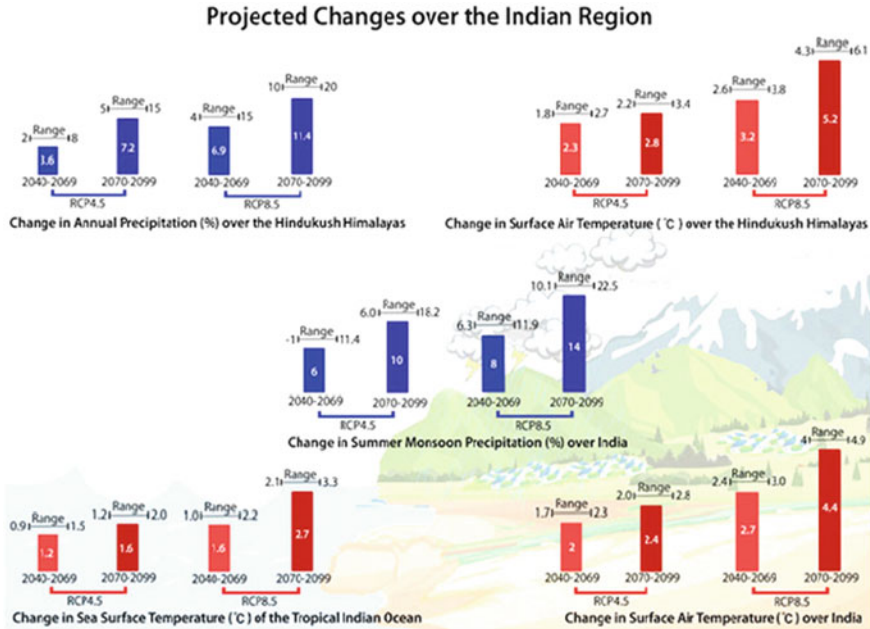


Fig. 6 Predicted trends in precipitation and temperature Source IITM

rainy spells in the summer monsoon season and it is well explained through predicted Fig. 6 provided by IITM [19].

## 6 Concluding Remarks

The springs are the significant and vital source of drinking water, and it is widely used for agricultural, irrigation, and other domestic works in rural or urban regions such as Himalayan states. Better understanding and awareness with Hill region communities will create better improvement of aquifers and groundwater to secure water security for the future generation. Under various Government or Non-Government agencies, watersheds, spring shed, soil-water management with proper engineering planning and execution activities should be carried out. The study of hydrogeology and rock construction should be implemented, which will prove better opportunities for recognizing and evolving groundwater recharge. National broad program on regeneration and reviving of springs along with capacity building training programs, complete mapping of Himalayan springs should be held in the Himalayan region. A comprehensive policy involving “Ministry of Water Resources, Ministry of Environment, Forests and Climate Change (MoEF&CC), Ministry of Tribal Affairs, Ministry of Rural Development, Ministry of Drinking Water and Sanitation, and key institutions

like State government groundwater agencies” along with scientific information’s need to be framed by the policymaker for such spring shed management works. Spring shed development is not just excavating ditches; it is a systematic procedure of mobilizing societies and comprising scientific study to help progress in decision-making and action. Concentrating on gathering real-time data on springs as well as on “scientific identification” of spring recharge regions.

## References

1. Losilla M (2001) Los acuíferos volcánicos y el desarrollo sostenible en América Central. Editorial Universidad de Costa Rica
2. Bredehoeft J (2007) It is the discharge. *Ground Water* 45(5):523–523
3. Korkmaz N (1990) The estimation of groundwater recharge from spring hydrographs. *Hydro Sci J* 35(2):209–217
4. Manga M (2001) Using springs to study groundwater flow and active geologic processes. *Annu Rev Earth Planet Sci* 29(1):201–228
5. Husain MS, Umar R, Ahmad S (2020) A comparative study of springs and groundwater chemistry of Beas and Parbati valley, Kullu district, Himachal Pradesh, India. *Hydro Research* 3:32–47. ISSN: 2589-7578. <https://doi.org/10.1016/j.hydrres.2020.04.003>
6. Singh HK, Sinha SK, Alam MA, Chandrasekharam D (2020) Tracing the evolution of thermal springs in the Hazaribagh area of Eastern Peninsular India through hydrogeochemical and isotopic analyses. *Geothermics* 85:101817. ISSN: 0375-6505. <https://doi.org/10.1016/j.geothermics.2020.101817>
7. Taloor AK, Pir RA, Adimalla N, Ali S, Manhas DS, Roy S, Singh AK (2020) Spring water quality and discharge assessment in the Basantar watershed of Jammu Himalaya using geographic information system (GIS) and water quality index (WQI). *Groundwater Sustain Dev* 10:100364. ISSN: 2352-801X. <https://doi.org/10.1016/j.gsd.2020.100364>
8. NITI Aayog, August 2018
9. Craig J, Absar A, Bhat G, Cadel G, Hafiz M, Hakhoo N, Kashkari R, Moore J, Ricchiuto TE, Thurrow J, Thusu B (2013) Hot springs and the geothermal energy potential of Jammu and Kashmir State, N.W. Himalaya, India. *Earth-Sci Rev* 126:156–177. ISSN: 0012-8252. <https://doi.org/10.1016/j.earscirev.2013.05.004>
10. <https://indiawaterportal.org/>
11. <https://geographyandyou.com/>
12. Chinnasamy P, Prathapar SA (2018) Methods to investigate the hydrology of the Himalayan Springs: a review. Working Papers id: 12844, eSocial Sciences
13. Guhathakurta P, Bhagwat PP, Satpute US, Menon P, Prasad AK, Sable ST, Advani SC (2020) *Met Monograph No.: ESSO/IMD/HS/Rainfall Variability/17(2020)/41* Observed rainfall variability and changes over Meghalaya State. India Meteorological Department, Pune
14. Ansari MA, Deodhar A, Kumar S, Khatti VS (2015) Water quality of few springs in outer Himalayas—a study on the groundwater–bedrock interactions and hydrochemical evolution. *Groundwater Sustain Dev* 1(1–2):59–67. ISSN: 2352-801X. <https://doi.org/10.1016/j.gsd.2016.01.002>
15. Tiwari SK, Rai SK, Bartarya SK, Gupta AK, Negi M (2016) Stable isotopes ( $\delta^{13}\text{C}_{\text{DIC}}$ ,  $\delta\text{D}$ ,  $\delta^{18}\text{O}$ ) and geochemical characteristics of geothermal springs of Ladakh and Himachal (India): evidence for  $\text{CO}_2$  discharge in northwest Himalaya. *Geothermics* 64:314–330. ISSN: 0375-6505. <https://doi.org/10.1016/j.geothermics.2016.06.012>
16. Mahamuni K, Upasani D (2011) Springs: a common source of a common resource. <http://hdl.handle.net/10535/7360>
17. <https://www.eea.europa.eu/>

18. Konapala G, Mishra AK, Wada Y et al (2020) Climate change will affect global water availability through compounding changes in seasonal precipitation and evaporation. *Nat Commun* 11:3044. <https://doi.org/10.1038/s41467-020-16757-w>
19. <https://indiaclimatedialogue.net/>

# Assessment of Digital Elevation Models Based on the Drainage Morphometric Parameters for the Tawi River Basin



Ravindra V. Kale, P. G. Jose, A. K. Taloor, and Rajat Kumar

**Abstract** Digital elevation models (DEMs) datasets are the fundamental input data for the conduction of the hydrologic, hydraulic, geomorphologic and ecohydrological modelling studies. Many practitioners from the hydrological, geomorphological and ecohydrological fields rely on open-access global digital elevation datasets due to their cost-effectiveness and sparse coverage of source at relatively high resolution. The recent literature replicates with a plethora of such studies that attempt to utilize various topographic datasets based on the various DEMs to study and access the physiographic characteristics as well as hydrological behaviour of the river basin. Now it is well-accepted fact that the basin's hydrological response (which is a reflection of the physiographic features of the basin) is closely related to fundamental geomorphic processes and landscape evaluations at local and regional scales. However, there is a fundamental question that arises about the accuracy and sensitivity of these topographic datasets based on the various available DEMs. Therefore, this study attempts to deals with five open-access DEMs viz., Shuttle Radar Topographic Mission (SRTM), ALOS Global Digital Surface Model "ALOS World 3D30m (AW3D30), Advanced Spaceborne Thermal Emission and Reflection Radiometer (ASTER), CartoDEM and ALOS PALSAR-Radiometric Terrain Correction (ALOS PALSAR-RTC), etc. All the DEMs except ALOS PALSAR-RTC are with a spatial resolution of 30 m whereas ALOS-RTC DEM is with a 12.5 m spatial resolution. Estimation of about 25 morphometric aspects parameters that includes linear aspects, areal aspects and relief aspects are carried out for the Tawi river basin up to its confluence with the Chenab River basin. All these five types of DEMs are verified with google earth maps. Results show that ALOS World 3D30m

---

R. V. Kale (✉) · P. G. Jose · R. Kumar  
Western Himalayan Regional Centre, National Institute of Hydrology, Satwari Cantt, Jammu,  
Jammu and Kashmir UT 180003, India  
e-mail: [rvkale.nihr@gov.in](mailto:rvkale.nihr@gov.in)

P. G. Jose  
e-mail: [pgjose.nihr@gov.in](mailto:pgjose.nihr@gov.in)

A. K. Taloor  
Department of Remote Sensing and GIS, University of Jammu, Jammu, Jammu and Kashmir UT  
180006, India

(AW3D30) DEM data possess high accuracy in the delineation of the river basin as well as the presentation of the stream network followed by the CartoDEM, particularly in the low-lying area. However, the performance of ALOS-RTC DEM is the worst among all the studied DEMs. Further, an attempt has been made to subdivide the whole watershed area into fourteen sub-watersheds. The hypsometric integral analysis for these fourteen sub-watersheds has been carried out to compare different sub-watersheds irrespective of scale. Results of the hypsometric integral analysis using the AW3D30 DEM dataset indicate that the Upper Tawi sub-watershed had a high hypsometric integral value of 0.373 whereas the sub-watershed Sohagni had a low value of 0.147. The hypsometric integral value for the whole watershed was found to be 0.18. It was also found that the sub-watersheds namely Upper Tawi, Sardhan, Ramnagar, Balini and Lower Tawi were with high hypsometric integral values which indicate that these sub-watersheds are at a late mature stage of the geomorphological evaluation.

**Keywords** DEM · SRTM · AW3D30 · CartoDEM · ALOS · ASTER · Morphometry

## 1 Introduction

Morphometry or Geomorphometry which deals with establishing geometric features of the landforms based on measurements is considered as the independent discipline in the Earth sciences [1, 2]. Nowadays, it is well-accepted fact that geomorphometry is a very important component in terrain analysis and surface modelling [3]. The morphometric analysis is done successfully through the measurement of linear, aerial, relief, the gradient of channel network and contributing ground slope of the basin [4, 5]. A plethora of studies [6–13] suggests that the drainage basin morphology reflects various geological and geomorphological processes over time which are essential to understand the landform processes, soil physical properties and basin erosional characteristics. A drainage basin or a watershed refers to the entire area of land confined inside the ridges and hills that drains all the streams and their tributaries and rainfall to a common outlet. Quantitative analysis of drainage network within a basin or watershed is essential to analyze various landforms and predominant hydrogeological processes essential for flood management, integrated watershed management, detection of landmass movement, tectonic activities [14, 15]. Horton's works [6, 16] on stream networks and drainage basin processes are classically identified as the precursor to this quantitative movement. Further, as suggested by Summerfield and Hulton [17] the topographical features are controlling the physical aspects of the drainage basin, therefore, topography should be analyzed quantitatively to determine the relative efficiency of its component [3].

The data for morphometric analysis were obtained mainly from measurements on the detailed topographic map or data from fieldwork. However, the use of the Digital Elevation Model (DEM) has many advantages over traditional topographical maps

as they can seamlessly cover the globe and very easily be processed in numerous GIS software. Digital Elevation Model (DEM) plays an important role in the representation of the topographic surfaces with respect to any defined datum which is an important dataset in the hydrological modelling studies. Although in the data-scarce developing countries, the unavailability of high-resolution DEM data is the prime limitation for simulating hydrological models, however nowadays many open-access DEMs with spatial resolutions of 30 m are available, e.g. open-access DEMs viz., Shuttle Radar Topographic Mission (SRTM), ALOS Global Digital Surface Model "ALOS World 3D-30m (AW3D30), Advanced Spaceborne Thermal Emission and Reflection Radiometer (ASTER), CartoDEM, etc. Further, ALOS PALSAR-Radiometric Terrain Correction (ALOS PALSAR-RTC) DEM is available with a spatial resolution of 12.5 m spatial resolution.

Many studies focus on drainage morphometric analysis using DEM all across the globe [14, 15, 17–23]. However, Dragut et al. [24] study argue that the scale of the parameters derived from geomorphological analysis is mainly governed by DEM resolution. Further, the study by Saran et al. [25] suggested that DEMs of high resolution have more accuracy and a higher extraction and traces for the watershed, tributaries and relief characteristics. Numerous studies attempt to assess the accuracies of the DEMs based on the extracted morphometric drainage parameters [21, 26, 27]. Particularly, Singh et al. [26] have carried out the hydrological analysis and morphometric evaluation by using SRTM DEM, multispectral satellite data and survey of India topographical sheets. They found that SRTM DEM based hydrological evaluation at the watershed scale is more applied and precise compared to other available techniques. Further, Bhatt and Ahmed [27] have applied Cartosat DEM to evaluate the morphometric parameters for the Upper Krishna basin. They found that systematic analysis of morphometric parameters derived from Cartosat DEM using GIS provides useful information about catchment characteristics with respect to flood management. Saran et al. [25] attempted to evaluate the quality of DEMs from four sources viz. topographic map (1:50,000), SRTM (90 m), ASTER (15 m) and CARTOSAT (2.5 m) based on the elevation accuracy and morphometric features analysis in Sitla Rao watershed (North India). Their study found that the ASTER and CARTOSAT DEMs provided higher vertical accuracies than the SRTM and topographic map-based DEM. The SRTM with a coarse resolution of 90 m provided vertical accuracy but better morphometry compared to a topographic map. Niyazi et al. [21] attempted to compare four types of DEMs (ASTER 30 m, SRTM 90 m, SRTM 30 m and ALOS 30 m) by using google maps and topographic maps of 1:50 k based on derived morphometric parameters of the Fatimah watershed (Makkah Province, KSA) to find the best DEM for geomorphometric analysis. They have found that the best DEM for geomorphometric analysis was SRTM 30 m as it matches the results of google maps and topographic maps of 1:50 k. Further, both the SRTM 30 and ASTER 30 are very closed to each other and also in accordance with the google maps and the topographic maps of 1:50k as of the slope aspect. Alganci et al. [28] have carried out an accuracy assessment of different digital surface models that includes freely available ASTER 30 m, SRTM 30 m and ALOS (AW3D30) DSM

30 m and commercially available 3 m and 1 m resolution DSMs produced from tri-stereo images from the SPOT 6 and Pleiades high-resolution (PHR) 1A satellites, respectively. This study results illustrated that PHR and SPOT DSMs shows higher accuracy values as their spatial resolution was higher. Particularly, the accuracy of the ALOS (AW3D30) DSM was very promising as compared to other freely available SRTM and ASTER DSMs which shows the worst accuracies. According to them, although the ALOS (AW3D30) DSM had a 30 m grid spacing, it possesses high accuracy due to the acquisition of strong signals from the original 5 m DSM, which was produced from the 2.5 m images. Further, they found that the DSMs able to produce better accuracy values for rare residential and road classes when the elevation differences were not considerable. Nikolakopoulos [29] has carried out the study to examine the accuracy of the ALOS Global Digital Surface Model (AW3D30) by comparing visually and statistically with DSMs created from ALOS stereo pairs at several areas of Greece with complex geomorphologic characteristics. He has observed that AW3D30 DSM presents two or three times lower Root Mean Square Error (RMSE) than the respective DSMs. Further, the AW3D30 DSM presents RMSE values of 2.69 and 14.0 m in the area of low (at Antiparos Island in the Cyclades complex) and high (at the Chania Prefecture in Western Crete) relief, respectively. Jain et al. [30] attempted to evaluate SRTMDEM-GL1, GDEM-V2, AW3D30 and CartoDEM-V3.1 DEMs of 30 m resolution with Dual Frequency GNSS for Lower Tapi Basin India and found that AW3D30 DEM was more accurate compared to the other three DEMs when terrain elevation accuracy is considered. When the vertical accuracies are considered then AW3D30 and SRTM-GL1 DEMS were performed better than CartoDEM-V3.1 and GDEM-V2. From this review, it could be inferred that although nowadays quite a good number of high-resolution DEMs are freely available, only a few studies particularly for the Himalayan watersheds attempt to compare these DEMs accuracies based on morphometric parameters analysis. Therefore, there is a need to study the accuracies of these freely available DEMs for the typical Himalayan watershed.

In view of the reviewed literature, the main objective of this study is to assess the accuracies of the available different types of DEMs (ASTER 30 m, SRTM 30 m, ALOS (AW3D30) 30 m, CartoDEM 30 m and ALOS PALSAR-RTC 12.5 m) with different resolutions based on drainage morphometric analysis for the Tawi river basin. The drainage morphometric parameters for the Tawi river basin are initially calculated from different DEMs and then finally compared and correlated to find the best-suited dataset of digital elevation model for geomorphometric analysis that could be potentially utilized for hydrological and hydraulic modelling purposes (Fig. 1).

## 2 Study Area

The Tawi River is an important tributary of the Chenab River in the Western Himalayan region. Tawi river originates from the lap of Kailash Kund glacier and adjoining area southwest of Bhadarwah in Doda district of the Union Territory of

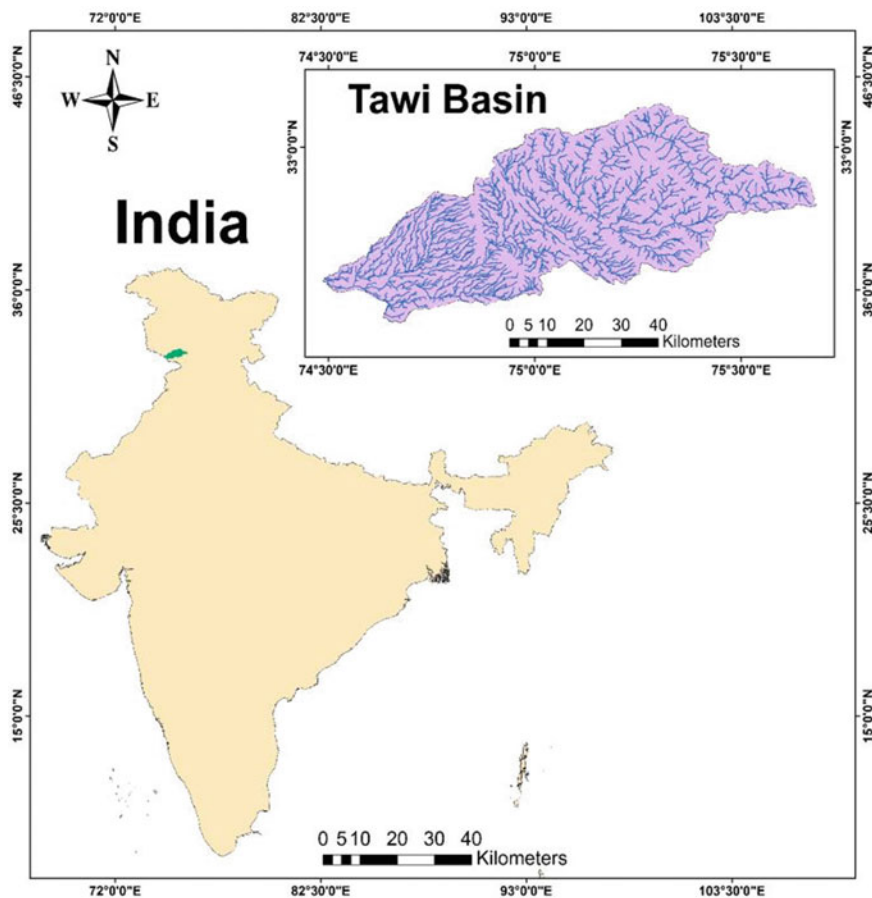


**Fig. 1** Location map of the Tawi river basin

Jammu and Kashmir, India. The catchment area of the Tawi river basin is bounded by latitude  $32^{\circ} 35' 20''$ - $33^{\circ} 6' 6''$  N and longitude  $74^{\circ} 29' 8''$ - $75^{\circ} 40' 54''$  E which varies between 239 and 4331 m. The total catchment area up to its confluence with the Chenab river is around 2964 km<sup>2</sup>. In Indian territory, this river basin falls in the districts of Jammu, Udhampur and a small part of Doda. This basin has an elongated shape in the upper part while it is broad circular shaped in the lower part. This river basin is characterized by rugged mountainous topography in the upper reaches while its lower reaches consist of low hills and aggradational plains. The slope of the basin is from east to west in the upper part and northeast to southwest in the lower part. Being a mountainous river Tawi has more than 2000 numbers of tributaries and sub-tributaries. However, there are nine numbers of predominant tributaries of the river Tawi. The Tawi River is comprised of streams of 1–6 orders.



The Tawi River basin is mainly falling under a subtropical monsoonal climate regime. The summer monsoon is more active in the plains, while winter monsoon rainfall is received in the hilly terrains. The middle portion of the Tawi River records the heaviest rainfall over the catchments. The annual rainfall varies from 900 to 1900 mm. Tawi river basin consists mainly of metamorphic terrain in the higher reaches associated with granite intrusions and sedimentary rocks in the lower reaches. The Tawi catchments have three meso-geomorphic regions; the upper one is in the north of the Panjal Thrust with a maximum elevation of 4331 m, the middle one is between the Panjal thrust to the Udhampur thrust with an elevation of 700 to 1900 m and the lower one is comprised of low-lying hillocks between Udhampur and Jammu. Only a small portion of the Tawi catchment, near its starting point, is snow-fed. However, a majority of the terrain consists of hilly tracts becoming plain areas after Jammu town and before its confluence with the Chenab River.

### 3 Data Used and Methodology

#### 3.1 Data Used

In the present study, the five freely available DEM datasets with different spatial resolutions namely ASTER 30 m, SRTM 30 m, ALOS (AW3D30) 30 m, CartoDEM 30 m and ALOS PALSAR – RTC 12.5 m have been used. It is well accepted that different indicators of the drainage network give an inference about the basin's hydrological and geological characteristics [31]. Therefore, these DEMs have been investigated by extracting geometric features like tributaries and topographic features and estimation of various drainage morphometric parameters. The drainage network extracted by using these DEM datasets is compared with those of the topographic map by Survey of India (SoI) LULC map and with google earth maps. The main characteristics of all the above-mentioned DEM datasets are provided briefly in the following section.

- **ASTER DEM with 30 m resolution:** ASTER Global Digital Elevation Model first version (GDEM-V1) with 30 m resolution and absolute accuracy of 20 m (95% confidence interval) was released in 2009. The second version (GDEM-V2) was released in 2011 and the third version (GDEM-V3) released in 2019 and available from NASA's Land Processes Distributed Active Archive Center (LP DAAC). Its land surface coverage extent range between 83°N and 83°S. The ASTER GDEM Version 3 was produced through automated processing of 2.3 million scenes (1 arc-second) from the ASTER archive in GeoTIFF format, with 30-m spatial resolution and  $1 \times 1$  tiles. It uses WGS84 geoid projection.
- **SRTM DEM with 30 m resolution:** SRTM 1 arc-second DEM with global coverage was first made available worldwide for public use by the US government on 23 September 2014. The National Aeronautics and Space Administration (NASA) and the National Geospatial-Intelligence Agency (NGA) participated in the international project to acquire radar data through the

Shuttle Radar Topography Mission (SRTM) which was flown aboard the space shuttle Endeavour February 11–22, 2000. Its land surface coverage extent range between 60° N and 56° S which cover about 80% of the Earth's surface.

- **CartoDEM with 30 m resolution:** Indian National DEM generated by the Indian Space Research Organization (ISRO) on May 5, 2005. Cartosat-1 or IRS-P5 is a stereoscopic Earth observation satellite in a sun-synchronous orbit satellite globally capture along-track stereo images (Forward + 26o, Aft -5o) with 2.5 m spatial resolution (ground sampling distance) with 27 km swath and the base-height ratio of 0.63 using two panchromatic charge-coupled device sensors. These stereo images (2.5 m resolution) were used for DEM generation using augmented stereo strip triangulation (ASST) with 10 m posting for Indian landmass. Freely Available CartoDEM V3.1 (30 m resolution) covering a geographical area of India for public use can be downloaded from the BHUVAN portal (<https://bhuvan.nrsc.gov.in>) of ISRO.
- **ALOS (AW3D30) DEM with 30 m resolution:** AW3D30 is a global digital surface model (DSM) development started with launch of the Advanced Land Observing Satellite (ALOS) by the Japan Aerospace Exploration Agency (JAXA) on Jan 24, 2006 with a spatial resolution of approx. 30 m (1 arc-second). The AW3D30 dataset covering the global land surfaces was produced using 3 million scene archives acquired by the PRISM panchromatic optical sensor on the Advanced Land Observing Satellite “DAICHI” (ALOS) operated from 2006 to 2011. The AW3D30 is a resampling of the 2.5-m mesh version of the “World 3D Topographic Data”. This DSM global dataset was made freely available for public use in May 2016. Presently, the AW3D30 version 3.1/3.2 can be downloaded from the JAXA website.
- **ALOS PALSAR- RTC Dem with 12.5 m resolution:** The Alaska Satellite Facility Distributed Active Archive Data Center (ASF DAAC) released geometrically and radiometrically terrain corrected data products derived from ALOS PALSAR, processed using the Gamma Remote Sensing software package in October 2014. ALOS PALSAR-RTC RT1 product with 12.5 m spatial resolution is produced using 1/3 arc-second National Elevation (NED) Dataset for the USA and 1 arc-second SRTM GL1 datasets for the rest of the globe excluding Antarctica, Greenland, Iceland and northern Eurasia. The dataset is available in the GeoTIFF format.

The detailed information about the data sources used in the present study is shown in Table 1.

### 3.2 Methodology

To achieve the basic objective of the study to assess the DEMs based on the drainage morphometric properties of the Tawi river basin, several morphometric parameters (linear, areal and relief aspects) need to be calculated and interpreted. Standard

**Table 1** General information about DEMs and topographical data used in this study

| Sr. No. | Production authority           | Topographic maps and DEMs details   | Survey year/date of release | Spatial resolution/scale | Source  |
|---------|--------------------------------|---|-----------------------------|--------------------------|---|
| 1       | Alaska Satellite Facility, USA | <b>ALOS PALSAR-RTC DEM:</b><br>AP_12569_FBD_F0640_RT1.dem.tif<br>AP_04342_FBS_F0640_RT1.dem.tif   | 2014                        | 12.5 m                   | <a href="https://asf.alaska.edu/data-sets/derived-data-sets/alos-palsar-rtc/alos-palsar-radiometric-terrain-correction/">https://asf.alaska.edu/data-sets/derived-data-sets/alos-palsar-rtc/alos-palsar-radiometric-terrain-correction/</a> |
| 2       | NASA, USA                      | <b>ASTER DEM:</b><br>ASTGTMV003_N32E074<br>ASTGTMV003_N32E075<br>ASTGTMV003_N33E074<br>ASTGTMV003_N33E075   | 2011                        | 30 m                     | <a href="https://e4ftl01.cr.usgs.gov/">https://e4ftl01.cr.usgs.gov/</a>   |
| 3       | EORC, JAXA                     | <b>AW3D30 DEM:</b><br>N032E074_AVE_DSM.tif<br>N032E075_AVE_DSM.tif<br>N033E074_AVE_DSM.tif<br>N033E075_AVE_DSM.tif  | 2016                        | 30 m                     | <a href="https://www.eorc.jaxa.jp/ALOS/en/aw3d30/data/index.htm">https://www.eorc.jaxa.jp/ALOS/en/aw3d30/data/index.htm</a>   |
| 4       | ISRO, INDIA                    | <b>CARTO DSM:</b><br>C1_DEM_16B_2005-2014_v3_R-1_74E32N_i43u<br>C1_DEM_16B_2005-2014_v3_R-1_74E33N_i43o<br>C1_DEM_16B_2005-2014_v3_R-1_75E32N_i43v<br>C1_DEM_16B_2005-2014_v3_R-1_75E33N_i43p | 2005                        | 30 m                     | <a href="https://bhuvan-app3.nrsc.gov.in/data/download/index.php?c=s&amp;s=C1&amp;p=cdv2">https://bhuvan-app3.nrsc.gov.in/data/download/index.php?c=s&amp;s=C1&amp;p=cdv2</a>   |
| 5       | NASA, USA                      | <b>SRTM DEM:</b><br>n33_e075_larc_v3.tif<br>n33_e074_larc_v3.tif<br>n32_e075_larc_v3.tif<br>n32_e074_larc_v3.tif  | 2000                        | 30 m                     | <a href="https://earthexplorer.usgs.gov/">https://earthexplorer.usgs.gov/</a>   |

(continued)

**Table 1** (continued)

| Sr. No. | Production authority | Topographic maps and DEMs details | Survey year/date of release | Spatial resolution/scale | Source                       |
|---------|----------------------|-----------------------------------|-----------------------------|--------------------------|------------------------------|
| 6       | SOI LULC Map         |                                   | 1982                        | Scale: 1:50,000          | Survey of India (SOI), India |

procedure was followed to extract the stream network, slope, drainage density and basin from all five DEMs datasets in the GIS environment (Arc GIS 10.8). These extracted features are projected to the regional projection using UTM projection and WGS 84 datum (WGS\_1984\_UTM\_Zone\_43\_N).

The extracted stream networks and basins from all five DEMs are used to calculate various drainage morphometric parameters (linear, areal and relief aspects) through a combination of geoprocessing tools available in Arc GIS and SAGA software. The calculated drainage morphometric parameters for each DEM are then compared with those of other data sources to assess the best-suited DEM. The details of the morphometric parameters compared and the methodologies adopted for the computation of these morphometric parameters are given in Table 2.

The drainage morphometric parameters as shown in Table 2 were derived from all selected DEMs and then compared with each other to find out the DEM datasets providing better results.

## 4 Results and Discussions

### 4.1 Comparison of the Stream Network and Sub-Watersheds

The stream drainage pattern in any watershed is a representation of spatial structure and attributes of geography and hydrology of that particular basin. In a hydrological environment, drainage pattern mainly depends on composite factors such as spatial pattern and hydrological features formulated by the surface runoff phenomenon occurring in that particular watershed. Therefore, the representation of the stream network is an important aspect of any hydrological modelling study. In the present study, the drainage networks extracted from all these DEMs have also been compared with drainage networks on the Land Use Land Cover maps by SoI (Scale: 1:50k) and on google earth map and shown in Fig. 2. Based on the visual interpretation of the results shown in Fig. 2, it can be seen that almost every stream network extracted from each DEM dataset follows an identical drainage pattern particularly upstream of the Jammu. As it can be noted that the elevation of the Tawi river basin upstream of the Sidhra gauging station at Jammu is ranging between approximately 294 to 4331 m. However, the stream network pattern extracted by using different DEM datasets downstream of the Jammu gauging site is significantly different. Among the five stream networks extracted from the selected different DEMs, the stream network extracted from the AW3D30 DSM is closely matched with those by the SoI LULC map and google earth topographic map used as a standard. Further, the stream network extracted from Carto DEM was very close to those by AW3D30 DEM. However, ASTER, SRTM and ALOS PALSAR-RTC DEMs were failed to represent the stream network in the Tawi river basin downstream of the Jammu gauging site.

As mentioned earlier there are major nine tributaries (nallahs) namely Balini, Chirwa, Duddar, Gambir, Jhajjar, Ramnagar, Sardhan, Balole and Sohagni that joins

**Table 2** Details of the drainage morphometric parameters and methodology adopted for their computations

| Morphometric aspects | Parameters                             | Formulae  | References   |
|----------------------|--|---|--------------|
| Linear aspect        | Stream order ( <i>u</i> )              | Hierarchical rank   | Strahler [8] |
|                      | Stream numbers (Nu)                    | $Nu = N1 + N2 + N3 + \dots Nn$                                  | Strahler [7] |
|                      | Bifurcation ratio (Rb)                 | $Rb = Nu/Nu + 1$  | Schumm [32]  |
|                      | Weighted Mean bifurcation ratio (WMRb) | $WMRb = \sum (Rbu/(Rbu + 1)) \times \frac{(Nu+(Nu+1))}{\sum N}$ | Strahler [7] |
|                      | Stream length (Lu)                     | $Lu = L1 + L2 + \dots Ln$                                       | Horton [6]   |
|                      | Mean stream length (Lum)               | $Lum = Lu/Nu$   | Horton [6]   |
|                      | Stream length ratio (R1)               | $R1 = Lu/Lu - 1$  | Horton [6]   |
| Areal aspect         | Basin area (A)                         | GIS software analysis   | Schumm [32]  |
|                      | Basin Length (L)                       | GIS software analysis   | Schumm [32]  |
|                      | Form factor (Ff)                       | $Ff = A/L^2$  | Horton [16]  |
|                      | Drainage basin perimeter (P)           | GIS software analysis   | Schumm [32]  |
|                      | Circulatory ratio (Rc)                 | $Rc = 4\pi A/P^2$   | Miller [33]  |
|                      | Elongation ratio (Re)                  | $Re = 2\sqrt{A/\pi}/L$  | Schumm [32]  |
|                      | Drainage density (Dd)                  | $Dd = L/A$  | Horton [6]   |
|                      | Constant of channel maintenance (CCM)  | $CCM = 1/Dd$  | Schumm [32]  |
|                      | Stream frequency (Fs)                  | $Fs = \sum_{i=1}^u Nu/A$  | Horton [6]   |
|                      | Drainage Texture (Rt)                  | $Rt = Nu/P$   | Horton [6]   |
| Relief aspect        | Maximum elevation (Hmax)               | GIS software analysis using DEM                                 |              |
|                      | Minimum elevation (Hmin)               | GIS software analysis using DEM                                 |              |
|                      | Highest relief (R)                     | GIS software analysis using DEM                                 |              |
|                      | Lowest relief (r)                      | GIS software analysis using DEM                                 |              |

(continued)

**Table 2** (continued)

| Morphometric aspects | Parameters                | Formulae  | References   |
|----------------------|---------------------------|---|--------------|
|                      | Relative relief (Rr)      | $Rr = R - r$  | Schumm [32]  |
|                      | Relief ratio (Rf)         | $Rf = (Rr/L)/100$   | Schumm [32]  |
|                      | Dissection index (Di)     | $Di = Rr/R$   | Schumm [32]  |
|                      | Ruggedness index (Ri)     | $Ri = Dd * Rr/1000$   | Schumm [32]  |
|                      | Hypsometric Integral (HI) | $HI = (Elev_{mean} - Elev_{min}) / (Elev_{max} - Elev_{min})$ | Strahler [7] |

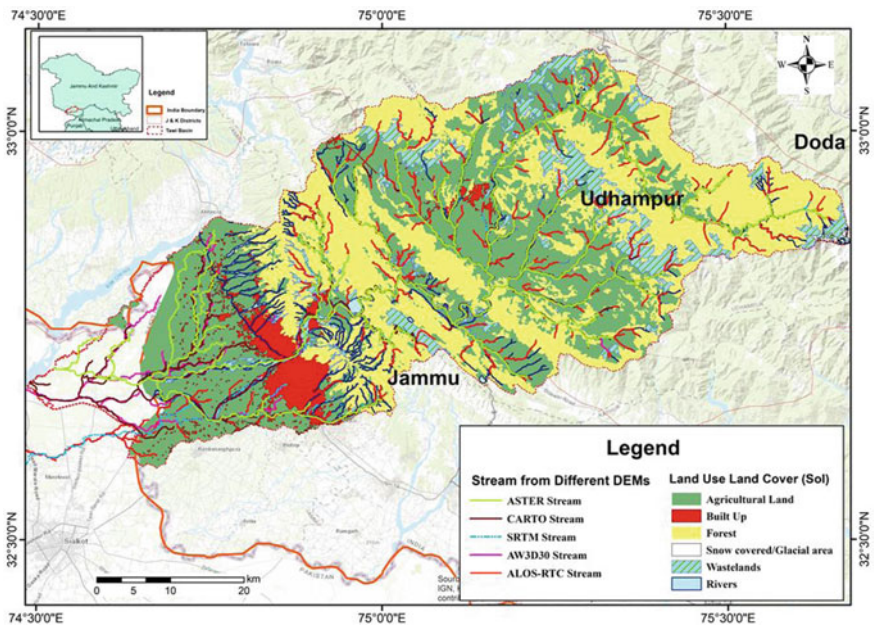


**Fig. 2** Drainage networks extracted from all five DEMs and overlaid on the LULC map by Sol

the main Tawi stream to form the drainage network of the river Tawi. Out of these nine tributaries, seven tributaries except Balole and Sohagni are drains into the main Tawi river located in the upstream catchment area from Sidhra gauging station at Jammu. Based on the discussion in the previous section, geomorphological properties of the Tawi river basin were analyzed separately for sub-watershed upstream and downstream of the Sidhra gauging site at Jammu and hence the complete Tawi river basin is subdivided into 14 sub-watersheds. The extracted drainage networks, sub-watershed extracted from all the five DEM datasets along with elevation overlaid on



the google earth map are shown in Fig. 3. The comparison of the sub-watersheds areas derived from different DEMs is shown in Fig. 4.

From the sub-watershed areas shown in Fig. 4, it can be inferred that the sub-watershed area extracted from selected five DEMs upstream of the Sidhra gauging site at Jammu are nearly the same. However, as there is a very large difference in the sub-watersheds area below the Sidhara gauging site. This conclusion can also be verified from the results shown in Fig. 3. Further, from the results shown in Fig. 3, it can be seen that the Sohagni sub-watershed is extracted from AW3D30, Carto and ASTER DEMs. SRTM and ALSO PALSAR-RTC DEMs do not able to extract

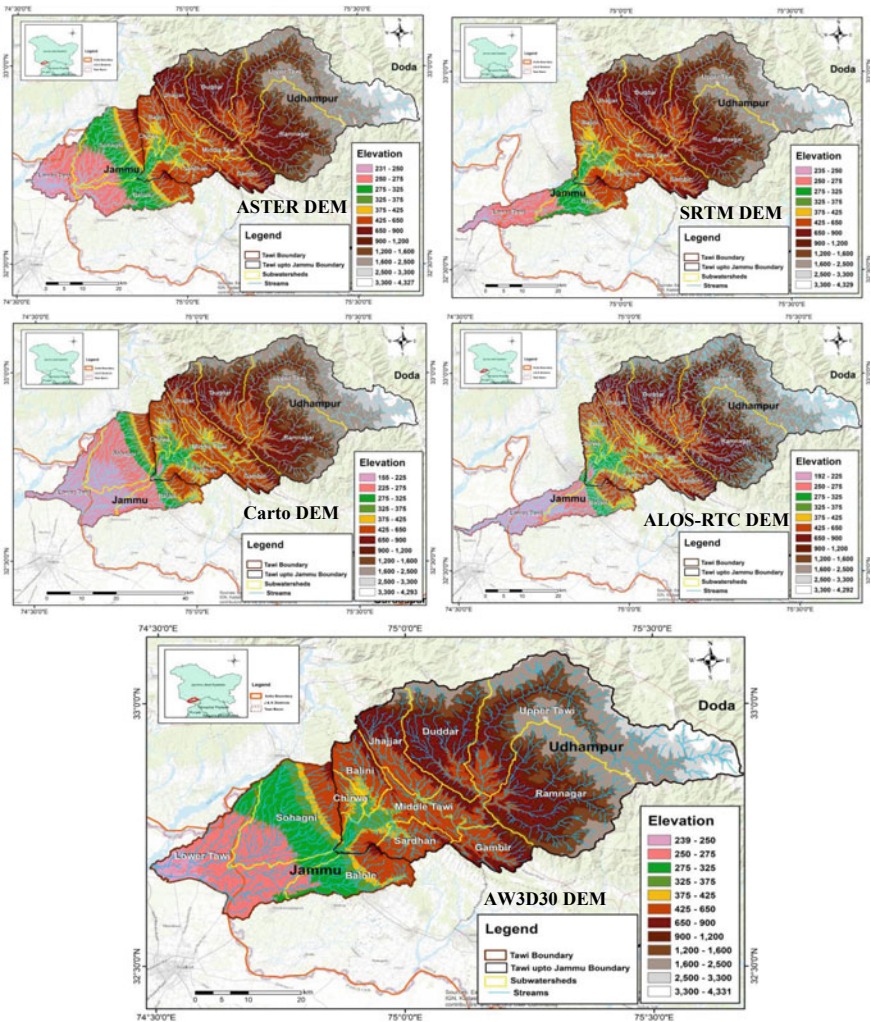
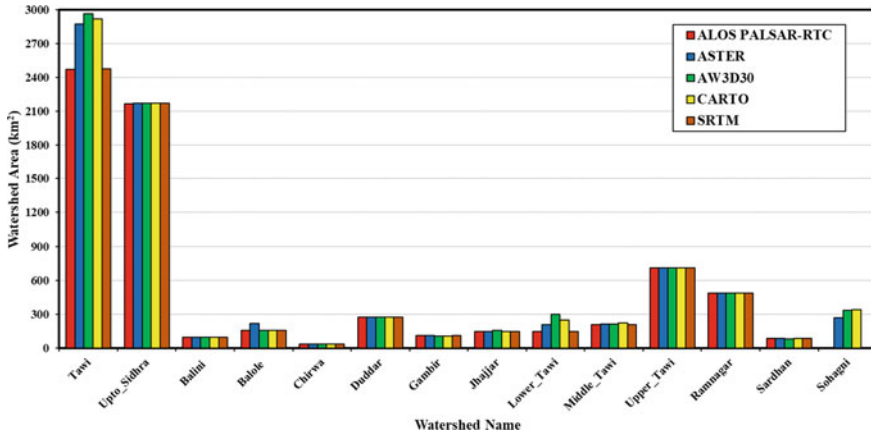


Fig. 3 Drainage networks and sub-watersheds extracted from all the five DEM datasets along with elevation overlaid on the google earth map





**Fig. 4** Comparison of sub-watershed areas computed by different DEMs

the Sohagni sub-watershed as these DEMs failed to represent the Tawi river stream accurately in the downstream reach.

## 4.2 Comparison of the Drainage Morphometric Properties

Several morphometric parameters (linear, areal and relief aspects) from all five selected DEM datasets were calculated in order to facilitate inter-comparison to choose the best DEM dataset. Linear aspect parameters computed were stream order, stream numbers, bifurcation ratio, weighted mean bifurcation ratio, stream length, mean stream length and stream length ratio. The areal aspect parameters computed were basin area, basin length, form factor, drainage basin perimeter, circularity ratio, elongation ratio, drainage density, constant of channel maintenance, stream frequency and texture ratio. The relief aspect parameters computed were maximum elevation, minimum elevation, highest relief, lowest relief, relative relief, relief ratio, dissection index and ruggedness index. These different morphometric properties of the Tawi river basin derived from selected five DEMs are shown in Table 3. Referring to Table 3, it can be seen that all the DEMs with a spatial resolution of the 30 m (AW3D30, SRTM, ASTER and CartoDEM) gave 6<sup>th</sup> as higher-order stream except ALOS PALSAR-RTC DEM which gave 7<sup>th</sup> as a higher-order stream. It is very interesting to see that the stream numbers and stream lengths derived from AW3D30, CartoDEM and ASTER DEMs were approximately the same as the watershed delineated with these DEMs were also approximately similar. Although, the stream numbers and stream lengths derived from SRTM were lower as compared to the former three DEMs as the SRTM DEM failed to accurately delineate the Tawi river watershed in the lower reaches. The highest stream numbers and stream lengths were derived from ALOS PALSAR-RTC DEM which means that the finer

**Table 3** Drainage Morphometric properties of the Tawi river basin derived from selected five DEMs

| Morphometric parameters                | ALOS PALSAR-RTC DEM | ASTER DEM | AW3D30 DEM | CARTO DEM | SRTM DEM |
|--|---------------------|-----------|------------|-----------|----------|
| <i>Linear aspect</i>                   |                     |           |            |           |          |
| Stream order ( <i>u</i> )              | 7                   | 6         | 6          | 6         | 6        |
| Stream numbers (Nu)                    | 7997                | 1861      | 1929       | 1861      | 1596     |
| Bifurcation ratio (Rb)                 | 0.24                | 0.26      | 0.17       | 0.41      | 0.09     |
| Weighted Mean bifurcation ratio (WMRb) | 3.09                | 3.57      | 4.13       | 2.64      | 6.88     |
| Stream length (Lu)                     | 4291.79             | 2580.66   | 2705.01    | 2636.41   | 2173.44  |
| Mean stream length (Lum)               | 0.56                | 1.39      | 1.44       | 1.64      | 1.64     |
| Stream length ratio (Rl)               | 0.73                | 0.98      | 0.80       | 0.85      | 0.87     |
| <i>Areal aspect</i>                    |                     |           |            |           |          |
| Basin area (A)                         | 2471.62             | 2870.21   | 2964.08    | 2919.02   | 2482.54  |
| Basin length (L)                       | 115.75              | 109.54    | 113.17     | 115.10    | 116.21   |
| Form Factor (Ff)                       | 0.184               | 0.239     | 0.231      | 0.220     | 0.183    |
| Drainage basin perimeter (P)           | 489.7               | 468.72    | 465.4      | 481.01    | 487.08   |
| Circulatory ratio (Rc)                 | 0.129               | 0.164     | 0.172      | 0.1586    | 0.131    |
| Elongation ratio (Re)                  | 1.35                | 1.36      | 1.30       | 1.32      | 1.33     |
| Drainage density (Dd)                  | 1.736               | 0.899     | 0.912      | 0.903     | 0.875    |
| Constant of channel maintenance (CCM)  | 0.576               | 1.112     | 1.096      | 1.107     | 1.142    |
| Stream frequency (Fs)                  | 3.23                | 0.648     | 0.650      | 0.637     | 0.642    |
| Drainage texture (Rt)                  | 5.608               | 0.582     | 0.593      | 0.575     | 0.562    |

(continued)

**Table 3** (continued)

| Morphometric parameters  | ALOS PALSAR-RTC DEM | ASTER DEM | AW3D30 DEM | CARTO DEM | SRTM DEM |
|--------------------------|---------------------|-----------|------------|-----------|----------|
| <i>Relief aspect</i>     |                     |           |            |           |          |
| Maximum elevation (Hmax) | 4292                | 4327      | 4331       | 4293      | 4329     |
| Minimum elevation (Hmin) | 192                 | 231       | 239        | 155       | 235      |
| Highest relief (R)       | 978                 | 826.38    | 1000.33    | 761.46    | 1017.56  |
| Lowest relief (r)        | 2.052               | 4.283     | 1.918      | 0.700     | 3.115    |
| Relative relief (Rr)     | 975.9               | 822.1     | 998.4      | 760.7     | 1014.4   |
| Relief ratio (Rf)        | 0.0084              | 0.0075    | 0.0088     | 0.0066    | 0.0087   |
| Dissection index (Di)    | 0.998               | 0.994     | 0.998      | 0.999     | 0.999    |
| Ruggedness index (Ri)    | 1.695               | 0.739     | 0.911      | 0.688     | 0.888    |

the resolution, the more stream counts will be derived from DEM. The bifurcation ratio for the highest order stream as well as the weighted mean bifurcation ratio for all the DEMs was significantly different. It can be noted that the bifurcation ratio is considered an important morphometric parameter as it denotes the water carrying capacity and related flood potentiality of any basin. Further, the mean stream length and stream length ratio derived from the AW3D30, SRTM, CartoDEM and ASTER DEMs were nearly close to each other. However, these values derived from ALOS PALSAR DEM are significantly lower.

The areal aspects seen from Table 3 reveals that the basin area derived from AW3D30 and CartoDEM were nearly the same which shows the highest basin area estimates. Although, the basin area derived from SRTM and ALSO PALSAR-RTC DEMs was approximately the same but significantly lower than those from the other three DEMs due to inaccurate delineation of the watershed area by these DEMs (see Fig. 3). Further, the basin length in kilometres derived from all five DEMs was approximately the same. The form factor values derived from all the DEMs are ranging between 0.183 to 0.239 with ASTER and AW3D30 DEMs shows higher values. These value of form factors suggest that the Tawi river catchment is elongated. Although the values of the other areal aspect parameters derived from AW3D30, CartoDEM, ASTER and SRTM are approximately very close to each other, the values derived from ASTER and CartoDEM are more close to AW3D30 DEM. The

drainage density, stream frequency and drainage texture parameters derived from the ALOS PALSAR-RTC DEM are significantly higher than those from the other four DEMs.

Referring to Table 3, the AW3D30 DEM shows higher values maximum as well as minimum elevation followed by SRTM, ASTER, ALOS PALSAR and CARTO DEMs, respectively. Interestingly the elevation values given by the AW3D30, ASTER and SRTM DEM are very close. The values of the highest relief, relative relief, relief ratio, dissection index and ruggedness index derived from Aw3d30 and SRTM DEMs are very close as compared to other DEMs. These results show that the DEM quality play important role in the extraction of the morphometric parameters.

### 4.3 Comparison Based on the Hypsometric Analysis

Topographical characteristics have a high influence on the hydrologic response of the drainage basin. The hypsometric tool developed by Strahler [7] is popularly used in the field of hydrology. The hypsometric curve and Hypsometric Integral (HI) values which are considered important indicators of the watershed conditions are commonly employed to analyze the topography of the basin [34]. Technically, hypsometry is related to the measurement of the heights. Hypsometric analysis (area-altitude analysis) provides an understanding of the stage of the development of the watershed. The hypsometric curve, which is essentially a graphical representation of the watershed area and elevation, is essentially a normalized cumulative frequency distribution of the elevation [7]. The hypsometric analysis is commonly used to understand the erosion status as well as the runoff potential of the watershed. The shape of the hypsometric curve is an important indicator in the determination of the role of topography in streamflow generation. According to Niyazi et al. [21], the hypsometric curve shape is the best parameter to select the suitable DEM for studying the hydrologic behaviour of the river basin.

The hypsometric integral is the area beneath the curve that relates the percentage of the total relief to the cumulative percentage area. The HI index can be estimated using the elevation-relief ratio method (see Table 2) proposed by Pike and Wilson [35]. Theoretically HI values range between 0 and 1. The HI index is important in identifying either tectonic or erosive forces which are predominant in the determination of the drainage basin shape [36, 37]. Further, due to its dimensionless nature, it is more effective in comparing the catchments and thus accuracy of the DEMs irrespective of their scale.

Figure 5a, b shows the results of the hypsometric curves of the Tawi river basin up to its confluence with Chenab river and up to Sidhra gauging site, Jammu, respectively. From Fig. 5a, it can be seen that the hypsometric curves derived from AW3D30, ASTER and CartoDEM were significantly different from those by SRTM and ALOS PALSAR-RTC DEMs. However, interestingly, there is no much noticeable difference between the hypsometric curves derived from all the five DEMs (Fig. 5b) of the Tawi river basin upstream of the Sidhra gauging site. It can be observed from the

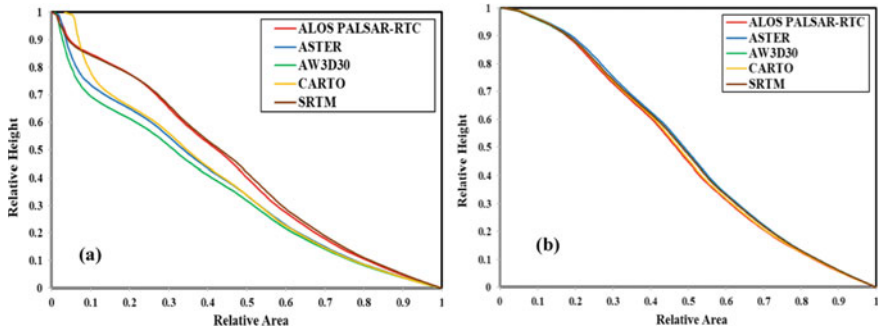


**Fig. 5** Hypsometric curves derived from five selected DEMs of the Tawi river basin, **a** up to its confluence with Chenab river and **b** up to Sidhra gauging site, Jammu

shape of these hypsometric curves that the drainage system of the Tawi river basin is in the younger stage of geomorphometric development.

Figure 6 shows the hypsometric integral values of the 14 sub-watersheds of the Tawi river basin derived from the selected five DEM datasets. From Fig. 6, it can be seen that the HI values derived from the SRTM and ALOS PALSAR-RTC DEMs of the whole Tawi basin were slightly higher as compared to those from other DEMs. However, the HI values of the Tawi basin up to the Sidhra gauging site were approximately the same. These results are confirming the results of hypsometric curves shown in Fig. 5. In the case of the lower Tawi sub-watershed, the HI values derived from AW3D30 DEM are significantly higher as compared to those given by the other DEMs. These results for the lower Tawi sub-watershed are important because in these lower reaches of the Tawi river only AW3D30 DEM following the stream as on the google earth map and is considered to be accurate. Particularly, the HI values derived from four DEMs except for ALOS PALSAR-RTC of the sub-watersheds

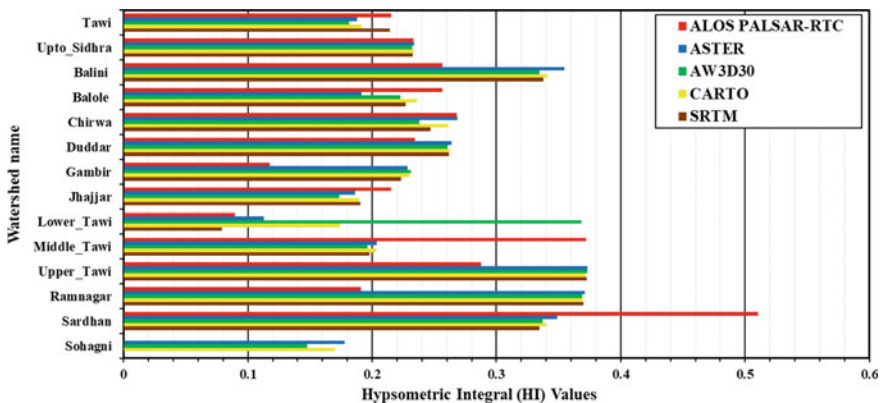


**Fig. 6** Hypsometric integral (HI) values of all the 14 sub-watersheds derived from five selected DEMs of the Tawi river basin up to its confluence with Chenab river

laying upstream of the Sidhara gauging site were very close to each other. From these hypsometric integral (HI) analyses, it can be seen that Ramnagar, Sardhan, Upper Tawi, Balini and lower Tawi sub-watersheds are in the late mature stage of erosion ( $0 < HI < 0.4$ ). The remaining sub-watersheds are in the old stage of erosion ( $0 < HI < 0.3$ ), representing a more incisive fluvial process.

## 5 Conclusions

The hydrologic, hydraulic, geomorphologic and ecohydrological modelling studies are necessary to analyze the impact of climate change on water resources as well as the integrated management of the water resources. However, the accuracy of the digital elevation model (DEM) datasets plays a prominent role in these modelling studies. Now-a-days, open-access global digital elevation datasets are extensively used due to their cost-effectiveness and sparse coverage of sources at relatively high resolution. As these DEM datasets are created using the data captured by various types of onboard sensors at different time periods and are processed using different algorithms, thus, the accuracy of each DEM dataset differs from others. Therefore, the researcher always faces the problem of using appropriate DEM datasets in modelling studies. Therefore, this study deals with the assessment of the accuracies of the available different types of DEMs (ASTER 30 m, SRTM 30 m, ALOS (AW3D30) 30 m, CartoDEM 30 m and ALOS PALSAR-RTC 12.5 m) with different resolutions based on drainage morphometric analysis for the Tawi river basin. This evaluation of the different DEMs derived from various sources provides insight into terrain and morphological characteristics analysis which are useful for hydro-ecological modelling studies.

In this study, the comparison of the stream network and sub-watersheds derived from these selected different DEMs has been carried. It was found that the ALOS World 3D-30 m (AW3D30) DEM is the best DEM for the hydrological and geomorphological study of the Tawi river basin as the stream network extracted from this DEM dataset matching well with those with google earth map and LULC map of the study basin. Results also show that AW3D30DEM data possess high accuracy in the delineation of the river basin followed by the CartoDEM, particularly in the low-lying area. However, the performance of ALOS-RTC DEM is the worst among all the studied DEMs. However, in the mountainous area upstream of the Sidhra gauging sites, the stream network and sub-watershed were derived using ASTER 30 m, SRTM 30 m, ALOS (AW3D30) 30 m, CartoDEM 30 m are approximately the same. The comparison of the drainage morphometric parameters derived from the selected five DEMs is suggesting that the AW3D30 DEM performed very well as compared to other DEM datasets.

Further, the comparison based on the hypsometric analysis has been carried out to assess the accuracies of the selected DEM datasets. The hypsometric curves derived from AW3D30, ASTER and CartoDEM of the whole Tawi basin up to its confluence with Chenab river were significantly different from those by SRTM and ALOS

PALSAR-RTC DEMs. However, there is no much noticeable difference between the hypsometric curves derived from all the five DEMs of the Tawi river basin upstream of the Sidhra gauging site. The shape of these hypsometric curves suggests that the drainage system of the Tawi river basin is in the younger stage of geomorphometric development. Further, the hypsometric integral values computed for 14 sub-watersheds of the Tawi river basin using the selected five DEM datasets are suggesting that the HI values derived from the SRTM and ALOS PALSAR-RTC DEMs of the whole Tawi basin were slightly higher as compared to those from other DEMs. However, the HI values of the Tawi basin up to the Sidhra gauging site were approximately the same. From the computed HI values, it can be concluded that the Ramnagar, Sardhan, Upper Tawi, Balini and Lower Tawi sub-watersheds are in the late mature stage of erosion ( $0 < HI < 0.4$ ). The remaining sub-watersheds are in the old stage of erosion ( $0 < HI < 0.3$ ), representing a more incisive fluvial process. The sub-watersheds at the old stage are in equilibrium and thus less prone to further erosion.

**Acknowledgements** The authors want to thank Dr. J. V. Tyagi, Director, NIH Roorkee and Dr. M. K. Goel, Scientist G and Head and Coordinator for supporting this research work.

## References

1. Clarke JI (1996) *Morphometry from Maps. Essays in geomorphology*. Elsevier, New York, pp 235–274
2. Szypuła B (2017) Digital elevation models in geomorphology. 5th Chapter in: *Hydro-Geomorphology—Models and trends*. Intech, pp 81–112. <https://doi.org/10.5772/intechopen.68447>
3. Pike RJ (2002) A bibliography of terrain modeling (geomorphometry), the quantitative representation of topography—supplement 4.0. USGS, Open File Report 02-465. US Department of the Interior, United States Geological Survey, Menlo Park, California
4. Nautiyal MD (1994) Morphometric analysis of a drainage basin, district Dehradun, Uttar Pradesh. *J Indian Soc Remote Sens* 22(4):251–261
5. Magesh NS, Jitheshlall KV, Chandrasekar N, Jini KV (2012) GIS based morphometric evaluation of Chimmuni and Mupily watersheds, parts of Western Ghats, Thrissur District, Kerala. *India Earth Sci Inf* 5(2):111–121
6. Horton RE (1945) Erosional development of streams and their drainage basins; hydrophysical approach to quantitative morphology. *Bull Geol Soc Am* 56:275–370
7. Strahler AN (1952) Hypsometric analysis of erosional topography. *Bull Geol Soc Am* 63:1117–1142
8. Strahler AN (1964) Quantitative geomorphology of drainage basins and channel networks. In: Chow VT (ed) *Handbook of applied hydrology*. New York, McGraw-Hill, pp 439–476
9. Muller JE (1968) An introduction to the hydraulic and topographic sinuosity indexes. *Ann Assoc Am Geogr* 58:371–385
10. Shreve RW (1969) Stream lengths and basin areas in topologically random channel networks. *J Geol* 77:397–414
11. Ohmori H (1993) Changes in the hypsometric curve through mountain building resulting from concurrent tectonics and denudation. *Geomorphology* 8:263–277

12. Oguchi T (1997) Drainage density and relative relief in humid steep mountains with frequent slope failure. *Earth Surf Process Land* 22:107–120
13. Hurtrez JE, Sol C, Lucazeau F (1999) Effect of drainage area on hypsometry from an analysis of small-scale drainage basins in the Siwalik hills (central Nepal). *Earth Surf Process Land* 24:799–808
14. Dikpal RL, Renuka Prasad TJ, Satish K (2017) Morphometric analysis and sub-watershed prioritization of Welmal watershed, Ganale-Dawa River Basin, Ethiopia: implications for sediment erosion. *Appl Water Sci* 7:4399–4414
15. Prabhakaran A, Jawahar Raj N (2018) Drainage morphometric analysis for assessing form and processes of the watersheds of Pachamalai hills and its adjoining, Central Tamil Nadu, India. *Appl Water Sci* 8–31
16. Horton RE (1932) Drainage basin characteristics. *Trans Am Geop Union* 14:350–361
17. Summerfield MA, Hulton NJ (1994) Natural controls of fluvial denudational rates in major world drainage basins. *J Geophys Res* 99(B7):13871–13883
18. Morris DG, Heerdegen RG (1988) Automatically-derived catchment boundaries and channel networks and their hydrological applications. *Geomorphology* 1:131–141
19. Lindsay JB, Evans MG (2008) The influence of elevation error on the morphometrics of channel networks extracted from DEMs and the implications for hydrological modelling. *Hydrol Process* 22(11):1588–1603
20. Wilton JP, Aggett G, Deng Y, Lam CS (2008) Water in the landscape: a review of contemporary flow routing algorithms. In: Zhou Q, Lees B, Tang G (eds) *Advances in digital terrain analysis. Lecture notes in geof ormation and cartography series, vol 3*. Springer, Berlin, pp 213–236
21. Niyaji B, Zaidi S, Masoud M (2019) Comparative study of different types of digital elevation models on the basis of drainage morphometric parameters (Case Study of Wadi Fatimah Basin, KSA). *Earth Sys Environ*. <https://doi.org/10.1007/s41748-019-00111-2>
22. Sharma S, Mahajan AK (2020) GIS-based sub-watershed prioritization through morphometric analysis in the outer Himalayan region of India. *Appl Water Sci* 10:163. <https://doi.org/10.1007/s13201-020-01243-x>
23. Mahala A (2020) The significance of morphometric analysis to understand the hydrological and morphological characteristics in two different morpho-climatic settings. *Appl Water Sci* 10:33. <https://doi.org/10.1007/s13201-019-1118-2>
24. Dragut L, Schauppenlehner T, Muhar A, Strobl J, Blaschke T (2009) Optimization of scale and parametrization for terrain segmentation: an application to soil-landscape modeling. *Comput Geosci* 35(9):1875–1883
25. Saran S, Sterk G, Peters P, Dadhwal VK (2010) Evaluation of digital elevation models for delineation of hydrological response units in a Himalayan watershed. *Geocarto Int* 25:105–122. <https://doi.org/10.1080/10106040903051967>
26. Singh P, Gupta A, Singh M (2014) Hydrological inferences from watershed analysis for water resource management using remote sensing and GIS techniques. *Egypt J Remote Sens Sp Sci* 17:111–121
27. Bhatt S, Ahmed SA (2014) Morphometric analysis to determine floods in the Upper Krishna basin using Cartosat DEM. *Geocarto Int* 29(8):878–894. <https://doi.org/10.1080/10106049.2013.868042>
28. Alganci U, Besol B, Sertel E (2018) Accuracy assessment of different digital surface models. *ISPRS Int J Geo-Inf* 7:114. <https://doi.org/10.3390/ijgi7030114>
29. Nikolakopoulos KG (2020) Accuracy assessment of ALOS AW3D30 DSM and comparison to ALOS PRISM DSM created with classical photogrammetric techniques. *Eur J Remote Sens* 1–14. <https://doi.org/10.1080/22797254.2020.1774424>
30. Jain AO, Thaker TK, Chaurasia A, Patel P, Singh AK (2017) Vertical accuracy evaluation of SRTMDEM-GL1, GDEM-V2, AW3D30, and CartoDEM-V3.1 of 30m resolution with dual frequency GNSS for Lower Tapi Basin India. *Geocarto Int*. <https://doi.org/10.1080/10106049.2017.1343392>
31. Singh P, Thakur JK, Singh UC (2013) Morphometric analysis of Morar River Basin, Madhya Pradesh, India, using remote sensing and GIS techniques. *Environ Earth Sci* 68(7):1967–1977



32. Schumm SA (1956) Evolution of drainage system and slope in badlands of Perth Amboy, New Jersey. *GSA Bull* 67:597–646
33. Miller VC (1953) A quantitative geomorphic study of drainage basin characteristics in the Clinch Mountain area, Virginia and Tennessee. Project NR, Technical report 3, Columbia University, Department of Geology, ONR, Geography Branch, New York, pp 389–442
34. Ritter DF, Kochel RC, Miller JR (2002) *Process geomorphology*. McGraw Hill, Boston, USA
35. Pike RJ, Wilson SE (1971) Elevation-relief ratio, hypsometric integral and geomorphic area—altitude analysis. *Geol Soc Am Bull* 82:1079–1084
36. Gopinath G, Swetha TV, Ashitha MK (2014) Automated extraction of watershed boundary and drainage network from SRTM and comparison with Survey of India toposheet. *Arab J Geosci* 7(7):2625–2632
37. Girish G, Ambili GK, Jesiya NP, Lemoon K (2016) Hydro-hypsometric analysis of tropical river basins, southwest coast of India using geospatial technology. *J Mt Sci* 13(5):939–946

# Comparison of HEC-HMS and SWAT Hydrological Models in Simulating Runoff at Machhu River Catchment, Gujarat, India



Kishanlal Darji, Dhruvesh Patel, and Indra Prakash

**Abstract** It is important in the hydrological study to correctly predict runoff in the river catchment for designing the civil engineering structures for irrigation, hydropower, flood control and erosion control. In this regard, several models have been developed by different researchers based on the precipitation and characteristics of the catchment for the estimation of runoff. However, selection of an appropriate model is essential considering its robustness and wide applicability in different topographical, geological, geo-environment and climate conditions. With this objective, we have applied two hydrological models namely Hydrologic Modelling System (HEC-HMS) and Soil and Water Assessment Tool (SWAT) at the Machhu River Catchment, Gujarat, India to estimate accurate runoff. In this study, hydrological data of 37 years period (1982–2017) was used for the simulation of models. Validation of the models was done using observed runoff data of Macchu dam-I. Regression analysis  $R^2$  ( $R$ -squared) of the observed and estimated runoff data was done to compare and evaluate the performance of the models. Results showed that  $R^2$  value for the HEC-HMS model was 0.89, whereas of the SWAT model 0.62 thus, the runoff prediction performance of the HEC-HMS model is better than the SWAT model. Therefore, HEC-HMS model can be used for the accurate estimation of runoff considering local geo-environmental and meteorological conditions in other catchments also for proper planning and management of the watershed.

**Keywords** Rainfall-runoff · HEC-HMS · SWAT · Regression analysis · HSG · Hydrological models

---

K. Darji (✉) · D. Patel

Civil Engineering Department, School of Technology, PDPU, Gandhinagar, Gujarat, India

D. Patel

e-mail: [dhruvesh.patel@sot.pdpu.ac.in](mailto:dhruvesh.patel@sot.pdpu.ac.in)

I. Prakash

Geological Survey of India, Gandhinagar, Gujarat, India

## 1 Introduction

Estimation of runoff of a river catchment plays a principal task in watershed management such as flood prediction, water quality management, hydropower production, land use planning and industrial development [1, 2]. Nowadays, rapid industrialization and population growth especially in developing countries like India require accurate estimation of runoff of river basins for optimum utilization of surface water resources in conjunction with ground water for the development of a region [3, 4].

With the advancement of technology, computer models that simulate hydrologic runoff processes are important tools to understand overall hydrologic cycle [5, 6]. Many hydrological and hydrodynamical models have been developed by researchers to simulate watershed and river hydrologic behaviour for better watershed management [7, 8]. These hydrological models include Agricultural Non-Point Source (AGNPS), Hydrological Engineering Centre—The Hydrologic Modelling System (HEC-HMS), Hydrological Simulation Program-Fortran (HSPF), System Hydrology European (MIKE SHE) and Soil and Water Assessment Tool (SWAT) [7]. These models help in water management, soil erosion, water quality assessment, land use land cover changes, flood inundation studies and many other forecasting applications. The success of current model development and subsequent hydrologic prediction lies in the proper selection of model input parameters [9]. The effects of spatial variability in precipitation, vegetation, topography, land use pattern and soils are to be considered in the models [10].

Main aim of the paper is to evaluate the performance of HEC-HMS and SWAT models in simulating runoff of Machhu River catchment (Gujarat, India) for the selection of the best suitable model for hydrological modelling of a river basin.

## 2 Study Area

Machhu River starts from Chotila hills of Surendranagar region, Gujarat at an altitude of 220 m (m.s.l). The Machhu basin is located between 22°10' to 23°10' North latitude and 70°40' to 71°15' East longitude. It flows in north westerly direction and debouches near Malia in the little Rann of Kachchh. This river with its tributaries flow 52% in the hilly area and 48% in plain region. Machhu drains an area of 2515 km<sup>2</sup>. Total span of Machhu river from its starting point to its outlet is 141.75 km [11]. In the Machhu River basin, three irrigation dams namely Machhu I, II and III are located across Main River (Fig. 1).

Climate of the area is semi-arid type. The monsoon season is from mid-June to early October. Average rainfall in the Machhu River catchment area is 533.5 mm, Average Maximum temperature is 41 °C and Average Minimum Temperature is 14 °C (<http://cwc.gov.in>). Land use patterns in the area include agriculture, built-up, forest, grass land, waste land and water bodies (Fig. 3). Geologically the area is occupied mainly by Deccan basalt rocks except in the lower reaches of the river

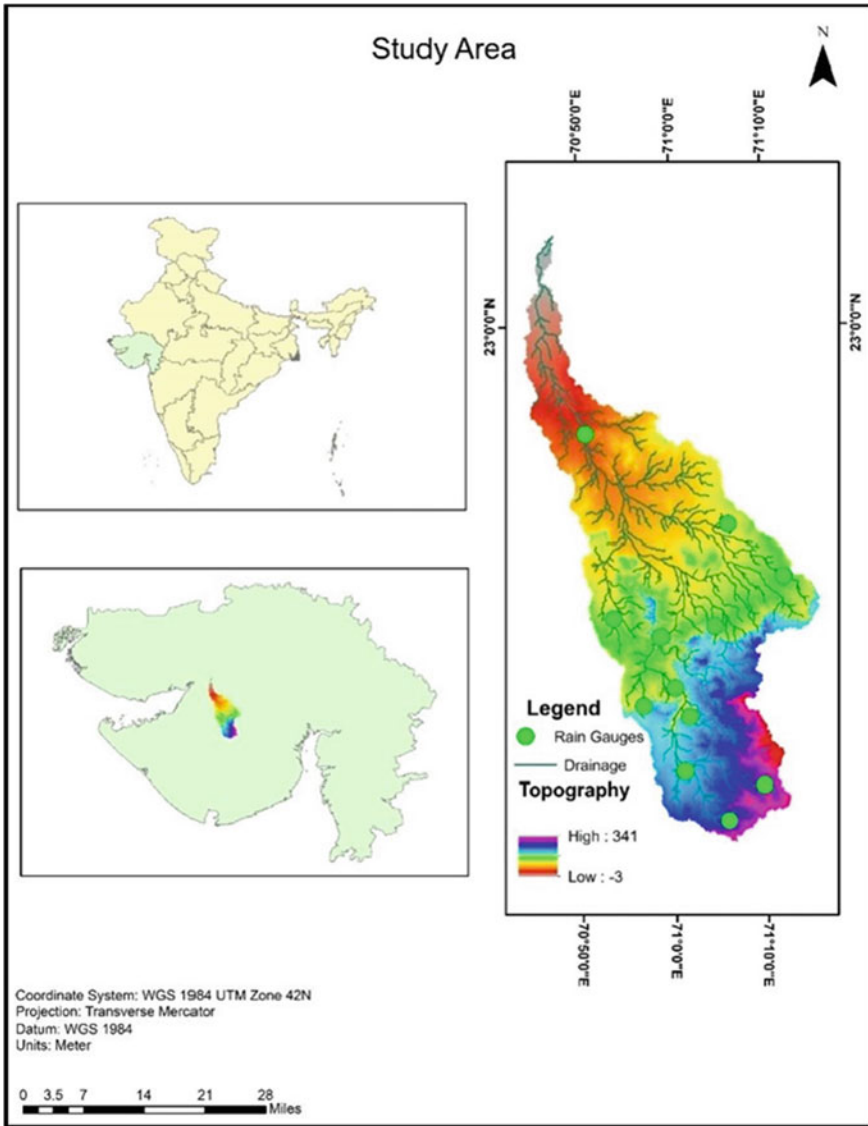


Fig. 1 Study area map of machhu river basin

where Dhrangadhra Sandstone is exposed and alluvium along the river valleys. Soil exposed in the catchment area belongs to Hydrological Soil group (HSG) C (clayey, clayey skeletal and fine loamy) and B (loamy and loamy skeletal) (Fig. 2).

### 3 Data Collection and Analysis

Meteorological data of the Machhu river basin was obtained from the State (SWDC) [11] and central (IMD) (<http://www.imd.gov.in/>) agencies. Thematic maps (topography, land cover, geology and soil) were prepared from the published literature [12, 13] in conjunction with the interpretation of the Landsat images, Google earth images and Aster DEM using remote sensing and GIS technology. Analysis of the data was done using HEC-HMS and SWAT models (Figs. 2, 3, 4 and 5).

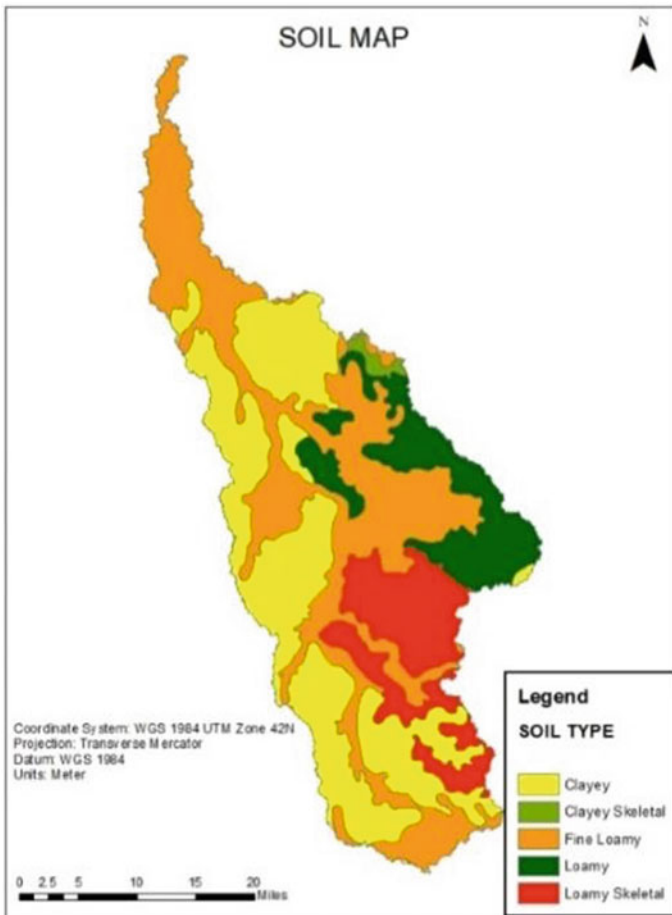


Fig. 2 Soil map of Machhu Basin

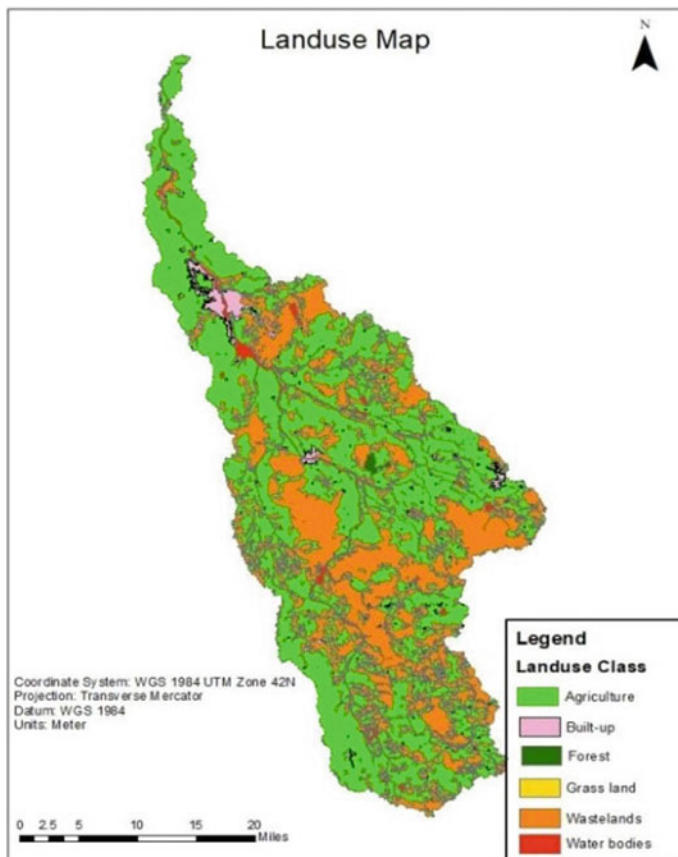


Fig. 3 Landuse map of Machhu Basin

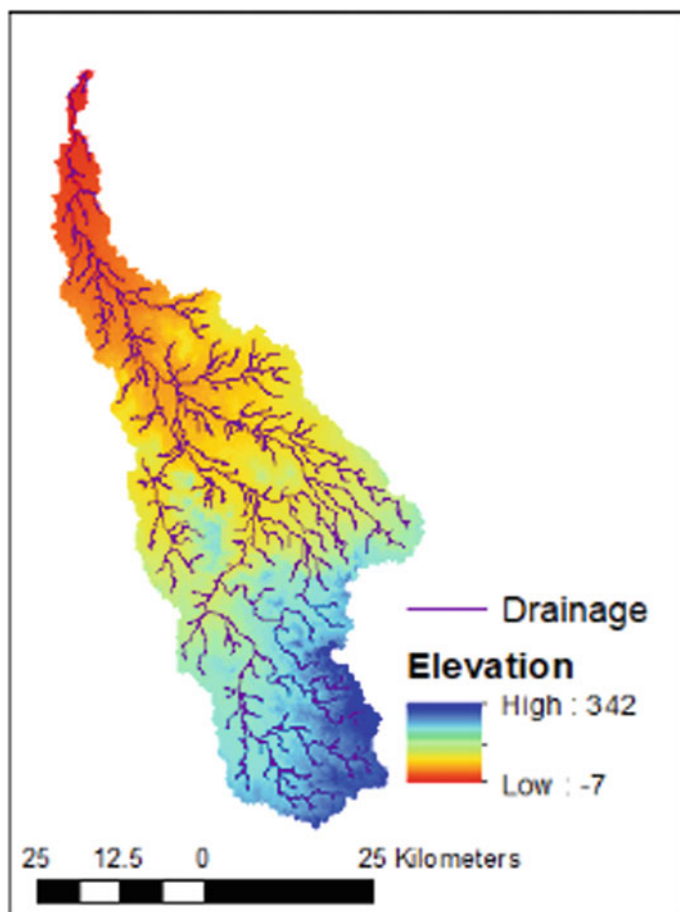


Fig. 4 Topography map of Machhu Basin

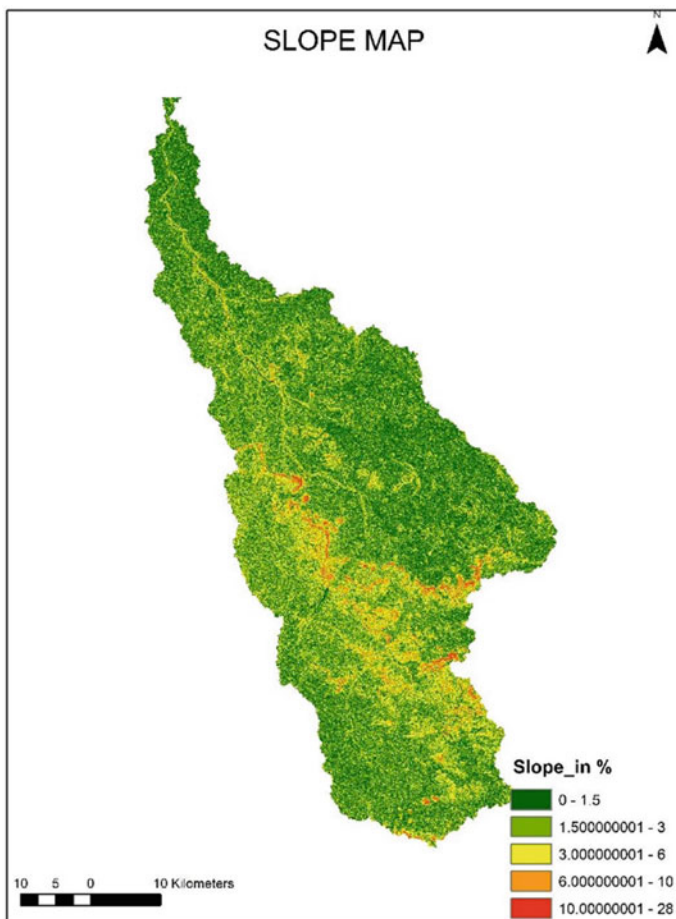


Fig. 5 Slope map of Machhu Basin



### 4 Methodology

Runoff of Machhu dam was estimated using HEC-HMS and SWAT models. Methodology adopted in this study is summarized below (Fig. 6).

Following is a summary of the main steps of HEC-HMS methodology adopted in the present study:

- Created river basin model from DEM, Loss method (Initial and constant) using HEC-geoHMS tool in Arc GIS.

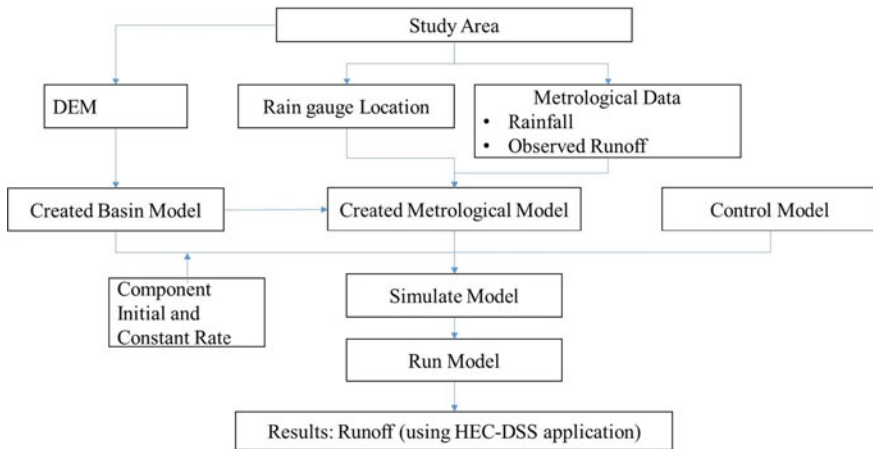


Fig. 6 HEC-HMS methodology flow diagram

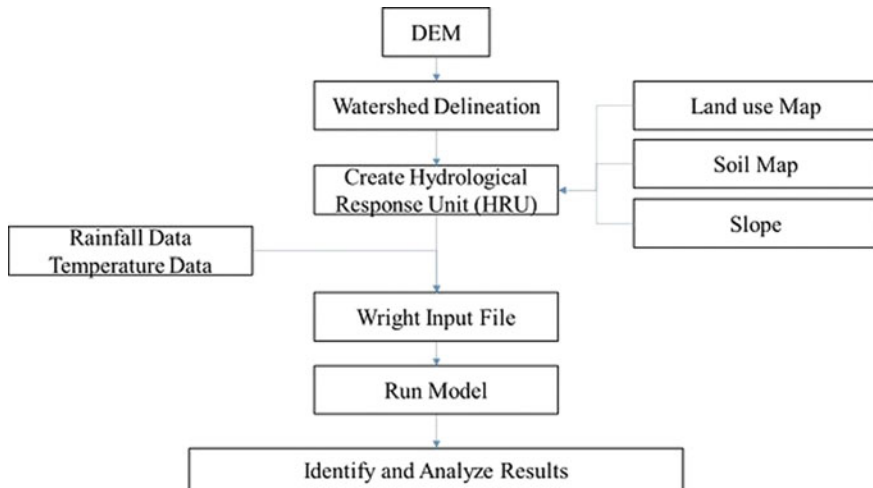


Fig. 7 SWAT model methodology flow diagram

- Created Metrological Model from precipitation data of rain gauges situated in the basin using HEC-geoHMS. Integrated basin and metrological models prepared above in HEC-HMS.
- Inputted time-series rainfall data (Precipitation) in HEC-HMS model.
- Created Control Model to provide simulation data.
- Created Simulation Runoff model by integrating basin, metrological and control models.
- Running of simulation Model.
- Analysis of Result Using HEC-DSS (Data Storage System) Application to obtain Runoff.

The HEC-DSS method was applied to analyze model results for obtaining runoff of the catchment.

### Steps for Running SWAT Model

- Created new project and input DEM tiff file
- Basin and sub-basins were delineated using Automatic Watershed Delineation tool of the SWAT
- Created hydrological response unit of Soil map
- Applied different thematic maps (Land cover, Slope and Soil) of Catchment in the models for the analysis
- Inputted weather data (Rainfall data) and Rain gauge Locations
- Created table for input parameters
- Running of the SWAT model to apply simulation Start and End date and Identify Result: Estimated Runoff value.

Validation of the models was done using observed runoff data of Macchu dam-I using statistical measures and performance of the models was evaluated by Regression analysis  $R^2$  ( $R$ -squared) of the observed and estimated runoff (Fig. 7).

## 5 Model Results

Average rainfall and estimated runoff of the Machhu River catchment was estimated using HEC-HMS and SWAT models.

### 5.1 Average Rainfall

Average rainfall is the quantity of precipitation received per annum. This is a means of rainfall noted in an area during several years. Annual rainfall or precipitation is the sum of daily rainfall in a year. Average rainfall was estimated for Machhu basin using HEC-HMS and SWAT by inputting 12 rain gauges daily Rainfall Data from

1982 to 2017 into the model process. Annual average Rainfall of Machhu basin was calculated by sum of daily rainfall in the particular year as shown in Figs. 8 9 and 10. Analysis of meteorological data of the Machhu River catchment for the period 1982–2017 indicated that the average annual rainfall differs during this period annually between 47 mm in year 1987 and 1058 mm in year 2017 as per HEC-HMS Model and 51 mm in year 1987 and 1137 mm in year 2017 as per SWAT Model.

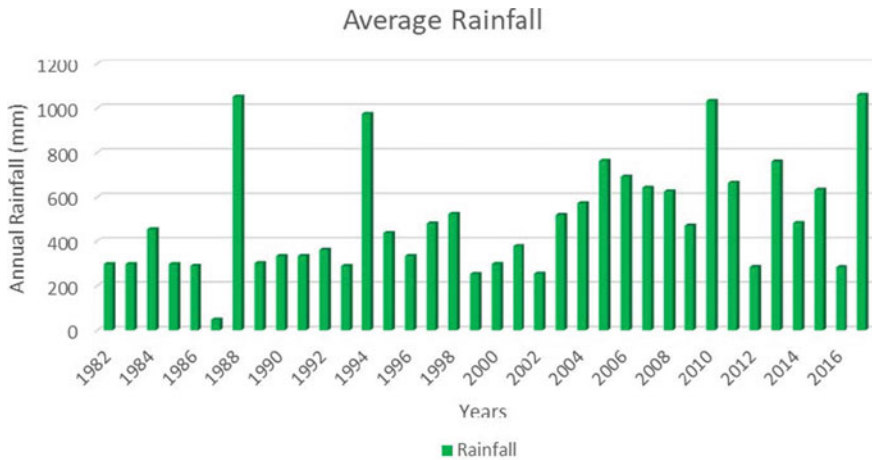


Fig. 8 Average rainfall as per HEC-HMS model

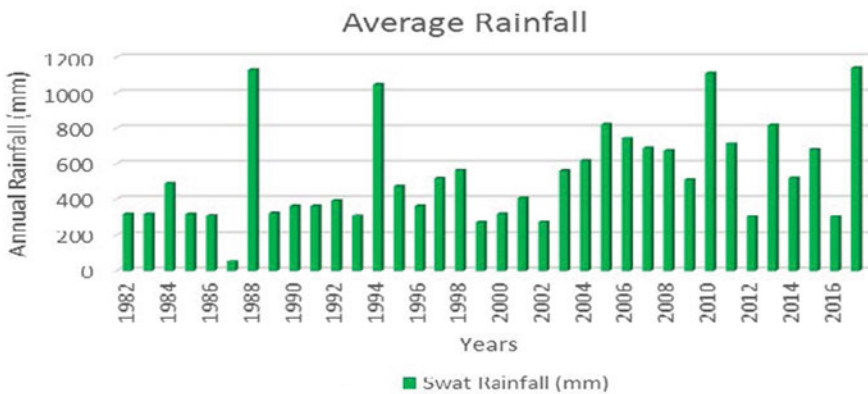


Fig. 9 Average rainfall as per SWAT model

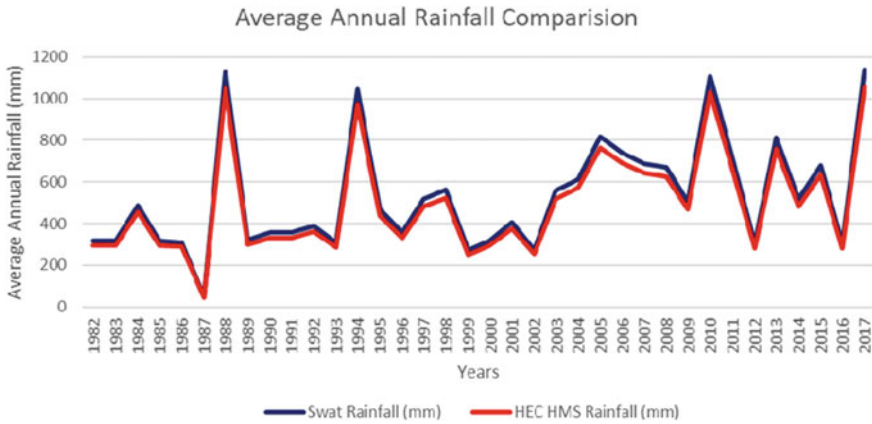


Fig. 10 Comparison of result of average rainfall calculated by SWAT and HEC-HMS models

### 5.2 Estimation of Runoff

Estimation of Runoff was done using HEC-HMS and SWAT Model and correlated with the rainfall data. Analysis of the runoff data indicates that that annual runoff during this period varies from 1 mm in year 1987 to 578 mm in year 1988 as per HEC-HMS model and 1 mm in year 1987–758 mm in year 1988 as per SWAT model. Rainfall and Runoff pattern is wavy indicating an increase and decrease of runoff depending on the rainfall. However, during the period 1985–1987, negligible to very less runoff has been observed corresponding to the rainfall. It is due to the fact that rainfall during this period was very less, hence most of the initial precipitation was absorbed in the ground before starting runoff. This corroborates the study of the other workers [14] (Figs. 11, 12 and 13).

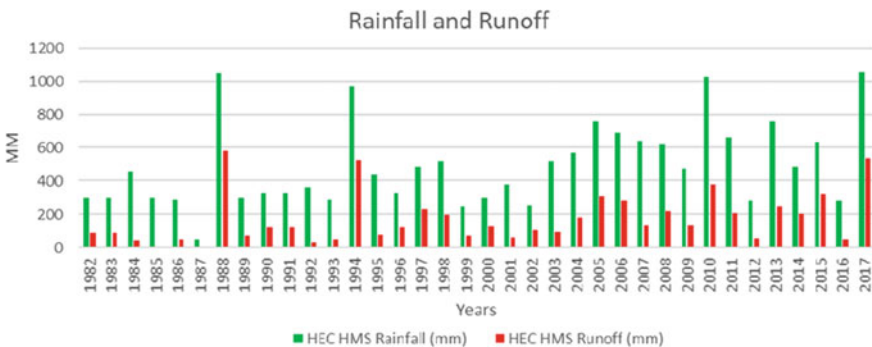


Fig. 11 Comparison of rainfall with estimated runoff obtained from HEC-HMS model

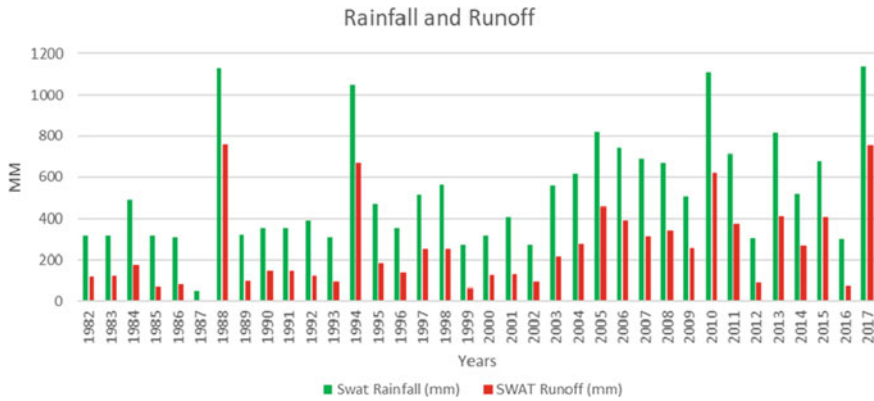


Fig. 12 Comparison of rainfall with estimated runoff obtained from SWAT model

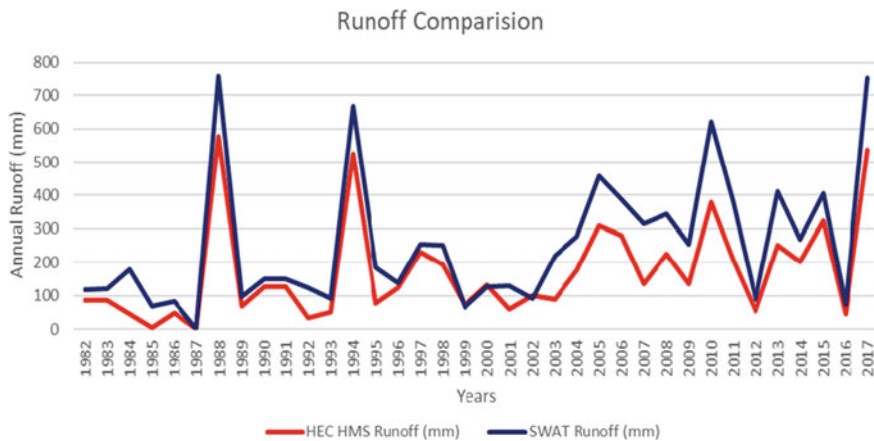


Fig. 13 Comparison of estimated runoff obtained from HEC-HMS and SWAT models

### 5.3 Evaluation of Rainfall-Runoff Relation

The relation between precipitation and surface runoff is complicated as it depends on many factors linking to the watershed and meteorology. Evaluation of the rainfall-runoff was done by the regression analysis. Following equation was obtained by regression analysis for the estimation of runoff (Y) of the Macchu catchment for given precipitation (X) (Figs. 14 and 15):

$$Y(\text{mm}) = 0.5396 * X(\text{mm}) - 95.808 \text{ As per HEC HMS model}$$

$$Y(\text{mm}) = 0.7218 * X(\text{mm}) - 129.47 \text{ As per SWAT model}$$

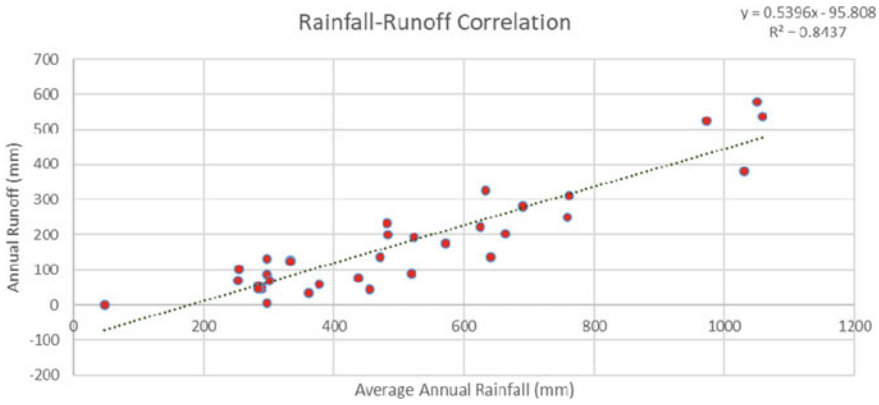


**Fig. 14** Rainfall-runoff correlation using HEC-HMS results of regression analysis:  $R^2$

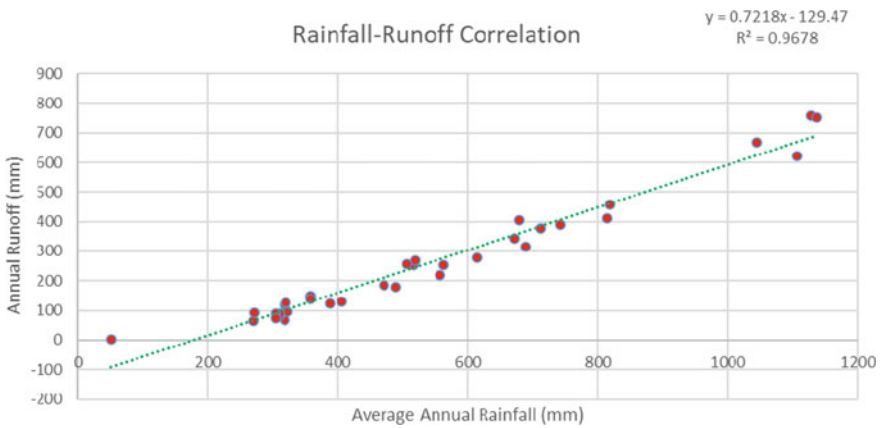


**Fig. 15** Rainfall-runoff correlation using SWAT results of regression analysis:  $R^2$

In this study,  $R^2 = 0.85$  as per HEC-HMS Model and  $R^2 = 0.97$  as per SWAT Model. These values mean that 85 and 97% of the total variation in the estimated runoff data can be correlated with the observed rainfall data, thus it can be considered a good correlation.

### 5.4 Evaluation of Performance of Models

Performance of the models was assessed by the regression study of the observed and simulated data of the runoff at Machhu Dam 1. The coefficient of determination is a degree of how well the regression curve /line expresses the data. Results of the regression analysis gave the coefficient of determination ( $R^2$ ) values equal to 0.89

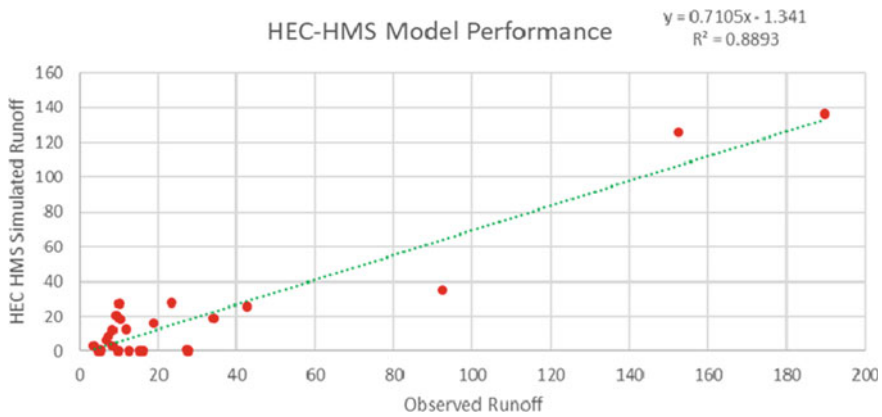


**Fig. 16** Performance evaluation of the HEC-HMS model using regression method

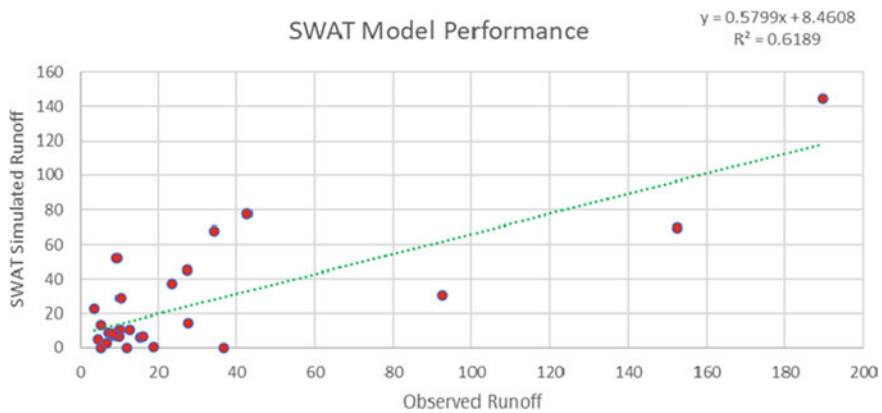


**Fig. 17** Performance evaluation of the SWAT model using regression method

and 0.62 for HEC-HMS and SWAT Model, respectively which is a good prediction value ( $0 < R^2 < 1$ ). It signifies the percent of the information which is the closest to the line of greatest match (Figs. 16 and 17).

That is  $R^2$ : 0.89 and 0.62 means that 89 and 62% of the total variation in simulated data can be correlated with the observed data.

## 6 Concluding Remarks

The principal aim of the analysis was to evaluate performance of two well-known hydrological models namely HEC-HMS and SWAT for the selection of one of the best simple models for accurate prediction of runoff. Machhu River catchment in

Gujarat was selected for the model study. Estimated runoff values were compared with observed values at Machhu dam-I. Regression analysis of rainfall-runoff data of the model's results indicated that both the model performed well but the prediction capability of the HEC-HMS model ( $R^2 = 0.89$ ) is the best in comparison to SWAT model ( $R^2 = 0.62$ ).

Therefore, HEC-HMS model can be used for the estimation of accurate runoff requiring relatively less input data, thus it is also suitable for data scarce regions. Results of this analysis showed that the proposed model performance is good even for large size watershed ( $>250 \text{ km}^2$ ). Limitation of the study is that climate change effect has not been considered in the models study.

## References

1. Darji K, Khokhani V, Dr. Prakash I, Mehmood K, Pham BT Rainfall-runoff modelling using HEC-HMS model: an application of regression analysis. *J Emerging Technol Innov Res* 6(5):226–234
2. Nguyen DT, Nguyen TQN (2014) Using HEC-HCM model to simulate the design floods for hydropower reservoirs in the Vu Gia—Thu Bon River System. *Univ Danang J Sci Technol* 5(78):91–95
3. Chow VT, Maidment DK, Mays LW (2002) *Applied hydrology*. McGraw-Hill Book Company, New York, USA
4. Kalin L, Hantush MM (2006) Hydrologic modeling of an Eastern Pennsylvania watershed. *J Hydrol Eng* 11:555–569. <https://doi.org/10.1061/ASCE1084-0699200611:6555>
5. Skinner C, Bloetscher F, Pathak C (2009) Comparison of NEXRAD and rain gauge precipitation measurements in South Florida. *J Hydrol Eng* 14:248–260
6. Dao NK (2012) Evaluating the impacts of climate change on streamflow in Srepok watershed. *VNU-HCM J Sci Technol Dev* 15(M2):18–32
7. Dogan S, Berktaş A (2008) Comparative study between various hydrological models for watershed management: robustness and suitability. *Ecol Environ Protect*
8. Dao NK, Chau NXQ (2015) Assessment of water resources in the Dong Nai River Basin. *Sci Technol J Agric Rural Dev* 5:54–59
9. Khoi DN (2016) Comparison of the HEC-HMS and SWAT hydrological models in simulating the streamflow. *J Sci Technol* 53(5A):189–195
10. Solanki VK, Bhatt N, Prakash I, Darji K, Pham BT (2019) Application of SWAT model in the estimation of runoff and sedimentation of Watrak River Basin, North Gujarat, India. *J Emerging Technol Innov Res* 6(5):556–566
11. <https://swhydrology.gujarat.gov.in>
12. <https://www.gsi.gov.in/>
13. <http://cgwb.gov.in/>
14. Subramanya K (2017) *Engineering hydrology (Book)*. TATA McGraw Hill Education Private Limited, New Delhi, India
15. Gajjar D, Darji K, Patel D, Prieto C, Han D (2018) A comparative study of delineated watershed through ASTER, SRTM and ALOS for evaluating morphological changes in Hathmati Basin, Gujarat, India (Abstract). *Euro. Geosci. Union* 20:2083
16. IMSD (1995) *Technical guidelines, integrated mission for sustainable development, national remote sensing center (NRSC)*. Department of Space, Government of India (1995)
17. USDA (1986) *Urban hydrology for small Watersheds, TR-55*. United States Department of Agriculture, pp 1–164



18. USDA (1972) Soil conservation service, national engineering handbook. Hydrology. Section 4. Chapters 4–10
19. US Army Corps of Engineers—Hydrologic modeling system HEC-HMS User’s manual version 4.0.

# Flood Hazard Assessment of Baitarani River Basin Using One-Dimensional Hydrodynamic Model



Aman Kumar and K. C. Patra

**Abstract** The research work concentrates over the use of imagery and topography, based on remote sensing in a GIS plat form for Baitarani River's integrated flood analysis, which is one of the most flood-prone zones in India. For flood data from 2001 to 2018, flood frequency analysis is performed. The work has been carried out using the maximum flood for the year 2015 with value of 7688 m<sup>3</sup>/s discharge. The current work uses a methodology that combines the HEC-RAS and Arc-GIS application tools for better vision of flood monitoring analysis, which is a non-structural measure of flood management system. The work is sorted in three phases; in the first preparation phase, TIN generation has been done from the DEM with other initial modifications; while in the second execution phase, pre-processing on HEC-GeoRAS Tool is carried out, and data is exported to the HEC-RAS for computing the water surface profiles for the unsteady flow. In the third phase, flood depth and its extent for the flood hazard analysis are done. The recommendations from this study are; either to increase height of banks or construct a retaining wall at certain sections in the downstream part of Jajpur town in Odisha state.

**Keywords** HEC-RAS · HEC-GeoRAS · Arc-GIS · Flood hazard analysis

## 1 Introduction

Natural disasters, as we know are the outcomes of events caused by natural hazards that exceed the capability of local intervention and adversely affect a Nation's socio-economic development. The most recurrent, widespread, calamitous and common natural hazards in the world are probably the floods affecting people at large. There have been 17 floods, 5 severe cyclones and 11 droughts in the last 24 years in Odisha state. On an average, Odisha suffers Rs. 3000 crores of financial loss in each year

---

A. Kumar (✉) · K. C. Patra  
Civil Engineering Department, NIT Rourkela, Rourkela 769008, India

K. C. Patra  
e-mail: [kcpatra@nitrkl.ac.in](mailto:kcpatra@nitrkl.ac.in)

due to natural calamities, which is not only massive, but also severely stresses the state's economy. The average State rainfall is 1451.2 mm. Approximately 75–80% per cent of the rainfall is received in the months of June to September, which causes remarkable damage to both crops and lives. Baitarani River floodwaters submerge over 40 villages in Jajpur Blocks of Jajpur district affecting some 22,000 residents. The water level in the Baitarani rises to 5.5 m as against the danger mark of 5.4 m at Akhuapada gauging station, very frequently.

After reviewing these flood effects, two types of flood management measures are proposed by the river authorities, i.e. structural and non-structural methods. The structural method, construction of embankments, levees, spurs and others have not proved to be completely successful in the long runs. In the non-structural approach, flood risk maps are prepared using a hydrological-hydraulic method, where in the flood depth, flood duration and flood area are computed with peak discharge of a specific return period. Various numerical models have been developed for flood plain delineation, flood inundation and simulation that could be used as a means to delineate flood plain zones adjacent to rivers and quantify the associated danger by taking into account the potential floods of different return periods.

In the past, the hydrodynamic modelling approach was adopted by various researchers to simulate flood inundation in the flood plain zones. Different arithmetical models have been proposed for floodplain delineation/flood inundation and flow modelling that can be instrumental to delineate floodplain areas adjoining the rivers and to quantify the associated risk or possibility, by taking into account the simulated floods with different periods of return.

Flood analysis helps in administering the prevention and prediction of flood occurrences. Modelling performed through computer techniques has supported the engineers and researchers with regulating more accurately by precisely defining the location and time of the flooding. Computer models for the assessment of impact of floods use the following four steps:

1. Hydrological modelling in which, from the past flow records, determination of the rainfall-run off relationship is developed.
2. Hydraulic modelling, which assist the runoff propagation through river/channel and generation of water surface profiles in a tabular and graphical form at a particular location across the cross section.
3. Floodplain mapping and monitoring devices.
4. Extraction of geospatial data.

Many of the techniques in hydraulic modelling use one-dimension tools of steady-state flow measured at a particular time. Since flows in streambeds are naturally random and unsteady, steady-state methods do not often show water surface profiles precisely [10].

Agrawal [2] had successfully studied steady and unsteady flow for Dudhuna river and prepared a 3D view of perceptive plot for single discharges for the given study area. The performance of calibrated model has been verified from the observed discharges from dam.

Patel et al. [9] developed a model that can be used to predict water levels along the river reach from Ichhapur to Dhamdachha village for different water flows conditions. Flood inundation area for the years 1984, 1994 and 2004 has been assessed and investigated that dykes breaching was the major causes of the flood events. Hence, it was recommended to improve the carrying capacity of Ambica River which could help to minimize the flood in surrounding of Navsari city.

HEC-RAS is a tool used by hydraulic engineers which are used to analyse water flow through channel and river and floodplain control [12]. HEC-RAS is a one-dimensional steady flow hydraulic modelling approach that is used by many government agencies. With the help of HEC-RAS, simulating water surface profile for steady flow is simple that quantify the effect of any obstructions such as over bank region, weir, bridges and culverts. HEC-RAS is used to predict the flood inundation maps for a given flood [8]. A combination of Arc-GIS and HEC-RAS tools is used to create flood plain maps using river geometry, historical flood records, river discharge records and channel roughness.

The objective of the study is to implement a one-dimensional hydrodynamic model for the Baitarani river basin between Anandpur Barrage to Jajpur using HEC-RAS (5.0.5) modelling software for the flood hazard analysis.

## 2 Study Area and Data Collection

### 2.1 Study Area

Baitarani River basin has a total catchment area of 14,218 km<sup>2</sup> spreading over the two states of Odisha and Jharkhand in India. A major portion of the river basin with 13,482 km<sup>2</sup> of catchment lies in the state of Odisha while Jharkhand have the rest of 736 sq. km. The river originates at the Gonasika/Guptaganga hills at 21° 32'20" N-85°30'48" E, and it begins to flow over a stone which looks like the nostril of the cow. The river at its origin has the elevation of 900 m (3000 ft) above sea level. The river traverses a total length of 360 km from its sources at Gonasika until it flows into the Bay of Bengal at the mouth of Dhamra near Chandabali after joining the Brahmani River. This river has a total of 65 tributaries, some of which are the major tributaries of the Baitarani River, Deo, Kanjhari, Kusei and Salandi [6].

The stretch of Baitarani River, considered in the study, is from Anandapur barrage (21° 13'35" N-86°07'00" E) to the Jajpur (2°51'19" N-86°25'13" E) which is witnessing frequent floods over the years. Its total length is 64.3 km from Anandapur barrage to Jajpur and is considered for 1D hydraulic modelling and mapping for flood inundation. Nearly 90% of the basin receives average annual rainfall between 1400 and 1600 mm. The analysis of rainfall indicates that the average annual rainfall in the basin is 1442.53 mm [7].

The basin is also rich in forest which constitutes around 34.36% of the total area. The forest class includes evergreen, deciduous and scrub forest. The Odisha State

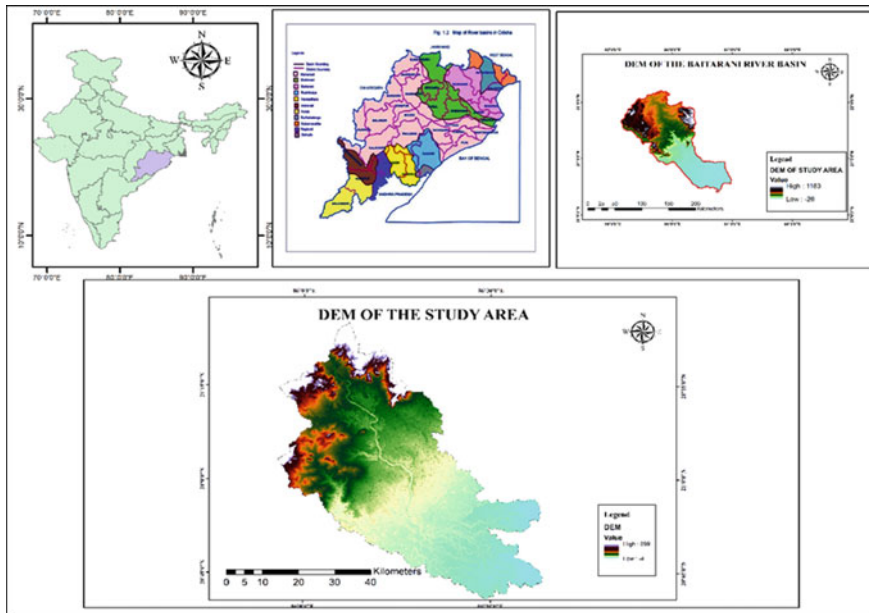


**Fig. 1** Location map of the study area

Government designates forests based on density requirements. About 538160 km<sup>2</sup> of land is categorized as quite dense forest with a canopy density of more than 70%, 27,656 km<sup>2</sup> of forests are categorized as relatively dense cover with a canopy density of 40–70% and 20,180 km<sup>2</sup> are identified as open forest with a canopy density of 10 to 40%. Major cropping pattern found in the region is Kharif [paddy (77%), vegetables (9%), oil seeds (5%), pulses (6%), fibres (2%) and species (1%)], while the Rabi crops include pulses (44), oil seeds (19%), vegetables (23%), spices (5%), sugarcane (1%) and paddy (8%). The current research location map is shown in Fig. 1.

## 2.2 Flood Frequency of Study Area in Baitarani River

Rainfall data used for this research work has been collected from the office of Central Water Commission (CWC), Bhubaneswar, Odisha. From the last 18 years of records, it is noted that severe flood events have occurred in 2009, 2012 and 2015, leading to immense damage to property and lives in the catchment. Year-wise maximum discharge in the study area is shown in Fig. 2. On 5 August 2015, the Baitarani river basin had very heavy rainfall in its catchment with 7688.5 m<sup>3</sup>/s discharge which is maximum among all the discharges from the year 2001–2018. Figure 3 depicts the inflow hydrograph used in the hydrodynamic model as an upstream boundary condition.

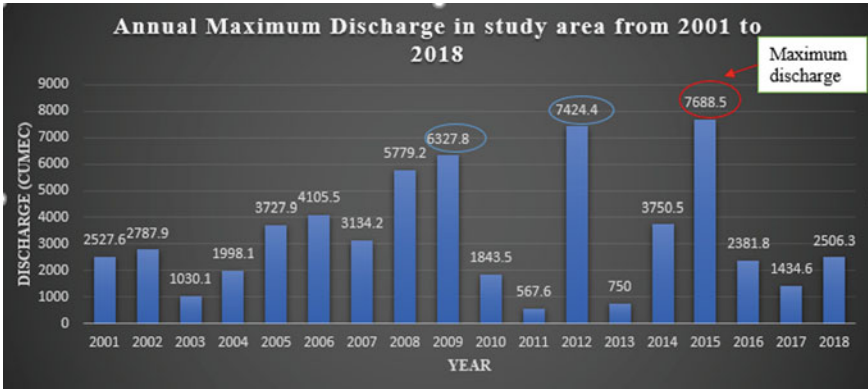


Fig. 2 Year-wise maximum discharge in Baitarani River at Anandpur barrage (upstream)

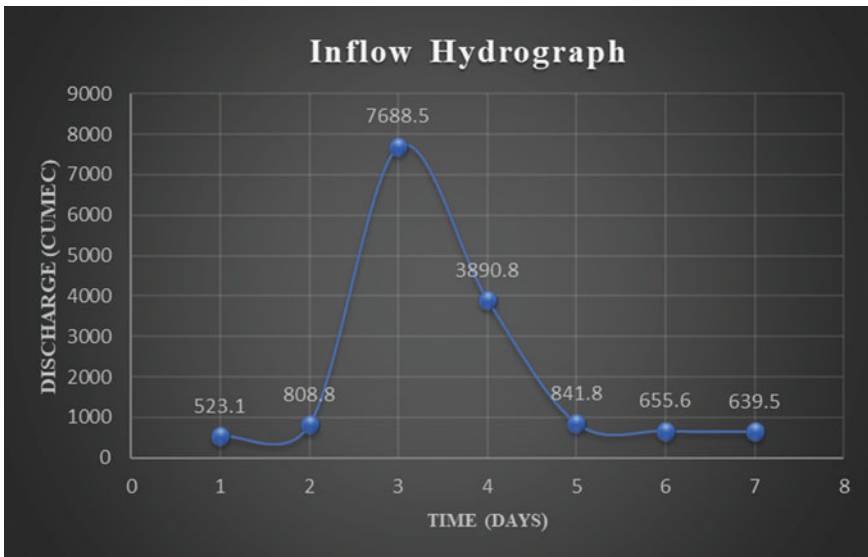


Fig. 3 Inflow hydrograph used as an upstream boundary condition in hydrodynamic model

### 2.3 Data Collection

- DEM is downloaded from the Bhuvan- Indian Geo Platform of ISRO from the satellite under the sub-category of Cartosat-1 with all its version of CartoDEM. After collecting the DEM tiles, data is modified in Arc-GIS for further use in HEC-GeoRAS and HEC-RAS. Different operations such as mosaic, shape-file and watershed delineation have been carried out.

- The research would use rainfall data from two meteorological stations and stream flow data from two gauging stations. The Central Water Commission, Bubaneswar, collected discharges at two gauging stations from 2001 to 2018 and daily rainfall data from two rainfall gauging stations for the same period [3]. These are the HEC-RAS model input data that provides inundation areas.

### 2.3.1 Arc-GIS Application

Arc-GIS is a geographic information system (GIS) for map and geographic information operations. It is used to build and map; compile geographical data; analyse mapped information; exchange and discover geographical information; use the maps and geographical information in a variety of applications; and manage geographical information in a database [4].

### 2.3.2 HEC-GeoRAS

HEC-GeoRAS is an extension of Arc View-GIS primarily developed for the use of geospatial data processes along with HEC-RAS. This HEC-GeoRAS extension creates a geometric attribute file which is an import file for further work in HEC-RAS [1].

### 2.3.3 HEC-RAS

HEC-RAS is an advanced software framework designed to be used interactively in a multi-task, multi-user network environment. A graphical user interface (GUI), different modules for hydraulic analysis, data storage and control features, displays and monitoring facilities compose the device (Brunner 2016). HEC-RAS can perform four 1D river analysis computations which are (1) steady flow water surface profile computations, (2) unsteady flow computations, (3) movable boundary sediment transport computations and (4) water quality analysis [12]. This user interface prepares information for operating the steady and unsteady model which further results in numerical computations.

#### One-Dimensional Unsteady Flow Calculations (HEC-RAS)

The flows are defined by the user in steady-state modelling, and the process measures water levels at specific cross sections. Two variables are determined in unstable modelling (stage and flow); therefore, two equations are required. The continuity and the momentum equations as partial differential equations are used in the simulations given in Eqs. 1 and 2.

$$\frac{\partial AT}{\partial x} + \frac{\partial Q}{\partial x} - q_1 = 0 \quad (1)$$

where  $q_1$  represents the lateral inflow per unit length and the distance  $x$  is measured along the river.  $Q(x,t)$  and  $A$  represent the flow and total flow area, respectively.

$$\frac{\partial Q}{\partial t} + \frac{\partial QV}{\partial x} + gA \left( \frac{\partial z}{\partial x} + S_f \right) = 0 \quad (2)$$

where  $S_f$  indicates the friction slope in Eq. 2. Flow and stage must be identified with the friction slope.

### 3 Methodology

The methodology consists of the following steps a. Pre-processing of Data (Arc-GIS and HEC-GeoRAS), b. Model Execution (HEC-RAS) and c. Post-processing in HEC-GeoRAS. The conceptual diagram of 1D hydrodynamic flood methodology is shown in Fig. 4.

#### 3.1 Pre-processing Application

RAS Geometry is an informative file setup in the HEC-GeoRAS condition, which is used to develop geometric information and extract the waterway catchment from the floodplain. This pre-processing option is provided for preparing required input for the HEC-RAS. The geometrical information mainly main channel banks, stream centreline, flow path along with its centreline and cross-section cut lines are constructed in HEC-GeoRAS.

**Main Channel Bank** is used to distinguish the main stream from the left bank or the right bank of the floodplain. The main channel bank is created by discretising it from the google maps.

**Stream Centreline** Centreline of the stream is created from the stream centreline option.

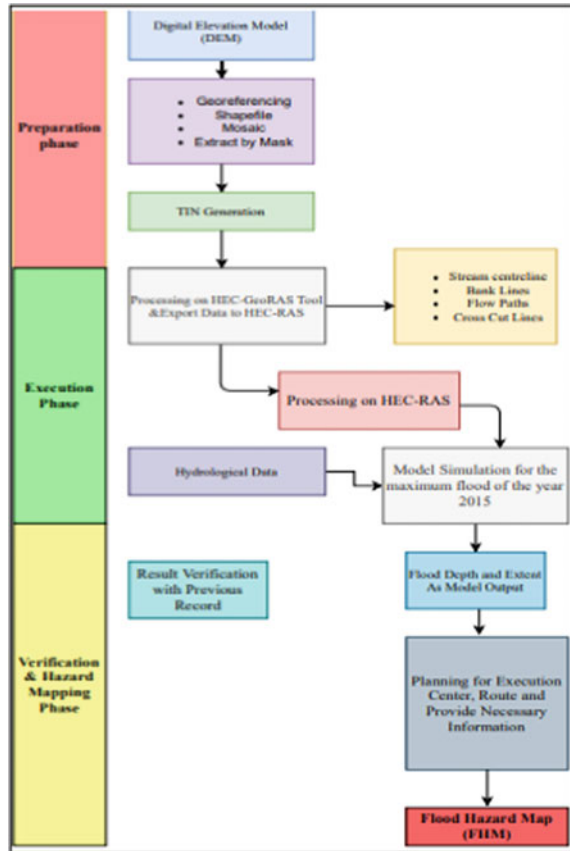
**Flow Path Along with Its Centreline** Paths of the flows have been created from upside to the downside of the stream along with its centreline.

**Cross Section Cutline** The cross-cut lines are drawn perpendicular to the direction of the flow. While creating cross-section cut lines, the average distance between two cross section was at 1500 m interval, and average width of cross section was given width of 2000 m.

Figure 5 represents the processes done in HEC-GeoRAS which is an extension of Arc-GIS.



**Fig. 4** Outline frame of methodology work



### 3.2 Model Execution in HEC-RAS

Model execution is the foremost operation in the work. The file made in HEC-GeoRAS is imported in HEC-RAS under the geometric data window. The section elevation data provided by HEC-RAS requires some modification in bank stations and editing in the geometry. As by adding geometry data, it gives only the section elevation data, and additional Manning’s value is assigned which is taken from the table of Chow’s roughness coefficients based on its land use and surface material. The values considered are: for the left bank as 0.035, right bank as 0.035 and main channel as 0.030 as per observation. Figure 6 representing the elevation and horizontal cross-sectional data at river station (RS) 68,703.07 and 228.07 along with the manning’s *n* value.

Boundary condition is given in unsteady flow data window. Flow hydrograph is selected for the upstream boundary condition at river station 68,703.07. Normal depth = 0.00042 derived from the manning’s equation is selected for the downstream boundary condition at river station 228.07.

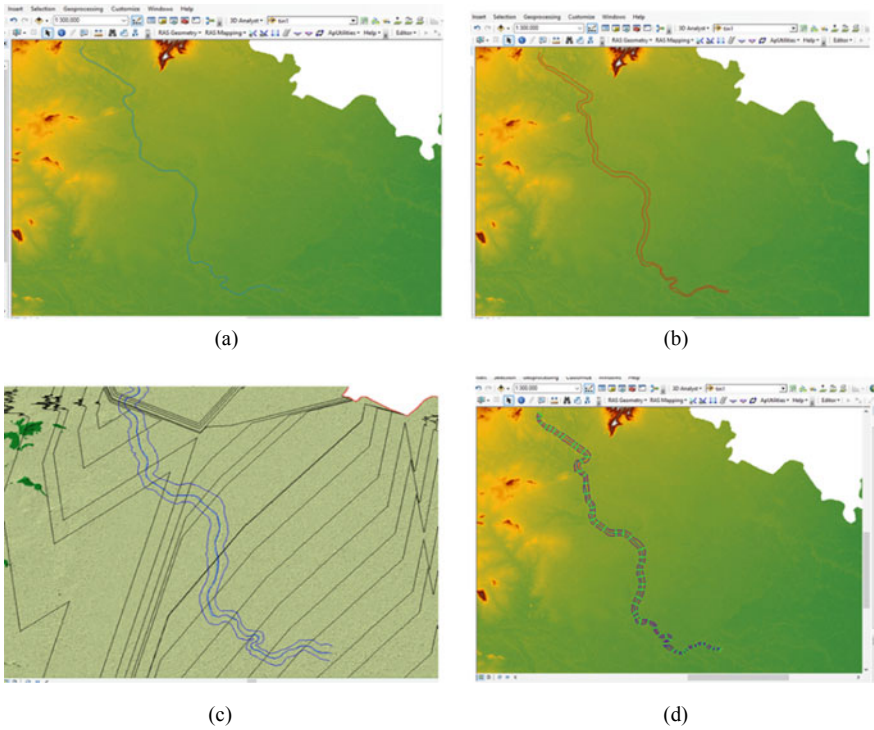


**Fig. 5** Processes **a** main channel bank, **b** stream centre line, **c** flow path and its centre line and **d** cross-section cut lines, respectively, in Pre-GeoRAS application performed in the Arc-GIS

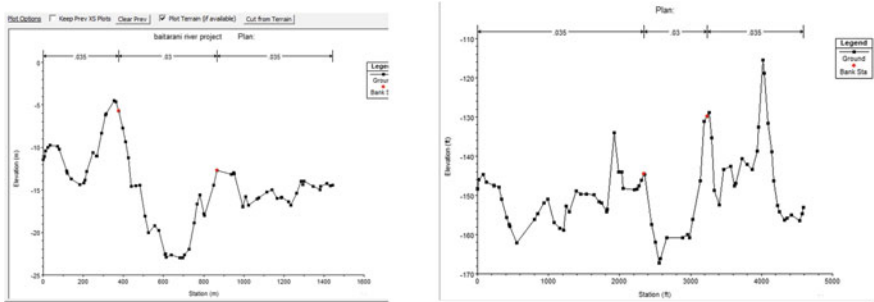


**Fig. 6** Elevation and horizontal cross section at different river stations entered in cross-section data. **a** RS 68,703.07, **b** RS 228.07

After running the unsteady flow analysis, water surface profiles are calculated. Once the simulation is finished, export file from HEC-RAS to HEC-GeoRAS is prepared for the post-processing.

### ***3.3 Post-processing in HEC-GeoRAS***

After exporting results from HEC-RAS, a GIS import file is developed and post-processing steps start [5]. The steps involved in the post-processing are:

- Generation of stream network, cross-cut lines and the bounding polygon: After finishing the theme setup and convert it into an appropriate extension, it will read RAS GIS export file and create primary data files. Automatically, the stream network, cross-cut lines, bank station points and the bounding polygon themes are generated.
- Water surface TIN generation: For every water surface profile, water surface TIN is created which depends on the water surface elevations of these cross-section cut lines and the created theme of bounding polygons,
- Delineation of the floodplains: The next step is delineation of the floodplain after generating the water surface TIN. The delineation of the floodplain forms a poly-line theme which identifies the floodplain and a grid of depth. After deducting the water surface TIN raster values from the Terrain TIN values, a water depth grid is produced.

### ***3.4 Flood Hazard Analysis***

Flood hazard is classified according to the degree of everyday life challenges and/or property loss. Flood hazard evaluation is the estimation of in general unfavourable impacts of flooding. It relies upon numerous parameters, for example, depth of flooding, flooding duration, flood wave velocities and rising rate of water level. At least one parameter can be considered in the hazard evaluation. In the current investigation, flooding depth is taken as chief factor for the hazard assessment evaluation. The intensity of flood risk is constantly given by a relative scale, which speaks to the level of danger and is known as a hazard rank. A littler hazard rank was given for a lower depth or low risk, while bigger danger rank was utilized to show a higher risk (Table 1).

The areas bounded by the flood polygons were calculated to make an assessment of the flood hazard level for the peak discharge having 10-year return period.

**Table 1** Hazard rank provided for depth of flooding

| Flooding depth (m) | Hazard category | Rank |
|--------------------|-----------------|------|
| Hazard free        | No hazard       | 0    |
| $0 < D \leq 1$     | Low             | 1    |
| $1 < D \leq 3$     | Medium          | 2    |
| $3 < D$            | High            | 3    |

## 4 Results Outcomes and Discussion

### 4.1 Results of Unsteady Flow Analysis

After importing the files from pre-process in HEC-GeoRAS to HEC-RAS with all the modifications in the river geometry, the water surface profiles in the graphical plan have been interpreted as the results of the computations of the model. Results from HEC-RAS give a 3D perspective view of the stretch of the river taken as the study area which is shown in Figs. 7 and 8 for the river discharge 7688.5 m<sup>3</sup>/s and 523.1 m<sup>3</sup>/s, respectively. According to the data of the Central Water Commission, at the high flows of the river, many of the cross sections are at risk especially the downstream cross-section no. 13, 16, 20, 25–33 as water coming out from its banks. These cross sections are safe at low or normal flows which is 25–40 m<sup>3</sup>/s.

The water surface profiles in Fig. 9 representing the flooding in the right and left banks at cross section 7 and 27.

After the execution phase in HEC-RAS model, the results are used for the further processing through HEC-GeoRAS for post-processing. Delineation of the floodplain

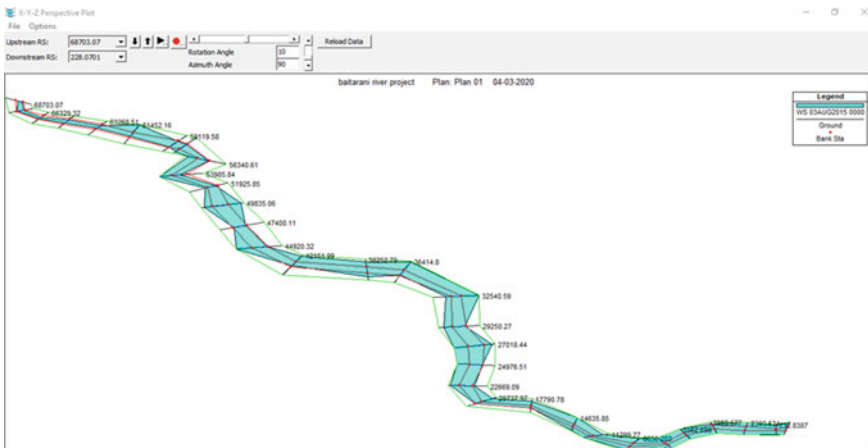


**Fig. 7** X-Y-Z perspective plot for the maximum river discharge 7688.5 m<sup>3</sup>/s



**Table 3** Flood depth area classification

| Water depth (m) | Total inundated area        |        |
|-----------------|-----------------------------|--------|
|                 | 10-year return period flood |        |
|                 | Area                        | Area   |
| <1              | 15.65                       | 6.168  |
| 1–1.5           | 9.70                        | 3.634  |
| 1.5–2           | 7.75                        | 3.315  |
| 2–2.5           | 6.72                        | 2.814  |
| 2.5–3           | 17.34                       | 6.353  |
| >3              | 192.23                      | 77.716 |
| Total           | 249.23                      | 100    |

flooded areas have water depths of more than 3 m. A very small area is flooded below the depth of 1–1.5 m. Results of flood hazard analysis are summarized in Table 3 and Fig. 11.

From the graph of Fig. 10 of depth-flooded area relationship, it can be seen that with the rise in flood intensity, the flooded area increased significantly under the water level more than 3 m. For 10-year flooding, the flooded area which is 192, 17, 6, 7, 9, 15 ha corresponding to the water depth >3, 2.5–3, 2–2.5, 1.5–2, 1–1.5, <1 m, respectively, indicate that with the increase in flooding intensity, the water depth exceeds beyond 3 m. Figure 11 shows the flood hazard map pf the study area.

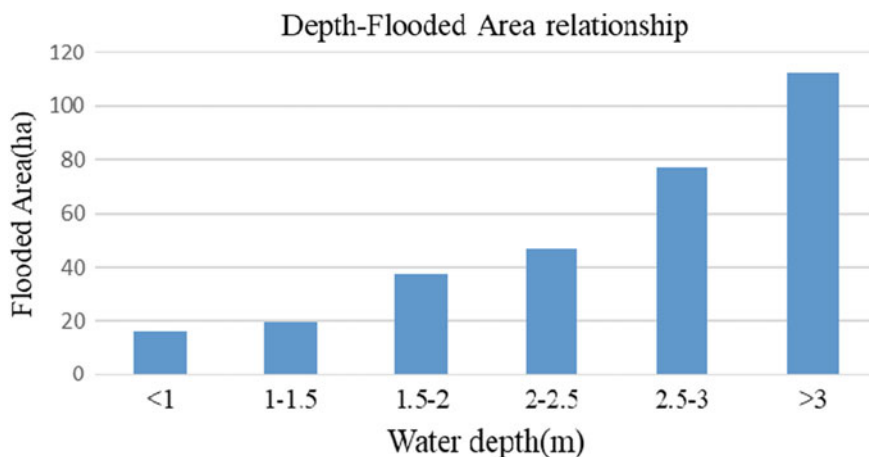


**Fig. 10** Depth-flooded area relationship

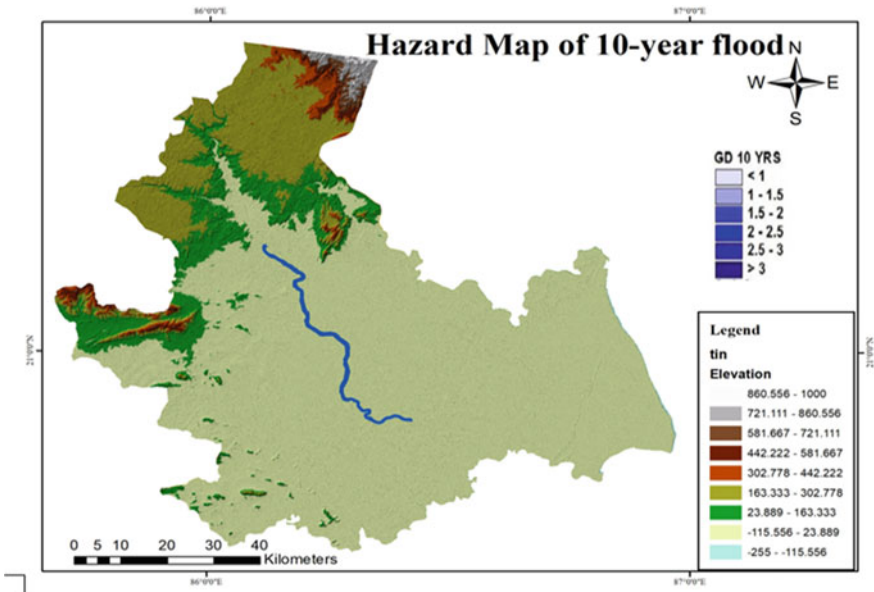


Fig. 11 Flood hazard map of 10-year flood

## 5 Conclusions

The study aims to look at how useful the combination of software Arc-GIS and HEC-RAS for the estimation of flooding at various cross sections which are likely to be submerged. A special flood study of the August 2015 flood has been done to the assessment of flood hazard of the area downstream of the Jajpur with the help of the one-dimensional hydrodynamic model HEC-RAS. It has been observed from the results of the post-processing part of HEC-GeoRAS that at high flows, most of the cross sections at downstream of the river are at high risk and need to implement river training and riverbank protection works at Jajpur, as it is affected more at high flood discharge. The research also analysed flood hazards with respect to flood return periods and their water depth. The correlation between the flood area and the discharge shows that the floodwater intensity rises at a medium rate, meaning that most of the areas under flood have a water depth greater than 3.0 m.

### Scope of Work

Flood vulnerability and flood risk maps of the study area can be planned with population and building material census data on the Arc-GIS network. With the help of vulnerability analysis and hazard analysis, risk analysis can be carried out. A topographic survey can be carried out for the measurements of the cross section in a better practical way.

**Acknowledgements** I am grateful to all the Central Water Commission, Bhubaneswar for providing necessary data for this research work.

## References

1. Ackerman CT (2009) HEC-GeoRAS GIS tools for support of HEC-RAS using ArcGIS User's Manual. US Army Corps of Engineers-Hydrologic Engineering Center (HEC), 4
2. Agrawal R (2016) Flood analysis of Dhudhana River in Upper Godavari Basin using HEC-RAS. *Int J Eng Res* 8(1):188–191
3. Chief Engineer Office CWC-Bhubaneswar (2006) Discharge data of Baitarani. Central Water Commission, Boinagar, Bhubaneswar
4. ESRI (1996) *Introducing ArcView: the geographic information system for everyone*. Environmental Systems Research Institute (ESRI), IncRedlands, California
5. Hydraulic Engineering Center (HEC) (2010) User manual. HECGeoRAS version 4.3. California, USA. [http://www.hec.usace.army.mil/software/hec-ras/documents/HEC-GeoRAS\\_43\\_Users\\_Manual.pdf](http://www.hec.usace.army.mil/software/hec-ras/documents/HEC-GeoRAS_43_Users_Manual.pdf). Accessed on 13 June 2010
6. INDIA-WRIS (2012) River basin Atlas of India
7. Kset DS, Thile EB, France B (2002) Version 2.0. Read 2002:2–5
8. Manandhar B (2010) Flood plain analysis and risk assessment of Lothar Khola. A thesis submitted in partial fulfillment of the requirements for the Degree of Master of Science in Watershed Management, Tribhuvan University, Institute of Forestry, Pokhara, Nepal
9. Patel SB, Mr. et al (2018) One dimensional hydrodynamic flood modeling for ambica river, South Gujarat, *JETIR*, ISSN-2349-5162
10. Snead D (2000) Development and application of unsteady flood models using geographic information systems. Technical report. University of Texas at Austin, Center for Research in Water Resources
11. Study, Target. Natural disasters—Cause and effects. Target study
12. US Army Corps of Engineers (2016) HEC-RAS River analysis system hydraulic reference manual version 5.0. Hydrologic Engineering Center, p 547



# River Geometry Extraction from Cartosat-1 DEM for 1D Hydrodynamic Flood Modeling Using HEC-RAS—A Case of Navsari City, Gujarat, India



Azazkhan Ibrahimkhan Pathan, Prasit Girish Agnihotri,  
and Dhruvesh Patel

**Abstract** Flooding is a worldwide phenomenon that occurs in casualties, property destruction, and it is possibly the most destructive, severe, and recurrent natural catastrophe. The main input parameter for any hydrodynamic modeling is river geometry. A discussion of a method to create river geometry by using the Cartosat-1 Digital Elevation Model (DEM) has been carried out. Many difficulties in distinguishing arise in hydraulic features, which requires pre-processing of the datasets before using it in the HEC-RAS model. The extracted geometry has been utilized in the Hydrological engineering Center-River Analysis System (HEC-RAS) mapper/GeoRAS to perform a 1D hydrodynamic flood modeling approach on the river Purna, Navsari, India. Earlier the river geometry was extracted with the HEC-GeoRAS extension tools available in ARC-GIS. The new HEC-RAS version 5 has been utilized in this study. The geometry of the river includes river centerline, bank lines, flow path lines, and cross-section cut lines which have been digitized in HEC-RAS mapper tool without ARC-GIS being used in the current study. The  $R^2$  value of the Cartosat-1 DEM was 0.7166 which showed the best match with the observed values. The model output was promising and demonstrated the strong potential to extract the river geometry using Cartosat-1 DEM especially in the data scarce regions.

**Keywords** Cartosat-1 DEM · River geometry · HEC-RAS · Modeling · Purna River

---

A. I. Pathan (✉) · P. G. Agnihotri  
Sardar Vallabhbhai National Institute of Technology, Surat, Gujarat, India

D. Patel  
Pandit Deendayal Petroleum University, Gandhinagar, Gujarat, India  
e-mail: [dhruvesh1301@gmail.com](mailto:dhruvesh1301@gmail.com)

## 1 Introduction

Flooding is undoubtedly regarded as the world's most destructive cause of natural catastrophes. During rainy seasons (June–September), the Himalayan Rivers cause flooding in 80% of the total flood-affected region in India. In many states of India such as Gujarat, Maharashtra, Andhra Pradesh, West Bengal, and Orissa extreme flooding is witnessed mostly annually during the monsoon season, affecting a tremendous loss in properties and lives. The primary causes of flooding in India are inadequate water systems particularly in the low land depositional area of the basins, inadequate river carrying capacity due to sedimentation, and inadequate flood management techniques. To minimize flood losses, appropriate flood management practices are needed, which in turn requires space-time flux flow variation in 1-D as well as 2-D. Few researchers have conducted studies on the hydrodynamic flood modeling with the integration of GIS of the Indian basin river floods [1–3].

An effective model of the river flood includes a proper river bed representation and the floodplains geometry, with a precise explanation of the model input parameters, for forecasting the magnitude of flow and the flood water level along the river path precisely [4]. At present, software techniques have been created and are now being modified to extract river geometry features, which are effective for hydrodynamic modeling based on the GIS database [5, 6]. Several studies have been conducted which attempt to address bathymetric data shortages in river flood modeling which highly depend on Digital Elevation Model (DEM) GIS integration obtained from remote sensing satellites or other data sets available globally [7–9]. Also, data assimilation techniques are used to recognize synthetic cross-sections similar to river geometry [10].

With the advent of the latest computers, 1D hydrodynamic flood inundation modeling has become simpler. Numerous studies have been performed in the past 20 years on different aspects of river hydraulics. The theory of hydraulic river flow routing was added to numerous river basins across the globe [11, 12]. The integrated approach of the hydraulic model such as Water RIDE, Mike 11, and HEC-RAS with Geographic Information Systems (GIS) are the latest advancement in flood modeling [7, 13, 14]. The Digital Elevation Model (DEM) is used for the HEC-RAS model extension with a GIS database to extract the river geometry for flood modeling [15]. Pathan and Agnihotri [16] have extracted the river cross-section by using the latest HEC-RAS mapper tools for 1D hydrodynamic modeling.

In the present study, the 1D hydrodynamic approach has been carried out using the latest HEC-RAS version 5. Cartosat-1 DEM is downloaded free of cost from the ISRO BHUVAN web portal. RAS mapper tool available in HEC-RAS was utilized to extract the river geometry such as center line of the river, bank lines, flow path lines, and cross-section lines. This research demonstrates the utility of DEM in flood modeling with the integration of GIS. This approach is the advancement of the 1D hydrodynamic flood modeling in the data-scarce region.

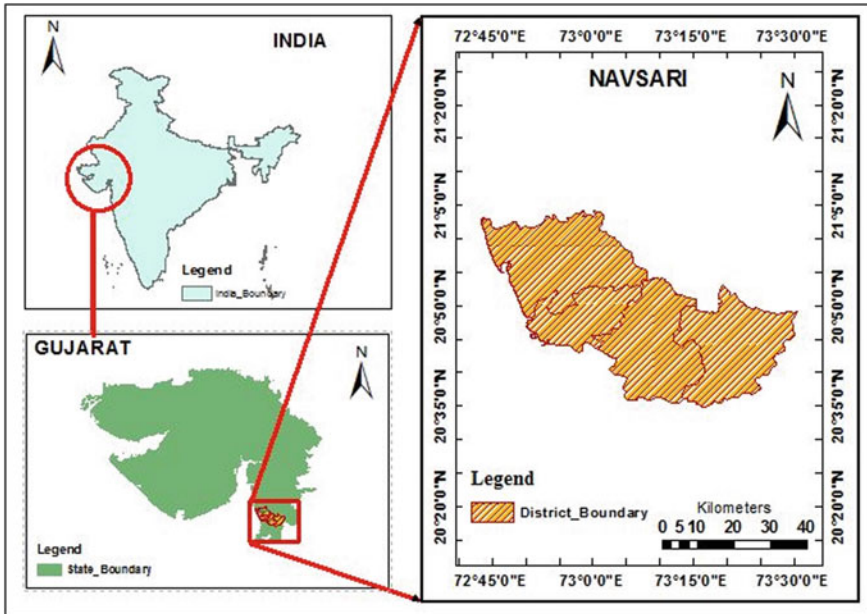


Fig. 1 Study area map

## 2 Study Area and Data

### 2.1 Study Area

Navsari city is situated on the coastal part of Gujarat near the Arabian Sea. The city is at 20° 32' and 21° 05' north latitude and 72° 42' and 73° 30' east longitude. The topographical area of the city is about 2210.97 km<sup>2</sup>. The study area map is illustrated in Fig. 1. Due to heavy precipitation, the water level may rise in the study area and the surrounding area gets inundated annually in monsoon. There is no setup provided by the government in this region to reduce the impact of the floods.

### 2.2 Data

The river flow data of the last 2 decades were obtained from the Navsari irrigation department. The two major flooding events which took place in the city of Navsari for the years 1968 and 2004. Cartosat-1 DEM was utilized for the extraction of river geometry which is freely available ([www.bhuvan.nrsc.gov.in](http://www.bhuvan.nrsc.gov.in)). The spatial projection needs to be set in Arc-GIS for coordinate systems used in HEC-RAS [17]. The 2004 year flood data is required for validating the model.

### 3 Methodology

RAS Mapper is a GIS function capable of collecting GIS datasets such as the center-line of the river, bank lines, flow direction lines, and cross-section lines by river digitalization. The following are presented input parameters for 1D hydrodynamic flood modeling in the HEC-RAS mapper. The flow chart of the region of study is illustrated in Fig. 2.

#### 3.1 Extracting River Geometry

To build the river alignment within the river reach, a light blue marked line which shows the river center line is shown in Fig. 3, which flows from upstream to downstream. To separate the primary river from the left and right banks of the floodplain, the red marked lines shows the river bank lines. To regulate the flow of the river, flow path lines were digitized presented by the red marked shown in Fig. 3. The Green marked line shows the elevation data which was extracted from DEM, which is perpendicular to river flow.

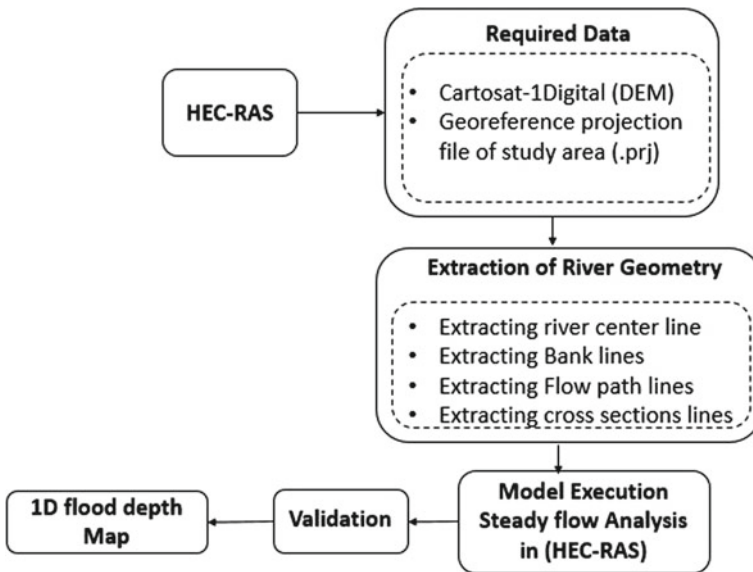
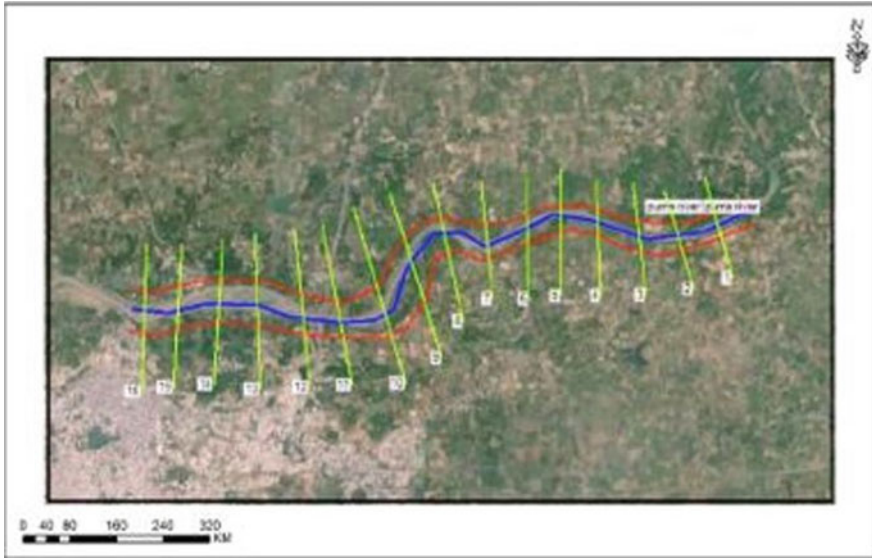


Fig. 2 Flowchart of methodology



**Fig. 3** Extraction of River geometry

### 3.2 *Hydrodynamic Flood Modeling Using HEC-RAS (Hydrological Engineering Center-River Analysis System)*

HEC-RAS is a software that describes water hydraulics flowing through common rivers and other channels. It is a computer-based modeling program for water moving through open channel systems and calculating profiles of water surfaces. HEC-RAS identifies specific applications viable in floodplain mitigation measures [18, 19]. Saint Venant’s equation is utilized in HEC-RAS to solve the energy equation for one-dimensional hydrodynamic flood modeling [20] expressed as,

$$Z_2 + Y_2 + \frac{\alpha_2 V_2^2}{2g} = Z_1 + Y_1 + \frac{\alpha_1 V_1^2}{2g} + h_e \tag{1}$$

where,  $Y_1, Y_2$  indicates the water depth at cross-sections,  $Z_1, Z_2$  expressed as the elevation of the main river channel,  $\alpha_1, \alpha_2$  demonstrates the velocity weighting coefficients,  $V_1, V_2$  shows the average velocities,  $g$  indicates the acceleration due to gravity, and  $h_e$  expresses it as energy head loss.

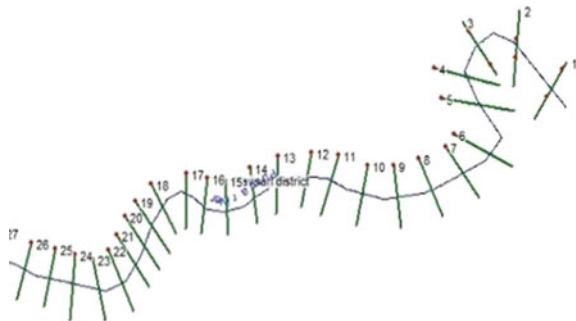
### 3.3 Model Execution in HEC-RAS

Cartosat-1 Dem was downloaded from the ISRO BHUVAN portal for the digitization of river geometry such as river centerline, river bank lines, flow path lines, and cross-section lines with the arrangement of the spatial coordinate system in HEC-RAS through the RAS mapper window along with Google map as shown in Fig. 4. The extraction of the cross-sections presents the station-elevation data through a geometric data window as illustrated in Figs. 5 and 6 represents river geometry in HEC-RAS. River maximum discharge of the 2004 year flood was used as an upstream condition and the normal depth of the Purna river was utilized as a downstream condition in HEC-RAS, the rugosity coefficient is taken as per [21], and steady flow analysis was carried out for flood modeling.



Fig. 4 Extraction of River geometry in RAS mapper with google base map

Fig. 5 Extracted river geometry in HEC-RAS



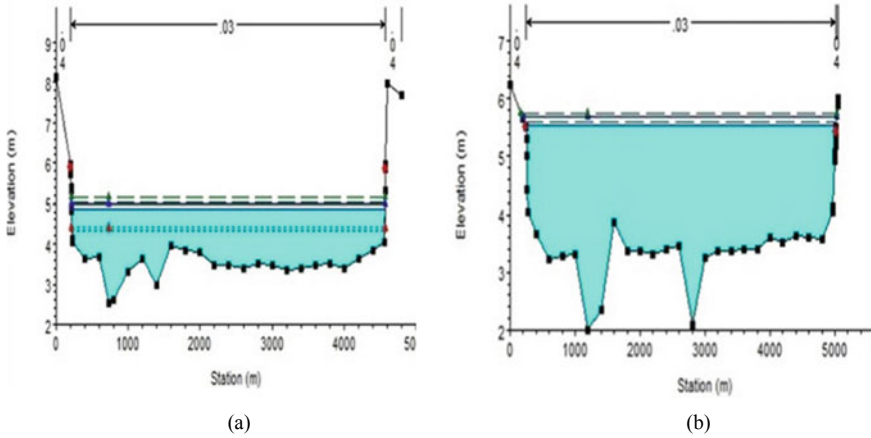


Fig. 6 a Water level at CS-1; b water level at CS-2

### 4 Results

This study is being performed in the lower part of the city. Discharge data for the 2004 year flood events has been used to simulate steady flow analysis. Due to data scarcity in the study area and only one gauging site is available, it is mandatory to simulate only 2004 year flood events to verify model accuracy. Cross-sections were extracted from DEM provides good results in the data deficient region. Flood modeling approach in such region would be effective during peak flood events [6, 17]. The results from the model for the present study indicate the depth of water at each cross-section. The discharge was measured from the gauge station near Kurel village about 1.5 km away from the downstream side. The depth of water was measured corresponding to the discharge of 8836 m<sup>3</sup>/s for 1D hydrodynamic flood modeling. Results obtained from the simulation indicated that the cross-section number 1 and 2 were quite affected during peak discharge, and cross-sections 19 and 20 close to Navsari city were more affected by the flood event. The results which were simulated show that the water level at cross-section one and cross-section twenty (Fig. 6). The water level at the downstream part of the study area demonstrates that the people surrounding cross-section number twenty were suffered more during peak discharge and there were lots of property and lives casualties during the 2004 year flood events. Figure 7 indicates simulated the one-dimensional flood depth map for the 2004 year flood event. 1D hydrodynamic flood modeling would be advantageous for the region where the flash flood is frequently occurring phenomenon annually (Fig. 8) [9].





Fig. 7 Simulated flood depth for the 2004 years flood event

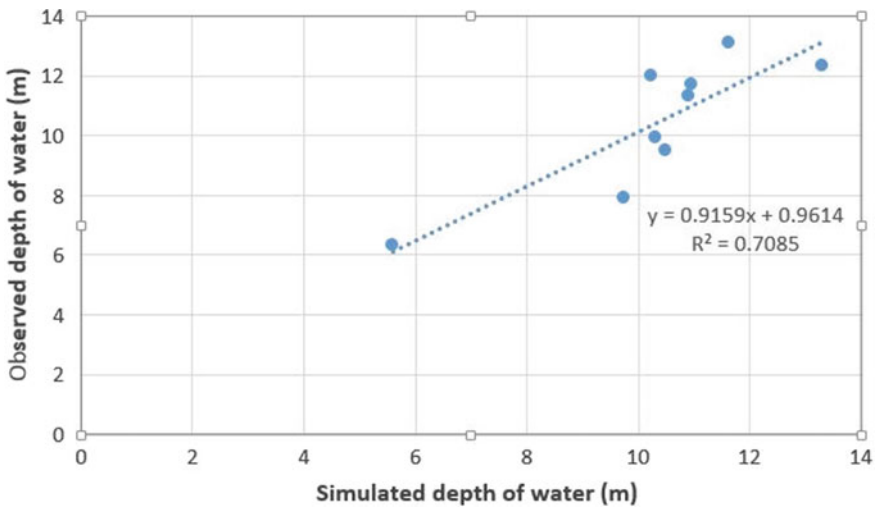


Fig. 8 Regression analysis



### 4.1 Error Analysis of Cartosat-1 DEM

The error analysis of Cartosat-1 DEM was determined by the comparative analysis of GPS elevation and DEMs grid height at 6 locations of the study area. The scatter plot of GPS elevation and DEM grid elevation is shown in Fig. 9. The linear regression analysis indicates a clear significant correlation between the elevation given by Cartosat-1 DEM and the GPS measured elevation at six locations. Additionally, the  $R^2$  value of the Cartosat-1 was 0.7166, which illustrates the accurate correlation. The gradient value of the regression line shown in Fig. 9 indicates that the value is near 1. The error was evaluated by the difference of the elevation grid of DEM and the GPS elevation of the six locations in the study area. The propagation of error corresponding to the elevation of the Cartosat-1 is shown in Fig. 10. It is noted that the negative errors were observed at two locations, which indicates that the elevation of the Cartosat-1 DEM is higher than the elevation of GPS points. Figure 11 shows the profile comparison between the GPS elevation and Cartosat-1 elevation. It is observed that the major elevation difference was found at GPS locations number two, five, and six. The selection of DEM will have been a great influence on flood modeling. From the output of the model, it is noted that the river geometry extraction from the Cartosat-1 DEM was promising and effective because the availability of DEM data is open source. Further research would be on 2D modeling with the use of different DEMs and comparative analysis would be required for the accuracy of the model.

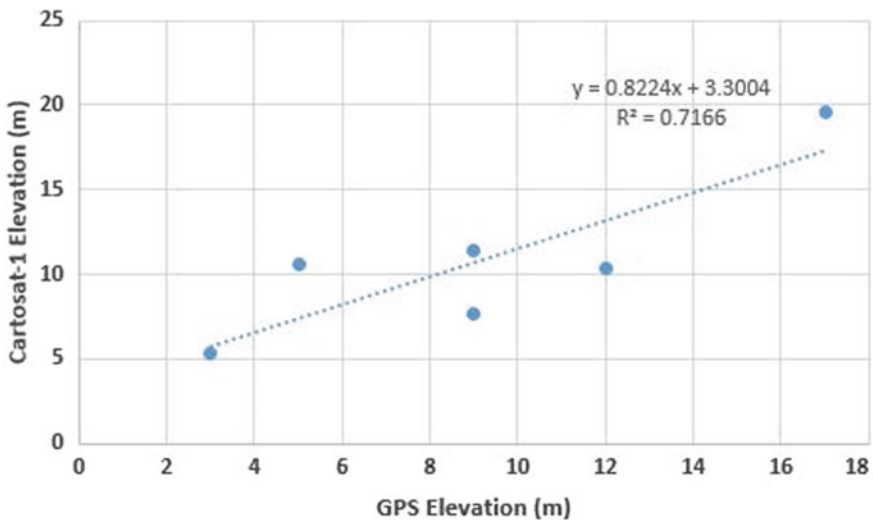


Fig. 9 Scatter plot of Cartosat-1 DEM elevation versus GPS elevation

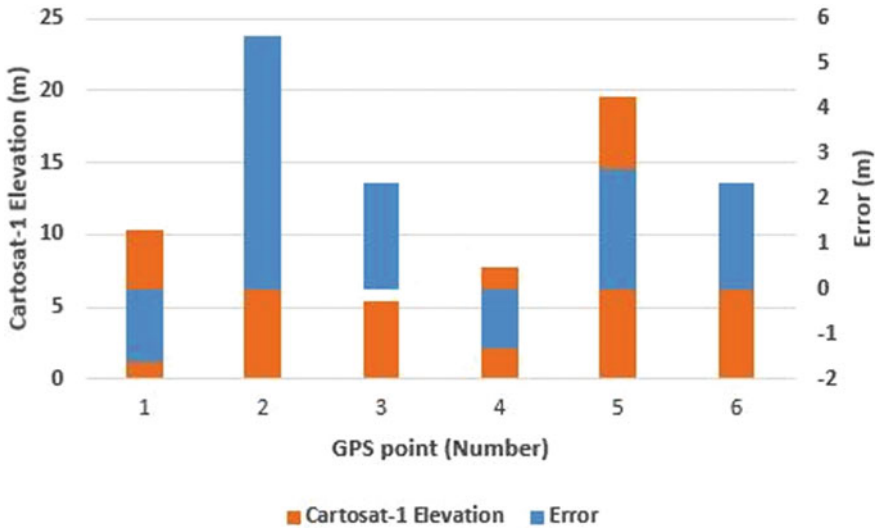


Fig. 10 Error propogation in Cartosat-1 DEM

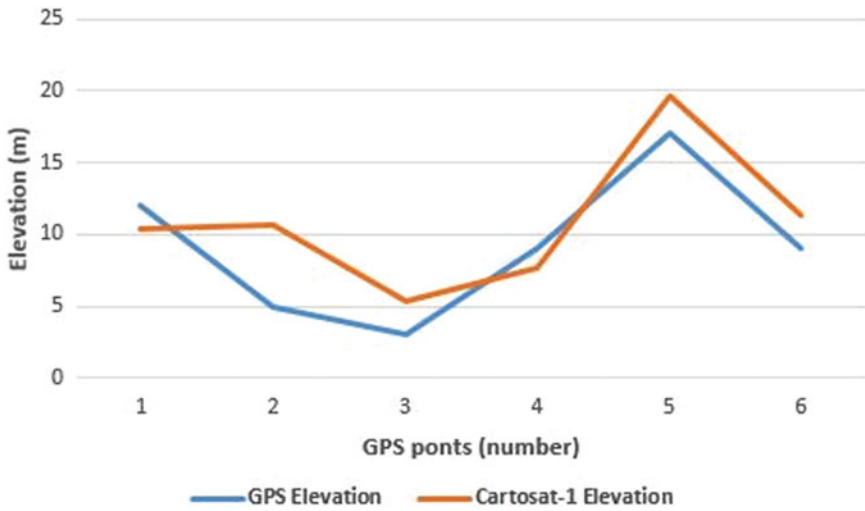


Fig. 11 Profile comparison between GPS elevation and Cartosat-1 Elevation

### 5 Discussion

The main objective of the study was to show the applicability of Cartosat-1 DEM to extract the river geometry and perform 1D hydrodynamic modeling using HEC-RAS. Newly released HEC-RAS version 5 can extract the GIS data from the DEM, which

indicates the advancement of the approach we have performed in the present study [22]. 30 m resolution DEM was used for 1D hydrodynamic modeling in the study. The 2004 year flood event is simulated and steady flow analysis was performed in the present study. Error analysis of the Cartosat-1 DEM demonstrated the scientific approach to the study. The present study showed the comparative analysis of the observed and simulated water depth. Improvement of the existing cross-section with the modification of error could be the research gap of the study [23, 24]. It is assumed that the precipitation, infiltration process were assumed to be neglected in the HEC-RAS. Due to the scarcity of data in the study region, less observed data were identified. The study would be more accurate if more data can be collected in the future. 2D model should be well recognized the flood extent, which was a limitation of the present study. The flooded cross-sections work were located in the HEC-RAS model was based on the base map as a google earth image. However, GPS surveys could be required to find the actual position of cross-sections.

## 6 Validation

The limitation of data in the study region was a major concern. The river geometry approach presented in the study is the advancement of geospatial techniques in flood modeling. Moreover, Only one gauging site is available near Kurel village, Navsari for validation of simulated results for the 2004 year flood event. Table 1 depicts the comparison between observed and simulated water depth at the gauging site, which indicates valued and efficient results as far as accuracy is concerned. The regression analysis of observed and simulated datasets at the gauging sites is shown in Fig. 8.

**Table 1** Differences between observed and simulated water depth at Gauge station

| Satellite  | Years | Observed depth of water (m) | Simulated depth of water (m) | Difference (m) |
|------------|-------|-----------------------------|------------------------------|----------------|
| Cartosat-1 | 2001  | 10.9                        | 11.3                         | 0.01           |
|            | 2002  | 10.23                       | 12                           | 0.27           |
|            | 2003  | 10.32                       | 9.92                         | -0.22          |
|            | 2004  | 11.64                       | 13.1                         | 1.6            |
|            | 2005  | 13.3                        | 12.32                        | 0.92           |
|            | 2006  | 10.5                        | 9.5                          | 0.37           |
|            | 2007  | 10.96                       | 11.69                        | -1.1           |
|            | 2008  | 9.75                        | 7.89                         | 0.02           |
|            | 2009  | 5.61                        | 6.3                          | 0.13           |
|            | 2010  | 10.9                        | 11.3                         | -0.06          |
|            | 2011  | 10.23                       | 12                           | 0.02           |
|            | 2012  | 13.8                        | 13.79                        | 0.01           |

## 7 Summary and Conclusions

The present study shows the applicability of the HEC-RAS for river geometry extraction with the application of geospatial techniques (HEC-RAS mapper tool). A 1D hydrodynamic flood modeling approach was presented using Cartosat-1 DEM on the Purna river, Navsari, Gujarat, India. The new version of HEC-RAS version 5 was utilized in the present study for GIS applications in flood modeling. River geometry includes: river centerline, bank lines, flow path lines, cross-section cut lines were digitized in RAS mapper tools without ARC-GIS being used in the present study. The error analysis of Cartosat-1 DEM was performed, in which vertical differences were evaluated between GPS elevation and Cartosat-1 elevation. The  $R^2$  value of the Cartosat-1 was found to be 0.7166, which indicates good results. The Validation of the model is being carried out by comparing the observed water depth with the simulated water depth at the location of the gauging site. The output of the model was promising and demonstrates strong potential in the area of data scarcity for using the suggested method. The applicability of open-source datasets would be an effective worldwide approach in flood modeling.

**Acknowledgments** The first author is sincerely obliged to Dr. Prasit Agnihotri his Research Supervisor at SVNIT, Surat, for inspiring him to perform research on flood modeling and providing all the help and advice with equal thanks to Director of SVNIT for using the Geospatial laboratories Facilities. The author would like to thank Dr. Dhruvesh Patel, Assistant Professor of Civil engineering Department, Pandit Deen Dayal Energy University for useful support in modeling and technical assessment of the study. The author would like to thanks Mr. Bhargav Kothiya, Deputy Executive, Navsari Irrigation Circle for given that the useful dataset, and help during the research period. The Author would like to thanks research colleagues Arshad Joseph for providing support in research work.

## References

1. Kale VS (1997) Flood studies in India: A brief review. J Geol Soc India (Online archive from Vol 1 to Vol 78), 49(4):359–370
2. Vijay R, Sargoankar A, Gupta A (2007) Hydrodynamic simulation of River Yamuna for riverbed assessment: a case study of Delhi Region, vol 130, no 1–3. Springer, pp 381–387. <https://doi.org/10.1007/s10661-006-9405-4>
3. Pathan AKI, Agnihotri PG (2020) 2-D unsteady flow modelling and inundation mapping for lower region of Purna Basin using HEC-RAS. Nat Environ Pollut Technol 19(1):277–285
4. Merwade V, Cook A, Coonrod J (2008) GIS techniques for creating river terrain models for hydrodynamic modeling and flood inundation mapping. Environ Model Softw 23(10–11):1300–1311. <https://doi.org/10.1016/j.envsoft.2008.03.005>
5. Schwanghart W, Kuhn NJ (2010) TopoToolbox: a set of Matlab functions for topographic analysis. Environml Model Softw 25(6):770–781
6. Tesfa TK, Tarboton DG, Watson DW, Schreuders KA, Baker ME, Wallace RM (2011) Extraction of hydrological proximity measures from DEMs using parallel processing. Environ Model Softw 26(12):1696–1709
7. Abdulkareem JH, Pradhan B, Sulaiman WNA, Jamil NR (2018) Review of studies on hydrological modelling in Malaysia. Model Earth Syst Environ 4(4):1577–1605

8. Pathan AI, Agnihotri PG (2019) A combined approach for 1-D hydrodynamic flood modeling by using Arc-Gis, Hec-Georas, Hec-Ras Interface-a case study on Purna River of Navsari City, Gujarat. *IJRTE*, 8(1):1410–1417
9. Maharjan LB, Shakya NM (2016) Comparative study of one dimensional and two dimensional steady surface flow analysis. *J Adv Coll Eng Manage* 2(c):15. <https://doi.org/10.3126/jacem.v2i0.16095>
10. Roux H, Dartus D (2008) Sensitivity analysis and predictive uncertainty using inundation observations for parameter estimation in open-channel inverse problem. *J Hydraul Eng* 134(5):541–549
11. Finaud-Guyot P, Delenne C, Guinot V, Llovel C (2011) 1D-2D coupling for river flow modeling. *Comptes Rendus - Mecanique* 339(4):226–234. <https://doi.org/10.1016/j.crme.2011.02.001>
12. Teng J, Jakeman AJ, Vaze J, Croke BFW, Dutta D, Kim S (2017) Flood inundation modelling: a review of methods, recent advances and uncertainty analysis. *Environ Model Softw* 90:201–216. <https://doi.org/10.1016/j.envsoft.2017.01.006>
13. Pathan AI, Gandhi PJ, Agnihotri PG, Scholar R (2019) Integrated approach for flood modeling using Arc-GIS, HEC-GeoRAS—A case study on Purna River of Navsari District of Gujarat State
14. Pathan AI, Agnihotri PG (2020) Use of computing techniques for flood management in a coastal region of South Gujarat—A case study of Navsari District. *Adv Intell Syst Comput* 1072:108–117. [https://doi.org/10.1007/978-3-030-33585-4\\_11](https://doi.org/10.1007/978-3-030-33585-4_11)
15. Gichamo TZ, Popescu I, Jonoski A, Solomatine D (2012) River cross-section extraction from the ASTER global DEM for flood modeling. *Environ Model Softw* 31:37–46
16. Pathan AI, Agnihotri PG (2021) Application of new HEC-RAS version 5 for 1D hydrodynamic flood modeling with special reference through geospatial techniques: a case of River Purna at Navsari, Gujarat, India. *Modeling Earth Systems and Environ* 7(2):1133–1144. <https://doi.org/10.1007/s40808-020-00961-0>
17. Gichamo TZ, Popescu I, Jonoski A, Solomatine D (2012) River cross-section extraction from the ASTER global DEM for flood modeling. *Environ Model Softw* 31:37–46. <https://doi.org/10.1016/j.envsoft.2011.12.003>
18. Ouma YO, Tateishi R (2014) Urban flood vulnerability and risk mapping using integrated multi-parametric AHP and GIS: methodological overview and case study assessment. *Water (Switzerland)* 6(6):1515–1545. <https://doi.org/10.3390/w6061515>
19. Ahmad HF, Alam A, Bhat MS, Ahmad S (2016) One dimensional steady flow analysis using HECRAS—A case of River Jhelum, Jammu and Kashmir. *Eur Sci J* 12:340–350
20. Brunner G (1995) HEC-RAS River analysis system. hydraulic reference manual. Version 1.0. <https://apps.dtic.mil/docs/citations/ADA311952>
21. Chow V, Maidment D, Og Mays LW (1988) Applied hydrology. International edition. McGraw-Hill, New York
22. Kumar N, Lal D, Sherring A, Issac RK (2017) Applicability of HEC-RAS & GFMS tool for 1D water surface elevation/flood modeling of the river: a Case Study of River Yamuna at Allahabad (Sangam), India. *Model Earth Systems and Environ* 3(4):1463–1475. <https://doi.org/10.1007/s40808-017-0390-0>
23. Bhuyian MNM, Kalyanapu AJ, Nardi F (2015) Approach to digital elevation model correction by improving channel conveyance. *J Hydrol Eng* 20(5):1–10. [https://doi.org/10.1061/\(ASCE\)HE.1943-5584.0001020](https://doi.org/10.1061/(ASCE)HE.1943-5584.0001020)
24. Pathan AI, Agnihotri PG, Patel DP, Eslamian S (2021) Comparative analysis of 1D hydrodynamic flood model using globally available DEMs a case of the coastal region. *Int J Hydrol Sci Technol* 1(1):1. <https://doi.org/10.1504/IJHST.2021.10034760>

# Impact Assessment of Environmental Flows Using CORDEX Regional Climate Models: Case Study of Nagarjuna Sagar Dam, Krishna River, India



Rajesh Maddu, Krishna Mohan Ganta, Rehana Shaik, and C. T. Dhanya

**Abstract** The quantity and quality of water flow in a river may significantly change from its normal condition between a reservoir and downstream, thus paving the way for drastic changes in the riverine ecosystem. Any disruption in the river's natural flow regime can alter the entire river ecosystem and socio-economic activities. Environmental flows are mainly defined based on hydrologic, hydraulic, and ecological conditions of a river system. Given the changes in precipitation and temperature patterns under climate change, the river flows are expected to alter, thereby impacting the hydrological and environmental flow conditions. The present study will articulate various hydrological methods currently available in the state-of-the-art, to determine the environmental flows. The study demonstrates how the climatological driven changes in river flows alter the hydrological, environmental flows, using the dynamically downscaled Coordinated Regional Downscaling Experiment (CORDEX) model outputs. A data-driven hydrological model has been used to study the river flow alterations for the projected precipitation patterns. The projected river flows have been used to study the changes in hydrological, environmental flows for future scenarios. The study has considered the Krishna river, emphasizing the Nagarjuna Sagar reservoir, and assessing downstream hydrological, environmental flows with the changes of precipitation under climate change. The decrease of rainfall over the reservoir's catchment has led to a significant decrease in reservoir inflows for the period of 1980 to 2011 and a consequent decrease of environmental flows in terms of 75, 80, 85, 90, 95% exceedance flows for Nagarjuna Sagar dam. The increasing projections of rainfall over the reservoir's catchment based on CORDEX outputs have resulted in lower magnitudes of decrease in low flow quantities.

---

R. Maddu · K. M. Ganta · R. Shaik (✉)

Hydroclimatic Research Group, Lab for Spatial Informatics, International Institute of Information Technology, Hyderabad 500032, India  
e-mail: [rehana.s@iiit.ac.in](mailto:rehana.s@iiit.ac.in)

C. T. Dhanya

Department of Civil Engineering, Indian Institute of Technology Delhi, Hauz Khas, Delhi 110016, India

**Keywords** Reservoirs · Inflows · Flow duration curves · Climate change · Regional circulation models

## 1 Introduction

River ecosystems play a significant role in cleansing, water-storing, landscape, transport, maintaining biodiversity, and offering aquatic faunas environments [1]. The river flows have been progressively being changed through anthropogenic alterations such as dams and weirs, and other hydraulic structures for flood control, withdrawals for cultivation, and industrial effluents [2]. Such interventions reduce the flow and cause alterations in the flow seasonality and flood frequency of rivers, impacting the environmental effects. Therefore, a balance between the river flow modifications for human and ecological needs is necessary [3]. The water that is allocated for such maintenance of ecological needs, such as maintaining aquatic habitats, is referred to as “Environmental flow (E.F.)” also called “Environmental flow requirement (EFR)” [3–5].

India is a tropical country where the rainfall is very seasonal, where the seasonal spread is different from tropical monsoons followed by summer (dry spell). But due to urbanization, industrialization, and the use of pesticides in agriculture, rivers are observed to receive a large number of effluents that are untreated or partially treated [6]. In India, the environmental flow releases are relatively low (often minimal) to store maximum volume upstream. Due to this, the downstream is remained to be almost dry, which allows them to be more polluted except for the monsoon season, where there will be a substantial flow. Rivers in India are considered religious, and they provide livelihoods and essential services. Still, there has been little or no appreciation of the nature of rivers. Along with several other factors, India is still behind many countries like Australia and the USA in the Environmental Flow Assessment [6].

In the past few decades, various methods were identified and developed to evaluate environmental flows, which is also called Environmental Flow Assessment (EFA). More than 200 approaches were developed for the environmental flow assessment to suggest minimum environmental flow requirements of a river in over 44 countries, and many countries preferred these assessments in water resources management. Overall, several approaches were used to estimate river ecosystems’ environmental flows, considering hydrology, hydraulic, and water quality criteria, as discussed in the following sections. The environmental flow allocation methodologies can be classified as hydrological, hydraulic, habitat, and holistic [4, 7, 8].

## ***1.1 Hydrological Methods***

Hydrological methods are widely used in environmental flow calculations due to their ease of use and are even considered the most straightforward approach. About 30% of all the techniques used are hydrological methods [7]. Hydrological methods, while developed, are given importance for full-scale planning and hence are recommended for the pre-assessment of E.F.'s in water management planning. For the assessment, hydrological methods use daily or monthly streamflow data with a priority to the daily data due to the ease in determining flow characteristics with the daily records [2]. Among all the methods that existed, the Tennant method is considered the best. The Tennant method identifies the minimum flow levels based on specified mean flow proportions [9]. Later, the Tennant method was modified in several other ways. In one such, each month's minimum flows were specified as a percentage of mean monthly flow to incorporate seasonal variations [10]. Tennant divided a hydrological year into two periods: October to March and April to September. But Tessman [11] considered 12 monthly periods for a year and classified them into three categories based on the Mean Monthly Flow (MMF) and Mean Annual Flow (MAF).

Few hydrological methods, such as the flow duration curve method and the Tennant method, discussed only the flows with little or no discussion on Temporal Variability. Hence Indicators of Hydrologic Alteration (IHA) method has been developed by Richter et al. [12] Based on a few parameters. A total of 32 hydrological Parameters with ecological considerations were considered the annual flow regime and were divided into groups such as magnitude, frequency, timing, duration, and rate of change. This method is widely used to compare the hydrological attributes of two situations or events like before and after the impacts or level of influence of two sites, etc. [12]. Apart from these hydrological methods, there are many other methodologies and methods developed by specific countries, such as the Alberta Desktop Method, Percentage of Flow method, and the BC-Instream Flow Threshold approved by British Columbia to meet their local demands.

## ***1.2 Hydraulic Rating Methods***

Hydrological methods widely discuss the flows and habitats with little or no consideration of the stream's hydraulic properties. They assume a relationship between discharge and a few hydraulic properties [7, 13]. Hydraulic methods, for the EFA, work with the qualitative and quantitative relationships between the flows and the habitats of fish species. Typically, any parameter can be used in these methods in the available large number of them, but widely involved parameters are wetted perimeter and maximum depth [14].

The wetted perimeter method is often the widely used hydraulic method for the EFA [15]. It considers fixed flow and wetted perimeter and their relationship with each other and is a fixed flow method. The minimum flow requirement considered



is the point of inflection, i.e., the point where the wetted perimeter becomes small [16]. But the method was in jeopardy at selecting critical breakpoints on the curve since there is no methodology available for it [14]. Another method called Toe-width Method was developed in Washington state in 1976, which is very similar to wetted perimeter considering water depth and velocity as hydraulic parameters but was not widely applied outside the Washington state [17]. Apart from the above-used methods, which widely considered wetted perimeter and depth as the hydraulic properties, there were few other methods with the other parameters such as, “adapted ecological hydraulic radius approach” [16], which was developed by considering the hydraulic radius as the hydraulic parameter and flow event method considering the flow recommendations.

### ***1.3 Habitat Simulation Methods***

Habitat simulation methods, as the name says, consider the conditions and aspects of the habitat requirements for the environmental flow assessment [18]. Physical habitat is directly or indirectly linked with the streams’ hydraulic conditions; hence, there is a need to consider these aspects too, which will make them an extension of the hydraulic methods with a consideration of the habitats [13]. Hence, there is a need to establish a relationship between the hydraulic and habitat properties, which habitat simulation methods do with a variety of models along with considering environmental aspects such as water quality [19–21].

Habitat simulation methods are developed to meet more demands than the hydrological and hydraulic methods but are not widely used due to their necessity in a comprehensive database, which may take a few years to collect. They give results with accuracy than others, but due to their time and high requirement money consumption, they are widely used for only high-risk projects. Instream flow Incremental methodology is the most widely adopted method in habitat simulation methods. To use the relationship between the flow and habitat, a set of computer models called the “Physical HABitat SIMulation Model” has been incorporated as the major component of IFIM [22]. Many such models were developed later to meet their specific requirements like habitat requirements, microhabitats, microhabitats, flow requirements, etc. such as MesoHABSIM [15]. IFIM works in stages, with each stage designated to a principle. The five stages of IFIM are as follows: problem identification, planning of the study, implementation, study of the alternatives, and resolving the problem [16].

### ***1.4 Holistic Methodologies***

In holistic methodologies, the term “holistic” refers to the whole system, which means these methods represent the entire riverine system by considering various

aspects of the river ecosystem like flow, living and non-living components for the environmental flow assessment [23]. Holistic methodologies are observed to be better than the other hydrological, hydraulic, and habitat methods due to their consideration of the complete river ecosystem, wetlands, and groundwater [24]. Building block methodology, Top-down process, and bottom-up process are the most recognized and widely accepted holistic methods.

Holistic methodologies have been described as two approaches, bottom-up and top-down methods. The bottom-up approach is designed to construct a flow regime from scratch by adding flow components to a baseline of zero flows. In contrast, the top-down approach works on the maximum acceptable degree of change in the riverine system before it starts degrading or noticeably changed. Building block methodology and Benchmarking methodology are examples of bottom-up and top-down approaches simultaneously [8]. Building Block Methodology was developed as an alternative for the IFIM method [25]. The river flow regime is divided into several components, called building blocks, where each block performs some function (ecological or geomorphological). BBM is an extensive and rigorous method that involves several documentations, rigorous field study, stakeholders in workshops, and intensive resources [8].

Recent studies stressed holistic approaches, including hydrology and water quality criterion to estimate environmental flows (e.g., [26]). Choudhary et al. [27] estimated water quality based minimum environmental flow under hypothetical scenarios of pollution by varying Biochemical Oxygen Demand (BOD) by using QUAL2K for the Tungabhadra river, India. Such studies emphasized the environmental flows are accounting for the fluctuations of water quality under climate change [28]. Few studies used General Circulation Model (GCM) outputs along with statistical down-scaling models to study the impacts of climate change on river water quality [29, 30]. However, assessment of hydrological, environmental flows under climate change are limited in the literature. The advantages of climate change projections at more satisfactory resolution have been progressed in terms of regional circulation model climate projections [31]. Combining such climate change projections in the estimation of environmental flows can be valuable to make the decision policies to maintain the ecological stability of river flows under climate signals [28].

The objectives of the present study are defined as to (1) study the various hydrological methods currently available to determine the environmental flows, (2) study the river flow alterations for the projected precipitation patterns by using the data-driven hydrological models, (3) assessing downstream hydrological, environmental flows (wide range of low flows Q75, Q80, Q85, Q90, and Q95 values) using CORDEX projections with the changes of precipitation under climate change by considering the Krishna river, emphasizing the Nagarjuna Sagar reservoir, India.

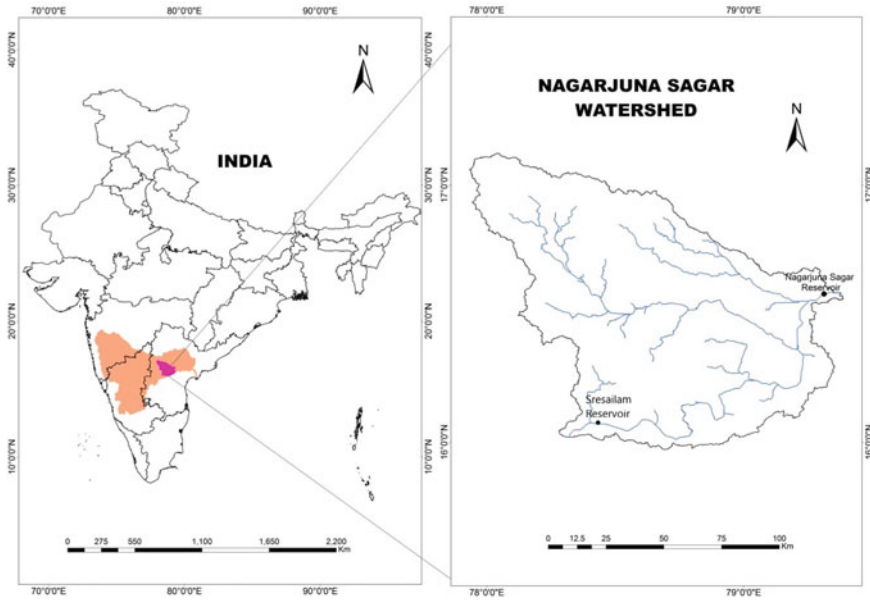


**Fig. 1** Map of Nagarjuna Sagar Watershed

## 2 Study Area

Nagarjuna Sagar is one of India's largest multipurpose projects, with a 215,000 sq. km catchment area. It is one of the major reservoirs on river Krishna along the border of Telangana and Andhra Pradesh and is located at a latitude of  $16^{\circ}34'33.6''$  N and a longitude of  $79^{\circ}18'44.64''$  E (Fig. 1). This project provides irrigation water to around nine districts in Andhra Pradesh and Telangana and Hydroelectric generation. It contains two canals (right canal and left canal), which irrigate up to 8500 km<sup>2</sup> in both states. Nearly 99% of the basin's annual rainfall occurs during the south-west monsoon (June to October). In summer, i.e., during March, April, and May, high temperatures will be experienced, ranging from 34 to 41 °C.

## 3 Methodology and Data

Climate change will Influence the intensity, type, duration, and variability of rainfall, which will affect the inflow to the reservoir and consequent releases [29]. The downstream reservoir releases are prominent in studying the environmental flows, which again depends on the reservoir inflows/water availability. The inflow of the reservoir depends on the amount of rainfall over the catchment of the reservoir. The following

methodology has been formulated to study the impact of precipitation changes on the environmental flows:

1. Developing a model to predict the reservoir inflows using the precipitation over the reservoir's upstream catchment area.
2. Developing a model to predict the downstream reservoir releases (outflows) with the predicted inflows from step 1.
3. Study the environmental flow analysis using the outflows modeled from step 2.
4. Implementing the trained and tested models from steps 1 and 2 with CORDEX climate projections of precipitation over the catchment area to study the environmental flows under climate signals.

The present study used multiple linear regression models to relate the precipitation-inflows and inflows-outflows, as explained in the following section.

### 3.1 Multiple Linear Regression

Multiple linear regression (MLR) is a statistical technique that uses several explanatory variables to predict a response variable's outcome. A multiple linear regression model describes the dependence and variation of the predictand variable ( $Y$ ) with two or more predictor variables ( $X$ ) with the coefficient of predictors as  $\beta$ 's as follows:

$$Y = \beta_0 X_0 + \beta_1 X_1 + \beta_2 X_2 \quad (1)$$

The overview of the modeling framework has been shown in Fig. 2. A catchment-scale rainfall-inflow model was developed to study the climate change impact on reservoir inflows.

Multiple linear regression model was developed with input as rainfall at various time steps (i.e.,  $R_t$ ,  $R_{t-1}$ ) and outflow of the previous period ( $I_{t-1}$ ) with an output of the model as the inflow at the time step  $t$ ,  $I_t$ .

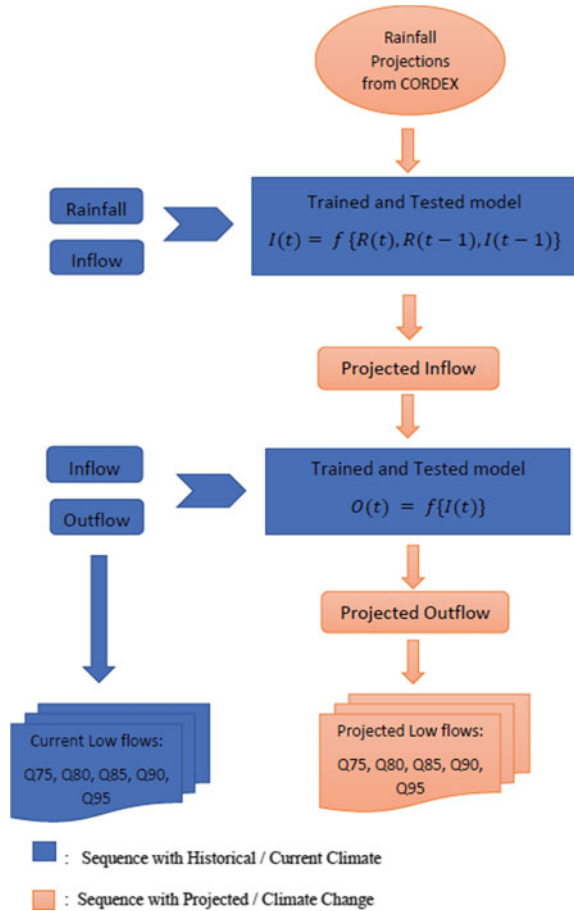
$$I_t = f\{R_t, R_{t-1}, I_{t-1}\} \quad (2)$$

$I_t$  is the inflow at time  $t$ ;  $R_t$  is the rainfall at time  $t$ ;  $R_{t-1}$  rainfall at time  $t - 1$ ;  $I_{t-1}$  Inflow at time  $t - 1$ ;  $t - 1$  is the one-step time lag of rainfall and inflow. Another linear regression model was developed to relate inflow and outflow/release of a reservoir to study the climate change impact on outflows. The reservoir outflow modeled from Eq. 1 will form the basis for the inflow-outflow model. The monthly reservoir inflow at the time  $t$ , ( $I_t$ ) as input and the reservoir discharge at the time  $t$ ,  $O_t$ , as the output variable as follows:

$$O_t = f\{I_t\} \quad (3)$$

where  $I_t$  is the monthly inflow at the time,  $t$ ;  $O_t$  is the monthly outflow at the time,  $t$ .

**Fig. 2** Overview of the modeling approach to estimate environmental flows under climate change of a reservoir system



### 3.2 Estimation of Environmental Flows Using Flow Duration Curve Method

The flow duration curve is another widely used method for analyzing the low flows of a river stream. A flow duration curve (FDC) represents the percent of the flow time exceeding a specified flow of interest. It uses daily, weekly, or monthly records of discharge for the E.F. calculations. FDC has been widely applied in recent years in environmental applications in controlling and maintaining healthy aquatic ecosystems. Several studies used various approaches to estimate the environmental flows as low flows estimated by FDC [30]. A range of 70–99% of the FDC generally specifies the lof flow range also stated as Q70 to Q99, low flow indices [28].

**Table 1** Available precipitation, reservoir Inflow, and Outflow data periods and sources

| Data                   | Data obtained | Data used |
|------------------------|---------------|-----------|
| Rainfall (IMD GRIDDED) | 1901–2015     | 1980–2011 |
| Rainfall (CORDEX)      | 1950–2060     | 2012–2050 |
| Inflow                 | 1967–2012     | 1980–2011 |
| Outflow                | 1967–2012     | 1980–2011 |

### 3.3 Data

The current study considered precipitation, reservoir inflow, and reservoir outflow data from 1980 to 2011 (Table 1). Historical gridded monthly precipitation data at  $0.25^\circ \times 0.25^\circ$  resolution from the Indian Meteorological Department. The gridded monthly precipitation data for the study period was then converted into single time-series data by taking the gridded data's arithmetic mean. The monthly inflow and outflow data were obtained from the Central Water Commission from 1967 to 2012. The projected monthly precipitation data were obtained from the Coordinated Regional Downscaling Experiment (CORDEX) available from 1950 to 2060. From the available 14 domains of CORDEX datasets, we incorporated the South-Asian domain of the CORDEX project. To demonstrate the use of CORDEX projections in the estimation of environmental flows, the present study used the daily precipitation data simulated by RCM, CORDEX ([www.cordex.org](http://www.cordex.org)). The CORDEX experiment applied is: 1) RegCM4(LMDZ), Regional Climatic Model version 4 (RegCM4), with deriving GCM as IPSL LMDZ4, from Centre for Climate Change Research (CCCR), Indian Institute of Tropical Meteorology (IITM), India.

## 4 Results and Discussion

The present study adopted a quantile-based mapping method of bias correction with a comparison of cumulative distribution functions. Figures 3 and 4 show the comparison of the monthly gridded rainfall data obtained from the Indian Meteorological Department (IMD) as observed data and RegCM4 for the study period of 1980–2011 after bias correction an  $R^2$  value of 0.34. From Fig. 4, which shows the distribution of observed rainfall and the RegCM4 data, we can infer that though the lower quartile (first 25% data points) is the same for both the data sets, the Interquartile (middle 50% data points) ranges from 0 to 100 mm and 0 mm to 150 mm respectively, while the upper quartile (last 25% data points) range from 100 to 220 mm and 150 mm to 300 mm respectively for observed and the RegCM4 data. The median lies around 20 mm for observed data, while it lies about 10 mm for the RegCM4 data for the historic period.

The annual inflow to the Nagarjuna Sagar varies over a wide range of values ranging from a maximum inflow of about 1683 Thousand Million Cubic (TMC)

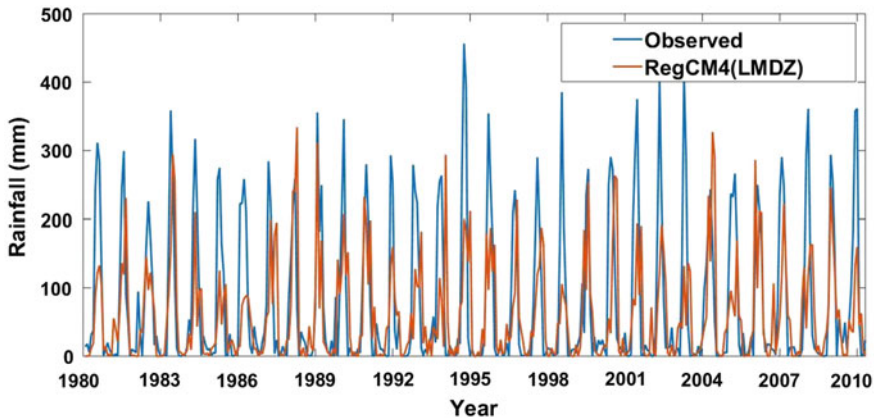


Fig. 3 Comparison of the observed and RegCM4 model rainfall data for the period 1980–2011

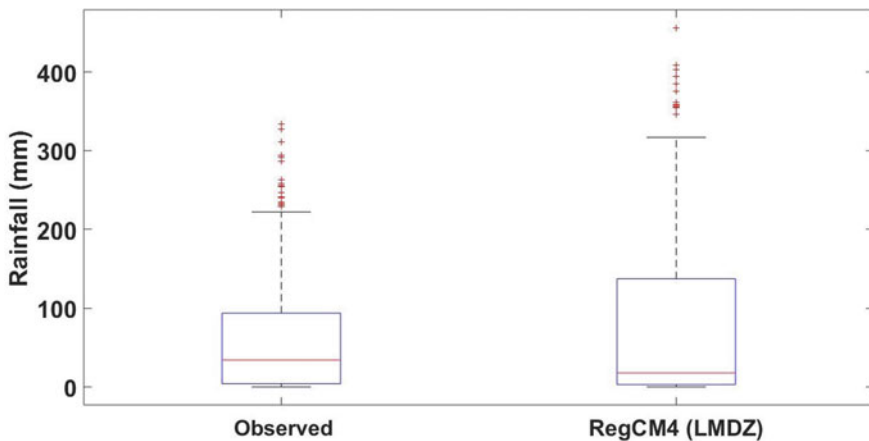


Fig. 4 Box plot of the observed and RegCM4 model rainfall data for the period 1980–2011

feet during the year 1998–99 and a minimum of about 149 TMC in the year 2003–04. A maximum monthly inflow of 769 TMC was received in October 1998. Peak inflows were observed from July to October every year. The annual outflow from the Nagarjuna Sagar varies over a wide range of values ranging from a maximum outflow of about 1750 TMC during 1981–82 and a minimum of about 158 TMC in the year 2003–04. A maximum monthly outflow of 770 TMC was received in October 1998. The average annual outflows from Nagarjunasagar Reservoir are around 600 TMC.

The climatic variables considered for the statistical models were the rainfall at the current and previous interval inflow to the reservoir while modeling the reservoir inflows. Similarly, for the Inflow—outflow model, input variables are the inflow to the reservoir at the current interval. The models used in the current study are the

multiple linear regression model and linear regression model, respectively, to project the inflow and outflow of the reservoir. The study used the IMD gridded monthly rainfall data and monthly reservoir inflow data to train and test the multiple linear regression model. Similarly, the study used the monthly inflow and outflow data of the reservoir to train the model, and the results were tested. The model’s validity and efficiency can be seen when the training dataset fits on the trained model and high accuracy in terms of high values of  $R^2$ . Based on the statistical results, both the rainfall-inflow model and inflow-outflow model produced the  $R^2$  values of 0.79, 0.89 for the training period, and 0.48, 0.73 for the testing period. Figures 5, 6, 7, and 8 show the comparison between the observed and the predicted inflow to the reservoir for both training and testing periods. Figures 9 and 11 shows the observed

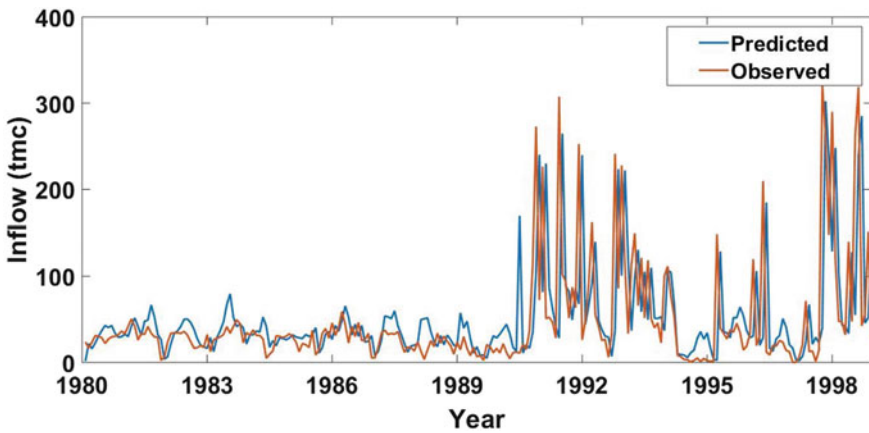


Fig. 5 Comparison graph of the observed and predicted inflow during training period

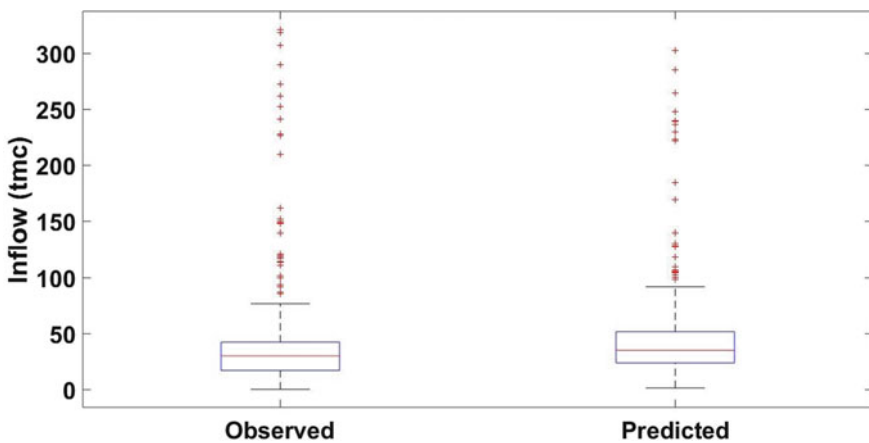


Fig. 6 Box plot of the observed and predicted inflow during training period



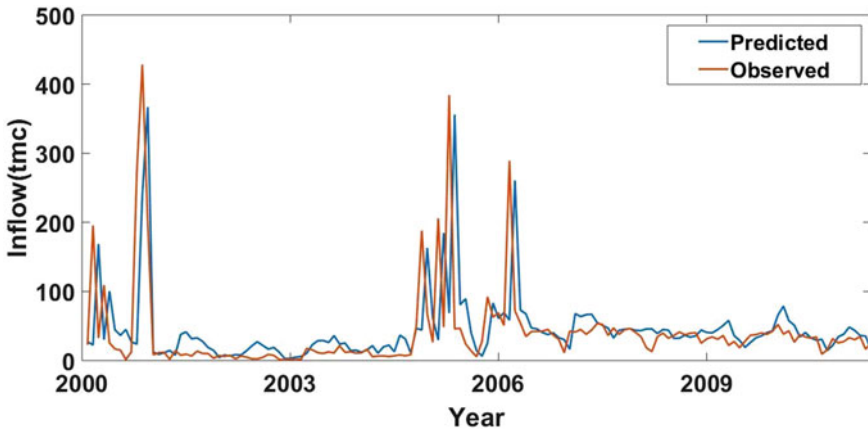


Fig. 7 Comparison graph of the observed and predicted inflow during the testing period

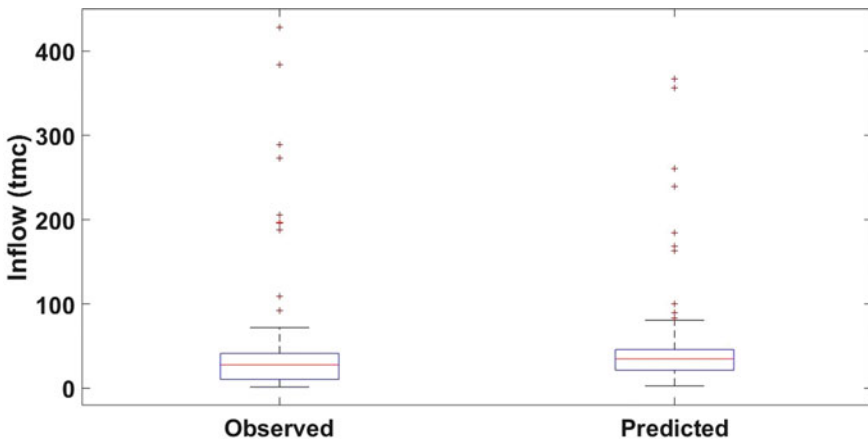


Fig. 8 Box plot of the observed and predicted inflow during the testing period

and predicted outflow for the training and testing period, respectively. Figures 10 and 12 show the distribution of the outflow of both the observed and the predicted data for the training and testing period, respectively. It can be inferred that the interquartile range between 0 to 50 TMC for both the observed and the predicted data.

A significant decrease in the inflow to the reservoir was observed for the period of 1980 to 2011. Furthermore, a considerable reduction in the outflow from the reservoir during 1996–2000 is due to the water and land conservation projects and major drought years during 2000–2004 [32]. The irrigated regions through rainfed and groundwater lower Krishna basin has been noted as increased by 44% over the last 50 years, which resulted in 58% of total water depletion during 1996–2000 and consequent decrease of inflow to the reservoir (IWMI).

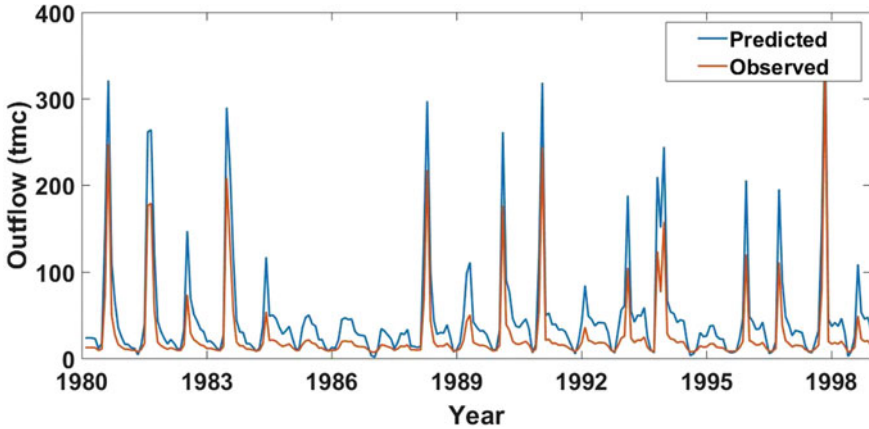


Fig. 9 Comparison graph of the observed and predicted outflows during training period

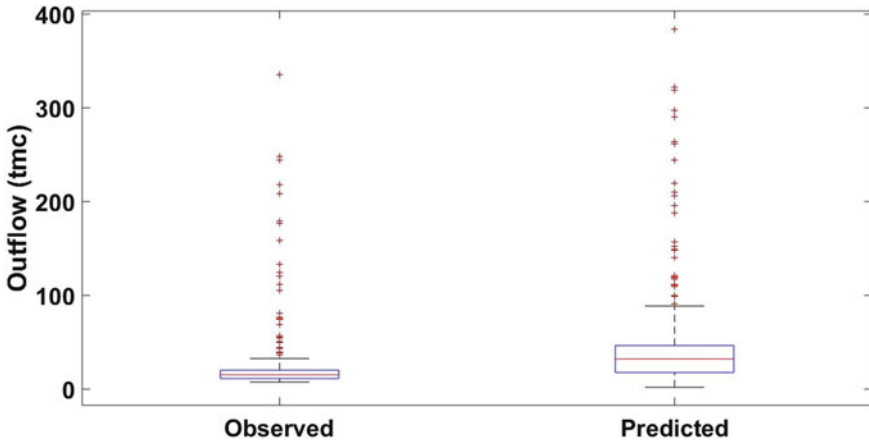


Fig. 10 Box plot of the observed and predicted outflows during training period

The trained and tested rainfall-inflow and inflow-outflow models were used with CORDEX model projections to study the catchment-scale rainfall, inflows, outflows for the projected scenarios. Various low flow quantiles estimated from FDCs have been chosen to analyze the trends of the environmental flows for Nagarjuna Sagar dam. In the current study, the flow duration curve was plotted for the available 32 years of outflow data from the 1980–2011 on *Y*-axis and percentage exceedance on the *X*-axis, as shown in Fig. 13. The outflow values for the corresponding 75, 80, 85, 90, 95% exceedances were taken as Q75, Q80, Q85, Q90, Q95 values from the plotted curve. Table 2 shows the flow values of the respective thresholds for the historic period.

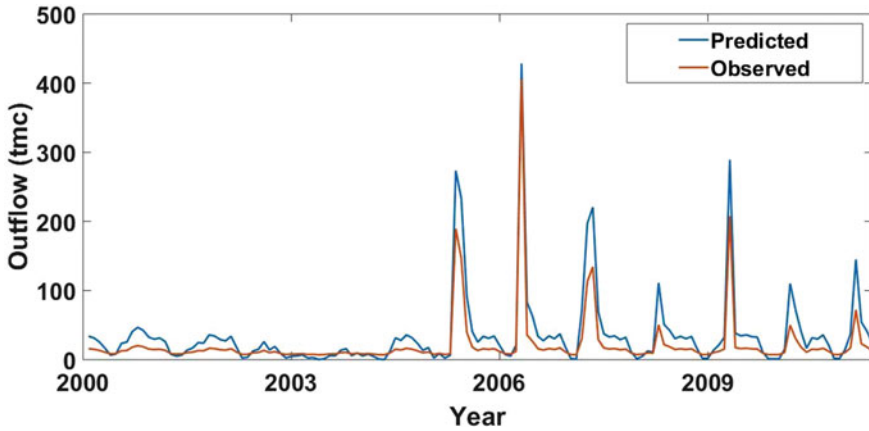


Fig. 11 Comparison graph of the observed and predicted outflows during the testing period

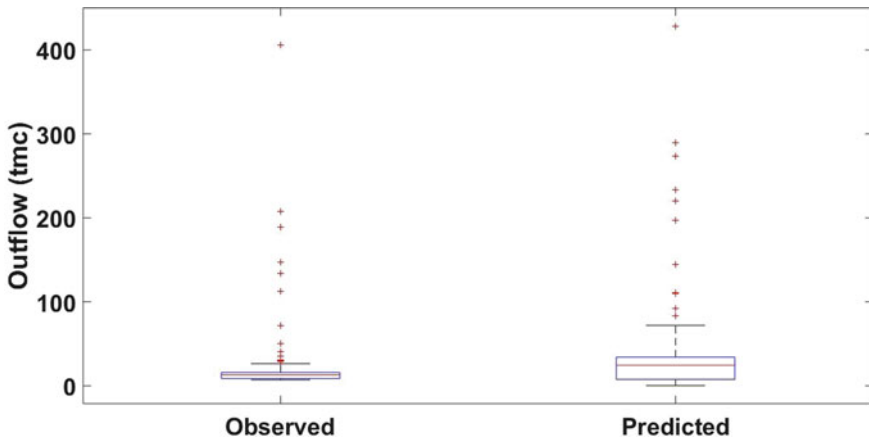
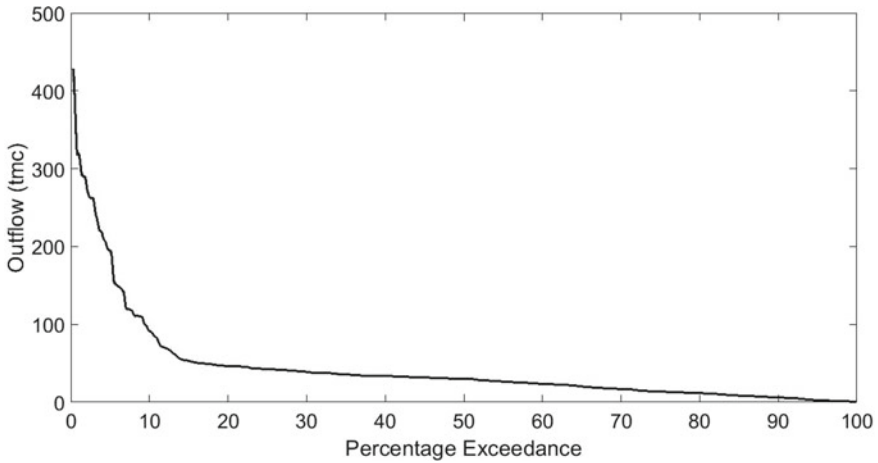


Fig. 12 Box plot of the observed and predicted outflows during the testing period

The outflows from 1980 to 2050 were obtained to determine environmental flows. The historical low flow values for various thresholds were given in Table 2—the low flow duration indices Q75, Q80, Q85, Q90 and Q95 for every decade starting from 1980 to 2050, as shown in Table 3. It has been observed that there is a considerable increase in the environmental flow values higher thresholds like Q75 and Q80 from 1980–89 decade to the 1990–99 decade while with a fall in the flow values of the lower thresholds due to the decrease in the inflow to the reservoir during 1996–2000 due to the water and land conservation projects.

The Q75 (16.54 TMC) and Q80 (13.24) flows from 1980 to 1989 were increased to 22.39 TMC and 16.46 TMC respectively from 1990 to 1999. The Q85, Q95, and Q95 flows have been noted to decrease from 1980–1989 to 1990–1999. Furthermore,



**Fig. 13** Flow duration curve

**Table 2** The low flow values of the basin for the period 1980–2011

| Threshold | Low flow values (TMC) |
|-----------|-----------------------|
| Q75       | 13.60                 |
| Q80       | 11.48                 |
| Q85       | 8.51                  |
| Q90       | 5.93                  |
| Q95       | 2.54                  |

a substantial decrease in environmental flows in the range of Q75 to Q95 (Table 3) in recent years for the Nagarjuna Sagar dam. However, the low flows estimated based on CORDEX model projections of rainfall have decreased with lower magnitudes. The low flow projections for the future are observed to range from 11 to 14, with a median of 11.89. Such results are evident in the context of the increase of rainfall projections over the catchment area. Also, it can be noted that as the rainfall was the primary contributing variable in the modeling framework of the rainfall-inflow-outflow model as demonstrated in the present study, increasing projections of rainfall have increased low flow quantiles. An environmental flow assessment model should consider various factors such as evapotranspiration, land-use changes, and soil properties of the catchment. Such detailed factors through a hydrological model can make better predictions over the catchment rainfall variability, resulting in inflows and consequent downstream releases from the dam. Furthermore, the study used one CORDEX model output to assess environmental flows, which can vary with other regional climate model outputs. Therefore, the study can be implemented for various CORDEX model projections of rainfall and temperatures, wind speed, and other climate variables.

The low flow values of the Nagarjuna Sagar basin for various decades

| Year    | Q75   | Q80   | Q85   | Q90   | Q95   |
|---------|-------|-------|-------|-------|-------|
| 1980–89 | 16.54 | 13.24 | 11.94 | 11.50 | 8.71  |
| 1990–99 | 22.39 | 16.46 | 10.14 | 7.69  | 6.66  |
| 2000–11 | 7.572 | 5.55  | 3.43  | 2.13  | 1.37  |
| 2012–19 | 12.24 | 11.94 | 11.67 | 11.57 | 11.40 |
| 2020–29 | 11.93 | 11.82 | 11.61 | 11.49 | 11.29 |
| 2030–39 | 12.18 | 11.96 | 11.81 | 11.59 | 11.28 |
| 2040–50 | 11.71 | 14.07 | 11.44 | 12.90 | 12.28 |

## 5 Conclusions

A modeling framework has been demonstrated to estimate the environmental flows under climate change using regional circulation model outputs. The flow duration curve estimated low flow quantiles in the 75–95% threshold were considered environmental flows. A catchment-scale rainfall-inflow-outflow modeling approach has been developed to assess the impacts of the environmental flows under climate signals. The present study has demonstrated a modeling approach to synthesize the regional circulation model outputs to estimate the downstream releases regarding environmental flow criteria in terms of low flows estimated using flow duration curves. Regression models were developed to protect the reservoir's inflow and outflow from the projected rainfall obtained from the regional circulation model outputs data. The observed and projected outflows were used to estimate the low flow values for 75-, 80-, 85-, 90-, 95-percent exceedances for the Nagarjuna Sagar dam. The models for projecting the inflow and outflow were developed using regression techniques, and the model performances were assessed using  $R^2$  estimates. An  $R^2$  value of 0.79 and 0.89 for the training period and 0.48 and 0.73 for the testing period were observed for the rainfall-inflow and inflow-outflow models. The Environmental flows of the basin were estimated for the historical and projected period. A substantial decrease in environmental flows in the range of Q75 to Q95 was observed in recent years for the Nagarjuna Sagar dam.

Furthermore, the low flows estimated based on regional circulation model projections of rainfall have decreased environmental flows with lower magnitudes. Such results are evident in the context of the increase of rainfall projections over the Nagarjuna Sagar reservoir catchment. Future directions towards estimation of environmental flows under climate change can implement adopting a holistic approach that can relate rainfall, temperature, and other climatic variables over the catchment along with catchment characteristics of soil, land use, and other water abstractions in the modeling of reservoir inflows. There should be a unique approach to convert the inflows to the reservoir releases or outflows with consideration of the reservoir's

storage. Further, the demonstrated approach can be integrated with various general circulation model outputs to study the uncertainty range in the environmental flows resulting from each climate model.

## References

1. Gao J, Gao Y, Zhao G, Hörmann G (2010) Minimum ecological water depth of a typical stream in Taihu Lake Basin, China. *Quat Int* 226(1):136–142. <https://doi.org/10.1016/j.quaint.2010.03.004>
2. Shaeri Karimi S, Yasi M, Eslamian S (2012) Use of hydrological methods for assessment of environmental flow in a river reach. *Int J Environ Sci Technol* 9(3):549–558. <https://doi.org/10.1007/s13762-012-0062-6>
3. Brown C, King K (2003) Water resources and environment technical note C1. In: *Environmental flows: concepts and methods*, p 28
4. Dyson M, Bergkamp G, Scanlon J (2008) *Flow : the essentials of environmental flows*. In: IUCN. <https://www.iucn.org/content/flow-essentials-environmental-flows-0>
5. Smakhtin VU, Revenga C, Doll P (2004) Taking into account environmental water requirements in global-scale water resources assessments. International Water Management Institute, Comprehensive Assessment Secretariat, Report. <https://cgspace.cgiar.org/handle/10568/39741>
6. Jain SK, Kumar P (2014) Environmental flows in India: towards sustainable water management. *Hydrol Sci J* 59(3–4):751–769. <https://doi.org/10.1080/02626667.2014.896996>
7. Tharme RE (2003) A global perspective on environmental flow assessment: emerging trends in the development and application of environmental flow methodologies for rivers. *River Res Appl* 19(5–6):397–441. <https://doi.org/10.1002/rra.736>
8. Arthington A, Tharme R, Brizga SO, Pusey B, Kennard M (2004) Environmental flow assessment with emphasis on holistic methodologies
9. Tennant DL (1976) Instream flow regimens for fish, wildlife, recreation and related environmental resources. *Fisheries* 1(4):6–10. [https://doi.org/10.1577/1548-8446\(1976\)001%3c0006:IFRFFW%3e2.0.CO;2](https://doi.org/10.1577/1548-8446(1976)001%3c0006:IFRFFW%3e2.0.CO;2)
10. Fraser JC (1978) Suggestions for developing flow recommendations for in-stream uses of New Zealand streams (a report to the National Water and Soil Organisation). Water and Soil Miscellaneous Publication—National Water and Soil Conservation Organisation, New Zealand. <https://agris.fao.org/agris-search/search.do?recordID=NZ7850169>
11. Tessmann SA (1979) Environmental use sector: reconnaissance elements of the western Dakotas region of South Dakota study. Water Resources Institute, South Dakota State University, Brookings, S.D.
12. Richter BD, Baumgartner JV, Powell J, Braun DP (1996) A method for assessing hydrologic alteration within ecosystems. *Conserv Biol* 10(4):1163–1174. <https://doi.org/10.1046/j.1523-1739.1996.10041163.x>
13. Jowett I (1989) River hydraulic and habitat simulation. RHYHABSIM computer manual
14. Książek L, Woś A, Florek J, Wyrębek M, Młyński D, Wałęga A (2019) Combined use of the hydraulic and hydrological methods to calculate the environmental flow: Wisłoka river, Poland: case study. *Environ Monit Assess* 191(4):254. <https://doi.org/10.1007/s10661-019-7402-7>
15. Parasiewicz P (2007) The MesoHABSIM model revisited. *River Res Appl* 23(8):893–903. <https://doi.org/10.1002/rra.1045>
16. Gopal B (2016) A conceptual framework for environmental flows assessment based on ecosystem services and their economic valuation. *Ecosyst Serv* 21:53–58. <https://doi.org/10.1016/j.ecoser.2016.07.013>
17. Swift CH (1975) Estimation of stream discharges preferred by steelhead trout for spawning and rearing in western Washington, [s.n.]. 75–155. <https://doi.org/10.3133/ofr75155>

18. Bovee KD, Lamb BL, Bartholow JM, Stalnaker CB, Taylor J, Henriksen J (1998) Stream habitat analysis using the instream flow incremental methodology. U.S. Geological Survey, Fort Collins, CO, Federal Government Series 1998-0004. <http://pubs.er.usgs.gov/publication/itr19980004>
19. Herricks EE, Braga MI (1987) Habitat elements in river basin management and planning. *Water Sci Technol* 19(9):19–29. <https://doi.org/10.2166/wst.1987.0063>
20. Stalnaker CB (1979) Myths concerning instream flows: a background to understanding instream uses. U.S. Fish and Wildlife Service, Western Energy and Land Use Team, Fort Collins, CO, Other Report FWS/OBS-79/03. <http://pubs.er.usgs.gov/publication/70119913>
21. Brown C, King J (2000) A summary of the drift process for environmental flow assessments for rivers. Southern Waters Information Report No. 01/00, Mowbray, South Africa
22. Bovee KD (1982) A guide to stream habitat analysis using the instream flow incremental methodology. IFIP No. 12, U.S. Fish and Wildlife Service, 82/26. [https://pubs.er.usgs.gov/publication/fwsobs82\\_26](https://pubs.er.usgs.gov/publication/fwsobs82_26)
23. Arthington A et al (1992) Development of an holistic approach for assessing environmental flow requirements for riverine ecosystems. In: Proceedings of an international seminar and workshop on water allocation for the environment, Jan 1992.
24. Arthington A (1998) Comparative evaluation of environmental flow assessment techniques: review of holistic methodologies, Jan 1998
25. King JM, Tharme RE (1994) Assessment of the instream flow incremental methodology (IFIM) and initial development of alternative instream flow methodologies for South Africa. Water Research Commission, Report No. 295/1/94. Pretoria, SA, p 590
26. Dhanya CT, Kumar A (2015) Making a case for estimating environmental flow under climate change. *Curr Sci* 109
27. Chaudhary S, Dhanya CT, Kumar A, Shaik R (2019) Water quality-based environmental flow under plausible temperature and pollution scenarios. *J Hydrol Eng* 24(5):05019007. [https://doi.org/10.1061/\(ASCE\)HE.1943-5584.0001780](https://doi.org/10.1061/(ASCE)HE.1943-5584.0001780)
28. Smakhtin VU (2001) Low flow hydrology: a review. *J Hydrol* 240(3):147–186. [https://doi.org/10.1016/S0022-1694\(00\)00340-1](https://doi.org/10.1016/S0022-1694(00)00340-1)
29. Rehana S, Mujumdar PP (2014) Basin scale water resources systems modeling under cascading uncertainties. *Water Resour Manag* 28(10):3127–3142. <https://doi.org/10.1007/s11269-014-0659-2>
30. Verma RK, Murthy S, Verma S, Mishra SK (2017) Design flow duration curves for environmental flows estimation in Damodar River Basin, India. *Appl Water Sci* 7(3):1283–1293. <https://doi.org/10.1007/s13201-016-0486-0>
31. Singh S, Ghosh S, Sahana AS, Vittal H, Karmakar S (2017) Do dynamic regional models add value to the global model projections of Indian monsoon? *Clim Dyn* 48(3):1375–1397. <https://doi.org/10.1007/s00382-016-3147-y>
32. Rehana S, Sireesha Naidu G, Monish NT, Sowjanya U (2020) Modeling hydro-climatic changes of evapotranspiration over a semi-arid river basin of India. *J Water Clim Change* no. jwc2020173. <https://doi.org/10.2166/wcc.2020.173>

# Trend Analysis of Annual, Seasonal, and Monthly Streamflow in Naula Watershed, Uttarakhand (India)



Anurag Malik and Anil Kumar

**Abstract** For optimal development and management of water resources, a study on trend analysis is crucial. The present study employed the Theil–Sen’s slope (TSS), simple linear regression (SLR), Kendall rank correlation (KRC), Mann–Kendall (MK), and modified MK (MMK) methods to investigate the magnitude (size of trend) and trend in annual, seasonal, and monthly streamflow of Naula and Kedar hydrological stations. Both stations are placed in the upper catchment of Ramganga River basin (RRB), state of Uttarakhand, India. The outcomes of KRC, MK, and MMK demonstrate the significant negative and positive trends in annual, seasonal, and monthly streamflow at 5%, 10%, and 1% levels of significance (LOS) for both stations. While the magnitude (ha-m/scale) was found falling at both stations for all timescales, except October month had rising magnitude at Kedar station. These findings would help in the efficient utilization of existing water resources under climate change in the study basin.

**Keywords** Streamflow · Trend analysis · Uttarakhand

## 1 Introduction

Recently, climate change and human activities have a considerable impact on hydro-meteorological variables, and streamflow is one of them and a vital component of the hydrologic cycle [6, 23, 25]. Devi et al. [4] reported that climate change becomes an international matter, challenging humanity by increasing extra pressure on the earth’s atmosphere which has consequences in heatwaves, floods, droughts, and forest fires and also leads to water shortages and agricultural and socio-economic failures [22]. Therefore, understanding the trends or sudden jumps in hydro-climatic

---

A. Malik · A. Kumar

Department of Soil and Water Conservation Engineering, College of Technology, G.B. Pant University of Agriculture and Technology, Pantnagar-263145, Uttarakhand, India

A. Malik (✉)

Punjab Agricultural University, Regional Research Station, Bathinda-151001, Punjab, India



variables is very important for the sustainable management of water systems [5]. A variety of methods such as Theil–Sen’s slope (TSS), simple linear regression (SLR), Spearman’s rho (SR), Kendall rank correlation (KRC), Mann–Kendall (MK), innovative trend analysis (ITA), and modified MK (MMK) are available for trend identification which has extensive application in numerous fields of water engineering [2, 3, 12, 13, 16–18, 20].

To related context, Diop et al. [7] exploited Pettitt, TSS, MK, and MMK techniques for detecting the change point, magnitude, and trend in three different time series of streamflow (i.e. seasonal, annual, and monthly) at Bafing Makana station situated in upper Senegal River basin (SRB), West Africa. The outcomes of applied methods were verified at 5% LOS. They observed a significant decreasing trend in annual and seasonal series and a non-significant decreasing trend in monthly series, except the June month. The change points were noted in 1976 and 1993 with varying magnitude.

Kale and Kumar [9] investigated trend and magnitude at five streamflow gauging stations located in the Tapi River basin, India, by applying the MK, MK with block bootstrapping, innovative trend (IT), and TSS methods. They found that the seasonal streamflow (i.e. winter, pre-monsoon, monsoon, and post-monsoon) had a significant negative trend at all study stations. Li et al. [15] deliberated how human interventions and climate change affect the run-off of the Mun River, Thailand, by applying MK, Morlet wavelet transforms, and double cumulative curve methods. They found abrupt variation (1999/2000) in the annual run-off with an increasing trend due to a decrease in the forest range, a small reduction in evaporation and farmland extent, and a dramatic increase in the garden area during 1999.

To this end, the present study was conducted to inspect the temporal trend and magnitude in long-term series of annual, seasonal, and monthly streamflow by employing the Kendall rank correlation (KRC), Mann–Kendall (MK), modified MK (MMK), Theil–Sen’s slope (TSS), and simple linear regression (SLR) methods at Naula and Kedar sites on 10, 5, and 1% levels of significance (LOS). The results of this research may help to formulate a reliable decision support system for sustainable water resources management in the study region. As authors noticed, no such study has been conducted in the study basin.

## 2 Materials and Methods

### 2.1 Study Site and Data Acquisition

The monthly streamflow data of 33-years (1975–2007) of two hydrological stations (i.e. Naula and Kedar) were gained from Forest and Soil Conservation Department (FSCD), Ranikhet (Uttarakhand). The annual series is comprising of the sum of January to December months, whereas the seasonal series include (1) December to February (winter), (2) March to May (pre-monsoon), (3) June to September (monsoon), and (4) October to November (post-monsoon). Figure 1 shows the

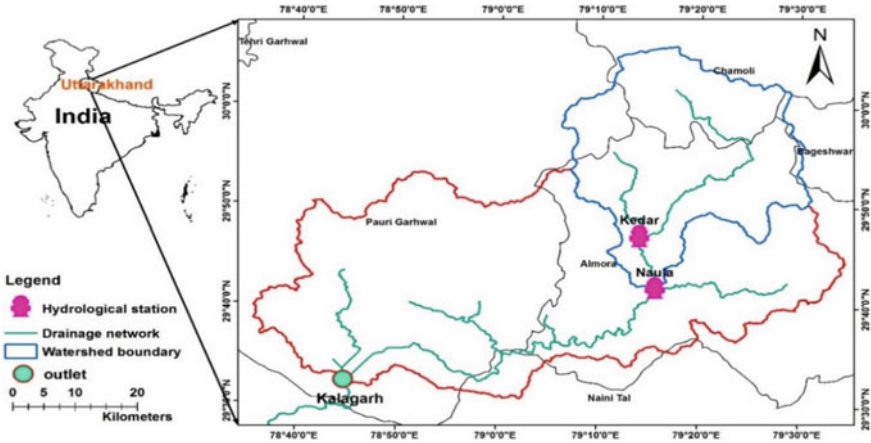


Fig. 1 Map of study basin

geographical coordinates of both stations with changing elevation from 724 m (Naula) to 929 m (Kedar) above the mean sea level. The area of the Naula watershed is 1071.26 km<sup>2</sup> with hilly terrain.

### 2.2 Mann–Kendall (MK) Method

For assessment of monotonic trend in climatic parameters, the MK method is extensively utilized and described as follows [10, 15]:

$$Z_{MK} = \begin{cases} \frac{S - 1}{\sqrt{Var(S)}}; & \text{if } S > 0 \\ 0; & \text{if } S = 0 \\ \frac{S + 1}{\sqrt{Var(S)}}; & \text{if } S < 0 \end{cases} \quad (1)$$

$$S = \sum_{i=1}^{n-1} \sum_{j=i+1}^n \text{sgn}(Q_j - Q_i) \quad (2)$$

$$\text{sgn}(Q_j - Q_i) = \begin{cases} 1; & \text{if } (Q_j - Q_i) > 0 \\ 0; & \text{if } (Q_j - Q_i) = 0 \\ -1; & \text{if } (Q_j - Q_i) < 0 \end{cases} \quad (3)$$

$$\text{Var}(S) = \frac{n(n-1)(2n+5) - \sum_{i=1}^P t_i(t_i-1)(2t_i+5)}{18} \quad (4)$$

in which  $Q_i$  and  $Q_j$  are the rank of  $i$ th ( $i = 1, 2, \dots, n - 1$ ) and  $j$ th ( $j = i + 1, 2, \dots, n$ ) observations,  $\text{Var}(S)$  indicates the variance,  $P$  is the number of tied groups,  $t_i$  shows tied cluster in data, and  $n$  specifies the streamflow ( $Q$ ) data points.

After that, two hypotheses are proposed, i.e.  $H_0$  (null hypothesis) = no trend in streamflow data and  $H_1$  (alternative hypothesis) = trend in streamflow data. The  $H_0$ , and  $H_1$  are tested at 1% ( $Z = \pm 2.33$ ), 5% ( $Z = \pm 1.96$ ), and 10% ( $Z = \pm 1.645$ ) levels of significance (LOS).  $H_0$  is discarded, and  $H_1$  is accepted when  $\pm Z_{MK} > \pm Z_{\alpha/2}$ . A decreasing and increasing trend in streamflow is nominated with negative and positive values of  $Z_{MK}$ ,  $Z_{MMK}$ , and  $Z_{KRC}$ .

### 2.3 Modified Mann–Kendall (MMK) Method

The MMK method is the extended form of MK, applied where lag-1 serial correlation is significant [8], and computed by using Eqs. (5–9)

$$Z_{MMK} = \begin{cases} \frac{S - 1}{\sqrt{\text{Var}(s)^*}}; & \text{if } S > 0 \\ 0; & \text{if } S = 0 \\ \frac{S + 1}{\sqrt{\text{Var}(s)^*}}; & \text{if } S < 0 \end{cases} \quad (5)$$

where  $\text{Var}(S)^*$  is the modified variance and computed using Eq. (6)

$$\text{Var}(S)^* = \text{Var}(S) \frac{n}{n_s} \quad (6)$$

in which  $\frac{n}{n_s}$  is a correction factor and determined using Eq. (7) given by Lettenmaier [14]

$$\frac{n}{n_s} = 1 + \frac{2}{n(n-1)(n-2)} \sum_{k=1}^{n-1} (n-k)(n-k-1)(n-k-2)r_k \quad (7)$$

where  $r_k$  = significant serial correlation at lag- $k$  and calculated using Eq. (8):

$$r_k = \frac{\frac{1}{(n-k)} \sum x_i x_{i+k} - \frac{1}{(n-k)^2} \sum x_i x_{i+k}}{\left\{ \frac{1}{(n-k)} \sum x_i^2 - \frac{1}{(n-k)^2} (\sum x_i)^2 \right\}^{1/2} \left\{ \frac{1}{(n-k)} \sum x_{i+k}^2 - \frac{1}{(n-k)^2} (\sum x_{i+k})^2 \right\}^{1/2}} \quad (8)$$

The significance of  $r_k$  value is tested using Eq. (9) given by [1, 20]

$$(r_k)_{\text{upper/lower}} = \left[ \frac{-1}{(n-k)} \right] \pm Z_{1-\alpha/2} \left[ \frac{\sqrt{n-k-1}}{(n-k)} \right] \quad (9)$$

When  $(r_k)_{\text{upper}} < r_k < (r_k)_{\text{lower}}$ , then  $H_0$  of no significant serial correlation is rejected, and  $H_1$  of a significant serial correlation is accepted at 90%, 95%, and 99% confidence limits (CL).

## 2.4 Kendall Rank Correlation (KRC) Method

Kendall [11] invented the concept of the KRC method, also known as Kendall's tau ( $\tau$ ) coefficient method. The KRC is employed for computing the rank correlation of data using Eqs. (10–12)

$$Z_{\text{KRC}} = \frac{\tau}{\sqrt{\text{var}(\tau)}} \quad (10)$$

$$\tau = \left[ \left\{ \frac{4P}{n(n-1)} \right\} - 1 \right] \quad (11)$$

$$\text{Var}(\tau) \left[ \frac{2(2n+5)}{9n(n-1)} \right] \quad (12)$$

where  $P$  is the numbers of times  $x_j > x_i$  in all pairs of data points.

## 2.5 Theil–Sen's Slope (TSS) Method

The TSS computes the magnitude of the trend of all pair-wise slopes among each pair of points in the time series data [21, 24]. The TSS with negative/positive value designates a falling/rising magnitude, while TSS with zero displays no trend. The TSS for  $N$  (odd and even) time series data is computed by Eqs. (13–14)

$$\text{TSS}_{ij} = \text{median} \left( \frac{Q_j - Q_i}{j - i} \right) \quad i < j \quad (13)$$

in which  $Q_j$  and  $Q_i$  represents the pair data values on  $j > i$ , respectively, for  $i = 1, 2, 3, \dots, N$ . The median TSS is computed as follows:

$$\text{TSS}_{\text{median}} = \begin{cases} \text{TSS}_{\left(\frac{N+1}{2}\right)} & \text{if } N \text{ is odd} \\ \frac{1}{2} \left[ \text{TSS}_{\left(\frac{N}{2}\right)} + \text{TSS}_{\left(\frac{N+2}{2}\right)} \right] & \text{if } N \text{ is even} \end{cases} \quad (14)$$

## 2.6 Simple Linear Regression (SLR) Method

The SLR is a parametric model, which examines the trend in data series using Eq. (15)

$$y = c + mx \tag{15}$$

where  $c$  = intercept,  $x$  = independent parameter,  $m$  = slope of regression line, and  $y$  = dependent parameter.

## 3 Results and Discussion

### 3.1 Trend Investigation at Naula and Kedar Stations

The results of parametric (i.e. SLR) and nonparametric (i.e. TSS, KRC, MK, and MMK) methods to inspect the trend in annual, seasonal, and monthly streamflow at Naula station during 1975–2007 are recorded in Table 1. The Z-statistics of MK, MMK, and KRC methods were verified at 10, 5, and 1% LOS. As can be seen from

**Table 1** Trend and magnitude pattern at Naula site

| Timescale    | Z <sub>MK</sub> | Z <sub>MMK</sub> | Z <sub>KRC</sub> | TSS (ha-m) | SLR (ha-m) |
|--------------|-----------------|------------------|------------------|------------|------------|
| January      | -2.557***       | -2.047**         | -2.572***        | -40.196    | -34.484    |
| February     | -1.565          |                  | -1.580           | -24.342    | -22.255    |
| March        | -1.720*         |                  | -1.735*          | -27.209    | -49.467    |
| April        | -2.371***       |                  | -2.386***        | -32.847    | -35.836    |
| May          | -2.185**        |                  | -2.200**         | -32.575    | -24.513    |
| June         | -1.534          | -1.235           | -1.549           | -32.135    | -51.460    |
| July         | -2.464***       | -1.986**         | -2.479***        | -279.019   | -304.820   |
| August       | -4.571***       | -3.528***        | -4.586***        | -739.898   | -768.510   |
| September    | -2.309**        |                  | -2.324**         | -288.601   | -294.150   |
| October      | -2.464***       |                  | -2.479***        | -94.971    | -123.760   |
| November     | -3.083***       | -2.406***        | -3.099***        | -53.525    | -60.489    |
| December     | -2.789***       | -2.218**         | -2.807***        | -43.098    | -60.215    |
| Winter       | -3.052***       | -2.402***        | -3.068***        | -126.997   | -116.950   |
| Pre-monsoon  | -2.464***       |                  | -2.479***        | -104.459   | -109.820   |
| Monsoon      | -3.300***       | -2.515***        | -3.316***        | -1348.234  | -1418.900  |
| Post-monsoon | -2.835***       |                  | -2.851***        | -152.121   | -184.240   |
| Annual       | -3.734***       | -2.769***        | -3.750***        | -1675.932  | -1830.000  |

Note \*, \*\*, \*\*\* statistically significant at 10, 5 and 1% LOS

Table 1, there was a significant negative trend in annual ( $-3.734$ ), seasonal (winter to post-monsoon), and monthly (January, April, July, August, October to December) at 1% LOS, for May ( $-2.185$ ) and September ( $-2.309$ ) at 5% LOS and for March ( $-1.720$ ) at 10% LOS by MK method. The MMK technique was implemented to those series of streamflow where serial correlation with lag-1 was found significant at 90%, 95%, and 99% confidence limits (CL). The serial correlation was found significant at 1% CL (annual and monsoon), 5% CL (August, November, December, and winter), and 10% CL (January, June, and July) on the study site. The projected values of  $Z_{MMK}$  are given in Table 1 which displays a significant negative trend in annual ( $-2.769$ ), seasonal (winter and monsoon), and monthly (August and November) at 1% LOS, for January ( $-2.047$ ), July ( $-1.986$ ), and December ( $-2.218$ ) at 5% LOS. Table 1 recaps the calculated value of  $Z_{KRC}$  (KRC-statistic), which exposed a similar pattern of the trend as detected by the MK test at the Naula site.

Similarly, magnitude (or size of trend) on three different scales of streamflow from 1975–2007 was investigated by employing the TSS and SLR methods, and their grades are enlisted in Table 1. It was clearly seen from Table 1 that the magnitude was found to be falling in annual, seasonal, and monthly timescales by both methods on the study station. Also, the obtained results of the SLR method for annual, seasonal, and monthly streamflow series are demonstrated graphically in Figs. 2a–e and 3a–l, respectively.

Likewise, Table 2 summarizes the computed value of  $Z_{MK}$ ,  $Z_{MMK}$ , and  $Z_{KRC}$  at Kedar station for annual, seasonal, and monthly streamflow over 33 years (1975–2007). The significant negative trend was investigated in annual, winter, January, February, April at 10% LOS, for March, and monsoon at 5% LOS, for May, August, and pre-monsoon at 1% LOS by MK and KRC tests. The application procedure of the MMK test is the same as stated earlier (for Naula station). The results of the MMK test (Table 2) disclose that May ( $-2.196$ ) and pre-monsoon ( $-2.070$ ) had a significant positive pattern at 5% LOS.

For Kedar station, the magnitude of streamflow on three different scales was examined with TSS and SLR methods, and their results are outlined in Table 2, which exposed the magnitude of the trend was falling on all timescales by both methods, except the October month had a positive magnitude of streamflow by TSS. Figures 4a–e and 5a–l show the variation of annual, seasonal, and monthly streamflow through the SLR method at Kedar station, respectively.

## 4 Conclusion

In the current study, the trend and magnitude in three different scales of streamflow were investigated on two hydrological stations (i.e. Naula and Kedar) by employing parametric (i.e. SLR) and nonparametric (i.e. MK, MMK, KRC, and TSS) methods at three levels significance (1, 5, and 10%). The results of the investigation demonstrate that annual, seasonal, and monthly streamflow had a significant negative trend with falling magnitude (slope) at both stations, except the October month displays the

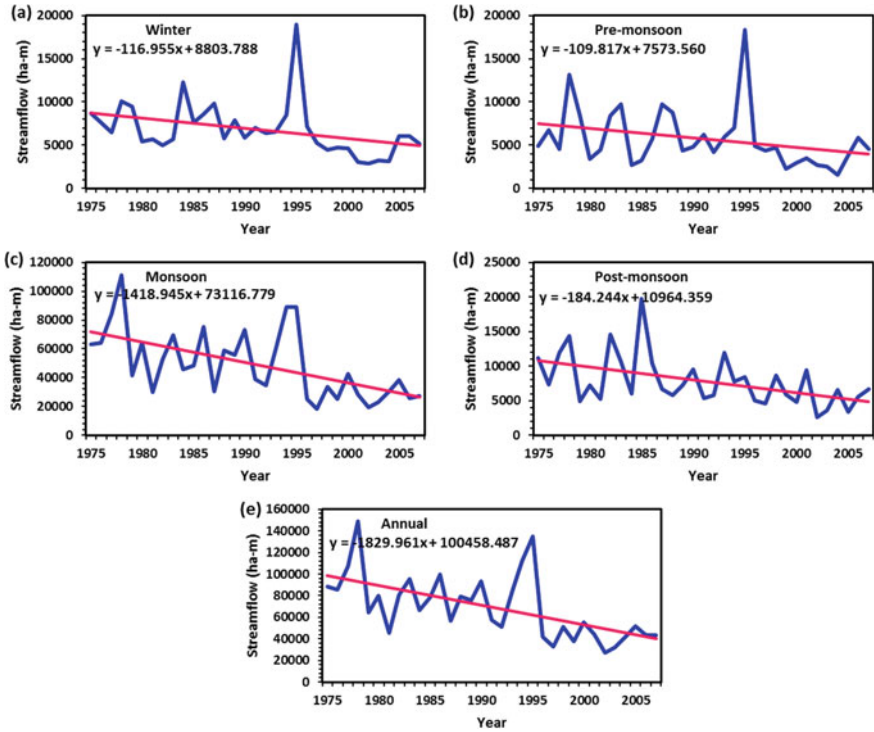


Fig. 2 a–e Seasonal and annual streamflow trend by SLR method on Naula site

rising magnitude at Kedar station by TSS method. Also, it was noted that both KRC and MK methods have identical patterns of trends in all streamflow scales for study stations. The water managers and hydrologists will get benefits from the outcomes of this research to tackle natural hazards like droughts and floods in the study basin.

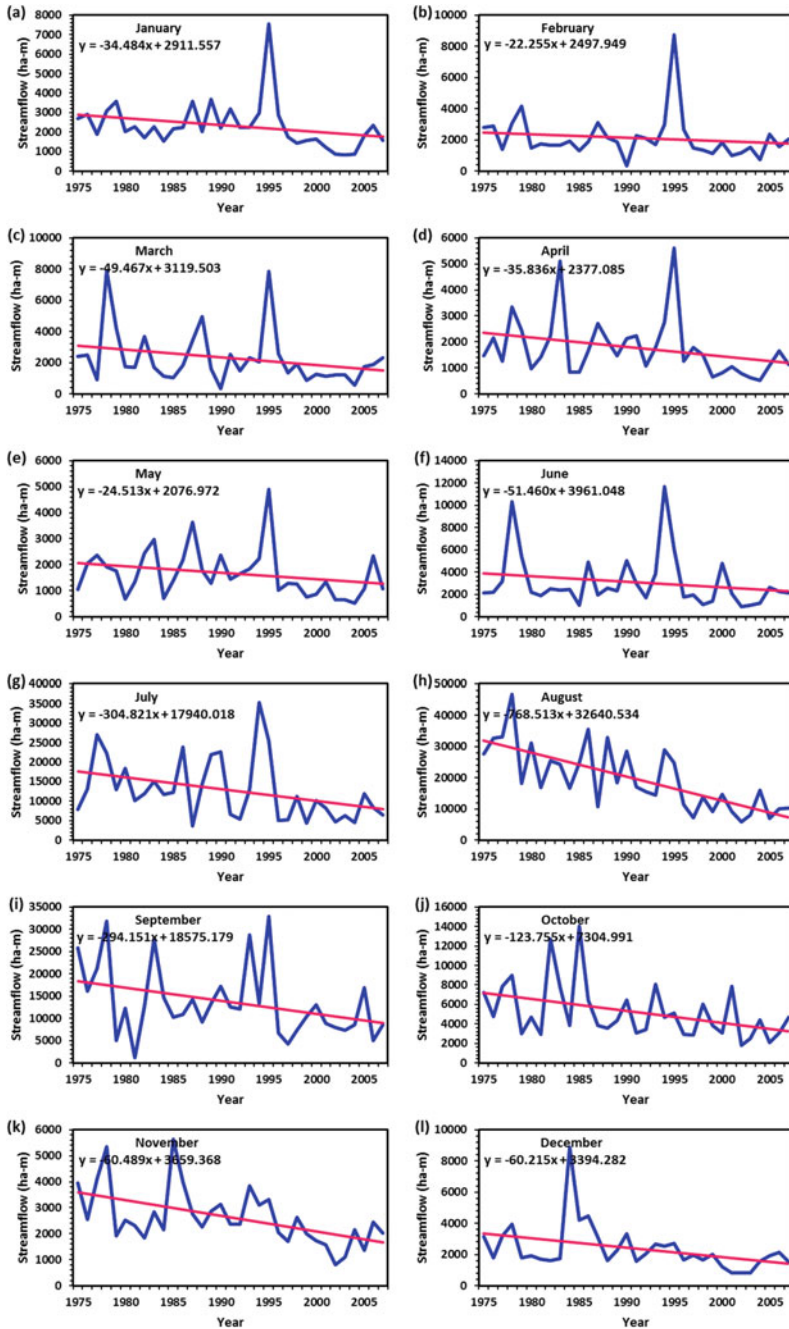


Fig. 3 a-l Monthly streamflow trend by SLR method on Naula site



**Table 2** Trend and magnitude pattern at Kedar site

| Time scale   | Z <sub>MK</sub> | Z <sub>MMK</sub> | Z <sub>KRC</sub> | TSS (ha-m) | SLR (ha-m) |
|--------------|-----------------|------------------|------------------|------------|------------|
| January      | -1.782*         |                  | -1.797*          | -8.059     | -8.560     |
| February     | -1.720*         |                  | -1.735*          | -8.401     | -7.726     |
| March        | -2.015**        |                  | -2.036**         | -10.310    | -10.686    |
| April        | -1.798*         |                  | -1.818*          | -7.452     | -10.097    |
| May          | -3.083***       | -2.196**         | -3.099***        | -12.687    | -16.820    |
| June         | -0.294          | -0.228           | -0.310           | -1.906     | -4.391     |
| July         | -0.821          |                  | -0.837           | -22.994    | -5.873     |
| August       | -2.928***       |                  | -2.944***        | -93.247    | -102.240   |
| September    | -0.170          |                  | -0.186           | -3.805     | -27.734    |
| October      | 0.077           |                  | 0.093            | 1.791      | -2.823     |
| November     | -0.651          |                  | -0.669           | -3.220     | -1.407     |
| December     | -0.496          |                  | -0.515           | -2.061     | -0.470     |
| Winter       | -1.875*         |                  | -1.890*          | -17.827    | -16.756    |
| Pre-monsoon  | -2.650***       | -2.070**         | -2.665***        | -36.220    | -37.603    |
| Monsoon      | -2.030**        |                  | -2.045**         | -141.812   | -140.240   |
| Post-monsoon | -0.201          |                  | -0.217           | -2.775     | -4.229     |
| Annual       | -1.937*         |                  | -1.952*          | -217.806   | -198.830   |

Note \*, \*\*, \*\*\* statistically significant at 10, 5 and 1% LOS

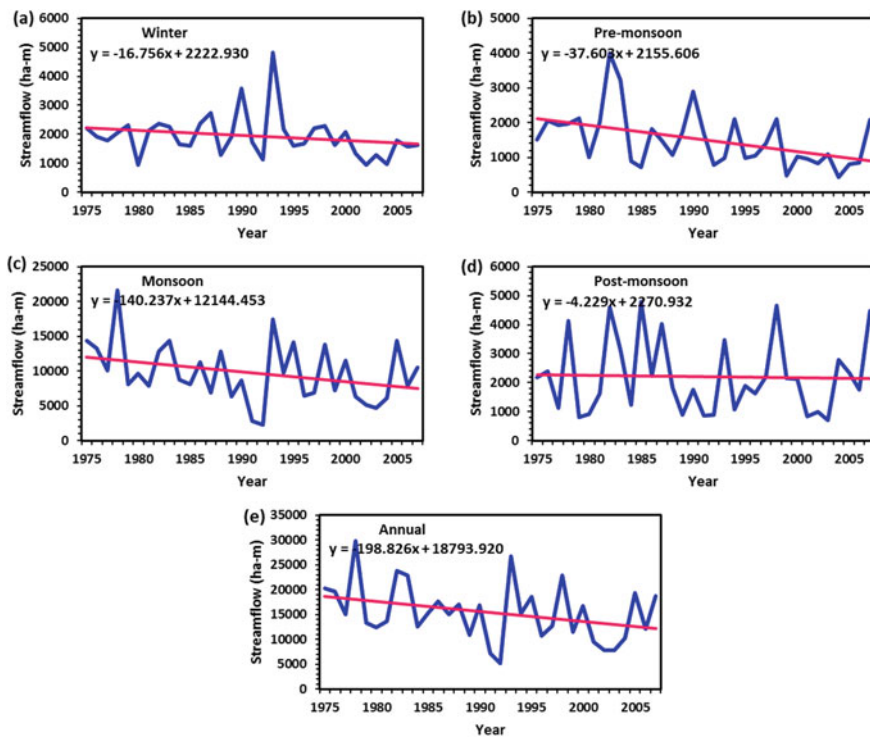


Fig. 4 a–e Seasonal and annual streamflow trend by SLR method on Kedar site

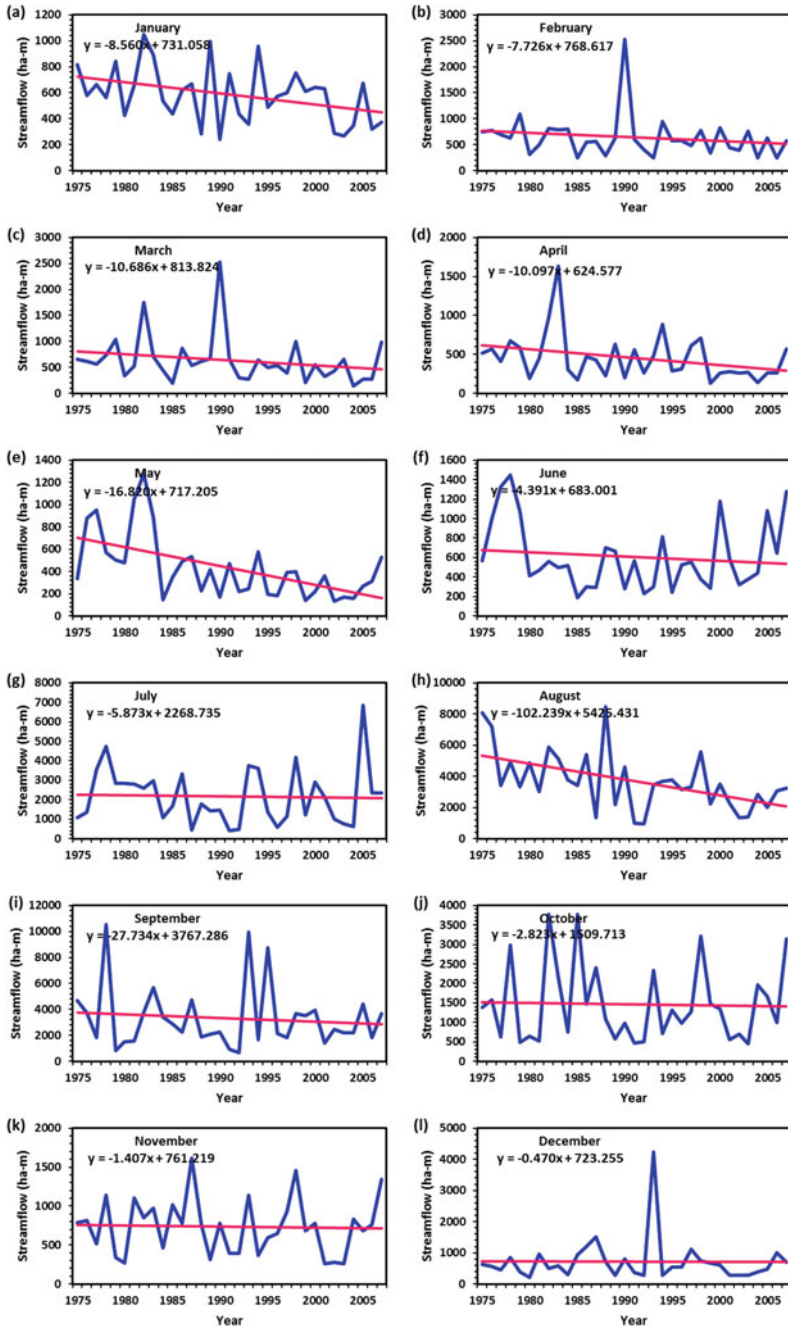


Fig. 5 a-l Monthly streamflow trend by SLR method on Kedar site

## References

1. Anderson RL (1942) Distribution of the serial correlation coefficient. *Ann Math Stat* 13:1–13. <https://doi.org/10.1214/aoms/1177731638>
2. Caloiero T (2018) SPI trend analysis of New Zealand applying the ITA technique. *Geosciences* 8:1–14. <https://doi.org/10.3390/geosciences8030101>
3. Dabanlı İ, Şen Z, Yeleğen MÖ et al (2016) Trend assessment by the innovative-Şen method. *Water Resour Manag* 30:5193–5203. <https://doi.org/10.1007/s11269-016-1478-4>
4. Devi RM, Patasaraiya MK, Sinha B et al (2020) Analyzing precipitation and temperature trends of Kanha and Satpura Tiger Reserve, Central India. *Theor Appl Climatol* 140:1435–1450. <https://doi.org/10.1007/s00704-020-03134-2>
5. Dinpashoh Y, Mirabbasi R, Jhajharia D et al (2014) Effect of short-term and long-term persistence on identification of temporal trends. *J Hydrol Eng* 19:617–625. [https://doi.org/10.1061/\(ASCE\)HE.1943-5584.0000819](https://doi.org/10.1061/(ASCE)HE.1943-5584.0000819)
6. Dinpashoh Y, Singh VP, Biazar SM, Kavehkar S (2019) Impact of climate change on streamflow timing (case study: Guilan Province). *Theor Appl Climatol* 138:65–76. <https://doi.org/10.1007/s00704-019-02810-2>
7. Diop L, Yaseen ZM, Bodian A et al (2018) Trend analysis of streamflow with different time scales: a case study of the upper Senegal River. *ISH J Hydraul Eng* 24:105–114. <https://doi.org/10.1080/09715010.2017.1333045>
8. Hamed KH, Rao RA (1998) A modified Mann-Kendall trend test for autocorrelated data. *J Hydrol* 204:182–196. [https://doi.org/10.1016/S0022-1694\(97\)00125-X](https://doi.org/10.1016/S0022-1694(97)00125-X)
9. Kale GD, Kumar ND (2019) Trend analyses of seasonal streamflows of the Tapi Basin. *Water Conserv Sci Eng* 4:1–11. <https://doi.org/10.1007/s41101-018-0062-6>
10. Kendall MG (1975) Rank correlation methods. 4th edn. Charles Griffin, London 6
11. Kendall MG (1938) A new measure of rank correlation. *Biometrika* 30:81–89
12. Kumar S, Machiwal D, Dayal D (2017) Spatial modelling of rainfall trends using satellite datasets and geographic information system. *Hydrol Sci J* 62:1636–1653. <https://doi.org/10.1080/02626667.2017.1304643>
13. Kuriqi A, Ali R, Pham QB et al (2020) Seasonality shift and streamflow flow variability trends in central India. *Acta Geophys* 68:1461–1475. <https://doi.org/10.1007/s11600-020-00475-4>
14. Lettenmaier DP (1976) Detection of trends in water quality data from records with dependent observations. *Water Resour Res* 12:1037–1046. <https://doi.org/10.1029/WR012i005p01037>
15. Li R, Huang H, Yu G et al (2020) Trends of runoff variation and effects of main causal factors in Mun River, Thailand during 1980–2018. *Water* 12:1–16. <https://doi.org/10.3390/w12030831>
16. Malik A, Kumar A (2020) Spatio-temporal trend analysis of rainfall using parametric and non-parametric tests: case study in Uttarakhand, India. *Theor Appl Climatol* 140:183–207. <https://doi.org/10.1007/s00704-019-03080-8>
17. Malik A, Kumar A, Guhathakurta P, Kisi O (2019) Spatial-temporal trend analysis of seasonal and annual rainfall (1966–2015) using innovative trend analysis method with significance test. *Arab J Geosci* 12:328. <https://doi.org/10.1007/s12517-019-4454-5>
18. Malik A, Kumar A, Najah Ahmed A et al (2020) Application of non-parametric approaches to identify trend in streamflow during 1976–2007 (Naula watershed). *Alexandria Eng J* 59:1595–1606. <https://doi.org/10.1016/j.aej.2020.04.006>
19. Mann HB (1945) Nonparametric tests against trend. *Econometrica* 13:245–259. <https://doi.org/10.2307/1907187>
20. Pingale SM, Khare D, Jat MK, Adamowski J (2014) Spatial and temporal trends of mean and extreme rainfall and temperature for the 33 urban centers of the arid and semi-arid state of Rajasthan, India. *Atmos Res* 138:73–90. <https://doi.org/10.1016/j.atmosres.2013.10.024>
21. Sen PK (1968) Estimates of the regression coefficient based on Kendall's Tau. *J Am Stat Assoc* 63:1379–1389. <https://doi.org/10.1080/01621459.1968.10480934>
22. Şen Z (2014) Trend Identification simulation and application. *J Hydrol Eng* 19:635–642. [https://doi.org/10.1061/\(ASCE\)HE.1943-5584.0000811](https://doi.org/10.1061/(ASCE)HE.1943-5584.0000811)

23. Şen Z (2012) Innovative trend analysis methodology. *J Hydrol Eng* 17:1042–1046. [https://doi.org/10.1061/\(ASCE\)HE.1943-5584.0000556](https://doi.org/10.1061/(ASCE)HE.1943-5584.0000556)
24. Theil H (1950) A rank-invariant method of linear and polynomial regression analysis, III. *Proc K Nederl Akad Wetensch* 53:1397–1412
25. Wang Y, Xu Y, Tabari H, et al (2020) Innovative trend analysis of annual and seasonal rainfall in the Yangtze River Delta, eastern China. *Atmos Res* 231:104673. <https://doi.org/10.1016/j.atmosres.2019.104673>

# Hydrologic Response Estimation Using Different Descriptors for Upper Baitarani River Basin



Avijit Bardhan and Chintalacheruvu Madhusudana Rao

**Abstract** This study demonstrates the hydrological response estimation of a river basin using two different descriptors, (1) landscape descriptors, and (2) climate descriptors. The landscape descriptors such as land use/land cover (LU/LC), geomorphologic, soil property and geology, and the climate descriptor of the river basin are estimated for Upper Baitarani river basin in India to identify the characteristic features of this basin. The required data is extracted from land use/land cover, soil, elevation profiles, and climatic conditions of the river basin. The Potential Dryness Index (PDI) and Actual Dryness Index (ADI) values are estimated to indicate soil moisture deficit in the study area. In order to assess the hydrological response of the river basin, the empirical relation between landscape descriptors and the climate descriptor is developed. The results obtained in this study have satisfactorily explained the hydrologic response of the river basin, and the developed descriptors are very much useful for future predictions of the hydrologic responses in the river basin.

**Keywords** Hydrologic response · Descriptors · Dryness index · Flow duration indices · Upper Baitarani

## 1 Introduction

Hydrological response study in river basin is a blend of many natural phenomena that occurs in it. The natural phenomenon includes the hydro-meteorological, geomorphologic, and changes in climate, land use land practice, droughts, etc., within the river basin. The natural phenomena of river basin can be described through many factors called descriptors. These descriptors, namely (1) landscape descriptors (land use/land cover (LU/LC), geomorphologic, soil property and geologic) and (2) climate descriptors.

---

A. Bardhan · C. M. Rao (✉)  
Department of Civil Engineering, National Institute of Technology Jamshedpur, Jamshedpur  
831014, India  
e-mail: [cmrao.civil@nitjst.ac.in](mailto:cmrao.civil@nitjst.ac.in)

In the past, many statistical and empirical equations have been developed for hydrological response studies on river basins (e.g., rational method equation as proposed by Kuichling [1], Inglis and DeSouza equation 1930 [2–4]). The rational method equation is widely used for runoff estimation in river basin [1]. One of the most used other empirical equation is soil conservation service method [5] equation, which in turn is represented as curve number (CN) method. This CN method is also in use as a module for runoff estimation in the widely used SWAT model [6].

In the past hydrological methods, the statistical equations and empirical equations are being developed using limited number of physical parameters of the river basin (e.g., rational method equation, etc.) pertaining to the estimation of runoff of river basin, whereas in recent research descriptors are developed based on use of more number of physical parameters of the river basin (e.g., landscape and climate characteristics etc.) to describe the natural phenomena of river basin accurately through many factors.

Earlier, many researchers have developed descriptors for assessment of hydrological response of river basins (e.g., [7–10]). Some other researchers (e.g., Berger, and Entekhabi [11], Laaha and Blöschl [12], Zacharias and Brutsaert [13], Mohamoud [14]) have developed the relationship between the descriptors and natural phenomena of river basin, i.e., hydrologic response of the river basin.

The relationship between the hydrologic responses of the river basin with either single or multiple descriptors has already been developed. For example, base flow recession curve characteristics [13], mean annual flow (MAF) [15], base flow index (BFI) [16, 17], runoff ratio [11], and  $Q_{95}$  [12] studies can be identified as single descriptor relationship with hydrological response of the river basin.

However, the work presented by Mohamoud [14] is an example case of multiple descriptor relationship with hydrological response of the river basin. He represented the flow duration indices (FDIs) as hydrologic response with multiple descriptors which contain the descriptors from different sources. Initially, Mohamoud [14] has developed linear relationship with FDIs, and at later stage, he modified it as a nonlinear relationship [18].

However, development of relationship between descriptors and natural phenomena occurs in river basin usually a complex approach [14, 19, 20]. Even though considerable studies were available in literature, none of these earlier studies have attempted to relate the landscape and climate descriptors directly to get runoff or flow duration indices though it is very important for assessment of hydrological response studies at ungauged river basins. In order to fill this gap of research, in the present study, an attempt is made to develop a relation between the landscape and climate descriptors for assessment of hydrologic response of Upper Baitarni river basin in India as this basin requires assessment of water resources potential for better management of water resources for drinking, agriculture, and other needs in the basin.

## 2 Study Area

Upper Baitarani river basin with Champua gauging station is located between the 21° to 22.5°N latitude and 85° to 86°E longitude in Odisha state of Eastern India (Fig. 1a). It consists of an area of 1812.83 km<sup>2</sup> with an elevation varying from 375 to 1116 m above MSL (Fig. 1b) showing high topographical variation in the study region.

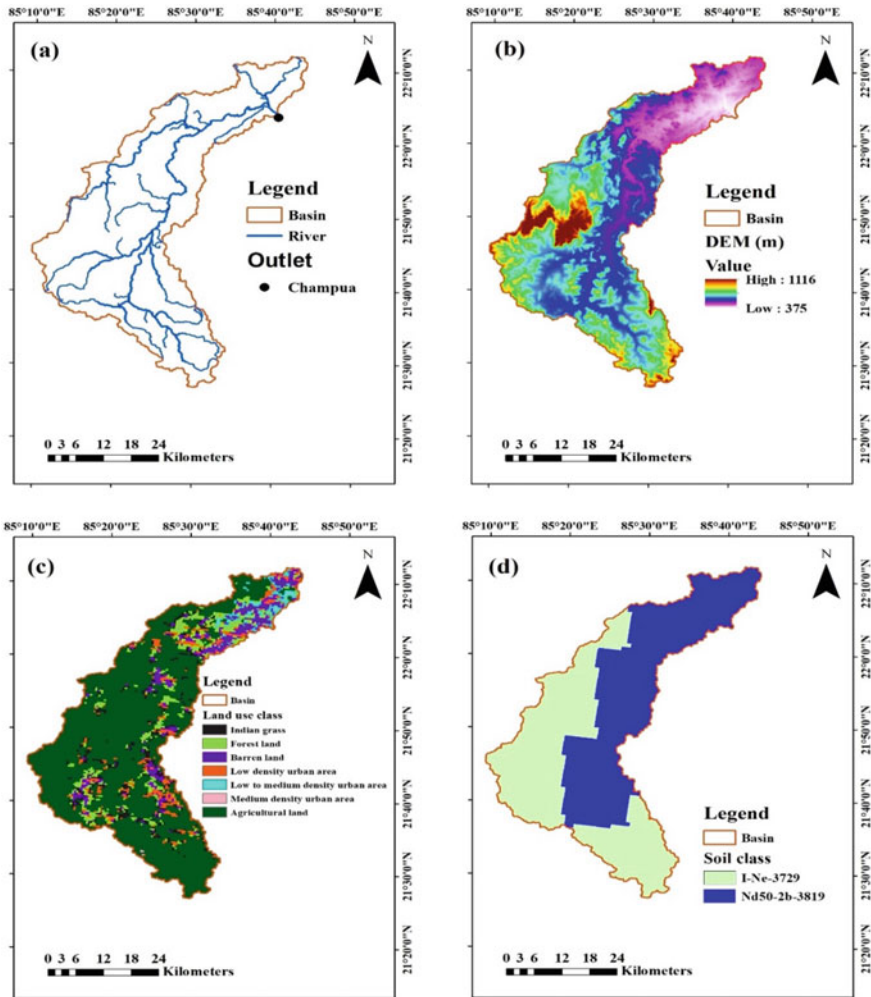


**Fig. 1** Upper Baitarani river basin details. **a** Location and basin map with gauging station, **b** DEM **c** LULC and **d** soil map



According to the India-WRIS report (2016), the Upper Baitarani river basin receives an average rainfall of 1534 mm in a year. The maximum and minimum monthly temperatures in the area vary from 35 °C observed in the month of May to 10 °C observed in the month of January, respectively.

The land use class map of the Upper Baitarani is given in Fig. 1c. There are seven major land use classes, namely Indian grass, forest land, barren land, low density urban area, low to medium density urban area, medium density urban area, and agriculture land available in the river basin. Among the seven land use classes, three land use classes such as agriculture land, forest land, and barren land covering the total area of about 71.48%, 8.38%, and 7.30%, respectively.

The other four land use classes covering a total of 12.84% of the area. The present study uses the global soil data (Harmonized World Soil Data viewer—HWSD, version 1.2) from FAO [21] soil database. Figure 1d shows the soil class of the Upper Baitarani river basin. There are two major kinds of loamy soils such as I-Ne-3729 and Nd50-2b-3819 contributing to 49.24% and 50.76%, respectively, of the study area.

### 3 Methodology

#### 3.1 SWAT Model Setup

The present study uses the soil and water assessment tool (SWAT) for hydrological model simulation. SWAT is a semi-distributed physically based model [6] which works on continuous time step. SWAT simulates the hydrological cycle based on the water balance equation (Eq. 1). The Upper Baitarani river basin was divided into 27 sub-basins which are further sub-divided into 178 Hydrological Response Unit (HRU).

The SWAT component methods such as soil conservation service (SCS) curve number method [5] for estimating surface runoff, Hargreaves method [22] for evapotranspiration, Muskingum-Cunge method [23] for flow routing, and SUFI-2 algorithm for sensitivity, and uncertainty analysis linked to SWAT-CUP [24] were used for calibrating the model.

$$SW_t = SW_0 + \sum_{i=1}^t (R_{\text{day}} - Q_{\text{surf}} - E_a - W_{\text{seep}} - Q_{\text{gw}}) \quad (1)$$

where  $SW_t$  is the final soil water content (mm),  $SW_0$  is the initial soil water content on day  $i$  (mm),  $t$  is the time (days),  $R_{\text{day}}$  is the amount of precipitation on day  $i$  (mm),  $Q_{\text{surf}}$  is the amount of surface runoff on day  $i$  (mm),  $E_a$  is the amount of evapotranspiration on day  $i$  (mm),  $W_{\text{seep}}$  is the amount of water entering the vadose zone from the soil profile on day  $i$  (mm), and  $Q_{\text{gw}}$  is the amount of return flow on day

$i$  (mm). SWAT model is simulated for 23 years (1989–2011). First 2 years (1989–1990) used as warm-up period. Next 16 years (1991–2006) selected as calibration period and the remaining 5 years (2007–2011) considered as validation period. The model performance is assessed using the statistical performance indices such as coefficient of determination ( $R^2$ ), Nash–Sutcliffe Efficiency (NSE), and percentage bias (PBIAS).

### 3.2 FDC and FDIs

The hydrologic response of river basins can easily be known from the flow duration curve (FDC) of the basin. The FDC synthesizes the long-term records of streamflow data of the river basin in the form of graphical display to relate the flow magnitudes and the frequency associated with each magnitude. The normalized FDC is developed according to usual procedure and statement of [25], which means the FDC, developed with frequency and magnitude of the streamflow.

But, the flow duration indices (FDI) designate a particular flow value related to corresponding frequency carried out to indicate high, median, and low streamflows. In the present study, thirteen FDIs were calculated such as,  $Q_{0.5}$ ,  $Q_1$ ,  $Q_5$ ,  $Q_{10}$ ,  $Q_{20}$ ,  $Q_{30}$ ,  $Q_{40}$ ,  $Q_{50}$ ,  $Q_{70}$ ,  $Q_{75}$ ,  $Q_{90}$ ,  $Q_{95}$ , and  $Q_{99}$ . Each of these FDIs represent different segment of flow duration represent descriptors of FDIs. All these FDIs indicate linked descriptors which explain the characteristics of the streamflow indices in the river basin.

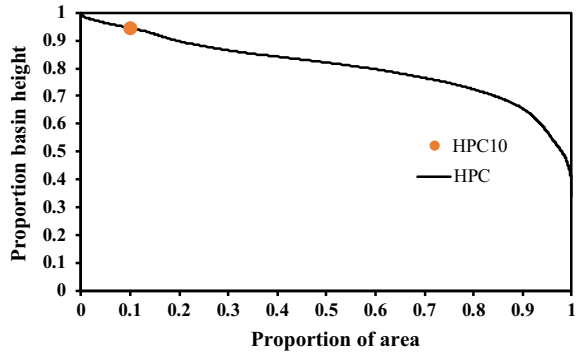
### 3.3 Landscape and Climate Descriptors

For flow indices calculation, this study uses the percentage cover of deciduous forest (FRSD) as one of the land use and land cover descriptors and three geomorphologic descriptors such as relief ratio (Rrat), hypsometric curve elevation corresponding to 10% of area (HPC10), and median watershed slope (MDSL). Relief ratio defined as the ratio between basin relief and longest reach length. Here the longest reach length considered through river reach.

The hypsometric curve is a plot between normalized area and normalized elevation of a watershed [26, 27]. Hypsometric curve explains about the coverage area corresponding to a particular elevation. Present study uses HPC10 as one of the geomorphologic descriptors, wherein HPC10 is defined as the corresponding normalized elevation of the hypsometric curve related to 10% normalized area.

The developed hypsometric curve of Upper Baitarani river basin is given in Fig. 2. Hypsometric curve is commonly used in geomorphological analysis. A total of six soil descriptors, namely SOLD, AWC2, CLAY2, SILT2, KSAT1, and KSAT2 were used in the present study. The detailed descriptions of these descriptors were given

**Fig. 2** Hypsometric curve of Upper Baitarani river basin



in Table 1. Further, the base flow index (BFI) is used as geologic descriptor in many studies [18, 28, 29].

The base flow index was estimated by hydrograph separation of daily stream-flow. The relationship between base flow index and landscape descriptors can also be examined for development of a set of qualitative geology-vegetation parameters and dimensionless topographic and climatic indices. The mean annual dryness index (actual) is defined as the ratio of actual evapotranspiration (AET) and precipitation

**Table 1** List of different descriptors used in the present study

| Descriptors                    | Variable description                                      | Units |
|--------------------------------|---|-------|
| <b>Landscape</b>               |   |       |
| <i>Land use and land cover</i> |   |       |
| FRSD                           | Deciduous forest  | %     |
| <i>Geomorphologic</i>          |   |       |
| Rrat                           | Relief ratio  | m/km  |
| HPC10                          | Hypsometric curve elevation corresponding to 10% of area  | %     |
| MDSL                           | Median watershed slope                                    | m/m   |
| <i>Soil (top two layers)</i>   |   |       |
| SOLD                           | Top two layers soil depth                                 | mm    |
| AWC2                           | Available moisture content at 2nd layer of the soil       | mm    |
| CLAY2                          | Clay content at 2nd layer of the soil                     | %     |
| SILT2                          | Silt content at 2nd layer of the soil                     | %     |
| KSAT1                          | Saturated hydraulic conductivity at 1st layer of the soil | mm/h  |
| KSAT2                          | Saturated hydraulic conductivity at 2nd layer of the soil | mm/h  |
| <i>Geology</i>                 |   |       |
| BFI                            | Base flow index   | –     |
| <b>Climate</b>                 |   |       |
| AET/PREC                       | Mean annual dryness index (actual)                        | mm/mm |

(PREC) which is also used as potential climate descriptor [14]. The step-wise regression method is being used to identify the influencing descriptors for different flow indices.

A linear relationship between the descriptors and flow duration indices were developed. Here, the relationship equation is expressed as:

$$Q_n = C_1 \pm C_2(x) \pm C_3(y) \tag{2}$$

where  $Q_n$  is percentile flow means flow duration indices,  $x$  and  $y$  are landscape and climate descriptor.  $C_1$ ,  $C_2$ , and  $C_3$  are coefficients related to the descriptors. These coefficients vary to relate with flow percentile.

### 3.4 Water Balance Component and Dryness Index

A conceptual water balance equation is used to quantify the monthly water balance components in the river basin. The monthly streamflows are quantified based on monthly quantities of precipitation, actual evapotranspiration, and change in soil moisture storage. The equation is express as:

$$R = P - AET - \Delta S \tag{3}$$

where

- $R$  streamflow (controlled by Geomorphologic, soil, land use and land cover, geology and climate components)
- $P$  precipitation (climate descriptor)
- AET actual evapotranspiration (controlled by climate and soil)
- $\Delta S$  change in soil moisture storage (controlled by geology, soil, climate, etc.).

Further, in order to examine the soil moisture condition, two different dryness indices are considered, namely potential dryness index (PDI) and actual dryness index (ADI). Potential dryness index is calculated as the ratio of potential evapotranspiration and average daily precipitation. And, the mean actual dryness index is expressed as the ratio between subtracted average daily discharge from average daily precipitation and average daily precipitation. Change in storage also calculated to check out the variation in moisture storage. The equations of those are mentioned below:

$$PET/\overline{PREC} = \text{Potential Dryness Index} \tag{4}$$

$$1 - \frac{\overline{Q}}{\overline{PREC}} = \text{Mean Actual Dryness Index} \tag{5}$$

$$\overline{\text{PREC}} - \text{PET} - \overline{Q} = \text{Change in storage} \quad (6)$$

The terms from Eqs. (4)–(6) are PET represents the potential evapotranspiration, PREC represents the precipitation,  $\overline{\text{PREC}}$  is the annual average precipitation, and  $\overline{Q}$  is annual average streamflow.

## 4 Results and Discussion

### 4.1 SWAT Model Performance

The performance of SWAT hydrological model in calibration and validation were acceptable, when the performance statistics reach desired limits between the observed and the final simulated data [30]. The performance statistics such as  $R^2$  (coefficient of determination), NSE (Nash-Sutcliff efficiency), and PBIAS (percentage bias correction) are estimated for calibration and validation periods and compared them with the widely used performance ratings as suggested by Moriasi et al. [31] to know the model performance levels in calibration and validation periods. The performance statistics ( $R^2$ , NSE, and PBIAS) of hydrological model simulations for streamflow estimation in Upper Baitarani river basin are given in Table 2. Results show that the model performance is very good in both calibration and validation periods.

### 4.2 Descriptor Identification and Relation

Flow duration curve plots are to represent the relationship between magnitude and frequency of the streamflow. Its components like percentile flow points that are called flow duration indices are symbolized with landscape – climate descriptors in the present study for Upper Baitarani river basin. To symbolize those flow duration indices with landscape – climate descriptors, first one must identify and analyze the sensitivity of those descriptors to the particular flow duration indices. The relationship equations are mentioned below:

$$Q_{0.5} = 286.096 + 0.095(\text{CLAY2}) - 2.04(\text{AET/PREC}) - 1.04(\text{BFI}) \quad (7)$$

$$Q_1 = 202.755 - 0.15(\text{AET/PREC}) - 0.25(\text{BFI}) + 0.095(\text{CLAY2}) \quad (8)$$

$$Q_5 = 143.53 - 5.82(\text{AET/PREC}) - 0.02(\text{Rrat}) - 1.389(\text{BFI}) - 1.976(\text{AWC2}) \quad (9)$$

**Table 2** Performance statistics of hydrological model simulations for streamflow estimation in Upper Baitarani river basin

| Performance indices | Calibration period (1991–2006) | Validation period (2007–2011) | Performance rating (according to Moriasi et al. [31])   |
|---------------------|--------------------------------|-------------------------------|---|
| $R^2$               | 0.88                           | 0.94                          | $0.75 < R^2 \leq 1.00$ (Very good)<br>$0.65 < R^2 \leq 0.75$ (good)<br>$0.50 < R^2 \leq 0.65$ (satisfactory)<br>$R^2 \leq 0.50$ (unsatisfactory)  |
| NSE                 | 0.87                           | 0.93                          | $0.75 < NSE \leq 1.00$ (Very good)<br>$0.65 < NSE \leq 0.75$ (good)<br>$0.50 < NSE \leq 0.65$ (satisfactory)<br>$NSE \leq 0.50$ (unsatisfactory)  |
| PBIAS               | 0.60                           | -9.80                         | $PBIAS < \pm 10$ (Very good)<br>$\pm 10 < PBIAS < \pm 15$ (good)<br>$\pm 15 < PBIAS < \pm 25$ (satisfactory)<br>$PBIAS > \pm 25$ (unsatisfactory) |

$$Q_{10} = 92.775 - 0.63(AET/PREC) - 1.05(Rrat) - 0.019(SILT2) - 0.087(KSAT1) \tag{10}$$

$$Q_{20} = 68.179 - 1.67(AET/PREC) - 0.09(CLAY2) - 0.011(SOLD) - 0.185(FRSD) \tag{11}$$

$$Q_{30} = 37.229 - 0.44(AET/PREC) - 0.09(CLAY2) - 0.273(FRSD) + 8.16(MDSL) \tag{12}$$

$$Q_{40} = 16.15 - 1.02(AET/PREC) + 0.851(BFI) + 0.09(CLAY2) - 3.99(FRSD) \tag{13}$$

$$Q_{50} = 2.138 - 0.36(AET/PREC) + 15.87(BFI) - 0.4(FRSD) - 0.077(CLAY2) \tag{14}$$

$$Q_{70} = 0.5 - 4.92(AET/PREC) + 0.22(BFI) - 3.98(HPC10) + 0.01(SOLD) \tag{15}$$

$$Q_{75} = 0.134 + 9.82(BFI) - 0.007(CLAY2) - 0.105(AWC2) \tag{16}$$

$$Q_{90} = -0.109 + 7.49(\text{BFI}) - 0.005(\text{CLAY2}) - 0.01(\text{Rrat}) \quad (17)$$

$$Q_{95} = -0.159 + 6.22(\text{BFI}) - 0.004(\text{CLAY2}) - 0.202(\text{AWC2}) \quad (18)$$

$$Q_{99} = -0.209 + 4.65(\text{BFI}) - 0.002(\text{CLAY2}) - 0.003(\text{KSAT1}) \quad (19)$$

The above Eqs. from (7) to (19) are developed based on the natural processes that occur in the river basin. This natural process is very much complex phenomena that include sensitive factors or descriptors like landuse land cover, soil, geomorphologic, and climatic changes in the river basin. The sensitive descriptors are given the present study. The normalized flow duration curve and flow duration indices are shown in Fig. 3. The step-wise regression analysis provides excellent predictions.  $Q_{0.5}$ ,  $Q_1$ ,  $Q_5$ , and  $Q_{10}$  are high flow indices (Fig. 3), where  $Q_{0.5}$  and  $Q_1$  indices stand for very high flow, which are mainly caused by sudden heavy storm. The  $Q_{0.5}$  and  $Q_1$  highly influenced by dryness index and base flow index with negative correlation (Eqs. 7 and 8). Both indices influenced by percentage of clay content in the 2nd soil layer with positive correlation.  $Q_5$  and  $Q_{10}$  are influenced by relief ratio (Rrat), whereas the correlation of relief ratio is negative for  $Q_5$  and positive for  $Q_{10}$ . The dryness index influences both  $Q_5$  and  $Q_{10}$  and is more influences for  $Q_5$ . Further,  $Q_5$  also strongly correlated geologic descriptor, base flow index, and soil descriptor available moisture content in the 2nd layer of the soil (Eq. 9).  $Q_{10}$  is influenced by two soil descriptors, namely percentage of silt content in the 2nd layer of the soil and saturated hydraulic

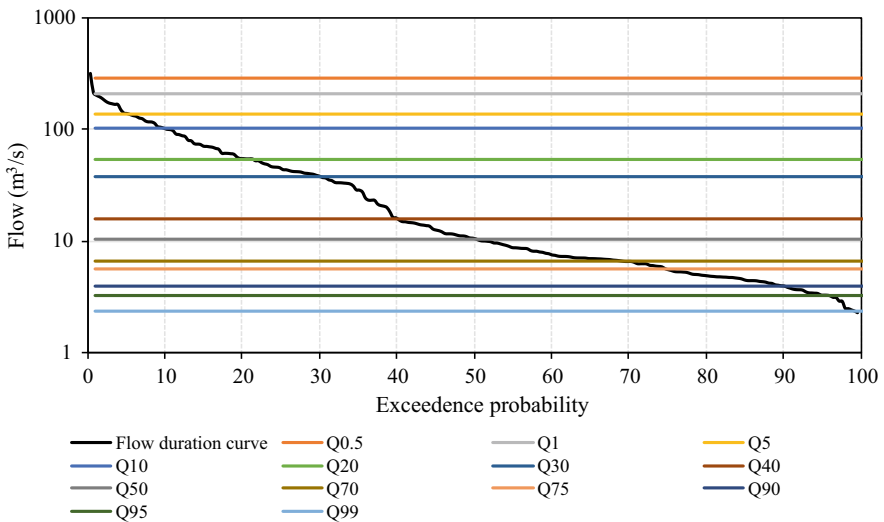


Fig. 3 Normalized flow duration curve and flow duration indices

conductivity at 1st layer of the soil (Eq. 10).  $Q_{20}$  and  $Q_{30}$  used to signify the high to medium flow magnitude.

$Q_{20}$  is more negatively correlated with dryness index than  $Q_{30}$ . Both indices are positively correlated with same coefficient with percentage of clay content in the 2nd soil layer. As the deciduous forest coverage used to control the normalized flow [14], this study used the percentage cover of deciduous forest as land use and land cover descriptor to symbolize both the indices (Eqs. 11 and 12).  $Q_{20}$  also influenced by a soil descriptor top two layers soil depth (Eq. 11).  $Q_{30}$  is strongly correlated with geomorphologic descriptor median watershed slope (Eq. 12).

The  $Q_{40}$  and  $Q_{50}$  indices stand for low end of the medium flow condition and high end of the low flow condition, respectively. Percentage of clay content in the 2nd soil layer has same influence on  $Q_{40}$  as  $Q_{20}$  and  $Q_{30}$ . Similar to  $Q_{20}$  and  $Q_{30}$ , the  $Q_{40}$  have negative correlation with deciduous forest cover but more effective (Eq. 13). As the  $Q_{40}$  indices cover 40% of the time, it comes under low end of the medium flow condition.

$Q_{50}$  covers 50% time of flow duration. It comes under high end of the low flow condition. Dryness index has negative correlation with it similar to  $Q_{40}$ . Among all indices,  $Q_{50}$  is one which is more effectively influenced by any descriptor. In this study,  $Q_{50}$  is more effectively influenced by the geological descriptor base flow index.

Percentage of deciduous forest cover and percentage of clay content in the 2nd soil layer has negative correlation with  $Q_{50}$  flow indices.  $Q_{70}$  comes under medium low flow condition and is the last indices to be effected by climate descriptor. It is most negatively correlated with the climate descriptor dryness index (Eq. 15). The  $Q_{70}$  is positively influenced by base flow index and top two layers soil depth (Eq. 15). It is negatively correlated with the most effective geomorphologic descriptor hypsometric curve elevation corresponding to 10% of area (HPC10), as the geomorphology has control over the end portion of the recession limb.

Further, the  $Q_{75}$  is negatively influenced by available moisture content at 2nd layer of the soil, whereas  $Q_{90}$  is negatively correlated with relief ratio.  $Q_{75}$ ,  $Q_{90}$ ,  $Q_{95}$ , and  $Q_{99}$  indices morally stands for low flow, and they represents the environmental flows in river basins. Climate descriptor influences very high to low medium flow and has negligible impact on low flow indices. The base flow index effectively influences the  $Q_{90}$  indices (Eq. 17).

The percentage of clay content in the 2nd soil layer and relief ratio has negative impact on  $Q_{90}$ . The  $Q_{95}$  and  $Q_{99}$  come under environmental flow condition, which indicates the required flow to maintain the ecosystem. Both indices strongly influenced by base flow index (Eqs. 18 and 19) and both are negatively correlated with percentage of clay content in 2nd soil layer. Available moisture content at 2nd layer of the soil negatively correlates  $Q_{95}$  indices (Eq. 18) as the moisture transfer to 2nd layer which reduces the environmental flow. The  $Q_{99}$  indices indicate the minimum flow condition in the channel. Along with the percentage of clay content in 2nd soil layer, the  $Q_{99}$  also effected by saturated hydraulic conductivity at 1st layer of the soil (Eq. 19).



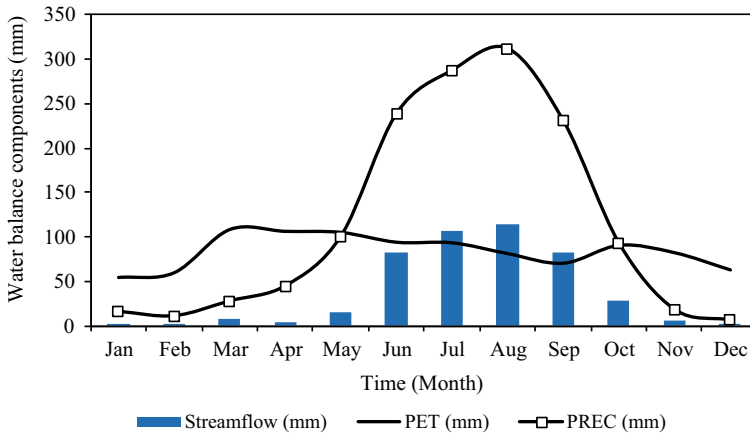


Fig. 4 Monthly water balance components PET and PREC of Upper Baitarani river basin

### 4.3 Water Balance Application

The conceptual approach of water balance is applied to the present study [32]. This study applies different approaches of water balance analysis to indicate the streamflow magnitude. In one of its approaches, if precipitation (PREC) is greater than the potential evapotranspiration (PET), the streamflow is said to be categorized as high flow in the river basin. In contrast, if  $PET > PREC$ , the streamflow is said to be categorized as low flow in the river basin. This observation is demonstrated in Fig. 4 developed for Upper Baitarani river basin. Low flow situation is seen from January to May and October to December periods, and high flow situation is seen from June to September period in the Upper Baitarani river basin.

Further, the potential dryness index (PDI) and the actual dryness index (ADI) are calculated as indicators to soil moisture deficit in the present study. The dryness index is one of the most effective climate descriptor. It is very effectively correlated with extreme flow to low medium flows. The dryness index and runoff index combine to unity.

In this study, the annual average runoff index shows 0.33 and mean actual dryness index shows 0.67. The potential dryness index is calculated according to Eq. 4. Higher precipitation and lower evapotranspiration will results a lower dryness index. To demonstrate this in the present study, comparisons of water balance components of Upper Baitarani river basin over a selected time period from November 2009 to May 2010 are considered. Figure 5 demonstrates the comparison of water balance components for a selected time period from November 2009 to May 2010 to demonstrate the lower dryness index in the Upper Baitarani river basin. The potential dryness index varies based on proportionality to temperature.

It is clear from Fig. 5 that if temperature decreases from November to February, the PDI also decreases, whereas it increases with the increase in temperature, i.e.,

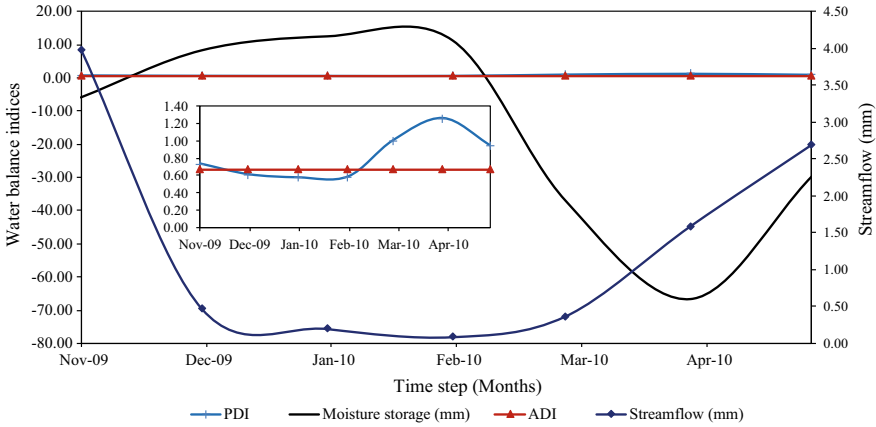


**Fig. 5** Comparison of water balance components of Upper Baitarani river basin over a selected time period from November 2009 to May 2010 for lower dryness index

from March to May months. The change in soil moisture is also presented in Fig. 5 according to Eq. 6. The mean actual dryness index calculated according to Eq. 5 assumes the net soil moisture storage as zero.

The soil moisture deficit occurs when the potential dryness index is greater than mean actual dryness index and surplus soil moisture exist when the Mean ADI > PDI (Fig. 5).

## 5 Conclusion

In this study, the FDCs and its duration indices are represented in terms different descriptors, namely geomorphologic, geologic, soil, climate, and land cover and land use descriptors instead of representing them in widely practiced conventional way of representation such as relationship between frequency and magnitude of streamflow. This way of novel representation of FDCs in the form of descriptors enables to correctly asses the hydrologic response of river basins in many ways. The hydrological response of Upper Baitarani river basin was satisfactorily assessed using two approaches (1) empirical flow duration curve approach and (2) water balance approach. Though the relationship between the descriptors was done here in the present work, and the identification of sensitive descriptors is beyond the scope of the work. The developed descriptors are very much useful for future predictions of the hydrologic responses in the river basin.

## References

1. Kuichling E (1889) The relation between the rainfall and the discharge of sewers in populous districts. *Trans ASCE* 20:1–60
2. Inglis CC, Desouza (1930) A critical study of runoff and floods of catchment of the Bombay Presidency with a short note on loss from lakes by evaporation. Bombay PWD Technical. Paper No. 30
3. Khosla AE (1949) Analysis and utilization of data for the appraisal of water resources. *The Central Board Irrigation and Power Journal*
4. Subramanya K (2008) *Engineering hydrology*, 3rd edn. Tata McGraw Hill, pp, 155–162
5. USDA-SCS (1972) *USDA soil conservation services national engineering handbook*, section 4: hydrology, U.S. Government Printing Office
6. Arnold JG, Srinivasan R, Mutiah RS, Williams JR (1998) Large area hydrologic modeling and assessment, Part I: model development. *J Am Water Resour Assoc* 34:73–89
7. Kaviya B (2013) Runoff estimation using SWAT model in Brahmani-Baitarani river basin. *Int J Biot Trends Technol* 3(2)
8. Padhiary J, Swain JB, Patra KC (2020) Optimized irrigation scheduling using SWAT for improved crop water productivity. *Irrig Drain*. <https://doi.org/10.1002/ird.2418>
9. Verma K, Jha MK (2015) Evaluation of a GIS-based watershed model for streamflow and sediment-yield simulation in the Upper Baitarani river basin of Eastern India. *J Hydrol Eng* 20(6). [https://doi.org/10.1061/\(ASCE\)HE.1943-5584.0001134](https://doi.org/10.1061/(ASCE)HE.1943-5584.0001134)
10. Uniyal MK, Jh, Verma AK (2015) Parameter identification and uncertainty analysis for simulating streamflow in a River Basin of Eastern India. *Hydrol Process* 29(17):3744–3766
11. Berger KP, Entekhabi D (2001) Basin hydrologic response relations to distributed physiographic descriptors and climate. *J Hydrol* 247:169–182
12. Laaha, Blöschl G (2007) A national low flow estimation procedure for Austria. *Hydrol Sci J* 52(4):625–644
13. Zacharias YB, Brutsaert W (1988) The influence of basin morphology on groundwater outflow. *Water Resour Res* 24:1645–1650
14. Mohamoud YM (2004) Comparison of hydrologic responses at different watershed scales. U.S. Environmental Protection Agency. EPA/600/R-04/103.
15. Reimers W (1990) Estimation hydrological parameters from basin characteristics for large semi-arid catchments. In: Beran MA, Brilly M, Becker A Bonacci O (eds) *Regionalization in hydrology*. In: Proceedings of Ljubljana symposium, April 1990, vol 191. IAHS Publications 191, pp 187–194. IAHS Press, Wallingford, UK. [http://iahs.info/redbooks/a191/iahs\\_191\\_0187.pdf](http://iahs.info/redbooks/a191/iahs_191_0187.pdf)
16. Lacey GC, Grayson RB (1998) Relating base flow to catchment properties in south-eastern Australia. *J Hydrol* 204:231–250
17. Nathan RJ, McMahon TA (1990) Identification of homogeneous regions for the purposes of regionalisation. *J. of Hydrol.* 121:217–238
18. Mohamoud YM (2008) Prediction of daily flow duration curves and streamflow for ungauged catchments using regional flow duration curves. *Hydrol Sci J* 53(4):706–724. <https://doi.org/10.1623/hysj.53.4.706>
19. Post A, Jones JA (2001) Hydrologic regimes at four long-term ecological research sites in New Hampshire, North Carolina, Oregon, and Puerto Rico. *Adv Water Resour* 24:1195–1210
20. McNamara JP, Kane DL, Hinzman LD (1998) An analysis of streamflow hydrology in the Kuparuk River basin, Arctic Alaska: a nested catchment approach. *J Hydrol* 206:39–57
21. FAO (2009) *Harmonized world soil database (version 1.1)*. In: *Global environmental change-human and policy dimensions*. FAO, Rome, Italy and IASA, Laxenburg, Austria
22. Hargreaves L, Hargreaves GH, Riley JP (1985) Irrigation water requirements for Senegal River Basin. *J Irrig Drain Eng-ASCE* 111(3):265–275
23. Cunge JA (1969) On the subject of a flood propagation method (Muskingum Method). *J Hydraulic Res IAHR* 7(2):205–230. <https://doi.org/10.1080/00221686909500264>

24. Abbaspour KC, Vejdani M, Haghight S (2007) SWAT-CUP: calibration and uncertainty programs for SWAT. In: Proceedings of the international congress on modelling and simulation (MODSIM 2007). Modelling and Simulation Society of Australia and New Zealand, New Zealand, pp 1596–1602
25. Vogel RM, Fennessey NM (1995) Flow duration curves. 2. A review of applications in water resources planning. *Water Resour Bull* 31:1029–1039.
26. N. Strahler. Hypsometric (area-altitude) analysis of erosional topography. *Geological Society of America Bulletin*. 1952, **63**(117).
27. Langbein WB et al (1947) Topographic characterization of drainage basins. U.S. Geological Survey. Paper no. 968-c. Washington, D.C
28. Potter KW (2001) A simple method for estimating baseflow at ungauged locations. *J Am Water Resour Assoc* 37(1):177–184
29. Miller MP, Johnson HM, Susong DD, Wolock DM (2015) A new approach for continuous estimation of baseflow using discrete water quality data: Method description and comparison with baseflow estimates from two existing approaches. *J Hydrol* 522:203–210
30. Madhusudana Rao C, Bardhan A, Patra JP (2020) Assessment of hydrological response in Subarnarekha river basin under anticipated climate change scenarios. *Global NEST J* 22(2):207–219
31. Moriasi N, Arnold JG, Van Liew MW, Bingner RL, Harmel RD, Veith TL (2007) Model evaluation guidelines for systematic quantification of accuracy in watershed simulations. *Trans ASABE* 50(3):885–900
32. Thornthwaite W, Mather JW (1955) The water balance. *Publ Climatol Drexel Inst Technol* 1:1–104

# Temperature and Precipitation Towards the End of the 21st Century in Pecan Producing Areas of Mexico



Arturo Corrales-Suastegui, Gerardo Martinez-Diaz, Osias Ruiz-Alvarez, Miguel Angel Gonzalez-Gonzalez, and Edgar G. Pavia

**Abstract** In northern Mexico, especially in the states of Chihuahua, Coahuila, Sonora, and Durango, pecan production is one of the main agricultural activities. Temperature and precipitation affect the development of crops since they influence their metabolic processes. In this work, we examine seasonal changes in maximum and minimum temperature, precipitation, and growing degree days with the Rossby Center Regional Atmospheric Climate Model (RCA4), for the Coordinated Regional Climate Downscaling Experiment (CORDEX) Central America domain, driven with different General Circulation Models (GCM) and for two Representative Concentration Pathway (RCP) scenarios. We consider two 30-year periods: “current conditions” (1981–2010) and “future scenario” (2070–2099). The results suggest an increase in both: maximum and minimum temperatures for the four seasons of the year by the end of the present century. This might have repercussions on an extension of the budbreak period, dehiscence of the pecan flowers and fruits, nut filling, and vivipary, which will affect the yield and quality of pecan orchards. Drier winters, springs, and summers will increase water stress on pecan trees; with wetter autumns over pecan producing regions are to be expected, which will lead to a reduction in quality due to vivipary. Under this evidence, the pecan industry may be affected since yield and quality may decrease, especially in areas where pecan already suffers from stress due to water scarcity, extreme temperatures, low chilling hour accumulation, and rainfall during nut maturity.

---

A. Corrales-Suastegui (✉) · O. Ruiz-Alvarez · M. A. Gonzalez-Gonzalez  
Laboratorio Nacional de Modelaje y Sensores Remotos, C. E. Pabellón, Instituto Nacional de Investigaciones Forestales, Agrícolas y Pecuarias (INIFAP), Pabellón de Arteaga, Aguascalientes, México  
e-mail: [corrales.arturo@inifap.gob.mx](mailto:corrales.arturo@inifap.gob.mx)

G. Martinez-Diaz  
C. E. Costa de Hermosillo, Instituto Nacional de Investigaciones Forestales, Agrícolas y Pecuarias (INIFAP), Hermosillo, Sonora, México

E. G. Pavia  
Departamento de Oceanografía Física, División de Oceanología, Centro de Investigación Científica y de Educación Superior de Ensenada (CICESE), Ensenada, Baja California, México

**Keywords** Pecan · Nut · Degree Days · RCA4 · RCP

## Abbreviations

|            |   |
|------------|---|
| $T_{\max}$ | Maximum temperature   |
| $T_{\min}$ | Minimum temperature   |
| Prec       | Precipitation   |
| GDD        | Growing degree days   |
| M0         | RCA4 forced by the ERA-Interim reanalysis                     |
| M1         | RCA4 forced by the MOHC-HadGEM2-ES model                      |
| M2         | RCA4 forced by the M-MPI-ESM-LR model                         |
| M3         | RCA4 forced by the MIROC-MIROC5 model                         |
| M4         | RCA4 forced by the ICHEC-EC-EARTH model                       |
| Eref       | The ensemble for the reference period                         |
| Ercp26     | The ensemble for the future period under the RCP 2.6 scenario |
| Ercp85     | The ensemble for the future period under the RCP 8.5 scenario |
| DJF        | Winter  |
| MAM        | Spring  |
| JJA        | Summer  |
| SON        | Autumn  |

## 1 Introduction

The pecan (*Carya illinoensis*) belongs to the Juglandaceae family, which comprises arboreal plants that produce a drupe. During the ripening season, the pericarp and mesocarp dry out, and the endocarp (shell) and seed (almond) are considered nut [30]. Mexico has positioned itself as one of the main exporters of pecan nuts in the international market, generating in 2015 a national trade surplus of more than 330 million dollars (SIAP 2016). In northern Mexico, primarily in the states of Chihuahua, Coahuila, Sonora, and Durango, pecan production is one of the leading agricultural activities. The climate in this region is arid to semi-arid, making water the main agricultural management factor that allows reaching a higher output. Pecan's water requirement is high compared to other crops, so introducing the degree-day concept in irrigation scheduling might lead to better control of the water's efficient use [2, 11, 36], compared to traditional irrigation scheduling.

Temperature and precipitation affect the development of pecan since they influence metabolic processes. The warming of the global climate system is unequivocal: air temperature near the terrestrial surface has increased an average of 0.85 °C during the period from 1880 to 2012; furthermore, continued greenhouse gas emissions

could cause even greater warming (up to 4.8 °C by the end of the century). Long-lasting changes in all climate system components increase the likelihood of severe, widespread, and irreversible impacts on people, agriculture, and ecosystems [16].

Previous works based on General Circulation Models (GCMs) have suggested a general increase in temperature (~4 °C) and reduction (increase) in summer (autumn) precipitation in the northwest of Mexico for the late twenty-first century [3, 4, 40]. Several works have shown that these changes in climate will produce significant impacts on the crops' performance. In this regard, Ruiz-Alvarez et al. (2011), based on observations over Mexico, showed that under a drought scenario, the irrigation requirements increase significantly with respect to a typical year due to the decrease in effective precipitation. Similarly Kang [18] and Mimi and Jamous [26] showed that under drought conditions irrigation requirements to optimize production increase, however, water productivity decreases. On the other hand, in northwest South America, Zhang and Cai [45] found significant increases in irrigation requirements in the last 30 years of the twenty-first century. For this reason, it is expected that projected changes in Mexico's climate will affect pecan crops in producing areas of northern Mexico.

Regional climate simulation can generally be improved by using a Regional Climate Model (RCM) nested within a coarser-resolution GCM [13]. Given the economic importance of the pecan producing region for the country, in this research we use the Rossby Centre Regional Atmospheric Climate Model (RCA4), for the so-called Central America domain of the Coordinated Regional Climate Downscaling Experiment (CORDEX) (Fig. 1) driven by several GCMs for different Representative Concentration Pathways (RCP), to analyze possible future changes in maximum and minimum temperature, precipitation, and degree days.

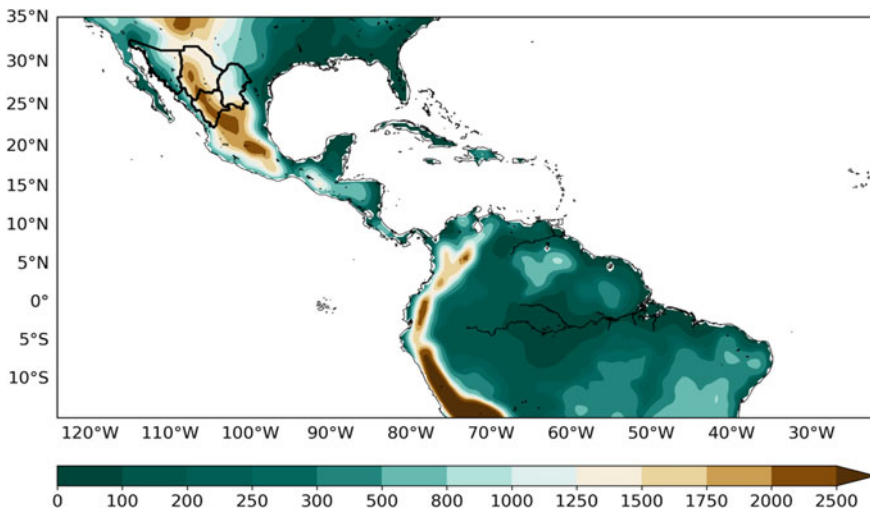


**Fig. 1** Model domain, topography (m), and study region in thick black contours

**Table 1** Mean annual temperature, annual total precipitation, and the pecan production in 2016 for the states of Chihuahua, Coahuila, Sonora, and Durango

| State     | Mean annual temperature | Annual total precipitation | Area (ha) |           | Production | Yield  |
|-----------|-------------------------|----------------------------|-----------|-----------|------------|--------|
|           | (°C)                    | (mm)                       | Sown      | Harvested | (t)        | (t/ha) |
| Chihuahua | 8–26                    | 200–1200                   | 70,587.5  | 49,903.7  | 91,987.7   | 1.8    |
| Coahuila  | 8–22                    | 200–500                    | 12,214.3  | 8897.5    | 18,326.1   | 2.1    |
| Sonora    | 8–28                    | 100–1000                   | 17,653.5  | 13,017.6  | 14,500     | 1.1    |
| Durango   | 8–26                    | 300–1500                   | 6562.7    | 5413.7    | 8921.3     | 1.7    |

## 2 Materials and Methods

### 2.1 Study Region

The main pecan producing regions are found in the northern Mexican states of Chihuahua, Coahuila, Sonora, and Durango (Fig. 1), represent 12.62, 7.73, 9.15, and 6.29% of Mexico's territory, respectively (INEGI 2020). As an example, the mean annual temperature, annual total precipitation, and the pecan production in 2016 of these states are shown in Table 1 [15, 29].

### 2.2 Observations

We use daily fields of maximum temperature ( $T_{\max}$ ), minimum temperature ( $T_{\min}$ ), and precipitation (Prec) from the Livneh observational data-set gridded to a  $1/16^\circ$  ( $\sim 6$  km) resolution covering Mexico, the United States of America, and southern Canada, for the period 1950–2013 [21].

### 2.3 Model

The RCA4 model is semi-lagrangian, semi-implicit with horizontal diffusion of sixth order applied to the prognostic variables, and executed for the initial CORDEX domain [8, 9, 34].



## 2.4 Regional Climate Simulations

We defined the 1981–2010 period as the reference for “current condition,” similarly, the 2070–2099 period as representative of a “future scenario.” As an evaluation of the model, we analyzed a simulation (M0) forced by the ERA-Interim reanalysis [6] of the European Center for Medium-Range Weather Forecast (ECMWF) for the reference period. We also analyzed four simulations driven by four GCMs from the Coupled Model Intercomparison Project 5 (CMIP5) [39]:

1. Met Office Hadley Centre MOHC-HadGEM2-ES (M1),
2. Max Planck Institute for Meteorology (MPI-M) M-MPI-ESM-LR (M2),
3. Model for Interdisciplinary Research On Climate MIROC-MIROC5 (M3),
4. European EC-Earth consortium ICHEC-EC-EARTH (M4).

Simulations M1, M2, M3, and M4 were performed for reference, and future periods for the lowest forcing level scenario, RCP2.6 [27, 43, 44] and the high-end scenario, RCP8.5 [27, 31, 43]. Simulations M1 to M4 were analyzed by Corrales-Suastegui [5] for southern Mexico and Central America for several RCPs, yielding acceptable results.

## 2.5 Growing Degree days

We use the canonical form for calculating the Growing degree days (GDD) [25]:

$$\text{GDD} = (T_{\max} + T_{\min})/2 - T_b \quad (1)$$

where  $T_{\max}$  and  $T_{\min}$  are the daily maximum and minimum temperatures, respectively,  $T_b = 4.4$  °C is the base temperature.

## 2.6 Ensembles

We defined ensembles of  $T_{\max}$ ,  $T_{\min}$ , Prec, and GDD for the reference (Eref) and future (Ercp26 and Ercp85) periods by averaging the corresponding daily field from simulations M1 to M4. From the ensembles, we calculate the annual cycle over the study region, seasonal mean for winter (December–February, DJF), spring (March–May, MAM), summer (June–August, JJA), and autumn (September–November, SON), see Corrales-Suastegui [5] for details.

### 3 Results and Discussion

#### 3.1 Reference period

We assessed the model performance by comparing M0 with the Livneh dataset. We found that the model reproduces spatial and temporal patterns similar to this observational data-set.

##### 3.1.1 Annual Cycle

In Fig. 2, we show the annual cycle from several datasets for  $T_{max}$  (Fig. 2a, b),  $T_{min}$  (Fig. 2c, d), Prec (Fig. 2e, f), and GDD (Fig. 2g, h).

##### Maximum Temperature

Simulations M0, M1 to M4, and Eref reproduced the annual cycle comparable to observations (Fig. 2a). Simulations M0 to M4, and Eref have a cold bias (Fig. 2b).

##### Minimum Temperature

Simulations M0, M1 to M4, and the ensemble (Eref) reproduced the annual cycle very close to observations (Fig. 2c). M0, M1 to M4, and Eref have a warm bias (Fig. 2d).

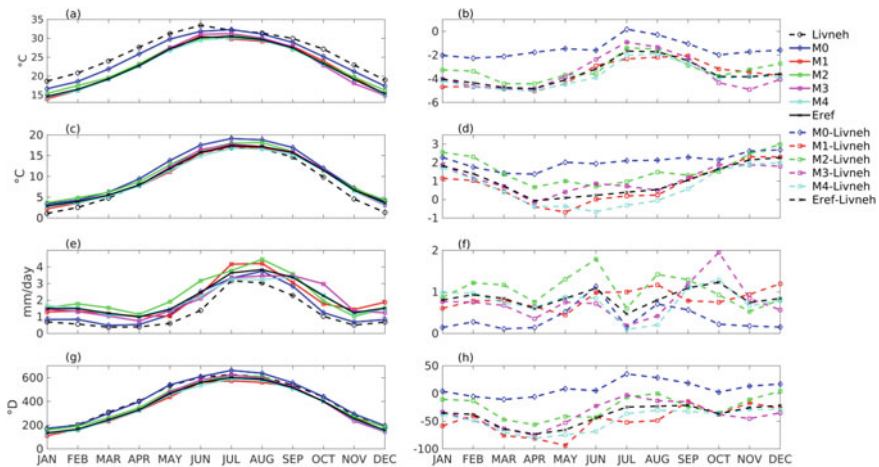


**Fig. 2** Annual cycle for reference period from observations and different simulations. The annual cycle was computed doing the spatial average of the monthly  $T_{max}$  (a),  $T_{min}$  (c), Prec (e), and GDD (g) over the pecan producing region. The dotted lines are the bias (model minus Livneh) in the  $T_{max}$  (b),  $T_{min}$  (d), Prec (f), and GDD (h) annual cycle

### Precipitation

The observed annual cycle of precipitation is well reproduced by M0, M1 to M4, and Eref, as well as the months of maximum precipitation (July, August, and September) (Fig. 2e). All simulations and the ensemble show a slight wet bias (~1 mm/d) (Fig. 2f).

### Growing Degree Days

Simulations M0, M1 to M4, and Eref reproduced the annual cycle close to observations (Fig. 2g). M0 shows a positive bias while M1 to M4 and Eref show a negative bias (Fig. 2h).

## 3.1.2 Seasonal Mean

### Maximum Temperature

Figure 3 shows the seasonal average of  $T_{max}$  for DJF, MAM, JJA, and SON during the reference period. In observations (Livneh, Fig. 3a–d), the maximum  $T_{max}$  (~24 °C) in winter (DJF, Fig. 3a) are mainly found over Sonora. For spring (MAM, Fig. 3b), the maximum  $T_{max}$  (~32 °C) was observed in Sonora and Coahuila. During summer (JJA, Fig. 3c), the maximum  $T_{max}$  was found in Sonora (> 34 °C), Coahuila (>32 °C), and northern Chihuahua (>32 °C). In autumn (SON, Fig. 3d),  $T_{max}$  reaches values of ~34 °C over Sonora. For the model evaluation (M0, Fig. 3e–h), the maximum values of  $T_{max}$  (~22 °C) during winter (DJF, Fig. 3e) are mainly over Sonora. For spring (MAM, Fig. 3f),  $T_{max}$ 's maximum value over Sonora and Coahuila is ~30 °C. In summer (JJA, Fig. 3g), the maximum  $T_{max}$  was found in Sonora (>34 °C), Coahuila (>30 °C), and northern Chihuahua (>30 °C). During autumn (SON, Fig. 3h),  $T_{max}$ 's maximum value over the region was located in Sonora (~32 °C). For simulations

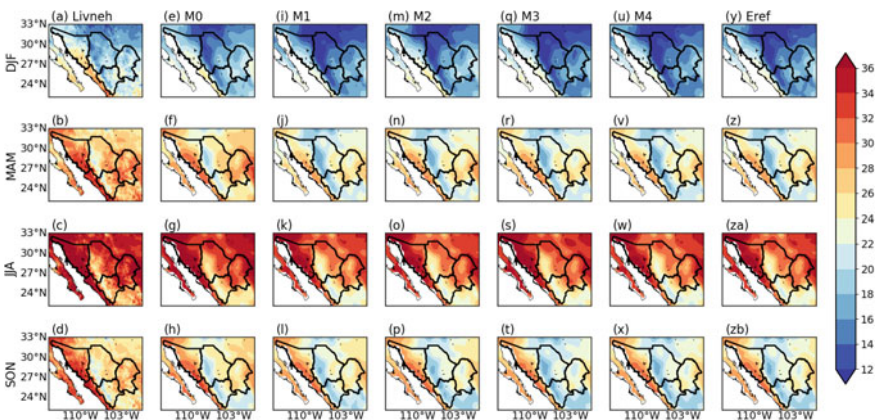


**Fig. 3** Average maximum temperature (°C) during 1981–2010 for **a** DJF, **b** MAM, **c** JJA, **d** SON for Livneh, **e–h** similar to **a–d** but for M0, **i–l** similar to **e–h** but for M1, **m–p** similar to **i–l** but for M2, **q–t** similar to **m–p** but for M3, **u–x** similar to **q–t** but for M4, and **y–zb** similar to **u–x** but for Eref

M1 to M4 and Eref (Fig. 3i–zb),  $T_{max}$ 's maximum value during DJF (Fig. 3i, m, q, u, y) is  $\sim 22^{\circ}\text{C}$  over Sonora. For MAM (Fig. 3j, n, r, v, z), the maximum value of  $T_{max}$  ( $\sim 28^{\circ}\text{C}$ ) was found over Sonora and Coahuila's states. During JJA (Fig. 3k, o, s, w, za), the maximum  $T_{max}$  was found in Sonora ( $>34^{\circ}\text{C}$ ), Coahuila ( $>28^{\circ}\text{C}$ ), and northern Chihuahua ( $>28^{\circ}\text{C}$ ). For autumn (SON, Fig. 3l, p, t, x, zb),  $T_{max}$ 's maximum value over the study area was located in Sonora ( $\sim 32^{\circ}\text{C}$ ).

**Minimum Temperature**

Figure 4 shows the average  $T_{min}$  for DJF, MAM, JJA, and SON during the reference period. Observations (Livneh, Fig. 4a-d) show that the lowest value of  $T_{min}$  ( $<0^{\circ}\text{C}$ ) during DJF (Fig. 3a) is found mainly in Chihuahua and high areas of Durango. For MAM (Fig. 4b), low  $T_{min}$  values ( $<2^{\circ}\text{C}$ ) were observed in mountainous areas of Chihuahua and Durango. During JJA (Fig. 4c) the maxima of  $T_{min}$  ( $>22^{\circ}\text{C}$ ) were found in Sonora and northeast of Coahuila. In autumn (SON, Fig. 4d),  $T_{min} < 4^{\circ}\text{C}$  was located over Durango and Chihuahua. The M0 simulation (Fig. 4e-h) reveals that low values of  $T_{min}$  ( $<2^{\circ}\text{C}$ ) during DJF (Fig. 4e) are located mainly over high areas of Chihuahua and Durango. For MAM (Fig. 4f), the maximum value of  $T_{min}$  over Sonora and Coahuila is  $\sim 30^{\circ}\text{C}$ . In JJA (Fig. 4g) the highest values of  $T_{min}$  were found in Sonora ( $>24^{\circ}\text{C}$ ), Coahuila ( $>20^{\circ}\text{C}$ ), and northern Chihuahua ( $>30^{\circ}\text{C}$ ). During SON (Fig. 4h), the maximum value of  $T_{min}$  over the region was located in Sonora ( $\sim 22^{\circ}\text{C}$ ). The simulations M1 to M4 and Eref (Fig. 4i–zb) show that the lowest value of  $T_{min}$  during DJF (Fig. 4i, m, q, u, y) is  $\sim 2^{\circ}\text{C}$  over Chihuahua and mountainous areas of Durango. In spring (MAM) (Fig. 4j, n, r, v, z), the minimum value of  $T_{min}$  ( $<4^{\circ}\text{C}$ ) was found in high areas of Chihuahua and Durango. During JJA (Fig. 4k, o, s, w, za) the maximum of  $T_{min}$  ( $>22^{\circ}\text{C}$ ) was found in Sonora and northeast of Coahuila. For SON (Fig. 4l, p, t, x, zb), the maximum value of  $T_{min}$  over the study area was located in Sonora ( $\sim 22^{\circ}\text{C}$ ).

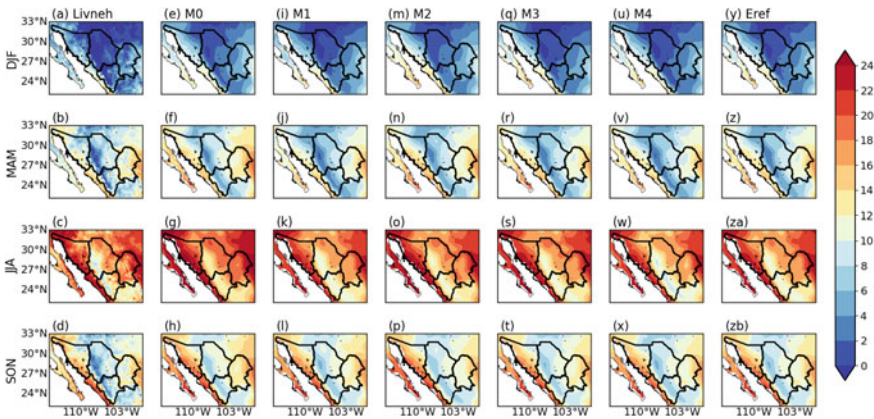


**Fig. 4** Similar to Fig. 3 but for minimum temperature ( $^{\circ}\text{C}$ )

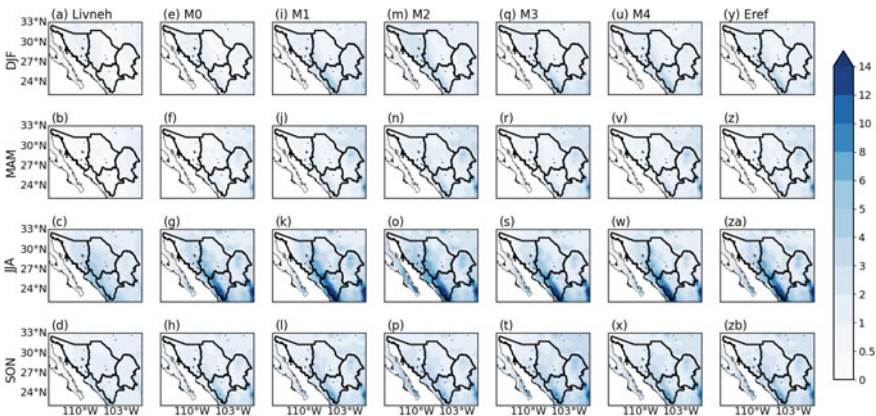
**Precipitation**

A climatological feature of this region (from 22° to 36° N and from 113° to 104° W) is the so-called North American Monsoon (NAM), with its onset in summer and its end in autumn [4, 40]. The NAM region covers three (Sonora, Chihuahua, and Durango) of the four states in the pecan producing region.

The seasonal Prec (DJF, MAM, JJA, and SON) during the reference period is shown in Fig. 5. In the Livneh observational data-set (Fig. 5a–d), the Prec for DJF (Fig. 4a) and MAM (Fig. 5b) is in the range of ~0.5 to ~1 mm/d over the NAM region. During JJA (Fig. 5c), the maximum Prec value (~2 to ~4 mm/d) is observed in the NAM region. For autumn (SON, Fig. 5d), Prec was observed in the range of ~1 to ~2 mm/d over the entire study area. M0 (Fig. 5e–h), during DJF (Fig. 5e) and MAM (Fig. 5f), shows the highest Prec values in the range of ~0.5 mm/d to ~1 mm/d in Sonora, Chihuahua, and Durango. For JJA (Fig. 5g), M0 generally overestimates Prec, mainly in mountainous regions of Durango; however, the maximum was also found over the NAM region. During SON (Fig. 5h), M0 showed the Prec in the range of ~1 to ~2 mm/d over the entire study area. M1 to M4, and Eref (Fig. 5i–zb), during DJF (Fig. 5i, m, q, u, y) and MAM (Fig. 5j, n, r, v, z), show the Prec in the range of ~0.5 to ~1 mm/d in Sonora, Chihuahua, and Durango, however, they overestimate in northern Coahuila. For JJA (Fig. 5k, o, s, w, za), similar to M0 (Fig. 5g), they generally overestimate Prec, mainly in high areas of Durango, although the maximum was also found over the NAM region. During SON (Fig. 5l, p, t, x, zb), simulations (M1–M4), and the reference ensemble (Eref) showed the Prec in the range of ~1 to ~2 mm/d over the whole study region.

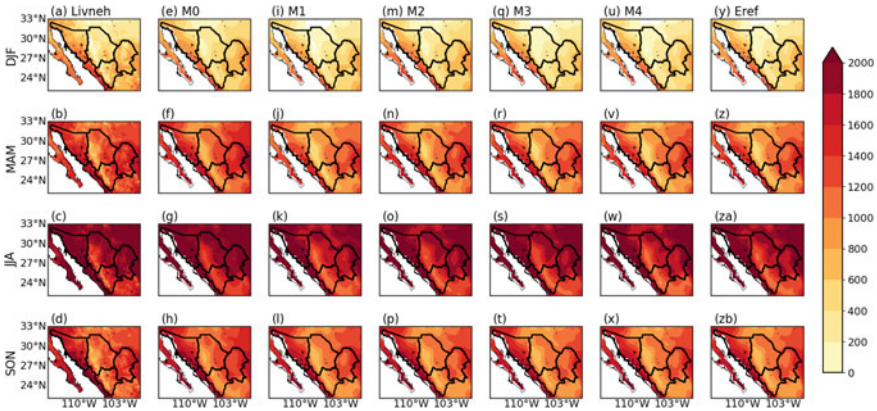
**Growing Degree Days**

Figure 6 shows the seasonal mean of Growing degree days for DJF, MAM, JJA, and SON during 1981–2010. In Livneh (Fig. 6a–d), the maximum GDD ranging from 1000 to 1200°D in DJF (Fig. 6a) was found in Sonora. For MAM (Fig. 6b), the maximum GDD (1400–1800 °D) was observed in Sonora and Coahuila. During



**Fig. 5** Similar to Fig. 4 but for precipitation (mm/d)





**Fig. 6** Similar to Fig. 5 but for GDD (°D)

JJA (Fig. 6c), the maximum GDD (>1800 °D) was found in Sonora, Coahuila, and northern Chihuahua. In SON (Fig. 6d), GDD reaches values of ~1600 °D over Sonora. M0 (Fig. 6e–h) shows the maximum value of GDD between 1000 to 1200°D over Sonora during DJF (Fig. 6e). For MAM (Fig. 6f), GDD’s maximum value (1400 < GDD < 1800 °D) was over Sonora, and Coahuila. In JJA (Fig. 6g), the maximum GDD was over Sonora, Coahuila, and northern Chihuahua (> 1800°D). During SON (Fig. 6h), GDD’s maximum value (~1600°D) was in Sonora. For simulations M1 to M4 and Eref (Fig. 6i–zb), GDD’s maximum value during DJF (Fig. 6i, m, q, u, y) is from 1000 to 1200°D over Sonora. For MAM (Fig. 6j, n, r, v, z), the maximum value of GDD (1200 < GDD < 1600 °D) was found over Sonora and Coahuila’s states. In JJA (Fig. 6k, o, s, w, za), the maximum GDD (>1800 °D) was found in Sonora, Coahuila, and northern Chihuahua. For autumn (SON, Fig. 6l, p, t, x, zb), GDD’s maximum value over the study area was in Sonora (~1400°D).

### 3.2 Future Period

In this section, we present the results for the 2070–2099 period under the low-emission and “business as usual” scenarios.

#### 3.2.1 Annual Cycle

We calculated the annual cycle for all simulations and the difference between the reference and the future scenario (Figs. 7 and 8).

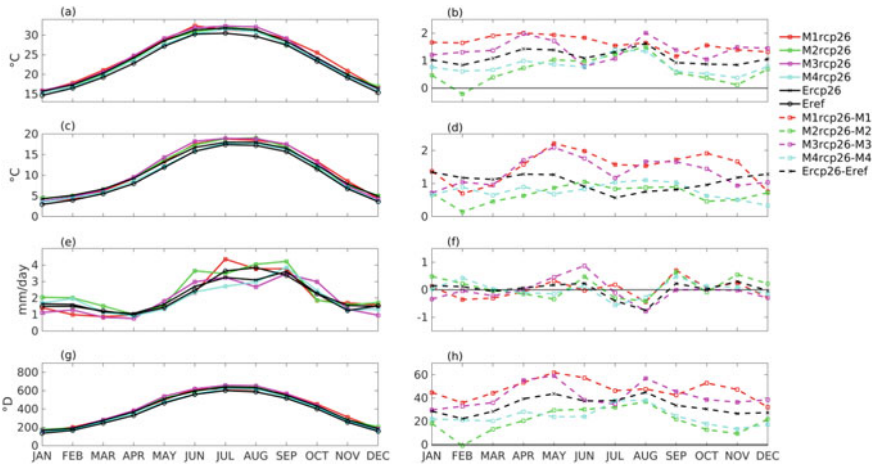


**Fig. 7** Annual cycle for future period. Black solid lines are the ensembles for Eref and Ercp26. Dashed lines indicate the change in the annual cycle of  $T_{max}$  (a, b),  $T_{min}$  (c, d), Prec (e, f), and GDD (g, h)

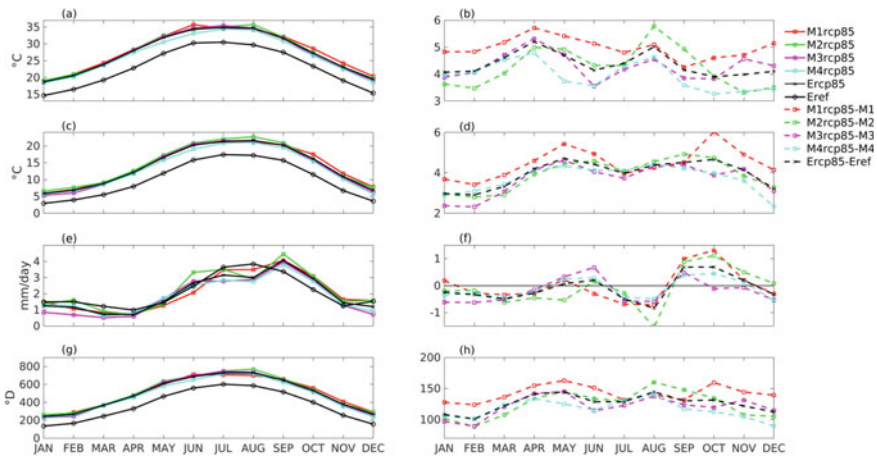


**Fig. 8** Annual cycle for the future period. Black solid lines are the ensembles for Eref and Ercp85. Dashed lines indicate the change in the annual cycle of  $T_{max}$  (a, b),  $T_{min}$  (c, d), Prec (e, f), and GDD (g, h)

RCP2.6

**Maximum Temperature**

We found an increase in  $T_{max}$  (Fig. 7a) for all months, especially in April and August (Fig. 7b).  $T_{max}$  increase from April to August will reduce net pecan photosynthesis

even if water is sufficiently supplied. This increase of  $T_{\max}$  is likely to cause problems in pecan pollination which occurs in April [10]. Then June drop will increase that will reduce nut set. On the other hand, the increase of  $T_{\max}$  on August may reduce floral induction.

### Minimum Temperature

Similarly, we found an increase in  $T_{\min}$  (Fig. 7b) through the year but more remarkably from December to May (Fig. 7c). Pecans from Sonora drop their leaves until December or January, after the first frost. An increase on  $T_{\min}$  in these months means that leaves that are partially active will not allow the tree to enter dormancy. Chilling hours may decrease as a consequence of the increase of  $T_{\min}$ . Then pecan trees will have a delayed and not uniform budbreak as mentioned by Sparks (1983). The increase of  $T_{\min}$  may not have the same effects in the other pecan areas since they accumulate much more chilling hours.

### Precipitation

We found an increased drying from July to August but a wetter June, and September (Fig. 7e, f). Higher precipitation in September will increase vivipary pecan problems in Sonora. Gibberellic acid seems to be related to nut vivipary but high humidity was the most important factor that promoted nut germination [23, 24].

### Growing Degree Days

We also found a general increase in GDD (Fig. 7g) for all months, but more noticeable in May and August (Fig. 7h). GDD determines duration of each stage of development. In addition, faster development leads to lower fruit size. Then it is likely that pecan quality will decrease because of reduction in size.

RCP8.5

### Maximum Temperature

We found an increase in  $T_{\max}$  (Fig. 8a) for all months, especially in April and August up to  $\sim 5$  °C (Fig. 8b).

### Minimum Temperature

Similarly, we found an increase in  $T_{\min}$  (Fig. 8b) through the year but more remarkably from September to November up to  $\sim 4$  °C (Fig. 8c).

### Precipitation

We found an increased drying from July to August, but a wetter October (Fig. 8e). This delayed end of the rainy season (Fig. 8f) has been previously reported in studies based on GCMs from CMIP3 and CMIP5 [4].

### Growing Degree Days

We also found a general increase in GDD (Fig. 8g) for all months, ranging from 100 °D (December to February) to 150 °D (April to August) (Fig. 8h).



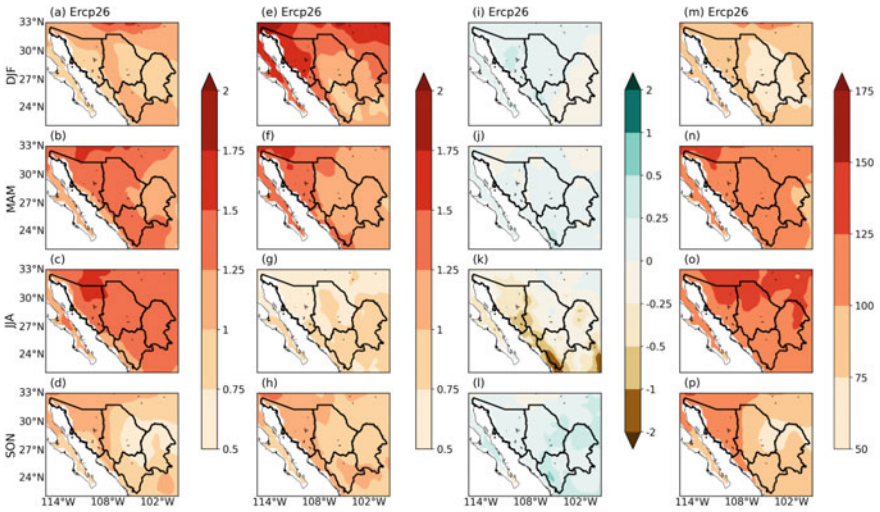


**Fig. 9** Change in seasonal  $T_{max}$  ( $^{\circ}C$ ) during 2070–2099 for Ercp26 for **a** DJF, **b** MAM, **c** JJA, **d** SON, **e–h** similar to **a–d** but for  $T_{min}$  ( $^{\circ}C$ ), **i–l** similar to **e–h** but for Prec (mm/d), **m–p** similar to **i–l** but for GDD ( $^{\circ}D$ )

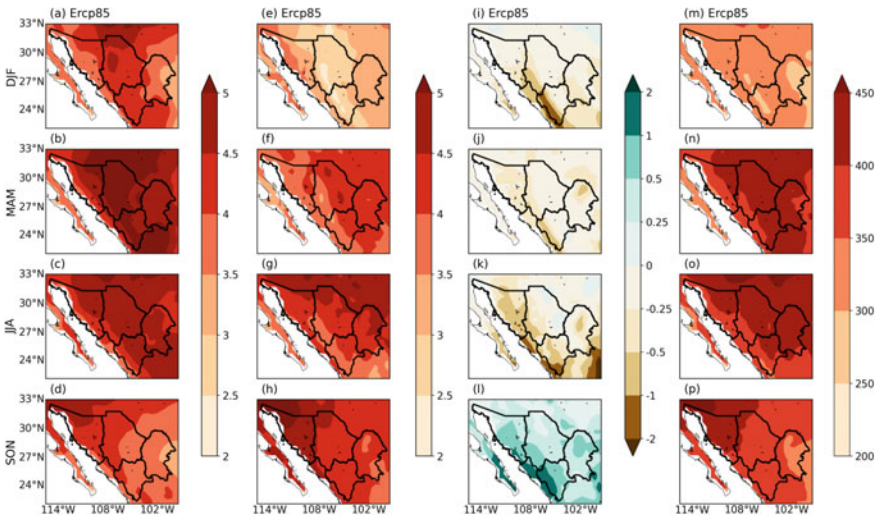


**Fig. 10** Change in seasonal  $T_{max}$  ( $^{\circ}C$ ) during 2070–2099 for Ercp85 for **a** DJF, **b** MAM, **c** JJA, **d** SON, **e–h** similar to **a–d** but for  $T_{min}$  ( $^{\circ}C$ ), **i–l** similar to **e–h** but for Prec (mm/d), **m–p** similar to **i–l** but for GDD ( $^{\circ}D$ )

### 3.2.2 Seasonal Mean

Figures 9 and 10 show the change in  $T_{\max}$  ( $\Delta T_{\max} = T_{\max_{\text{future}}} - T_{\max_{\text{reference}}}$ ),  $T_{\min}$  ( $\Delta T_{\min} = T_{\min_{\text{future}}} - T_{\min_{\text{reference}}}$ ), Prec ( $\Delta \text{Prec} = \text{Prec}_{\text{future}} - \text{Prec}_{\text{reference}}$ ), and GDD ( $\Delta \text{GDD} = \text{GDD}_{\text{future}} - \text{GDD}_{\text{reference}}$ ) under the low-level and “business as usual” scenario.

#### RCP2.6

##### Maximum Temperature

In Fig. 9a–d, the Ercp26 reveals that the pecan region shows the highest values of  $\Delta T_{\max}$  in MAM (Fig. 9b) and JJA (Fig. 9c).

##### Minimum Temperature

In Fig. 9e–h, the Ercp26 reveals that the highest values of  $\Delta T_{\min}$  will be in DJF (Fig. 9e) and MAM (Fig. 9f).

An increase in both,  $T_{\min}$  (see Fig. 9e–h) and  $T_{\max}$  (see Fig. 9a–d) could induce premature germination. This disorder is associated with delayed shuck opening and high temperature during nut ripening. High temperatures, besides promoting germination, retard shuck opening [38].

##### Precipitation

From the ensemble of the future simulations, we found the change in precipitation (Fig. 9i–l) that in summer  $\Delta \text{Prec}$  will be negative over the region (Fig. 9k). In autumn positive values of  $\Delta \text{Prec}$  could be over the whole region (Fig. 9l).

##### Growing Degree days

In Fig. 9m–p, the Ercp26 reveals that the pecan region shows the highest values of  $\Delta \text{GDD}$  in MAM (Fig. 9n) and JJA (Fig. 9o).

#### RCP 8.5

##### Maximum Temperature

Ercp85 reveals that over the study region the change in  $T_{\max}$  for DJF (Fig. 10a) could be between 3 and 4.5 °C. During MAM (Fig. 10b), Durango and Chihuahua show the highest values (>5 °C) of  $\Delta T_{\max}$ , followed by Sonora and Coahuila (4 °C <  $\Delta T_{\max}$  < 5 °C). During the summer (JJA, Fig. 10c), the change in  $T_{\max}$  could be between 4 and 4.5 °C on the coast of Sonora, in the rest of the region between 4.5 and 5 °C. During SON (Fig. 10d) the highest values of  $\Delta T_{\max}$  (between 4 and 4.5 °C) are shown in Sonora. These results are consistent with that reported in Colorado-Ruiz [4] for mean temperature using CGMs.

### Minimum Temperature

Similar to  $T_{\max}$ , the future ensemble shows, in general, an increase in  $T_{\min}$  over the entire region. For DJF (Fig. 10e), Ercp shows that  $\Delta T_{\min}$  will be in the range of 2.5–4 °C. During MAM (Fig. 10f),  $\Delta T_{\min}$  could be between 3 and 4.5 °C. The change in  $T_{\min}$  during JJA (Fig. 10g) will be between 3.5 and 5 °C. During SON (Fig. 10h), Ercp85 shows the highest values in Sonora ( $\Delta T_{\min} > 5$  °C), followed by Chihuahua, Durango and Coahuila ( $4$  °C  $< \Delta T_{\min} < 5$  °C). The increase expected in  $T_{\min}$  is consistent with that reported in Colorado-Ruiz [4] for mean temperature based on CGMs.

### Precipitation

In general, Ercp85 shows a reduction in Prec in high areas of Durango of up to ~2 mm/d during DJF (Fig. 10i) and ~1 mm/d for MAM (Fig. 10j). During the summer (JJA, Fig. 10k), the lowest values (between –0.5 and –2 mm/d) of  $\Delta$ Prec are shown in Sonora, Durango, and Chihuahua, which are within the NAM region. During SON (Fig. 10l), Ercp shows an increase in Prec ( $0.5 < \Delta$ Prec  $< 2$  mm/d) in Durango, and in Sonora, Chihuahua, and Coahuila between 0.5 and 1 mm/d. The increase in precipitation during SON is consistent with results based on GCMs reported in Torres-Alavez [40]. The dryness expected by the end of the century over the region during DJF, MAM, and JJA is consistent with those results reported in Cavazos and Arriaga-Ramírez [3] and Torres-Alavez [40].

### Growing Degree Days

We found that over the study region the change in GDD for DJF (Fig. 10m) could be between 300 and 350 degree days (DD). During MAM (Fig. 10n), Durango, Coahuila, and Chihuahua show the highest values of  $\Delta$ GDD ( $> 450^{\circ}$ D). During the summer (JJA, Fig. 10o), the change in GDD could be between 350 and  $400^{\circ}$ D on the coast of Sonora, in the rest of the region between 400 and 450 DD. During SON (Fig. 10p) the highest values of  $\Delta$ GDD (between 400 and 450 DD) are shown in Sonora.

## 3.3 Possible Causes of Changes on Temperature and Precipitation

Simulations suggest that temperature increases in both: low and high emissions. This means that perhaps, even adopting laws and policies for reducing greenhouse gasses emissions, the climatic system of pecan producing areas in Mexico will tend to warm up. One possible reason for which the temperature of these areas will continue to increase irrespective of the scenario is the intensification of human activities during 2000–2070, and therefore the policies to reduce emissions will not yield the expected results, and we will continue emitting greenhouse gasses. For example, the high demand for essential products obligates industries to operate intensively (EPA 2020). High population projected for the XXI century will force the habilitation of extensive

agricultural surface for food production; this change in land use might promote the warming of the terrestrial surface due to the greater radiation absorption [42]. Modifications on the atmosphere chemistry by natural and anthropogenic causes could be responsible for the nightly clouds promotion, which impedes that the air close to the soil loses heat, increasing nocturnal/minimum temperature [17].

By the end of the century, both ensembles (Ercp26 and Ercp85) suggest warming in the entire region. The warming could be partially due to increments in warm extremes and feedbacks from the projected drying from winter to summer [4, 19].

It was observed a difference in the precipitation pattern for each scenario. Under the scenario with policies for constraint emissions, in the whole study area, precipitation decreases in summer and increases in autumn, while for winter and spring, some regions present increases and decreases. In the scenario without emissions policies, precipitation increases in September, October, and November; and decreases through December to August. Emission of anthropogenic aerosol and particles to the atmosphere can continue even under the low-emissions scenario. These particles can contribute to the precipitation decrease during 2070–2099. Aerosols promote water vapor condensation in small drops and given their weight instead of precipitating re-evaporate [12]. This phenomenon has been documented as a critical cause of precipitation decrease in several regions of the world. Nut-producing areas are immersed within the most important Mexican deserts. It has been reported that desert dust is also responsible for precipitation decrease [32], this condition is significant enhanced by an increase in wind speed caused by land-use changes, mainly when forests are removed. On the other hand, precipitation increases at the end of the century could be promoted by the same warming of the atmosphere that was found in this research. It is proven that a warmer atmosphere has a greater capacity for absorbing water vapor, which is explained by the Clausius-Clapeyron relationship [41].

In a more regional context according to Torres-Alavez [40] during winter, under the RCP85 scenario, an intensification and eastward expansion of the jet stream by the end of the century results in stronger subsidence and reduced precipitation over north-western Mexico. During summer regional changes in precipitation could be linked to a decrease in the mid-tropospheric Land-Sea Thermal Contrast (LSTC), enhanced atmospheric stability, and a southward displacement of the Inter-Tropical Convergence Zone. At the end of the twenty-first century, the surface LSTC is projected to increase during the NAM season, with an earlier onset of continental warming in MAM. On the other hand, autumn might result in more precipitation in the late twenty-first century under both scenarios, suggesting a delay of the end of the rainy season in agreement with previous works based on GCMs from CMIP5 (e.g., [4, 20, 22, 40], among others).

### ***3.4 Potential Implications of Temperature and Precipitation Changes***

The temperature increase and the precipitation decrease/increase at the end of the twenty-first century may bring a series of implications in pecan crops in northern Mexico. The temperature increase brings with it a greater evaporative capacity of the atmosphere. Under conditions of temperature increase, under both scenarios, more water consumption is expected by the pecan crop; this is due to the influence of maximum temperature on reference evapotranspiration (ET<sub>0</sub>), and in turn, on actual crop evapotranspiration (ETC) [1]. Under conditions of greater crop water demands, an increase in groundwater extractions is expected. This case would be critical since groundwater aquifers of northern Mexico are already overexploited. It is expected that at the end of the century pecan production will add up to the increase in pressure on water resources. This condition is especially crucial in “La Costa de Hermosillo”, where wells experience the saline intrusion phenomenon. Under the two scenarios, the temperature increase could trigger important changes around the pecan agronomy. The temperature increase is responsible for increasing the GDD [28]. Under both scenarios, a GDD increase in the whole area cropped with pecan is expected. As temperatures increase in winter (autumn) late (early), trees’ active period could be extended. That is to say, they could take more time to start the dormancy period, and the dormancy period could be broken earlier. While the active period of trees increases, needs and maintaining costs increase also, that is to say, greater use of fertilizers, herbicides, pesticides, irrigation, etcetera is required. During the growing cycle, it could increase the periods with better conditions for the proliferation of weeds, plagues, and diseases [46], significantly increasing the cost to farmers.

In the case of the low-emissions scenario, the precipitation decrease in summer could significantly enhance the water requirements increase (which originally had already been affected by the temperature increase); this would coincide with the higher water consumption season of the crop. The precipitation decrease would promote a decline of the effective precipitation, which is a significant parameter in irrigation management so that irrigation requirements would increase and the problem of agricultural water management could get even more critical. Under the low-emissions scenario, the increase of fall-precipitation at the moment of harvest could bring high moisture content on the nut. For this same scenario, precipitation increases in June and September could decrease irrigation requirements; however, they could promote the presence of weeds and obligate the farmer to invest more resources for controlling them. Under the scenario “business as usual”, from December to August, the precipitation decrease most likely would be compensated by increased irrigation.

## 4 Conclusions

The RCA4 model reproduced the spatial patterns of the variables analyzed and their main values realistically. This study shows that towards the end of the century, an increase in maximum and minimum temperatures under both the low-emission and the “business as usual” scenarios are expected in all seasons. The latter will have repercussions on an extension of the budding period, dehiscence of the pecan flowers and fruits, nut filling, and vivipary, which will affect the yield and quality of pecan orchards. Also, the expected increase in temperature for the late twenty-first century will enhance premature germination disorder. The temperature increase is responsible for increasing the Growing degree days in the whole area cropped with pecan. As the Growing degree days increase in winter (autumn) late (early), trees’ active period could be extended taking more time to start the dormancy period. Over the pecan producing region, summers will be drier, a decrease in precipitation could increase the irrigation requirements, and autumns will be wetter, promoting weeds apparition obligating the farmer to take actions for controlling them. Under this evidence, the pecan industry may be affected since yield and quality may decrease, especially in areas where pecan already suffers from stress due to water scarcity, extreme temperatures, low chilling hour accumulation, and rainfall during nut maturity.

**Acknowledgments** The first author gratefully acknowledges the Instituto Nacional de Investigaciones Forestales Agrícolas y Pecuarias (INIFAP), experimental station Pabellon, for all support in carrying this research out. EGP’s research is supported by CONACYT (Mexico). We also gratefully acknowledge the two anonymous reviewers for helping us to improve this work.

## References

1. Allen RG, Pereira L, Raes D, Smith M (1998) Crop evapotranspiration: guidelines for computing crop water requirements. In: FAO irrigation and drainage paper 56. Food and Agriculture, Rome, Italy
2. Barboza DS, Ferreira JA, Rammana TV, Rodríguez VP (2007) Crop water stress index and water use efficiency for melon (*Cucumidmelo* L.) on different irrigation regimes. *Agric J.* 2(1):31–37
3. Cavazos T, Arriaga-Ramírez S (2012) Downscaled climate change scenarios for Baja California and the North American Monsoon during the twenty-first century. *J Climate* 25:5904–5915. <https://doi.org/10.1175/JCLI-D-11-00425.1>
4. Colorado-Ruiz G, Cavazos T, Salinas JA, De Grau P, Ayala R (2018) Climate change projections from Coupled Model Intercomparison Project phase 5 multi-model weighted ensembles for Mexico, the North American monsoon, and the mid-summer drought region. *Int J Climatol* 38:5699–5716. <https://doi.org/10.1002/joc.5773>
5. Corrales-Suastegui A, Fuentes-Franco R, Pavia EG (2020) The mid-summer drought over Mexico and Central America in the 21st century. *Int J Climatol* 40:1703–1715. <https://doi.org/10.1002/joc.6296>
6. Dee DP, Uppala SM, Simmons AJ, Berrisford P, Poli P, Kobayashi S, Andrae U, Balmaseda MA, Balsamo G, Bauer P, Bechtold P, Beljaars AC, van de Berg L, Bidlot J, Bormann N, Delsol C, Dragani R, Fuentes M, Geer AJ, Haimberger L, Healy SB, Hersbach H, Hólm EV,

- Isaksen L, Källberg P, Köhler M, Matricardi M, McNally AP, Monge-Sanz BM, Morcrette J, Park B, Peubey C, de Rosnay P, Tavolato C, Thépaut J, Vitart F (2011) The ERA-Interim reanalysis: configuration and performance of the data assimilation system. *QJR Meteorol Soc* 137:553–597. <https://doi.org/10.1002/qj.828>
7. EPA (2020) <https://www.epa.gov/ghgemissions/sources-greenhouse-gas-emissions>
  8. Giorgi F, Gutowski WJ (2015) Regional dynamical downscaling and the cordex initiative. *Annu Rev Environ Resour* 40(1):467–490
  9. Giorgi F, Jones C, Asrar GR (2009) Addressing climate information needs at the regional level: the cordex framework. *Bull World Meteorol Organ* 58(3):175–183
  10. Grageda J, Sabori R, Fú A, Jiménez A, Morales M., Barrón R (2008) El clima y la producción de nogal. CECH-CIRNO-INIFAP. Reunión Técnica Internacional de Nogal Pecanero. Memoria técnica 27:57–63
  11. Godoy-Avila C, López-Montoya I (2000) Desarrollo de la almendra y germinación del fruto del nogal pecanero bajo cuatro calendarios de riego. *Terra Latin* 18(4):305–311
  12. Gunn R (1956) The ratio of the positive and negative light ion conductivities in a neutral aerosol space. *J Colloid Interf Sci* 11:691–696
  13. Guo D, Wang H (2016) Comparison of a very-fine-resolution GCM with RCM dynamical downscaling in simulating climate in China. *Adv Atmos Sci* 33:559–570. <https://doi.org/10.1007/s00376-015-5147-y>
  14. INEGI (2020) <http://cuentame.inegi.org.mx/monografias/default.aspx?tema=me>
  15. INEGI (2018) Anuario estadístico y geográfico por entidad federativa
  16. IPCC (2013) Climate Change 2013: the physical science basis. In: Stocker TF, Qin DH, Plattner GK, Tignor M and others (eds) Contribution of working group I to the 5th assessment report of the Intergovernmental Panel on Climate Change. Cambridge University Press, Cambridge
  17. Jhajharia D, Singh VP (2011) Trends in temperature, diurnal temperature range and sunshine duration in northeast India. 1367:2010 June 1353–1367. <https://doi.org/10.1002/joc.2164>
  18. Kang Y, Khan S, Ma X (2009) Climate change impacts on crop yield, cop water productivity and food security—A review. *Prog Nat Sci* 19(2009):1665–1674
  19. Kharin VV, Zwiers FW, Zhang X, Wehner M (2013) Changes in temperature and precipitation extremes in the CMIP5 ensemble. *Clim Change* 119:345–357. <https://doi.org/10.1007/s10584-013-0705-8>
  20. Lee J, Wang B (2014) Future change of global monsoon in the CMIP5. *Clim Dyn* 42:101–119. <https://doi.org/10.1007/s00382-012-1564-0>
  21. Livneh B, Bohn T, Pierce D et al (2015) A spatially comprehensive, hydrometeorological data set for Mexico, the U.S., and Southern Canada 1950–2013. *Sci Data* 2:150042. <https://doi.org/10.1038/sdata.2015.42>
  22. Maloney ED, Camargo SJ, Chang E, Colle B, Fu R, Geil KL, Hu Q, Jiang X, Johnson N, Karnauskas KB, Kinter J, Kirtman B, Kumar S, Langenbrunner B, Lombardo K, Long LN, Mariotti A, Meyerson JE, Mo KC, Neelin JD, Pan Z, Seager R, Serra Y, Seth A, Sheffield J, Stroeve J, Thibeault J, Xie S, Wang C, Wyman B, Zhao M (2013) North American climate in CMIP5 experiments: part III: assessment of twenty first-century projections. *J Clim* 27:2230–2270. <https://doi.org/10.1175/JCLI-D-13-00273.1>
  23. Martínez-Díaz G (2011) El ácido giberélico incrementa la germinación prematura en nogal pecanero (*Carya illinoensis* Koch.). *Tecnociencia Chihuahua* 5(3):148–155
  24. Martínez-Díaz G, Miranda-Blanco JL, Vieira-Figueiredo F, Núñez-Moreno JH (2014) Avances en el estudio de la viviparidad de la nuez. Simposio Internacional de nogal Pecanero CEC-CIRNO-INIFAP. Memoria científica 5:39–43
  25. McMaster G, Wilhelm WW (1997) Growing degree-days: one equation, two interpretations. *Agric For Meteorol* 87(4):291–300. [https://doi.org/10.1016/s0168-1923\(97\)00027-0](https://doi.org/10.1016/s0168-1923(97)00027-0)
  26. Mimi ZA, Jamous SA (2010) Climate change and agricultural water demand: Impacts and adaptations. *Afr J Environ Sci Technol* 4(4):183–191
  27. Moss R, Edmonds J, Hibbard K et al (2010) The next generation of scenarios for climate change research and assessment. *Nature* 463:747–756. <https://doi.org/10.1038/nature08823>



28. Ojeda-Bustamante W, Sifuentes-Ibarra E, Iñiguez-Covarrubias M, Montero-Martinez MJ (2011) Climate change impact on crop development and water requirements. *Agrociencia* 45:1–11
29. Orona Castillo I, Sangerman-Jarquín D, Cervantes Vázquez M, Espinoza Arellano J, Núñez Moreno J (2019) La producción y comercialización de nuez pecanera en México. *Revista Mexicana De Ciencias Agrícolas* 10(8):1797–1808. <https://doi.org/10.29312/remexca.v10i8.1833>
30. Retes-López R, Nasaimea Palafox AR, Moreno Medina S, Denogean Ballesteros FG, Martín Rivera M (2014) Análisis de rentabilidad del cultivo de nogal pecanero en la Costa de Hermosillo. In: *Revista Mexicana de Agronegocios*, vol 34, enero-junio, pp 872–882
31. Riahi K, Rao S, Krey V, Cho C, Chirkov V, Fisher G, Kindermann G, Nakicenovic N, Rafaj P (2011) RCP8.5: a scenario of comparatively high greenhouse gas emissions. *Clim Change* 109:33–57. <https://doi.org/10.1007/s10584-011-0149-y>
32. Rosenfeld D, Rudich Y, Lahav R (2001) Desert dust suppressing precipitation: a possible desertification feedback loop. *Proc Natl Acad Sci* 98(11):5975–5980. <https://doi.org/10.1073/pnas.101122798>
33. Ruiz-Álvarez O, Arteaga-Ramírez R, Vázquez-Pena MA, Lopez-Lopez R, Ontiveros-Capurata RE (2011) Requerimiento de riego y predicción del rendimiento en gramíneas forrajeras mediante un modelo de simulación en Tabasco. México. *Agrociencia* 45(7):745–760
34. Samuelsson P, Jones CG, Will En U, Ullerstig A, Gollvik S, Hansson U, Jansson E, Kjellström MC, Nikulin G, Wyser K (2011) The rossby centre regional climate model rca3: model description and performance. *Tellus A: Dyn Meteorol Oceanogr* 63(1):4–23
35. SIAP (2016) SAGARPA, México. <http://www.gob.mx/siap/>
36. Sifuentes Ibarra E, Samaniego Gaxiola JA, Anaya Salgado A, Núñez Moreno JH, Valdez Gascón B, Gutiérrez Soto RG, Ruelas Islas JD, Macías Cervantes J (2015) Irrigation scheduling in pecan (*Carya illinoensis*), through an integrated model based on thermal time. *Revista mexicana de ciencias agrícolas* 6(8):1893–1902. Recuperado en 05 de septiembre de 2020, de [http://www.scielo.org.mx/scielo.php?script=sci\\_arttext&pid=S200709342015000801893&lng=es&tlng=en](http://www.scielo.org.mx/scielo.php?script=sci_arttext&pid=S200709342015000801893&lng=es&tlng=en)
37. Sparks D (1993) Chilling and heating model for pecan budbreak. *J Am Soc Hort Sci* 118:29–35
38. Sparks D (2000) Pecan in warm climate. In: Erez A (eds) *Temperate fruit crops in warm climates*. Springer, Dordrecht. [https://doi.org/10.1007/978-94-017-3215-4\\_14](https://doi.org/10.1007/978-94-017-3215-4_14)
39. Taylor KE, Stouffer RJ, Meehl GA (2012) An overview of CMIP5 and the experiment design. *Bull Am Meteor Soc* 93(4):485–498
40. Torres-Alavez A, Cavazos T, Turrent C (2014) Land-sea thermal contrast and intensity of the North American monsoon under climate change conditions. *J Climate* 27:4566–4580. <https://doi.org/10.1175/JCLI-D-13-00557.1>
41. Trenberth KE, Day A, Rasmussen RM, Parsons DB (2003) The changing character of precipitation. *Am Meteorol Soc* 84:1205–1218. <https://doi.org/10.1175/BAMS-84-9-1205>
42. USGCRP (2018) In: Reidmiller DR, Avery CW, Easterling DR, Kunkel KE, Lewis KLM, Maycock TK, Stewart BC (eds) *Impacts, risks, and adaptation in the United States: fourth national climate assessment, vol II*. U.S. Global Change Research Program, Washington, DC, USA, 1515 pp. <https://doi.org/10.7930/NCA4.2018>
43. van Vuuren DP, Edmonds J, Kainuma M et al (2011) The representative concentration pathways: an overview. *Clim Change* 109:5. <https://doi.org/10.1007/s10584-011-0148-z>
44. van Vuuren DP, Stehfest E, den Elzen MGJ et al (2011b) RCP2.6: exploring the possibility to keep global mean temperature increase below 2 °C. *Clim Change* 109:95. <https://doi.org/10.1007/s10584-011-0152-3>
45. Zhang X, Cai X (2013) Climate change impacts on global agricultural water deficit. *Geophys Res Lett* 40(6):1111–1117
46. Ziska LH (2003) Evaluation of the growth response of six invasive species to past, present and future atmospheric carbon dioxide. *J Exp Botany* 54:395–404. <https://doi.org/10.1093/jxb/erg027>



# **Water Resources System Planning and Management**

# Effect of Water Distribution Network Pipes Size on Flow Rate of a House Connection and Its Hydraulic Analysis



C. R. Suribabu and P. Sivakumar 

**Abstract** Supply of water from the distribution pipeline to the house service connection varies street to street due to variation of water pressure. It is commonly noticed that houses located near to the service tank or pumping station get more supply than the houses located far away from the source or at dead-end users despite the house service connection pipe diameter is being the same. Supply at the outlet point of house connection directly depends on the pressure available at that point. In general water distribution analysis, the demand in the particular street will be divided into two quantities after clubbing the demand estimated in the street and assigned as a nodal demand. So, the demand is fixed and for which analysis will be carried out using hydraulic simulation. But, actual supply to the house is difficult to ascertain in this method. In the present study, how to determine the actual supply to the house service connection point through a hydraulic simulation is illustrated using a sample network. The study illustrates how simulation can be done without fixing nodal demand in the hydraulic simulation engine for house service connection having intermittent water by treating it as open orifice and water is being collected directly in the sump. The result of the study depicts that the diameter of water distribution lines and loss of pressure head poses unequal distribution of water to the consumer. Further, the study reveals that equity of supply can be ensured unless the flow at the house service level is controlled.

**Keywords** House service connection · Hydraulic simulation · Water pressure

---

C. R. Suribabu (✉)

School of Civil Engineering, Centre for Advanced Research in Environment, SASTRA Deemed University, Thanjavur, Tamil Nadu 613401, India  
e-mail: [suribabu@civil.sastra.edu](mailto:suribabu@civil.sastra.edu)

P. Sivakumar

Department of Civil Engineering, North Eastern Regional Institute of Science and Technology (Deemed to be University), Nirjuli (Itanagar), Arunachal Pradesh 791109, India

## 1 Introduction

Intermittent water supply systems are very common mode of providing water supply to the public in most developing countries. Supply will be generally done 2–3 h per day in the morning time and in some places, water will be supplied for a few hours during the evening time. It is a general tendency of public to store as much water available at their service point. This has let an uneven distribution of water supply among the public. Most of the intermittent water supply systems are designed for low source head (varies from 8 to 15 m). Due to low source heads, the availability of residual pressure head often falls below 3 m in case of 8 m source head and 6 m for 15 m source head. Large variation of residual pressure head will be noticed for the system having huge coverage area. Under such a circumstance, more flow goes to high pressure zone and a meager water supply happens at low pressure zone and sometimes low pressure zone does not get adequate supply [1, 5]. Though this aspect is well known to the design, municipal, and operational engineers, there is no good mechanism to control the flow at house service level. Equal distribution of water to the consumer is found to be a challenging task among municipal authorities through pipeline designed for estimated nodal demand with proper future projection. Non-uniform availability of pressure possesses a major concern during operation of water distribution network. Though water metering is one of the effective mechanisms to control the usage of water and reduce the wastage of water, effectiveness of the system depends on its reliability of functioning. Collecting meter readings for payment based on consumption requires additional manpower. It is important to design a network which delivers only specified quantity per day with high reliability. Such a design cannot be obtained directly from hydraulic analysis alone as maintaining constant pressure certainly requires an additional valve operation to control the flow remotely.

Hence, automatic control device at the house connection point is essential to maintain the equal supply to all the house service connections. In the present scenario of the intermittent supply, while supplying water at few hours, more water will be delivered to the houses located at high pressure zones. While designing network, the pipe diameter is obtained by considering demand occurs at nodal point instead along the pipeline. Due to summing up of demand occurring along the pipe to the node, hydraulic analysis provides the pressure at nodal points and flow rate through a pipeline. No details will be available on what could be the actual supply of water at the house service connection. In the intermittent water supply system, most of the consumer collects the water in the underground sump constructed in their premises. Later, water will be pumped to over tank available on the terrace of the building for internal supply by gravity. The house service connection pipeline at the outlet point to the sump behaves as an orifice opening. For highly intermittent water supply systems, the outflows at the demand nodes behave as uncontrolled orifice-based demands [5]. It is a general tendency for the customers to draw the maximum available water during intermittent water supply periods and water will be stored in the underground storage system more than required for the consumers expecting that there will not be supply in coming days [3, 6]. The actual outflows at each nodal point during the supply hour

in case of intermittent water distribution network (WDN) are the useful indicator to assess the performance of highly intermittent WDNs [5]. Due to non-availability of adequate water for supply, intermittent or discontinuous water distribution, and rationing the available water is widely adopted not only in developing countries and also in developed countries [1]. Assessment of house service supply is very important to understand the actual supply of water. This can be assessed by creating a node to each house connection point and connecting a sump (reservoir) to that node. This method requires large creation of nodal points and also reservoir needs to be connected to each house service node. This actually increases the complexity to the hydraulic analysis. However, for small networks, it is possible to create such a detailed network and can be analyzed using hydraulic simulation software. Paez et al. [2] has shown that a network with large number of nodes connected with reservoirs can easily be analyzed using any software. In the present work, a network with house service connected with a reservoir is analyzed to assess the supply to each house. The influence of main and distribution pipes on water supply to the house connections is observed from the hydraulic analysis of the network.

## 2 Methodology

Fontanazza, et al. [1] introduces an index to evaluate the equity in the distribution during intermittent operational conditions. The equity index (EQ) defined as the ratio between volume of water actually supplied to the users in a service cycle and the user demand. Its value represents the ability of supplying water against user demand and helps to identify the advantaged and dis advanced users in the system. This equity index is used to assess how equity of supply is getting affected when intermittent supply system is adopted.

$$\text{Equity Index} = \frac{\text{Volume of water supply}}{\text{User demand volume}} \quad (1)$$

Delivery or withdrawal of water from the house connection may not happen as per design quantity. Particularly, if the water is being collected in the sump, the pipe outlet behaves as uncontrolled orifice and entire quantity will be supplied quickly than design duration of supply.

The ratio of duration of supply of actual quantity and designed supply duration can be defined as Supply duration index.

$$\text{Supply duration index} = \frac{\text{Duration of supply}}{\text{Designed duration}} \quad (2)$$

The following steps need to be followed to carry out the hydraulic analysis of the network with HSC.

1. Draw the network layout and create nodal point for each house service connection. For connection to opposite houses, same node can be utilized.
2. Connect a sump (reservoir) to all the house service nodal point by 2.5 m length 12 mm diameter pipe (if 12 mm service connection is adopted in the system) with necessary roughness coefficient. The exact length of house service connection can be used if data is available. Otherwise, it is taken as half the width of the road plus 1 m inside from house compound boundary.
3. Assign sump elevation as that of the nodal elevation.
4. By performing an extended period simulation for supply duration, the flow to the house connection and change in water level at the source and also emptying time of the source can be calculated through the simulation.
5. By changing the main pipe diameter, the flow at each house service can be studied. This will show how the diameter affects the flow rate to the house service level.
6. Calculate equity index and supply duration index for all the nodes to assess the degree of equity for the system.

## ***2.1 Example Network***

A small rural water supply network is used for illustration of proposed approach to study the equity in water distribution and effects of pipe size on supplying capability. An overhead tank (OHT) shall supply water intermittently to 100 houses of a well-planned small hamlet (Fig. 1). The bottom level of OHT is eight meter above the ground level and it can store water to a maximum depth of 3 m. The inner diameter of OHT is 3.66 m. The supply will be made for 1 h with a design supply rate of 5 L per minutes (LPM). The per capita consumption for small hamlet is considered as 60 L and with 5 people per house. The quantity of water to be supplied to each house is 300 L. The house service connections (HSCs) are made with 12 mm diameter pipe and connected directly to underground sump to collect water. The length of the distribution pipe between HSCs is taken as 12 m by considering each plot width 12 m (40 ft). The main pipe connecting tank and node is taken 100 m and the remaining length of the pipe between nodes is considered 50 m. Controlled flow is possible if the water tap is set in such a way that consumers draw water at the rate of 5 LPM. Since the supply is intermittent, the general practice adopted in a country like India is to store the water in the sump and pump the water to house OHT. Under this kind of practice, the customer keeps the tap fully open to collect water in the storage system.

Figure 1 shows the rural water supply network with house service connections. Each house connection node connects with a reservoir having elevation same as that of distribution line. The length of house connection pipeline is taken as 2.5 m. The hydraulic simulation of the network is performed using EPANET 2 [3] by changing the main and distribution pipe size to examine the effect of pipe size on supply. Table 1 gives the details of pipe sizes for main and distribution pipes. Extended period simulation is carried out until water in the tank gets empty. Single filling of water in

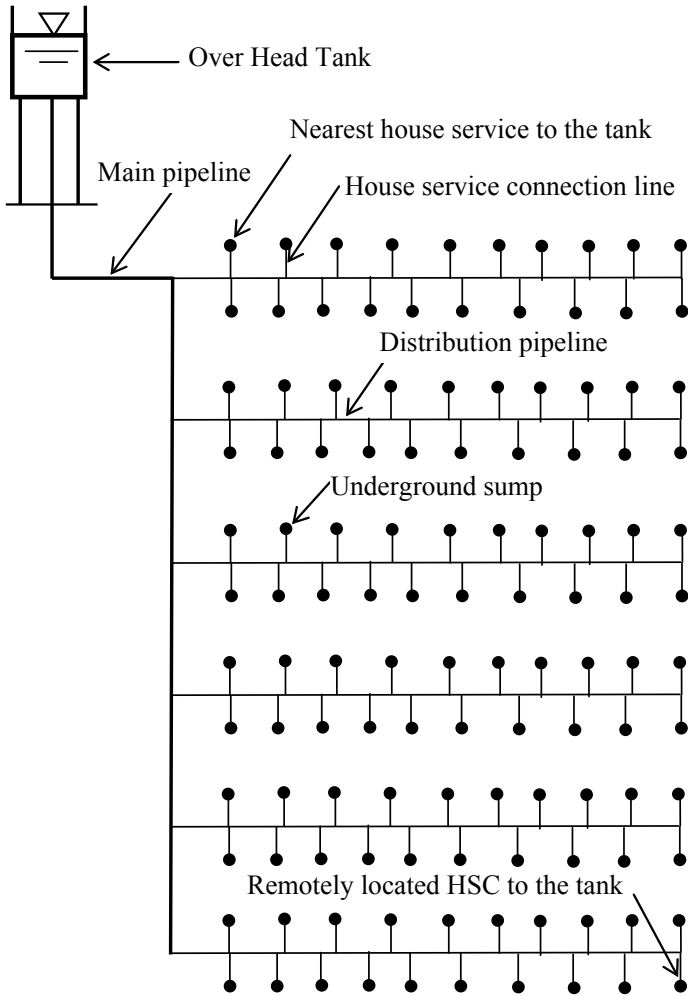


**Fig. 1** Layout of a rural water distribution network

the tank can satisfy the demand of 60 L per capita. Double time filling will be able to satisfy with 120 L per capita demand. It can be seen from the Table 1 that HSCs located near to the tank and remotest point to the tank has distinct value when the simulation is performed without restriction to the supply (uncontrolled flow). Another important observation is that when the size of the pipe for main and distribution lines is higher, more quantity of water gets delivered for all the connections. The time to delivery increases when the pipe sizes selected for both main and distribution are small. It is clear that more delivery of water takes place while pressure loss in the main and distribution pipes is less. In all the eight options (Table 1), no option is able to supply equal quantity of water to the consumers.

**Table 1** Initial flow rate at the house service connection and duration of supply

| Sl. No. | Main pipe diameter in mm | Distribution pipe diameter in mm | Initial flow at HSC located near source (LPM) | Initial Flow at HSC located far away (LPM) | Duration of supply to meet out demand (min) |
|---------|--------------------------|----------------------------------|---|--|---|
| 1       | 150                      | 100                              | 54.24   | 27.13                                      | 8   |
| 2       | 100                      | 100                              | 26.57   | 9.12                                       | 23  |
| 3       | 100                      | 75                               | 26.93   | 9.20                                       | 23  |
| 4       | 150                      | 75                               | 38.35   | 25.33                                      | 12  |
| 5       | 150                      | 50                               | 38.08   | 13.16                                      | 17  |
| 6       | 100                      | 50                               | 28.84   | 7.06                                       | 27  |
| 7       | 75                       | 50                               | 22.00   | 2.78                                       | 48  |
| 8       | 75                       | 75                               | 19.94   | 2.54                                       | 44  |

Controlled withdrawal of water can alone maintain the equity of the supply. There are large variations of flow between HSC located near the tank and far away from the tank. It can be seen from the Table 2 that equity of the supply with respect to 300 L per connection is unachievable under uncontrolled flow. From Table 2, it can be observed that the interval between maximum and minimum equity index values increases when the network pipe sizes decrease. Smaller pipe sizes offer more resistance to flow and supply more water at nearest nodes to the tank than that of with higher pipe sizes. Time taken to empty the tank is more if the network with smaller sizes. This aspect highlights the importance of the selection of appropriate pipe sizes for both main and distribution pipes. For small size networks, the best combination pipe sizes can arrive through a permutation and combination. But, for larger size networks, the optimization model provides a better solution. If the same network is simulated by setting nodal demand as 5 LPM, then, demand for all nodes will be satisfied as per hydraulic simulation and equity of one will be achieved. But, in reality, this won't happen at all HSCs unless consumers draw water 5 LPM

**Table 2** Equity and supply duration indices for different pipe configured network

| Sl. No. | Main pipe diameter in mm | Distribution pipe diameter in mm | Equity index |         | Supply duration index |
|---------|--------------------------|----------------------------------|--------------|---------|-----------------------|
|         |                          |                                  | Maximum      | Minimum |                       |
| 1       | 150                      | 100                              | 1.46         | 0.73    | 0.13                  |
| 2       | 100                      | 100                              | 1.92         | 0.66    | 0.38                  |
| 3       | 100                      | 75                               | 1.95         | 0.67    | 0.38                  |
| 4       | 150                      | 75                               | 1.45         | 0.95    | 0.20                  |
| 5       | 150                      | 50                               | 2.04         | 0.70    | 0.28                  |
| 6       | 100                      | 50                               | 2.44         | 0.60    | 0.45                  |
| 7       | 75                       | 50                               | 3.32         | 0.42    | 0.80                  |
| 8       | 75                       | 75                               | 2.76         | 0.35    | 0.73                  |

only. Supplying equal amount of water among all the consumers is not possible hydraulically without any control device. A control device should be developed in such a way that whatsoever change in pressure, the device should be able to control the pressure automatically and maintain constant pressure in order to ensure constant supply to all the consumers of the system.

### 3 Conclusion

The study reveals that equity of supply is hardly possible without any control device at house service connection level particularly intermittent water supply or consumer themselves should draw the water as per designed demand. The degree of supply to the consumer depends on the main and distribution pipe sizes. The study illustrates how main pipe sizes influence the rate of flow at house service connection. The network composed with smaller pipe sizes could take longer the supply duration to meet out the volumetric demand than the same network composed of higher diameter. If the supply is administrated as uncontrolled flow, then large deviation in the supply between the HSC located near to OHT and far away from the OHT is observed. Water supply to all populace is possible effectively once a control device is provided at HSC point.

### References

1. Fontanazza CM, Freni G, La Loggia G (2007) Analysis of intermittent supply systems in water scarcity conditions and evaluation of the resource distribution equity indices. *W IT Trans Ecol Environ* 103. <https://doi.org/10.2495/WRM070591> (Water Resources Management IV)
2. Paez D, Suribabu CR, Filion Y (2018) Method for extended period simulation of water distribution networks with pressure driven demands. *Water Resour Manage* 32:2837–2846
3. Rossman LA (2000) EPANET user's manual. Risk Reduction Engineering Laboratory. U.S. Environmental Protection Agency, Cincinnati
4. Reddy LS, Elango K (1989) Analysis of water distribution networks with head-dependent outlets. *Civ Eng Syst* 6(3):102–110
5. Mohan S, Abhijith GR (2020) Hydraulic analysis of intermittent water-distribution networks considering partial-flow regime. *J Water Resour Plann Manage* 146(8):04020071
6. Andey SP, Kelkar PS (2009) Influence of intermittent and continuous modes of water supply on domestic water consumption. *Water Resour Manage* 23(12):2555–2566. <https://doi.org/10.1007/s11269-008-9396-8>



# Leakage Optimization of Water Distribution Network Using Artificial Intelligence



Sejal Desai and Gargi Rajapara

**Abstract** In water distribution system, maintaining adequate pressure and uninterrupted water supply for an efficient distribution to the consumers is very important. Main objective of the recent study was to analyze water distribution system by simulating flow in the network using hydraulic model and optimization tools in form of genetic algorithm (GA) using MATLAB for minimizing leakage. Novel tools and strategies were used in the form of advanced hydraulic simulation models and its optimization for precise prediction of the behavior of flow in the system. Hydraulic model developed in EPANET 2.0 was used to simulate the pressure and discharge at various nodes known as junction and links of pipes which gave the hypothesis that the leakage in the system has been encountered. Genetic algorithm (GA) is a part of artificial intelligence (AI) which is a fast and precise method for single or multiple targets of optimization. The leakage model was formulated and coded in genetic algorithm and optimized. Genetic algorithm is the optimization technique in MATLAB adopted to minimize the leakages at the critical nodes. The results obtained by genetic algorithm reduce the amount of the leakages to an optimum value. The amount of leakages obtained by genetic algorithm in the network is reduced to 73% from the actual leakage calculations. The proposed novel methodology was very effective in optimizing the leakage scenario, thereby minimizing the leakage and wastage of water, thus resulting into augmented storage of the water.

**Keywords** Artificial intelligence · Genetic algorithm · Leakage · Optimization · Water distribution system

---

S. Desai (✉)

Sal Institute of Technology and Engineering Research, Ahmedabad, Gujarat, India

G. Rajapara

LDRP, Kadi Sarva Vishwavidyalaya University, Gandhinagar, Gujarat, India

## 1 Introduction

Water is next to air which is the most essential commodity for all the living being to sustain and maintain their life [1]. As per recent survey, around 2.2 billion people around the world lacks safely managed drinking water, 3 billion population lack basic hand washing facilities [2]. Ever increasing population demand for water increment, industrialization, and irrigation requirements leads to over exploitation of this treasure, leading to scarcity. Water Distribution System (WDS) network receives treated water, and then it is supplied to the consumers. Hence, in any efficient Water Distribution Network (WDN), it is very essential that water reaches the end point with sufficient pressure, flow, and potable water standards as per CPHEEO standards [3]. Distribution network consists of network of various diameters of pipes, overhead tanks, pumps, control valves, disinfectant dosing stations, etc. The majority of the WDS elements are either hidden beneath the ground or unnoticeably placed [4].

Models of the water distribution network have been widely accepted like a tool for simulation of hydraulic as well as water quality scenarios in the network [5]. According to WHO/UNICEF, water supplied in pipe was considered as an improvisation in living standards when drinking water was supplied to the various buildings, plots areas, etc. [6, 7]. It was predicted that 50% of piped water supply in the Asian countries were having intermittent water supply [6, 8]. However, pilot projects were gradually rising in few of the cities in India [9].

An efficient and sustainable water distribution system relies on the service given by the supplier and the generation of income from the consumers [10]. Continuous water supply reduced the queuing of the people at public taps [11].

## 2 Case Study

According to the research of American Water Works Association (AWWA), leakage discovering agency in the year 1996 recommended 10% as a benchmark for unaccounted for water (UFW) of the losses incurred during the supply in the water distribution network [12, 13]. This was one of the major losses of precious treated potable water in piped network [3].

### 2.1 Study Location

Research for study area located in Ahmedabad city was conducted. Objective of selecting present case study is to analyze and optimize leak in the continuous distribution network. Ahmedabad is one of the largest city in Gujarat state with semi-arid climate, located at 23°2'1" N and 72°35'6" E Gujarat, in western India on the banks

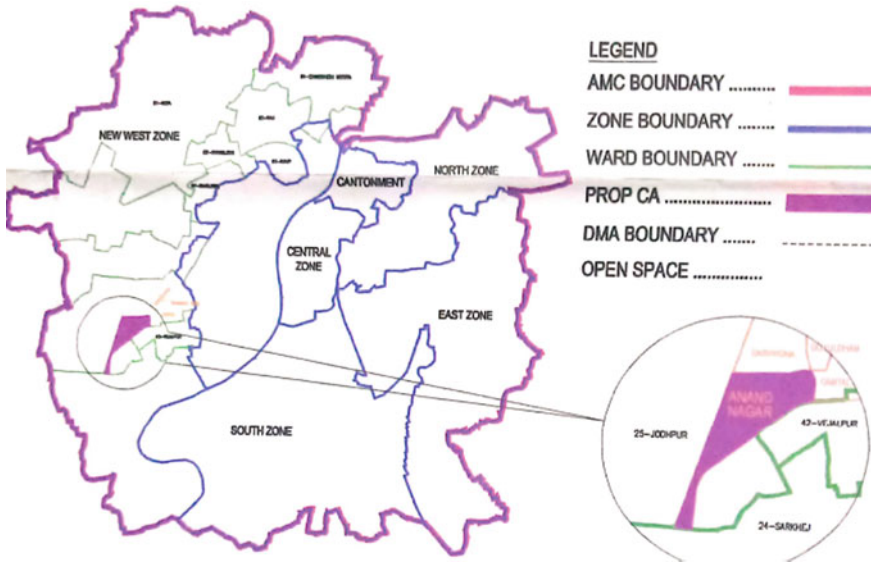


Fig. 1 Site location of the area under study

of Sabarmati river having average annual rainfall of 450–800 mm during monsoon. The city has an area of 466.00 sq km consisting of approximate 56 lakh residents.

Reduced level of Ahmedabad was found to be 52.500 m. City had been divided in to various six zones like North, East, Central, South, West, and New West zones. Jodhpur, having ward number 25, was identified with the circle, which was as shown in Fig. 1. Study area was further divided into district metering area having an area of 181.44 ha.

## 2.2 Study Area Data Collected

The data available were of the test results conducted during the implementation period of the distribution system. Still complete execution of the continuous network was under operation. The Jodhpur comes under New West zone, and it was developed in year 2007. Hence, the population as per the census survey for year 2011 has been considered as 95,444. The population prediction of this research area has been calculated using various numerical methods as suggested in CPHEEO manual [14]. Maximum population is obtained by incremental increase method in the year 2041 which was taken for the further calculations.

Water was supplied to Ahmedabad city through various water sources and then treated at four water treatment plants. Treated water from these water treatment plants was supplied to six zones of Ahmedabad. Jaspur WTP gets water from Dholka branch canal from Narmada River. Jaspur supply water to New West Zone which is divided

into two zones North West zone and South west zone. Since Jodhpur lies under New West Zone, it received water from Jaspur water treatment plant. Per capita water supply was approximately 140–160 lpcd. The water quality was checked and it meet the standard, set by World Health Organization WHO. There was intermittent water supply in most of the city. Looking to the experience of  $24 \times 7$  water supplies in other cities of India, Ahmedabad Municipal Corporation has taken initiative toward converting intermediate water supply to continuous supply.

### 3 Methodology

Nowadays, with the inventions in the software technology utility of models is more convenient and powerful for water distribution network. Hence, the results obtained through computer simulations are more acceptable. Model results can be compared to the field operations, and the distribution network operator can identify the various causes of the problems in the system and get the solutions in the first attempt itself, instead of making changes in the real distribution system through trial and error. The ability to explore all the possible alternatives for a wide range of options results in an economic and robust designs of models in a speedy and easy way [3, 15]. The modeling has a vital function for the progress and application of water quality and hydraulic modeling in the whole world [16]. These models were highly improved in 1990 with the preface of EPANET model [17–19] and many other commercially available water distribution model [5]. Studying various problems is caused by the water distribution system design; it was very difficult and expensive for the large-scale working system. Hence, pilot project was taken under the study. Firstly, identification of the problem for given study area, collection of the data was done. Then hydraulic model was generated for the study area using EPANET. Secondly, in order to solve the problem of leakages, critical nodes were identified in the network. Thirdly, an appropriate solution for the minimization and optimization of leakages was carried out utilizing genetic algorithm.

Methodology adopted in this study is represented in detail in the flowchart as shown in Fig. 2. Area under study received treated potable water from water treatment plant. This water was distributed in the pipe network having varied pipe diameters and different pipe lengths. Study area was distributed into five small district measuring areas (DMA). But the data for critical nodes at DMA 2, 3, 4, 5 were only available. Hence, only four critical points were taken in the study. For hydraulic simulation in EPANET model, various input parameters were set, and pressure was obtained as output. Actual pressure was measured on field at various critical nodes in this DMA and was compared to the simulated results obtained from EPANET. The difference in the actual and simulated results detected leakages in the network. Hence, to minimize the predicted leakages, optimization of the leakages was carried out using genetic algorithm. For leak optimization, mathematical model was generated giving the parameters and constraints to the model. Then using MATLAB, genetic algorithm

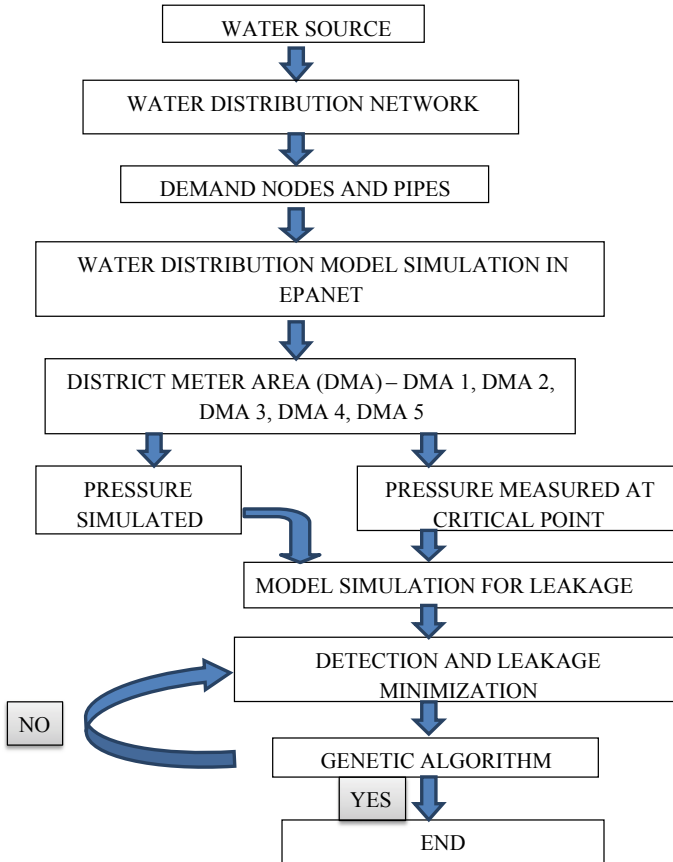


Fig. 2 Flowchart for optimizing water distribution system

code was developed giving various input parameters, and ultimately, the leakages were minimized which is discussed further in detail in this research.

### 3.1 Hydraulic Model Parameters

Considering all the input data like length of pipe, pipe roughness, elevation, and demand of water in the area, the results of output obtained in form of velocity, pressure, and discharge of water at different pipe links and junctions were received. Computational outcome of hydraulic parameters acquired, by means of EPANET, precisely matched with the outcome received by the computation made with EXCEL. It was inferred from this outcome that EPANET can be compared and validated with any other water distribution system [20, 21]. Pressure dependent demands (PDD),

which incorporate nodal demand to the pressure function, was derived by Walski [22]. To analyze distribution network using EPANET, following input data were required.

### **3.1.1 Junction Input Parameters**

In the distribution system, the points where links join collectively were junctions. At this point, water leaves or enters the system. At all the junctions, input data had required elevation higher than any reference viz. water demand and mean sea level (MSL).

### **3.1.2 Output Result of Junction**

It computes hydraulic head, pressure in the water distribution network.

### **3.1.3 Pipes Input Parameters**

Pipes are also called as links which transmits water from one point to another point in a network. In EPANET, it was assumed that all the pipes were under pressure and full at all times. At the same time, flow direction of water was from elevated hydraulic head to the lesser hydraulic head. The essential hydraulic parameters for the pipes input were starting nodes and ending nodes, pipe roughness coefficient, length of the pipe, and diameter of the pipe.

### **3.1.4 Output Result of Pipes**

The computed output given by EPANET was flow rate, velocity, and headloss.

## ***3.2 Hydraulic Model Simulation by EPANET***

Following steps were carried out in EPANET for hydraulic model simulation:

1. Water distribution network was drawn in the software or imported from AutoCAD or basic explanation of network in text file. Appropriate scale for the network drawing was taken.
2. Properties of the objects that made up the system were edited. Various properties and required data entry in various objects like junction, reservoirs, and pipes were made.
3. Description of the operation of the system.

4. Set options selected for the analysis.
5. Hydraulic analysis is obtained by the 'RUN' option.
6. View option shows the outcome of the hydraulic analysis in forms of various tables and graphs.
7. Same steps can be repeated for the other water distribution networks.

Three equations commonly used for pipe friction head loss were Manning's equation, Hazen-Williams, and Darcy-Weisbach. All these equations relate friction loss or head in the pipes to the length of pipe, velocity of the pipe, roughness of the pipe, and diameter of the pipe.

### 3.3 Hydraulic Model Performance for the Study Area

The hydraulic performance of the study network can be enhanced using EPANET. As depicted in Fig. 3, tank was the inlet to the distribution network taken under study. Various input data like diameter of the pipe, ground elevation, and maximum and minimum water level were feed in the EPANET model. The input data of water demand and reduced level for each junction or node at which water enters or leaves were inserted. Input information for the pipe diameter and roughness factor was entered at each of the links. The model calculates the output pressure at all the nodes. Also, simulation results obtained at each link were velocity, unit head loss, and flow rate as shown in Fig. 3. The water flow direction was from elevated hydraulic head to the lower hydraulic head. In this research, EPANET pipe network consists of total 118 numbers of links and 88 numbers of nodes. A control valve is provided at the starting of the water distribution system.

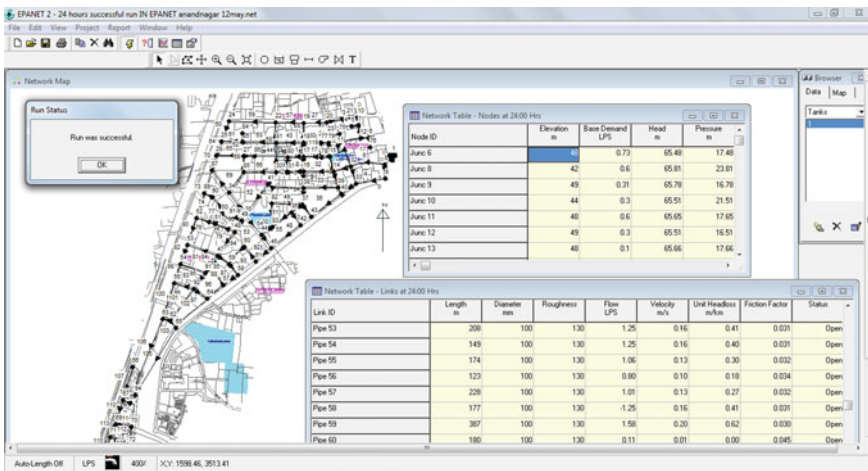


Fig. 3 Successful run of hydraulic model in EPANET

Once all the input parameters are entered in the model to check the validity and correctness of the model, 'RUN' command is given to the model [20, 21]. If the generated model is proper considering all the input parameters, it would give the confirmed output result as 'Run Successful' as shown in Fig. 3. Also, nodes and link tables are generated after the successful run of the model which is inserted as shown in Fig. 3. This gives the verification of the simulated hydraulic model.

### ***3.4 Comparative Study of Hydraulic Models by EPANET and WaterGEMS***

EPANET and WaterGEMS are the two softwares that are extensively used for designing and analysis in water industry. A comparative study was conducted to check the variations in different parameters of EPANET and WaterGEMS.

#### **3.4.1 EPANET**

It is a computer program which performs extended period simulation of hydraulic and water quality behavior within pressurized pipe networks. A distribution network consists of pipes, nodes (pipe junctions), pumps, valves, and storage tanks or reservoirs.

#### **3.4.2 WaterGEMS**

It uses results of hydraulic model to help and optimize the design of complex water distribution systems and utilize built in scenario and management features to keep track of design alternatives. WaterGEMS can also optimize the design using the inbuilt Darwin Designer network optimization tool. Input data of nodes, pipes for the study network are entered, and the simulated results obtained after running the EPANET software are shown in sample Table 1 for 94 nodes in the network.

The pressure results obtained from the 'Successful Run' of the EPANET and WaterGEMS software are summarized in Table 1. Figure 4 represents pressure readings obtained from EPANET and WaterGEMS software which are varying between 0.01m and 0.21 m.

### ***3.5 Mathematical Model for Optimization***

Main objective was to obtain set of pipe network and/or outflow parameters such that the difference between the observed and computed variable such as nodal head,



**Table 1** Comparison of pressure in EPANET and WaterGEMS

| Nodes | Pressure obtained in EPANET (m) | Pressure obtained in WaterGEMS (m) | Difference of pressure in % |
|-------|---------------------------------|------------------------------------|-----------------------------|
| 3     | 19.51                           | 19.5                               | 0.05                        |
| 4     | 18.5                            | 18.4                               | 0.54                        |
| 5     | 5.12                            | 5.1                                | 0.39                        |
| 6     | 17.48                           | 17.4                               | 0.46                        |
| 8     | 23.81                           | 24                                 | 0.79                        |
| 9     | 16.78                           | 16.8                               | 0.12                        |
| 10    | 21.51                           | 21.4                               | 0.51                        |
| 11    | 17.65                           | 17.5                               | 0.86                        |
| 12    | 16.51                           | 16.5                               | 0.06                        |
| 13    | 17.66                           | 17.7                               | 0.23                        |
| 14    | 20.71                           | 20.6                               | 0.53                        |
| 15    | 20.7                            | 20.8                               | 0.48                        |
| 16    | 22.66                           | 22.7                               | 0.18                        |
| 17    | 21.67                           | 21.7                               | 0.14                        |
| 18    | 19.68                           | 19.8                               | 0.61                        |
| 19    | 20.58                           | 20.7                               | 0.58                        |
| 20    | 20.59                           | 20.7                               | 0.53                        |
| 22    | 18.52                           | 18.6                               | 0.43                        |
| 23    | 18.64                           | 18.7                               | 0.32                        |
| 24    | 18.28                           | 18.3                               | 0.11                        |
| 25    | 16.28                           | 16.4                               | 0.73                        |
| 26    | 16.32                           | 16.4                               | 0.49                        |
| 27    | 19.36                           | 19.5                               | 0.72                        |
| 28    | 16.28                           | 16.4                               | 0.73                        |
| 30    | 19.6                            | 19.5                               | 0.51                        |
| 31    | 21.65                           | 21.6                               | 0.23                        |
| 32    | 20.74                           | 20.7                               | 0.19                        |
| 33    | 20.73                           | 20.6                               | 0.63                        |
| 34    | 21.49                           | 21.5                               | 0.05                        |
| 35    | 23.58                           | 23.5                               | 0.34                        |
| 36    | 22.59                           | 22.6                               | 0.04                        |
| 89    | 20.33                           | 20.4                               | 0.34                        |
| 90    | 21.35                           | 21.3                               | 0.23                        |
| 91    | 22.52                           | 22.5                               | 0.09                        |
| 92    | 24.51                           | 24.3                               | 0.80                        |
| 94    | 25.39                           | 25.2                               | 0.75                        |

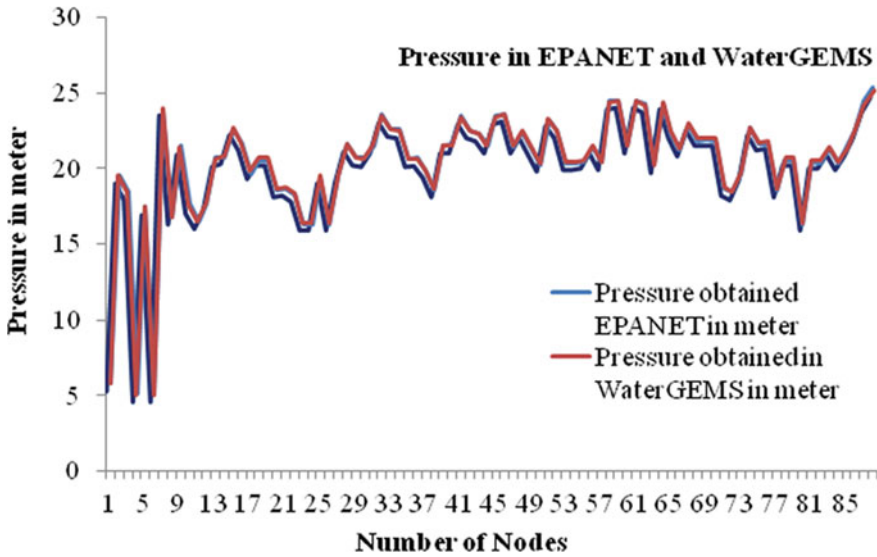


Fig. 4 Pressure variations in EPANET and WaterGEMS

pipe discharge were minimum. Although alternate formulations were possible, the sum of weighted squared error was used in the present analysis. If the variations between the simulated and actual discharge reduces, it was assumed that the leakage will be minimum in the network. Hence, the leakage would be calculated based on the difference between variation of actual and simulated values of pressure, and head was taken as the hypothesis for the study area as it was the test run done in WDS. Lesser the difference minimum would be the leakage.

### 3.5.1 Objective Function

The objective function to be minimized was written as shown in Eq. 1.

$$\text{Min} \sum_{t=1}^n (X) \tag{1}$$

Minimizing leakage amount was in m<sup>3</sup>/h, m<sup>3</sup>/day, m<sup>3</sup>/s, l/s, l/h.

Leakage factor is represented by the parameter vector *X* and is determined by minimizing the objective function *F(X)*:

$$F(X) = \sum_{t=1}^n [W_H \sum_i (H_i(t; x) - H_i(t))^2 + W_Q \sum_i (Q_j(t; x) - Q_j(t))^2] \tag{2}$$

where  $t$ ,  $i$ , and  $j$  denote the time, index of a junction with a pressure sensor, and index of a conduit with a flow meter, respectively. The measured head that is the sum of pressure head and elevation is shown by  $H_i(t)$ , and flow rate is denoted by  $Q_j(t)$ . Their corresponding model forecasted was shown with the parameter vector  $X$  as  $H_i(t; x)$  and  $Q_j(t; x)$ . The character  $W_H$  and  $W_Q$  denoted the weights for flow rate and pressure head, respectively. The choice of weight was an important consideration in objective function specially where two measurements had different physical unit and had large variation in their magnitude. The ordinary least square method was based on the use of  $W_H$  or  $W_Q = 1$  [23]. Equation 2 represented the variation between the readings measured on field by the sensors and the results obtained from hydraulic simulation model.

### 3.5.2 Constraints of Leakage

In this research, leakage ( $L_i$ ) is less than 3 l/s approximated, and hypothesis was made for the model formation as a constraint as shown in Eq. 3. This constraint of leakage value was considered after referring to various researches [24].

$$\sum_{t=1}^n L_i \leq 3 \tag{3}$$

Pipe length, diameter, roughness, discharge, and velocity were taken as the major parameters which directly affected the leakages, flow, and pressure in the water distribution system. These parameters were taken into considerations in coding of genetic algorithm for optimization of leakages.

### 3.5.3 Total Demand Parameters

The demand  $q_i(t)$  of  $i$  junction of the simulated model consists of authorized demand  $d_i(t)$  and leakage as  $X_a k_i (p_i(t))^\alpha$  pressure reliant demand observed in Eq. 4 and referring to research of Adachi [25] and Maskit [26].

$$q_i(t) = d_i(t) + X_a k_i (p_i(t))^\alpha \tag{4}$$

where the symbol denotes  $p_i(t)$  the pressure junction ‘ $I$ ,’ at time ‘ $t$ .’ The symbol  $X_a, k_i$ , and  $\alpha$  represents the scale factor parameter for the area ‘ $a$ ,’ spatial factor of junction ‘ $i$ ,’ and the emitter exponent ‘ $\alpha$ ,’ where  $\alpha$  value was 0.5 for the cast iron pipe or ductile iron pipe [24]. The authorized demand  $d_i(t)$  represented the authorized water consumption, which was assigned based on the flow rate measurement and meter reading. Leakage was modeled as an emitter type pressure reliant demand. Leak emitter coefficient was the product of area scale factor  $X_a$  and junction spatial factor  $k_i$ . Area spatial factors were the elements of the vector parameter  $X$ . Spatial factor

was given by  $k_i = \sum \beta$ . Here  $\beta$  was a risk component that depends on distribution pipes and service connection.

### 3.5.4 Leakage Discharge

Leakage was calculated with the given Eq. 5.

$$\text{Leakage discharge} = X_a k_i (p_i(t))^\alpha \quad (5)$$

Taking  $X_a k_i = \text{emitter coefficient} = 0.92$  and  $\alpha = 0.5$  [25, 26] from orifice meter formula calculated and generalized for different pipe material. Pressure simulated hydraulically and actual pressure leakage discharge was found by  $[X_a k_i (p_{\text{sim}}(t))^\alpha - X_a k_i (p_{\text{act}}(t))^\alpha]$ , where  $p_{\text{sim}}$  and  $p_{\text{act}}$  were the pressure simulated by the hydraulic model and pressure actual measured in the study area. Leakage discharge presumed by the leakage formula is between 0.80 and 0.85 l/s. Using leakage optimization model Eq. 2, the objective function of leakage minimization was obtained as 0.32 l/s.

## 3.6 Optimization Using Genetic Algorithm (GA)

Genetic algorithm provided a solution space compassing of high proportion of good solution. The GA involved three steps that were selection, crossover, and mutation which created new generation from initial population [27]. The process started by consideration of the current population as an initial population up to the termination criteria. GA had an ability to solve multi-model function, multi objectives nonlinear discreet, and continuous functional problems [28]. The individual bits were considered as genes. The mutation and crossover rates were adapted to the generation's fitness statistics for each generation [29].

Objective of pressure monitoring in the network was to find out the relation between pressure changes and leakage rate. It was done to optimize the accuracy and complexity of the network [30]. Optimizing energy consumption costs and environmental emissions by dynamically arranging pumping cycles was a nonlinear and multi-objective problem with significant constraints. For solving this kind of problems, genetic algorithm was suitable [31]. Recently artificial intelligence-based techniques like genetic algorithms have received increased attention worldwide [32]. The genetic algorithm was utilized to find out operating water levels for reservoirs, diameters of new and duplicate pipes, and status of valve control. As a result, the estimated expansion costs of the system were minimized [33].

Research was carried out to find the most appropriate optimization method for the water distribution network. Various optimization techniques like genetic algorithm, differential evolution, particle swarm optimization, and ant colony optimization were compared, and among them, most appropriate system for leakage optimization can be ascertained. The study concluded that genetic algorithm was the most appropriate

method for leakage optimization for the district measuring area (DMA) taken under study [34]. Main purpose of this research was to find out the most suitable method of optimizing and thereby minimizing leakages in the water distribution system. By appropriate selection of an optimization method with hydraulic simulated model, it would result in maintaining of adequate pressure and assuring the proper flow in the network and reduction of leakages and losses of water. A set of solutions presented by chromosomes were named as population. These set of solutions were utilized to form a new better population as offspring. Further selection and reproduction of offspring were based on the fitness. This procedure was repeated till some condition was satisfied. Vital steps of genetic algorithm were as follows:

1. (START) For the proper any problem to obtain solution, first create a random population of 'n' number of chromosomes.
2. (Fitness) For each 'X' chromosome estimate the fitness function  $f(X)$ . It was also called as an objective function.
3. (New population) Novel population was generated by replicating procedure till new required population was obtained.
  - i. (Selection) Two parent chromosomes were chosen from the population as per their robustness.
  - ii. (Crossover) Parents were crossed over to obtain offspring.
  - iii. (Mutation) Each locus point in chromosome new offspring was mutated.
  - iv. (Accepting) In new population, new offspring was placed.
4. (Replace) Now new produced population was used for advanced run of the algorithm.
5. (Test) STOP if end situation was obtained.
6. (Loop) Go to step 2 if end results were not obtained.

During crossover and mutation, there were chances that paramount chromosome might be vanished which are of good quality. So, Elitism was utilized in which best chromosome was first copied to a new population, and thus, it prevents losing of best found output solution at the end.

### ***3.7 Genetic Algorithm (GA) Flow Chart in MATLAB for Optimization***

Flowchart of genetic algorithm was prepared as shown in Fig. 5 to make the systematic analysis using GA.

Genetic algorithm in MATLAB was set as follows:

1. The node discharge was converted into binary numbers using eleven digits to store discharges from 0.000 l/s (binary: 00000000000) to 2.047 l/s (binary: 11111111111).
2. The initial population was generated arbitrarily.

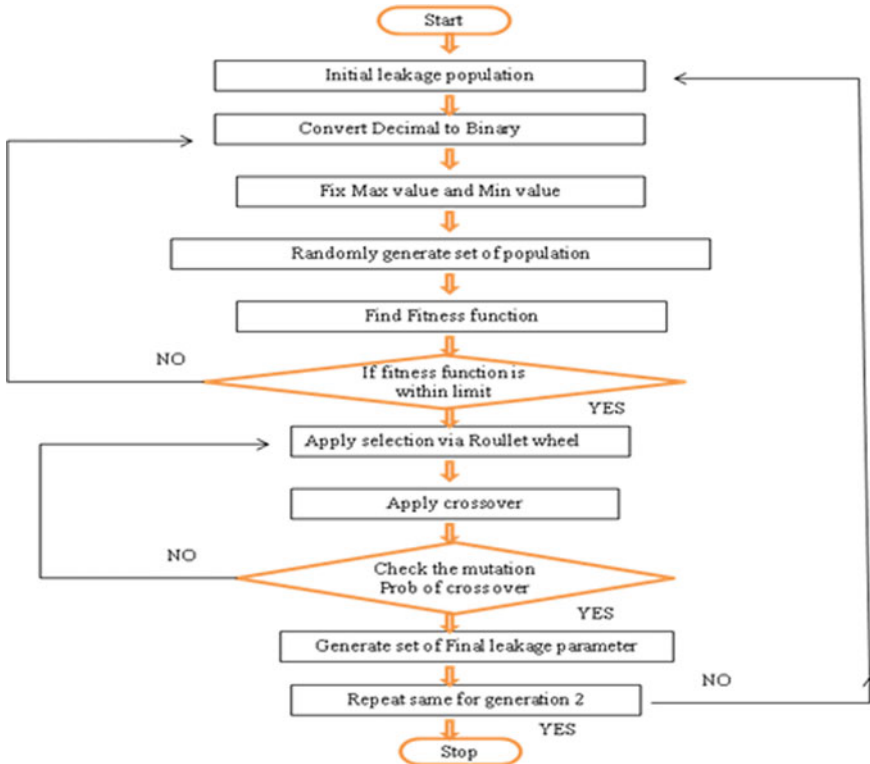


Fig. 5 Flowchart for optimization by genetic algorithm

3. Evaluation of the objective function was done for each and every individual of the population.
4. Crossover was utilized for 20 numbers of generations to create the next population, with a number of the paramount individuals being kept without altering (elitism).
5. Points 3 and 4 were repeated until required number of iteration was arrived.
6. The basic parameters of genetic algorithm are shown in Table 2.

### 3.7.1 Population

It was observed that very large population size does not improved functioning of the genetic algorithm in the terms of pace of finding the result. Population size was generally kept fixed. Population size about 20–30 was good. In general, GA uses the population size of 30–200 was the best [35]. Hence in this study, population size of 40 chromosomes was taken for the analysis.

**Table 2** Basic parameters of genetic algorithm

| GA parameter             | Description |
|--------------------------|-------------|
| Population size          | 40          |
| Chromosome length        | 11          |
| Probability of crossover | 0.5         |
| Probability of mutation  | 0.5         |
| Iterations               | 2000        |
| Selection method         | Roulette    |
| Crossover                | 1point      |

### 3.7.2 Mutation Probability

Mutation rate was taken as very low. Excellent results were obtained if the mutation values were around 0.5–1% [35]. Hence, the mutation probability rate was taken as 0.5 for this study as shown in Table 2.

### 3.7.3 Selection Method

From existing population, best chromosomes were selected and placed in the matting pool in the probabilistic manner. There were various methods to select the chromosomes for parents for the crossover. One of the methods which were best suited for the study area was Roulette-wheel for rank selection.

### 3.7.4 Crossover Probability

In GA, crossover was found out by the ratio of number of pairs of chromosomes to be crossed over to some fixed population. Its probability ranges from 0 to 1. As per the study, it was found that for the population of size 30–200, crossover probability lies in 0.5–1 range. Hence, the researcher had taken crossover probability as 0.5.

### 3.7.5 Crossover Point

It was a single point selected on two parent chromosomes which was picked up randomly and named as ‘crossover point.’ The bits to right hand side of that point were swapped between parents to give two offspring consisting of genetic information over it and were better than their parents. As per the study for the population of size 30–200 [35], researcher had taken crossover point taken as 1.

### 3.7.6 Chromosome Length

Chromosome characterized as binary string of 0 and 1. Hence, the length of the chromosome in the coding of the program in this research was taken as 11.

### 3.7.7 Iterations

This repetitive computation was done to get the best solution in GA. The number of iterations conducted for this research of leakage optimization was taken as 2000.

The input values for optimization of the leakages were written in the code of MATLAB which was given as in Table 2, and also, the constraint of leakage for less than or equal to 3 l/s was considered in code. The pipe material used was ductile iron or cast iron pipe for which the pipe resistance was taken in the calculations. Length of the pipe, elevation of the pipe laid, diameter of the pipe, and water demand of the particular area all these parameters were considered for the calculations in EPANET, and these simulated values of pressure and discharge or flow were taken in the calculation of optimization problem, and hence, these parameters were incorporated and inbuilt in the optimization calculations. Main parameters taken for the genetic algorithm were pressure and flow, hydraulically simulated and actual measured during test run. These hydraulically simulated results were indirectly correlated to parameters like reduced level, water demand at nodes, pipe diameter, pipe length, and roughness factor taken within the maximum and minimum ranges and were coded to get perfect optimization results for the study area.

## 3.8 Genetic Algorithm Code in MATLAB

For the optimization of leakage, actual code was written in genetic algorithm in MATLAB. The code was 'Successfully Run.' Genetic algorithm code after its successful run was programmed to generate graph automatically. In Fig. 6, successful run of code with minimum leak value is depicted. As depicted in Fig. 7, successful run of GA code with fitness graph is shown.

## 3.9 Parameters for Genetic Algorithm

Parameters such as pipe resistance, pipe impedance, pipe decay, pipe leakage and length of the pipe, diameter of the pipe, pipe material, and gradient of the pipe are the various parameters which could be taken into the considerations while considering the optimization. The pipe material used was ductile iron pipe for which the pipe resistance was taken in the calculations. Length of the pipe, elevation of the pipe laid, diameter of the pipe, and water demand of the particular area all these parameters



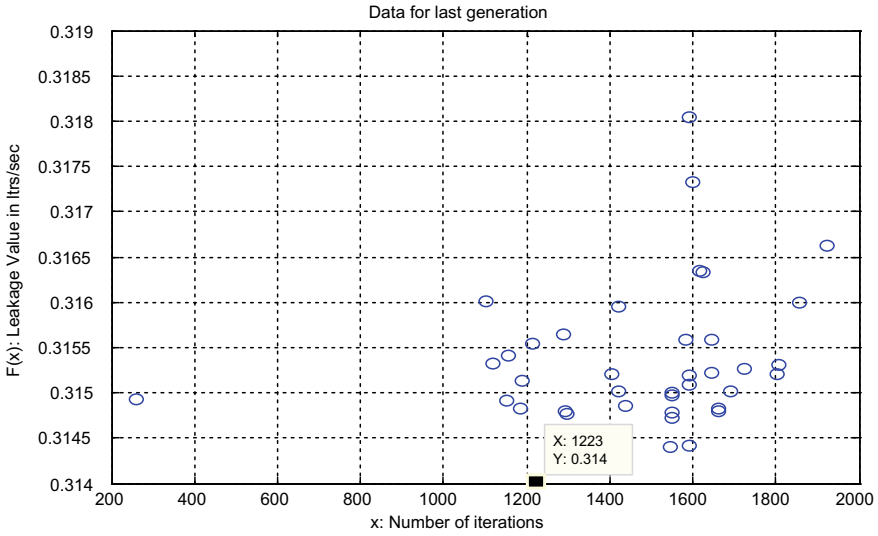


**Fig. 6** Graph of number of iterations versus leakage

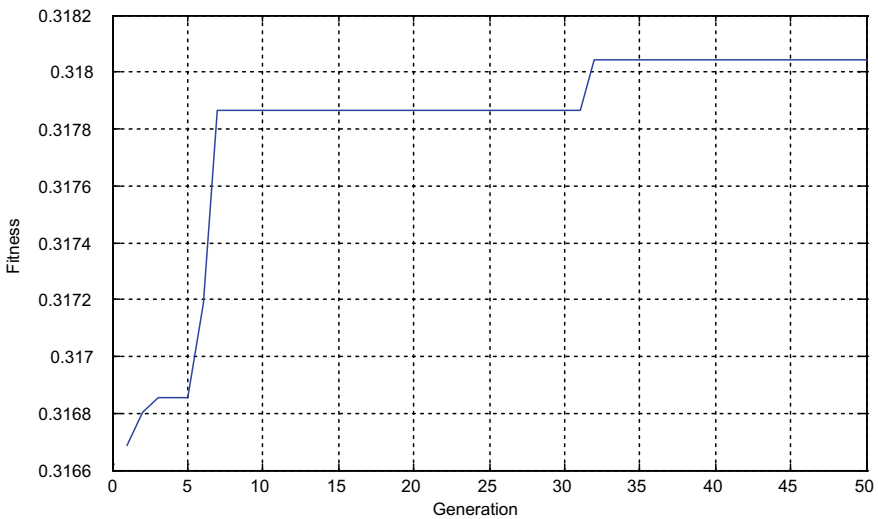


**Fig. 7** Graphical presentation of generation versus fitness

were considered for the calculations in EPANET, and those simulated values of pressure and discharge or flow were taken in the calculation of optimization problem, and hence, those parameters were incorporated and inbuilt in the optimization calculations. Main parameters taken for the genetic algorithm were pressure and flow, hydraulically simulated and actual measured during test run. These hydraulically

simulated results were indirectly correlated to parameters like reduced level, water demand at nodes, pipe diameter, pipe length, and roughness factor taken within the maximum and minimum ranges.

Figure 6 shows the number of iteration up to 2000 numbers on  $x$  axis and optimized model leakage values on  $y$  axis. The graph depicts that with least number of iterations of 1223, the minimum leakage that is optimized leakage value was 0.3144 l/s. Figure 7 shows the generations on  $x$  axis and optimized fitness function values on  $y$  axis. The graph depicts that at the 50th generation, fitness stabilizes between 0.318 and 0.3182 l/s.

## 4 Results and Interpretations

Firstly, results obtained from hydraulic simulation of model in EPANET after entering various input data gave pressure head at various nodes in the network after the successful run, while at links output data like velocity, discharge, etc., were obtained which is tabulated in this study. The model also showed the direction of flow in the distribution network. Secondly, in this research, pressure results of EPANET and WaterGEMS are compared. It was observed from the graph that pressure readings obtained from EPANET and WaterGEMS are varying between 0.01 and 0.21 m. Also, the pressure results showed average 0.37% of variation between two softwares. From the acquired results, it was interpreted that both the softwares are competent for the hydraulic simulation of model. Hence, EPANET software is selected for the hydraulic model simulation as it is available as 'open source.'

Thirdly, mathematical model generated was found to be competent enough to serve the objective of optimization. Fourthly, the coding of genetic algorithm was done in MATLAB, and then, the code was run successfully giving the output results in the graph pattern. The results showed that the graph depicted the minimum leakage of 0.3144 l/s in the least number of iterations of 1223, while the actual leakage value calculated was 0.85 l/s. This satisfied the constraint of leakage which was taken as, less than or equal 3 l/s. So, it was interpreted from the results that the objective function  $F(X)$  to minimize the leakage in the water distribution system was obtained. Thus, optimization of the leakage parameter was achieved, and the aim of the study project was completed. Hence, a novel concept of leakage optimization using coding program by genetic algorithm in MATLAB computer programming language was adopted.

## 5 Conclusions

Research showed that pressure obtained in the network at various junctions was adequate in almost 94% of the pipes than the minimum pressure requirement as suggested by Central Public Health and Environmental Engineering Organization

(CPHEEO) manual. EPANET 2.0 consumed a smaller amount of time and obtained more precise results. It could be utilized in various complicated distribution networks. This hydraulic simulation runs successfully, which showed that the system was competent with the continuous water distribution system maintaining pressure and flow in the network.

The amount of leakage to be minimized had been estimated by optimization model. Genetic algorithm was the optimization technique in MATLAB adopted to minimize the leakages at the critical nodes. The amount of leakages obtained by genetic algorithm in the network was reduced to 73% from the actual leakage calculations. Thus, the leakages were minimized to the optimum value. Thus, prior study of any water distribution network will help the authorities that can supply an efficient water distribution system with minimum water losses and required pressure and flow. In absence of SCADA system and precise leakage measurement instruments, data acquisition had a limitation. Laboratory model of the network could be framed, and experimental setup can be studied as future scope.

**Acknowledgements** Authors are thankful to AMC for providing necessary data for study purpose.

## References

1. Bhave PR, Gupta R (2012) Analysis of water distribution networks. Textbook Published by Narosa Publishing House
2. World Bank (2019) worldbank.org. Overview
3. Desai SD (2020) Analysis and optimization of water distribution system using computational techniques. Ph.D. thesis, submitted to Kadi Sarva Vishwavidyalaya, Gandhinagar, Gujarat
4. Goyal RV, Patel HM (2015) Analysis of residual chlorine in simple drinking water distribution system with intermittent water supply. *Appl. Water Sci Springer* 311–319
5. U.S. Environmental Protection Agency (USEPA) (2005) Water distribution system analysis: field studies, modeling and management—A reference guide for utilities. Research and Development National Risk Management Research Laboratory Water Supply and Water Resource Division
6. Hastak S, Labhasetwar P, Kundley P, Gupta R (2017) Changing from intermittent to continuous water supply and its influence on service level benchmarks: a case study in the demonstration zone of Nagpur, India. *Urban Water J Taylor & Francis* 14(7):768–772
7. World Health Organization (2011) Guidelines for drinking-water quality, 4th edn.
8. Danilenko A, Vanden Berg C, Macheve B, Moffitt L (2014) The IBNET water supply and sanitation blue book 2014. The International Benchmarking Network for Water and Sanitation Utilities Databook Default Book Series, The World Bank Publications
9. Kumpel E, Nelson KL (2013) Comparing microbial water quality in an intermittent and continuous piped water supply. *Water Res Elsevier* 1–13
10. Zerah MH (1998) How to assess the quality dimension of urban infrastructure: the case of water supply in Delhi cities. *Science Direct* 15(4):285–290
11. Water and Sanitation Program (WSP) (2010) 24×7 Water supply is achievable the Karnataka urban water sector improvement project. Water and Sanitation Program, p 24
12. Gungao V (2017) Using performance indicators for non-revenue water reduction: a case study in a Small Island State (Mauritius). *Int J Sci: Basic Appl Res (IJSBAR)*

13. Naikikartiki S, Glickfeld M (2015) Water distribution system efficiency—an essential or neglected part of the water conservation strategy for Los Angeles county water retailers. In: Institute of Environment and Sustainability (UCLA), pp 1–36
14. CPHEEO Manual (1999) Manual on water supply and treatment. Central Public Health and Environmental Engineering Organization CPHEEO, Ministry of Urban Development, New Delhi
15. Walski T, Chase DV, Grayman DA, Beckwith S, Koelle E (2003) Advanced water distribution modeling and management. Civil and Environmental Engineering and Engineering Mechanics Faculty Publications University of Dayton eCommons, p 800
16. Clark RM (2015) The USEPA, distribution system water quality modelling program: a historical perspective. *Water Environ J* 320–330
17. Goyal RV, Patel HM (2016) Decision support models for managing chlorine disinfection in drinking water distribution system. Ph.D. thesis, submitted to M.S. University
18. Rossman LA (2000) EPANET 2 users manual. Soc Stud Sci
19. Rossman LA, Paul F, Altman T (1993) Discrete volume element method for network water quality models. *ASCE J Water Resour Plan Manage* 119(5):505–517
20. Desai SD, Rajpara G (2018) Analysis of drinking water distribution system of Ahmedabad City, using EPANET 2.0—A case study. *Int J Tech Innov Mod Eng Sci (IJTIMES)* 4(10):217–222
21. Desai SD, Rajpara G (2018) Validating hydraulically simulated model for continuous water distribution system. *Int J Adv Res Eng Technol (IJARET)* 9(6):15–18
22. Walski T, Blakley DE, Matthew WB (2017) Verifying pressure dependent demand modelling. *Procedia Eng Elsevier*
23. Rajpara G (1999) Analysis, performance evaluation, water quality modeling, estimation of parameters and control of water distribution networks. Ph.D. thesis, submitted to IIT Bombay
24. Mashford J, Dhammika S, Donovan M, Stewart B (2009) An approach to leak detection in pipe networks using analysis of monitored pressure values by support vector machine. In: Proceeding of 3rd international conference on network system security. *IEEE Journal*
25. Adachi S, Takahashi S, Kurisu H, Tadokoro H (2014) Estimating area leakage in water networks based on hydraulic model and asset information. In: 16th Conference on water distribution system analysis, vol 89. WDSA, Science Direct, Elsevier, *Procedia Engineering*, vol 278–285
26. Maskit M, Ostfeld A (2014) Leakage calibration of water distribution networks. In: 16th Conference on water distribution system analysis. WDSA, Science Direct, *Procedia Engineering*, pp 664–671
27. Paszkowicz W (2009) Genetic algorithms, a nature inspired tool survey of application in materials science and related field. *J Mater Manuf Process* 24:174–197
28. Deb K (2001) Multi objective optimization using evolutionary algorithm, 1st edn. Wiley (2002)
29. Badar A, Umre BS (2012) Reactive power control using dynamic particle swarm optimization for real power loss minimization. *Int J Electr Power Energy Syst* 41(1):133–136
30. Jalalkamali A, Mehdi E (2012) Estimating water losses in water distribution networks using a hybrid of GA and neuro-fuzzy model, Kerman Province (Iran). *World Appl Sci J* 18(4):528–537
31. Peter V (1999) Artificial intelligence-based electrical machines and drives: application of fuzzy, neural, fuzzy-neural and genetic algorithm based techniques. Oxford University Press
32. Seyed Mohsen SA (2014) Evaluation of genetic algorithms using discrete and continuous methods for pump optimization of water distribution systems. Elsevier
33. Murphy LJ., Gransbury J, Simpson AR, Dandy GC (1998) Optimization of large-scale water distribution system design using genetic algorithm. In: Water tech. conference. AWWA, Brisbane
34. Desai SD, Rajpara G (2019) Comparative study of optimization techniques in drinking water distribution system—A review. *J Emerging Technol Innov Res* 6(4):61–67
35. Rajasekaran, S., Vijayalakshmi, G.A., *Neural Networks, Fuzzy Logic and Genetic Algorithms, Synthesis and Applications, PHI Learning Private Limited Publishers* (2011)

# The Effect of Pipe Age and Piping Materials on Chlorine Decay in a Pilot Loop Water Distribution Network



C. Ramprasad and C. R. Suribabu

**Abstract** Chlorination is one of the most widely used methods of disinfectant in many developing countries water distribution network due to its inexpensive, highly effective, and stable nature. In the transmission and distribution network, the water quality can deteriorate with age due to various factors like pipe wall materials, biomass growth, and reaction with ammonia, iron, and organic compounds. In the present study, the impact of service age of the pipe and the pipe materials on the chlorine decay in a pilot loop water distribution network was performed. The two distinct zones in South India with a partial water distribution network with dissimilar water source and piping material were selected for the study. The network 1 has 35 piping with 24 junction was constructed with galvanized steel material with a Hazen Williams roughness coefficient as 120. In network 2, there were 60 piping system with 33 junctions and were constructed with cast iron material having Hazen Williams roughness coefficient as 100. The results show that the chlorine first order wall decay is highly governed by the pipe service age and the piping material. The results indicate that quality of the residual chlorine above the standard value of 0.2 mg/L was maintained at a constant rate immediately after the flow in the galvanized steel pipe. However, in the cast iron piping due to the roughness and aging factor, it takes more time to achieve the desired concentration of above 0.2 mg/L. Additionally, in the cast iron pipe, the quality is changing periodically. Therefore, the study concludes that chlorine decay is not affected in the galvanized steel pipe and recommended for the pipe networks in South India.

**Keywords** Water distribution · EPANET · Chlorine decay · Hazen Williams · Disinfectant

---

C. Ramprasad (✉) · C. R. Suribabu  
School of Civil Engineering, SASTRA Deemed To Be University, Thanjavur, India  
e-mail: [ramprasad@civil.sastra.edu](mailto:ramprasad@civil.sastra.edu)

C. R. Suribabu  
e-mail: [suribabu@civil.sastra.edu](mailto:suribabu@civil.sastra.edu)

© The Author(s), under exclusive license to Springer Nature Singapore Pte Ltd. 2022  
C. M. Rao et al. (eds.), *Advanced Modelling and Innovations in Water Resources Engineering*, Lecture Notes in Civil Engineering 176,  
[https://doi.org/10.1007/978-981-16-4629-4\\_20](https://doi.org/10.1007/978-981-16-4629-4_20)

285

## 1 Introduction

The drinking water obtained from the surface water sources has to be treated in the treatment plant with an addition of disinfectant before the distribution. The most common and quite extensively used disinfectant is chlorine due to its cost effectiveness and stable nature. Chlorine is widely used for treating the drinking water because it prevents the re-growth of bacterial contamination like *E. Coli* [1]. Consequently, the chlorine concentration needs to be maintained with a minimum level of above 0.2 mg/L in the entire water distribution network. Mohapatra et al. [2] throughout the water network is a significant aspect of water quality management. Nonetheless, the residual chlorine concentration in a water transmission system varies with various physical properties [2]. In the water distribution network, the free chlorine concentration can be obsessive in the wall properties, bulk liquid phase, or reaction with organic biofilm or bio-materials formed with ammonia and iron deposits. Additionally, the free chlorine evaporates as it interacts with the deposits or scale formed, and it reacts with the corrosive layers and developed organic biomass on the inner pipe walls, roughness of the piping materials, and with the piping age [3–7]. Zhang [6] illustrated that it is difficult to estimate the chlorine decay in real-time water distribution systems, especially if they work under deprived hydraulic conditions (like aged pipes, small velocities, looping nodes, etc.). As a result, the evaluation of chlorine decay in the simulated water distribution system seems to be easier, if the bulk liquid reactions can be separated from the pipe wall and its materials associated reactions.

It is a necessity that maintaining the water quality in the distribution system especially the chlorine disinfection levels at constant minimum dosage of 0.2 mg/L in the entire distribution system to avoid the growth of bacterial contamination. If the quality is not maintained, then there are chances of humans get infected with water borne diseases. The factors that affect the chlorine decay in the distribution network need to be identified, and modeling the residual chlorine levels and its decay rate in treated and distributed water should be developed. The recent studies on the chlorine decay and its by-products' formation in the water distribution system are meagre concerned to piping age [8, 9] flow velocity [10, 11] and pipe materials [4, 5, 6, 12] for the simulated water networks. Kim et al. [13] demarcated a strong relationship between the decay coefficient and the Reynolds number (Re) for a generalized chlorine prediction model. A balance between a chlorine disinfectant dosage remaining after certain time (say 60 h or 80 h after pumping) and decay of pathogens numbers in the drinking water is essential, and hence, it is essential to identify with the mechanism as well as the factors governing the chlorine decay in distribution networks [14].

In the real-time water distribution network, the chlorine decay predominantly governed by the reaction kinetics that happens between the bulk water and biofilm attached and grown at the sides of the pipelines. In the water distribution network, the initial chlorine concentrations from the source of water (like rivers, lakes or reservoirs) are the vital one that determines the chlorine bulk decay rate, whereas chlorine wall decay rate depends on the pipe age, organic biofilm thickness, inorganic scale

formed, and pipe material. The following Eq. 1 represents the overall chlorine dissipation within the distribution network. The overall decay rate constant is equivalent to the summation of bulk and wall decay rate, as shown in the equation below.

$$\frac{dc}{dt} = -K_{\text{total}}C = -(K_{\text{bulk}} + K_{\text{wall}})C \quad (1)$$

The rate of wall reaction ( $K_{\text{wall}}$ ) is governed by the wall rate constant, the water flow velocity through the pipes, and surface–volume geometry of pipe or the pipe diameter [11]. Therefore, overall wall decay constant could be expressed as follows,

$$K_{\text{wall}} = \frac{4(k_f * k_w)}{D(k_f + k_w)} \quad (2)$$

where

- $D$  is the diameter of the pipe measured in meter
- $k_w$  is the wall constant and measured in meter per day
- $k_f$  is the mass transfer rate constant and measured in meter per day.

The chlorine decay follows the first order rate reaction kinetics, where the rate constant  $K_{\text{total}}$  plays a vital role. The chlorine residual concentrations at any junction or node in the water distribution system were determined by EPANET [15] software model. The EPANET program was employed by many researchers to estimate the chlorine reaction for simulated and real-time water networks [4, 5, 6, 11]. The reactions of chlorine in any water distribution network are affected by three vital parameters, and the reaction models are programmed into EPANET 2.0 software. Initially, the quality of chlorine in the reservoir has to be fed into the software, and the bulk decay rate has to be provided next and finally the decay rate limited to wall properties. The bulk decay rate allows modeling using first and second order rates or even for concentration limited rates [11]. The wall decay rate can be modeled by taking into account the disinfectant like chlorines molecular mass transfer rate, the concentration of chlorine available in the bulk solution, the rate of wall decay, and the hydraulic radius of the pipe. Therefore, the study was conducted for a real-time water distribution network in South India to study the influence of piping material and its age. The objective of the present study was to first to examine the effect of piping materials (galvanized steel and cast iron) on the chlorine decay and secondly to investigate the effect of piping age on the chlorine decay.

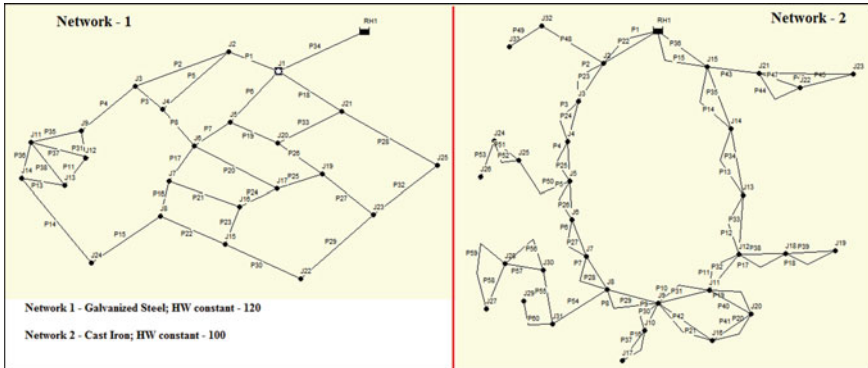


Fig. 1 Water distribution network layout

## 2 Materials and Methods

### 2.1 EPANET Model and Water Distribution Network

The real-time water distribution network of Ambur municipality in South India was selected and supported by the EPANET 2.0 version to illustrate and simulate the process of calibrating using the water quality model. The EPANET 2.0 software program was developed by the US environmental protection agency (USEPA) using a C language and made it freely available for wide use as well as it is found to be a highly reliable for water distribution simulation. The EPANET program employs a gradient method to model the residual chlorine decay by combining the mass balance and advective transport mechanism at junctions as well as in the storage tanks.

The water distribution networks of two distinct places were selected and were imported to EPANET 2.0 (Fig. 1). The loop network 1 has a reservoir at an elevation of 36.4 m above the ground level supplying water through 35 pipes with 24 junctions to a particular zone, and other junction points have an elevation varies from 6 to 13.9 m. The piping were made with galvanized steel material covering an areal extends of 0.84 sq. km. The initial quality of chlorine in the reservoir was maintained at 0.5 mg/L. The loop network 2 has a reservoir at 85 m elevated from the ground surface, and the system is 10 year old one and has 60 pipes and 33 junctions. The type of pipe materials is cast iron.

### 2.2 Water Quality Modeling

The chlorine water quality modeling is developed from the general mass balance principle at any selected point/node (i) in the network as explained by the following Eq. 3. The bulk decay coefficient in both the network was taken equal to  $-0.018$  per



hour which has the highest regression coefficient ( $R^2 = 0.974$ ) and corresponds to  $-0.45$  per day, and the wall decay was  $-0.20$  per day [16]. The negative sign refers to reduction of chlorine residuals with time. The first order rate reaction was considered for the chlorine decay, and an initial concentration of  $0.5$  mg/L was maintained in the reservoirs.

$$\frac{\partial C}{\partial t} = \nabla J_i + r_i \tag{3}$$

where

- $C$  represents the mass of free residual chlorine at any selected point
- $\nabla$  represents the gradient operator
- $r_i$  represents the rate of total decay of chlorine (including the bulk and wall decay)
- $J_i$  represents the mass flux of the chlorine decay and
- $J_i = C * v_i$  where  $v_i$  stands for flow of velocity in meter per second.

### 2.3 Water Distribution Network Operation

The EPANET software has the following demand-driven assumption that is,

1. The nodal demands are already calculated/fixed values and
2. The quandary is to find pipe flows and nodal pressures that are hydraulically consistent with the nodal demands [2].

$$h_L = 4.727C^{-1.852}d^{-4.871}q^{1.852}L \tag{4}$$

where

- $h_L$  is the head loss within the pipe and measured in m
- $C$  is the roughness coefficient
- $d$  is the pipe diameter and measured in m
- $q$  is the flow rate is measured in liters per second (LPS)
- $L$  is the pipe length measured in m

The Monte Carlo Simulation (MCS) technique was used to estimate the diurnal water demand and was incorporated into the EPANET software under the pattern tab. The water demand for a city in India is generated based on socio-economic status of the people living in the region, and time-series distribution graph was plotted [17]. The quantity of water consumed for day-to-day activities viz. drinking, cloth washing, gardening, cooking, housecleaning, bathing, toilet flushing, utensils washing, and sanitation and hygiene, in different time series 1, 2, 3, etc., to 24 h were obtained and plotted as the time-series distribution graph. Table 1 shows the elevation, base demand, and pressure for different nodes and the reservoir of the network 1 and 2.

**Table 1** Water distribution pipe network nodal demand

| Network 1—Nodes at start (0:00 h) |           |             |          | Network 2—Nodes at start (0:00 h) |           |             |          |
|-----------------------------------|-----------|-------------|----------|-----------------------------------|-----------|-------------|----------|
|                                   | Elevation | Base Demand | Pressure |                                   | Elevation | Base Demand | Pressure |
| Node ID                           | m         | LPS         | m        | Node ID                           | m         | LPS         | M        |
| J1                                | 6.4       | 15          | 11.97    | J2                                | 25.5      | 9.24        | 43.09    |
| J2                                | 7         | 15          | 10.7     | J3                                | 25.5      | 9.24        | 23.99    |
| J3                                | 6         | 15          | 10.41    | J4                                | 25.5      | 8.82        | 17.94    |
| J4                                | 8.4       | 11          | 7.83     | J5                                | 25.5      | 8.82        | 12.07    |
| J5                                | 7.4       | 18          | 10.15    | J6                                | 25        | 8.82        | 8.97     |
| J6                                | 9         | 15          | 8.12     | J7                                | 25        | 8.82        | 2.63     |
| J7                                | 9.1       | 5           | 7.51     | J8                                | 25        | 8.82        | -1.36    |
| J8                                | 9.5       | 5           | 6.85     | J9                                | 22        | 17          | 0.81     |
| J9                                | 8.4       | 15          | 7.25     | J10                               | 22        | 10          | 0.58     |
| J11                               | 10.5      | 5           | 4.66     | J11                               | 22        | 17          | 1.27     |
| J12                               | 9.6       | 5           | 6        | J12                               | 22        | 11.7        | 4.58     |
| J13                               | 11.7      | 15          | 2.68     | J13                               | 25        | 11.7        | 7.94     |
| J14                               | 12.3      | 7           | 2.67     | J14                               | 25.5      | 9.24        | 22.92    |
| J15                               | 10.6      | 7           | 5.49     | J15                               | 25.5      | 9.24        | 38.67    |
| J16                               | 10.1      | 7           | 5.67     | J16                               | 22        | 17          | -0.3     |
| J17                               | 9.5       | 5           | 6.42     | J17                               | 22        | 5.75        | 0.35     |
| J19                               | 10.2      | 7           | 6.43     | J18                               | 22        | 11.7        | 0.88     |
| J20                               | 9.6       | 7           | 7.52     | J19                               | 22        | 11.7        | 0.05     |
| J21                               | 9.1       | 7           | 8.36     | J20                               | 22        | 17          | -0.14    |
| J22                               | 13.9      | 15          | 1.43     | J21                               | 25        | 11.7        | 28.36    |
| J23                               | 11.1      | 5           | 4.93     | J22                               | 22        | 11.7        | 30.07    |
| J24                               | 11.7      | 8           | 4.15     | J23                               | 22        | 11.7        | 30.14    |
| J25                               | 10        | 5           | 5.75     | J24                               | 25        | 5.2         | -0.48    |
| RH1                               | 36.4      | #N/A        | 0        | J25                               | 25        | 5.2         | 6.56     |
|                                   |           |             |          | J26                               | 25        | 5.2         | -4.62    |
|                                   |           |             |          | J27                               | 22        | 5.5         | -79.56   |
|                                   |           |             |          | J28                               | 22        | 5.5         | -78.95   |
|                                   |           |             |          | J29                               | 22        | 5           | -65.22   |
|                                   |           |             |          | J30                               | 22        | 5.5         | -75.16   |
|                                   |           |             |          | J31                               | 22        | 5.5         | -63.36   |
|                                   |           |             |          | J32                               | 25.5      | 8.82        | 20.28    |
|                                   |           |             |          | J33                               | 25.5      | 8.82        | 15.2     |
|                                   |           |             |          | RH1                               | 85        | #N/A        | 0        |

## 3 Results and Discussion

### 3.1 *Effect of Pipe Age*

The important parameter that contributes to the decay in the chlorine concentrations is the pipe age. As the age of pipes increases, the friction factor as well as the pipe flow resistance increases. In the present study, the roughness coefficient only of the network 1 was increased from 120 to 130 and found that chlorine concentrations tend to decrease. The results are in concurrence with [16, 18, 19, 20]. In the network 1, node 22 was selected to express the effect of piping age, because the node is at the dead end of the network with higher point of elevation than the other nodes and found to be highly susceptible due to aging. The above scenario was evident from the previous research that the end nodes are vulnerable due to age [21]. It was observed that at one of the end node 22, with the roughness value of 120, the chlorine concentration after 120 h was 0.46 mg/L; whereas with a roughness of 130, the chlorine concentration in the same node was found to be 0.23 mg/L. There is a reduction in the concentrations and found to follow the WHO prescribed standard of 0.2 mg/L. It is to be noted that aging of pipe increases the roughness increases, and corresponding Hazen William roughness factor will be less than initial value. The resistant to flow owing the aging brings down the velocity of flow in the pipeline. The slow movement of water in the system due to less pressure makes opportunity water to react with pipe wall.

### 3.2 *Effect of Piping Material*

In the network 1 and 2, with the continuous supply of water, the residual chlorine concentrations in the nodes (node 14 for network 1 and node 17 for network 2) of both the network remain above the recommended standard value of 0.2 mg/L. The concentration of chlorine reached the WHO recommended value of 0.2 mg/L faster than the stipulated time in the network 1 compared to network 2 as shown in the frequency plot created for the node after the 120 h of flow (Fig. 2). For example in network 1, less than 50% of the nodes have achieved the residual concentration of 0.47 mg/L; whereas in network 2 for the same 0.47 mg/L of residual concentration in the nodes, only less than 20% have achieved. As the other parameters for the networks remaining the same, piping material plays a vital role. Hence, the study concludes that cast iron piping material shows some resistance to chlorine concentration, and hence, the decay is more. The obtained results were in good agreement with [12, 16, 21]. Therefore, the usage of galvanized steel pipe in the water distribution network is more advisable. It was also observed from Table 1 that in the network 1, there were no negative pressures attained in any of the junctions; whereas in the network 2, there were several loops having negative pressure (like J26 to J31). Hence, it

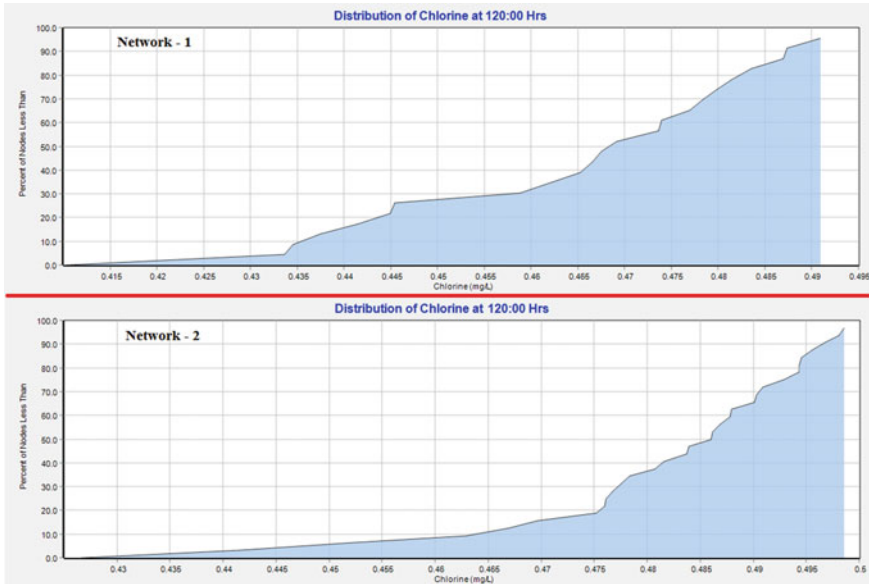


**Fig. 2** Frequency plot showing the distribution of chlorine after 120 h in the nodes

is recommended to have an over hand tank with a pump to eliminate the negative pressure and allow the water to flow to the dead ends.

It was also seen in Table 2 that the velocities in the pipes for the network 1 were predominantly more than 0.2 m/sec. It was also seen that a sudden decrease in the velocity as water travels from pipe 2 to pipe 3 (0.94–0.38 m/s), and it could be due to sudden contraction in diameter of pipe from 290 to 100 mm. Similar trend in the velocity were seen with respect to the pipe diameters in both the networks. The minimum velocity of 0.09 m/s was observed in Pipe 37 of network 2, and it is mainly due to the length of the pipe, and the selected diameter corresponding to the elevation is not appropriate. Hence, the recommendation of changing the pipe diameter or providing a small booster pump should be provided to boost pressure. Figure 3 shows the chlorine concentration at one of the dead end one, in network 1, the node 14 is selected; whereas for the network 2, the node 17 was selected. The above nodes from each of the networks were found to be one of the end nodes, and the water to the node arrives from many interconnected pipe networks as see in Fig. 1. These nodes were the one present at the dead end and pumped water from the reservoir reaches these nodal points with time delay. As researchers show that water taking a longer path in a network showed a significant changes in the pollutants concentrations [22], it was clearly visible that node 14 gets to the desirable chlorine concentration with 2 h of flow, while the node 17 takes more than 10 h to reach the desirable concentration (0.12 mg/L). Figure 3 shows clearly that chlorine decay is more in the cast iron pipe than galvanized steel pipe, and hence, the required concentration of 0.2 mg/L of chlorine has not reached the end nodes. Therefore, a

**Table 2** Water distribution pipe network nodal demand

| Network 1—Table—Links at end (120:00 h) |        |          |        |          |                |          |         |        |          |        | Network 2—Table—Links at end (120:00 h) |                |          |  |  |  |  |  |  |  |  |
|---|--------|----------|--------|----------|----------------|----------|---------|--------|----------|--------|---|----------------|----------|--|--|--|--|--|--|--|--|
| Link ID                                 | Length | Diameter | Flow   | Velocity | Unit head loss | Chlorine | Link ID | Length | Diameter | Flow   | Velocity                                | Unit head loss | Chlorine |  |  |  |  |  |  |  |  |
|   | m      | mm       | LPS    | m/s      | m/km           | mg/L     |         | m      | Mm       | LPS    | m/s                                     | m/km           | mg/L     |  |  |  |  |  |  |  |  |
| P1                                      | 200    | 327      | 81.84  | 0.97     | 3.38           | 0.49     | P1      | 1160   | 204      | 83.75  | 2.56                                    | 49.22          | 0.5      |  |  |  |  |  |  |  |  |
| P2                                      | 350    | 290      | 62.41  | 0.94     | 3.67           | 0.49     | P2      | 1980   | 204      | 68.11  | 2.08                                    | 33.57          | 0.48     |  |  |  |  |  |  |  |  |
| P3                                      | 120    | 100      | 2.36   | 0.3      | 1.53           | 0.48     | P3      | 730    | 204      | 62.74  | 1.92                                    | 28.83          | 0.46     |  |  |  |  |  |  |  |  |
| P4                                      | 380    | 290      | 45.04  | 0.68     | 2.01           | 0.48     | P4      | 830    | 204      | 57.61  | 1.76                                    | 24.62          | 0.45     |  |  |  |  |  |  |  |  |
| P5                                      | 300    | 100      | -4.43  | 0.56     | 4.89           | 0.48     | P5      | 860    | 204      | 43.41  | 1.33                                    | 14.58          | 0.43     |  |  |  |  |  |  |  |  |
| P6                                      | 250    | 368      | 110.03 | 1.03     | 3.29           | 0.49     | P6      | 1910   | 204      | 38.28  | 1.17                                    | 11.55          | 0.41     |  |  |  |  |  |  |  |  |
| P7                                      | 180    | 327      | 68.11  | 0.81     | 2.41           | 0.49     | P7      | 960    | 204      | 43.24  | 1.32                                    | 14.47          | 0.38     |  |  |  |  |  |  |  |  |
| P8                                      | 200    | 100      | 4.21   | 0.54     | 4.44           | 0.48     | P8      | 1250   | 204      | 16.07  | 0.49                                    | 2.31           | 0.35     |  |  |  |  |  |  |  |  |
| P11                                     | 100    | 100      | 7.24   | 0.92     | 12.15          | 0.47     | P9      | 960    | 204      | 9.16   | 0.28                                    | 0.82           | 0.31     |  |  |  |  |  |  |  |  |
| P13                                     | 120    | 100      | 4.44   | 0.57     | 4.91           | 0.44     | P10     | 1120   | 204      | -12.45 | 0.38                                    | 1.44           | 0.36     |  |  |  |  |  |  |  |  |
| P14                                     | 820    | 100      | -1.96  | 0.25     | 1.08           | 0.41     | P11     | 1450   | 204      | -31.28 | 0.96                                    | 7.95           | 0.39     |  |  |  |  |  |  |  |  |
| P15                                     | 250    | 164      | -9.96  | 0.47     | 1.97           | 0.47     | P12     | 1220   | 204      | -48.83 | 1.49                                    | 18.13          | 0.41     |  |  |  |  |  |  |  |  |
| P16                                     | 180    | 290      | -37.72 | 0.57     | 1.44           | 0.48     | P13     | 2410   | 204      | -54.68 | 1.67                                    | 22.35          | 0.44     |  |  |  |  |  |  |  |  |
| P17                                     | 250    | 290      | -45.59 | 0.69     | 2.05           | 0.48     | P14     | 2110   | 204      | -59.3  | 1.81                                    | 25.98          | 0.47     |  |  |  |  |  |  |  |  |
| P18                                     | 320    | 164      | 12.13  | 0.57     | 2.84           | 0.49     | P15     | 1550   | 204      | -81.47 | 2.49                                    | 46.78          | 0.49     |  |  |  |  |  |  |  |  |
| P19                                     | 220    | 229      | 23.92  | 0.58     | 1.96           | 0.49     | P16     | 2640   | 204      | 5.4    | 0.17                                    | 0.31           | 0.2      |  |  |  |  |  |  |  |  |
| P20                                     | 420    | 100      | 3.31   | 0.42     | 2.85           | 0.47     | P17     | 3120   | 204      | 21.98  | 0.67                                    | 4.13           | 0.37     |  |  |  |  |  |  |  |  |
| P21                                     | 380    | 100      | 2.88   | 0.37     | 2.2            | 0.46     | P18     | 2400   | 204      | 11.25  | 0.34                                    | 1.2            | 0.27     |  |  |  |  |  |  |  |  |

(continued)

**Table 2** (continued)

| Network 1—Table—Links at end (120:00 h) |        |          |        |          |                |          | Network 2—Table—Links at end (120:00 h) |        |          |        |          |                |          |
|---|--------|----------|--------|----------|----------------|----------|---|--------|----------|--------|----------|----------------|----------|
| Link ID                                 | Length | Diameter | Flow   | Velocity | Unit head loss | Chlorine | Link ID                                 | Length | Diameter | Flow   | Velocity | Unit head loss | Chlorine |
|   | m      | mm       | LPS    | m/s      | m/km           | mg/L     |   | m      | Mm       | LPS    | m/s      | m/km           | mg/L     |
| P22                                     | 250    | 258      | 22.76  | 0.44     | 1              | 0.47     | P19                                     | 1440   | 204      | 19.87  | 0.61     | 3.43           | 0.36     |
| P23                                     | 190    | 100      | 2.51   | 0.32     | 1.71           | 0.46     | P20                                     | 3840   | 204      | 3.52   | 0.11     | 0.14           | 0.18     |
| P24                                     | 200    | 100      | -1.61  | 0.21     | 0.75           | 0.43     | P21                                     | 2640   | 204      | -12.53 | 0.38     | 1.46           | 0.29     |
| P25                                     | 250    | 100      | -3.3   | 0.42     | 2.84           | 0.46     | P22                                     | 1160   | 180      | 60.26  | 2.37     | 49.22          | 0.5      |
| P26                                     | 220    | 204      | -18.88 | 0.58     | 2.22           | 0.48     | P23                                     | 1980   | 180      | 49.01  | 1.93     | 33.57          | 0.47     |
| P27                                     | 400    | 164      | 8.58   | 0.41     | 1.49           | 0.46     | P24                                     | 730    | 180      | 45.14  | 1.77     | 28.83          | 0.46     |
| P28                                     | 650    | 100      | 3.18   | 0.4      | 2.64           | 0.45     | P25                                     | 830    | 180      | 41.45  | 1.63     | 24.62          | 0.45     |
| P29                                     | 800    | 100      | 1.75   | 0.22     | 0.88           | 0.39     | P26                                     | 860    | 180      | 31.23  | 1.23     | 14.58          | 0.43     |
| P30                                     | 400    | 184      | 13.25  | 0.5      | 1.91           | 0.46     | P27                                     | 1910   | 180      | 27.54  | 1.08     | 11.55          | 0.41     |
| P31                                     | 120    | 258      | 14.79  | 0.28     | 0.45           | 0.47     | P28                                     | 960    | 132      | 13.76  | 1.01     | 14.47          | 0.38     |
| P32                                     | 300    | 100      | 1.82   | 0.23     | 0.95           | 0.43     | P29                                     | 1250   | 132      | 5.11   | 0.37     | 2.31           | 0.33     |
| P33                                     | 320    | 100      | -1.96  | 0.25     | 1.08           | 0.46     | P30                                     | 960    | 180      | 6.59   | 0.26     | 0.82           | 0.3      |
| P34                                     | 1532   | 368      | -219   | 2.06     | 11.77          | 0.49     | P31                                     | 1120   | 204      | -12.45 | 0.38     | 1.44           | 0.36     |
| P35                                     | 200    | 184      | 15.25  | 0.57     | 2.48           | 0.47     | P32                                     | 1450   | 204      | -31.28 | 0.96     | 7.95           | 0.39     |
| P36                                     | 180    | 184      | 9.48   | 0.36     | 1.03           | 0.46     | P33                                     | 1220   | 204      | -48.83 | 1.49     | 18.13          | 0.41     |
| P37                                     | 250    | 100      | -2.55  | 0.33     | 1.76           | 0.46     | P34                                     | 2410   | 204      | -54.68 | 1.67     | 22.35          | 0.44     |

(continued)

**Table 2** (continued)

| Network 1—Table—Links at end (120:00 h) |        |          |      |          |                |          | Network 2—Table—Links at end (120:00 h) |        |          |        |          |                |          |
|---|--------|----------|------|----------|----------------|----------|---|--------|----------|--------|----------|----------------|----------|
| Link ID                                 | Length | Diameter | Flow | Velocity | Unit head loss | Chlorine | Link ID                                 | Length | Diameter | Flow   | Velocity | Unit head loss | Chlorine |
|   | m      | mm       | LPS  | m/s      | m/km           | mg/L     |   | m      | Mm       | LPS    | m/s      | m/km           | mg/L     |
| P38                                     | 270    | 100      | 3.32 | 0.42     | 2.87           | 0.46     | P35                                     | 2110   | 204      | -59.3  | 1.81     | 25.98          | 0.47     |
|   |        |          |      |          |                |          | P36                                     | 1550   | 204      | -81.47 | 2.49     | 46.78          | 0.49     |
|   |        |          |      |          |                |          | P37                                     | 2640   | 72       | 0.35   | 0.09     | 0.31           | 0.09     |
|   |        |          |      |          |                |          | P38                                     | 3120   | 72       | 1.42   | 0.35     | 4.13           | 0.25     |
|   |        |          |      |          |                |          | P39                                     | 2400   | 60       | 0.45   | 0.16     | 1.2            | 0.13     |
|   |        |          |      |          |                |          | P40                                     | 1440   | 60       | 0.79   | 0.28     | 3.43           | 0.27     |
|   |        |          |      |          |                |          | P41                                     | 3840   | 60       | 0.14   | 0.05     | 0.14           | 0.05     |
|   |        |          |      |          |                |          | P42                                     | 2640   | 72       | -0.81  | 0.2      | 1.46           | 0.17     |
|   |        |          |      |          |                |          | P43                                     | 855    | 150      | 35.1   | 1.99     | 43.97          | 0.48     |
|   |        |          |      |          |                |          | P44                                     | 1225   | 150      | 9.18   | 0.52     | 3.67           | 0.44     |
|   |        |          |      |          |                |          | P45                                     | 750    | 150      | -2.5   | 0.14     | 0.33           | 0.37     |
|   |        |          |      |          |                |          | P46                                     | 1255   | 180      | 14.2   | 0.56     | 3.39           | 0.44     |
|   |        |          |      |          |                |          | P47                                     | 1000   | 12       | -0.01  | 0.12     | 4.5            | 0.28     |
|   |        |          |      |          |                |          | P48                                     | 2177   | 120      | 17.64  | 1.56     | 36.46          | 0.46     |
|   |        |          |      |          |                |          | P49                                     | 1752   | 120      | 8.82   | 0.78     | 10.1           | 0.4      |
|   |        |          |      |          |                |          | P50                                     | 2135   | 150      | 15.6   | 0.88     | 9.79           | 0.41     |

(continued)

**Table 2** (continued)

| Network 1—Table—Links at end (120:00 h) |        |          |      |          |                |          | Network 2—Table—Links at end (120:00 h) |        |          |       |          |                |          |
|---|--------|----------|------|----------|----------------|----------|---|--------|----------|-------|----------|----------------|----------|
| Link ID                                 | Length | Diameter | Flow | Velocity | Unit head loss | Chlorine | Link ID                                 | Length | Diameter | Flow  | Velocity | Unit head loss | Chlorine |
|   | m      | mm       | LPS  | m/s      | m/km           | mg/L     |   | m      | Mm       | LPS   | m/s      | m/km           | mg/L     |
|   |        |          |      |          |                |          | P51                                     | 825    | 70       | 3.83  | 0.99     | 29.72          | 0.36     |
|   |        |          |      |          |                |          | P52                                     | 1722   | 100      | 6.57  | 0.84     | 14.24          | 0.34     |
|   |        |          |      |          |                |          | P53                                     | 1560   | 100      | 5.2   | 0.66     | 9.23           | 0.28     |
|   |        |          |      |          |                |          | P54                                     | 2820   | 120      | 27    | 2.39     | 80.21          | 0.36     |
|   |        |          |      |          |                |          | P55                                     | 1275   | 120      | 16.5  | 1.46     | 32.22          | 0.33     |
|   |        |          |      |          |                |          | P56                                     | 2170   | 100      | 4.15  | 0.53     | 6.06           | 0.26     |
|   |        |          |      |          |                |          | P57                                     | 855    | 100      | -6.85 | 0.87     | 15.39          | 0.3      |
|   |        |          |      |          |                |          | P58                                     | 925    | 100      | 2.46  | 0.31     | 2.31           | 0.23     |
|   |        |          |      |          |                |          | P59                                     | 1525   | 120      | -3.04 | 0.27     | 1.4            | 0.21     |
|   |        |          |      |          |                |          | P60                                     | 755    | 100      | 5     | 0.64     | 8.58           | 0.32     |



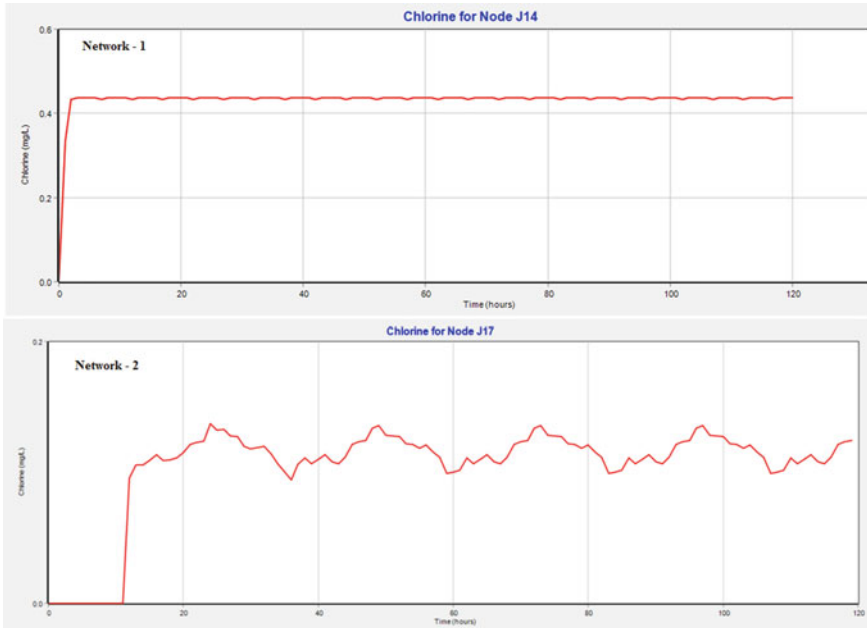


**Fig. 3** Time-series plot showing the distribution of chlorine in the node for network 1 and 2

chlorine injection is required to chlorinate the water at those nodes as well as the pipe where the concentrations have reduced down to 0.2 mg/L.

In the realistic circumstances, the pipelines are laid and dwell in position for longer time (more than 15–20 years), as the year progresses the piping network gets adversely affected due to the formation of scale deposits and corrosion, resulting in dropped flow velocity, quality decline, and head losses. The pipe roughness drops significantly resulting in reduced quality of water at the end nodes, in-order to maintain a desired quality the initial quality of water is increased to an elevated concentration (more than 5.0 mg/L). Hence, the nodes closer to the source will have higher concentrations, leading to many health effects. Therefore, to overcome the issues providing a booster pump at the desired locations are advisable.

## 4 Conclusion

In this study, two distinct water distribution networks in the South India were selected, and the effect of piping material and pipe age on chlorine decay was examined. The network 1 was constructed using a galvanized steel pipe with a roughness of 120, while the 2<sup>nd</sup> network was made of cast iron with a roughness of 100. The bulk wall decay coefficient and bulk liquid decay coefficient are taken as  $-0.2$  and  $-0.045$  per

day, respectively, negative sign denotes the reduction in chlorine values with time. It is attributed from the present study that the residual chlorine quality of above 0.2 mg/L as per WHO recommendations can be maintained in the networks configured with galvanized steel piping material, while it have not reached the desired concentrations in few nodes of cast iron pipes. Subsequently, as the piping age increases, the friction factor also increased leading to a slight decrease in the chlorine concentration. This study concludes that the end nodes in the networks (node 22 of network 1) have showed a significant change in chlorine concentration from 0.46 mg/L to 0.23 mg/L as the roughness increased from 120 to 130, respectively. In addition, the effect of piping material showed a variation in the residual chlorine concentration in the end nodes 14 (network 1) and 17 (network 2). A constant residual concentration of 0.4 mg/L was maintained in network 1, whereas the network 2 saw a very less residual concentration (0.2 mg/L). Hence, the study concludes that use of galvanized steel pipe is more suitable than cast iron pipe to maintain the minimal chlorine levels in the nodes. Additionally, providing booster pump at the negative pressure regions with a chlorine addition will eliminate the decay of chlorine.

## References

1. Termini D, Viviani G (2015) Spatial diversity of chlorine residual in a drinking water distribution system: application of an integrated fuzzy logic technique. *J Hydroinform* 17(2):293–306
2. Mohapatra S, Sargaonkar A, Labhasetwar PK (2014) Distribution network assessment using EPANET for intermittent and continuous water supply. *Water Resour Manag* 28(11):3745–3759
3. Nagatani T, Yasuhara K, Murata K, Takeda M, Nakamura T, Fuchigami T, Terashima K (2008) Residual chlorine decay simulation in water distribution system. In: *The 7th international symposium on water supply technology*. Yokohama, Japan, pp 22–24
4. Ecura J, Okot-Okumu J, Okurut TO (2011) Monitoring residual chlorine decay and coliform contamination in water distribution network of Kampala, Uganda. *J Appl Sci Environ Manage* 15(1):167–173
5. Wang H, Hu C, Hu X, Yang M, Qu J (2012) Effects of disinfectant and biofilm on the corrosion of cast iron pipes in a reclaimed water distribution system. *Water Res* 46(4):1070–1078
6. Zhang C, Li C, Zheng X, Zhao J, He G, Zhang T (2017) Effect of pipe materials on chlorine decay, trihalomethanes formation, and bacterial communities in pilot-scale water distribution systems. *Int J Environ Sci Te* 14(1):85–94
7. Nono D, Odirile PT, Basupi I, Parida BP (2019) Assessment of probable causes of chlorine decay in water distribution systems of Gaborone city, Botswana. *Water SA* 45(2):190–198
8. Castro P, Neves M (2003) Chlorine decay in water distribution systems case study—Lousada network. *Electron J Environ J Agric Food Chem* 2(2):261–266.
9. Kim H, Kim S (2017) Evaluation of chlorine decay models under transient conditions in a water distribution system. *J Hydroinform* 19(4):522–537
10. Menaia J, Coelho ST, Lopes A, Fonte E, Palma J (2003) Dependency of bulk chlorine decay rates on flow velocity in water distribution networks. *Water Sci Tech: W Sup.* 3(1–2):209–214
11. Jamwal P, Kumar MM (2016) Effect of flow velocity on chlorine decay in water distribution network: a pilot loop study. *Curr Sci* 2016:1349–1354.
12. Al-Jasser AO (2011) Pipe service age effect on chlorine decay in drinking water transmission and distribution systems. *CLEAN—Soil Air Water* 39(9):827–832
13. Kim H, Koo J, Kim S (2015) A general framework of chlorine decay modeling at a pilot-scale water distribution system. *J Water Supply: Res T—AQUA* 64(5):543–557

14. Kowalska BEATA, Kowalski DARIUSZ, Musz ANNA (2006) Chlorine decay in water distribution systems. *Environ Prot Eng* 32(2):5–16
15. Rossman LA (2000) EPANET 2: users manual. USEPA, pp 1–200
16. Tiruneh AT, Debessai TY, Bwembya GC, Nkambule SJ, Zwane L (2019) Variable chlorine decay rate modeling of the Matsapha town water network using EPANET program. *J Water Resour Prot* 11(01):37
17. Jethoo AS, Poonia MP (2011) Water consumption pattern of Jaipur city (India). *Int J Environ Sci Develop.* 2(2):1–4
18. Neelakantan TR, Suribabu CR, Lingireddy S (2008) Optimisation procedure for pipe-sizing with break-repair and replacement economics. *Water SA* 34(2):217–224
19. Ratnasooriya AHR, Wijesekara NTS (2009) Ageing of pipes and sustainability of water supply, *Engineer. J Inst Eng Sri Lanka* 2009:42(3)
20. Mostafa NG, Matta ME, Halim HA (2013) Simulation of chlorine decay in water distribution networks using EPANET—Case study. *Simulation* 3(13)
21. Ramana GV, Chekka VS (2018) Validation and examination of existing water distribution network for continuous supply of water using EPANET. *Water Resour Manag* 32(6):1993–2011
22. Philip L, Ramprasad C, Krithika D (2019) Sustainable wastewater management through decentralized systems: case studies. In: *Water scarcity and ways to reduce the impact*. Springer, Cham, pp 15–45

# Hydraulic Analysis of Drinking Water Distribution Network Using WaterCAD Simulation: Case of Purba Medinipur in West Bengal



Koushik Debnath, Subhasish Das, and Biprodip Mukherjee

**Abstract** Water distribution network design is going through many developments. Today, simulation software programs are essentially being used to design the whole network of water distribution systems to reduce the overall cost while meeting the water demand at adequate terminal pressure and maintaining CPHEEO standard water quality. In this study, we have used WaterCAD software to design and to analyze the proposed water distribution network of Bhogpur gram panchayat of Panskura 2 block of Purba Medinipur District in West Bengal. The analytic study is based on a surface water-based pipeline water delivery scheme, executed by the Public Health Engineering Department, Government of West Bengal at Purba Medinipur district of West Bengal. The outputs of the above-noted study are also verified theoretically. It was computed and ensured that the minimum pressure head available in the water distribution network is 8.82 m and the maximum flow velocity of 0.9 m/s. The study exercised in this paper is enthralled to support both academicians with industry-versed hydraulics engineer.

**Keywords** Water supply · Pipe network · WaterCAD · Hydraulic simulation · Headloss

## 1 Introduction

One of the most important issues in modern times has been the provision of quality water and value. A reliable source of water for drinking and agriculture is given to the inhabitants by a river as the groundwater table is running out day by day. New advanced systems for surface water treatment and distribution are emerging as water is a vital part of the socioeconomic development of a nation. And for a nation like India where about 70% of people breaths in rural areas, efficient, and sufficient water supply in those areas is very much exigent along with urban water supply. West Bengal, one of the states of India, has an area of 8,875,200 hectares including

---

K. Debnath (✉) · S. Das · B. Mukherjee  
School of Water Resources Engineering, Jadavpur University, Kolkata 700032, India

© The Author(s), under exclusive license to Springer Nature Singapore Pte Ltd. 2022  
C. M. Rao et al. (eds.), *Advanced Modelling and Innovations in Water Resources Engineering*, Lecture Notes in Civil Engineering 176,  
[https://doi.org/10.1007/978-981-16-4629-4\\_21](https://doi.org/10.1007/978-981-16-4629-4_21)

301

8,362,643 hectares rural and 5,12,557 hectare urban areas. A large population of these rural areas is mostly dependent on the groundwater source or untreated surface water for drinking. These unhygienic practices had increased incidents of the epidemic which has been reported various times in newspapers and different studies.

The government is endeavoring in implementing different schemes to provide the rural areas potable piped water supply for sustainable development. There are two types of structures in West Bengal by which water supply systems are being delivered. The straightforward structure is one of two structures, with PHED staff at various levels of management. Another horizontal framework is consisting of Gram Panchayats (GP), Panchayat Samiti (PS), and Zilla Panchayats (ZP). Our study is based on a surface water-based pipeline water supply system (PWSS), operated by the Public Health Engineering Department, West Bengal Government at Bhogpur gram panchayat in Purba Medinipur District. Some of the works previously done on pipe network analysis and design using various software programs are discussed in connection with the present study for better understanding.

A study had been carried out for measuring time-varying decay of chlorine concentration for a PWSS at Dakshin Raipur, West Bengal [1, 2]. Where it is aimed to simulate the present condition through a computer model which would act as a base for any modifications in the network if required and then modifications are suggested to achieve the flow in such a way that all the overhead reservoirs and ground-level reservoirs fill up almost simultaneously. After hydraulic simulation and analysis, it is found that the different overhead reservoirs are taking distinct time to engulf fully. Research has been done on a pipeline networking design and analysis for Dhapa PWSS by EPANET and waterhammer analyzing software programs [3]. Comparative research on the actual operation was also conducted on the emergence of hydraulic analysis in the pipeline networking between EPANET and waterhammer analyzing software programs [4]. The output of the study is that in both the software programs the flow output remains more or less the same.

A study conducted at the El-Nozha water delivery network at the Alexandria Governorate in Egypt revealed that through improved software programs like WaterCAD, it is likely to maintain a percentage of residual chlorine concentrations in various areas without relying on chlorine plant supplementation for water treatment only [5]. A study was carried on the real-life operation of Garfa Boosting Station, Kolkata, under Borough 12 of Kolkata Municipal Corporation (KMC) by hammer and WaterGEMS software programs [6]. The study of comparison between LOOP and EPANET software programs is using a gravitational transmission network in the Panskura block of Purba Medinipur District showed the results were similar up to 96% [7]. A study was performed to analyze the drinking water supply network of the Panskura 2 zone 1 boosting station using WaterGEMS software and by observing the pressures at endpoints and hydraulic grade markings of the complete system along with only some undulations of geography air valves were suggested at different nodes of the pipe network. Stresses in pipeline systems are caused due to transient as a result of global loss of frictional force as is accessed by many hydraulic simulation software programs such as waterhammer and EPANET programs [8–10]. In almost every study, it is accessed that higher than sixty percent of head losses occur in valves

with appurtenances and pipes which plays an important role in hydraulic engineering [11, 12].

The aim of the implementation of the drinking water supply is to improve supply for rural people and services of sanitation by advancing decentralization, public participation, improved accountability, and policy. The PHED, WB in Panskura 2 block also enhances the actual capacity of Panskura 2 PWSS with the objective to close the present difference between actual demand and actual supply then to satisfactorily meet the perceived local require to be covered by 2043 through PWSS. The proposed PWSS will have proviso for a few street hydrants besides a supply of water through house connection for benefiting the housing for low-income groups. Most importantly in a future perspective, the leakage study and also pump selection study can be done like one of the previous research studies [13].

The purpose of this study is to perform the hydraulic analysis of Panskura 2, Bhogpur gram panchayat (Zone-III) of Purba Medinipur District water distribution network using WaterCAD simulation software. The following points are part of the research (a) to establish a network model of pipe based on simulating software and (b) to suggest some measures if the present network does not fulfill the present and future demand and to analyze the existing water distribution system using simulating software. In Fig. 1, the total pipe network from the elevated storage reservoir (ESR) (T-1) to the consumer's end of Bhogpur GP (Zone-III) is shown.

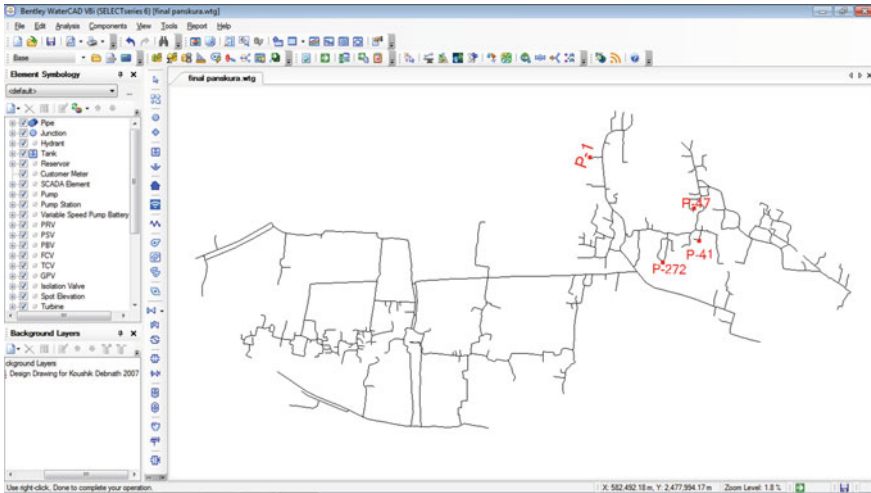
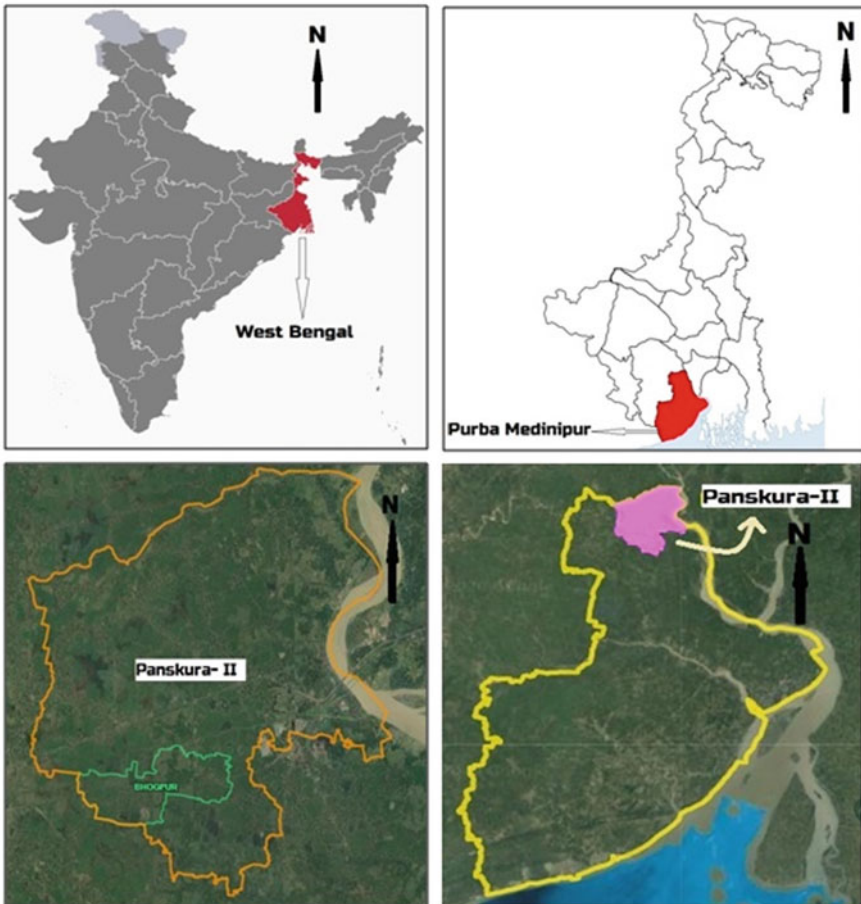


Fig. 1 WaterCAD software interface

## 2 Study Area

The country India now has 29 states and eight Union Territories, and West Bengal is a state in eastern India. There are 23 districts in West Bengal, and the location of our study is in Purba Medinipur District. The district is further divided into 25 community development (CD) blocks. The surface water-based water supply scheme has been implemented at Panskura 2 block of Purba Medinipur. The Panskura 2 block consists of 13 number of gram panchayats, viz. Amalhanda, Bhogpur, Baisnabchak, Brindabanchak, Gopal Nagar, Deriachak, Khanyadihi, Kola 1, Kola 2, Pulsita, Siddha 1, Siddha 2, and Sagarbarh. Figure 2 completely shows the study area.



**Fig. 2** Location map of West Bengal in India; Purba Medinipur District in West Bengal; Panskura 2 block in Purba Medinipur District; Bhogpur gram panchayat in Panskura 2 block (clockwise from the top left corner)



**Fig. 3** Command area details of surface water-based PWSS for Panskura 2 block. *Source* WPHED Purba Medinipur

The command area of the proposed water supply scheme stretches from Panskura 1 in the southwest, along the western bank of river Rupnarayan toward north–south, block Daspur 2 in the north, and block Sahid Matangini in the south (Fig. 3). The entire command area of the scheme stretches up to 14,343.27 hectares. The ESR and the pipe network drawn and analyzed using WaterCAD simulating software in the study serve the area of Bhogpur GP (Zone-III). The Bhogpur GP is surrounded by Siddha 1 and Siddha 2 GP in the north, Deriachak GP at the southwest, Sagarbarh GP at the northwest, and Pratappur 1 and Raghunathbari GP at the east and southeast. Total seven Mouzas of Bhogpur GP that is Narayanpakuria, Namalbarh, Kishor Chak, Benia, Kotalia, Bhogpur, and Nandai Gajan get the treated water from Zone-III boosting station. The area of Bhogpur GP is 193.74 hectares with a population of 7,559 people (as per the 2011 census) residing in 1582 households.

The upper phase of the Rupnarayan River is known as Dhaleswari (Dhalkisor), and it begins from plateau Chhota Nagpur on riverbank foothills northeast of town Purulia. Then with the name Dwarakeswar River, it follows a meandering southeasterly course through Bankura town. Near Ghatal town, it is joined by the Shilabati River, from which it derives the name Rupnarayan. Eventually, the river joins the Hoogli River and reaches the Bay of Bengal. To draw raw water from the river Rupnarayan which is a perennial source flowing adjacent to the area, Chhatinda mouza jurisdiction list number 285 is selected as the location for the construction of intake arrangement. The coordinates of the intake site are N 22°27'48.66", E 87°52'45.64".



### 3 Overview of Simulation Software

WaterCAD from Bentley Systems is a well-designed program that assists engineers with planning, designing, and analyzing complex pressurized piping systems. A powerful and user-friendly graphical interface (equally in AutoCAD and stand-alone mode) builds it simple to quickly set up complex networking of tanks, pumps, pipes, valves, and more. Some of the hydraulic model capabilities of the software are mentioned herein.

The simulating software is able to redact steady-state piping analysis of PWSS with pumps, reservoirs, tanks, junctions, and several controlling valves. Software is able to execute extended time period simulations for examining the piping system response to different supply and node demand schedules. Software is able to execute water quality simulative modeling to work out a water resource and age or tracking the expansion or degradation of chemical constituents for the entire PWSS network. Software is able to execute fire flow analytics with the network system for determining how the system will work under critical conditions. The software is capable of configuring umpteen groups of physical and hydraulic properties, operational and start-up settings, fire flow, costing, and water quality choices. Software's flexible scenario management feature gives easy access to create and use any numeral of situations by integrating and properly matching substitutes, then outlook and evaluate outcomes swiftly and effortlessly. It is able to connect to GIS data using shapefiles and connections of the database.

### 4 Methodology

The steps involved in drawing, designing, and analyzing the water distribution network using simulating software WaterCAD is shown in Fig. 4.

Few assumptions were made for running the software analysis, viz. the fluid is homogeneous and incompressible. The elasticity of pipe material and fluid ensures a linear outline. The flow-through piping units is one-dimensional. This software exercises mean velocity. The points considered for network design are addressed herein. The Class 3 uPVC pipelines and ductile iron class K7 pipelines are used depending on the analysis of the soil type, topography accessibility, etc. Hazen-Williams constant (C) for Class 3 uPVC pipelines is taken 145, and class K7 ductile iron pipelines is taken 140. The losses due to bends and specials are taken a maximum of 2.0 m. Elevation differences are duly considered in the design.

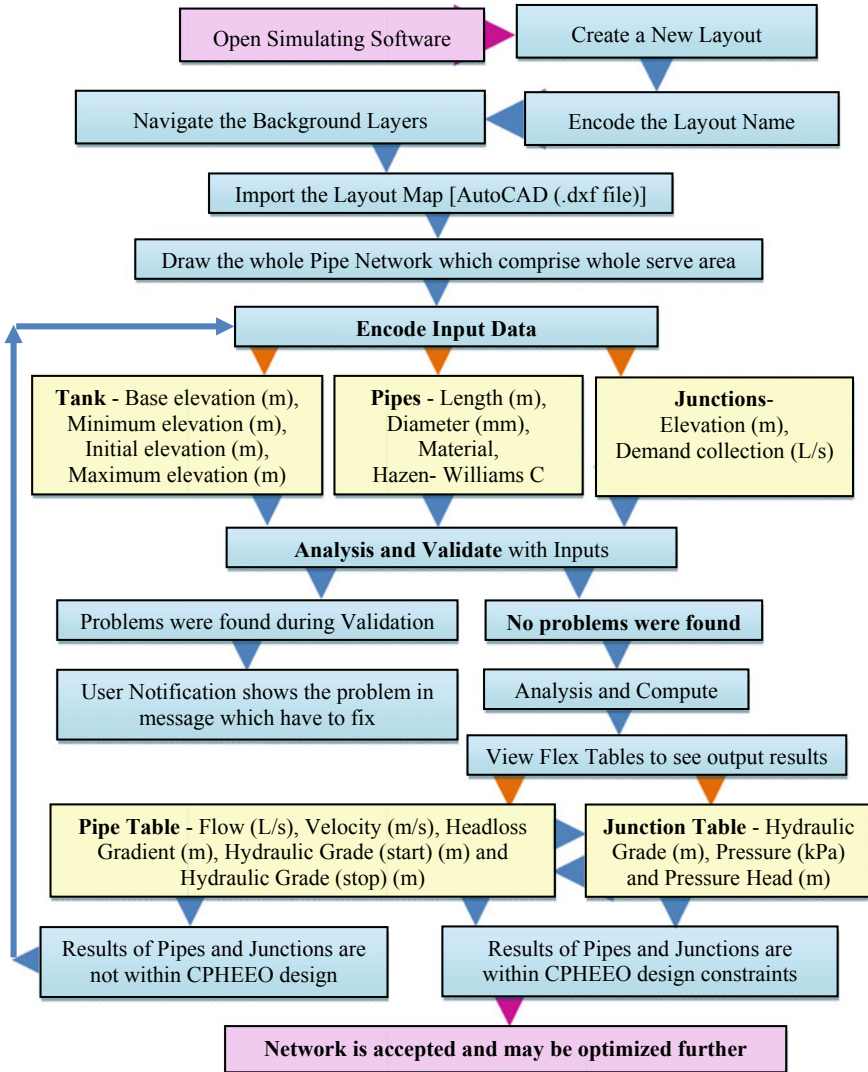


Fig. 4 Flowchart of drawing, designing, and analyzing in simulating software

## 5 Results and Discussion

As per Indian standards CPHEEO manual of 1999, the two main design constraints for piped water supply that have to be maintained by designers are minimum residual pressure at ferrule or consumer endpoints and minimum velocity at end-user points. According to this manual, a minimum residual pressure of 7 m and a minimum velocity of 0.6 m/s have to be maintained. However, where inevitable due

to minimum pipe diameter criteria or other hydraulic constraints—lower velocities may be adopted with adequate provision of scouring. Selection of a proper diameter of a pipe is the main criteria to maintain a minimum system pressure of 7 m. The whole pipe network has a length of 51.092 km consisting of 334 numbers pipes of various diameters and 310 number junctions or nodes. It is to be noted that the pipes are denoted with an ID P-1, 2, 3...334, junctions are denoted by J-1, 2, 3...310, and the ESR is denoted by T-1.

From the analysis in simulating software, it reflects that the lowest hydraulic pressure in the network is 8.82 m at junction ID J-168 as shown in Fig. 4. The shortest path between tank (T-1) and the junction J-168 is 6.448 km as shown in Fig. 5. The maximum velocity in the network is found out to be 0.9 m/s at pipe ID P-92 and minimum velocity of 0.0042 m/s at pipe ID P-41, P-47, and P-272 as shown in Fig. 6. The result from the simulating software and also from Fig. 7 mentioned in the study depicts that the maximum and minimum head losses are 2.36 m and 0.00 m at pipe ID P-93, and P-179, respectively. The pressure head is a maximum of 18.47 m at J-1 and a minimum of 8.82 m at J-168. The critical variation of concerned parameters such as fluctuating pressure head, velocity deviation, and headloss inconsistency is shown in the profile plots Figs. 8, 9, and 10. Keeping in view the overall survey drawing of the pipeline network, the reservoir balancing head of 23.003 m holds great to undertake water losses contained by 15%. The noted staging height given for pressurizing reservoir is supposed to manage up the overall major and minor losses in the form of frictional losses plus fittings losses correspondingly in the concerned pipeline network. In addition to the above information here, it can be said that around 2 m total losses are nearly 10% losses with regard to the reservoir staging height of 20 m above ground level as eventually considered to construct the master reservoir.

The initial survey of the command area suggests that there is an uneven landscape in the PWSS network of 51.092 km. With the aid of Fig. 11, four air valves positioning

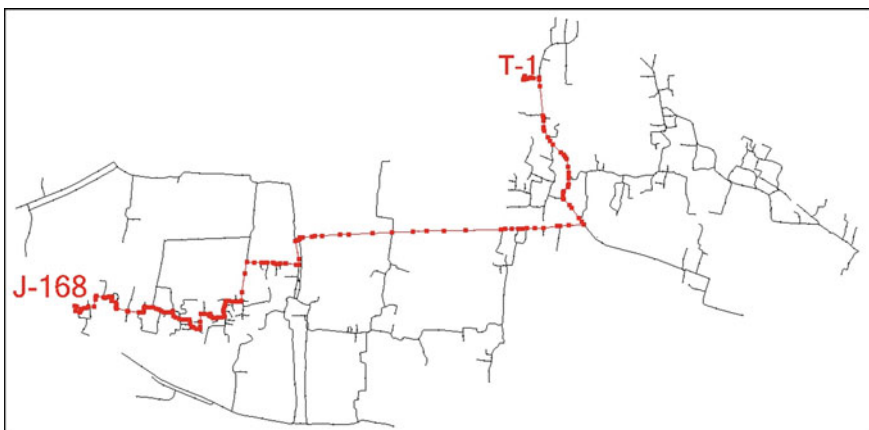


**Fig. 5** Illustration showing Junction-168 and the shortest path between T-1 and J-168

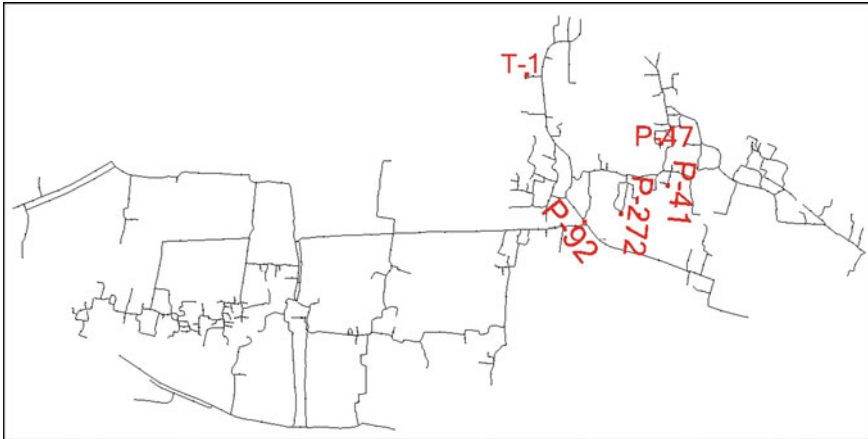


Fig. 6 Illustration showing the pipes having maximum and minimum velocities

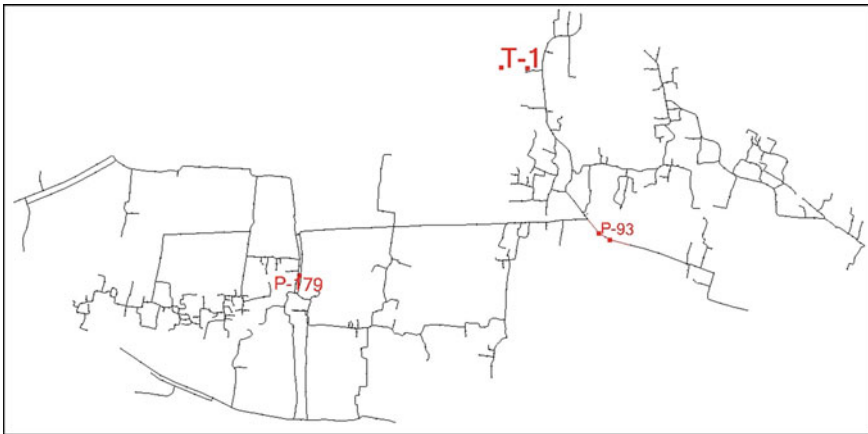
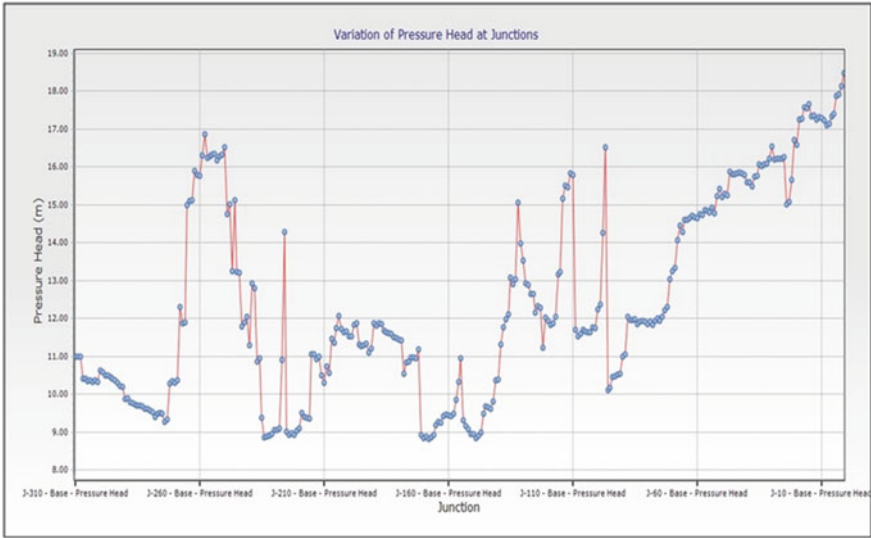


Fig. 7 Illustration showing pipes having maximum and minimum headloss

is suggested to exhaust the entrapped air blocking pipe cross sections in the pipes due to terrain undulations. If air valves are not given in such locations, then the headloss gradient increases in the continuous flow of water through the network. This in turn causes leakages in joints. From Table 1, the locations of the air valves can be judged out and those nodes are addressed in Fig. 11. While suggesting the locations for the considered network minimum elevation fluctuations was about 0.5 m between pipes and the air valve to be positioned in the highest elevation junction of the pipes.

Double acting or single orifice valves and triple acting, or double orifice valves are the most commonly used air valves as per IS and BS codes are been manufactured in order to aid support to the pipe network. Triple acting kinetic air valves are generally used at high points, long horizontal pipelines (spacing of 400–750 m), long descents



**Fig. 8** Variation of pressure heads at different junctions

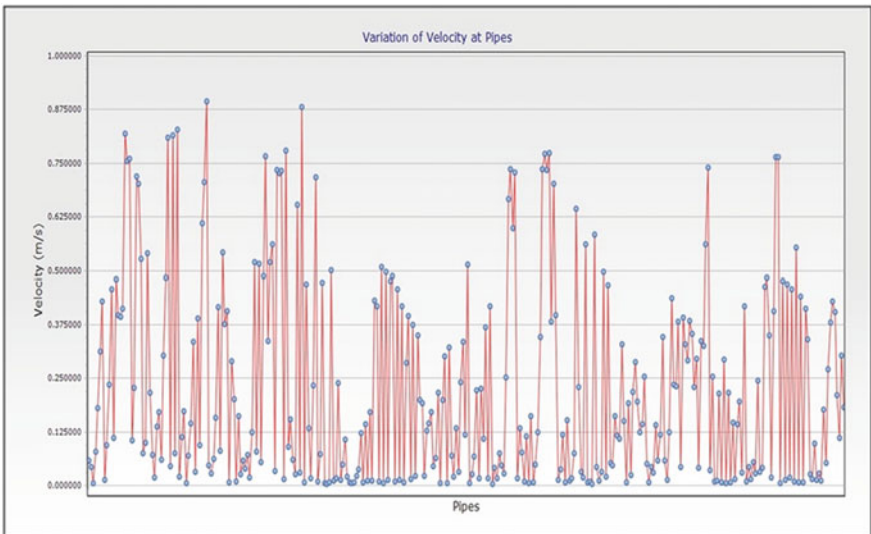


**Fig. 9** Variation of velocity in pipes

(spacing of 400–750 m) in a pipeline. Double-acting kinetic air valves are generally used in long ascents (spacing of 400–750 m).

In a PWSS network scour valves are technically used to eject sediments found accumulated in the PWSS pipes of lower elevation and low flow and for draining off

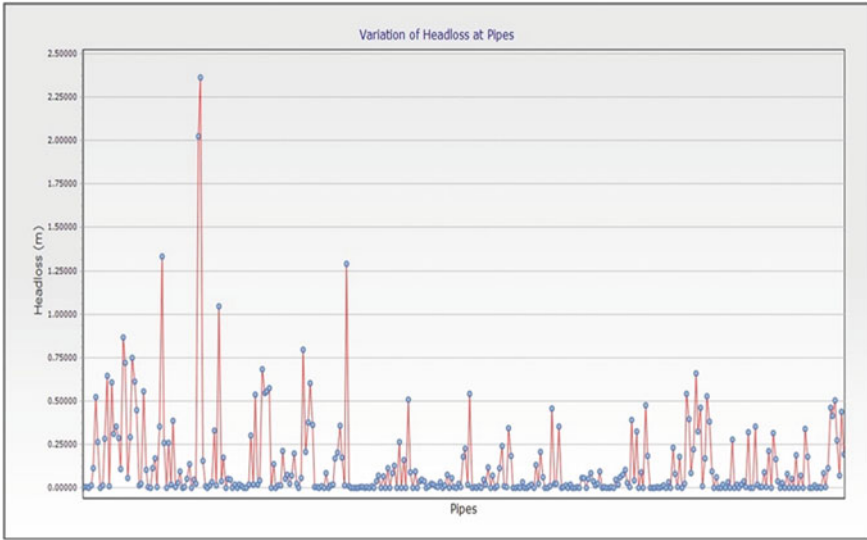


**Fig. 10** Variation of head loss in pipes



**Fig. 11** Position of air valves highlighted in red square bullets

**Table 1** Air valve locations

| S. no | Air valve position respecting node number |
|-------|---|
| 1     | J-53                                      |
| 2     | J-73                                      |
| 3     | J-146                                     |
| 4     | J-215                                     |

**Table 2** Scour valve locations

| S. no. | Scour valve locations with respect to Node ID | Node elevation (m) |
|--------|---|--------------------|
| 1      | J-99  | 2.290              |
| 2      | J-154   | 2.301              |

**Fig. 12** Position of scour valves highlighted in red square bullets

pressurized water when pipelines get contaminated. Keeping these facts into consideration two numbers of scouring valves is suggested at two nodes of the network mentioned in Table 2 and in Fig. 12. The time to empty water from connected all PWSS pipes as speedily as feasible is the key governing aspect linked with designing a scouring valve in any large PWSS. It is customary to locate the scouring valves at the lowest elevated nodes of the PWSS network and near a water body or barren land where the water can easily be disposed of. From our initial survey, a water body was found near end node J-154 only. And for node J-99, it is proposed that proper arrangements have to be made to carry drained water to a distant water body or barren land.

## 6 Conclusions

The present study deals with a hydraulic analysis of a PWSS drinking water zone for Bhogpur GP of Panskura 2 block in Purba Medinipur. A total area of 193.74 hectares will be benefited after installing this 51.092 km of network pipelines that interact with 310 junctions in terms of hydraulic design module. Hydraulic simulations were performed to assess the flow as per water demand and CPHEEO standard pressure in the nodes. Therefore, the analysis satisfies the above condition. In the hydraulic

analysis of the study, the minimum findings of 8.82 m pressure indicate that the system is above the normal CPHEEO pressure standard of 7 m. This buffer of pressure in the system will allow flexibility to install more required appurtenances like sluice and control valves. Since the ground undulation is a feature of air entrapment in the pipes, four optimized air valves are placed throughout the network that will be able to capture the entrapped air exhaustion. Scour valve plays a major role in PWSS distribution networks for draining out at the time of maintenance. Similarly, draining of water and repairing of broken elements like pipes, valves, and other appurtenances or to perform repair work for customary maintenance are often required, and two scour valves are suggested in the PWSS pipe network. The study would have been more effective if the design data could be compared with the actual data. From an overall perspective, this study is a good academic practice of juggling hydraulic parameters at the design phase, before the start of the operation phase, and the maintenance of the entire piped water network.

**Acknowledgements** The authors warmly thank PHED, GoWB, and NCC, Hyderabad, for their cherished help by giving the data for the research study. The master's thesis work of Shri Koushik Debnath helped in a great way to suggest the research work.

## References

1. Das S (2006) Study of pipe network & temporal decay of chlorine for the water treatment plant (WTP) at Dakshin Raipur, West Bengal, India (M.E. Thesis). School of Water Resources Engineering, Jadavpur University, Kolkata, India
2. Das S, Roy PK, Mazumdar A (2008) Analysis of pipe flow & head loss of a modeled network based on EPANET in a water treatment plant at Raipur, West Bengal. *J Inst Public Health Eng India*. 2008–2009(3):21–28
3. Mukherjee B (2012) Pipeline design and analysis of distribution network of Dhapa water treatment plant, KMC by EPANET and HAMMER software (M.E. Thesis). School of Water Resources Engineering, Jadavpur University, Kolkata, India
4. Mukherjee B, Das S, Mazumdar A (2012) Comparison of pipeline hydraulic analysis between EPANET and HAMMER softwares. *Int J Adv Sci Tech* 4(6):52–63
5. Hamdy D, Moustafa MAE, Elbakri W (2014) Free residual chlorine calibration by water-CAD at El-Nozha water network in Alexandria Governorate, Egypt. *J. Environ. Protect.* 5:845–861
6. Sarkar PK (2014) Extended period simulations of pipeline distribution network of Garfa boosting station by hammer and WaterGEMS softwares (M.E. Thesis). School of Water Resources Engineering, Jadavpur University, Kolkata, India
7. Halder K (2016) Comparison between EPANET and LOOP Softwares using a Gravity Flow Water Supply Network (M.E. Thesis). School of Water Resources Engineering, Jadavpur University, Kolkata, India
8. Mukherjee B, Kuila A, Das S (2019) Optimized hydraulic design of an water distribution network at West Medinipur in West Bengal: A case study. *J Assoc Eng India* 89(1 & 2):19–32
9. Das S, Mukherjee B, Mazumdar A (2013) Analysis of hammer head at increased flow demand in pipe networks: A case study. *Int Rev Mech Eng* 7(4):757–766
10. Mukherjee B, Das S, Mazumdar A (2015) Transient analysis of a pipeline network for drinking purpose in Assam, India. *J Inst Public Health Eng India* 2014–2015(4):26–32
11. Mukherjee B, Das S, Maity S (2020) Optimum process of pipeline selection in water distribution network: Case study. *Appl Mech Materials Civ, Arch, Struct Constr Eng III* 897:137–141



12. Das S, Mukherjee B, Mazumdar A (2018) Comparison of outcomes through EPANET and LOOP softwares using a gravity flow water supply network at East Medinipur in West Bengal. *J Indian Chem Soc* 95(3):313–324
13. Mukherjee P, Das M, Mukherjee B, Das S (2020) Optimization of irrigation design technique for pumping units through software simulation analysis for varied landscapes. *IOP Conf Ser: Earth Environ Sci* 505:012025

# Comparison Model Study Using WaterGEMS and EPANET Software Programs for Clearwater Rising Main at Bhangar in West Bengal



Biprodip Mukherjee, Prasun Das, and Subhasish Das

**Abstract** To handover, a glass of pure drinking water to the general population a huge water infrastructure is required for all water supply projects. In the general concept for a surface-based water supply project, the raw untreated water is been conveyed from a surface water source like a river, lake, reservoirs, or pond to a water treatment plant. Thereafter portable treated water is been conveyed to the overhead reservoir through clearwater rising main pipes. Most importantly no tapings from the clearwater pipes are exercised to maintain target flow and pressure. The study here is envisaged for the pipeline balancing network of proposed rising main alignment of the ground-level reservoir (GLR) II to overhead reservoirs for surface water-based water supply scheme at Bhangar 2 block in South 24 Parganas under West Bengal. Presently, the work is being monitored by West Bengal PHED. To carry out this study, a line network diagram has been drawn with necessary input such as elevation of nodes, details of pumps, pipes line diameter, length, and elevated storage reservoir details to operate the system and obtain outputs like pressure head, flow, velocity, hydraulic grade, and losses. Today many water simulation software programs are available to perform a hydraulic flow study. For this purpose, EPANET and WaterGEMS software programs have been used to get the desired output with simulation. After getting the output, both the software results have been compared with various parameters to show the merits and limitations of both the systems and to understand how the system can be optimized economically. The percentage of head loss for the clearwater network was computed 0.18398 and 0.18394 using EPANET and WaterGEMS, respectively. The variation is negligible. In the matter of user friendly, the WaterGEMS software prevails over EPANET software since in the former software accurate length can be fed in which designing of small, short piece pipes also which are joining valves and pumps.

**Keywords** Optimization · Hydraulic grade · Pump selection · Valve adjustment · Pipe diameter selection

---

B. Mukherjee (✉) · P. Das · S. Das  
School of Water Resources Engineering, Jadavpur University, Kolkata 700032, India

© The Author(s), under exclusive license to Springer Nature Singapore Pte Ltd. 2022  
C. M. Rao et al. (eds.), *Advanced Modelling and Innovations in Water Resources Engineering*, Lecture Notes in Civil Engineering 176,  
[https://doi.org/10.1007/978-981-16-4629-4\\_22](https://doi.org/10.1007/978-981-16-4629-4_22)

315

## 1 Introduction

The state of West Bengal is one of the most populous states in India with 1029 people per km<sup>2</sup> [1]. Its average urban size is very high at about 7500 people per km<sup>2</sup>. West Bengal (WB) has free access to water as a natural resource that supports large-scale rain-fed agriculture. However, the pressure on urban water resources has been growing for some years due to population growth, low investment in supply output, and the declining status of existing systems. An overall loss of frictional force that immediately causes transients in pressure and produces stress in the piping system is all judged by applying a variety of hydraulically simulating software such as waterhammer and EPANET programs [2–4]. Analysis of pipeline age is one of the most intriguing facts and was well discussed in a previous study [5].

The state WB includes three distinctive regions concerning water resources—Eastern Bhagirathi, Western Rarh, and North Bengal. The basins in northern Bengal contain 63% of the state's water resources while Rarh and the eastern plains carry 22% and 15%, respectively. Depending on urban water supply, WB has been segregated into two distinct regions—the Metropolitan Area of Kolkata (KMA) and the non-metropolitan area (non-KMA). This KMA area has 41 urban entities (three numbers of municipal corporations counting Kolkata Municipal Corporation along with 38 other municipalities) among 127 in the WB, the remaining municipalities being under non-KMA area. Necessary supply of water in urban municipalities like KMA area is accounted for by Kolkata Metropolitan Development Authority, whereas the department of public health engineering (PHED) takes care of water supply in non-KMA area until shortly before the decentralization of power to the area. After the amendment of the 74th constitution in 1992 and financial programs like Jawaharlal Nehru National Urban Renewal Mission (JNNURM) from the central government, the gradual adoption has taken place in local government. According to JNNURM's report from WB, the burden of operating and repairing water and sanitation needs has been transferred to 88 of the 127 urban local entities (ULE). And other ULEs such as the Nabadiganta Industrial Township Authority with mainly industrial buyers and retailers in the IT industry have entered into programs with independent players to stop and maintain water and sanitation. The KMA covers 185 km<sup>2</sup> areas with a population density of 24,306 persons per km<sup>2</sup> as per the 2011 Census [6]. It turned out that higher than 60% of the losses occurred in the pipes and valves network. Therefore, understanding the fundamentals of hydraulic engineering is important [7, 8]. Water in the KMA area is derived from two sources—the Hooghly River, the only source of surface water, and the rest is found in groundwater. The portable water from the river is supplied by pipelines to the KMA boundary area, many areas depending on the source water from the deep tube springs connected to the network of ponds and pipelines as addressed in the development plan for Kolkata City. If measurement approaches are thoroughly taken up in water supply systems, then the mobility found in most openings will be significantly high. Previously conducted several transient analyses address transient behavior of the concerned raw water pipelines involved

in water supply [9, 10]. The discussion has been made about the control of open and closed-loop pressure to reduce pipe leaks [11, 12].

An appendix to the state of water supply in the province is presented in Table 1. Water demand was analyzed of Public Water Supply in Municipalities using pipeline modeling for providing effective scheduling, expansion, and process of water delivery and distribution networking is one of the priorities of urban infrastructure [13]. The reliability and adaptability of various pipeline modeling have also been tested [14]. There is a growing shortage of water demand in the WB state. So, it is meaningful for examining the long-term efficiencies of involved water supply systems in the WB state. Another appealing point to note is that only 56% of the population is provided with surface water, the rest relying on fast-flowing groundwater resources. And, according to access, only 53% of people have access to water inside their buildings. Therefore, depending on the necessity of groundwater resources there is an additional impact on issues of health in WB state. Details of the need for water and service delivery in WB are shown for 2000, 2011, and 2025 in Table 1. It reflects that the water service deficit will be 11% more from 2011 to 2025. In line with the objectives set out under “VISION 2020,” PHED aims to meet the requirements of “VISION 2020,” a piped-supplied water supply system, which provides adequate and sufficient drinking water in blocks affected by arsenic contamination of great importance. The current paid project looks at end-to-end family metering solutions regularly for each home in rural areas, with access to bulk water at national levels limited to urban renewal facilities.

The distribution systems were designed according to the district metering area (DMA), reached a high level of housing including community and government institutions (Anganwadis, schools, etc.) are filled with district metering devices and domestic metering devices, and subsequently integrated by supervisory control arrangement along with data acquisition technique named SCADA. The mass water supply networks are linked to a grid-type supply system where possible.

To carry out this study, a line network diagram has been drawn with the necessary input to operate the system and obtain outputs like pressure head, flow, velocity, hydraulic grade, and losses. Today many water simulation software programs are available to carry out the hydraulic flow study. For this purpose, EPANET and WaterGEMS software programs have been used to get the desired output with simulation. After getting output, both the software results have been compared with various parameters to show the merits and limitations of both the systems and to understand how the system can be optimized economically.

**Table 1** Need for water and service delivery in West Bengal

| Year | Water requirement (hectare meter $\times 10^6$ ) | Deficit (in %) |
|------|--|----------------|
| 2000 | 10.85  | 38             |
| 2011 | 13.02  | 48             |
| 2025 | 16.60  | 59             |

The objectives of the study are to analyze the network of secondary rising mains of Bhangar 2 block under PHED of West Bengal. This study was carried out in the following parts:

- i. To draw a network in EPANET and WaterGEMS softwares as per collected data from PHED.
- ii. To carry a simulation to optimize the system.
- iii. To determine the desired flow, velocity, head losses, and requirement of valves in an optimized way.
- iv. To compare the hydraulic outcomes obtained through EPANET and WaterGEMS software simulations and validate the obtained outcomes with field data, if available plus to the outcomes whether these are following CPHEEO manual guidelines.

## 2 Study Area

### 2.1 Piped Water Supply Scheme Detail

The proposed surface-based piped water supply scheme (PWSS) for the Haroa blocks and Rajarhat blocks of North 24-Parganas and Bhangar 2 of South 24-Parganas was thought-about to mitigate the arsenic-related health issues. The PWSS was considered with Hooghly River as the source, with a total ultimate design capacity of 66 MLD, to serve the three blocks.

Treated water is proposed to be pumped to block-level ground-level storage reservoirs, from where the treated water through rising pipes is pumped for respective overhead storage tanks, for further distribution. A plan showing the proposed command area of the three blocks (of Haroa, Rajarhat, and Bhangar 2) is shown in Fig. 1.

The total area covered under the PWSS is nearly 347.70 sq. km, covering 728 habitations (and a population of 525,644, as per Census 2011) in 170 villages. The total ultimate design population was calculated at 806,588 for the year 2046. The estimated cost of the PWSS for the Haroa, Rajarhat, and Bhangar 2 blocks was Rs. 686.93 crores.

The name of the piped water supply scheme is integrated surface-based PWSS for arsenic affected areas of Haroa, Rajarhat, Barasat 2 in North 24-Parganas and Bhangar 2, 1 block in South 24-Parganas West Bengal. It covers Haroa, Rajarhat, Barasat 2 of North 24-Parganas, and Bhangar 1, Bhangar 2 blocks of South 24-Parganas district. Details of this scheme have been given in Table 2. The base year for this design was 2016, and the intermediate design year of the design was considered 2031. The ultimate design year was taken in 2046. With 70 lpcd water demand, the plant gross water demands for the years 2016, 2031, and 2046 were considered 99.4 MLD, 120.7 MLD, and 145.0 MLD, respectively. The availability of three-phase electricity for 24 h (substation proposed at the water treatment plant (WTP) and all the ground-level reservoir (GLR) cum booster pumping station (PS) was confirmed.

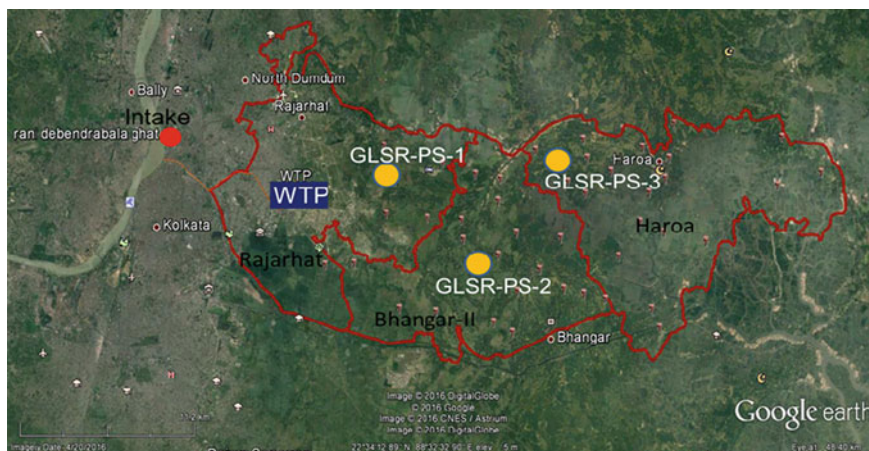


**Fig. 1** Proposed PWSS for Haroa, Rajarhat, and Bhangar 2 blocks

**Table 2** Blockwise detail of villages, habitations, and population under the concerned PWSS

| Description  | Details    |         |            |            |
|--|------------|---------|------------|------------|
|  | block      | Village | Habitation | Population |
| Population of villages/habitations (covered under PWSS)<br>(Village list is as per district Census handbook) | Haroa      | 8       | 110        | 214,401    |
|  | Rajarhat   | 6       | 43         | 189,893    |
|  | Bhangar 2  | 10      | 60         | 246,708    |
|  | Barasat 2  | 6       | 69         | 171,250    |
|  | Bhangar 1  | 5       | 47         | 142,568    |
|  | Total      | 35      | 329        | 964,820    |
| Groundwater contaminant  | Arsenic    |         |            |            |
| Groundwater affected by arsenic in village/habitation/population   | Block name | Village | Habitation | Population |
|  | Haroa      | 110     | 112        | 96,485     |
|  | Rajarhat   | 43      | 99         | 95,488     |
|  | Bhangar 2  | 60      | 104        | 92,146     |
|  | Barasat 2  | 69      | 78         | 76,673     |
|  | Bhangar 1  | 47      | 33         | 35,361     |
|  | Total      | 329     | 426        | 396,153    |

The proposed source of raw water is River Hooghly near Debednrabala Ghat. Three numbers (two working and one standby) of intake raw water pumps are already installed to serve the purpose. The raw water pumping main was proposed to design with spirally welded mild steel pipe conforming to IS 3589: 2000 with 10,500 m length of pipe; 1829 mm pipe outer diameter and 10 mm thickness. The proposed capacity of the WTP is 100 MLD. Materials for primary transmission mains from

WTP to PS and primary transmission mains; from boosting PS to block-level GLR cum PS were DI (ductile iron) pipe conforming to IS:8329:2000 for pipe diameters 1000 mm and below with length of pipe 65 km and 600 mm to 1000 mm diameter, respectively.

Total five numbers of GLRs taking one in each block were considered. The capacities of such reservoirs are 3200 m<sup>3</sup> for Haroa, 1000 m<sup>3</sup> for Rajarhat; 4100 m<sup>3</sup> for Bhangar 2, 2400 m<sup>3</sup> for Barasat 2; and 3200 m<sup>3</sup> for Bhangar 1. Total 80 numbers of overhead storage reservoirs have been employed with staging height—20 m, capacity varying from 250 100 kl to 1000 kl. The material for secondary transmission mains—from block-level GLR via PS to overhead storage reservoirs are DI pipe conforming to IS 8329: 2000 with a length of pipe 199 km and diameter 150–700 mm.

The water supply distribution network is consisted of DI pipe material having diameter of 250 mm and above, high-density polyethylene (HDPE) pipes of diameter 200 mm and below with a total length of 1767.99 km. Rs 3510 for HH (household) service connection (15 mm) was set to charge for consumer water per family whereas Rs 4200 was set for commercial connection (20 mm) as connection line cost per entity also explained in Table 2.

## 2.2 Location of the Study Area

Consolidated CD block of Bhangar 1 is attached to the CD block of Bhangar 2 in the northern side, Minakhan block under North 24-Parganas in the eastern region, block Canning 2 in the southern side, and the block Sonarpur in the western side. A schematic diagram showing the water distribution for the scheme location of the Bhangar 2 block is shown in Fig. 2.

The analysis shown in this paper is mainly focused on the highlighted red portion in Fig. 2, i.e., conveyance of water from Bhangar 2 GLR to 18 elevated storage reservoirs (ESRs). In this study, the pipe length is considered based on ESR locations. The ESR locations were fixed concerning land availability. A total pipe length of 178 km has been considered in the hydraulic design analysis of clear water rising main from Bhangar 2 GLR to 18 ESRs.

The River Hooghly, which is a perennial river, is the source of raw water. The intake is also constructed near Debendrabala Ghat (Fig. 3), for supplying 500 MLD to the WTP complex, owned by WB Housing Infrastructure Development Corporation (WBHIDCO), jointly maintained by State Government and PHED.

## 3 Methodology

Throughout the whole layout—hydraulic modeling is done by the following process. First, the reservoir location was fixed and drawn then associated pumps were drawn. The intermediate connecting links such as main pipes, branch pipes, and valves were

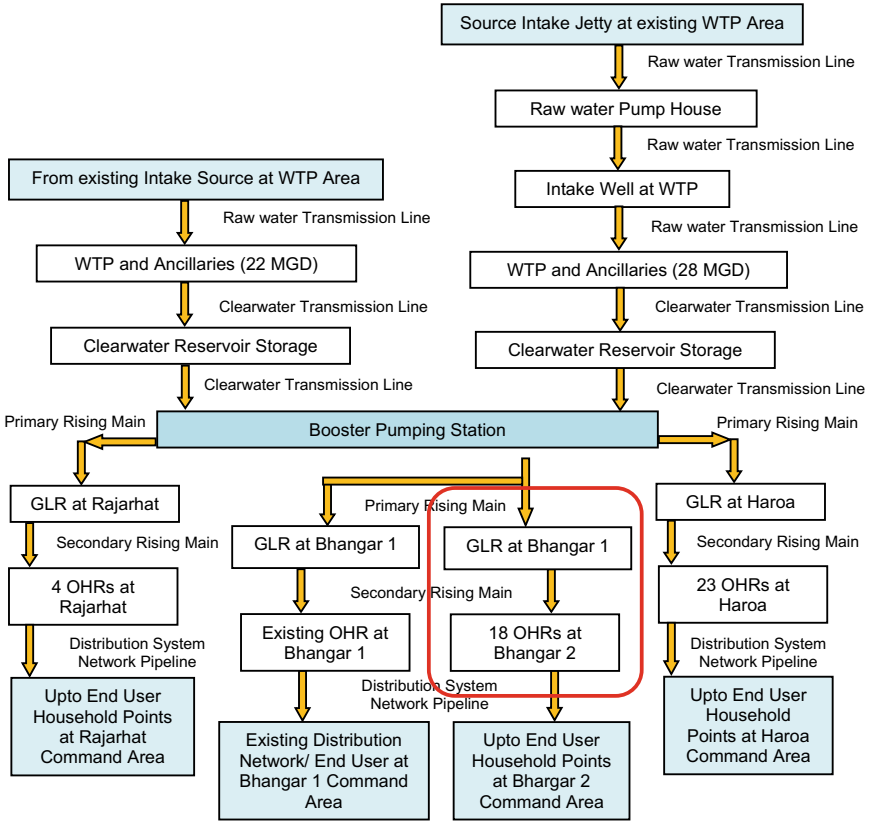


Fig. 2 Schematic diagram of the PWSS network

Fig. 3 Intake location at Debendrabala Ghat





drawn to connect the pumps to the reservoir using the toolbar next to the software drawing window. Then the tanks (headworks or elevated storage reservoirs in real) were drawn, and connecting pipes and valves were connected along with intermediate junctions to the pumps. By selecting the reservoirs, values of elevation were entered. Same input has been given to the intermediate nodes. By selecting the pumps, the values of flow rate, power were entered. By selecting all the main pipes and branch pipes, the values of pipe lengths, diameters, and roughness coefficients have been included. By selecting the required valves, the critical parameters of the valves like their diameter, type, and settings were included and adjusted.

By selecting the tanks, the values of elevation, minimum elevation, initial elevation, maximum elevation, tank volume, and tank diameter were included. After the entire network model was completed, the operation of the network was performed with results like pressure, the hydraulic grade lines in concerned junctions and unit headloss, inflow velocity, flow discharge in the pipes were inspected and saved.

By analyzing, a few software considerations were made. The liquid under concern is said to be homogeneous. The elasticity property of the concerned liquid and material of pipelines is assumed to follow a linear model. Here the concerned flow is set one-dimensional, and moving fluid is incompressible. The software by default uses mean velocity. Due to the rareness of data for valves like their setting-related parameters at the distributing end—the system is modeled devoid of valves. The pipe elevations in many areas were unknown so these were interpolated.

With the exception, a few more details have been taken under consideration. All the pipes were taken as new pipes having the same roughness coefficient as 140 and a maximum amount of pipe material as DI. The average temperature of internal liquid was assumed to be 20 °C. The pump data for giving input are being rated data devoid of having important pump curves. Water quality parameters simulation for these networks using both EPANET and WaterGEMS software programs was outside the scope of the current study.

## 4 Result and Discussions

Both EPANET and WaterGEMS software are used for pipe network analysis. In both the system, three hours simulation has been done to ensure the filling of all the water tanks. Here a rising main network of Bhangar 2 boosting station has been analyzed to compare the results of the software also. During the present study, various data were assumed as per normal design aspects and desired output in view of the demand. Some valves had to be provided to analyze the network with the desired output which was not provided in our collected data. Figures 4 and 5 reveal the variation of hydraulic head and pressure head with time for both EPANET and WaterGEMS software programs, respectively.

For a clearer view, Node 10 (nearest node to delivery pumps near GLR Bhangar 2) and Node 60 (farthest node from delivery pumps near 18 ESRs) had been considered for analysis. This selection had been considered purposely so that the total pipeline

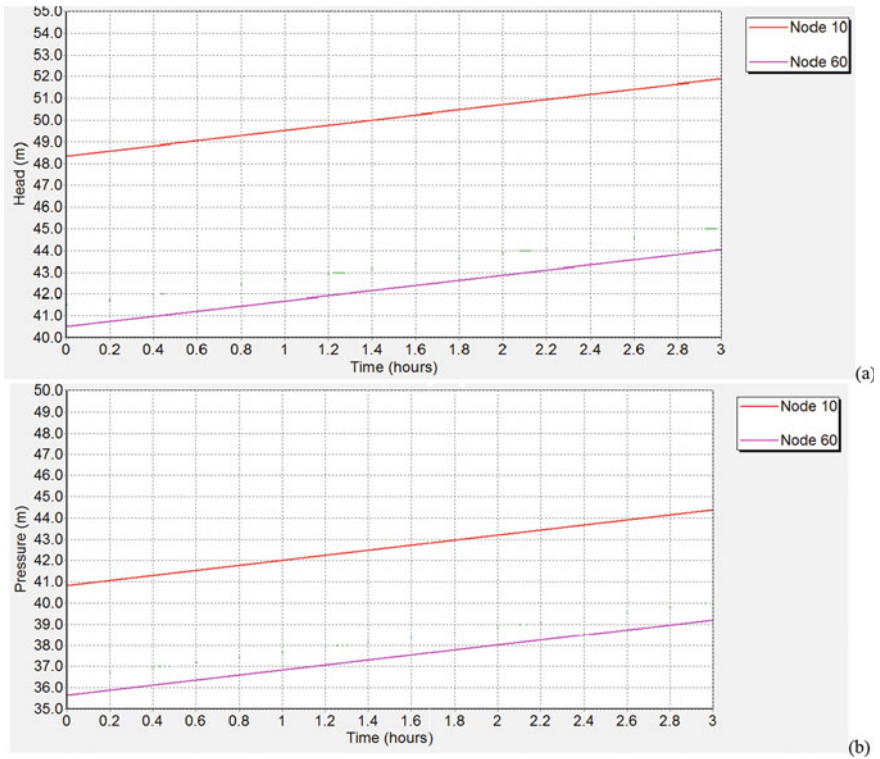


**Fig. 4** Time variation of hydraulic parameters in EPANET for node 10 and 60 **a** Hydraulic grade; **b** Pressure head

hydraulics can be considered by the way. Hydraulic grade and pressures are the important criteria to decide about the conveyance of waters from the pumping station to the ESRs. Henceforth the comparative study of softwares on the said parameters would be an important call for the designer or management about which software to choose.

Both EPANET and WaterGEMS software programs are used for pipe network analysis. In both the system, three hours simulation has been done to ensure the filling of all the water tanks since the main motto of the secondary main is to convey the water from GLR Bhangar to 18 ESRs to be filled up. The analysis can be only hoped to be completed when the tanks are filled which also serves as a justification of the duration of the analysis. Here a rising main network of Bhangar 2 boosting station has been analyzed to compare the results of both the software also. During the present study, various data were assumed as per normal design aspects and desired output in view of the demand. Some valves had to be provided after properly designed to analyze the network with the desired output which was not provided in the collected data.

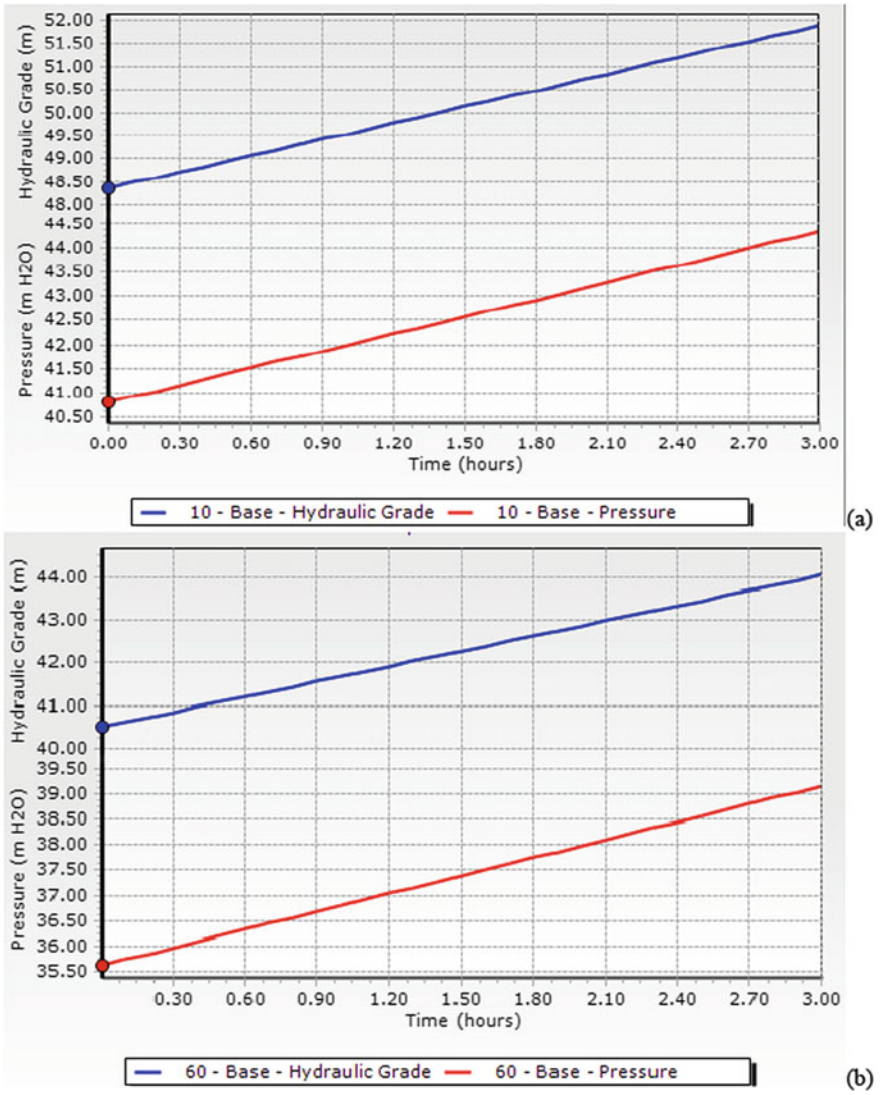


**Fig. 5** Variation of hydraulic parameters in WaterGEMS with time for node 10 and 60 **a** Hydraulic grade; **b** Pressure head

A separate hydraulic analysis simulation for three hours duration was done, and hydraulic parameters such as pressure and unit headloss gradient are viewed. From Fig. 6, it can be observed that roughly pressure higher than 40 m is within 20% time and below 40 m in the 80% time in the network. The pressure 25–40 m is obtained 10 to 80% time, whereas pressure more than 10 m was observed 98.5% time.

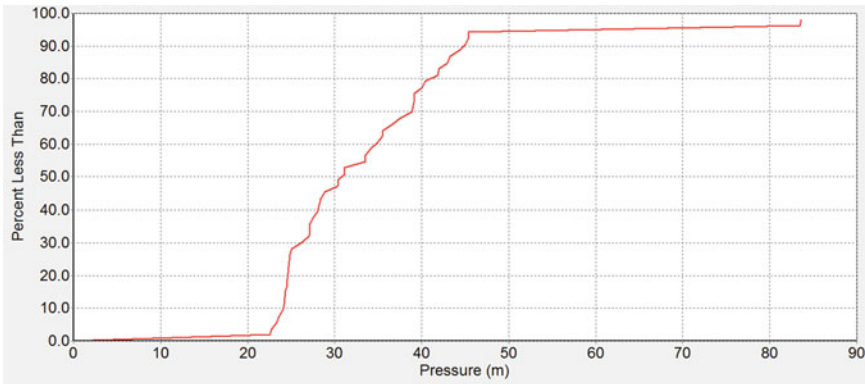


**Fig. 6** Distribution of pressure at 3:00 h

After three hours of simulation from the subsequent observations on headloss following Fig. 7, it can be easily configured that chances of more than 3 m/km unit headloss are only 10%. The maximum observed headloss is 16.6 m/km. The headloss below 2 m/km and 1 m/km was found in 63% and 20% pipelines, respectively.

Henceforth when the headloss gradient is under normal range for the PWSS water network considered hereafter for such network, whichever software is used—the accuracy and similarity of results are high. To justify the above losses in the pipeline, simulation results were compared in both EPANET and WaterGEMS software programs. For a detailed understanding of the above analysis in the network, the selected nodes, i.e., starting from Bhangar GLR to 18 ESRs, are shown in Fig. 8. In the figure, it is clearly shown that the drinking water is routed from Bhangar 2 GLR through a combination of three pumps to 18 ESR located at various water command areas.

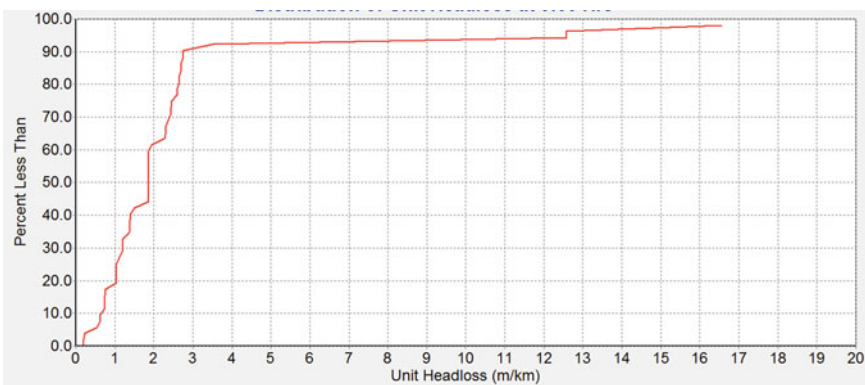


**Fig. 7** Distribution of unit headloss at 3:00 h

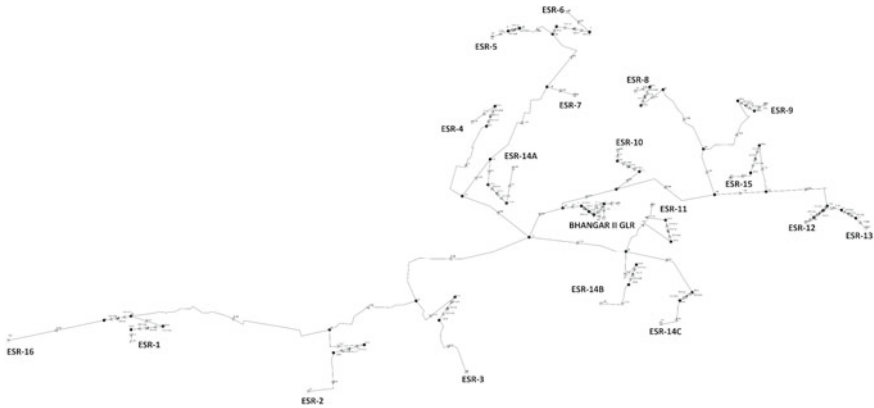


Fig. 8 Pipe network for the clearwater rising mains from Bhangar 2 GLR to 18 ESRs

### 5 Comparison of Losses

The hydraulic analysis was carried out on two softwares EPANET and WaterGEMS. The percentages of losses were compared for analysis in both above-mentioned softwares. The percentage of losses was computed from the hydraulic results as per Eq. (1)

$$\text{Percentage of losses} = \frac{\sum (\text{Unit headloss} \times \text{length of the pipe})}{\sum \text{length of the pipe}} \times 100 \quad (1)$$

$$\text{Percentage of losses in EPANET system} = \frac{112.729 \text{ (m)}}{61270 \text{ (m)}} \times 100 = 0.18398\%$$

$$\text{Percentage of losses in WaterGEMS system} = \frac{112.811 \text{ (m)}}{61330 \text{ (m)}} \times 100 = 0.18394\%$$

From the computed percentage of losses for both softwares, it is observed that the variation is negligible. In the matter of user-friendly, the WaterGEMS software prevails over EPANET software since in the former software accurate length can be fed in which designing of small, short piece pipes also which are joining valves and pumps.

### 6 Conclusions

A comparative study revealed that both softwares can be parallelly used in the simulation of a water supply network system. Various extra features like annotation, prototypes, navigator, and active topology are available in WaterGEMS. Both the

softwares are user-friendly but EPANET has the lesser layout tools and options than WaterGEMS. The WaterGEMS occupies more space in the central processing unit (CPU) but EPANET needs less space in the CPU to analyze a network. The WaterGEMS can consider the value of the length of the pipe of the valve and pump on both sides. So, it can provide a more accurate output of a pipeline network, whereas in the EPANET platform, there is no provision to provide the length of pipe of the pump on both sides.

For the clearwater network, the difference between the calculated percentage of head losses using EPANET and WaterGEMS has been found to only 0.021% which is nearly negligible. In WaterGEMS, the differences between hydraulic grade line and pressure line are not the elevation of the point because it calculates some losses also in the pipe but in EPANET, the elevation of a junction is the difference between hydraulic grade line and pressure line. Although having such differences in both the system, after analyzing the losses it can easily justify that there is less variation in both the software. WaterGEMS can give more detailed results than EPANET. Moreover, in WaterGEMS there are options for selecting the water temperature, detailed material characteristics that directly affect the results, and the percentage of headloss between WaterGEMS and other software like EPANET. As because of having marginally better accuracy in WaterGEMS, nowadays it has become more popular software in water supply network analysis in every stage of academics and industry.

**Acknowledgements** The authors heartily thank PHED, GoWB for their esteemed support by providing the data for the research study. The master's thesis work of Sri Prasun Das helped in a great way to reflect the research work.

## References

1. Government Website: [https://censusindia.gov.in/2011-prov-results/prov\\_data\\_products\\_wb.html](https://censusindia.gov.in/2011-prov-results/prov_data_products_wb.html)
2. Das S, Mukherjee B, Mazumdar A (2013) Analysis of hammer head at increased flow demand in pipe networks: A case study. *Int Rev Mech Eng* 7(4):757–766
3. Mukherjee B, Kuila A, Das S (2019) Optimized hydraulic design of a water distribution network at West Medinipur in West Bengal: A case study. *J Assoc Eng India* 89:19–32
4. Mukherjee B, Das S, Mazumdar A (2015) Transient analysis of a pipeline network for drinking purpose in Assam, India. *J Inst Public Health Eng* 2014-2015(4):26–32
5. Koppel T, Vassiljev A (2009) Calibration of a model of an operational water distribution system containing pipes of different age. *Adv Eng Soft* 40:659–664
6. Census of India 2011, West Bengal. District Census Handbook, Kolkata. 20(XII B):26
7. Mukherjee B, Das S, Maity S (2020) Optimum process of pipeline selection in water distribution network: Case study. *Appl Mech Materials Civ, Arch, Struct Constr Eng III* 897:137–141
8. Das S, Mukherjee B, Mazumdar A (2018) Comparison of outcomes through EPANET and LOOP softwares using a gravity flow water supply network at East Medinipur in West Bengal. *J Indian Chem Soc* 95(3):313–324
9. Mukherjee B, Das S, Mazumdar A (2017) Simulation of composite pipedwater supply by EPANET and LOOP softwares: A case study. *J Inst Public Health Eng India* 45:44–54

10. Mukherjee B, Das S, Mazumdar A (2015) Transient analysis of a pipeline network for drinking purpose in Assam, India. *J Inst Public Health Eng India* 2014–15:26–32
11. Ulanicki B, Bounds PLM, Rance JP, Reynolds L (2000) Open and closed loop pressure control for leakage reduction. *J. Urban Water.* 2:105–114
12. Mukherjee P, Das M, Mukherjee B, Das S (2020) Optimization of irrigation design technique for pumping units through software simulation analysis for varied landscapes. *IOP Conf Ser: Earth Environ Sci* 505:012025
13. Arunkumar M, Nethaji MVE (2011) Water demand analysis of municipal water supply using EPANET software. *Int J Appl Bioeng* 5:9–19
14. Chandramouli S, Malleswararao P (2011) Reliability based optimal design of a water distribution network for municipal water supply. *Int J Eng Tech* 3:13–19

# A Conceptual Approach toward Water Management with Aquaponics



Sana Kaja, Rajasekar Veeramani, and Mohammad Tanveer

**Abstract** Increasing population and urban areas expedite the depletion of water resources at an unsustainable rate and the urban regions are demanding more resources. The realization of imminent water crisis with the exploitation of resources has paved way for the consent of community toward environmentally sustainable techniques in urban water management. Water, being a critically inevitable resource for agriculture, needs to be managed effectively. Globally, aquaculture is recognized as an essential source for proteinaceous food production in animal food production sector to meet the food demand. However, nutrient pollution caused by aquacultural effluent let into rivers lead to amplified growth of certain phytoplankton as a consequence declines the water quality. As freshwater availability is limited, complete utilization of water, i.e., doing more with less, is necessary to ensure resources for the future. To resolve this, ‘Aquaponics’ an efficient technique that ensures a maximum reuse of water. Aquaponics integrates ecological cycles by combining fish culture with plant culture and proves to be advantageous in water scarce areas. The essence of aquaponics is recirculating water, which can be exercised for urban strategies. In this paper, media-based aquaponics system is designed due to its availability of significant surface area for microbial activity than floating raft and nutrient film technique. This paper manifests the likelihood of water management buttoned by aquaponics in food production. The conclusions are applicable, sustainable and significantly water saving.

**Keywords** Water management · Aquaponics · Sustainability · Dissolved solids · Food production

---

S. Kaja (✉)

Fisheries Engineering, College of Fisheries Engineering, TNJFU, Nagapattinam, India

R. Veeramani · M. Tanveer

Department of Aquacultural Engineering, College of Fisheries Engineering, TNJFU, Nagapattinam, India

e-mail: [mohammadtanveer@tnfu.ac.in](mailto:mohammadtanveer@tnfu.ac.in)



## 1 Introduction

The concept of sustainable cities has prime objective of driving cities greener and healthier for humans with sustainability engaging economic viability, social solidity and wise use of natural assets [10]. Vlachos and Braga [23] insisted that cities of both developing and developed countries need urgent decisions concerning the methods in urban water management. S. Postel [15] pondered that in industrial countries, with adequate living standards renewable supply of water must be at least 2000 m<sup>3</sup> per year. In acquiring the maximum water management, different facets of the urban water system should be considered in orienting urban toward sustainability. Retreatment and reuse from the agricultural and industrial effluent are the best solution to conserve water. Water management in agriculture and aquaculture should be coordinated as water is a critically inevitable resource for both [13]. Growing population and food demand necessitate the understanding of crop water management in irrigation. Water sustainability in agriculture can be achieved only through appropriate management practices [16]. There is a rise in the consumption of fish and meat, increasing the benefits of income for industrial livestock production. However, it creates more pressure on water [13]. Planned reuse of water and resource recovery is the befitting course of action to administer the necessities of this age. Currently, water resource management is undergoing participatory and combined managerial approach. Effluent from both agriculture and aquaculture are generated in larger amount and the treatment of it costs high hence to resolve this aquaponics is the best strategy to retreat and reuse the effluent. Aquaponics is a vivacious relationship between the fishes, the plants and the bacteria with its aquatic environment [8].

It is the symbiotic cultivation of fishes and plants in a recirculating water system. Plant bed media acts as biofilter which is a means of filtration, facilitated by nitrogen cycle. Aquaponics averts the outflow of aquacultural effluent [22]. Visions for building-based food production in urban areas of temperate regions are emerging [2]. Utilization of terrace area provides space for farming activities in urban regions with limited space. This eco-friendly technique can be adopted in the urban areas with minimal water requirement and at the same time it generates considerable profit. In this research aquaponics system is designed in a small scale which can be operated in the urban terrace for the efficient management of water in urban areas. Among the different types of aquaponics systems, media-based aquaponics system was selected based on its flexibility and sustainability. The developed design was applicable for a MIG (Middle Income Group) and HIG (High Income Group) category folks.

## 2 Condition of Urban Waters and Water Reuse Potency

Unpredictable climate change threatens water security and food security [5]. Disruptions in availability and timing of water flow in inland capture fisheries due to climate change, directly or indirectly affect fisheries productivity and transitional shift of

domestic stakeholders from capture fisheries to culture fisheries can be seen [21]. The demand for culture fisheries exist in society with concern for marine pollution. In most cases, the effluent water is not treated properly and when it is let into water bodies they affect the good quality water by nutrient pollution. Secondly, the non-point sources of pollution such as pesticide runoff from agriculture affect water bodies including groundwater. These effluents need intense water treatments which are expensive and complex [1]. Due to this high expense only few farmers treat the water before discharging into the water bodies. Larsen and Gujer [9] insisted that utilization of resources in an efficient manner would create a minimal increase of entropy which leads to an active approach instead of reactive treatment. To counter these issues aquaponics technique can be adopted, which is the combination of plants and fish culture. Here the effluent from fish culture serves as a nutrient source for plant growth where the plant roots acts as a filter in absorbing the feed and fish waste, hence the water is well treated and reused. In this technique pesticides are not used as it affects the fish growth and it also eliminates the agriculture runoff.

### 3 Aquaponics System

The combination of aquaculture and hydroponics is known as aquaponics, in which both the plant and fish species can be cultured at the same time [24]. It is a soilless agriculture system. Nutrients required for plant growth was provided by fish feed and its waste [14]. In the aquaponics system water, energy and fish feed are the three main physical inputs in any type of production system of different sized animals [11]. According to FAO [6], among the three general types of aquaponics systems (media filled bed system, floating raft and nutrient film technique) media filled bed system is majorly successful in growing plants, like tomato, chili, ladies finger, beans, etc. as the plant growing media is fixed and bear the weight of these plants on it. There is no requirement of a separate biofiltration system in this technique. Hence, the cost of operation can also be minimized.

Water quality parameters are essential for fish growth and survival. The change in water quality parameters affects the plant and fish growth, feed efficiency, leading to pathological changes and even mortality under extreme conditions. Water quality monitoring is substantially less for an aquaponics system than a hydroponic or recirculating aquaculture system [18]. Fish reared in aquaponic systems require good quality water in terms of dissolved oxygen, temperature, ammonia, nitrate, nitrite, alkalinity and pH within permissible species-specific limits. Indeed, tilapia became a versatile species for aquaponics systems, which is now practiced in most developed countries worldwide [17].

## 4 Proposed Methodology

The proposed model was designed to address the MIG (Middle Income Group) and HIG (High Income Group) category allotted space by the Tamil Nadu Housing Board, which is an individual house of 1250 ft<sup>2</sup> area. Tamil Nadu Housing Board is one of the most prominent institutions in India catering to the shelter needs of various income groups of the society. To effectively utilize the area, plant bed (25 m<sup>2</sup>) was mounted on the terrace and the fish culture tank (9.6 m<sup>3</sup>) at the backyard. The ratio of fish culture unit to plant culture unit was taken as 1:2 [19]. The following components are needed for the construction of an aquaponics system in an individual house of 50 feet × 25 feet area (Table 1, Figs. 1 and 2).

The brick masonry fish culture tank of dimension 5 m × 1.7 m × 2.25 m was chosen. The inner thickness of fish culture tank was kept as 0.25 m. The effective volume of the tank was 9.6 m<sup>3</sup> excluding freeboard. Bird fencing can be provided at the top of any issue encountered by birds. The provision of steps outside the fish culture tank at the height of 1.2 m facilitates harvest. To tackle uncertain weather conditions, a setup of Polyurethane Sandwich PUF Panel of dimension 5 m × 1.7 m should be arranged separately. The slope of 1:100 was provided at the bottom of the tank. Two rectangular FRP tanks were mounted at an area of 25 m<sup>2</sup> in the terrace, each of dimensions 5 × 2 × 0.8 m<sup>3</sup>, thickness of 0.05 m and had a surface area of 10 m<sup>2</sup>. The spacing of 0.7 m was provided between the plant beds, which helps to operate freely and maintain the system effectively. The FRP plant culture bed has greater impact resistance and elasticity with adequate thermal insulation. The outlet of the plant bed should be organized according to the slope of the terrace so that gravitational flow of the treated return water is possible. Media provides support and surface area for plant growth, promotes bacterial growth for nitrification, aerates the roots by voids and purifies the effluent water. The selection of media was based on the diameter, specific surface area, cost, availability and weight per unit volume. Commonly available, any small media like river sand, crushed stones, granite grit and fine gravels can be used as a media for plant growth, recommending particle sizing

**Table 1** Components of an integrated aquaponics system

| Items   | Description            |
|---|------------------------|
| Rectangular Fiber Reinforced Plastic tank - Plant culture | 5 m × 1.7 m × 112.25 m |
| Rectangular brick cement tank- Fish culture               | 5 m × 4 m × 10.8 m     |
| Submersible pump  | 15–20 m head           |
| Pipelines–0.75"   | 30 m                   |
| Elbow 90°–0.75"   | 13 Nos                 |
| Elbow 45°–0.75"   | 1 No                   |
| Tee joint–0.75"   | 8 Nos                  |
| Control valve–0.75"                                       | 3 Nos                  |

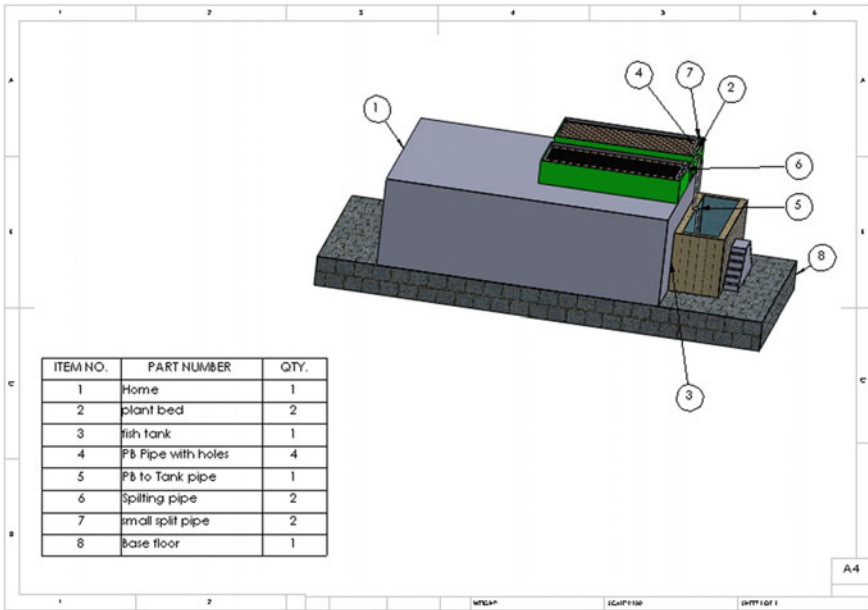


**Fig. 1** Three-dimensional view of the aquaponics integrated individual house of MIG and HIG category

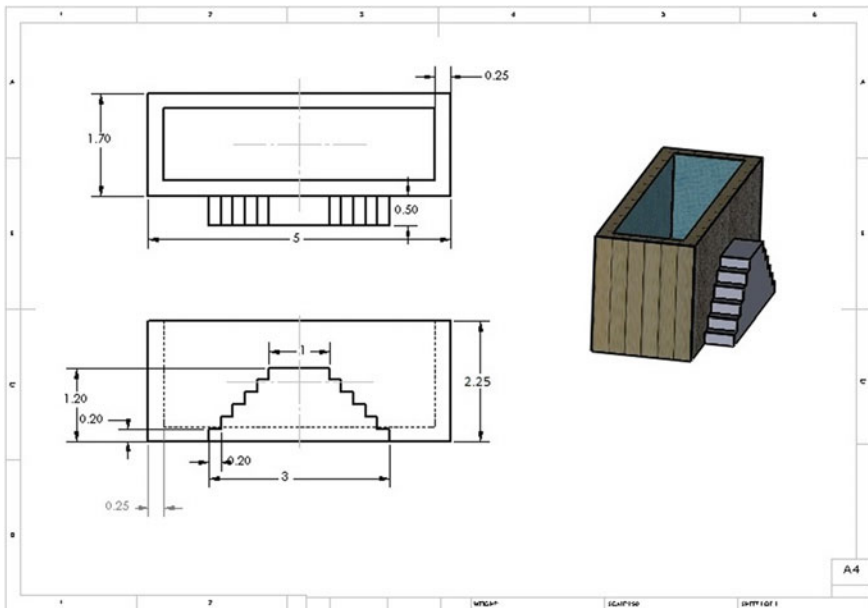


**Fig. 2** Proposed dimensions of fish culture tank for MIG and HIG category

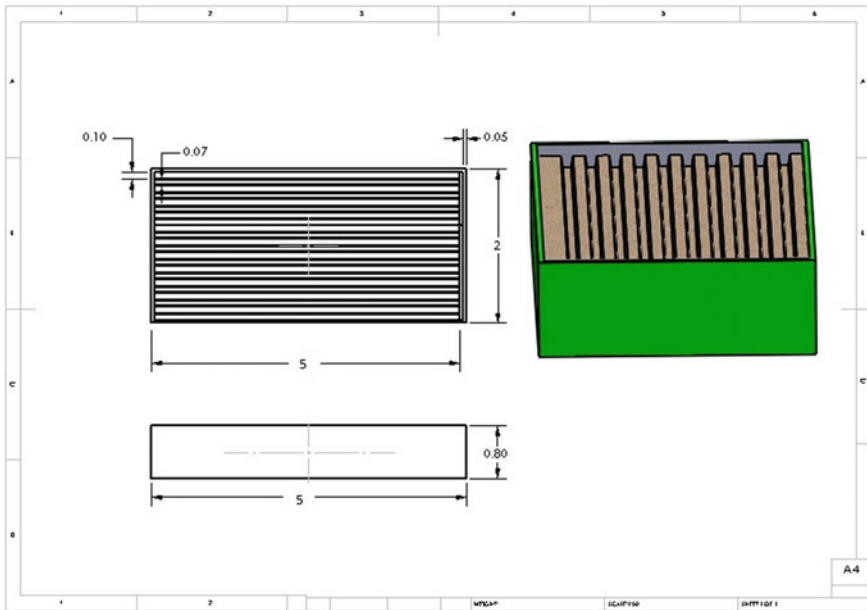


**Fig. 3** Proposed dimensions of terrace plant culture area for MIG and HIG category

ranging from 2 to 4 mm was highly preferable. Large sized media provides more voids space comparatively which do not retain the water for longer periods. Before using the media, it must be well washed and rinsed to remove unnecessary contaminants into the closed-loop system. Ridges and furrows are critical consideration in plant bed, and generally, it is based on the plant species. Here is an assumption made that for lightweight plants, the roots are too small; hence the dimensions of ridges (10 no's for 2 m) be 0.05 m height, 0.05 m crest. For medium weight plants, the roots are a little deeper and hence the dimensions of ridges (6 nos for 2 m) be 0.1 m height, 0.05 m crest (Fig. 3).

The submersible pump is suitable for pumping effluent and the main advantage of this type of pump is that it prevents pump cavitation. V Guard 0.5 HP, Open well Submersible Pump, was chosen for this design based on market availability. The head requirement is 15m and discharge 85–150 lpm and economically best. The inlet and outlet pipelines are fitted with control valves of their respective size to control the recirculating flow rate and retention period respectively. For the design, 13 number of Elbow 90° and One Elbow 45° is assumed. Elbow at 45° is considered for the particular purpose that it makes the water delivers in a fall manner to the plant bed hence even distribution of water is achieved. A 1m length pipe delivered it (4 no's) which was holed with the spacing of 0.1m (9 holes) at 0.015m diameter. Fishes can be chosen based on consumer preference. The tolerance capacity and stocking density suggesting hardy fishes like Carps, Tilapia and Catfish should be analyzed. Fishes like seabass, common carp, silver perch, trout, cod and other ornamental fishes can

also be cultured. The concentration of dissolved oxygen less than 2 mg/L retard the growth of nitrifying bacteria and thereby decreases the nitrification rate in nitrifying filters [12]. The optimum range of pH for nitrification can generally be between 7.0 and 9.0 [3, 7]. For hardy fishes, the optimum preferred temperature range is 27–30 °C and the preferred feeding rate is 2% of their body weight. The optimum stocking density ranges from 0.5 to 1.0 fish/ft<sup>2</sup> (“Tank Culture of Tilapia”) [20]. Seasonal plants can be chosen based on the need, demand and the available nutrient concentration of cultured water [4]. Most types of veggies, greens, herbs, fruits and flowers can be cultured under the recommended conditions of the specified species. In terms of the floriculture, ratio of fish culture unit to plant culture unit can be increased to 1:3 and 1:4 because floriculture requires only less amount of nutrients since there is no fruiting. Spinach-Fast-growing within 30–35 days. Vegetables like cucumber, snake guards are fast growers, i.e., In a 5 m × 2 m area over the ten ridges, 65 plants can be cultured in a single plant bed. The spacing for each plant can be provided at 0.6m (based on the plant it varies) which makes seven plants in one ridge and six plants in another ridge in an alternate manner, provided over the ridges throughout the area promotes proper growth. For vines trained on a trellis, plant spacing will be reduced to 0.3m so that more plants can be cultured.

## 5 Discussion

With the advent of globalization, the world is becoming urbanized and there is no room for agriculture and aquaculture with space and resources being limited. This emphasizes the need for accretion of agricultural facet into urban water management. Aquaponics is generally carried out in both large and small scales. Large-scale aquaponics demands many other factors like land, water source, and high capital investment but the production will be high. In terms of small-scale aquaponics system, it requires less land, investment and water source and the production is also less. Whereas, in the proposed model, the system is designed on medium scale which yields acceptable profit through vegetation and fishes. Since this model is designed for the home terrace, the land requirement is completely minimized. In urban areas, the economic standards of the community are divided into three, viz. LIG (Low Income Group), MIG (Middle Income Group), HIG (High Income Group). It is been found that this type of aquaponics system is not affordable for LIG (Low Income Group). This design is found to be fruitful and ease of operation for both HIG & MIG category of community compared to the other. Also aquaponics is a sustainable technique to be operated in the urban areas with minimal water requirement. Initiatives with this kind of home terrace aquaponics with polyhouse structure would provide ease of management during the imminent climate change crisis. The participation of the public in this kind of water management enables them to learn the significant aspects of this approach. Collection of data would facilitate planning and monitoring of the system digitally for further advancement.

## 6 Summary

Urban policy makers and the government should recognize the reality that aquaponics helps to achieve the urban water management which makes the cities healthier and promote mixed land use. Agricultural subsidies for infrastructure establishment can be applied judiciously as a means to promote this technique in water management in public and aquaculture industries. Even though this activity is not on a global scale, the local activities aggregates for global sustainability. It is evident from this pandemic situation that apartments with rooftop gardening were able to withstand on self for a certain extend when transportation was closed and every commodities were limited. Therefore, there is an ineluctable predestine for the upcoming generation to reflect and train on water management strategies.

## References

1. Bouwer H (2000) Integrated water management: Emerging issues and challenges. *Agric Water Manag* 45(3):217–228
2. Caplow T (2009) Building integrated agriculture: Philosophy and practice. *Urban Futur* 2030:48–51
3. Chen S, Ling J, Blancheton J-P (2006) Nitrification kinetics of biofilm as affected by water quality factors. *Aquacult Eng* 34(3):179–197
4. Diver S (2006) Aquaponic-integration hydroponic with aquaculture. National Centre of Appropriate Technology. Department of Agriculture's Rural Bussiness Cooperative Service. P.
5. Eastham J, Mpelasoka F, Mainuddin M, Ticehurst C, Dyce P, Hodgson G, Ali R, Kirby M (2008) Mekong river basin water resources assessment: impacts of climate change. Australian Commonwealth Scientific and Research Organization: Water for a Healthy Country National Research Flagship
6. FAO (Food and Agriculture Organization of the United Nations) (2014) The state of world fisheries and aquaculture: Opportunities and challenges. FAO, Rome, Italy.
7. Haug RT, McCarty PL (1972) Nitrification with submerged filters. *J (Water Pollut Control Fed)*, 2086–2102
8. Klinger-Bowen RC, Tamaru CS, Fox BK, McGovern-Hopkins K, Howerton R (2011) Testing your aquaponic system water: A comparison of commercial water chemistry methods. Center for Tropical and Subtropical Aquaculture (CTSA), University of Hawaii, College of Tropical Agriculture and Human Resources
9. Larsen TA, Gujer W (1997) The concept of sustainable urban water management. *Water Sci Technol* 35(9):3–10
10. Leitmann J (1999). *Sustaining cities: Environmental planning and management in urban design*. McGraw-Hill Professional Publishing
11. Love DC, Fry JP, Li X, Hill ES, Genello L, Semmens K, Thompson RE (2015) Commercial aquaponics production and profitability: Findings from an international survey. *Aquaculture* 435:67–74
12. Michaud L, Blancheton J-P, Bruni V, Piedrahita R (2006) Effect of particulate organic carbon on heterotrophic bacterial populations and nitrification efficiency in biological filters. *Aquacult Eng* 34(3):224–233
13. Molden D (2013) *Water for food water for life: A comprehensive assessment of water management in agriculture*. Routledge

14. Nelson RL, Pade JS (2008) Aquaponic food production: Growing fish and vegetables for food and profit
15. Postel S (1992) Last Oasis. Worldwatch Institute, Washington, DC
16. Postel SL (2000) Entering an era of water scarcity: The challenges ahead. *Ecol Appl* 10(4):941–948
17. Salam MA, Jahan N, Hashem S, Rana KMS (2014) Feasibility of tomato production in Aquaponic system using different substrates. *Progress Agric* 25:54–62
18. Sfetcu L, Cristea V, Oprea L (2008) Nutrients dynamic in an aquaponic recirculating system for Sturgeon and Lettuce (*Lactuca Sativa*) production. *Lucr Științifice-Zooteh Și Biotehnol, Univ Științe Agric Și Med VetĂ Banat Timișoara* 41(2):137–143
19. Shete AP, Verma AK, Chadha NK, Prakash C, Chandrakant MH (2015) A comparative study on fish to plant component ratio in recirculating aquaponic system with common carp and mint. *J Environ Biol Sci* 29(2):323–329
20. “Tank Culture of Tilapia” (n.d). Accessed December 4, 2020. <https://thefishsite.com/articles/tank-culture-of-tilapia>.
21. Timmers B (2012) Impacts of climate change and variability on fish value chains in Uganda
22. Verdegem MCJ (2013) Nutrient discharge from aquaculture operations in function of system design and production environment. *Rev Aquac* 5(3):158–171
23. Vlachos E, Braga B (2001) The challenge of urban water management. *frontiers in urban water management: deadlock or hope*. IWA Publishing, London, pp 1–36
24. Zou Y, Zhen Hu, Zhang J, Xie H, Guimbaud C, Fang Y (2016) Effects of PH on nitrogen transformations in media-based Aquaponics. *Biores Technol* 210:81–87



# Water Distribution Network Analysis Using EPANET: A Case Study of Surat City



Nitin Singh Kachhawa and Surendra Borana

**Abstract** The rapid growth of population increases the demand of water supply for domestic, irrigation and industrial purposes. Therefore, optimal utilization and conservation of water are of utmost importance. The supply of water to an increasing population with limited water resources is becoming challenging year by year. To solve this problem, design of new or updating existing water distribution network (WDN) is needed. Thus, such types of problems can be resolved using STANET, LOOP 4.0, EPANET 2.0 and WATERGEMS software. Combined WDN of elevated storage reservoir (ESR)-21 belonging to water distribution system (WDS)-7 is consisting of a newly laid and proposed pipe network situated in west and southwest zone of the Surat City. This combined network is designed corresponding to the population of the year 2044. Analysis of WDN of ESR-21 situated in west and southwest zone of the Surat Municipal Corporation (SMC) is carried out to ascertain that water in sufficient quantity and pressure is delivered to the different consumers in the year 2044, and analysis of this combined WDN is performed for the population of the year 2044 by using EPANET software. Results of EPANET reveal that the pressures, flows and velocities at all pipes are adequate to supply water in complete WDN. The results of this study will be helpful for hydraulic engineers to analyse WDN in a fast manner and will also serve as a decision support tool.

**Keywords** EPANET · Elevated storage reservoir · Water distribution network

## 1 Introduction

For the socio-economic development of a country, water is a key element. For domestic as well as industrial uses, essential infrastructure like water distribution network (WDN) is required. Water distribution system establishes a connection between the consumers and the source of water using the hydraulic components such as valves, tanks, pumps and pipes.

---

N. S. Kachhawa (✉) · S. Borana

Department of Civil Engineering, Sardar Vallabhbhai National Institute of Technology, Surat 395007, India

© The Author(s), under exclusive license to Springer Nature Singapore Pte Ltd. 2022  
C. M. Rao et al. (eds.), *Advanced Modelling and Innovations in Water Resources Engineering*, Lecture Notes in Civil Engineering 176,  
[https://doi.org/10.1007/978-981-16-4629-4\\_24](https://doi.org/10.1007/978-981-16-4629-4_24)

339

Water distribution system can be divided into two parts, i.e. intermittent system and continuous system. In the intermittent system, the water may be supplied for few hours or at regular intervals throughout the day, which results in the development of negative pressure and may result in the deterioration of water quality because of polluted groundwater ingress as compared to the continuous water distribution system. In a continuous system, the system is pressurized continuously and does not allow contaminated water to enter in the water pipelines in the event of small leakages.

WDNs are designed to distribute water from a source in sufficient quantity and at required pressure to the different customers. To resolve any problem, design of new or updating existing WDN is required. Thus, such type of problems can be solved using LOOP 4.0, STANET, EPANET 2.0 and WATERGEMS software.

The program EPANET is developed for the Windows platform and is public domain software. Extended period simulation of the water quality and hydraulic behaviour within pressurized pipe networks can be performed using EPANET.

Combined WDN of ESR-21 belonging to water distribution system (WDS)-7 is consisting of a newly laid and proposed pipe network serving west and southwest zone of the Surat City. This combined network is designed for the population of the year 2044. None of the earlier studies reviewed have performed the analysis of WDN of ESR-21 situated in west and southwest zone of the Surat Municipal Corporation (SMC). So, to ascertain that water in sufficient quantity and pressure is delivered to the different customers in the year 2044, analysis of this combined WDN is performed for the population of the year 2044 by using EPANET software.

The objective of this study is to perform the analysis of combined WDN consisting of a newly laid and proposed pipe network of ESR-21 (WDS-7) for the year 2044 by using EPANET software and to indorse some measures if the present WDN does not fulfil the future demand.

## 2 Study Area

Surat City is located in the state of Gujarat in the western part of India. It is one amongst the most vibrant cities of India with one amongst the fastest growth rate because of migration from different parts of the Gujarat and other states of India. Surat is one amongst the cleanest cities of India and is also known by various other names like “The DIAMOND CITY”, “THE SILK CITY”, and “THE GREEN CITY”. It has the most dynamic present and similarly varied past heritage. The area of the Surat City is 326,515 sq. km. The population of the Surat City in the year 2011 was 4,466,826. Surat City has eight zones. Figure 1 shows the southwest zone of Surat City.

WDN of ESR-21 (WDS-7) is located in west and southwest area of the Surat. The area of WDN of ESR-21 (WDS-7) is 137.87 ha. The population of the area served by WDN of ESR-21 for the years 2014 and 2021 is 15,167 and 24,128, respectively. Demand for WDN of ESR-21 for the years 2014 and 2021 is 2.73 MLD and 4.85



**Fig. 1** Southwest zone of Surat City

MLD, respectively, and this demand will be raised to 11.17 MLD in the year 2044 (Hydraulics Department, SMC, Surat).

### 3 Overview of EPANET Software

US Environmental Protection Agency had developed an application to model water distribution systems named EPANET. The developed application can be used to design size and optimize new water infrastructure, optimize tanks and pump operation, prepare for emergencies, retrofit existing ageing infrastructure, investigate problems of water quality and reducing energy usage. EPANET may also be used to evaluate resilience to natural disasters or security threats and modelling contamination threats.

The program EPANET is developed for windows platform and is public domain software. Extended period simulation of the water quality and hydraulic behaviour within the pressurized pipe networks can be performed using EPANET. The pressurized pipe network comprises reservoirs, storage tanks, nodes, pumps, valves and pipes. The model can track the pressure at each node, a chemical concentration, flow of water in each pipe, the age of the water, source tracing and height of water in each tank throughout the entire network during a simulation period. The graphical user interface of EPANET consists of a visual network editor, which simplifies the process of editing and building a pipe network model, its properties and associated data. Data reporting and visualization tools are provided to assist in interpreting the

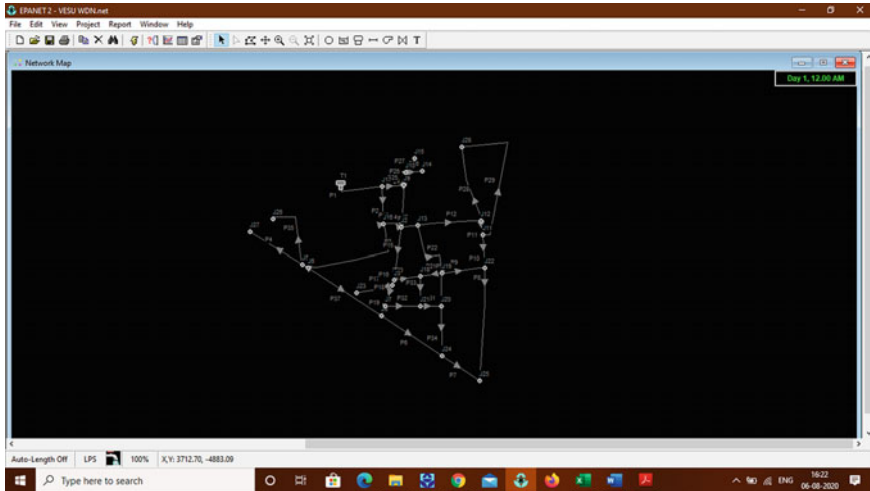


**Fig. 2** Layout of water distribution network drawn

results obtained from network analysis. The data reporting and visualization tools include energy usage, data tables, colour-coded network maps, calibration, reaction, profile, contour plots and time series graphs. Figure 2 shows the layout of water distribution network drawn in EPANET.

### ***3.1 Modelling Capabilities of EPANET***

The hydraulic analysis engine of the EPANET contains state-of-the-art modelling capabilities which include the following System operation based on complex rule-based controls, timer controls or simple tank level. The modelling capabilities of EPANET are limitless network size can be analysed, compute friction head loss using Chezy–Manning, Darcy–Weisbach or Hazen–Williams, and include minor head losses for fittings, bends, etc., models variable speed or constant speed pumps, computes cost and pumping energy, models various types of valves, including check, flow control, pressure regulating and shutoff, permits storage tanks to be of any shape, considers multiple categories of demand at nodes, each having its time variation pattern, models flow from emitters, which are pressure-dependent.

### ***3.2 Applications of EPANET***

EPANET has its utilities in maintaining and improving the quality of water delivered to the consumers. It finds its application in the following areas. The applications

of EPANET are vulnerability studies, minimization of energy, analysis of fire flow, assist with pump, pipe and valve placement and sizing, planning and improving the hydraulic efficiency of a system, design of sampling programs, carry out consumer exposure assessments, study disinfectant loss and by-product formations, assess alternate strategies for improving the quality of water, application of booster disinfection stations at key positions to maintain residual targets, alter tank filling/emptying and pumping schedules to decrease water age.

## 4 Methodology

This includes the data required for the simulation of WDN in EPANET, and data collected from SMC department which includes the pipe report, junction report and ESR report.

### 4.1 Data Required

The following data is required for analysis of WDN, which include junction report data, pipe report data and ESR report data.

#### (a) Junction report

Junctions are the points in the WDN where two or more than two links join together and where water either enters or leaves the WDN. The input parameters required for the junctions are elevation above some reference (usually mean sea level), water demand (withdrawal rate from the network).

#### (b) Pipe report

Pipes are the links that convey water from one node to the other node in the WDN. The input parameters related to pipes needed in the analysis are start node and end nodes, diameter of pipe, length of pipe and roughness coefficient.

#### (c) ESR report

The input parameters of ESR required in the analysis by using EPANET software are elevation above some reference (usually mean sea level), initial water level, maximum water level, minimum water level, diameter of tank.

### 4.2 Data Collected

The following data is collected from SMC, Hydraulics Department which includes the junction report, pipe report and ESR report.

(a) **Junction report**

The junction report of WDN is obtained from SMC, Hydraulics Department. The elevation data is provided by SMC, Hydraulics Department. The distribution system of ESR-21 contains 28 junctions. The allocation of demand at each node plays a crucial role in the design of WDN. In the present study, demand at each node was calculated by distributing the total demand evenly throughout the length of the pipe.

Total demand of area = 11.17 MLD = 129.28LPS.

Total length of distribution network = 10,648 m.

Demand per unit length of pipe = 0.0121 lps/m.

Pipe demand is calculated by multiplying the demand per unit length of the pipe to the length of the pipe. Pipe demand represents the demand which is associated with a pipe, which will transfer to the consumers through distribution pipes, which are laid parallel to the main pipes. Table 1 shows the length and demand for each pipe of the WDN of ESR-21.

Now, this pipe demand is converted into node demand by summing the pipe demand, when water flows towards the junction. The elevation and demand data at each node of the WDN of ESR-21 (WDS-7) are tabulated below in Table 2. The water demand in the WDN is varied throughout the day, to account for this variation in the design peak factor is considered. The peak factor is the ratio of the maximum flow during some specified time to the average flow. The peak factor depends on various parameters like the number of users, the service areas, and the duration of the peak flow of a WDN. In the current study, a peak factor equal to 3 is considered to calculate the peak demands.

(b) **Pipe report**

Pipe report of WDN is obtained from SMC, hydraulics department which consists of the length, diameter and roughness coefficient of all the pipes. The distribution system of ESR-21 consists of 31 pipes, made up of ductile iron (DI pipe). Pipe report data is shown in Table 3.

(c) **ESR report**

The detailed project report (DPR) of ESR-21 (WDS-7) was obtained from the hydraulics department of SMC, which includes maximum water level, minimum water level, staging height and volume of the tank. These details are given in Table 4.

The water distribution network of ESR-21 is shown in Fig. 3 which consists of 28 junctions and 37 pipes and 1 ESR.

**Table 1** Length and demand for each pipe of the WDN of ESR-21

| Sr. No | Pipe number | Length (m) | Pipe demand (LPS) |
|--------|-------------|------------|-------------------|
| 1      | P-1         | 329        | 3.99              |
| 2      | P-2         | 249        | 3.02              |
| 3      | P-3         | 731        | 8.88              |
| 4      | P-4         | 410        | 4.98              |
| 5      | P-5         | 44         | 0.53              |
| 6      | P-6         | 502        | 6.10              |
| 7      | P-7         | 286        | 3.47              |
| 8      | P-8         | 755        | 9.17              |
| 9      | P-9         | 283        | 3.44              |
| 10     | P-10        | 216        | 2.62              |
| 11     | P-11        | 93         | 1.13              |
| 12     | P-12        | 427        | 5.18              |
| 13     | P-13        | 117        | 1.42              |
| 14     | P-14        | 28         | 0.34              |
| 15     | P-15        | 353        | 4.29              |
| 16     | P-16        | 34         | 0.41              |
| 17     | P-17        | 246        | 2.99              |
| 18     | P-18        | 150        | 1.82              |
| 19     | P-19        | 70         | 0.85              |
| 20     | P-20        | 181        | 2.20              |
| 21     | P-21        | 150        | 1.82              |
| 22     | P-22        | 445        | 5.40              |
| 23     | P-23        | 110        | 1.34              |
| 24     | P-24        | 255        | 3.10              |
| 25     | P-25        | 131        | 1.59              |
| 26     | P-26        | 90         | 1.09              |
| 27     | P-27        | 114        | 1.38              |
| 28     | P-28        | 518        | 6.29              |
| 29     | P-29        | 988        | 12.00             |
| 30     | P-30        | 223        | 2.71              |
| 31     | P-31        | 152        | 1.85              |
| 32     | P-32        | 235        | 2.85              |
| 33     | P-33        | 199        | 2.42              |
| 34     | P-34        | 341        | 4.14              |
| 35     | P-35        | 500        | 6.07              |
| 36     | P-36        | 108        | 1.31              |
| 37     | P-37        | 585        | 7.10              |

**Table 2** Elevation and demand data at each node of the WDN of ESR-21

| Junction | Node elevation (m) | Demand (lps) | Peak Demand (lps) (considering peak factor = 3) |
|----------|--------------------|--------------|---|
| J1       | 8                  | 4.52         | 13.55   |
| J2       | 8                  | 0.34         | 1.02  |
| J3       | 8                  | 4.29         | 12.86   |
| J4       | 8                  | 0.41         | 1.24  |
| J5       | 8                  | 0.53         | 1.6   |
| J6       | 8                  | 8.88         | 26.63   |
| J7       | 8                  | 1.82         | 5.46  |
| J8       | 8                  | 7.95         | 23.86   |
| J9       | 8                  | 1.59         | 4.77  |
| J10      | 8                  | 1.09         | 3.28  |
| J11      | 8                  | 1.13         | 3.39  |
| J12      | 8                  | 5.18         | 15.55   |
| J13      | 8                  | 1.34         | 4.01  |
| J14      | 8                  | 1.31         | 3.93  |
| J15      | 8                  | 1.38         | 4.15  |
| J16      | 8                  | 3.02         | 9.07  |
| J17      | 8                  | 3.99         | 11.98   |
| J18      | 8                  | 4.02         | 12.06   |
| J19      | 8                  | 5.4          | 16.21   |
| J20      | 8                  | 4.55         | 13.66   |
| J21      | 8                  | 5.27         | 15.81   |
| J22      | 8                  | 6.06         | 18.18   |
| J23      | 8                  | 2.99         | 8.96  |
| J24      | 8                  | 10.24        | 30.71   |
| J25      | 8                  | 12.64        | 37.92   |
| J26      | 8                  | 6.07         | 18.21   |
| J27      | 8                  | 4.98         | 14.93   |
| J28      | 8                  | 18.29        | 54.86   |

## 5 Results and Discussion

After collecting data of the water distribution network of ESR-21 of west and south-west zone which includes pipe report and junction report pressure at each junction, velocity and flow in each pipe are computed using EPANET. Frictional head loss in the pipe is calculated using the Hazen–Williams formula. Table 5 shows the simulated head and pressure at each node in the distribution system, and Table 6 shows the simulated flow, velocity, unit head loss, and friction factor for each pipe in the distribution network.



**Table 3** Pipe report data

| Label | Scaled length (m) | Start node | Stop node | Diameter (mm) | Hazen–Williams C |
|-------|-------------------|------------|-----------|---------------|------------------|
| P-1   | 329               | T-1        | J-17      | 600           | 140              |
| P-2   | 249               | J-17       | J-16      | 350           | 140              |
| P-3   | 731               | J-16       | J-6       | 350           | 140              |
| P-4   | 410               | J-5        | J-27      | 150           | 140              |
| P-5   | 44                | J-6        | J-5       | 200           | 140              |
| P-6   | 502               | J-8        | J-24      | 150           | 140              |
| P-7   | 286               | J-24       | J-25      | 150           | 140              |
| P-8   | 755               | J-22       | J-25      | 250           | 140              |
| P-9   | 283               | J-19       | J-22      | 150           | 140              |
| P-10  | 216               | J-11       | J-22      | 250           | 140              |
| P-11  | 93                | J-12       | J-11      | 250           | 140              |
| P-12  | 427               | J-13       | J-12      | 350           | 140              |
| P-13  | 117               | J-16       | J-1       | 150           | 140              |
| P-14  | 28                | J-1        | J-2       | 500           | 140              |
| P-15  | 353               | J-2        | J-3       | 250           | 140              |
| P-16  | 34                | J-3        | J-4       | 200           | 140              |
| P-17  | 246               | J-4        | J-23      | 150           | 140              |
| P-18  | 150               | J-4        | J-7       | 200           | 140              |
| P-19  | 70                | J-7        | J-8       | 200           | 140              |
| P-20  | 181               | J-3        | J-18      | 150           | 140              |
| P-21  | 150               | J-19       | J-18      | 250           | 140              |
| P-22  | 445               | J-13       | J-19      | 350           | 140              |
| P-23  | 110               | J-2        | J-13      | 450           | 140              |
| P-24  | 255               | J-9        | J-1       | 500           | 140              |
| P-25  | 131               | J-17       | J-9       | 500           | 140              |
| P-26  | 90                | J-9        | J-10      | 150           | 140              |
| P-27  | 114               | J-10       | J-15      | 150           | 140              |
| P-28  | 518               | J-12       | J-28      | 250           | 140              |
| P-29  | 988               | J-11       | J-28      | 200           | 140              |
| P-30  | 223               | J-19       | J-20      | 250           | 140              |
| P-31  | 152               | J-21       | J-20      | 250           | 140              |
| P-32  | 235               | J-7        | J-21      | 150           | 140              |
| P-33  | 199               | J-18       | J-21      | 200           | 140              |
| P-34  | 341               | J-20       | J-24      | 250           | 140              |
| P-35  | 500               | J-5        | J-26      | 200           | 140              |
| P-36  | 108               | J-10       | J-14      | 150           | 140              |
| P-37  | 585               | J-6        | J-8       | 200           | 140              |

**Table 4** Elevated storage reservoir data

| S.N | Parameters          | Value       |
|-----|---------------------|-------------|
| 1   | Maximum water level | 31.9 m      |
| 2   | Minimum water level | 27 m        |
| 3   | Volume of tank      | 1,500,000 L |
| 4   | Diameter of tank    | 19.74 m     |



**Fig. 3** water distribution network of ESR-21

The pressure profile of the distribution network is shown in Fig. 4, which represents the pressure variation at each junction in the distribution system. At the farthest point junction J25, the pressure head available is 26.69 m, which shows the availability of sufficient pressure at the farthest point of the WDN. Velocity in pipe P6, P19, P20, P27, P29, P31, P32, and P36 is less than 0.5 m/sec. as the water distribution network is designed as a continuous system, even low velocity will not distort water quality. The head loss for pipe P4 is found to be quite high as compared to other pipes, result in significant head loss.

## 6 Conclusions

In this study, EPANET software is used to analyse the newly laid and proposed water distribution network of ESR-21 located in west and southwest zone of SMC. Results of EPANET software disclose that the newly laid and proposed water distribution network performs well, and pressure at all junctions is above the minimum residual

**Table 5** Simulated head and pressure at nodes in EPANET

| Node ID  | Head (m) | Pressure (m) |
|----------|----------|--------------|
| Junc J1  | 38.04    | 30.04        |
| Junc J2  | 37.97    | 29.97        |
| Junc J3  | 36.61    | 28.61        |
| Junc J4  | 36.46    | 28.46        |
| Junc J5  | 36.90    | 28.90        |
| Junc J6  | 37.15    | 29.15        |
| Junc J7  | 36.12    | 28.12        |
| Junc J8  | 36.06    | 28.06        |
| Junc J9  | 38.73    | 30.73        |
| Junc J10 | 38.47    | 30.47        |
| Junc J11 | 36.01    | 28.01        |
| Junc J12 | 36.36    | 28.36        |
| Junc J13 | 37.65    | 29.65        |
| Junc J14 | 38.42    | 30.42        |
| Junc J15 | 38.42    | 30.42        |
| Junc J16 | 38.44    | 30.44        |
| Junc J17 | 39.12    | 31.12        |
| Junc J18 | 36.43    | 28.43        |
| Junc J19 | 36.59    | 28.59        |
| Junc J20 | 36.03    | 28.03        |
| Junc J21 | 36.04    | 28.04        |
| Junc J22 | 35.63    | 27.63        |
| Junc J23 | 35.99    | 27.99        |
| Junc J24 | 35.40    | 27.40        |
| Junc J25 | 34.69    | 26.69        |
| Junc J26 | 36.04    | 28.04        |
| Junc J27 | 34.92    | 26.92        |
| Junc J28 | 35.00    | 27.00        |

pressure requirement of 7 m (for single-storied building) and 17 m (for three-storied building) as suggested by CPHEEO manual. This study will be helpful to the water supply engineers for analysis of the distribution network, as this process is fast and less tedious. This study will serve as a decision support tool, for the upgradation of the present distribution network. A scenario of leakage/losses in the WDN and its impact would help to analyse the robustness of the design.

**Table 6** Simulated flow, velocity, unit head loss and friction factor in EPANET

| Link ID  | Flow (LPS) | Velocity (m/s) | Head loss Gradient (m/km) | Friction Factor |
|----------|------------|----------------|---------------------------|-----------------|
| Pipe P1  | 387.86     | 1.37           | 2.36                      | 0.015           |
| Pipe P2  | 101.83     | 1.06           | 2.73                      | 0.017           |
| Pipe P3  | 80.40      | 0.84           | 1.77                      | 0.017           |
| Pipe P4  | 14.93      | 0.84           | 4.84                      | 0.020           |
| Pipe P5  | 34.74      | 1.11           | 5.70                      | 0.018           |
| Pipe P6  | 7.36       | 0.42           | 1.31                      | 0.022           |
| Pipe P7  | 10.46      | 0.59           | 2.51                      | 0.021           |
| Pipe P8  | 27.46      | 0.56           | 1.24                      | 0.019           |
| Pipe P9  | 12.37      | 0.70           | 3.42                      | 0.021           |
| Pipe P10 | 33.27      | 0.68           | 1.77                      | 0.019           |
| Pipe P11 | 50.37      | 1.03           | 3.82                      | 0.018           |
| Pipe P12 | 107.07     | 1.11           | 3.00                      | 0.017           |
| Pipe P13 | 12.36      | 0.70           | 3.41                      | 0.021           |
| Pipe P14 | 256.73     | 1.31           | 2.67                      | 0.015           |
| Pipe P15 | 50.48      | 1.03           | 3.84                      | 0.018           |
| Pipe P16 | 31.25      | 0.99           | 4.68                      | 0.019           |
| Pipe P17 | 8.96       | 0.51           | 1.88                      | 0.022           |
| Pipe P18 | 21.05      | 0.67           | 2.25                      | 0.020           |
| Pipe P19 | 12.19      | 0.39           | 0.82                      | 0.021           |
| Pipe P20 | 6.36       | 0.36           | 1.00                      | 0.023           |
| Pipe P21 | 25.23      | 0.51           | 1.06                      | 0.020           |
| Pipe P22 | 94.16      | 0.98           | 2.36                      | 0.017           |
| Pipe P23 | 205.23     | 1.29           | 2.94                      | 0.016           |
| Pipe P24 | 257.92     | 1.31           | 2.69                      | 0.015           |
| Pipe P25 | 274.05     | 1.40           | 3.01                      | 0.015           |
| Pipe P26 | 11.36      | 0.64           | 2.92                      | 0.021           |
| Pipe P27 | 4.15       | 0.23           | 0.45                      | 0.024           |
| Pipe P28 | 41.15      | 0.84           | 2.63                      | 0.018           |
| Pipe P29 | 13.71      | 0.44           | 1.02                      | 0.021           |
| Pipe P30 | 40.35      | 0.82           | 2.54                      | 0.018           |
| Pipe P31 | 7.13       | 0.15           | 0.10                      | 0.024           |
| Pipe P32 | 3.41       | 0.19           | 0.31                      | 0.025           |
| Pipe P33 | 19.53      | 0.62           | 1.96                      | 0.020           |
| Pipe P34 | 33.82      | 0.69           | 1.83                      | 0.019           |
| Pipe P35 | 18.21      | 0.58           | 1.72                      | 0.020           |
| Pipe P36 | 3.93       | 0.22           | 0.41                      | 0.024           |
| Pipe P37 | 19.03      | 0.61           | 1.87                      | 0.020           |

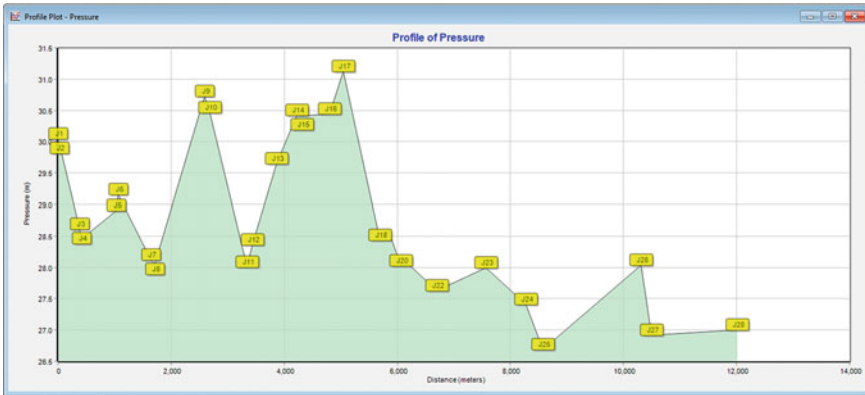


**Fig. 4** Pressure profile of WDN – ESR-21 in EPANET

**Acknowledgements** The authors are grateful to Surat Municipal Corporation for providing the data and support to carry out the present study.

## Bibliography

1. Batish R (2003) A new approach to the design of intermittent water supply networks. World Water & Environ Resour Congr 2003:1–11
2. Dave BH, Rajpara G, Patel A, Kalubarme MH (2015) Continuous water distribution network analysis using geo-informatics technology and EPANET in Gandhinagar city, Gujarat state, India. Int J Sci Eng Res 6(4):1587–1594
3. Dhumal JR, Danale MS, Jadhav GH (2018) Design of continuous water supply system by using watergems. NCETET-2018
4. Giustolisi O, Walski TM (2012) Demand components in water distribution network analysis. J Water Resour Plan Manag 138(4):356–367
5. Ingeduld P, Pradhan A, Svitak Z, Terrai A (2006) Modelling intermittent water supply systems with EPANET. Water Distrib Syst Anal Symp 2006:1–8
6. Jumanalmath SG, Shivapur AV (2017) Analysis of 24 × 7 water distribution network of Gabbur zone in Hubballi city, Karnataka state, India using EPANET software. Int Res J Eng Technol 4(2):478–485
7. Mehta DJ, Prajapati KJ (2017) Simulation of existing water distribution network at punagam area of Surat city using WATERGEMS software. In: Urbanization challenges in emerging economies: Energy and water infrastructure; transportation infrastructure; and planning and financing, 312–321.
8. Mehta DJ, Yadav V, Waikhom SI, Prajapati K (2017) Design of optimal water distribution systems using WATERGEMS: a case study of Surat city. J Glob Anal 2(4):90–93

# Impact of Different Parameters in the Development of Operating Policies of a Reservoir Using Stochastic Dynamic Modelling Technique



Ashrumochan Mohanty, Satish Chandra Bhuyan, and Sangeeta Kumari

**Abstract** Stochastic dynamic programming (SDP) has been used for several decades to develop the operating policies for the reservoir. But there is a need to study in depth about how the SDP-derived operating policies perform with respect to different parameters. In this study, we have used a real-world problem to study the effect. There are different aspects in SDP model which influences the development of the decision policies. The study majorly focuses on four different areas, i.e. (a) influence of the inflow transition probability matrix (ITPM) on the outcome of SDP model, (b) influence of different assumption taken in development of ITPM, (c) influence of serial correlation in the performance of a reservoir operated using SDP-derived operating policies and (d) applying SDP modelling technique to a real-world problem and comparing its performance with conventional operating rules used by the reservoir. The dependency of the convergence criteria was analysed on the basis of the inflow transition probability matrix. Influence of the inflow assumption in SDP model has been studied thoroughly. After conducting different sensitivity analysis, it was concluded that the SDP model is insensitive towards ITPM. Results produced by Markov I and independent assumption performed better than deterministic assumption which was used to develop ITPM. When comparisons are made in-between Markov I and independent assumption, it was found that Markov I performs better when the serial correlations are high and independent assumptions perform better when serial correlations are low. A reservoir when operated with SDP policies gives 14% more hydropower energy than the conventional rule curve method.

**Keywords** Stochastic dynamic programming · Operating policies · Inflow transition probability matrix · Serial correlation

---

A. Mohanty (✉)

Civil Engineering Department, NIT Jamshedpur, Jamshedpur, Jharkhand 831014, India

S. C. Bhuyan · S. Kumari

Civil Engineering Department, VSSUT, Burla, Odisha 768018, India

## 1 Introduction

Reservoir is an expensive structure that is built to store water. It helps to solve a single or multiple purposes in both dry and wet seasons. Nowadays, the effective use of the reservoir system has become very important. It has been found that reservoir contributes 12–16% of the total food production worldwide by helping in irrigation [1]. Hydropower is the main source of clean energy. World's 19% of the energy produced is clean energy or renewable energy. Nearly 97% of clean energy is produced from water stored in the reservoirs [1, 2]. It has been predicted that world's population will reach 9 billion at the end of 2050, and the food production needs to be increased by 70% [3]. For proper function of a reservoir or we can say that to get the maximum output, reservoir operation rules are important. Many reservoirs use rule curve for the operation of reservoir, which is generally static in nature. It does not account for the probabilistic nature of the inflow. So, there is a need to develop operating rules that could incorporate the inflow variation. For many years, the reservoir operation was done on the basis of the rule curve. The rule curve shows the level of the reservoir to be maintained at each month to satisfy different purposes of the dam. If the water level in the reservoir was above the level of the rule curve, then the releases from the reservoir shall be increased and vice versa. To reduce the inefficiency of the rule curve, many additional policies have been developed. These rules have been incorporated in the dam to increase the efficiency of the reservoir. These operation policies are used when the condition is ideal. But when the conditions are not ideal (when it becomes difficult to maintain the storage level), then the decision to be made for various combinations of hydrological and the reservoir storage condition can easily be managed by the operating rules. Nowadays, the operating rules have already been overtaken by the rule curve, and it is acting as the main principal rule for the operation of the reservoir.

The two optimization techniques have been widely used by the researcher, i.e. linear programming and dynamic programming techniques. Other methods have also been used by the researchers such as soft computing techniques. These all techniques have been used to derive the operating policies. *Linear programming (LP)*: As the name of the technique explains itself, the technique uses a linear relationship between the reservoir variable and the reservoir constraints to derive the optimal policies. But in the real life, the variables used in the reservoir operation are not linear in nature. This has been a major obstacle in the success of this technique. Although LP can be employed in the development of the operation policies, the degree of approximation in LP could seriously affect the outcome. *Dynamic programming (DP)*: In this method, a multi-decision is divided into sequence of small multi-decision. It is highly effective in solving the time-related decision-making. So, this technique comes in very handy in deriving the reservoir operation policies. Hall and Dracup (1970) said that there is a substantial advantage of solving a system with DP technique. It can treat a non-convex, nonlinear discrete variable and can take stochastic inputs [4]. Generally, there are three stochastic models that can take the serial correlations assumption into consideration. The models are policy iteration, stochastic LP (SLP) and stochastic

DP (SDP). Many studies have been done comparing the result of the explicit methods. All the studies said that SDP model has an advantage over other models. Although the optimal policies that have been derived have nearly same policy, the efficiencies calculated are different. Apart from that, computational time for SDP is very less as compared to the other models. From an analysis, it was seen that the time taken by the SDP model is 1/12 of the time taken by SLP [5]. But at the end, the accuracy of the model matters the most than the solving time. While solving a group of linear equation, the computer rounds off different values which may result in the truncation error. This may end up making a feasible solution to an infeasible solution. This becomes a constraint which leads to the limiting on the size of the problem which uses the SLP and policy iteration methods.

There are many mathematical models on the reservoir operation modelling. Goulter and Tai (1985) gave a detailed and thorough procedure for the optimization using DP to various water system problems. Reznicek and Cheng (1991) worked on the incorporation of the uncertainties in the reservoir modelling [6]. The earliest study on the stochastic reservoir optimization study was published in 1955 by Little who used a simplified reservoir system for the analysis purpose. Little (1955) went for the deterministic reservoir operation. In his analysis, he assumed that the inflow follows a stochastic sequence. Then the simulation was carried out by a recursive equation, and the inflow transition probability matrix was formed on the base of the 39 years of the historical data. After simulation, his model gave an operational policy, and the operational policy was based on the storage decision variable. Later the operational policy was compared with the rule curve of the reservoir, and a relative development was achieved on the operational policy [7]. Schweig and Cole (1968) took forward the model proposed by Little (1955) and applied it to a multi-reservoir problem, which was in fact a two-reservoir system problem. Then they applied the SDP and realized that there are several computational difficulties associated with the technique [8]. Loucks et al. (1970) studied three types of the stochastic reservoir operation. Models were based on the serially correlated Markov inflow: linear, dynamic and policy iteration. All models lead to the generation of same optimal policy, but the time for the simulation was different. SDP model approach was the fastest among all [9]. Arun Kumar and Yeh (1973) used the SDP modelling technique to maximize the hydropower output by introducing a penalty function for not meeting the specified firm power level. They proposed a heuristic decomposition approach for a multi-reservoir system and further used decomposition algorithm for two parallel reservoirs which were in the California Centre valley, USA [10]. Klemes (1977) focused on to study the effect of the discretization of the storage on stochastic model development. He stated that the number of storage discretization is subjected to some constraints. He suggested the storage discretization should increase linearly as the reservoir capacity increases to incorporate the result which is assured. He also theoretically and mathematically proved that too many storage discretization can seriously affect the accuracy and can disturb the real-time operation of the reservoir [11]. Turgeon (1980) stated two methods to overcome the difficulty of dimensionality. The two methods were named as “one at a time”, and the other was named as “decomposition method”. In one at a time, the method consists of dividing the



problem into one state variable with sub-problem, and then it is solved by DP. Then in second method known as decomposition in which the original  $n$  state variable DP problem is divided into  $N$  stochastic optimization sub-problem with two state variable and then it is solved with DP [12].

Loucks (1981) developed an SDP model which was completely different that was developed in the 1971 by Butcher. In Loucks model, the policy that was developed at the simulation end was the final storage volume which was the function of the known initial storage and the inflow which is unknown till the end of the period. The policy needed to be formulated in such a way that it does not depend upon the future inflow. Then the problem can be solved in two ways such that it can be applied in the real-world reservoir operation. In the first way, the final storage should be known subjected to the limitation to the release or in the other way by knowing the release target and subjected to limitation in the final storage in each time period. In the second process, the method can be implemented if the inflow can be obtained by using any inflow for casting problem. There may be error involved in the forecasting, but this opens a way for the application of the SDP model in the real world [13]. Stedinger (1984) prepared a SDP model which was inspired by Loucks (1981) model. He used the best forecast of the current period for the development of SDP model. The use of the historical data as the inflow state variable improved the model performance instead of forecasted data [14]. Bogardi (1988) applied the SDP model on single and multiple reservoirs. Mainly, the study was on impact of the storage and inflow discretization on the performance. The study found that as the number of class intervals is increased after a certain limit, the performance of the system will not improve dramatically. Emphasis was given on proper combination of storage and inflow class interval [15]. Kelman (1990) develop a model known as sampling stochastic dynamic programming (SSDP). It was modification over the SDP model. This captures the temporal and the spatial streamflow by using the simplex streamflow sequence. Then the best hydrological state variable was included in the model, which lead to the development of the SDP policies [14].

After studding lot of development in the recent past, it has been observed that the stochastic dynamic programming (SDP) modelling is gaining popularity among the researchers as it can incorporate the stochastic nature and the inflow, different inflow assumption and inflow serial correlation. A lot of studies have been done on operation modelling using SDP modelling technique. But very less studies have been done how the parameters influence the outcome of the SDP model. In our study, we will majorly focus on three-parameter inflow transition probability matrix (ITPM), inflow assumption while developing the ITPM and serial correlation.

## 2 Methodology and Development of Model

Stochastic dynamic programming (SDP) is a development over conventional dynamic programming (DP). It incorporates the stochastic nature of the parameters. SDP model is defined by its stages, state, decision variable, the objective function (the purpose that to be optimized), constraints and a recursive function which is used to develop the optimal policy. The probability of the inflow is calculated by observing the historical data. Then an objective function is defined keeping the purpose of the dam in view. Thereafter, an optimal policy is derived by iterating the recursive equation on each stage. An optimal policy is reached when the performance index becomes stable or converse. The below section will explain how the model is developed in detailed and stepwise manner.

### 2.1 Stage

During the model formulation using SDP for reservoir operation problem, stage is one of the important parameters. Stage is generally taken as week or month or combination of some continuous series of week or month. The total stages in one year are called the cycle period. One is " $n$ " and " $T$ ".  $n$  is absolute index which counts the period or stage that has been passed backward, and  $T$  takes care of the stages passed within the cycle.

### 2.2 Discretization of Inflow and Storage

Discretization of the inflow is done by observing the maximum and minimum inflow in the past (historical data). Generally, two types of the discretisation schemes are followed. First one is the scheme in which the inflow is divided into several zones such that the number of inflows falling in each interval becomes the same. In the second scheme, the inflow is divided into equal intervals. The former is of non-uniform interval, but the latter is of uniform interval. The characteristic value is defined as the average of the boundary value.

Discretization of storage means to divide the total storage volume in to discrete number of zones. Here in reservoir modelling, the storage volume is the difference between the maximum storage volume and the minimum storage volume. Generally, equally spaced discretization is preferred. After discretization, each zone is represented by a value known as the characteristic value or representative value. Each characteristic value is the halfway between the upper and the lower boundaries. Generally, discretization is done for the live storage of the reservoir.

### 2.3 Different Inflow Serial Correlation Assumptions

Markov process is mostly used to assume inflow serial correlation while doing a SDP model. It is one of the key aspects to understand the inflow serial correlation assumption. Markov chain is the process of discretized process of representing Markov process. Generally, when a Markov process is described by a single step dependence, then it is called a first-order Markov process. This means that the present inflow depends on one past value. Similarly, if the present inflow has a dependency of two past values, then it is known as the second-order Markov chain process.

### 2.4 The Markov I Inflow Process Assumption

The above relation represents a first-order Markov chain process. In a Markov chain, the movement from a state (time period) to another state is known as transition. Assume that in an inflow (Q) process, the inflow can assume any inflow value  $q$  ( $q = q_1, q_2, q_3 \dots$ ).  $P_{ij}$  is a conditional inflow transition probability which shows the transition of the inflow from state  $t$  to  $t + 1$ . Mathematically, we can write it as shown in Eq. (1).

$$P_{t+1}(Q_{t+1}|Q_t, Q_{t-1}, Q_{t-2}, \dots) = P_t(Q_t|Q_{t-1}) \tag{1}$$

Mathematically, the value of  $P_{ij}$  can be calculated by Eq. (2)

$$P_t(Q_t = q_j|Q_{t-1} = q_i) = \frac{N(Q_t = q_j|Q_{t-1} = q_i)}{N(Q_{t-1} = q_i)} \tag{2}$$

The inflow transition satisfies the rules of the probability, i.e.  $0 \leq P_{ij}^t \leq 1$  for all feasible  $i, j$  and  $\sum P_{ij}^t = 1$  for all  $I$ , where  $q_i$  is the inflow in the state  $t$  and  $q_j$  is the inflow in the state  $t + 1$ .

#### 2.4.1 Independent Assumption

The process in which the existing process is not correlated with the previous time period is known as independent process. It can be represented as

$$P_{t+1}(Q_{t+1}|Q_t, Q_{t-1}, Q_{t-2}, \dots) = P_t(Q_t) \tag{3}$$

The number of elements in the matrix is equal to the inflow class discretization. It will form a one-dimensional matrix. We can say that it is a row matrix. It can be mathematically calculated by Eq. (4)

$$P_t(Q_t = q_j) = \frac{N(Q_t = q_j)}{N(Q_t)} \tag{4}$$

**2.4.2 Deterministic Assumption**

The deterministic assumption means that it is assumed that the inflow of that time period is known at that time. That means the probability of occurrence of that flow is 100%. Generally, the flow is taken as the average of that period. Mathematically, it can be written as

$$P_{t+1}(Q_{t+1}|Q_t, Q_{t-1}, Q_{t-2}, \dots) = P_t(Q_t) \tag{5}$$

**2.4.3 Inflow Serial Correlation**

It is quite a common thing that a process at a time period is related to another time period of the process. The relation between the processes at different lag is known as the serial correlation or autocorrelation. Here in our study, we have taken the inflow as our process. Serial correlation can exist between different time observations ( $k = 1,2,3$ ). It is also known as population correlation which is denoted by  $\rho(k)$ , where  $k$  represents the time lag. It can be calculated by Eq. (6).

$$\rho(k) = \frac{\sum_{i=1}^{n-k} Q_i * Q_{i+k} - \frac{\sum_{i=1}^{n-k} Q_i * \sum_{i=1}^{n-k} Q_{i+k}}{n-k}}{\left[ \sum_{i=1}^{n-k} Q_i^2 - \frac{\left(\sum_{i=1}^{n-k} Q_i\right)^2}{n-k} \right]^{1/2} * \left[ \sum_{i=1}^{n-k} Q_{i+k}^2 - \frac{\left(\sum_{i=1}^{n-k} Q_{i+k}\right)^2}{n-k} \right]^{1/2}} \tag{6}$$

**2.5 State Transformation Equation**

State continuity equation of a reservoir follows conservation of mass. State continuity equation of SDP can be written as follows:

$$S_{t+1} = S_t + Q_t - R_t - Spill_t - E_t \text{ for all } t \tag{7}$$

where  $t$  represents the stages in a cycle,  $S_{t+1}$  is the storage of the reservoir at the time  $t + 1$ ,  $S_t$  represents the storage of the reservoir at time  $t$ ,  $Q_t$  represents the inflow

to the reservoir in the period  $t$ ,  $R_t$  represents the release from the reservoir in the period  $t$ ,  $Spill_t$  represents the spill from the reservoir, and  $E_t$  represents the evaporation loss from the reservoir catchment in the time period  $t$ . The relation between the variables is clearly shown in Eq. 7.

## 2.6 Physical Constraints

For storage in the reservoir, the storage at any time period must lie

$$S_{t,min} \leq S_t \leq S_{t,max} \text{ for all } t \quad (8)$$

where  $S_{t,min}$  is the minimum live storage at any time  $t$ ,  $S_{t,max}$  is the maximum live storage at time  $t$ , and  $S_t$  is the live storage at any time  $t$ .

Reservoir release constraints are as follows:

$$R_{t,min} \leq R_t \leq R_{t,max} \text{ for all } t \quad (9)$$

where  $R_t$  is the release at any time period  $t$  and  $R_{t,min}$  and  $R_{t,max}$  represent the minimum and the maximum water that can be released. The minimum and the maximum release depends upon many factors such as the purpose of the dam, downstream condition and the spillway capacity. Different constraints have been used in the experiment like maximum and minimum head to the turbine, maximum and minimum firm energy, etc.

## 2.7 Objective Function

A reservoir is designed keeping many things in vision. The reservoir may be designed for single purpose or multi-purpose. The purpose of the reservoir can be supplying drinking water and domestic water, supplying water for irrigation, reducing the flood peak, keeping the minimum depth of water for navigation purpose, providing energy, etc. A properly formulated objective function will show the purpose of the reservoir. Reservoir has been designed to solve the purpose of hydropower generation and to supply irrigation water. The objective function can be formulated to minimize the energy deficit or to maximize energy generation for a year, and for the irrigation water supply, the objective function can be defined to deviate minimum from the target.

$$\text{Max} \sum_{t=1}^N \text{Energy} \quad (10)$$

The above equation is represented to maximize the energy generation in a year. N is the number of periods in a year.

### 2.8 Recursive Equation

There are different ways to write the recursive equation depending upon the factors that influence the recursive equation. Different factors that influence the recursive equation are as follows:

- Correlation characteristics (time dependent or time independent)
- Decision variable (storage or release)
- Inflow state variable dependency (previous inflow or present inflow)
- Objective pattern (maximization or minimization)

$$f_n^t(S_t, Q_t) = \text{Opt}_{(\min, \max)} \left[ \sum_{n=1}^{n=t} P_{ij} B(S_t, Q_t) + f_{n-1}^{t+1}(S_{t+1}, Q_{t+1}) \right] \quad (11)$$

$\forall S_t, Q_t, D_t$  feasible

subjected to reservoir continuity equation, i.e.

$$R_t = S_t + Q_t - S_{t+1} - SP_t - E_t \quad (12)$$

$$f_1^T(S_t, Q_t) = \text{Opt}_{(\min, \max)} [f_{n=1}^{t-T}(S_{t+1}, Q_{t+1})] \quad (13)$$

the notation used in Eqs. (11), (12) and (13) has been explained in Sect. 2.5. The notation *n* represents the time period that have passed (*n* = 1,2, 3...). *D<sub>t</sub>* represents the decision variable which can be storage at time period *t* or the inflow at the time period *t* or *t-1* (*S<sub>t</sub>*, *Q<sub>t</sub>* or *Q<sub>t-1</sub>*), *P<sub>ij</sub>* is a conditional inflow transition probability which shows the transition of the inflow from state *t* to *t + 1*, *B(S<sub>t</sub>, Q<sub>t</sub>)* is the increment over the objective function starting from the time period *t* to the end of the time period *t*, and *f<sub>n-1</sub><sup>t+1</sup>(S<sub>t+1</sub>, Q<sub>t+1</sub>)* is the sub-optimal value of the recursive function at the stage *n*. For solving the recursive Eq. (11), a backward dynamic programming (DP) algorithm is taken into account. The computer solves the equation backward till the recursive equation produces a stable policy, and the performance value becomes constant. In other words, the convergence criteria need to be satisfied (Sect. 2.9). The SDP model is always solved in the backward direction because solving in forward has no sense because the expectation over the future state has to be considered.

## 2.9 The Convergence Conditions

There are two conditions when we can say that the policy has been converged or we can say that the policy has reached “steady state”.

- The first condition emphasizes the stabilization of the policy. After each stage of the computation of the algorithm, we could generate the operating policies. After continuing the computation in the backward direction every time, we will get operating policies, but after computation operating policies for certain years, the policies will become constant. The policies will not change over period. Here we can say that we have reached a steady-state policy or the policies have converged.
- The second condition for the convergence or to reach at the steady state is to have a constant performance value. After the computation of the SDP algorithm at each stage, the algorithm returns a performance value or expects annual performance value. After computation for several years, the expected value becomes constant, i.e.

$$f_i^{T+n}(S_t, SQ_t) - f_i^n(S_t, SQ_t) = \text{Const} \quad (14)$$

The condition in which above equation becomes constant is known as steady state. The phenomenon is called stabilization of objective function value.

## 3 Case Study

Rengali Reservoir, a multi-purpose reservoir, was selected for conducting the experiments. It is built on Brahmani River. The main aim of the Rengali Reservoir is to store water for the purpose of the irrigation and hydropower generation. It also helps to reduce the severity of the flood by reducing the mood peak. As it serves multiple reasons, it is called as *multi-purpose* reservoir. On 29 km of the downstream side of the Rengali Reservoir, Samal Barrage is located from which different canals are connected which solves the purpose of the irrigation. Different hydropower mechanism is present at the Rengali Reservoir to generate energy.

### 3.1 Reservoir Characteristics

- Maximum water level (MWL): 125.40 m (Elevation)
- Full reservoir level (FRL): 123.50 m (Elevation)
- Dead storage level (DSL): 109.72 m (Elevation)
- Storage capacity at MWL: 5,150 Mm<sup>3</sup>
- Storage capacity at FRL: 4,400 Mm<sup>3</sup>
- Storage capacity at DSL: 986.29 Mm<sup>3</sup>

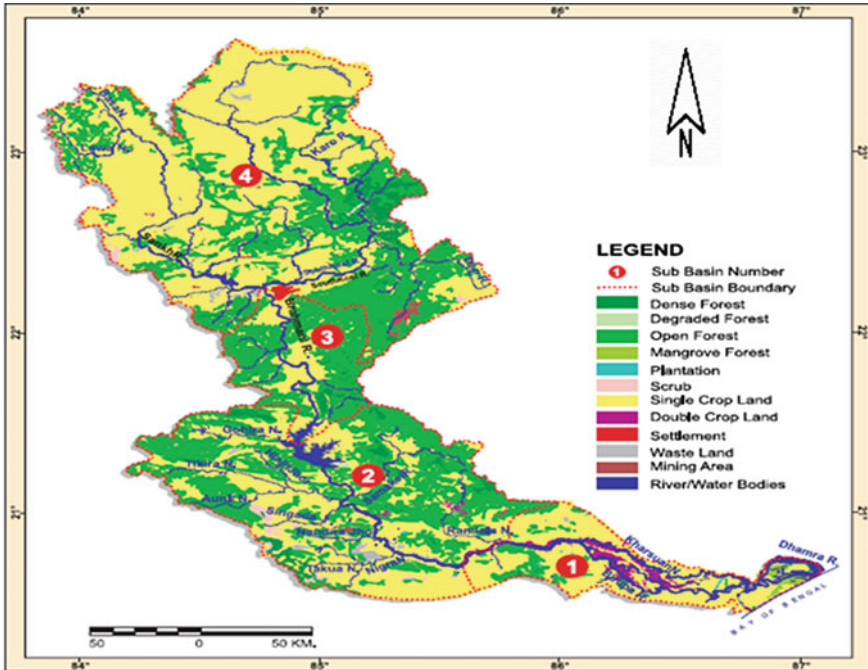


**Fig. 1** Brahmani River Basin with different land cover

- Live storage capacity of reservoir: 3413.71 Mm<sup>3</sup>
- Water spread area at MWL: 414 Mm<sup>2</sup>
- Water spread area at FRL: 378.40 Mm<sup>2</sup>
- Water spread area at DSL: 143.0861 Mm<sup>2</sup> (Fig. 1).

It has maximum rainfall (annual) of 2850 mm, minimum rainfall (annual) of 890 mm and mean rainfall (annual) 1870 mm. It has maximum run-off (annually) of 36,500,000 Mm<sup>3</sup>, minimum run-off (annually) of 5,670 Mm<sup>3</sup>, mean annual run-off (Annually) of 14,900 Mm<sup>3</sup>, 1000-year return period flood of 27,800 m<sup>3</sup>/s, probable maximum flood (PMF): 55,540 m<sup>3</sup>/s 75% dependability (run-off): 9150 Mm<sup>3</sup> and 90% dependability (run-off): 7430 Mm<sup>3</sup>.

#### 4 Experiment Result and Discussion

While working on the SDP model, different assumptions are taken into consideration. First assumption is that stochastic process is a stationary process. Hence, the inflow transition probability matrix does not change over time. Secondly, the design parameters are constant which means parameters like dead storage, live storage, target release to be met, etc., remain unchanged during entire study. Third assumptions are



that the model follows a continuous discretization method. Hence, time, capacity and inflow are approximated by discrete units. In upcoming sections, different experiments have been conducted to know the effect of different parameters on the outcome of the SDP model.

#### 4.1 Experiment 1

The multi-purpose reservoir was selected for the study of the effect of the inflow transition probability matrix (ITPM). But for comparing the effect of ITPM, only single objective was used, i.e. to maximize the hydropower generation. This was assumed to reduce the effect of different objective of the reservoir on modelling. In this study, first three transition probability matrices were constructed. The first matrix (ORIGINAL) was formulated using the historical data of 30 years, and then other two hypothetical matrices were formulated using different flow regimes. Second matrix (EQLELT) was constructed in such a way that the elements in the inflow transition probability matrix were equal. Then a third matrix (HIGH DEVIATION) was constructed taking large variation in the historical inflow data, but it was made sure that the mean variation of the original flow pattern of the hypothetical inflow pattern does not vary more than 5%. This will help us to know the effect of the ITPM on the SDP model if a reservoir is operated with large deviation in the inflow or there is error in collection in inflow data (Fig. 2).

*Result Analysis:* From the result, we can see that there is a limited impact of the ITPM on the SDP model as the objective is concerned. We could conclude that inherent inaccuracy in the development of the ITPM does not have considerable impact on the SDP model performance. The cumulative difference between the three-model hydropower energy output is less than 5%. This shows that ITPM is insensitive towards SDP-derived policies. From the above experiment, we could conclude few points.

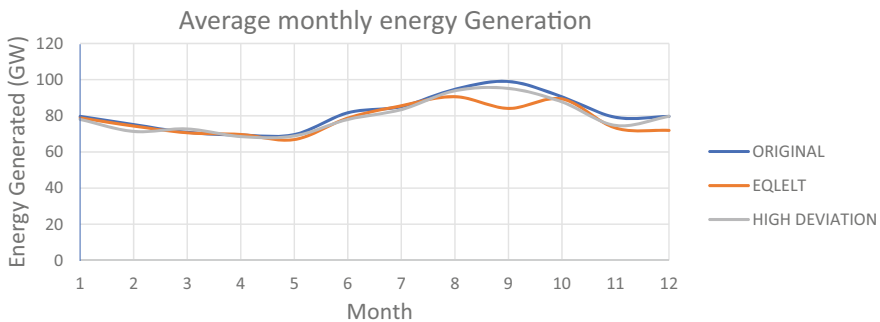


**Fig. 2** Simulated result of average monthly reservoir storage using three different ITPM (X-axis is representing months starting from January to December with time step of one month)

- ITPM with large variation may result in the same operating policies. There may be little variation in the operating policies, but the hydropower generated remains nearly the same.
- The main reason behind the derivation of the nearly the same operating policies is due to iteration of the SDP model.
- The derived policy may result in the little different operating policies but could solve similar objective almost to the same extent.

## 4.2 Experiment 2

The purpose of the study is to know the influence of the inflow assumptions on the SDP model. As discussed, inflow assumptions play an important role on the model development as it influences the ITPM. The experiment is conducted to know the best inflow assumption that suites the SDP model. For this, we will conduct experiments taking three assumptions, i.e. Markov I, independent and the deterministic assumption.

Markov chain II assumption has been ignored because of the following reasons:

- When the ITPM was constructed assuming Markov II process, the matrix generated was a three-dimensional matrix. If we will construct a matrix  $4 \times 4 \times 4$  (say), then the matrix contains 64 elements. But we have taken historical inflow data of 30 years. This implies that  $\frac{1}{2}$  of the elements in the matrix is zero, which will not satisfy the convergence criteria. It becomes a difficult task to construct ITPM with Markov II assumption of size more than  $3 \times 3 \times 3$ .
- Markov II assumption leads to the development of a three-dimensional matrix which will increase the complexity of the model. If we have  $n \times n \times n$  matrix, then we have to solve  $n^2$  equations at a state to achieve the optimal policy.

*Result analysis:* The simulated performance of the hydropower generation is shown in Fig. 3. We can clearly see that the Markov I and the independent SDP model assumption have completely outperformed the deterministic model. The Markov model and the independent models have produced 13–14% more hydropower energy (annual average). But it is difficult to know which is better between the Markov I model and the independent model as the difference between these two averages yearly hydropower generation is less than 2%. Further another experiment 3 is conducted to know which is better among them by taking different inflow assumption in a single SDP model set-up.

## 4.3 Experiment 3

An attempt has been made to find the best among the two assumptions: Markov I and independent models. This experiment was conducted taking the serial correlation

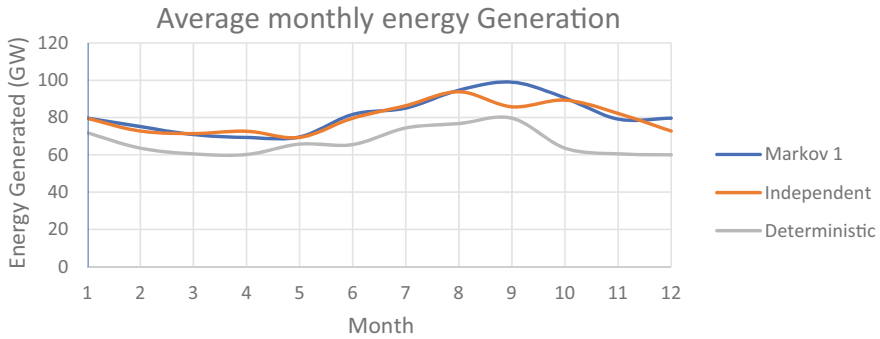


**Fig. 3** Simulated result of average monthly power generation using three assumptions, i.e. Markov I, independent and deterministic. (X-axis is representing months starting from January to December with time step of one month)

into consideration. For this experiment, four points were selected, i.e. 0, 0.3, 0.6 and 1. For instance, a point 0.3 is selected, and the experiment will be performed taking Markov chain I assumption, wherein the serial correlation is greater than 0.3 and all the serial correlation less than or equal to 0.3 will take an assumption of independent relation and same in the case of 0.6. Now coming to serial correlation point 1, serial correlation cannot be greater than one, so in all the steps independent assumption is taken. In our study, no month has serial correlation less than zero. So, in case of serial correlation point 0, the model will completely operate on Markov I assumption (Fig. 4).

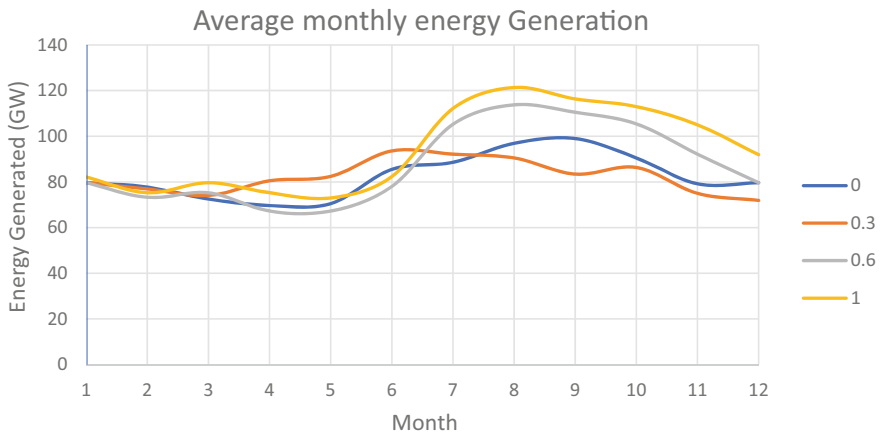


**Fig. 4** Simulated hydropower power generation for Experiment 3 using different correlation coefficients (0, 0.3, 0.6 and 1). (X-axis is representing months starting from January to December with time step of one month)

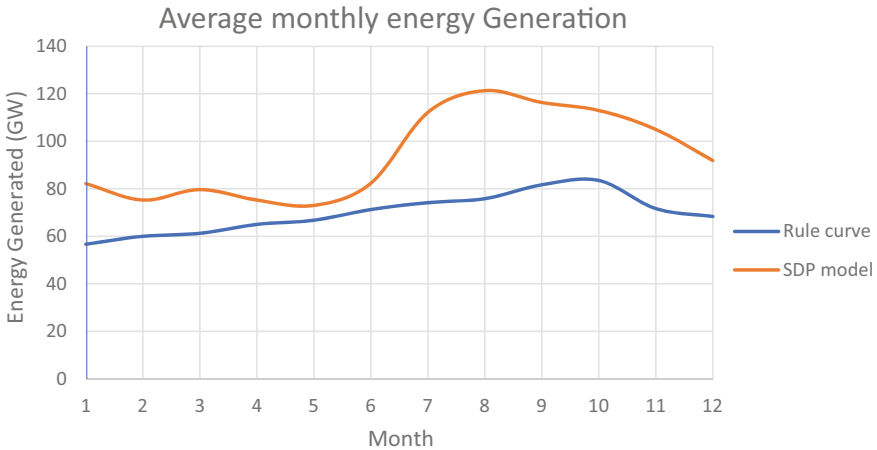


**Fig. 5** Hydropower generated using rule curve and SDP model (X-axis representing months starting from January to December with time step of one month)

*Result Analysis:* We can see that the difference between the performances of the four models is minimal. A gradual improvement in the performance is observed as we go from lower point to higher serial correlation point. There is little jump in the model from point 0.6 to 1. We can conclude that the model performs better when there is an assumption of Markov I when the serial correlation is high and of independent assumption when the serial correlations are low.

#### 4.4 Experiment 4

The main purpose of this experiment is to apply the above concluded result to a real-world problem. For this, the rule curve was used to find the performance of the reservoir. Here the performance was measured on the basis of hydropower generation. Then an SDP model was developed for reservoir operation. Then the performance of the reservoir was evaluated (Fig. 5).

*Result Analysis:* It was found that the SDP model performed way better than the conventional rule curve operation method. It was found that nearly 14% of excess average yearly hydropower was generated.

## 5 Conclusion

The study mainly focuses on three major aspects in the SDP model development, i.e. the influence of the inflow transition probability matrix in the development of the

SDP model, the best inflow assumption that can be used for model formation and the effect of serial correlation. It was found that the ITPM was insensitive towards the SDP model. There was no much influence in the operating policy of the SDP model. But after simulation, minor variation in average yearly power generation was noticed though it was under 5%. Thereafter, several experiments were done on the basis of assumption of the inflow assumption. Three assumptions were taken, viz. Markov chain I, independent assumption and deterministic assumption. It is difficult to take the assumption of the Markov chain II due to less inadequate length of historical data. It was observed that the ITPM formulated using Markov II was having higher numbers of zero elements. These zero elements made convergence criteria difficult to satisfy. Therefore, three assumptions were made, and it was found that the Markov chain of order 1 and the independent assumptions were the best. The deterministic assumption failed to achieve the desired result. Then many experiments were conducted to determine the best among the two (Markov chain I and independent) assumptions. It was found that the Markov chain I performs better when the serial correlation is high, and independent assumptions hold good when the serial correlation is low.

## References

1. The World Commission on Dams (2000) Dams and development: A framework for decision making. Earthscan, London, UK
2. Demirbas A (2007) Focus on the world: Status and future of hydropower. Energy Sources Part B Econ Plan Policy 2:237–242
3. Bruinsma J (2009) The resource outlook to 2050: By how much do land, water and crop yields need to increase by 2050? Food and Agriculture Organization of the United Nations, Rome, Italy
4. Hall W, Dracup J (1970) Water resources systems engineering. McGraw-Hill, New York
5. Loucks DP, Falkson LM (1970) A comparison of some dynamic, Linear and policy iteration methods for reservoir operation. Water Resour Bull 6(3):384–400
6. Goulter IC, Tai F-K (1985) Practical implications in the use of stochastic dynamic programming for reservoir operation. Water Res Bulletin, AWRA 21(1):65–74
7. Little JDC (1955) The use of storage water in a hydroelectric system. Operation Res 3(2):657–669
8. Schweig Z, Cole A (1968) Optimal control of linked reservoirs. Water Resour Res 4(3):479–498
9. Stedinger JR, Sule BF, Loucks DP (1984) Stochastic dynamic programming models for reservoir operation optimization. Water Resour Res 20(11):1499–1505
10. Arun kumar S, Yeh WWH (1973) Probabilistic models in the design and operation of a multi-purpose reservoir system Contributions 144. University of California, Davis, US, California Water Resources Centre
11. Klemes V (1977) Discrete representation of storage for stochastic reservoir optimization. Water Resour Res 13(11):149–158
12. Turgeon A (1980) Optimal operation of multi-reservoir power systems with stochastic inflows. Water Resour Res 16(2):275–283
13. Gablinger M, Loucks DP (1970) Markov models for flow regulation. J Hydraulic Division, ASCE, 96:165–181
14. Kelman J, Stedinger JR, Cooper H, Yuan ESQ (1990) Sampling stochastic dynamic programming applied to reservoir operation. Water Resour Res 26(3):447–454

15. Kularathna MDUP, Bogardi JJ (1990) Simplified system configurations for stochastic dynamic programming based optimization of multireservoir systems. In: Proceedings, International Symposium on Water Resources Systems Application, Winnipeg, Canada.
16. Deepti R, Madalena MM (2010) Simulation–optimization modeling: A survey and potential application in reservoir systems operation. *Springer Water Resources Manag* 24:1107–1138
17. Arash A, Reza A, Majd M (2009) Optimization of reservoir volume by yield model and simulation of it by dynamic programming and Markov chain method. *American-Eurasian J Agric & Environ Sci*
18. Husain A (2012) An overview of reservoir systems operation techniques. *Int J Engineering Res Develop* 4(10):30–37
19. Celeste AB, Billib M (2012) Improving implicit stochastic reservoir optimization models with long-term mean inflow forecast. *Springer Water Res Manag* 26:2443–2451
20. Laabs H, Harboe R (1988) Generation of Operation Rules with Stochastic Dynamic Programming and Multiple Objectives. *Water Resour Manage* 2:221–227
21. Loaiciga HA, Marino AM (1986) Risk Analysis for reservoir operation. *Water Resour Res* 22(4):483–488
22. Loucks DP (1968) Computer models for reservoir regulations. *J Sanitary Manag*, 156–218
23. Moy WS, Cohon JL, ReVelle CS (1986) A Programming Model for Analysis of the Reliability, Resilience and Vulnerability of a Water Supply Reservoir. *Water Resour Res* 22(4):489–498
24. Nandalal KDW (1986) Operation policies for two multipurpose reservoirs of the mahaweli development scheme in Sri Lanka. M.Eng. Thesis, No. WA-86–9, ATT, Bangkok, Thailand
25. Liu P, Zhao J, Li L, Shen Y (2012) Optimal reservoir operation using stochastic dynamic programming. *Scientific Research*
26. ReVelle C, Joeres E, Kirby W (1969) The Linear Decision Rule in Reservoir Management and Design 1: Development of the Stochastic Model. *Water Resour Res* 5(4):767–777
27. Reznicek K, Cheng TCE (1991) Stochastic Modelling of Reservoir Operations. *Eur J Oper Res* 50:235–248
28. Tai FK, Goulter IC (1987) A Stochastic Dynamic Programming Based Approach to the Operation of a Multi-reservoir System. *Water Resour Bull* 23(3):371–377
29. Yakowitz S (1973) A Stochastic Model for Daily River Flows in an Arid Region. *Water Resour Res* 9(5):1271–1285
30. Yakowitz S (1982) Dynamic Programming Application in Water Resources. *Water Resour Res* 18(4):673–696

# Feasibility Analysis and Design of Water Distribution System for Ghadara (East Singhbhum District) Using Water Gems



Abu Rashid and Sangeeta Kumari

**Abstract** Water Supply in Ghadara is not equally distributed due to regular terrain and increase in bulk population. This study is proposed to suggest measures for upgrading of the distribution network. In this paper the analytical results are carried out using WATERGEMS software. This paper includes the reorganizational measures needed in future for its optimal design using Water Gems. This pipeline is proposed to ensure the service standard of 135 l-pcd and satisfy the pressure limits between 35 and 80 psi. Water Gems (Bentley) is found to be user friendly for addressing systems with varying demands, pipe conditions and Design horizons. During Hydraulic simulation different valves have been placed to satisfy the pressure requirement and proper placement of Diameter is also ensured to minimize the head loss. It also supports graphical interface which makes analysis real and further reduces time for reanalyzing the network. To control the flow rate of water from Water Treatment Plant to overhead tank SCADA is installed at the Water Treatment Plant and PFC valve is installed at the overhead tank which prevents the overflow of water from overhead tank and therefore reduces the energy cost of pumping water from reservoir to water treatment plant and finally to overhead tank.

**Keywords** WDN · Water gems · Ghadara · East-Singhbhum district

## 1 Introduction

Water is an essential element for the living being and also a vital element for the economic development of a country. Water has always been a problem specially to areas which are far away from coastal region and also to land locked countries where there is a complete scarcity of water. The infrastructure for water distribution system is important for industrial as well as domestic uses. It connects users to sources of water, using hydraulic components, such as links, nodes, orifice, pumps, valves, and tanks. The infrastructure of WDN design of such systems is a tremendous task

---

A. Rashid (✉) · S. Kumari  
NIT Jamshedpur, Jamshedpur, Jharkhand, India

© The Author(s), under exclusive license to Springer Nature Singapore Pte Ltd. 2022  
C. M. Rao et al. (eds.), *Advanced Modelling and Innovations in Water Resources Engineering*, Lecture Notes in Civil Engineering 176,  
[https://doi.org/10.1007/978-981-16-4629-4\\_26](https://doi.org/10.1007/978-981-16-4629-4_26)

371

involving numerous factors, therefore the designing for such system is done carefully. Design parameters include water demand, minimum pressure requirements, velocity requirement, topography and head loss. The primary goal of all water distribution system engineers is the delivery of water to meet the demands as per the standards and satisfy the pressure as well as velocity criteria. Unfortunately, it is seen that in new as well as old water distribution system the ability to transport water reduces due to high head loss and therefore the demands of such networks increases. This leads to the insufficient performance of the network which hampers the economy.

Elements which constitute water distribution system are pipes, valves (PRV, PBV, FCV), Orifice meter, Over-head tanks. Distribution systems carries water from reservoir to Water Treatment Plant under pumping pressure and from WTP to overhead tank and finally to consumers.

Water distribution system can be categorized into two main parts: (1) Continuous system: In this type of system, there is continuous supply of water so dirty ground water cannot enter into the water pipelines even there are some small escapes in the system. (2) Intermittent System: In this type of system there is no continuous supply of water throughout the day. Water is generally supplied for a few hours in the morning or in evening. Due to adverse pressure, the quality of water is not as good as continuous water supply system and therefore causes health issue. Using commercial software such as Bentley it helps to simulates pressures and head loss in the networks and flows in and out to/from the tank. The main moto is to deliver water at the required quantity to individual users as per government standards under standard pressure throughout the distribution network.

The distribution of drinking water in DMA-02, Ghadara region network, Jharkhand is a technical challenge. It is important that each node of the distribution network be supplied with a sufficient flow of water so as to meet the demands. In Indian cities water is available for a few hours per day, with irregular pressure, and the quality of the water is also compromised. For this study area Ghadara area (DMA-02) of East Singhbhum District, Jharkhand has been identified and the network model for the area under consideration will be prepared and studied to meet the demand per users.

The objective of this study is to study the real network performance of Water Distribution Network of Ghadara (DMA-02) zone, East Singhbhum District, Jharkhand and to report any improvements required in existing network to reduce the overall head loss and satisfy the pressure constraints without increasing the total head loss as per the standards by using hydraulic simulation software like Water GEMS.

Water GEMS is a product of Bentley which is an American-based software development company which develops, sells and supports computer software which renders services including design, operation and construction of infrastructure. Their software products are generally used to design, build, and operate large building assets such as roads, railways, power plants, and Water and Sewer utility networks. Water-Gems is superior to Water-CAD and EPANET software's in distribution network as it is easy to export from google earth. It supports modelling elements such as variable speed pump battery, CAD and GIS interoperability and it has advanced hydraulic features such as pipe renewal planner and Water Hammer.



## 2 Model Development

### **The following steps are followed:**

The introduced methods are simple and practical based mainly on the simulation procedures used to handle the water shortage conditions in the distribution network of quite a large and complex WDS.

### **2.1 Collection of Data**

Collection of real network data of Chhotagovindpur and Bagbera Water Supply Project, Jharkhand is done. The data collected is pressure at nodes, velocity in link, head loss in link, reduced level at nodes, pump details and diameter as well as length of links.

### **2.2 Filling Input Data**

The input parameters are Pipe data such as pipe types (C.I, PVC, D.I etc.), pipe diameter (inches), Valve Data, Hazen Williams Co-efficient ( $C = 140$ ), Reservoir capacity and Tank (minimum and maximum level) as well as elevation reading at nodes, tanks are filled or Flex Table can be used to generate input data of any component where-ever required.

### **2.3 Validation of the Network**

Validation of network is performed only after the input of all the parameters is done. If there is no error in the network then engine information message displays that no problems found and if there is an error it should be rectified by changing the parameters and again validated.

Validation of network is performed only after the input of all the parameters is done. If there is no error in the network then engine information message displays that no problems found and if there is an error it should be rectified by changing the parameters and again its validated.

## 2.4 Computation

Once the validation is over the computation is performed and the results can be obtained in Flex Tables of each and individual data. From flex tables the results can also be represented in terms of graph or it can be exported from Flex Tables to Excel.

**The following steps are followed for the development of the model in Water GEMS:**

Step 1: Collection of Data from the Drinking water and Sanitation Department.

Step 2: Input Hydraulic Parameters such as Pipes, Junctions, Tanks, Valves, Pumps and Reservoir with their corresponding elevations.

Step 3: Perform the validation of the network. If there is error in validation go back to step 2 and change the parameters else if there is no error found during validation go to Step 4.

Step 4: Compute the network.

Step 5: Go to Analysis and then to Flex Tables to obtain the results.

Step 6: From the Flex Tables (Results) are exported the MS-Excel where graph are plotted between Real and Revised Network as shown in Figs. 4 and 5.

## 3 Study Area

**East Singhbhum** is one of the twenty-four districts of Jharkhand which lies in Kolhan Division. It has a total area of 3533 km<sup>2</sup>. The total population recorded as per 2011 census is 2,293,919. This district is bounded by the districts of West-Bengal on east and north. On west, Seraikela Kharsawan district and south by Mayurbhanj district of Odisha. The study area which is selected for the design of Water Distribution is Ghadara which is a census town in Purbi or East Singhbhum district in the state of Jharkhand, India. Ghadara has a latitude of 22.75° N and has a longitude of 8.25° E.

The type of pipe used in entire water distribution network is Ductile Iron varying from four inches up to eighteen inches. The entire hydraulic simulation is done through Water-Gems. The main source of water is Subarnarekha River and it flows through the Indian States of West Bengal, Odisha and Jharkhand. The entire length of distribution network in my study area (DMA-02, Ghadara) is 7293 ft from Over-head tank to consumers and the length from Reservoir up to Over-Head tank is not considered in this study.

Figure 1, shows the Purbi Singhbhum area in the state of Jharkhand, India which is done in Arc GIS. The study area Ghadara is marked as circle inside the Jharkhand Map.

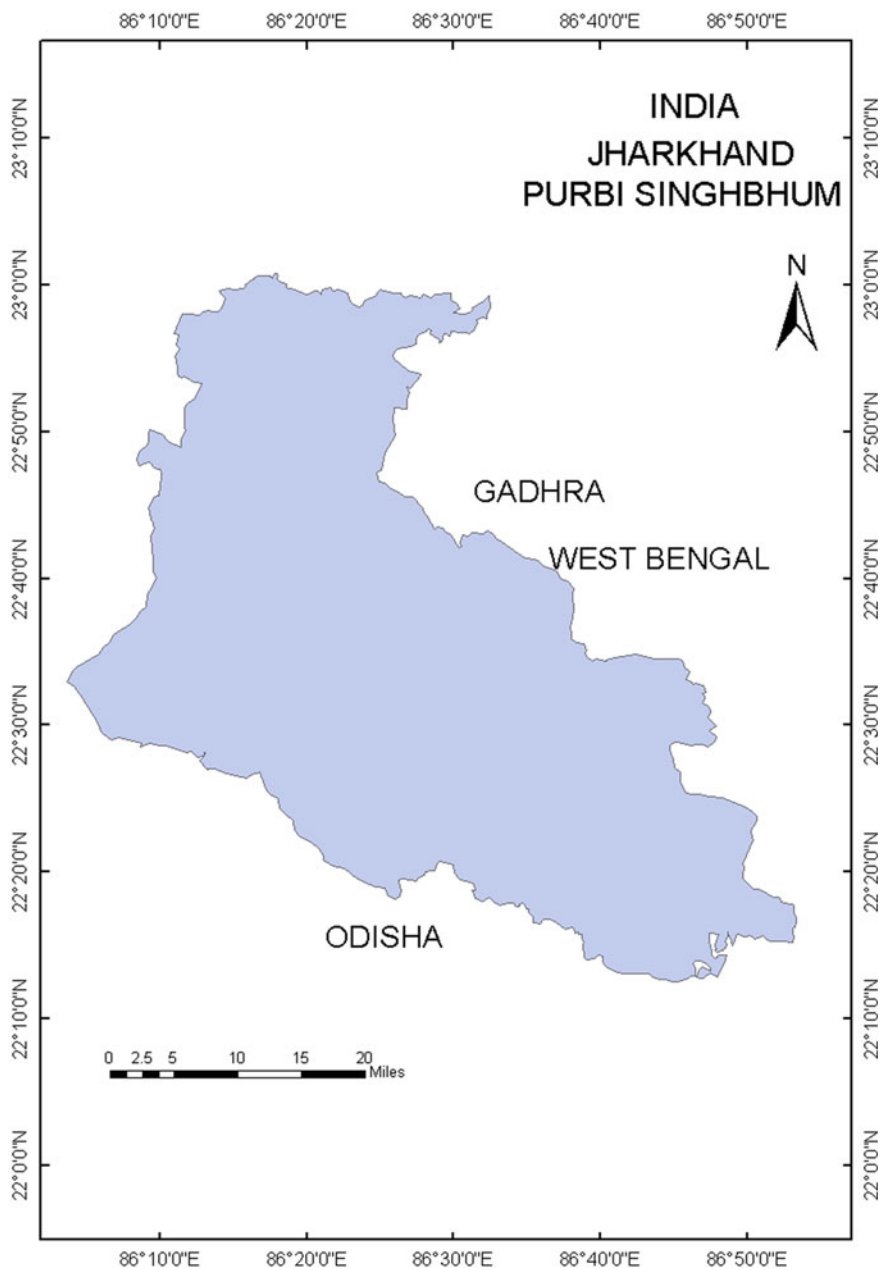


**Fig. 1** Location map of study area

## 4 Results and Discussion

In this study, the part of the real network is considered DMA-02 (Ghadara) in East Singhbhum District, Jharkhand which is having a network of 7293ft with diameter varying from four inches up to eighteen inches.

As, per the Indian Standards the pressure should be within 35–80 psi when there is no fire. After hydraulic computation in Water Gems we have observed that this standard pressure is not achieved in real network so there is need for a revised network which will satisfy the pressure criteria as per the standards while keeping in note that there should be no increase in total head loss in the entire network.

In revised network one Pump and one Pressure Break Valve is added in the hydraulic network as compared to the real network to satisfy the pressure criteria within 35–80 psi and there is also no increase in Total Head Loss which is 0.244 ft/ft similar to real network.

Simulation network is represented in figure and computational Results are represented in Tables for both real and revised network. Reservoir Table, Tank Table and Orifice between pipe is similar for both real and revised network in terms of its character sticks. whereas Pipe Table and Junction Table is represented differently for real and revised network and Pressure Break Valve and Pump Tables are presented only for revised network.

In this study we have considered the flow from Tank (overhead tank) to consumers whereas the flow from reservoir up to Overhead tank is not considered in our study area as it is under pumping pressure whereas the flow from Tank (overhead tank) to consumers is under the flow of gravity.

Figures 2 and 3, represents hydraulic network simulation is represented for real and revised network—Water GEMS.

The Head Loss is calculated noting Hazen Williams Equation where the value of Hazen Williams Coefficient is taken to be 140 for both the real and revised network and the elevation used for all the Junctions is same for both the networks.

In the Real Network as shown in Fig. 3, during Simulation in Water GEMS it was found to have no error but on validation the results obtained from Flex Tables shows that out of 24 Junction or node which is used in the entire network pressure was not found to be in the desired range of 35- 80 psi which is represented in terms of graph between Junction ID in the horizontal axis and pressure in the vertical axis so redesign of this network is must to bring the pressure limits within the standards. Here the elevation in the entire nodes and demand of 36 gpm is set same in both networks.

In the Revised Network as shown in Fig. 4, where 01 Pump and 01 Pressure Break Valve is added in the network between tank (T-1) and Junction (J-1) during simulation in Water GEMS it was found to have no error but on validation results obtained from Water GEMS results obtained from Flex Tables showed that the pressure is found to be within specified limits of 35–80 psi. Here pump characteristics is defined as standard 3 point and its efficiency are set to best efficiency, Breakeven point is set to 85% and NPSH (Net Positive Suction Head) warning safety factor is set to 1. In

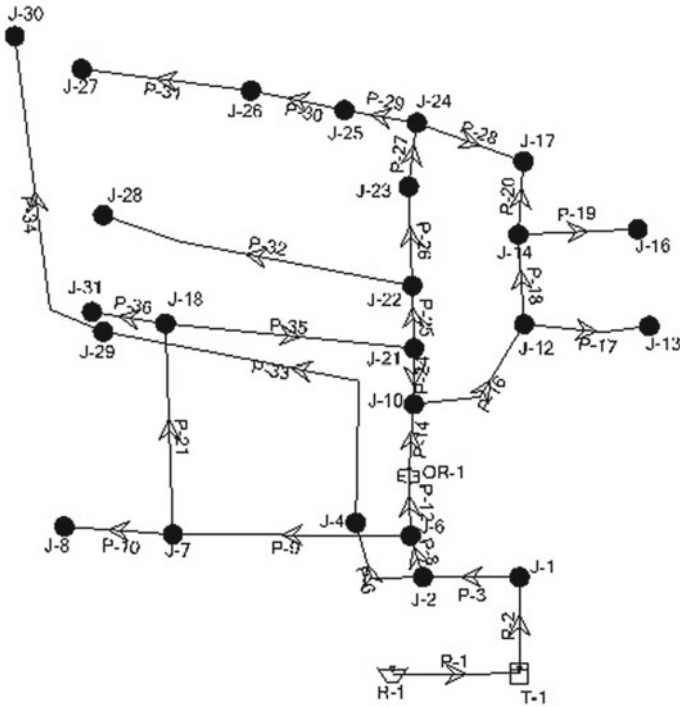


Fig. 2 Real network simulation

Pressure Reducing Valve (PRV) its settings are set to 100 psi to make pressure within standard limit of (35–80 psi). The results obtained is represented in terms of graph which is plotted as Junction ID in horizontal Axis and Pressure (psi) in the vertical axis. The elevation in both the networks (real and revised) are kept same for each node but here in the revised network it was found the hydraulic grade increases since there is increase in pressure compared to real network.

In both the real as well as revised network diameter of the pipe remains the same for both network varying from 4 inch up to 18 inch, selected on the basis of distribution mains and transmission mains. The quality of the pipe used in the entire network is Ductile Iron. Here the graph is obtained between Pipe ID in the horizontal axis and the Head Loss in the vertical axis.

In the Real Network Fig. 3, on simulation no error was found but after validation the results obtained from Flex Table showed that Head Loss obtained in the network was high which validates the basis principle of Conservation of Energy: Sum of head loss must be equal to zero ( $\sum H_L - \sum H_{PUMP} = 0$ ) which violates this statement to a greater extent as the Head Loss obtained using this real network is 0.244 ft/ft.

In the Revised Network Fig. 4, on addition of 01 Pump and 01 PRV (Pressure Reducing Valve) during simulation no error was found but after validation results obtained from Flex Tables shows that the Head loss is reduced to 0.175 ft/ft compared

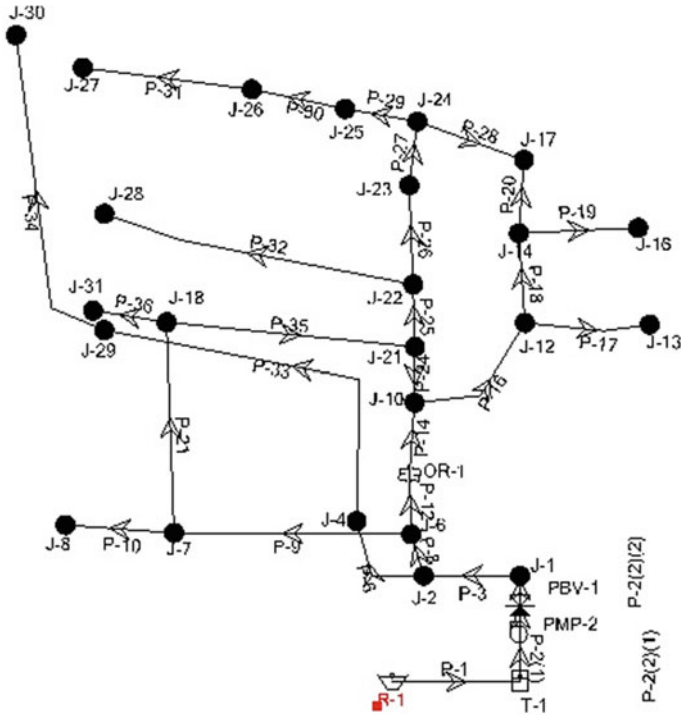


Fig. 3 Revised network simulation

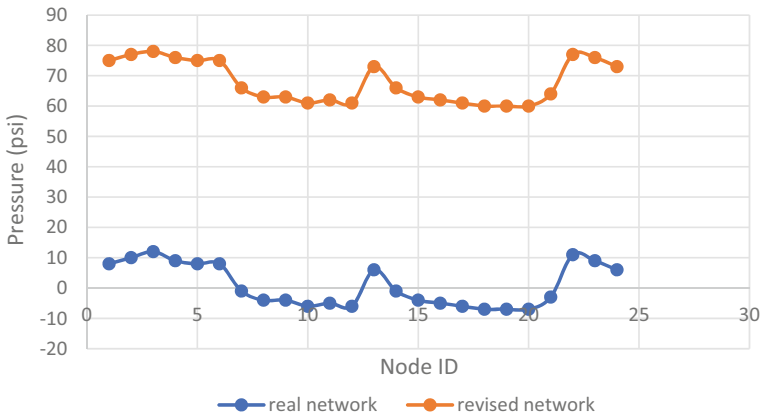
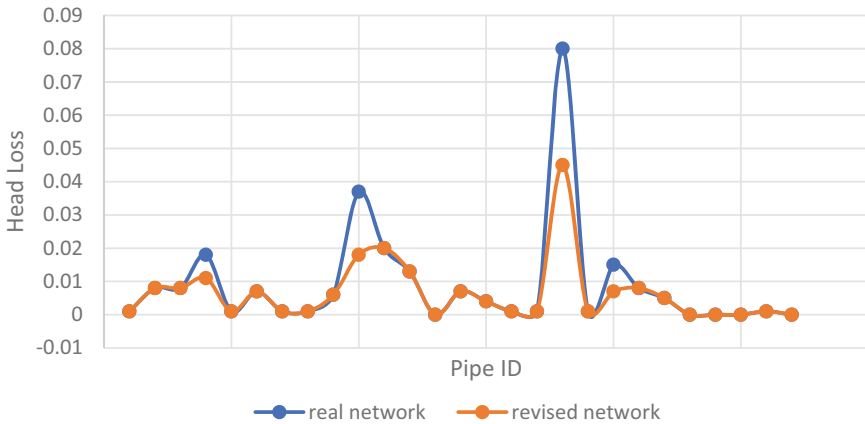


Fig. 4 Node ID versus pressure (psi)



**Fig. 5** Pipe ID versus head loss (ft/ft)

to 0.244 ft/ft in the real network which means that basic violation of conservation of energy is less in Revised Network as compared to Real Network which clearly indicates that revised network performs better than real network (Fig. 5).

Subarnarekha river is the Reservoir for both Real and Revised Network of Ghadara (DMA-02) and the water is supplied to Tank with an outflow of 2700 gpm. With an elevation of 181.44 ft. Tank Table represents overhead tank which stores water for the entire network of Ghadara including all DMA's. Here we observe that 2700 gpm is supplied from reservoir to tank and 1844 gpm is stored in the tank and the rest 856 gpm is the entire demand for the network which is to be supplied. Here the volume stored in the tank is 130,000 MG whereas the stage height is the difference between initial elevation and minimum elevation and the diameter of the tank is 30 ft. Orifice is placed between pipe nos 12 and 14 for both real and revised network during hydraulic simulation. The advantages of orifice meter is that it can be installed either horizontal, vertical or inclined. It is suitable for line sizes 6 mm up to 800 mm. The accuracy that we are getting with orificemeter is  $\pm 0.5%$  up to  $\pm$  up to 3%. Pump is added as a hydraulic parameter in the revised network to satisfy the pressure standards of 35-80 psi. So, here pump character is defined as standard 3 point. Pump efficiency is set to best efficiency, Breakeven point is set to 85% and NPSH (Net Positive Suction Head) warning safety factor is set to 1.

PBV (Pressure Break Valve) is placed between pump and Junction 1 in the revised network to reduce the excess pressure at nodes downstream of PBV. This excess pressure is caused by the installation of pump in between Tank and Junction 1. To reduce this excess pressure caused by the pump one PBV is used in the entire network of 7293 ft between pump and junction 1 as shown in Fig. 3 and its Pressure settings is set to 100 psi to make pressure within standard limit of (35–80 psi).

## 5 Conclusion

Here after considering two networks real and revised networks the nodes where the pressure is not met is predicted through hydraulic simulation through Water Gems software in the real network and by adding certain hydraulic parameters such as Pump and PBV (Pressure Break Valve) in the revised network satisfies the pressure standard limit of 35–80 psi and meet the required demands of 135 l-pcd for individuals without increasing the total head loss in revised network when compared it with real network. It is obvious that by the addition of pump and PBV the overall cost will increase but it is also important to satisfy the individual demand per capita of water.

## Bibliography

1. Araujo LS, Ramos H, Coelho ST (2006) Pressure control for leakage minimization in water distribution systems Management. *Water Resour Manage* 20(1):133–149
2. Agathokleous A, Christodoulou SE (2016) Vulnerability of urban water distribution networks under intermittent water supply operations. *Water Resour Management*. 30:4731–4750
3. Bhave PR, Lam CF (1983) Optimal layout for branching distribution networks. *J Transp Eng (ASCE)* 4:534–547
4. Batish R (2003) A new approach to the design of intermittent water supply networks. In: *Proceedings of the World Water and Environmental Resources Congress, Philadelphia, PA, USA, 23–26 June*
5. Chandapillai J, Sudheer KP, Saseendran S (2012) Design of water distribution network for equitable supply. *Water Resour Management* 26(2):391–406
6. Zhang C, Ding W, Li Y, Guangtao F (2019) Cost-benefit framework for optimal design of water transfer systems. *ASCE*
7. Mehta DJ, Prajapati KJ (2018) Simulation of existing water distribution network at Punagam Area of Surat City using WATERGEMS software. *ASCE* (2018)
8. Eyath SA (2016) Master plan for water management and distribution. In: SA Eyath, Area of responsibility; Corporate Report. Thessaloniki, Greece, 2016 (in Greek)
9. Fontanazza C, Freni G, La Loggia G (2007) Analysis of intermittent supply systems in water scarcity conditions and evaluation of the resource distribution equity indices. *Des Nat III Comp Des Nat Sci Eng*, 103
10. Alighalehbabakhani F, Miller CJ, Elmurry SM, Mohsen S, Abkenar S (2013) A case study of energy cost optimization in Monroe water distribution system. In: *International Green Computing Conference Proceedings*
11. Praveen Kumar G, Geetha P, Shanmugasundaram GA (2016) Real time water utility model using GIS: A case study in Coimbatore district. Springer, Switzerland
12. Switnicka K, Suchorab P, Kowalska B (2017) The optimization of a water distribution system using Bentley Water GEMS software. *ITM Web of Conferences* 15:03009
13. Lansey KE, Duan N, Mays LW (1989) Water distribution system design under uncertainties. *ASCE J. Water Resources Planning & Management* 5:630–644
14. Aral MM, Guan J, Maslia ML, Optimal design of sensor placement in water distribution networks
15. Morosini AF, Caruso O, Veltri P, Costanzo F (2015) Water distribution network management in emergency conditions. *Procedia Eng*. 119:908–917
16. Pathan SS, Kahalekar UJ (2015) Optimal design of water distribution network by using WATERGEMS. *Int J Pure Appl Res Engineering Tech* 3:308–319



17. Chandramouli S, Malleswararao P (2011) Reliability based optimal design of a water distribution network for municipal water supply. *Int J Engineering Tech*
18. Gebremedhin Berhane T, Areg TT, Optimization of water distribution system using Water gems: the case of Wukro Town, Ethiopia. *Civil and Environmental Research*. ISSN 2224–5790 (Paper) ISSN 2225–0514
19. Vairavamoorthy K, Gorantiwar SD, Mohan S (2007) Intermittent water supply under water scarcity situations. *Water Int* 32:121–132
20. Wu ZY, Wang RH, Walski TM, Yang SY, Bowdler, D, Baggett CC (2006) Efficient pressure dependent demand model for large water distribution system analysis. In: *Proceedings of the 8th Annual Water Distribution System Analysis Symposium*
21. Wu ZY, Walski TM (2006) Pressure dependent hydraulic modelling for water distribution systems under abnormal conditions. In: *Proceedings of the IWA World Water Congress, Beijing, China, 10–14 September*

# **Remote Sensing/Geospatial Techniques in Water Resources**

# Identification of Flood Vulnerable Area for Kharun River Basin by GIS Techniques



Bhupendra Kumar Dhiwar, Shashikant Verma, and A. D. Prasad

**Abstract** Floods are natural disasters which cause the loss of human life and property. The natural disasters that cause the loss of human life and property are floods. The important tool for defining the flood zone of any region and its control is flood plain mapping. Flood plain mapping is important to educate and inform people living in flood prone regions about the risk of flooding and to prevent potential settlements and developments. The benefits of this flood inundation mapping of any flood region are that users can easily access the information and make special plans to minimize flood losses by using advanced technology such as GIS and remote sensing, i.e., flood control. This study offers a fundamental approach by using HEC-RAS and GIS methods to classify flood prone areas of the Kharun River basin Peak discharge released from both the gauge and discharge site of the Kharun river basin has been taken for flood modeling. The modeling results promote the detection of the flood prone area and the magnitude of the flood for various flow conditions via the flood maps.

**Keywords** Introduction · Review of literature · Methodology · Flood modeling · Flood conditions · Flood inundation maps · Validation

## 1 Introduction

Water is an essential ingredient of life. Rain is the major component of the hydrologic cycle. It reaches the earth's surface after condensation of water droplets present in the atmosphere. When the soil exceeds the capacity of infiltration and has no ability to capture water, water flows in the form of runoff over the surface of the earth. It

---

B. K. Dhiwar (✉)

Civil Engineering Department, Chhattisgarh Swami Vivekanand Technical University, Bhilai 490009, India

S. Verma · A. D. Prasad

Civil Engineering Department, National Institute of Technology, Raipur 492001, India  
e-mail: [sverma.phd2018.ce@nitrr.ac.in](mailto:sverma.phd2018.ce@nitrr.ac.in)

can cause water overflows that can cause flooding if there is any obstruction in the flow path.

Floods are one of the world's most natural catastrophes, resulting in loss of life, livelihood systems, infrastructure, livelihood systems, production, productivity in agriculture, and public utilities. Floods are normally triggered by the increasing occurrence of heavy rainfall, inadequate drainage capacity, and drainage system maintenance failure, water resource structure failure such as dam break, etc. As water falls on the surface of the earth as precipitation in different forms such as rain, snow, etc. it penetrates into their previous voids into the ground. But in the case of an impermeable base, or if the ground is frozen and the soil is completely saturated, water will not be freely drained before it falls, causing immense problems. Flood inundation mapping is the operational tool to forecasts flood risks, the primary purpose of those are not only for public safety but also to understand the natural process change that produces hazards, to develop the hazard mitigation strategies and technology and to reduce vulnerability and to prevent repetition of loss of infrastructure [1, 2].

Flood plains are those areas which are adjacent to the river or stream due to exceeding (overflowing) of water in rainy season. This causes tremendous problems in the region for both living and non-living species, such as water logging, land submergence, relocation of people living along the river, etc. Flood inundation/vulnerable mapping is nothing but the identification of the flood region using different software tools by mapping.

### ***1.1 Factors of Flood***

Both human and natural activities are responsible for the event of flooding. Natural phenomenon includes a very high rate of rainfall for a short period of time (incessant rains), cloud bursting and man-made causes that include collapse of infrastructure such as a bank, dam canal, dam, etc. It also happens due to the insufficient capacity of the drains and the lack of maintenance of the drainage system, the degradation of the structure of the water resource, such as the dam break, etc. In case of flooding in river, high intensity precipitation, landslides, sediment deposition are most common reasons.

### ***1.2 Flood Inundation Mapping***

There are both structural and non structural measures to control the floods. As a result of developments in computer technology, numerous software tools for flood prediction, flood hazard mapping/flood inundation mapping have been developed [3]. Flood plains are those areas that are adjacent to the river or stream due to it creates huge problems for all living and non-living organisms in surrounding area such as water logging, submergence of land area, displacement of the people living

**Table 1** Characteristic of the Kharun River Basin

| Study area     | Kharun Basin               |
|----------------|----------------------------|
| Latitude       | 20° 33' 30" N–21°33' 38" N |
| Longitude      | 81° 17' 51" E–81° 55'25" E |
| Catchment area | 4112 km <sup>2</sup>       |
| Length         | 164 km                     |

near the river, etc. flood inundation mapping is the one of the non structural measure, the primary purpose of which to identify the flood prone area through mapping. Flood inundation mapping is the operational tool to forecasts the flood risks and the purpose of those are not only for public safety but also to understand the natural process change that produces hazards, to develop the hazard mitigation strategies and technology, and to reduce the vulnerability, and to prevent repetition of loss of infrastructure [4]. Improved understanding and visualization of flood inundation map and flood vulnerability analysis, flood and mitigation insurance, flood management, emergency action plans can be developed [5].

### 1.3 Study Area

The Kharun River Basin is chosen as a study area in this research work. All parts of study area occupy within the Chhattisgarh state. It is a major tributary of the Seonath River which is also the tributaries of the Mahanadi River. The geographical coordinates of the study area lie between the latitudes of 20° 33' 30" N–21° 33' 38" N and 81° 17' 51" E–81° 55' 25" E. Origin point of Kharun River situates at Petechua village of Balod block in southeast of Durg district and after flowing about 164 km, it meets to Seonath River near Somnath. Kharun River plays a vital role to fulfill the public, domestic, and industrial water supply. Kharun Basin is a part of lower basin of Mahanadi river basin in Chhattisgarh state of India. This basin is having 5.42% of catchment area of Mahanadi basin in Chhattisgarh state. Table 1 and Fig. 1 show the characteristic and index map of the Kharun River Basin respectively.

### 1.4 Data Used

Digital Elevation Model (DEM)—Digital Elevation Model is a digital representation of elevation variations on earth surfaces. The DEM 30 m resolution of ASTER has been used for this work. In order to obtain the DEM needed for this study area, the entire Kharun basin is delineated. The maximum and minimum elevations of this study area are 451 and 249 m above the mean sea level. The DEM of the Kharun River Basin is shown in Fig. 2.

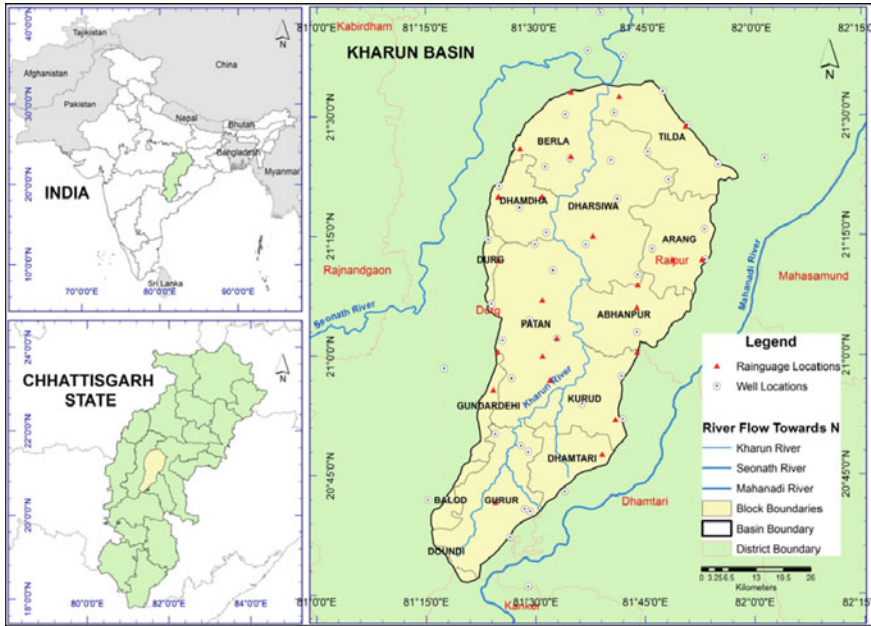


Fig. 1 Index map of Kharun River Basin. Source Arab J Geosci (2016) 9: 98

### 1.5 Gauge and Discharge Data

The water level and discharge at the point of the cross section of the river are observed daily for Pathardih and Amdi Gauge and the discharge site for monsoon and non-monsoon times. Initially, the G&D site at Pathardih was set up by the Central Water Commission under the Ministry of Water Resources, Government of India in 1989. After that Amdi G&D site began by Water Resources Department of Chhattisgarh’s Government in 2001. Discharge data are available from 1989 to 2015 for Pathardih and from 2001 to 2015 for Amdi G&D site. Figure 3 shows the Gauge and discharge site of Kharun River Basin (Pathardih and Amdi site).

### 1.6 Land Use Land Cover (LULC)

LULC of the study area was obtained from BHUVAN. According to LULC map, Kharun river basin consists of five features, i.e., water bodies, forest, wastelands, built up area, and agricultural area. Figure 4 shows the land use land cover of Kharun river basin (Table 2).

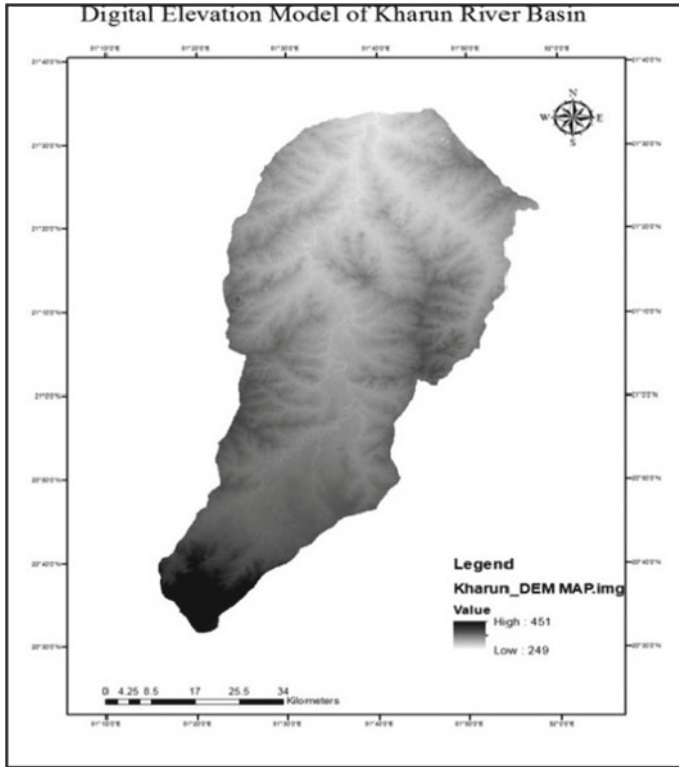


Fig. 2 Kharun River Basin DEM

## 2 Review of Literature

**Goodell, C. et al. (2006)** have presented a paper in 2006 based on flood inundation mapping of Cameron Run Watershed, located in eastern Fairfax County, in the Commonwealth of Virginia, USA. The results obtained in the form of flood inundation maps are useful for municipal planning purposes, flood insurance rates, emergency action plans, and ecological studies.

**G. Shrinivasa Rao et al. (2006)** has done research work on Flood Inundation Modeling of Godavari River Basin. In this work, part of Godavari floodplain was chosen as a study area which is located in Andhra Pradesh, India. An attempt was made to simulate the flood inundated area of Godavari River Basin part. HEC-RAS and HEC-GeoRAS with the companion of ArcGIS model were taken for flood inundation mapping. Simulated results obtained from modeling are according to satellite observation. A further study of this research work can be carried out for early warning system of floods in the country.

**Mr. Praveen Kumar Thakur et al. (2006)** have carried out research work on Flood Inundation Mapping and 1-D Hydrodynamic modeling by using remote

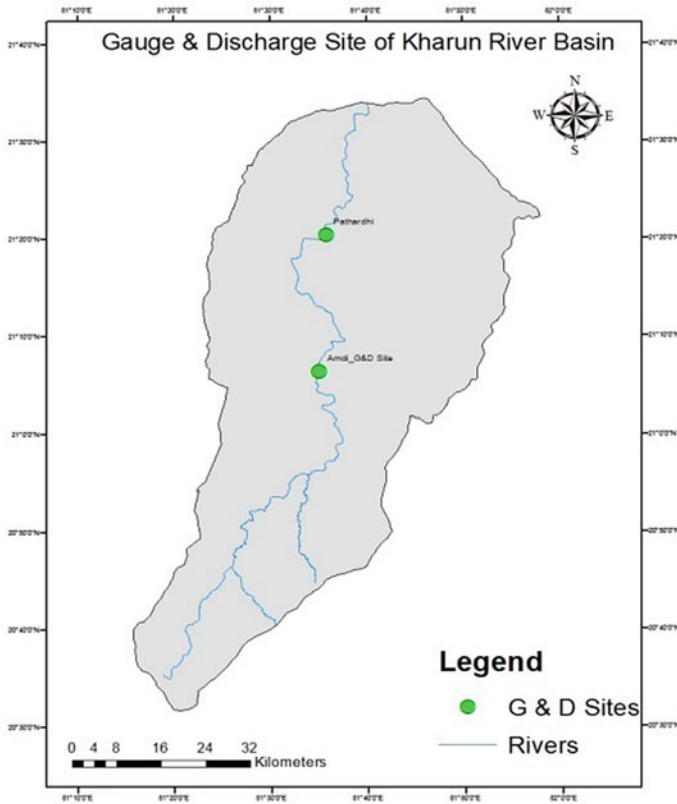


Fig. 3 Gauge and discharge site of Kharun River Basin

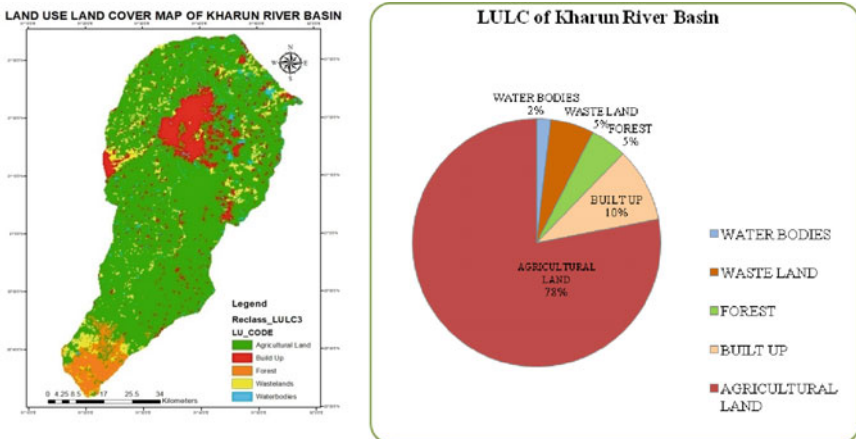


Fig. 4 Land use land cover of Kharun River Basin



**Table 2** Land use of Kharun River Basin

|                         | Agricultural land | Forest area | Urban area | Waste land | Water bodies | Total area |
|-------------------------|-------------------|-------------|------------|------------|--------------|------------|
| Area in km <sup>2</sup> | 3269.96           | 199.55      | 405.98     | 237.38     | 76.52        | 4189.39    |
| Area in % age           | 78.05             | 4.76        | 9.69       | 5.67       | 1.83         | 100        |

sensing and GIS technique. Objective of this study was to develop flood inundation maps of flood event occurred in 2003 in Puri District, Orissa, India. Digital elevation model (DEM) of the study area was taken from ASTER to extract the cross section required for flood modeling also the cross section data were collected from six different places by field visit to Puri district to adjust the cross section obtained from DEM. Rating curve had also been established using observed G&D data at the site chosen for the study. Hydrodynamic model HEC-RAS (Hydraulic Engineering Center-River Analysis System) was used to found out the water surface profile of the river. Again with the help of HEC-GeoRAS with the companion of the GIS flood inundation area are identified. After the end flood inundation maps are compared with the flood extent maps derived from RADARSAT SAR satellite images (4, 11, 13 September 2003).

**Nanshan Zheng et al. (2008)** has carried out research work on a distributed flood inundation model integrating with Rainfall-Runoff processes using GIS and Remote Sensing Data. This paper presents development of distributed model for simulation of flood inundation integrating with rainfall-runoff processes. This model takes a 1-D diffusion wave represent channel flow and 2-D diffusion wave approximation of overland flow which was solved by the application of an explicit finite difference scheme. Simulated results help to identify and delineate the flood vulnerable area.

**Dr. D. P. Vijayalakshmi et al. (2010)** evaluated in his work different methodology and advance technologies that are incorporating for hydraulic and hydrologic analysis which could be useful for prediction of flood water surface elevation of any ungauged catchment. They found out that the rainfall-runoff modeling can be effectively carried out by HEC-HMS software and HEC-GeoRAS and GIS an ideal package for flood inundation modeling.

**T. Z. Gichamo et al. (Dec 2011)** gives an approach in his study to extract the River cross section from the ASTER global DEM which is generally used for flood modeling. This extracted cross section of river could be used in 1-D River modeling tool in HEC-RAS/HEC-GeoRAS to simulate the flooding on Tisza River, Hungary. A Bias correction has been carried out for comparison of elevation point of DEM for improvement of cross section data of the corresponding DEM.

**Marina Mazlan et al. (March 2014)** presented the general approach, methodology, and some usual practices for the development of flood inundation model. Model generation covers the availability of data; method adopted, and flood modeling using either (1-D) one-dimensional and (2-D) two dimensional hydrodynamic model with approach for flood mapping. For hydrodynamic model and flood mapping, Sembong River and for flood inundation modeling, Kota Tinggi site was chosen.

**Sunil Kute et al. (June 2014)** has carried out a research work on the Flood modeling of River Godavari using HEC-RAS. In this paper, Gangapur dam is at the upstream side of Godavari River reach selected for flood inundation modeling. This dam is constructed at the upstream part of the Nasik city at a distance of 14 km. This work is based on consideration of worst flood discharge in the year of 1969. For this modeling fourteen bridges that come across the river are considered. This flood model shows the development of flood plain and its extension for flood prevention measure and their management. Flood modeling using HEC-RAS facilitates an effective tool for control of disaster management measures.

**F. V. Silva et al. (Sept 2014)** has explained flood inundation mapping of urban areas by HEC-RAS model companion with the GIS. Rio dos Cedros urban area, located in medium Itajaí River Valley, Santa Catarina, Southern Brazil are selected for mapping of flood plain areas. These flood plain maps were very useful for decision makers in the field of urban land use development plan, growth of awareness between the people related to risk areas, and improvement of understanding of the overflow water dynamics to riparian areas regarding rescue evacuation routes and defining the safety areas to allocate affected person. A future study can be carried out in the field of hydrologic rainfall-runoff modeling studies to analyze the different influences on the dam by the dam.

**Evan, T. A. et al. (2015)** has presented a new feature HEC-GeoRAS with the integration of GIS for pre and post processing of HEC-RAS during hydraulic model. It includes the importing the roughness value along with the cross section exporting the bank station of river in GIS and velocities across different cross section of the river. These manning coefficients of correlated with the land use and land cover of area in the attribute table.

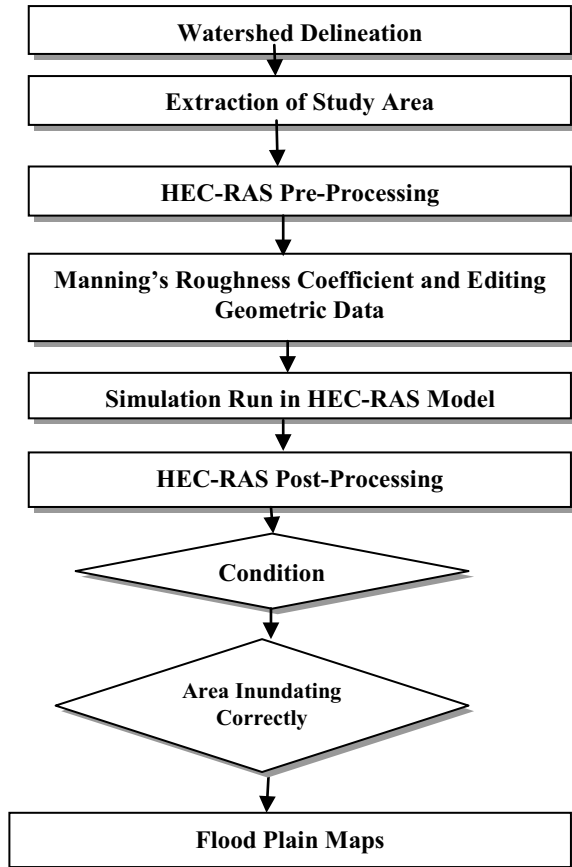
**Da-wei Zhang et al. (2015)** made a case study on Xiapu River Basin, China which is focused on flash flood hazard mapping. In this study, the headwater catchment of the Xiapu River Basin in china was selected for their study. Flash flood hazard analysis gives an estimation of the extent and intensity of design flash flood scenarios. A new conceptual distributed hydrological model for the simulation of flash floods was developed by this study.

**Faghih Mina et al. (2015)** showed some GIS Techniques for Flood Plain Modeling and Flood Inundation Mapping. In this paper, application of GIS for developing flood plain and flood inundation maps are described. So many researchers conducted various flood models for flood vulnerability analysis and flood forecasting. GIS with the integration of HEC-RAS model is becoming an effective tool for flood plain mapping. In this research work, HEC-RAS and HEC-GeoRAS were used for floodplain delineation and identification of flood prone areas of Dalaman Plain. HEC-RAS and HEC-GeoRAS were used for hydraulic modeling and companion of the GIS to get the HEC-RAS result respectively.

### 3 Methodology

In this study, ArcGIS, HEC-GeoRAS, HEC-RAS software are used to develop the flood vulnerability maps. Methodology consists of three phases: (i) Preparation of digital elevation model of the study area by using watershed delineation process using ArcGIS (ii) Model simulation run using flow values recorded at gauge and discharge station. (iii) Development of flood maps for different flow conditions. Flow chart (Fig. 5) shows the methodology to develop the flood inundation maps of Kharun River basin.

Fig. 5 Flow chart of methodology



## 4 Flood Modeling

Hydrological Engineering Center-River Analysis System (HEC-RAS) model—This is public domain software which was developed by US ARMY CORPS OF ENGINEERS. It has various applications such as one and two dimensional steady and unsteady flow calculation, sediment transport, water temperature modeling and water quality modeling, Quasi unsteady and full unsteady flow sediment transport-mobile bed modeling, etc [6].

This software is built after some improvement in HEC-2 and has the ability to share data with ArcGIS via HEC-Georas. This program is normally designed to perform a 1-D mathematical hydraulic calculation for a natural and built channel and through which stream morphology can be presented by a sequence of cross sections of a river flow. This model typically relies on two mathematical equations, one for continuity equations and the other for momentum equations [7].

Continuity equation used in HEC-RAS is given by:

$$\frac{\partial Q}{\partial x} + \frac{\partial A}{\partial t} = 0 \quad (1)$$

Similarly, momentum equation used in HEC-RAS is given by:

$$\frac{\partial Q}{\partial t} + \frac{\partial(QV)}{\partial x} + gA \left( \frac{\partial h}{\partial x} + S_f \right) = 0 \quad (2)$$

where,

|          |                               |
|----------|-------------------------------|
| $A$      | Cross Sectional Area of flow, |
| $Q = AV$ | Discharge,                    |
| $V$      | Velocity of flow,             |
| $H$      | Head,                         |
| $S_f$    | Friction Slope.               |

HEC-RAS is multitasking software which uses 1-D saint-vecant equation for flow computation in any stream/river.

Saint Vecant equation can be expressed as:

$$\frac{\partial u}{\partial t} + u \frac{\partial u}{\partial x} + g \frac{\partial h}{\partial x} + g(s - s_f) = 0 \quad (3)$$

where,

|     |                              |
|-----|------------------------------|
| $u$ | velocity in $x$ direction,   |
| $t$ | time,                        |
| $g$ | acceleration due to gravity, |
| $h$ | head,                        |

$s$  bed slope,  
 $S_f$  energy slope.

To perform this equation, requires making a number of assumptions. For this research work, hydraulic modeling and simulation are performed in HEC-RAS. The key input required to work on the HEC-RAS is geometric data and flow data of the river [8]. Variations in the water level of the river are calculated by HEC-RAS. After that Depth of water is then overlaid on the DEM of the study area so that it will give the probable extent of flood areas [7].

**HEC-GeoRAS**

HEC-GeoRAS is a set of procedures, tools, and utilized for processing geospatial data in ArcGIS using a graphical user interface (GUI). This was also developed by the Hydraulic Engineering Center (US Army Corps of Engineers) which is widely used in civil engineering applications [9]. HEC-GeoRAS develops stream network, flow path lines, cross sections, ineffective flow areas, storage areas, Manning’s n values, etc. This acts as HEC-RAS model input. Water surface profile of basin and velocity data can be exported from HEC-RAS simulation that may be processed by HEC-GeoRAS for GIS analysis for flood inundation mapping, flood vulnerability analysis, ecosystem restoration, flood warning system, and preparedness.

The data specifications as main input for HEC-RAS are imported from ArcGIS by operating with the interface known as HEC-GeoRAS. Geometric data of the study area, such as area, length, slope, etc. are extracted using HEC-GeoRAS. RAS geometry is useful for creating a different function class, e.g., stream centerline, bank lines, flowpath centerlines, cross section cutlines, etc. This layer helps to obtain the elevation data of the river [10, 11]. In order to obtain this geometric data, the terrain model (TIN) has been used that can be created by using DEM. After getting the geometric data of the river; this data is used as key input in HEC-RAS. Flow data which is one of the key input of HEC-RAS requires to set a boundary condition also [12]. There are many options for boundary conditions are available, that can be chosen as per the suitability and data availability. In the end, model is run for simulation to get the desired result [13].

**Conditions**

In order to identify the flood prone area along with the variation in the flow value of the river, the flood vulnerable maps of the Kharun River Basin are created by considering the flow values along with the different flow conditions. Peak discharge values have been used to classify vulnerable flood areas. Table 3 shows the peak discharge reported at both the gauge and the discharge site.

**Table 3** Peak discharge recorded at gauge and discharge sites

| G&D site                      | Pathardih  | Amdi       |
|-------------------------------|------------|------------|
| Discharge (m <sup>3</sup> /s) | 2000       | 1600       |
| Occurrence date               | 14/09/2005 | 23/07/2014 |

**Table 4** Discharge for different conditions at both gauge and discharge sites

| Gauge and discharge site                        | Pathardih | Amdi |
|---|-----------|------|
| Peak discharge (m <sup>3</sup> /s)              | 2000      | 1600 |
| 0.1 times of peak discharge (m <sup>3</sup> /s) | 200       | 160  |
| 1.1 times of peak discharge (m <sup>3</sup> /s) | 2200      | 1760 |
| 1.5 times of peak discharge (m <sup>3</sup> /s) | 3000      | 2400 |

On the basis of twenty-five years of discharge data available for the Pathardih site and fifteen years of data for the Amdi site, the generation of flood prone maps is used. In order to classify flood variations, various conditions are used to produce flood vulnerability maps by adjusting corresponding maximum discharges such as 0.1, 1.1, and 1.5 times the peak discharge. Table 4 displays the flow values for the different conditions used to produce flood vulnerability maps.

## 5 Results and Discussion

In this work, ArcGIS 10.2.2, HEC-Georas 10.2, HEC-RAS 4.1.0, MS Excel 2007 were used for the preparation of flood maps, the extraction of river geometric properties, the hydraulic modeling, and the preparation of pie charts showing the percentage of flood vulnerable areas. Once the geometric properties of the river have been obtained by processing the HEC-Geo RAS, for each cross section of the river, the manning coefficient was entered [6]. The manning coefficient for the stretch of the Kharun River and the area surrounding the flood plains is 0.030 and 0.035. These values are intended for a clean, straight full stage with stones and weeds, as well as canals with heavy weeds and a scattered brush in the floodplain. Manning's n value is integrated as 0.035 for the left and right bank, and 0.03 for the main channel for all the cross sections of the river.

Flow values for both Gauge and Discharge have been entered for the simulation run of the model that calculates the water level for each cross section. At last, HEC-Geo RAS post processing was carried out in ArcGIS with the HEC-GeoRAS companion to create flood inundation maps for different flow conditions [9, 14, 15]. Pie chart displays the percentage of different areas inundated by different flow conditions. Figures 6, 7, 8, 9, 10, 11, 12, 13, 14, 15, 16 and 17 shows the flood vulnerable maps and percentage of flood affected areas of the Kharun River basin for different conditions.

In rainy season, when high intensity rainfall occurs, there is a problem of overflowing of water from bank station to the dry area, adjacent to the river. Flood vulnerability maps for different flow conditions have been prepared by intersecting the land use land cover of the Kharun basin with the flood area polygon for each flood event modeled. Out of the total flooded areas, about 76–77% of the region comes from agricultural areas and the remaining area consists of urban areas, forest areas including tree-clad areas, wastelands, water bodies, etc. 40.90 km<sup>2</sup>, 1.83 km<sup>2</sup>, 43.27

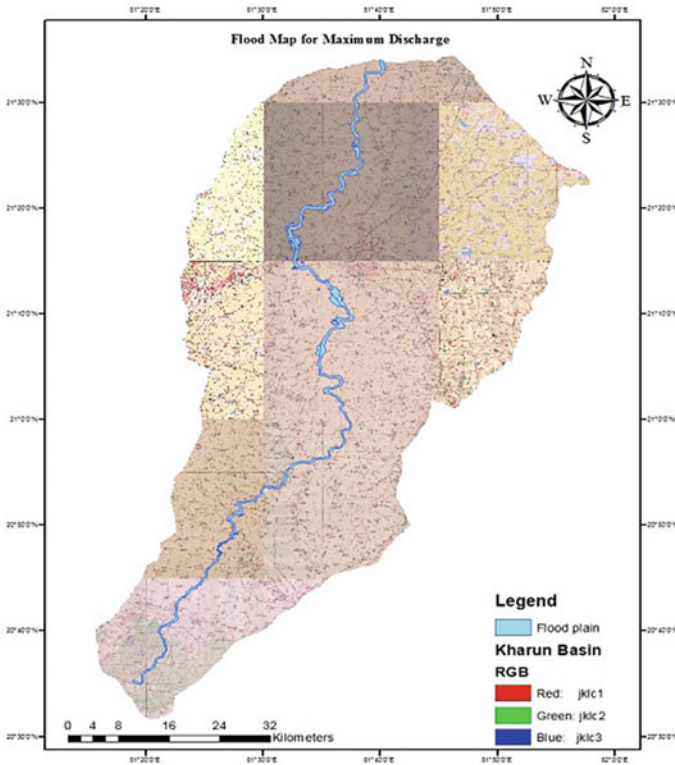


Fig. 6 Flood map for maximum discharge

km<sup>2</sup>, 55.87 km<sup>2</sup> of flooded areas under different conditions, i.e., peak discharge, 0.1 times peak, 1.1 times peak, and 1.5 times peak. Results obtained after running the model for each case have been presented through the pie chart. The degree of flood vulnerability is highly associated with the agricultural area followed by water bodies, urban area, waste land, and forest area. Different areas coming under inundation for various flow conditions are illustrated in Table 5.

## 6 Validation

To confirm the results obtained after hydraulic modeling: first previous year of the flood record of the catchment area, including Raipur, Dhamtari, Balod, Durg district, is taken from the Revenue and Disaster Department, Raipur C.G. and Second, the results were compared with the flood vulnerability index map of the state of Chhattisgarh produced by the National Remote Sensing Center (NRSC) available on the BHUVAN website.

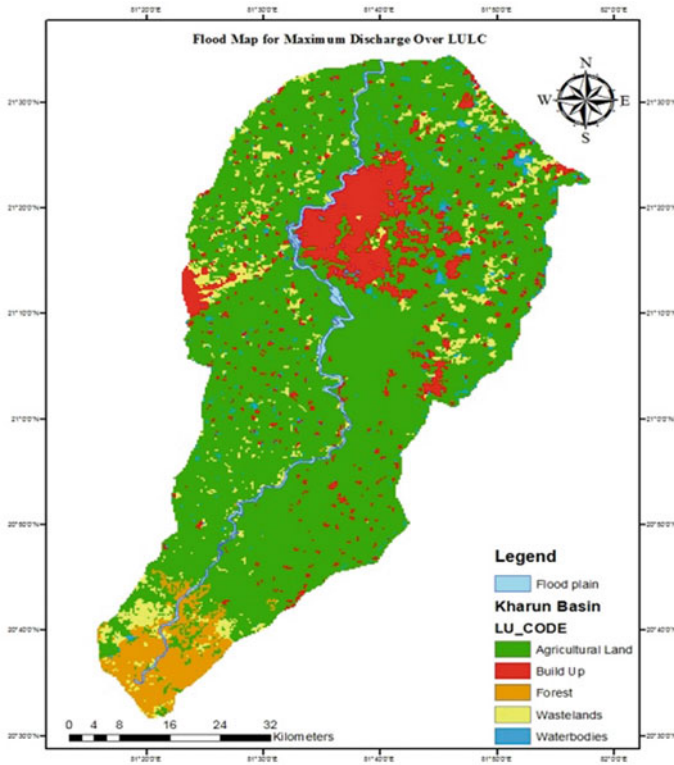


Fig. 7 Flood map for maximum discharge over LULC

The National Remote Sensing Center has developed flood vulnerability maps to evaluate vulnerable areas by combining various layers using multi-criteria assessment techniques. Using these maps, we compared the model results with the flood vulnerability index. According to both results, the maximum area near the Durg district is flooded. Maps of the Flood Risk Index have been established to assess flood prone areas. Table 6 demonstrates the validation of the findings of the model.

It is clear from the above table that the flood vulnerable area derived from the model is exactly same as the area reported by the Department of Revenue and Disaster also as flood vulnerability index established by the NRSC. So the model gives a satisfactory result (Fig. 18).



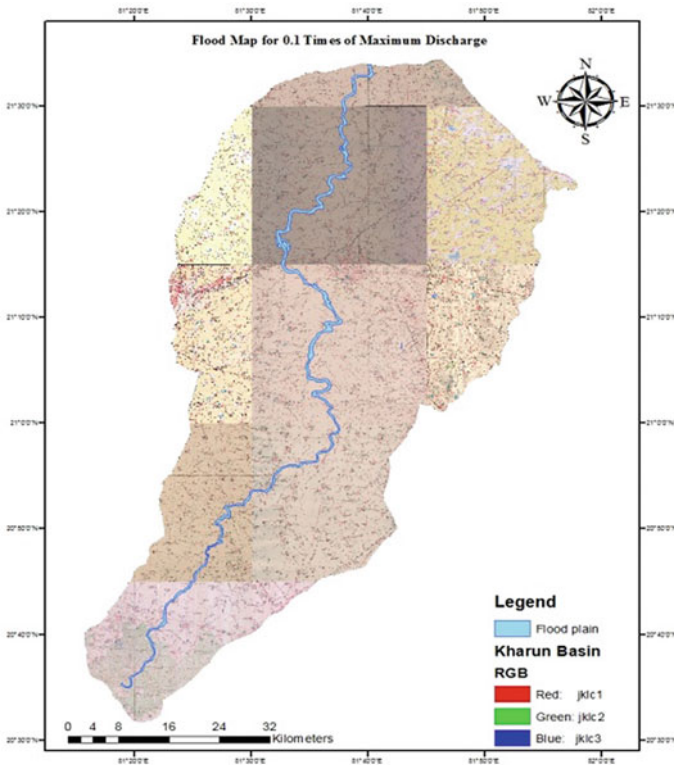
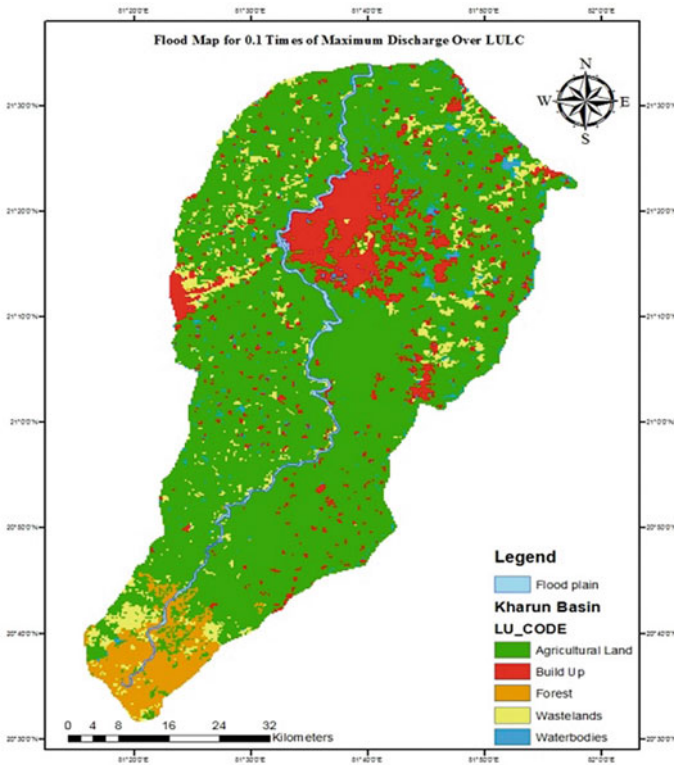


Fig. 8 Flood map for 0.1 times of maximum discharge

## 7 Conclusion

This study demonstrates a systematic approach to the development of flood maps to identify flood vulnerability areas by using a steady flow model with the help of a one-dimensional HEC-RAS numerical model, ArcGIS for data processing, data management, and HEC-GeoRAS serving as an interface between two other applications. The inference to be drawn from that review is as follows:

- Hydrological factors should be considered for the implementation of any project, otherwise, they can cause natural disasters such as floods.
- Development of flood inundation maps can be improved by using high resolution DEM and by increasing no. of cross section in the stream/river.
- HEC-RAS and ArcGIS with the companion of HEC-GeoRAS are useful tools in the development of flood inundation maps.
- Assessment of flood vulnerability areas for Kharun River Basin was very successful.
- HEC-RAS and HEC-GeoRAS are very time efficient tools for flood modeling.



**Fig. 9** Flood map for 0.1 times of maximum discharge over LULC

- The accuracy of our model simulation results depends on different factors, such as DEM accuracy, hydrological and hydraulic model structures, etc.
- HEC-RAS is a very strong, open package program for people. It is very easy to use and helps to assess the water surface profile for a number of streams.
- Flood inundation modeling can be done for both steady and unsteady flow conditions.
- Flood inundation maps produced using the HEC-RAS flood modeling method are useful for identifying vulnerable flood areas and planning flood mitigation steps.
- Emergency Action Plans, Municipal Planning Purposes, Ecological and Economic Research, Inundation Insurance Rate can be carried out using flood inundation maps.

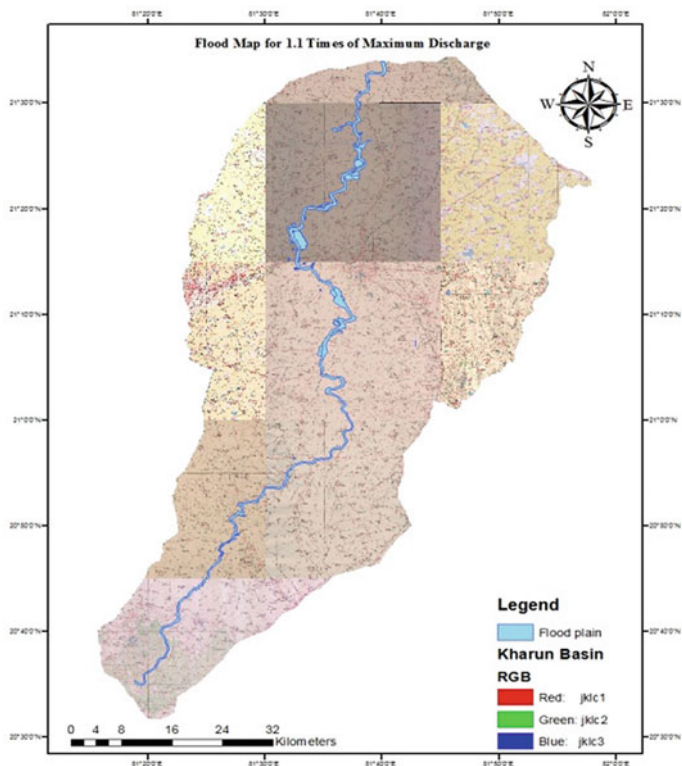
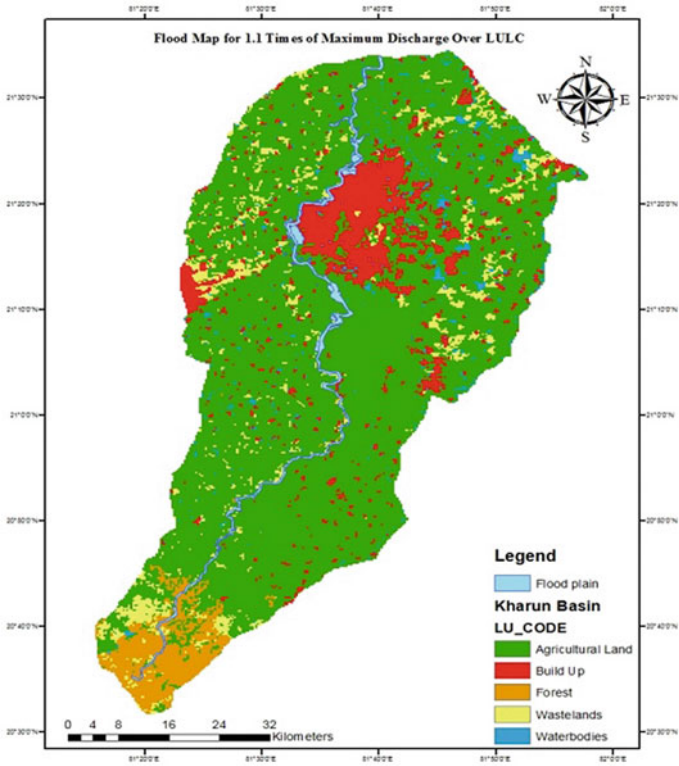


Fig. 10 Flood map for 1.1 times of maximum discharge



**Fig. 11** Flood map for 1.1 times of maximum discharge over LULC

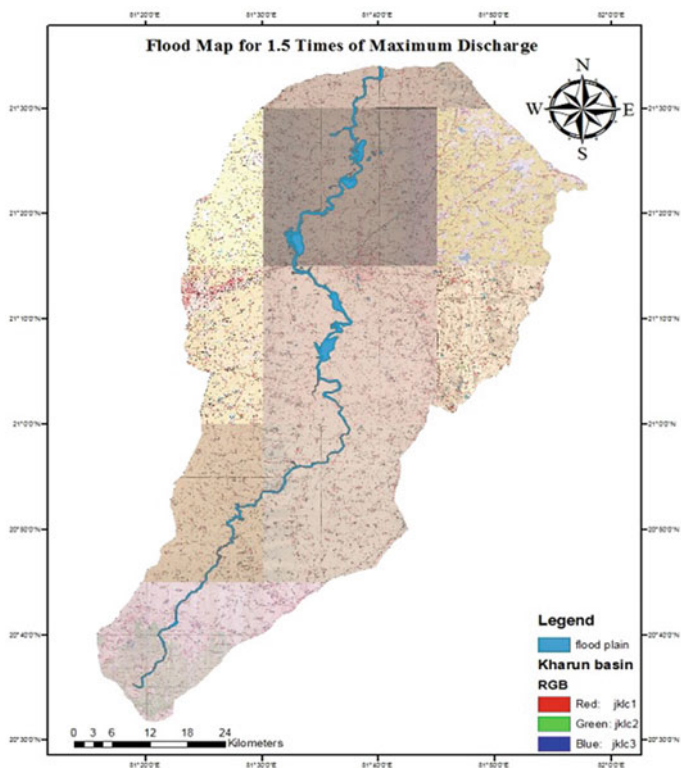


Fig. 12 Flood map for 1.5 times of maximum discharge

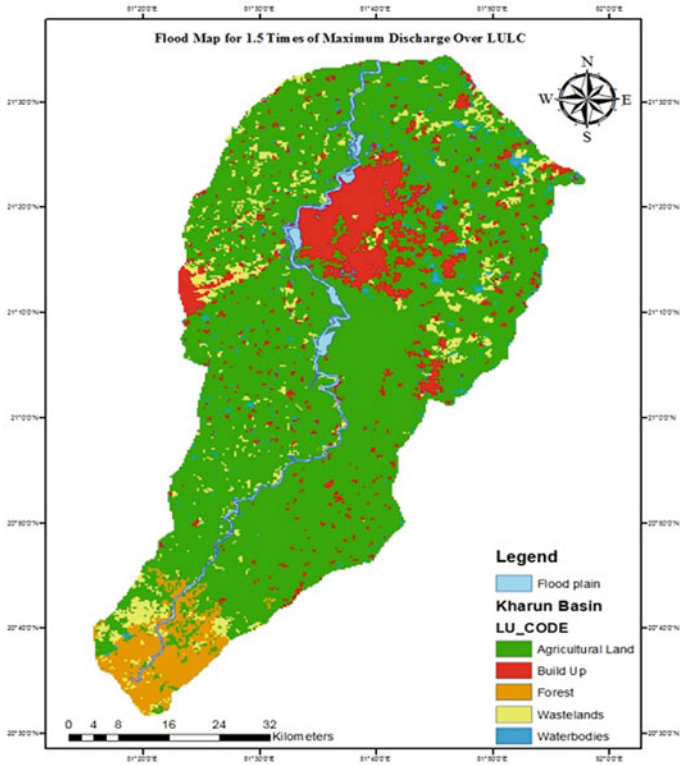
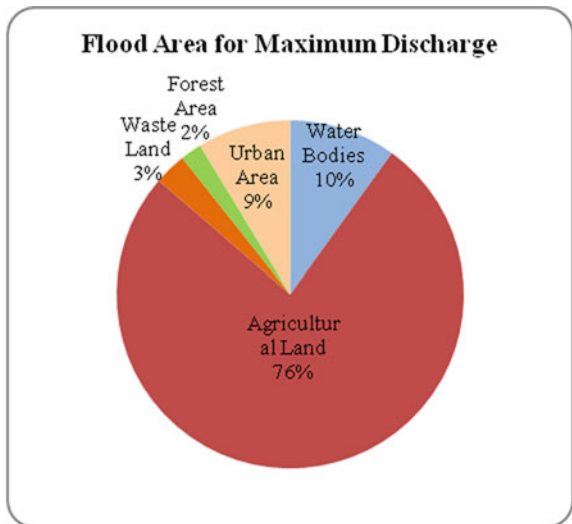
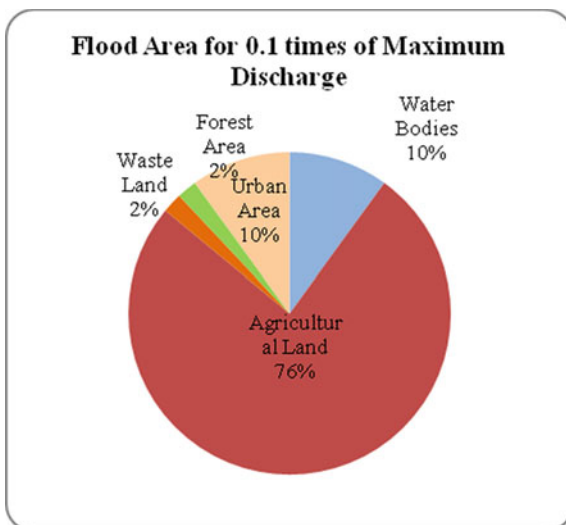


Fig. 13 Flood map for 1.5 times of maximum discharge over LULC

Fig. 14 Flood affected area for max. discharge condition



**Fig. 15** Flood affected area for 0.1 times of max. discharge condition



**Fig. 16** Flood affected area for 1.1 times of max. discharge condition

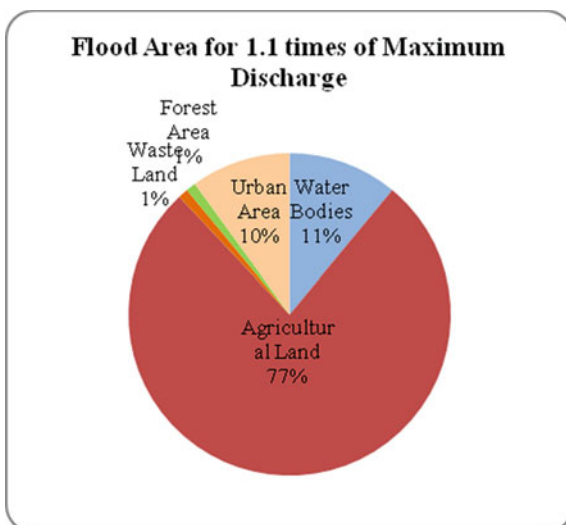


**Fig. 17** Flood affected area for 1.5 times of max. discharge condition

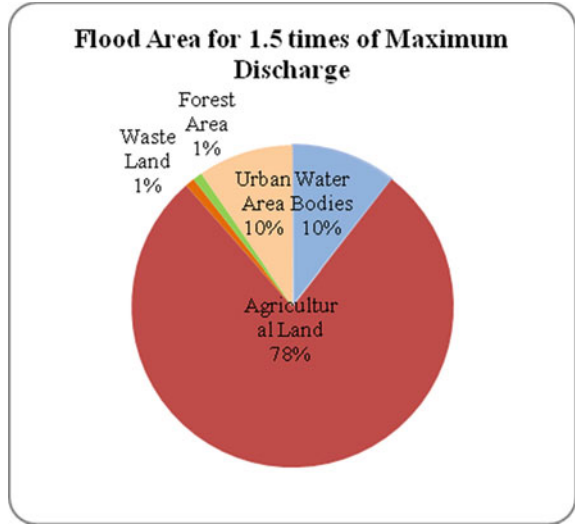


**Table 5** Flood affected area for different flow conditions

| Condition      | Agricultural land (km <sup>2</sup> ) | Water bodies (km <sup>2</sup> ) | Urban area (km <sup>2</sup> ) | Waste land (km <sup>2</sup> ) | Forest area (km <sup>2</sup> ) | Total inundated area (km <sup>2</sup> ) |
|----------------|--------------------------------------|---------------------------------|-------------------------------|-------------------------------|--------------------------------|---|
| Peak discharge | 31.31                                | 4.01                            | 3.56                          | 1.21                          | 0.41                           | 40.90                                   |
| 0.1 times peak | 1.02                                 | 0.13                            | 0.13                          | 0.27                          | 0.28                           | 1.83                                    |
| 1.1 times peak | 33.31                                | 4.76                            | 4.31                          | 0.47                          | 0.42                           | 43.27                                   |
| 1.5 times peak | 43.59                                | 5.89                            | 5.32                          | 0.53                          | 0.54                           | 55.87                                   |



**Table 6** Flood inundation area of different district of Kharun River Basin

| S. no. | District | Inundated area by model result   | Inundated area recorded by Bhuvan and Revenue and Disaster Department, Raipur (C.G.)   |
|--------|----------|--|--|
| 1      | Durg     | Khurmuda (Bhathagaon)  | Khurmuda, Patan  |
| 2      | Balod    | Tarri (Gurur), Some parts of Balod region  | Tarri, Gurur, Gunderdehi, Balod  |
| 3      | Dhamtari | Hathband   | Hathbandh  |
| 4      | Raipur   | Chandnidih, Pathardih, Kathadih, Kumhi, Tila, Bahesar, Kumhari, Murethi, Khairghut, few part of Amdi | RAIPUR-Pathardih, Bendri, Gomchi, Sarona, Raipura, Bhathagaon, Kathadih, Changorabhatha, Murethi, Bahesar, Baratnara, Kumhari, Bhura, Bhairwa, Chandnidih<br>ABHANPUR- Amdi, Tila, Dhondhara, Bagdehi, Joudi |

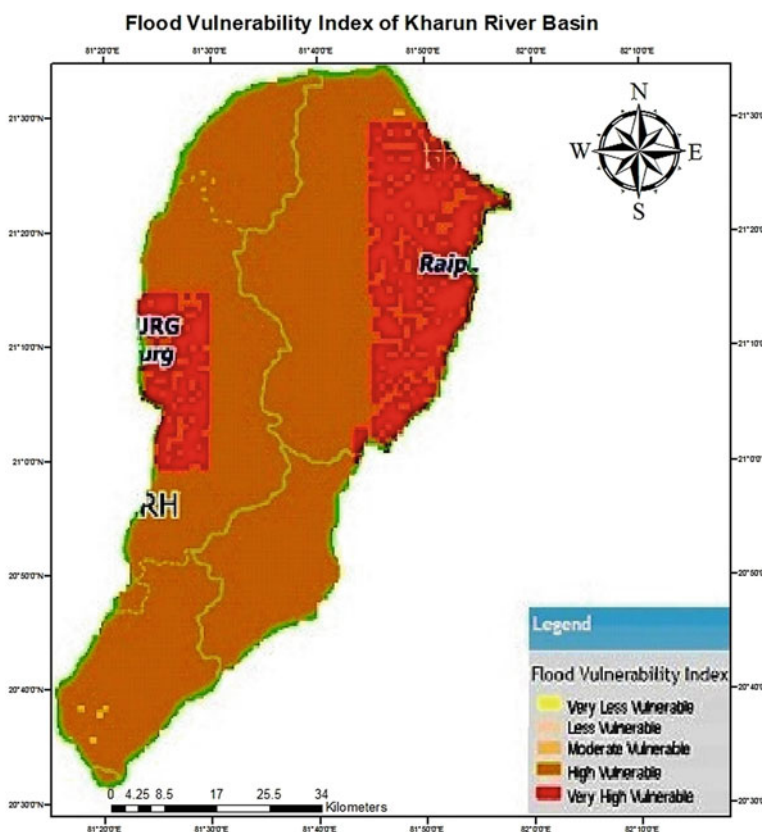


**Fig. 18** Flood vulnerability index of Kharun River Basin. *Source* [Bhuvan.com](#)

## References

1. Le HN, Perminov AV, Kozyr IE (2016) Modeling of floods and flood control water reservoirs for evaluation of inundation Da Nang province of Vietnam. In: 12th international conference on hydroinformatics, HIC 2016. *Procedia Eng* 154:1319–1323. <https://doi.org/10.1016/j.proeng.2016.07.478>
2. Kale VS (1997) Flood studies in India: a brief review. *J Geol Soc India* 49:359–370
3. Timbadiya PV, Patel PL, Porey PD (2014) One-dimensional hydrodynamic modelling of flooding and stage hydrographs in the lower Tapi River in India. *Curr Sci* 106(708)
4. Mujiburrehman K (2015) Preparation of flood inundation map in Ganga river at Baraka Bridge, Malda, West Bengal, India. *Int J Res Geogr (IJRG)* 1(1):1–7. [www.arcjournals.org](http://www.arcjournals.org)
5. Goodell, C., et al. Flood inundation mapping using HEC-RAS, West Consultants 2601, 25th St. SE, Suite 450, Salem, OR 97302, pp 18–23
6. USACE (2010) HEC-RAS, User manual, US Army Corps of Engineers (USACE), Hydrological Engineering Center, Davis, California
7. USACE (2010) HEC-RAS, Hydraulic Reference Manual, US Army Corps of Engineers (USACE), Hydrological Engineering Center, Davis, California
8. Floodplain modelling materials and methodology. In: Proceeding of international conference on advances in civil engineering (2010)
9. Ackerman NL, Cameron T (2011) HEC-GeoRAS, User Manual-Version 4.3.93, US Army Corps of Engineers (USACE), Institute for Water Resources, Hydrological Engineering Center, Davis, California
10. Domeneghetti A, Vorogushyn S, Castellarin A, Merz B, Brath A (2013) Probabilistic flood hazard mapping: effects of uncertain boundary conditions. *Hydrol Earth Syst Sci* 17:3127–3140. [www.hydrol-earth-syst-sci.net/17/3127/2013/](http://www.hydrol-earth-syst-sci.net/17/3127/2013/). <https://doi.org/10.5194/hess-17-3127-2013>
11. Thakur PK, Sumangala A, Flood inundation mapping and 1-D hydrodynamic modeling using remote sensing and GIS technique
12. Leon AS (2016) Tutorial on using HEC-GeoRAS 10.1 (or newer) with ArcMap 10.1 (or newer) and HEC-RAS 5.0.3 (or newer) for flood inundation mapping in Steady and Unsteady Flow Conditions (1D and 2D). WRE Department of Civil and Environmental Engineering, University of Houston
13. Meena RS (2012) Simulation of runoff and flood inundation in Kosi River Basin using hydrological models, ANN, Remote Sensing and GIS, Master of Technology (Research), Department of Civil Engineering, National Institute of Technology Rourkela-769008
14. Duvvuri S, Narasimhan B (2013) Flood inundation mapping of Thamiraparani River Basin using HECGeo RAS and SWAT. *Int J Eng Res Technol (IJERT)* 2(7). ISSN: 2278-0181. V2IS70510
15. Venkatesh M (2012) Tutorial on using HEC-GeoRAS with ArcGIS 10 and HEC-RAS modeling. School of Civil Engineering, Purdue University [vmerwade@purdue.edu](mailto:vmerwade@purdue.edu)

# Seepage of Water Quality Analysis of a Concrete Gravity Dam Using Langlier and Aggressive Index



Satish Chandra Bhuyan, Jyotirmaya Behera, Jyoti Kar,  
and Prakash Kumar Barik

**Abstract** This study deals with the impact of water quality on the dam structure. Seepage water samples were collected from different blocks of left spillway of dam and water samples were collected from reservoir site. Various parameters such as temperature, pH value, electrical conductivity, total suspended solids, total hardness, and total alkalinity have been studied in this work. The test result shows that the pH value of seepage water is more acidic than reservoir water. To know the water quality of reservoir, the water quality index value which offers a useful representation of overall quality of water has been calculated. Also, the Langlier Index which is an approximate measure of the degree of saturation of calcium carbonate in water has been studied. The paper also presents a systematic calculation of the Aggressive Index of the seepage water which indicates the corrosiveness of water. The result of the water quality index analysis of the reservoir site was found to be poor and the Langlier Index of various blocks indicated the corrosiveness or scaling effect on the dam structure. Likewise, the leaching effect was observed in different locations. The calculated Aggressive Index value also indicated the aggressive nature of the water. However, this paper concludes that the seepage water quality has a harmful effect on the dam structure which increases in the form of cracks in various blocks of the spillway, and also more hardness shows the scaling effect on the surface of various blocks of dams.

**Keywords** Water quality index · Langlier Index · Aggressive Index

---

S. C. Bhuyan  
Civil Engineering Department, VSSUT, Burla, Odisha 768018, India

J. Behera (✉)  
Model Studies & Research Division, Burla, Odisha 768017, India

J. Kar · P. K. Barik  
Civil Engineering Department, GCE, Keonjhar, Odisha 758002, India

## 1 Introduction

A seepage measuring system is a vital part of any concrete gravity dam's monitoring system. Many existing seepage monitoring systems are not however sensitive enough to detect small changes in the seepage flow. The physical and chemical characteristics of a major concrete gravity dam water and water from cracked areas have been investigated to compare the reservoir water and seepage water collected from the cracked areas to evaluate any chemical changes between them [2]. A concrete gravity dam is constructed by large blocks divided by joints. Joints are grouted after the dam is cooled and this type of construction can help to reduce thermal stress [1]. Water in the reservoir upstream of the dam pushes horizontally against the dam, and the weight of the gravity dam pushes downward to counteract the water pressure. Concrete gravity dam has weight as its strength. The raw material for the construction process is concrete and reinforcement. Concrete is mixer of water, cement, and aggregates. When water reacts with concrete chemical reaction takes place and it makes the concrete hard. It also releases heat which can cause cracks on the surface of the dam and it can cause seepage [3]. Seepage through concrete gravity dam can cause loss of concrete mass and cause removal of material from surface of concrete. It can also cause internal change in strength due to internal expansion. Due to alkali reacts with cement and silica present in aggregate internal expansion happens on the dam. Cementitious material present on the concrete picks by water due to seepage through the dam body which intensity depends aggressively on water. Monitoring and chemical analysis of quality of reservoir water we can analyze the degree of aggressiveness caused by the seepage water and leached material and also the degree of damage caused by the loss of cementitious material.

The analysis of aggressiveness depends on parameters like temperature, and other chemical properties of water. Langlier Index depends on the corrosivity of water which is not directly related to corrosion [8]. Both the Aggressive Index and Langlier Index have a proper scale and a particular graph type which can decide the water seepage water quality of concrete gravity dam. Chemical properties like hardness and alkalinity is the measure thing that one can calculate for deciding the quality. So determining the extent and nature of mineral concentration should be a priority in dam safety assessment where seepage is a concern. By chemical analysis of leached material samples, the nature of deterioration and the quality of deterioration can directly be determined.

## 2 Area of Investigation

Seepage water quality is monitored for some time. To know the degree of aggressiveness a comparison of changes of mineral dissolution is done in between the seepage water and the reservoir water. Seepage water collected from the cracks of operation gallery and foundation gallery of a major dam [4]. Water sample of left and right side

of reservoir is collected for chemical analysis. Leakage sample from different blocks in upstream and downstream side of operation and foundation gallery of left and right side of spillway was collected on random selection basis. The samples collected in polythene bottles were collected from different stations. Each bottle was washed in nitric acid and cleaned by distilled water. There is no air space present in the bottle and they were properly sealed to avoid leakage. Then all the samples were sent to lab to analyze the parameters for the IS code 3025-1989.

### 3 Role of Chemical Analysis

Carbonization is the major problem of acid attacks on concrete. Concrete contains calcium hydroxide which is alkaline in nature and alkaline material present in set cement makes the cement strongly alkaline. This calcium carbonate generally protects the reinforcement from corrosion. Within the concrete soluble calcium hydroxide by dissolving in seepage water carries to the exposed face of the concrete surface. When the water evaporates calcium carbonate deposited on the surface and white crystalline substances form. These deposits are formed by reaction of carbon dioxide. These carbonates should be monitored as it can indicate the amount of seepage find in its way through thin cracks in the concrete and inadequate drainage and concrete deterioration [5]. As a result of bicarbonation in concrete shrinkage and drop of pH from 13 to 9 of the pore water takes place due to which the embedded steel is susceptible to corrosion. The excess  $\text{CO}_2$  convert calcium carbonate to calcium bicarbonate which is more soluble in water and reach the surface of concrete more rapidly [6].

### 4 Chemical Analysis of Seepage Water

The seepage water collected from operation gallery of left spillway is highly alkaline than the reservoir water and its value ranges from 6.5 to 8. A no. of factors such as permeability of concrete, amount of total Ca and  $\text{Ca}(\text{OH})_2$  in concrete, carbonation, hardness, amount of carbonic acid which is free to attack the concrete may influence the leaching of lime from concrete. In comparison of Ca and Mg in reservoir water and leaked water, it is indicating the appreciable loss of cementitious material [7]. Sample from 3 different blocks (39, 47, 57) was tested and results are tabulated in Table 1. Again the pH value is recorded in the range of 5.7–6.2 and value increases after passing through the concrete portion and is regarded as corrosive. The conductivity of seepage water fell between 812 and 1100 Micro-mhos/cm. and is considering being very high for block 47. Hardness level of water is associated with geological construction contact throughout the year and values in water samples ranged from 44.61 to 60.6 mg/lit. Total alkalinity in leakage areas showed in the range of 12.1–231.8 mg/lit. Again Ca and Mg content in reservoir water and leaked water are

**Table 1** Chemical analysis of water sample from seepage areas in operation gallery of left spillway

| S. no. | Parameters                                     | Block no. 39 | Block no. 47 | Block no. 57 |
|--------|--|--------------|--------------|--------------|
| 1      | Electrical conductivity (micro-mhos/cm)        | 812          | 1100         | 865          |
| 2      | Total dissolve solid (TDS) (mg/lit)            | 441          | 525          | 406          |
| 3      | Calcium (Ca) (mg/lit)                          | 35           | 41           | 41           |
| 4      | Magnesium (Mg) (mg/lit)                        | 9.61         | 19.6         | 13.6         |
| 5      | Total hardness (TH) (mg/lit)                   | 44.61        | 60.6         | 54.6         |
| 6      | Carbonate group (CO <sub>3</sub> ) (mg/lit)    | 6            | –            | –            |
| 7      | Bicarbonate group (HCO <sub>3</sub> ) (mg/lit) | 6.1          | 231.8        | 128.1        |
| 8      | Total alkalinity (TA) (mg/lit)                 | 12.1         | 231.8        | 128.1        |
| 9      | pH   | 6.2          | 5.7          | 5.9          |

compared and content is not the same thereby indicating an appreciable loss of cementing material.

Results of chemical parameters of water seepage through different crack areas on reservoir side wall of operation gallery of right spillway are shown in Tables 2 and 3. Again pH values are recorded in the range 6.2–7.5. The conductivity of seepage water fell between 422 and 1254 micro-mhos/cm which is an approximate measure of dissolved salts in water. Total alkalinity is in the range of 24.4–176.8 mg/lit.

The physical-chemical parameters of water samples collected from foundation gallery of right spillway are shown in Table 4. The pH value for all samples is between 5.7 and 6.6 and this indicates the pH of seepage water is highly acidic in nature. The electrical conductivity varied from 350 to 850 Micro-mhos/cm. which is an approximate measure of dissolved salt in water which indicates the presence of inorganic matters. The seepage water of leaked section is increased after passage through the cracks of the dam structure. The total alkalinity is 45.7–158.6 mg/lit which is beyond the permissible limit of WHO standard. Total hardness varied from

**Table 2** Results of chemical parameter of water seepage through different crack areas on reservoir side wall of operation gallery of right spillway

| S. no. | Parameters                                     | Block no. 51 | Block no. 53 | Block no. 49 |
|--------|--|--------------|--------------|--------------|
| 1      | Electrical conductivity (micro-mhos/cm)        | 517          | 492          | 562          |
| 2      | Total dissolve solid (TDS) (mg/lit)            | 293          | 247          | 225          |
| 3      | Calcium (Ca) (mg/lit)                          | 37           | 39           | 55           |
| 4      | Magnesium (Mg) (mg/lit)                        | 9.57         | 7.29         | 13.6         |
| 5      | Total hardness (TH) (mg/lit)                   | 46.57        | 46.29        | 68.6         |
| 6      | Carbonate group (CO <sub>3</sub> ) (mg/lit)    | –            | 5            | –            |
| 7      | Bicarbonate group (HCO <sub>3</sub> ) (mg/lit) | 24.4         | 61           | 59.4         |
| 8      | Total alkalinity (TA) (mg/lit)                 | 24.4         | 66           | 59.4         |
| 9      | pH   | 7.5          | 7.3          | 6.5          |

**Table 3** Chemical parameter of water of reservoir side wall of operation gallery of right spillway

| S. no. | Parameters                                     | Block no. 37 | Block no. 55 | Block no. 54 |
|--------|--|--------------|--------------|--------------|
| 1      | Electrical conductivity (micro-mhos/cm)        | 422          | 445          | 1254         |
| 2      | Total dissolve solid (TDS) (mg/lit)            | 201          | 261          | 714          |
| 3      | Calcium (Ca) (mg/lit)                          | 35           | 37           | 77           |
| 4      | Magnesium (Mg) (mg/lit)                        | 10.25        | 10.38        | 8.25         |
| 5      | Total hardness (TH) (mg/lit)                   | 45.25        | 47.87        | 85.25        |
| 6      | Carbonate group (CO <sub>3</sub> ) (mg/lit)    | –            | 6            | 18           |
| 7      | Bicarbonate group (HCO <sub>3</sub> ) (mg/lit) | 54.9         | 170.8        | 152.5        |
| 8      | Total alkalinity (TA) (mg/lit)                 | 54.9         | 176.8        | 170.5        |
| 9      | pH   | 6.2          | 6.4          | 7.4          |

**Table 4** The physical-chemical parameter of water samples collected from foundation gallery of right spillway

| S. no. | Parameters                              | Block no. 51 | Block no. 50 | Block no. 49 | Block no. 53 |
|--------|---|--------------|--------------|--------------|--------------|
| 1      | Electrical conductivity (micro-mhos/cm) | 427          | 357          | 818          | 290          |
| 2      | Total dissolve solid (TDS) (mg/lit)     | 214          | 189          | 449          | 587          |
| 3      | Calcium (Ca) (mg/lit)                   | 41           | 47           | 47           | 35           |
| 4      | Magnesium (Mg) (mg/lit)                 | 10           | 22           | 14.8         | 10.87        |
| 5      | Total hardness (TH) (mg/lit)            | 51           | 69           | 61.8         | 45.87        |
| 6      | Carbonate group (CO <sub>3</sub> )      | –            | 3            | –            | –            |
| 7      | Bicarbonate group (HCO <sub>3</sub> )   | –            | –            | –            | –            |
| 8      | Total alkalinity (TA) (mg/lit)          | 54.9         | 45.7         | 158.6        | 158.6        |
| 9      | pH                                      | 5.7          | 6.6          | 6.3          | 5.8          |

45.87 to 69 mg/lit which is below the permissible limit of WHO standard. The bicarbonate is not traceable in water samples from foundation gallery. The leaked water picked up Calcium and when passed through cracks of the dam as shown in Table 4. Bicarbonate is absent in all the samples indicating alkalinity is due to carbonates only. The seepage water in the foundation gallery becomes more alkaline as compared to reservoir water in the respective section. Thus in the process of seepage, the water picked up certain salts and become alkaline in nature.

## 5 Study Methodology

### 5.1 Langlier Index

International commission on large dams (ICOLD) bulletin number 71 has recommended the calculation of Langlier Index (LI) as a means of evaluating potential soft water attacks [9]. Soft water is aggressive to concrete structure because of its ability to dissolve certain salts from concrete, mainly the strength giving calcium [10, 11]. It is observed worldwide that structures are made by taking utmost care and precautions due to soft water attacks and consequent leaching. LI is calculated as

$$LI = pH + \text{Log } C + \text{Log } A - 0.025 \times T - 0.011 \times S - 12.30 \quad (1)$$

where,

- pHs is the pH of water.
- C calcium hardness.
- A alkalinity.
- T temperature of water in degree Celsius.
- S total dissolved solids.

### 5.2 Aggressive Index

The Aggressive Index (AI) originally developed for monitoring water in asbestos pipe is sometimes substituted for the Langlier Index as an indicator of corrosivity of water. The AI derived from actual pH, calcium hardness, and total alkalinity [12]. Where it is applicable, it is simpler and more convenient than LI [13]. Because the AI does not include the efforts of temperature or dissolved solids, it is less accurate as an analytical tool than the LI [14] (Table 5).

$$AI = \text{pH actual} + C + D$$

$$C = \log_{10}(\text{Ca}_2 + \text{as CaCO}_3) - 0.4$$

$$D = \log_{10}(\text{alkalinity as CaCO}_3)$$

**Table 5** Corrosive characteristics

| Corrosive characteristics | Langlier Index | Aggressive Index |
|---------------------------|----------------|------------------|
| Highly aggressive         | <-2.0          | <10.0            |
| Moderately aggressive     | -2.0 to 0.0    | 10.0-12.0        |
| nonaggressive             | >0.0           | >12.0            |



## 6 Results

From the analysis of seepage water of concrete gravity dam, we can get the Langlier Index value and the Aggressive Index value and derive the drinking water standard of the water.

It is seen from Table 6 that there is possibility of soft water leaching attack since out of 13 samples all water samples have negative values for LI and are classified as aggressive to moderately aggressive. From Table 7 results show out of 13 samples, 6 water samples have AI values less than 10 and are classified as highly aggressive. These may cause corrosion/leaching of calcium carbonate mass if the expose of concrete to such water is prolonged.

## 7 Conclusions

Based on the research work carried out on the seepage water quality from crack areas of concrete gravity dam following conclusions are drawn.

The seepage samples collected from the dam side are generally highly aggressive by nature. This shows water is hard water. The pH value of seepage water sample is generally more acidic in nature as compared to reservoir water and has started leaching due to the deposition of lime on concrete surface. Langlier Index value for majority of water sample fall into negative values shows the moderately aggressive characteristics which indicate the corrosivity of sample. Generally, the Langlier Index value of most of the sample varies between  $-1.5$  and  $2$ . This value not indicates directly corrosive property but is related to the calcium carbonated deposition on a large scale. The Aggressive Index value indicates moderately aggressive in nature which means it has a less corrosive property.

**Table 6** Classification of degree of aggressiveness based on LI of water sample from crack areas

| S. no. | Block no. | pH  | Calcium (mg/lit) | Magnesium (mg/lit) | Calcium hardness (mg/lit) | Tds (mg/lit) | Temperature (degree celcius) | Carbonate (degree) | Carbonate (mg/lit) | Bicarbonate (mg/lit) | Alkalinity (mg/lit) | Langlier Index (LI) |
|--------|-----------|-----|------------------|--------------------|---------------------------|--------------|------------------------------|--------------------|--------------------|----------------------|---------------------|---------------------|
| 1      | 39        | 6.2 | 35               | 9.61               | 127.5                     | 441          | 29                           | 6                  | 6                  | 6.1                  | 15                  | -2.4                |
| 2      | 47        | 5.7 | 41               | 19.6               | 184.1                     | 525          | 28                           | -                  | -                  | 231.8                | 190                 | -1.67               |
| 3      | 57        | 5.9 | 41               | 13.6               | 159.1                     | 406          | 28                           | -                  | -                  | 128.1                | 105                 | -1.72               |
| 4      | 37        | 6.2 | 35               | 10.25              | 130.2                     | 201          | 29                           | -                  | -                  | 59.4                 | 48.68               | -1.85               |
| 5      | 55        | 6.4 | 37               | 10.38              | 135.7                     | 261          | 30                           | 6                  | 6                  | 170.8                | 150                 | -1.13               |
| 6      | 54        | 7.5 | 77               | 8.25               | 226.8                     | 714          | 28                           | 18                 | 18                 | 152.5                | 155                 | -0.13               |
| 7      | 51        | 7.5 | 37               | 9.57               | 132.3                     | 293          | 29                           | -                  | -                  | 24.4                 | 20                  | -0.93               |
| 8      | 53        | 7.3 | 39               | 7.29               | 127.8                     | 247          | 28                           | 5                  | 5                  | 61                   | 58.33               | -0.7                |
| 9      | 49        | 6.5 | 55               | 13.6               | 194.1                     | 225          | 30                           | -                  | -                  | 59.4                 | 48.68               | -1.36               |
| 10     | 51        | 5.7 | 41               | 10                 | 144.1                     | 214          | 28                           | -                  | -                  | 59.4                 | 48.68               | -2.33               |
| 11     | 50        | 6.6 | 47               | 22                 | 209.1                     | 189          | 29                           | 3                  | 3                  | 42.7                 | 40.02               | -1.31               |
| 12     | 49        | 6.3 | 47               | 14.8               | 179.8                     | 449          | 29                           | -                  | -                  | 158.6                | 130                 | -1.21               |
| 13     | 53        | 5.8 | 35               | 10.87              | 132.7                     | 587          | 30                           | -                  | -                  | 158.6                | 130                 | -1.83               |

**Table 7** Classification of degree of aggressiveness based on AI of water sample from crack areas

| S. no. | Block no. | pH  | Calcium (mg/lit) | Magnesium (mg/lit) | Calcium hardness (mg/lit) | Temperature (degree celcius) | Carbonate (mg/lit) | Bicarbonate (mg/lit) | Alkalinity (mg/lit) | Aggressive Index (AI) |
|--------|-----------|-----|------------------|--------------------|---------------------------|------------------------------|--------------------|----------------------|---------------------|-----------------------|
| 1      | 39        | 6.2 | 35               | 9.61               | 127.5                     | 29                           | 6                  | 6.1                  | 15                  | 9.07                  |
| 2      | 47        | 5.7 | 41               | 19.6               | 184.1                     | 28                           | -                  | 231.8                | 190                 | 9.83                  |
| 3      | 57        | 5.9 | 41               | 13.6               | 159.1                     | 28                           | -                  | 128.1                | 105                 | 9.77                  |
| 4      | 37        | 6.2 | 35               | 10.25              | 130.2                     | 29                           | -                  | 59.4                 | 48.68               | 9.59                  |
| 5      | 55        | 6.4 | 37               | 10.38              | 135.7                     | 30                           | 6                  | 170.8                | 150                 | 10.3                  |
| 6      | 54        | 7.5 | 77               | 8.25               | 226.8                     | 28                           | 18                 | 152.5                | 155                 | 11.64                 |
| 7      | 51        | 7.5 | 37               | 9.57               | 132.3                     | 29                           | -                  | 24.4                 | 20                  | 10.52                 |
| 8      | 53        | 7.3 | 39               | 7.29               | 127.8                     | 28                           | 5                  | 61                   | 58.33               | 10.76                 |
| 9      | 49        | 6.5 | 55               | 13.6               | 194.1                     | 30                           | -                  | 59.4                 | 48.68               | 10.06                 |
| 10     | 51        | 5.7 | 41               | 10                 | 144.1                     | 28                           | -                  | 59.4                 | 48.68               | 9.13                  |
| 11     | 50        | 6.6 | 47               | 22                 | 209.1                     | 29                           | 3                  | 42.7                 | 40.02               | 10.10                 |
| 12     | 49        | 6.3 | 47               | 14.8               | 179.8                     | 29                           | -                  | 158.6                | 130                 | 10.26                 |
| 13     | 53        | 5.8 | 35               | 10.87              | 132.7                     | 30                           | -                  | 158.6                | 130                 | 9.86                  |

## References

1. Bhandari NS, Nayal K (2008) Correlation study on physico-chemical parameters and quality assessment of Kosi River water, Uttarakhand. *J Chem* 5(2):342–346
2. Behera J (2019) Assessment of water quality parameters of seepage water from crack areas of Hirakud Dam. In: International dam safety conference, DRIP, Bhubaneswar, 13th–14th Feb, vol 1, pp 351–358
3. Deep PR, Bhattacharyya S, Nayak B (2013) Cyano bacteria in wetlands of the industrialized Sambalpur District of India. *Aquat Biosyst* 9(1):14
4. Baboo B (1992) Technology and social transformation: the case of Hirakud multi-purpose dam project in Orissa. Concept Publishing Company
5. Ichwana I, Syahrul S, Nelly W (2016) Water quality index by using national sanitation foundation-Water quality index (NSF-WQI) method at kruengtamiangaceh. In: International conference on technology, innovation, Universitas Syiah Kuala, Indonesia
6. Reza R, Singh G (2010) Application of water quality index for assessment of pond water quality status in Orissa, India. *Curr World Environ* 5(2):305
7. Effendi H, Romanto WY, Wardiatno Y (2015) Water quality status of Ciambulawung River, Banten Province, based on pollution index and NSF-WQI. *Procedia Environ Sci* 24(4):228–237
8. Aazami J, Esmaili-Sari A, Abdoli A, Sohrabi H, Van den Brink PJ (2015) Monitoring and assessment of water health quality in the Tajan River, Iran using physicochemical, fish and macro invertebrates indices. *J Environ Health Sci Eng* 13(1):29
9. Langlier WF (1936) The analytical control of anti-corrosion water treatment. *J Am Water Works Assoc* 28(10):1500–1521
10. Osepchuk JM (1984) A history of microwave heating applications. *IEEE Trans Microw Theory Tech* 32(9):1200–1224
11. Kar PK, Pani KR, Pattanayak SK, Sahu SK (2010) Seasonal variation in physico-chemical and microbiological parameters of Mahanadi river water in and around Hirakud, Orissa (India). *The Ecoscan* 4(4):263–271
12. Chung WS, Yu MJ, Lee HD (2004) Prediction of corrosion rates of water distribution pipelines according to aggressive corrosive water in Korea. *Water Sci Technol* 49(2):19–26
13. Koszelnik P, Kaleta J, Bartoszek L (2018) An assessment of water quality in dam reservoirs, considering their aggressive properties. In: E3S web of conferences, vol 45, p 00035. EDP Sciences
14. Mason PJ (1990) The effects of aggressive water on dam concrete. *Constr Build Mater* 4(3):115–118

# Application of GIS and Geostatistical Interpolation Method for Groundwater Mapping



Ashesh Chakma, Tridip Bhowmik, Santanu Mallik, and Umesh Mishra

**Abstract** Geographic Information System (GIS) is a cost effective computer based tool used to visualize, analyze and display geospatial data. GIS interpolation method has been widely used in various domains to predict values of unknown points by using the similarity of nearby sample points. GIS based groundwater mapping is one such area, where interpolation is used for the mapping of various parameters such as microbial contamination, physiochemical concentrations, water level, and so on so forth. Two types of interpolation techniques are used in GIS, i.e., deterministic and geostatistical. Deterministic techniques make use of mathematical functions to interpolate while geostatistics uses both statistical and mathematical methods to create surfaces as well as to assess the uncertainty present in the predictions. Although, there is some confusion associated with the selection of these methods. So, in this paper, a comparison between geostatistics and deterministic methods has been shown. This study will help the GIS users to get a better insight into both the interpolation methods.

**Keywords** GIS · Groundwater · Interpolation · Deterministic · Geostatistic · IDW · Kriging

## 1 Introduction

Groundwater is an important natural resource serving as a boon for mankind. The persistent rise in population and anthropogenic activities such as irrigation, urbanization, land use, mining activities, disposal of sewage, etc. has proved to be a major concern for the degrading groundwater. Hence, it is very important to keep a check on the groundwater level, usage, contamination, and other factors that can lead to its deterioration. One of the ways to do it is through determining the spatio-temporal variation of the groundwater quality and the pollutants present in it. The GIS (geographic

---

A. Chakma (✉) · T. Bhowmik · S. Mallik · U. Mishra  
Department of Civil Engineering, National Institute of Technology Agartala, Barjala, Jirania,  
Tripura (W), India

© The Author(s), under exclusive license to Springer Nature Singapore Pte Ltd. 2022  
C. M. Rao et al. (eds.), *Advanced Modelling and Innovations in Water Resources Engineering*, Lecture Notes in Civil Engineering 176,  
[https://doi.org/10.1007/978-981-16-4629-4\\_29](https://doi.org/10.1007/978-981-16-4629-4_29)

419

information system) based interpolation methods are very useful in these studies since they help in providing an estimate of the values at random locations [13, 15, 31].

Two types of interpolation techniques mostly used in GIS are deterministic and geostatistics. Geostatistical methods use both mathematical and statistical functions for analysis and estimation of data based on their relation in space or time. In geostatistical methods to predict values at the unsampled location and to create the surface autocorrelation within the measured values are considered [15]. The advantage of geostatistical method over the deterministic method is that along with spatial mapping it also evaluates the uncertainty associated with it [12, 19]. The evaluation of the uncertainties associated with the prediction is quantified by the cross validation technique which indicates the accuracy of the surface model created. Whereas, deterministic methods use mathematical functions based on the degree of similarity with measured values and it does not consider the statistical properties of the measured values. Globally various deterministic methods are available such as Inverse Distance Weighted (IDW), Global Polynomial Interpolation (GPI), Local Polynomial Interpolation (LPI), Radial Basis Function (RBF). Among these methods, IDW is one of the most preferred deterministic techniques [5].

Formerly, various other interpolation techniques such as a closest neighbor, moving average and linear triangulation were used but nowadays their usage is very minimal as kriging and inverse distance weighting methods have been proven to have greater accuracy. While preparing the spatial interpolation surface one major question arises that is which method to select and what is the accuracy of the selected method, is there any pre-processing required this review paper could possibly help to address all such questions.

In this review, the performance of commonly used interpolation methods in groundwater applications like IDW, OK (ordinary kriging), and CK (cokriging) have been studied using the information from comparative studies of the methods in groundwater mapping. The results obtained from the selected articles were checked to find out which method has been preferred the most.

## 2 Overview of Interpolation Methods

### 2.1 *Inverse Distance Weighted (IDW)*

IDW is one of the simplest interpolation methods [10]. IDW estimates the surface based on the assumption that points that are close to each other are more similar than those that are far apart. Interpolating points that are closer to the interpolation point are assigned more weight and points that are further have less weight [5]. When  $\beta$  is higher the nearest points have more weight and when it is lower the weight is distributed more uniformly between neighboring points [13].

$$Z(x_0) = \frac{\sum_{i=1}^n \frac{x_i}{h_{ij}^\beta}}{\sum_{i=1}^n \frac{1}{h_{ij}^\beta}} \quad (1)$$

where,  $Z(x_0)$  is the interpolated value,  $n$  is the total number of sample data values,  $x_i$  is the  $i$ th data value,  $h_{ij}$  is the separation distance between interpolated value and the sample data value, and  $\beta$  denotes the weighting power [5].

## 2.2 Ordinary Kriging (OK)

Kriging is a geostatistical interpolation technique that uses the spatial autocorrelation between the sampled points to predict the surface. The strength of spatial autocorrelation is measured as a function of distance by the semivariogram. The spatial autocorrelation exists up to a certain distance called range, beyond which it vanishes. The spatial autocorrelation assumes that the points that are closer have properties more similar than those that are far apart. To examine the spatial distribution a semivariogram  $\gamma(h)$  is used, expressed as

$$\gamma(h) = \frac{1}{2N(h)} \sum_{i=1}^{N(h)} [Z(x_i) - Z(x_i + h)]^2 \quad (2)$$

where  $h$ , called the lag distance, is the separation between the values at  $Z(x_i)$  and  $Z(x_i + h)$  [19, 32].

Kriging estimate  $Z^*(x_0)$  at any point  $x_0$  it can be calculated as

$$Z^*(x_0) = \sum_{i=1}^n \lambda_i Z(x_i) \quad (3)$$

where  $\lambda_i$  is the weight and  $Z(x_i)$  is the known value at  $x_i$  [5, 19].

An empirical semivariogram model is to be fitted over the experimental semivariogram and numerous iterations of parameters such as (range, sill, and nugget) are used to select the empirical semivariogram model. Various empirical models are available in literature and the best model is selected based on leave one out cross validation technique. A sample figure with different empirical model and their associated parameters is shown in Fig. 1. If any data trend or outlier is observed in the experimental data then it is good practice to remove them before carrying out OK interpolation method to get better results.

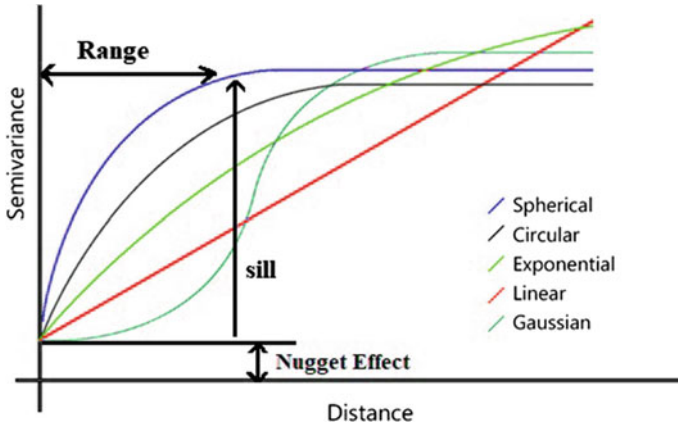


Fig. 1 Different empirical semivariogram [36]

### 2.3 CoKriging (CK)

CoKriging contains a primary and a secondary variable and the measurement of the primary variable at the unsampled location is quantified using the effect of secondary variable. Both autocorrelation and cross-correlations between the primary and secondary variables are used to improve the prediction result [17, 20]. CK is generally preferred when secondary variable is easily available or measured and reasonably well correlated with primary variable.

$$z_{CK}^*(\mathbf{u}) = \sum_{\alpha=1}^{n(\mathbf{u})} \lambda_{\alpha}(\mathbf{u}) z(\mathbf{u}_{\alpha}) + \sum_{\alpha'=1}^{m(\mathbf{u})} \lambda_{\alpha'}(\mathbf{u}) y(\mathbf{u}_{\alpha'}) \tag{4}$$

where  $z_{CK}^*$  is sample value at  $\mathbf{U}$  location,  $\lambda_{\alpha}(\mathbf{U})$  and  $\lambda_{\alpha'}(\mathbf{U})$  are the weight associated with  $z(\mathbf{u}_{\alpha})$  and  $y(\mathbf{u}_{\alpha'})$ ,  $n(\mathbf{u})$  and  $m(\mathbf{u})$  are the number of sample used to estimate the sample value at  $\mathbf{u}$  location [20].

## 3 Literary Survey Methods

Relevant publications were searched using several online scientific search engines, electronic libraries, and databases. The search was restricted to articles that were published in the referred journals for the time period of 2015–2020. It was done by searching each website for relevant terms: groundwater interpolation GIS. Any article having the relevant search terms was deemed as possible for inclusion in this review paper.



Manual search was also done by searching the reference sections of the selected papers. Any relevant references in those papers were manually searched and followed upon. The factors for inclusion in the review were any theoretical or applied work concerning the use of the methodologies integrating GIS. Out of all the papers identified in the search, 30 papers that serve the requirements for this review were chosen.

Figure 2 shows the number of articles obtained for search term ‘groundwater interpolation GIS’ from the websites searched for the time period 2015–2020. Figure 3 shows the number of publications for each year from 2015 to 2020. The number of publications was similar from 2015 to 2017, since 2016 there is increase in the number of publications for each year. The total number of articles from the five websites searched for IDW was 5189, for OK was 4723 and for CK was 1257. Figure 4 shows the number of articles published every year from 2015 to 2020 for each method. For the year 2020, the number of articles published till August is the same as the number of publications in 2015. The increase in number of publications

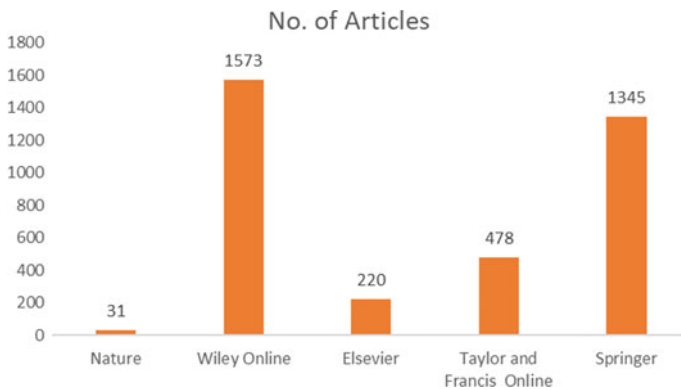
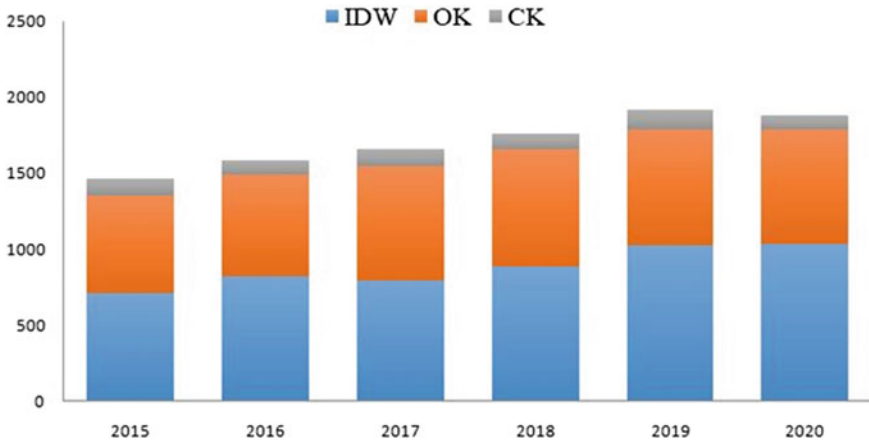


Fig. 2 Total number of articles per website using relevant search terms from 2015 to 2020



Fig. 3 Total number of articles using relevant search terms for each year from 2015 to 2020



**Fig. 4** Year wise paper for each keyword (IDW, OK, CK)

can be attributed to more focus being given on groundwater conservation as there is possibility of water scarcity in the future.

#### 4 Comparison of IDW, OK, and CK

Kriging in theory is considered to be better than IDW as kriging method combines the effects of distance and direction parameters [28]. In this review, a total of 30 papers that compare these three methods were selected. Table 1 lists the preferred method in each of the papers reviewed. Out of the reviewed papers OK was considered to be better in 15 [3, 7, 8, 10, 11, 16,17, 21, 24, 27, 29, 28, 30, 31], IDW was considered better in 6 [2, 4, 13, 22,26, 36] and CK was the better in 4 [6, 9, 14, 25] for the purpose of spatial distribution mapping of groundwater quality. For groundwater level assessment kriging was found to be better in 4 [15, 34, 35, 37] and IDW was the better in 2 [1, 23]. The three methods were cross validated in the reviewed papers by root mean square error (RMSE), mean absolute error (MAE), mean error (ME), coefficient of determination ( $R^2$ ) and other methods. Cross validation is a statistical method that analyzes the accuracy of interpolation model [28]. In this paper, RMSE value is considered for comparison of the results as it was the most commonly used method in the reviewed papers. In some cases, the RMSE of IDW with power of 1, 2, 3, and 4 were compared, in such cases the power which provided the least error was chosen for comparison with OK and CK. Figure 5 shows graphical comparison between IDW and OK, the values were chosen from papers that were found suitable due to closeness of their values for graphical representation. CK was not included for graphical comparison due to small amount of data available. The figure shows that OK was found to be better than IDW, in most of the papers the difference was very small except [1, 12, 16, 18, 22, 24, 28, 34, 37]. Although OK has been superior

**Table 1** Summary of 30 studies reviewed

| S. no. | Methods used | Pre-processing | Preferred method | Reference |
|--------|--------------|----------------|------------------|-----------|
| 1      | IDW, OK      | Yes            | IDW              | [22]      |
| 2      | IDW, OK, CK  | No             | CK               | [15]      |
| 3      | IDW, CK      | No             | IDW              | [13]      |
| 4      | IDW, OK, CK  | Yes            | CK               | [6]       |
| 5      | OK, IDW      | Yes            | OK               | [37]      |
| 6      | OK, IDW      | Yes            | OK               | [18]      |
| 7      | OK, IDW      | Yes            | OK               | [29]      |
| 8      | OK, IDW      | Yes            | OK               | [31]      |
| 9      | OK, IDW      | Yes            | IDW              | [23]      |
| 10     | OK, IDW      | No             | IDW              | [1]       |
| 11     | OK, IDW      | Yes            | OK               | [21]      |
| 12     | OK, IDW      | Yes            | OK               | [16]      |
| 13     | OK, IDW      | Yes            | IDW              | [12]      |
| 14     | IDW, CK      | No             | CK               | [14]      |
| 15     | OK, IDW      | Yes            | OK               | [28]      |
| 16     | OK, IDW      | Yes            | OK               | [11]      |
| 17     | OK, IDW      | Yes            | OK               | [34]      |
| 18     | OK, IDW      | Yes            | OK               | [3]       |
| 19     | OK, IDW      | Yes            | OK               | [35]      |
| 20     | OK, IDW      | Yes            | IDW              | [36]      |
| 21     | OK, IDW, CK  | Yes            | CK               | [25]      |
| 22     | OK, IDW      | Yes            | OK               | [30]      |
| 23     | OK, IDW      | No             | IDW              | [2]       |
| 24     | OK, IDW      | Yes            | OK               | [24]      |
| 25     | OK, IDW      | No             | OK               | [7]       |
| 26     | OK, IDW      | No             | OK               | [10]      |
| 27     | OK, IDW      | No             | OK               | [27]      |
| 28     | OK, IDW      | Yes            | IDW              | [26]      |
| 29     | OK, IDW, CK  | No             | CK               | [9]       |
| 30     | OK, IDW      | No             | OK               | [8]       |

in most of the studies it also has certain disadvantages. If the datasets are very small then OK cannot be performed, in that case, most of the studies implement IDW technique since the method is directly dependent on the measured values and the interpolation is done based on mathematical function, so can be applied for smaller datasets as well. There are other instances as well when the autocorrelation within the datasets are poor and in such case, either IDW method or secondary variables can be considered for determining the primary variable using CK method.

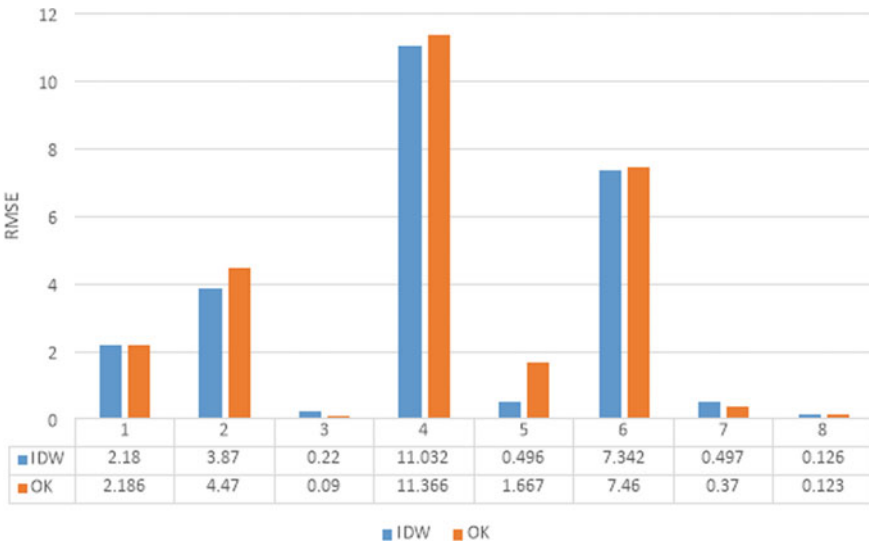


Fig. 5 Graphical comparison of OK and IDW

### 5 Conclusion

The 30 reviewed papers show that geostatistical methods provide more accurate results when compared to deterministic methods. Although the difference in accuracy is minimal sometimes it can be large enough to induce significant error as shown in Fig. 5. Among the geostatistical methods, OK is the most widely used method but sometimes CK has been found to outperform OK. The reason behind popularity of geostatistical method over deterministic method is because of not only production of interpolate surface but also measure the amount of uncertainty involved in field sampling. This will help to redesign the sampling density if further sampling is required. This review on geostatistical interpolation methods helps to answer the question that for preparing more accurate spatial interpolation surface geostatistical methods should be used, where deterministic methods have used the results obtained can be cross checked using deterministic methods for finding out the best result.

### References

1. Ali MH, Al-Adili AS, Sivakugan N (2018) Comparison between deterministic and stochastic interpolation methods for predicting ground water level in Baghdad. *Eng Technol J* 36, Part A(12):1222–1225
2. Almodaresi SA, Mohammadrezaei M, Dolatabadi M, Nateghi MR (2019) Qualitative analysis of groundwater quality indicators based on Schuler and Wilcox diagrams: IDW and Kriging models. *J Environ Health Sustain Dev (JEHSD) Sustain Dev* 4(4):903–912

3. Amah VE, Agu FA (2020) Geostatistical modelling of groundwater quality at Rumuola Community, Port Harcourt, Nigeria. *Asian J Environ Ecol* 12(1):37–47
4. Arslan H, Turan NA (2015) Estimation of spatial distribution of heavy metals in groundwater using interpolation methods and multivariate statistical techniques; its suitability for drinking and irrigation purposes in the Middle Black Sea Region of Turkey. *Environ Monit Assess* 187:516
5. Bhunia GS, Shit PK, Ramkrishna M (2016) Comparison of GIS-based interpolation methods for spatial distribution of soil organic carbon (SOC). *J Saudi Soc Agric Sci* 17. <https://doi.org/10.1016/j.jssas.2016.02.001>
6. Boufekane A, Saighi O, Assessing groundwater quality for irrigation using geostatistical method—case of wadi Nil Plain (North-East Algeria). *Groundwater for Sustainable Development*
7. Elumalai V, Brindha K, Sithole B, Lakshmanan E (2017) Spatial interpolation methods and geostatistics for mapping groundwater contamination in a coastal area. *Environ Sci Pollut Res* 24:11601–11617
8. Fallahzadeh RA, Almodaresi SA, Dashti MM, Fattahi A, Sadeghnia M, Eslami H, Khosravi R, Minaee RP, Taghavi M (2016) Zoning of nitrite and nitrate concentration in groundwater using geographic information system (GIS), Case Study: Drinking Water Wells in Yazd City. *J Geosci Environ Protect* 4:91–96
9. Feizia Z, Keshkara AR, Afzalia A (2019) Using geostatistical and deterministic modelling to identify spatial variability of groundwater quality. *Desert* 24–1:143–151
10. Galal Uddin M, Moniruzzaman M, Quader MA, Hasan MA, Spatial variability in the distribution of trace metals in groundwater around the Rooppur nuclear power plant in Ishwardi, Bangladesh. *Groundwater Sustain Dev* 7:220–231
11. Gidey A (2018) Geospatial distribution modeling and determining suitability of groundwater quality for irrigation purpose using geospatial methods and water quality index (WQI) in Northern Ethiopia. *Appl Water Sci* 8:82
12. Goovaerts P, AvRuskin G, Meliker J, Slotnick M, Jacquez G, Nriagu J (2005) Geostatistical modeling of the spatial variability of arsenic in groundwater of southeast Michigan. *Water Resour Res* 41:1–19. <https://doi.org/10.1029/2004WR003705>
13. Gunarathna MHJP, Nirmanee KGS, Kumari MKN, Are geostatistical interpolation methods better than deterministic interpolation methods in mapping salinity of groundwater? *Int J Res Innov Earth Sci* 3(3). ISSN (Online): 2394-1375
14. Gunarathna MHJP, Kumari MKN, Nirmanee KGS, Evaluation of interpolation methods for mapping pH of groundwater. *Int J Latest Technol Eng Manag Appl Sci V(III)*
15. Hassan I, Lawal IM, Mohammed A, Abubakar S, Analysis of geostatistical and deterministic techniques in the spatial variation of groundwater depth in the North-western part of Bangladesh. *Am J Eng Res* 5(3):29–34
16. Javari M (2017) Comparison of interpolation methods for modeling spatial variations of Precipitation in Iran. *Int J Environ Sci Educ* 12(5):1037–1054
17. Johnson K, Ver Hoef JM, Krivoruchko K, Lucas N (2001) Using ArcGIS geostatistical analyst, GIS by ESRI, Redlands, USA
18. Khosravi K, Nejad Roshan MH, Safari A (2017) Assessment of geostatistical methods for determining distribution patterns of groundwater resources in Sari-Neka Coastal Plain, Northern Iran. *Environ Resour Res* 5(2):123–134
19. Mallik S, Mishra U, Paul N (2021) Groundwater suitability analysis for drinking using GIS based fuzzy logic. *Ecological Indicators* 121:107179. <https://doi.org/10.1016/j.ecolind.2020.107179>
20. Mallik S, Bhowmik T, Mishra U, Paul N (2020) Mapping and prediction of soil organic carbon by an advanced geostatistical technique using remote sensing and terrain data. *Geocarto International* 1–17. <https://doi.org/10.1080/10106049.2020.1815864>
21. Mirzaei R, Sakizadeh M (2016) Comparison of interpolation methods for the estimation of groundwater contamination in Andimeshk-Shush Plain, Southwest of Iran. *Environ Sci Pollut Res* 23:2758–2769

22. Moghaddama A, Moteallemib A, Joulaeic F, Peirovi R (2018) A spatial variation study of groundwater quality parameters in the Gonabad Plain using deterministic and geostatistical models. Desalination and water treatment, pp 261–269
23. Njeban HS (2018) Comparison and evaluation of GIS-based spatial interpolation methods for estimation groundwater level in AL-Salman District—Southwest Iraq. *J Geogr Inf Syst* 10:362–380
24. Safarbeiranvnd M, Amanipoor H, Battaleb-Looie S, Ghanemi K, Ebrahimi B (2018) Quality evaluation of groundwater resources using geostatistical methods (Case Study: Central Lorestan Plain, Iran). *Water Resour Manage* 32:3611–3628
25. Salari M (2018) Investigating the spatial variability of some important groundwater quality factors based on the geostatistical simulation (case study: Shiraz plain)
26. Seyedmohammadi J, Esmaeelnejad L, Shabanpour M (2016) Spatial variation modeling of groundwater electrical conductivity using geostatistics and GIS. *Modell Earth Syst Environ* 2:169
27. Shekhar C, Rohilla K, Kumar P, Sihag P, Sood A (2020) Spatial variability of ground water quality for irrigation of Mansa District, Punjab. *Int J Agric Sci*:9448–9450 (2020)
28. Shin W-J, Ryu J-S, Kim R-H, Min J-S (2020) First strontium isotope map of groundwater in South Korea: applications for identifying the geographical origin. *Geosci J*
29. Shyamala G, Arun Kumar B, Manvitha S, Vinay Raj T, Assessment of spatial interpolation techniques on groundwater contamination. In: International conference on emerging trends in engineering (ICETE), pp 262–269
30. Talebnia M, Zehtabian G, Malekian A, Khosravi H, Monitoring of groundwater contamination of Sagzi plain for drinking use. *Int Res J Appl Basic Sci* 10(5):538–554
31. Towfiqul Islam ARM, Shen S, Bodrud-Doza M, Atiqur Rahman M, Das S (2017) Assessment of trace elements of groundwater and their spatial distribution in Rangpur district, Bangladesh. *Arab J Geosci*
32. Wang Y, Shao M (2013) Spatial variability of soil physical properties in a region of the Loess Plateau of PR China subject to wind and water erosion. *Land Degr Devel* 24. <https://doi.org/10.1002/ldr.1128>
33. Web page. <https://gisgeography.com/wp-content/uploads/2016/11/kriging-models-1.png>. Accessed on 06 Aug 2020
34. Xiao Y, Gu X, Yin S, Shao J, Cui Y, Zhang Q, Niu Y (2016) Geostatistical interpolation model selection based on ArcGIS and spatio-temporal variability analysis of groundwater level in piedmont plains, northwest China. *SpringerPlus* 5:425
35. Yin S, Gu X, Xiao Y, Wu W, Pan X, Shao J, Zhang Q (2017) Geostatistics-based spatial variation characteristics of groundwater levels in a wastewater irrigation area, northern China. *Water Supply* 17(5):1479–1789
36. Zhang Y, Xu, B, Guo Z, Han J, Li H, Jin L, hen F Xiong Y (2019) Human health risk assessment of groundwater arsenic contamination in Jinghui irrigation district, China. *J Environ Manag* 237:163–169
37. Zirakbash T, Admiraal R, Boronina A, Anda M, Bahri PA (2020) Assessing interpolation methods for accuracy of design groundwater levels for civil projects. *J Hydrol Eng* 25(9):04020042

# Estimation of Glacier Ice Velocity and Thickness Using Optical Remote Sensing



Sunita and Amanpreet

**Abstract** The velocity of glaciers impacts many aspects of glaciology. Glacier velocity measurement is one of the prime aspects as it is closely related to the glacier mass balance. The variations in velocity occur in the different zones of the glacier also these variations can be observed on yearly basis. Measuring the glacier velocity has become an important aspect because it can be easily affected by the increase of snow mass in the accumulation zone of the glacier. Two images of ‘different times’ are compared using correlation techniques to derive glacier displacement over the period of time. LANDSAT TM data with 30 m of spatial resolution is used. In order to obtain an optimum correlation between the images, it was ensured that the images were accurately coregistered and free from cloud cover. By use of correlation image, we obtained three output images: an ‘East/West displacement’ image, a ‘North/South displacement’ image, and ‘Signal to Noise ratio’ image (SNR). The quality of the correlation is defined by SNR image. Finally, Eulerian norms were used to calculate the resultant velocity. Further, an attempt has also been made to find out the thickness using surface velocities. The mean annual velocity for the Gangotri glacier for year 2009–2010 is  $55.32 \text{ ma}^{-1}$  and the mean annual Ice thickness 235.12 m. For the period of 2010–2011, mean annual velocity is  $56.25 \text{ ma}^{-1}$  and the mean annual ice thickness is 239.62 m.

**Keywords** Gangotri glacier · Ice velocity · Ice thickness

## 1 Introduction

The Glacier dynamics have been categorized depending upon majorly two parameters namely; Surface Velocity and Ice Thickness. It has been observed in the past couple of decades that the temperature of the globe has started to rise and it may continue to rise in the coming years, as we know that sea level is very sensitive to even little changes in ‘ice-sheet volume’, i.e., 1% decrease, increases the sea level by about

---

Sunita (✉) · Amanpreet  
Department of Civil Engineering, Punjabi University, Patiala, India

1 m. It is evident that any change in the dynamics of ice can affect such changes very swiftly, so, the analysis of glacier dynamics has become so important and necessary far beyond the level as suggested by the small size of the glaciological community. Velocity measurement is a very important aspect as it is closely related to the glacier mass balance. Velocity variations occur in the different zones of the glacier also the variations can be observed on yearly basis. Hydro metrological or geomorphology can be observed as the causes for the variation of the glacier velocities. Measuring the glacier velocity becomes important because it's likely to get easily affected by the increase of snow mass in the zone of accumulation of glacier. The dominating factor governing the 'Flow rates' is 'temperature', i.e., the rate at which the ice at 0 °C flows is nearly 10 times faster than the rate at which ice flows at -10 °C, and which is 100 times faster than the rate at which the ice flows at -25 °C. For better and accurate results of study, theoretical models of glaciers and ice sheets have to get both dynamics and thermodynamics correctly.

## 2 Study Area

The Gangotri Glacier (Fig. 1) is a valley type Glacier located in Uttarkashi District of Garhwal Himalaya, Uttarakhand India in a region bordering China. It is between 30° 44'–30°56' N 79° 04'–79° 15' E flows in Northwest direction. It is counted as one of the largest Glaciers of Himalayas. It is about 30.2 km long and 0.20–2.35 km wide and its surface elevation ranges between 4000 and 7000 mean above sea level [6, 13] with a surface area of about 140 km<sup>2</sup>.

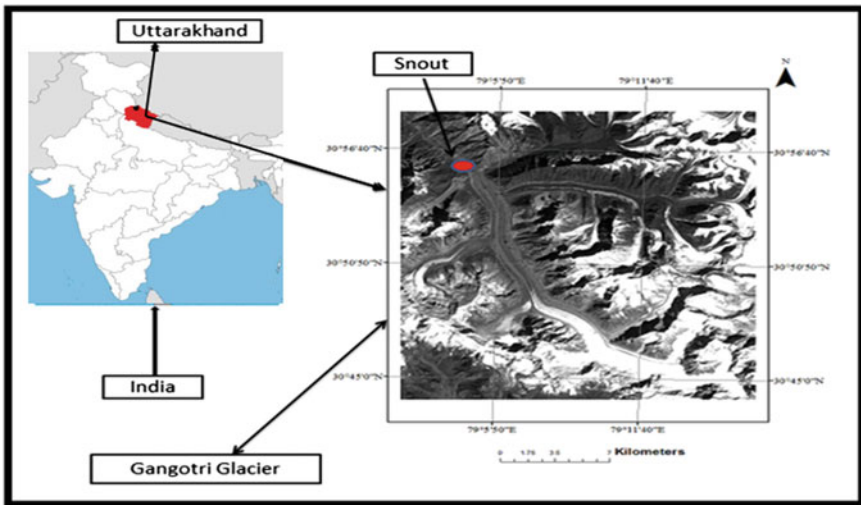


Fig. 1 Depicting location of the 'Gangotri Glacier'



**Table 1** Data sets used for Gangotri glacier

| Date of pass    | Satellite/sensor | Spatial resolution (m) | No. of bands |
|-----------------|------------------|------------------------|--------------|
| 30 July 2009    | LANDSAT-5 TM     | 30                     | 7            |
| 21 October 2010 | LANDSAT-5 TM     | 30                     | 7            |
| 24 October 2011 | LANDSAT-5 TM     | 30                     | 7            |

### 3 Data Used

Landsat TM imagery (30 m spatial resolution) was obtained for 2009–2011 during October, i.e., at the end of the melting season. The post-monsoon months were chosen to ensure minimum cloud cover over the area of interest. Pair used are July 2009–Oct 2010 and Oct 2010–Oct 2011. All images used in this study are downloaded from <http://earthexplorer.usgs.gov>. The Images are selected ensuring minimum cloud cover, however. In general, USGS satellite-based cloud cover algorithm tends to overestimate cloud cover. A set of Landsat images for Gangotri glacier as shown in Table 1 was selected.

### 4 Overview of Methodology (Surface Velocity)

The objective is to measure the surface motion of Gangotri glacier. Based on the software-module COSI-Corr (Coregistration of Optically Sensed Images and Correlation) integrated into the software ENVI, we avail a semi-automated feature tracking procedure. For the creation of the velocity fields, the individual displacement measurements generated by COSI-Corr were processed. The velocity fields obtained through this method are used for estimating the ice thickness distribution of Gangotri Glacier using Glen's flow law in conjunction with slope obtained using Advanced Spaceborne Thermal Emission and Reflection (ASTER) digital elevation model [6].

The processing chain for adopted methodology for measuring surface velocity is made up of basic steps depicted in flowchart below (Fig. 2).

#### 4.1 Pre-processing

The first task group consists of orthorectification, coregistration, and satellite imagery correlation (Fig. 3), followed by post processing of the results of the correlation using COSI-Corr. Images used to derive displacements have to be orthorectified before matching them, or alternatively, the displacements obtained when matching non-orthorectified original images have to be rectified. This requires knowledge of camera position, camera look direction, lens distortion, and ground topography. The

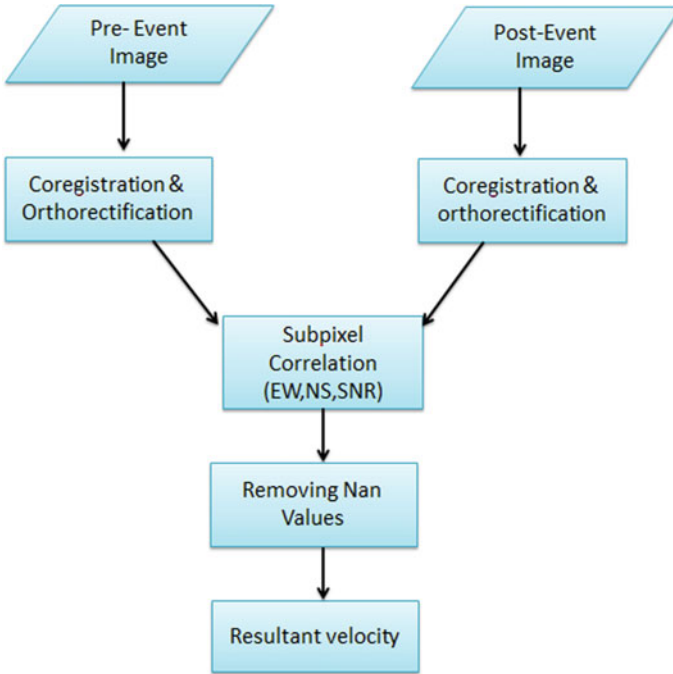


Fig. 2 Flow chart of methodology showing basic steps for estimating surface velocity of glacier using Cosi-corr

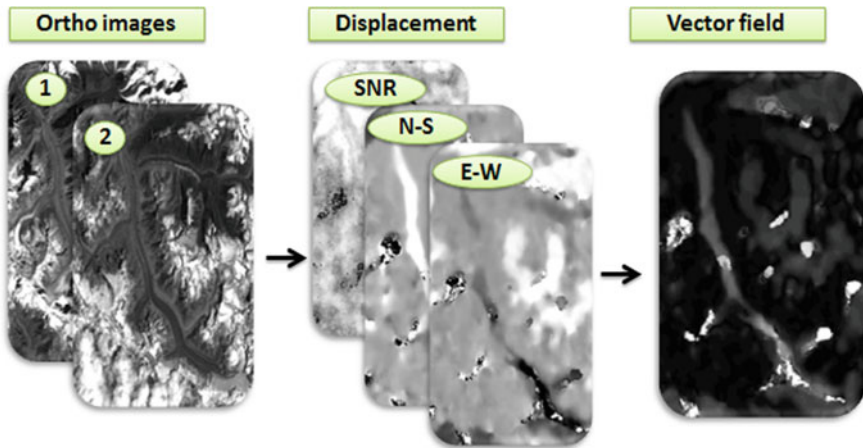


Fig. 3 Orthorectification and coregistration of multi temporal satellite images

orthorectification quality limits the exactness of the displacement field. Incorrect values of camera position, direction of look, distortion of the lens, and atmospheric effects give horizontal shifts in the ortho images which can be mistakenly identified as dislocation. Likewise, vertical errors in digital elevation models (DEMs) used to orthorectify the images are translated into horizontal shifts in the orthorectified images [2].

## ***4.2 Image Pair Selection***

The properties of the chosen images have a big impact on the quality of the output. Images are selected based on three main criteria:

(i) coverage, (ii) coverage in the cloud, and (iii) acquisition geometry. Images should include the area of interest and surrounding area. A significant area is required around the region of interest, as these areas are used to reduce distortions in coregistration process. Additionally, images near the region of interest must be free from cloud cover. Last but not least, the geometry of acquisition must be favorable.

## ***4.3 Coregistration and Orthorectification***

The struggle in accurate coregistration of satellite images is may be due to the spacecraft's changing altitude, accurate resampling, and DEM errors. A UTM, i.e., Universal transfer ground projection Mercator is used to project images on a common reference system independent of the viewing geometry of image coregistration by the sensor [11]. Following parameters were determined for precise and accurate coregistration and orthorectification.

### **4.3.1 Ancillary File**

It contains satellite altitudes, positions, and looks directions while capturing an image, along with numerous lines and columns, ground resolution, elevation, and solar azimuth. Since all Landsat scenes are geo-referred, hence all ancillary information is lost and the only solution lies in directly correlating the images.

### **4.3.2 Selections of GCP's**

Before deriving displacements from the raw satellite images, they must be orthorectified and coregistered which requires selecting tie points manually on a master image (already orthorectified) with respect to a slave image then a set of ground control points are established for the automatic registration and orthorectification of the slave

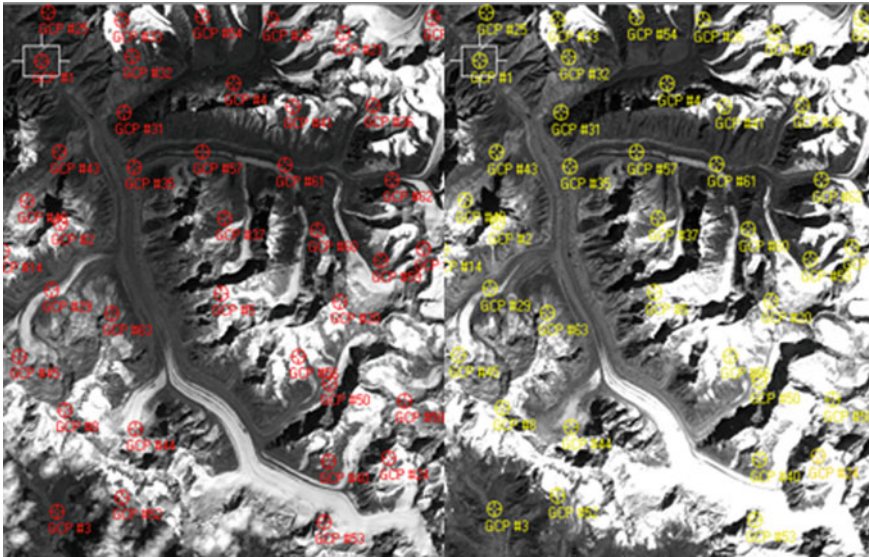


**Fig. 4** Image to the left depicts ground control points on master image and right image depicts GCPs on slave image

image with respect to the master. Tie points are precisely selected on areas of zero displacements (principally off-glacier) scattered in the scene, and mostly located in the valleys to minimize stereoscopic effect. The orthorectified image is further used to rectify other images [10]. Here we have used Landsat images since all Landsat scenes are geo-referred, hence all ancillary information is lost and the only solution lies in directly correlating the images. The generation of GCPs was made by taking Google Earth reference to get ortho image pre event, then this image was used as a reference to orthorectify image post event. For both the raw images and reference images, more than 40 tie points were generated automatically. The root means square spatial error equivalent of the standard deviation is used to estimate the quality of the coregistration. RMS should have a value of less than or equal to 0.5. Points with higher RMS values were deleted and final points in the text file were saved. The lower the RMSE, the more accurate the orthorectification will resemble reality. In our study, the RMSE (root mean square error) reached a total value of 0.268 (Fig. 4).

### 4.3.3 Resampling

By selecting one of the four available resampling methods; nearest neighbor, Bilinear interpolation, cubic convolution, and bi cubic spline an image according to the mapping matrices was recreated with inverse mapping matrices by which ground coordinates are associated with raw pixel coordinates. After taking into account

satellite attitude variations without adding any aliasing the coregistered orthorectified image with an accuracy of 1/50 of image pixel size is acquired [9]. Another image was coregistered in the same manner.

### 4.3.4 Cross Correlation

To derive surface movement of the Gangotri glacier between the two orthorectified scenes, we used a feature tracking algorithm operating at sub-pixel level that tracks the displacement of surface features. However, feature tracking can only be accomplished on coregistered single band image pairs. The pre-event optical image and the post-event optical image containing horizontal ground displacement were retrieved using a frequential correlator using process of estimating phase plane in the Fourier domain.

Pre-event and post-event ortho rectified optical images sub-pixel correlation gives ground horizontal displacements through estimating phase plane process in Fourier domain [3, 5]. Two correlation images showing ground horizontal displacement components, i.e., East–West and North–South resulted from the process.

The process of estimating the phase plane in the Fourier domain which is an iterative, unbiased method results in image correlation. Two correlation images representing horizontal ground displacement component (East–West and North–South), and Signal to Noise Ratio (SNR) for each measurement were obtained from the process, assessing the confidence of the results.

Frequential and statistical are the two types of correlators available. The frequency correlator is more accurate based on the Fourier domain than the statistical correlator. Due to the sensitivity to noisy images of frequency correlator, it is adopted for sub-pixel correlation. Coarser results are obtained from statistical correlator which is more robust than frequency correlator because it results in maximization of the absolute value of correlation coefficient. To obtain better results statistical correlator is preferred for noisy optical images (Fig. 5).

For Gangotri glacier, the Landsat images used for correlation were obtained from USGS. Images used for studying glacier dynamic behavior. They were acquired on 30th July 2009, 21st October 2010, and 24th October 2011. After image coregistration, a correlation was performed Table 2. Band 4 nadir viewing near infrared region (NIR) was selected for all the images. Best correlations were obtained using a small

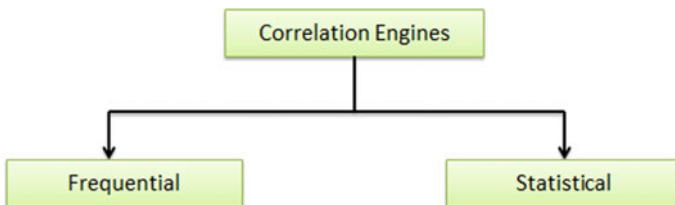
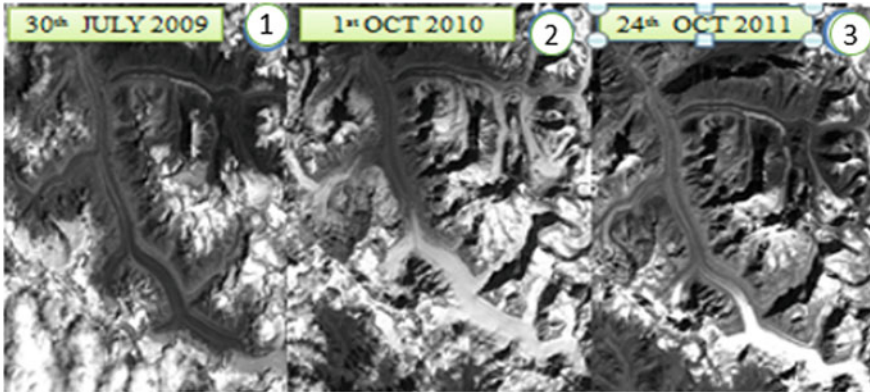


Fig. 5 Two types of correlation engines

**Table 2** List of image pairs (Gangotri) used

| S. no. | Image pair selected for correlation |
|--------|-------------------------------------|
| 1      | 30th July 2009–21st October 2010    |
| 2      | 21st October 2010–24th October 2011 |

**Fig. 6** Image pair of Gangotri glacier used for Coregistration of Gangotri glacier

32 × 32 pixel correlation window, a 2-pixel step size, and a 3-robustness iteration (Fig. 6).

### 4.3.5 Post Processing

After correlation, three band images are attained based on which a series of operations is obtained, that further lead to production of the velocity field. These post-processing procedures are dedicated to the assessment and removal of errors made in the data processing or related to the data itself.

### 4.3.6 Data Filtering

The displacements derived from the COSI-Corr technique are filtered to eliminate miscorrelations, signal to noise ratio (SNR) image that is derived from the above technique and this helps in deciding poorly as well as good correlation over the image. The correlation quality is evaluated by the SNR value, reportedly; lower the SNR value poorer will be the correlation. 0 represents no correlation whereas 1 represents perfect correlation. Hence all pixels with SNR less than 0.9 were discarded. Image with original SNR values and corrected SNR image of Gangotri region for a correlation between 2009 and 2010 scenes are shown in Fig. 7a, b respectively. Using a tool ‘discard/replace image values’, the miscorrelations produced due to change in

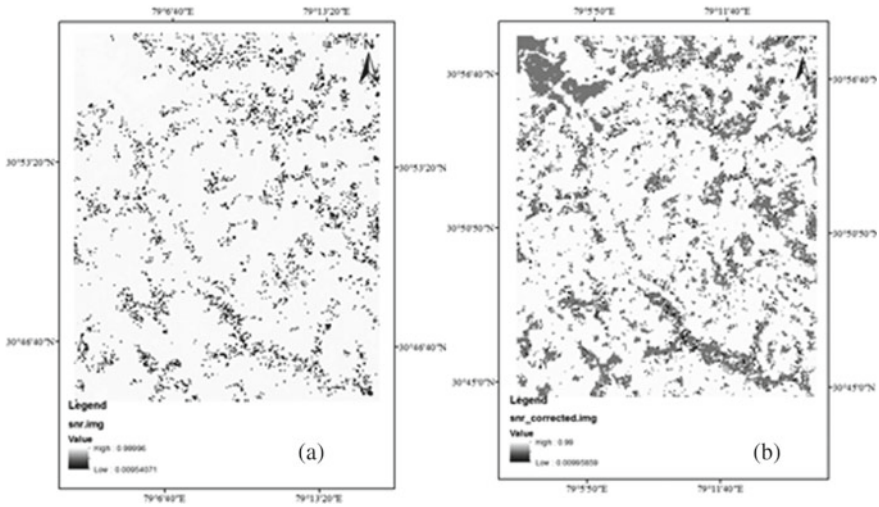


Fig. 7 a Original SNR image; b SNR image corrected

shadow pattern between the images of a pair were discarded. It allows to filter and to change the pixel values of an image based on their values [1].

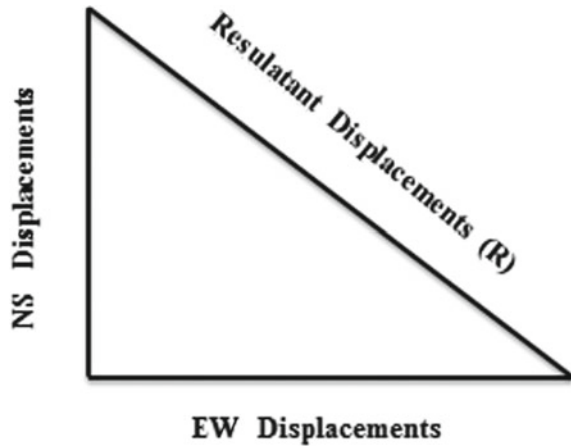
### 5 Measuring Displacements

The displacement values attained from the resulting filtered correlation file over the time period between two images should be converted into annual displacements and then combined into a single image [8, 9]. After correlation, take a  $32 \times 32$  pixel sliding window, three-pixel step size, correlation mask parameter  $m = 0.9$ , with four iterations, we obtain three output images: A North/South displacement image, an East/West displacement image, and a Signal to Noise image ratio (SNR) that defines the correlation quality. Correlation pixels having a value  $< 0.9$  have been chunked out. Finally, the resultant displacement was calculated using Eulerian norms. The time span difference between two images is used for calculating the field of velocity. These annual displacements can be converted into annual displacements as shown by Eq. 1, while the direction can be given by Eq. 2. Resultant annual velocities were obtained by multiplication of displacement values by 365 and dividing it by number of days of separation between the two images. The calculations for obtaining absolute velocities are explained by Fig. 8.

$$R = \sqrt{NS^2 + EW^2}$$



**Fig. 8** Calculation of absolute displacement



$$\theta = \tan^{-1} \frac{NS}{EW}$$

## 6 Analysis and Interpretation

The methodology used to carry out this study uses different methodological parameters which are available in *cosi-corr* software, summarized above. To analyze and interpret the results, different products in ArcMap, ENVI, Erdas imagine and MS excel software was prepared. Previously done research were compared with the present research for evaluating the coregistration, correlation, and correlators with different window size, step size between two correlating windows, iterations, threshold values etc.

By getting the results of correlation, three output images were brought out, i.e., a North/South displacement image, an East/West displacement image, and Signal to Noise ratio image (SNR) which elaborates the quality of correlation. Pixels of correlation which were having value  $<0.9$  were chunked out. For further processing, vector field results for each correlated image were also exported as jpeg and text files. From the 'exported vector field text files' numerous different calculations were done for the calculation of resultant displacement values and their directions from East–West and North–South direction. For each correlated image, the average of displacement values was made and counted for different time intervals. This entire process was repeated for other sets of images.



## 7 Depth Estimation

After measuring surface velocity, we find Gangotri Glacier ice thickness using surface velocities and slope. For topographic analysis the ASTER digital elevation model (30 m resolution DEM) was used [10]. Assuming that the basal velocity is 25% of the surface velocity, the thickness was estimated by the relationship [4].

Using the Laminar Flow equation, Ice Thickness can be estimated as

$$U_s = U_b + \frac{2A}{n + 1} \tau_b^n H \tag{1}$$

where,  $U_s$  and  $U_b$  are surface and base velocities resp. The basal velocity of these Glaciers has not been accurately estimated till now but we can assume  $U_b$  to be 25% of  $U_s$ . ‘ $n$ ’ is the Glen’s flow law [7] exponent in the Laminar’s Flow equation, we assume it to be 3, wherein  $H$  is the thickness of ice and  $A$  is the creep parameter which depends majorly on three factors that are impurity content, grain size, and temperature which has a value of  $3.24 \times 10^{-24} \text{ Pa}^{-3} \text{ s}^{-1}$  for temperate glaciers.

The basal stress is modeled as

$$\tau_b = f \rho g H \sin \alpha \tag{2}$$

where  $\rho$  denotes the density of ice which has a constant value of  $900 \text{ kgm}^{-3}$ ,  $g$  denotes acceleration due to gravity which has a constant value of  $9.8 \text{ ms}^{-2}$ ,  $f$  denotes the scale factor which is the ratio between the driving stress and basal stress along a glacier, and the range for this scale factor is 0.8–1 for temperate glaciers. Here, we use  $f = 0.8$ .  $\alpha$  denotes the slope that is being estimated from ASTER (Advanced Spaceborne Thermal Emission and reflection radiometer) at 100 m intervals DEM elevation contours. The interval of 100 m was chosen to average the surface slope over a reference distance which can be larger than the local ice thickness.

$$H = \sqrt[4]{\frac{1.5U_s}{Af^3(\rho g \sin \alpha)^3}} \tag{3}$$

## 8 Results

The Velocity maps in Fig. 9a–b show that accumulation zone that is the upper part of glacier shows variation in velocities, whereas lower part of the glacier shows lesser velocities. Decorrelation was observed in the upper part of the glacier due to cloud cover and excessive snowfall. Further fall in velocity near the snout was observed

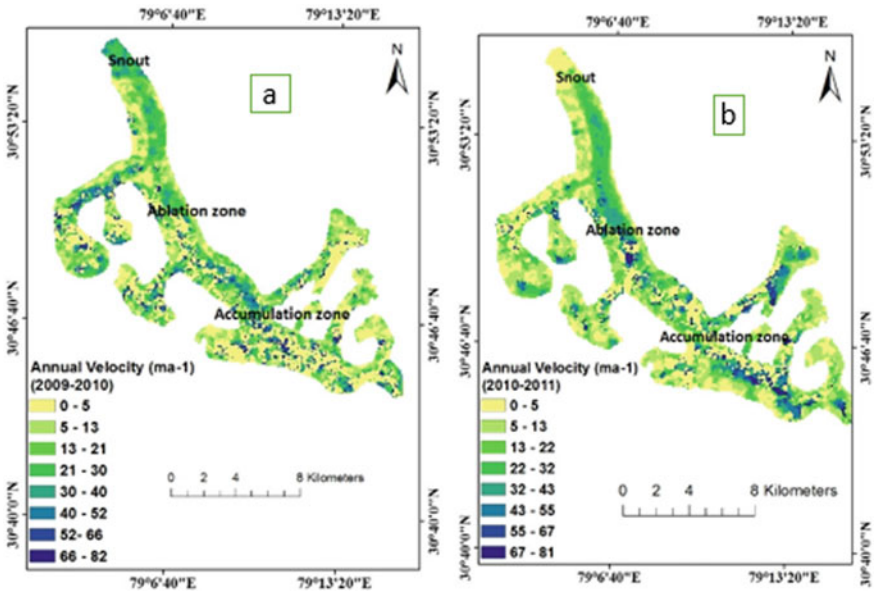


**Fig. 9** **a** Annual velocity ( $\text{ma}^{-1}$ ) 2009–2010 Gangotri glacier; **b** Annual velocity ( $\text{ma}^{-1}$ ) 2010–2011 Gangotri glacier

**Table 3** Mean annual velocities for different pairs

| S. no. | Duration                       | Mean velocities ( $\text{ma}^{-1}$ ) |
|--------|--------------------------------|--------------------------------------|
| 1      | 30th July, 2009–21st Oct. 2010 | 55.32                                |
| 2      | 21st Oct. 2010–24th Oct. 2011  | 56.25                                |

due to the change in orientation of the glacier. The mean velocities of the glacier for each period are illustrated in Table 3.

### 8.1 Snout of Gangotri Glacier

Velocity maps of Gangotri are shown in Fig. 10a–b depict that the Variation of velocity for the period 2009–2010 lies between ( $\sim 12\text{--}40 \text{ ma}^{-1}$ ) whereas velocity of 2010–2011 have shown with a significant part of glacier flowing with velocities of the order ( $\sim 22\text{--}40 \text{ ma}^{-1}$ ). However, the end part of snout observed to be flowing with very low velocity in all cases except 2009–2010.

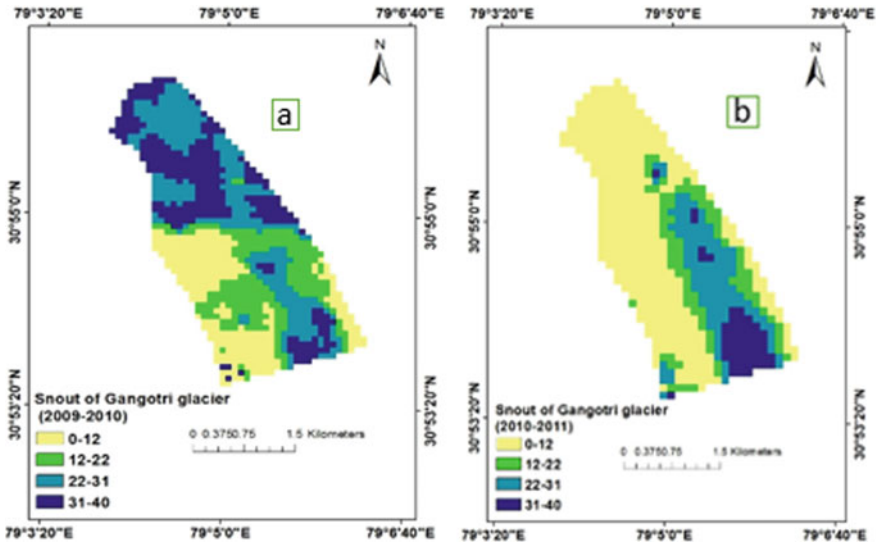


Fig. 10 a Annual velocity near Snout (2009–2010); b Annual velocity near Snout (2010–2011)

### 8.2 Ablation Zone of Gangotri Glacier

Velocity distribution in Fig. 11a for 2009–2010 period have shown velocities of ( $\sim 30\text{--}70\text{ ma}^{-1}$ ) in both upper and lower reaches. Velocity distribution for the period of the year 2010–2011 in Fig. 11b shows velocities of order ( $\sim 60\text{--}70\text{ ma}^{-1}$ ) in upper region of the ablation zone and patches of high velocity in lower region of ablation zone that is velocity ranges between ( $\sim 70\text{--}81\text{ ma}^{-1}$ ).

### 8.3 Accumulation Zone of Gangotri Glacier

Velocity maps illustrated in Fig. 12a and b clearly indicates the fast movement of glacier in the center with respect to glacier margins. The velocity of ice flowing at the edges vary about ( $\sim 0\text{--}30\text{ ma}^{-1}$ ). Velocity variation can be seen in the center of accumulation zone these fluctuations in velocity can be due to the steep slopes of the accumulation region of the glacier. Velocity profiles measured from the upper portion of accumulation zone of various periods are Very high velocities ( $\sim 60\text{--}80\text{ ma}^{-1}$ ) are observed for the period of 2010–2011.

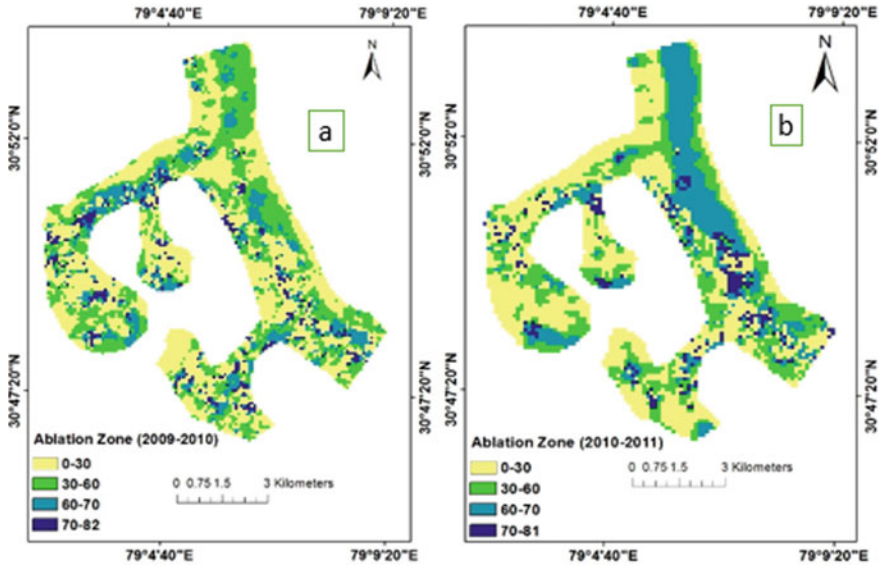


Fig. 11 a Annual velocity in ablation Zone (2009–2010); b Annual velocity in ablation Zone (2010–2011)

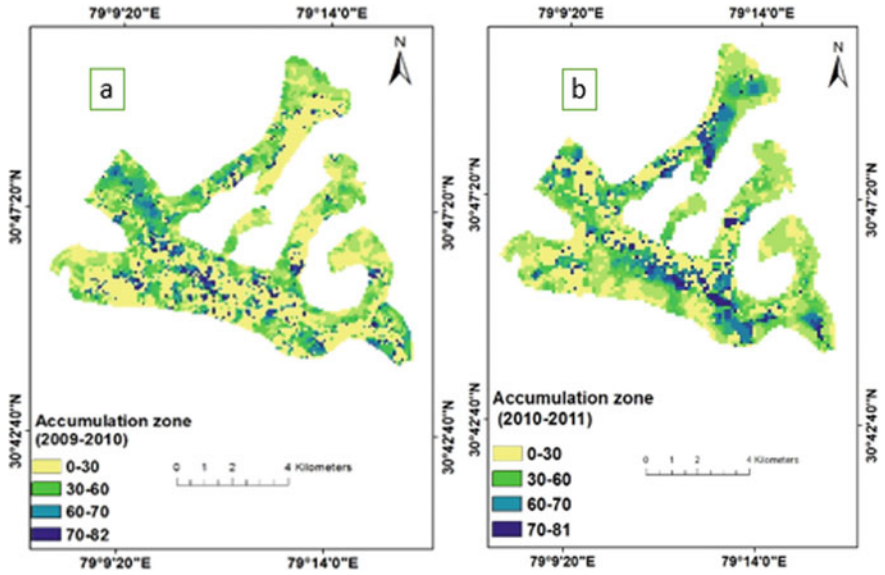
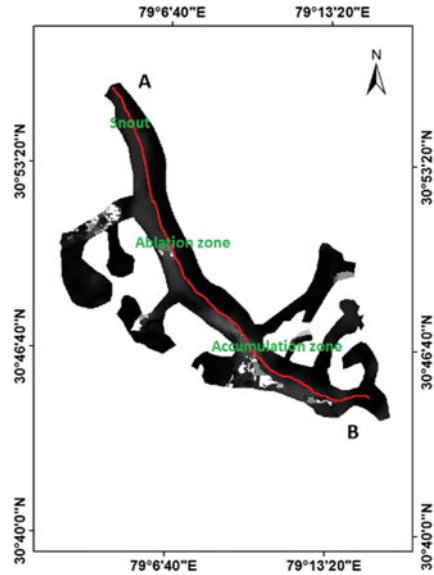


Fig. 12 a Annual velocity in accumulation Zone (2009–2010); b Annual velocity in accumulation Zone (2010–2011)

**Fig. 13** Longitudinal profiles of Gangotri glacier



### 8.4 Velocity Profile Along the Center Line of the Glacier

Velocities were also computed longitudinally along the central line (A–B) of the glacier as shown in Fig. 13. The velocity field (30th July, 2009–21st Oct. 2010), the velocities of Gangotri in the accumulation zone ranges from 56–82  $\text{ma}^{-1}$ , 33–58  $\text{ma}^{-1}$  in ablation zone and 18–32  $\text{ma}^{-1}$  near the snout, highest velocities were recorded in accumulation zone. For the second velocity field (21st Oct. 2010–24th Oct. 2011) velocity in the accumulation zone ranges from 55 to 81  $\text{ma}^{-1}$  and in the middle region of the glacier, velocities of the order of 22–55  $\text{ma}^{-1}$  are observed. Velocities around 5–28  $\text{ma}^{-1}$  are observed near snout.

## 9 Ice Thickness Estimation for Gangotri Glacier

There was an attempt to estimate the glacier’s thickness using surface velocities. For topographic analysis, the ASTER digital elevation model (30 m resolution DEM) was used [12]. By taking into assumption basal velocity as 25% of the surface velocity, thickness was estimated by the relation given by ‘Cuffey and Paterson’ [4]. The proposed technique comprises of estimating a distribution of the apparent mass balance, from which an ice flux for chosen ice flow lines is computed. The flux is converted into an ice thickness using an integrated form of Glen’s flow law [7] and interpolated over the entire glacier. The equations used for estimation of ice thickness have already been discussed in previous chapters. Final equation used for

estimation of ice depth is given below.

$$H = \sqrt[4]{\frac{1.5U_s}{Af^3(\rho g \sin \alpha)^3}} \tag{4}$$

Figure 14a–b presents the result for thickness distribution along the length of the glacier. Images of different periods have shown similar trends for thickness. Thickness is less at edges as compared to the thickness computed at the center of the glacier. The average thickness of glaciers varying from 105 to 280 m and in accumulation zone it varies from 350 to 539 m. Average values of thickness are presented in Table 4.

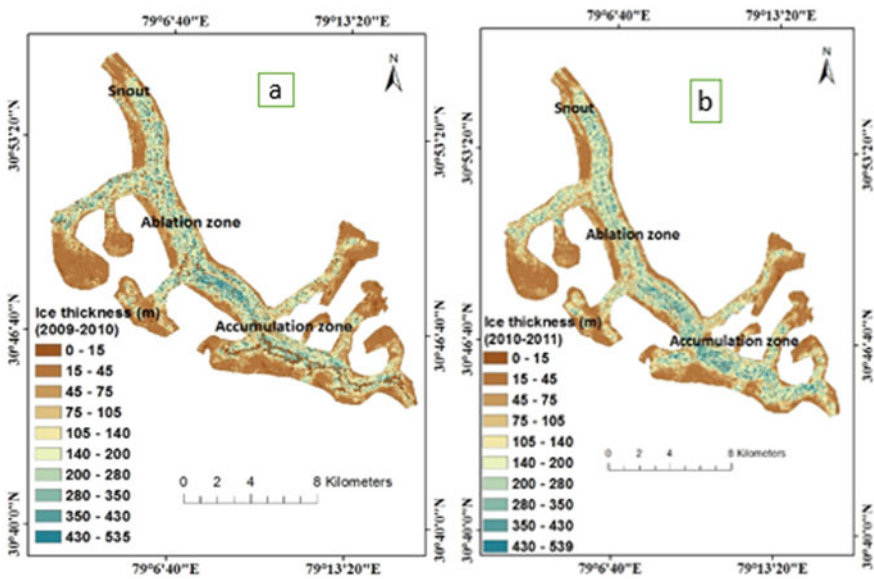


**Fig. 14** a Ice Thickness distribution of Gangotri (2009–2010); b Ice Thickness distribution of Gangotri (2010–2011)

**Table 4** Mean annual ice thickness for different pairs

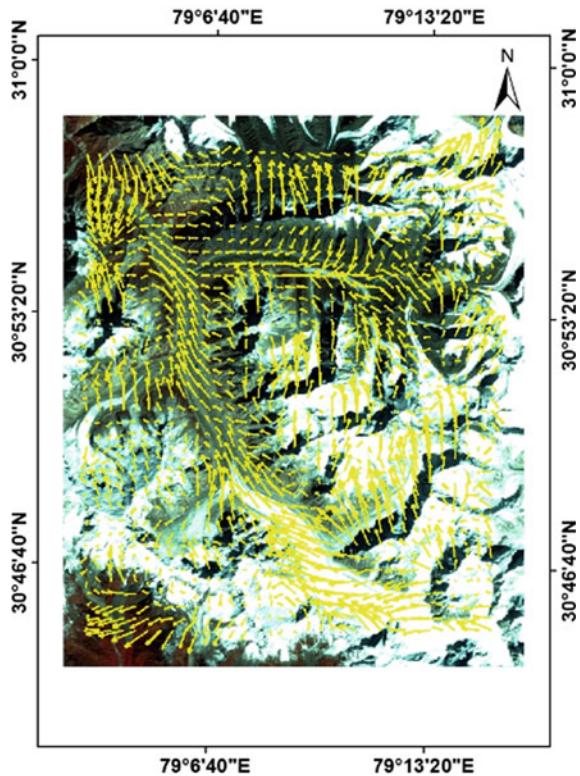
| S. no. | Duration                           | Mean thickness (m) |
|--------|------------------------------------|--------------------|
| 1      | 30th July, 2009 and 21st Oct. 2010 | 235.12             |
| 2      | 21st Oct. 2010 and 24th Oct. 2011  | 239.62             |

### 10 Results Validation

Since the Gangotri Glacier has never been the subject of any field-based velocity estimation, hence field observed data is not available for evaluation of computed results. However, the accuracy and precision of outcomes can still be assessed using different analytic methods. The obtained results possess a series of tests to assess their quality. Firstly, assessment of velocity magnitudes was carried out. In general, velocity decreases from the glacier centerline to the margin. The velocity profile drawn along the center line of the glacier shows that velocity increases from accumulation zone to snout. Further for glacier displacement direction assessment was performed on obtained velocity vectors. From this, a good correlation was found as velocity vectors indicate a consistent and realistic glacier motion (Fig. 15).

The final velocity for the Gangotri glacier for year 30th July. 2009–21st Oct. 2010, the velocities in the accumulation zone ranges from  $56\text{--}82\text{ ma}^{-1}$ ,  $33\text{--}58\text{ ma}^{-1}$  in ablation zone and  $18\text{--}32\text{ ma}^{-1}$  near the snout. The Ice thickness distribution attains a maximum of 535 m in central part of glaciers main body, 340–460 m in the accumulation zone. Ice thickness near the snout was 38–64 m. For the period of 21st Oct. 2010–24th Oct. 2011, Resultant velocity in the accumulation zone ranges from

**Fig. 15** Flow direction of Gangotri glacier





55–81  $\text{ma}^{-1}$  and in the middle region of the glacier, velocities of the order of 22–55  $\text{ma}^{-1}$  are observed. Velocities around 5–28  $\text{ma}^{-1}$  are observed near snout of the glacier. The ice thickness of the glacier has been estimated in the range of 25–68 m near terminus and thickness increases to 539 m in the middle part and accumulation zone of the glacier.

## References

1. Ayoub F, Leprince S, Keene L (2009) User's guide to COSI-Corr, co-registration of optically sensed images and correlation. California Institute of Technology, USA, pp 1–38. <http://www.caltech.edu>
2. Berthier E, Vadon H, Baratoux D, Arnaud Y, Vincent C, Feigl KL, Rémy F, Legrésy B (2005) Surface motion of mountain glaciers derived from satellite optical imagery. *Remote Sens Environ* 95(1):14–28
3. Brown LG (1992) A survey of image registration techniques. *ACM Comput Surv* 24:12–14
4. Cuffey KM, Paterson WSB (2010) *The physics of Glaciers*, 4th edn. Butterworth Heinemann Publications. Burlington, USA
5. Fitch AJ, Kadyrov A, Christmas WJ, Kittler J (2002) Orientation correlation. In: *British machine vision conference*, Cardiff, UK, pp 133–142
6. Gantayat P, Kulkarni AV, Srinivasan J (2014) Estimation of ice thickness using surface velocities and slope case study at Gangotri glacier, India. *J Glaciol* 60(220):277–282
7. Glen JW (1955) The creep of polycrystalline ice. In: *Proceedings of Royal Society*, vol 228(1175):519–538
8. Herman F, Anderson B, Leprince S (2011) Mountain glacier velocity variation during retreat/advance cycle quantified using sub pixel analysis of aster images. *J Glaciol* 57(202):197–206
9. Leprince S, Barbot S, Ayoub F, Avouac JP (2007) Automatic and precise orthorectification, coregistration and subpixel correlation of satellite images, application to ground deformation measurements. *IEEE Trans Geosci Remote Sens* 45(6):1529–1558
10. Negi HS, Saravana G, Rout R, Snehmani (2013) Monitoring of great Himalayan Glaciers in Patsio region, India using remote sensing and climatic observations. *Curr Sci* 105(10)
11. Quincey DJ, Copland L, Mayer C, Bishop M, Luckman A, Belo M (2009) Ice velocity and climate variations for Baltoro Glacier, Pakistan. *J Glaciol* 55(1194):1061–1071
12. Tiwari RK, Gupta RP, Arora MK (2014) Estimation of surface ice velocity of Chotta Shigri glacier using sub-pixel ASTER image correlation. *Curr Sci* 106(6):853–859
13. Jain S (2008) Impact of retreat of Gangotri Glacier on the flow of Ganga River. *Curr Sci* 95:1012–1014



# Groundwater Quality Indexing Using Weight Overlay Analysis and GIS—A Case of Rel River Catchment



Tulansi Patel, Heli Patel, Meet Trada, Jay Hirpara, Prateek Bhura, Akshesh Prajapati, Dhruv Tavethia, Dhruvesh Patel, and Naimish Bhatt

**Abstract** Ground water quality assessment is an important parameter for identification of water quality in watershed. Recently, RS and GIS techniques are important tool to do a spatial analysis of the watershed. Water quality index (WQI) will provide meaningful insight for the health and assessing water quality. In the case of Gujarat floods in 2017, Banaskantha's Rel river region was one of the most vulnerable regions. To check the water quality many attempts have been made to develop WQI with some selected parameters along four bore wells at different locations. Weighted arithmetic water quality index method and Pearson's R Matrix method were the main methods used to identify WQI. Furthermore, the obtained result is analyzed using GIS analytical techniques using IDW interpolation, the maps have been prepared detailing WQI, so it is possible to get the WQI of pinpoint locations within the study area. The results are compared with Bureau of Indian Standards IS code 10500:2012 and World Health Organization (WHO). The result will be helpful to decision makers to improve the quality of groundwater in Rel river catchment. It would provide better watershed management practice.

**Keywords** Groundwater · Water Quality Index · GIS · WHO

## 1 Introduction

Water is the most vital element of life and it is essential for humanity and its welfare. Since the last few years, the demand for water for Domestic, Industrial and Agricultural purposes is increasing exponentially where sources of water are being depleted extensively. Surface sources and subsurface sources are limited and entirely depends on climatic conditions and surrounding eco-system. Groundwater sources tend to be reliable where surface water sources are not available. Besides the quality of groundwater is deteriorating due to uncontrolled anthropogenic activities, geogenic activities, etc. usage of such contaminated water may lead to severe health problems

---

T. Patel (✉) · H. Patel · M. Trada · J. Hirpara · P. Bhura · A. Prajapati · D. Tavethia · D. Patel · N. Bhatt

Civil Engineering Department, School of Technology, PDPU, Gandhinagar, India

© The Author(s), under exclusive license to Springer Nature Singapore Pte Ltd. 2022  
C. M. Rao et al. (eds.), *Advanced Modelling and Innovations in Water Resources Engineering*, Lecture Notes in Civil Engineering 176,  
[https://doi.org/10.1007/978-981-16-4629-4\\_31](https://doi.org/10.1007/978-981-16-4629-4_31)

447

as well as economic losses, hence monitoring of ground water quality is crucial for its potential use.

A grade like single number provides a unique numerical rating to the overall quality of the water which can be used by the concerned regulatory bodies to alter policies [1]. It is defined as a rating that represents the composite influence of different water quality parameters for Water Quality Index (WQI) calculation. The standard water quality tests include the tests of various physico-chemical parameters like Alkalinity,  $\text{Cl}^-$ ,  $\text{SO}_4^{-2}$ ,  $\text{NO}_x$ , total hardness,  $\text{Ca}^{+2}$ ,  $\text{Mg}^{+2}$ , EC, DO, BOD, TDS and TSS. For estimating the Water Quality Index, the two different methods that are used are Weighted Arithmetic Index and Pearson's R. Matrix. In this study, the weighted arithmetic mean method for determining the Water Quality Index (WQI) was used. To assess co-relationship and the interrelationship between the parameters selected, the Pearson's R Matrix was used [2].

ArcGIS 10.5 software was used for interpolation of data. It is well known software that is used for viewing, editing, managing and analyzing geographic data. In GIS, spatial interpolation technique was applied to create a raster surface with estimates made for all raster cells. Spatial interpolation process helps in estimating values of unknown points by using values of known points. In order to generate continuous maps, Inverse Distance Weighted (IDW) Interpolation has been used.

IDW is an interpolation method that helps to find the cell values by averaging each sample points values with the nearest processing cell. By specifying search distance, power setting, closest points & barriers unknown values can be estimated.

## 2 Study Area

This study is conducted in Rel region of Banaskantha District of Gujarat and aims to provide Water Quality Index (WQI) of region. Rel River originates from the Aravalli hills of Rajasthan and flows to Gujarat. Rel River basin is Northern basin of Gujarat, with Latitude lies between  $24^\circ 50' 0''$  N and  $25^\circ 15' 0''$  N and longitude lies between  $72^\circ 0' 0''$  E and  $72^\circ 45' 0''$  E. Annual precipitation was 191 mm in the region during 2017 flood, which leads to heavy damage to the region and to the water bodies [14].

The region has mostly sandy soil, which is p medium in fertility and water retention capacity. Banaskantha district gets more water during monsoon periods and then the region gets dried up because the region comes under semi-arid type of climate. Region has a vast difference in temperature from  $45^\circ\text{C}$  in summer to  $12^\circ\text{C}$  in winter. Since the region has limited water available on the surface, so they use groundwater more for their daily activities, even for drinking and irrigation activities. Gujarat had recorded a heavy rainfall during July 2017, which led to a heavy inflow into the dams, which leads to flooding in many parts of the state, i.e. Aravalli, Banaskantha, Morbi, Patan, Surendranagar districts were badly affected [3, 4] (Fig. 1).

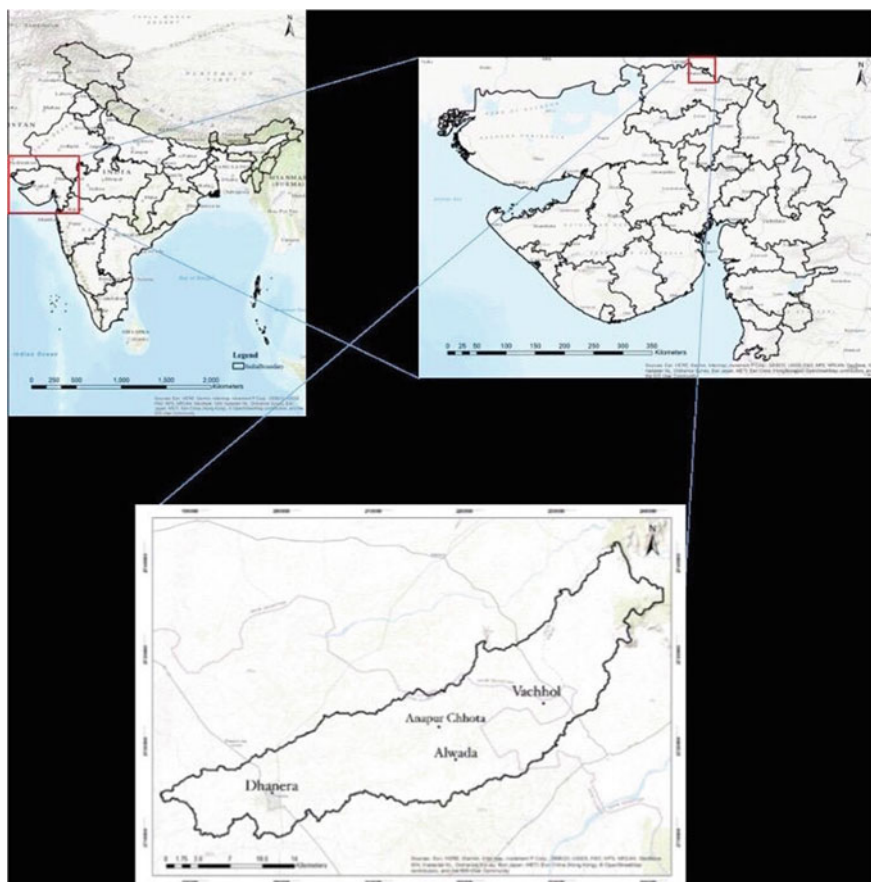


Fig. 1 Study area map

### 3 Methodology

#### 3.1 Data Sampling

Groundwater samples were collected from 4 tube wells located in Anapur Chhota, Alwada, Dhanera and Vachhol. These tube wells are maintained by Gujarat Water Resources Development Corporation (GWRDC). During the collection of samples, latitude and longitude of tube wells were noted with the help of GPS device. Samples collected from the sites were stored in air tight plastic bottles sealed by lock mechanism and opened with the help of Allen key. Samples were properly labelled with all the necessary information as well a field book was maintained, which included date and time of collection, site name, location of sampling sites, depth of water table, etc. Samples were transported from sampling site to labs with utmost care. The samples

were stored for a significant period of time in which all the specific study necessary experiments were carried out.

## **3.2 Testing**

### **3.2.1 pH**

The pH electrode consists of a combined glass electrode used for pH measurement. Electrode systems have a sensing half-cell and a reference half-cell. The sensing half-cell is a thin pH sensitive semi permeable membrane that separates the two solutions. pH value gives hydrogen ion activity of the water. pH value can be determined by using electrometric method. The hydrogen electrode is the absolute standard for the measurement of pH. An electric potential develops inside and another potential develops outside, this difference between the potential measured gives the pH value [5].

### **3.2.2 Total Hardness**

Hardness of water means water containing high mineral content. Determination of hardness of a water sample can be done through two methods (a) Ethylenediamine Tetra-acetic Acid (EDTA) and (b) analytical data method [6].

In EDTA method, calcium and magnesium salts react with ethylenediamine tetra-acetic acid or its disodium salt. In this method, Ethylenediamine Tetra-acetic Acid or its disodium salt forms a stable complexes with calcium and magnesium ions. A water sample is buffered to pH 10.0 and an indicator Eriochrome Black T (EBT) is added to water sample containing calcium and magnesium ion which turns the colour of the sample to wine red. Eriochrome black T (EBT) is used for indication of the end point for the titration of given water sample. On adding Ethylenediamine Tetra-acetic Acid (EDTA), the titrant, forms complexes with calcium and magnesium ions. When all the ions of calcium and magnesium react with EDTA, it forms complexes that change the colour of indicator to blue. End point of the titration is reached [6].

### **3.2.3 Total Dissolved Salt**

Solids refer to any material either dissolved or suspended in water that can be physically isolated either through filtration or through evaporation. Total solids are defined as the residue left in the crucible after evaporating water at a definite temperature generally 103–105 °C in an oven.

The given water sample is evaporated in a weighed dish and then dried to a constant mass in an oven at 103–105 °C. Total solids are calculated from increase in mass. Then water sample is filtered using filter paper, filtered water is taken in

a dry crucible and oven dried at 103–105 °C. The solids remaining in crucible are Dissolved solids [7].

### 3.2.4 Chloride

Chlorides are one of the major inorganic anions present in the water. In water, chlorides are widely distributed as salts of calcium, potassium and sodium. In potable water, chloride concentration also produces a salty taste depending upon its chemical composition and its quantity. A high chloride content in water may harm metallic pipes, growing plants as well as structures. In a given water sample, the amount of chloride can easily be determined by titrating it with silver nitrate solution. Take potassium chromate as an indicator, which will turn the sample into light yellow colour. The one mole of silver nitrates reacts with one mole of chloride to produce white precipitate of silver chloride. The concentration of titrant is generally 0.02 M. The formation of silver chromate colour indicates the end of titration, which is red in colour due to excess of silver nitrate [8].

### 3.2.5 Sulphate

Sulphates are widely distributed minerals in nature. Sulphate occurs naturally in forms of various minerals, including barite and gypsum. Turbidimetric method is used for measuring the concentration of sulphate ions in water sample.

By addition of a highly acidified solution of barium chloride to water sample sulphate ions present in water are precipitated in the form of barium sulphate crystals. Then the same water sample is placed in turbidity meter (nephelometer) and turbidity of water sample is measured. Based on turbidity of water, concentration of sulphate ion is determined by comparing with standard curve [9].

### 3.2.6 Alkalinity

Alkalinity of water is determined by calculating the amount of acid required to get the sample to a pH of 4.2 (e.g. sulfuric acid). Initially, phenolphthalein indicator is added to sample, if pH is greater than 8.3 solution changes to pink colour which indicates presence of hydroxyl ions. Now on titration with sulphuric acid pink colour disappears due to neutralization of  $\text{OH}^-$  ions. Now on addition of mixed indicator colour of solution changes to blue colour due to presence of  $\text{CO}_3^{2-}$  and  $\text{HCO}_3^-$ . On titrating with sulphuric acid solution changes to red in colour due to neutralization of all  $\text{CO}_3^{2-}$  and  $\text{HCO}_3^-$  ions which is the end point [10].

## 4 Result and Discussion

### 4.1 Mathematical Modelling

The experimental data acquired from water samples collected from the field are tabularized in Table 1.





It can be directly identified that the values of Water quality exceed the acceptable limits provided by the BIS IS 10500:2012 (Table 2) and World Health Organization (Table 3) for Drinking Water.

For estimating the Water Quality Index two different methods has been used: (1) Weighted Arithmetic Index (2) Pearson's R. Matrix.

#### 4.1.1 Weighted Arithmetic Index

By using this method, quality of water in terms of tested parameters against the acceptable limits of respective parameter Water Quality Index was calculated. Mathematical representation of WQI:

**Table 1** Data of Rel-River Region Water Quality

| Well No | Village       | Lat       | Long      | pH   | Total hardness (mg/L) | TDS (mg/L) | Chloride (mg/L) | Sulphate (mg/L) | Alkalinity (mg/L) | WQI    | WQ Status  | Colour   |
|---------|---------------|-----------|-----------|------|-----------------------|------------|-----------------|-----------------|-------------------|--------|------------|--|
| S1      | Anapur Chhota | 24°34'54" | 72°12'07" | 7.4  | 147                   | 373.12     | 110             | 5.91            | 25.2              | 35.44  | Good       |    |
| S2      | Alwada        | 24°32'59" | 72°13'14" | 6.8  | 670                   | 1536       | 618             | 107.25          | 5.5               | 146.67 | Unsuitable |   |
| S3      | Dhanera       | 24°30'48" | 72°01'25" | 7.11 | 337                   | 1052.48    | 356.57          | 72.42           | 28.11             | 87.81  | Very Poor  |  |
| S4      | Vachhol       | 24°36'26" | 72°18'50" | 6.91 | 150                   | 325.56     | 79.56           | 3.89            | 14.9              | 27.56  | Good       |  |

**Table 2** BIS drinking water std. [11]

| S. no. | Parameter      | Unit | Requirement (Acceptable) | Permissible limit |
|--------|----------------|------|--------------------------|-------------------|
| 1      | pH             | —    | 6.5–8.5                  | No relaxation     |
| 2      | Total hardness | mg/L | 200                      | 600               |
| 3      | TDS            | mg/L | 500                      | 2000              |
| 4      | Chloride       | mg/L | 250                      | 1000              |
| 5      | Sulphate       | mg/L | 200                      | 400               |
| 6      | Alkalinity     | mg/L | 200                      | 600               |

**Table 3** WHO drinking water guidelines [12]

| S. no. | Parameter      | Unit | Threshold |
|--------|----------------|------|-----------|
| 1      | pH             | –    | <8        |
| 2      | Total hardness | mg/L | <500      |
| 3      | TDS            | mg/L | <1000     |
| 4      | Chloride       | mg/L | <250      |
| 5      | Sulphate       | mg/L | <500      |
| 6      | Alkalinity     | mg/L | <120      |

$$WQI = \sum q_p W_p / \sum W_p \tag{1}$$

where,

$q_p$  Sub Index.

$W_p$  Relative weight.

$$q_p = 100[V_p - V_i] / [S_p - V_i] \tag{2}$$

$V_p$  Experimental value of  $p$ th parameter.

$V_i$  Ideal value of  $p$ th parameter in pure water (i.e. Except for pH(7) all other parameters are taken 0).

$S_p$  Standard permissible value of the  $p$ th parameter.

Relative weight is inversely proportional to standard permissible value and which can be expressed as follows:

$$W_p = K / S_p \tag{3}$$

where,

$W_p$  relative weight or unit weight for the  $p$ th parameter.

$S_p$  standard value for  $n$ th parameters.

$K$  constant for proportionality.

Relative weight is assigned as per standard permissible value of parameter, the parameter having low standard permissible value is allotted high relative weight. As even little fluctuation can influence water quality to large extent and vice versa. Relative weight of respective parameters is tabulated in Table 4. Further, they are converted into unit weight [1].






The overall Water Quality Index was calculated by aggregating the quality rating linearly with the unit weight.

Based on WQI, Water quality is rated into 5 grades which are tabulated in Table 5. The ranges are verified with previous studies conducted by K. Yogendra and E.T. Puttaiah [13].

**Table 4** Relative weight and unit weight

| S. no. | Parameter      | Relative weight | Unit weight |
|--------|----------------|-----------------|-------------|
| 1      | pH             | 3               | 0.13        |
| 2      | Total hardness | 5               | 0.21        |
| 3      | TDS            | 2               | 0.08        |
| 4      | Chloride       | 4               | 0.17        |
| 5      | Sulphate       | 5               | 0.21        |
| 6      | Alkalinity     | 5               | 0.21        |

**Table 5** Scale of water quality based on WQI

| Water Quality Status | WQI    | Colour  |
|----------------------|--------|---|
| Excellent            | 0-25   |  |
| Good                 | 26-50  |  |
| Poor                 | 51-75  |  |
| Very Poor            | 76-100 |  |
| Unsuitable           | >100   |  |

Based on the above-mentioned formula, Water Quality Index was calculated for each water sample (Table 1).

#### 4.1.2 Pearson's R. Matrix

Further, Pearson's R. Matrix method has been used to get the correlation between the tested parameters and estimate the extent by which the values of each parameter are interrelated for all the possible combinations. The matrix formed after calculating all the combinations will give the correlation coefficient of the parameters in rows with the parameters in columns. The Matrix is tabulated in Table 6.

**Table 6** Pearson's R. Matrix

|                | pH        | Total hardness | TDS       | Chloride  | Sulphate  | Alkalinity |
|----------------|-----------|----------------|-----------|-----------|-----------|------------|
| pH             | 1         |                |           |           |           |            |
| Total hardness | -0.634740 | 1              |           |           |           |            |
| TDS            | -0.550038 | 0.970977       | 1         |           |           |            |
| Chloride       | -0.563001 | 0.987958       | 0.995558  | 1         |           |            |
| Sulphate       | -0.542563 | 0.954100       | 0.997743  | 0.987013  | 1         |            |
| Alkalinity     | 0.819275  | -0.648031      | -0.461381 | -0.524744 | -0.417031 | 1          |



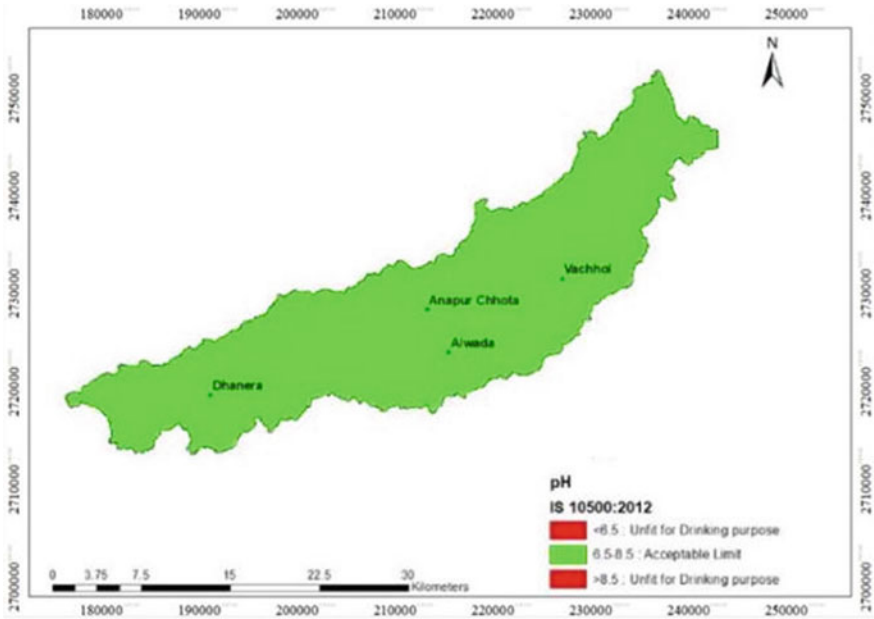


Fig. 2 pH

### 4.2 Geospatial Techniques

The data collected was run through the GIS software to allow for the analysis and visual representation of the contrast in the quality of water over the geographical area of Rel River Region in a map format as shown in Figs. 2, 3, 4, 5, 6, 7 and 8 for each parameter. The topographic data presents sites of interest in the district which have undergone and have higher concentrations of each parameter and with IDW interpolation, the tool allows to ascertain the nearby areas with similar concentrations in the topographical depiction of the district.

Based on WQI of tested samples, Water Quality of Annapur Chhota (S1) and Vachhol (S4) is Good whereas that of Dhanera (S3) is very poor and that of Alwada (S2) is Unacceptable. Further pH of water samples ranges from 6.8 to 7.4 indicating water of rel river region is almost neutral to sub-alkaline. TDS of sample ranges from 373 to 1536 mg/L for samples S1 and S4 it is within acceptable limit while for S2 and S3 it is between acceptable limit and permissible limit this might be due to concentration of chloride as for the same sample the concentration of chloride falls between acceptable limit and permissible limit. Also, for each sample Total hardness is greater than total alkalinity hence Total alkalinity is carbonaceous hardness and difference between TH and TA is non carbonaceous hardness. Hence a major portion of TH is non carbonaceous hardness which is mainly due to chloride concentration. Concentration of sulphate ranges from 3.9 to 107 mg/L which is within acceptable

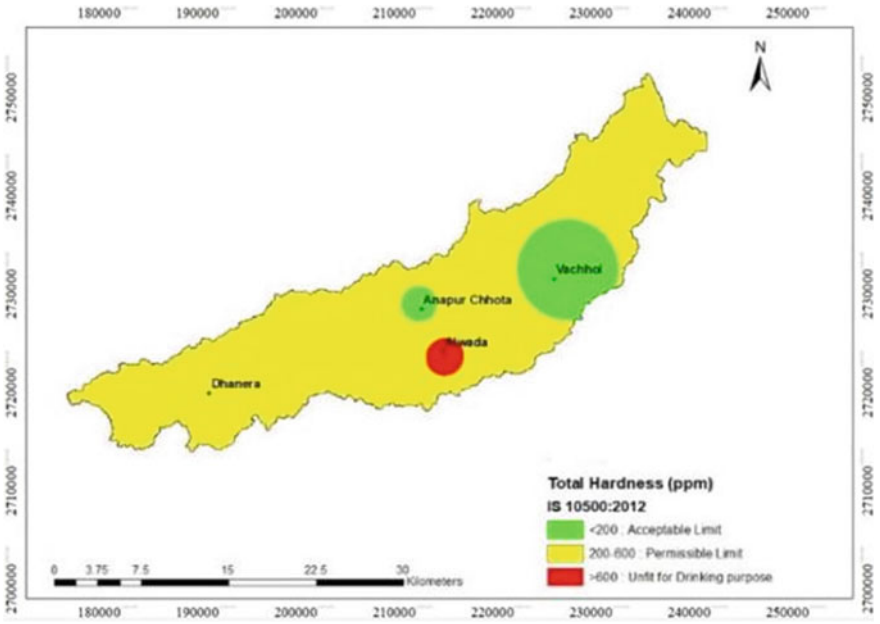


Fig. 3 Total hardness

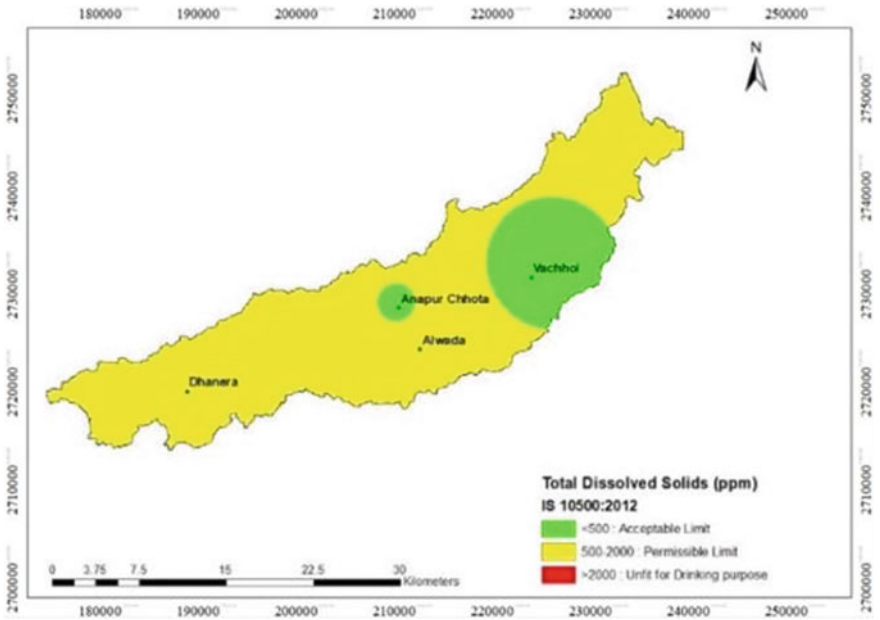


Fig. 4 Total dissolved solid

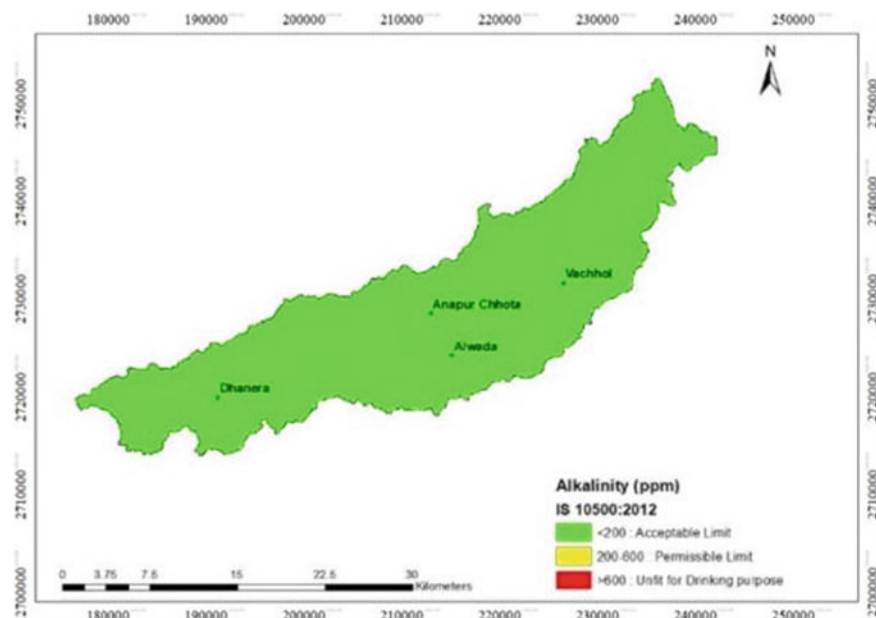


Fig. 5 Alkalinity

limit. And also, from the Pearson's Matrix the regression between TH and Chloride is 98.79%, TH and Sulphate is 95.41% which indicates a strong correlation.

## 5 Conclusion

The present study is conducted to determine the water quality of the study area; however, it would not be possible to show WQI and its spreading area through mathematical modelling. Hence to visualize the change in the spatial pattern of water quality GIS technique has been utilized. The water quality index map reveals that the overall quality of water is very poor as 39.67% area falls under very poor, 25.88% poor and 7.90% unsuitable range where remaining 26.55% area falls under good range. From the tested parameters maximum value of Total hardness, TDS and Chloride was seen in the region of Alwada (S2). From the Pearson R Matrix, the correlation is strong as the regression between TH and Chloride is 98.75% and TDS and Chloride is 99.56%. Hence the direct consumption of water is not suitable, it should be treated properly before utilization. Suitable treatment processes like water softening methods should be adopted to reduce the level of hardness, Reverse Osmosis to reduce the concentration of contaminants like TDS and Chloride in the study area. In this study, the developed water quality index map is straightforward for understanding and communicating water quality information to recipients and

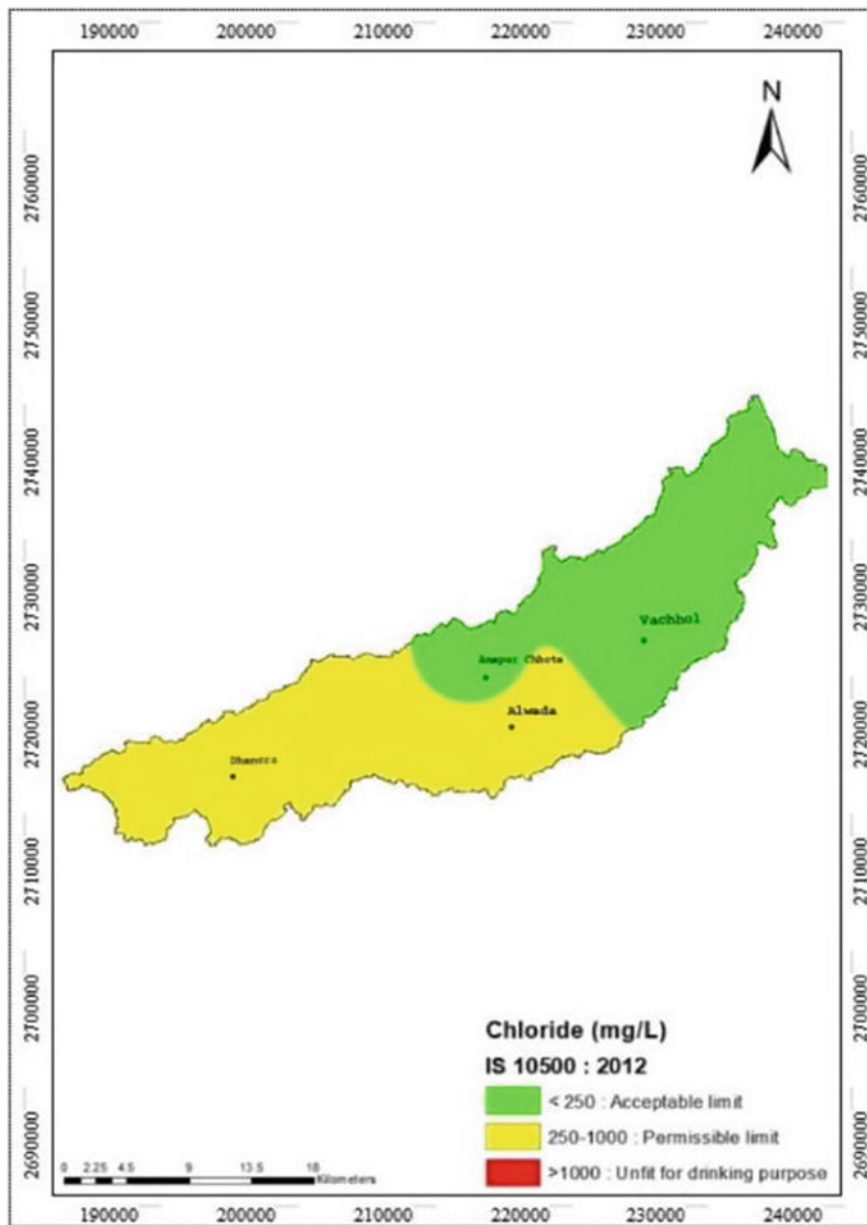


Fig. 6 Chloride

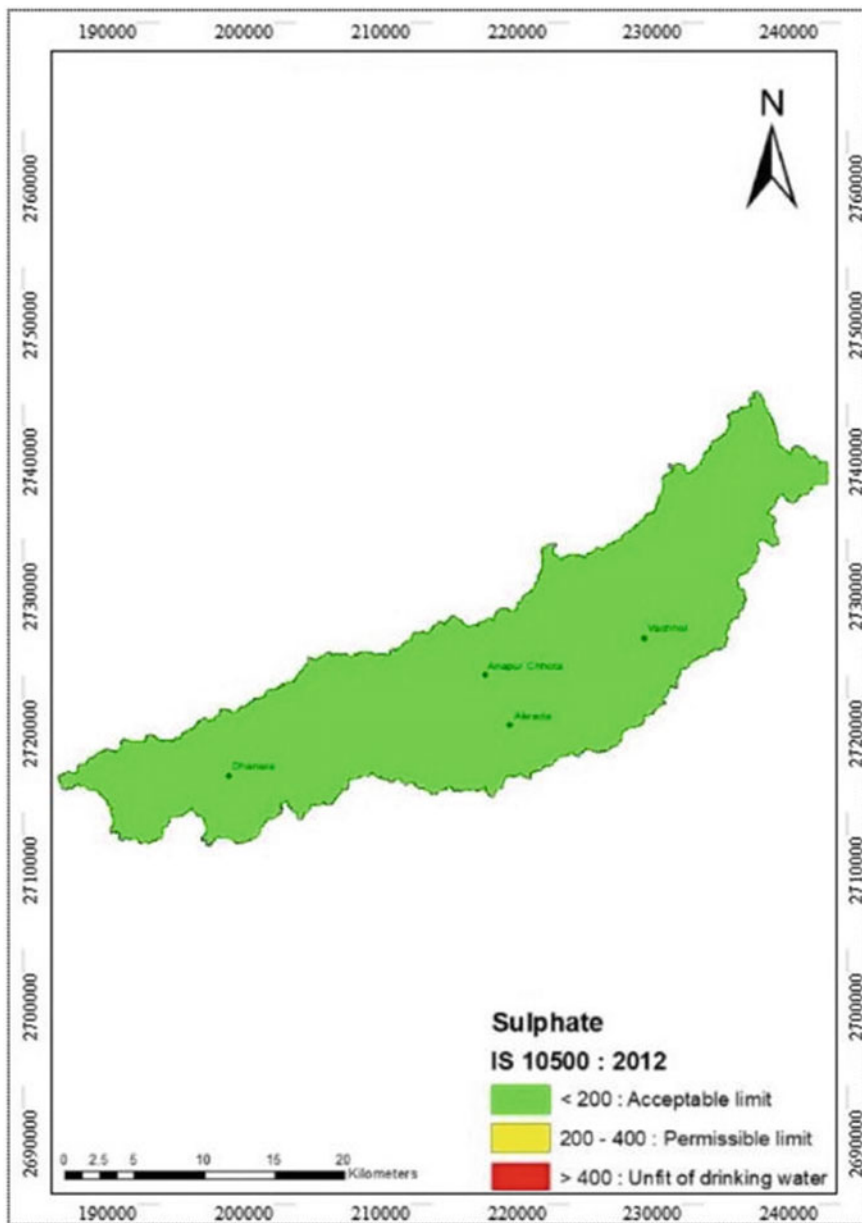


Fig. 7 Sulphate

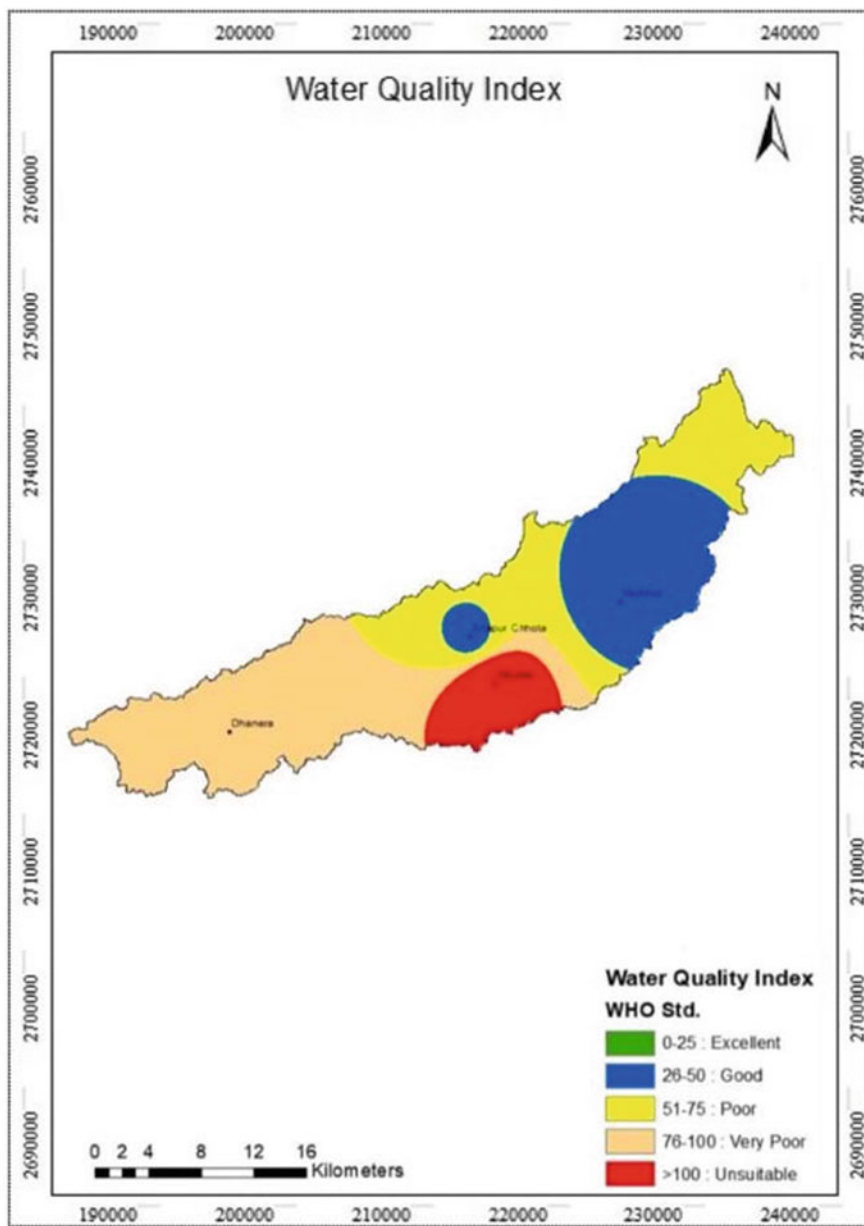


Fig. 8 Water Quality Index

local management so that they can properly regulate water consumption and its management. The approach adopted in this study can be easily applied to other areas to improve and refine the ability to use and maintain water quality in order to ensure proper use and avoid depletion of water quality. Therefore, it can be learned from this analysis that the GIS and water quality index are the possible methods for handling and mapping parameters of water quality, assessing water quality and recommending appropriate treatment.

## References

1. Brown RM, McClelland NI (1970) A water quality index; do we dare? *Water & Sewage Works* 117:339–343
2. Etim EE, Odoh R, Itodo AU, Umoh SD, Lawal U (2013) Water quality index for the assessment of water quality from different sources in the Niger Delta Region of Nigeria. *Front Sci* 3(3):89–95. <https://doi.org/10.5923/j.fs.20130303.02>
3. Narmada (2010) Water Resources, Water Supply and Kalpsar Department
4. Nimrabanu Memon DNS (2020) Integrated framework for flood relief package (FRP) allocation in semiarid region: a case of Rel River flood, Gandhinagar, Gujarat, India. *Nat Hazards* 100:279–311. <https://doi.org/10.1007/s11069-019-03812-z>
5. IS Code 3025 Part 11 pH value (1983) Reaffirmed (2002) Methods of sampling and test (physical and chemical) for water and waste water part II pH value (first revision), 1983
6. IS Code 3025 Part 21 Hardness (2009) Methods of sampling and test (Physical and Chemical) for water and wastewater: Part 21 hardness (Second Revision)
7. IS: 3025 (Part 32) (1988) (Reaffirmed 2003) Methods of sampling and test (physical and chemical) for water and wastewater part 32 chloride (first revision)
8. IS: 3025 (Part 16) (1984) (Reaffirmed 2006) Methods of sampling and test (physical and chemical) for water and waste water
9. IS: 3025 (Part 24) (1986) (Reaffirmed 1002) Methods of sampling and test (physical and chemical) for water
10. IS: 3025 (Part 23) (1986) (Reaffirmed 2003) Methods of sampling and test (physical and chemical) for water and wastewater part 11 alkalinity (first revision)
11. IS 10500 (2012) Drinking water—specification (second revision)
12. World Health Organization (WHO): Guidelines for Drinking—Water Quality. WHO/SDE/WSH/07.01/1, WHO/SDE/WSH/03.04/16, ISBN 92 4 154503 8 (v. 3), WHO/SDE/WSH/03.04/114, WHO/SDE/WSH/03.04/03
13. Yogendra K, Puttaiah ET (2007) Determination of water quality index and sustainability of an urban waterbody in Shimoga Town, Karnataka. In: *Taal: The 12th World Lake conference*, pp 342–346
14. Dave RN, Patel DP (2019) Identification of vegetation growth potential area and soil conservation area using morphometric analysis, p 134

# Flood Damages Assessment Using Remote Sensing and GIS: A Case Study of 2018 Kodagu Floods



**Jagadish Vengala, Manish S. Dharek, Prashant Sunagar, K. S. Sreekeasha, Kilabanur Pramod, Darshan Baliga, P. S. Haripriya, and Poornachandra Thejaswi**

**Abstract** Flood being the highest occurring natural phenomenon has large social consequences for communities and individuals and have a negative impact on the economy. Quantification of damage caused due to floods is the most important post flood procedure. In the present study, assessment of flood damages that had occurred in Kodagu district of Karnataka during August 2018, has been studied through application of concepts relating to Remote Sensing and GIS. Microwave Remote Sensing data was chosen to be the most accurate and has been utilized which was captured by Sentinel-1 satellite and the data accessed through Copernicus Access Hub. Pre-processing of microwave data has been done using SNAP tool and QGIS was used for the post processing. The results obtained after analyzing in QGIS include generation of flood map, Quantification of area of inundation due to flood was obtained for the Kodagu districts and its taluks namely Virajpet, Somwarpet and Madikeri. Comparison of area of inundation was done on the basis of corresponding land uses. The study concludes that amongst the three taluks Virajpet taluk was majorly affected due to the floods.

---

J. Vengala (✉)

Department of Civil Engineering, PVP Siddhartha Institute of Technology, Vijayawada, Andhra Pradesh, India

M. S. Dharek

Department of Civil Engineering, BMS College of Engineering, Bengaluru, India

P. Sunagar

Department of Civil Engineering, Ramaiah Institute of Technology, Bengaluru, India

K. S. Sreekeasha

Department of Civil Engineering, Jyothy Institute of Technology, Bengaluru, India

K. Pramod

Department of Civil Engineering, JSPM's RSCOE, Pune, India

P. Thejaswi

Department of Civil Engineering, Bengaluru Institute of Technology, Bengaluru, India

D. Baliga · P. S. Haripriya

Department of Civil Engineering, BMS Institute of Technology and Management, Bengaluru, India



**Keywords** Kodagu · SNAP · QGIS · Microwave data · Area of inundation

## 1 Introduction

Of all the natural disasters that have taken place, floods are the most hazardous and disturbing natural disasters which affect and disrupt the safety of society. Floods are large amounts of water overflowing over land either by submerging the land surface completely or causing damages. Floods are difficult to predict because they are caused due to local factors like heavy precipitation, slope of terrain, overflowing rivers, dam breaking [1]. In this paper, Kodagu district in Karnataka state of India was taken as the study area as it was prone to flash floods in August 2018 [10]. Flash floods generally occur within a very short time span and are generally due to heavy rains or snow melt [3]. Flash floods are the most destructive and can be fatal. There is a need to know the total damages that have occurred. Damages can be classified into agricultural damages and property damages [8]. The main purpose of the present study is to generate a flood map for the overall Kodagu district, to know the total area of submergence and quantifying it taluk wise. Since floods cannot be avoided but can be mitigated proper measures have to be taken to mitigate them [9]. In this fast moving technology, GIS and remote sensing can be the methodology adopted for monitoring and for the damage assessment due to its high accuracy [2, 4].

Geographic Information System (GIS) based spatial analysis and visual elements are generally used in recent times for flood to be prone and flood prone areas and also prepare a flood map [7, 5]. GIS can analyze and recognize the spatial relationships that exist within digitally stored spatial data [11–13].

In this study, the Kodagu district has been handled which is situated in the lower western part of Karnataka cradled in the Western Ghats between the 12.3375° N latitude and 75.8069° E longitude which covers an area of 4102 km<sup>2</sup>. This study area comprises the major river Cauvery originating at Talakaveri, located on the eastern side of the Western Ghats.

Extreme rainfall in the first half of August 2018 had caused widespread floods in the Kodagu district of Karnataka causing severe damage to mankind. Experts had predicted that this was due to heavy precipitation, the change in the rainfall pattern and climate changes. Therefore there is a need to know about the danger that could be expected and necessary mitigation steps have to be implemented. This can be done with the help of GIS and Remote Sensing.

## 2 Literature Review

Elkhrach [3] studied the mapping of flash floods using GIS tools and satellite imageries for Najran city, Saudi Arabia. SPOT and SRTM DEMs data for accurate assessment was used by making use of check points obtained from GPS observations. Analytical Hierarchical Process was used to determine the relative impact weight of flood causative factors in order to obtain a composite Flood hazard index. The flood risk zone was obtained by making use of these models. Haq et al. [6] studied about the application of supervised classification—maximum likelihood algorithm in ERDAS imagine to detect land cover/land use changes observed in Simly watershed using multispectral satellite data obtained from Landsat 5 and SPOT 5 for the years 1992 and 2012 respectively. The watershed was classified into five major land cover/land use classes, i.e. Agriculture, Bare soil/rocks, Settlements, Vegetation and water. Resultant land cover/land use and overlay maps were generated in ArcGIS 10 which showed the shrinking of Vegetation and water cover to agriculture, bare soil/rock and settlements cover by 38.2 and 74.3%. Data were processed in ERDAS imagine for geo referencing, mosaicking and sub setting of the image on the basis of Area of Interest (AOI). For each of the predetermined land cover/use type, training samples were selected by delimiting polygons around representative sites. Supervised classification is done and to improve classification accuracy and reduction of misclassifications, post-classification refinement was therefore used for simplicity and effectiveness of the method. These land cover/use transformations posed a serious threat to watershed resources. Hence, proper management of these water resources is required. Few recommendations can be done like an effective water management practice could be breaking down major river basins into sub-watersheds and prioritizing the sub-watershed for conservation and management based on degradation level so as to conserve and minimize the human induced impacts faced by it. Effective land use planning should be performed for the watershed before any construction activity is carried out in the region and a suitable environmental impact assessment (EIA) should precede it.

Following objects were part of the present study indicated below

- Generate flood map for overall Kodagu and its taluks based on August 2018 floods using Microwave Remote sensing.
- Quantifying Area of inundation for each land use.
- Comparing taluk wise flood trends and identifying the highly affected region due to flood.

### 3 Methodology Adopted

#### 3.1 Inputs Given in the Study

The following inputs were taken for the study. Figure 1 gives the methodology adopted for the study.



Fig. 1 Methodology adopted in the present study

**Data Acquisition:**

- Data Type: Microwave; Satellite: SENTINAL—1
- Satellite number: A; Ingestion Date: 2018-08-14
- Ingestion Time: 00:48:13; Polarization: VV VH
- Instrument: SAR-C; Instrument mode: IW
- Product level: L1; Product type: GRD
- Operator: European Space Agency; Source: scihub.copernicus.eu.

**Land Use Classification Data**

- Type: L-1; Source: Karnataka State Remote Sensing Application Center.

### ***3.2 Downloading the Data***

Initially for downloading SENTINEL-1, microwave imagery data was provided by Copernicus open access Hub. Once the required data was obtained, with the help of SNAP tool the raw sentinel data was processed. Data consisted of 2 polarizations, VV + VH and HH + HV with 2 bands namely Amplitude and Intensity. For the current case study, VV + VH polarization with Intensity band was chosen.

### ***3.3 Pre-processing Using Snap***

Subset of the Kodagu region was created to remove the unwanted areas (removal of ocean or other water bodies) by digitizing a new vector with the boundaries that are required. Orbit file was applied to improve the geocoding and other SAR processing results. As the information can have a high influence on the quality of several processing steps, hence orbit file was applied and the new layer was formed. Thermal noise correction was applied to products of Sentinel-1 Level-1 Single Look Complex (SLC), as well as to products of Level-1 Ground Range Detection (GRD). Based on the label annotations, one may also delete this correction. Product notations will be revised to allow the correction to be re-applied. Calibration is an important process as it encompasses the entire system, from sensor performance to the derivation of the data products. It plays a critical role in measurements that involve several sensors and orbit either simultaneously or sequentially. This was done to transform the pixel values from the digital values recorded by the sensor into backscatter coefficient values and create a new image with the backscatter coefficient. The Speckle function eliminates speckle and smooth out noise in radar datasets and preserves edges and sharp image features. Speckle is the high-frequency noise produced by laser, ultrasound and synthetic aperture radar (SAR) systems in radar images that is subject to noise due to interference from multiple surfaces scattered electromagnetic waves that return. The Sentinel-1 image that was downloaded had geographic

coordinates, so a coordinate system had to be applied to view it in a GIS with other data. While terrain correction removed the effects of side looking geometry of SAR images and Range Doppler terrain correction was done to the given study area to shift all pixels to their correct location according to an input digital elevation model as it increased the location accuracy. Since Kodagu terrain was elevated because of hills and valleys, Time of the signal to travel to the earth's surface and back to the sensor was distorted, leading to geometric shifts in the image: layover and shadow. Once the pre-processing was done, the final layer was converted to GEOTIFF format to carry out the post processing in QGIS.

### ***3.4 Post processing Using QGIS***

The final flood map and classification can be obtained using QGIS. The converted VV and VH bands as a TIFF file used in a new layer in QGIS. Then the newly formed layer has to be classified into water and non-water bodies and also classified as supervised and unsupervised classification. Supervised classification was chosen for the respective case study and plugins used for classification are semi-automatic Classification Plugin and DZETSAKA Classification Plugins. Render type was changed to multi-band pseudo colour by modifying minimum and maximum values for each band. Based on the maximum and minimum values, classification was done as water and non-water bodies. The raster layer was vectorised, by modifying the raster conversion properties to Polygonize The layer formed was saved as a shape file layer. Slope was obtained using SRTM DEM with elevation model of 30 m resolution. The DEM values were vectorized from the obtained raster slope values and slopes were classified into slope below  $12^\circ$  and slope above  $12^\circ$ . In the generated flood map, the slope vector was intersected and the water layer present above  $12^\circ$  was clipped out. The flood map consisted of unnecessary water bodies which are out of the Kodagu region. Hence to remove these unnecessary water bodies, clipping was done. After clipping the lulc layer, the slope below  $12^\circ$  layer had to be intersected to get a single layer. Data obtained was in two different parts namely (top & bottom) layer which had to be combined to get one final map. Different shape files were combined using union option and final flood map was generated in QGIS. The flood map was intersected with the generated lulc classified map by updating the attribute table of the intersected layers which is later exported as spread sheet (format as.xls). Finally, we proceed with Taluk wise mapping. Using query builder, shape files were extracted for Madikeri, Virajpet and Somwarpet Taluks. By using Clip tool on the flood map, extracted individual flood maps for the taluks were extracted and updated attribute table for individual taluks which were exported as spread sheet.

**Table 1** Final damage assessment of Kodagu (Inundated area) as on 14th August 2018

| Land use class                                 | Area of inundation (acres) |
|--|----------------------------|
| <b>Agriculture</b>                             |                            |
| Agricultural plantation                        | 1305.89                    |
| Crop land                                      | 13,811.82                  |
| Fallow land                                    | 45.92                      |
| <b>Forest</b>                                  |                            |
| Evergreen/semi evergreen forest                | 156.73                     |
| Forest plantations                             | 15.28                      |
| Degraded forest                                | 42.02                      |
| Moist and dry deciduous forest                 | 141.84                     |
| Tree groves                                    | 552.71                     |
| Grass land/grazing land                        | 63.74                      |
| <b>Settlements</b>                             |                            |
| Town/cities                                    | 7.58                       |
| Village  | 23.97                      |
| <b>Other vegetation</b>                        |                            |
| Sandy area                                     | 4.17                       |
| Habitation with vegetation                     | 5.09                       |
| Land with scrub                                | 20.29                      |
| Mixed vegetation                               | 27.19                      |
| <b>Total area loss due to flood (in acres)</b> | <b>16,224.24</b>           |

## 4 Results

Based on the studies conducted, results have been presented in Tables 1, 2, 3 and 4. Figure 2 shows the final flood map of Kodagu district as on 14th August 2018. Figure 3 gives the highest flood region of Virajpet Valley as on 14th August 2018.

## 5 Discussions

- The flood-inundated regions are shown in Fig. 2. The overall area of inundation is 16224.24 acres. Out of which total agricultural land inundated is 15163.63 acres, total forest lands inundated is 972.32 acres and total settlements inundated is 31.55 acres.
- Land use Percentage area inundated for agriculture is 93.46%, forest—5.99%, settlements—0.19% and other vegetation—0.35%. From this, it can be seen that highest loss was found in Agricultural lands, which comes up to 93.46% of the

**Table 2** Final damage assessment of Madikeri taluk (Inundated area) as on 14th August 2018

| Land use class                                 | Area of inundation (acres) |
|--|----------------------------|
| <b>Agriculture</b>                             |                            |
| Agricultural plantation                        | 230.68                     |
| Crop land                                      | 2766.73                    |
| Fallow land                                    | 3.04                       |
| <b>Forest</b>                                  |                            |
| Evergreen/semi evergreen forest                | 84.52                      |
| Forest plantations                             | 4.00                       |
| Tree groves                                    | 130.18                     |
| Grass land/grazing land                        | 32.85                      |
| <b>Settlements</b>                             |                            |
| Town/cities                                    | 5.68                       |
| Village  | 1.03                       |
| <b>Other vegetation</b>                        |                            |
| Habitation with vegetation                     | 2.14                       |
| Land with scrub                                | 4.28                       |
| Mixed vegetation                               | 0.99                       |
| <b>Total area loss due to flood (in acres)</b> | <b>3266.11</b>             |

total loss. The same is shown in Fig. 3 as below. Based on Taluk wise area of submergence, Fig. 4 shows the taluk wise submergence (Fig. 5).

## 6 Conclusion

GIS based mapping and analysis carried out in order to arrive at the quantified inundated area based on the flash floods that occurred in August 2018 in Kodagu district of Karnataka showed that the highest Agricultural land submerged was in Virajpet, i.e. 9196.81 acres and highest Settlement damaged is in Virajpet, i.e. 12.29 acres. Overall highly affected area in terms of flood and submergence was Virajpet.

**Table 3** Final damage assessment of Somwarpet taluk (Inundated area) as on 14th August 2018

| Land use class                                 | Area of inundation (acres) |
|--|----------------------------|
| <b>Agriculture</b>                             |                            |
| Agricultural plantation                        | 213.23                     |
| Crop land                                      | 2777.70                    |
| <b>Forest</b>                                  |                            |
| Evergreen/semi evergreen forest                | 9.28                       |
| Forest plantations                             | 2.90                       |
| Degraded forest                                | 5.58                       |
| Moist and dry deciduous forest                 | 95.41                      |
| Tree groves                                    | 311.11                     |
| Grass land/grazing land                        | 11.16                      |
| <b>Settlements</b>                             |                            |
| Town/cities                                    | 0.71                       |
| Village  | 10.10                      |
| <b>Other vegetation</b>                        |                            |
| Sandy area                                     | 0.02                       |
| Habitation with vegetation                     | 1.56                       |
| Land with scrub                                | 14.37                      |
| Mixed vegetation                               | 26.21                      |
| <b>Total area loss due to flood (in acres)</b> | <b>3479.36</b>             |



**Table 4** Final damage assessment of Virajpet taluk (Inundated area) as on 14th August 2018

| Land use class                                 | Area of inundation (acres) |
|--|----------------------------|
| <b>Agriculture</b>                             |                            |
| Agricultural plantation                        | 872.94                     |
| Crop land                                      | 8280.44                    |
| Fallow land                                    | 43.43                      |
| <b>Forest</b>                                  |                            |
| Evergreen/semi evergreen forest                | 53.12                      |
| Forest plantations                             | 8.50                       |
| Degraded forest                                | 36.91                      |
| Mixed and dry deciduous forest                 | 47.07                      |
| Tree groves                                    | 89.39                      |
| Grass land/grazing land                        | 16.89                      |
| <b>Settlements</b>                             |                            |
| Town/cities                                    | 1.21                       |
| Village  | 11.02                      |
| <b>Other vegetation</b>                        |                            |
| Land with scrub                                | 1.67                       |
| <b>Total area loss due to flood (in acres)</b> | <b>9462.59</b>             |

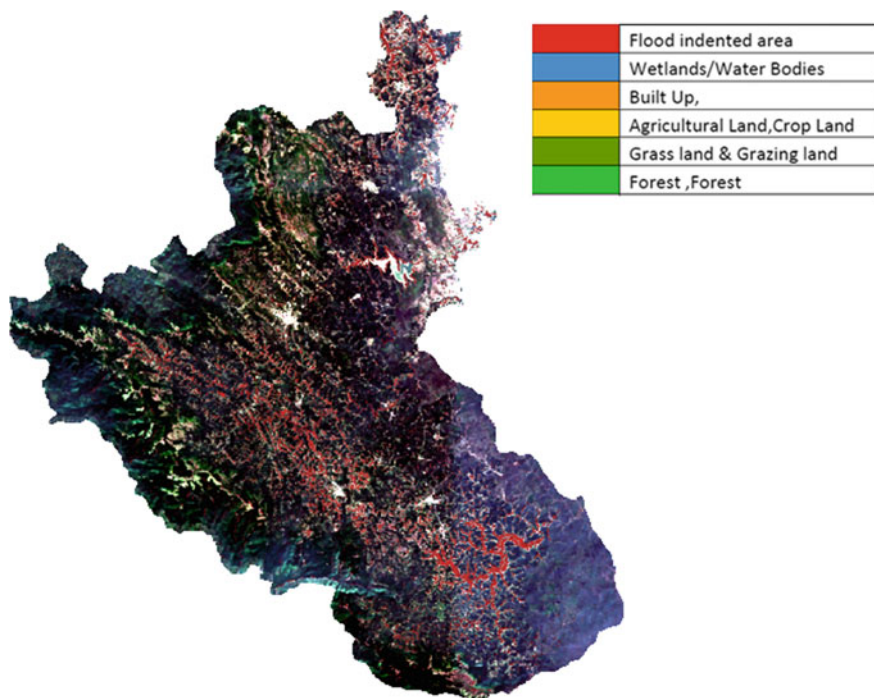


Fig. 2 Final flood map of Kodagu district as on 14th August 2018

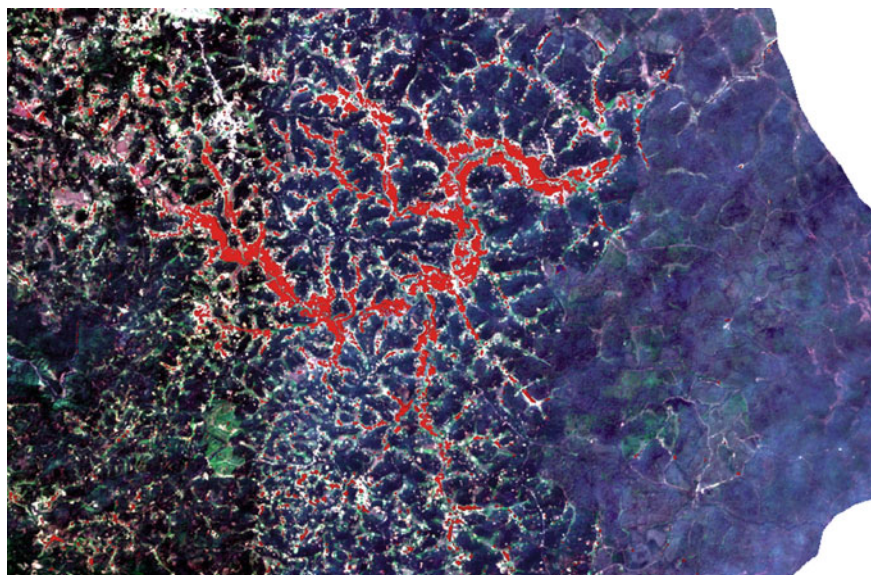


Fig. 3 Highest flood region of Virajpet Valley as on 14th August 2018

### Percentage area submerged

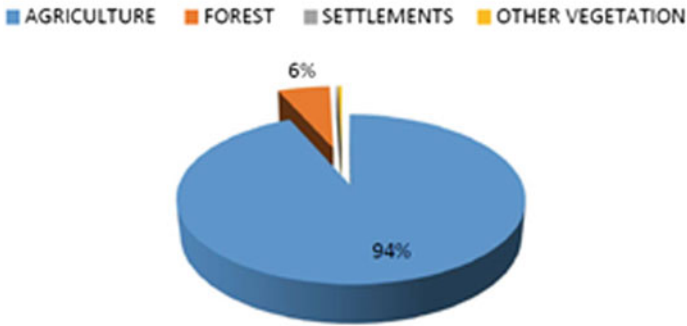


Fig. 4 Percentage area submerged

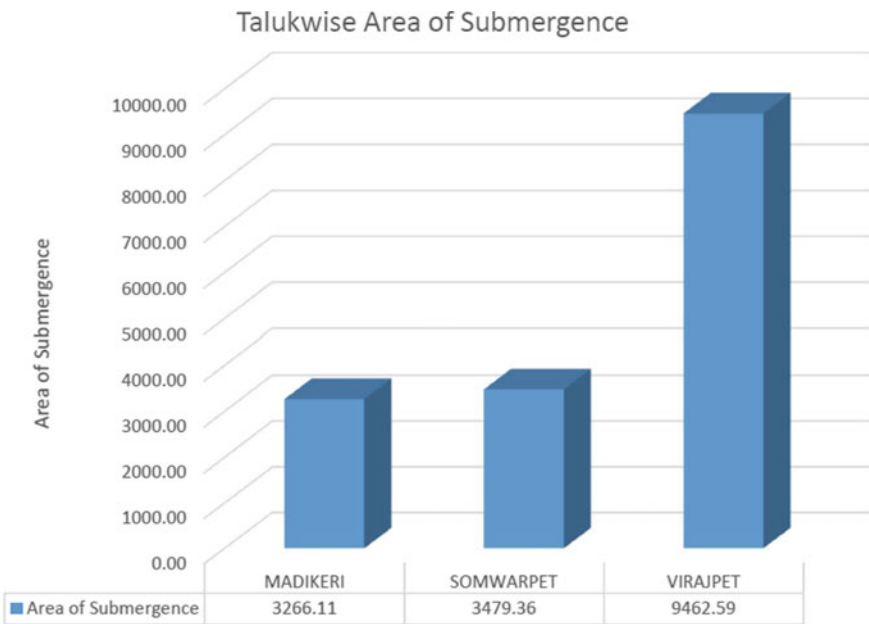


Fig. 5 Taluk wise submergence

### References

1. Ajin RS, Krishnamurthy RR, Jayaprakash M, Vinod PG (2013) Flood hazard assessment of Vamanapuram River Basin, Kerala, India: an approach using remote sensing & GIS techniques. Adv Appl Sci Res 4(3):263–274 (2013)

2. Mathur DK, Udan PM (2017) Application of remote sensing and GIS for flood vulnerability and mitigation: a case study of flood affected villages of Mahi River. *Scholars Research Library, Arch Phys Res* 8(2):07–11 (2017)
3. Elkhrachy I (2015) Flash flood hazard mapping using satellite images and GIS tools: a case study of Najran City, Kingdom of Saudi Arabia (KSA). *Egypt J Remote Sens Space Sci* 18:261–278
4. Bera K, Pal M, Bandyopadhyay, J (2012) Application of RS & GIS in flood management a case study of Mongalkote blocks, Burdwan, West Bengal, India. *Int J Sci Res Publ* 2(11) (2012). ISSN 2250-3153
5. Lingadevaru DC, Govindaraju, Jayakumar PD, Somesha GS, Vinaya M (2019) Flood inundation mapping using microwave remote sensing and GIS data integration: a case study of Tungabhadra and Hagari River sub-catchments in North-East Karnataka, India. *IOSR J Eng (IOSRJEN)* 09(2) (2019)
6. Haq M, Akhtar M, Muhammad S, Paras S, Rahmatullah J (2012) Techniques of remote sensing and GIS for flood monitoring and damage assessment: a case study of Sindh province, Pakistan. *Egypt J Remote Sens Space Sci* 15:135–141 (2012)
7. Pawar Amol D, Sarup J, Mittal SK (2016) Application of GIS for flood mapping: a case study of Pune city. *Int J Mod Trends Eng Res* (2016)
8. Suriya S, Mudgal BV, Nelliyat P (2012) Flood damage assessment of an urban area in Chennai, India, part I: methodology. Flood damage assessment of an urban area in Chennai, India, part II: results and discussions. *Springer Science + Business Media B.V. Nat Hazards* 62:149–167 (2012)
9. De Groeve T, Riva P (2009) Early flood detection and mapping for humanitarian response. In: *Proceedings of the 6th international ISCRAM conference—Gothenburg, Sweden* (2009)
10. <https://kgis.ksrsac.in/kgis/>
11. Dharek MS, Sunagar PC, Kadalli MV, Sreekeshava KS, Pujar AG (2021) Assessment of solar power potential mapping in Telangana state using GIS. In: *Narasimhan MC, George V, Udayakumar G, Kumar A (eds) Trends in civil engineering and challenges for sustainability. Lecture Notes in Civil Engineering, vol 99. Springer, Singapore.* [https://doi.org/10.1007/978-981-15-6828-2\\_63](https://doi.org/10.1007/978-981-15-6828-2_63)
12. Rao KR, Sreekeshava KS, Dharek MS, Sunagar P (2020) Issues on planning of solid waste management scheme through evaluation in integrated data information system. In: *Proceedings of the 35th international conference of the polymer processing society (pps-35).* <https://doi.org/10.1063/1.5141548>
13. Rao KR, Sreekeshava KS, Dharek MS, Sunagar PC, Ganesh CR (2020) Spatial variation of climate change issues using remote sensing technique. *IOP Conf Ser Mater Sci Eng* 814:012042. <https://doi.org/10.1088/1757-899x/814/1/012042>

# Groundwater Heavy Metal Contamination Mapping Using Geographic Information System (GIS): A Case of Nashik Thermal Power Station, Eklahare, Nashik (M.S.), India



Vrushali V. Sasane and Alka S. Kote

**Abstract** Coal-based thermal power plants generate a significant amount of fly ash and are facing fly ash management problems, which is emerging as a major environmental concern. Commonly, fly ash is disposed of in an unlined earthen pond, which may lead to contamination of groundwater in surrounding areas due to the leaching of heavy metals through fly ash. In the present study, hydro-geochemical analysis is carried out on groundwater samples from the proximity of Nashik Thermal Power Station, Eklahare village, to assess the impact. The heavy metals, i.e. Cd, Hg, and Pb, are selected and analysed in groundwater samples during pre-monsoon and post-monsoon seasons due to its high concentration in coal and fly ash samples. The analysis results showed that the maximum concentration of Cd is 0.0068 mg/l and 0.017 mg/l; Hg is 0.36 mg/l and 0.032 mg/l; and Pb is 0.23 mg/l and 0.075 mg/l during the pre-monsoon and post-monsoon seasons, respectively. Around 33.33%, 58.33%, and 41.67% of samples in pre-monsoon have concentration beyond desirable limit of the Bureau of Indian Standard, 2012 for Cd, Hg, and Pb, respectively. While 58.66%, 66.67%, and 50% of samples in the post-monsoon season have exceeded desirable limits. Spatial distribution maps for selected heavy metals are prepared using the IDW data interpolation technique in GIS. The maps showed that the ash pond is adversely affecting the groundwater quality in the village, thereby creating a threat to the health of residents and indicate the need for corrective measures to check the infiltration of leachate from the ash pond. Based on contamination zones, the location of a new groundwater source can be planned.

**Keywords** Thermal power station · Groundwater · Heavy metal contamination · Integrated distance weighing · Geographic information system

---

V. V. Sasane (✉) · A. S. Kote  
Dr. D Y Patil Institute of Technology, SPPU, Pimpri, Pune, Maharashtra 411018, India

© The Author(s), under exclusive license to Springer Nature Singapore Pte Ltd. 2022  
C. M. Rao et al. (eds.), *Advanced Modelling and Innovations in Water Resources Engineering*, Lecture Notes in Civil Engineering 176,  
[https://doi.org/10.1007/978-981-16-4629-4\\_33](https://doi.org/10.1007/978-981-16-4629-4_33)

477

## 1 Introduction

India is the largest user of groundwater in the world. It uses an estimated 230 cubic kilometres of groundwater per year—over a quarter of the global total. More than 60% of irrigated agriculture and 85% of drinking water supplies are dependent on groundwater [1]. This overexploitation of groundwater resources is also combined with deteriorated groundwater quality due to the increasing level of a variety of toxic substances resulting from natural and man-made activities. Groundwater quality is a growing social and environmental concern. Thus, groundwater conservation concerning availability and quality has attained prime concern. In addition to this, industrialization and urbanization have increased energy demand leading to a global energy crisis. In the context of India, this demand is mainly met by coal-based thermal power plants with its share of 53.7% of total electricity generation [2]. This conventional fossil fuel-based energy generation results in serious implications on surrounding water resources and the ecosystem.

Effluents from thermal power plants mainly include ash disposal, thermal discharges, wastewater effluents, and coal storage run-off. The coal fly ash has varying composition and volume of major constituents, *namely* CaO, MgO, Na<sub>2</sub>O, K<sub>2</sub>O, SiO<sub>2</sub>, Fe<sub>2</sub>O<sub>3</sub>, MnO, TiO<sub>2</sub>, and P<sub>2</sub>O<sub>5</sub>. Besides, ash is also rich in trace elements such as Cd, Pb, Ni, Cu, and Cr [3]. The disposal of ash is carried out by a wet method, where ash-loaded water slurry is carried to the ash pond. In most of the cases, leaching of heavy metals is due to the unlined construction of the ash ponds. Heavy metal-enriched leachate from ash pond penetrates the groundwater and increases the turbidity of water due to the release of ash in surrounding water bodies. Looking at the serious effects of heavy metals on human health, the efficient tool to manage the groundwater quality becomes necessary.

The spatial distribution of heavy metals in groundwater plays a vital role in delineating potential contamination zones. And it to assess the impacts of ash pond on surrounding groundwater resources. It will help in identifying the extent of contamination and plan future groundwater resources. The groundwater quality analysis and Geographic Information System (GIS)-based mapping are essential components in devising groundwater management strategy. A GIS has a variety of applications in different disciplines to solve spatial queries, analysis, and interpretation. It has gained special reference in the groundwater-related studies which include the determination of potential sites for groundwater evaluation and groundwater quality mapping. In India, GIS integrated with statistical tools has been extensively used in many groundwater modelling and assessment studies successfully [4–9]. However, limited studies are available presenting its applications for assessment and mapping the impact of thermal power plants on groundwater resources in India.

The present paper delineates the spatial variation of heavy metals, *viz.* Cd, Hg, and Pb in groundwater in Eklahare, Nashik, Maharashtra. Contamination mapping for selected heavy metals is carried out using GIS to develop maps for pre-monsoon and post-monsoon seasons that describe existing groundwater quality. It is carried

out using groundwater quality data obtained by analysing samples from the area under study.

## 2 Material and Methods

### 2.1 Study Area

Eklahare village is located in the Nashik district of Maharashtra (India), and it has a total geographical area of 9.15 km<sup>2</sup>. It houses the Nashik Thermal Power Station (NTPS). It commenced in the year 1970 and is situated on the left bank of the Godavari river. The thermal power station has a rated capacity of 630 MW and has 3 units of 210 MW each. It uses a coal-fired boiler to produce steam for power generation. The location of Eklahare village and thermal power plant is shown in Fig. 1.

Deccan trap basalt is the main water-bearing formation in the Nashik district. Basaltic rocks contain minerals rich in trace elements, *namely* Ag, As, Hg, Si, Mn, Pb, Cu, Zn, Cr, Fe, Ti, V, Ni, Zr, and Nb. Weathering of basaltic rock releases the trace elements in groundwater from low to high concentration and becomes a geogenic source of heavy metals in groundwater. Some baseline concentrations of these heavy metals can be observed in groundwater at greater depth in the district [10, 11].

The field survey and interview with the residents of Eklahare village suggest that the residents are facing many health issues and a decline in agricultural yield. Groundwater quality in Eklahare village is not addressed and monitored for heavy metal contamination due to fly ash disposal. Therefore, it is necessary to predict heavy metals for initiating preventive measures.

### 2.2 Groundwater Sampling and Analysis

The groundwater quality in Eklahare village is assessed by collecting four samples from dug well and bore well during the pre-monsoon season, i.e. March 2018 to May 2018 and post-monsoon season, i.e. October 2017 to December 2017. The samples are collected from bore well and hand pump in sterilized polyethylene bottles and analysed for heavy metals. These sources are designated as sampling stations S1, S2, S3, and S4. The stations S1 and S2 are bore wells, while S3 and S4 are hand pumps. The location of each sampling station is recorded using a handheld global positioning system (GPS) instrument GARMIN model eTrex-VISTA-H, USA receiver. Details of sampling stations are presented in Table 1. The procedure for analysis is adopted as prescribed by the APHA manual. Before water quality analysis, the coal and fly ash samples are analysed for heavy metals, *namely* Cd, As, Hg, Pb, Zn, Al, Mn, Cu, Fe, Mg, Cr, Ni, and Ba. It is carried out to determine their concentration and to select







**Table 1** Details of groundwater sampling stations

| Sampling station | Description                            | Source    | Depth (m) | Co-ordinates     |                  |
|------------------|--|-----------|-----------|------------------|------------------|
|                  |  |           |           | Latitude         | Longitude        |
| S1               | Ratna Shivram Dushing (Godavari hotel) | Bore well | 42.67     | N 19° 59' 32.4"  | E 73° 54' 28.02" |
| S2               | Gram panchayat                         | Bore well | 60.96     | N 19° 59' 35.88" | E 73° 54' 8.46"  |
| S3               | At Gaothan (Anganwadi)                 | Hand pump | –         | N 19° 59' 33.48" | E 73° 54' 8.28"  |
| S4               | Siddharthnagar (Slum area)             | Hand pump | 60.96     | N 19° 58' 30.54" | E 73° 52' 27.18" |

the heavy metal for groundwater analysis that has a high concentration in coal and fly ash samples.

### 2.3 Groundwater Quality Mapping for Heavy Metals

The hydro-chemical analysis of the groundwater quality variables can describe potentially contaminated resources. GIS can then utilize this analysis data to identify areas affected by groundwater contamination and other information regarding the existing groundwater quality scenarios that are necessary for the effective implementation of the groundwater management programme.

Generally, spatial distribution maps are prepared using inverse distance weighted (IDW) interpolation algorithm. The IDW algorithm is widely used in spatial interpolation of the groundwater quality due to its intuitive and efficient characteristics. Besides, it is simple, easy to understand, and accurate compared to other spatial interpolation algorithm like kriging and spline [12]. IDW algorithm assumes that every measured point has its local influence that diminishes with the distance. The amount of weights depends upon the distance between the measured point and the point to be measured (unknown point); and the weights are assigned to the unknown points. The higher weights are given to the neighbourhood points, while small weights are assigned two farthest points. The points of equal distances have the same weights. Thus, weights assigned are inversely proportional to the distance [13, 14]. The general formula of IDW interpolation for 2-D problems is as given in Eq. (1) [15].

$$w(x, y) = \sum_{i=1}^N w_i f_i \quad (1)$$

where

$$f_i = \frac{\left(\frac{1}{D_i}\right)^P}{\sum_{i=1}^N \left(\frac{1}{D_i}\right)^P}$$

$$D_i = \sqrt{(x - x_i)^2 + (y - y_i)^2}$$

where  $w(x, y)$  is the predicted value at the location  $(x, y)$ ,  $N$  is the number of nearest scatter known points surrounding  $(x, y)$ ,  $f_i$  is the weights assigned to each known point value  $W_i$  at the location  $(x_i, y_i)$ ,  $D_i$  is the 2-D Euclidean distances between each  $(x_i, y_i)$  and  $(x, y)$ , and  $P$  is power parameter, which controls the significance of known points on the interpolated values based on their distance from the unknown point. The power parameter is assigned as 2.

Digitized map of study area is obtained from the Maharashtra Remote Sensing Application Centre, Nagpur. Groundwater quality analysis data of sampling station are attached to the generated station location map in the form of an attribute table. Further, point interpolations using IDW in open-source QGIS software are performed, which interpolate data spatially and estimate the values between the measurements. Each such estimated value is a weighted average of the surrounding sample station to obtain spatial distribution maps for selected heavy metals. The spatial distribution maps of Cd, Hg, and Pb for Eklahare are prepared in open-source QGIS software.

### 3 Results and Discussion

#### 3.1 Analysis of Coal, Fly Ash, and Groundwater Samples

##### Analysis of coal and fly ash samples

The analysis of coal and fly ash samples shows that Cd, Hg, and Pb concentration in coal samples is 0.46 mg/l, 8.15 mg/l, and 23.56 mg/l, respectively, while it is 1.89 mg/l, 24.95 mg/l, and 62.86 mg/l in fly ash samples. Other heavy metals are observed to have lower concentrations compared to these heavy metals. Moreover, a significant increase in concentration is observed in fly ash than coal. Therefore, Cd, Hg, and Pb are analysed in the collected groundwater samples. The coal and fly ash analysis results are presented in Table 2.

##### Analysis of groundwater samples

Comprehensive groundwater analysis results for Hg and Pb concentration during the pre-monsoon and post-monsoon seasons are presented in Table 3. Its descriptive statistics facilitate in understanding the percentage of samples affected by these contaminations, and it is presented in Table 4.

**Table 2** Analysis of coal and fly ash samples

| Sr. No. | Description    | Concentration in mg/l |         |
|---------|----------------|-----------------------|---------|
|         |                | Coal                  | Fly ash |
| 1       | Aluminium (Al) | 0.22                  | 2.87    |
| 2       | Arsenic (As)   | 0.011                 | 0.11    |
| 3       | Barium (Ba)    | 0.008                 | 0.0092  |
| 4       | Cadmium (Cd)   | 0.46                  | 1.86    |
| 5       | Chromium (Cr)  | 27.14                 | 43.96   |
| 6       | Copper (Cu)    | 0.063                 | 0.011   |
| 7       | Iron (Fe)      | 0.32                  | 0.15    |
| 8       | Mercury (Hg)   | 8.15                  | 24.95   |
| 9       | Lead (Pb)      | 23.56                 | 62.86   |
| 10      | Magnesium (Mg) | 0.011                 | 0.69    |
| 11      | Manganese (Mn) | 0.0067                | 0.0087  |
| 12      | Nickel (Ni)    | 0.039                 | 0.011   |
| 13      | Zinc (Zn)      | < 0.01                | 0.011   |

**Table 3** Comprehensive analysis of groundwater quality

| Heavy metal                              |     | Cd          | Hg     | Pb     | Cd            | Hg     | Pb     |
|--|-----|-------------|--------|--------|---------------|--------|--------|
| Water quality standards BIS:10500 (2012) | DL  | 0.003       | 0.001  | 0.01   | 0.003         | 0.001  | 0.01   |
|  | MPL | NR          | NR     | NR     | NR            | NR     | NR     |
| Season                                   |     | Pre-monsoon |        |        | Post-monsoon  |        |        |
| Sr. No                                   |     | March 2018  |        |        | October 2017  |        |        |
| S1                                       |     | 0.0068      | 00     | 0.23   | 0.0049        | 0.019  | 0.0051 |
| S2                                       |     | 0.0001      | 00     | 0.018  | 00            | 0.012  | 0.0018 |
| S3                                       |     | 0.0008      | 00     | 0.09   | 00            | 0.022  | 0.012  |
| S4                                       |     | 0.0006      | 0.0038 | 0.045  | 0.0026        | 0.032  | 00     |
|  |     | April 2018  |        |        | November 2017 |        |        |
| S1                                       |     | 0.0041      | 0.017  | 0.017  | 0.0067        | 0.0083 | 0.0093 |
| S2                                       |     | 0.0008      | 0.0260 | 0.0019 | 0.0012        | 0.0074 | 0.027  |
| S3                                       |     | 0.0009      | 0.0097 | 0.0016 | 0.00095       | 0.0091 | 0.034  |
| S4                                       |     | 0.0036      | 0.3600 | 0.0041 | 0.0043        | 0.0098 | 00     |
|  |     | May 2018    |        |        | December 2017 |        |        |
| S1                                       |     | 0.0011      | 0.0017 | 0.0031 | 0.017         | 00     | 0.044  |
| S2                                       |     | 0.0009      | 0.0021 | 0.0038 | 0.0045        | 00     | 0.075  |
| S3                                       |     | 0.0034      | 0.0009 | 0.0026 | 0.011         | 00     | 0.04   |
| S4                                       |     | 0.0023      | 0.0002 | 0.0036 | 0.006         | 00     | 00     |

**Table 4** Descriptive statistics of comprehensive the groundwater quality analysis

| Water quality variables    | BIS:10500 (2012) |     | Min     | Max    | Mean  | SD     | % of samples with a concentration |                      |       |
|----------------------------|------------------|-----|---------|--------|-------|--------|-----------------------------------|----------------------|-------|
|                            | DL               | MPL |         |        |       |        | < DL                              | between DL-MPL > MPL |       |
| <i>Pre-monsoon season</i>  |                  |     |         |        |       |        |                                   |                      |       |
| Cd                         | 0.003            | NR  | 0.00015 | 0.0068 | 0.002 | 0.0019 | 66.67                             | 00                   | 33.33 |
| Hg                         | 0.001            | NR  | 0.000   | 0.36   | 0.035 | 0.102  | 41.67                             | 00                   | 58.33 |
| Pb                         | 0.01             | NR  | 0.0016  | 0.23   | 0.035 | 0.066  | 58.33                             | 00                   | 41.67 |
| <i>Post-monsoon season</i> |                  |     |         |        |       |        |                                   |                      |       |
| Cd                         | 0.003            | NR  | 0.0001  | 0.017  | 0.004 | 0.0049 | 41.67                             | 00                   | 58.33 |
| Hg                         | 0.001            | NR  | 0.0001  | 0.032  | 0.01  | 0.0107 | 33.33                             | 00                   | 66.67 |
| Pb                         | 0.01             | NR  | 0.0001  | 0.075  | 0.020 | 0.0236 | 50.00                             | 00                   | 50.00 |

All units are in mg/l; *DL* Desirable limit, *MPL* Maximum permissible limit, *NR* No relaxation

### Pre-monsoon season

**Cadmium:** During all three months of pre-monsoon, Cd content is observed to be low, as 66.67% of samples showed Fl value below and 33.33% samples exceed the permissible limit of 0.003 mg/l. The Cd value ranged from 0.00069 mg/l to 0.0068 mg/l with mean and SD of 0.002 and 0.00197, respectively. This less concentration is might be due to lack of water to take away the leachate from the ash pond to the groundwater during the pre-monsoon season. The groundwater is suitable for drinking purposes.

**Mercury:** Effect of occurrence of high concentration of Hg in the fly ash is observed in analysis as 58.33% of groundwater samples exceeded the permissible level of 0.001 mg/l by BIS (2012) with mean and SD of 0.035 and 0.102, respectively. As compared to March and May, the April month showed high values in all four samples varied from 0.009 to 0.36 mg/l which is above the permissible limit. The occurrence of Hg is not consistent throughout the pre-monsoon season, but wherever it occurs it is with high value.

**Lead:** The Pb is emerging as a potential contaminant as 41.67% of samples have a value more than the permissible level of 0.01 mg/l with mean and SD of 0.066 and 58.33, respectively. The Pb content in March is above the desirable limit, and in April and May, it is below the desirable limit of 0.01 mg/l. The Pb is observed in the range of 0.0016–0.23 mg/l. In March, Pb contamination is more significant as it varied from 0.018 to 0.23 mg/l. It indicated that contamination is initiated in Eklahare village.

### Post-monsoon season

**Cadmium:** The concentration level of Cd during post-monsoon rose gradually, having a lower concentration in October month and higher in December. The Cd values are between 0.00095–0.017 mg/l with mean and SD of 0.004 and 0.0049, respectively. About 41.67% of samples have values below 0.003 mg/l, and 58.33% of samples exceeded this permissible level. It indicates the alarming situation in the study area as these percentages are 66.67% and 33.33%, respectively, in the pre-monsoon season. An increased Cd may cause tubular dysfunction, kidney stones, and osteomalacia.

**Mercury:** The effect of a high concentration of Hg in the fly ash is reflected in the groundwater. The scenario continued during the post-monsoon season also. The concentration in four samples is above the acceptable limit of 0.001 mg/l (BIS) and varied from 0.0074 mg/l to 0.32 mg/l in October, and November with mean, and SD of 0.01, and 0.0107, respectively. About 66.67% of samples exceed the permissible limit, which is a matter of concern. Whereas in December, Hg is unexpectedly absent in all four samples.

**Lead:** The Pb values varied between 0.0001–0.075 mg/l during post-monsoon season, which is 0.0016–0.23 mg/l in pre-monsoon season. While 50% of samples have exceeded the maximum permissible limit. It indicates that the concentration range decreases during the post-monsoon season, but an increase in the percentage of samples affected with Pb is also observed. The rainwater infiltrated during the monsoon carried Pb to the groundwater reserves, which started accumulating, gives rise to a high concentration in the groundwater. Some baseline concentrations of Pb in the groundwater may exist due to the parent rock, and this increased concentration

**Table 5** Criteria for the classification of spatial maps of the groundwater quality for heavy metal contamination

| Criteria    |             |               | Class                  |
|-------------|-------------|---------------|------------------------|
| Cd          | Hg          | Pb            |                        |
| < 0.001     | < 0.001     | < 0.0025      | <i>Safe</i>            |
| 0.001–0.002 | 0.001–0.003 | 0.0025–0.0075 | <i>Moderately safe</i> |
| 0.002–0.003 | 0.003–0.006 | 0.0075–0.01   | <i>Unsafe</i>          |
| > 0.003     | > 0.006     | > 0.1         | <i>Very unsafe</i>     |

is an indication of the ingress of Pb through the leaching action of fly ash of the thermal power station.

### 3.2 Spatial Distribution Mapping of Heavy Metals in the Groundwater

The spatial distribution mapping of Cd, Hg, and Pb concentration in the groundwater of Eklahare villages is carried out to delineate the potential zones of contamination which will facilitate to see the extent of the impact by ash pond on the groundwater resources. Moreover, the mapping of heavy metals helps to understand the spatial pattern of contamination in the groundwater. The analysis of spatial pattern will also help to identify potentially contaminated the groundwater resources and to demarcate the vulnerable resources. It will assist in deciding the future strategy for the development of the groundwater resources (i.e. dug well and bore well) in the study area. The spatial distribution maps of selected heavy metals are prepared for pre-monsoon and post-monsoon seasons. The groundwater quality is classified in different categories based on the BIS (2012) guidelines and is presented in Table 5. Referring to the classification, the interpretation of generated pre-monsoon and post-monsoon season maps is discussed in the following section.

#### Pre-monsoon season

**Cadmium:** Referring to Fig. 2, it is observed that sample station S1 and S4 fall under a *very unsafe* category indicating Cd concentration above the desirable limit. Whereas station S2 and S3 fall under the *safe* category due to concentration below 0.001 mg/l. The groundwater is found to be affected mainly in the eastern and western parts of the village, while the effect is lowered in the northern part. But the groundwater of S2 and S3 stations should be analysed regularly to check the contamination and to plan future the groundwater source around these stations. Approximately, 40% of the area is covered with high Cd concentration.

**Mercury:** Almost the entire area of villages is observed to be adversely contaminated with Hg contamination with a concentration range of 0.003–0.006 mg/l, making it *unsafe* for drinking and irrigation as seen from Fig. 3. However, the lower contamination is found to be in the isolated pocket around the S3 station. Around 98% of the area falls in an *unsafe* zone.

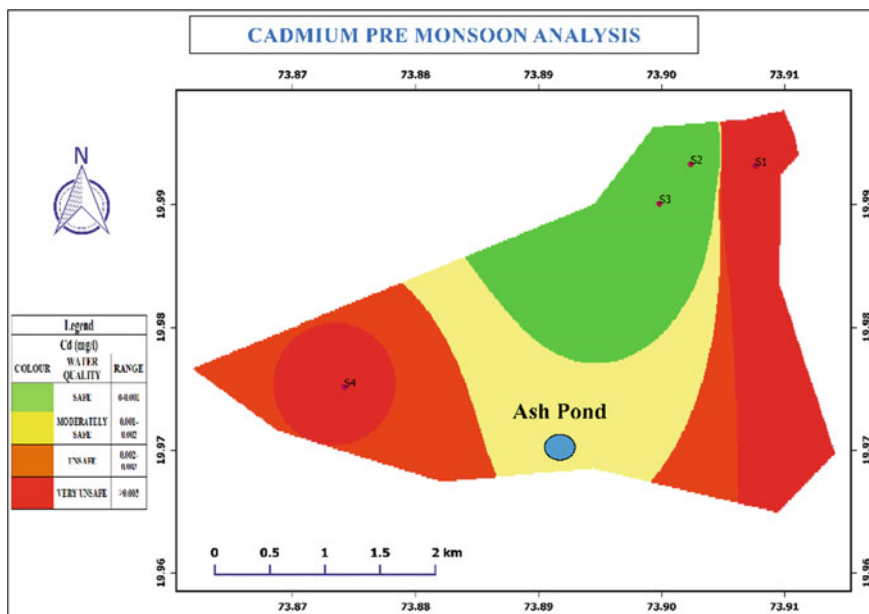


Fig. 2 Spatial distribution of Cd during pre-monsoon season

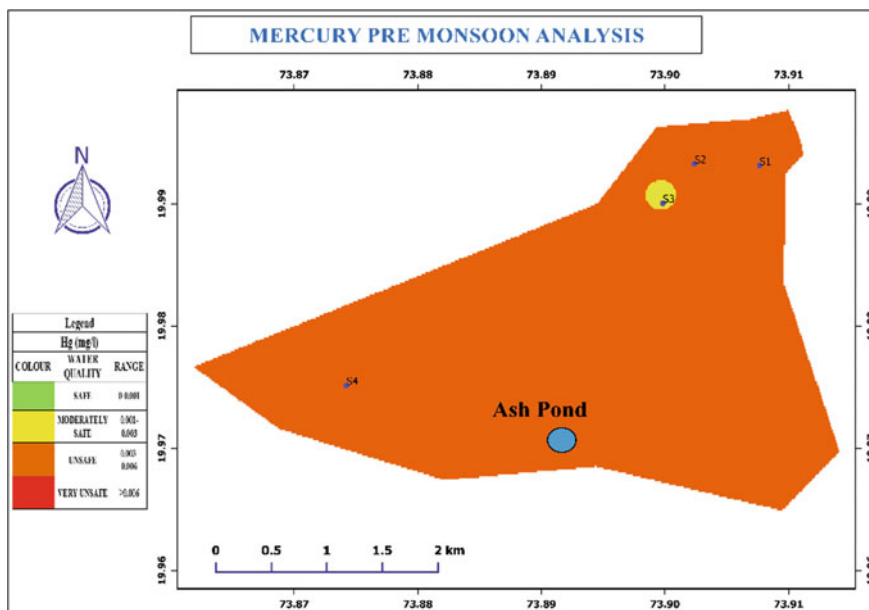


Fig. 3 Spatial distribution of Hg during pre-monsoon season

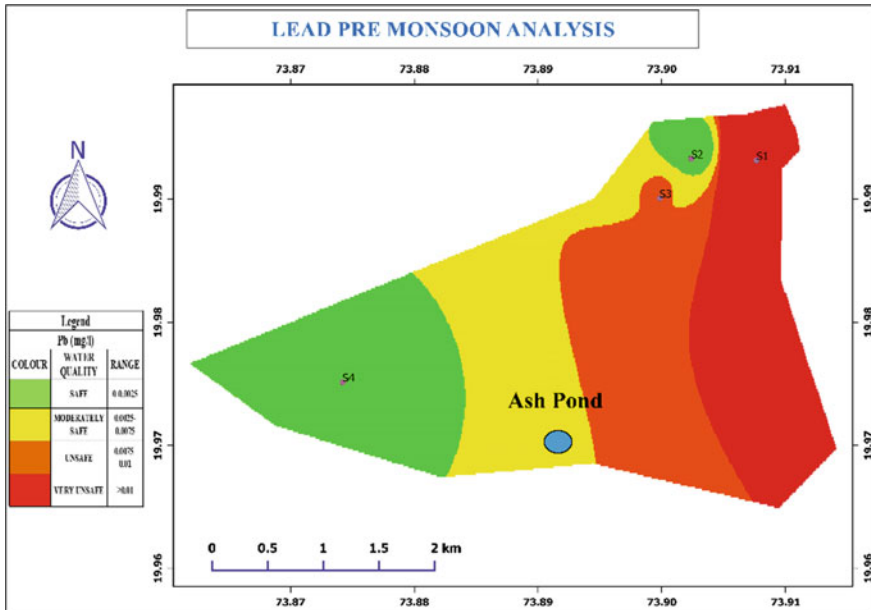


Fig. 4 Spatial distribution of Pb during pre-monsoon season

**Lead:** Figure 4 describes the distribution of Pb; according to it, eastern part of the village is severely affected by the Pb concentration. The two distinct zones of the *unsafe* and *very unsafe* category of the groundwater are observed in this part covering S1 and S3 stations. Whereas the scenario is improved in the middle and western parts of the village due to lowered Pb concentration covering the S2 and S4 stations. *Unsafe* and *very unsafe* zones constitute 48% of the entire area.

**Post-monsoon season**

**Cadmium:** During the post-monsoon season, the Cd distribution in the groundwater has been changed drastically as shown in Fig. 5. According to Figure station, S2 alone has a concentration in the range of 0.001–0.002 mg/l, making it *safe* for drinking. The stations S1, S3, and S4 fall under the *very unsafe* category. These stations have Cd concentration above BIS limit, i.e. > 0.003 mg/l. Thus, around 98% of the area is comprised of *very unsafe* groundwater quality. This changing trend in the post-monsoon season might be due to the infiltration of Cd-loaded leachate into the groundwater resources.

**Mercury:** From Fig. 6, it has been observed that the 100% area of the village is severely affected with very high Hg concentration, i.e. > 0.006 in the groundwater, resulting in the groundwater *very unsafe* for drinking. The change of distribution during the post-monsoon period indicates that rainwater takes up the Hg from the ash pond to groundwater resources.



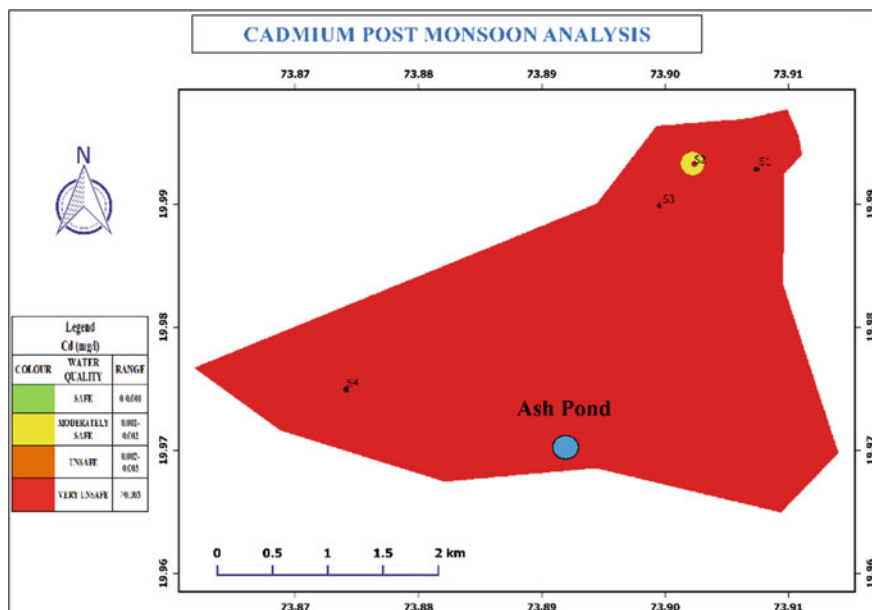


Fig. 5 Spatial distribution of Cd during post-monsoon season

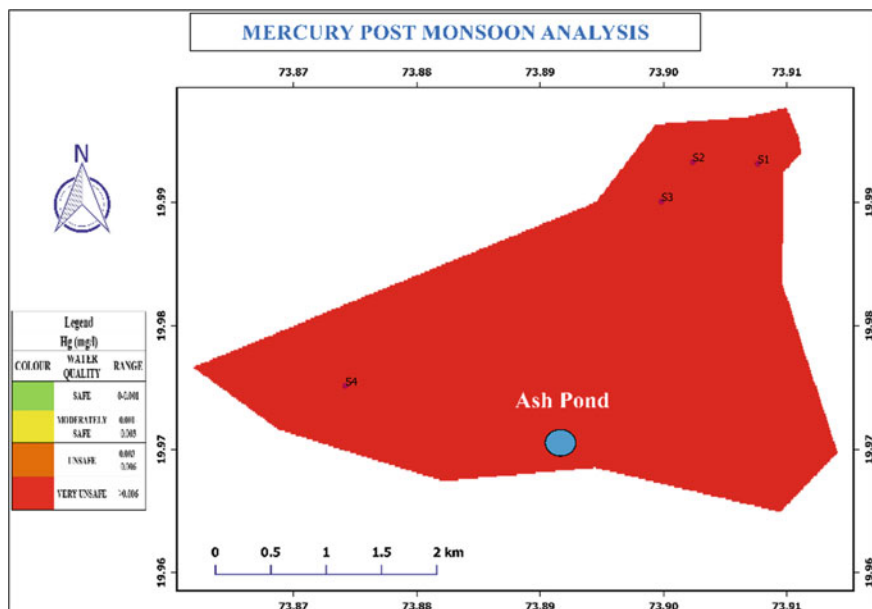


Fig. 6 Spatial distribution of Hg during post-monsoon season

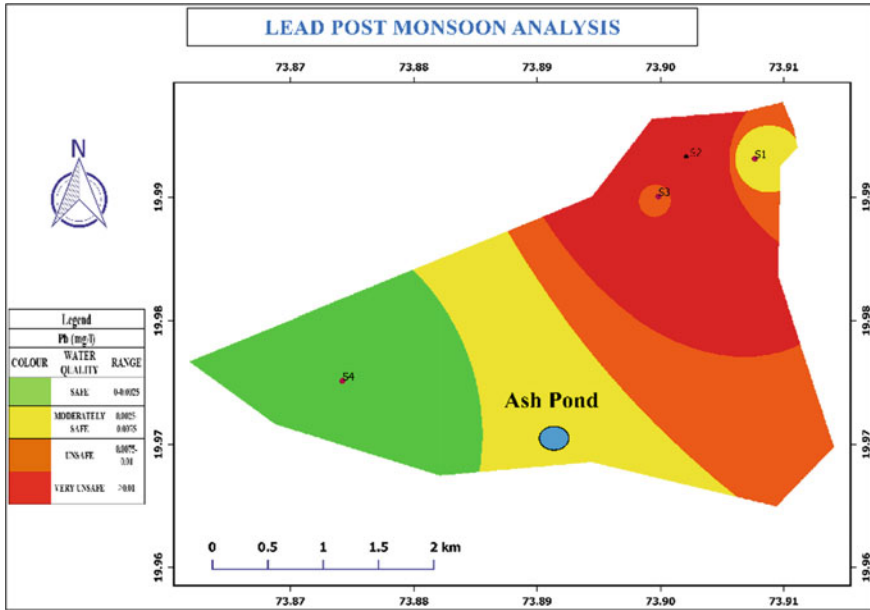


Fig. 7 Spatial distribution of Pb during post-monsoon season

*Lead:* During the post-monsoon, Pb distribution changed significantly and is presented in Fig. 7. Contamination has become severe in the north-east part of the village. The groundwater in this part is *very unsafe* and comprises about 50% of the area of the village. It is mainly due to the natural gradient of the ground caused by the Godavari River. However, in the western part comprised of S4 station, the groundwater quality is *safe* for drinking. While in isolated patches covering S1, S2, and S3 station, water quality is *moderately safe to unsafe category*, respectively.

### 4 Conclusions

In the present study, groundwater analysis at Eklahare showed the occurrence of heavy metals. Dug wells and bore wells around the ash pond found with high Cd, Hg, and Pb concentrations. The high concentration may have harmful effects on the health of residents. The GIS technique successfully mapped the impact of NTPS ash pond on groundwater resources. It shows that ash pond is the principal cause of contamination in the area. However, such a high concentration of Cd, Hg, and Pb in groundwater is generally observed at very great depth to relate it with the geologic source. The unlined ash pond of NTPS, Eklahare, has adversely affected the groundwater quality by the Cd, Hg, and localized contamination by Pb. Especially scenario gets worse during the post-monsoon season due to the infiltration of heavy metal-laden rainwater

to the groundwater resources. The contamination is predominant in the northern part of the area due to the natural gradient of the ground caused by the Godavari River. The groundwater is not suitable for drinking purpose and require regular monitoring of the dug well and bore well, and quality should be judiciously monitored before planning new groundwater resources in the area. There is an urgent need for decision-makers to plan corrective action to check the contamination resulting from the leaching of ash in the disposal pond.

**Acknowledgements** We would like to thank the Head of Civil Engineering Department and Director, SRES Sanjivani College of Engineering, Kopargaon, Ahmednagar (M.S.), for institutional facilities. We would also like to thank the authorities of Nashik Thermal Power Station, Eklahare and Eklahare Gram panchayat for permitting us for collection of samples and field surveys.

## References

1. The World Bank (2012) Feature story on India groundwater: a valuable but diminishing resources. <https://www.worldbank.org/en/news/feature/2012/03/06/india-groundwater-critical-diminishing#:~:text=the%20global%20total>
2. Ministry of Power, Government of India (2020) Power sector at a glance All India. National Informatics Centre (NIC). <https://powermin.nic.in/en/content/power-sector-glance-all-india>
3. Deshmukh N, Shah KC, Srivastava BN (1994) Impact of rainy season (monsoon) on fly ash dispersal—a case study of Koradi thermal power plant, Maharashtra. *Gondwana Geol Mag* 8:1–17
4. Ratnakanth MJ, Das IC, Jaisankar G, Dhananjaya EN, Rao P, Kumar A (2011) Assessment of the groundwater pollution in parts of Guntur district using remote sensing & GIS. *Int J Earth Sci Eng* 4(6):024–1030
5. Magesh NS, Chandrasekar N (2013) Evaluation of spatial variation in the groundwater quality by WQI and GIS technique: a case study of Virudunagar, District, Tamilnadu, India. *Arab J Geosci* 6:1883–1898. <https://doi.org/10.1007/s12517-011-0496-z>
6. Adhikary PP, Dash CJ, Chandrasekharan H, Rajput TBS, Dubey SK (2012) Evaluation of the groundwater quality for irrigation, and drinking using GIS and geostatistics in a peri-urban area of Delhi, India. *Arab J Geosci* 5:1423–1434. <https://doi.org/10.1007/s12517-011-0330-7>
7. Yammani S (2007) The groundwater quality suitable zones identification: application of GIS, Chittoor area, Andhra Pradesh, India. *Environ Geol* 53:201–210. <https://doi.org/10.1007/s00254-006-0634-1>
8. Rao YS, Jugran DS (2013) Delineation of the groundwater potential zones, and zones of the groundwater quality suitable for domestic purposes using remote sensing, and GIS. *Hydrolog. Sci. J.* 48(5):821–833. <https://doi.org/10.1007/s12517-011-0496-z>
9. Demirel Z (2007) Monitoring of heavy metal pollution of the groundwater in a phreatic aquifer in Mersin-Turkey. *Environ Monit Assess* 132:15–23. <https://doi.org/10.1007/s10661-006-9498-9>
10. Pawar NJ, Nikumbh JD (1999) Trace element geochemistry of the groundwater for Behedi basin, Nashik District, Maharashtra. *J Geol Soc India* 54:501–514
11. Pawar NJ, Pawar JB (2016) Intra-annual variability in the heavy metal geochemistry of the groundwaters from the Deccan basaltic aquifer of India. *Environ Earth Sci* 75:654. <https://doi.org/10.1007/s12665-016-5450-7>
12. Wu Y, Hung M (2016) Comparison of spatial interpolation techniques using visualization and quantitative assessment. Book chapter-2 in *Applications of spatial statistics*. <https://doi.org/10.5772/65996>

13. Sapna K, Thangavelu A, Mithran S, Shanthi K (2018) Spatial analysis of river water quality using inverse distance weighted interpolation in Noyyal watershed in Coimbatore, Tamilnadu, India. *Res J Life Sci Bioinf Pharm Chem Sci*. <https://doi.org/10.26479/2018.0401.13>
14. Balkrishna P, Saleem A, Mallikarjun ND (2011) The groundwater quality mapping using geographic information system (GIS): a case study of Gulbarga City, Karnataka, India. *Afr J Environ Sci Technol* 5(12):1069–1084. <https://doi.org/10.5897/AJEST11.134>
15. Shashi S, Xiong H (2008) *Encyclopedia of GIS: constraint databases and data interpolation*, 2nd edn. Springer, Berlin, p 150. ISBN 978-3-319-17885-1

# Using Earth Observations and GLDAS Model to Monitor Water Budgets for River Basin Management



Chiranjit Singha and Kishore C. Swain

**Abstract** Using the hydrologic decision support system water quality monitoring is also the most significant approach for sustainable hydrological cycle of any catchment region. Even with the uncertainties, earth observation remote sensing (RS) and Global Land Data Assimilation System (GLDAS) data employed to assess inter-annual and seasonal variability in individual water mechanisms and to get signs of decrease/increase in water availability for relatively large river basins. Evaluation of empirical methodology or local knowledge with the RS and GLDAS data may help in assessing the usefulness of best agricultural practice management system in the watershed. RS can contribute to understanding, predicting, and monitoring the water balance of large, poorly instrumented basins. There is power in merging data streams, through both multi-sensor algorithm and data assimilation system. Uncertainties are substantial and should not be understated. Collaborative analysis can, sometimes, overcome skepticism of remotely sensed products. Our research focuses on amounts of precipitation, evapotranspiration, storm surface runoff and change in terrestrial storage in the river basin for dry and wet seasons were calculated from remote sensing-based GPM IMERG, MODIS, and GRACE/GRACE-FO-derived GLDAS-CLSM model during the wet and dry seasons on 2004–2005, 2009–2010, 2014–2015, and 2018–2019 in Mahanadi river basin, India. More accurate, quantitative estimation of water budget continues to be a challenge for a variety of reasons such as climate change, land cover dynamics, anthropogenic water diversions, etc. The spread of estimates can be used for assessing the uncertainty.

**Keywords** River basin management · Remote Sensing · Precipitation · Water budget · GLDAS

---

C. Singha (✉) · K. C. Swain

Department of Agricultural Engineering, Institute of Agriculture, Visva-Bharati, Sriniketan, West Bengal 731236, India

## 1 Introduction

Due to climatic changes, there is a need of water supply constant monitoring because an increasing of the global hydrological cycle is extremely determined by a global warming, land use changes, and anthropogenic interference. The high population explosion, urbanization, and industrialization in South and Southeast Asia region have also negative impact on extreme hydrologic changeability more than 75% of the total precipitation rate occurring during the wet season June to September of the southwest monsoon, causing water stress, flood occurrence, and drought severity increasing to be a consistent yearly incident [1, 2]. Water allocation, distribution, and sharing have been carried out among states/regions within a country or even among various countries sharing the same river basin. River basin management is crucial aggregating effect of climatic change and anthropogenic water diversions from rivers and extensive ground water withdrawals from any geographical region through accelerated drought and flood severity [3, 4]. In India, greater than 80% of total annual groundwater draft is utilized for agricultural irrigation purpose [5]. Widely accepted land surface model (LSM) is most significant and valuable alternative decision support system for water management in regions which make the detailed analysis of the hydrological variability and quantification of the associated physical problem which identifying the better understanding earth's water cycle changing pattern in a spatial or temporal scale [6]. Different forcing data, remote sensing-based approaches and models, and output results may differ from different regions environmental factors such as solar radiation, evapotranspiration (ET), meteorological data, and vegetation indices [7]. LSMs are outperformed in hydrological variable estimation that can be excellent and effective tool for calculating the ET difference [8]. Global Land Data Assimilation System (GLDAS) model outputs quantified by the LSM measure for availability water in the world's major river basins [9]. Hanington et al. [10] reported that hydrological models are effective tool for water resource management in sustainable agricultural planning at Mekong delta region.

The Gravity Recovery and Climate Experiment (GRACE)-derived GLDAS simulations' terrestrial water storage changes (TWSCs) are good agreement for numerous key features of spatial and temporal land water storage differences in major river basin in the world [11]. GRACE output monitors the changeability of groundwater storage anomaly at regional to global scale [12].

Combined GRACE satellites and GLDAS identify the decreasing trend of ground water table levels to compensate for human withdrawals and excessive lost through evapotranspiration during 2003–2012 in UAE [13]. Water resource management discipline soil water storage disturbs the separating of energy fluxes and water at the terrestrial surface, with inferences for rainfall recovering, hydrologic excesses including occurrence of flood and drought which negatively impacted on land memory progressions [14]. River basin management involves policies and decisions at the river basin scale, which guides actions at sub-basin levels including (I) sustainable water supplies for all stakeholders (domestic, industrial, and agricultural), (II) flood and drought management, (III) improved land and ecosystem management,

and (IV) improved sanitation. Terrestrial surface water storage influences rates of freshwater, nutrient, and sediment transportation which plays a significant role in greenhouse gas (GHG) emissions to the environment [15]. Satellite-based GRACE and MODIS observations could examine the influences of land use cover change on water budget components such as soil ET, discharge rate, and soil moisture without expelling anthropogenic water budget issue [16]. The anthropogenic interferences like inter-basin water diversion and irrigation withdrawals could negatively impact on global hydrological cycle expressively over river basins that could be special attention for water budget estimation [17–19]. Widespread use of GRACE-derived GLDAS LSM system in South and Southeast Asian regions identifies ground water storage changing pattern and groundwater table fluctuations levels [3, 20, 21]. Singh et al. [22] reveal that the combined remote sensing-based GRACE signal can be better explored on reservoir volume water storage change dynamics by the hybrid method at Aral Sea and Lake Mead region.

Globally, mean terrestrial water storage changing pattern depends upon the evapotranspiration rate. Wan et al. [23] use GRACE-derived TWSC total water balance-based ET for quantifying the residual ET in the water balance component. However, the uncertainty of GRACE-derived TWSC evaluates the reconstructed ET by the root-mean-square difference (RMSD), and they did not take irrigation into account for high and comparable measure [24]. Long et al. (2014) establish that the lowest uncertainty LSMs and ET products are North American Land Data Assimilation System (NLDAS), GRACE, MODIS, and AVHRR. Mostly, LSMs do not consist of anthropogenic actions [26]. Thus, ET products are supplementary essential component for river basin water resource management in agricultural purpose of withdrawal of more water results in declined stream flow and increased ET [27–29].

## 1.1 GRACE-FO

GRACE has monitoring at least five years' time-variable element of earth's gravity field at monthly temporal resolution and also first evaluations of land water storage differences in the earth. GRACE mission is a joint undertaking between the DLR and NASA launched in March 2002. The monthly New GRACE-FO started coverage from 2018 June [30]. GRACE has estimated first time TWS (Terrestrial water storage) variations of their changing pattern extended river basin region [31], Winsemius et al. [32] used global LSMs for the improvement and validation of the terrestrial water storage balance in land surface hydrology estimation [33, 34]. The basin-scale terrestrial water budget assumes no lateral base flow of groundwater across a river basin border [23, 35]. Total runoff is estimated as follows, Eq. 1:

$$R_{\text{total}} = P - ET - \Delta S / \Delta t \quad (1)$$

$$\frac{\Delta S}{\Delta t} = \frac{TWSA(t) - TWSA(t - 1)}{\Delta t} \quad (2)$$

Where,  $\Delta S/\Delta t$  (cm/t) is estimated by the GRACE-derived terrestrial water storage anomaly (TWSA) (e.g.), [25],  $P$  (cm/t)—precipitation, and  $ET$  (cm/t) = actual evapotranspiration,  $t$ - time span. The  $R_{\text{total}}$  (cm/t) conditional from Eq. (1) is occupied to signify the total basin discharge, which comprises not only the surface water but also the groundwater storage anomaly [36]. These components are available from remote sensing-based earth observations and Global Land Data Assimilation System (GLDAS) model. Water budgets' estimation for ten larger river basins across the world is using earth observation RS or in situ measurement of  $P$ ,  $R$ ,  $ET$ , and GRACE-derived TWSA; however, large water budget non-closure errors fluctuate from 5 to 25% of  $P$  [37, 38].

## 1.2 GLDAS

GLDAS is to present land surface states and fluxes. There are two versions: GLDAS 2.1 and GLDAS 2.2. Both the models use a Vegetation mask, Land/Water mask, and Leaf Area Index (LAI) from MODIS. Both use forcing precipitation, meteorological data, and surface radiation from different sources. GLDAS 2.2 assimilates GRACE terrestrial water storage anomaly data in Catchment-F2.5 Land Surface Model (CLSM) for simulation of land surface fields, while GLDAS 2.1 does not. GLDAS 2.1 is accessible from January 2000, where GLDAS 2.2 from January 2003 to present [39]. The GLDAS model has numerous versions with many LSMs parameterizations such as Noah, CLSM, VIC with their strengths, restrictions, and varying spatial resolutions.

GLDAS observation allocates mainly water budget component and energy mechanisms [40, 41]. GLDAS is designated in a procedure of four LSMs sub-models—Mosaic Land Surface Model and CLM (Common Land Surface model), NOAH (National Centers for Environmental Prediction/Oregon State University/Air Force/Hydrologic Research Lab Model), and VIC (Variable Infiltration Capacity Model) [42]. Newer versions of GLDAS (i.e., GLDAS2) and ECMWF model are in better performance of accuracy in water balance estimation compared to The Routing Application for Parallel computation of Discharge (RAPID) in transboundary river basins at South and Southeast Asia [43]. Chen et al. [44] and Bi et al. [45] compared in situ station mean soil moisture and GLDAS LSM-derived soil moisture with the Advanced Microwave Scanning Radiometer Earth Observing System (AMSR-E) in the Tibetan Plateau. Output result showed that the GLDAS LSMs outperformed over the RS satellite-derived product because LSMs generally underestimated soil moisture. NLDAS and GLDAS-derived hydro-meteorological forcing data use global soil moisture estimation and simulations with in situ soil moisture data that found good agreement between the anomalies of observed and modeled soil moisture [46].

Our research work investigated the temporal and spatial variations of terrestrial water storage changes (TWSA) from GRACE satellite and compared with the simulated Global Land Data Assimilation System (GLDAS) product in Mahanadi river



basin region. Also examine and compare dry and wet seasons' water budget components of RS based on IMERG precipitation, MODIS Evapotranspiration (ET), and GRACE terrestrial water storage (TWS) for estimate seasonal, basin-averaged, and sub-basin level water budget components to understand the source of uncertainties involved in estimating water budgets for a river basins.

## 2 Materials and Method

### 2.1 Study Area

The Mahanadi river basin lies between of 80°30' to 86°50' East longitudes and 19°20' to 23°35' North latitudes geographical co-ordinates with a study area border of nearly 14,258.6 km<sup>2</sup> (Fig. 1). Mahanadi is the major river in Orissa; the lower part of the delta region have more potential of flood occurrence. The average elevation is 426 m mean sea level. The mean temperature in the region is 20–35 °C in summer which goes down to 4 °C in winter. Mahanadi basin has tropical monsoon-type climate with average annual rainfall of 1360 mm. Most of the rainfall up to 86% is received in four months from mid-June to end September mostly due to southwest monsoon [47]. The highest relative humidity of the region varies between 68 and 87% during July–August. The study area has yellow mixed red, black soils and laterite soils. The area comprises of rich clay percentage in the middle and lower part of the region.

Rice is the principle crop of the basin, where the interior dryer parts growing millets. Sugarcane, mung, gram, black gram, pea, jute, mustard, groundnut, and linseed are other miscellaneous crops of the study area.

Mahanadi watershed boundaries' layer is obtained from the Hydrological Data and Maps Based on Shuttle Elevation Derivatives at Multiple Scales (HydroSHEDS) [48].

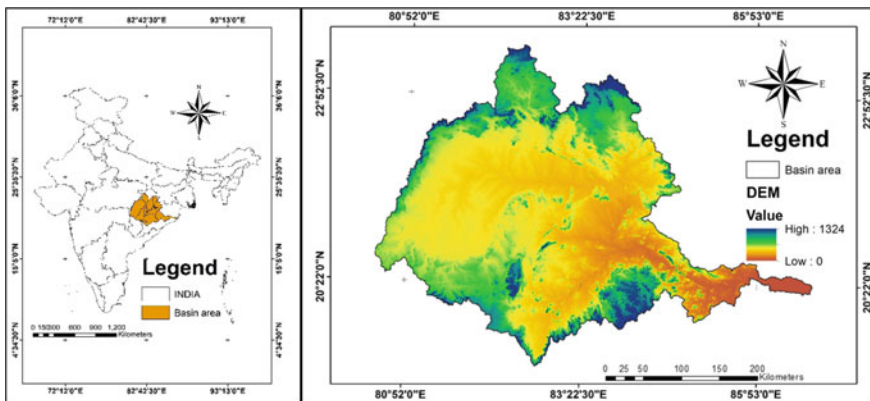


Fig. 1 Study area location map

**Table 1** Sub-basin areas of the Mahanadi river basin

| Sub-basin | District  | Area in km <sup>2</sup> |
|-----------|---|-------------------------|
| 1         | Angul, Bauda, Cuttak, Ganjam, Kandhamal, Kendrapara, Khordha                        | 1794.477                |
| 2         | Balangir, Kalahandi, Nabarangapur, Nuapada, Rayagada                                | 2368.467                |
| 3         | Bargarh, Sambalpur  | 1072.477                |
| 4         | Debagarh  | 118.7151                |
| 5         | Jangir-champa, Raigarh  | 1403.875                |
| 6         | Jashpur, Simdega, Jharsuguda, Sudargarh, Debagarh                                   | 1322.65                 |
| 7         | Mahasamund  | 515.8151                |
| 8         | Anuppur, Surjapur, Surguja, Korba, Koriya   | 1068.506                |
| 9         | Balod, Bemetara, Bilaspur, Durg, Raipur, Rajnandgaon, Shahdol, Gondiya, Garhchiroli | 3196.962                |
| 10        | Dhamtari, Garaband, Kondagaon, Uttar Baster Kanker                                  | 1396.655                |
|           | Total   | 14,258.6                |

The coarse river network was derived from the upscaled 0.1° HydroSHEDS grid [49]. Monitoring water availability in river basins depends on the precipitation, evaporation and transpiration, infiltration, surface water and groundwater storage, and runoff. The fine-resolution geo-referenced datasets were derived from the HydroSHEDS 15 arc second product level5 ESRI vector format in WGS84 (<https://www.hydrosheds.org/>). The Mahanadi river basin is divided into ten sub-basins (Table 1).

Performance of LSMs depends on the computed basin-averaged mean annual precipitation, evapotranspiration, storm surface runoff, and base runoff. GLDASv1 was first used with same forcing in different LSMs. In the LSMs, precipitation basic input variable and other input meteorological sources are uncertainty in simulated stream flow. The Noah LSM outputs forced by four meteorological version; GLDAS, GLDASv2.0, GLDASv2.1, and GLDASv2.2. GLDAS-2 products are existing 0.25° and 1° spatial resolutions where 1° resolution for LSMs used for reliability with GLDAS product. The GLDASv2.1 (Noah LSM) model have 0.25° and 1° spatial resolution and temporal resolution is 3 h.

## 2.2 Earth Observation Remote Sensing

Download the monthly final IMERG precipitation data mm/month for the selected months December to February (DJF) for dry season and June to August (JJA) for wet season in the years of 2004–2005, 2009–2010, 2014–2015, and 2018–2019, respectively, from <https://giovanni.gsfc.nasa.gov/giovanni/> for water budget estimation in the study area. Eight-day composite MODIS ET data products (MOD16) for the selected months with considering Julian days of respective year are acquired from <https://lpdaacsvc.cr.usgs.gov/appears/>.

**Table 2** Satellite data products used for estimation of water budget

| Product  | Description  | Spatial and temporal resolutions   | Source   |
|--|--|--|--|
| HydroSHEDS vector watershed boundaries   | Hydrological data and maps based on Shuttle Elevation Derivatives at multiple Scales level5        | Digital elevation model the Shuttle Radar Topography Mission (SRTM) 15 arc-sec | HydroSHEDS   |
| Integrated Multi-satellite Retrievals for GPM (IMERG) Precipitation mm/month                                     | GPM Microwave Imager (GPM IMERG Final Precipitation L3 1 month 0.1 degree $\times$ 0.1 degree V06) | 0.1° $\times$ 0.1° Monthly   | Giovanni   |
| MODIS ET (MOD16A2)   | MODIS  | 500 m 8-Daily  | Application for Extracting and Exploring Analysis Ready Samples (AppEEARS) |
| GRACE-FO   | Microwave Radar (K-Band)   | 1.0° $\times$ 1.0° Monthly   | JPL GRACE Tellus   |
| GRACE-DA1 V2.2 Water Budget Components (evapotranspiration surface/sub-surface runoff terrestrial water storage) | Catchment-F2.5 in Land Information System (LIS) Version 7  | 0.25° $\times$ 0.25° Daily   | GES DISC   |
| GLDAS Noah Land Surface Model L4   | GLDAS_NOAH025_3H   | 0.25° $\times$ 0.25° hourly V2.1   | Giovanni   |
| Annual Land cover Product  | MCD12Q1) Version 6   | Spatial resolution 500mt   | AppEEARS   |

The GRACE-derived TWSA product is obtained from three sources such as Jet Propulsion Laboratory (JPL), the Center for Space Research (CSR), and GeoForschungs Zentrum (GFZ). Download monthly GRACE-FO TWS anomaly data for December to March (dry season) and June to September (wet season) of the study area. All GRACE-FO TWS anomaly product is acquired from [https://podaactools.jpl.nasa.gov/drive/files/allData/tellus/L3/gracefo/land\\_mass/RL06/v03/JPL](https://podaactools.jpl.nasa.gov/drive/files/allData/tellus/L3/gracefo/land_mass/RL06/v03/JPL) (Table 2).

### 2.3 Land Surface Models of GLDAS-2.2

Use GLDAS 2.2 data for water budget estimation in the Mahanadi river basin for the wet and dry seasons during 2004–2005, 2009–2010, 2014–2015, and 2018–2019 (Table 2). ET ( $\text{kg m}^{-2} \text{s}^{-1}$ ), TWS (mm), and Storm surface runoff ( $\text{kg m}^{-2}$  per 3-h) data are obtained from GLDAS 2.2 for the selected months by NASA GES DISC

(<https://daac.gsfc.nasa.gov/>). All data acquired by the subset get data link in GES DISC subsetter tool for refine the parameters. Spatial resolution of the GRACE-derived TWSA and GLDAS-2.0 LSMs is  $1.0^\circ \times 1.0^\circ$  (Table 2) [40]. Total precipitation hourly data derived from GLDAS Noah LSM L4 3 0.25° × 0.25° V2.1 product [50].

## 2.4 Land use Map

The Terra and Aqua combined Moderate Resolution Imaging Spectroradiometer (MODIS) Land Cover Type (MCD12Q1V6) yearly data product provides at interval year of 2005, 2010, 2015, and 2019. NASA AppEEARS tool extracted the all LULC Type 1-International Geosphere-Biosphere Program (IGBP) classification data for the respective year.

## 3 Results and Discussion

### 3.1 MODIS Land cover

Land cover map was carried out using International Geosphere-Biosphere Program (IGBP) classification for four alternate years, 2005, 2010, 2015, and 2019 for the Mahanadi river basin (Fig. 2). Majority of the area is distributed under cropland category with 64% for all the years except 2005 (Table 3). However, there is decreasing trend in cropland area in 2005–2019. Similarly, the area is distributed under forest category with (15%) for the years of 2010–2015 except 2005 and 2019. Interestingly, the area under built-up area has been increased from 57.74 to 64.48 km<sup>2</sup> during the study period (Table 3). Similarly, the area under wetland area has been increased from 10.90 to 17.92 km<sup>2</sup>.

The water budget component changing pattern was closely observed and compared with the corresponding climate inputs such as precipitation distribution in the study area. The satellite-gauge precipitation for monthly estimated average was used to plot the quarterly precipitation (Fig. 3). The highest rainfall occurs in the month of June to August quarter and lesser values in December–February quarters. The major precipitation occurs in the years 2012 and 2018 where the least values in the years 2010 and 2015. However, the precipitation level also attained decreasing trend for the wet season June–August quarter years 2005–2019 in the study region.

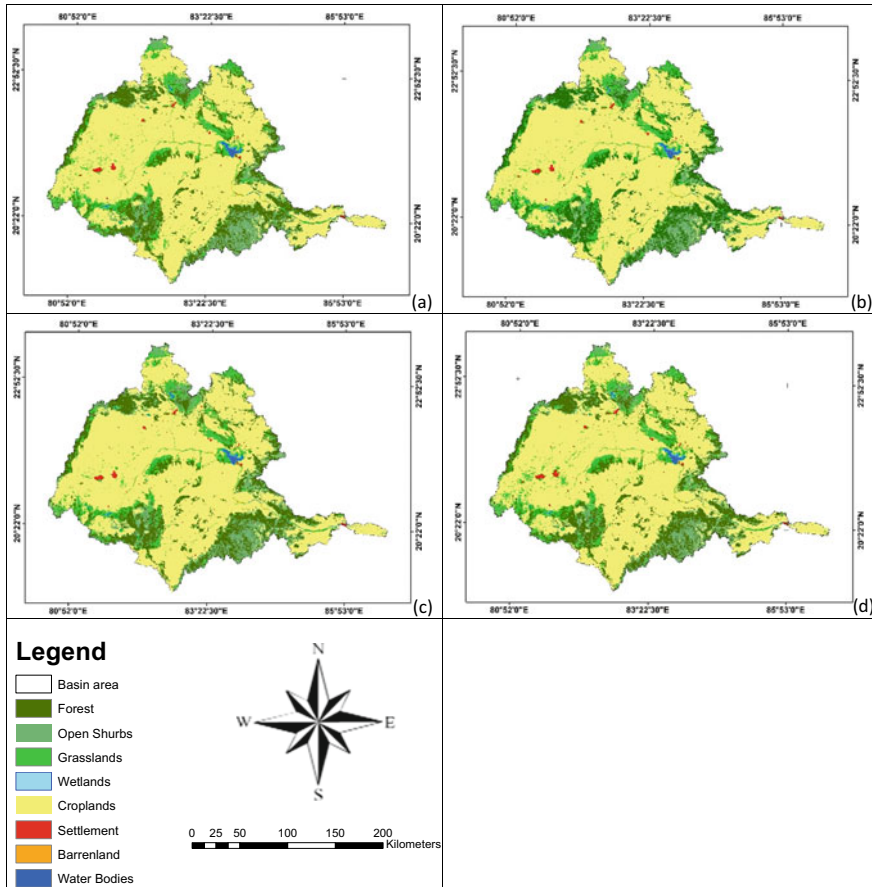


Fig. 2 Land cover map of Mahanadi river basin of the year a 2005, b 2010, c 2015, and d 2019

### 4 Earth Observation Remote Sensing

Remote sensing-based model IMERG precipitation mm/month and MODIS ET for dry and wet season difference are shown in Figs. 4 and 5 for selected years. To sum all the ET over the wet and dry seasons, we first reclassify all fill values in each dataset and assign a new value of 0. Fill values in each dataset corresponding to unclassified, water body, urban, wetland, barren or sparsely vegetated. All the ET images reclassify values (range) by run as batch process then using raster calculator to sum of the all images both the dry and wet season using ArcGIS 10.5 software. The GRACE-FO data represent DTWS anomalies are in meters. To find seasonal TWS change, take the difference between TWS anomalies for March and December for the wet season and multiply by 1000 mm/meter to convert in mm (Figs. 6 and 7). Here we compare dry and wet season precipitation, ET, and TWS change. Estimate

**Table 3** Land cover map of the study area during 2005–2019

|               | 2005                    |        | 2010                    |        | 2015                    |        | 2019                    |        |
|---------------|-------------------------|--------|-------------------------|--------|-------------------------|--------|-------------------------|--------|
|               | Area in km <sup>2</sup> | Area % | Area in km <sup>2</sup> | Area % | Area in km <sup>2</sup> | Area % | Area in km <sup>2</sup> | Area % |
| Forest        | 2113.72                 | 14.82  | 2265.85                 | 15.89  | 2226.65                 | 15.62  | 2313.55                 | 16.23  |
| Shrub land    | 1621.78                 | 11.37  | 1536.85                 | 10.78  | 1744.36                 | 12.23  | 1559.37                 | 10.94  |
| Grass land    | 1046.94                 | 7.34   | 1032.44                 | 7.24   | 908.65                  | 6.37   | 1073.77                 | 7.53   |
| Wetland       | 10.90                   | 0.08   | 12.53                   | 0.09   | 16.00                   | 0.11   | 17.92                   | 0.13   |
| Cropland      | 9310.76                 | 65.30  | 9257.41                 | 64.92  | 9210.37                 | 64.60  | 9143.86                 | 64.13  |
| Built-up area | 57.74                   | 0.40   | 59.81                   | 0.42   | 60.88                   | 0.43   | 64.48                   | 0.45   |
| Barren land   | 26.10                   | 0.18   | 24.70                   | 0.17   | 20.45                   | 0.14   | 15.64                   | 0.11   |
| Water bodies  | 70.71                   | 0.50   | 69.06                   | 0.48   | 71.28                   | 0.50   | 70.04                   | 0.49   |
| Total         | 14,258.6                | 100.00 | 14,258.64               | 100.00 | 14,258.64               | 100.00 | 14,258.64               | 100.00 |

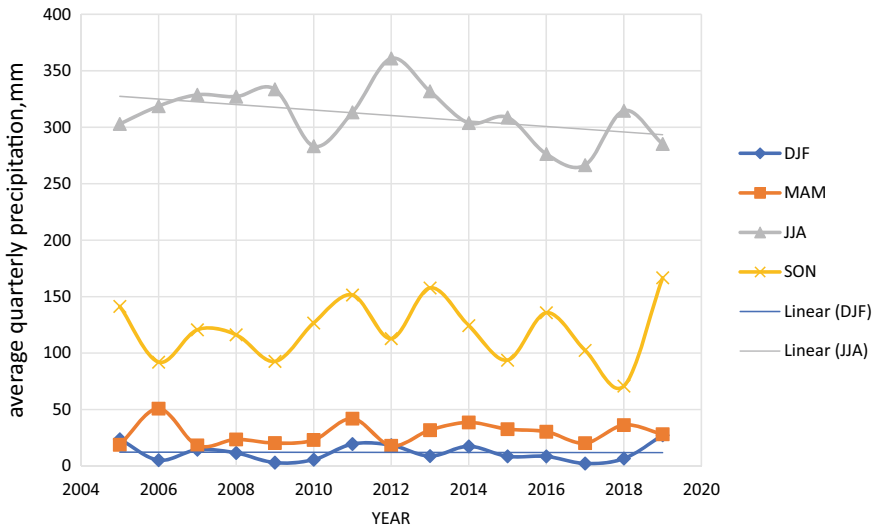


**Fig. 3** Average merged satellite-gauge precipitation estimate (0.1° resolution, mm/month); *Note* DJF: December, January, and February; MAM: March, April, and May; JJA: June, July, and August; SON: September, October, and November

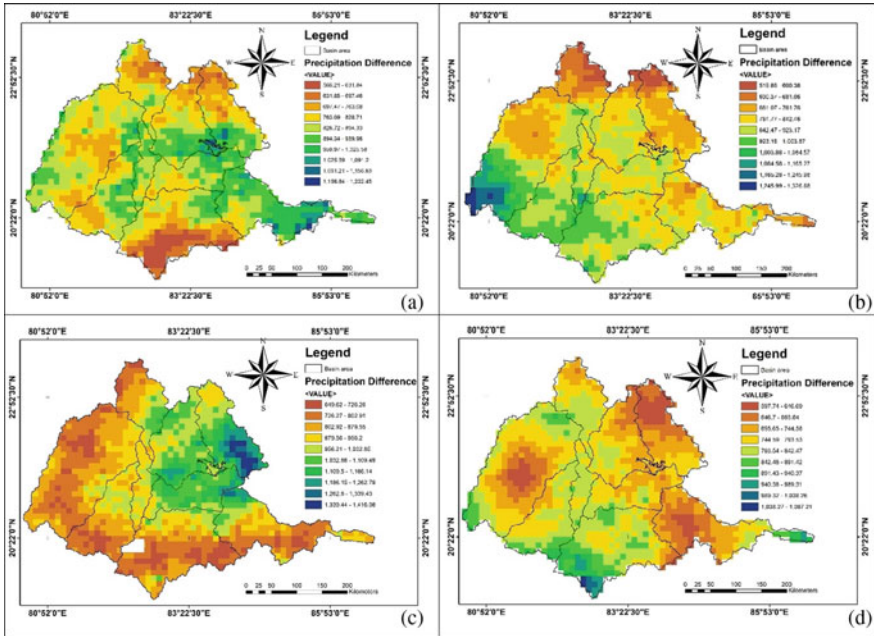


Fig. 4 Precipitation (Pr) difference map of dry and wet seasons a 2005, b 2010, c 2015, d 2019

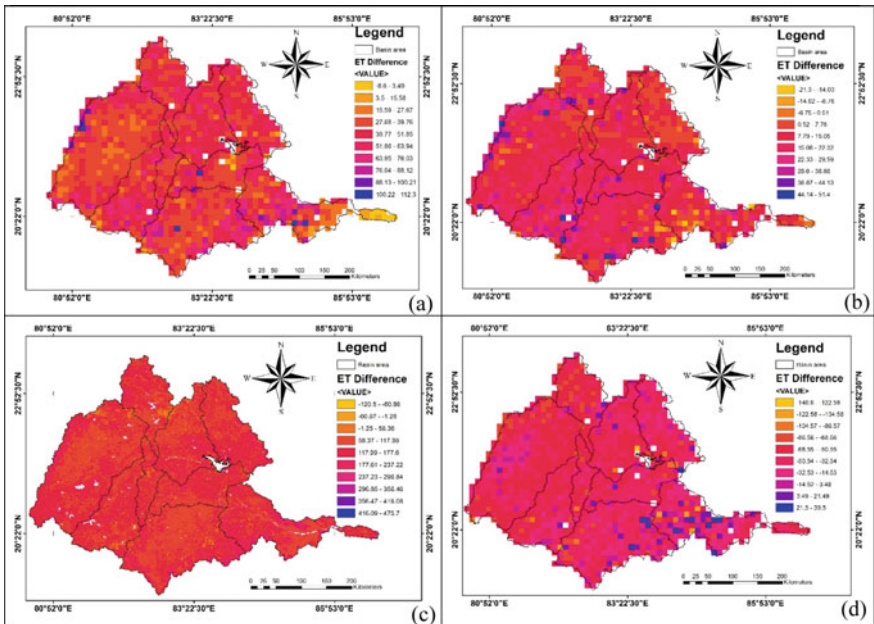


Fig. 5 Evapotranspiration (ET) difference map of dry and wet seasons a 2005, b 2010, c 2015, d 2019



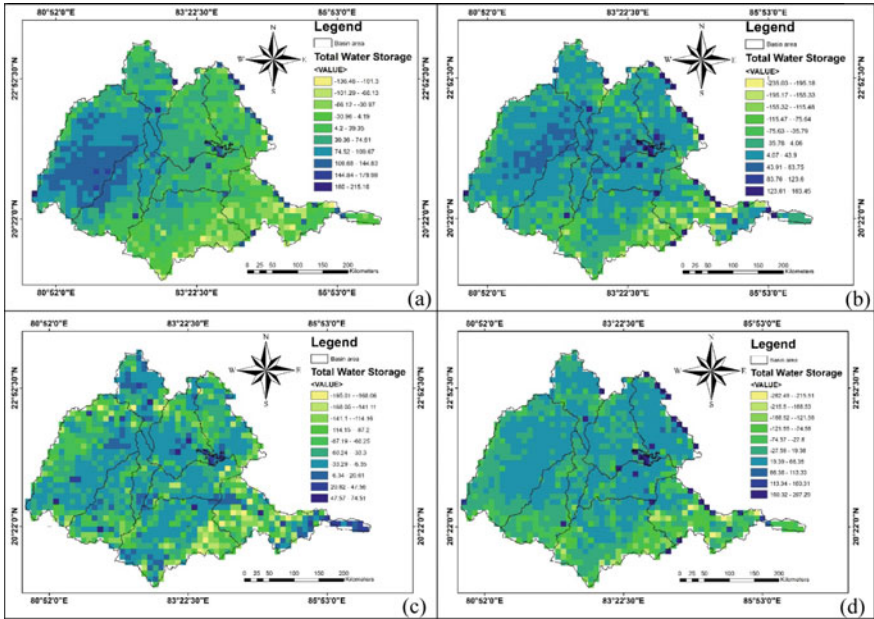


Fig. 6 Total water storage change (DTWS) map of dry season a 2005, b 2010, c 2015, d 2019

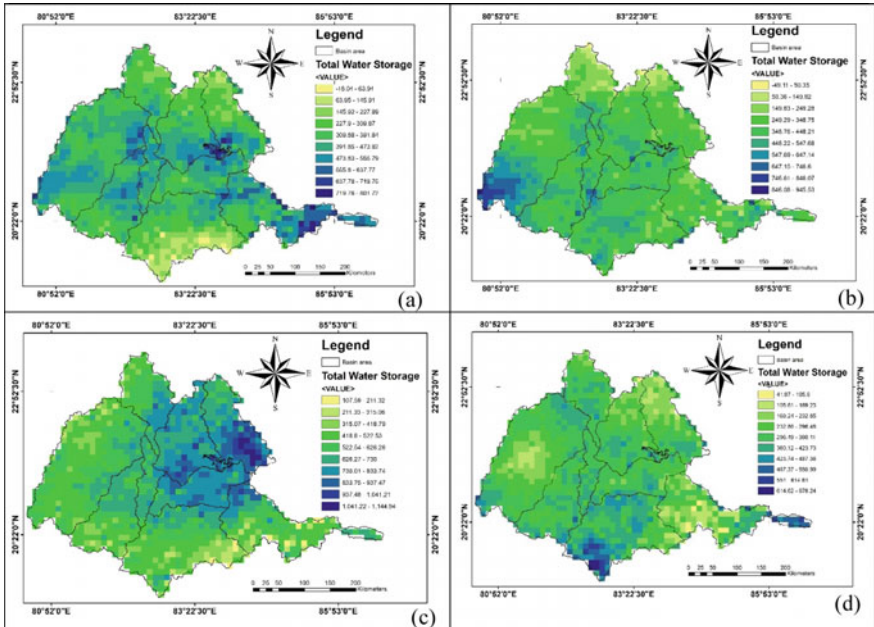


Fig. 7 Total water storage change (DTWS) map of wet season a 2005, b 2010, c 2015, d 2019



seasonal water budget components using zonal statistics to get the total seasonal precipitation, ET, and TWS change amount averaged over the Mahanadi sub-basins. All sub-basin region seasonal water amount will convert the units from mm to m<sup>3</sup>. Finally, total seasonal water amount estimation and examine seasonal water budget components multiply the sum by 10<sup>-9</sup> to calculate billions of cubic meters. Variation of total seasonal water amount estimation is using Eq. (2).

$$R_{\text{total}} = \text{Pr} - \text{ET} - \text{DS} \quad (2)$$

where

- Pr    Precipitation,
- T     Evapotranspiration,
- DS    Water storage change in the river basin (soil moisture, snow) and sub-surface (root zone moisture, groundwater component).

## 5 GLDAS 2.2 Observation

Examine and compare dry and wet seasons' water budget components from GLDAS 2.2 and estimate seasonal, basin-averaged, and sub-basin level total water balance mechanisms in study area through the periods of 2004–2005, 2009–2010, 2014–2015, and 2018–2019. All water balance variables such as precipitation (Pr), evapotranspiration (ET), and storm surface runoff (RO) units convert to mm/month. This three water budget components' difference map for dry and wet seasonal pattern is shown in Figs. 8, 9, and 10. Final total seasonal water budget is shown in Figs. 11 and 12. ArcGIS zonal statistics tool to estimation the total seasonal water amount over the Mahanadi sub-basins uses the shapefile attributes/calculator to get the area of the sub-basins. The open attribute table will have sub-basin numbers, characteristics, and columns with count and spatial mean for the seasonal all water budget component rasters. Mahanadi sub-basin region seasonal water amount will be converted from mm unit to m<sup>3</sup>. Finally, total seasonal water amount is estimated and the component is multiplied by 10<sup>-9</sup> to calculate in billions of cubic meters. Variation of total seasonal water amount estimation is done using Eq. (2).

Higher precipitation difference shown on 2005 and 2015 in the northeastern part of the region, similarly 2010 and 2019 found that western part of the basin (Fig. 8). Negative ET difference found in southeastern region sub-basin 6, 1, 2 where positive ET difference showing in the region mainly western part (sub-basin 5, 7, 8, 9, 10) of the entire region (Fig. 9). High runoff estimate in central (sub-basin 1) and eastern (sub-basins 2 and 3) part of the river basin where very low runoff estimate in western (sub-basins 9 and 10) part (Fig. 10).

Dry season highly total water storage deficit area found sub-basin 1 eastern part in the year 2005, similarly in the year of 2015 northern (sub-basin 6, 5, 8) and 2019 (sub-basin 7, 8, 9, 10) western part of the region (Fig. 11). In wet season, higher

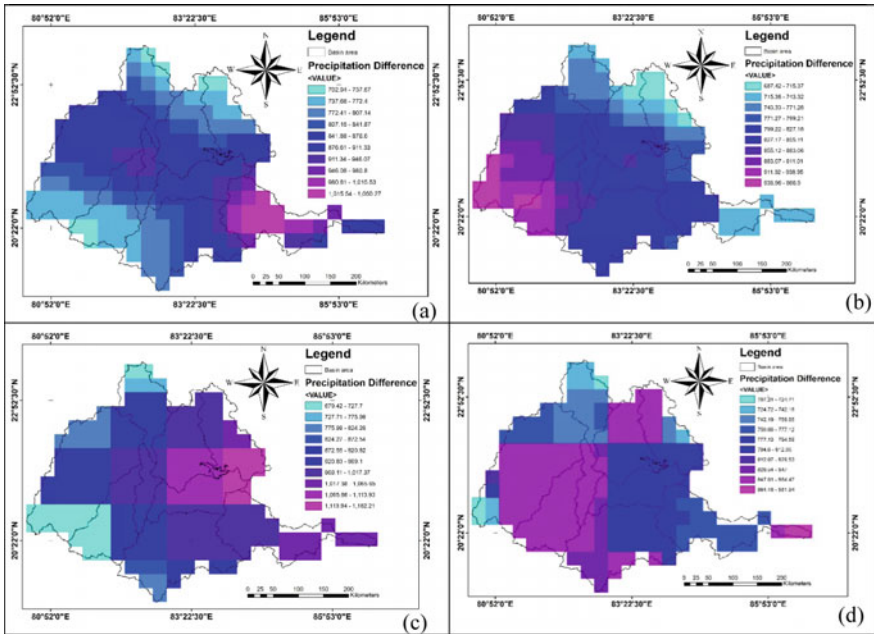


Fig. 8 Precipitation (Pr) difference map of dry and wet seasons a 2005, b 2010, c 2015, d 2019

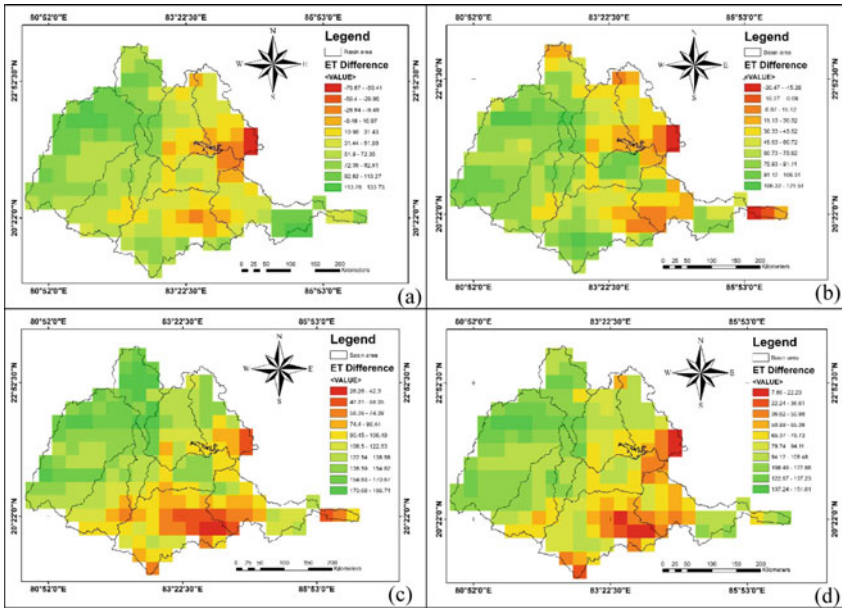


Fig. 9 Evapotranspiration (ET) difference map of dry and wet season a 2005, b 2010, c 2015, d 2019

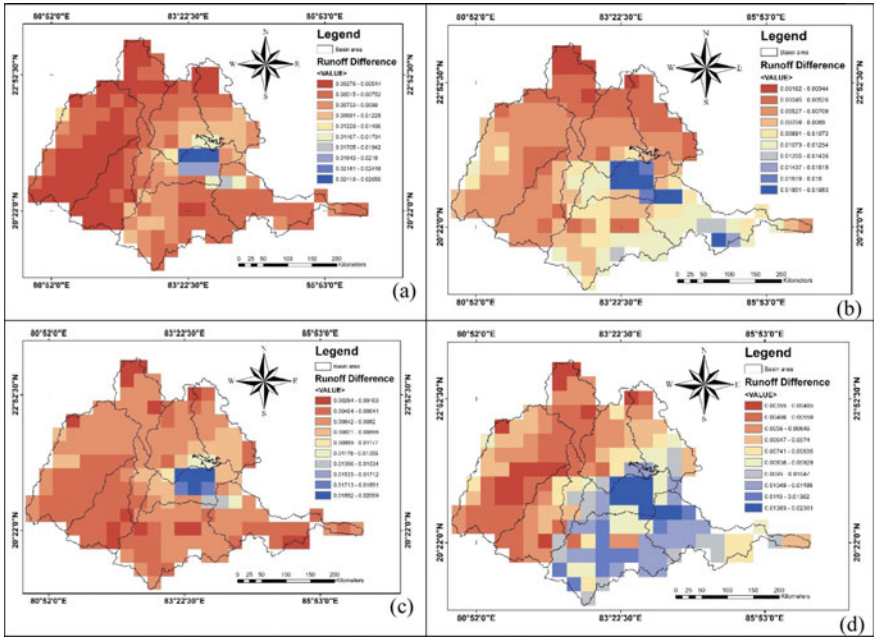


Fig. 10 Runoff difference in dry and wet seasons a 2005, b 2010, c 2015, d 2019

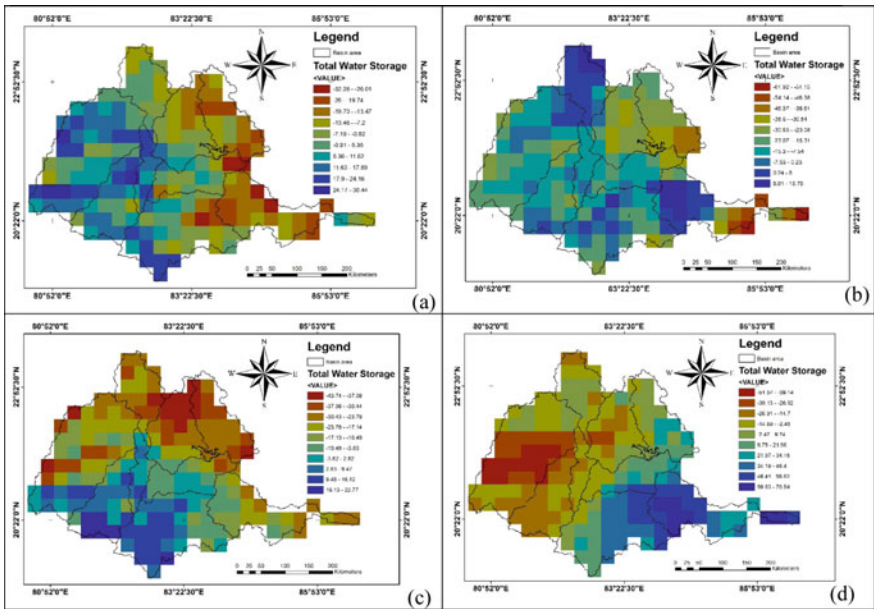
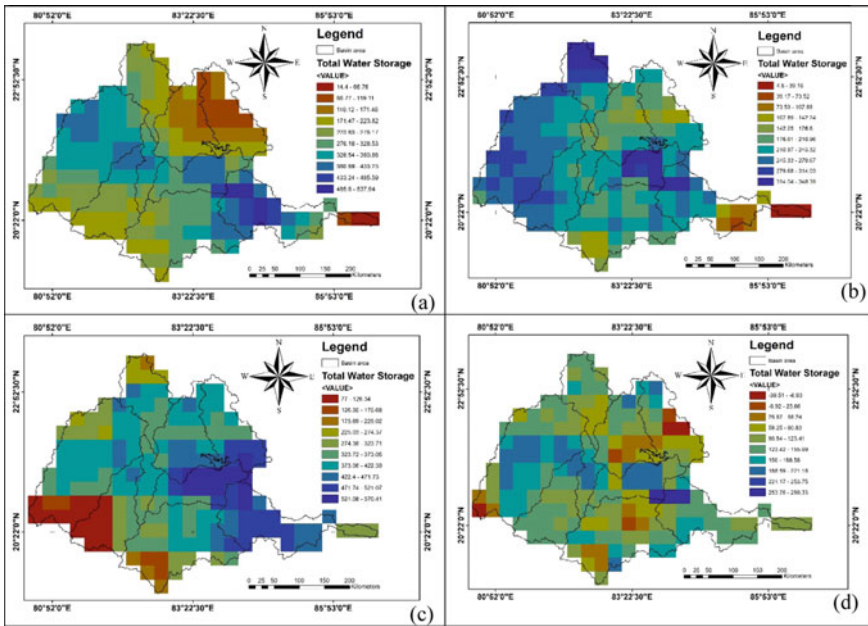


Fig. 11 Total water storage map of dry season a 2005, b 2010, c 2015, d 2019



**Fig. 12** Total water storage map of wet season a 2005, b 2010, c 2015, d 2019

level of total water storage mainly found in sub-basin 3 and 1 located in the eastern side of the entire basin. High water deficit is shown in basin 6 for the year 2005 for northern part and sub-basin 9 and 10 for 2015 in the southern part (Fig. 12).

All the water budget component is estimated in billion cubic meter (BCM). Highest precipitation rate and ET occurred in wet season of the year 2015 (133.65 and 41.73) estimated by GLDAS 2.2 model (Table 4). DTWS measured higher value 64.34 in the year of 2019 by GLDAS 2.2 where in dry season water deficit is more -18.61 in the year of 2015. Lowest DTWS value is 14.16 measured by RS based observation in the year of 2015 during wet season. However, the groundwater storage level also attained decreasing trend all over the study region except for fewer part in the eastern and western regions of the entire basin. Similarly, the period of the wet season follows an adverse trend over the common of the region except for the central part (Fig. 12). Cropland area covered by higher percentage in the region where the increasing trend for built-up area is due to anthropogenic interference. This can be aggregating effect of climate change and land use land cover changes which specify a minor changing in the monsoon period of the entire basin. This is extensive distress groundwater recharge from precipitation over the region.

Remote sensing observation and GLDAS 2.2 model estimated that total water storage decreasing trend in wet periods accept the year of 2015 in the Mahanadi river basin (Table 5). Dry season deficit water is more due to more ET over precipitation; similarly wet periods of precipitation is high over ET. So, both the seasons of entire basin precipitation rate dominate over ET; there are more water losses to the

**Table 4** Total water storage in dry and wet seasons' entire basin in BCM

|     | 2005   |          |        | 2010     |        |          | 2015   |          |        | 2019     |        |          |
|-----|--------|----------|--------|----------|--------|----------|--------|----------|--------|----------|--------|----------|
|     | RS Obs | GLDAS2.2 | RS Obs | GLDAS2.2 | RS Obs | GLDAS2.2 | RS Obs | GLDAS2.2 | RS Obs | GLDAS2.2 | RS Obs | GLDAS2.2 |
| Dry | Pr     | 10.02    | 7.76   | 2.14     | 1.69   | 3.28     | 4.87   | 11.48    | 8.63   |          |        |          |
|     | ET     | 17.64    | 25.41  | 20.41    | 21.48  | 14.54    | 25.44  | 23.64    | 24.33  |          |        |          |
|     | DTWS   | -13.43   | -17.63 | -17.47   | -17.99 | -4.29    | -18.61 | -11.73   | -16.19 |          |        |          |
| Wet | Pr     | 122.93   | 122.99 | 115.47   | 113.49 | 126.35   | 133.65 | 115.05   | 118.51 |          |        |          |
|     | ET     | 23.52    | 32.98  | 22.30    | 29.86  | 30.83    | 41.73  | 17.74    | 36.85  |          |        |          |
|     | DTWS   | 48.71    | 51.29  | 42.96    | 52.79  | 14.16    | 42.30  | 55.33    | 64.34  |          |        |          |

*Note* Pr Precipitation, ET Evapotranspiration, DTWS Terrestrial water storage change

atmosphere compared to how much receive precipitation. Using Eq. 2 in GLDAS 2.2 model, we get the total runoff or discharge so that is more like a residual because there are different datasets different resolution so they have all error characteristics but this adopted methodology could give idea and interpret overall changing the water budget scenario of season to season and year to year basis. There are substantial variances between the total of accumulated precipitation and their concentrations from diverse precipitation datasets [51, 52]. In the global hydrological models, ET is the most uncertain parameters [53]. Overestimation of ET acts as major role and underestimation of potential water mass and vice versa. This adopted methodology would indicate that wet seasons might expect higher runoff compared to that of dry seasons in the entire basin (Table 5).

## 6 Discussion

Remote sensing-based data together with GIS analysis helps in assessing the water budget estimation in Mahanadi river basin management. Monthly/seasonal and inter-annual variations can be utilized in soil water resources management in the river basin, while all the information calibrated in this session is validated with selected surface measurements, regional and local assessment is recommended. In addition to the water budget component, information about socio-economic characteristics and in situ data (e.g., river discharge, soil moisture, ecosystems) are required for sustainable river basin management.

Our research focuses on amounts of precipitation rate, evapotranspiration, and terrestrial water storage change in the Mahanadi river basin during dry and wet seasons. All the water budget components are calculated from remote sensing based GPM IMERG, MODIS, and GRACE/GRACE-FO observations GLDAS-CLSM model during 2004–2005, 2009–2010, 2014–2015, and 2018–2019. More accurate, quantitative estimation of water budget continues to be a challenge for a variety of reasons. The spread of estimates can be used for assessing the uncertainty. This study illustrates and investigates the temporal and spatial variability of water storage variations over Mahanadi river basin, with consequences for a better understanding of the basin hydrologic cycle mechanism due to climate change and anthropogenic interference. Simulation of GRACE-based TWSC with GLDAS model also emphasizes the possible for improving and validating global LSMs GRACE data [54]. There are barriers in estimating total water budget using remote sensing and GLDAS data due to limitations in observing/modeling all the water components and anthropogenic effects (e.g., stream flow, irrigation, ground water pumping, and diversion). Terrestrial water storage anomalies from GRACE and GRACE-FO have coarse resolutions and cannot provide accurate information for micro-watersheds. The ET reconstruction system is robust and effective for different LSMs of GLDAS model with diverse climatic condition; and it can be very useful to other LSMs to provide an alternative assessment of authentic ET over the human-control river basin. Uncertainty becomes larger for smaller area of study and depends on the shape and latitude of

**Table 5** Total water storage in dry and wet seasons' entire study area

|      | Dry (Pr-ET) |          | Wet (Pr-ET) |          | Dry (Pr-ET-DTWS) |          | Wet (Pr-E-DTWS) |          |
|------|-------------|----------|-------------|----------|------------------|----------|-----------------|----------|
|      | RS Obs      | GLDAS2.2 | RS Obs      | GLDAS2.2 | RS Obs           | GLDAS2.2 | RS Obs          | GLDAS2.2 |
| 2005 | -7.62       | -17.64   | 99.41       | 90.01    | 5.81             | -0.02    | 50.71           | 38.72    |
| 2010 | -18.28      | -19.79   | 93.17       | 83.62    | -0.80            | -1.80    | 50.21           | 30.83    |
| 2015 | -11.26      | -20.57   | 95.52       | 91.92    | -6.97            | -1.96    | 81.37           | 49.62    |
| 2019 | -12.16      | -15.70   | 97.32       | 81.67    | -0.42            | 0.50     | 41.99           | 17.33    |

*Note* Pr Precipitation, ET Evapotranspiration, DTWS Terrestrial water storage change

the area. MOD16 evapotranspiration may have significant uncertainties depending on watershed characteristics [e.g., 55, 56]. GRACE-derived TWSC data and other remote sensing-based product such as precipitation, evapotranspiration, runoff are used to solving water-related issues for water budget estimation in any river basin. Future recommendation a customized, ensemble modeling approach (e.g., Land Information System, <https://lis.gsfc.nasa.gov/> using in situ and remote sensing data), with appropriate stream flow routing model would yield better water component estimates. A newer version of GRACE Mascon product, GRACE-FO combination JPL, GeoForschungsZentrum Potsdam (GFZ), etc., is used for better water budget estimation.

## 7 Conclusion

Using the Hydrologic Decision Support System, water quality monitoring is also the most significant approach for sustainable hydrological cycle of any catchment region. This research work estimating and examines the spatial–temporal variations of total water budget in Mahanadi basin region, India. Understand the source of uncertainties involved in water budgets for river basins. Compare dry and wet seasons' water budget components based on IMERG precipitation, MODIS ET, and GRACE-derived TWS with GLDAS2.2 model for estimate seasonal, basin-averaged, and sub-basin level water budget. This research work focuses only application of earth observation RS based data for monitoring the water budget components in Mahanadi river basins. Despite the uncertainties, RS and GLDAS model can be applied to assess temporal and spatial variations in individual water budget components and to get better signs of changing pattern of water availability for a relatively river basins. In situ measurements, such as soil moisture, precipitation rate, observed stream flow, and vegetation information, should be validated with the RS and GLDAS data. Evaluation of empirical methodology or local knowledge with the RS and GLDAS data may help in assessing the usefulness of best agricultural practice management system in the watershed. Remote sensing can contribute to understanding, monitoring, and predicting the water balance of large, poorly instrumented basins. There is power in merging data streams, both through multi-sensor approaches and data assimilation. Uncertainties are substantial and should not be understated. Collaborative analysis can, sometimes, overcome skepticism of remotely sensed products.

**Acknowledgements** The authors do hereby acknowledged the contribution Visva-Bharati (A Central University), West Bengal, India, for facilitating this research work.



## References

1. Mirza MMQ (2011) Climate change, flooding in South Asia and implications. *Region Environ Change* 11:95–107. <https://doi.org/10.1007/s10113-010-0184-7>
2. Hoang LP, Vliet MTH, Kummu M, Lauri H, Koponen J, Supit I et al (2019) The Mekong's future flows under multiple drivers: how climate change, hydropower developments and irrigation expansions drive hydrological changes. *Sci Tot Environ* 649:601–609. <https://doi.org/10.1016/j.scitotenv.2018.08.160>
3. Khandu FE, Schumacher M, Awange JL, Schmied HM (2016) Exploring the influence of precipitation extremes and human water use on total water storage (TWS) changes in the Ganges–Brahmaputra–Meghna river basin. *Water Resour Res* 52:2240–2258. <https://doi.org/10.1002/2015WR018113>
4. UNEP (2016) Transboundary River Basins Status and Trends SUMMARY FOR POLICY MAKERS. United Nations Environment Programme (UNEP). <http://www.geftwap.org/publications/river-basins-spm>. Accessed on 17 June 2020
5. Food and Agriculture Organization (FAO) (2012) Irrigation in Southern and Eastern Asia in Figures. FAO, Land and water division, Water Reports. 37
6. Murshed SB, Kaluarachchi JJ (2018) Scarcity of fresh water resources in the Ganges Delta of Bangladesh. *Water Secur* 4–5:8–18. <https://doi.org/10.1016/j.wasec.2018.11.002>
7. Mao Y, Wang KC, Liu XM, Liu CM (2016) Water storage in reservoirs built from 1997 to 2014 significantly altered the calculated evapotranspiration trends over China. *J Geophys Res Atmos* 121:10097–10112
8. Xue BL, Wang L, Li XP, Yang K, Chen DL, Sun LT (2013) Evaluation of evapotranspiration estimates for two river basins on the Tibetan Plateau by a water balance method. *J Hydrol* 492:290–297
9. Lakshmi V, Fayne J, Bolten J (2018) A comparative study of available water in the major river basins of the world. *J Hydrol* 567:510–532. <https://doi.org/10.1016/j.jhydrol.2018.10.038>
10. Hanington P, To QT, Van PDT, Doan NAV, Kiem AS (2017) A hydrological model for interprovincial water resource planning and management: a case study in the Long Xuyen Quadrangle, Mekong Delta. *Vietnam J Hydrol* 547:1–9. <https://doi.org/10.1016/j.jhydrol.2017.01.030>
11. Syed TH, Famiglietti JS, Rodell M, Chen J, Wilson CR (2008) Analysis of terrestrial water storage changes from GRACE and GLDAS. *Water Resour Res* 44:W02433. <https://doi.org/10.1029/2006WR005779>
12. Hassan A, Jin S (2016) Water storage changes and balances in Africa observed by GRACE and hydrological models. *Geod. Geodyna* 7–1:39–49. <https://doi.org/10.1016/j.geog.2016.03.002>
13. Gonzalez R, Ouarda T, Marpu P, Allam M, Eltahir E, Pearson S (2016) Water Budget Analysis in Arid Regions, Application to the United Arab Emirates. *Water* 8(9):415. <https://doi.org/10.3390/w8090415>
14. Eltahir EAB, Bras RL (1996) Precipitation recycling. *Rev Geophys* 34(3):367–378
15. Richey JE, Melack JM, Aufdenkampe AK, Ballester VM, Hess LL (2002) Outgassing from Amazonian rivers and wetlands as a large tropical source of atmospheric CO<sub>2</sub>. *Nature* 416:617–620
16. Panday PK, Coe MT, Macedo MN, Lefebvre P, Castanho ADDA (2015) Deforestation offsets water balance changes due to climate variability in the Xingu River in eastern Amazonia. *J Hydrol* 523:822–829. <http://dx.doi.org/https://doi.org/10.1016/j.jhydrol.2015.02.018>
17. Long D, Yang Y, Wada Y, Hong Y, Liang W, Chen Y, Yong B, Hou A, Wei J, Chen L (2015) Deriving scaling factors using a global hydrological model to restore GRACE total water storage changes for China's Yangtze River Basin. *Remote Sens Environ* 168:177–193. <https://doi.org/10.1016/j.rse.2015.07.003>
18. Penatti NC, Almeida TIRD, Ferreira LG, Arantes AE, Coe MT. Satellite based hydrological dynamics of the world's largest continuous wetland. *Remote Sens. Environ.* 2015, **170**: 1–13. <https://doi.org/10.1016/j.rse.2015.08.031>

19. Lv M, Ma Z, Yuan X, Lv M, Li M, Zheng Z (2017) Water budget closure based on GRACE measurements and reconstructed evapotranspiration using GLDAS and water use data for two large densely-populated mid-latitude basins. *J Hydrol* 547:585–599. <https://doi.org/10.1016/j.jhydrol.2017.02.027>
20. Rodell M, Velicogna I, Famiglietti JS (2009) Satellite-based estimates of groundwater depletion in India. *Nature* 460:999–1002. <https://doi.org/10.1038/nature08238>
21. Chinnasamy P, Maheshwari B, Prathapar S (2015) Understanding groundwater storage changes and recharge in Rajasthan, India through remote sensing. *Water* 7:5547–5565. <https://doi.org/10.3390/w7105547>
22. Singh A, Seitz F, Eicker A, Güntner A (2016) Water budget analysis within the surrounding of prominent lakes and reservoirs from multi-sensor earth observation data and hydrological models: case studies of the Aral Sea and Lake Mead. *Remote Sens* 8(11):953
23. Wan Z, Zhang K, Xue X, Hong Z, Hong Y, Gourley JJ Water balance based actual evapotranspiration reconstruction from ground and satellite observations over the conterminous United States. *Water Resour Res* 51:6485–6499. <https://doi.org/10.1002/2015wr017311>
24. Landerer FW, Swenson SC (2012) Accuracy of scaled GRACE terrestrial water storage estimates. *Water Resour Res* 48:W04531. <https://doi.org/10.1029/2011wr011453>
25. Long D, Longuevergne L, Scanlon BR (2014) Uncertainty in evapotranspiration from land surface modeling, remote sensing, and GRACE satellites. *Water Resour Res* 50:1131–1151. <https://doi.org/10.1002/2013wr014581>
26. Swain KC, Singha C, Nayak L (2020) Flood susceptibility mapping through the GIS-AHP technique using the cloud. *Int J Geo-Inf* 9:720. <https://doi.org/10.3390/ijgi9120720>
27. Haddeland I, Lettenmaier DP, Skaugen T (2006) Effects of irrigation on the water and energy balances of the Colorado and Mekong river basins. *J Hydrol* 324:210–223. <https://doi.org/10.1016/j.jhydrol.2005.09.028>
28. Siebert S, Burke J, Faures JM, Frenken K, Hoogeveen J, Döll P, Portmann FT (2010) Groundwater use for irrigation—a global inventory. *Hydrol Earth Syst Sci* 14(10):1863–1880. <https://doi.org/10.5194/hess-14-1863-2010>
29. Wada Y, van Beek LPH, Bierkens MFP (2012) Nonsustainable groundwater sustaining irrigation: a global assessment. *Water Resour Res* 48:W00L06. <https://doi.org/10.1029/2011WR010562>
30. Landerer F (2020) CSR TELLUS GRACE Level-3 Monthly Ocean Bottom Pressure Anomaly Release 6.0 VERSION 03 in netCDF/ASCII/GeoTIFF Formats. Ver. RL06 v03. PO.DAAC, CA, USA. 2020. Accessed on 01 June 2020. <https://doi.org/10.5067/TEOCN-3AC63>
31. Singha C, Swain KC, Swain SK (2020) Best crop rotation selection with GIS-AHP technique using soil nutrient variability. *Agriculture* 10:213. <https://doi.org/10.3390/agriculture10060213>
32. Winsemius HC, Savenije HHG, vandeGiesen NC, vandenHurk BJM, Zapreeva EA, Klees R (2006) Assessment of gravity recovery and climate experiment (GRACE) temporal signature over upper Zambezi. *Water Resour Res* 42:W12201. <https://doi.org/10.1029/2006WR005192>
33. Niu GY, Yang ZL (2006) Assessing a land surface model's improvements with GRACE estimates. *Geophys Res Lett* 33:L07401. <https://doi.org/10.1029/2005GL025555>
34. Swenson SC, Milly PCD (2006) Climate model biases in seasonality of continental water storage revealed by satellite gravimetry. *Water Resour Res* 42:W03201. <https://doi.org/10.1029/2005WR004628>
35. Wang G, Pan J, Shen C, Li S, Lu J, Lou D, Hagan DFT (1884) Evaluation of Evapotranspiration Estimates in the Yellow River Basin against the Water Balance Method. *Water* 2018:10
36. Syed TH, Famiglietti JS, Chen J, Rodell M, Seneviratne SI, Viterbo P, Wilson CR (2005) Total basin discharge for the Amazon and Mississippi River basins from GRACE and a land-atmosphere water balance. *Geophys Res Lett* 32:L24404. <https://doi.org/10.1029/2005gl024851>
37. Sahoo AK, Pan M, Troy TJ, Vinukollu RK, Sheffield J, Wood EF (2011) Reconciling the global terrestrial water budget using satellite remote sensing. *Remote Sens Environ* 115(8):1850–1865
38. Pan M, Sahoo AK, Troy TJ, Vinukollu RK, Sheffield J, Wood EF (2011) Multisource estimation of long-term terrestrial water budget for major global river basins. *J Clim* 25(9):3191–3206

39. Li B, Beaudoin H, Rodell M (2020) NASA/GSFC/HSL GLDAS Catchment Land Surface Model L4 daily  $0.25 \times 0.25$  degree GRACE-DA1 V2.2, Greenbelt, Maryland, USA, Goddard Earth Sciences Data and Information Services Centre (GES DISC) 2020. Accessed on 15 June 2020. <https://doi.org/10.5067/TXBMLX370XX8>
40. Rodell M, Houser PR, Jambor U, Gottschalck J, Mitchell K, Meng CJ, Arsenault K, Cosgrove B, Radakovich J, Bosilovich M, Entin JK, Walker JP, Lohmann D, Toll D (2004) The Global land data assimilation system. *Bullet Am Meteor Soc* 85(3):381–394
41. Zaitchik BF, Rodell M, Olivera F (2010) evaluation of the global land data assimilation system using global river discharge data and a source to sink routing scheme. *Water Resource Res* 46:W06507. <https://doi.org/10.1029/2009WR007811>
42. Pennemann PCS, Rivera JAR, Saulo ACE, Penalba OCP (2016) A comparison of GLDAS soil moisture anomalies against standardized precipitation index and multisatellite estimations over South America. *J Hydrometeorol* 16. <https://doi.org/10.1175/JHM-D-13-0190.1>
43. Sikder MS, David CH, Allen GH, Qiao X, Nelson EJ, Matin MA (2019) Evaluation of available global runoff datasets through a river model in support of transboundary water management in South and Southeast Asia. *Front Environ Sci* 7:171. <https://doi.org/10.3389/fenvs.2019.00171>
44. Chen Y, Yang K, Qin J, Zhao L, Tang W, Han M (2013) Evaluation of AMSR-E retrievals and GLDAS simulations against observations of a soil moisture network on the Central Tibetan Plateau. *J Geophys Res* 118:4466–4475. <https://doi.org/10.1002/jgrd.50301>
45. Bi H, Ma J, Zheng W, Zeng J (2016) Comparison of soil moisture in GLDAS model simulations and in situ observations over the Tibetan Plateau. *J Geophys Res* 121:2658–2678. <https://doi.org/10.1002/2015JD024131>
46. Berg AA, Famiglietti JS, Rodell M, Reichle RH, Jambor U, Holl SL et al (2005) Development of a hydrometeorological forcing data set for global soil moisture estimation. *Int J Climatol* 25:1697–1714. <https://doi.org/10.1002/joc.1203>
47. GOI (Government of India Ministry of Water Resources), Mahanadi Basin 2014, pp.1–100. [www.india-wris.nrsc.gov.in](http://www.india-wris.nrsc.gov.in). Accessed on 20 July 2020
48. Lehner B, Verdin K, Jarvis A (2008) New global hydrography derived from spaceborne elevation data. *Eos Trans Am Geophys Union* 89:93–104. <https://doi.org/10.1029/2008EO100001>
49. Snow AD (2015) A new global forecasting model to produce high-resolution stream forecasts [Master's thesis]. Brigham Young University, Provo, UT, United States
50. Beaudoin H, Rodell M (2020) NASA/GSFC/HSL, GLDAS Noah Land surface Model L4 3 hourly  $0.25 \times 0.25$  degree V2.1, Greenbelt, Maryland, USA, Goddard Earth Sciences Data and Information Services Centre (GES DISC), 2020. Accessed on 14 June 2020. <https://doi.org/10.5067/E7YRXPJKWOQ>
51. Negrón Juárez RI, Li W, Fu R, Fernandes K, de Oliveira Cardoso A (2009) Comparison of precipitation datasets over the Tropical South American and African continents. *J Hydrometeorol* 10:289–299
52. Shin DB, Kim JH, Park HJ (2011) Agreement between monthly precipitation estimates from TRMM satellite, NCEP reanalysis, and merged gauge-satellite analysis. *J Geophys Res Atmospheres* 116
53. Schumacher M, Eicker A, Kusche J, Schmied HM, Döll P (2015) Covariance analysis and sensitivity studies for GRACE assimilation into WGHM. In: Rizos C (ed) International association of geodesy symposia. Springer, Berlin/Heidelberg, Germany, pp 1–7
54. Lettenmaier DP, Famiglietti JS (2006) Water from on high. *Nature* 444:562–563
55. Dziki et al (2019) Comparison of two remote sensing models for estimating evapotranspiration: algorithm evaluation and application in seasonally arid ecosystems in South Africa 2019: Comparison. *J Arid Land* 11:495–512. <https://doi.org/10.1007/s40333-019-0098-2>
56. Souza et al (2019) Evaluation of MOD16 algorithm over irrigated rice paddy using flux tower measurements in Southern Brazil. *Water* 11. <https://doi.org/10.3390/w11091911>

# Utility of Geomatics in Land Use Land Cover Change Detection and Accuracy Analysis



G. Padmaja and M. V. S. S. Giridhar

**Abstract** Unprecedented growth and rapid urbanization resulted in remarkable changes in the land use and land cover patterns which altered the global environmental scenario and also affected ecosystem services. Continuous monitoring of land use and land cover changes is extremely important to systematically plan various infrastructure projects and their land requirements to meet demands from various sectors, especially in an urban context. Timely and reliable information on the spatial and temporal behavior of land use land cover patterns is, therefore, a prerequisite and realizing the potential of geospatial technologies in providing such information, a study has been taken up in the Hussain Sagar catchment area, a part of Hyderabad City. The present study includes land use land cover (LULC) classification of various satellite images taken at different periods for comparison and checking for their accuracy assessment. The results indicated a spectacular increase in settlements/built-up land to the tune of 50.34 km<sup>2</sup> accounting for 48.38% of the proposed study area. Contrastingly, a significant shrinkage in the areal extent of vegetation, barren land, and water bodies has been noticed over the past one and half decades. It is noted from various sources and findings that the Kappa value greater than 0.75, is rated to be considerable. The results obtained from the present study indicated an overall classification accuracy of 87.33% with kappa value ( $K$ ) = 0.84 which are found to be satisfactory and therefore the classified images can be used for further analysis.

**Keywords** LULC classification · Change detection · Kappa statistics

## 1 Introduction

Most of the cities in developing countries are often distressed due to environmental and socioeconomic problems. Human activities coupled with greed have not only altered the natural ecosystems but also degraded the natural environment. Land and water have become scarce natural resources. Consequently, there is immense pressure

---

G. Padmaja (✉) · M. V. S. S. Giridhar  
CWR, IST, JNTUH, Hyderabad, Telangana, India

© The Author(s), under exclusive license to Springer Nature Singapore Pte Ltd. 2022  
C. M. Rao et al. (eds.), *Advanced Modelling and Innovations in Water Resources Engineering*, Lecture Notes in Civil Engineering 176,  
[https://doi.org/10.1007/978-981-16-4629-4\\_35](https://doi.org/10.1007/978-981-16-4629-4_35)

517

from various sectors such as agriculture, industries, residential, commercial in most of the urban areas. The pragmatic changes observed in land use such as the conversion of forests into agricultural lands, agricultural lands into human settlements, the encroachment of wetlands have adversely affected the ecosystem services, thus posing a challenge at local and global scales. These changes in land use mostly occur due to growing population density, demand for agriculture, industries, and continuous economic growth. The exponential increase in population over the decades with the simultaneous increase in economic activities had elicited changes in land use patterns, thereby leading to immense pressure on the availability of resources and the natural environment. The existing land use land cover patterns are the outcome of several natural, socioeconomic influences, their exploitation by humans over the decades. Therefore, the information about land use land cover is essential for selecting, planning, and implementation of land use schemes to meet the increasing demand for basic human needs and welfare of the society. This information also helps in estimating the dynamics of land use as a result of increasing population and their changing demands. In the present study, many projects have embarked in the city which has attracted a lot of people's attention, thus contributing to the physical expansion of the city in terms of buildings, roads, commercial spaces, IT sector, and industries, all these had led to changes in the land use pattern. Remote sensing data and GIS analysis help in detecting the land consumption rate; therefore, an attempt had been made to predict the same [1, 2].

### ***1.1 Objectives of the Present Study***

The main objective of the present study is to generate land use land cover maps of Hussain Sagar catchment area present in Hyderabad region at different epochs for detecting changes that have occurred during the past one and half decades especially in the built-up land due to urbanization and concretization, compare the results and assess the change detection matrix for the above said period.

### ***1.2 Study Area and Data Input***

Hussain Sagar catchment is about 287 km<sup>2</sup>, falling into 5 major sub-watersheds, viz. Bowenpally, Banjarahills, Kukatpally, Dulapally, and Yusufguda. The highest peak in the catchment is at 642 m which lies north of Nizampet while the lowest is about 500 m at the confluence of the stream outlet adjoining with Musi River in downstream of Hussain Sagar Lake. Due to encroachments, the watershed area has shrunk from 540 to 450 hectares and the majority of water that enters into the lake is from Kukatpally Nala along with effluents from industries and domestic sources.

### 1.3 Data Input

In the present study, LISS III and Landsat satellite images of the Hyderabad region were acquired from Bhuvan open data source and USGS Earth Explorer for eight different Epochs, namely 2005, 2007, 2009, 2011, 2013, 2015, 2017, and 2019 as shown in Table 1.

## 2 Methodology

To study the change detection for Hussain Sagar catchment, 8 satellite images were acquired for different periods, i.e., 2005, 2007, 2009, 2011, 2013, 2015, 2017, and 2019 with 30 and 24 m resolutions, respectively. The images were clipped to get the area of interest (AOI) and then using the combined method; i.e., by using both unsupervised and supervised classifications, LULC was performed. In the combined approach, firstly we classified the area of interest using an unsupervised method by taking 100 classes. Once the classes are automatically defined by the system, then the recode option present in the raster menu was initiated and each class was manually checked by comparing the satellite image of that particular period for its spectral signature, and then it is finally re-coded into five major classes. Though this approach was time-consuming, it had given accurate results and this approach is more suitable for complex terrains with varied land uses in small areas. Once land use land classification maps for all the above-mentioned periods were generated, the change detection was initiated in ERDAS imagine using matrix union overlay analysis for comparison (Fig. 1).

**Table 1** List of satellite images acquired for LULC classification

| Satellite data                    | Acquisition date | Spatial resolution (m) | Source              |
|-----------------------------------|------------------|------------------------|---------------------|
| Landsat 4–5 TM C1<br>Level-1      | 2005/03/06       | 30                     | USGS Earth Explorer |
| Landsat 4–5 TM C1<br>Level-1      | 2007/03/28       | 30                     | USGS Earth Explorer |
| Landsat 7 ETM + C1<br>Level-1     | 2009/03/09       | 30                     | USGS Earth Explorer |
| Landsat 4–5 TM C1<br>Level-1      | 2011/03/07       | 30                     | USGS Earth Explorer |
| LISS III                          | 2013/03/03       | 24                     | Bhuvan              |
| LISS III                          | 2015/03/17       | 24                     | Bhuvan              |
| Landsat 8 OLI/ TIRS C1<br>Level-1 | 2017/03/23       | 30                     | USGS Earth Explorer |
| Landsat 8 OLI/ TIRS C1<br>Level-1 | 2019/03/29       | 30                     | USGS Earth Explorer |

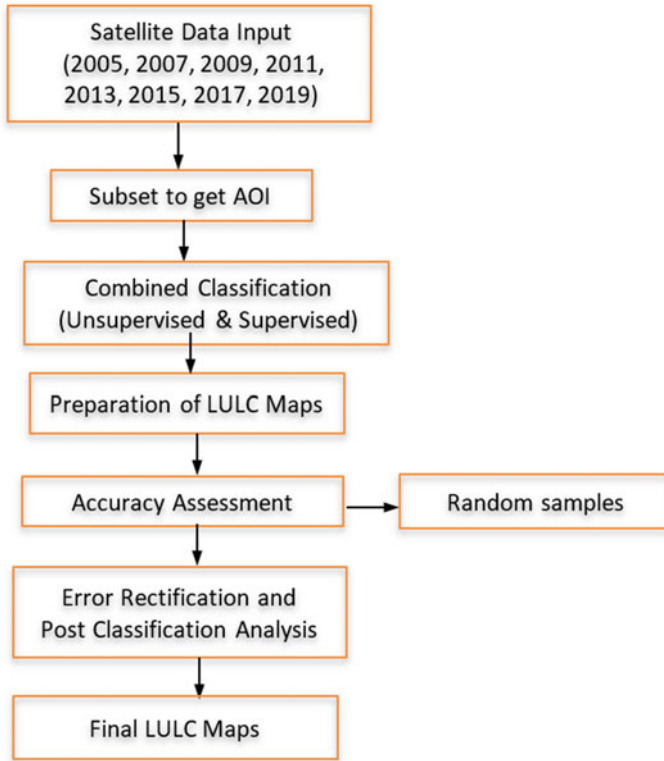


**Fig. 1** Methodological workflow used for LULC classification and accuracy assessment

### ***2.1 Change Detection Using Satellite Images***

Change detection is a process in which numerous land use land cover classified images acquired at different instances are meticulously compared to identify significant changes that have occurred over a period. It is a process in which two different satellite images taken at different times are compared pixel by pixel to estimate the temporal changes that have occurred, in a sense it is to detect which land use is changing to which land use. In the present study, pixel-to-pixel comparison has been initiated to study changes observed over the years, i.e., from 2005 to 2019 by using matrix union overlay process using ERDAS imagine. The information obtained during the process helps to easily identify changes that occurred over time in a particular area.

## 2.2 Accuracy Assessment

Assessing the accuracy of classified images is a desirable procedure and is primarily used to determine the quality and reliability of images that were classified [3]. It is performed by comparing classified images produced by using remote sensing and GIS techniques with the original satellite imagery by choosing some random pixels and manually checking for any inconsistencies. Once all the inconsistencies are checked and corrected manually for all the chosen pixels, the kappa statistics is initiated. In this process, the results obtained are the overall classification accuracy and kappa statistics. Form research, it is noted that if the Kappa value is less than 0.40, it indicates poor performance, while a kappa ranging between 0.40 and 0.75 indicates a good kappa value with moderate performance, and incase the kappa value is higher than 0.75, it indicates an exceptional kappa value with good performance of the classified images [4].

## 3 Results and Conclusions

Remote sensing and GIS play a significant role to determine changes that have occurred in the land use pattern over the years [5]. In the present-study area, remarkable changes were noticed during the past one and half decades which were seen evidently from the generated LULC maps for different years which were compared in Table 2 and Fig. 2. The analysis is performed by comparing classified LULC images chosen for eight instances of alternate periods during the 15 year period, i.e., between 2005 and 2019 which were shown in the figures (Fig. 3a–h).

In the present study, land use and land cover classification was performed by taking multiple satellite images acquired during different periods, and later these classified images were compared with the original satellite images to assess the accuracy of the classified images. The accuracy of all the classified images was checked by using the stratified random sample method which creates some random points for visual comparison of all the randomly selected points with the original satellite image for its accuracy. In the current study, 50 random points for each classified image were taken into consideration and all points were visually compared with the raw satellite images of the same period, and in case any discrepancies were found those were manually corrected, and then the accuracy statistics were computed.

The results obtained were overall classification accuracy, overall kappa index, kappa for each class were summarized for understanding the accuracy performed in a better way. The calculated accuracy assessment for each classified satellite image, the total accuracy, and overall kappa statistics for each satellite image during the years 2005–2019 were shown in Table 3. Also, the comparison of areas under different LULC classes from 2005–2019 was shown in Table 4a and the overall changes in the land use, i.e., what percentage of land use class has changed to the another has been shown in Table 4b. From the results obtained, it is found that the overall accuracy



**Table 2** Details of LULC during 2005, 2007, 2009, 2011, 2013, 2015, 2017, 2019

| Sl. No.                       | Class name        | Area covered (km <sup>2</sup> ) |        |        |        |        |        |        |        |  |  |
|-------------------------------|-------------------|---------------------------------|--------|--------|--------|--------|--------|--------|--------|--|--|
|                               |                   | 2005                            | 2007   | 2009   | 2011   | 2013   | 2015   | 2017   | 2019   |  |  |
| 1                             | Water bodies      | 7.77                            | 7.45   | 7.52   | 7.47   | 6.91   | 6.69   | 6.91   | 6.62   |  |  |
| 2                             | Urban settlements | 104.05                          | 106.49 | 110.19 | 114.53 | 124.48 | 125.42 | 143.38 | 154.39 |  |  |
| 3                             | Vegetation        | 78.20                           | 72.08  | 92.42  | 90.66  | 74.65  | 77.09  | 73.18  | 67.18  |  |  |
| 4                             | Agriculture       | 8.12                            | 9.36   | 4.26   | 4.13   | 3.68   | 4.44   | 3.14   | 3.92   |  |  |
| 5                             | Barren land       | 88.88                           | 91.62  | 72.64  | 70.21  | 77.28  | 73.37  | 60.41  | 54.92  |  |  |
| Total area (km <sup>2</sup> ) |                   | 287.03                          | 287.00 | 287.03 | 287.00 | 287.00 | 287.01 | 287.03 | 287.03 |  |  |

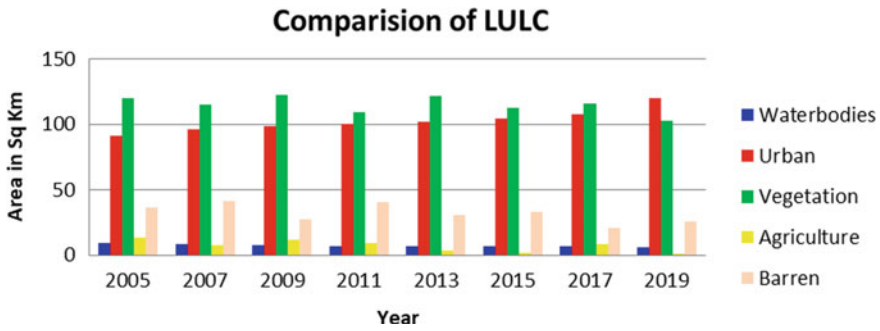


Fig. 2 LULC Pattern during 2005, 2007, 2009, 2011, 2013, 2015, 2017, 2019

was found to be satisfactory, and further, these classified images could be used for future analysis.

From Tables 4a, b the negative change is seen evidently, i.e., a reduction in the areal extent of water bodies, vegetation was observed during the years 2005 and 2019. The reduction in the water bodies and green cover could be primarily due to tremendous population growth, changes in lifestyle practices, huge economic development in the city, and enormous expansion in the IT industry all leading to an upsurge in the built-up area over the decades. The period during 2005–2019 has witnessed an increase in the built-up area by 50.34% due to the physical expansion of the city. Also, it was observed that there was a decrease of 51.75% in agricultural land, 14.10% decrease in vegetation cover, and 38.20% decrease in the barren land mostly contributing to an increase in the built-up area and road networks. Furthermore, water bodies have shrunk by 14.81% from 2005 to 2019 mainly due to construction activities and encroachment of the low-lying areas. The change detection analysis presented in this study was based on the findings obtained from developed eight land use land cover classified maps for the proposed study as shown in Fig. 3a–h. On a whole, there were significant changes observed in the study area between 2005 and 2019 periods which were easily identified by analyzing the maps shown in the figures.

## 4 Conclusions

The present study uses remote sensing and GIS approach for the spatial and temporal analysis and findings which is unlikely through any other conventional mapping techniques. The research findings help in the identification of natural resources that are rapidly depleting, detect environmentally sensitive areas, recognize pragmatic changes occurring in the hydrology in vast areas due to transformations in the land use. Also, these findings would be very helpful to the urban planners in designing better infrastructure keeping in view the goals of sustainable development for better planning and decision making.

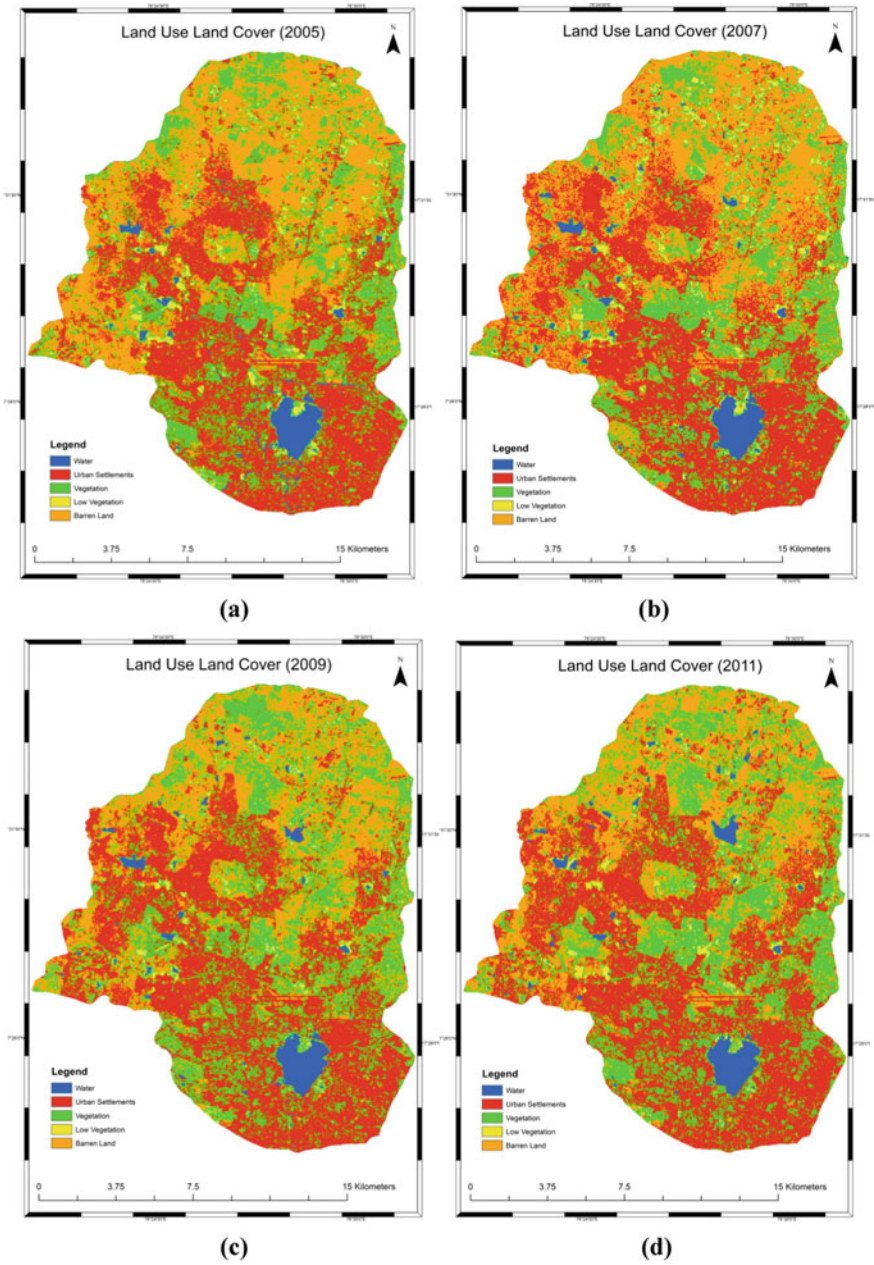


**Fig. 3** a LULC 2005; b LULC 2007; c LULC 2009; d LULC 2011; e LULC 2013; f LULC 2015; g LULC 2017; h LULC 2019

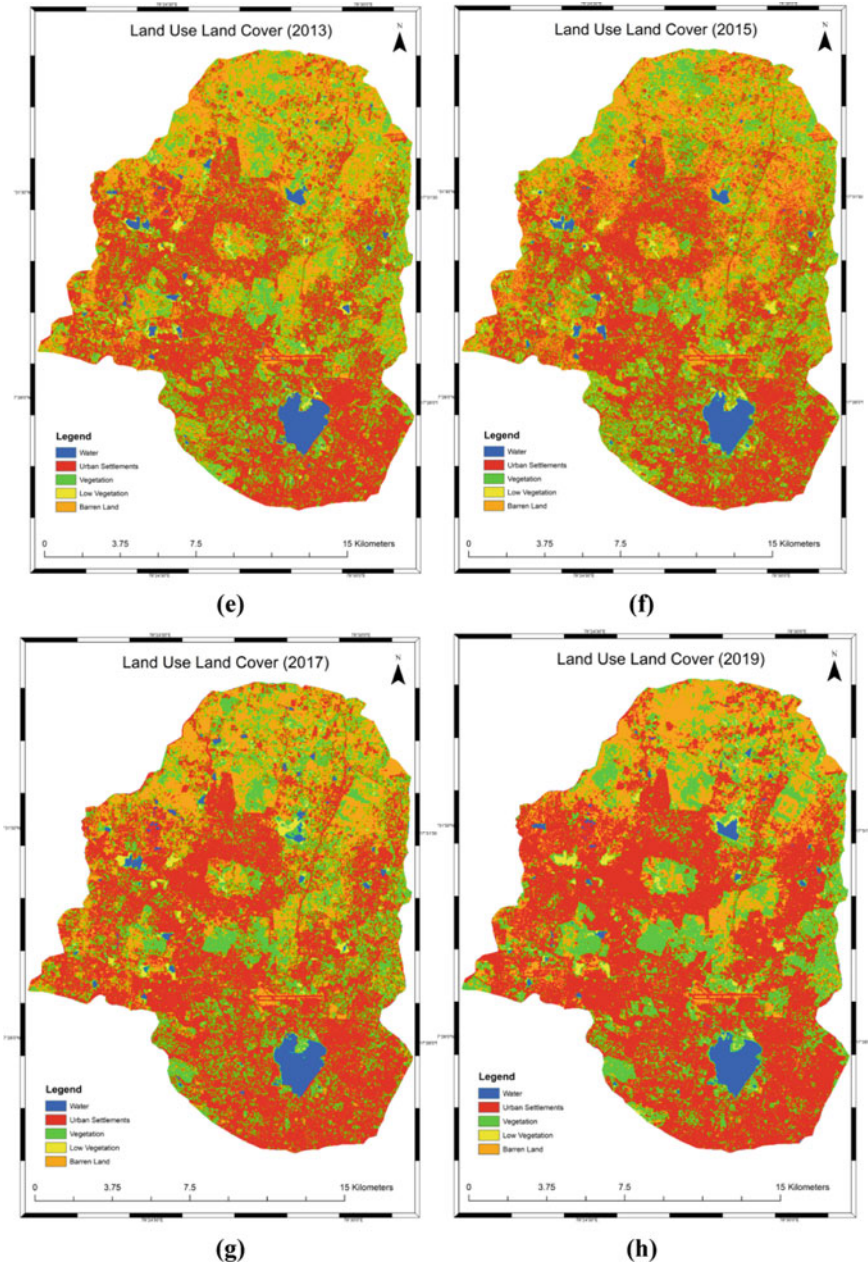


Fig. 3 (continued)

**Table 3** Accuracy assessment of classified images (2005, 2007, 2009, 2011, 2013, 2015, 2017, 2019)

| Year | Overall classification accuracy (%) | Overall Kappa statistics | Kappa        |       |            |             |        |
|------|-------------------------------------|--------------------------|--------------|-------|------------|-------------|--------|
|      |                                     |                          | Water bodies | Urban | Vegetation | Agriculture | Barren |
| 2005 | 84.00                               | 0.80                     | 0.878        | 0.750 | 0.625      | 0.878       | 0.868  |
| 2007 | 88.00                               | 0.85                     | 1.000        | 0.750 | 1.000      | 0.762       | 0.756  |
| 2009 | 88.00                               | 0.85                     | 1.000        | 0.535 | 0.868      | 1.000       | 0.872  |
| 2011 | 88.00                               | 0.85                     | 1.000        | 1.000 | 0.524      | 1.000       | 0.756  |
| 2013 | 84.00                               | 0.80                     | 1.000        | 1.000 | 0.432      | 0.762       | 0.875  |
| 2015 | 78.00                               | 0.72                     | 1.000        | 0.865 | 0.167      | 0.878       | 0.861  |
| 2017 | 92.00                               | 0.90                     | 1.000        | 0.872 | 0.875      | 1.000       | 0.756  |
| 2019 | 96.67                               | 0.96                     | 1.000        | 1.000 | 0.896      | 0.898       | 1.000  |

**Table 4 a** Comparison of areas under different LULC classes from 2005–2019. **b** Land use changes observed from 2005–2019

| (a)          |                                      |                                      |                                    |                                 |                           |                               |
|--------------|--------------------------------------|--------------------------------------|------------------------------------|---------------------------------|---------------------------|-------------------------------|
| Class name   | Area covered (km <sup>2</sup> ) 2005 | Area covered (km <sup>2</sup> ) 2019 | Changes in LULC (km <sup>2</sup> ) | Changed area as % of total area |                           |                               |
| Water bodies | 7.77                                 | 6.62                                 | – 1.15154                          | – 14.812                        |                           |                               |
| Urban        | 104.05                               | 154.39                               | 50.344                             | 48.3849                         |                           |                               |
| Vegetation   | 78.20                                | 67.18                                | – 11.0261                          | – 14.0995                       |                           |                               |
| Agriculture  | 8.12                                 | 3.92                                 | – 4.20397                          | – 51.7477                       |                           |                               |
| Barren       | 88.88                                | 54.92                                | – 33.9548                          | – 38.2042                       |                           |                               |
| (b)          |                                      |                                      |                                    |                                 |                           |                               |
| Class name   | Water bodies (km <sup>2</sup> )      | Urban (km <sup>2</sup> )             | Vegetation (km <sup>2</sup> )      | Agriculture (km <sup>2</sup> )  | Barren (km <sup>2</sup> ) | Total 2019 (km <sup>2</sup> ) |
| Water bodies | 4.779                                | 0.325                                | 0.177                              | 0.105                           | 0.948                     | 6.335                         |
| Urban        | 0.967                                | 90.219                               | 25.885                             | 2.336                           | 35.069                    | 154.475                       |
| Vegetation   | 0.777                                | 10.482                               | 36.168                             | 3.467                           | 16.366                    | 67.26                         |
| Agriculture  | 0.928                                | 0.207                                | 1.246                              | 0.795                           | 0.744                     | 3.92                          |
| Barren       | 0.05                                 | 2.85                                 | 14.814                             | 1.424                           | 35.822                    | 54.959                        |
| Total 2005   | 7.502                                | 104.082                              | 78.289                             | 8.126                           | 88.949                    | 286.95                        |

**Acknowledgements** The authors express sincere gratitude to Bhuvan, an open data platform, and also to USGS Earth Explorer for satellite data which were used in the present study.

## References

1. Fichera CR, Modica G, Pollino M (2012) Land cover classification and change-detection analysis using multi-temporal remote sensed imagery and landscape metrics. *Eur J Remote Sens* 45(1):1–18. <https://doi.org/10.5721/EuJRS20124501>
2. Rwanga SS, Ndambuki JM (2017) Accuracy assessment of land use/land cover classification using remote sensing and GI. *Int J Geosci* 8:611–622
3. Bharatkar<sup>1</sup> PS, Patel R (2013) Approach to accuracy assessment for RS image classification techniques. *Int J Sci Eng Res* 4(12). ISSN 2229-5518
4. Congalton RG (2011) Accuracy assessment and validation of remotely sensed and other spatial information. *Int J Wildland Fire* 10:321–328. <https://doi.org/10.1071/WF01031>
5. Shrivaya S, Sridhar P (2017) Land use and land cover change detection for Delhi region through remote sensing approach. *Int J Sci Res Dev (IJSRD)* 4(11). ISSN (online): 2321-0613

# **Ground Water and Water Quality Models**

# Urbanization Implications on Local Climate and Groundwater Levels Using Index-Based Techniques



V. Shiva Chandra and T. Reshma

**Abstract** Unplanned urbanization and tremendous pressure of increased human activities are often resulting in more stress on urban surface water resources and augmentation of groundwater resources and subsequent dependence on transporting of water from large distances. Our current study aims at determining the impact of spatiotemporal characteristics of urban growth on hydrometeorological parameters in the Northern and Eastern regions of Extended Hyderabad City of the Indian state of Telangana. The rate of change of urbanization is calculated using various indices such as normalized difference built-up index (NDBI), normalized difference vegetation index (NDVI), built-up index (BUI), modified built-up index (MBUI). The spatial distribution of rainfall, temperature, and groundwater levels is determined by using techniques of Inverse distance weighting (IDW). The results reveal an increase of 197 sq.km of the built-up area from 2009–2020 and a considerable increase in the depth to groundwater levels in areas like Nagole, Uppal, Saroor Nagar, Hayatnagar, and LB Nagar. The groundwater table is increased during the monsoon period and decreased in the pre-monsoon period. The maximum depth to groundwater level increased from 15.1 mbgl to 22.8 mbgl during the pre-monsoon period and from 13.5 mbgl to 19 mbgl during the monsoon period under the period of consideration. The maximum temperature increased from 29.2 to 38.7 °C between 2009 and 2020, and annual rainfall has decreased from 936 to 844 mm between 2009–10 and 2019–20. The study reveals that there is a strong correlation between the variables. Correlation between the expansion of the built-up area and population, temperature, rainfall, pre-monsoon groundwater, and post-monsoon groundwater levels is 0.989, 0.867, – 0.900, 0.982, and 0.782, respectively. The study revealed that enormous efforts required in determining the built-up area using conventional supervised classification techniques can be minimized using indices-based techniques.

**Keywords** Urbanization · Spectral indices · Rainfall · Groundwater

---

V. Shiva Chandra (✉) · T. Reshma  
CED, NIT Andhra Pradesh, West Godavari, India

T. Reshma  
e-mail: [reshma@nitandhra.ac.in](mailto:reshma@nitandhra.ac.in)



## 1 Introduction

Rapid urbanization in an unplanned and unsystematic manner can cause profound impacts on the environment, especially toward land and water. Understanding the dynamics of urbanization-induced land cover change at a deeper level is thus necessary for facilitating sustainability as these urban areas are the potential consumer of world energy and leading to severe environmental issues. Urbanization is very critical in India, which contributes nearly 16% of the world's population against a geographical area of 2.5%. India recorded a 3.3% increase in urbanization during 2001–2011 against an increase of 2.1% during 1991–2001 [1]. The urban population of India is projected to be around 600 million by 2031 [3]. Unhealthy living conditions are the outcomes of drastic urbanization, because of changes in land use and land cover [4]. Rapid urbanization and changes in the environment enhance the curiosity of a researcher to know how land use and land covers, temperature, rainfall, and groundwater depths change and how well these changes are related to each other. Many researchers found that anthropogenic activities influence the urban environment considerably, and hence, it attracts greater interest in studying the changes in land use and land cover in urban areas [7, 8]. In addition to changes in the hydrology of the area, the quality and quantity, and recharge of groundwater were impacted adversely due to urbanization [2]. Till now many researchers have concentrated only on examining how the relationships are varying between urbanization and land use land cover, urbanization and temperature, urbanization and groundwater, but there are very few studies on how these all are related to each other. Many researchers depended on supervised classification techniques in the preparation of land use land cover maps, which is time-consuming and the accuracy is user-dependent.

Various indices such as NDBI, BUI, enhanced built-up and Bareness Index (EBBI), normalized difference impervious surface index (NDISI) were proposed by many researchers and proved that the results are satisfactory. The current research attempts to examine the changes in the urban built-up area using various indices and establish the correlation between built-up area, temperature, rainfall, groundwater levels, and population. It is expected the findings of the research would assist in effective decision making for sustainable urban development [5, 6, 9, 10].

## 2 Study Area

Uppal, Ghatkesar (Medchal–Malkajgiri district), Saroor Nagar, and Hayatnagar mandals (Ranga Reddy district) which are adjacent to Hyderabad City (North and Eastern Hyderabad) are selected as the study area. There have been huge developments going on in the above areas as it is most near to the Hyderabad City, and there is a huge increase in the available means of transportation facilities. People can reach the city center within 30 min by METRO, MMTS, RTC, etc. There is a huge increase in the population in these mandals, as most of the people from the

adjoining districts like Warangal and Nalgonda are migrating for higher education and better employment opportunities. This increase in population is causing huge pressure on the existing natural resources in the study area, and one of the Mandal named Uppal is having the highest population density of 19,000 people for one square kilometer. Doubling of the population was observed between 2001–2011, and a further exponential increase is expected shortly. The study area lies between 17°20'41.7" North Latitude and 17°27'17.4" North Latitude and 78°30'57.9" East Longitude and 78°40'51.4" East Longitude (Figs. 1 and 2).

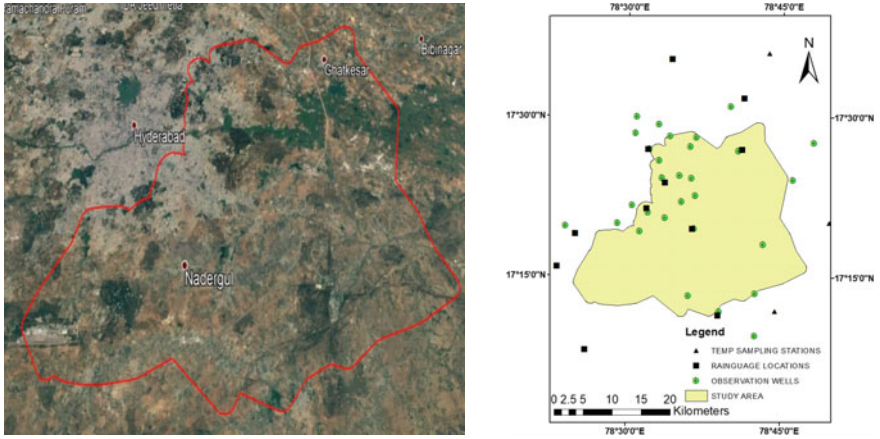


Fig. 1 Google Earth image and map showing observation stations of the study area

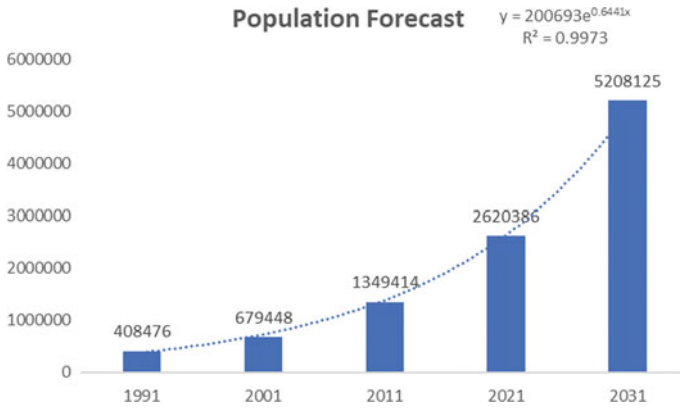


Fig. 2 Forecast of population

**Table 1** Details of satellite imagery

| S. No | Date of Imagery | Source of data  | Spatial Resolution | Path/row |
|-------|-----------------|-----------------|--------------------|----------|
| 1     | 25 March 2009   | Landsat 7, USGS | 30                 | 144/48   |
| 2     | 18 March 2015   | Landsat 8, USGS | 30                 | 144/48   |
| 3     | 31 March 2020   | Landsat 8, USGS | 30                 | 144/48   |

### 3 Data and Methodology

#### 3.1 Data

The following data sets were used in the present study (Table 1).

- Landsat imageries of 30 m resolution were collected from USGS for the years 2009, 2015, 2020
- Data on temperature is taken from the National Aeronautics and Space Administration.
- Rainfall data is collected from the District Collectorate of Ranga Reddy and Medchal–Malkajgiri districts.
- Groundwater data is collected from the Telangana State Ground Water Department and Central Ground Water Department
- Data on population is collected from Census and District Collectorate.

#### 3.2 Methodology

The following indices were calculated from the satellite imageries:

##### 3.2.1 Normalized Difference Vegetation Index

NDVI is the most commonly used vegetation index. It is calculated as below.

$$\text{NDVI} = [\text{NIR} - \text{RED}] / [\text{NIR} + \text{RED}] \quad (1)$$

The values of NDVI range from  $-1$  to  $1$ . The lower values represent water bodies, whereas the higher values represent dense vegetation and tropical forest.

##### 3.2.2 Normalized Difference Built-Up Index

NDBI is used to identify the built-up areas (impervious) from remote sensing satellite images. It is calculated as below.

$$\text{NDBI} = [\text{SWIR} - \text{NIR}] / [\text{SWIR} + \text{NIR}] \quad (2)$$

NDBI values lie between  $-1$  to  $+1$ . The lower value represents water bodies, vegetation, etc., whereas the higher value represents built-up and barren areas.

### 3.2.3 Built-Up Index

Urban pattern is identified by using the built-up index which is calculated as below. A higher positive value indicates a built-up and barren area and thus allows BUI to map the built-up area automatically.

$$\text{BU} = \text{NDBIDVI} \quad (3)$$

### 3.2.4 Modified Normalized Difference Water Index

MNDWI helps in separating water areas and wetlands from built-up areas by suppressing noise from built-up land, vegetation, and soil effectively. It is calculated as below.

$$\text{MNDWI} = [\text{GREEN} - \text{SWIR}] / [\text{GREEN} + \text{SWIR}] \quad (4)$$

### 3.2.5 Modified Built-Up Index

MBUI helps in extracting built-up areas more distinctively by separating it from wetlands and water bodies. It is calculated as the arithmetic difference between BUI and MNDWI.

$$\text{MBUI} = \text{BUI} - \text{MNDWI}. \quad (5)$$

### 3.2.6 Analysis of Hydrometeorological and Hydrogeological Parameters

The impact of changes in the built-up area on spatial and temporal variation of temperature, rainfall, and groundwater levels, is determined by using IDW interpolation tools available in ARC GIS software, and a correlation test is performed to determine the relationship between built-up area, rainfall, temperature, and groundwater levels.

## 4 Interpretation of Results

### 4.1 Analysis of Changes in Built-Up Area

From the study it is observed, there is a considerable increase in the built-up area at the cost of other land-use features such as agriculture land, vegetation, water bodies, and barren lands. The built-up area was 239 km<sup>2</sup> in the year 2009 which increased to 312 km<sup>2</sup> in 2015 and the current built-up area as per 2020 is 436 km<sup>2</sup>. There was an increase of 197 km<sup>2</sup> in the built-up area between 2009 and 2020, and most of the changes are observed in localities like Nagole, Uppal, LB Nagar, and Hayatnagar and along the outer ring road. The accuracy of the work was estimated by selecting hundred pixels randomly from the classified Modified Build-Up index image using Create Accuracy Assessment Points Tool in Arc Map and verified their authenticity by human interpretation of high-resolution imagery available in Google Earth for all the years under consideration. The accuracy was 79%, 72%, 83%, respectively, during 2009, 2015, and 2020. Statistics related to the built-up area are provided in Table 2 (Figs. 3, 4, 5, 6, 7, 8, 9, and 10; Tables 3, 4, and 5).

**Table 2** Details of built-up area

| Year | Total area (km <sup>2</sup> ) | Built-up area (km <sup>2</sup> ) | Percentage (%) |
|------|-------------------------------|----------------------------------|----------------|
| 2009 | 852                           | 239                              | 28             |
| 2015 | 852                           | 312                              | 37             |
| 2020 | 852                           | 436                              | 51             |

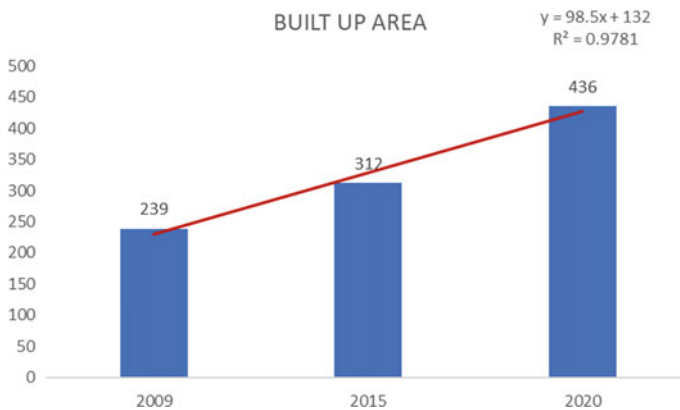


**Fig. 3** Changes in the built-up area in 2009, 2015, 2020

Fig. 4 Built-up area—2009

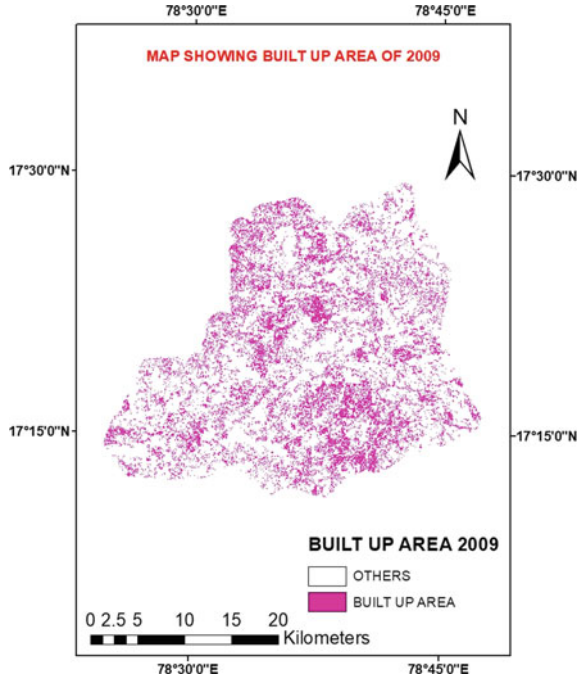


Fig. 5 Built-up area—2015

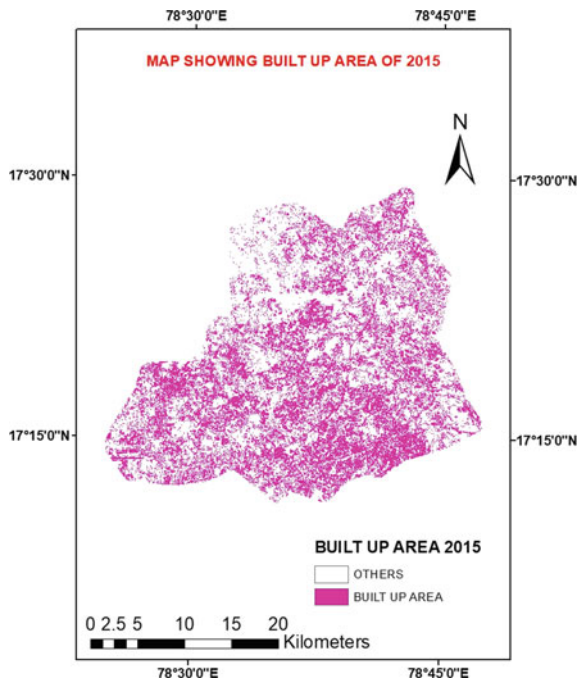
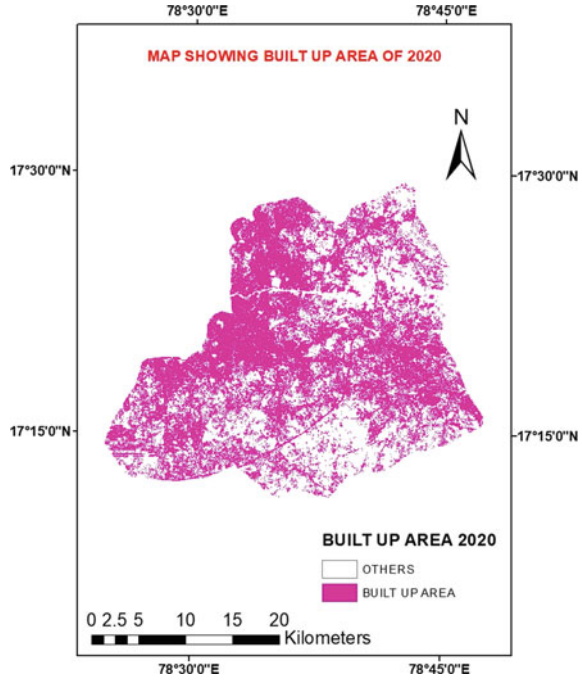


Fig. 6 Built-up area—2020



### 4.2 Spatial and Temporal Distribution of Temperature

The present study reveals that there is a considerable increase in temperature from 2009 to 2020. The average maximum temperature in the study area varies from 27.5 to 29.2 °C in the year 2009. The temperatures were high in the areas like Uppal and LB Nagar when compared to other parts of the study area. In the year 2015, the average maximum temperature varies from 32.12 to 32.92 °C. From the map, it is observed, the temperature is almost the same all across the study area. The temperature has increased by 3 °C from 2009 to 2015. In the year 2020, the average maximum temperature varies from 30.1 to 38.7 °C, a drastic increase in temperatures compared to 2009 and 2015 due to a huge increase in the built-up areas which is also supported by NDBI and BUI Maps. The highest temperatures of 38.7 °C were recorded in the areas like Saroor Nagar, Kothapet where there is a huge increase in the built-up areas due to an increase in commercial establishments, residential activity, and improved transportation facilities like the metro. Spatial variation maps of temperature for the years 2009, 2015, and 2020 are shown in Figs. 12 and 13.

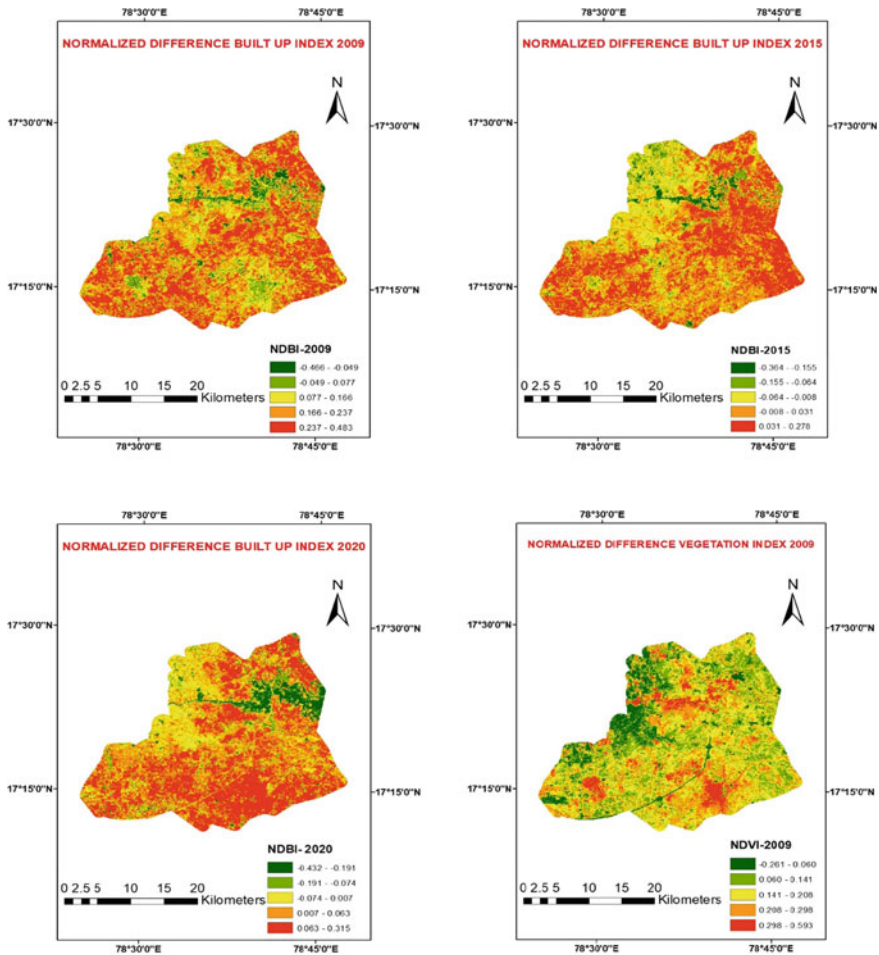


Fig. 7 NDBI and NDVI Maps of the study area of various years

### 4.3 Spatial and Temporal Distribution of Rainfall

Spatial distribution of annual rainfall of 2009, 2015, and 2020 is shown in Figs. 12 and 13. There is a sharp decrease in the amount of rainfall under the period of consideration. The study area recorded maximum rainfall of 936 mm in 2009–10, and it decreased to 884 mm in 2015–16 and further reduced to 844 mm in 2019–20. From the maps, it is observed there is an increase in the amount of rainfall in high-density built-up areas when compared to low-density built-up areas.



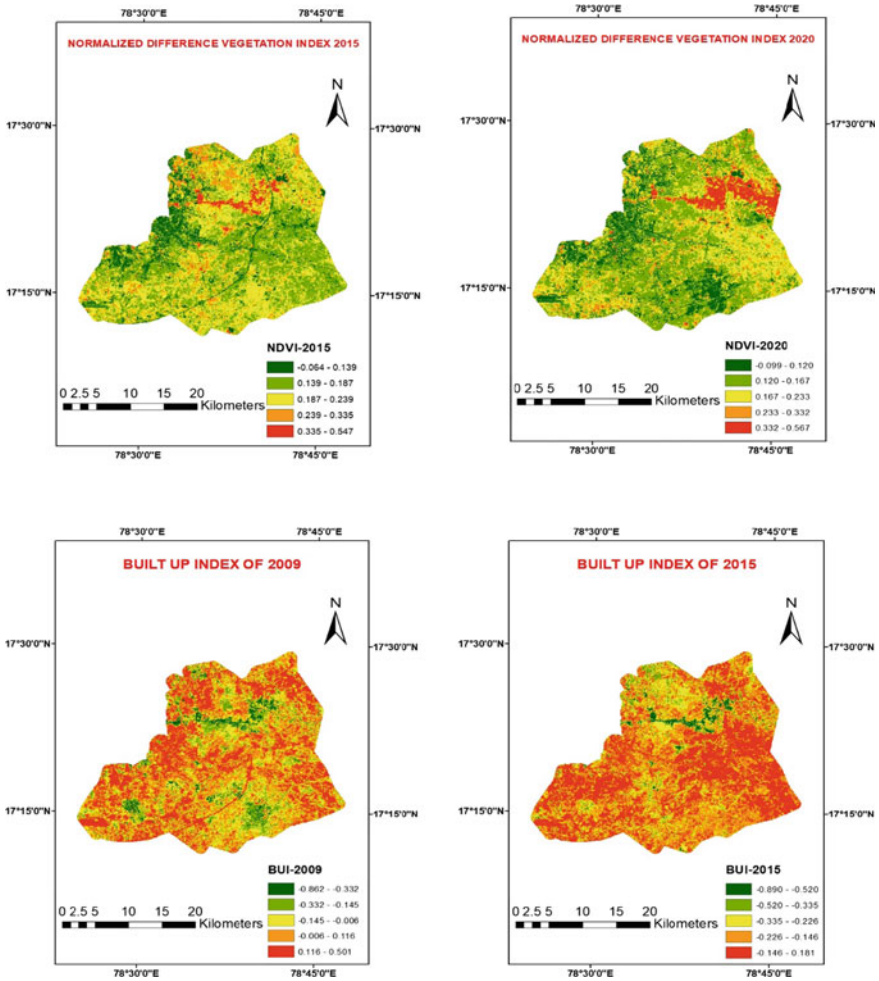
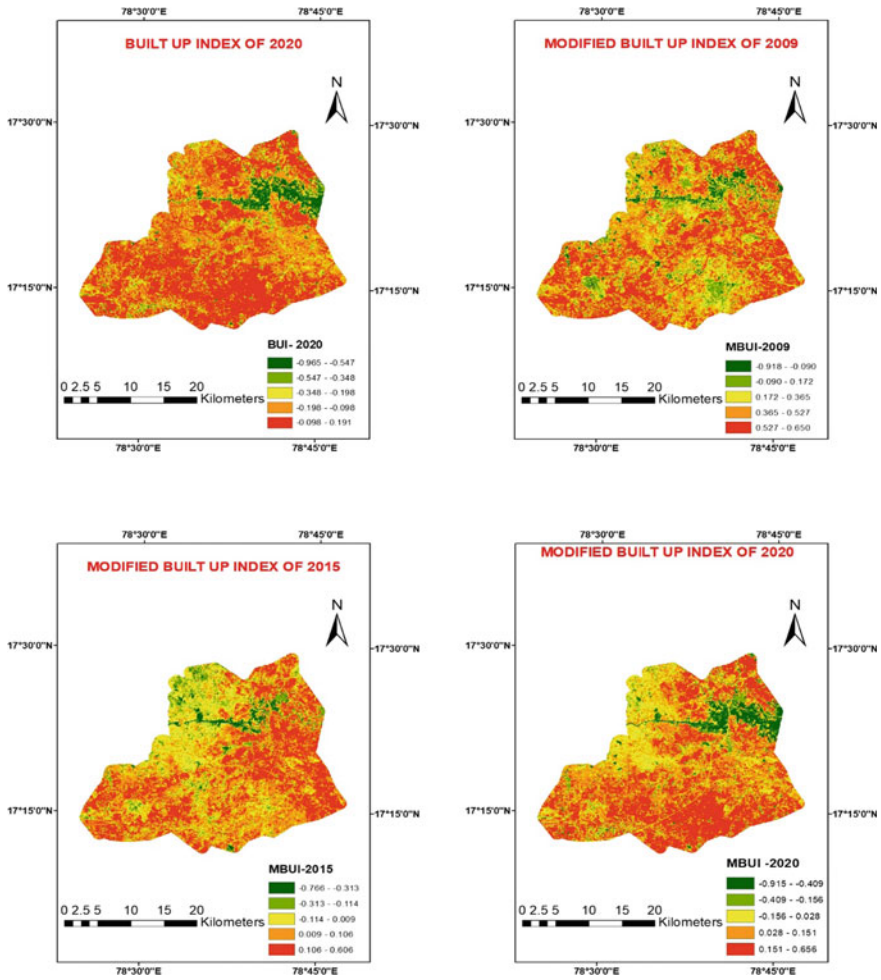


Fig. 8 NDVI and BUI Maps of study area of various years

### 4.4 Spatial and Temporal Distribution of Groundwater Levels

#### 4.4.1 Analysis of Pre-monsoon Groundwater Levels

Groundwater levels decreased radically between 2009–10 and 2019–20. The maximum depth to groundwater level was 15.16 mbgl during 2009–10, and it increased to 19.26 mbgl in 2015–16 and further increased to 22.83 mbgl in 2019–20. The comparison of rainfall versus groundwater levels reveals that there is a drastic decrease in groundwater levels even for almost the same amount of rainfall, which



**Fig. 9** BUI and MBUI Maps of Study area of various years

can be attributed to an increase in the built-up area, runoff, and decrease in infiltration due to concrete cover and increase in exploration of groundwater for the day-to-day needs. The maximum difference between average pre-monsoon and average monsoon groundwater levels was 5.23 m in the year 2016–17. Rainfall was excess in seven years from 2009 to 2020. Areas under different ranges of groundwater depths are shown in Fig. 11 and Table 6.

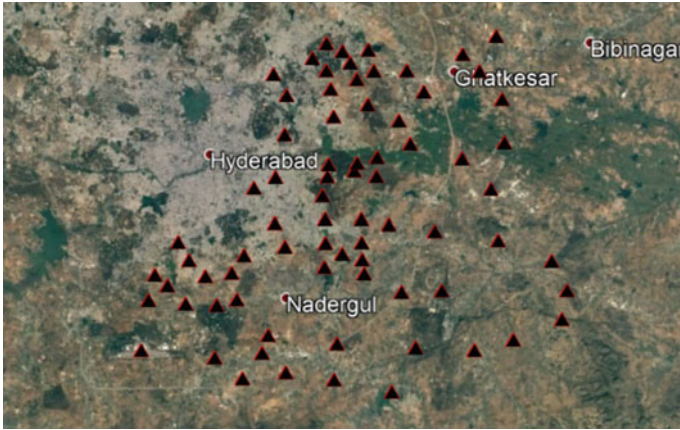


**Fig. 10** Google Earth image overlaid with accuracy assessment points

**Table 3** Statistics of various indices for the year 2009

| Indices    | Max  | Min    | Mean   | SD   |
|------------|------|--------|--------|------|
| NDVI-2009  | 0.59 | - 0.26 | 0.16   | 0.09 |
| NDBI-2009  | 0.48 | - 0.46 | 0.18   | 0.09 |
| BUI-2009   | 0.50 | - 0.86 | 0.01   | 0.15 |
| MNDWI-2009 | 0.56 | 0.52   | - 0.34 | 0.09 |
| MBUI-2009  | 0.65 | - 0.91 | 0.40   | 0.21 |

**Table 4** Statistics of various indices for the year 2015

| Indices    | Max  | Min    | Mean   | SD   |
|------------|------|--------|--------|------|
| NDVI-2015  | 0.54 | - 0.06 | 0.19   | 0.05 |
| NDBI-2015  | 0.27 | - 0.36 | 0.01   | 0.05 |
| BUI-2015   | 0.18 | - 0.89 | - 0.19 | 0.10 |
| MNDWI-2015 | 0.20 | - 0.45 | - 0.21 | 0.05 |
| MBUI-2015  | 0.60 | - 0.76 | 0.02   | 0.13 |

**Table 5** Statistics of various indices for the year 2020

| Indices    | Max  | Min    | Mean   | SD   |
|------------|------|--------|--------|------|
| NDVI-2020  | 0.56 | - 0.09 | 0.17   | 0.07 |
| NDBI-2020  | 0.31 | - 0.43 | 0.01   | 0.09 |
| BUI-2020   | 0.19 | - 0.96 | - 0.15 | 0.15 |
| MNDWI-2020 | 0.31 | 0.46   | - 0.20 | 0.07 |
| MBUI-2020  | 0.65 | - 0.91 | 0.04   | 0.19 |

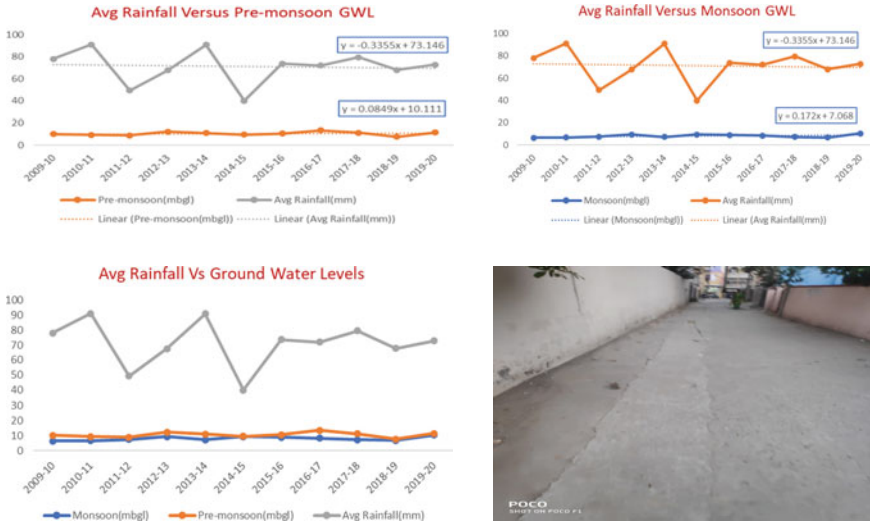


**Fig. 11** Comparison of rainfall versus groundwater levels and image showing concrete cover leaving no scope to infiltration

**Table 6** Area occupied by different groundwater levels (pre-monsoon)

| GWL(m) | 2009–10 |                 | 2015–16 |                 | 2019–20 |                 |
|--------|---------|-----------------|---------|-----------------|---------|-----------------|
|        | Area    | % of total area | Area    | % of total area | Area    | % of total area |
| < 5    | 0       | 0               | 32      | 4               | 12.8    | 1.5             |
| 5–10   | 298.26  | 35              | 320     | 37.5            | 301.4   | 35.2            |
| 10–15  | 553.6   | 64.9            | 410     | 48              | 512     | 60              |
| 15–20  | 0.15    | 0.1             | 90      | 10.5            | 23.2    | 3               |
| > 20   | 0       | 0               | 0       | 0               | 2.6     | 0.3             |

**4.4.2 Analysis of Post-monsoon Groundwater Levels**

Groundwater levels declined from 2009–10 to 2019–20 during post-monsoon. The maximum depth to groundwater level was 13.5 mbgl in 2009–10, and it increased to 19 mbgl in 2015–16 and 2019–20, respectively. However, it is observed that groundwater levels raised by 2 m to 3 m during monsoon. The area under different ranges of groundwater depths is shown Table 7.

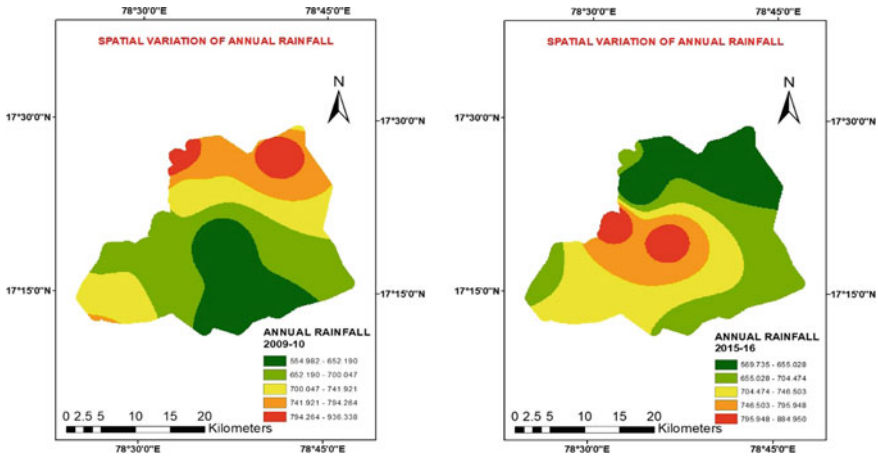


Fig. 12 Maps showing the spatial variation of annual rainfall

#### 4.5 Relationship Between Urbanization and Other Variables

To identify the relationship between the built-up area, population, rainfall, temperature, and groundwater levels, correlation analysis is performed. The rapid increase in the built-up area has led to increased temperatures and a decline in rainfall and groundwater levels. The study reveals that there is a strong correlation between the variables. Correlation between the expansion of built-up area and population, temperature, rainfall, pre-monsoon groundwater, and post-monsoon groundwater levels are 0.989, 0.867,  $-0.900$ , 0.982, and 0.782, respectively (Figs. 12, 13, 14, and 15).

## 5 Conclusions

In the present paper, an attempt has been made to determine the changes in the built-up area and its impact on hydrometeorological and hydrogeological parameters in the study area during 2009 and 2020. The analysis shows an increase of 7% and 14% in the built-up area between 2009 and 2015 and 2015–19, respectively. The increase in the built-up areas has resulted in an increase of maximum and minimum temperature and a subsequent decrease in rainfall in the study area. It is found that, though the decrease in rainfall is less, the change in groundwater levels is more, which can be due to reduced infiltration and increased runoff because of an increase in concrete cover. The method of estimation of the built-up area using various spectral indices is much easier than compared to supervised classification techniques. Comprehensive and strategic planning is the need of the hour for overcoming the consequences of unplanned, unsystematic, and rapid urbanization to

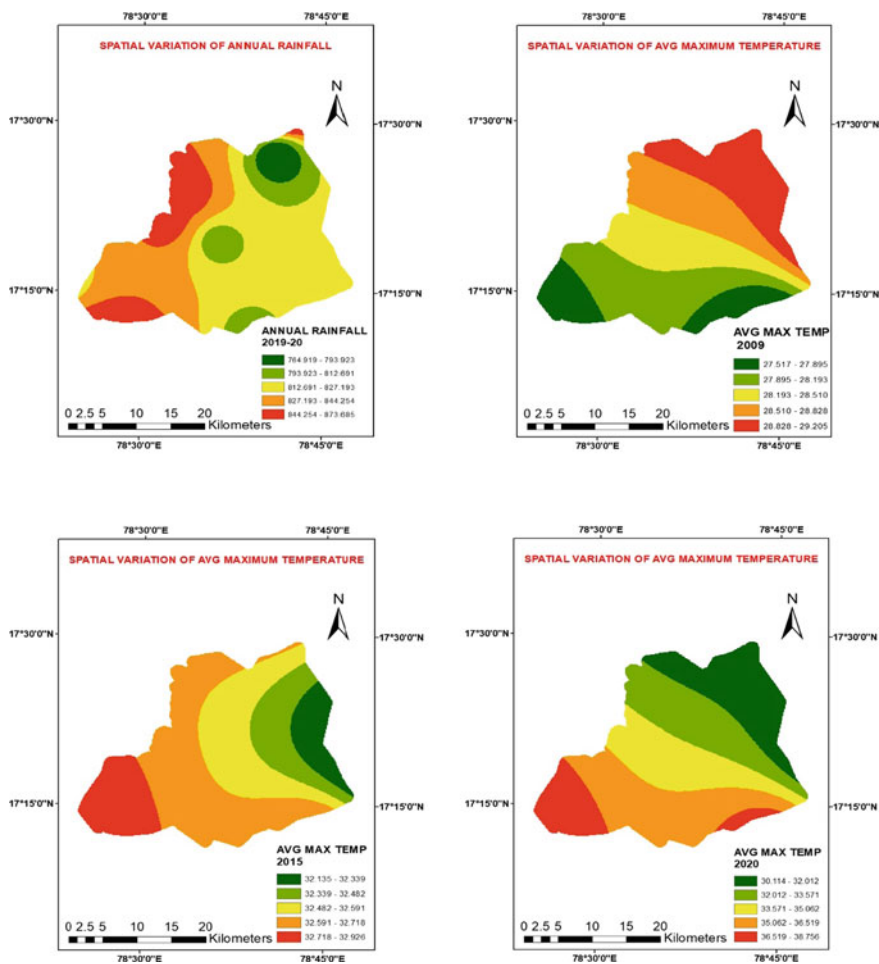


Fig. 13 Maps showing the spatial variation of annual rainfall and avg max temp

Table 7 Area occupied by different groundwater levels (monsoon)

| GWL(m) | 2009–10 |                 | 2015–16 |                 | 2019–20 |                 |
|--------|---------|-----------------|---------|-----------------|---------|-----------------|
|        | Area    | % of Total Area | Area    | % of Total Area | Area    | % of Total Area |
| < 5    | 136     | 16              | 37      | 4.5             | 45.7    | 5.5             |
| 5–10   | 685.6   | 80.5            | 521     | 61              | 358.8   | 42              |
| 10–15  | 30.4    | 3.5             | 265     | 31              | 437.7   | 51.3            |
| 15–20  | 0       | 0               | 29      | 3.5             | 9.8     | 1.2             |
| > 20   | 0       | 0               | 0       | 0               | 0       | 0               |

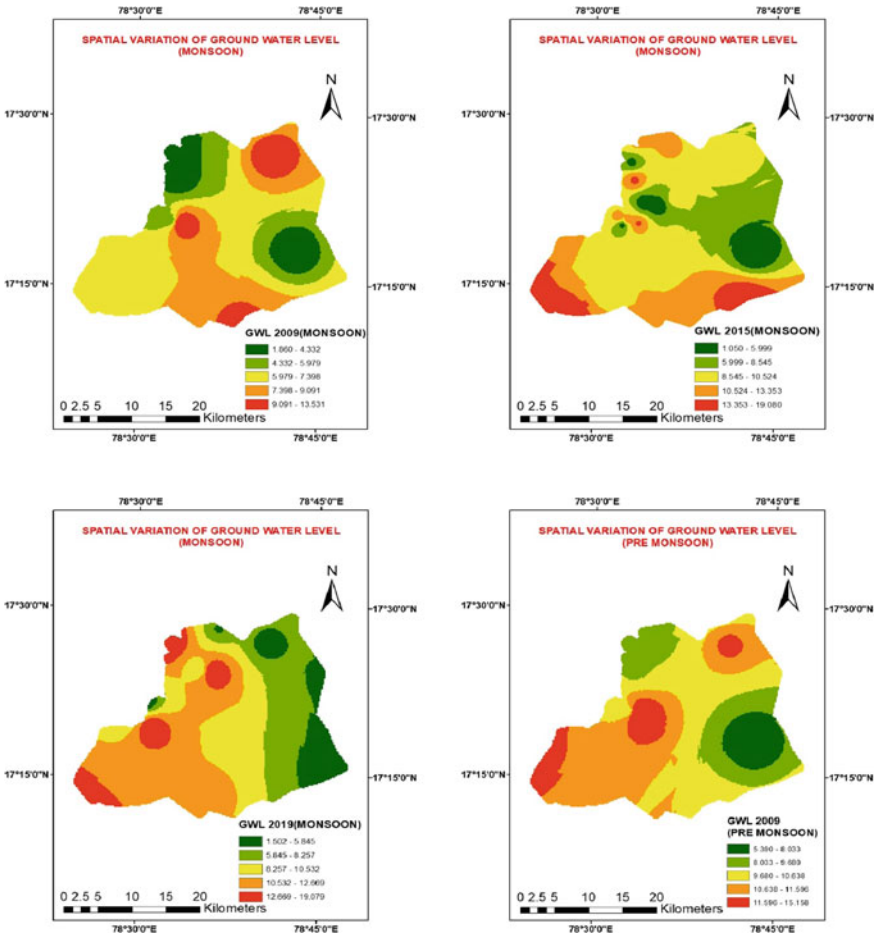


Fig. 14 Maps showing the spatial variation of groundwater levels

realize the sustainable development of cities by conserving natural resources and maintaining better urban health.



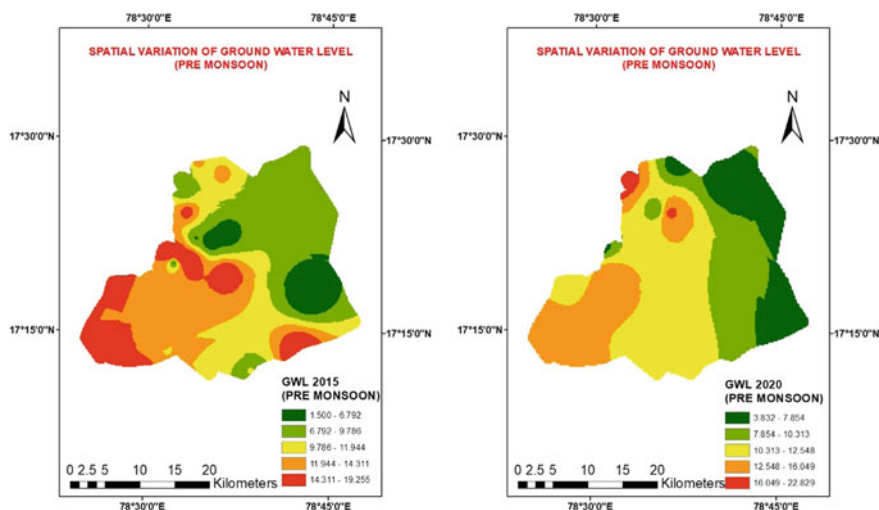


Fig. 15 Maps showing the spatial variation of groundwater levels

**Acknowledgements** The authors express their gratitude to Telangana Ground Water Department and Ranga Reddy District Collectorate for providing data related to Ground Water Levels and Rainfall.

## References

1. Bhagat RB (2011) Emerging pattern of urbanisation in India. *Econ Polit Weekly* 46:10–12
2. Graniel CE, Morris LB, Carrillo-Rivera JJ (1999) Effects of urbanization on groundwater resources of Merida, Yucatan, Mexico. *Environ Geol* 37(4):303–312
3. Heilig GK (2012) World urbanization prospects: the 2011 revision. United Nations. Department of Economic and Social Affairs (DESA), Population Division, Population Estimates and Projections Section, New York
4. Kantakumar LN, Kumar S, Schneider K (2016) Spatiotemporal urban expansion in Pune metropolis, India using remote sensing. *Habitat Int* 51:11–22
5. Lee J, Lee SS, Chi KH (2010) Development of an urban classification method using a built-up index. In: *Proceedings of 6th WSEAS international conference on remote sensing*, pp 39–43
6. Prasomsup W, Piyatadsananon P, Aunphoklang W, Boonrang A (2020) Extraction technic for built-up area classification in landsat 8 imagery. *Int J Environ Sci Dev* 11(1):15–20
7. Shiva Chandra V, Reshma T, Rajkumar (2019) Impact of urbanization on water resource of eastern part of Hyderabad using geomatics. In: *8th APHW international conference on emerging technologies in urban water management organized by IIT Roorkee on 21–23 Nov 2019*, p 49
8. Stow DA, Chen DM (2002) Sensitivity of multitemporal NOAA AVHRR data of an urbanizing region to land-use/land-cover changes and misregistration. *Remote Sens Environ* 80(2):297–307



9. Patra S, Sahoo S, Mishra P, Mahapatra SC (2018) Impacts of urbanization on land use/cover changes and its probable implications on local climate and groundwater level. *J Urban Manag* 7(2):70–84
10. Zha Y, Gao J, Ni S (2003) Use of normalized difference built-up index in automatically mapping urban areas from TM imagery. *Int J Remote Sens* 24(3):583–594

# Seasonal Groundwater Table Depth Prediction Using Fuzzy Logic and Artificial Neural Network in Gangetic Plain, India



Kusum Pandey and Anurag Malik

**Abstract** Modelling and forecasting of groundwater level fluctuation are essential for sustaining groundwater availability. Therefore, it is necessary to carry out mechanisms and methods that can predict the groundwater level precisely. This study investigates the comparative potential of FL (Fuzzy Logic) and ANN (Artificial Neural Network) to predict the seasonal groundwater table depth (GWTD) between the Ganga and Hindon rivers area located in Uttar Pradesh State, India. The groundwater recharge (GWR), groundwater discharge (GWD), and the antecedent groundwater level data of 21-years (1994–2014) have been utilized to formulate 18 models (nine for pre-monsoon, and nine for post-monsoon) for training and testing of FL and ANN techniques. The outcomes of FL-based models were evaluated against the ANN models based on performance indicators and graphical inspection for the prediction of seasonal GWTD. The comparison of results reveals that the FL-based models performed better than the ANN models during both seasons for GWTD prediction in the study region. The results derived from this study would help the hydrologists and policymakers to formulate a better plan of action for governance under extreme conditions and conservation of groundwater resources in the study region.

**Keywords** Groundwater table · Fuzzy logic · Uttar Pradesh

## 1 Introduction

Groundwater is the prime source of water for drinking, irrigation, and industrial use in many countries [1]. In the last two decades, groundwater depletion has become very rapid in many regions that affect the groundwater storage and groundwater levels and resulting in water scarcity and groundwater contamination [2, 3]. Hence,

---

K. Pandey

Department of Soil and Water Engineering, Punjab Agricultural University, Ludhiana 141004, Punjab, India

A. Malik (✉)

Punjab Agricultural University, Regional Research Station, Bathinda 151001, Punjab, India

the knowledge about groundwater table fluctuations is very important for optimal utilization and management of groundwater resources [4, 5]. The conceptual and physical-based models are typically the key methods for groundwater simulation; but they have certain limitations, which includes a large set of data requirement, detailed knowledge about the study area, its boundary conditions, physical characteristics, and input specification, which are not generally available [6]. In this context, precise predictions are more significant than knowing the fundamental mechanisms, so, the soft computing techniques prove as an effective alternative [7, 4, 8, 9].

In recent time, soft computing (SC) techniques (i.e. artificial neural network: ANN, support vector machine: SVM, FL, genetic algorithm: GA, adaptive neuro-fuzzy inference system: ANFIS, radial basis function network: RBFN, co-active neuro-fuzzy inference system: CANFIS, etc.) have been successfully exploited in water resources engineering [10–22]. Also, several effective applications of SC methods have been found in groundwater modelling [23–30].

To date, few studies have explored the potential of SC models in groundwater quality modelling [2, 31–33]. Gong et al. [34] analysed the predictive ability of SVM, ANN, and ANFIS to predict the groundwater fluctuation near Lake Okeechobee in Florida, USA. They found that SVM and ANFIS models provided more precise outcomes than the ANN model. Yu et al. [35] forecasted groundwater depth in the Ejina Basin (China), for one, two, and three months lead times by employing the ANN, SVR (support vector regression), W-ANN (Wavelet-ANN), and W-SVR models. They found the superior performance of the SVR model than the other models for all time scales. Nadiri et al. [29] applied three models of FL (i.e. Larsen, Sugeno, and Mamdani) and three multiple models of these with simple averaging, weighted averaging, and committee machine techniques implemented with ANN to predict the groundwater levels in the Duzduzan-Bilverdi area of Iran. They found that the multiple models improve the prediction performance than the other models in the study region.

Pradhan et al. [36] studied the comparative performance of the CANFIS, FL, and RBFN to predict the fluctuations of groundwater table depth in the lower Ganga-Ramganga inter-basin (India). They found that the FL-based models outperformed the other models. Rajasekhar et al. [37] examined the feasibility of FL, analytical hierarchy process (AHP), and Fuzzy-AHP (F-AHP) models for groundwater mapping in Anantapur district of Andhra Pradesh (India), and they concluded that the F-AHP model was best for estimating the groundwater potential in the study region. Banadkooki et al. [24] forecasted the groundwater level in Iran by using the genetic programming (GP), and the hybrid of whale optimization algorithm (WOA) embedded the multilayer perception (WOA-MLP) and radial basis function (WOA-RBF). They found that the WOA-MLP model outperformed the other models. Jha et al. [2] assessed groundwater quality on spatio-temporal scales during pre- and post-monsoon seasons in Tiruchirappalli district of Tamil Nadu State (India) by employing the hybrid FL-GIS-based GQI (Fuzzy Logic-Geographical Information System-based Groundwater Quality Index). The results of the analysis demonstrate the better feasibility of the hybrid FL-GIS-based GQI model for assessing the suitability of groundwater for drinking purposes in both seasons.

The main objective of this study was to inspect the predictive efficacy of FL (fuzzy logic) and ANN (artificial neural network) for predicting seasonal groundwater table depth in the area between the Ganga-Hindon rivers. The predicted models were compared with the observed values of GWTD by using performance indicators and through graphical inspection.

## 2 Materials and Methods

### 2.1 Study Region and Data

The study region lies between the Ganga-Hindon rivers basin consisting of an alluvial shelter of Gangetic plain covering an area of approximately 563,647 ha with varying elevations from 215 to 273 m above the MSL (mean sea level). The study zone located in the latitude of 28° 66' N and 29° 92' N and longitude of 77° 46' E and 78° 02' E comprising of 24-blocks, i.e. 12-blocks of Meerut district (Sardhana, Rohta, Daurala, Mawana, Meerut, Janikurd, Saroorpur, Paricchitgarh, Hastinapur, Rajpura, Kharkhoda, Macchra), 3-blocks of Saharanpur district (Baliakheri, Nagal, Deoband), 6-blocks of Muzaffarnagar district (Charthawal, Purkaji, Muzaffarnagar, Shahpur, Jansath, Khatauli), and 3 blocks of Ghaziabad district (Muradnagar, Razapur, Bhojpur) of Uttar Pradesh State, India (Fig. 1). The annual rainfall ranges from 933 to 1204 mm with a sub-tropical climate over the study region.

The 21-years (1994–2014) daily rainfall data were acquired from the headquarters of Nazarat district, whereas pre- and post-monsoon groundwater depth were obtained from the department of groundwater Uttar Pradesh (India) for the same period. The statistical data, i.e. minor irrigation structures information, minor and major crops occupied area, minor irrigation structures irrigated area, livestock, and human population were seeking from the respective district statistical departments. These statistical data were utilized to calculate the net groundwater recharge (GWR) and net groundwater discharge (GWD) in the study area by using Eqs. (1) and (2) given by the Ministry of Water Resources, India [38]:

$$GWR = R_R + R_{SC} + R_{RFIW} + R_{GIA} + R_{ISR} + R_{STP} \tag{1}$$

$$GWD = E_{ESR} + O_{GOA} + ET_{GR} + T_{GPW} \tag{2}$$

In which,  $R_R$  = recharge due to rainfall,  $R_{SC}$  = recharge due to seepage from canals,  $R_{RFIW}$  = recharge due to return flow of irrigation water,  $R_{GIA}$  = groundwater inflow into the zone,  $R_{ISR}$  = influent seepage from rivers,  $R_{STP}$  = recharge because of seepage from tanks and ponds,  $E_{ESR}$  = effluent seepage to rivers,  $O_{GOA}$  = groundwater outflow from the extent,  $ET_{GR}$  = evapotranspiration loss from groundwater reservoir, and  $T_{GPW}$  = groundwater pumpage through wells.

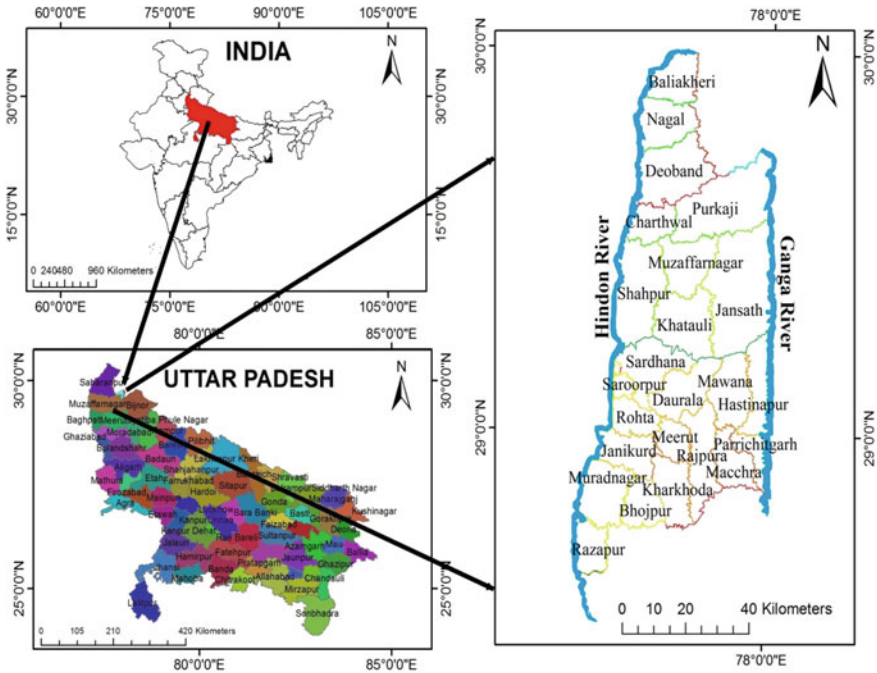


Fig. 1 Location map of the study area

### 2.2 Fuzzy Logic (FL)

In this study, the complete FL exercise was carried out using MATLAB R2018a software. The Mamdani-type (M-type) fuzzy inference system (FIS) was applied to process the training and testing datasets. The structure of M-type FL is presented in Fig. 2. The methodology of FIS is as follows: first, the fuzzification system transforms crisp input to fuzzy with the help of the membership functions (MFs). The selection of MFs depends on the availability of input data and user-defined. In the present, the trapezoidal and triangular MFs are selected to define both input and output variables, because they are simple to use, computationally efficient, and their ability to represent ambiguities and uncertainties and widely used in literature [39]. Figure 3 illustrates the MFs for the input and output variables. Second, the formulations of fuzzy rule, which define the relationship between MFs and combining the fuzzified inputs using fuzzy rules and output membership function. Fuzzy rules are constructed using linguistic variables and based on the status of indicators in each component. The number of fuzzy rules in a system depends on the possibility of combinations of all possible states of the input variables. The input and output variables were divided into nine different subsets, i.e. very extremely low (VEL), extremely low (EL), very low (VL), low (L), medium (M), high (H), very high (VH), extremely high (EH) and very extremely high (VEH). These fuzzy rules are stated

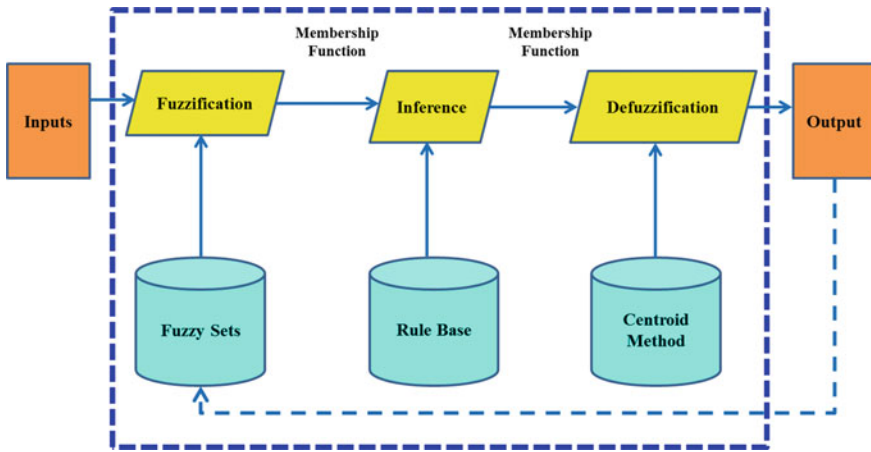


Fig. 2 Architecture of Mamdani-type FL

in the IF–THEN format [40, 41] and given in Table 1. Finally, defuzzification of output distribution giving crisp output. The CENTROID defuzzification technique was presumed to defuzzify the fuzzy sets. The final output ( $FL_{out}$ ) was determined using the following equation [29]:

$$FL_{out} = \frac{\sum_{i=1}^n w_i \overline{FL}}{\sum_{i=1}^n w_i} \tag{3}$$

where  $w_i$  = weight of the  $i$ th rule, and  $\overline{FL}$  = output of the  $i$ th rule.

### 2.3 Artificial Neural Network (ANN)

The ANN is analogous to the biological nervous system, comprising of an immensely parallel-distributed system made up of huge interlinked neural computing elements that possess the capability to learn the entire system [42]. The MLP neural network was utilized to predict the seasonal GWTD, comprises an input layer, a single hidden layer, and an output layer in this study. The input signal passed from input nodes to the output nodes through the hidden nodes only in the forward direction, which helps to accomplish useful intermediary computations. The whole network of MLP was built by logistic sigmoid transfer function and Levenberg–Marquardt training algorithm with a hit-and-trail procedure for finding the optimal number of neurons for the hidden layer [43, 44].

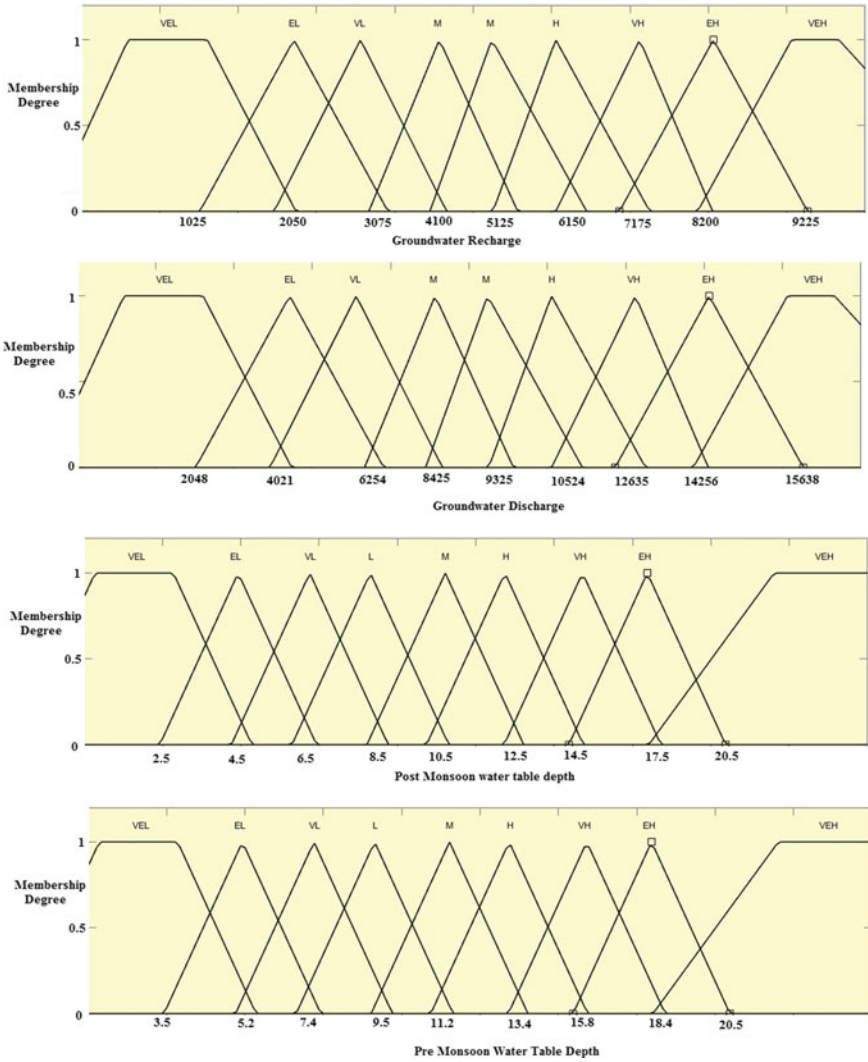


Fig. 3 Membership functions for the input and output variables

### 2.4 Development and Evaluation of Models

For the prediction of pre-monsoon (Pr) and post-monsoon (Ps) seasons GWTD, the input series of the time lagged groundwater recharge (GWR), groundwater discharge (GWD), and groundwater table depth (GWTD) were arranged in eighteen combinations (i–ix for pre-monsoon and x–xviii for post-monsoon): (i) GWR ( $n - 1$ ) GWD ( $n - 1$ ) GWTD Pr ( $n - 1$ ), (ii) GWR ( $n - 1$ ) GWD ( $n - 1$ ) GWTD Pr ( $n - 1$ ) GWTD Ps ( $n - 1$ ), (iii) GWR ( $n - 1$ ) GWD ( $n - 1$ )  $\Delta$ GWTD(Pr–Ps) ( $n - 1$ ), (iv)

**Table 1** Fuzzy rule for the developed FL models

| IF recharge | And discharge | And post-monsoon groundwater table | THEN pre-monsoon groundwater table |
|-------------|---------------|------------------------------------|------------------------------------|
| L           | L             | L                                  | VL                                 |
| L           | VL            | M                                  | L                                  |
| L           | VL            | EL                                 | L                                  |
| VEL         | L             | M                                  | VL                                 |
| VL          | M             | VL                                 | VL                                 |
| M           | VEL           | M                                  | M                                  |
| L           | H             | EL                                 | M                                  |
| L           | M             | H                                  | M                                  |
| H           | L             | M                                  | M                                  |
| L           | H             | H                                  | H                                  |
| H           | EH            | H                                  | H                                  |
| H           | M             | H                                  | H                                  |
| M           | M             | H                                  | M                                  |
| H           | VH            | H                                  | H                                  |
| VH          | H             | VH                                 | VH                                 |
| EH          | H             | H                                  | VH                                 |
| VH          | H             | VH                                 | VH                                 |
| VEH         | EH            | H                                  | EH                                 |
| H           | VEH           | H                                  | EH                                 |
| EH          | VH            | VEH                                | VEH                                |

Note L Low, M Medium, H High, VL Very Low, VH Very High, EH Extremely High, EL Extremely Low, VEH Very Extremely High, VEL Very Extremely Low

GWR  $(n - 1)(n - 2)$  GWD  $(n - 1)(n - 2)$  GWTD Pr  $(n - 2)$ , (v) GWR  $(n - 1)(n - 2)$  GWD  $(n - 1)(n - 2)$  GWTD Pr  $(n - 2)$  GWTD Ps  $(n - 2)$  GWTD Pr  $(n - 1)$  GWTD Ps  $(n - 1)$ , (vi) GWR  $(n - 1)(n - 2)$  GWD  $(n - 1)(n - 2)$   $\Delta$ GWTD (Pr-Ps)  $(n - 1)$   $\Delta$ GWTD (Pr-Ps)  $(n - 2)$   $\Delta$ GWTD (Pr-Ps)  $(n - 1)$ , (vii) GWR  $(n - 1)(n - 2)(n - 3)$  GWD  $(n - 1)(n - 2)(n - 3)$  GWTD Pr  $(n - 3)$ , (viii) GWR  $(n - 1)(n - 2)(n - 3)$  GWD  $(n - 1)(n - 2)(n - 3)$  GWTD Pr  $(n - 3)$  GWTD Ps  $(n - 3)$  GWTD Pr  $(n - 2)$  GWTD Ps  $(n - 2)$  GWTD Pr  $(n - 1)$  GWTD Ps  $(n - 1)$ , (ix) GWR  $(n - 1)(n - 2)(n - 3)$  GWD  $(n - 1)(n - 2)(n - 3)$  WT(Pr-Ps)  $(n - 3)$   $\Delta$ GWTD (Pr-Ps)  $(n - 2)$   $\Delta$ GWTD(Pr-Ps)  $(n - 1)$ , (x) GWR  $(n - 1)$  GWD  $(n - 1)$  GWTD Ps  $(n - 1)$ , (xi) GWR  $(n - 1)$  GWD  $(n - 1)$  GWTD Ps  $(n - 1)$  GWTD Pr  $(n)$ , (xii) GWR  $(n - 1)$  GWD  $(n - 1)$   $\Delta$  GWTD (Ps-Pr)  $(n - 1)$ , (xiii) GWR  $(n - 1)(n - 2)$  GWD  $(n - 1)(n - 2)$  GWTD Ps  $(n - 2)$  (xiv) GWR  $(n - 1)(n - 2)$  GWD  $(n - 1)(n - 2)$  GWTD Ps  $(n - 2)$  GWTD Pr  $(n - 1)$  GWTD Ps  $(n - 1)$  GWTD Pr  $(n)$ , (xv) GWR  $(n)$   $(n - 1)(n - 2)$  GWD  $(n)$   $(n - 1)(n - 2)$   $\Delta$ GWTD (Ps-Pr)  $(n - 2)$   $\Delta$ GWTD (Pr-Ps)  $(n - 1)$   $\Delta$ GWTD (Ps-Pr)  $(n)$ , (xvi) GWR  $(n)$   $(n - 1)(n - 2)(n - 3)$  GWD  $(n)$   $(n - 1)(n -$



2)(n - 3) GWTD Ps (n - 3), (xvii) GWR(n) (n - 1)(n - 2)(n - 3) GWD(n) (n - 1)(n - 2)(n - 3) GWTD Ps (n - 3), GWTD Pr (n - 2) GWTD Ps (n - 2) GWTD Pr (n - 1) GWTD Ps (n - 1) GWTD Pr (n), (xviii) GWR(n) (n - 1)(n - 2)(n - 3) GWD(n) (n - 1)(n - 2)(n - 3) ΔGWTD (Ps-Pr) (n - 3) ΔGWTD (Pr-Ps)(n - 2) ΔGWTD (Ps-Pr) (n - 1) ΔGWTD (Pr-Ps) (n - 1) ΔGWTD(Ps-Pr)(n).

These developed models were skilled by FL and ANN algorithms with a dataset from 1994–2008 for training and 2009–2014 for testing in MATLAB R2018a environment. The predictive efficacy of these developed models was assessed through six statistical indicators viz. R<sup>2</sup> (coefficient of determination), CE (coefficient of efficiency), MAD (mean absolute deviation), RMSE (root mean square error), CVRE (coefficient of variation of error residuals), and APE (absolute prediction error). The R<sup>2</sup>, CE, MAD, RMSE, CVRE, and APE are defined as:

$$R^2 = \left\{ \frac{\sum_{i=1}^n (O_{GWTD,i} - \overline{O_{GWTD}})(P_{GWTD,i} - \overline{P_{GWTD}})}{\left[ \sum_{i=1}^n (O_{GWTD,i} - \overline{O_{GWTD}})^2 \right]^{0.5} \left[ \sum_{i=1}^n (P_{GWTD,i} - \overline{P_{GWTD}})^2 \right]^{0.5}} \right\}^2 \tag{4}$$

$$CE = 1 - \frac{\sum_{i=1}^n (O_{GWTD,i} - P_{GWTD,i})^2}{\sum_{i=1}^n (O_{GWTD,i} - \overline{O_{GWTD}})^2} \tag{5}$$

$$MAD = \frac{1}{n} \sum_{i=1}^n |P_{GWTD,i} - O_{GWTD,i}| \tag{6}$$

$$RMSE = \sqrt{\frac{1}{n} \sum_{i=1}^n (P_{GWTD,i} - O_{GWTD,i})^2} \tag{7}$$

$$CVRE = \frac{1}{\overline{O_{GWTD}}} \sqrt{\frac{\sum_{i=1}^n (P_{GWTD,i} - O_{GWTD,i})^2}{n}} \tag{8}$$

$$APE = \frac{\sum_{i=1}^n |O_{GWTD,i} - P_{GWTD,i}|}{\sum_{i=1}^n O_{GWTD,i}} \tag{9}$$

where  $O_{GWTD,i}$  = observed GWTD values,  $P_{GWTD,i}$  = predicted GWTD values,  $n$  = number of data points,  $\overline{O_{GWTD}}$  = average of observed GWTD values,  $\overline{P_{GWTD}}$  = average of predicted GWTD values.

### 3 Results and Discussions

#### 3.1 Prediction GWTD Using FL and ANN Methods

The M-type FIS was set in MATLAB R2018a using fuzzy logic toolbox with the help of three input parameters, i.e. GWR, GWD, and antecedent groundwater table depth to predict the current GWTD (i.e. output). Table 2 outlines the values of performance indicators for both seasons (i.e. pre- and post-monsoon) in the testing period. It was noted from Table 2 that the FL-8 and FL-17 models were found to be better for both seasons. In addition, the FL-8 model had maximum value of  $R^2 = 0.95$ , and CE = 0.94, and minimum value of MAD = 0.79, RMSE = 1.20, CVRE = 0.13, and APE = 0.08 during pre-monsoon season, while in post-monsoon season FL-17 model had maximum value of  $R^2 = 0.95$ , and CE = 0.95, and minimum value of MAD = 0.76, RMSE = 1.09, CVRE = 0.13, and APE = 0.09, respectively. Therefore, the FL-8 and FL-17 models were chosen the best to forecast the pre- and post-monsoon GWTD in the study area. Figures 4a-i and 5a-i shows the distribution of observed versus

**Table 2** Performance indicators values of FL models for pre- and post-monsoon seasons during the testing period

| Model               | $R^2$ | CE   | MAD  | RMSE | CVRE | APE  |
|---------------------|-------|------|------|------|------|------|
| <i>Pre-monsoon</i>  |       |      |      |      |      |      |
| FL-1                | 0.86  | 0.86 | 1.05 | 1.87 | 0.19 | 0.37 |
| FL-2                | 0.73  | 0.41 | 2.95 | 3.82 | 0.41 | 0.32 |
| FL-3                | 0.91  | 0.91 | 0.99 | 1.53 | 0.16 | 0.11 |
| FL-4                | 0.82  | 0.81 | 1.24 | 2.14 | 0.23 | 0.13 |
| FL-5                | 0.53  | 0.08 | 4.01 | 5.17 | 0.55 | 0.43 |
| FL-6                | 0.33  | 0.29 | 4.24 | 5.64 | 0.61 | 0.45 |
| FL-7                | 0.73  | 0.73 | 1.61 | 2.58 | 0.27 | 0.17 |
| FL-8                | 0.95  | 0.94 | 0.79 | 1.20 | 0.13 | 0.08 |
| FL-9                | 0.51  | 0.51 | 2.71 | 3.49 | 0.37 | 0.28 |
| <i>Post-monsoon</i> |       |      |      |      |      |      |
| FL-10               | 0.91  | 0.91 | 1.02 | 1.49 | 0.17 | 0.12 |
| FL-11               | 0.94  | 0.94 | 0.91 | 1.18 | 0.14 | 0.11 |
| FL-12               | 0.13  | 0.90 | 3.63 | 4.65 | 0.54 | 0.42 |
| FL-13               | 0.81  | 0.81 | 1.19 | 2.14 | 0.24 | 0.14 |
| FL-14               | 0.94  | 0.93 | 0.91 | 1.26 | 0.14 | 0.15 |
| FL-15               | 0.47  | 0.99 | 4.18 | 5.18 | 0.59 | 0.48 |
| FL-16               | 0.80  | 0.81 | 1.45 | 2.18 | 0.25 | 0.17 |
| FL-17               | 0.95  | 0.95 | 0.76 | 1.09 | 0.13 | 0.09 |
| FL-18               | 0.10  | 0.09 | 3.79 | 4.66 | 0.54 | 0.44 |

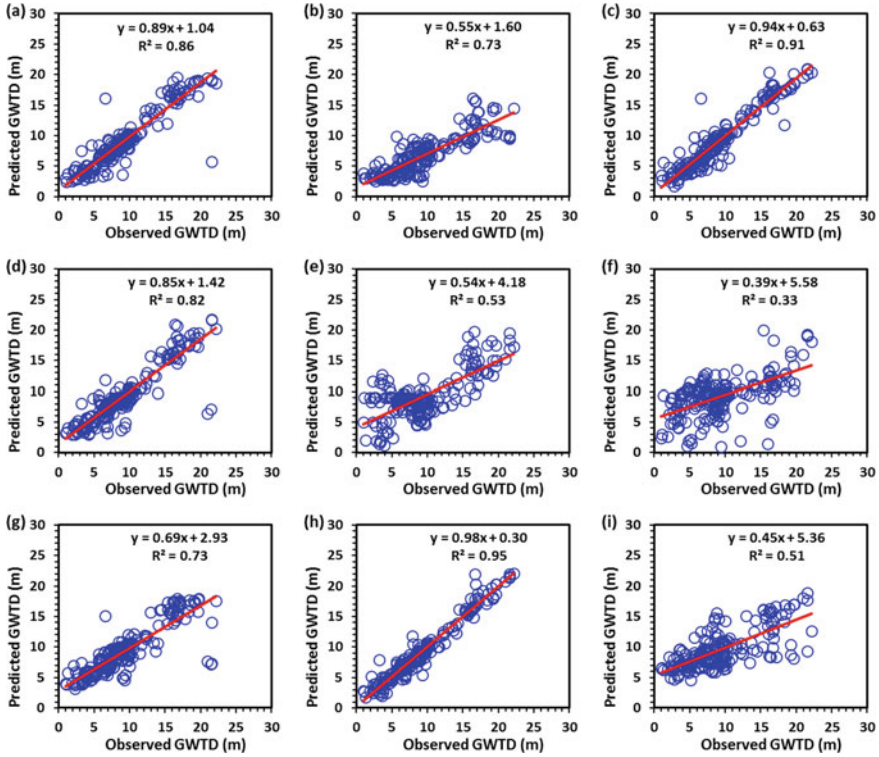


**Fig. 4** Scatter plot of observed vs predicted GWTD values by **a** FL-1, **b** FL-2, **c** FL-3, **d** FL-4, **e** FL-5, **f** FL-6, **g** FL-7, **h** FL-8, and **i** FL-9 models for pre-monsoon season in the testing period

predicted GWTD values yielded by FL-1 to FL-18 models in pre- and post-monsoon seasons.

Similarly, the ANN model was organized in MATLAB R2018a with the help of a formulated combination of different inputs as listed earlier (Sect. 2.4). For the testing period, the value of performance indicators of ANN models for pre- and post-monsoon seasons are mention in Table 3, which shows that the performance of ANN-8 and ANN-17 were found to be better in both seasons. The values of  $R^2$  and CE for the ANN-8 (8-9-1) were 0.90, and 0.93, and MAD, RMSE (m), CVRE, and APE were 0.96, 1.54, 0.16, and 0.10 in the pre-monsoon season during testing, while for the post-monsoon season the values of  $R^2$  and CE for the ANN-17 (8-9-1) were 0.94, and 0.94, and MAD, RMSE (m), CVRE and APE were 0.91, 1.24, 0.14 and 0.10, respectively. Figures 6a–i and 7a–i demonstrates the scatter plots among the observed and predicted values of GWTD during pre- and post-monsoon seasons of ANN-1 to ANN-18 models in the testing period, respectively.

Finally, the overall outcomes of the study support the application of the fuzzy logic technique for monthly groundwater table depth prediction in the Ganga-Hindon rivers area in pre- and post-monsoon seasons with varying input variables.

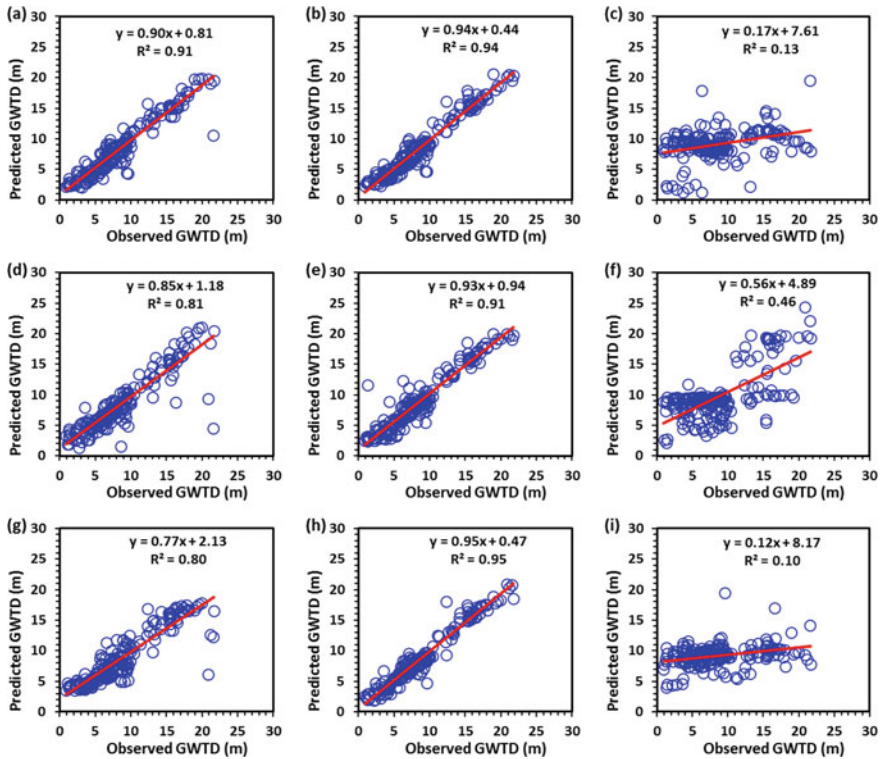


**Fig. 5** Scatter plot of observed vs predicted GWTD values by **a** FL-10, **b** FL-11, **c** FL-12, **d** FL-13, **e** FL-14, **f** FL-15, **g** FL-16, **h** FL-17, and **i** FL-18 models for post-monsoon season in the testing period

## 4 Conclusion

The current study investigates the comparative potential of fuzzy logic (FL) and artificial neural network (ANN) models to predict the seasonal GWTD in the area between the Ganga-Hindon rivers in Uttar Pradesh, India. The feasibility of developed models was assessed based on six performance indicators along with the visual inspection. The results of the quantitative and qualitative analysis showed that the performance of ANN and FL-based models were found to be acceptable, whereas the FL rule-based models outperformed the ANN models. In addition, the input combination 8 and 17 correspondings to FL-8 and FL-17 were found optimal for predicting the seasonal groundwater depth in the study region. Furthermore, it was noted that the maximum number of input variables increased the prediction accuracy. Thus, the outcomes of this study would help the researches for modelling groundwater level in data scarce conditions for optimal utilization of groundwater resources.

**Table 3** Performance indicators values of ANN models for pre- and post-monsoon seasons during the testing period

| Model               | Structure | $R^2$ | CE   | MAD  | RMSE | CVRE | APE  |
|---------------------|-----------|-------|------|------|------|------|------|
| <i>Pre-monsoon</i>  |           |       |      |      |      |      |      |
| ANN-1               | 3-4-1     | 0.86  | 0.86 | 1.05 | 1.84 | 0.19 | 0.11 |
| ANN-2               | 4-6-1     | 0.89  | 0.89 | 0.89 | 1.58 | 0.17 | 0.09 |
| ANN-3               | 3-5-1     | 0.04  | 0.04 | 3.84 | 4.86 | 0.52 | 0.41 |
| ANN-4               | 3-6-1     | 0.79  | 0.79 | 1.4  | 2.29 | 0.24 | 0.15 |
| ANN-5               | 6-7-1     | 0.87  | 0.87 | 1.03 | 1.78 | 0.19 | 0.11 |
| ANN-6               | 5-8-1     | 0.08  | 0.50 | 3.76 | 4.74 | 0.51 | 0.40 |
| ANN-7               | 3-6-1     | 0.72  | 0.72 | 1.64 | 2.64 | 0.28 | 0.18 |
| ANN-8               | 8-9-1     | 0.90  | 0.90 | 0.96 | 1.54 | 0.16 | 0.10 |
| ANN-9               | 7-8-1     | 0.47  | 0.47 | 2.73 | 3.60 | 0.38 | 0.29 |
| <i>Post-monsoon</i> |           |       |      |      |      |      |      |
| ANN-10              | 3-7-1     | 0.89  | 0.88 | 0.98 | 1.56 | 0.18 | 0.11 |
| ANN-11              | 4-7-1     | 0.93  | 0.93 | 0.92 | 1.25 | 0.14 | 0.11 |
| ANN-12              | 3-8-1     | 0.05  | 0.05 | 3.80 | 4.79 | 0.03 | 0.44 |
| ANN-13              | 3-6-1     | 0.81  | 0.81 | 1.29 | 2.14 | 0.25 | 0.15 |
| ANN-14              | 6-8-1     | 0.90  | 0.89 | 0.96 | 1.56 | 0.18 | 0.11 |
| ANN-15              | 5-12-1    | 0.07  | 0.07 | 3.79 | 4.76 | 0.55 | 0.44 |
| ANN-16              | 3-7-1     | 0.77  | 0.77 | 1.42 | 2.34 | 0.27 | 0.16 |
| ANN-17              | 8-9-1     | 0.94  | 0.94 | 0.91 | 1.24 | 0.14 | 0.10 |
| ANN-18              | 7-8-1     | 0.13  | 0.13 | 3.68 | 4.56 | 0.52 | 0.42 |

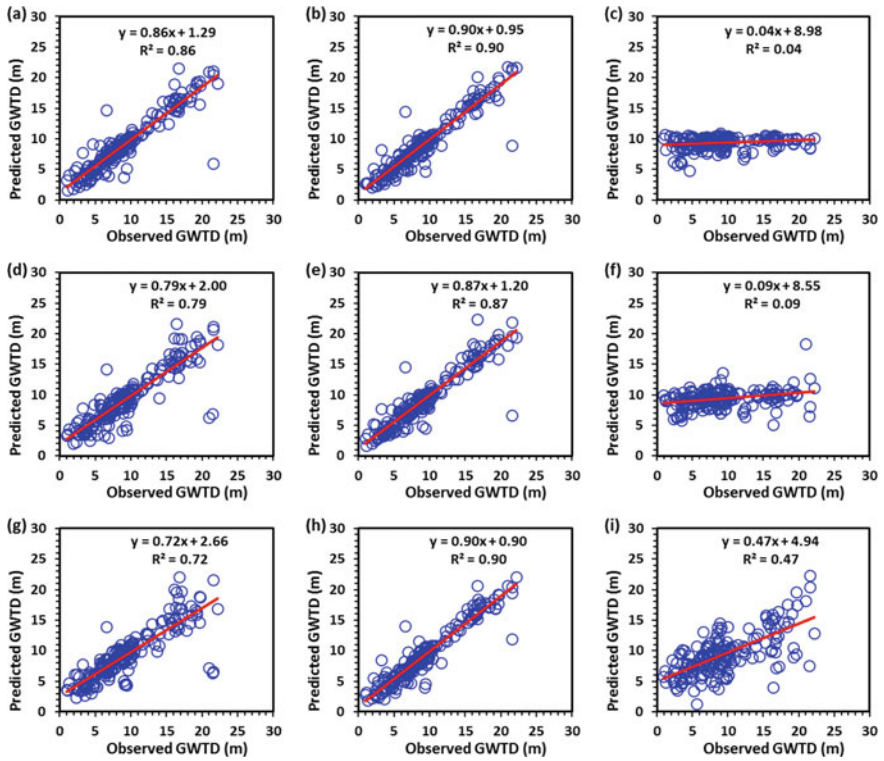


**Fig. 6** Scatter plot of observed vs predicted GWTD values by **a** ANN-1, **b** ANN-2, **c** ANN-3, **d** ANN-4, **e** ANN-5, **f** ANN-6, **g** ANN-7, **h** ANN-8, and **i** ANN-9 models for pre-monsoon season in the testing period

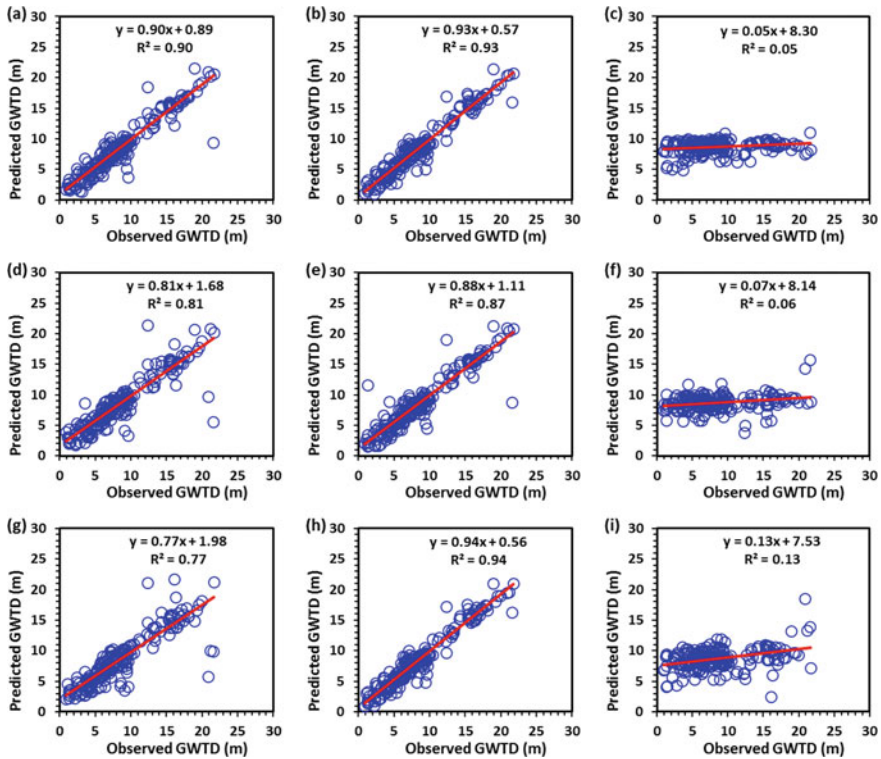


**Fig. 7** Scatter plot of observed vs predicted GWTD values by **a** ANN-10, **b** ANN-11, **c** ANN-12, **d** ANN-13, **e** ANN-14, **f** ANN-15, **g** ANN-16, **h** ANN-17, and **i** ANN-18 models for post-monsoon season in the testing period

## References

1. Mohamed A, Dan L, Kai S et al (2019) Hydrochemical analysis and fuzzy logic method for evaluation of groundwater quality in the North Chengdu Plain, China. *Int J Environ Res Public Health* 16:302. <https://doi.org/10.3390/ijerph16030302>
2. Jha MK, Shekhar A, Jenifer MA (2020) Assessing groundwater quality for drinking water supply using hybrid fuzzy-GIS-based water quality index. *Water Res* 179:115867. <https://doi.org/10.1016/j.watres.2020.115867>
3. Theodoridou PG, Varouchakis EA, Karatzas GP (2017) Spatial analysis of groundwater levels using Fuzzy logic and geostatistical tools. *J Hydrol* 555:242–252. <https://doi.org/10.1016/j.jhydrol.2017.10.027>
4. Di Nunno F, Granata F (2020) Groundwater level prediction in Apulia region (Southern Italy) using NARX neural network. *Environ Res* 190:110062. <https://doi.org/10.1016/j.envres.2020.110062>
5. Zhang J, Zhu Y, Zhang X et al (2018) Developing a long short-term memory (LSTM) based model for predicting water table depth in agricultural areas. *J Hydrol* 561:918–929. <https://doi.org/10.1016/j.jhydrol.2018.04.065>
6. De Filippis G, Margiotta S, Caruso F, Negri SL (2020) Open questions about the hydrodynamic behaviour of the deep, coastal aquifer of the Salento peninsula (south-eastern Italy): coupling



- expert knowledge, data, and numerical modelling for testing hydrogeological conceptual models. *Sci Total Environ* 715:136962. <https://doi.org/10.1016/j.scitotenv.2020.136962>
7. Chang J, Wang G, Mao T (2015) Simulation and prediction of suprapermafrost groundwater level variation in response to climate change using a neural network model. *J Hydrol* 529:1211–1220. <https://doi.org/10.1016/j.jhydrol.2015.09.038>
  8. Panahi M, Sadhasivam N, Pourghasemi HR, et al (2020) Spatial prediction of groundwater potential mapping based on convolutional neural network (CNN) and support vector regression (SVR). *J Hydrol* 588:125033. <https://doi.org/10.1016/j.jhydrol.2020.125033>
  9. Shiri J, Kisi O, Yoon H et al (2020) Prediction of groundwater level variations in coastal aquifers with tide and rainfall effects using heuristic data driven models. *ISH J Hydraul Eng* 26:1–11. <https://doi.org/10.1080/09715010.2020.1729876>
  10. Elbeltagi A, Deng J, Wang K, et al (2020) Modeling long-term dynamics of crop evapotranspiration using deep learning in a semi-arid environment. *Agric Water Manag* 241:106334. <https://doi.org/10.1016/j.agwat.2020.106334>
  11. Malik A, Kumar A (2015) Pan evaporation simulation based on daily meteorological data using soft computing techniques and multiple linear regression. *Water Resour Manag* 29:1859–1872. <https://doi.org/10.1007/s11269-015-0915-0>
  12. Malik A, Kumar A (2020) Meteorological drought prediction using heuristic approaches based on effective drought index: a case study in Uttarakhand. *Arab J Geosci* 13:1–17. <https://doi.org/10.1007/s12517-020-5239-6>
  13. Malik A, Kumar A, Ghorbani MA et al (2019) The viability of co-active fuzzy inference system model for monthly reference evapotranspiration estimation: case study of Uttarakhand State. *Hydrol Res* 50:1623–1644. <https://doi.org/10.2166/nh.2019.059>
  14. Malik A, Kumar A, Kisi O (2018) Daily pan evaporation estimation using heuristic methods with Gamma test. *J Irrig Drain Eng* 144:04018023. [https://doi.org/10.1061/\(ASCE\)IR.1943-4774.0001336](https://doi.org/10.1061/(ASCE)IR.1943-4774.0001336)
  15. Malik A, Kumar A, Kisi O, Shiri J (2019) Evaluating the performance of four different heuristic approaches with Gamma test for daily suspended sediment concentration modeling. *Environ Sci Pollut Res* 26:22670–22687. <https://doi.org/10.1007/s11356-019-05553-9>
  16. Malik A, Kumar A, Piri J (2017) Daily suspended sediment concentration simulation using hydrological data of Pranhita River Basin, India. *Comput Electron Agric* 138:20–28. <https://doi.org/10.1016/j.compag.2017.04.005>
  17. Malik A, Kumar A, Salih SQ, et al (2020a) Drought index prediction using advanced fuzzy logic model: Regional case study over Kumaon in India. *PLoS One* 15:e0233280. <https://doi.org/10.1371/journal.pone.0233280>
  18. Malik A, Kumar A, Singh RP (2019) Application of heuristic approaches for prediction of hydrological drought using multi-scalar streamflow drought index. *Water Resour Manag* 33:3985–4006. <https://doi.org/10.1007/s11269-019-02350-4>
  19. Malik A, Rai P, Heddarn S et al (2020) Pan evaporation estimation in Uttarakhand and Uttar Pradesh states, India: validity of an Integrative data intelligence model. *Atmosphere (Basel)* 11:1–26. <https://doi.org/10.3390/atmos11060553>
  20. Malik A, Tikhamarine Y, Souag-Gamane D et al (2020) Support vector regression optimized by meta-heuristic algorithms for daily streamflow prediction. *Stoch Environ Res Risk Assess.* <https://doi.org/10.1007/s00477-020-01874-1>
  21. Singh A, Malik A, Kumar A, Kisi O (2018) Rainfall-runoff modeling in hilly watershed using heuristic approaches with gamma test. *Arab J Geosci* 11:1–12. <https://doi.org/10.1007/s12517-018-3614-3>
  22. Tikhamarine Y, Malik A, Kumar A et al (2019) Estimation of monthly reference evapotranspiration using novel hybrid machine learning approaches. *Hydrol Sci J* 64:1824–1842. <https://doi.org/10.1080/02626667.2019.1678750>
  23. Adamowski J, Chan HF (2011) A wavelet neural network conjunction model for groundwater level forecasting. *J Hydrol* 407:28–40. <https://doi.org/10.1016/j.jhydrol.2011.06.013>
  24. Banadkooki FB, Ehteram M, Ahmed AN et al (2020) enhancement of groundwater-level prediction using an integrated machine learning model optimized by whale algorithm. *Nat Resour Res* 29:3233–3252. <https://doi.org/10.1007/s11053-020-09634-2>



25. Khedri A, Kalantari N, Vadiati M (2020) Comparison study of artificial intelligence method for short term groundwater level prediction in the northeast Gachsaran unconfined aquifer. *Water Suppl* 20:909–921. <https://doi.org/10.2166/ws.2020.015>
26. Malekzadeh M, Kardar S, Saeb K et al (2019) a novel approach for prediction of monthly ground water level using a hybrid wavelet and non-tuned self-adaptive machine learning model. *Water Resour Manag* 33:1609–1628. <https://doi.org/10.1007/s11269-019-2193-8>
27. Mohanty S, Jha MK, Kumar A, Sudheer KP (2010) Artificial neural network modeling for groundwater level forecasting in a river island of eastern India. *Water Resour Manag* 24:1845–1865. <https://doi.org/10.1007/s11269-009-9527-x>
28. Mohanty S, Jha MK, Raul SK et al (2015) Using artificial neural network approach for simultaneous forecasting of weekly groundwater levels at multiple sites. *Water Resour Manag* 29:5521–5532. <https://doi.org/10.1007/s11269-015-1132-6>
29. Nadiri AA, Naderi K, Khatibi R, Gharekhan M (2019) Modelling groundwater level variations by learning from multiple models using fuzzy logic. *Hydrol Sci J* 64:210–226. <https://doi.org/10.1080/02626667.2018.1554940>
30. Natarajan N, Sudheer C (2020) Groundwater level forecasting using soft computing techniques. *Neural Comput Appl* 32:7691–7708. <https://doi.org/10.1007/s00521-019-04234-5>
31. Maroufpoor S, Jalali M, Nikmehr S et al (2020) Modeling groundwater quality by using hybrid intelligent and geostatistical methods. *Environ Sci Pollut Res* 27:28183–28197. <https://doi.org/10.1007/s11356-020-09188-z>
32. Norouzi H, Moghaddam AA (2020) Groundwater quality assessment using random forest method based on groundwater quality indices (case study: Miandoab plain aquifer, NW of Iran). *Arab J Geosci*. <https://doi.org/10.1007/s12517-020-05904-8>
33. Shwetank S, Chaudhary JK (2020) A comparative study of fuzzy logic and WQI for groundwater quality assessment. *Procedia Comput Sci* 171:1194–1203. <https://doi.org/10.1016/j.procs.2020.04.128>
34. Gong Y, Zhang Y, Lan S, Wang H (2016) A comparative study of artificial neural networks, support vector machines and adaptive neuro fuzzy inference system for forecasting groundwater levels near Lake Okeechobee, Florida. *Water Resour Manag* 30:375–391. <https://doi.org/10.1007/s11269-015-1167-8>
35. Yu H, Wen X, Feng Q et al (2018) comparative study of hybrid-wavelet artificial intelligence models for monthly groundwater depth forecasting in extreme arid regions, Northwest China. *Water Resour Manag* 32:301–323. <https://doi.org/10.1007/s11269-017-1811-6>
36. Pradhan S, Kumar S, Kumar Y, Sharma HC (2019) Assessment of groundwater utilization status and prediction of water table depth using different heuristic models in an Indian interbasin. *Soft Comput* 23:10261–10285. <https://doi.org/10.1007/s00500-018-3580-4>
37. Rajasekhar M, Sudarsana Raju G, Sreenivasulu Y, Siddi Raju R (2019) Delineation of groundwater potential zones in semi-arid region of Jilledubanderu river basin, Anantapur District, Andhra Pradesh, India using fuzzy logic, AHP and integrated fuzzy-AHP approaches. *HydroResearch* 2:97–108. <https://doi.org/10.1016/j.hydres.2019.11.006>
38. MWRI (2009) Report of the ground water resource estimation committee. *Minist Water Resour New Delhi, India*, p 133
39. Zadeh LA (1965) Fuzzy sets. *Inf. Control* 8:338–353. [https://doi.org/10.1016/S0019-9958\(65\)90241-X](https://doi.org/10.1016/S0019-9958(65)90241-X)
40. Chen M-S, Wang S-W (1999) Fuzzy clustering analysis for optimizing fuzzy membership functions. *Fuzzy Sets Syst* 103:239–254. [https://doi.org/10.1016/S0165-0114\(98\)00224-3](https://doi.org/10.1016/S0165-0114(98)00224-3)
41. Chiu SL (1994) Fuzzy Model Identification Based on Cluster Estimation. *J Intell Fuzzy Syst* 2:267–278. <https://doi.org/10.3233/IFS-1994-2306>
42. Haykin S (1999) *Neural networks-a comprehensive foundation* (2nd eds.) London. Prentice-Hall, Up Saddle River, NJ 26–32
43. Daliakopoulos IN, Coulibaly P, Tsanis IK (2005) Groundwater level forecasting using artificial neural networks. *J Hydrol* 309:229–240. <https://doi.org/10.1016/j.jhydrol.2004.12.001>
44. Dawson CW, Wilby RL (2001) Hydrological modelling using artificial neural networks. *Prog Phys Geogr Earth Environ* 25:80–108. <https://doi.org/10.1177/030913330102500104>

# An Identification of Suitable Location to Construct Underground Sump for Rooftop Rainwater Harvesting in the Campus of Debre Tabor University



G. Venkata Ramana, Ch.V. S. S. Sudheer, and R. Suresh Kumar

**Abstract** Many centralized water supply schemes with advanced technologies came by replacing rainwater harvesting. It is the process of collecting, preserving and diverting of rainwater collected for irrigation, household activities and other uses in both large and small scales. Besides, several advantages are noticed from harvesting of rainwater such as increase in groundwater levels, reduction of salt accumulation in the soil, off-site flooding, supply of water to crops during deficiency and erosion. Even though the limitations of rainwater harvesting are a very few, which can be met with a proper design and planning rainwater may be captured by adopting many different methods, of which the most common practice is that rainwater falling on roofs of houses and other buildings is collected through a system of pipes and semicircular channels (artificial) made of galvanized iron, PVC or concrete and is stored in tanks suitably located on the ground or underground. This practice is at the development phase at individual household level for hilly areas with high rainfall and also in some semi-arid areas in the plains where the scheme of water supply is intermittent or insufficient to meet the daily demands for public. Dimensions of storage tank were mainly influenced by the parameters like rainfall, temperature, population, type of usage and its corresponding demands, time period for supplying of water without rainfall, etc. and sociological parameters. Authors were mainly focused to convey the importance of rainwater harvesting at Debre Tabor University (DTU), Debre Tabor, Ethiopia. DTU is located in the heart of Debre Tabor town with a main motto to provide research-oriented and transfer of innovative technologies for the students. Study area is located at an elevation of 2700 m above mean sea level, with an average annual rainfall of 1250–1400 mm. It may be noted that a difference of only 400–450 mm depth of rainfall between dry and wet seasons. As mentioned earlier, rainfall is one of the most influencing factors to fix the capacity of storage tank; therefore, rainfall data of the study area was taken and forecasted for 20 years using Thomas–Fiering model. On the other hand, demands and total quantity of water collected from

---

G. V. Ramana (✉)

Aurora's Technological and Management Academy, Moula-Ali, Hyderabad, Telangana, India

Ch.V. S. S. Sudheer · R. Suresh Kumar

Department of Civil Engineering, Institute of Aeronautical Engineering, Dundigal, Hyderabad, Telangana 500043, India

all the tops of roofs were also estimated manually to fix the capacity of storage tank. Therefore, based on the forecasted data of rainfall and total demand calculations a storage tank is provided with a capacity of 0.77 m<sup>3</sup> which acts as supplementary source for the improved living at DTU.

**Keywords** Rainwater harvesting · Thomas–Fiering model · Intermittent water supply · Synthetic flow data · Probabilistic modelling

## 1 Introduction to Rainwater Harvesting (RWH)

Water is one of man’s basic and precious resources. Harvested rainwater plays an important role in various phases like a source for drinking, landscape watering and for agricultural activities. Water-harvesting is the process of capturing the rainwater, diversion, and storage of the same rainwater for various purposes. It is an effective and economical tool for the conservation of the water. This practice is most suitable for the places, where groundwater is limited, the problems of seawater intrusion are observed, topography of land is uneven or rugged for smooth distribution of water, etc.

On the other hand, at a very small scale the process of capturing the rainwater shall be applied even at a very small scale such as in schools, public parks, offices; due to reason that it is a low-cost technique and requires a basic expertise [1]. The application of rainwater harvesting spreads across the globe and is widely used both rural and urban areas of many countries like China, Germany, Sri Lanka, Singapore, Thailand and Tokyo [2]. In a broad view, there are various methods for collecting the rainwater as shown in Fig. 1.

A brief description of microcatchments and macrocatchments is discussed below.

- **On farm systems**—In this type of catchments, the rainwater will be collected from a small catchment of an area approximately 1000 sq. m. Following are the various types of on farm systems which are widely adopted like contour ridges, semicircular and trapezoidal bunds, small pits, small run-off basins, run-off strips, inter-row systems, Meskat system and contour bench terraces.

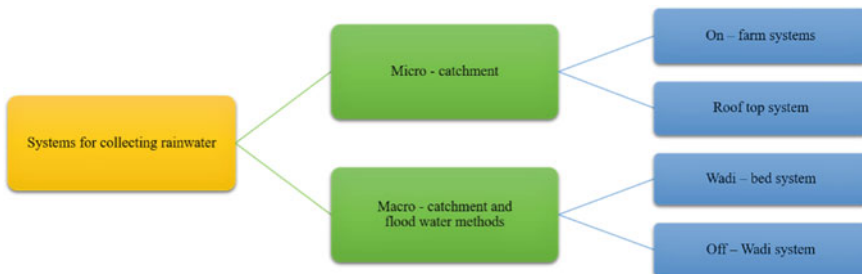


**Fig. 1** Methods involving the collection of rainwater

- **Rooftop systems**—A general and common way for collecting the rainwater from the roof of the houses or large buildings through gutters shall be collected in a small artificial reservoir. The collected water is thus purified according to its usage and gets distributed for various activities.
- **Wadi-bed systems**—In this type of catchments, the surface run-off water is collected from relatively large catchments or a mountainous region. These catchments have a capacity to capture the run-off ranging from very low to 75% of annual rainfall in the catchment. Therefore, in steeped areas these types of catchments shall also be called as floodwater—harvesting systems. Wadi, an Arabic term which represents a valley. Following are different types of Wadi-bed systems like small farm reservoirs, Wadi-bed cultivation and Jessour.
- **Off-Wadi systems**—In this system, the rainwater harvesting in the above system (Wadi-bed system) is applied outside by the construction of suitable structures for the conservation of water. Following are various types of off-Wadi bed systems like water-spreading systems, large bunds, tanks and Hafair, cisterns and hill side—run-off systems.

The choice of selecting the choosing the suitable system of rainwater harvesting mainly depends on [3, 4].

- The topographical condition of the study area.
- Soil characteristics, occurrence of rainfall.
- Nature of lands (dry or wet).
- Improper management of land use and land cover (LU & LC).
- Type of roofs for buildings in case of rooftop rainwater harvesting and
- Availability of groundwater below the earth surface, etc.
- Of all the different methods which were discussed above, authors choose rooftop rainwater harvesting techniques for the conservation of rainwater due to the following observations. [5].
- The study area lies in mountainous region at an elevation of 2700 m approximately above mean sea level (MSL).
- Occurrence of rainfall is high during the months of May to August of every year.
- Roofs of the buildings are sloped for the easy collection of rainwater, and all the roofs are properly connected to artificial channels through gutters which were shown in Fig. 2.
- Availability of groundwater is at greater depths (approximately 150–175 m) rather than shallow depths, therefore making it costlier for the extraction of groundwater. Therefore, authors suggested the officials of university for the construction of storage tank at a depth of 4–5 m, as it was more economical rather than artificial recharge of groundwater.
- Rainwater is a clean, salt-free source of water for plants. Therefore, the treatment of rainwater collected is not required. Also, it is not strongly endorsed for drinking purposes instead it shall be used for various uses such as landscaping, washing of clothes and flushing of toilets.
- Therefore, by considering all the above-said advantages, authors proposed the officials to construct a conservation tank for collecting rainwater.



**Fig. 2** Various buildings in study area with sloped roof and suitably connected to channels with pipes to conserve rainwater

### ***1.1 Generation of Synthetic Flow Data***

Stochastic hydrology is the statistical branch of hydrology that deals with the probabilistic modelling of those hydrological processes which have random components associated with them [6]. Models to generate stochastic monthly streamflow data can be applied to generate monthly rainfall data. Applications of stochastic hydrology can be broadly expanded to numerous fields such as designing of hydraulic structures, estimation of missing data, operational forecasting's and complex system operations. Numerous time series modelling approaches have been adopted by various hydrologists depending on type and quantum of historic data for future forecasting. Basically, two models were developed, namely one for rainfall and the other for potential evapotranspiration (PET) for the generation of rainfall data and PET sequences at a larger scale [7]. Monthly rainfall data is highly useful for the process of simulation to forecast the future data. The process involving the forecasting of the future data is an important and challenging task for many of hydrologists nowadays. In view of water resources system design, several models were existing stochastic hydrology was first implemented by Thomas & Fiering in 1962. This model uses a monthly time series model in combination with Monte Carlo techniques to generate synthetic streamflow data. In this research, authors used the concept of Thomas & Fiering model for the generation of rainfall data [8].

### ***1.2 Justification for Hydrological Modelling***

The forecasting of data based on historical values is having a great significance in planning and designing of any hydraulic structure. In the current situations,

most of the hydrologic systems are complex due to the association of mathematical techniques and the presence of constraints. Following are the main reasons for hydrological modelling [9].

- Generalization of data is very much required for understanding the behaviour of system.
- Modelling the hydrological data supports to gain a knowledge of various hydrological parameters and their influence in the system.
- The chances for the generation of synthetic data of historical hydrological data shall be enhanced. Therefore, by the consideration of the above benefits, hydrological modelling of data was implemented in this research.

## 2 Objectives

The main objectives of this research include:

- To determine the total demand of water for the students of Debre Tabor University (DTU) in order to meet their daily demands.
- To estimate the total volume of water can be collected from various blocks of the university through rooftops.
- To forecast the rainfall data based on the historical data collected using Thomas–Fiering model.
- To validate the synthetic flow data using historical data for present conditions.
- To assess suitable structure for the collection and conservation of rainwater from the top of roofs of various buildings in the university.

## 3 Study Area

Study area is considered as Debre Tabor University (DTU), which lies at  $11^{\circ} 51' N$  latitude and  $38^{\circ} 1 E$  longitude which was shown in Fig. 3a, b. Debre Tabor town and a woreda in north-central Ethiopia of Amhara zone. DTU lies at 2700 m approximately above mean sea level. This campus serves with the main motto to provide a better



**Fig. 3** a Map of Debre Tabor town. b Aerial view of Debre Tabor University (DTU)—study area

**Table 1** Demand calculations from various buildings based on per capita demand for various blocks in Debre Tabor University campus

| S. No                                    | Block No | Population (No's) | Per capita demand | Total demand (L) |
|--|----------|-------------------|-------------------|------------------|
| 1  | 53       | 204               | 40                | 8160             |
| 2  | 54       | 204               | 40                | 8160             |
| 3  | 55       | 204               | 40                | 8160             |
| 4  | 56       | 204               | 40                | 8160             |
| 5  | 57       | 204               | 40                | 8160             |
| 6  | 58       | 204               | 40                | 8160             |
| 7  | 61       | 320               | 40                | 12,800           |
| 8  | 62       | 120               | 40                | 4800             |
| 9  | 63       | 320               | 40                | 12,800           |
| 10                                       | 64       | 120               | 40                | 4800             |
| 11                                       | 67       | 320               | 40                | 12,800           |
| 12                                       | 68       | 320               | 40                | 12,800           |
| 13                                       | 144      | 320               | 40                | 12,800           |
| Total demand per day (L)                 |          |                   | 138,760           |                  |
| Total demand per annum (L)               |          |                   | 40,240,400        |                  |
| Total demand per annum (m <sup>3</sup> ) |          |                   | 40,240.4          |                  |

technical and quality education for more than 5000 students and teachers. The climate in the study area is mostly warm and moderate with an average daily temperature of 14.8 °C. The precipitation in the study area generally occurs from mid of May to mid of September with an average precipitation value of 1350–1450 mm. Monthly rainfall data collected from 1992 to 2016 which was collected from metrological department of Debre Tabor town was shown in Table 1a, b [5]. Based on the data available from Central Statistical Agency (CSA), the total population in town is 72,937 no's. The main livelihood of the study area was agriculture and Teff.

## 4 Methodology

The following methodology was adopted for the assessment of suitable rainwater harvesting structure in the study area using Thomas–Fiering model.

- In the first step, the total demand required by the students of DTU was calculated individually per block by the consideration of both floating and fixed population.
- The demand was assumed as follows, for floating population it is considered as 10 L per capita per day (LPCD) and for fixed population as 40 LPCD. In this case, the demand was assumed only for the working days of the university.



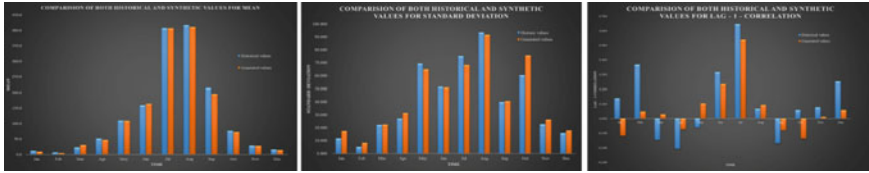


**Fig. 4** Validation of mean, standard deviation, correlation between historic and synthetic rainfall data

- Thus, based on the total demand obtained from the above two steps the final capacity of the collecting tank is fixed as 0.77 m<sup>3</sup>. The plan for proposed collecting tank was shown in Fig. 4.
- A value of 0.75 was taken as run-off coefficient for calculating the total volume of surface run-off from buildings of the university. A lower value was considered due to the reason that surface of channels, pipes connected from buildings to channels are very rough.
- On the other hand, monthly rainfall data was collected for the past 25 years (1992–2016) from the metrological station of Debre Tabor town.
- Using Ms Excel collected data was processed for the errors, if any and to find the missing of rainfall data.
- Required parameters such as mean ( $\mu$ ), standard deviation ( $\rho$ ) and correlation ( $\sigma$ ) values were calculated based on the historical data.
- The values of  $\mu$ ,  $\rho$  and  $\sigma$  show a larger impact during the forecasting of rainfall data.
- At this stage, based on the inputs available Thomas–Fiering models are used for the forecasting of rainfall data. The following formula was used [8]:

$$X_{i,j+1} = \mu_{j+1} + (\rho_j) * \frac{\sigma_{j+1}}{\sigma_j} * (X_{i,j} - \mu_j) + (t_{i,j+1}) * (\sigma_{j+1}) * \sqrt{1 - \rho_j^2} \tag{1}$$

- The above equation is also called as first-order stationary Markov model. Some of the following assumptions are made in the process of estimating the rainfall data such as
- The process is stationary in mean, variance, and lag-one autocorrelation.
- This model is generalized to account for stationarity in hydrological data.
- Assumes standard deviation ( $\mu$ ) is equal to forecasted value for the first month ( $X_1$ ).
- The values generated using the above formula are purely statistical only.
- Values for the forecasted rainfall shall be considered as zero (0), when the negative values are obtained by using the above formula.
- Therefore, by the forecasted values obtained through the above equation and considering the demand in the study area, tank capacity is determined.



- The data thus forecasted is then validated by using mean, variance and correlation of the historic data which was collected from metrological department.
- The detailed procedure for the determination of demand from individual blocks of the university is shown in Table 1.

## 5 Results and Discussion

A stochastic modelling procedure was implemented to simulate monthly rainfall data using Thomas–Fiering model. The values obtained from the above formula help to fix the capacity of the tank for collecting and conservation of the rainwater. The values of forecasted rainfall for a period of 20 years (2017–2036) and graphs for validation of the forecasted data based on historic data were presented in Table 2 and Fig. 4. Following are some of the observations made based on the historic and synthetic rainfall values (Table 3).

As mentioned above, the average values of rainfall in the study area lie between 1350 and 1450 mm, which is the same for both the historic and synthetic data of rainfall with an intensity of 1359.51 mm and 1396.26 mm, respectively.

Further, the other additional parameters used in the above formula such as mean ( $\mu$ ), standard deviation ( $\rho$ ) and correlation ( $\sigma$ ) for both historic and synthetic rainfall

**Table 2** Demand calculations from various buildings based on per capita demand for dormitories in Debre Tabor University campus

| S. No                                    | Block No       | Population (No's) | Per capita demand | Total demand ( litres) | Remarks  |
|--|----------------|-------------------|-------------------|------------------------|--|
| 1  | 47             | 50                | 10                | 500                    | Registrar block—floating population                            |
| 2  | 48             | 240               | 10                | 2400                   | Lecture hall—floating population                               |
| 3  | 49             | 240               | 10                | 2400                   | Lecture hall—floating population                               |
| 4  | 51             | 50                | 10                | 500                    | Dean block—floating population                                 |
| 5  | 52             | 240               | 10                | 2400                   | Lecture hall—floating population                               |
| 6  | 143            | 50                | 10                | 500                    | H & WRE—department—floating population                         |
| 7  | Student Lounge | 750               | 10                | 7500                   | Floating population  |
| Total demand per day (lit)               |                |                   |                   | 138,760                | No. of days considered are 290, due to vacation in summer time |
| Total demand per annum (lit)             |                |                   |                   | 40,240,400             |  |
| Total demand per annum (m <sup>3</sup> ) |                |                   |                   | 40,240.4               |  |

**Table 3** Data for forecasted rainfall using Thomas-Fiering model from 2017 to 2036

| Year           | Jan.  | Feb.  | Mar.  | Apr.   | May    | Jun.   | Jul.   | Aug.   | Sep.   | Oct.   | Nov.  | Dec.  | Sum     | Average (mm) |
|----------------|-------|-------|-------|--------|--------|--------|--------|--------|--------|--------|-------|-------|---------|--------------|
| 2017           | 8.86  | 0.00  | 17.21 | 78.88  | 60.47  | 143.90 | 443.70 | 495.31 | 225.05 | 114.63 | 20.33 | 38.77 | 1647.12 | 137.26       |
| 2018           | 0.00  | 11.46 | 33.20 | 74.11  | 91.89  | 164.51 | 304.43 | 341.62 | 204.73 | 194.00 | 18.24 | 0.00  | 1438.21 | 119.85       |
| 2019           | 0.94  | 5.14  | 71.09 | 30.10  | 95.44  | 116.95 | 452.42 | 374.05 | 154.67 | 129.72 | 34.40 | 34.54 | 1499.45 | 124.95       |
| 2020           | 0.00  | 2.10  | 14.98 | 104.41 | 174.99 | 108.41 | 385.83 | 447.42 | 202.42 | 104.71 | 0.00  | 12.20 | 1557.46 | 129.79       |
| 2021           | 11.65 | 11.14 | 0.00  | 34.92  | 46.41  | 106.92 | 301.54 | 200.49 | 222.12 | 40.43  | 40.67 | 45.57 | 1061.86 | 88.49        |
| 2022           | 0.00  | 0.00  | 6.20  | 0.00   | 248.64 | 206.53 | 357.11 | 417.41 | 154.03 | 15.44  | 52.70 | 20.66 | 1478.72 | 123.23       |
| 2023           | 0.00  | 0.00  | 2.16  | 53.95  | 187.98 | 113.12 | 359.85 | 464.02 | 239.88 | 62.22  | 0.00  | 0.00  | 1483.16 | 123.60       |
| 2024           | 18.16 | 5.78  | 29.20 | 82.55  | 155.71 | 162.27 | 379.02 | 304.20 | 207.77 | 0.00   | 0.00  | 28.12 | 1372.77 | 114.40       |
| 2025           | 21.03 | 17.29 | 37.80 | 42.76  | 121.18 | 184.47 | 326.92 | 203.52 | 278.63 | 74.68  | 44.70 | 45.80 | 1398.77 | 116.56       |
| 2026           | 20.10 | 3.08  | 9.54  | 84.34  | 247.34 | 133.10 | 473.94 | 537.53 | 212.64 | 135.38 | 35.03 | 18.43 | 1910.43 | 159.20       |
| 2027           | 34.57 | 6.77  | 0.00  | 74.39  | 160.61 | 182.72 | 499.02 | 463.65 | 207.74 | 66.64  | 15.51 | 56.52 | 1768.14 | 147.35       |
| 2028           | 8.10  | 6.82  | 0.00  | 46.59  | 6.46   | 137.78 | 420.45 | 516.03 | 206.52 | 97.10  | 10.36 | 0.00  | 1456.22 | 121.35       |
| 2029           | 31.47 | 0.00  | 0.00  | 64.92  | 152.71 | 100.97 | 373.40 | 358.56 | 218.07 | 122.21 | 35.43 | 7.05  | 1464.79 | 122.07       |
| 2030           | 18.08 | 0.00  | 0.00  | 66.95  | 0.00   | 145.83 | 368.81 | 345.27 | 187.44 | 175.76 | 30.90 | 16.07 | 1355.10 | 112.93       |
| 2031           | 3.76  | 14.17 | 29.92 | 105.93 | 79.14  | 191.20 | 416.70 | 455.94 | 299.25 | 70.04  | 52.66 | 1.95  | 1720.67 | 143.39       |
| 2032           | 11.49 | 5.75  | 0.00  | 46.44  | 84.40  | 222.68 | 535.98 | 589.75 | 276.38 | 0.00   | 33.57 | 0.00  | 1806.44 | 150.54       |
| 2033           | 15.28 | 0.00  | 27.94 | 24.61  | 173.07 | 23.12  | 366.78 | 421.02 | 226.36 | 163.94 | 31.73 | 0.00  | 1473.84 | 122.82       |
| 2034           | 21.42 | 7.96  | 9.55  | 59.34  | 97.06  | 230.58 | 502.82 | 371.75 | 129.67 | 0.00   | 3.27  | 19.71 | 1453.13 | 121.09       |
| 2035           | 0.00  | 0.00  | 33.51 | 34.63  | 146.15 | 151.88 | 511.97 | 465.76 | 186.72 | 85.97  | 32.22 | 8.82  | 1657.64 | 138.14       |
| 2036           | 18.02 | 13.45 | 10.95 | 54.66  | 86.58  | 140.95 | 472.55 | 561.63 | 226.80 | 33.14  | 0.00  | 10.19 | 1628.92 | 135.74       |
| Average        | 11.75 | 6.92  | 23.30 | 51.54  | 109.66 | 159.41 | 407.43 | 417.17 | 214.62 | 77.68  | 28.50 | 16.15 |         |              |
| Std. deviation | 11.75 | 5.24  | 22.22 | 27.00  | 69.40  | 51.56  | 75.07  | 93.63  | 39.88  | 59.13  | 22.70 | 15.90 |         |              |

(continued)

**Table 3** (continued)

| Year        | Jan. | Feb. | Mar.  | Apr.  | May   | Jun. | Jul. | Aug. | Sep.  | Oct. | Nov. | Dec. | Sum | Average (mm) |
|-------------|------|------|-------|-------|-------|------|------|------|-------|------|------|------|-----|--------------|
| Correlation | 0.14 | 0.37 | -0.15 | -0.21 | -0.06 | 0.31 | 0.65 | 0.07 | -0.17 | 0.07 | 0.08 | 0.25 |     |              |

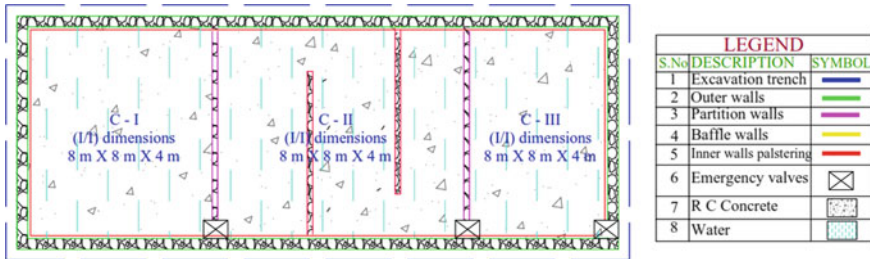


**Fig. 5** Plan for the collecting tank in the study area for the collection of rainwater

data are approximately same with an intensity of 126.948, 41.217, 0.111 and 124.432, 43.007, 0.059, respectively.

Hence based on the topography of the study area and the frequency of occurrence of precipitation, a common collecting tank was constructed by connecting all the channels in the university with a total capacity of 0.77 m<sup>3</sup> on gravity basis for easy collection of rainwater which was shown in Fig. 5.

Collecting tank was divided into three partitions as C—I, C—II and C—III for which the primary treatment of water is provided for the collected water in order to settle down the dust particles from the water.

## 6 Conclusions

Following are some of the conclusions drawn from this study:

- The forecasted values obtained using the above formula help to fix the capacity of tank by calculating the total volume of water required.
- The volume of the water collected from the roofs of various buildings in the university is sufficient to meet the demands of students and teachers.
- The values obtained from this model are purely statistical, and also, this does not consider the influence of metrological parameters except rainfall.
- It can also be concluded that concluded the generated rainfall data is statistically fit when compared with the historic values as the mean, standard deviation and correlation are approximately same.
- The other advantage being that it can be acted as a supplement for the existing water available already and shall also be used for irrigation use, indoor non-potable water use.
- Hence, it can be concluded that Thomas–Fiering model was most suitable to simulate monthly rainfall data even for a large period of time and also able to generate a synthetic rainfall data which was similar to original data.

## References

1. Harvesting rainwater for landscape use, cooperative extension, College of Agriculture and Life Sciences, The University of Arizona, 2nd edn, October 2004, Revised 2006
2. <http://www.rainwaterharvesting.org/international/thailand.htm>, last accessed 2017/08/22
3. Harvesting rainwater for landscape use, cooperative extension, College of Agriculture and Life Sciences, The University of Arizona, 2nd edn, October 2004, Revised 2006, pp 15–25
4. <https://www.watercache.com/faqs/rainwater-harvesting-benefits>. Last accessed 15 Oct 2018
5. Halefom A, Teshome A, Sisay E, Ahmad I (2018) Dynamics of land use and land cover change using remote sensing and GIS: a case study of Debre Tabor Town, South Gondar, Ethiopia. *J Geogr Inf Syst* 10(2) April 2018
6. Soltani S, Modarres R, Eslamian SS (2007) The use of time series modeling for the determination of rainfall climates of Iran. *Int J Climatol* May 2007. <https://doi.org/10.1002/joc.1427>
7. Zahabiyou B (1999) Stochastic generation of daily streamflow data incorporating land use and/or climate change effects. Newcastle University Library, UK, pp 100–125
8. Mujumdar PP (2015) Stochastic hydrology - Parameter estimation, Lecture 7 - NPTEL
9. Xu C (2002) Textbook of hydrologic models. Uppsala University, Sweden, pp 50–59

# A Novel Statistical Approach for Infiltration Model Analysis



Sunith John David, K. U. Abdu Rahiman, and V. Subha

**Abstract** Infiltration of water below ground surface is one of the major components of hydrological cycle which impart significant role in calculation of runoff volume associated with any catchment area. Also, infiltration is the only method through which groundwater replenishment is made possible thereby directly affecting the groundwater table of a particular location. The hydrological component infiltration is affected by various parameters, among which soil properties and hydraulic conductivity predominantly affect the natural process. Even though conventional method of infiltration measurement is available, various infiltration models can also be used to find the percolation of water into soil. The consistency of such infiltration models with conventional field experiment method needed to be evaluated and analyzed for recommending better infiltration models for specific geographic conditions. The present work analyzes the consistency between infiltration values estimated using various infiltration models and field experiment with the aid of one-way ANOVA analysis as statistical tool. Also, work is extended to determine the most reliable infiltration model with filed infiltration data using statistical approach. Statistical analysis shows Kostiakov model having better agreement with field infiltration data in terms of significance level and decision factor.

**Keywords** Infiltration · Infiltration models · One-way ANOVA · Statistical approach

---

S. J. David (✉) · K. U. Abdu Rahiman · V. Subha  
Department of Civil Engineering, School of Engineering, CUSAT, Kochi, India  
e-mail: [sunithjohndavid@mgits.ac.in](mailto:sunithjohndavid@mgits.ac.in)

K. U. Abdu Rahiman  
e-mail: [arku@cusat.ac.in](mailto:arku@cusat.ac.in)

V. Subha  
e-mail: [v.subha@cusat.ac.in](mailto:v.subha@cusat.ac.in)

## 1 Introduction

Infiltration capacity denotes the capacity of soil at particular land cover to seepage or percolation water till a constant rate is achieved over a period of time usually expressed as depth per rate. Infiltration capacity of a place normally depend on the soil properties of the terrain and meteorological combinations over the basin or catchment area [1]. The conventional method of estimation of infiltration comprises of double ring infiltrometer with two concentric rings inserted into soil and infiltration of water measured manually with respect to time using any conventional depth measuring device. Infiltration models like Green-Ampt Model, Kostiakov Model, Horton's Model, Modified Kostiakov Model, etc. are available to describe the process of infiltration with respect to time [1]. One of the main drawbacks of field infiltration test is that this process is too time consuming and tedious. Sometimes it is better to rely on infiltration models to elaborate the variation of infiltration for particular land use pattern than going for field infiltration test as it has mentioned disadvantages. Development of new infiltration models by modifying existing ones are most commonly adopted practice in hydrological investigations. Even though there are possible methods to develop such models, these models need to be analyzed with field infiltration values to confirm the results obtained [2]. Hence, the consistency infiltration models to be evaluated with conventional field test [3]. The objective of the present study is to find the significance value of different infiltration models with field data using one-way ANOVA test and to suggest most reliable infiltration model with filed infiltration data using statistical approach.

## 2 Methodology

The preliminary procedures commence with double ring field infiltrometer test which is one of the most commonly adopted experimental method to determine the field infiltration values. The method is equipped with a double ring infiltrometer of 30 cm inner diameter and 60 cm outer diameter respectively. The depth of water infiltrated in the inner ring can be continuously recorded however the outer ring water helps to prevent the lateral infiltration could happen from inner ring. The method was continued till a constant rate of infiltration for the particular soil is reached [4].

### 2.1 Infiltration Models

Infiltration models explain the variation of field infiltration value with respect to time over a terrain. The present work focuses following infiltration models for the comparative analysis.

- Horton's model

The rate of infiltration and its exponential variation is mathematically explained by

$$f = f_c + (f_0 - f_c)e^{-kt} \tag{1}$$

where

- $f$  Variation of infiltration value over the time
- $t$  Time from the start of infiltration
- $f_0$  Infiltration capacity of soil at beginning
- $f_c$  Constant infiltration capacity
- $k$  Hydraulic conductivity of soil

- Green-Ampt Model

Green and Ampt presented an approach that is based on fundamental physics and the equation is given as follows.

$$f = K[\Psi \Delta\theta / F + 1] \tag{2}$$

where

- $f$  Variation of infiltration value over the time
- $F$  Cumulative Infiltration value from beginning till constant rate is achieved
- $\Psi$  Suction head of soil at wetting front
- $\Delta\theta$  Representation of moisture Content
- $K$  Hydraulic conductivity of soil

- Kostiakov’s model

Kostiakov assumes the variation of infiltration over a time reduces with arbitrary power function

$$f = Kt^{(-m)} \tag{3}$$

where

- $K, m$  Arbitrary power functions
- $f$  Variation of infiltration value over the time
- $t$  Time from the start of infiltration



## 2.2 Statistical Parameters

### One-way ANOVA

The one-way analysis of variance (ANOVA) compares the means of an independent group and related dependent groups using the fundamental expression, Total sum of squares = Sum of squares between groups + Sum of squares within groups.

### Correlation Coefficient and Standard Error of Correlation Coefficient

The strength of two or more values in fundamental statistics and relationship between them varies in degree based on the value of the correlation coefficient. Also, very low value of standard error indicates the low precision between the parameters that under consideration.

### Decision factor ( $D_f$ )

Mathematically it is the difference between correlation coefficient and standard error. Highest value of decision factor always implies better correlation or reflects information toward best fit model in the relevant analysis.

## 3 Results and Discussion

The field infiltration test was performed in an agricultural land use area at Puthencruz panchayath, Kochi, Kerala and with respect to obtained values infiltration models was also developed. The various model parameters such as hydraulic conductivity, soil suction head and moisture content are determined based on soil parameters after performing hydrometer analysis [2, 3, 5]. Kostiakov model parameters are derived from logarithmic graphical representation between infiltration and time [6]. The respective values are tabulated in Table 1.

The variation in infiltration rate between field and models are plotted in Fig. 1.

One-way analysis of variance was performed to determine significance analysis and were tabulated in Table 2. All the data that we obtained are within the permissible significance level of 0.05 and therefore the field infiltration values are reliable and comparable with various infiltration models.

By performing the pearson correlation analysis, various statistical parameters were also determined and tabulated in Table 3. After pearson analysis it is observed that the infiltration values obtained from filed when compared with the models doesn't follow a linear variation. A best fit line was attempted to relate the same parameters which detailed in Fig. 2 ultimately reflects the linear relationship between various infiltration values.

**Table 1** Field infiltration and model values

| Time (min) | Field infiltration rate (cm/h) | Horton's infiltration (cm/h) | Green Ampt's infiltration model (cm/h) | Kostiakov's infiltration model (cm/h) |
|------------|--------------------------------|------------------------------|--|---------------------------------------|
| 5          | 59.63                          | 65.56                        | 29.795                                 | 61.53                                 |
| 10         | 45.9                           | 59.48                        | 26.814                                 | 47.84                                 |
| 15         | 37.46                          | 54.27                        | 25.83                                  | 41.37                                 |
| 20         | 35.78                          | 49.91                        | 25.35                                  | 37.43                                 |
| 25         | 33.97                          | 45.85                        | 25.04                                  | 34.44                                 |
| 30         | 32.28                          | 42.42                        | 24.84                                  | 32.23                                 |
| 35         | 32.28                          | 39.58                        | 24.71                                  | 30.56                                 |
| 40         | 33.97                          | 37.11                        | 24.6                                   | 29.17                                 |
| 45         | 28.07                          | 34.71                        | 24.51                                  | 27.85                                 |
| 50         | 25.54                          | 32.86                        | 24.45                                  | 26.86                                 |
| 55         | 28.91                          | 31.14                        | 24.39                                  | 25.92                                 |
| 60         | 25.54                          | 29.69                        | 24.34                                  | 25.11                                 |
| 65         | 22.28                          | 28.49                        | 24.3                                   | 24.43                                 |
| 70         | 23.85                          | 27.36                        | 24.27                                  | 23.75                                 |
| 75         | 23.61                          | 26.43                        | 24.24                                  | 23.18                                 |
| 80         | 22.04                          | 25.65                        | 24.21                                  | 22.66                                 |
| 85         | 25.54                          | 24.97                        | 24.19                                  | 22.19                                 |
| 90         | 21.8                           | 24.31                        | 24.16                                  | 21.7                                  |
| 95         | 20.36                          | 23.8                         | 24.15                                  | 21.3                                  |
| 100        | 20.36                          | 23.32                        | 24.13                                  | 20.89                                 |
| 105        | 20.36                          | 22.93                        | 24.11                                  | 20.53                                 |

**Fig. 1** Comparison of Infiltration Capacity Curves

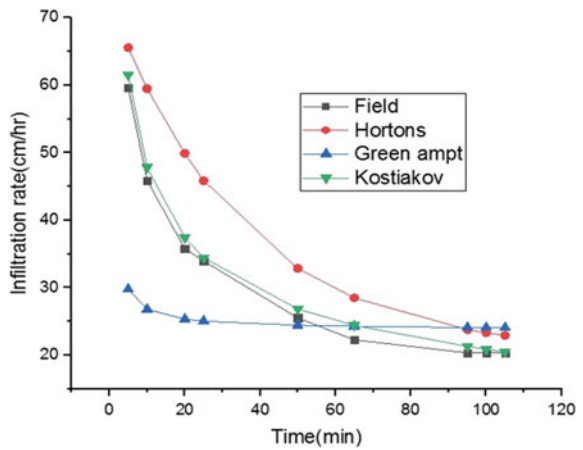


**Table 2** Significance analysis of field infiltration values with models

| Models       | Significance |
|--------------|--------------|
| Kostiakov's  | 0.001        |
| Green Ampt's | 0.006        |
| Horton's     | 0.001        |

**Table 3** Statistical Parameters after analysis

| Models       | Correlation coefficient ( <i>R</i> ) | Coefficient of determination ( <i>R</i> <sup>2</sup> ) | Number of observations ( <i>n</i> ) | Standard error | <i>D<sub>f</sub></i> |
|--------------|--------------------------------------|--|-------------------------------------|----------------|----------------------|
| Horton's     | 0.952                                | 0.906  | 21                                  | 0.070          | 0.836                |
| Green Ampt's | 0.945                                | 0.893  | 21                                  | 0.075          | 0.818                |
| Kostiakov's  | 0.982                                | 0.964  | 21                                  | 0.043          | 0.921                |

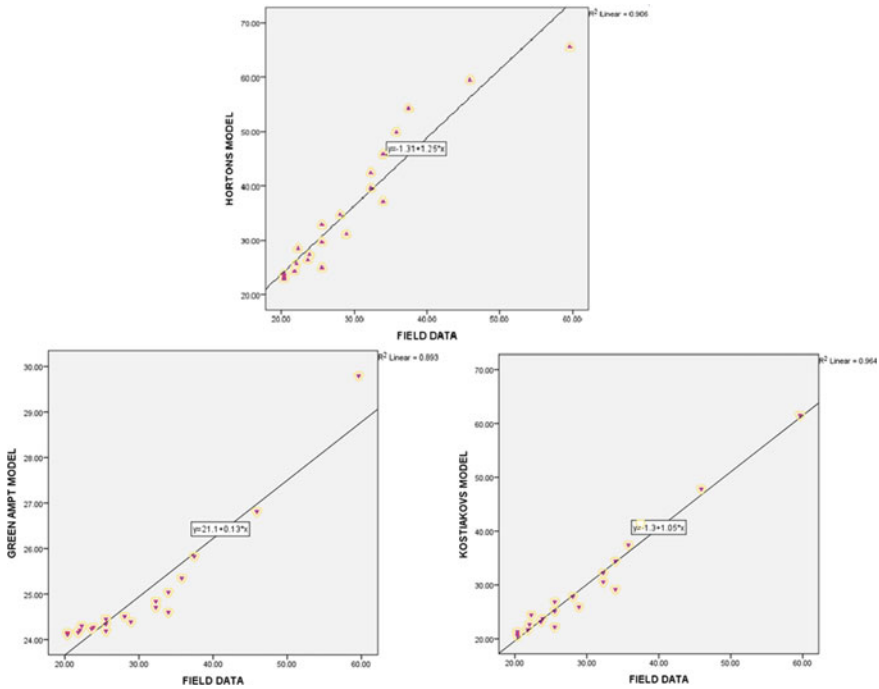


**Fig. 2** Line of best fit between field data and infiltration models

## 4 Conclusion

In the proposed methodology an attempt was made to study the significance of field infiltration with other standard infiltration models during Rabi crop season period.

Using statistical approach, the significance analysis and best fit model suggestion was made by analyzing the field and infiltration model values. Based on statistical analysis, Kostiakov's model shows good agreement with field infiltration values for the land use under study area with one-way ANOVA significance value less than 0.05 and maximum decision factor 0.921.

## References

1. Ma Y, Feng S, Sua D, Gao G, Huo Z (2019) Modeling water infiltration in a large layered soil column with a modified Green–Ampt model and HYDRUS-1D. *J Comput Electron Agric* 71S (2010):S40–S47
2. Mao L, Lia Y, Hao W, Zhou X, Xu C, Lei T (2016) A new method to estimate soil water infiltration based on a modified Green–Ampt model. *J Soil Tillage Res* 161:31–37
3. Fu Q, Hou R, Li T, Li Y, Liu D, Li M (2017) A new infiltration model for simulating soil water movement in canal irrigation under laboratory conditions. *Agric Water Manag* 213:433–444
4. Punmia BC (2009) *Irrigation and water power engineering*, 16th edn. Laxmi Publication (P) Ltd, pp 145–155
5. Su L, Wang J, Qin X, Wang Q (2017) Approximate solution of a one-dimensional soil water infiltration equation based on the Brooks-Corey model. *J Geoderma* 297: 28–37
6. Cui G, Zhu J (2017) Prediction of unsaturated flow and water backfill during infiltration in layered soils. *J Hydrology*

# Assessment of Groundwater and Lake Water Quality at S. Bingipura Dumpsite



R. Manjunath, B. Umadevi, and E. T. Arasu

**Abstract** The study focuses on physical, chemical and biological parameters of water and determining the Water Quality Index. Unscientific dumping of wastes from commercial, industrial and anthropogenic activities has resulted in unscientific dumping of waste at S. Bingipura dumpsite, South Bangalore. The seepage of leachate and heavy metals are responsible for contamination of ground and surface water at the site. Water samples were collected from all the four directions of dumpsite at a radial distance of 0.5 km, 1 km away from the dumpsites to assess contaminant flow and degree of contamination. The samples were analyzed for pH value, electrical conductivity, total dissolved solids, total alkalinity, chloride, dissolved oxygen, BOD<sub>5</sub>, sulfate and nitrate. Heavy metals like manganese, iron, zinc, arsenic, lead, and cadmium were analyzed as per the standard procedures of CPCB. Concentrations of contaminants were higher for manganese of 0.9 mg/l, iron of 1.8 mg/l, arsenic of 0.08 mg/l and cadmium of 0.06 mg/l, respectively. The Weighted Arithmetic Index method was used for the calculation of Water Quality Index of ground and lake water. The WQI for groundwater ranges between 75 and 100 indicating the water quality is very poor and treatment is required before consumption. The Water Quality Index for lake water exceeds 100 hence unsuitable for drinking as per drinking Water Quality Standards.

**Keywords** Physical · Chemical · Industrial waste · Total dissolved solids · Heavy metals · Water Quality Index

## 1 Introduction

Water quality is one of the important key parameters in selecting sources for domestic use, industrial uses, agricultural practices, recreational activities, etc. (1). The Water

---

R. Manjunath (✉) · B. Umadevi · E. T. Arasu  
Department of Civil Engineering, M S Ramaiah Institute of Technology, Bangalore, India

E. T. Arasu  
e-mail: [arasuet@msrit.edu](mailto:arasuet@msrit.edu)

Quality Index is a representation of assessment of water resources which directly depends on many parameters. It is an indicator pollution level in any water body and one of the ways to express the quality of water for different purposes (4). Groundwater and surface water are the important natural resources. The heavy dumping of solid waste in and around the S. Bingipura site has led to deterioration of groundwater quality and lake water quality around it.

### Study Area

S. Bingipura village is located in Anekal taluk, adjacent to Bettadasanapura main road to the south of the Bangalore. Latitude:  $12^{\circ} 50'6''$  N Longitude:  $77^{\circ} 37'38''$  E. It is spread over the area of around 40 acres. The land is owned by Bruhat Bengaluru Mahanagara Palike (BBMP). S. Bingipura is 22 km away from district headquarter Bengaluru. S. Bingipura's gram panchayat is Hulimangala. The total area of the village is 418.57 hectares. The population of the village is 1851 according to 2011 census and there are almost 463 houses in the village. The soil composition for S. Bingipura dumpsite was well-graded silty sand (13). The soil classification carried out according to Indian soil classification system.

## 2 Materials and Methods

The water samples were collected at all the 12 locations. The water samples were collected in two seasons pre-monsoon and post-monsoon seasons. Two liters of water sample were collected from each sampling point and were immediately tested in the laboratory for analysis of all the considered parameters.

Water Quality Index represents the quality of particular source of water which can be understood by any concerned authorities. The WQI incorporates data from multiple parameters into a mathematical equation that rates the quality of water bodies with numbers from 1 to 100 which can be separated in five classes, each class with a different quality state and with a different usage domain (6, 7) (Tables 1, 2; Fig. 1).

**Table 1** Index value intervals and the corresponding quality

| WQI VALUE | Rating of water quality         | Grading |
|-----------|---------------------------------|---------|
| 0–25      | Excellent water quality         | A       |
| 26–50     | Good water quality              | B       |
| 51–75     | Poor water quality              | C       |
| 76–100    | Very poor water quality         | D       |
| Above 100 | Unsuitable for drinking purpose | E       |

**Table 2** Sampling locations near and around S. Bingipura dumpsite

| Sl. No | Sampling point                               | Location                   | Latitude    | Longitude   |
|--------|--|----------------------------|-------------|-------------|
| 1      | GW 1 (south 1.0 km radius, bore well 690 ft) | Bingipura village (temple) | 12° 49'26"N | 77° 36'29"E |
| 2      | GW2 (south 1.0 km radius, bore well 780 ft)  | Bingipura village (home)   | 12° 49'41"N | 77° 38'19"E |
| 3      | GW3 (west 0.5 km radius, bore well 840 ft)   | Bingipura village (hotel)  | 12° 50'06"N | 77° 37'38"E |
| 4      | GW4 (west 1.0 km radius bore well 810 ft)    | Bingipura village (home)   | 12° 50'24"N | 77° 37'41"E |
| 5      | GW5 (north 1.0 km radius bore well 820 ft)   | Bingipura village (home)   | 12° 50'26"N | 77° 37'39"E |
| 6      | GW6 (north 0.5 km radius, bore well 860 ft)  | Bingipura village (home)   | 12° 50'23"N | 77° 37'43"E |
| 7      | GW7 (north 0.5 km radius, bore well 720 ft)  | Bingipura village (farm)   | 12° 50'24"N | 77° 37'45"E |
| 8      | GW8 (east 0.5 km radius, bore well 840 ft)   | Bingipura village (home)   | 12° 49'53"N | 77° 38'34"E |
| 9      | GW9 (east 1.0 km radius, bore well 880 ft)   | Bingipura village (home)   | 12° 50'22"N | 77° 38'23"E |
| 10     | GW10 (east 1.0 km radius, bore well 860 ft)  | Bingipura village (home)   | 12° 50'20"N | 77° 38'24"E |
| 11     | SW (at lake)                                 | Bingipura village (lake)   | 12° 49'57"N | 77° 38'11"E |
| 12     | SW (at lake)                                 | Bingipura village (lake)   | 12° 49'56"N | 77° 38'08"E |

### 3 Results and Discussions

The water samples from the water body will be collected at different time intervals. Analysis of 12 physiochemical parameters by following the established procedures. The parameters like- pH, electrical conductivity, dissolved oxygen, total dissolved solids, total alkalinity, total hardness, total suspended solids, calcium, magnesium, chloride, nitrate, sulfate and biochemical oxygen demand are analyzed in the laboratory as per the standard procedures. Even heavy metal analysis is to be carried out. The WQI is calculated by using the standards of drinking water quality recommended by World Health Organisation (WHO), Bureau of Indian Standards (BIS) and Indian Council for Medical Research (ICMR) and Central Pollution Control Board (CPCB). The weighted arithmetic index method will be used for the calculation of WQI of the water body. Further the quality rating or sub-index "Qn" is calculated using the following expression

$$Q_n = (V_n - V_{io}) * 100 / (S_n - V_{io}) \quad (1)$$

where



**Fig. 1** Water Sampling locations near and around S. Bingipura

- $Q_n$  Quality rating for the  $n$ th water quality parameter.
- $V_n$  Estimated value of the  $n$ th parameter at a given sampling Station.
- $S_n$  Standard permissible value of the  $n$ th parameter
- $V_{io}$  Ideal value of  $n$ th parameter in pure water [i.e., 0 for all other parameters except pH and DO (7 and 14.6 mg/l respectively)]. Unit weight was calculated by a value inversely proportional to the recommended standard value  $S_n$  of the corresponding parameter. The unit weight ( $W_n$ ) values in the present study are taken from Krishnan et al. (2013)

$$W_n = K/S_n \tag{2}$$

where

- $W_n$  Unit weight for the  $n$ th parameters.
- $S_n$  Standard value for the  $n$ th parameters
- $K$  Constant for proportionality.



**Table 3** Calculation of constant of proportionality (*K*) and unit weight (*W<sub>n</sub>*)

| Sl. No. | Parameters              | Standard values |        |                       |
|---------|-------------------------|-----------------|--------|-----------------------|
| 1       | pH                      | 8.5             | 1.7365 | 0.2042                |
| 2       | Electrical conductivity | 300             |        | 0.005786              |
| 3       | Total alkalinity        | 200             |        | 0.00868               |
| 4       | Total hardness          | 300             |        | 0.005786              |
| 5       | Total dissolved solids  | 500             |        | 0.003472              |
| 6       | Calcium                 | 75              |        | 0.02314               |
| 7       | Magnesium               | 30              |        | 0.05786               |
| 8       | Sulfate                 | 200             |        | 0.00868               |
| 9       | Nitrate                 | 45              |        | 0.03857               |
| 10      | Chloride                | 250             |        | 0.006944              |
| 11      | BOD                     | 5               |        | 0.3472                |
| 12      | DO                      | 6               |        | 0.28941               |
|         |                         |                 |        | $\sum W_n = 0.999718$ |

$$k = \frac{1}{\sum \left(\frac{1}{S_n}\right)} \quad K = \frac{1}{\sum \left(\frac{1}{S_n}\right)} \tag{3}$$

The overall Water Quality Index is calculated by aggregating the quality rating with the unit weight linearly (Table 3).

$$WQI = \sum W_n * Q_n / \sum W_n \tag{4}$$

### 3.1 Calculation of WQI for Lake Sample (L1)

After the calculation of Quality Rating (*Q<sub>n</sub>*) of all the parameters of the sample (for location L1, S. Bingipura lake) and substituting it in WQI formula

$$WQI = \sum W_n * Q_n / \sum W_n \tag{5}$$

where *W<sub>n</sub>* = Unit weight for the *n*th parameters.

We found  $\sum Q_n * W_n = 116.1219$  and  $\sum W_n = 0.999718$ .

Hence,  $WQI = 116.1547$ .

According to the suitability of WQI values for human consumption, the above-found WQI exceeds the limit for drinking purpose. Same procedure of calculation is adopted for all the sampling locations. For the calculation of WQI of the water, the

weighted arithmetic index method has been used. For quality rating and sub index ( $q_n$ ) was calculated according to the following.

BOD in all the samples varies with the maximum value of 8.35 mg/l [L1] for first sample and for second sample is 8.5 mg/l [N1 (0.5)]. The minimum value for the pre-monsoon sample is 5 mg/l [E1] having the mean value for first sample as 6.34 mg/l and that for post-monsoon is 5.1 mg/l [N1] having the mean value for post-monsoon sample as 6.7 mg/l. BOD is an important indicator of overall water quality (Fig. 3).

**Table 4** Pre-monsoon sampling results Water Quality Index

| Sl no | pH  | EC  | TA  | TH  | Ca  | Mg  | Cl     | S   | NO <sub>3</sub> | DO  | TDS | BOD  | WQI    |
|-------|-----|-----|-----|-----|-----|-----|--------|-----|-----------------|-----|-----|------|--------|
| L1    | 7.3 | 780 | 340 | 196 | 9.4 | 5.5 | 177.5  | 5.0 | 12.5            | 0.5 | 450 | 8.35 | 97.71  |
| L2    | 7.2 | 850 | 326 | 170 | 8.6 | 4.0 | 88.75  | 0.8 | 27              | 3.5 | 509 | 8.01 | 105.22 |
| S3    | 7.6 | 560 | 185 | 210 | 5.5 | 2.0 | 177.5  | 0.8 | 19              | 6.6 | 255 | 1.2  | 63.27  |
| N2    | 6.8 | 280 | 282 | 231 | 6.8 | 3.0 | 230.75 | 2.1 | 22              | 5.3 | 301 | 7.2  | 109.79 |
| N1    | 7.2 | 650 | 277 | 187 | 8.6 | 4.5 | 315.95 | 2.8 | 35.3            | 3.2 | 350 | 5.6  | 97.24  |
| E3    | 7.5 | 980 | 253 | 181 | 7.0 | 2.5 | 71.0   | 3.5 | 30.1            | 5.4 | 314 | 5.9  | 103.66 |
| S2    | 6.9 | 960 | 311 | 214 | 8.1 | 4.5 | 106.5  | 4.0 | 16.2            | 7.1 | 361 | 6.2  | 92.74  |
| E1    | 6.5 | 430 | 280 | 197 | 6.7 | 3.0 | 195.25 | 5.9 | 43              | 4.9 | 235 | 5.4  | 72.46  |
| W2    | 7.4 | 560 | 296 | 218 | 8.6 | 4.5 | 142    | 5.7 | 36.5            | 6.1 | 321 | 5.3  | 71.63  |
| E1    | 6.7 | 860 | 270 | 205 | 9.5 | 5.5 | 88.75  | 3.1 | 32.2            | 5.8 | 241 | 5.0  | 87.69  |
| N1    | 7.9 | 730 | 290 | 240 | 9.3 | 4.5 | 195.25 | 3.4 | 14.7            | 5.0 | 351 | 7.7  | 113.81 |
| W1    | 7.2 | 970 | 302 | 153 | 6.2 | 3.0 | 124.25 | 2.7 | 38              | 6.0 | 327 | 6.0  | 96.24  |

**Table 5** Post-monsoon sampling results of Water Quality Index

| Sl.no | pH  | EC  | TA  | TH  | Ca  | Mg  | Cl     | S   | No <sub>3</sub> | DO  | TDS | BOD | WQI    |
|-------|-----|-----|-----|-----|-----|-----|--------|-----|-----------------|-----|-----|-----|--------|
| L1    | 6.5 | 890 | 357 | 205 | 4.9 | 2.5 | 102.95 | 0.5 | 15.0            | 4.1 | 515 | 7.2 | 108.38 |
| L2    | 7.7 | 550 | 316 | 191 | 4.3 | 2.1 | 85.2   | 1.1 | 24.2            | 3.8 | 498 | 7.7 | 120.2  |
| S3    | 6.3 | 650 | 285 | 202 | 3.9 | 1.5 | 198.8  | 1.5 | 22.1            | 4.2 | 355 | 6.9 | 59.50  |
| N2    | 6.8 | 830 | 298 | 212 | 2.8 | 1.2 | 17.75  | 0.5 | 17.0            | 4.9 | 324 | 7.5 | 95.20  |
| N1    | 7.1 | 460 | 258 | 241 | 1.8 | 1.1 | 159    | 1.0 | 24.7            | 3.0 | 314 | 5.1 | 80.45  |
| E3    | 7.2 | 930 | 265 | 200 | 6.9 | 3.6 | 124.25 | 6.2 | 29.0            | 5.7 | 351 | 5.6 | 81.88  |
| S2    | 6.6 | 870 | 283 | 224 | 2.5 | 1.3 | 230.75 | 0.5 | 21.1            | 6.4 | 333 | 6.7 | 93.48  |
| E1    | 6.5 | 970 | 264 | 209 | 5.3 | 2.2 | 88     | 1.0 | 34.0            | 4.4 | 257 | 5.9 | 61.26  |
| W2    | 7.5 | 540 | 309 | 219 | 5.9 | 2.5 | 159    | 0.5 | 32.2            | 5.8 | 365 | 7.6 | 67.24  |
| E1    | 6.9 | 930 | 248 | 195 | 1.9 | 0.9 | 159    | 1.0 | 37.6            | 5.4 | 298 | 5.4 | 77.73  |
| N1    | 7.7 | 930 | 294 | 225 | 5.5 | 2.6 | 71     | 0.5 | 22.4            | 5.3 | 345 | 8.5 | 120.83 |
| W1    | 7.2 | 650 | 329 | 190 | 3.5 | 1.5 | 142    | 2.5 | 19.4            | 6.5 | 419 | 7.2 | 88.19  |

**Table 6** Pre-monsoon sampling results of heavy metals

| Sl no             | Na  | CO <sub>3</sub> | As        | Pb       | Cd         | Zn   | Fe       | Mn      | Cu       |
|-------------------|-----|-----------------|-----------|----------|------------|------|----------|---------|----------|
| Permissible limit | 20  | 60              | 0.01–0.05 | 0.01–0.1 | 0.003–0.01 | 5–15 | 0.03–0.3 | 0.1–0.3 | 0.05–1.5 |
| L1                | 1.1 | 15              | 0.03      | 0.03     | 0.05       | 0.6  | 0.6      | 0.7     | 0.02     |
| L2                | 0.4 | 15              | 0.05      | 0.02     | 0.06       | 0.2  | 1.2      | 0.9     | 0.01     |
| S3                | 0.5 | 15              | 0.08      | 0.02     | 0.04       | 0.2  | 1.2      | 0.1     | 0.02     |
| N2                | 0.9 | 15              | 0.02      | 0.05     | 0.02       | 0.8  | 1.8      | 0.2     | 0.01     |
| N1                | 1.0 | 30              | 0.01      | 0.02     | 0.03       | 0.6  | 1.6      | 0.3     | 0.05     |
| E3                | 1.1 | 75              | 0.02      | 0.06     | 0.06       | 0.5  | 0.5      | 0.2     | 0.03     |
| S2                | 0.5 | 186             | 0.03      | 0.02     | 0.05       | 0.6  | 1.6      | 0.6     | 0.01     |
| E1                | 0.3 | 15              | 0.05      | 0.01     | 0.06       | 0.3  | 0.3      | 0.9     | 0.02     |
| W2                | 0.8 | 30              | 0.02      | 0.03     | 0.02       | 0.2  | 0.2      | 0.9     | 0.03     |
| E1                | 0.2 | 15              | 0.03      | 0.05     | 0.05       | 0.3  | 0.3      | 0.4     | 0.01     |
| N1                | 1.1 | 45              | 0.05      | 0.02     | 0.06       | 0.4  | 0.4      | 0.5     | 0.02     |
| W1                | 1.1 | 30              | 0.02      | 0.04     | 0.01       | 0.4  | 0.4      | 0.8     | 0.04     |

**Table 7** Post-monsoon sampling results of heavy metals

| Sl. No.           | Na    | CO <sub>3</sub> | As        | Pb       | Cd         | Zn   | Fe       | Mn      | Cu       |
|-------------------|-------|-----------------|-----------|----------|------------|------|----------|---------|----------|
| Permissible limit | 20    | 60              | 0.01–0.05 | 0.01–0.1 | 0.003–0.01 | 5–15 | 0.03–0.3 | 0.1–0.3 | 0.05–1.5 |
| L1                | 18.15 | 0.3             | 0.02      | 0.04     | 0.01       | 0.4  | 1.7      | 1.6     | 1.1      |
| L2                | 24    | 0.9             | 0.04      | 0.01     | 0.02       | 0.01 | 1.0      | 0.9     | 0.4      |
| S3                | 19    | 0.4             | 0.04      | 0.02     | 0.03       | 0.02 | 1.3      | 0.8     | 0.2      |
| N2                | 29    | 0.3             | 0.03      | 0.02     | 0.07       | 0.01 | 3.0      | 0.6     | 0.2      |
| N1                | 67    | 0.4             | 0.01      | 0.02     | 0.03       | 0.03 | 1.5      | 1.6     | 0.2      |
| E3                | 48    | 1.6             | 0.04      | 0.03     | 0.06       | 0.01 | 1.5      | 1.9     | 0.3      |
| S2                | 102   | 1.8             | 0.03      | 0.04     | 0.03       | 0.02 | 1.8      | 0.9     | 0.2      |
| E1                | 65    | 1.6             | 0.02      | 0.01     | 0.01       | 0.01 | 1.5      | 1.5     | 0.1      |
| W2                | 12    | 0.6             | 0.02      | 0.01     | 0.02       | 0.02 | 1.7      | 1.7     | 0.2      |
| E1                | 19    | 0.2             | 0.01      | 0.04     | 0.02       | 0.02 | 1.8      | 0.7     | 0.1      |
| N1                | 36    | 1.2             | 0.05      | 0.01     | 0.01       | 0.01 | 1.9      | 0.6     | 0.2      |
| W1                | 49    | 0.5             | 0.01      | 0.05     | 0.05       | 0.02 | 1.2      | 1.2     | 0.2      |

pH in all the samples varies with the maximum value of 7.9 [S3 and N1 (0.5)] for the first sample and that for pre-monsoon sample is 7.5 [W2 (0.5)]. The minimum value for pre-monsoon sample is observed to be 6.5 [E1 and N2 (0.5)] having the mean value for pre-monsoon sample as 7.27 and the minimum value for post-monsoon sample is 6.3 [S3] having the mean value for post-monsoon sample as 6.94. Beyond

**Table 8** Standard values of water quality parameter

| Parameters                                 | Observed value ( $V_n$ ) | Ideal value ( $V_{io}$ ) | Standard values ( $S_n$ ) | Quality rating ( $Q_n$ ) | Unit weigh ( $W_n$ ) | $Q_n * W_n$               |
|--|--------------------------|--------------------------|---------------------------|--------------------------|----------------------|---------------------------|
| pH   | 7.3                      | 7                        | 8.5                       | 20                       | 0.2042               | 4.08                      |
| EC( $\mu$ s/cm)                            | 780                      | 0                        | 300                       | 260                      | 0.00578              | 1.50                      |
| Total alkalinity (mg/l)                    | 340                      | 0                        | 200                       | 170                      | 0.00868              | 1.47                      |
| Total hardness as CaCO <sub>3</sub> (mg/l) | 196                      | 0                        | 300                       | 65.33                    | 0.00578              | 0.37                      |
| Total dissolved solids (mg/l)              | 450                      | 0                        | 500                       | 90                       | 0.00347              | 0.31                      |
| Calcium (mg/l)                             | 9.4                      | 0                        | 75                        | 12.53                    | 0.02314              | 0.29                      |
| Magnesium (mg/l)                           | 5.5                      | 0                        | 30                        | 18.33                    | 0.05786              | 1.06                      |
| Chlorides (mg/l)                           | 177.5                    | 0                        | 250                       | 71                       | 0.00694              | 0.49                      |
| Nitrate (mg/l)                             | 12.5                     | 0                        | 45                        | 27.77                    | 0.03857              | 1.07                      |
| Sulfate (mg/l)                             | 5.0                      | 0                        | 200                       | 2.5                      | 0.00868              | 0.02                      |
| DO (mg/l)                                  | 0.5                      | 14.6                     | 6                         | 163.95                   | 0.2894               | 47.44                     |
| BOD (mg/l)                                 | 8.35                     | 0                        | 5                         | 167                      | 0.3472               | 57.78                     |
|  |                          |                          |                           |                          | $\sum W_n = 0.99$    | $\sum W_n * Q_n = 116.12$ |

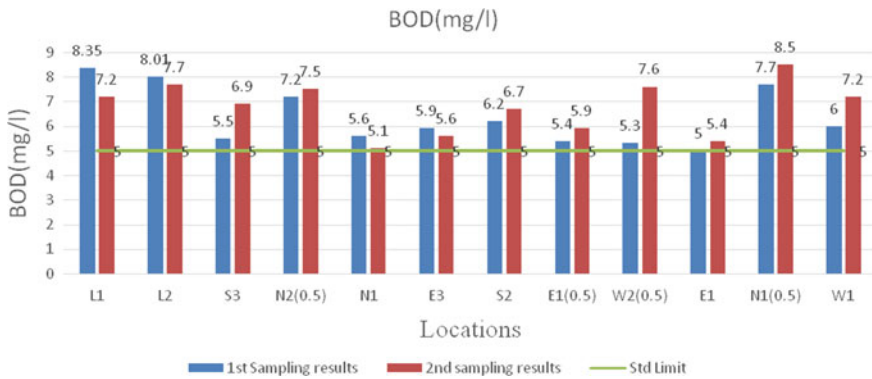
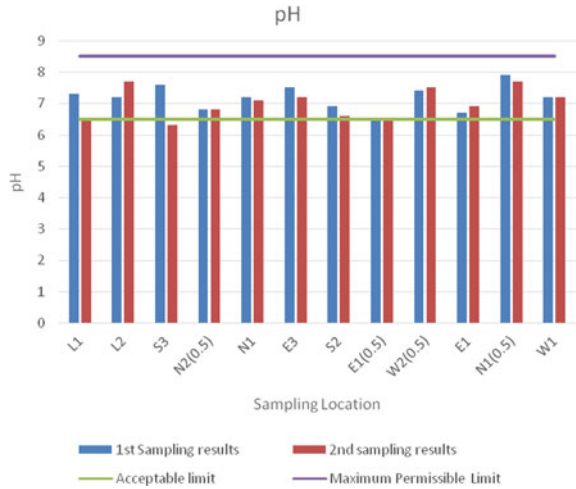


**Fig. 2** Variation of BOD along different locations

**Fig. 3** Variation of pH along different locations



the limit, the water will affect the mucous membrane. Drinking water with an elevated pH above 11 can cause skin and eye irritation (Fig. 4).

Magnesium in all the samples varies with the maximum value of 5.5 mg/l [L1] and [E1] for the pre-monsoon sample and that for the post-monsoon sample is 3.6 mg/l [E3]. The minimum value of pre-monsoon sample is 2 mg/l [S3] having the mean value of pre-monsoon sample as 3.875 mg/l and the minimum value for post-monsoon sample is 0.9 mg/l [E1] having the mean value for post-monsoon sample as 1.91 mg/l. Magnesium can cause suppression of the Central Nervous System when ingested in the large amounts. Ingestion of a combination of magnesium and sulfate can result in diarrhea (Fig. 5).

Manganese in all the samples varies with the maximum value of 0.9 mg/l [L2, E1 (0.5), W2 (0.5)] and that of post-monsoon sample is 1.9 mg/l [E3]. The minimum

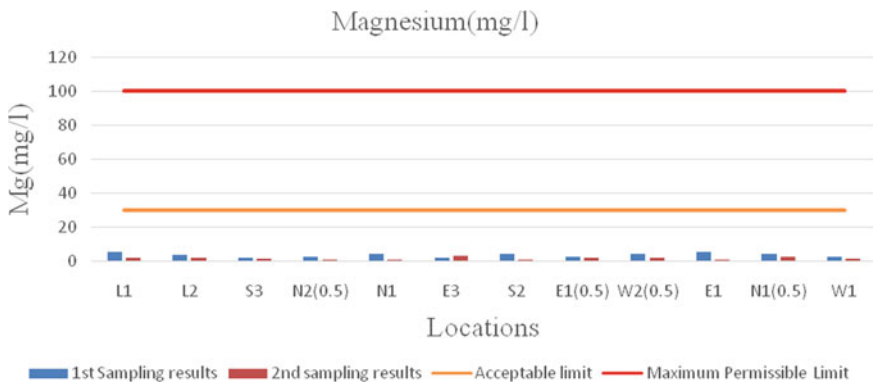


**Fig. 4** Variation of magnesium along different locations

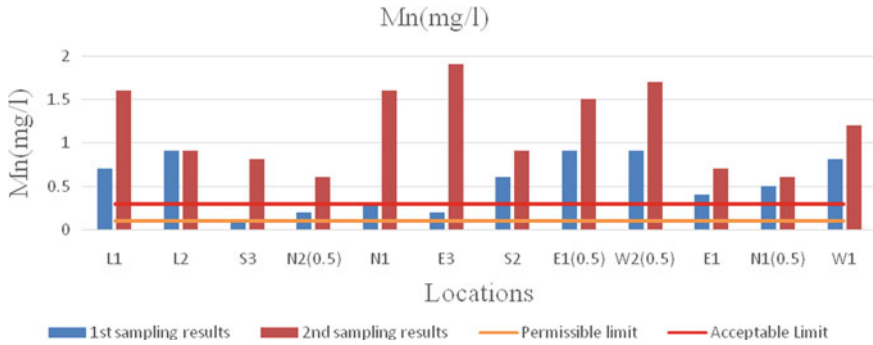


Fig. 5 Variation of manganese along different locations

value of pre-monsoon sample is 0.1 mg/l [S3] having the mean value of pre-monsoon sample as 0.54 mg/l and the minimum value of post-monsoon sample is 0.6 mg/l [N1 (0.5), N2 (0.5)] having the mean value of second sample as 1.16 mg/l. Presence of manganese causes Osteoporosis. It causes Anemia. Also it causes tremors (Fig. 6).

Iron in all the samples varies with the maximum value of 1.8 mg/l [N2 (0.5)] and that of post-monsoon sample is 3.0 mg/l [N2 (0.5)]. The minimum value of pre-monsoon sample is 0.2 mg/l [W2 (0.5)] having the mean value of pre-monsoon sample as 0.84 mg/l and the minimum value of post-monsoon sample is 1.0 mg/l [L2] having the mean value of post-monsoon sample as 1.65 mg/l. Presence of Iron causes blood vomiting and also may cause death from liver failure. It gives nausea feeling and causes vomiting (Fig. 7).

Arsenic in all the samples varies with the maximum value of 0.08 mg/l [S3] and that of post-monsoon sample is 0.05 mg/l [N1 (0.5)]. The minimum value of pre-monsoon sample is 0.01 mg/l [N1] having the mean value of first sample as 0.031 mg/l and the minimum value of post-monsoon sample is 0.01 mg/l [N1, W1, E1] having the mean

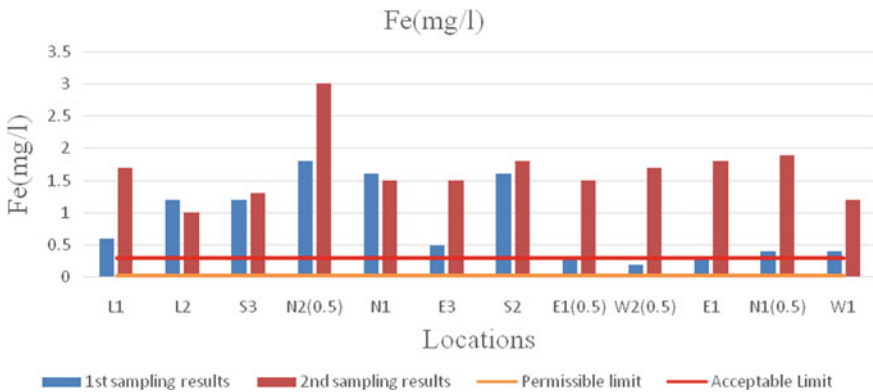


Fig. 6 Variation of iron along different locations

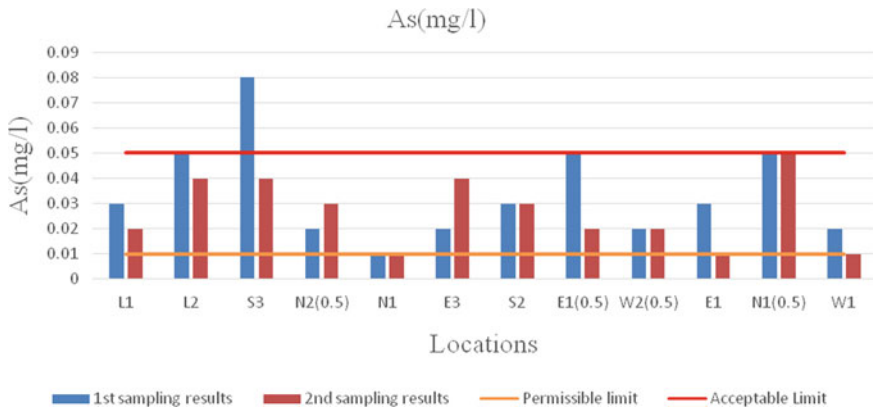


Fig. 7 Variation of arsenic along different locations

value of post-monsoon sample as 0.026 mg/l. Presence of Arsenic causes Breathing problems and can also cause death if exposed to high levels. It also causes known human carcinogen like lung and skin cancer, peripheral nervous system problems, nausea, diarrhea and vomiting. Also results in Decreased intelligence (Fig. 8).

Lead in all the samples varies with the maximum value of 0.06 mg/l [E3] and that of post-monsoon sample is 0.05 mg/l [W1]. The minimum value of pre-monsoon sample is 0.01 mg/l [E1 (0.5)] having the mean value of pre-monsoon sample as 0.030 mg/l and the minimum value of post-monsoon sample is 0.01 mg/l [E1 (0.5), L2, W2 (0.5), N1 (0.5)] having the mean value of post-monsoon sample as 0.025 mg/l. Lead causes behavioral problems, kidney damage, high blood pressure, anemia. It also causes Miscarriage and decreased sperm production. It leads to Memory and learning difficulties and Reduced IQ (Fig. 9).

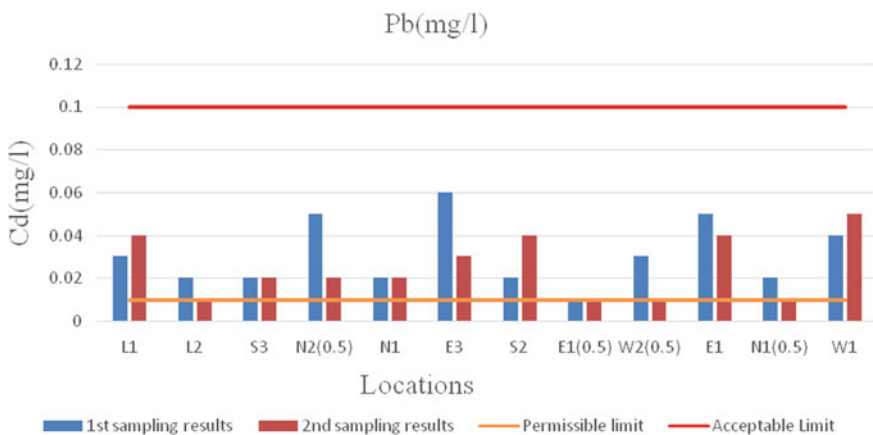


Fig. 8 Variation of lead along different locations

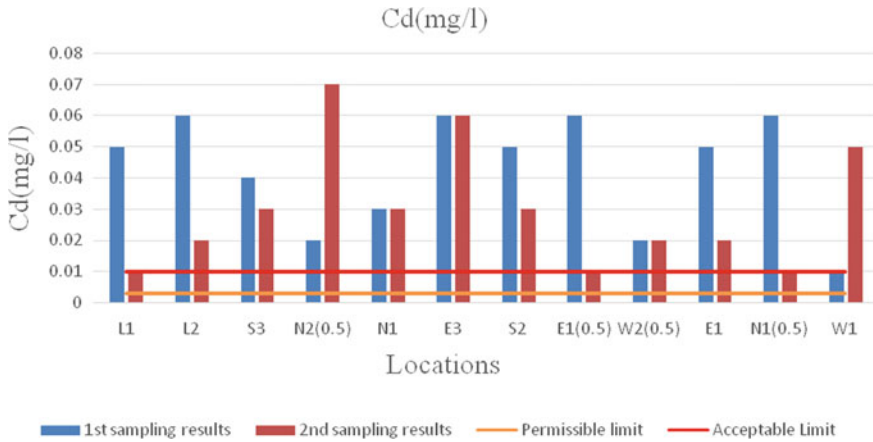


Fig. 9 Variation of Cadmium along different locations

Cadmium in all the samples varies with the maximum value of 0.06 mg/l [E3, L2, E1 (0.5), N1 (0.5)] and that of post-monsoon sample is 0.07 mg/l [N2 (0.5)]. The minimum value of pre-monsoon sample is 0.0425 mg/l and the minimum value of post-monsoon sample is 0.01 mg/l [E1 (0.5), L1, N1 (0.5)] having the mean value of post-monsoon sample as 0.03 mg/l. Ingesting very high levels severely irritates the stomach, leading to vomiting and diarrhea. Long term exposure to lower levels leads to build up in the kidneys and possible kidney disease, lung damage and fragile bones. Regulatory limits.

### 4 Conclusions

- It was found that for the first sampling locations the Water Quality Index exceeds 100 for the locations L1 (surface water), L2 (surface water) and hence they are unsuitable for drinking as per drinking standards For W2 (0.5 km) (Groundwater), E1 (0.5 km) (Groundwater) and S3 (Groundwater), N2 (0.5 km) (Groundwater), N1 (0.5 km)(Groundwater), N1 (Groundwater), S2 (Groundwater), E1 (Groundwater), E3 (Groundwater) and W1 (Groundwater), WQI lies between 75 and 100 the water quality is very poor and treatment is required before consumption.
- It was found that for second sampling locations the Water Quality Index exceeds 100 for the locations L2 (surface water) and N1 (0.5 groundwater), hence they are unsuitable for drinking as per drinking standards.
- For L1 (surface water) N2 (0.5) (Groundwater), E1 (0.5 km) (Groundwater) N1 (Groundwater), S3 (Groundwater), S2 (Groundwater), E3 (Groundwater), W2 (0.5 km)(Groundwater), W1 (Groundwater), E1 (Groundwater) WQI lies



between 75 and 100 the water quality is very poor and treatment is required before consumption.

## Bibliography

1. Venkatramanan S, Chung SY, Lee SY, Park N (2014) Assessment of river water quality via environmental multivariate statistical tools and water quality index: a case study of Nakdong River Basin, Korea. *Carpathian J Earth Environ Sci* 9(2):125–132
2. Milanovic M, Urosev M, Milijasevic D (2006) Use of the RHS method in GolijaskaMoravica river basin. *Bull Serb Geogr Soc* 86(2):53–61
3. Milanovic M, Milijasevic D, Brankov J (2011) Assessment of polluting effects and surface water quality using water pollution index: a case study of hydro-system Danube-Tisa-Danube, Serbia. *Carpathian J Earth Environ Sci* 6(2): 269–277
4. Parvulescu L, Hamchevici C (2010) The relation between water quality and the distribution of *Gammarus balcanicus sch*“afern 1922 (Amphipoda: Gammaridae) in the Anina mountains. *Carpathian J Earth Environ Sci* 5(2):161–168
5. Ionus O (2010) Water quality index—assessment method of the Motru River water quality (Oltenia, Romania). *Ann Univ Craiova Ser Geogr* 13:74–83
6. Tyagi S, Sharma B, Singh P, Dobhal R (2013) Water quality assessment in terms of water quality index. *Am J Water Resour* 1(3):34–38
7. Bordalo A, Teixeira RW, Wiebe WJ (2006) A water quality index applied to an international shared river basin: the case of the Douro River. *J Environ Manag* 38(6):910–920
8. Behmanesh A, Feizabadi Y (2013) Water quality index of parameters Babolrood River in Mazandaran, Iran. *Int J Agric Crop Sci IJACS* 5(19):2285–2292
9. Chowdhury RM, Muntasir SY, Hossain MM (2012) Water quality index of water bodies along Faridpur- Barisal road in Bangladesh. *Glob Eng Technol Rev* 2(3):1–8
10. Kalavathy S, Rakesh Sharma T, Sureshkumar P (2011) Water quality index of river cauvery in Tiruchirappalli district, Tamilnadu. *Arch Environ Sci* 5:55–61
11. Yogendra K, Puttaiah ET (2007) Determination of water quality index and suitability of an urban water body in Shimoga Town, Karnataka. In: *Proceedings of Taal2007: The 12th World Lake Conference*. pp 342–346
12. Manjunath R, Umadevi B, Arasu ET (2020) Physico chemical properties and heavy metal concentration of soils in two major dumpsites. *Gis Sci J* 7(7):701–7101
13. Ramesh N, Krishnaiah S (2013) Scenario of water bodies (lakes) in urban areas—a case study on Bellandur Lake of Bangalore Metropolitan city. *IOSR J Mech Civ Eng (IOSRJMCE)* 7(3):6–14. e-ISSN 2278-1684, p-ISSN 2320–334X

# Assessment of Contaminant Migration Using MT3DMS Model



P. Anil Kumar, G. N. Pradeep Kumar, and M. J. Nandan

**Abstract** Tentacles of modelling are omnipresent. This has become more so with the present day very fast and efficient computers with user demand being the final output, which may be numerical, graphical or 3 D pictorial. Mass transport models to study and analyze pollutant migration find enormous applications in the field of environmental management. Rapid industrialization aggravated water pollution, especially subsurface waters. This paper presents the results and inferences drawn from studies on pollutant migration from chemical and pharmaceutical industries established around the Choutuppal Industrial Area near Hyderabad. Partially effluents whether treated or untreated are being discharged from these industries directly onto the surface, into streams, polluting surface and groundwaters. In order to estimate the extent of pollution, an experimental study integrated with the application of MT3DMS was carried out. As a part of experimental investigation, the close monitoring of groundwater level and water quality was carried out. The preparation of Mass transport models was made using visual MODFLOW software with a discussion on the spatial (vertical and horizontal) and temporal expansion of plume of contamination of groundwater at different subsurface formations in the study area.

**Keywords** MT3DMS · Contaminant migration · TDS concentration · Pollutant transport · Choutuppal

---

P. A. Kumar (✉)

Department of Civil Engineering, Sree Vidyanikethan Engineering College, Tirupati 517502, India  
e-mail: [anilkumar.p@vidyanikethan.edu](mailto:anilkumar.p@vidyanikethan.edu)

G. N. P. Kumar

Department of Civil Engineering, S.V.U. College of Engineering, S.V. University, Tirupati 517502, India

M. J. Nandan

National Geophysical Research Institute, Hyderabad 500007, India

## 1 Introduction

An upcoming problem in the present day is that of groundwater pollution. The causes of pollution of water resources are such as indiscriminate disposal of industrial waste, extensive use of fertilizers and pesticides and human interventions. Pollution after affecting soils and surface water further reaches the free aquifer through downward movement also lateral dispersion and advective migration. Fractures, fissures, joints, etc. provide additional preferred pathways for a faster migration of pollutants. Groundwater should be managed effectively. The ability which we require is to predict subsurface flow and transport of solutes and the response of fluid and solute flux to changes in natural and manmade stresses. With the increase in industrialization and there is sharp increase in usage of groundwater, it is very essential to study the movement of contaminants in an aquifer to predict their migration [1]. It is immensely helpful for planners in working out necessary remedial and preventive measures. Such studies also help evolve better directions for future planning of waste disposal operations and for controlling the existing pollution plumes.

The evolution of popular tool during last three decades is MT3DMS which is deterministic, distributed parameter and a computer simulation model for solute transport in groundwater systems [2, 3]. The add-ons such as pre-processing and post-processing facilities made it more versatile. Present study illustrates the significance of mass transport modelling for estimating groundwater contamination [4].

## 2 Materials and Methods

### 2.1 Study Area

Choutuppal Mandal, one of the drought prone mandals of Nalgonda district, Telangana State lies between longitude  $78^{\circ}45'$  and  $79^{\circ}E$  and latitude  $17^{\circ}10'$  and  $17^{\circ}24'$  N. Some villages of the mandals are affected with high concentration of fluoride in groundwater. Temperature in summer differs from  $30$  to  $46.5^{\circ}C$  and in winter from  $16$  to  $29^{\circ}C$ . Highest elevation in the study area is  $447$  m (m) and the lowest elevation is  $323$  m (MSL). Cotton, Paddy, Red grams and Castor are important crops. Since surface water availability is less, dependency on groundwater for irrigation is more. High dependency on groundwater is the major cause for the depletion of water table. Toposheets (No: 56 k/15 and 56 k/16) collected from Survey of India are used in the present study [5]. As shown in Fig. 1, nineteen (19) observation wells are selected at random to collect the data for development of the model.

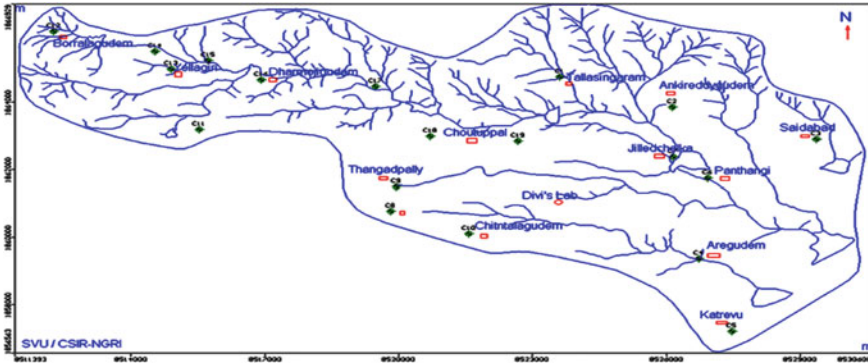


Fig. 1 Location of observation wells in the study area

### 2.2 Geology and Hydrogeology

Study area is covered with weathered, medium to coarse grained, pink to grey coloured granite, gneiss and dolerite rocks. Granitic rocks are found to be well jointed. Further, the vertical distribution of the geology of the study area is obtained through VES using Schlumberger method.

Top 19–21 m layer is made up of weathered rock overlain by a fractured rock of same thickness. A relatively hard and impervious bed lies below fractured rock. Therefore, for the development of MODFLOW and MT3DMS for the study area, a conceptual model of two layers (weathered and fractured rocks) each of thickness 20 m is used in the present study. Significant deformation has produced a network of intersecting fractures to facilitate hydraulic continuity between the two systems. Study area contains unconfined and confined aquifers. Groundwater is present in both weathered and fractured zones. Since precipitation is the primary source of groundwater recharge, rainfall data were collected from Agriculture office, Choutuppal.

### 2.3 Analysis Using Spectrophotometer

Using Spectrophotometer, groundwater quality parameters such as pH, TDS, Fluorides, Nitrates and Sulphates are determined in the NGRI laboratory as listed in Table 1. Results have shown that the TDS and Fluoride concentrations are high [6]. Several persons were found affected from dental cavities and bone deformation.

**Table 1** Various water quality parameters

| Observation Well No | Location       | pH  | TDS (mg/l) | Fluoride (mg/l) | Nitrates (mg/l) | Sulphates (mg/l) |
|---------------------|----------------|-----|------------|-----------------|-----------------|------------------|
| 1                   | Tallasingaram  | 7.3 | 430        | 1.1             | 6               | 50               |
| 2                   | Ankireddygudem | 8.0 | 410        | 0.45            | 26.5            | 40               |
| 3                   | Saidabad       | 7.4 | 600        | 0.55            | 26.5            | 105              |
| 4                   | Aregudem       | 7.6 | 920        | 3.65            | 4.5             | 50               |
| 5                   | Katrevu        | 7.6 | 790        | 5.3             | 7.5             | 55               |
| 6                   | Panthangi      | 7.3 | 820        | 0.85            | 8.5             | 120              |
| 7                   | Jilledchelka   | 7.6 | 760        | 1.3             | 6.5             | 260              |
| 8                   | Damera         | 7.1 | 720        | 2.15            | 30              | 105              |
| 9                   | Thangadpally   | 7.2 | 730        | 1.35            | 29.5            | 85               |
| 10                  | Chintalagudem  | 7.1 | 740        | 2.05            | 8               | 80               |
| 11                  | Koyyalagudem   | 7.1 | 930        | 0.45            | 60.5            | 310              |
| 12                  | Borrolagudem   | 7.6 | 540        | 1               | 43.5            | 65               |
| 13                  | Yellagiri      | 7.6 | 730        | 0.75            | 34              | 175              |
| 14                  | Mukudonibavi   | 8.2 | 550        | 1.1             | 19              | 130              |
| 15                  | Yellambavi     | 7.3 | 650        | 1.35            | 23.5            | 135              |
| 16                  | Dharmojigudem  | 7.1 | 1050       | 1               | 43.5            | 345              |
| 17                  | Lakkaram       | 7.5 | 990        | 1.3             | 27              | 270              |
| 18                  | Choutuppal (1) | 7.2 | 900        | 0.65            | 14.5            | 135              |
| 19                  | Choutuppal (2) | 7.6 | 970        | 1.95            | 4               | 125              |

### 3 Solute Transport Model

Partial differentiation equation describing three-dimensional transport of contaminant in groundwater is given by

$$\frac{\partial(C)}{\partial t} = \frac{\partial}{\partial x_i} \left( D_{ij} \frac{\partial C}{\partial x_j} \right) - \frac{\partial}{\partial x_j} (C V_j) + \frac{q_s}{n} C_s + \sum_{k=1}^N R_k \quad (1)$$

where  $C$  is the concentration of contaminants dissolved in groundwater,  $t$  is the time,  $x_j$  is the distance along  $x$ -axis,  $D_{ij}$  is the hydrodynamic dispersion coefficient,  $V_j$  is the seepage velocity,  $q_s$  is the volumetric flux of water per unit volume of aquifer representing sources (positive) and sinks (negative),  $C_s$  is the concentration of the sources or sinks,  $n$  is the porosity and  $R_k$  is the chemical reaction.

Transport of TDS has been investigated by using MT3DMS, which is a computer model for simulation of advection, dispersion and chemical reactions of soluble

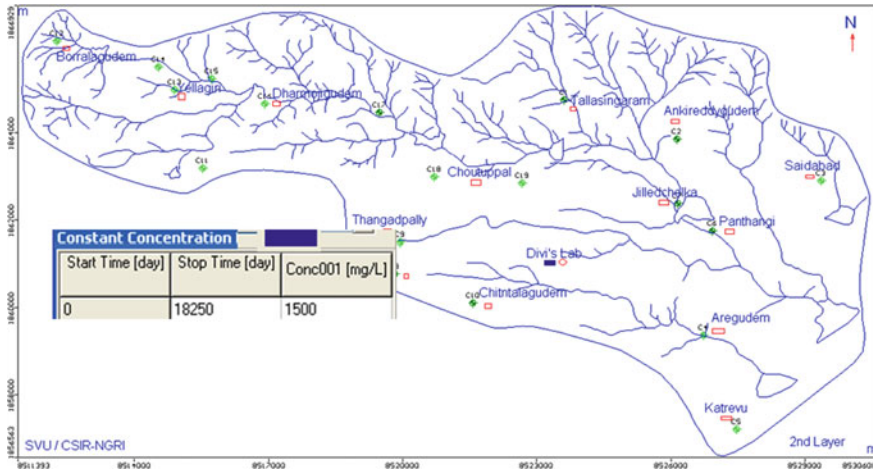


Fig. 2 Source location and TDS concentration near Divi's industries

contaminants in three-dimensional groundwater flow systems [7, 8]. The groundwater velocity field has been computed from the flow model by assuming an effective porosity of 0.1. The computed groundwater velocity field indicates a maximum groundwater velocity of 80 m/y and a minimum of 7 m/y. The same velocity field is used for computing contaminant migration in the study area in the development of mass transport model considering dispersion of contaminant. In the model, longitudinal dispersivity was assumed as 20 m and the ratio of horizontal/longitudinal and vertical/longitudinal dispersivity was assumed as 0.1 and 0.01 respectively [9].

In Choutuppal Mandal, Divis industry is the one which is in part of the watershed area. The pollutant movement in the area and its variation with time, unit rate of TDS concentration is assumed to be applied from a point where the industry is located. Maximum TDS concentration was assigned of about 1500 mg/l reaching groundwater table during its respective active period [10] (Fig. 2).

Computed TDS plume originating from the source have been found increasing initially. The predicted TDS concentrations for various years present that the TDS plume migration is limited to a small area not exceeding 200 m<sup>2</sup> in the downstream of Divis area. The concentration is shown in two layers for 1, 5, 20 and 50 years [11].

Mass transport modelling has demonstrated the contaminant migration from the source location [12, 13]. The migration pattern of contaminant plume from the MT3DMS model indicated that it may take about 20 years to attain the natural background condition. The vertical migration was predicated along Column 50 indicates migration pattern with the depth is very slow and hardly restricted to 200–300 m from the source area [14, 15].

Figure 3a, b illustrate the extent of plume formation pertaining to 1-year period for the layers-I and II. A very close observation of the nature of plume indicates that the colour concentration is NOT the same over the entire plume area. At the centre of the plume, a very small extent of RED colour is found, indicating the area of spread

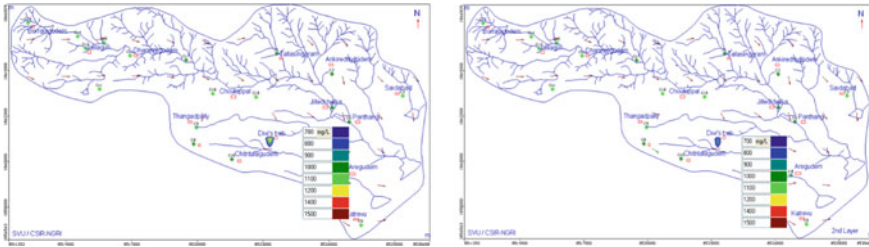


**Fig. 3** Predicted TDS (mg/l) plume in the mass transport model for 1 year in **a** 1st layer and **b** 2nd layer

of TDS of 1400 mg/l in one year. Around this RED coloured area, is the area with LIGHT GREEN spread over a relatively larger area. This indicates that, over this area, the concentration of TDS in 1 year will be around 1100 mg/l. Further, around this LIGHT GREEN area, there is a plume with DARK GREEN colour, indicating the areal extent of TDS of 1000 mg/l [16, 17].

Similar to earlier observations the nature of plume indicates that plume has different colour concentrations for different years in different layers.

Figure 5a, b indicates horizontal dispersion of pollutant, in terms of TDS, over a period of 5 years in layer I and layer II respectively. The spreading of contaminants over a greater region is clearly visible for 5 years.

It is noted that the spreading of contaminants over the same region is reduced when reaches 50 years.

## 4 Results and Discussions

A simulation period of 18250 days (50 years) was applied. The same time was subdivided into four time intervals. The contaminant plume was obtained for 1, 5, 20 and 50 years (365, 1800, 7300 and 18250 days). The results obtained from the model are shown in Figs. 3, 4, 5, 6, 7, 8, 9, 10 and 11 near Divis Industries. From the results, it is noted that the extent of the plume area varies for different years. The groundwater velocity is so small as the change in the conductivity affects the velocity.

## 5 Conclusions

This paper presents a thorough understanding of the contaminant migration and the factors governing the quality of groundwater in the aquifer system. The modelling study has helped in gaining a better insight into the assessment of contamination

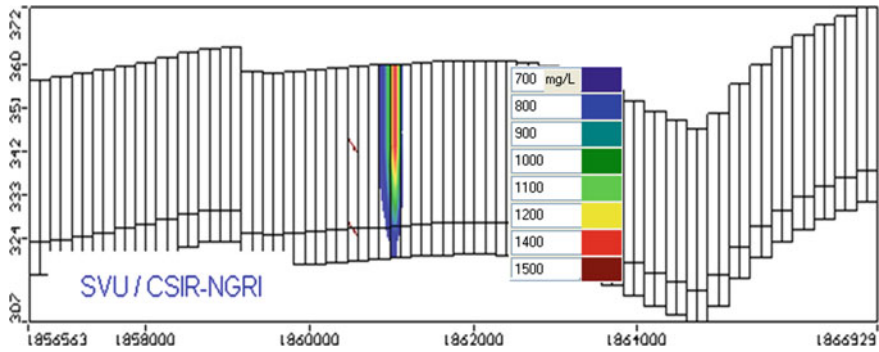


Fig. 4 Predicted TDS (mg/l) plume along column 50 after 1 year

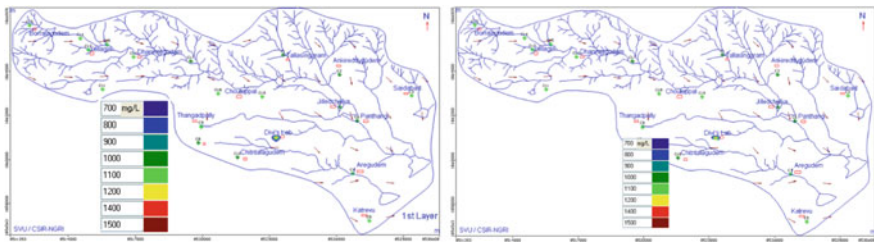


Fig. 5 Predicted TDS (mg/l) plume in the mass transport model for 5 years in a 1st layer and b 2nd layer

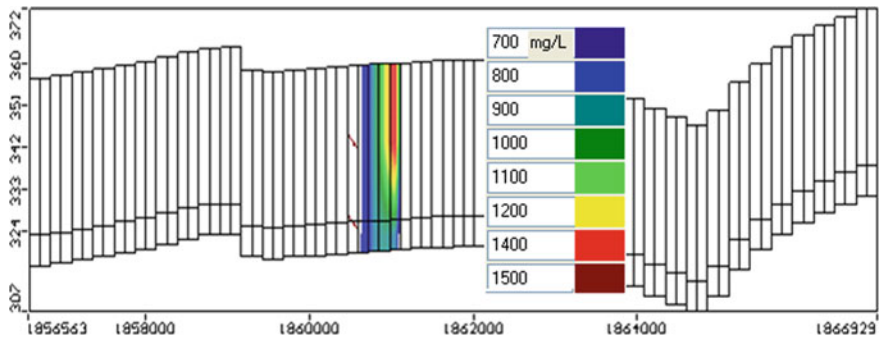
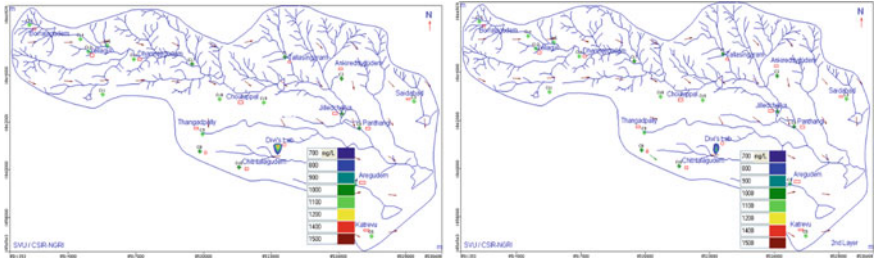


Fig. 6 Predicted TDS (mg/l) plume along column 50 after 5 years

migration due to mass transport processes. It is observed that the higher concentration of TDS and Fluoride in the study area; due to various activities like domestic effluents, agriculture and local anthropogenic activities are directed into the groundwater, which would be the principal cause of increasing the concentration of the ions in the water. Groundwater models are tools frequently used in studying aquifer





**Fig. 7** Predicted TDS (mg/l) plume in the mass transport model for 10 years in **a** 1st layer and **b** 2nd layer

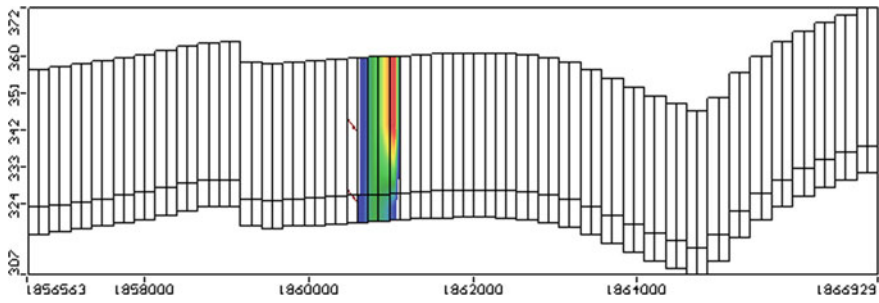


**Fig. 8** Predicted TDS (mg/l) plume along column 50 after 10 years

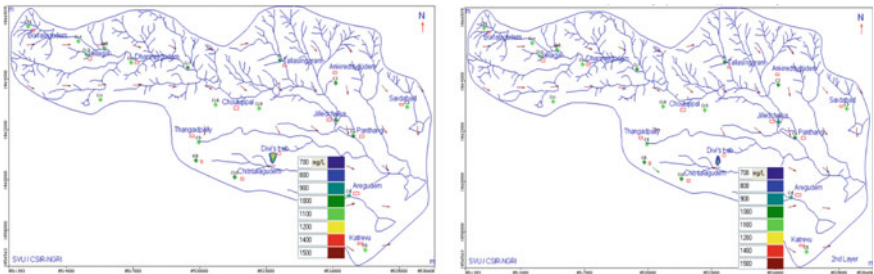


**Fig. 9** Predicted TDS (mg/l) plume in the mass transport model for 20 years in **a** 1st layer and **b** 2nd layer

systems. Though the effect of contaminant migration is currently minimal, the model which is developed in this study area shows the contamination of the well field. It is found from the mass transport model predictions that migration of the plume is very slow and hardly restricted to 200–300 m<sup>2</sup> from the source area only.

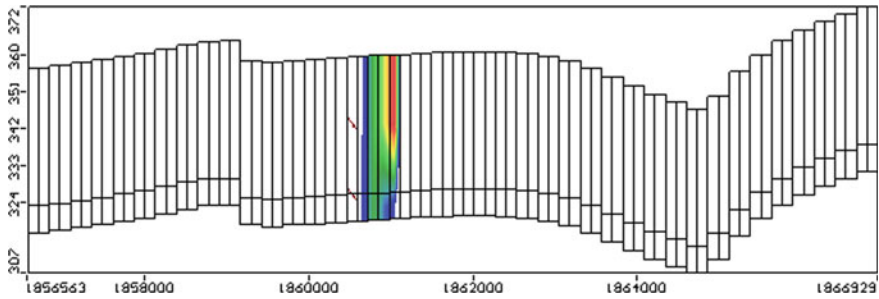


**Fig. 10** Predicted TDS (mg/l) plume along column 50 after 20 years

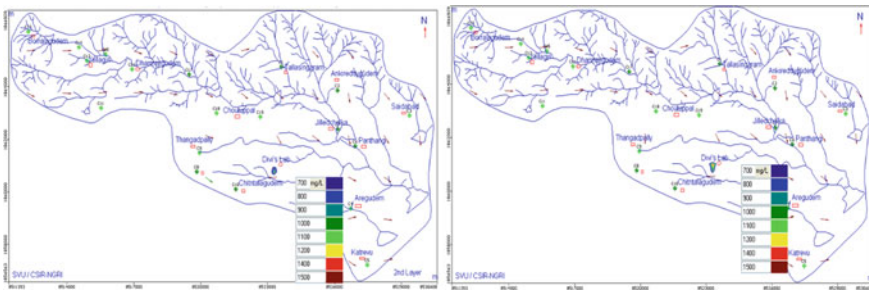


**Fig. 11** Predicted TDS (mg/l) plume in the mass transport model for 50 years in **a** 1st layer and **b** 2nd layer

**Acknowledgements** The authors express their thankfulness to the director of NGRI for his imminent support and great encouragement. The authors are thankful to V.V.S. Gurunadha Rao Deputy Director (Retd.) Environmental Hydrology Group for completion of the work.

**References**

1. Subba Rao N, Gurunadha Rao VVS (1999) Pathlines of pollutant migration in groundwater of the Visakhapatnam urban area, India. *Hydrol Process* 13:1381–1389
2. Varghese GK, Alappat BJ, Samad MSA (2015) MT3DMS and genetic algorithm in environmental forensic investigations. *Procedia Environ Sci* 30:85–90
3. Shuwei Q, Xiujuan L, Changlai X, Bo L, Jinfeng L (2013) Solving for dispersivity in field dispersion test for unsteady flow in mixing flow fluid: mass transport modeling. *Procedia Earth Planet Sci* 7:709–712
4. Gurunadha Rao VVS, Dhar RL, Subrahmanyam K (2001) Assessment of contaminant migration in groundwater from an industrial development area, Medak district, Andhra Pradesh, India. *Kluwer Academic Publishers*, vol 128, pp 369–389
5. Kumar D, Mondal S, Nandan MJ, Harini P, Soma Sekhar BMV, Sen MK (2016) Two-dimensional electrical resistivity tomography (ERT) and time-domain-induced polarization (TDIP) study in hard rock for groundwater investigation: a case study at Choutuppal Telangana, India. *Arab J Geosci* 9:355

6. BIS (Bureau of Indian Standards) 10500, Indian Standard Drinking Water— specification, 2nd revision (2012)
7. Rahnama MB, Zamzam A (2013) Quantitative and qualitative simulation of groundwater by mathematical models in Rafsanjan aquifer using MODFLOW and MT3DMS. *Arab J Geosci* 6:901–912
8. Zhang H, Xu WL, Hiscock KM (2013) Application of MT3DMS and geographic information system to evaluation of groundwater contamination in the sherwood sandstone aquifer, UK. *Water Air Soil Pollution* 224:1438
9. Ghoraba SM, Zyedan BA, Rashwan IMH (2013) Solute transport modeling of the groundwater for quaternary aquifer quality management in Middle Delta, Egypt. *Alexandria Eng J* 52:197–207
10. Chen C-S, Chia-Huei Tu, Chen S-J, Chen C-C (2016) Simulation of groundwater contaminant transport at a decommissioned landfill site—a case study, Tainan City, Taiwan. *Int J Environ Res Public Health* 13:467
11. Mondal NC, Singh VS (2009) Mass transport modeling of an industrial belt using visual MODFLOW and MODPATH: A case study. *J Geogr Reg Planning* 2(1):001–019
12. Abu-El-Sha WY, Hatamleh RI (2007) Using Modflow and MT3D groundwater flow and transport models as a management tool for the Azraq groundwater system. *Jordan J Civ Eng* 1(2)
13. Zhang H, Yang R, Guo S et al (2020) Modeling fertilization impacts on nitrate leaching and groundwater contamination with HYDRUS-1D and MT3DMS. *Paddy Water Environ* 18:481–498
14. Hussein EE, Fouad M, Gad MI (2019) Prediction of the pollutants movements from the polluted industrial zone in 10th of Ramadan city to the Quaternary aquifer. *Appl Water Science* 9:20
15. Guo Z, Fogg GE, Brusseau ML et al (2019) Modeling groundwater contaminant transport in the presence of large heterogeneity: a case study comparing MT3D and RWhet. *Hydrogeol J* 27:1363–1371
16. Rajamanickam R, Nagan S (2010) Groundwater quality modeling of Amaravathi river basin of Karur District, Tamil Nadu, using visual Modflow. *Int J Environ Sci* 1(1)
17. Seyed RS, Saari M (2011) Prediction of contamination migration in an unconfined aquifer with visual MODFLOW: a case study. *World Appl Sci J* 14 (7):1102–1106

# Water Quality Analysis at Mancherial, Jagdalpur and Konta Using Non-parametric Methods



Chintalacheruvu Madhusudana Rao, Prakhar Modi, and D. Jhajharia

**Abstract** The present work aims to gain a better understanding of water quality aspect in Godavari River, for which the temporal and spatial variations in the concentration levels of Ca, Cl and Na is analyzed. A total of 3 gauging stations namely Mancherial, Jagdalpur and Konta are chosen and their records of 25 years spanning from 1981 to 2005, divided into Pre-Monsoon, Monsoon and Post-Monsoon seasons annually is used. Normality test using Kolmogorov-Smirnov and Shapiro-Wilk test is conducted which indicates the use of non-parametric Mann-Kendall's and Sen's slope test to detect the presence of statistically significant trend in the concentrations and its magnitude, respectively. The results of M-K test show a significant increasing trend in Ca at Mancherial and Jagdalpur gauging station during all seasons, whereas a significant decreasing trend is observed in concentrations of Cl in different seasons. No significant trend is detected in the concentrations of Na. It is found out that no parameter behaves similarly during all three seasons. The Sen's slope test shows that there is an average increase of 0.65 unit per year in the concentration of Ca and an average decrease of 2.2 unit per year in the concentration of Cl seasonally. The present study also uses a second order auto-regressive model (AR (2)) to generate and forecast the concentrations of various water quality parameters. The concentrations of parameters were forecasted for the next 25 years using AR (2) model. The accuracy of AR (2) model to generate the concentrations is assessed using NSE and  $R^2$  values which are found to be more than 0.85 in both calibration and validation periods. The value of MSE was also found well within the limits to verify the accuracy of the model. So, the results of the present study may provide some guidance to monitor the water quality in Godavari river.

**Keywords** Normality test · Mann-Kendall test · Sen's Slope test · Auto-regression model · Godavari river

---

C. M. Rao (✉) · P. Modi

Department of Civil Engineering, National Institute of Technology Jamshedpur, Jamshedpur, India  
e-mail: [cmrao.civil@nitjsr.ac.in](mailto:cmrao.civil@nitjsr.ac.in)

D. Jhajharia

Department of Soil and Water Conservation Engineering, College of Agricultural Engineering and Post-Harvest Technology, Sikkim, India

## 1 Introduction

The assessment of river water quality is a subject of great concern in the present times. The understanding of various processes and factors that affect river water quality is of major importance. It is very important to understand the pattern in the variations of various water quality parameters in order to understand and predict the changes in various hydrological processes. However, the process of analyzing changes in long term water quality parameters can be a very exigent task. One of the major developments in the field of river water quality analysis is thus acquisition and storage of reliable long term water quality data records, which can possibly be used to detect significant trends [10]. To detect temporal and spatial changes in water quality parameters is the most important task in river water quality monitoring. Trend analysis in the concentrations of water quality parameters can be used to identify the deterioration in river water quality and accordingly can be used to rectify the causes. The detection and estimation of possible trends are complicated by problems related to characteristics of water quality data. These characteristics are presence of seasonality, skewness, kurtosis, correlation, non-normal data, outliers and missing values [11, 12], therefore some special statistical tests are developed to deal with these possibilities.

The primary purpose of trend analysis is to determine whether the values of random variable generally increases (or decreases) over a period of time in statistical terms [9]. Various statistical approaches broadly, parametric and non-parametric tests, are currently available to detect and estimate trends present in a time series. If a parametric test is used, it requires data to be normally distributed and it restricts analysis for annual data series, for which independence assumptions are acceptable [9]. In non-parametric test, fewer assumptions are made about the data [15] and it is not necessary to assume a distribution. However, many of these tests still trust assumptions of independence. Several researchers have used the non-parametric methods with fewer assumptions to detect trends in the water quality parameters [12, 19, 21, 22]. Antonopoulos et al. [1] detected trends in water quality and quantity data for Strymon river in Greece. Drapela and Drapelova [5] used Mann-Kendall test and Sen's Slope estimates to detect trend in deposition data.

Predicting the potential change in the concentrations of water quality parameters could be a vital step in preparing oneself for unforeseen future water quality problems. In fact, it will be much convenient if the concentrations of these water quality parameters can be forecasted for the future. Various time series model has been used to simulate the observed concentration of water quality parameters so that the model can be used to forecast with high accuracy. ARIMA models have been used for time series analysis to study the water quality in rivers [6, 8, 16]. Jalal Kamali [13] also used time series models to evaluate monthly inflows in Jiroft dam. Dalme and Yalcin [3] applied time series model in Mississippi River for flood forecasting. Jassby et al. [14] formulated a time series model considering inter annual variability for Secchi depth in Lake Tahoe, the USA for Secchi depth. The time series method can be used to determine concentration that is measured over certain time intervals.

Auto-Regressive (AR) is one of the widely used time series methods, that can be used for forecasting the concentrations of water quality parameters. In the present study, water quality analysis has been conducted in Godavari River. Trend analysis in the concentration of Ca, Cl and Na have been conducted using non-parametric methods at three water quality gauging stations. Second order auto-regressive model is used to generate and forecast the concentrations of water quality parameters.

## 2 Study Area

In the present study, three stations are chosen from three different sub-basins namely Godavari lower sub-basin, Indravati sub-basin and Pranhita and other sub-basin which comprises of Konta, Jagdalpur and ManCherial stations respectively as shown in Fig. 1.

Godavari lower sub-basin incorporates around 14.7% of area whereas the Indravati and Pranhita incorporates 12.6% and 11.9% area respectively of total Godavari basin [2]. ManCherial is located on Godavari river whereas Jagdalpur lies on Indravati river and Konta lies on Sabari river which are the two major tributaries of Godavari. There are various industries and mines situated near the gauging stations which

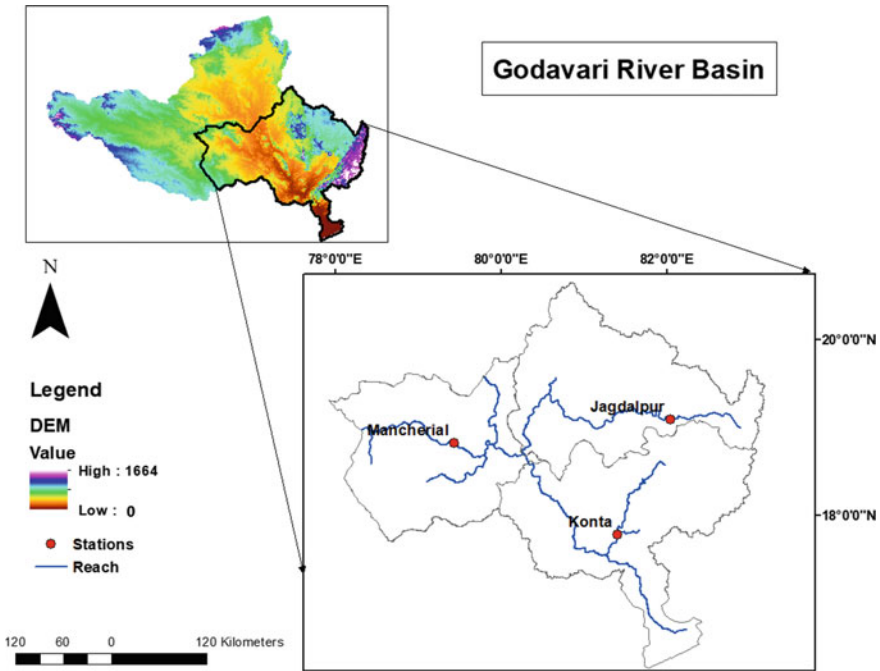


Fig. 1 Location map of study area

causes heavy disposal of wastes, due to which parameters Ca, Cl and Na is selected for the water quality analysis. From the observed data, Mancherial shows highest concentration of all parameters as compared to other two stations. It may be due to the various industries situated upstream of Mancherial in Maharashtra and Andhra Pradesh and also due to the presence of mines in Mancherial district. The principal source of Godavari river pollution is sewage which constitutes about 84–92% and industrial waste which constitute about 8–16% [4].

### 3 Methodology

A total of 25 years (1981–2005) of water quality data, which includes Calcium (Ca), Chlorine (Cl) and Sodium (Na), were collected seasonally at Mancherial, Jagdalpur and Konta station for water quality monitoring in Godavari River basin. The data have been collected annually for three seasons namely Pre-Monsoon (March–May), Monsoon (June–October) and Post-Monsoon (November–February).

As it is important to check the normality of a data distribution because it provides a sense in selecting proper trend detection method. In the present study, the most commonly used Kolmogorov-Smirnov (K-S) test and Shapiro-Wilk (S-W) test is employed to check the normality of the time series. Both the test compares the distribution of the time series with normal distribution with same mean and standard deviation as of the given time series to determine the normality within the significance level. Although, some researchers have recommended the S-W test as best for testing the normality of a distribution [18, 20].

The series of seasonal annual concentrations of Ca, Cl and Na are then tested for monotonic increasing or decreasing trend using the non-parametric Mann-Kendall trend test [7]. The Sen's Slope test [17] is used to test the magnitude of the M-K test. It is used to estimate the change per unit time in time series that shows a monotonic trend. The M-K test can be used if the possible trend in the data series can be considered monotonic and should not be characterized by seasonality. If the p-value of the test is smaller than the significance level than the null hypothesis  $H_0$  of no trend is rejected and alternate hypothesis  $H_1$  of presence of increasing or decreasing trend is accepted. In the present study, the null hypothesis has been tested against 5% significance level.

In the present study, second order auto-regressive model (AR (2)) is used to generate and forecast the concentration of water quality parameters. The auto-regressive model AR (2) can be expressed as,

$$x_t = \varphi_1 x_{t-1} + \varphi_2 x_{t-2} + \xi_t \quad (1)$$

Here, the  $\varphi_1$ ,  $\varphi_2$  are the parameter of the process which depends on serial correlation coefficient of respective order and  $\xi_t$  is an independent process, i.e. a random variate that follows normal distribution. The  $x_{t-1}$  and  $x_{t-2}$  are the concentrations at previous time levels.

The AR (2) model is used to generate and forecast the concentration of water quality parameters. A total period of 25 years was divided into 10 years (1981–1990) as calibration period and 15 years (1991–2005) as validation period for AR (2) model. The model is also used in forecasting the concentrations for next 25 years (2006–2030) and the performance of the model was assessed using indicators such as Nash-Sutcliffe efficiency (NSE) and Coefficient of Determination ( $R^2$ ). To evaluate forecast accuracy, Mean Square Error (MSE) is computed.

## 4 Result and Discussion

The concentrations of all the parameters were tested for normality conditions using Kolmogorov-Smirnov and Shapiro-Wilk test at a significance level of 5%. The results of K-S test with Lilliefors significance correction and S-W test are presented in Table 1. It can be seen that both the tests show similar results for most of the concentrations, unlike Konta in post-monsoon season for Ca shows normality only as per the S-W test, also Jagdalpur in post-monsoon season for Cl and Konta in pre-monsoon season for Na shows normality only in accordance with K-S test. The difference in K-S and S-W tests may be due to the fact that K-S test has been applied using Lilliefors significance correction. The normality test highlights non-normal distribution seasonally for a parameter. At a particular station, a parameter shows normal distribution for a season and non-normal distribution for another season.

As most of the stations have non-normal distribution, so non-parametric trend tests such as Mann-Kendall's test and Sen's Slope test is used to detect a trend in concentrations of water quality parameters seasonally. The results of non-parametric Mann-Kendall's and Sen Slope tests are summarized in Table 1. If the p-value found is less than or equal to significance level 0.05, then the corresponding estimates of Sen Slope are statistically significant, else it is statistically insignificant and no trend condition exists.

A significant increasing trend is only detected in the concentrations of Ca at Mancherial and Jagdalpur stations for all three seasons. The Sen slope estimates show the increase in concentrations of Ca at an average rate of 0.65 units per year seasonally. The increase in concentration of Ca at Mancherial may be caused due to the limestone mine situated in Mancherial district and at Jagdalpur, it may get dissolved from most of the soil and rocks found there. On the other hand, in Konta the increasing trend in Ca only prevails during the pre-monsoon season. A significant decreasing trend is observed in Cl for all stations in different seasons. The decrease in concentration of Cl was estimated at an average rate of 2.2 units per year seasonally. The decrease in Cl concentration can be the result of reduction in agricultural activities or due to dilution factors. No statistically significant trend was found in concentrations of Sodium (Na) at all three stations in all seasons. The concentration of sodium shows an independent behaviour and its concentration cannot be predicted with any proper evidence.



**Table 1** Normality test, M-K trend and Sen’s slope estimator results for all parameter

| Parameter | Station    | Season       | K-S test<br>( <i>p</i> -value) | S-W test<br>( <i>p</i> -value) | Kendall’s test<br>( <i>p</i> -value) | Sen’s slope estimates | Nature of trend |
|-----------|------------|--------------|--------------------------------|--------------------------------|--------------------------------------|-----------------------|-----------------|
| Ca        | Mancherial | Pre-monsoon  | <b>0.200*</b>                  | <b>0.690</b>                   | <b>0.026</b>                         | 0.442                 | <b>I</b>        |
|           |            | Monsoon      | <b>0.099</b>                   | <b>0.721</b>                   | <b>0.020</b>                         | 0.6                   | <b>I</b>        |
|           |            | Post-monsoon | <b>0.200*</b>                  | <b>0.209</b>                   | <b>0.003</b>                         | 0.833                 | <b>I</b>        |
|           | Jagdapur   | Pre-monsoon  | 0.015                          | 0.007                          | <b>0.000</b>                         | 0.782                 | <b>I</b>        |
|           |            | Monsoon      | <b>0.200*</b>                  | <b>0.080</b>                   | <b>0.000</b>                         | 0.341                 | <b>I</b>        |
|           |            | Post-monsoon | 0.002                          | 0.014                          | <b>0.000</b>                         | 0.892                 | <b>I</b>        |
|           | Konta      | Pre-monsoon  | <b>0.068</b>                   | <b>0.213</b>                   | 0.013                                | 0.178                 | <b>I</b>        |
|           |            | Monsoon      | 0.005                          | 0.043                          | 0.096                                | 0.049                 | N               |
|           |            | Post-monsoon | 0.024                          | <b>0.070</b>                   | 0.308                                | 0.077                 | N               |
| Cl        | Mancherial | Pre-monsoon  | 0.009                          | 0.001                          | 0.543                                | -0.116                | N               |
|           |            | Monsoon      | 0.001                          | 0.000                          | <b>0.045</b>                         | -0.228                | <b>D</b>        |
|           |            | Post-monsoon | <b>0.200*</b>                  | <b>0.506</b>                   | 0.112                                | -0.19                 | N               |
|           | Jagdapur   | Pre-monsoon  | 0.030                          | 0.022                          | <b>0.042</b>                         | -0.183                | <b>D</b>        |
|           |            | Monsoon      | <b>0.200*</b>                  | <b>0.682</b>                   | 0.401                                | -0.1                  | N               |
|           |            | Post-monsoon | <b>0.200*</b>                  | 0.027                          | 0.123                                | -0.1                  | N               |
|           | Konta      | Pre-monsoon  | 0.023                          | 0.000                          | 0.096                                | -0.121                | N               |
|           |            | Monsoon      | 0.010                          | 0.000                          | 0.304                                | -0.065                | N               |
|           |            | Post-monsoon | <b>0.157</b>                   | <b>0.142</b>                   | <b>0.006</b>                         | -0.2                  | <b>D</b>        |
| Na        | Mancherial | Pre-monsoon  | <b>0.200*</b>                  | <b>0.586</b>                   | 0.283                                | -0.306                | N               |
|           |            | Monsoon      | <b>0.200*</b>                  | <b>0.516</b>                   | 0.362                                | -0.254                | N               |
|           |            | Post-monsoon | <b>0.200*</b>                  | <b>0.703</b>                   | 0.375                                | -0.132                | N               |
|           | Jagdapur   | Pre-monsoon  | 0.024                          | 0.005                          | 0.167                                | 0.044                 | N               |
|           |            | Monsoon      | 0.004                          | 0.000                          | 0.591                                | 0.031                 | N               |
|           |            | Post-monsoon | <b>0.200*</b>                  | <b>0.212</b>                   | 0.722                                | 0.017                 | N               |
|           | Konta      | Pre-monsoon  | <b>0.078</b>                   | 0.010                          | 0.590                                | -0.021                | N               |
|           |            | Monsoon      | 0.000                          | 0.000                          | 0.325                                | 0.033                 | N               |
|           |            | Post-monsoon | 0.004                          | 0.000                          | 0.859                                | 0.013                 | N               |

\*Lower bound value of true significance *I* increasing trend, *D* Decreasing trend, *N* No trend  
 The bold *p*-values shows statistically significant results. Statistically significant shows that the results are caused not only by chance. It shows the validity of null hypothesis, which hypothesizes that there is nothing more than random chance

Table 2 show the details of performance indicators used namely N-S efficiency and  $R^2$  to assess the potential of the AR (2) model to simulate the concentration of water quality parameters. The AR (2) model is used to generate and forecast the concentrations of water quality parameters. A calibration period of 10 years (1981–1990), validation period of 15 years (1991–2005) and forecasting period of

**Table 2** Performance indicators and MSE of AR (2) model

| Parameter | Station    | Season       | NSE   |       | $R^2$ |       | MSE   |       |
|-----------|------------|--------------|-------|-------|-------|-------|-------|-------|
|           |            |              | Cal   | Val   | Cal   | Val   | Cal   | Val   |
| Ca        | Mancherial | Pre-monsoon  | 0.994 | 0.991 | 0.997 | 0.993 | 0.152 | 0.228 |
|           |            | Monsoon      | 0.994 | 0.994 | 0.994 | 0.994 | 0.15  | 0.191 |
|           |            | Post-monsoon | 0.993 | 0.996 | 0.994 | 0.996 | 0.175 | 0.162 |
|           | Jagdalpur  | Pre-monsoon  | 0.966 | 0.996 | 0.973 | 0.996 | 0.142 | 0.208 |
|           |            | Monsoon      | 0.924 | 0.972 | 0.929 | 0.983 | 0.219 | 0.22  |
|           |            | Post-monsoon | 0.96  | 0.998 | 0.978 | 0.998 | 0.117 | 0.142 |
|           | Konta      | Pre-monsoon  | 0.982 | 0.954 | 0.983 | 0.959 | 0.139 | 0.175 |
|           |            | Monsoon      | 0.925 | 0.879 | 0.948 | 0.936 | 0.163 | 0.165 |
|           |            | Post-monsoon | 0.963 | 0.97  | 0.968 | 0.971 | 0.151 | 0.182 |
| Cl        | Mancherial | Pre-monsoon  | 0.995 | 0.993 | 0.996 | 0.993 | 0.141 | 0.187 |
|           |            | Monsoon      | 0.987 | 0.966 | 0.995 | 0.967 | 0.227 | 0.275 |
|           |            | Post-monsoon | 0.988 | 0.983 | 0.99  | 0.984 | 0.145 | 0.105 |
|           | Jagdalpur  | Pre-monsoon  | 0.966 | 0.973 | 0.967 | 0.976 | 0.234 | 0.253 |
|           |            | Monsoon      | 0.899 | 0.963 | 0.935 | 0.966 | 0.149 | 0.228 |
|           |            | Post-monsoon | 0.878 | 0.978 | 0.967 | 0.98  | 0.17  | 0.191 |
|           | Konta      | Pre-monsoon  | 0.962 | 0.991 | 0.968 | 0.992 | 0.1   | 0.088 |
|           |            | Monsoon      | 0.882 | 0.962 | 0.946 | 0.964 | 0.085 | 0.109 |
|           |            | Post-monsoon | 0.977 | 0.978 | 0.979 | 0.979 | 0.068 | 0.105 |
| Na        | Mancherial | Pre-monsoon  | 0.999 | 0.998 | 0.999 | 0.998 | 0.141 | 0.151 |
|           |            | Monsoon      | 0.998 | 0.998 | 0.999 | 0.998 | 0.104 | 0.14  |
|           |            | Post-monsoon | 0.996 | 0.992 | 0.996 | 0.995 | 0.174 | 0.188 |
|           | Jagdalpur  | Pre-monsoon  | 0.954 | 0.952 | 0.956 | 0.962 | 0.203 | 0.158 |
|           |            | Monsoon      | 0.919 | 0.965 | 0.951 | 0.967 | 0.202 | 0.149 |
|           |            | Post-monsoon | 0.964 | 0.957 | 0.974 | 0.959 | 0.106 | 0.141 |
|           | Konta      | Pre-monsoon  | 0.961 | 0.903 | 0.964 | 0.923 | 0.073 | 0.097 |
|           |            | Monsoon      | 0.935 | 0.96  | 0.942 | 0.964 | 0.072 | 0.076 |
|           |            | Post-monsoon | 0.953 | 0.961 | 0.981 | 0.975 | 0.074 | 0.112 |

25 years (2006–2030) is adopted in AR (2) model simulations. It is evident from the results of N-S efficiency and  $R^2$  that the model is capable of simulating the observed concentrations to a satisfactory level. The values of NSE and  $R^2$  is more than 0.90 during both calibration and validation periods except at some stations where the values are above 0.85. It can be inferred that the model is performing well in both calibration and validation periods for all seasons at all three stations. Table 2 also show the details of errors associated with the evaluating forecast accuracy of AR (2) model using MSE. It shows that as the value of MSE is less than 0.2 for most of

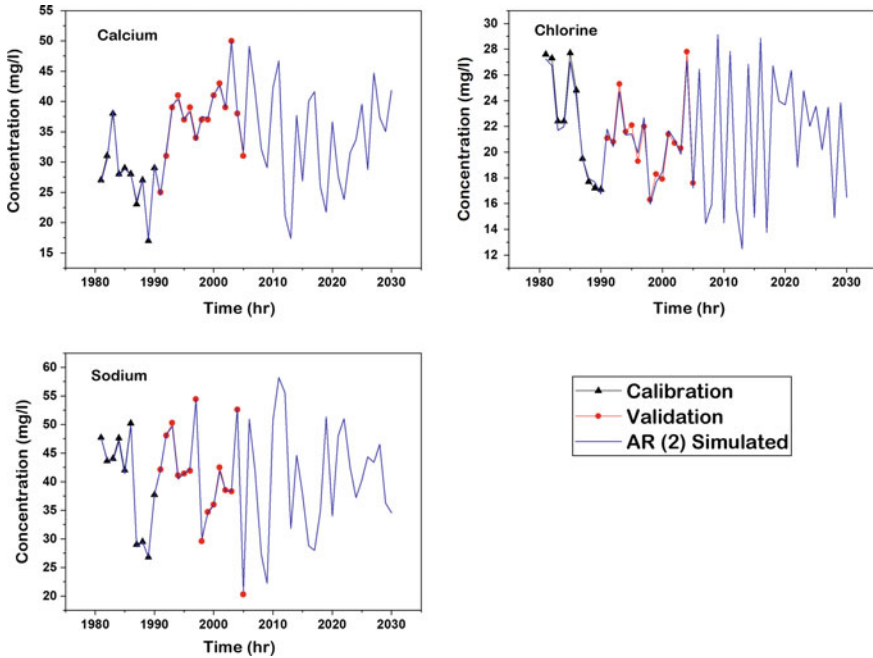


Fig. 2 Results of AR (2) simulation at Mancherial station in monsoon season

the concentrations, so it can be inferred that model can also be used for forecasting purposes.

Figures 2, 3 and 4 shows sample result plots of AR (2) simulation at Mancherial, Jagdalpur and Konta for monsoon, pre-monsoon and post-monsoon season respectively of all three parameters. It can be inferred that AR (2) model is capable to simulate the concentrations of water quality parameters with acceptable level of accuracy.

## 5 Conclusions

The water quality analysis in Godavari river basin using Ca, Cl and Na at three gauging stations shows quite a variety of results. The result of K-S and S-W test reveals non-normal distribution in the concentrations of various water quality parameters, which suggests the use of non-parametric test. The Mann-Kendall test detects significant increasing trend for Ca and significant decreasing trend for Cl at various stations. The increase in Ca concentration may lead to an increase in hardness and also may form some toxic compound which is harmful to living organisms. Also, as Cl is used for purifying water, its decreasing trend is also an alarming issue. The Sen’s slope test estimates the magnitude of significant trends. It is seen that the trends

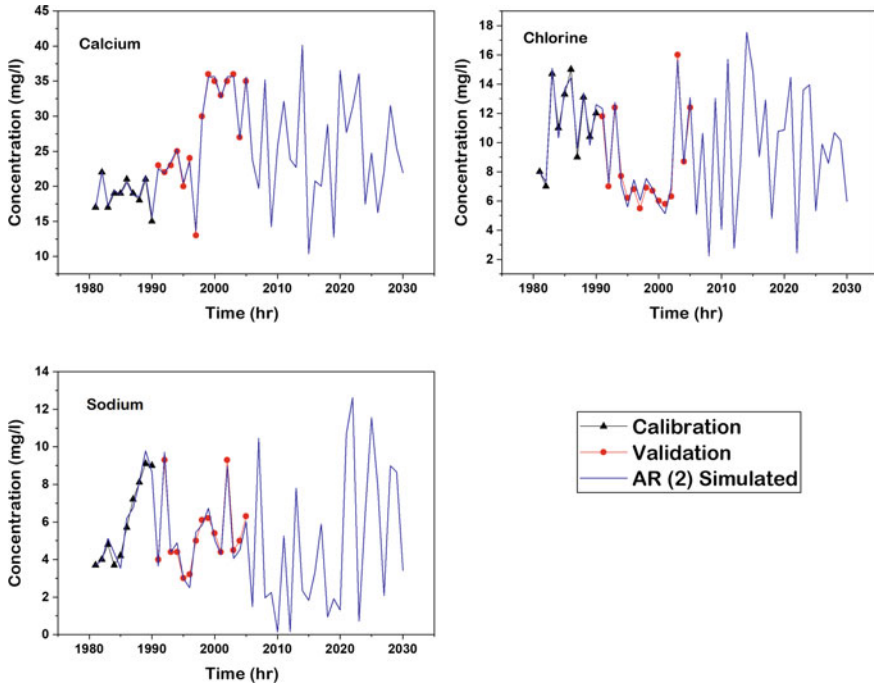
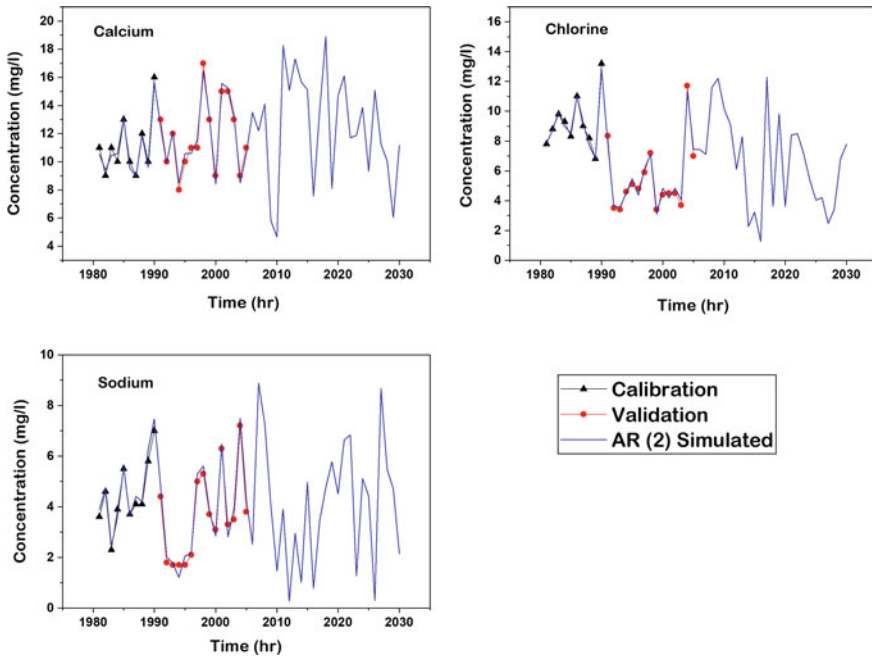


Fig. 3 Results of AR (2) simulation at Jagdalpur station in pre-monsoon season

in a parameter vary from season to season at a particular station. The concentration of Na does not show any trend. Finally, the second order auto-regressive AR (2) model is successfully used to generate and forecast the concentrations in succeeding time steps.



**Fig. 4** Results of AR (2) simulation at Konta station in post-monsoon season

## References

1. Antonopoulos VZ, Papamichail DM, Mitsiou KA (2001) Statistical and trend analysis of water quality and quantity data for the Strymon River in Greece. *Hydrol Earth Syst Sci* 5(4):679–691
2. CWC report on Godavari basin (2014)
3. Dalme C, Yalcin A (2007) Flood prediction using time series data mining. *J Hydrol* 333:305–316
4. Dhirendra MJ, Kumar A, Agrawal N (2009) Studies on Physicochemical parameters to assess the water quality of river Ganga for drinking purpose in Haridwar district. *Rasayan J Chem* 2:195–203
5. Drapela K, Drapelova I (2011) Application of Mann-Kendall test and the Sen's slope estimates for trend detection in deposition data from Bily Kriz 1997–2010. *Beskydy* 4(2):133–146
6. Faruk DO (2010) A hybrid neural network and ARIMA model for water quality time series prediction. *Eng Appl Artif Intell* 23:586–594
7. Gilbert RO (1987) *Statistical methods for environmental pollution monitoring*. Wiley, New York, USA
8. Hanh PTM (2010) Analysis of variation and relation of climate, hydrology and water quality in the lower Mekong River. *Water Sci Tech* 62(7):1587–1594
9. Helsel DR, Hirsch RM (1992) *Statistical methods in water resources*. Elsevier, The Netherlands
10. Hirsch RM, Alexander RB, Smith RA (1991) Selection of methods for the detection and estimation of trends in water quality. *Water Resour Res* 27:803–813
11. Hirsch RM, Slack JR, Smith RA (1982) Techniques of trend analysis for monthly water quality data. *Water Resour Res* 18:107–121
12. Hirsch RM, Slack JR (1984) A nonparametric trend test for seasonal data with serial dependence. *Water Resour Res* 20:727–732

13. Jalal Kamali N (2006) Forecasting the variations of inflow to Jiroft Dam using Time Series Theories. In: 6th international seminar on River Engineering, Shahid Chamran University, Ahvaz, Iran
14. Jassby AD, Reuter JE, Goldman CR (2003) Determining long term water quality change in the presence of climate variability. Lake Tahoe (USA). *Can J Fisheries Aquatic Sci* 60:1452–1461
15. Kundzewicz ZW, Robson AJ (2004) Change detection in river flow records—a review of the methodology. *Hydrol Sci J* 49(1):7–19
16. Lehmann A, Rode M (2001) Long-term behaviour and cross-correlation water quality analysis of the River Elbe, Germany. *Water Res* 35:2153–2160
17. Sen PK (1968) Estimates of the regression coefficient based on Kendall's tau. *J Am Stat Assoc* 63:1379–1389
18. Thode HJ (2002) Testing for normality. Marcel Dekker, New York
19. Van Belle G, Hughes JP (1984) Nonparametric tests for trend in water quality. *Water Resour Res* 20(1):127–136
20. Yap BW, Sim CH (2011) Comparisons of various types of normality test. *J Stat Comput Simul* 81(12):2141–2155
21. Yu Y.-S., Zou S. and Whittemore D. (1991). Trend analysis of surface-water quality of the upper and lower Arkansas River basin in Kansas; Contribution No. 291, Kansas Water Resources Research Institute.
22. Yu Y-S, Zou S, Whittemore D (1993) Non-parametric trend analysis of water quality data of rivers in Kansas. *J Hydrol* 150:61–80

# Assessment of Water Quality of River Mutha for Onsite Treatment of Polluted River Water



Rohini More and Sameer Shastri

**Abstract** Water is one of the elements of Panch Mahabhutas and precious gift by the nature. Rivers play an important role in social and economic development. Rivers are frequently worshiped in India, however even with this greater recognition closer to rivers, we are unable to preserve their purity, cleanliness, and bodily well-being. Human activities are the primary sources for the contamination of water bodies like rivers, lakes, seas, and groundwater. The pollution in the river has direct as well as indirect impacts on the living species. The solution to reduce pollution of rivers can be proposed by providing online non-mechanized treatment system. Rivers downstream of the Dams, when flow through Pune city, receives discharge of partially treated or untreated sewage. Proper water quality assessment of such polluted rivers is the basic step before implementing any treatment system. This work highlights the water quality assessment carried out for polluted River Mutha which will be the basis for the proposed online treatment. There are many conventional methods for treatment of water which have been designed and used. All the treatment methods require high capital cost, maintenance cost, and labor cost. Therefore, a non-mechanized system needs to be evolved and studied. Like many cities, Pune also has sewerage network as well as STPs. However, 100% collection, conveyance, and treatment of sewage is not happening and untreated sewage finds its way into the River Mutha. There is a possibility of online treatment of rivers which will result in considerable improvement in water quality. The present findings of water quality will be helpful to check the feasibility of proposed system.

**Keywords** Water pollution · River Mutha · Water quality assessment · Non-mechanized system

---

R. More (✉) · S. Shastri  
Sinhgad College of Engineering, Pune 411041, India

S. Shastri  
e-mail: [ssshastriscoe@sinhgad.edu](mailto:ssshastriscoe@sinhgad.edu)

## 1 Introduction

Rivers play an important role in social and economic development [1]. Human activities are the number one reasserts for the infection of water bodies like rivers, lakes, seas, and groundwater. Human societies have settled down at the bank of rivers, this is the primary reason for pollution of rivers. The flowing rivers are getting polluted due to human activities and effluents from industries [2]. Around 80% of the domestic used water comes as waste water. The most important reason for pollution is untreated domestic waste water discharged into the river due to inadequate sewerage system, ascent of population still as open evacuation on watercourse banks.

Due to rapid increase in Globalization and Industrialization, providing quality water to the public is the main challenge faced by the country. The disposal of untreated point and non-point sources pollutants into the rivers causing more number of rivers to get polluted. The performing our bodies including municipalities are dealing with the issues to deal with river water to secure degrees and distribute it to human beings for domestic use. In terms of its fast growth and development, increasingly more humans from outside towns and cities are migrating into Pune metropolis, as it is one of the fastest developing cities in India. During the last two decades, the population rate has increased by 29% in Pune city and is particularly rapid with resultant impact at the boom of water pollutants level [3]. As per Pune Municipal corporation, 744 million liters per day (MLD) of waste generated by Pune through sewage and different means. Out of 744 MLD, 177 MLD of waste is entering the river without any treatment [4]. Total 9 sewage treatment plants are there in Pune city to serve the vast population of 7.4 million in the city, which is 2nd biggest city in the state of Maharashtra and 8th most popular metropolis in India [4]. The untreated effluent is commonly discharged into River Mutha.

River Mutha is one of every of the foremost vulnerable watercourse of Pune city from pollution perspective [3]. The River Mutha watercourse is flowing in western Maharashtra, India. It arises in the Western ghats and it flows eastward till it merges with a River Mula in the city of Pune [1]. River Mutha originates from Khadakwasla dam and it passes through Nanded City, Vitthalwadi, Rajaram Bridge, Mhatre Bridge, Z-bridge, Junabazzar, Pune RTO and ends at Sangamwadi. River Mula originates from Mulshi Dam and it passes through Paud, Wakad, Balewadi, Baner, Aundh, Khadki, Vishrantwadi and ends at Sangamwadi. Each River Mula and River Mutha merged at Sangamwadi and in addition, joined through River Indrayani and River Bhima [3]. River Mutha is flowing through the foremost areas of Pune city. Due to population growth as well as settlement on the banks of river, the pollutants load into river Mutha has been increased. Various large scale industries, as well as small scale industries, are not maintaining the effluent standards before discharging it into the River Mutha which may lead to pollution.

As increasing water pollution may be a major issue in Mutha river, there is a need to reduce the pollution level of river. Non-Mechanized treatment ways like phytoremediation [1], oxidation ponds, etc. can be used to minimize the load of sewage treatment plants. However, it requires more space. The model can be designed



in which the construction of bunds with staggered openings will be provided in such a way that the water is allowed to flow in zigzag pattern with maintained velocity. It is essential to study out analysis of hydraulic parameters like velocity, discharge of the flow, it may cause harmful effect on banks of river which further may cause severe damages to the banks. Proper water quality assessment of such polluted rivers is the basic step before implementing any treatment system.

## 2 Study Area

Pune is situated at 18°31' N and 73°51' E, is the city with three rivers (Mula, Mutha, and Pavana) flowing through heart of the city [5]. River Mutha is a lifeline of Pune town. It arises inside the Western Ghats and flows eastward and merges with the River Mula in the Pune City. Panshet Dam is constructed on the Ambi River which is used as a supply of ingesting water for Pune town and irrigation. The water launched right here is dammed once more at Khadakwasla and is an essential supply of ingesting water for Pune City [6]. One greater dam has been constructed while on the River Mutha at Temghar. After becoming a member of the River Mula in Pune, it flows as a River Mula-Mutha to enroll in the River Bhima. River Mutha starts from downstream of Khadakwasla dam to Sangamwadi Bridge. The Total distance from downstream of Khadakwasla dam to Sangamwadi Bridge is around 22 km (Fig. 1).

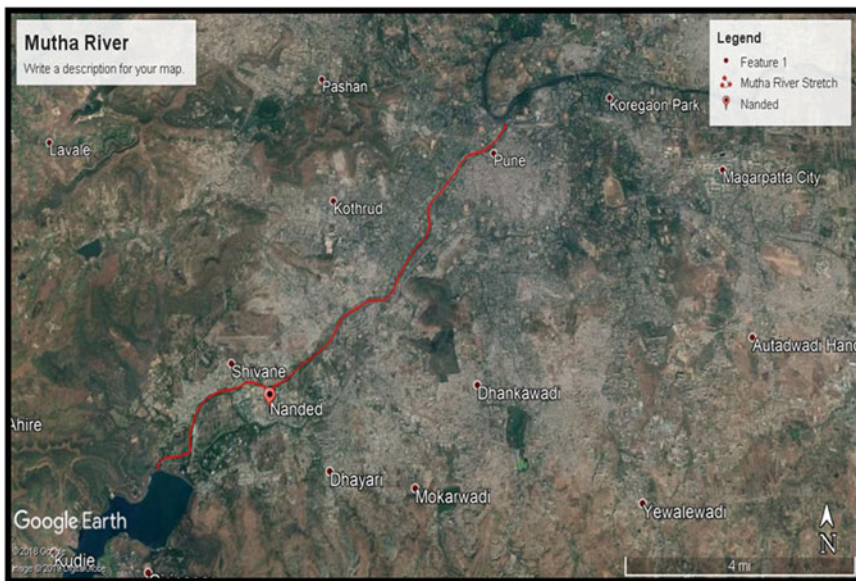


Fig. 1 Stretch of River Mutha source Google earth

### 3 Water Quality Assessment

The overall method of evaluation of the physical, chemical, and biological characteristics of the water is understood as Water quality assessment. Water quality of stream could vary due to Environmental conditions, Climatic conditions, Vegetation cover, and so on [4]. Assessment can be carried out by testing the parameters such as TS, TSS, TDS, pH, D.O., B.O.D., and C.O.D. There are several standard ways for treatment of impure water is used, however these treatment methods need high capital value, maintenance cost, and labor cost. Therefore, a non-mechanized system has to be evolved and studied. Proper water quality assessment of such polluted rivers is that the basic step before implementing any treatment system.

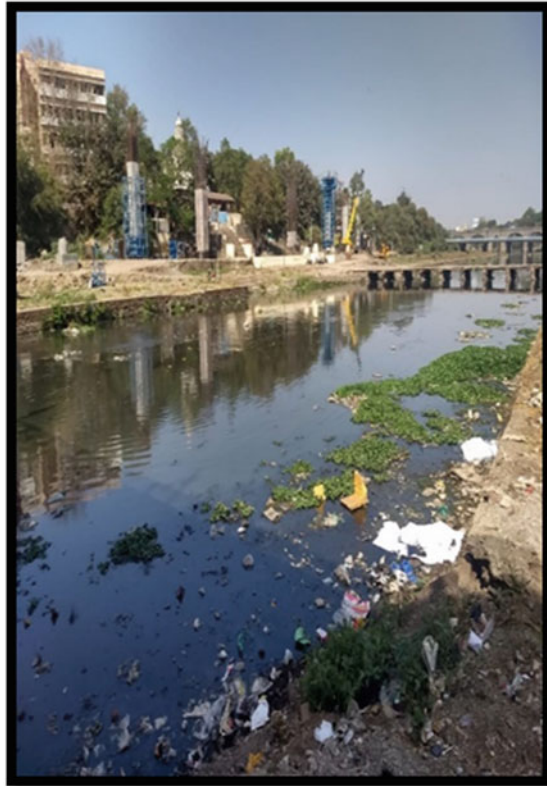
#### 3.1 Sample Collection

Environmental testing is carried out on collected samples from Onkareshwar, a place in Pune City. The river water samples were collected in Summer Season on 13/02/2019, 15/02/2019, 05/03/2019, and 07/03/2019 and for rainy season on 13/06/2019, 20/06/2019, 21/06/2019, and 24/06/2019 examined withinside the laboratory for specific Physical, Chemical, and bacteriological parameters. Figure 2 shows the sampling station, i.e., onkareshwar from where the water samples were collected at morning and Fig. 3 shows the collected sample from onkareshwar before the testing was done in the laboratory.

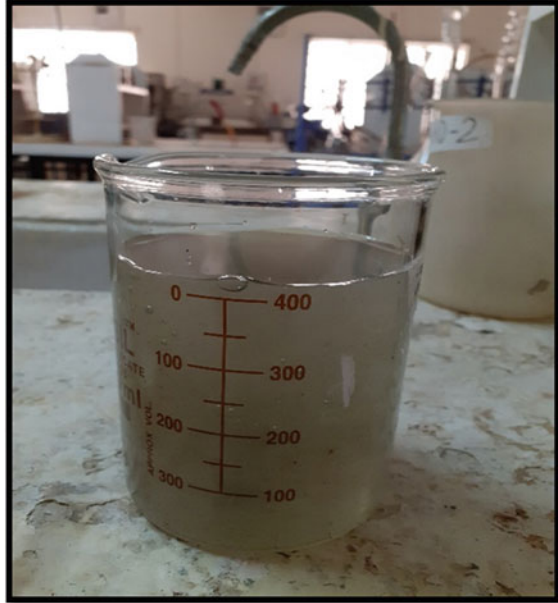
#### 3.2 Parameters for Water Quality Assessment

Water Quality is classed through chemical parameters including pH, D.O, B.O.D, and C.O.D. Physical evaluation is executed through parameters including Total Dissolved Solids, Total suspended solids, and total solids.

- TS—Total Solids determination classifies wastewater as weak (350 mg/l), moderately strong (around 700 mg/l), and strong (around 1200 mg/l). Total solids for selected sampling stations are in the range of 460–720 mg/l for Summer Season, whereas the range is 360–510 mg/l for Rainy Season.
- TSS—Total Suspended Solids constitute the whole suspended stable which are undissolved in water. After experimentation, observed values for TSS are 40–260 mg/l for Summer Season and 35–310 mg/l for Rainy Season.
- TDS—Total Dissolved Solid way general awareness of dissolved solids in shape water. TDS shows the suitability of wastewater for irrigation and fish culture. After experimentation, observed values for TDS are 260–460 mg/l for Summer Season and 155–365 mg/l for Rainy Season.

**Fig. 2** Sampling station

- pH—pH is an important parameter as it determines the acidity and alkalinity of waters [7]. The pH of selected sampling station is in the range of 6.80–7.12 for Summer Season and 6–6.25 for Rainy Season. The permissible value for pH is 6.5–8.5. pH tiers commonly range because of environmental effects specifically Alkalinity.
- C.O.D.—It is any other key indicator parameter to evaluate the diploma of pollution. By the action of strong oxidation agent, the amount of oxygen (mg/l) which is consumed under specified conditions in the oxidation of organic and oxidizable inorganic matter, the range of COD observed at sampling stations are 136 mg/l to 244 mg/l for Summer Season and 187–217 mg/l for Rainy Season.
- DO—Dissolved oxygen refers to the extent of free, non-compound oxygen found in water. It is an important parameter for assessment of water quality. DO value decreases with a rise in temperature, rise in salt concentration, and rise in organic concentration. DO below 3 mg/l is not suitable for aquatic life. The range of DO Observed at sampling stations is 1.084–2.956 mg/l for Summer Season and 18–2.1 mg/l for Rainy Season.

**Fig. 3** Collected sample

- B.O.D.—The quantity of dissolved oxygen utilized by aerobic microorganisms, while oxidizing decomposable natural matter found in wastewater. Permissible limit for BOD is 2–3 mg/l. The range of BOD Observed at sampling stations are 59 and 112 mg/l for Summer Season and 54–75 mg/l for Rainy Season.

#### 4 Results and Discussion

Increasing Water pollution is the first rate difficulty in the rivers of India. Pollution is the contamination of water which is the biggest health risk for humans as well as for aquatic life. Total solids, Total Suspended Solids and Total Dissolved Solid for selected sampling station are in the range of 460 mg/l to 720 mg/l for Summer Season and 360 mg/l to 510 mg/l for Rainy Season, 40 mg/l to 260 mg/l for Summer Season and 35 mg/l to 310 mg/l for Rainy Season, 260 mg/l to 460 mg/l for Summer Season and 155 mg/l to 365 mg/l for Rainy Season respectively. The pH of selected sampling station is in the range of 6.80–7.12 for Summer Season and 6–6.25 for Rainy Season. The range of COD, DO and BOD observed at sampling stations are 136 mg/l to 244 mg/l for Summer Season and 187 mg/l to 217 mg/l for Rainy Season, 1.084 mg/l to 2.956 mg/l for Summer Season and 18 mg/l to 2.1 mg/l for Rainy Season, 59 mg/l to 112 mg/l for Summer Season and 54 mg/l to 75 mg/l for Rainy Season respectively. The evaluation and results sincerely show that river water quality of River Mutha has deteriorated mainly due to discharge of domestic treated, untreated, and partially treated waste water. It clearly indicates that there

**Table 1** Results of environmental testing for summer season

| Environmental parameters | 13/02/2019 | 15/02/2019 | 05/03/2019 | 07/03/2019 |
|--------------------------|------------|------------|------------|------------|
| pH                       | 7.12       | 7          | 6.80       | 7.1        |
| DO                       | 1.084      | 2.956      | 1.87       | 2.76       |
| COD                      | 136        | 244        | 232        | 240        |
| BOD                      | 59         | 96         | 110        | 112        |
| TS                       | 460        | 540        | 720        | 580        |
| TDS                      | 420        | 300        | 460        | 260        |
| TSS                      | 40         | 240        | 260        | 320        |

is a load of pollution in the River Mutha. There is very much need to do a proper collection of waste and treatment of sewage to regulate and modify the flow. Tables 1 and 2 shows the results for Water Quality Assessment for Summer Season and Rainy season respectively. Figures 4, 5, 6, 7, 8, 9, 10, 11, 12, 13, 14, 15, 16 and 17 shows the

**Table 2** Results of environmental testing for rainy season

| Environmental parameters | 13/06/2019 | 20/06/2019 | 21/06/2019 | 24/06/2019 |
|--------------------------|------------|------------|------------|------------|
| pH                       | 6          | 6.12       | 6.25       | 6.19       |
| DO                       | 2.06       | 1.8        | 2.20       | 2.1        |
| COD                      | 187        | 217        | 192        | 205        |
| BOD                      | 64         | 75         | 62         | 54         |
| TS                       | 360        | 510        | 480        | 400        |
| TDS                      | 155        | 200        | 195        | 365        |
| TSS                      | 205        | 310        | 285        | 35         |

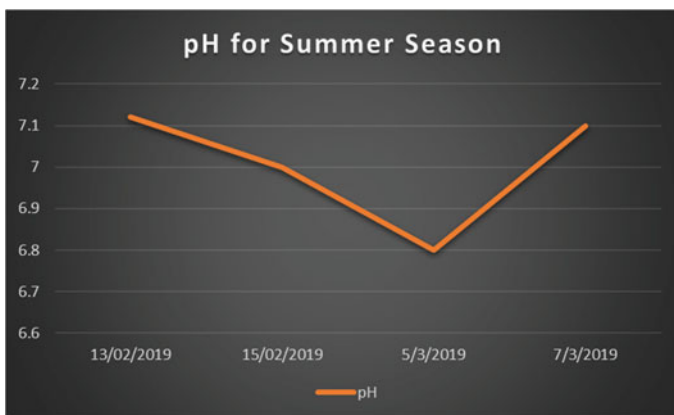


**Fig. 4** pH for summer season

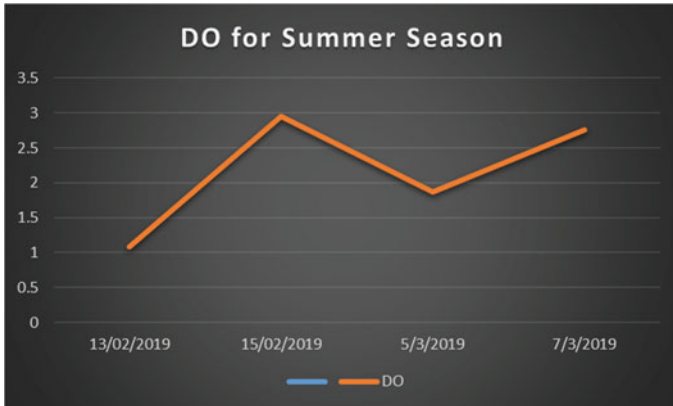


Fig. 5 DO for summer season

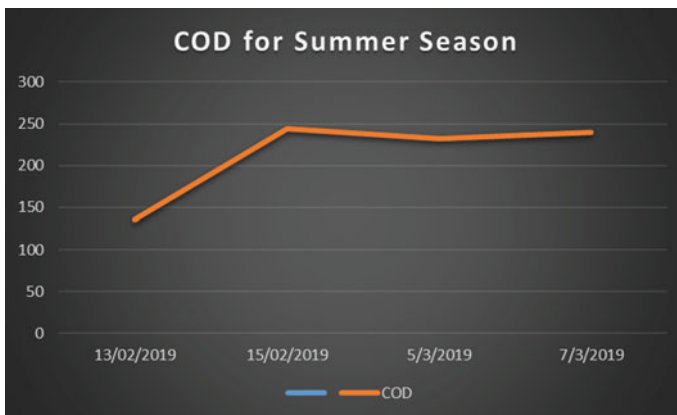


Fig. 6 COD for summer season

graphical variation of all Environmental Parameters for Summer Season and Rainy Season. Water Quality Assessment shows following results:

- The Water Quality Assessment done in Rainy Season does not show much difference of Assessment done in summer season, due to delayed monsoon.
- River Mutha is highly polluted. Hence, some measures like 100% collection, conveyance, and treatment of sewage should be practiced.
- This being an extremely difficult task, some alternatives like online treatment could be a feasible option for which the first step is characterization of River Water, same has been carried out in the current study. This will act as a base for further study.

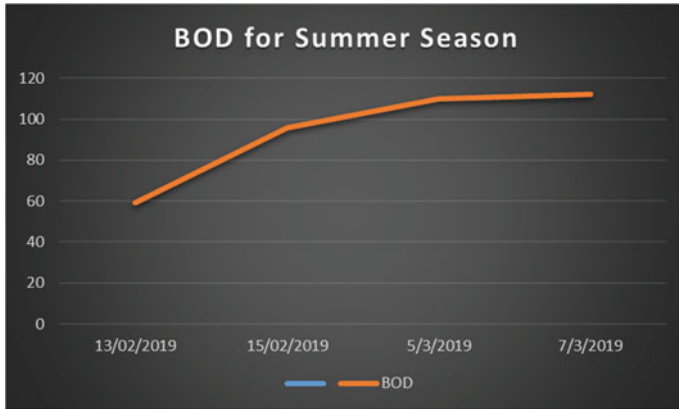


Fig. 7 BOD for summer season

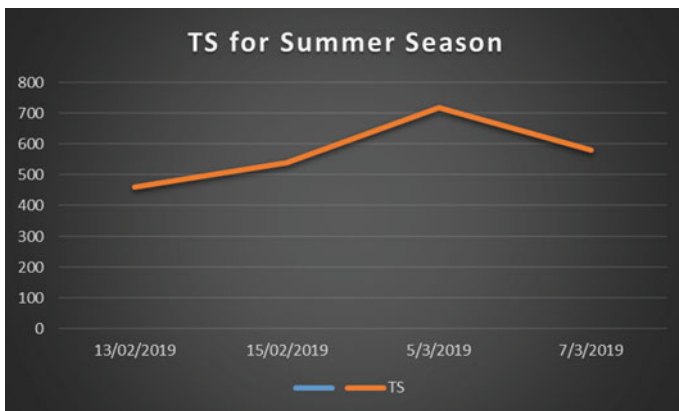


Fig. 8 TS for summer season

## 5 Conclusion

It is concluded that, except pH, all other parameters are on the unacceptable side, e.g., DO is less than 3 mg/l, which is not suitable for the survival of aquatic life. BOD, COD, and Solids, all values are higher than recommended values as per MOEFCC. As there is no water available for dilution, the untreated water goes further to Ujjani dam. Farmers are using this water for agriculture as well as drinking purposes which can be harmful to the health of humans.

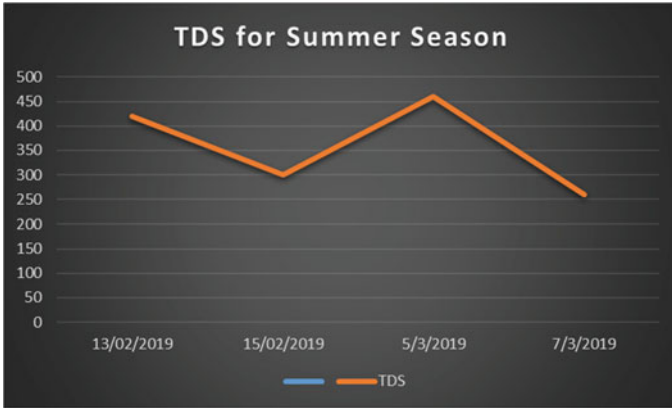


Fig. 9 TDS for summer season

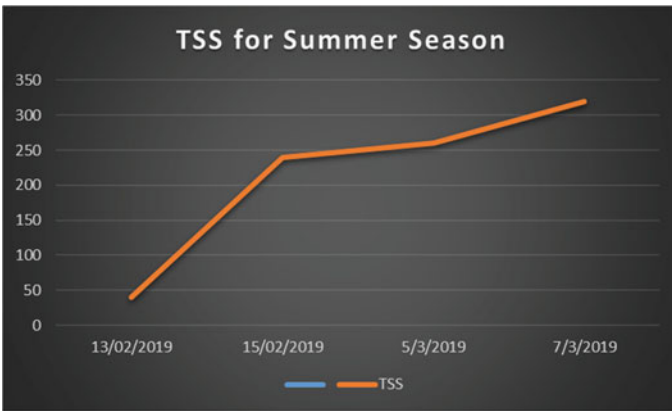


Fig. 10 TSS for summer season

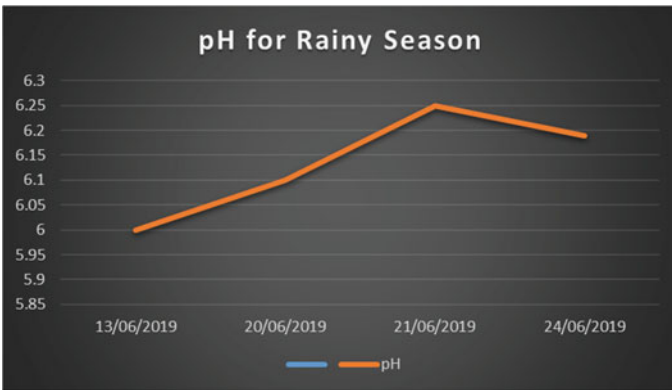


Fig. 11 pH for rainy season



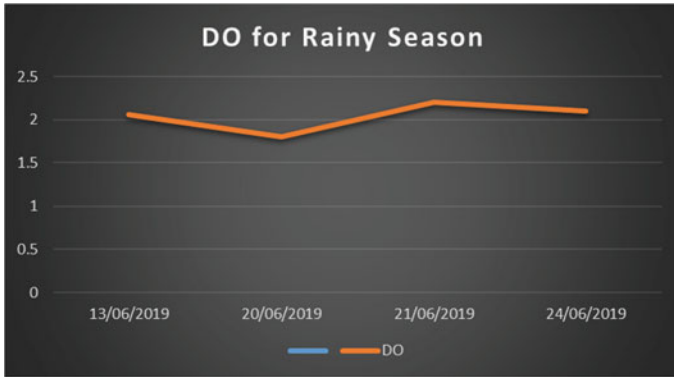


Fig. 12 DO for rainy season

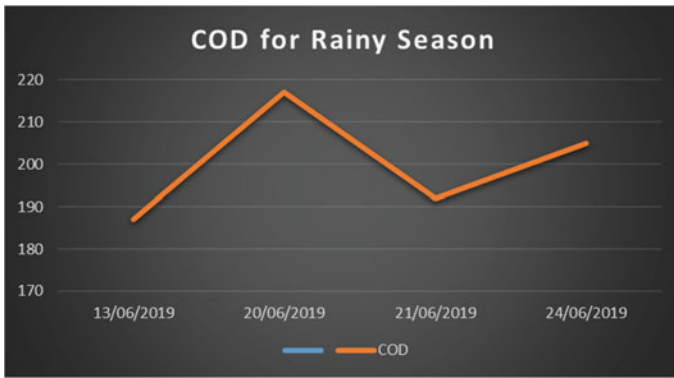


Fig. 13 COD for rainy season

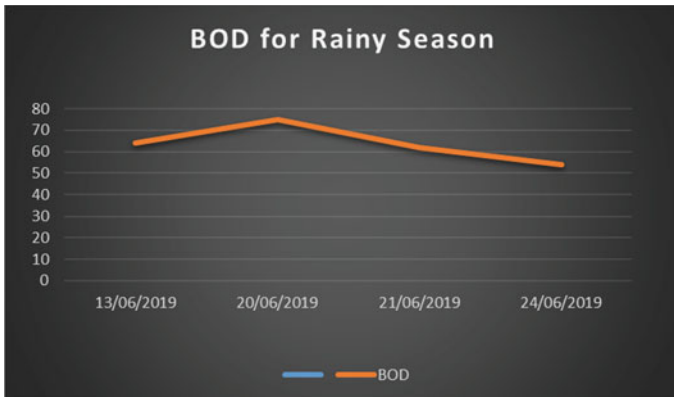


Fig. 14 BOD for rainy season

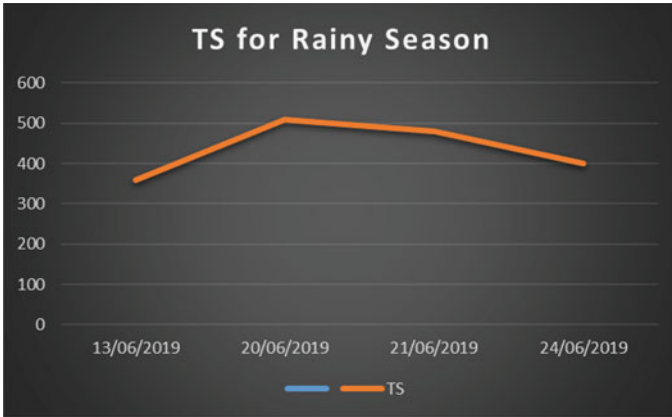


Fig. 15 TS for rainy season

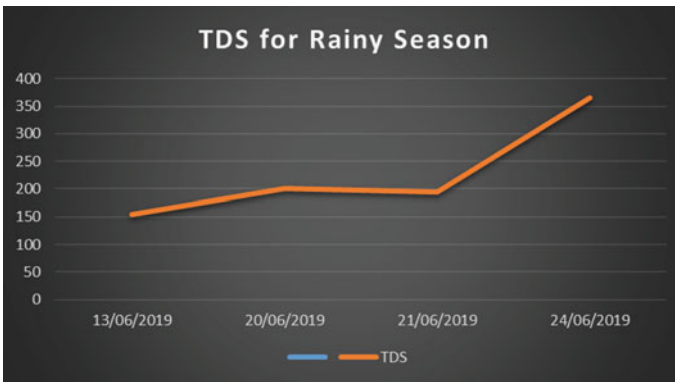


Fig. 16 TDS for rainy season

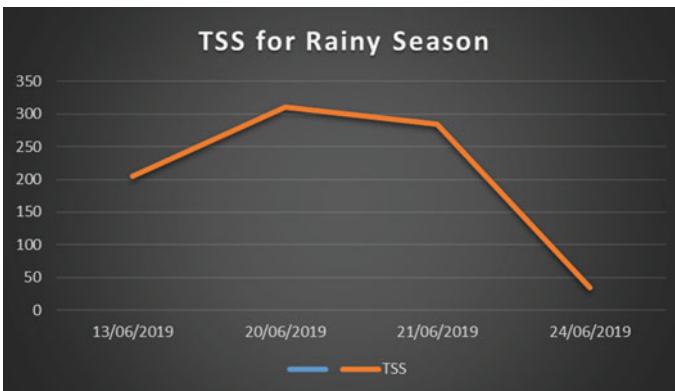


Fig. 17 TSS for rainy season

**Acknowledgements** All the authors are thankful to the organization of Sinhgad Technical Education Society's, SCOE, Pune-41, and the Lab Incharge and lab Assistant of Environmental lab of the Department of Civil Engineering, Pune-41 for their co-operation during the testing of sample. The first author is also thankful to Dr. S. S. Shastri, Head and Professor of Department of Civil Engineering, SCOE, Pune-41 for sharing their valuable knowledge during the entire work done.

## References

1. Jagtap SS, Manivanan R (2019) Water pollution status of Mula-Mutha rivers in Pune city: review. *Int J Trend Sci Res Dev* 4(1)
2. Anaokar GS, Kalgapurkar AP (2013) Control of major pollutants in river by bioremediation: a case study—River Mutha—Pune. *Int J Eng Res Technol* 2(3). ISSN 2278-0181
3. Sahu P, Sonali K, Sagar C, Sourabh K (2015) Physicochemical analysis of Mula Mutha river Pune. *Civ Eng Urban Plan Int J* 2(2)
4. Kulkarni E, Aswale S, Dhut P, Dhaygude A, Shinde S (2018) Water quality assessment and mapping of parameters for Mutha river: a review. *Int J Innov Res Sci Eng Technol* (5)
5. Fadtare VV, Mane TT (2007) Studies on water pollution of Mula, Mutha and Pawana rivers in summer season in the Pune city region. *Nat Environ Pollut Technol* 6(3):499–506
6. Wagh VM, Ghole VS, Wavde PN, Todkar VV, Kokate KK (2008) Assessment of water quality of Mutha river in Pune city. In: *GCE 2008: Indo-Italian international conference on green and clean environment*, March 20–21
7. Jadhav SD, Jadhav MS (2017) Analysis of water quality using physico chemical parameters of Mula-Mutha river, Pune (Maharashtra). *Int J Trend Sci Res Dev* 1(6)

# Comparative Study of Physical and Chemical Parameters of Lakes in Medchal District



R. Suresh Kumar, Ch.V. S. S. Sudheer, G. Venkata Ramana,  
and N. Sri Ramya

**Abstract** In present project, four lakes selected in such a way that Dundigal lake in growing village, Nizampet lake in city, and Bowrampet lake in village. Water quality characteristics were determined for four lakes (Dundigal, Nizampet, Mallampet, and Bowrampet) in the Quthbullapur mandal of Medchal district, Telangana state. In this study, water quality was determined on the basics of various physical–chemical parameters like pH, color, turbidity, alkalinity, hardness, suspended solids, dissolved solids, total solids, dissolved oxygen, chloride content, chemical oxygen demand, biological oxygen demand, and total load of bacteria. The process involves various methods/experiments/equipment's for evaluation of contaminants in the above-selected four lakes to know the presence of various contaminants. Therefore, it offers as a significant value to physio-chemical water quality standards.

**Keywords** Temperature · pH · Color · Turbidity · Alkalinity · Biological oxygen demand · Chemical oxygen demand · Dissolved oxygen

## 1 Introduction

Throughout the years, expanding populace urbanization and development in farming has head in the logical misuse of groundwater making a water pressure condition the basic issues of ecological contamination in view of over urbanization and just as industrialization it prompts water shortage issues. The groundwater quality has been sullied because of contamination and amount is additionally diminished because of overexploitation. The over extraction of groundwater drives inability to revive the groundwater table. Water quality testing has an answer job since it prevents water-borne illness and distinguishes contaminants. Majorly, water quality test makes

---

R. S. Kumar · Ch.V. S. S. Sudheer · G. V. Ramana (✉)  
Department of Civil Engineering, Institute of Aeronautical Engineering, Dundigal, Hyderabad,  
Telangana 500 043, India

N. S. Ramya  
Aurora's Technological and Management Academy, Moula—Ali, Hyderabad, Telangana, India

conformation that water is portable and satisfies neighborhood and international water standards [1, 4]. Water assessment results can give the second qualities and help in deciding of particular water body with a best game-plan, regardless of whether a treatment is required or an air circulation framework ought to be introduced [6].

Water quality assessment is considered as basic issue as of late particularly where freshwater getting one of scant asset in future. Water quality appraisal at the bowl scale requires not just countless variable and relating assessment factors, yet additionally a spatial dissemination of contamination levels dependent on each factor and assessment factor. Generally, quality water implies to the physical, pathogenic, chemical, and radiological characteristics of water [2].

The most normal gauges utilized to water quality evaluation identify with ecosystems being good level, safety for contacting with social beings, and drinking water [3, 7]. These risks are engaged with evaluation of water quality not only complex but also vast. They are contrasted with a chain of around twelve connections, and the disappointment of every last one of them can debilitate the entire evaluation.

### ***1.1 Parameters for Drinking Water Quality***

Quality of drinking water typically falls within three groups:

- Physical parameters: These included (turbidity, taste, temperature, odor, etc.) are finding by impressions of sight, touch, smell, and taste.
- Chemical parameters: The chemical parameters of water are pH, total solids (TS), total dissolved solids (TDS), total suspended solids (TSS), total hardness, calcium hardness, magnesium hardness, nitrates, phosphates, sulfates, chlorides, dissolved oxygen (DO), biological oxygen demand (BOD), and chemical oxygen demand (COD) [2, 5].
- Biological parameters show the presence of coliform and other microorganisms.
- The degree temperature of water influences qualities and some significant physical properties of water: warm limit, thickness, consistency, explicit weight, surface strain, saltiness and dissolvability, and so on. Concoction and natural counteraction rates rise with expanding temperature.
- Color of water is basically a concern to water quality for esthetic explanation. Colored water will give appearance of unpleasant to drink, despite the truth that water capability be totally ok for free use, color shows closeness of natural particles, for example, humid mixes, or algae.
- Odors and taste are human consideration of quality of water. Human consideration to taste incorporates salty (sodium chloride), sweet (sucrose), sour (hydrochloric acid), and bitter (caffeine).
- Human detect organic substances dispersed straightforwardly into water, for illustration, shedding leaves, spillover, and so on, which are some reasons of tastes and smell—making fusion release during microorganisms degradation [9, 10].

## 2 Objectives

The main objectives of this research include:

- To determine water quality characteristics of lakes namely (Dundigal, Nizampet Mallampet, and Bowrampet) in the Quthbullapur mandal of Medchal district, Telangana state.
- Present study was intended to find out water quality (physical and chemical parameters) of a lake in order to ascertain the quality of water for public and mention contamination control measures if needed.
- To classify lake water quality with respect to water quality index.

## 3 Study Area

- **Dundigal:** It is in Malkajgiri revenue division of Medchal district. Outer ring road (ORR) is nearby village with population 13,465 in 2011. Dundigal lake is located in geographical south of village and is 2 km far from our college. Outer ring road construction duly increased cost of Barren lands and residential area expenditure. This village has noticeable transportation facility. Usually, Dundigal lake water is used for cleaning heavy vehicles and domestic animals (cow, buffalo). Less quantity of water is used for agriculture purpose. Great assortments to freshwater are as of now experiencing floods of phosphorus and nitrogen from outside sources. The developing centralization of attainable phosphorus helps plants to acclimatize high nitrogen before the phosphorus is washed out into quarter, and some portion of Dundigal lake is secured with vegetation.
- **Mallampet:** It is located in Quthbullapur mandal, Medchal locale, Telangana, India. It is 2 km away Bachupally, 6 km from Nizampet intersection, and 10 km far from Kukatpally, with population of 2832 as per 2011. This lake is located in northeast direction of village. Prevailing quality of a peri-urban site is its progress out of an agrarian economy because of industrialization and urbanization. This generally shows itself as agrarian land either left desolate or sold for formative exercises and ranchers and farming workers searching for an elective wellspring of vocation. One of our examination towns, Mallampet, presents a valid example in Mallampet, and the move has happened through a blend of the two sorts of variables. In the mid-2000s, the outer ring road (ORR) came up near Mallampet, with which came a surge of industrialization and commercialization in and around the town. By then, a great deal of ranchers was lured into selling their territory for a singular amount measure of cash. Ranchers would take a very long time to make that measure of cash through farming, and henceforth, this is filled in as the most grounded pull factor that pulled in them out of agriculture. Lake act as internal storage for Infiltration of Water.
- **Nizampet:** The once desolate lake is secured with greenery now all around. In one year, they planted more than 6000 plants which have developed well.

The lake where once in a while walker ought to visit has present gotten one of most loved strolling points of the Nizampet zone containing very nearly 300 footfalls consistently. Additionally, one able to watch various types of feathered creatures and butterflies near to lake which unquestionably makes that appealing. Quiet, plantations and trees are to the center of our ecosystem, they can change our lives familiar, and they have changed Nizampet lake. It is quickest developing rural areas around IT hallway of Hyderabad, in light of moderately contamination free situations with just issue of water shortage; big haulers convey water to lofts and other lodging states which is normal sight here. It has a populace of 6931 individuals in 2011.

- **Bowrampet:** It is a village in Medchal district, Telangana. It is a panchayat under Quthbullapur municipality. Village is forming into a significant private and business rural in light of outer ring road, nearness to the IT passageway of city and contamination-free condition. Bowrampet lake is situated in the focal point of the village. In the present mechanical social orders, prerequisites for water, a lot of which is gotten from lakes, incorporate its utilization for weakening and evacuation of metropolitan and modern squanders, for cooling purposes, for water system, for power age, and for neighborhood entertainment and stylish showcases. It has a population of 2247 as per 2011. In Bowrampet village, three lakes are present; water sample for this project is collected from larger lake, and one side of lake is nearer to road which connects Suraram to Bowrampet village. Lake water is not used for any of domestic purpose. The bird eye view of all the lakes mentioned above are shown in Fig. 1.



**Fig. 1** Bird eye view of the study area

## 4 Methodology

The following methodology was adopted and shown in the figure below for the identification of physical, chemical, biological, and other properties of the water samples collected through the four lakes mentioned above. Surface water samples are gathered from the lakes. The collected samples are checked for the potentiality to use as alternate water source. Water quality observed assist specialists with anticipating formal procedures on the land and decide human trappings upon biological system. These figuring endeavors can likewise assist reconstruction methods that are assured natural principles which are able to meet. These measurements are sententious not elegantly to surface water explorations of the lakes, sea, and waterways, with regard to groundwater and prevailing procedures too [8].

- Initially each lake water samples are collected in plastic bottle of volume 1000 ml.
- Inspecting, safeguarding, transportation, and examination of water tests will be done by the individual tests.
- Based on water quality index, four samples are analyzed for their water quality.
- It is suggested that whether lake water is suitable or not as alternative source of water.
- All the bottles were washed with diluted water in order to make bottles clean.
- In laboratory, samples will be tested for physical, chemical, and biological parameters with suitable equipments (Fig. 2).

## 5 Results and Discussion

It is extremely basic and essential to try things out ahead it is outlined for drinking, domestic, agrarian, or modern probability. Water should be beat with various physio-compound framework. Water contains various kinds of coasting, broke down, suspended, and microbiological just as bacteriological impurities. Some physical test ought to execute the examining its physical appearance such as pH, turbidity, and temperature where chemical analysis must be conducted to determine dissolved oxygen, alkalinity, biological oxygen demand, chemical oxygen demand, and other characters.

### 5.1 Physical Parameters

- **Temperature:** Temperature has control on aquatic life. On the off chance that general water internal heat level is modified, oceanic network move might exist normal. Higher when water is more than 300 °C, a concealment to every benthic creature can be normal. Additionally, assortment tiny fish gatherings will develop under various temperatures. After downpours, lake temperature varies in range



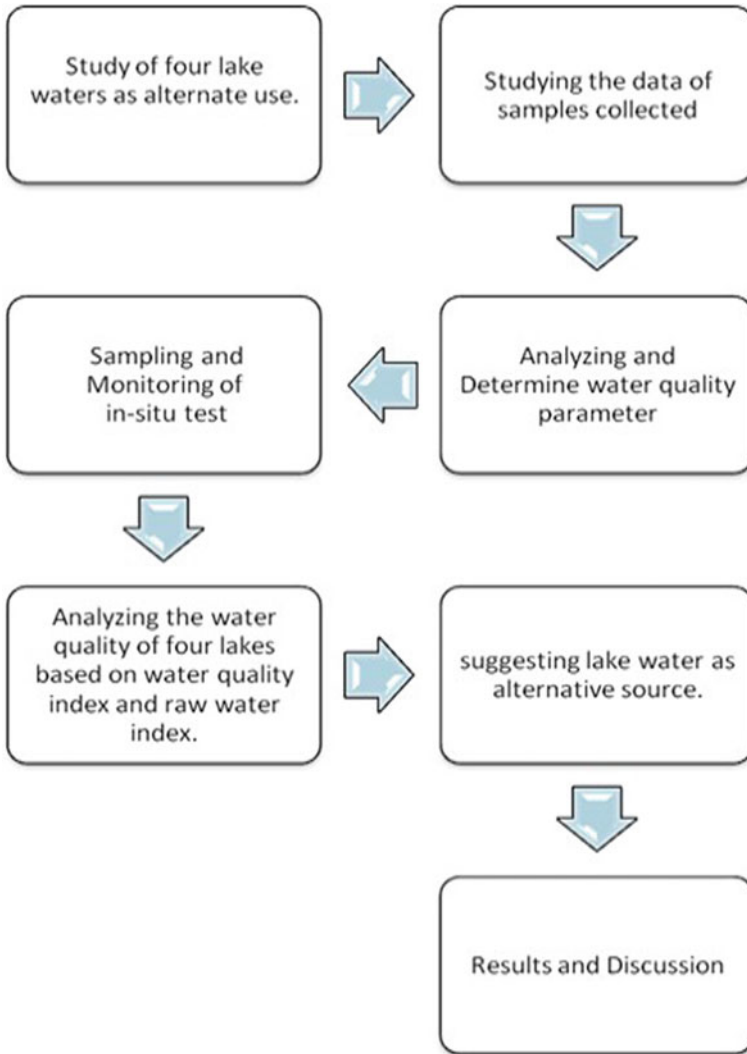


Fig. 2 Flowchart for the methodology

of 27.2–28.6 °C. For instance, green algae exist at 30–35 °C, cyano-microbes live above 35 °C, and diatoms exist at 20–25 °C.

- **pH:** The concentration of hydrogen ion assumes critical job in the natural procedures of practically all amphibian life forms. For nearness of sea-going life, pH range ought to be exist in between 6.5 and 8.5, and for water system, it ought to be 6.0–8.5. In the current examination, the Dundigal, Nizampet, and Bowrampet

**Table 1** Physical properties of the lakes

| S. no | Lake name | Color    | Odor          | Temperature | Turbidity |
|-------|-----------|----------|---------------|-------------|-----------|
| 1     | Dundigal  | Greenish | Objectionable | 29.5        | 24.8      |
| 2     | Mallampet | Greenish | Objectionable | 31.1        | 19.9      |
| 3     | Nizampet  | Greenish | Objectionable | 27.5        | 16.3      |
| 4     | Bowrampet | Greenish | Objectionable | 28.6        | 49.8      |

lakes show that this is because of expanded photosynthetic osmosis of disintegrated inorganic carbon by tiny fishes. After the underlying downpours, the pH esteem is from 6.94 to 8.53.

- **Turbidity:** Turbidity is a proportion of water which loses its straightforwardness due to presence of suspended particulates. The more the absolute suspended particles in water, the muddier it appears and the higher the turbidity (Table 1).

The chemical properties of the four lakes are presented in Table 2.

## 6 Conclusions

Water quality test adds advantage in water quality and purpose where it can be used; preventive measure and remedy can draw from water parameter results.

This process is very essential for new or existing water bodies as a source of water consumption for various purposes.

- The water quality of four lakes can be utilized as a helpful apparatus for watershed the board and amphibian body checking. Based on the above-mentioned conversations, it is presumed that the water quality index (WQI) for all the four lakes were found as unsatisfactory for drinking reason.
- Release of untreated metropolitan sewage, modern waste water into these lakes, and strict exercises like inundation of Gods and Goddess icons made by Plaster of Paris (POP) are answerable for the sullyng of these four lakes.
- From those numerical, it is seen that the water of lakes is not consumable without treatment because of the low dissolved oxygen (DO), and high nitrates and phosphates fixations, however, can be utilized for universally useful just as recreational reason.
- Higher values were recorded after starting downpours because of characteristic and anthropogenic sources, for example, run-off containing salts, land fill leachates, septic tank effluents, and creature takes care of is higher in first flush.
- It is additionally seen that the nitrate, water turbidity, and phosphorous levels are great in four lakes.
- It is because of the expansion of supplement level and the water hyacinth nearness in the lakes. In this manner, it is important to expel the water hyacinth from the lakes to clear the water.

**Table 2** Chemical properties of the lakes

| S. no | Name of the lake | Alkalinity mg/l | pH   | TDS mg/l | TSS mg/l | Do mg/l | BOD mg/l | COD mg/l | Nitrate mg/l | Phosphate mg/l | Coliform mpn |
|-------|------------------|-----------------|------|----------|----------|---------|----------|----------|--------------|----------------|--------------|
| 1     | Dundigal         | 183.5           | 9.38 | 687      | 236.9    | 424     | 8.9      | 0.8      | 49           | 9.7            | 3.72         |
| 2     | Mallampet        | 216             | 7.76 | 1986     | 158.9    | 509     | 5.5      | 1.0      | 52           | 9.2            | 3.1          |
| 3     | Nizampet         | 492             | 8.16 | 1501     | 203.4    | 531     | 7.2      | 1.2      | 32           | 9.8            | 3.5          |
| 4     | Bowrampet        | 143             | 8.26 | 357      | 173.4    | 601     | 8.1      | 3.0      | 41           | 8.2            | 3.8          |

## References

1. Yan CA, Zhang W, Zhang Z, Liu Y, Deng C, Nie N "Assessment of water quality and identification of polluted risky regions based on field observations & gis in the honghe river watershed, China". Published on March 13, 2015
2. Carlson RE[1] (1977) A trophic state index for lakes. *Limnol Oceanogr* 22:361–369
3. Das AK, Shrivastva NP (2003) Ecology of sarni reservoir (M. P.) in the contexts of fisheries. *Poll Res* 22(4):533–539
4. Faragallah HM, Askar AI, Okbah MA, Moustafa HMs[4] (2009) Physicochemical characteristics of the open Mediterranean Sea water far about 60 Km from Damietta harbor, Egypt. *J Ecol Nat Environ* 1:106–119
5. Rani H, Bahri D, Neupane P, Kothari K (Apr 2017) Water quality analysis: a case study in Byramangala Lake water and surrounding ground water Assistant Professors, Department of Civil Engineering, SET, Jain University, India [Rani et. al., vol 5 (Iss.4: RASM)]
6. Joshi PC, Singh A (2001) Analysis of certain physicochemical parameters and plankton of freshwater hill stream at Nanda devi biosphere reserve. *Uttarpradesh j. Zool*, 21:177–179
7. India Kaiser Manzoor, Raj P, Sheoran R, Dey S, Gupta EJ, Dr. Zaman B (Nov 2017) Water quality assessment through gis: a case study of Sukhna Lake, Chandigarh, E-ISSN: 2395–0056 04(11)
8. Lohani BN, Todino G (1984) Water quality index for Chao Phraya river. *J Environ Eng* 110:1163–1176
9. Mahmoud TH, Masoud MS, Shaltout NA (2005) Physico-chemical characteristics of different water types in El-Mex bay, Alexandria, Egypt. In *Proceedings of Oceans 2005 MTS/IEEE*, pp 2838–2849
10. Murugesan A, Ramu, Kannan N (2006) Water quality assessment from Uthamapalayam municipality in Theni District, Tamil Nadu, India *Poll Res* 25(1):163–166

# **Environmental Modelling**

# An Experimental Study on Removal of Cadmium Using *Annona Squamosa* Seed Powder and *Phyllanthus Acidus* Seed Powder



T. Aruna Devi, R. Jeykumar, and R. Ilangoan

**Abstract** Groundwater is a major source of freshwater which is being effectively used for various purposes such as in household works and in industries. India is the larger extractor of groundwater in the world. Increase in industrialization has resulted in the over exploitation of groundwater. Due to this, the concentration of contaminants is increased in the groundwater and resulted in the heavy metal pollution in the groundwater. Heavy metals such as cadmium, chromium, arsenic, lead, nickel, and mercury are the major threat present in the water. Cadmium from the aqueous solution was adsorbed using *Annona squamosa* seed powder and *Phyllanthus acidus* seed powder as biosorbents. The biosorbent was characterized by X-ray diffraction (XRD) technique. The optimum dosage, initial concentration of cadmium, and contact time of the solution were examined in a systematic manner. Adsorption kinetics was performed namely pseudo-first-order kinetics and pseudo-second-order kinetics. Among them, pseudo-second-order kinetics was found to be effective. The equilibrium data were analyzed using adsorption isotherm models. Results concluded that *Annona squamosa* was effective in removing cadmium compared to *Phyllanthus acidus*, and both biosorbents were economically of low cost and eco-friendly.

**Keywords** *Annona squamosa* · *Phyllanthus acidus* · Cadmium · Adsorption isotherms · Adsorption kinetics

## 1 Introduction

Water, which covers about two-third of the Earth's surface, is declared as a scarce source for drinking. The main sources of water to the people are groundwater and surface water. The groundwater in India had been depleted due to the over usage of

---

T. A. Devi

Department of Civil Engineering, University College of Engineering (BIT Campus),  
Tiruchirappalli 600 024, India

R. Jeykumar (✉) · R. Ilangoan

University College of Engineering, Panruti Campus, Cuddalore 607106, India

the groundwater. Increase in industrialization is also a major cause for ground water depletion and groundwater contamination [1]. Heavy metals pollution in groundwater is a major problem due to the direct disposal of effluents from the industries into the environment [2].

The well-known fact is that the industrial effluents containing heavy metals have adverse effects on human and aquatic life. Metals are notable for their wide environmental dispersion from industries and their tendency to accumulate in tissues of the human body and their overall potential to be toxic even at relatively minor levels of exposure.

The seventh most toxic metal as per Agency for Toxic Substances and Disease Registry (ASTDR) is cadmium [3]. It is generally a by-product from the zinc production. It is found naturally as an impurity of zinc or lead. Nowadays, it is used in rechargeable batteries, for production of special type of alloys, and is present in tobacco smoke. Cadmium is more toxic compared to lead and chromium.

The cadmium is mixed with the natural groundwater due to the fertilizers that are sprayed on the ground. The concentration of cadmium should be less than 1 mg/l in the groundwater. If the permissible limit of cadmium is more than 1 mg/L, it may cause diseases like kidney damage, increase in blood pressure level, itai—itai disease, and flu disorders [4]. The cadmium in water can be removed by the locally available indigenous plants.

## 2 Materials and Methods

AAS is used for the analysis of cadmium present in the aqueous solution. Microsoft Excel is used for plotting the graphs. XRD analyses are done to determine the characteristics of the biosorbents before and after adsorption process.

## 3 Preparation of *Annona Squamosa* and *Phyllanthus Acidus* Seed Powder and Synthetic Solution

The seeds were air dried at 40° C for two days. The seeds were then grounded to convert them into powder form. The seed powders are then heated in a furnace to remove the moisture content. The seed powders are then sealed in an air-tight container until usage. Standard cadmium solution is prepared by mixing 1.7911 g of CdCl<sub>2</sub> in 1000 ml of double distilled water.

## 4 Result and Discussion

After the calibration of AAS, batch adsorption study is carried out for the determination of optimum dosage, initial concentration of cadmium, and contact time for the maximum adsorption of cadmium. The percentage of adsorption obtained by both the adsorbents are determined. XRD analysis is done for the biosorbents before and after adsorption process to determine the characteristics of the adsorbents. Adsorption kinetics model and adsorption isotherm models are also analyzed for the design of the adsorption process.

### 4.1 XRD Analysis of *Annona Squamosa*

XRD analysis is done for *Annona squamosa* seed powder before and after treatment. The XRD patterns of *Annona squamosa* before adsorption process and after adsorption of cadmium are shown below.

Figure 1 represents the XRD patterns of untreated *Annona squamosa* seed powder. This shows that the seed powder is amorphous, that is, it does not have a regular shape. Figure 1a represents the XRD patterns of *Annona squamosa* seed powder after adsorption of cadmium. The powdered sample before adsorption is found to be poorly crystalline, whereas, after adsorption, the powdered sample obtained a peak at an angle  $68.1319^\circ$  with d spacing is found to be  $1.37517^\circ$  which indicates the adsorption of cadmium by the adsorbent. The relative intensity is found to be 100%.

### 4.2 XRD Analysis of *Phyllanthus Acidus*:

XRD analysis is done for *Phyllanthus acidus* seed powder before and after treatment. The XRD patterns of *Phyllanthus acidus* before adsorption process and after adsorption of cadmium are shown below.

The measurement conditions for the analysis of the seed powder are,

- Minimum step size : 0.001
- 2 theta angle start position : 10.0084
- 2 theta angle end position : 79.9804
- Step size : 0.0170
- Scan step time : 5.7150 s
- Scan type : Continuous
- Measurement temperature :  $25^\circ\text{C}$

Figure 2 represents the XRD pattern of *Phyllanthus acidus* seed powder before adsorption of the heavy metals. It is shown that the seed powder is amorphous or poorly crystalline before the adsorption process. Figure 2 represents the XRD pattern



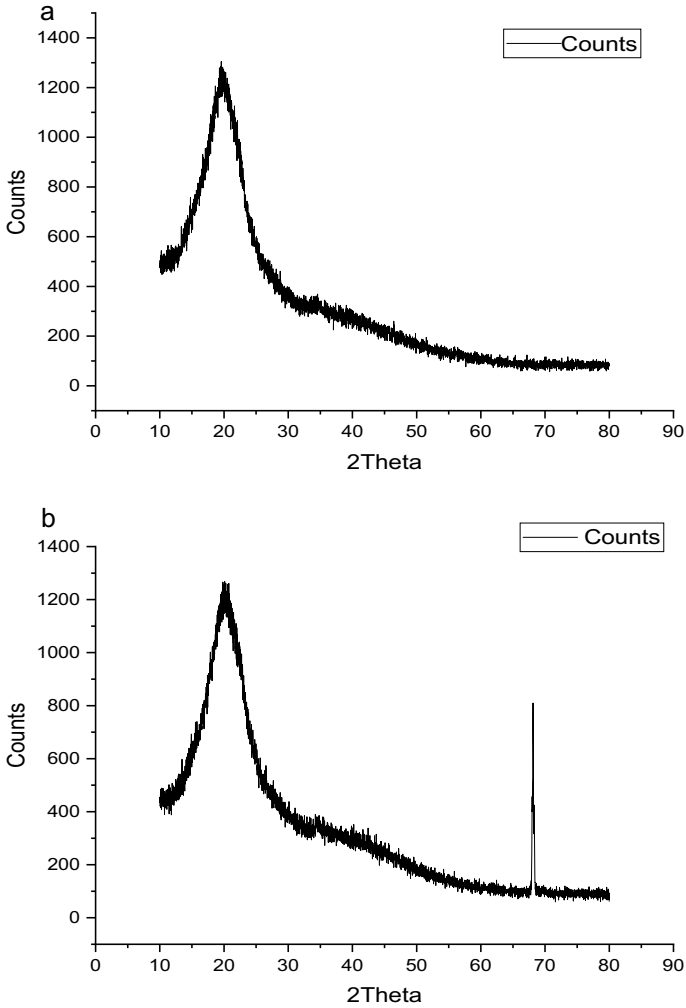


**Fig. 1** XRD analysis of *Annona squamosa* seed powder before adsorption process. XRD analysis of *Annona squamosa* seed powder after adsorption of cadmium

of *Phyllanthus acidus* seed powder after adsorption of cadmium. The peak is obtained at an angle of  $26.6077^\circ$  at a height of 674.55 cm with d spacing  $3.34746^\circ$  and the relative intensity is found to be 100%. This indicates the adsorption of cadmium by the adsorbent. The graph is compared between the adsorbent before and after adsorption process.

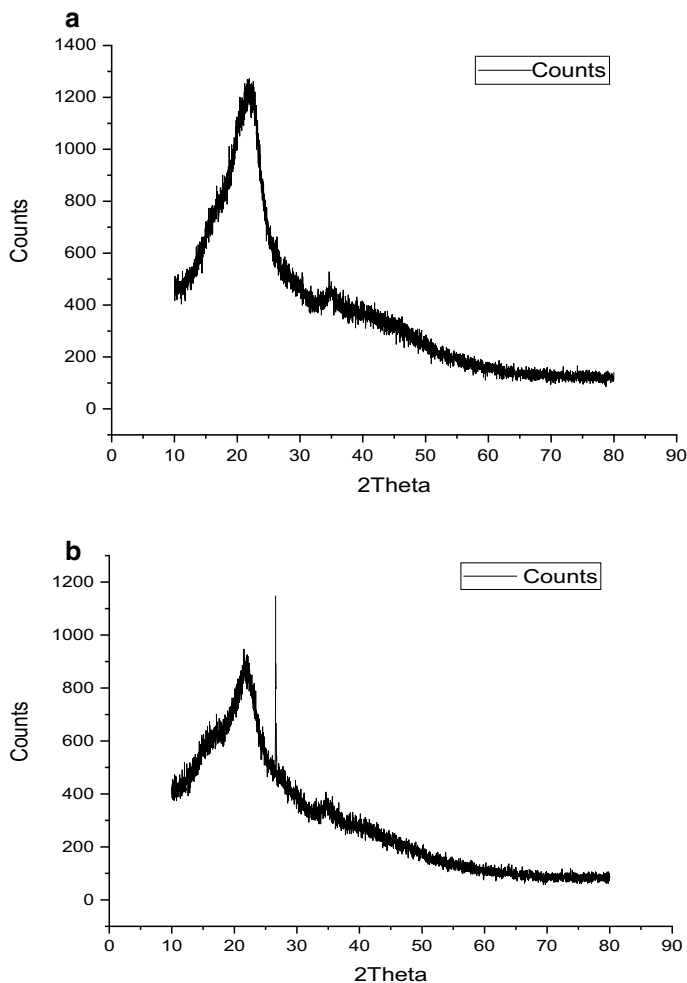


**Fig. 2** **a** XRD pattern of *Phyllanthus acidus* seed powder before adsorption. **b** XRD pattern of *Phyllanthus acidus* seed powder after adsorption of cadmium

### 4.3 Determination of Optimum Dosage

The optimum dosage for adsorption of cadmium by *Annona squamosa* seed powder is found to be 5 g, and the percentage adsorption of cadmium by the seeds is 80.3%. Here, the agitation rate, temperature, and pH is kept constant as 120 rpm, 32 °C and 4, respectively. The optimum dosage for adsorption of cadmium by *Phyllanthus acidus* seed powder is found to be 1.0 g and the percentage adsorption of cadmium by the seeds is 80.12%. Here, the agitation rate, temperature, and pH are kept constant as 120 rpm, 32 °C, and 4, respectively. The decrease in efficiency at higher biosorbent

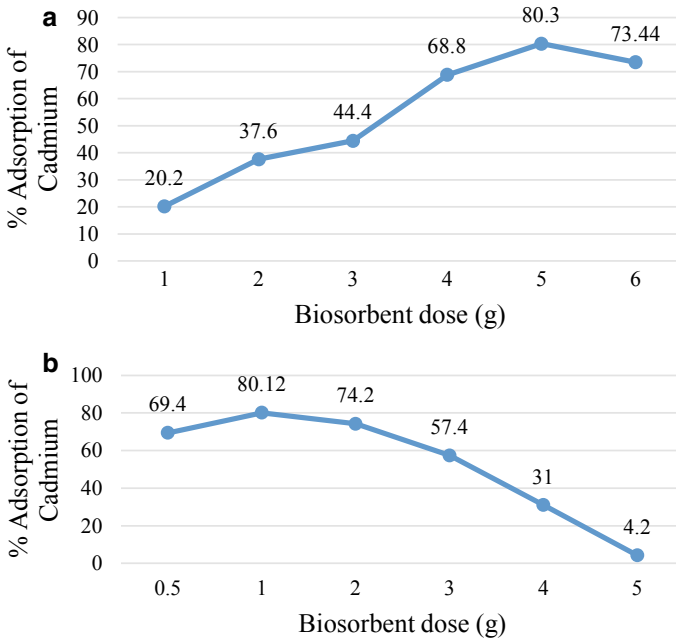


**Fig. 3** **a** Graphical representation of cadmium adsorption by *Annona squamosa* seed powder, **b** Graphical representation of cadmium adsorption by *Phyllanthus acidus* seed powder

concentration could be explained as a consequence of partial aggregation of adsorbent which results in a decrease in effective surface area of the metal uptake.

Figure 3a, b represents the graphical representation of cadmium adsorption by *Annona squamosa* seed powder and *Phyllanthus acidus* seed powder, respectively.

#### 4.4 Determination of Initial Concentration of Cadmium

The initial concentration of cadmium for the maximum adsorption of *Annona squamosa* seed powder is found to be 5 ppm, and the percentage adsorption of cadmium by the seed powder is 80.86%. Here, the dosage of the biosorbent, agitation rate, temperature, and pH are kept constant as 5 g, 120 rpm, 32° C, and 4, respectively. The initial concentration of cadmium for the maximum adsorption of *Phyllanthus acidus* seed powder is found to be 5 ppm, and the percentage adsorption of cadmium by the seed powder is 80.8%. Here, the dosage of the biosorbent, agitation rate, temperature, and pH is kept constant as 1.0 g, 120 rpm, 32° C, and 4, respectively. The decrease in adsorption of hexavalent chromium at higher concentration is due to the saturation of active binding sites.

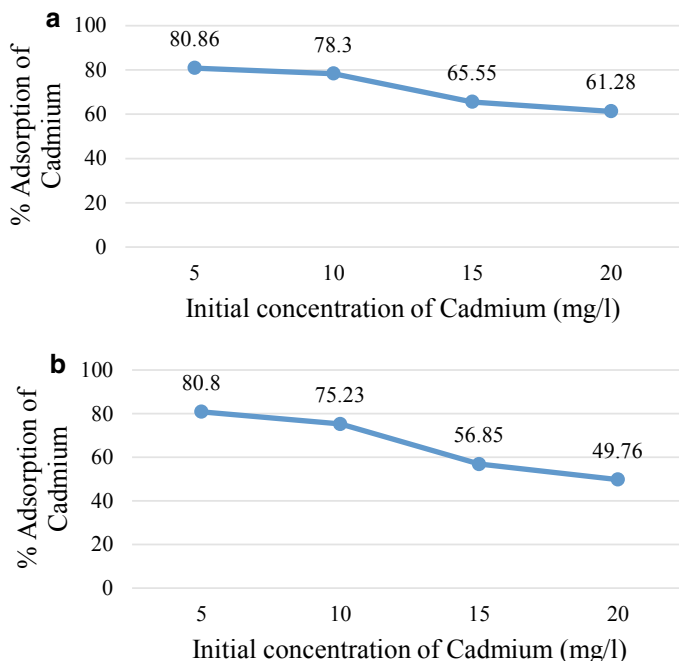


**Fig. 4** **a** Graphical representation of percentage adsorption of cadmium with respect to its concentration when *Annona squamosa* is used as a biosorbent, **b** Graphical representation of percentage adsorption of cadmium with respect to its concentration when *Phyllanthus acidus* is used as a biosorbent

Figure 4a, b represents the graphical representation of percentage adsorption of cadmium with respect to its concentration when *Annona squamosa* seed powder and *Phyllanthus acidus* seed powder are used as biosorbents, respectively.

#### 4.5 Determination of Time of Contact for Cadmium Adsorption

The contact time is varied from 30 to 240 min. The optimum time required for the maximum adsorption of cadmium is found to be 180 min. Here, the agitation rate, temperature, and pH is kept constant as 120 rpm, 32 °C, and 4, respectively. The concentration of cadmium contact time is varied from 30 to 240 min. The optimum time required for the maximum adsorption of cadmium is found to be 180 min. Here, the agitation rate, temperature, and pH is kept constant as 120 rpm, 32 °C, and 4, respectively. The concentration of cadmium is also varied. The adsorption rate is found to be constant after the equilibrium condition. This indicates that adsorption rate is more in *Annona squamosa* seed powder compared to *Phyllanthus acidus* seed

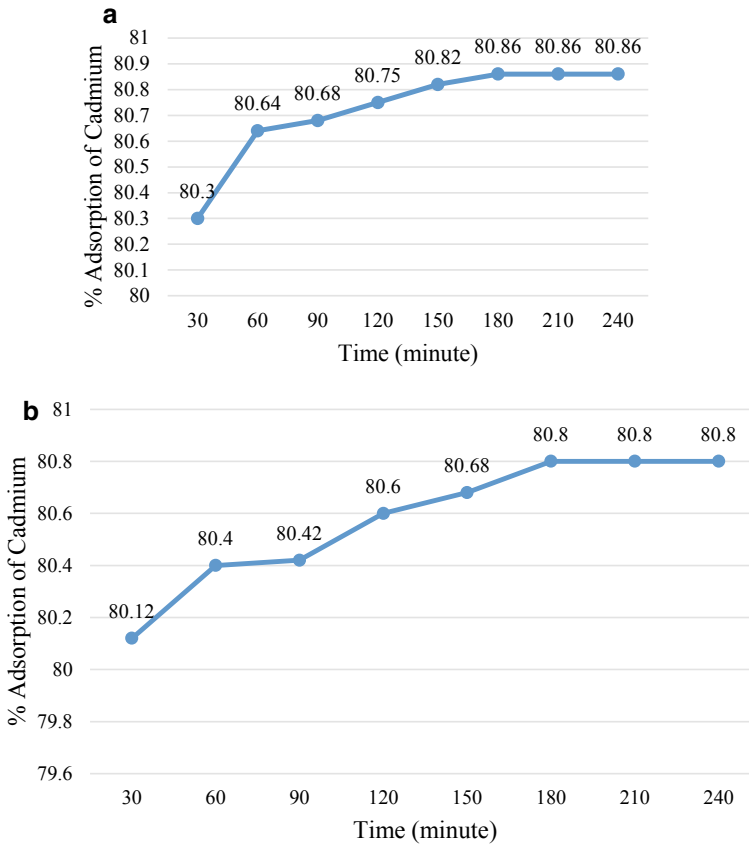


**Fig. 5** **a** Graphical representation of percentage adsorption of cadmium with respect to time when *Annona squamosa* is used as a biosorbent. **b** Graphical representation of percentage adsorption of cadmium with respect to time when *Phyllanthus acidus* is used as a biosorbent

powder. The optimum time required for getting the maximum adsorption of cadmium when both the biosorbents are used is represented in Fig. 5a, b.

#### 4.6 Freundlich Adsorption Isotherm Model for Cadmium

The constants in the Freundlich adsorption isotherm can be determined by plotting  $\log(x/m)$  versus  $\log C_e$  (to get the linear form) or by plotting  $x/m$  versus  $C_e$  (for nonlinear form).

$$\text{Log}(x/m) = \log K_f + 1/n \log C_e \quad (1)$$

The constants  $K_f$  and  $n$  are determined by slope ( $1/n$ ) and intercept ( $\log K_f$ ).

In Fig. 6a, the  $q_e$  or  $x/m$  value increases gradually. This is because the adsorption of cadmium occurred later at maximum adsorbent dosage. The correlation coefficient value is 0.984, and the constants such as  $K$  and  $n$  are determined from the equation in the graph. In Fig. 7a, the slope is found to be negative as the  $x/m$  value decreases with the  $C_e$ . This is because, the optimum dosage of the seed powder is obtained earlier, and hence, the adsorption rate decreases with increase in adsorbent dosage. Table 1 represents the Freundlich parameters for cadmium when both the biosorbents are used.

The  $n$  value indicates the degree of nonlinearity between the concentration of the solution and adsorption. If 'n' value is equal to 1, then the adsorption is said to be linear; if 'n' value is less than 1, the adsorption is said to be a chemical process; if 'n' value is greater than 1, the adsorption is then said to be a physical process. A relatively slight slope and small value of  $1/n$  indicate that the biosorption is good over the entire range of adsorption. The value of 'n' when *Annona squamosa* is used as a biosorbent is 9.12 which is greater than 1, and hence, the adsorption is said to be a physical process. The value of 'n' when *Phyllanthus acidus* is used as a biosorbent is 0.62 which is less than 1, and hence, the adsorption process for this seed powder is found to be a chemical process.

#### 4.7 Langmuir Adsorption Isotherm Model for Cadmium:

Langmuir adsorption isotherm model is a monolayer adsorption model on homogeneous adsorbent surface. The adsorbent reaches the maximum adsorption capacity when a saturated monolayer occurs on the adsorbent surface. The constants in the Langmuir adsorption isotherm can be determined by plotting  $1/q_e$  versus  $1/C_e$ .

$$x_m \text{ or } q_e = \frac{q_m b C_e}{1 + b C_e} \quad (2)$$

where

- $q_e$  is the mass of adsorbate adsorbed per unit mass of adsorbent, (mg adsorbate/g adsorbent).
- $b$  is an empirical constant.
- $C_e$  is the equilibrium concentration of adsorbate in the solution after adsorption (mg/l).
- $q_m$  is the maximum biosorbent capacity of the adsorbent (mg/g)

$$\frac{1}{q_e} = \frac{1}{q_m b C_e} + \frac{1}{q_m} \quad (3)$$

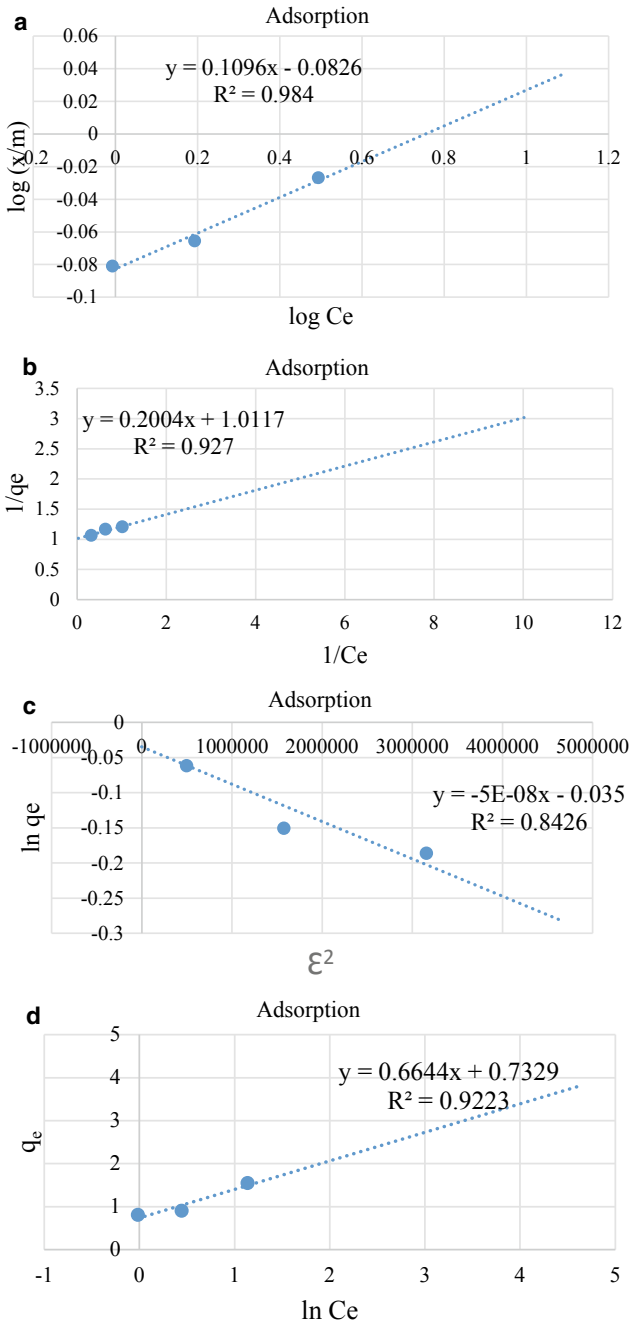


**Fig. 6** **a** Freundlich adsorption isotherm model for cadmium when *Annona squamosa* seed powder is used as a biosorbent. **b** Langmuir adsorption isotherm model for cadmium when *Annona squamosa* seed powder is used as a biosorbent. **c** Dubinin–Kaganer–Radushkevich adsorption isotherm model for cadmium when *Annona squamosa* seed powder is used as a biosorbent. **d** Temkin adsorption isotherm model for cadmium when *Annona squamosa* is used as a biosorbent

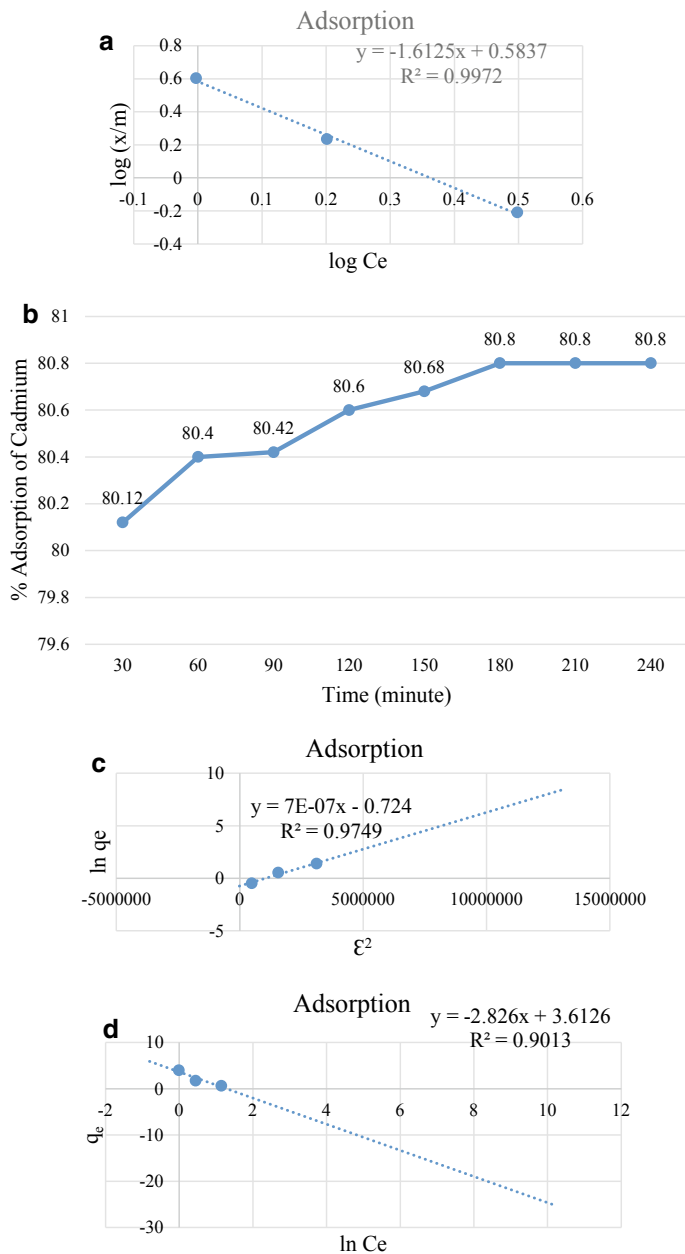


**Fig. 7** **a** Freundlich adsorption isotherm model for cadmium when *Phyllanthus acidus* seed powder is used as a biosorbent, **b** Langmuir adsorption isotherm model for cadmium when *Phyllanthus acidus* seed powder is used as a biosorbent, **c** Dubinin–Kaganer–Radushkevich adsorption isotherm model for cadmium when *Phyllanthus acidus* seed powder is used as a biosorbent, **d** Temkin adsorption isotherm model for cadmium when *Phyllanthus acidus* is used as a biosorbent



**Table 1** Freundlich parameters for cadmium

| Freundlich parameters         |                |        |
|-------------------------------|----------------|--------|
| For <i>Annona squamosa</i>    | K              | 0.827  |
|                               | 1/n            | 0.1096 |
|                               | R <sup>2</sup> | 0.984  |
| For <i>Phyllanthus acidus</i> | K              | 3.83   |
|                               | 1/n            | 1.6125 |
|                               | R <sup>2</sup> | 0.9972 |

The constants  $q_m$  and  $b$  are determined from the intercept ( $1/q_m$ ) and slope ( $1/q_m b$ ) of the line, respectively. The essential characteristics of the Langmuir isotherm parameters can be used to predict the affinity between the biosorbate and biosorbent which is calculated using following equation [5–8];

$$R_L = \frac{1}{1 + bC_i} \quad (4)$$

where

$b$  is the Langmuir constant.

$C_i$  is the maximum initial concentration of hexavalent chromium.

The value of separation parameters  $R_L$  provides important information about the nature of adsorption. The value of  $1/q_2$  indicated the type of Langmuir isotherm separation factor or dimensionless equilibrium parameters,  $R_L$  expressed as in the following equation: to be irreversible ( $R_L = 0$ ), favorable ( $0 < R_L < 1$ ), linear ( $R_L = 1$ ), or unfavorable ( $R_L > 1$ ) [9–14].

In Fig. 7b, the slope is found to be negative because the adsorption of cadmium decreases with increase in the adsorbent dosage as the optimum dosage of one of the biosorbent is obtained earlier. In Fig. 6b, the slope is found to be positive because the adsorption of cadmium increases with increase in the adsorbent dosage as the optimum dosage of one of the biosorbent is obtained later. Table 2 represents the Langmuir parameters for both the adsorbents. The value of  $R_L$  is found to be in the range of 0.038–0.009 for the concentration of 5–20 ppm of cadmium when *Annona*

**Table 2** Langmuir parameters for cadmium

| Langmuir parameters           |                |        |
|-------------------------------|----------------|--------|
| For <i>Phyllanthus acidus</i> | $q_m$          | 0.4357 |
|                               | $b$            | 1.036  |
|                               | R <sup>2</sup> | 0.8776 |
| For <i>Annona squamosa</i>    | $q_m$          | 0.988  |
|                               | $b$            | 5.048  |
|                               | R <sup>2</sup> | 0.927  |

*squamosa* is used as a biosorbent, since they are in the range between 0 and 1, which indicates the favorable condition. The value of  $R_L$  is found to be in the range of 0.16–0.046 for the concentration of 5–20 ppm of cadmium when *Phyllanthus acidus* is used as a biosorbent since they are in the range between 0 and 1, which indicates the favorable condition.

#### 4.8 Dubinin—Kaganer—Radushkevich (DKR) Adsorption Isotherm Model for Cadmium

DKR is a multilayer adsorption isotherm. The equation for Dubinin—Kaganer—Radushkevich adsorption isotherm can be written as,

$$\ln q_e = \ln q_m - \beta \varepsilon^2 \quad (5)$$

where

$q_m$  is the maximum biosorption capacity,

$\beta$  is the activity coefficient related to mean biosorption energy.

$\varepsilon$  is the Polanyi potential

$$\varepsilon = RT \ln(1 + 1/C_e) \quad (6)$$

Equilibrium data for the adsorption is plotted as  $\ln q_e$  versus  $\varepsilon^2$ . The two constants such as  $\beta$  and  $\ln q_m$  are determined from the slope ( $\beta$ ) and intercept ( $\ln q_m$ ). The values of adsorption energy ( $E$ ) is obtained from the following relationship,

$$E = \frac{1}{\sqrt{-2\beta}} \quad (7)$$

The mean free energy gives information about biosorption mechanism whether it is physical or chemical biosorption. If  $E$  value is between  $8 \text{ KJmol}^{-1}$  and  $16 \text{ KJmol}^{-1}$ , then the biosorption takes place chemically. If  $E$  value is less than  $8 \text{ KJmol}^{-1}$ , then the biosorption process is physical in nature [15–19].

Figure 6c and 7c represents the Dubinin—Kaganer—Radushkevich adsorption isotherm for cadmium when *Annona squamosa* and *Phyllanthus acidus* seed powders were used as biosorbents, respectively. Table 3 represents the parameters of Dubinin—Kaganer—Radushkevich adsorption isotherm.

Based on the adsorption capacity, the biosorption energy is varied, and so the activity coefficient also gets varied. In Fig. 7c, the  $\beta$  value is found to be positive as the adsorption capacity increases with increase in the Polanyi potential. In Fig. 6c, the  $\beta$  value is found to be negative as the adsorption capacity decreases with increase

**Table 3** Dubinin–Kaganer–Radushkevich parameters for cadmium

| Dubinin–Kaganer–Radushkevich parameters |         |        |
|---|---------|--------|
| For <i>Phyllanthus acidus</i>           | $\beta$ | 7E-07  |
|   | $q_m$   | 0.485  |
|   | $E$     | 0.845  |
|   | $R^2$   | 0.9749 |
| For <i>Annona squamosa</i>              | $\beta$ | -5E-08 |
|   | $q_m$   | 0.9656 |
|   | $E$     | 3.162  |
|   | $R^2$   | 0.8426 |

in the Polanyi potential. The mean free energy ( $E$ ) value for cadmium when *Phyllanthus acidus* is used as a biosorbent is 0.845 kJ/mol. Since it is less than 8 kJ/mol, biosorption of hexavalent chromium ions onto *Phyllanthus acidus* seed powder is of physical in nature. The mean free energy ( $E$ ) value for hexavalent chromium when *Annona squamosa* is used as a biosorbent is 3.162 kJ/mol. Since it is less than 8 kJ/mol, biosorption of hexavalent chromium ions onto *Annona squamosa* seed powder is of physical in nature [20–24].

#### 4.9 Temkin Adsorption Isotherm Model for Cadmium

The Temkin isotherm equation presumes that the adsorbent and adsorbate interactions cause a linearly decrease in heat of adsorption of all the molecules in the layer. Linearized Temkin adsorption isotherm is given by the equation,

$$q_e = \frac{RT}{b_T} \ln A_T + \frac{RT}{b_T} \ln C_e \quad (8)$$

where

- $b_T$  is the Temkin constant related to heat of biosorption (J/mol).
- $A_T$  is the Temkin isotherm constant (L/g).
- $R$  is the universal gas constant.
- $T$  is the temperature in kelvin.

Equilibrium data for the adsorption is plotted as  $q_e$  versus  $C_e$ . The two constants  $b_T$  and  $A_T$  are calculated from the slope  $\left(\frac{RT}{b_T}\right)$  and intercept  $\left(\frac{RT}{b_T} \ln A_T\right)$ , respectively.

Figures 6d and 7d represents the Temkin adsorption model for cadmium when *Annona squamosa* and *Phyllanthus acidus* seed powders are used as biosorbents, respectively. Table 4 represents the Temkin parameters for adsorption of cadmium when the seed powders are used as a biosorbent.

**Table 4** Temkin parameters for cadmium

| Temkin parameters             |       |         |
|-------------------------------|-------|---------|
| For <i>Annona squamosa</i>    | $b_T$ | 3816.63 |
|                               | $A_T$ | 3.013   |
|                               | $R^2$ | 0.9223  |
| For <i>Phyllanthus acidus</i> | $b_T$ | 897.3   |
|                               | $A_T$ | 0.278   |
|                               | $R^2$ | 0.9013  |

#### 4.9.1 Adsorption Kinetics for Cadmium

Adsorption kinetic study for the cadmium provides valuable information regarding the mechanism of adsorption process and the reaction pathways. The mechanism of adsorption depends on the physical and chemical characteristics of the adsorbents. The kinetics of adsorption explains the rate of uptake of cadmium onto the biosorbents such as *Annona squamosa* seed powder and *Phyllanthus acidus* seed powder and its rate control at the equilibrium time. The kinetic model is explained with the help of pseudo-first-order kinetics and pseudo-second-order kinetics.

##### Pseudo-First-Order Kinetic Model for Cadmium

The pseudo-first-order kinetic model for adsorption of cadmium is determined by the formula [25–29],

$$\ln(q_e - q_t) = \ln q_e - K_1 t \quad (9)$$

where

$q_e$  is the adsorption capacity of the biosorbent in the solid phase concentration at equilibrium (mg/g).

$q_t$  is the adsorption capacity of the adsorbent in the solid phase concentration (mg/g) at time,  $t$  (minute).

$K_1$  in (1/minute).

For the determination of pseudo-first-order kinetics, the graph is plotted between  $\ln(q_e - q_t)$  and time ( $t$ ). If the adsorption follows pseudo-first-order kinetic model, then the plot should be a straight line. Kinetic biosorption of pseudo-first-order model occurs chemically and involves valency forces through ion sharing or exchange of electron between biosorbent and the ions adsorbed onto it [30]. The values of  $K_1$  and  $\ln q_e$  are calculated from the slope ( $K_1$ ) and intercept ( $\ln q_e$ ), respectively. Figures 8a and 9a represents the pseudo-first-order kinetic model for cadmium when both the biosorbents are used. Table 5 represents the parameters of pseudo-first-order model for cadmium when *Annona squamosa* seed powder and *Phyllanthus acidus*

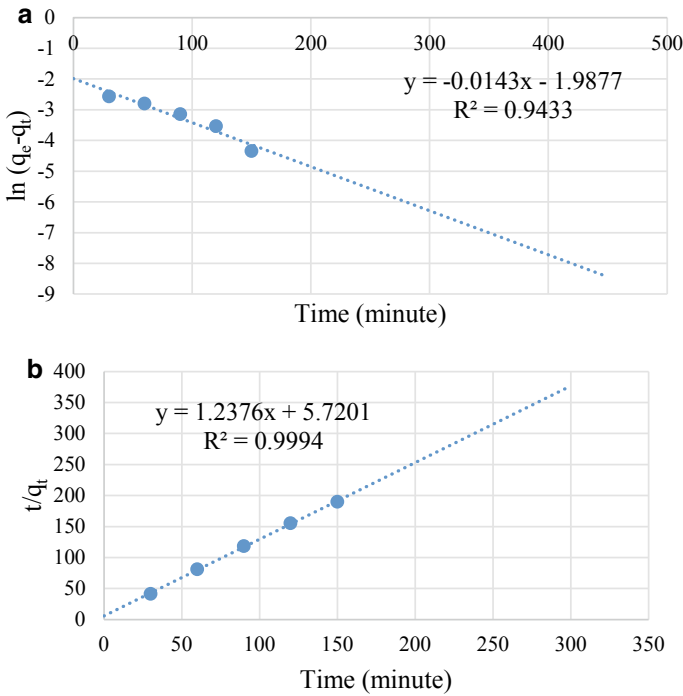


**Fig. 8** **a** Pseudo-first-order kinetic model for cadmium when *Annona squamosa* is used as a biosorbent, **b** pseudo-second-order kinetic model for cadmium when *Annona squamosa* is used as a biosorbent

seed powder are used as biosorbents, respectively. The correlation coefficient of *Phyllanthus acidus* seed powder is found to be 0.9867 which is higher than *Annona squamosa* seed powder.

Pseudo-Second-Order Kinetic Model for Cadmium

Pseudo-second-order kinetics is determined by the formula,

$$\frac{t}{q_t} = \frac{1}{K_2 q_e^2} + \frac{t}{q_e} \tag{10}$$

where  $K_2$  is in  $(g \cdot mg^{-1} \cdot min^{-1})$ .

The graph is plotted between  $t/q_t$  and time (t). The values  $K_2$  and  $q_e$  are calculated from the slope ( $1/q_e$ ) and intercept ( $1/K_2 q_e^2$ ), respectively. Figures 8b and 9b represents the pseudo-first-order model for cadmium when *Annona squamosa* seed powder and *Phyllanthus acidus* seed powder are used as biosorbents, respectively. In

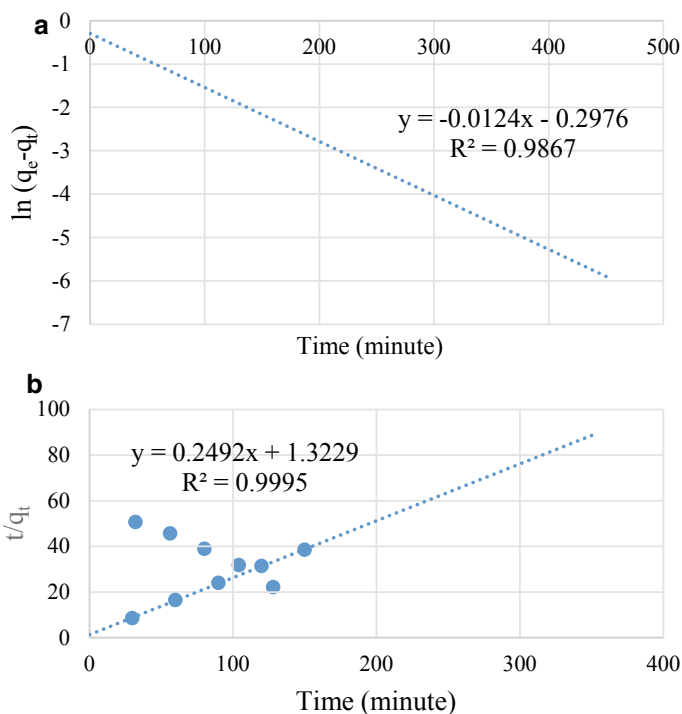


**Fig. 9** **a** Pseudo-first-order kinetic model for cadmium when *Phyllanthus acidus* is used as a biosorbent, **b** pseudo-second-order kinetic model for cadmium when *Phyllanthus acidus* is used as a biosorbent

**Table 5** Pseudo-first-order model parameters for cadmium

| Pseudo-first-order model      |       |        |
|-------------------------------|-------|--------|
| For <i>Annona squamosa</i>    | $K_1$ | 0.0143 |
|                               | $q_e$ | 0.137  |
|                               | $R^2$ | 0.9433 |
| For <i>Phyllanthus acidus</i> | $K_1$ | 0.0124 |
|                               | $q_e$ | 0.743  |
|                               | $R^2$ | 0.9867 |

this kinetic model, the value of  $t/q_t$  changes linearly with respect to time. This shows that the adsorption process obeys pseudo-second-order model. Table 6 represents the pseudo-second-order kinetic model for cadmium when both the biosorbents are used. It is found that the correlation coefficient is higher in pseudo-second-order kinetic model for cadmium compared to pseudo-first-order kinetic model for cadmium.

**Table 6**  
Pseudo-second-order model  
parameters for cadmium

| Pseudo-second-order model     |       |        |
|-------------------------------|-------|--------|
| For <i>Annona squamosa</i>    | $K_2$ | 0.27   |
|                               | $q_e$ | 0.81   |
|                               | $R^2$ | 0.9994 |
| For <i>Phyllanthus acidus</i> | $K_2$ | 0.047  |
|                               | $q_e$ | 4.01   |
|                               | $R^2$ | 0.9995 |

## 5 Conclusion

From the experiment, it is concluded that the efficiency of *Annona squamosa* seed powder is higher than *Phyllanthus acidus* seed powder. From the batch adsorption study, the adsorption of cadmium by *Annona squamosa* seed powder is found to be greater than *Phyllanthus acidus* seed powder. XRD analysis of the biosorbents is done, and the characteristics of the biosorbents are identified. The biosorbents are best suited for the removal of cadmium from the water sample. Freundlich adsorption isotherm is found to be best suited for the design of adsorption process as the correlation value is higher. Adsorption kinetic models are also analyzed and pseudo-second order is found to be suitable for the adsorption of cadmium.

## References

1. Verma R (2021) Two-third of the world population lives in water-scarce areas. [online] Downtoearth.org.in
2. Malik A, Alam I, Faridi MR, Ayub,S (2019) Corporate social irresponsibility towards the planet: a study of heavy metals contamination in groundwater due to industrial wastewater. Soc Responsib J
3. Atsdr.cdc.gov. 2021. [online]
4. Rahimzadeh MR, Rahimzadeh MR, Kazemi S, Moghadamnia AA (2017) Cadmium toxicity and treatment: an update. Caspian J Intern Med 8(3):135
5. Elavarasan A (2018) EDX and XRD, FT-IR spectra, analysis containing hexavalent chromium metal ion adsorption present in aqueous solution on to phosphoric acid ( $H_3PO_4$ ) activated *Mimusops elengi* leaves carbon. J Drug Delivery Therapeutics 8(5):132–138
6. Vaza, JS, Bhalerao SA (2018) ‘Removal of hexavalent chromium by using citric acid modified Tamarind Pod Shell powder (*Tamarindus indica L.*)’, Int J Trend Sci Res Dev 3
7. Fatma EE, Behzat B, Turan ES (2018) ‘Adsorption of hexavalent chromium by *Eucalyptus camaldulensis* bark/ maghemite nano composite’, Int J Chem Reactor Eng
8. Chandran PJI, Sivakumar A (2013) ‘Removal of lead and cadmium ions from water using *Annona squamosa* shell: kinetic equilibrium studies’, Desalination Water Treatment, 51
9. Chakresh kumar, J, Davendra Singh, M and Anuj Kumar, Y, (2016), ‘Applicability of plant based biosorbents in the removal of heavy metals: a review’, Environ Process
10. Santanu, M, Deepa Kumari, Madhvi Joshi, Alicia Kyoungjin and Manish Kumar, (2020), ‘Low cost bio-based sustainable removal of lead and cadmium using a polyphenollic bioactive Indian curry leaf (*Murraya koengii*) powder’, Int J Hygiene Environ Health

11. Moafi HF, Ansari R, Ostovar F (2016) Ag<sub>2</sub>O/Sawdust nanocomposite as an efficient adsorbent for removal of hexavalent chromium ions from aqueous solutions. *J Mater Environ Sci* 7(6):2051–2068
12. Khan EA, Shahjahan, Khan TA (2018) ‘Adsorption of methyl red on activated carbon derived from custard apple (*Annona squamosa*) fruit shell: Equilibrium isotherm and kinetic studies’, *J Molecular Liquids* 1195–1211
13. Seshadri N, Ramesh Naik B, Sandeep Kumar NV, Venkata Ramana DK, Seshaiiah K (2018) Application of citric acid modified *annona squamosa* (custard apple) bark powder as biosorbent to remove ni (ii) from waste water. *Indian J Adv Chem Sci* 3:1–10
14. Castaldi P, Santona L, Enzo S, Melis P (2008) Sorption processes and XRD analysis of a natural zeolite exchanged with Pb<sup>2+</sup>, Cd<sup>2+</sup> and Zn<sup>2+</sup> cations. *J Hazard Mater* 156:428–434
15. Kumar S, Meikap BC (2014) ‘Removal of chromium (VI) from waste water by using adsorbent prepared from green coconut shell’, *Desalination and Water Treatment*
16. Shahadat M, Rafatullah M, Teng TT (2015) ‘Characterization and sorption behavior of natural adsorbent for exclusion of chromium ions from industrial effluents’, *Desalination and Water Treatment*
17. Parate VR, Waghrukhar SS, Talib MI (2016) ‘Utilization of custard apple (*Annona squamosa*) seeds for heavy metal (Ni (II)) removal’, *Int Conf Global Trends Eng Technol Manage*
18. Vardhan KH, Panda RC, Saravanan A (2018) Removal of Zn(II) ions from aqueous solution using chemically modified *Annona reticulata* seeds: kinetics, isotherm and thermodynamics. *Desalin Water Treat* 122:66–77
19. Padmaja M, Bhavani R, Pamila R (2018) ‘Adsorption of cadmium from aqueous solutions using low cost materials-a review’, *Int J Eng Technol* 7(4.2):26–29
20. Perez-Marin AB, Meseguer Zapata V, Ortuno JF, Aguilar M, Saez J, Llorens M (2007) ‘Removal of cadmium from aqueous solutions by adsorption onto orange waste’, *J Hazardous Mater* 122–131
21. Collins Arun Prakash V, Karthika V, Masi M, Xavier Rajarathinam SR (2014) ‘Adsorption Study of Cr (VI) from Aqueous Solution Using *Annona Reticulata* and *Pouteria Sapota*’, *Int J Sci Res* 3
22. Sivakumar, R, Sri Renganathan, P, Mary Helan, H and Rajachandrasekar, T, (2019), ‘Removal of Copper ion from aqueous solution using seeds of sugar apple (*Annona squamosa* L.)’, *Res J Life Sci Bioinf Pharmaceutical Chem Sci* 5(2)
23. Anwar J, Shafique U, Waheed-uz-Zaman MS, Dar A, Anwar S (2010) Removal of Pb (II) and Cd (II) from water by adsorption on peels of banana. *Biores Technol* 101:1752–1755
24. Amoo IA, Emenike AE, Akpambang VOE (2008) Compositional evaluation of *Annona cherimoya* (Custard apple) fruit. *Trends Appl Sci Res* 3:216–220
25. Grassi M, Kaykioglu G, Belgiorio V, Lofrano G (2012) ‘Removal of Emerging Contaminants from Water and Wastewater by Adsorption Process’, *Green Chemistry for Sustainability*
26. Nisar MF, He J, Ahmed A, Yang Y, Li M, Wan C (2018) ‘Chemical components and biological activities of the genus phyllanthus: a review of the recent literature’, *Molecules* 23
27. Sree Devi O, Ravindhranath K (2013) ‘Affinity of bio-adsorbents derived from *annona squamosa*, *cassia auriculata* and *ficus religiosa* towards chromate in polluted waters’. *Asian J Res Chem* 6(2)
28. Suchitra MR, Prathasarathy S (2015) ‘Sitaphal: reemergence’. *Res J Pharm Biol Chem Sci* 6(3)
29. Munichandran M, Gangadhar B, Ramakrishna Naidu G (2019) Removal of nickel, cadmium and lead ions from aqueous solutions using combination of sapidilla (*manilkara zapota*), custard apple (*annona squamosa*) seeds powder. *J Appl Chem* 8(1):245–252
30. Vaza JS, Bhalariao A (2018) Phytochemistry, medicinal values and pharmacological potential of *Datura stramonium* L. review. *Int J Pharmac Drug Anal* 540–544. Chicago



# A Comparative Study on Environmental Impact Assessment of Recirculating Aquaculture System and Raceway System



Pradeep Ramesh, Mohammad Tanveer, R. S. Dharani Shree, and R. Gokul

**Abstract** The aquaculture industry is one of the sunshine industries, growing all over the world. India is a peninsula country with large coastal areas of about 8120 sq. km, which relies significantly on marine resources. The aquaculture industries serve as the most promising way of meeting the demand for a variety of seafood. Technological advancement leads to the adoption of upcoming technology in the aquaculture sector to boost production to fulfill the food requirement of the increasing population. However, the actual concern for policymakers or government is to utilize the marine and freshwater resources in an eco-friendly manner. Hence, the machinery used in the aquaculture industry must be evaluated for its impact on environmental sustainability. In this study, the focus has been made mainly on two major aquaculture and its allied production units viz recirculating aquaculture systems and raceways. The results obtained from the present study show that there is a significant impact by these systems to the environment viz ionizing radiation ( $107.12 \times 10^{-2}$  KBqU-235 eq), aquatic eco-toxicity ( $426.54 \times 10^{-2}$  kg TEG eq to water), and water scarcity ( $166.9 \times 10^{-2}$  m<sup>3</sup> world eq). Thus, it necessitates us to understand and improve our process condition to develop and adopt machinery in a manner to mitigate adverse impacts on the environment.

**Keywords** Environmental impact assessment · Aquaculture · Recirculating aquaculture system · Raceway system

## 1 Introduction

India has a significant interest on aquaculture. Besides having a vast coastal line, Indian fisheries have a considerable potential to bloom in culture fisheries by

---

P. Ramesh (✉) · M. Tanveer · R. S. D. Shree  
Department of Aquacultural Engineering, College of Fisheries Engineering, TNJFU,  
Nagapattinam, India

R. Gokul  
College of Fisheries Engineering, TNJFU, Nagapattinam, India

employing aquaculture. It helps in attaining the nutritional stability of the country, providing employment for various groups of people associated with its activity, and sustaining the livelihood of the fishers. The aquaculture advancement made its technical side stronger. It helps in increasing productivity by reducing the risk of culture in every possible way by employing scientific solutions. Some of the advanced systems are recirculating aquaculture system, raceway, biofloc, aquaponics, etc. In the recent trends of zero water exchange and low toxicity level, recirculating aquaculture system (RAS) is introduced with advanced biofiltration techniques. Other filtration equipments and environmental control are also necessary to maintain quality water and provide a suitable habitat for fish [2]. The main benefit of RAS is the ability to reduce the water exchange and maintaining a healthy habitat for fish. The commercial RAS with higher stocking densities are economically profitable [13]. Thus, many researchers are currently engaged in determining the RAS as a viable form of intensive aquaculture. It is also imperative to find the impacts caused by types of machinery used in the RAS system. Hence, the environmental impact assessment for the RAS system can be examined by using the life cycle assessment (LCA) tool for improvement of the system. A raceway is a culture unit used for raising aquatic animals. Raceway systems are one among the oldest aquaculture techniques used for inland aquaculture [7]. A raceway consists of rectangular basins or canals made of concrete, constructed with an inlet and outlet. A water recirculation mode is maintained to retain the standards of water quality to raise aquatic animals at higher stocking density within the raceway. In its process, it is essential to assess the impacts caused by the machinery used in the raceway [4]. Besides, advantages and needs for EIA study on types of machinery used [1], it is essential to note that several kinds of research have already been carried out in both the systems in EIA aspects.

d'Orbcastel et al. [8] conducted study on the EIA of rainbow trout in RAS using the SimaPro—life cycle assessment tool. Environmental impacts were analyzed using the following categories viz eutrophication potential, acidification potential, global warming potential, net primary production use, and non-renewable energy use. Pelletier et al. [10] analyzed salmon feeds using the SimaPro life cycle assessment tool to analyze the gross nutritional energy result with the system. Pelletier and Tyedmers [11] conducted a study on EIA of tilapia culture system to find out the gross nutritional energy based on the previous studies conducted in the year 2009. Gronroos et al. [3] conducted research on EIA on the net cage system to find out the gross nutritional energy. The functional unit was set as a metric ton of un-gutted rainbow trout after slaughtering. This process includes raw material production for feed, feed manufacturing, packaging production, manufacturing, package, hatchery, fish farming, and operation of slaughtering. The environmental impact categories include climate change, acidification, aquatic eutrophication, tropospheric ozone formation, and depletion of fossil fuels.

Shaine et al. [12] conducted study on EIA of the net cage system to analyze the economics of the system. Iribarren et al. [5] conducted study on EIA of the raft system to find out the environmental impacts. Other studies are as integrated farming system to analyze its economics, and Papatryphon et al. [9] assessed environmental impacts associated with different feed for rainbow trout production. The study was

based on the amount of feed required for the production of one metric ton of rainbow trout. The four analyzed feeds were considered in terms of a normalized nutrient profile to allow comparison on equivalent basis.

Hence, the present study aims to access the environmental impacts caused by the types of machinery used for the production of fishes using advanced aquaculture systems like raceway and recirculating aquaculture systems. The detailed system description was given in the next section.

## **2 Material and Method**

### ***2.1 Site Information***

The environmental impact study was carried out at the raceway and recirculating aquaculture system available at Advanced Research Farm Facility owned and administered by Tamil Nadu Dr. J. Jayalalithaa Fisheries University, Nagapattinam. The facility is established at Madhavaram region of Chennai city, Tamil Nadu, India. The site possessed with suitable environmental conditions for culturing aquatic organisms and enough water facility. Since it is entirely an indoor facility, the research work can be carried out without the influence of external conditions at any cost.

### ***2.2 System Description***

The raceway and recirculating aquaculture system do not differ significantly on their structural designs. Only, the operating conditions and the machinery capacity are the responsible variables in deciding the effectiveness of both the systems. As discussed, the raceway has the advantage of washing out the feed waste and fecal waste effectively, and it can give an active environment for the fishes to grow. As the fishes belong to the category called nektons, it always tends to move against the water current, and thereby, raceway helps in maintaining the active growth of fishes.

The recirculating aquaculture system has advantage of removing all the waste material with the help of mechanical and biological filters. Hence, it makes the culture easier and improves growth by maintaining the quality of water. The operations are similar in both the cases, except the machinery capacity and waterway structure in raceway which allows the water to flow through it. However, recirculating aquaculture system (RAS) and raceway systems are essentially a technology for farming fish or other aquatic organisms by reusing the water meant for better production strategies. These technologies take such advantage by the usage of mechanical and biological filters. Hence, these can be applied for any aquaculture species such as finfishes, crustaceans, and oysters [6]. The process flow and descriptions of both the system where inventories contributed are discussed in detail.

### **2.2.1 Culture Tank**

The culture tank must help the fish in the sense of quality of water it contains and tank design. Hence, to design a tank, the parameters viz size, shape, water depth, and the self-cleaning process should be considered with at most priority. In a circular or square tank with cut corners, the water moves in the circular pattern making the whole water in the tank move around the center. The self-cleaning effect depends on tank design and its hydraulic patterns. A vertical inlet having horizontal adjustment is a significant way to control the water currents. Hence, in this study, a tank with an inlet at the upper slope side and an outlet at the lower slope side was used. All the inlet and outlet are provided with a vertical axis in this study.

### **2.2.2 Drum Filter**

A drum filter is a mechanical filter, to remove the solid waste from the outlet water of the culture tank. Almost all recirculating aquaculture system filters the outlet water from the tanks with the so-called microscreen fitted with filter cloth of typically 35 to 100 microns. This filter consists of a drum, rotating in a tank of liquid to be filtered. The water to be filtered enters the drum and filtered through the drum's filter elements. The difference in water level inside/outside of the drum acts as the driving force for the filtration. As the drum rotates through the water, the vacuum sucks liquid and solids on to the drum precoat surface. Then, the solid particles present in the water get trapped by the filter elements, and then, the filtrate will be pumped away.

### **2.2.3 Biofilter**

Biofilters used in recirculating systems can be of two types, either fixed bed or moving bed type. It can be worked in submerged water. In the fixed bed filter, the plastic media present is fixed, and it is not moving. The water in the media runs through in laminar flow to make contact with the bacterial film. In the moving bed filter, the plastic media moves inside the biofilter by current created by air pumping. Because of the constant movement of the media, a moving bed filter gives a higher turnover rate per  $m^3$  of the biofilter. A fixed bed filter removes microscopic organic material and leaving the water very clear. It helps to maintain the water quality by removing ammonia, nitrates, and dissolved organic solids in the water.

### **2.2.4 UV Sterilization Unit**

UV sterilization unit works by applying light of a particular wavelength to destroy the DNA of biological organisms. Especially, pathogenic bacteria and one-celled organisms are targeted in aquaculture. The best control in the UV sterilization unit is

achieved when effective mechanical filtration is combined with thorough biofiltration to effectively remove organic matter from the process water, making the UV radiation work effectively. The efficiency depends on size, species to be targeted, and turbidity of the water. In order to inactivate about 90% of the microorganisms, the water needs to be treated with 2000–10,000  $\mu\text{Ws}/\text{cm}^2$ . Fungi require 10,000–100,000  $\mu\text{Ws}/\text{cm}^2$ , and small parasites require 50,000–200,000  $\mu\text{Ws}/\text{cm}^2$ . UV lighting used in this aquaculture system works underwater to give maximum efficiency.

### 2.2.5 Cartridge Filter

The cartridge filter is an auto oil filter, having replaceable plastic media to trap solids. It has a specialized application in recirculating aquaculture systems (RAS) to remove sediment, metal components, and microorganisms from the water. The filter should be correctly sized for the required flow of water. Otherwise, the water blockage may happen. Filters containing very loose media need to be used, where there is a significant quantity of sediment in the water or higher concentrations of iron and manganese components.

The schematic diagram of raceway and recirculating aquaculture system is given in Figs. 1 and 2.

### 2.2.6 Waterway Channel—Raceway

Figure 2 shows an exclusive structure of raceway system. The waterway structure is designed to allow the flow of water along the length of the tank. The depth of the tank is allowed to be at a considerable level, and it was kept as 1.5 m in this study. The baffle-type waterway is usually followed for this raceway system since it occupies minimum space. The waterway channel is fitted with a pump, water inlet, aerator, and water outlet structure.

## 2.3 *Environmental Impact Assessment (EIA)*

EIA is a broad term, which includes many aspects related to the impact characterization for a particular system. The life cycle analysis was carried out as per the standards of ISO 14,040–2006, which defines to include the goal and scope definition, inventory analysis, impact assessment, and interpretation of the result. The OpenLCA software v(1.9) is used for this study, and it contains the necessary database to carry out the study.

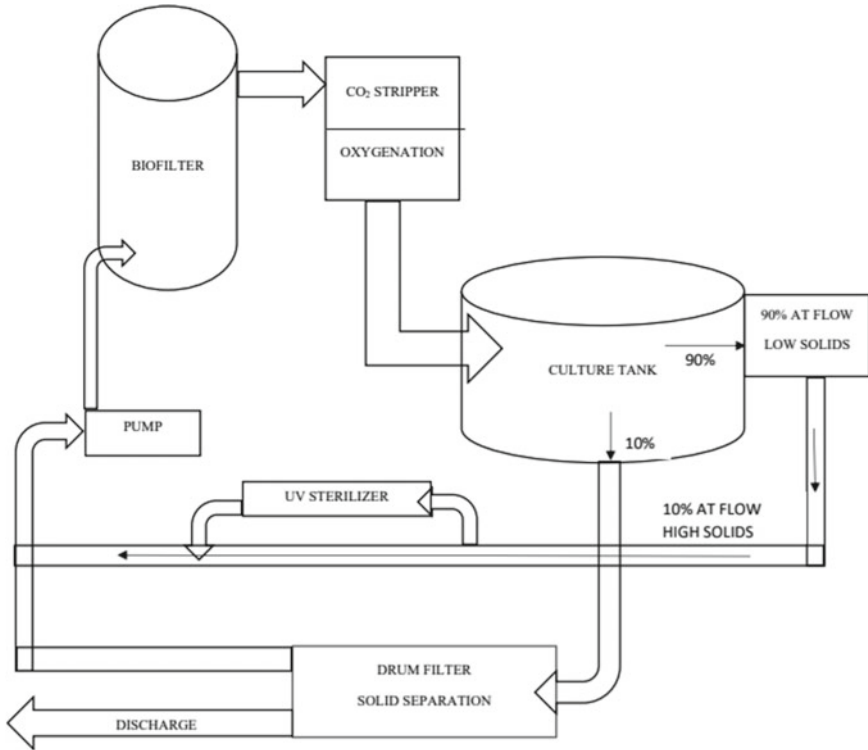


Fig. 1 Schematic diagram of RAS setup

### 2.3.1 Goal and Scope Definition

The principal goal of this impact analysis study is to analyze the impacts caused by the types of machinery mentioned above with an ultimate aim to evaluate the efficiency of the system in terms of its environmental sustainability. Furthermore, this will help in identifying the potential component causing more significant impacts to improve the system sustainability.

### 2.3.2 System Boundaries

The present study focuses on the manufacturing part, components used, and end-of-life product types of machinery used in the systems. The used phase of the component is also considered with utmost concentrations to analyses the impact in particular.

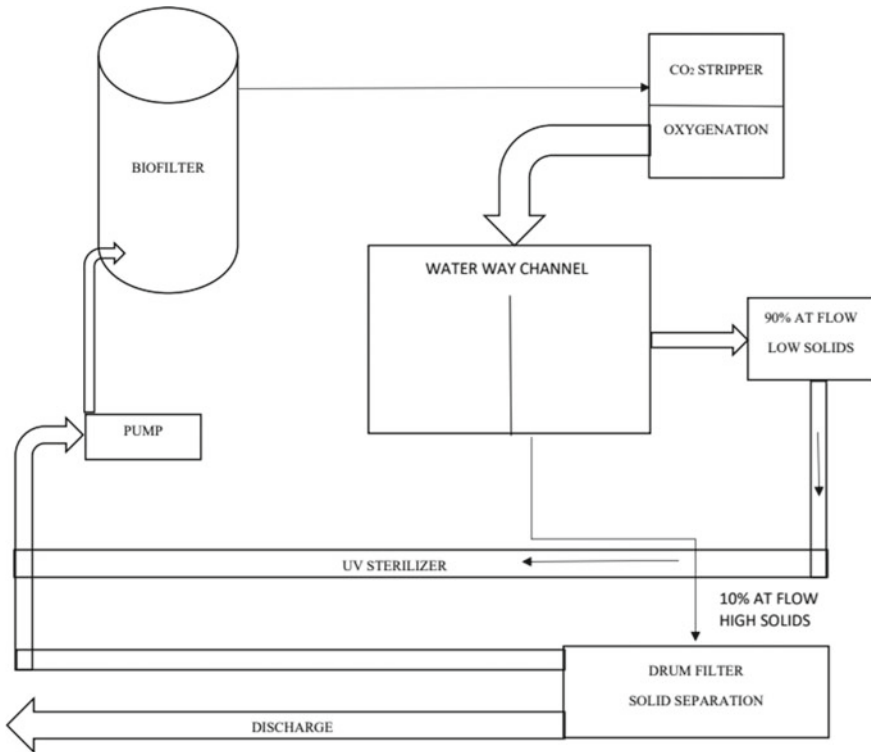


Fig. 2 Schematic diagram of raceway setup

### 2.3.3 Methods

There are two LCA impact methods used to analyse the data viz environmental footprint indicator method and Impact 2002. The impact analyzed with endpoint indicators like acidification terrestrial and freshwater, cancer under human health effects, climate change, and ionizing radiation.

### 2.3.4 Functional Unit

The functional unit of 15 years of operation was set as the standard value. It helps in conducting the study during the process of operation in 15 years. The 15 years of product lifespan is based on the practical experience and reliable assumption. The types of machinery analyzed mainly includes complex components and structural components. Hence, the detailed analysis was carried out in that aspect, and the main parameters used for manufacturing and the process are cement, steel, plastics, alloy material, UV light, copper, bronze, aluminum, rubber, and water.

**Table 1** Primary inventories for the life cycle analysis

| S. no | Category       | RAS                | Raceway            |
|-------|----------------|--------------------|--------------------|
|       |                | Quantity used      | Quantity used      |
| 1     | Steel          | 380 kg             | 30 kg              |
| 2     | Copper         | 18 kg              | 22 kg              |
| 3     | Bronze         | 7 kg               | 10 kg              |
| 4     | Aluminum       | 105 kg             | 86 kg              |
| 5     | Plastic        | <1 kg              | 3 kg               |
| 6     | Cement         | 250 m <sup>3</sup> | 425 m <sup>3</sup> |
| 7     | Concrete       | 515 m <sup>3</sup> | 680 m <sup>3</sup> |
| 8     | Electricity    | 810 Kwh            | 740 Kwh            |
| 9     | Water          | 580 m <sup>3</sup> | 380 m <sup>3</sup> |
| 10    | Estimated life | 15 years           |                    |

### 2.3.5 Inventory Analysis

It is the foremost and important step in every environmental impact analysis study. It comprises of all the element which takes part in the process of production of components, uses, and final discard. The total life span of types of machinery used is assumed based on reliable assumption of 15 years as discussed in 2.3.4. The inventories are described in Table 1.

## 3 Environmental Impact Assessment and Result Interpretation

As discussed in Sect. (2.3), the impact analysis was carried out with the machinery used in the culture systems. The results obtained with environmental footprint indicator were mentioned below in Table 2 and with Impact 2002 are mentioned in Table 3. Focusing on the issues of environmental factors, for the assessment of the aforementioned impact categories, databases called Agribylase and Ecovinent v2.2 are used.

The results obtained in the analysis and the combined classification of impacts are depicted in Figs. 3 and 4. The figure clearly shows that the impacts are not very different and almost same in every category except eco-toxicity, which results because of the improper accumulation of waste and other solids. Then impactful factors caused by the usage of machinery are classified into two such categories called human-associated impacts and ecological issues. Both the systems render almost common impacts with approximately the same values.

The land use impact will be higher in case of raceway since it is a flow-through channel, which is given in Table 2. The material and components used to categorize the major impacts when compared to the use of case impacts. It is clearly shown

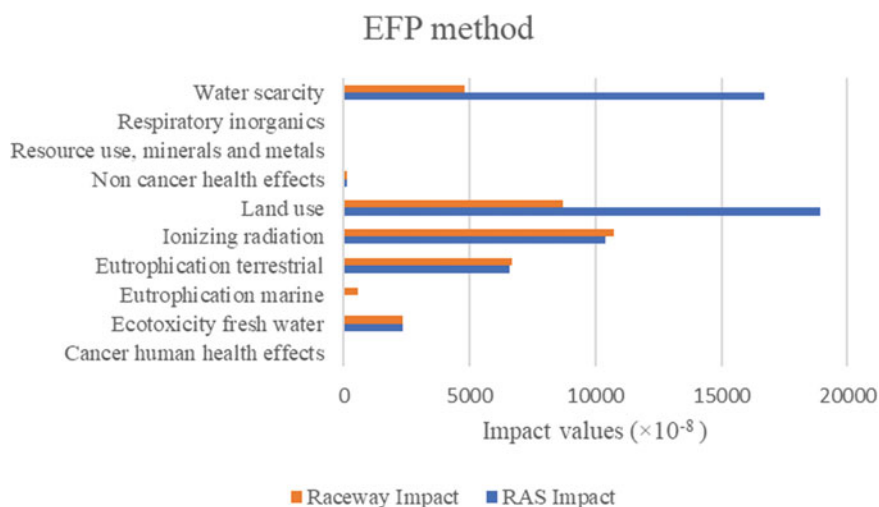


**Table 2** Impact assessment with environmental footprint indicator method

| S. no | Impact category                    | RAS impact             | Raceway impact          | Indicator/Unit          |
|-------|------------------------------------|------------------------|-------------------------|-------------------------|
| 1     | Cancer human health effects        | $1.59 \times 10^{-8}$  | $1.534 \times 10^{-8}$  | CTUh                    |
| 2     | Eco-toxicity freshwater            | $23.35 \times 10^{-4}$ | $2.357 \times 10^{-4}$  | CTUe                    |
| 3     | Eutrophication marine              | $5.86 \times 10^{-7}$  | $5.9 \times 10^{-7}$    | Kg N eq                 |
| 4     | Eutrophication terrestrial         | $6.61 \times 10^{-4}$  | $6.68 \times 10^{-5}$   | Mole of N eq            |
| 5     | Ionizing radiation                 | $10.4 \times 10^{-4}$  | $107.12 \times 10^{-4}$ | KBqU-235 eq             |
| 6     | Land use                           | $1.89 \times 10^{-4}$  | $0.087 \times 10^{-4}$  | Pt                      |
| 7     | Non cancer health effects          | $1.1 \times 10^{-6}$   | $1.12 \times 10^{-6}$   | CTUh                    |
| 8     | Resource use, minerals, and metals | $3.45 \times 10^{-8}$  | $3.4 \times 10^{-9}$    | Kg Sb eq                |
| 9     | Respiratory inorganics             | $4.6 \times 10^{-7}$   | $4.6 \times 10^{-7}$    | Death                   |
| 10    | Water scarcity                     | $166.9 \times 10^{-4}$ | $48.12 \times 10^{-4}$  | m <sup>3</sup> world eq |

**Table 3** Impact assessment with Impact 2002 method

| S. no | Impact category          | RAS impact              | Raceway impact         | Indicator/Unit                                |
|-------|--------------------------|-------------------------|------------------------|---|
| 1     | Aquatic eco-toxicity     | $426.54 \times 10^{-2}$ | $13.02 \times 10^{-2}$ | Kg TEG eq to water                            |
| 2     | Aquatic eutrophication   | $1.25 \times 10^{-4}$   | $1.2 \times 10^{-4}$   | Kg PO <sub>4</sub> eq to water                |
| 3     | Carcinogen               | $7.18 \times 10^{-1}$   | $20.2210^{-1}$         | Kg C <sub>2</sub> H <sub>3</sub> cl eq to air |
| 4     | Ionizing radiation       | $106.89 \times 10^{-2}$ | $10.45 \times 10^{-2}$ | Bq C-14 eq to air                             |
| 5     | Non-carcinogen           | $1.83 \times 10^{-1}$   | $1.832 \times 10^{-1}$ | Kg C <sub>2</sub> H <sub>3</sub> cl eq to air |
| 6     | Respiratory effect       | $3.512 \times 10^{-3}$  | $3.548 \times 10^{-3}$ | Kg PM-2.5 eq to air                           |
| 7     | Terrestrial eco-toxicity | $52.55 \times 10^{-2}$  | $5.68 \times 10^{-2}$  | Kg TEG eq to soil                             |

**Fig. 3** Graphical representation of impacts by EFP method

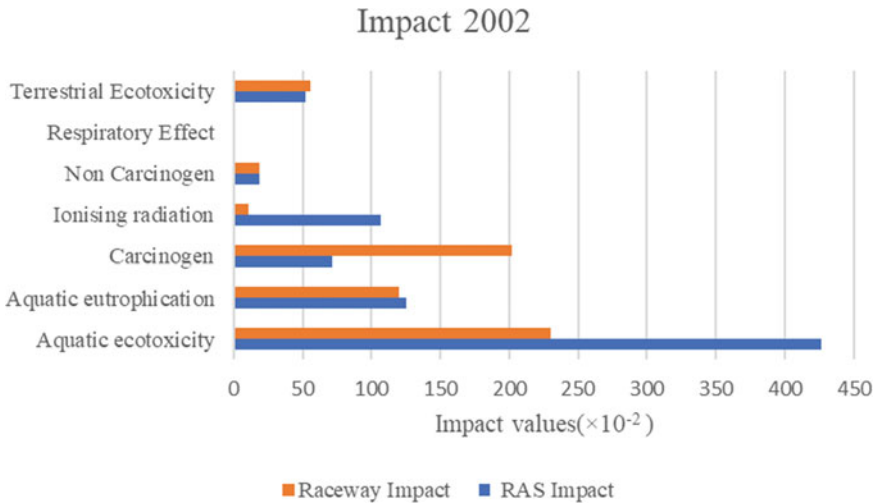


**Fig. 4** Graphical representation of impacts by Impact 2002 method

in Fig. 3 that terrestrial eco-toxicity, respiratory effects, ionizing radiation, resource use, minerals, and metal impacts are the categories which are purely dependent on the machinery components.

The human-associated impact categories such as ionization, a carcinogen is found to be present in the considerable limit; however, it is under the limit as shown in Fig. 4. Since these production systems are ultimately aiming to produce seafood for human consumption, it gives considerable nutritional output with minimum impactful categories. When compared the impacts of both the systems, it has no such significant difference in machinery aspects. However, the impact values of culture practices in both the systems vary considerably.

## 4 Conclusion

In this study, the detailed machinery and product description were analyzed, and the most important of any system from its environmental aspects called environmental impact assessment were also studied. The Open LCA tool, which is the reliable open-source software used with Agribylase and Ecovinent v2.2 databases was used, and the results are analyzed. From the results,

1. As a whole, it is observed that there is no such significant difference in systems, and the systems are not considerably impacting when compared to its advantage of producing protein food for the country. However, the process of systems has to be improved or altered with some innovative techniques viz precision farming, Aqua Intelligent to decrease the impacts even lower. The results help

in understanding the environmental suitability of the systems along with its direct output benefit.

2. The results help to prove the systems analyzed which are eco-friendly in nature, and it can be outreached across the length and breadth of the country making the fisheries community self-reliant.
3. This paper helps to understand the aquaculture systems properly and obtain intuition on its working and impact causing nature to the environment.
4. The future scope of the study can include the increased boundary limits, and also the analysis can be carried out for outdoor units by considering culture variables also.

**Acknowledgements** The authors are grateful to the faculties of College of Fisheries Engineering, Tamil Nadu Dr.J. Jayalalithaa Fisheries University, Nagapattinam, for their continuous motivation toward research and support.

## References

1. Bortolini M, Mora C, Cascini A, Gamberi M (2014) Environmental assessment of an innovative agricultural machinery. *Int J Oper Quantit Manag.* 20(3):243–258
2. Chen S, Xuejun Yu, He X, Xie D, Fan Y, Peng J (2009) Simplified pesticide multiresidues analysis in fish by low-temperature cleanup and solid-phase extraction coupled with gas chromatography/mass spectrometry. *Food Chem* 113(4):1297–1300
3. Gronroos J, Seppala J, Silvenius F, Makinen T (2006) Life cycle assessment of finnish cultivated rainbow trout. *Boreal Environ Res* 11(5):401
4. Huggins DL, Piedrahita RH, Rumsey T (2004) Analysis of sediment transport modeling using computational fluid dynamics (cfd) for aquaculture raceways. *Aquacult Eng* 31(3–4):277–293
5. Iribarren D, Moreira MT, Feijoo G (2010) Life cycle assessment of fresh and canned mussel processing and consumption in galicia (NW Spain). *Resour Conserv Recycl* 55(2):106–117
6. Lin CK, Yi Y (2003) Minimizing environmental impacts of freshwater aquaculture and reuse of pond effluents and mud. *Aquaculture* 226(1–4):57–68
7. Maillard VM, Boardman GD, Nyland JE, Kuhn DD (2005) Water quality and sludge characterization at raceway-system trout farms. *Aquacult Eng* 33(4):271–284
8. Orbcastel ER, Blancheton JP, Aubin J (2009) Towards environmentally sustainable aquaculture: comparison between two trout farming systems using life cycle assessment. *Aquacult Eng* 40(3):113–119
9. Papatryphon E, Petit J, Kaushik SJ, van der Werf HMG (2004) “Environmental impact assessment of salmonid feeds using life cycle assessment (LCA).” *AMBIO: A J Hum Environ* 33(6):316–323.
10. Pelletier F, Garant D, Hendry AP (2009) Eco-evolutionary dynamics. *The Royal Society London*
11. Pelletier N, Tyedmers P (2010) Life cycle assessment of frozen tilapia fillets from indonesian lake-based and pond-based intensive aquaculture systems. *J Ind Ecol* 14(3):467–481
12. Shainee M, Ellingsen H, Leira BJ, Fredheim A (2013) Design theory in offshore fish cage designing. *Aquaculture* 392:134–141
13. Ying L (2011) Research progress on marine industrial recirculating aquaculture technology. *J Agric Sci Technol* 13(5):50–53

# Exploring the Efficacy of Anammox Hybrid Reactor Technology Towards Nitrogen Removal: A Promising Alternative to Conventional Nitrogen Removal Systems



Swati Tomar, S. K. Gupta, and R. K. Verma

**Abstract** Successful application of anammox has revolutionised the field of biological nitrogen removal and offers potential promise over conventional nitrification–denitrification processes owing to considerable saving in aeration costs, absence of external carbon sources and significantly low sludge production. For the purpose of study, anammox process was established in a hybrid reactor configuration, which integrates the concept of attached and suspended microbial growth for the treatment of nitrogen-laden effluents. To evolve the most economical design of bioreactor, HRT study was performed at different HRTs varying from 3.0 to 0.25 days. The study revealed best reactor performance at an optimal HRT of 1 day with a corresponding nitrogen removal efficiency (NRE) of 95.1%. Filter media (FM) in anammox hybrid reactor (AHR) benefitted the overall reactor performance in terms of additional 15.4% ammonium removal and enhanced biomass retention. The mass balance of nitrogen in AHR dictated major chunk (79.1%) of influent nitrogen conversion to  $N_2$  gas, in addition to 11.25% accounting for biomass synthesis. The novel anammox process offers immense opportunities for dealing with nitrogen-rich wastewater; however, the field-scale applications are restricted by organic matter (OM) presence in wastewater streams. To overcome this, a novel strategy of seeding anaerobic granular sludge was investigated to achieve simultaneous OM and nitrogen removal in AHR. The study deciphered outstanding performance of AHR at optimal COD/N ratio of 0.54 accounting for both OM and nitrogen removal of 94.8% and 96.8%, respectively. Haldane model was used to investigate the kinetics of substrate inhibition in AHR, which was attributed to the presence of OM, nitrite and free ammonia. The inoculation strategy of anaerobic granular sludge not only proved to be a boon for anammox sustenance in severely high organic loads but also expedited simultaneous removal of both the pollutants.

---

S. Tomar (✉) · R. K. Verma  
BIT Sindri, Dhanbad, Jharkhand, India

R. K. Verma  
e-mail: [rkverma.phy@bitsindri.ac.in](mailto:rkverma.phy@bitsindri.ac.in)

S. K. Gupta  
IIT(ISM), Dhanbad, Jharkhand, India

**Keywords** Anammox · Hybrid reactor · Nitrogen removal · Organic matter · Inhibition modelling

## 1 Introduction

Nitrogenous compounds, particularly, ammonium from various industrial, agricultural and domestic sources, finds its way to our precious water bodies leading to eutrophication and their subsequent contamination. The effluent from these industries, viz., leachate, coke oven, hoggery and meat processing companies, pharmaceuticals, tanneries, monosodium glutamate and fertiliser wastewaters is rich in ammonium content, found in the range 116 to 2600 mg-NH<sub>4</sub>-N/L [1–6, 30–32]. This nitrogen-laden wastewater is not only detrimental to human health but also poses severe threat to aquatic flora and fauna. Thus, industries are looking forward to viable nitrogen elimination technologies in terms of higher removal efficiency and sound economic viability.

The conventional nitrification and denitrification process demands high energy with organic carbon donors and is characterised by increased operational cost and limitation of sludge disposal. Ammonium stripper shows limited applicability owing to relatively reduced efficiency of stripping (50–65%) coupled with the menace of air pollution. ANaerobic AMMonium Oxidation (anammox) is a novel microbial process that has revolutionised the field of conventional nitrogen removal and industrial wastewater treatment by carrying out single-step oxidation of ammonium under strictly anaerobic environment using nitrite, and the process is accomplished in complete absence of external carbon sources.

The intensified application of anammox technology is attributed to low sludge production, significantly reduced cost of aeration coupled with exogenous electron donor saving which makes this process competent and economically viable over conventional technologies. Various laboratory-scale anammox reactors have demonstrated super high-rate performance with a nitrogen removal rate (NRR) of 26.0–76.7 kgN/m<sup>3</sup>d [7, 8], indicating anammox as a most suitable approach for the treatment of nitrogen laden wastewaters. Present study investigated anammox process in a unique configuration of hybrid reactor, which conglomerates the promising features of both attached and suspended growth systems. Filter media (FM) constitutes attached growth and facilitates enhanced biomass retention and boosts nitrogen removal performance many folds.

While this novel microbial process offers immense opportunities for the treatment of nitrogen laden wastewater, its industrial applications are restricted by the presence of various inhibitors, such as dissolved oxygen (DO), nitrite, free ammonia (FA), other toxic and recalcitrant organic matter (OM) compounds, heavy metals, sulphide and phosphate in the effluent streams [9]. Moreover, the process is also limited by its delayed start-up in biological systems due to long start-up period of

anammox bacteria. Hence, there is an acute need to evolve a strategy for early start-up and efficient control of inhibiting factors to facilitate industrial application of the technology.

Integrating anammox with organic pre-treatment is a viable approach to deal with actual industrial effluent [10]. However, stable process performance coupled with higher substrate removal efficiency is still the major bottleneck of this process owing to the sensitivity of anammox bacteria to various factors, viz., DO, influent organic matter, suspended solids other refractory organics [11–13]. Several researchers emphasised that the strategy of extensive acclimation coupled with intermittent seeding can greatly reduce the impact of inhibition factors on anammox activity. Ni et al. [14] demonstrated the robust application of granular anammox sludge in his bio-setup and achieved ammonium removal efficiency (ARE) of 80% at higher C/N ratio of 3:1 owing to high tolerance of acclimatised consortia to OM. Henceforth, a novel strategy of seeding anaerobic granular sludge was devised in the study to establish proficient symbiosis amongst different bacterial communities and facilitate simultaneous removal of both OM and nitrogen. None of the researchers have so far attempted this strategy to achieve degradation of both the pollutants and establish its industrial acceptance. Furthermore, the inhibition kinetics was evaluated employing OM, free ammonia (FA) and nitrite as inhibitors with the help of Haldane model.

## 2 Material and Methods

### 2.1 Bioreactor Set-Up and Inoculum Sludge

The bioreactor set-up used for experimental analysis (Fig. 1B) was fabricated as per the guidelines of [15], using a sheet of transparent acrylic plastic of diameter 10 cm and height 65 cm. The capacity of the reactor was 5 L. Polyvinyl chloride (PVC) carriers (55 nos.) served as filter media and constituted attached growth system in anammox hybrid reactor (AHR). The bioreactor conglomerated the advantages of both attached and suspended growth. FM in the uppermost section provides an active surface area for attachment of biofilms while sludge blanket in the lower section forms suspended growth system (Fig. 1A). To avoid the algal growth and oxygen evolution, AHR was covered with black sheet all across its surface (Fig. 1B). Synthetic wastewater was fed to the reactor [16], and a constant flow rate was ensured using a peristaltic pump. Activated and anoxic sludge in the ratio 1:1 (v/v) served as an inoculum for early start-up of AHR. The mixed seed culture was grey in colour and contained VSS of 1.68 g/l.

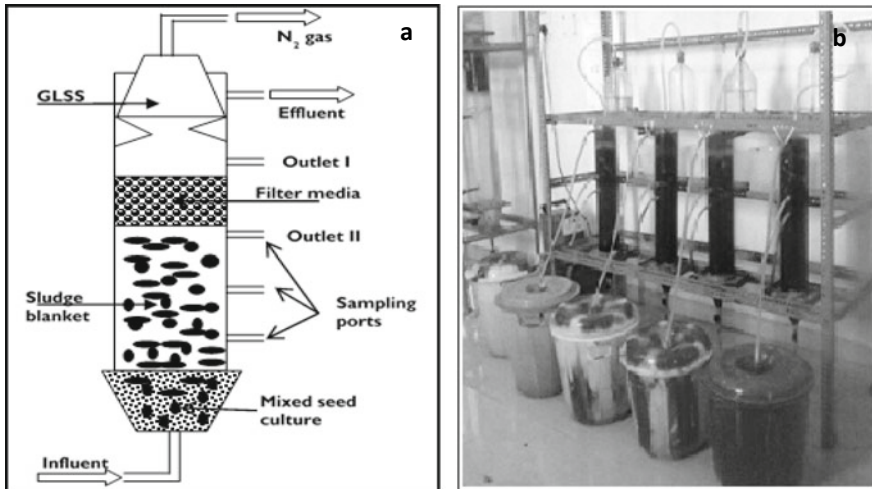


Fig. 1 Anammox hybrid reactor A Diagrammatic illustration B Bioreactor set-up for experiment

## 2.2 Strategy of Reactor Operation

To establish anammox activity in AHR, optimal  $\text{NO}_2/\text{NH}_4$  ratio (1:1) was maintained at an HRT of 1d, and bioreactors were fed with ammonium and nitrite concentration each of 100 mg/l. The performance of the reactors was monitored till pseudo-steady state (PSS) was achieved, which was apparently a period of 30 days. Later, the influent concentration (ammonium and nitrite) were stepped up to 600 mg/l each and maintained constant thereafter. For HRT study, bioreactor performance was analysed at different HRTs (3.0–0.25 d), so as to explore the optimal HRT for its efficient design and economical operation. To achieve the objective, the reactors performance was monitored for 15 days, after which stable performance was reached and the average values of the PSS removal was reported pertaining to each HRT. The contribution of FM towards nitrogen removal and reduced sludge washout was worked out by collecting effluent samples from outlets I and II, one above and one below the filter media. Mass balance of nitrogen was assessed to analyse the fate of input nitrogen and determine its conversion into different forms using Eq. (1):

$$N_{inf} = N_{eff} + N_{gas} + N_{syn} \quad (1)$$

where  $N_{inf}$  and  $N_{eff}$  represent the nitrogen concentrations in the influent and effluent, respectively, and  $N_{gas}$  refers to the nitrogen contributing towards nitrogen gas production, while  $N_{syn}$  indicates utilisation of nitrogen for biomass synthesis.

After HRT study, the reactors were inoculated with anaerobic granular sludge (1:5 v/v), from a high-rate UASB reactor treating coke oven wastewater. The mixture was then acclimatised to higher influent COD (50 to 1000 mg/L) with gradual supplement

of simulated wastewater fed with glucose and COD/TN ratio was varied from 0.04 to 0.83, till the attainment of process inhibition in AHR. Haldane model was used in the study to investigate inhibition kinetics employing nitrite, FA and COD as inhibitors.

### 2.3 *Methods of Analysis*

The analysis of physico-chemical parameters, viz., pH, alkalinity, ammonium, COD, nitrite, nitrate, VSS and TSS was carried out in the experimental study [17]. Water displacement method was used to measure the volume of gas liberated in AHR, and its composition was checked using gas chromatograph (GC), operated at injector and detector temperatures of 120 °C and 150 °C, respectively. The carrier gas used was H<sub>2</sub> @ 20 ml/min, and the detector to analyse gas samples was thermal conductivity detector.

### 2.4 *Quality Assurance /quality Control Procedure (QA/QC)*

Triplicate sample analysis was used to maintain the precision during the entire experimental study. Relative percentage difference (RPD) was calculated and cross verified between two parallel samples. In case of RPD value >5%, the samples were re-analysed. The final value marked the average of the triplicate readings. Injection of every ten samples was followed by continuous calibration checks. If the RPD was >10%, the instrument was recalibrated.

### 2.5 *Haldane Inhibition Kinetics*

Haldane model to describe bacterial inhibition kinetics is illustrated by Eq. (2):

$$q = \frac{q_{max}}{1 + \frac{K_s}{S} + \frac{S}{K_i}} \quad (2)$$

where  $q$  represents specific conversion rate (1/d) and  $q_{max}$  denotes maximum specific conversion rate (1/d);  $K_s$  is half saturation constant (mg/L);  $K_i$  represents substrate inhibition constant (mg/L) with  $S$  as the substrate concentration (mg/l).



### 3 Results and Discussion

#### 3.1 Investigating the Impact of HRT on Bioreactor Performance

Optimal HRT is essential to benefit the design of bioreactor in terms of higher efficiency and cost effective operation. Figure 2 depicts the bioreactor performance under varying HRTs from 3 to 0.25d. At an HRT of 2.25 day, AHR achieved maximum nitrogen removal of 97.5% at a NLR of 0.53 kg N/m<sup>3</sup>d. However, further decline in HRT (from 2.25 days to 1 day) resulted depreciation in nitrogen removal efficiency (NRE), but the rate was marginal. Hence, optimal performance of AHR was registered at an HRT of 1.0 day deciphering nitrogen removal of 95.1%. With further drop in HRT to < 1 day, NRE showed a sharp decline to 78.6% corresponding to an HRT of 0.25 day. Ammonium removal also depicted a similar profile. However, there was no appreciable change in nitrite removal efficiency (NiRE) with decline in HRT. The substrate removal efficiency observed in our study is found to be appreciably higher than reported [18, 19], which might be attributed to the role of filter media, which significantly enhances the biomass retention in AHR.

Xing et al. [20] also observed a similar occurrence in multi- and single-fed UASB reactors, wherein NRE declined for both the reactors and were found to be 55.7% and 60.4%, respectively, with decrease in HRT. A possible reason could be sudden increase in NLR at a lower HRT, which could have perturbed the reactor performance, indicating susceptibility of anammox bacteria to hydraulic shocks. Furthermore, other operational parameters including, pH of the reactor was  $8.8 \pm 0.2$  at an HRT of < 1 day, which might have elevated the FA concentration (9.4 mg/l to 15.7 mg/l) in AHR, resulting decline in ARE. However, the strategy of extensive acclimation adopted in our study led to high nitrogen removal coupled with weakened FA inhibition.

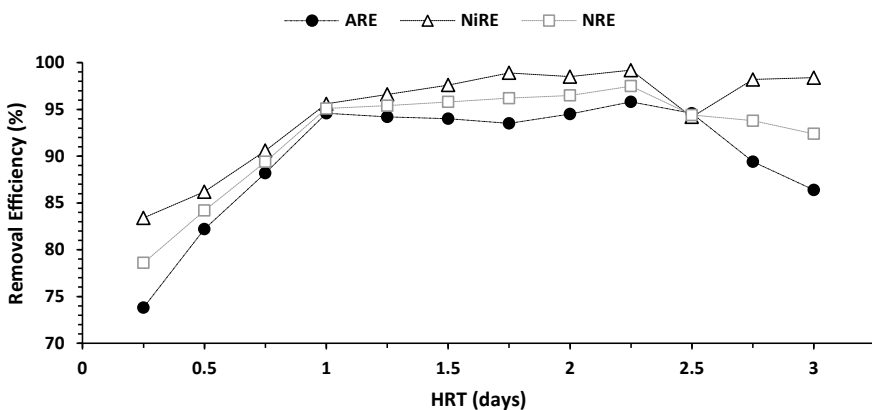


Fig. 2 Bioreactor performance at variable HRTs

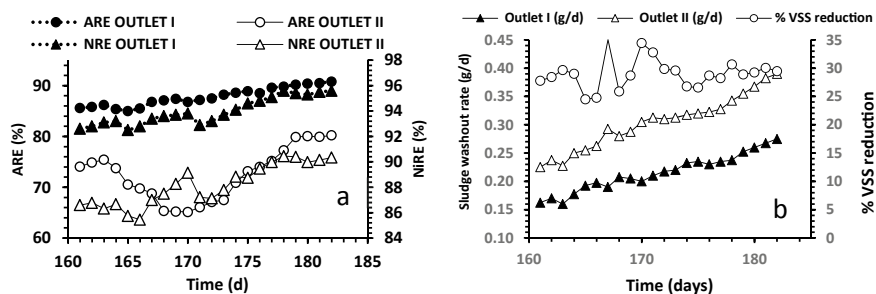


Fig. 3 Role of FM in AHR **A** Nitrogen removal **B** Sludge washout

### 3.2 Effect of Filter Media on Nitrogen Removal and Biomass Retention

Filter media in AHR provides active surface area for attachment of the biofilms and fosters enhanced biomass retention. Figure 3A depicts ammonium removal (ARE) and nitrite removal (NiRE) profile of AHR at two different outlets. The average ARE at outlets I (87.8%) was significantly higher than at outlet II (72.4%), and NiRE also showed a similar profile at both the outlets. This might be due to the evolved feature of FM in AHR, which enhanced ammonium removal by 15.4%. The sludge washout rate, which pertains to biomass retention and governs the overall process efficiency, was also determined at both the outlets. The results indicated that the average value of sludge washout rate was reported lower for outlet I (0.22 g/d) than outlet II (0.30 g/d) (Fig. 3B). A possible reason could be the presence of the FM, which catches the active biomass cells and leads to considerable reduction (29%) in the sludge washout from AHR. Thus, hybrid configuration of the bioreactor adopted in this study not only improved nitrogen elimination from the effluent but also reduced the washout of active biomass from AHR. Several researchers have advocated the applicability of hybrid reactors over conventional UASB systems for the treatment of variable refractory organics such as TCE, phenols, cyanides and other toxic organic compounds. Duan et al. [19] adopted hybrid reactor configuration with non-woven carrier as FM and reported pronounced biomass retention (2.8%) in addition to high NRR (8.1%). In a similar study attempted in an upflow biofilter (UBF), string-shaped plastic filter media enhanced the nitrogen removal to 89.5% [21].

### 3.3 Stoichiometry of Nitrogen Conversion in AHR

Mass balance was performed to analyse the fate of nitrogen and its utilisation into different forms in AHR by defining its stoichiometry. The study revealed major chunk (79.1%) of influent nitrogen was converted into  $N_2$  gas (79.1%), followed by 11.25% accounting for biomass synthesis and 4.56% going into the treated effluent as nitrate

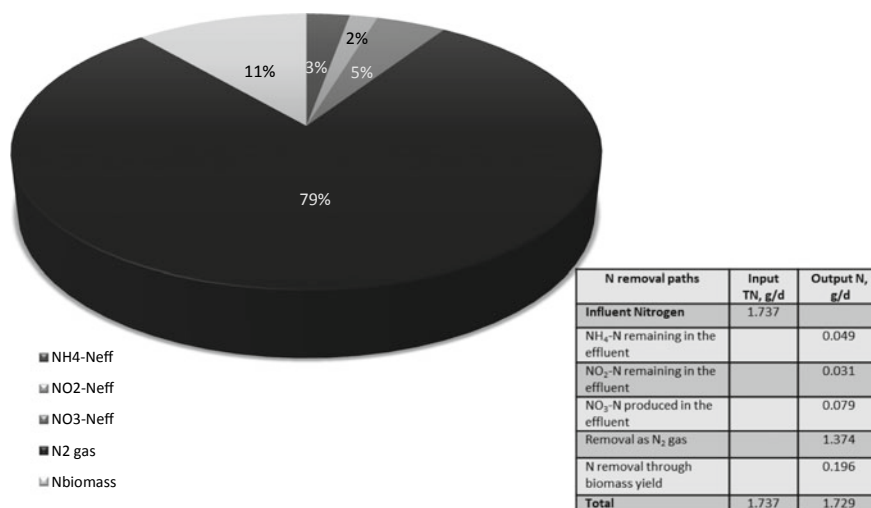


**Fig. 4** Mass balance of nitrogen in AHR

(Fig. 4). Very meagre amount was remaining in the effluent as NH<sub>4</sub>-N (2.82%) and NO<sub>2</sub>-N (1.81%) and 0.51% remained unclassified. Limited research focussed on evaluating the mass balance of nitrogen in anammox chemistry. However, in a study by Ni et al. [22], relatively lower fraction (68.5%) of influent nitrogen was found to be converted into N<sub>2</sub> gas and a comparatively larger portion (15.4%) got eliminated as nitrate. Higher fraction of input nitrogen being converted into N<sub>2</sub> gas was possible in our study due to the hybrid reactor configuration, and the use of the FM in AHR. The FM increases the active surface area to enable attachment of the biofilms and subsequently enhances the biomass retention, which results in higher conversion efficiency of influent nitrogen into N<sub>2</sub> gas, and minimises nitrate production in the treated effluent. Formation of nitrate is triggered by excess concentration of nitrite in the treated effluent. The possibility of nitrite conversion into nitrate was ruled out in our study due to consistently higher NiRE.

### 3.4 Impact of Inoculation Strategy on OM and Nitrogen Removal

Extensive acclimation of sludge coupled with intermittent seeding can greatly improve the tolerance of anammox bacteria to OM concentrations. COD/TN ratio is considered instrumental in controlling the process performance and efficiency of the bioreactor. The study indicated that there was no appreciable change in NRE observed as the COD/TN ratio was increased from 0.04 to 0.54 (Fig. 5). On the contrary, the COD removal efficiency (CRE) registered an increment consistently up to a

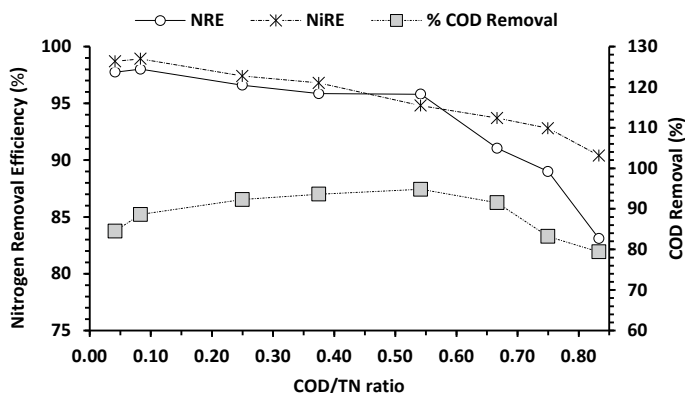


Fig. 5 Effect of COD/TN ratio on the performance of AHR

COD/TN ratio of 0.54. Both the pollutants were removed simultaneously in the study. This could have been possible due to the association of symbiosis existing between bacterial communities such as anammox, denitrifiers and anaerobes. However, with further increase in COD concentration (>650 mg/l), both nitrogen and OM removal registered a decline as observed with decrease in NRE and CRE, respectively. This suggested that optimal COD/TN ratio for simultaneous removal of both the pollutants was 0.54. Anammox activity registered a decline with increase in organic load as was observed by decreased nitrate in the treated effluent coupled with increase in alkalinity in the effluent samples. Several researchers advocated the adverse impact of OM load on anammox activity with inhibitory COD concentration reported in the range of 292 to 300 mg/L [23, 24]. However, the anammox activity in AHR showed a robust tolerance and outcompeted others with a COD sustaining capacity of 650 mg/L. A possible reason could be an appropriate inoculation strategy which might have fostered the optimal ratio of anaerobes, anammox and denitrifiers in the anaerobic granular sludge, leading to attainment of proficient symbiosis between operational the pathways. Not only this, the robustness of the bioreactor to sustain high COD load was evident from comparatively higher COD removal in our study than others [25, 26].

### 3.5 Investigating Inhibition Kinetics Using Haldane Model Along with Model Validation

Kinetics of inhibition for various substrates, primarily COD, nitrite and FA was evaluated using Haldane model. The model plot indicated highest correlation for COD and was followed by  $\text{NH}_4\text{-N}$  and  $\text{NO}_2\text{-N}$  (Fig. 6). The maximum specific conversion attained in our study (for  $\text{NH}_4\text{-N}$  and  $\text{NO}_2\text{-N}$ ) was comparatively lower than the values reported in literature (Table 1). A possible reason could be OM

inhibition in addition to low nitrogen loading rate (NLR). Half saturation constant was appreciably higher for NO<sub>2</sub>-N [29] and was almost similar for NH<sub>4</sub>-N. This could have been possible due to excess nitrite utilisation in denitrification and anammox pathways. The bioreactor demonstrated highest tolerance for NH<sub>4</sub>-N followed by COD and nitrite as is evident from their respective K<sub>i</sub> values, which were in line with the ones reported [14, 24, 28, 29]. Suitably, the Haldane model fit for different substrates viz., ammonium, nitrite and COD can be well depicted by Eqs. (3–5)

$$q = \frac{17.49}{1 + \frac{45.81}{S} + \frac{S}{930.2}} \tag{3}$$

$$q = \frac{22.56}{1 + \frac{73.55}{S} + \frac{S}{220.8}} \tag{4}$$

$$q = \frac{32.92}{1 + \frac{184.2}{S} + \frac{S}{354.9}} \tag{5}$$

The models validation was performed taken into consideration ammonium, nitrite and COD in the effluent. Figure 7 demonstrates a very strong correlation between

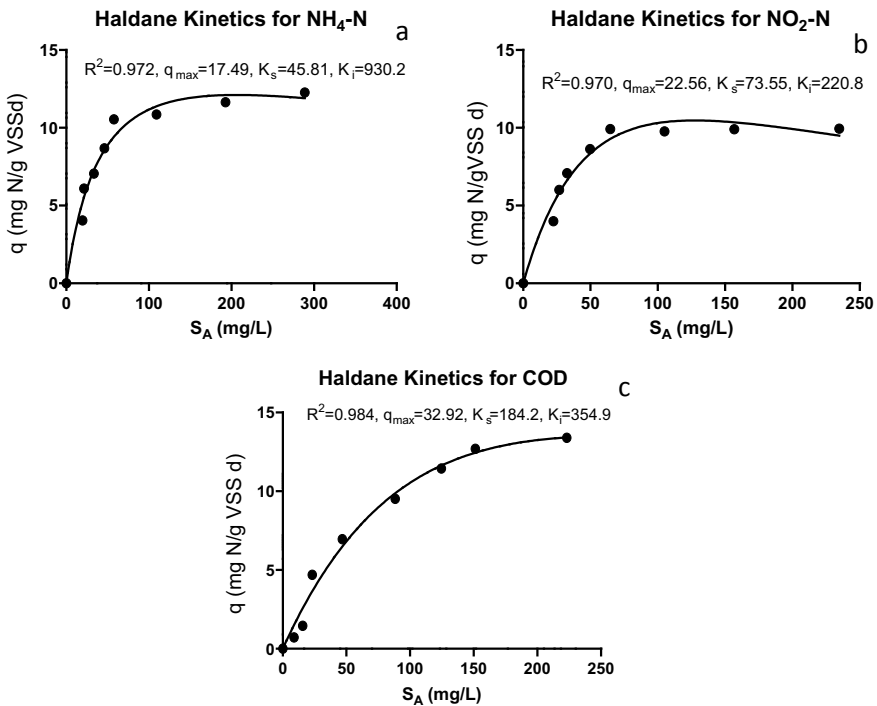


**Fig. 6** Substrate inhibition kinetics by Haldane model (A) NH<sub>4</sub>-N (B) NO<sub>2</sub>-N (C) COD

**Table 1** Model coefficients from inhibition kinetics

| Kinetic constants             | NH <sub>4</sub> -N |             | NO <sub>2</sub> -N |             | COD   |         | References      |
|-------------------------------|--------------------|-------------|--------------------|-------------|-------|---------|-----------------|
|                               | Obs                | Rptd        | Obs                | Rptd        | Obs   | Rptd    |                 |
| q <sub>max</sub> (mgN/gVSS.d) | 17.49              | 38.65–297.2 | 22.56              | 202.9–304.7 | 32.92 | –       | [14, 24, 27–29] |
| K <sub>s</sub> (mg/l)         | 45.81              | 48.41–87.1  | 73.55              | 6.552–15.39 | 184.2 | –       |                 |
| K <sub>i</sub> (mg/l)         | 930.2              | 887.1–1123  | 220.8              | 159.5–720.6 | 354.9 | 292–400 |                 |

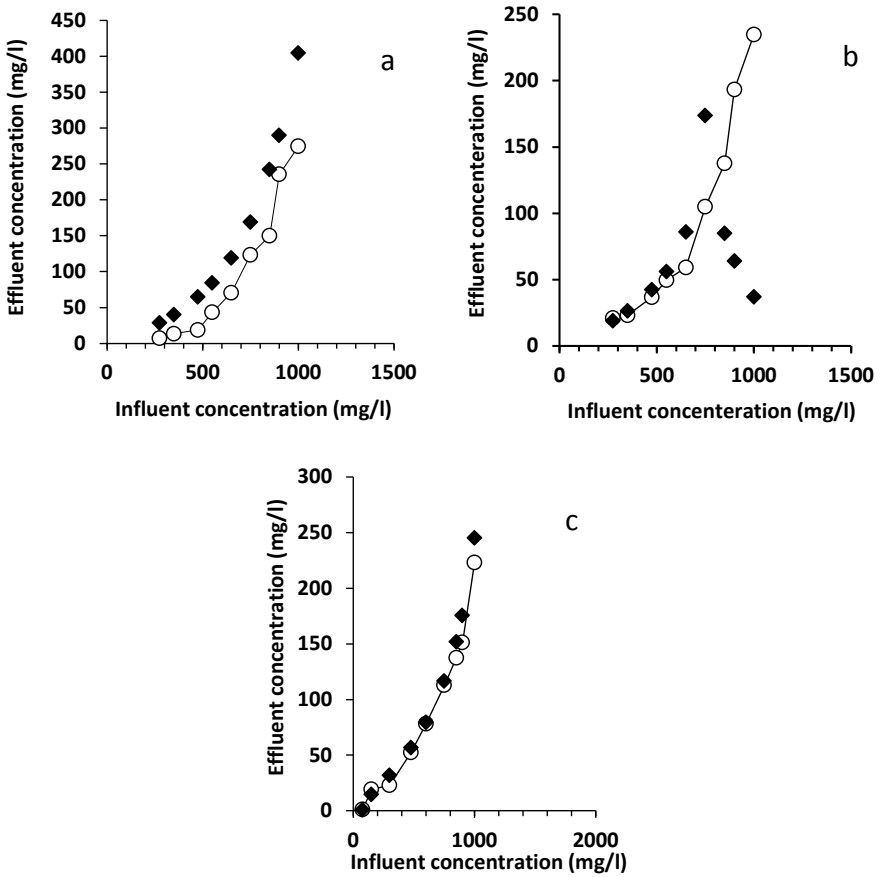


Fig. 7 Haldane model validation A NH<sub>4</sub>-N B NO<sub>2</sub>-N C COD

observed and predicted values for COD followed by NH<sub>4</sub>-N, indicating COD as the most influential parameter which is responsible for causing bacterial inhibition in AHR. The value registered in case of NO<sub>2</sub>-N was appreciably poor. This can be explained with the fact that nitrite was continuously utilised in anammox and denitrification pathways, leading to its higher removal, and hence, the possibility of nitrite inhibition can also be curtailed in the study. FA inhibition was minimised in the study due to optimal pH conditions maintained in the reactor. Thus, Haldane model can could perform well in determining the fate of COD inhibition in AHR.

## 4 Conclusion

The bioreactor offers immense potential for nitrogen removal (95.1%) in its hybrid configuration at optimal HRT of 1 day. FM contributes to additional 15.4% nitrogen removal and leads to enhancement in biomass retention by 29%. The major chunk of the input nitrogen was converted into nitrogen gas followed by some portion utilised in biomass synthesis, and a relatively small fraction going as nitrate in the effluent. The strategy of seeding granular anaerobic sludge facilitated symbiosis between anammox and anaerobes resulting in appreciable removal of both the pollutants. The bioreactor showed robust performance up to an influent COD load of 650 mg/l, beyond which substrate inhibition was observed. Haldane model could suitably be used to evaluate inhibition kinetics in AHR with COD as the prime inhibitor. The study works out a novel strategy to overcome OM inhibition in laboratory-scale and opens the door for industries and academicians for its field-scale implementation.

## References

1. Iaconi CD, Pagano M, Ramadori R, Lopez A (2010) Nitrogen recovery from a stabilized municipal landfill leachate. *Bioresour Technol* 101:1732–1736
2. Saran R, Singh G, Gupta SK (2009) Adsorption of phenol from aqueous solution onto fly ash from a thermal power plant. *Adsorpt Sci Technol* 27(3):267–279
3. Keluskar R, Nerurkar A, Desai A (2013) Development of a simultaneous partial nitrification, anaerobic ammonia oxidation and denitrification (SNAD) bench scale process for removal of ammonia from effluent of a fertilizer industry. *Bioresour Technol* 130:390–397
4. Murat S, Insel G, Artan N, Orhon D (2006) Performance evaluation of SBR treatment for nitrogen removal from tannery wastewater. *Water Sci Technol* 53(12):275–284
5. Magrí A, Béline F, Dabert P (2013) Feasibility and interest of the anammox process as treatment alternative for anaerobic digester supernatants in manure processing—an overview. *J Environ Manage* 131:170–184
6. Gupta SK, Sharma R (1996) Biological oxidation of high strength nitrogenous wastewater. *Water Res* 30(3):593–600
7. Tsushima I, Ogasawara Y, Kindaichi T, Satoh H, Okabe S (2007) Development of high-rate anaerobic ammonium-oxidizing (anammox) biofilm reactors. *Water Res* 41(8):1623–1634
8. Tang CJ, Zheng P, Wang CH et al (2011) Performance of high loaded ANAMMOX UASB reactors containing granular sludge. *Water Res* 45(1):135–144
9. Arora AS, Nawaz A, Qyyum MA, Ismail S, Aslam M, Tawfik A et al (2021) Energy saving anammox technology-based nitrogen removal and bioenergy recovery from wastewater: inhibition mechanisms, state-of-the-art control strategies, and prospects. *Renew Sustain Energy Rev* 135:110–126
10. McCarty PL (2018) What is the best biological process for nitrogen removal: when and why? ACS Publications
11. Collison R, Grismer M (2018) Upscaling the zeolite-anammox process: treatment of anaerobic digester filtrate. *Water* 10(11):553
12. Daverey A, Hung NT, Dutta K, Lin JG (2013) Ambient temperature SNAD process treating anaerobic digester liquor of swine wastewater. *Bioresour Technol* 141:191–198
13. Li X, Sun S, Yuan H, Badgley BD, He Z (2017) Mainstream upflow nitrification-anammox system with hybrid anaerobic pretreatment: long-term performance and microbial community dynamics. *Water Res* 125:298–308



14. Ni SQ, Ni JY, Hu DL, Sung S (2012) Effect of organic matter on the performance of granular anammox process. *Bioresour Technol* 110:701–705
15. Lettinga G, Pol LH (1991) UASB-process design for various types of wastewaters. *Water Sci Technol* 24(8):87–107
16. Van de Graaf AA, de Bruijn P, Robertson LA, Jetten MSM, Kuenen JG (1996) Autotrophic growth of anaerobic ammonium-oxidizing micro-organisms in a fluidized bed reactor. *Microbiology* 142(8):2187–2196
17. APHA AWWA, WEF (2012) *Standard Methods for Examination of Water and Wastewater*. 22nd ed, United Book Press, USA
18. Ni SQ, Lee PH, Sung S (2010) The kinetics of nitrogen removal and biogas production in an anammox non-woven membrane reactor. *Bioresour Technol* 101:5767–5773
19. Duan X, Zhou J, Qiao S, Yin X, Tian T, Xu F (2012) Start-up of the anammox process from the conventional activated sludge in a hybrid bioreactor. *J Environ Sci* 24:1083–1090
20. Xing BS, Qin TY, Chen SX, Zhang J, Guo LX, Jin RC (2013) Performance of the ANAMMOX process using multi- and single-fed upflow anaerobic sludge blanket reactors. *Bioresour Technol* 149:310–317
21. Jin RC, Zheng P (2009) Kinetics of nitrogen removal in high rate anammox upflow filter. *J Hazard Mater* 170:652–656
22. Ni BJ, Smets BF, Yuan Z, Nacher CP (2013) Model based evaluation of the role of Anammox on nitric oxide and nitrous oxide productions in membrane aerated biofilm reactor. *J Membr Sci* 446:332–340
23. Chamchoi N, Nitisorvut S, Schmidt JE (2008) Inactivation of ANAMMOX communities under concurrent operation of anaerobic ammonium oxidation (ANAMMOX) and denitrification. *Bioresour Technol* 99:3331–3336
24. Molinuevo B, Garcia MC, Karakashev D, Angelidaki I (2009) Anammox for ammonia removal from pig manure effluents: effect of organic matter content on process performance. *Bioresour Technol* 100:2171–2175
25. Nhat PT, Biec HN, Mai NTT, Thanh BX, Dan NP (2014) Application of a partial nitrification and anammox system for the old landfill leachate treatment. *Int Biodeterior Biodegradation* 95:144–150
26. Chen C, Huang X, Lei C, Zhang TC, WW (2013) Effect of organic matter strength on anammox for modified greenhouse turtle breeding wastewater treatment plant. *Bioresour Technol* 148:172–179
27. Tang CJ, Zheng P, Mahmood Q, Chen JW (2009) Start-up and inhibition analysis of the Anammox process seeded with anaerobic granular sludge. *J Ind Microbiol Biotechnol* 36:1093–1100
28. Chen T, Zheng P, Shen L, Ding S, Mahmood Q (2011) Kinetic characteristics and microbial community of anammox-ESGB reactor. *J Hazard Mater* 190:28–35
29. Zu B, Zhang DJ, Yan Q (2008) Effect of traceNO<sub>2</sub> and kinetic characteristics for anaerobic ammonium oxidation of granular sludge. *Environ Sci* 29:683–768
30. Galleguillos M, Vassel JL (2011) Landfill leachate characterization for simulation of biological treatment with activated sludge model no. 1 and activated sludge model no. 3. *Environ Technol* 32(11):1259–1267.
31. Deng LW, Zheng P, Chen ZA (2006) Anaerobic digestion and post-treatment of swine wastewater using IC-SBR process with bypass of raw wastewater. *Process Biochem* 41:965–969
32. Shen LD, Hu AH, Jin RC, Cheng DQ, Zheng P, Xu XX, Hu BL (2012) Enrichment of anammox bacteria from three sludge source for the startup of monosodium glutamate industrial wastewater treatment system. *J Hazard Mater* 199(200):193–199

# Smart and Water-Efficient Automatic Drip Irrigation System



Sanmit P. Nalawade and Pravin A. Manatkar

**Abstract** In the farming or agricultural sector, water shorting was one of the big and common problems which all farmers are facing nowadays all over the country. So it is very important to improve and increase the efficiency of irrigation methods so that the maximum farm area will be covered and irrigate will be done with less water quantity. The improved method will also reduce the wastage of water. Presently farmers are using drip irrigation method to minimize the water use and irrigate maximum area of field. But technically this method was not efficient as all. We can improve and increases the efficiency of this irrigation method by taking the help of technology and installing some useful sensors on our farm. But existing system has lot of disadvantages. It only irrigates the land by sensing moisture of soil. The new improved method is named as “smart and water-efficient automatic drip irrigation system.” This system provides facilities to the farmers to irrigate the land equally with the available water quantity at resources. This system also provides the facility of selecting rate of water discharging, choosing water requirements of crops, etc. It has few new sensors that analyze the weather condition and control the system.

**Keywords** Automatic drip irrigation system · Forecasting of weather · Moisture content · Weather conditions · Water requirements · Sustainable irrigation · Smart farming

## 1 Introduction

In nowadays, all the farmers along the country in need to apply water and irrigate there is farm very efficiently, due to the current water lacking issue. With respect to that there are numbers of research to find a solution and make irrigation as possible as more efficient to overcome this problem. The current condition of water shorting in India is very critical; the water shorting issue was already affected on large number of population. There are many international places which suffering from same problem

---

S. P. Nalawade · P. A. Manatkar (✉)  
Trinity Academy of Engineering, Pune, Maharashtra, India  
e-mail: [pravinmanatkar.tae@kjei.edu.in](mailto:pravinmanatkar.tae@kjei.edu.in)

© The Author(s), under exclusive license to Springer Nature Singapore Pte Ltd. 2022  
C. M. Rao et al. (eds.), *Advanced Modelling and Innovations in Water Resources Engineering*, Lecture Notes in Civil Engineering 176,  
[https://doi.org/10.1007/978-981-16-4629-4\\_48](https://doi.org/10.1007/978-981-16-4629-4_48)

693

but they had overcome this problem nicely by effective use of water. Comparing this issue with those countries, we have to need to find some solution and overcome that issue. So we can able to use available water for 12 months without facing any issue.

Irrigation was the main factor for cultivating and harvesting the crops to meet our daily needs of food. In agricultural sector, there are number of irrigation methods like surface irrigation method, flood irrigation method, sprinkler and drip irrigation method. The flood irrigation method is not as efficient because of uneven spreading and distribution of water taken place. Also, the quantity of water required is more. Drip irrigation method and sprinkles irrigation method are the efficient in some way due to less water requirement. In drip irrigation method, water was pumped and directly applies near the roots of crops, and in sprinkler irrigation method, water was pumped in high pressure with a special pump and passes over toward the sprinkler. Sprinklers are equipped with nozzles which spray the water toward the sky in the air, when sprayed comes down toward the earth it falls like a rain. But if the water contains some dissolved impurities, salt damages the plant. It is very big drawback of this system. A disadvantage of sprinkler irrigation is that many plants are touchy to foliar damage when sprinkled with saline waters. Also, the installation cost maintains and repairing cost of sprinkler irrigation method was much more therefore farmers who have less land cannot afford it [1].

In drip irrigation method, water was distributed at very less discharging rate, i.e., approximately 5–20 L/Hour. The water will be directly distributed nears the roots of crops so the water requirement was very less. In drip irrigation method, water is continuously supplied at root zone in form of droplets by the help of plastic drip pipes and plastic drippers. In drip irrigation method, there is negligible water loss, and due to this, we can achieve about 85%-90% efficiency [1–5] (Fig. 1).

## 2 System Module

### 2.1 Working Steps

The following steps are involved in the proposed “Smart, Water-Efficient Automatic Drip Irrigation System.”

Step i. —Installation of Sensors.

The various useful necessary sensors are placed in appropriate location. Soil moisture content counting sensor will be installed below the top surface inside the soil at square, pentagonal, and hexagonal forms, it continuously observing the value of moisture content in the soil. Rain sensors, temperature sensor, and humidity measuring sensors are installed above the ground level. This all sensors reordered various counts and forward this counts to the microprocessor.

Step ii. —Data Processing.

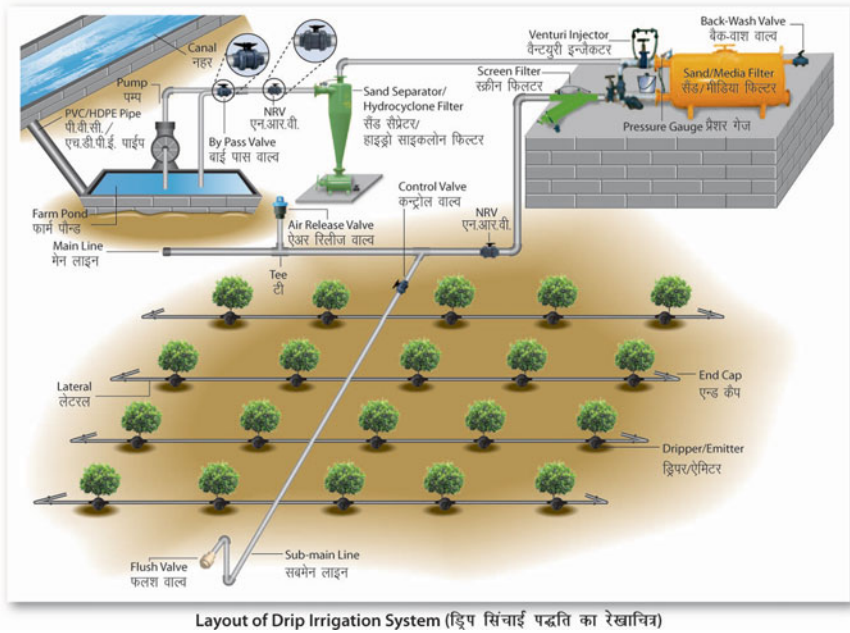


**Fig. 1** Typical layout of existing drip irrigation system [9]

The processing unit was analyzed and processes the received data, and the readable counts send to the farmers on his mobile. Then farmers give them any command about switching on and switching off the water pumps. After getting command from the farmers, these commands send to the microcontroller. Microcontroller controls the water pumps by switching them on and off.

If the farmer gives auto control command then microprocessor reprocesses the obtained values. If the obtained values were less than specified values, then it informs to microcontroller about switching on the water pumps. If the obtained values were more than specified values, then it informs to microcontroller about switching off the water pumps. The all the information and status off water pumps and sensors values are sent to the farmers on his mobile.

Step iii. —Switching On/Off the pumps.

As per the instruction given by data processing unit, the microcontroller switching on and off the water pump. Also, it was sent back the status of the water pump to the data processing unit.

## **2.2 Working Principle off Automatic Mode**

- If the sensors observed and detect the less value count of moisture content of soil and humidity present in the air, the microprocessor analyzed the count and send the command to the microprocessor, microcontroller will automatically start the water pump.
- After getting the water to the crops, till value reaches the specified value the water pump remains in on condition. When values reached at specified limit, the microprocessor sends the command about turning off to the microcontroller. It will automatically turn off the water pump.
- If the automatic mode is turned on, and it sensors detected more temperature and less humidity than specified values, system was also start the pump and stay as on “ON” condition till the valves of moisture content of soil reach the specified limit.
- If the weather forecasting or climate prediction system turn on, and it receives the information about the possibility of rain, the microcontroller automatically turns off the water pump and the information and status of pumps to the farmers on their mobiles. It will avoid the damage of crops and also avoid the deposition of excess water in farms.
- There is facility of energy backup. By providing recharging battery with the solar energy harvesting system, the automatic irrigation system stays as on if the supply of electric energy is cut. This method is also useful in remote area where the creating of network of electricity is and very difficult and costly. By using solar harvested energy, we can reduce in electric energy supply bill.

## **2.3 Hardware Requirements**

We can require the following hardware components for use and run the proposed smart, water-efficient automatic drip irrigation system [8].

- (a) Microcontroller
- (b) Processing unit
- (c) Various sensors
- (d) Voltage regulator
- (e) GSM module
- (f) Motor starter and relay
- (g) Electromagnetic valve

## **2.4 Software Requirements**

We can require the following software installed in microprocessor for use and run the proposed smart, water-efficient automatic drip irrigation system [8].

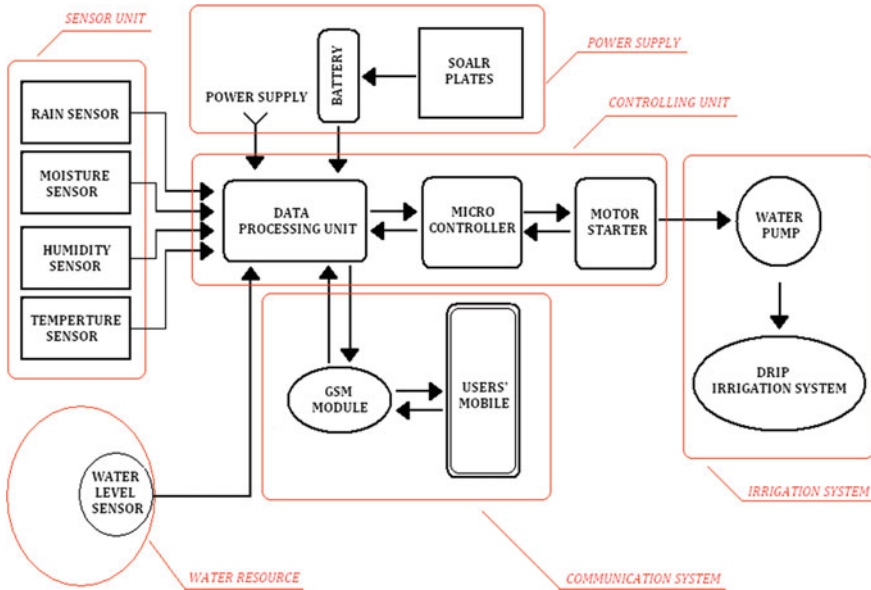


Fig. 2 Flow diagram of “smart, water-efficient automatic drip irrigation system”

- (a) Keil compiler
- (b) Language: Embedded C (Fig. 2).

### 3 Physical and Hydrological Parameters of System

#### 3.1 Physical Parameters

This proposed smart and water-efficient automatic drip irrigation system is designed by considering the low-cost materials available in the local market. The following materials are required for experimental setup. [10]

1. Submersible Pump:

A pump is used to lift the water from the sources by mechanical energy. This pump requires 12 V DC of power supply. The whole assembly is submerged in the water. The main advantage of this type of pump is that it prevents pump cavitations, a problem associated with a high elevation difference between the pump and the fluid surface. Submersibles pumps are more efficient than jet pumps.

2. Emitters/Drippers:

This dripper can be connected to the tubing or can be inside the tubing and deliver water at a slow, consistent rate, usually, 5–20 L/Hour.

### 3. Drip Pipe:

There are generally two types of pipes, polyethylene tubing and rigid PVC which are used. The internal diameter of pipe “1/4 inch,” “1/2 inch,” “3/4 inch” which delivers the water to the emitters.

### 4. Electromagnetic Valves:

We can use automatically operated electromagnetic control valves to control the water supply on and off. This valve needs to connect to the microcontroller.

### 5. Pressure Regulator:

These pressure regulators reduce the pressure of arriving water to the ideal pressure for the smooth working of drip irrigation system. This pressure is usually less than 20 PSI.

### 6. Filter:

All drip irrigation systems have needed some type of water filter to remove dirt and debris from clogging the emitters. For this proposed system, we can use any suitable filter. The size of filter is 1.5” × 20” and approximate filter capacity is 10 m<sup>3</sup>/hr.

## 3.2 *Hydrological Parameters*

There are mainly two sources of irrigation water, and they are canal water and well water. This water contains considerable amount of unnecessary or unwanted impurities dissolved from that may ill affect on soil and reduce soil fertility and crop growth [11].

These unwanted impurities resulted reduce in the water quality. The main parameters are as follows:-

1. Electrical conductivity (EC)
2. Total dissolved solids (TDS)
3. Sodium adsorption ratio (SAR)
4. Residual sodium carbonate (RSC) (Table 1).

## 4 Future Implementations of System

By using this automatic drip irrigation system, we can reduce the consumption of the water, electricity, and manpower considerably. The smart, water-efficient automatic drip irrigation system will request and encourage more farmers to install it in their farm for the purpose of increasing productivity and reduced the maintaining

**Table 1** Irrigation water quality standards [11]

| Water quality    | EC @ 25 °C<br>(Micromhos/cm) | TDS<br>(mg/L) | SAR<br>(meq/L) | RSC<br>(meq/L) |
|------------------|------------------------------|---------------|----------------|----------------|
| <b>Excellent</b> | <250                         | <160          | <10            | <1.25          |
| <b>Good</b>      | 250–750                      | 160–500       | 10–18          | 1.25–2.5       |
| <b>Medium</b>    | 750–2250                     | 500–1500      | 18–26          | >2.5           |
| <b>Bad</b>       | 2250–4000                    | 1500–2500     | >26            | -              |
| <b>Very Bad</b>  | >4000                        | >2500         | >26            | -              |

cost. After the number of experiment performed on it, it is seen that the automatic drip irrigation method consumes less water and less electric energy. Also, very less manpower is required to run this system. The installation cost of the systems was also affordable and maintains that cost is also low. In future, it is possible to add more sensors [7].

Major challenges nowadays to develop the automatic drip irrigation system that also runs on low water pressure and provides the uniform flow rate with pressure compensating emitters. This problem is very common problem all over. So we need to find out the solution and overcome this problem by redeveloping this system. During design process of this system, the main pressure of water at inlet, size of network pipes, filtration rate of water, and pressure at vacuum vents are considered [8].

Also, there are scopes to develop the proposed automatic drip irrigation system which drives the water pumps and maintains water distribution based on the requirement of water of crops. These water requirements are varying with the types of soil and types of crops. Due to variation in that this is required to give an option of selecting type of seasons, type of field, type of plants, and delta required for that crops to the users. Also scope to devolve this system in that way, the system is run and controls on voice commands of the farmers. The proposed system makes decisions based on the growth period of the crop [8].

As one step ahead built a system that senses the interruption of wild and domestic animals in the field, and automatically starting to honking and making sound makes scary environment so the animals go away, as well as system sends information of that animals. The possible damage of the field and loss of crops are easily avoided.

One more step ahead in developing of this proposed system, we can make this system capable to measure the quantity of soil parameters and analyze the physical properties and chemical properties of soil. By this data, users can easily understand the requirement of soil and mix the fertilizers as per requirements. Due to this, the excess cost on fertilizer and damages of land due to the fertilizer can be avoided.

There is also scope to develop this system which observing the breeding of any diseases spreading insects, larvae, and other crops eating flies and gives the information about that to the users. So the users can easily apply suitable medicine or insecticides and avoid loss.



The system should also be capable to prevent damage of the water pump from dry and over load, as well as problems like failure of energy supply. This system controls the water supply by switching and operating specially equipped valves made by electromagnet or valves that are connected to small motor. The operation of system is totally depending upon the observation and data collecting by sensors. Also, the role of farmers is very important, because no one who understands more than farmers about his field. A farmer was well known, well aware, and well updated about condition of his field. This system supports real-time information system, and the users can receive real-time information. So he is well known and updated about the status of the water pump and conditions of the field.

## **5 Benefits of Proposed Smart, Water-Efficient Automatic Drip Irrigation System**

Traditional irrigation methods are not suitable to handle the water shorting situation. Now this advanced irrigation technique with modern technology will be beneficial to all farmers and meet the all requirements of all farmers. It has the following advantages [6].

- Productivity increases.
- Water efficient.
- Reduce rate of nutrient leaching and soil erosion.
- Low maintains cost.
- High-quality crop production.
- All weathers sustainable system.
- Reduce cost of fertilizations.
- Reduce loss due to various diseases.
- Reduce cost of insecticides.
- Reduction in the electricity bills.
- Reduce weeds growths.
- Reduce runoff of fertilizers into groundwater.

## **6 Acknowledgements**

This was a small attempt to express my gratitude to all the teachers, professor who has assisted, encourage me and significantly motivate me to make and ready this paper.

I am profoundly grateful to the Guide Mr. Pravin A. Manatkar. For his expert guidance and continuous encouragement in this work till completion of this paper.

I am also grateful to the principal, HOD of Civil Engineering Department, Trinity Academy of Engineering, Pune, for their invaluable guidance and support in this work.

At last, I must express my sincere heartfelt gratitude to all the staff members of Civil Engineering Department who helped me directly or indirectly during this course of work and also I would like to give a big thanks to the library department.

## 7 Conclusion

The system has low maintains and installation cost. It should also be capable to prevent damage of the water pump from dry and over load, as well as problems like failure of energy supply. Also, this advanced irrigation technique with modern technology will be beneficial to all farmers and meets the all requirements of all farmers. This system is water-efficient and increases the productivity of crops. Reduce the rate of nutrient leaching and soil erosion also reduces the cost of fertilizations.

With advanced techniques, the system detects the breeding of diseases causing insects and informs the users so the users can apply suitable insecticides so the cost of that was decreased. It results in high-quality products from field. The system was all weathers' system. So by using solar power, it reduces the electricity bills.

## References

1. Munoth P. "Sensor based irrigation system: a review", (IJERT), Proceedings of NCACE-2016 conference
2. Suzden S, Dursun M. "An efficient improved photovoltaic irrigation system with artificial neural network based modeling of soil moisture distribution—a case study in Turkey"
3. Siqueira JA, Dias PC (2013) A high sensitivity single-probe heat pulse soil moisture sensor based on a single npn junction transistor. *Comput Electron Agric* 96:139–147
4. Dr. Jegathesh Amalraj J (Dec 2019) "A study on smart irrigation systems for agriculture using iot" (IJST), 8(12)
5. Mr. Dhanaji Baravade (Apr 2019). *Study paper on smart irrigation system*, ijesrt, ISSN: 2277–9655
6. Anitha K (05 Nov 2016) Automatic irrigation system, ISITSEM-16
7. Bjorneberg DL (2013) "Irrigation methods", Elsevier Inc
8. "Low cost design of automated drip irrigation system with gsm". *Int Journal of Recent Technology and Engineering*, 2019
9. Reddy J (13 Mar 2015) Drip irrigation vs. sprinkler irrigation, hrssystems.com
10. Drip Irrigation the Basic, The University of Arizona, College of Agriculture and life sciences
11. Arshad MG (Oct 2017) Irrigation water quality. Res Gate

# Analytical Study of Scour Mechanism Around Immersed Rectangular Vane Structures



Priyanka Roy, Subhasish Das, Anupama Dey, and Rajib Das

**Abstract** The intricacy of sedimentation and its transport in alluvial channels is a matter of great apprehension in the arena of hydraulic engineering. In this perspective, a submerged vane plays a dynamic part by providing an effective and efficient solution of sediment management. An immersed vane structure acts as a vortices-generating contrivance that can be employed for controlling the channel bed erosion in streams. The flow pattern downstream of the vane can be transformed by fixing the vanes on the stream bed at a certain angle, resulting in the modification of shear stress and sediment redistribution on the channel bed. Immersed vanes have found numerous functions in channel hydraulics, but commonly, immersed vanes are applied to generate optimal riverbed depth, to diminish unnecessary scour or sediment deposition, and an overall improvement of navigability. In the present study, four clearwater experiments are performed using rectangular single, double, and triple vanes arrangements to analyze the equilibrium scour pattern around the vanes positioned at  $15^{\circ}$  angle of attack. The contours of scouring holes developed around the immersed vanes are plotted. From the evaluation of the scour geometries and contours morphology around such arrangements of submerged vanes, it is observed that for each set of arrangement, there is a variation in the scour formation in the upstream and downstream side of the flow, which in turn gives a clear idea about the scour patterns around them. The scours are observed to be more for the downstream vanes in the case of multiple vanes in comparison with a single vane. The horseshoe vortex and wake vortex are much stronger at the place near to the vane. The experimental study provides an insight into the proper design and placement of vanes which could be further utilized for more effective channelizing of sediments toward the bank, enhancing the navigability of the channel.

**Keywords** Scour mechanism · Submerged rectangular vane · Scour contour · Sediment channelizing

---

P. Roy · S. Das (✉) · A. Dey · R. Das  
School of Water Resources Engineering, Jadavpur University, Kolkata, India

© The Author(s), under exclusive license to Springer Nature Singapore Pte Ltd. 2022  
C. M. Rao et al. (eds.), *Advanced Modelling and Innovations in Water Resources Engineering*, Lecture Notes in Civil Engineering 176,  
[https://doi.org/10.1007/978-981-16-4629-4\\_49](https://doi.org/10.1007/978-981-16-4629-4_49)

703

# 1 Introduction

An immersed vane is a vortices-generating mechanism that is able to control the emergence of a channel bed at natural streams. The immersed vane is basically a baffle of low height placed at the bottom of the river or channel at a certain diversion angle that redirects flow movement of the concerned channel and thus produces resulting currents in main-stream channels. As a result, the intensity of redirected flow and bottom shear stresses directions are simultaneously modified, and thereby, sediments are reallocated throughout the channel cross section. Therefore, these immersed vane structures have received numerous applications for channel hydraulics, for instance protecting banks from curved sections, protecting bridge pillars, and preventing sediment drifting in hydro-power and irrigation channel sections. In addition, they can produce an optimal depth of riverbed, also reduce unnecessary flooding or erosion, improve river flow completely, settle braided and wandering rivers by removing bars and debris, and thereby form suitable habitation for aquatic animals.

An immersed vane is an effective way to manage sediment in alluvial rivers. By inserting multiple vanes in the streambed angling to flow, the pattern of flow movement at the bottom of the immersed vane is transformed and shear pressure on the channel bed is newly redistributed. Accordingly, the bed sediments are moved randomly across the section across the channel. With the proper arrangement of immersed vanes, a definite segment of streambed influenced by immersed vanes can sensibly be updated into any pre-designated profile which is highly preferred for channel managing. The effectiveness of controlling sediment using an immersed vane is associated with its three dimensions, submergence nature, and form. Most immersed vanes in-ground applications are basically rectangle plates, mainly owing to their plainness for designing and constructing. Some difficult designs tested in laboratory studies have air-foil type sectional profiles. It is evident that vanes are structures to divert the flow of a river, however, like a structure placed on the riverbed and local scour around which is also a common phenomenon. Local scouring forming around structures is the prime cause of the obliteration of countless manmade structures inside channels. An approximation of maximum probable scouring surrounding any manmade structure is essential for channels' safe design.

In many smaller channels, it is noticeable that due to the deposition of sediment, the depth of the channel reduces a great extent. This makes it difficult to navigate. Hence, if the sediments could be shifted to one side of the bank of the smaller channels, it can help to navigate. And the proliferation of bank erosion and deposition in smaller channels is a prime resource managing problem. Bank erosion usually occurs at the curves of stream channels, where definite interaction between the vertical grade of velocity and subsequent curvature of flow produces a purported secondary or rotational flow.

Numerous researches report on predicting the geometries of scouring and flow characteristics around structures and various estimates developed by various investigators [1–15]. Extensive research was presented that contains the temporary emergence of large flow elements around the circular structures placed in a sedimentary

bed [2, 3]. Similar results were obtained from a semi-circular structure arrangement placed next to the channel bank wall [4]. Experimental investigation of the scour hole geometries and circulations for horseshoe and wake vortex system at circular structures, with data measured by a velocimeter [5–7]. Velocity vector structures and vorticity pathways of the developed flow field in the upper and lower plane of measurement were presented. Vortex characteristics around circular, square-like structures was compared [8]. The variations of geometry of scouring at structures having diverse effectual widths were observed [9, 10]. Other investigations on many structures were extended to double identical structure configurations like inline, sidewise, eccentric, focused on the predicting velocity fields, turbulence fields, scour geometries, etc. [11–15]. How eccentric structures placed inline, can increase sediment movement rate considerably toward channel bank flowing downward was well described [14–16].

The above-mentioned works of literature confirm that numerous studies on scouring around structures had been carried out, however, especially scour around vanes are very less. Most of the studies are mainly about scouring around bridge pier-like structures. Few studies carried out earlier showed that vanes can be efficiently used for controlling the movement of sediments [17–19]. A procedure was expanded for rational designing of immersed vanes system to manage proper depth in alluvial channels and rivers. The vane structures were vertical frames with small characteristic ratio foils mounted on channel bed at  $10^{\circ}$ – $15^{\circ}$  diversion angle concerning the flow. Their total height was 1/5 to 1/2 times the depth of water in the flow design. The process described for banking protections was a feasible and sensible approach to traditional strategies like riprap, rock, spur dikes, etc. Also, flow field measurements at immersed vanes at a high diversion angle were performed [19]. The immersed vane for about  $40^{\circ}$  diversion angle develops the strongest circulation. Flow features that cause sediment transportation were reported for vane structures with diversion angles of a wide range [20].

The effect of the immersed vane was studied as a counter-strategy on the local scale on the cylindrical structure [21]. An attempt was made where single-arm rock vane structures angled with flow through the pitch streambed in such a way that the tip of the vane is immersed yet at low flow [22]. The focus was on developing a morphological simulation system capable of simulating the effect of immersed vanes on the alluvial bed [23]. The maximum scouring reduction was obtained with an  $8.5^{\circ}$  diversion angle and 20 cm flow depth for a 0 cm immersed vane height while the maximum lift occurred with an  $18.5^{\circ}$  diversion angle and 10 cm flow depth for 5.7 cm height of an immersed vane. The investigation was continued using  $20^{\circ}$  diversion angle to observe the effect of the immersed vane position on the protection of river banks [24]. The angled type and curved type vanes compared to plane type vanes are found more effectual in protecting river banks by 20 and 35%, correspondingly. Four types of immersed vanes were hydraulically tested at the leading edges in  $30^{\circ}$ ,  $45^{\circ}$ , and  $60^{\circ}$  concerning the base [25]. An attempt was made to check whether the sediment particles could be transported and shifted to one side of the vane attached structure at four vane alignments of  $0^{\circ}$  (with no vane),  $15^{\circ}$ ,  $30^{\circ}$ , and  $45^{\circ}$  [26]. Several laboratory experiments were done without and with immersed vane structures. A

single immersed vane fixed with abutment upstream nose was found effective in reducing, modifying, and protecting erosion [27]. The attempt was made to evaluate and confirm the findings on immersed vanes in [17] using CFD [28].

From the literature, it is clear that most of the studies are mainly about the flow fields around the pier-like structures of different shapes. But some previous studies showed that vanes can be efficiently used to control the movement of sediments. It can be done by proper design and location of vanes on the riverbed. The efficient design of vanes also helps in bank protection.

In the present study, a rectangular immersed vane structure is used to find out the flow structure around it along with its scour geometry. Single vane, double vanes, and triple vanes are placed on a sand bed of a flume at a constant angle, depth, and flow condition to observe the scour geometry. Analysis of velocity pattern made around the vane which enables us to understand why the bed materials are shifted from the upstream side and deposited to the downstream, which in turn gives a clear idea of the scour phenomena, and we can be able to understand and diminish the non-navigability of stream in the practical field. The experiments were carried out with a fixed angle of  $15^\circ$  with the direction of the flow at a constant flow depth of 10.5 cm and constant discharge of 25 l/sec. The study also aims at the determination of the velocity profiles and the contours of the longitudinal, lateral, and vertical velocities at four horizontal planes 6, 4, 2, and 1 cm above the bed before the experimental run while observing the comparison between scouring pattern around vane.

## 2 Materials and Methods

The analytical study reported herein is based on experiments carried out in Fluvial Hydraulics Laboratory of School of Water Resources Engineering at the Jadavpur University using a physical hydraulic model. A recirculating flume of 11 m (length)  $\times$  0.81 m (width)  $\times$  0.60 m (height) size was used (Fig. 1). The study is confined to uniform cohesionless bed material and clearwater flow conditions. Three vanes having identical dimensions of 157.5 mm length, 84 mm height, and 5 mm thickness

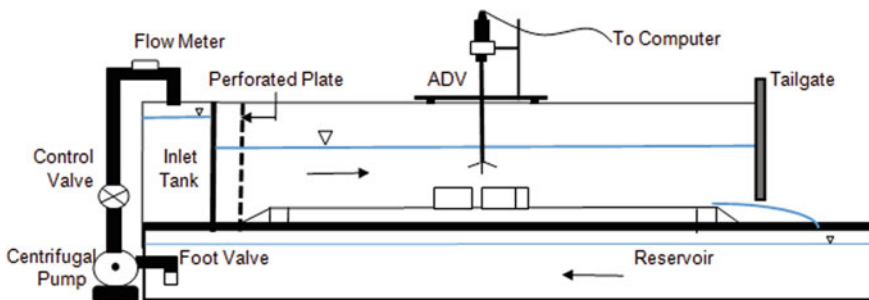


**Fig. 1** Sectional view of the recirculating flume

were used for this study. All experiments were carried out for 24 h of flow duration with a vane having a dimension of 157.5 mm (length)  $\times$  84 mm (height)  $\times$  5 mm (thickness) placing at a constant angle of  $15^\circ$  with the direction of the flow with constant water depth and discharge of 105 mm and 25 l/sec correspondingly. A tailgate was used to fix the water-surface depth ( $h$ ) as 105 mm for all immersed vane experiments at bed slope maintained consistently at 0.00042. Using Manning's equation, mean-flow velocity was determined.

Here, the coefficient of roughness ( $n$ ) was determined by using Strickler's formula. The average diameter ( $d$ ) of sand is set as 0.825 mm. Considering the constant flow of uniformity in a rectangular flume, the working bed shear stress ( $\tau$ ) is calculated by  $\gamma B h S / (B + 2 h)$  for the channel with a small bed slope where  $B$  is flume internal width. At air-water interfaces, the resistance is reasonably small for a smooth water surface that can be expediently neglected. The critical stress ( $\tau_c$ ) was determined using the Shields parameter expression. Then, equation of critical stress becomes as  $\tau_c = 0.0319 \Delta \rho \gamma d / \rho = 0.4084 \text{ N/m}^2$ .

The height of the functioning vane is calculated by the vane height-to-water depth ratio according to [17]. The angle of attack is kept  $15^\circ$  as for this angle, separation of the flow is minimum, and the scour is maximum for a specific width (effective width) of the vane [17–20]. The length of the vane ( $L$ ) is calculated by the effective vane width ( $W$ ) and angle of attack ( $\theta$ ). The formula for calculating vane length is  $W/L = \sin \theta$ . These tests were performed under precise conditions clearwater scouring. When a small ( $\leq 1$  mm) difference in scouring depth was recorded within two hours interval, it was thought to have reached the equilibrium phase of the scouring hole. Though, the minimum experiment duration was 24 h long enough to achieve the quasi-equilibrium scouring. Past the experiment, the maximum scouring was noticed at the bottom of the immersed vane and was precisely assessed by a Vernier gage with a round nose point having 0.1 mm precision. The contour plots of scouring at the immersed vane/vanes are plotted using a software tool. Velocity vector and velocity contour lines of the different velocities around the vane are plotted by OriginPro software 9.1 version. The flume water was drained from the scouring zone around the vane structure. When the scouring sand bed became convincingly dry, water mixed glue was sprinkled homogeneously over the scouring zone for stabilizing and solidifying. The scouring sand bed was adequately moistened with the diluted glue when left to sit for a minimum of three days. After drying for up to four days, the profile of the scouring bed became stiff, making it easier to use a velocimeter. The salinity of the water was measured ( $=0.63$  ppt) by a portable multi-parameter water analysis kit, and the value was given as an input to ADV to measure the velocities considering it.

An azimuthal coordinate system for a single immersed vane experiment has been used for representing the flow patterns. A four-beam down-looking Vectrino-Plus probe (ADV laboratory model with 10 MHz acoustic frequency), by Nortek, was taken for measuring immediate velocity components around a single immersed vane arrangement only. The 100 Hz sample rate and the variable sample volume of 5.5 mm wide with a sample height of 2–5 mm are chosen for gauging. The 2 and 5 mm height samples are used to measure in and out of the interfacial layer, respectively

[29]. The measuring area was 0.05 m below the velocimeter probe. The sample time of 120–300 s is considered as a guarantee of the velocity of the independent time scale. Sample times were taken too long near the bed. The continuous horizontal adjustment of the ADV scales was 10 mm. Vector profiles in Fig. 7 do not illustrate all test data in the lowest degree for avoiding overlaps or very congested plotting. Measurement made with velocimeter was beyond the range 3 mm above the scouring bed, as velocimeter requires a minimum 90 mm<sup>3</sup> measuring volume. Velocimeter outputs are with minimum SNR and correlation of 17 and 65%, correspondingly. The external radius of the velocimeter was around 30.25 mm with four transducers, to receive velocimeter signals, fixed on small arms at 90° gaps, making it easy to measure the flow at a distance of 30 mm from the immersed vane boundary. The case of measuring with velocimeter at 20 mm away from the vane was done by rotating it 45°.

### 3 Results and Discussion

Experiments were carried out for the scour geometry and scour morphology with a single vane, double vane, and triple vane arrangement with 15° diversion angle to the longitudinal direction of flow [Fig. 3]. The longitudinal center to center spacing between the two successive sets of vanes (one at the upper end and another one at the lower end) was  $0.75E_{ls}$  where  $E_{ls}$  is the net lengths of scouring and sediment deposition for a single immersed vane arrangement [12, 14]. The eccentric gap between to lower vanes was three times their width [5, 6]. Also, the flow field pattern around the scour hole was measured. In the case of flow field measurement test around the single placing vane, the ADV velocimeter was taken for measuring longitudinal, transverse, vertical, and time-averaged absolute velocities at different planes. Table 1 lists the scouring values acquired from Vernier gauge measurements for the three different arrangements of vanes. The scour-affected zone around the different vane arrangements and the respective contours, plotted with Surfer, of the scouring holes around the immersed vanes are shown in Fig. 2(a-c), and Fig. 3(a-c), respectively.

In the case of the single immersed vane layout, it was detected that the scouring at the upstream and dune at the lower end of the immersed vane is symmetric. Also from

**Table 1** Scour geometry for single vane, double vane, and triple vane arrangement

| Vane arrangement | Vane angle (degree) | Flow depth (cm) | Discharge (lit/sec) | Maximum scour depth (cm) | Maximum scour length (cm) | Maximum scour width (cm) |
|------------------|---------------------|-----------------|---------------------|--------------------------|---------------------------|--------------------------|
| Single vane      | 15                  | 10.5            | 25                  | 3.5                      | 122                       | 27                       |
| Double vane      | 15                  | 10.5            | 25                  | 3.1                      | 111                       | 25                       |
| Triple vane      | 15                  | 10.5            | 25                  | 1.8                      | 64                        | 20                       |



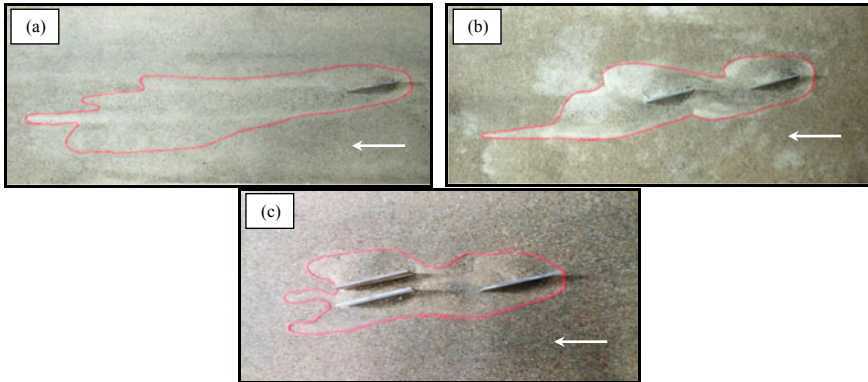


**Fig. 2** Scour-affected zones around the **a** single vane, **b** double vane, and **c** three vanes arrangement

the contour map, it can be concluded that the scour is higher toward the upstream tip of the vane.

For double vane arrangement, the scour occurred at the upstream sides of both the vanes and dune formed toward the downstream sides of both the vanes. It was observed from the contour map that the depth of scouring is higher at the upstream sides of the second vane (which is situated at the downstream side of the flow) than the first vane (which is situated upstream of the flow).

The scour width of the second vane is also greater than the scour width of the first vane. In the case of triple vane arrangement, scouring occurred at the upstream sides of both the vanes and dune formed toward the downstream sides of both the vanes. From the contour map, it can be addressed that the flow separation is more in this arrangement than the double vanes arrangement. Also, the scouring depth is more in the upstream tip of the second immersed vanes set (which is situated at the downstream side of the flow) than the first immersed vane (which is situated at the upstream side of the flow). The deposition heights for single, double, and triple immersed vanes are 0.83 cm, 1.21 cm, and 1.75 cm, respectively. Therefore, the deposition height is maximum for the immersed triple vanes structure. The scouring heights for single, double, and triple immersed vanes are 3.5 cm, 3.1 cm, and 1.8 cm.

Single vane causes maximum scouring that helps to increase and maximize sediment transportation compared to double and triple vanes. It also shifts sediment efficiently toward the bank wall as well. The deposition is also lowest for single vane, but it spreads on a large area compared to double and triple vanes. It may cause aggradations of larger areas of bed which may trouble the navigation facility. On other hand, to cause more erosion for transporting sediments and keeping the bed navigable at larger areas as well, double vane arrangement (Fig. 2) is better than single and triple vanes as it removes sediment almost at equal depth to single vane but with a much smaller deposition area. Therefore, double vane arrangement is the actually optimum choice, here, compared to single and triple vanes for both increasing erosion to move the sediment along the lower channel and shift sediment

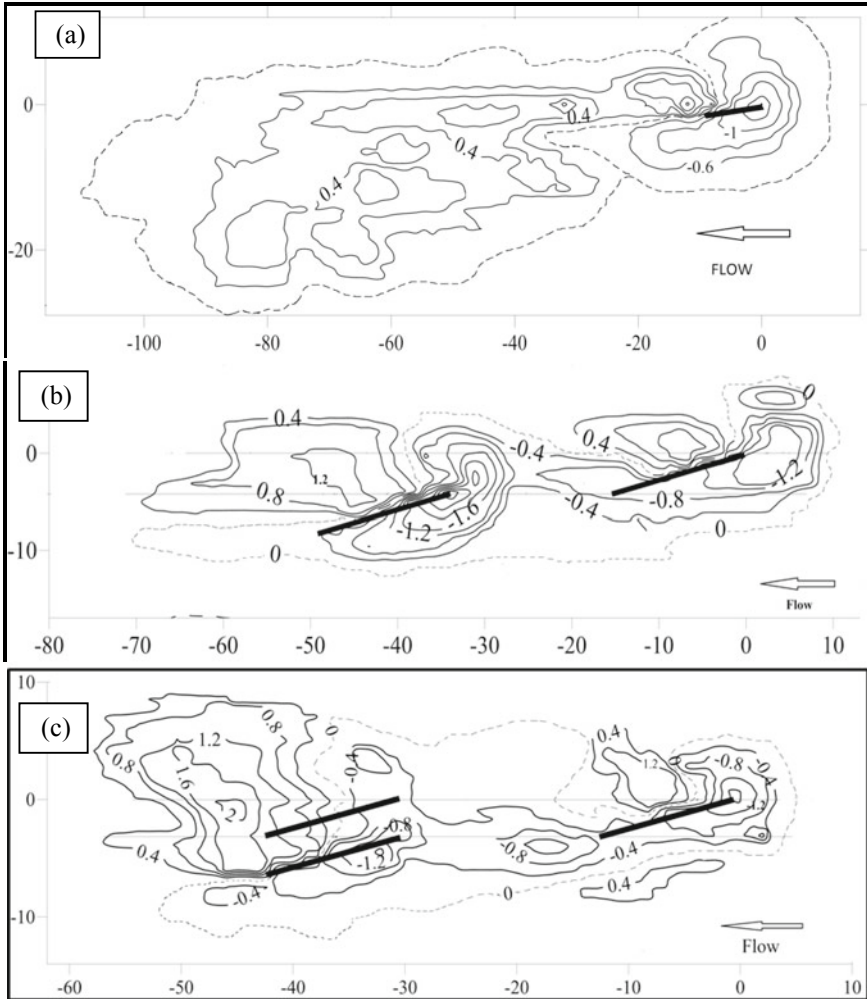


**Fig. 3** Contour map of the scour for **a** single vane, **b** double vane, and **c** triple vane arrangement, respectively (units: cm)

simultaneously near the channel bank wall. Double vane is also better for channels promoting navigational support as it deposits less sediment in height compared to triple vane and less sediment is spread in terms of bed area.

## 4 Flow Fields for Single Vane Arrangement

### 4.1 Longitudinal Flow Velocity (U)

Here, from Fig. 4, it is observed that for longitudinal velocity contour the velocities away from the vane (in transverse directions) are higher compared to the area which is closer to the immersed vane (for all the horizontal planes). Since the flow is obstructed at the vane, so the longitudinal component of the velocity ( $u$ ) gets very low in that region. It is also observed that the corresponding velocities are getting lower with the water depth toward the bed level. For the first two planes from the free water surface, the values of longitudinal velocities varied less, but in the other two bottom planes, the longitudinal velocities reduced by 50–60% compared to the upper planes. It is because of viscous effect is predominant at the bottom compared to the turbulence effect. It is observed that the variation of velocities is less away from the vanes in all planes as there are no considerable obstructions.

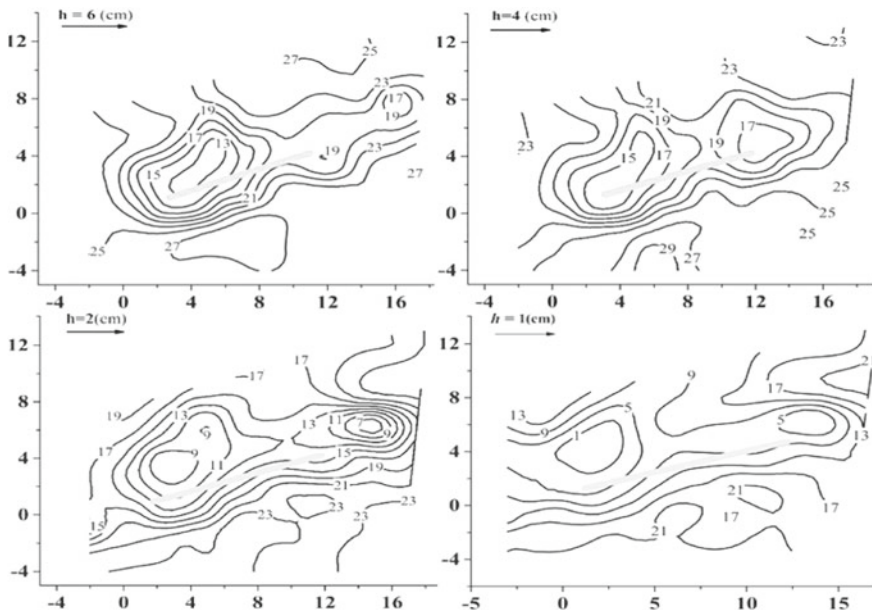


**Fig. 4** Longitudinal velocity contours plotted for the plane  $h = 6$  cm, 4 cm, 2 cm, and 1 cm, respectively (Here, abscissa and ordinate denote  $x$ -axis and  $y$ -axis with units in cm)

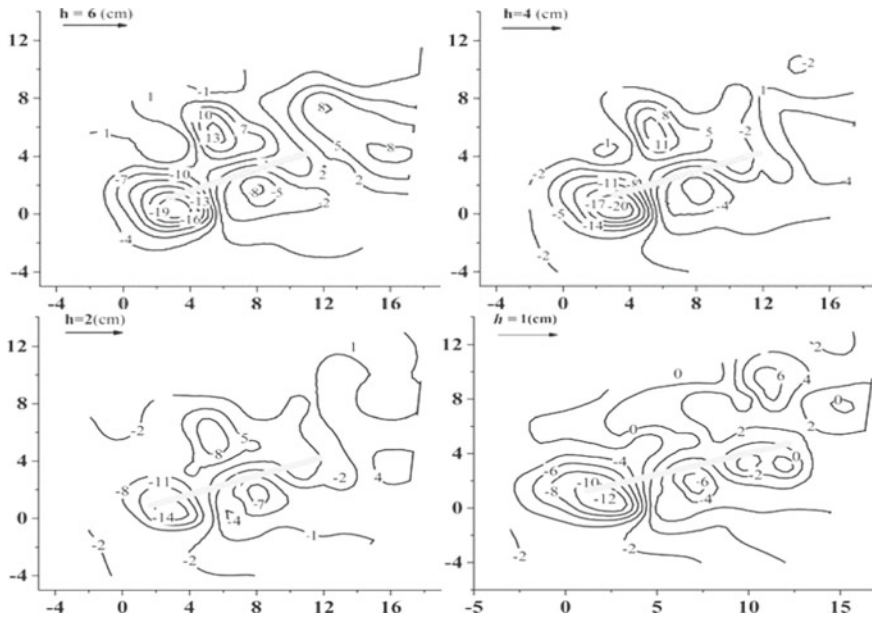


**Fig. 5** Transverse velocity contours plotted for the plane  $h = 6$  cm, 4 cm, 2 cm, and 1 cm, respectively

### 4.2 Transverse Flow Velocity ( $V$ )

From Fig. 5, it is observed that the flow is obstructed by the vane and it gets separated and the velocities are positive at the left bank of the vane and negative on the right bank and give the idea of separation of the flow with the help of the right-hand thumb rule.

(Here abscissa and ordinate denote  $x$ -axis and  $y$ -axis with units in cm).

Velocities are higher at the starting point of flow separation (upstream edge of vane), and then, it decreases gradually away from the vane. Separation velocities are higher at the upper planes compare to the bottom. The velocity of the upper-most plane increases by almost 60–70% compared to the bottom plane.

### 4.3 Vertical Flow Velocity ( $W$ )

It is observed from Fig. 6, that the vertical velocity  $-w$  is positive in the right bank of the immersed vane and negative in the left bank of the immersed vane for all the planes. A positive value means the velocity is in an upward direction, and a negative is in a downward direction. So from the contour plot of this velocity in different planes, it is observed that in the scour-affected zone the vertical velocity is in a downward

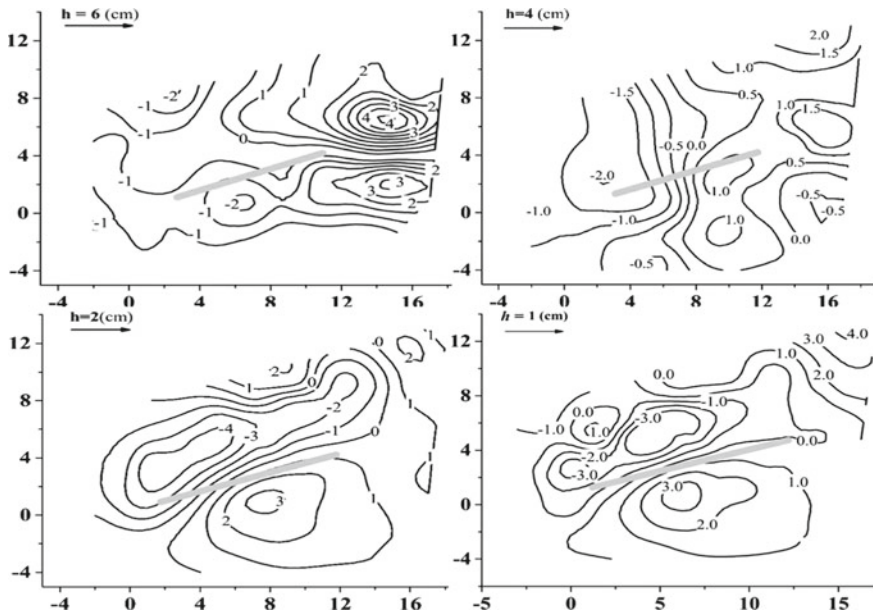


**Fig. 6** Vertical velocity contours plotted for the plane  $h = 6$  cm, 4 cm, 2 cm, and 1 cm, respectively (Here abscissa and ordinate denote  $x$ -axis and  $y$ -axis with units in cm)

direction, whereas in the dune part it is in an upward direction. Though, it is very obvious as horseshoe vortices form in the contact part of the immersed vane, so,  $w$  moves downward helping to scour the bed particles and for the up-flow event, a dune is formed in the lower side of immersed vanes, which is known as wake vortex. It is observed from the contour plots that the velocity increases gradually toward the bottom planes compare to the upper plane.

#### 4.4 Velocity Vector

From Fig. 7, it can be determined that the vector velocity pattern around the vane gets more deviated in the bottom two planes compared to the other upper two planes. It gives a clear idea about the direction in which the fluid particles (water) are moving along the horizontal. From the time-averaged absolute velocity contours (not shown here), it is evident that the velocity away from the vane (in lateral directions) is much higher compared to the area close to the vane (for all the horizontal planes). As the flow is restricted to the vane, so the longitudinal portion of the velocity ( $u$ ) decreases significantly in that region, so that the effect is also reduced. The absolute velocity decreases from the top horizontal plane to the bottom-most horizontal plane. In the first two planes, the values of absolute velocities vary slightly, but when for the third

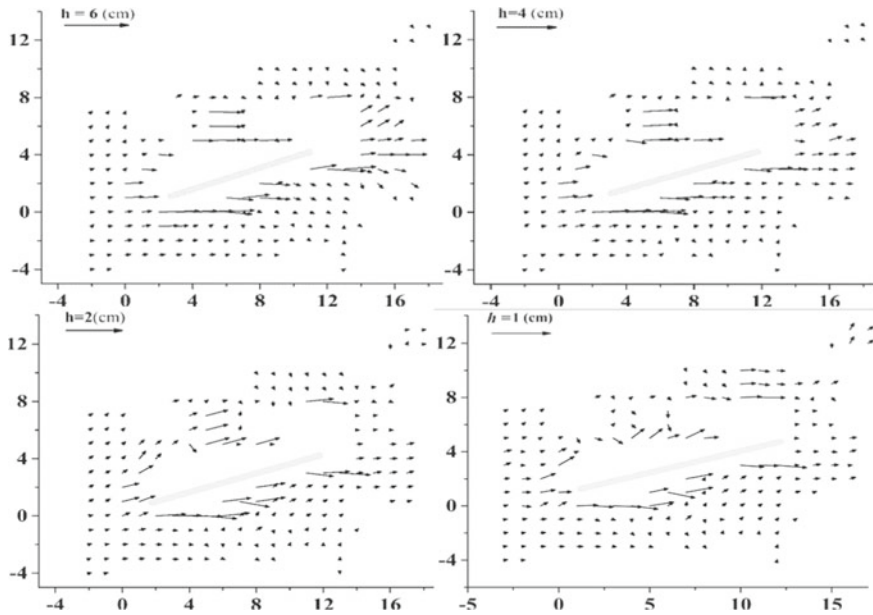


**Fig. 7** Horizontal velocity vector plotted for the plane  $h = 6$  cm, 4 cm, 2 cm, and 1 cm, respectively (Here abscissa and ordinate denote  $x$ -axis and  $y$ -axis with units in cm)

and fourth planes, it decreases significantly. In some places of third and fourth planes, time absolute velocities are reduced by 50–70% compared to the higher planes. It is due to the shear effect of the near-top layer on the lower plane.

Immersed vanes usually cause sediment deposition immediately at the downstream nose of vanes, cause scouring around them, and shift the sediment particles with the downflow. Vane alignment, size ratio, submergence, and intermediate densities (spacings) all play an important role in these cases. In the present study, vane was aligned at  $15^\circ$  to maintain similarity [19, 20, 26], vane height-flow ratio was set 0.8 following the range of 0.35–0.85 given in [30]; size ratio of 0.53 was also set keeping parity with the range 0.5–1.5 [30]. The majority of the parameters were set following the conditions adopted during the field experiments conducted earlier [17–20, 30]. For all immersed vane experiments, the scour was 25–35% less in the right bank compared to the left bank. This observation was consistent with previous field research [20]. However, when using the present results directly into the field experiments, the scaling issue may make a deviation between the views as made in the present study. Quantitative analysis should be performed to address the scaling issue. Moreover, the present study was performed under clearwater, whereas in the field less scour forms under live-bed conditions compared to clearwater. Therefore, on the scouring aspect, the present study may be useful. In the future, however, field experiences, as well as additional exploratory and theoretical studies, will lead to an improved understanding of the immersed vane functioning and improved designing.

## 5 Conclusion

From the scouring geometry measurements, morphology, and flow field measurement around the different layouts of immersed vanes, it can be reached in many interesting conclusions. Different directions—longitudinal, transversal, and vertical—velocities of different magnitude and directions around the vanes have been observed. It also provides a clear view of the scour pattern and flow pattern around the immersed vanes structures.

The maximum scour depth and width were observed to be the highest near single immersed vane structures, compared to immersed double and triple vane structures. In single vane structure, there was a similarity between the upstream scour and downstream dune. Also, more scour occurred near the upstream tip of the vane. With double vane structure, the scour and dune were formed upstream and downstream, respectively, for both vanes. More scour depth was observed upstream of the immersed double vane rather than the immersed single vane. For the triple vane structure, more flow separation was seen compared to the double vane structure. Also, more scour depth was found in the upstream tip of the double vane structure than the single vane. The scour was found more near the lower vanes of the three vane structure. From these observations, it is clear that for both increasing erosion to move the sediment along the lower channel and shift sediment simultaneously near the channel bank wall, the double vane structure is the best choice among the single, double, and triple vane structures. Double vane structure is also better for channels that improve maritime support as it incorporates less sediment deposition compared to triple vane structure and a smaller spread of sediment across the bed area.

The separation of transverse velocity was significantly increased in presence of the vanes. The longitudinal velocity was disturbed more or less away from the vane structures. It confirms no appreciative effect of the immersed vane on flow. From the observed size of the vertical velocity component in vortex areas, it can be concluded that the horseshoe vortices and wake vortices are the strongest in the vicinity of the immersed vane. In this experimental process, different vane configurations were considered and followed by subsequent scour patterns and velocity patterns surrounding the vanes.

On the riverbed, it can be done by finding the best location and proper construction of such flow guiding vanes. The well-designed vanes also help protect the riverbed and banks. With the proper design and layout, sediments can be properly directed to the bank with the vane structures that can increase or maintain the channel navigability and flow.

## References

1. Breusers HNC, Nicollet G, Shen HW (1977) Local scour around cylindrical piers. *J Hydraul Res* 15(3):211–252
2. Dargahi B (1990) Controlling mechanism of local scouring. *J Hydraul Eng* 116(10):1197–1214

3. Pandey M, Sharma PK, Ahmad Z, Karna N (2017) Maximum scour depth around bridge pier in gravel bed streams. *Nat Haz* 91(2):819–836
4. Barbhuiya AK, Dey S (2004) Local scour at abutments: a review. *Sadhana* 29:449–476
5. Das S, Mazumdar A (2018) Evaluation of Hydrodynamic Consequences for Horseshoe Vortex System developing around two eccentrically arranged Identical Piers of Diverse Shapes. *KSCE J. Civil Eng.* 22(7):2300–2314
6. Das R, Khwairakpam P, Das S, Mazumdar A (2014) Clear-water local scour around eccentric multiple piers to shift the line of sediment deposition. *Asian J Water Environ Pollut* 11(3):47–54
7. Rout A, Sarkar A (2020) Local scour around submerged tandem and offset cylinders due to change in alignment angle. *Proc Inst Civil Eng: Water Manag* 173(1):14–30
8. Das S, Mazumdar A (2015) Turbulence flow field around two eccentric circular piers in scour hole. *Int J River Basin Manag.* 13(3):343–361
9. Das S, Das R, Mazumdar A (2014) Variations of clear water scour geometry at piers of different effective widths. *Turk J Eng Environ Sci* 38(1):97–111
10. Das S, Das R, Mazumdar A (2014) Vorticity and circulation of horseshoe vortex in equilibrium scour holes at different piers. *J Inst Eng India Ser A* 95(2):109–115
11. Voskoboinick V, Nikishov VI, Voskoboinick A, Voskoboinick A (2014) Influence of grouping of the bridge piers on scour. *Sci Based tech* 22(2):229–235
12. Jaman H, Das S, Das R, Mazumdar A (2017) Hydrodynamics of flow obstructed by inline and eccentrically-arranged circular piers on a horizontal bed surface. *J Inst Eng India Ser A* 98(1–2):77–83
13. Das S, Ghosh S, Mazumdar A (2014) Kinematics of horseshoe vortex in a scour hole around two eccentric triangular piers. *Int J Fluid Mech Res* 41(4):296–317
14. Jaman H, Das S, Kuila A, Mazumdar A (2017) Hydrodynamic flow patterns around three inline eccentrically arranged circular piers. *Arab J Sci Eng* 42(9):3973–3990
15. Solaimani N, Amini A, Banejad H, Ghazvinei PT (2017) The effect of pile spacing and arrangement on bed formation and scour hole dimensions in pile groups. *Int J River Basin Manag* 15(2):219–225
16. Das S, Das R, Mazumdar A (2016) Comparison of local scour characteristics around two eccentric piers of different shapes. *Arab. J Sci Eng* 41(4):1193–1213
17. Odgaard AJ, Spoljaric A (1986) Sediment control by submerged vanes. *J Hydraul Eng* 112(12):1164–1180
18. Odgaard AJ, Mosconi CE (1987) Streambank protection by submerged vanes. *J Hydraul Eng* 113(4):520–536
19. Odgaard AJ, Wang Y (1991) Sediment management with submerged vanes. I: theory. *J Hydraul Eng* 117(3):267–283
20. Odgaard AJ, Wang Y (1991) Sediment management with submerged vanes. II: applications. *J Hydraul Eng* 117(3):284–302
21. Marelius F, Sinha SK (1998) Experimental investigation of flow past submerged vanes. *J Hydraul Eng* 124(5):542–545
22. Johnson PA, Hey RD, Tessier M, Rosgen DL (2001) Use of vanes for control of scour at vertical wall abutments. *J Hydraul Eng* 127(9):772–778
23. Flokstra C (2006) Modelling of submerged vanes. *J Hydraul Res* 44(5):591–602
24. Ghorbani B, Kells JA (2008) Effect of submerged vanes on the scour occurring at a cylindrical pier. *J Hydraul Res* 46(5):610–619
25. Bejestan MS, Azizi R (2012) Experimental investigation of scour depth at the edge of different submerged vanes shapes. *World Environ Water Resour Cong ASCE* 1376–1385
26. Das S, Mukherjee R, Das R, Mazumdar A (2017) Enhancement of sediment transportation by increasing scour around a square pier with vane attached on one side. *Proc 37th IAHR World Congress Malaysia*, 565–574
27. Bejestan MS, Khademi K, Kozeymehnezhad H (2015) Submerged vane-attached to the abutment as scour Countermeasure. *Ain Shams Eng. J.* 6(3):775–783
28. Sharma H, Jain B, Ahmad Z (2016) Optimization of submerged vane parameters. *Sadhana* 41(3):327–336



29. Das S, Das R, Mazumdar A (2015) Velocity profile measurement technique for scour using ADV. Int Conf testing and measurement: techniques and applications (TMTA)—Chan (ed), Taylor and Francis Group, London, 249–252
30. Ouyang H (2009) Investigation on the dimensions and shape of a submerged vane for sediment management in alluvial channels. *J Hydraul Eng* 135(3):209–217

# Riverbank Erosion for Different Levels of Impurity of Water—A Micro-analysis



Debasish Biswas, Arijit Dutta, Sanchayan Mukherjee, and Asis Mazumdar

**Abstract** The mechanism of riverbank erosion is largely impacted by wide varieties of forces acting on the soil grains as well as some micro-level parameters, e.g. water content index angle, inter-granular distance, wetted surface area and contact angle. All these players make the entire mechanism of extremely complex nature. Here, role of all these parameters has been studied for the determination of escape velocity of the sediments in micro-level. This velocity is indicative of volumetric erosion rate in macro-level. The dominant forces that are considered here are the force of cohesion, pore-pressure force, force due to weight of the sediment grains and hydrostatic force. The already-established “Truncated Pyramid Model (TPM)” has been applied to envisage the micro-structural arrangement of the grains. The quantitative effect of the contact angle on sediment escape velocity for different wetted surface areas has been studied and plotted for different inter-granular distances. The varying contact angle is a measure of impurity of water. The results show the adverse effect of the contact angle on sediment escape velocity and, consequently, the bank erosion.

**Keywords** Escape velocity · Inter-granular distance · Contact angle · Water content index angle

## 1 Introduction

For its predominant impact on the way of life, economy and agricultural land, river morphology is a subject of incredible enthusiasm to the researchers for long. Riverbank erosion is significant as the bank disintegration wrecks the agrarian land as the human habitat depends on the stream. The erosion mechanism of the riverbank

---

D. Biswas (✉) · A. Dutta · S. Mukherjee  
Department of Mechanical Engineering, Kalyani Government Engineering College, Kalyani  
741235, India

A. Mazumdar  
School of Water Resources Engineering, Jadavpur University, Kolkata 700032, India

© The Author(s), under exclusive license to Springer Nature Singapore Pte Ltd. 2022  
C. M. Rao et al. (eds.), *Advanced Modelling and Innovations in Water Resources Engineering*, Lecture Notes in Civil Engineering 176,  
[https://doi.org/10.1007/978-981-16-4629-4\\_50](https://doi.org/10.1007/978-981-16-4629-4_50)

719

surface is, to a great extent, affected by wide varieties of micro-structural parameters including forces acting on the soil grains and the flowing water impurity. So, it throws up an immense challenge to the researchers to build up a summed up idea for a generalized investigation of bank erosion.

For quantifying erosion of the bank, numerous analysts have performed rigorous experimentation [1-3]. These experimental analyses differ from case to case as river morphology changes. But micro-scale analysis for the investigation of the different forces acting on the soil grains and the effect of the different physical parameters and water salinity or impurity on the bank erosion are not so familiar as yet. In this study, the primary focus is on the micro-scale analysis and to evolve on generalized hypothesis for the bank erosion. Here, amount of erosion of the bank surface has been determined in terms of sediment escape velocity which is the essential variable for measuring volume of bank erosion in macro-scale. Higher sediment escape velocity suggests higher force requirement by the soil grains to get displaced from the surface of the bank. This signifies lower rate of the erosion of bank surface in macro-scale. For the microstructural arrangement of the soil grains, the well-established TPM developed by Mukherjee and Mazumdar [4] has been utilized in the present investigation. The forces which are considered in the present study are the inter-granular force of cohesion, pore-pressure force, force due to weight of the soil grains under suspension and the hydrostatic force due to entrapped water. The micro-structural view of the soil grain in TPM is shown in Fig. 1.

Stability of the bank surface has been analysed by Darby and Thorne [5] and Osman and Thorne [6] by considering pore-pressure force and hydrostatic force. Cohesive force between two soil grains has been described by Soulie et al. [7] through the following expression

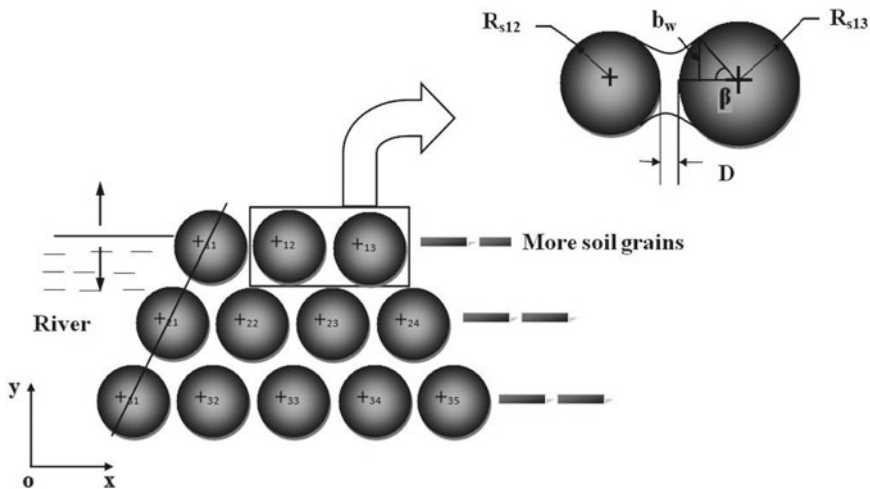


Fig. 1 TPM with adjacent soil grains magnified view (Mukherjee and Mazumdar [4])

$$F_{Cs} = \pi \sigma \times R_s \times \left[ \exp\left(a_l \times \frac{D}{R_s} + b_l\right) + c_l \right] \quad (1)$$

Here,  $R_s$  is the larger radius between those of two soil grains. In the present analysis, it has been assumed that both grains have the same radius. The radius of the soil grain has been chosen as 400  $\mu\text{m}$  going by Duan [8]. Also, the value of the surface tension coefficient  $\sigma$  for impure water has been considered to be 0.0681 N/m as per Poorni et al. [9]. The coefficients  $a_l$ ,  $b_l$  and  $c_l$  are strong functions of the volume of the liquid bridge as below

$$a_l = -1.1 \left( \frac{\forall_l}{R_s^3} \right)^{-0.53} \quad (2a)$$

$$b_l = \left[ -0.148 \ln\left(\frac{\forall_l}{R_s^3}\right) - 0.96 \right] \phi^2 - 0.0082 \ln\left(\frac{\forall_l}{R_s^3}\right) + 0.48 \quad (2b)$$

$$c_l = 0.0018 \ln\left(\frac{\forall_l}{R_s^3}\right) + 0.078 \quad (2c)$$

Here,  $\phi$  is the contact angle, and it depends on the impurity (e.g. salinity) of the liquid (i.e. water). In the present investigation, variation of contact angle has been chosen from 15° to 50°, as proposed by Bakker et al. [10], to study the effect of salinity. Again, in the analysis done by Mu and Su [11] it has been shown that the volume of liquid bridge depends on wetted surface area as follows:

$$\forall_l = \frac{\pi R_s}{2} \times [H^2(b_w) - D^2] \quad (3a)$$

Here,  $H(b_w)$  is a function of inter-granular distance ( $D$ ) and wetted surface radius ( $b_w$ ) as follows:

$$H(b_w) = D + \frac{b_l^2}{2} \quad (3b)$$

and the wetted surface radius ( $b_w$ ) from the Fig. 1 can be determined as a function of water content index angle ( $\beta$ ) as

$$b_w = R_s \times \sin \beta \quad (3c)$$

Likos and Lu [12] have expressed micro-scale pore-pressure force as

$$F_{Pw} = \pi \times r_2 \times (2 \times \sigma + P_w \times r_2) \quad (4a)$$

Pore-water pressure ( $P_w$ ) value from Likos and Lu [12] has been taken as 10 kPa (1.02 m of water column). And  $r_2$  in the above equation can be determined as a function of water content index angle ( $\beta$ ) and radius of the soil grain ( $R_s$ ) as

$$r_2 = R_s \times [1 + \tan \beta - \sec \beta] \tag{4b}$$

## 2 Forces on a Soil Grain

The soil grain 11 in Fig. 1 is of the primary concern for analysis as it is in direct contact with free surface of water. Free body diagram of the soil grain 11 has been depicted on Fig. 2.

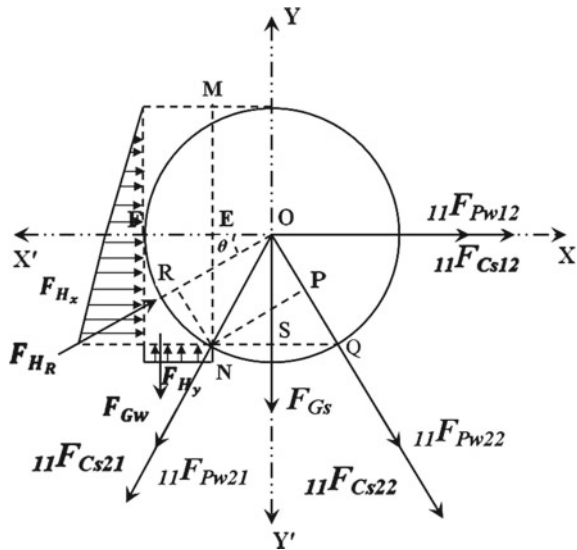
Here,  $F_{Gs}$  is the submerged weight of the soil grain,  $F_{Gw}$  is the fluid block weight, and  $F_{HR}$  is the resultant hydrostatic force which makes an angle  $\theta$  with the abscissa.

### 2.1 Escape Velocity Calculation

Conservation of angular momentum principle has been applied for finding soil grain escape velocity. In Fig. 2, point  $N$  is the contact point of the grain 11 with the grain 21. So the point  $N$  is the topple point of the soil grain 11. So, moment of momentum has been taken about the point  $N$  to calculate escape velocity. So, taking moment and applying angular momentum principle,

$$F_{Gs} \times \overline{NS} + F_{Cs} \times (\overline{NE} + \overline{NP}) + F_{HR} \times \overline{NR} + F_{Pw} \times (\overline{NE} + \overline{NP}) = I_N \times \alpha_s \tag{5}$$

**Fig. 2** Forces acting on soil grain 11 after submergence



Planar analysis has been considered to calculate hydrostatic force. Horizontal hydrostatic force can be calculated as:

$$F_{H_x} = P_{avg} \times A_x = h_c \times \rho_w \times g \times A_x \quad (6)$$

Vertical hydrostatic force (upward) can be calculated as:

$$F_{H_y} = h \times \rho_w \times g \times A_y \quad (7)$$

Liquid block weight (downward) can be calculated as:

$$F_{Gw} = \rho_w \times g \times \left[ \overline{FE} \times \overline{NE} - \frac{\pi R_s^2}{6} \right] \quad (8)$$

So, upward directional net vertical hydrostatic force:

$$F_{H_v} = F_{H_y} - F_{Gw} \quad (9)$$

$$F_{H_R} = \sqrt{F_{H_x}^2 + F_{H_v}^2} \quad (10)$$

and

$$\theta = \tan^{-1} \left( \frac{F_{H_v}}{F_{H_x}} \right) \quad (11)$$

Solving Eq. (5), the final expression for the soil grain angular acceleration is given by

$$\alpha_s = \frac{\frac{F_{G_s}}{2} + \sqrt{3} \times (F_{C_s} + F_{P_w}) + F_{H_R} \times \sin(60 - \theta)}{\frac{7}{5} \left( \frac{4}{3} \pi R_s^4 \rho_s \right)} \quad (12)$$

Here, soil grain density ( $\rho_s$ ) has been taken as 2650 kg/m<sup>3</sup>, and density of saline water ( $\rho_w$ ) has been considered to be 1025 kg/m<sup>3</sup> as suggested by Bakker et al. [10]. Now the expression for soil grain acceleration is

$$f_s = \alpha_s \times R_s \quad (13)$$

Now, from the work of Duan [8], the final expression of soil grain escape velocity is

$$V_{es} = [2 \times 10^{-6} \times f_s \times R_s]^{1/2} \quad (14)$$

Here, in the above expression, the value of  $R_s$  is taken as 400  $\mu$ m.

### 3 Results and Discussion

In the present investigation, variation of soil grain escape velocity with the contact angle has been studied for different inter-granular distances ( $D$ ) and for different water content index angles ( $\beta$ ), for both the situations of falling and rising water level for submerged soil grains. Four different variations (145, 155, 165 and 175  $\mu\text{m}$ ) of inter-granular distance and three different variations ( $15^\circ$ ,  $30^\circ$  and  $45^\circ$ ) of water content index angle have been investigated. The graph of these variations has been plotted subsequently.

#### 3.1 Sample Calculation

A sample calculation for 145  $\mu\text{m}$  inter-granular distance and  $\beta = 15^\circ$  is shown below.

Cohesive force between two soil grains

$$F_{Cs} = 3.68999 \times 10^{-5} \text{ N.}$$

Pore-pressure force

$$F_{P_w} = 2.9207 \times 10^{-4} \text{ N.}$$

Horizontal hydrostatic force

$$F_{H_x} = 3.7347 \times 10^{-3} \text{ N.}$$

Vertical hydrostatic force

$$F_{H_y} = 1.5011 \times 10^{-3} \text{ N.}$$

Liquid block weight

$$F_{G_w} = 4.47948 \times 10^{-4} \text{ N.}$$

So, upward directional net vertical hydrostatic force

$$F_{H_v} = 1.0531 \times 10^{-3} \text{ N.}$$

$$F_{H_r} = 3.88 \times 10^{-3} \text{ N.}$$

$$\text{And } \theta = 44.25^\circ.$$

Now, soil grain angular acceleration  $\alpha_s = 8246254.9 \text{ rad/s}^2$ .

Impending acceleration  $f_s = 3298.5 \text{ m/s}^2$ .

And escape velocity  $V_{es} = 1.6244389 \text{ m/s}$ .

Variation of soil grain escape velocity with contact angle for different conditions has been shown in all the above figures. Rising water level situation has been depicted in Figs. 3, 4 and 5; Similarly, Figs. 6, 7 and 8 show the falling water level situation. From all the figures, it is clear that the contact angle has an adverse effect on soil grain escape velocity. This implies that the increase in impurity or salinity will reduce the soil grain escape velocity, hence loosen the grain structure and, consequently, enhance the bank erosion in macro-scale. Four variations of inter-granular distance show the adverse effect of it on soil grain escape velocity. Again, if a comparison is made between the conditions of water level rising and falling, it can be seen

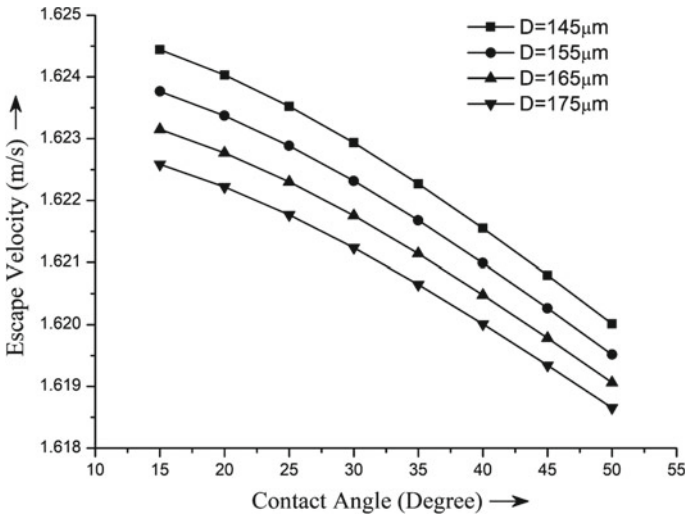


Fig. 3 Escape velocity versus contact angle for  $\beta = 15^\circ$

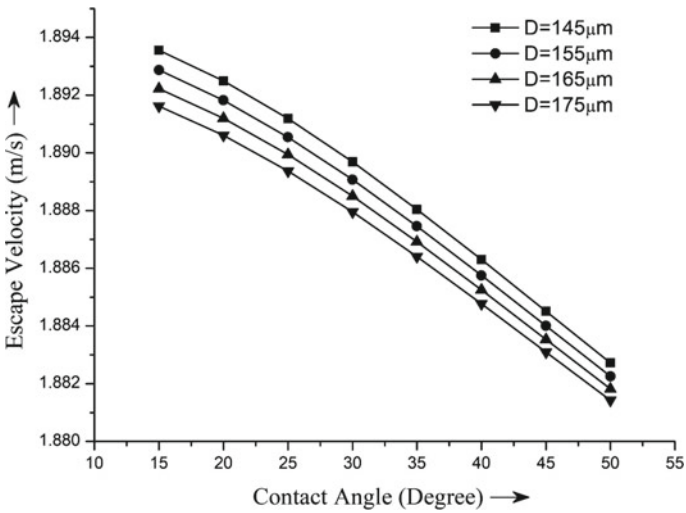


Fig. 4 Escape velocity versus contact angle for  $\beta = 30^\circ$

that the soil grain escape velocity is less for falling condition. A positive moment prevents detachment of a grain when the water is on the rise. On the other hand, gravity is responsible for dislodging a grain when the water level drops. This results in less escape velocity. From the above analysis, it is also clear that water content index angle has a favourable effect on the soil grain escape velocity. These findings



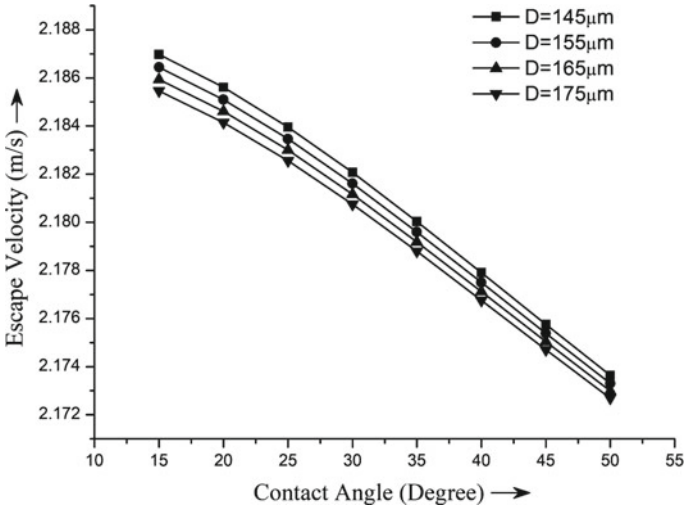


Fig. 5 Escape velocity versus contact angle for  $\beta = 45^\circ$

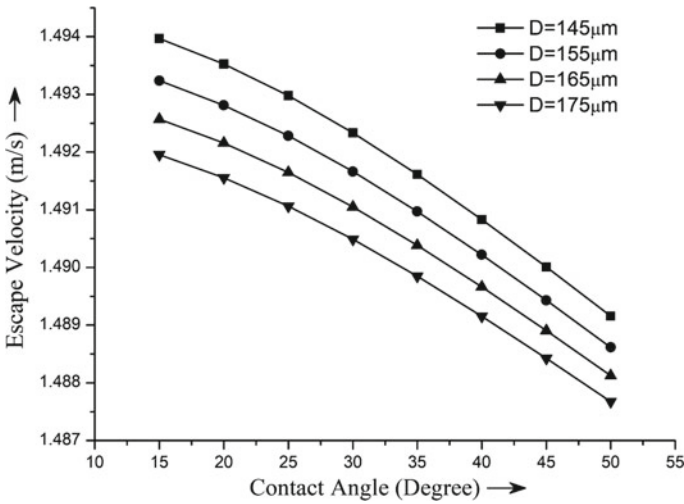


Fig. 6 Escape velocity versus contact angle for  $\beta = 15^\circ$

have a practical implication as the higher contact angle reduces the capillary pressure weakening the capillary action and, ultimately, enhancing bank erosion.

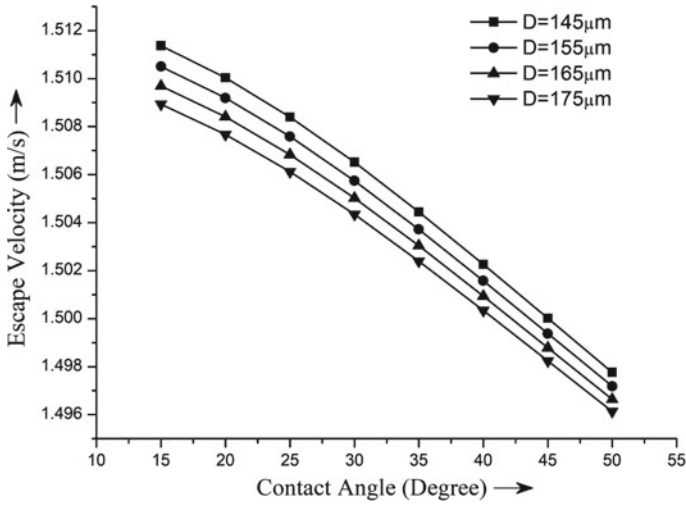


Fig. 7 Escape velocity versus contact angle for  $\beta = 30^\circ$

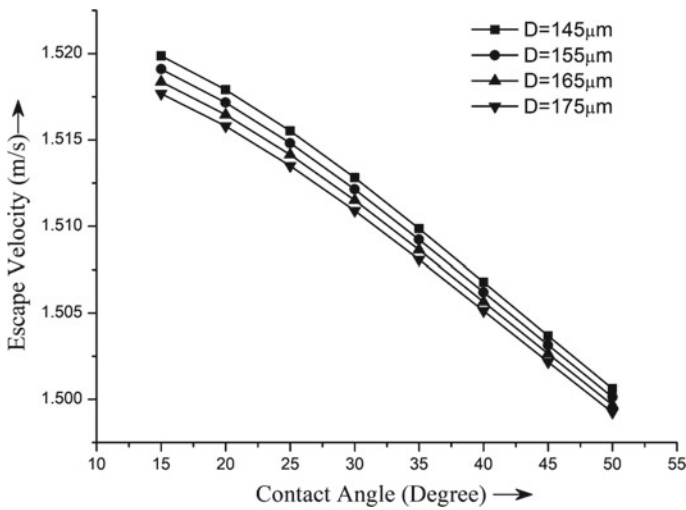


Fig. 8 Escape velocity versus contact angle for  $\beta = 45^\circ$

## 4 Conclusions

Conclusions that can be drawn from the present analysis are as follows:

- It is clear that the contact angle has an adverse effect on soil grain escape velocity. This is because higher contact reduces the capillary pressure weakening the capillary action. This results in reduction in soil grain escape velocity. This, in turn, enhances the riverbank erosion in macro-scale.
- Inter-granular distance has a negative impact on soil grain escape velocity. As the gap between the soil grains increases, capillary cohesion between the grains drops.
- While comparing the conditions of water level rising and falling, it is found that the soil grain escape velocity is less in falling condition. This is because the negative moment helps the grain to get dislodged from the bank surface during fall of water level.
- Water content index angle has a positive impact on the soil grain escape velocity. Increase in the water contact index angle increases the wetted surface area, which enhances the binding force between two grains. This increases the escape velocity of the soil grain and reduces the erosion of the bank surface.

## References

1. Odgaard AJ, Mosconi CE (1987) Streambank protection by submerged vanes. *J Hydraul Eng ASCE* 113(4):520–536
2. Carroll RWH, Warwick JJ, James AI, Miller JR (2004) Modeling erosion and overbank deposition during extreme floods conditions on carson river Nevada. *J Hydrol* 297(1–4):1–21
3. El Kadi AK, Moran AD, Mosselman E, Bouchard JP, Habersack H, Aelbrecht D (2014) A physical, movable-bed model for non-uniform sediment transport, fluvial erosion and bank failure in rivers. *J Hydro-Environ Res* 8(2):95–114
4. Mukherjee S, Mazumdar A (2010) Study of effect of the variation of inter-particle distance on the erodibility of a riverbank under cohesion with a new model. *J Hydro-Environ Res* 4(3):235–242
5. Darby SE, Thorne CR (1996) Stability analysis for steep, eroding, cohesive riverbanks. *J Hydraul Eng* 122:443–454
6. Osman AM, Thorne CR (1988) Riverbank stability analysis, I: theory. *J Hydraul Eng* 114(2):134–150
7. Soulie F, El Youssoufi MS, Cherblanc F, Saix C (2006) Capillary cohesion and mechanical strength of polydisperse granular materials. *Eur Phys J E* 21:349–357
8. Duan JG (2005) Analytical approach to calculate rate of bank erosion. *J Hydraul Eng* 131(11):980–990
9. Poorni S, Miglani R, Srinivasan MR, Indira R (2009) Comparative evaluation of the surface tension and the ph of calcium hydroxide mixed with five different vehicles: an in vitro study. *Indian J Dent Res* 20(1):17–20
10. Bakker DP, Klijnstra JW, Busscher HJ, Van der Mei HC (2003) The effect of dissolved organic carbon on bacterial adhesion to conditioning films adsorbed on glass from natural seawater collected during different seasons. *Biofouling* 19(6):391–397
11. Mu F, Su X (2007) Analysis of liquid bridge between spherical particles. *China Particool* 5:420–424
12. Likos JW, Lu N (2–5 Jun 2002) Hysteresis of capillary cohesion in unsaturated soils. 15th ASCE Engineering Mechanics Conference. New York, Columbia University, pp 1–8

# Optimizing Irrigation Requirement of Soil Test-Based Fertilizer Recommendation Models for Targeted Yields of Cabbage and Broccoli in a Typic Fluvaquept Soil



Kallol Bhattacharyya, Agnibha Sinha, Sudip Sengupta, Shubhadip Dasgupta, Sanmay Kumar Patra, Pradip Dey, and Debasis Mazumdar

**Abstract** Yield target-based fertilizer recommendation, on the basis of soil test values, remained the most logical platform which avoids possibilities of over application of fertilizers and related environmental pollution. This model is successful with assured irrigation and good crop management. The arsenic pollution of the groundwater and risk of accumulation of the pollutant in crops through irrigation water drives us to relook to further optimization of irrigation requirement without compromising yields significantly. In this purview, an attempt has been made in the present study, to manipulate moisture flexibility in yield target-based fertilizer recommendation models. Field experiments were conducted in a *Typic Fluvaquept* soil (23°N, 89°E) of West Bengal, India, with broccoli and cabbage in two consecutive winters of 2015–16 and 2016–17. With due cognizance of STCR recommended NPK doses, elevated and reduced fertilizer levels were administered across varied available soil moisture deficits (ASMD). To assume a possible crisp crop–nutrient–moisture relationship, we adopted the fuzzy linear regression model. Yields of broccoli and cabbage under applied nutrient and moisture interventions ranged from 3.90 (no fertilizer, 60% ASMD)—21.8 (NPK-285:40:115; 40% ASMD)  $\text{tha}^{-1}$  and 14.0 (no fertilizer, 30% ASMD)—84.0 (NPK-350:175:300; 30% ASMD)  $\text{tha}^{-1}$  respectively. The water productivity (WP) also varied widely (from 13.4 to 35.75  $\text{kgm}^{-3}$  in broccoli and 4.57–109.97  $\text{kgm}^{-3}$  in cabbage). Interestingly, a moderate moisture stress was observed to manage a good balance among WP and yield. Such water

---

K. Bhattacharyya · A. Sinha · S. Sengupta (✉) · S. Dasgupta · S. K. Patra  
Department of Agricultural Chemistry and Soil Science, Faculty of Agriculture, Bidhan Chandra Krishi Viswavidyalaya, Mohanpur, Nadia, West Bengal 741252, India

P. Dey  
ICAR-Indian Institute of Soil Science, Nabibagh, Berasia Road, Bhopal, Madhya Pradesh 462038, India

D. Mazumdar  
Department of Agricultural Statistics, Faculty of Agriculture, Bidhan Chandra Krishi Viswavidyalaya, Mohanpur, Nadia, West Bengal 741252, India

flexible fertilizer models designed toward a compromisable yield target may help in rendering environmental safeguard by reducing use of contaminated groundwater.

**Keywords** STCR · Moisture · Fuzzy linear regression modeling · Broccoli · Cabbage

## 1 Introduction

Possibility of “prescription method” of fertilizer use for obtaining high yields, empirical values of nutrient availability from soil and fertilizer was first illustrated by Truog [1]. Field-specific balanced amounts of N, P and K were prescribed based on crop-based estimates of the indigenous supply of N, P and K and by modeling the expected yield response as a function of nutrient interaction [2, 3]. Simple linear model for fertilizer recommendation was first introduced by Ramamoorthy during 1965–67 [4]. Later, Ramamoorthy and Velayutham [5] have elaborated this inductive approach and the soil test crop response (STCR) field design, also quoted by Black [6]. The experimental data from STCR were used for developing fertilizer recommendations for desired yield targets of crops [7–9].

In targeted yield approach, it is assumed that there is a linear relationship between grain yield and nutrient uptake by the crop, as for obtaining a particular yield, the plant must take up a definite amount of nutrients. Once the requirement is known for a given yield level, the fertilizer needed can be estimated taking into consideration the contribution from soil available nutrients [10]. Conceptually, targeted yield equations for fertilizer recommendations on the basis of soil test results are functional where adequate irrigation facilities are available, and such protocols have never been tested in moisture stresses. Imposition of moisture stresses has pronounced effect on nutrient availabilities either from native or from applied fertilizers [11]. Consequently, there may be chances of over/under-estimation of fertilizer prescriptions through soil test-based targeted yield equations until moisture component is considered when the model equations are generated. No attempt was taken in any level to incorporate the moisture component in conjunction with fertilizer for developing prescription equations. But rational fertilizer rate was determined to a large extent by soil water supply. Bolton [12] suggested a recommendation rate of N fertilizer for wheat based on precipitation. It is evident that there is an intense interaction between available water and fertilizer, and one being changed will likewise lead to the change of the other [13]. For promoting water and nutrient to fully play their role, one of the important things is to fully understand and utilize water-nutrient positive interaction [14, 15].

Full potentiality of such model equations is, thus, unexplored and achieving fixed target in many cases remained inconsistent. The present investigation will make a modest attempt to include the soil moisture as a factor in the conventional STCR-based fertilizer adjustment equations to extract the full advantage of such equations by increasing the efficiencies of fertilizer and water in upcoming climate change

scenario. This study further aims at addressing the priorities of environmental safeguard as well. Optimizing the levels of irrigation water ensures better use efficiency of the nutrients and minimizes percolation loss of nitrate and other nutrients to groundwater aquifer and pollution thereof. Further, the current study area lies in a zone deeply ravaged by arsenic contamination. The high water use by the crops renders entry of the contaminant into soil–plant–human food chain continuum [16]; thus, optimizing the crop water requirement in the arsenic endemic zone can obtain greater dividends.

Cabbage (*Brassica oleracea* var. *capitata*) is an important winter season vegetable grown throughout the country. It is one of the most important energy vegetable crops throughout the world and consumed fresh as salad and cooked as vegetable or utilized as processed product. West Bengal is the largest producer of cabbage (2207.24 MT) with a productivity of 28.10% and occupies 20.7% of the total cabbage growing area; Nadia is the second leading cabbage-producing district and accounts 16% of the total cabbage-growing area [17]. India is the second largest cauliflower- and broccoli-producing country next to China, accounting 36% of the world's production [17]. Realizing the tremendous potential of broccoli (*Brassica oleracea* var. *italica*) in domestic and foreign markets, the cauliflower growers of Terai zone of West Bengal, India, are gradually adopting the broccoli cultivation [18].

Considering the present importance and future prospects, we have selected these two vegetables for our experiment with existing STCR-based targeted yield equation to address the importance of balancing moisture and nutrient component for augmenting agricultural productivity while safeguarding the environment through nutrient and water use efficiency under varying levels of moisture and operative fertilizer-moisture-yield equations for selected vegetables in a Typic Fluvaquept soil.

## 2 Materials and Methods

### 2.1 Selection of Experimental Site

Field experiments were conducted in Research Farm of Bidhan Chandra Krishi Viswavidyalaya (latitude 23°N and longitude 89°E) with broccoli in 2015–16 and with cabbage in 2016–17 to develop fertilizer adjustment (targeted yield) equations flexible to available moisture in soil. The initially collected soil sample was air-dried, ground and stored in packet, and various physico-chemical characterizations of the soil were carried out following their standard methodologies. The surface soil (0–15 cm) of this research site is characterized by sandy clay loam texture (*Typic Fluvaquept*) with about 24.49% clay [19], a neutral pH (7.2) and electrical conductivity (EC) of 0.35 dSm<sup>-1</sup> [24] and medium range of oxidizable organic carbon (0.72%) [20]. Further, the soil has low-to-medium levels of plant-available alkaline potassium permanganate (KMnO<sub>4</sub>-N) nitrogen [21] varied 190–225 kg ha<sup>-1</sup>; Olsen extracted (NaHCO<sub>3</sub>-P) phosphorus [22] from 15–22 kg ha<sup>-1</sup> and ammonium acetate

extracted (NH<sub>4</sub>OAc-K) potassium [23] from 140 to 155 kg ha<sup>-1</sup>. The study area represents sub-humid tropic where the average annual rainfall usually diverges from 1200 to 1500 mm, relative humidity from 36 to 85%, and the maximum and minimum temperature by average is about 37.5 °C and 12 °C.

## 2.2 Experimental Details

The soil of the experimental field pertains to New Alluvial Zone of West Bengal is characterized by good drainage and water holding capacity. Elevated and reduced levels of NPK fertilizers were administered along with standard (STCR recommended) levels to both the vegetables which were simultaneously subjected to varied levels of available soil moisture deficits (ASMD). The available moisture of the experimental plots was determined with an AQUAPRO sensor-based soil moisture meter every day, and moisture stresses were allowed up to 20/30, 40/50 and 60/70 per cent available moisture for broccoli/cabbage. The available moisture has been calculated on the basis of values of field capacity (20.07% w/w) and permanent wilting point (9.54% w/w) determined in priori of the experiments. The standard levels of N, P and K fertilizers were applied based on STCR-recommended doses calculated on the basis of the targeted yield equations: FN = 1.24 T- 0.45SN; FP<sub>2</sub>O<sub>5</sub> = 0.47 T- 0.23SP and FK<sub>2</sub>O = 0.53 T- 0.16SK [for broccoli (cv. Centauro)] and FN = 0.79 T- 0.56SN; FP<sub>2</sub>O<sub>5</sub> = 0.68 T- 0.30SP; FK<sub>2</sub>O = 0.64 T- 0.16SK [for cabbage (cv. Millennium 101)]. Apart from the standard fertilizer dose of 285:60:115 kg ha<sup>-1</sup> for broccoli and 350:175:300 kg ha<sup>-1</sup> for cabbage, two lower levels of fertilizers, viz. 200:40:70 and 250:50:90 kg ha<sup>-1</sup> for broccoli and 250:100:200 and 300:125:250 kg ha<sup>-1</sup> for cabbage (designated as N<sub>1</sub>,P<sub>1</sub>,K<sub>1</sub> and N<sub>2</sub>,P<sub>2</sub>,K<sub>2</sub>) and one higher level of fertilizer 325:75:140 kg ha<sup>-1</sup> for broccoli and 400:200:350 kg ha<sup>-1</sup> for cabbage (designated as N<sub>3</sub>,P<sub>3</sub>,K<sub>3</sub>), were employed in 15 different combinations of 3 m × 4 m plots. The same 15 combinations were subjected to normal irrigation and moisture stresses of 20%, 40% and 60% ASMD for broccoli and 30, 50 and 70% ASMD for cabbage. Half of N and full dose of P and K (broccoli) and one-third of N and full dose of P and K (cabbage) were applied as basal, while the remaining N was applied in 1 and 2 split doses for broccoli and cabbage, respectively.

## 2.3 Irrigation Water Use and Potential Arsenic Entry

Employing stress condition to the cultivated crops resulted in a decrease in the number of irrigations and corresponding water use as elucidated in Table 1. Consequently for a specific concentration of arsenic in irrigation water of the site, the potential entry of the carcinogen arsenic into the plant system was calculated by multiplying the arsenic concentration with the total water use by the two crops under study.

**Table 1** Irrigation and water use by the crops

| Broccoli (2015–16) |           |          |          |          |
|--------------------|-----------|----------|----------|----------|
|                    | No stress | 20% ASMD | 40% ASMD | 60% ASMD |
| No of irrigation   | 5         | 4        | 2        | 1        |
| Water use (ha-mm)  | 310       | 248      | 124      | 59       |
| Cabbage (2016–17)  |           |          |          |          |
|                    | No stress | 30% ASMD | 50% ASMD | 70% ASMD |
| No of irrigation   | 6         | 4        | 2        | 1        |
| Water use (ha-mm)  | 350       | 235      | 117      | 55       |

## 2.4 Sampling of Plants and Analytical Techniques Adopted

Plant samples of broccoli/cabbage were collected at three sampling stages (45/48 DAT, 75/60 DAT and 86/92 DAT). Heads were harvested from the area earmarked for yield recording of each plot at maturity, and economic yield was recorded in  $\text{tha}^{-1}$ . Plant samples were dried, ground and analyzed for accumulation/uptake of nutrients. Total N was estimated by digesting plant samples with concentrated  $\text{H}_2\text{SO}_4$  accelerated with a digestion mixture for 1-2 h at  $420^\circ\text{C}$  and back-titrated with 0.005 N  $\text{H}_2\text{SO}_4$ . For total plant P and K measured, amount of plant samples was digested with tri-acid mixture ( $\text{HNO}_3$ :  $\text{H}_2\text{SO}_4$ :  $\text{HClO}_4$ :: 10:1:4), filtered and analyzed through a standard spectrophotometer or flame photometer, respectively, following Jackson [24]. A number of efficiency parameters have been determined while categorizing the experiment, viz.

### a. Nutrient Use Efficiency [25, 26]

Agronomic efficiency (AE)  $\cong$  kg crop yield increase per kg nutrient applied.  
 Partial factor productivity (PFP)  $\cong$  kg crop yield per kg nutrient applied.

### b. Water Productivity

Estimates of water productivity are appearing with increasing frequency in the issues relating to water management and water policy. Water productivity is crop (economic) yield per volume of water supplied or used, say,  $\text{kg m}^{-3}$  or  $\text{kg ha}^{-1} \text{mm}^{-1}$  [27].

## 2.5 Development of Targeted Yield Equation Under Simulated Moisture Domains Through Linear Regression Models

Although linear regression has many applications, problems can occur when observations are inadequate (small dataset), vagueness of the relationship between input and



output variables, ambiguity of events or degree to which they occur and inaccuracy and distortion introduced by linearization.

Development of targeted yield equation through soil test crop response correlation has been postulated by Ramamoorthy [28] through multiple linear regression relationship of targeted yield with soil–plant–fertilizer indices under assured irrigation. We assumed that subjecting such models to simulated moisture stresses (domains) may lead to vagueness of the relationship of targeted yield with soil–fertilizer–plant parameters, and outputs may not be crisp as it was in the previous model. Due to the assumption of crisp relationship, some information may be lost; therefore, the technique “fuzzy regression” is well suited to this type of situation which can be applied to solve agricultural problems [29].

Fuzzy regression analysis [30] is an extension of the classical regression analysis that is used in evaluating the functional relationship between the dependent and independent variables in a fuzzy environment. In general, fuzzy regression models the input and output data are fuzzy, the relationship between the input and output data is given by a fuzzy function and the distribution of the data is probabilistic. In the usual regression model, deviations between the observed values and the estimated values are supposed to be due to observation errors. We assume, on the contrary, that these deviations depend on the indefiniteness of the system structure. We regard these deviations as the fuzziness of system parameters. In fuzzy regression methodology, parameters are estimated by minimizing total vagueness in the model, i.e., sum of radii of predicted intervals. Simplex procedure [31] is usually employed to minimize such vagueness of the linear programming.

In the present experiment, the multiple linear and fuzzy linear regressions for dependent variable yield with soil nutrient, fertilizer nutrient and volumetric moisture content were generated through Statistical Analysis System (SAS version 9.2) in OPTMODEL linear programming module. In order to compare performance of both approaches, viz. multiple linear regression methodology and fuzzy regression methodology, width of prediction intervals corresponding to each observed value of response variable is computed.

### 3 Results and Discussion

#### 3.1 *Crop Nitrogen Dynamics Under Simulated Moisture Condition*

The availabilities of nitrogen and accumulation by broccoli and cabbage, subjected to simulated moisture stresses and administered with graded doses of NPK fertilizers, have been recorded in Table 2. We observed better N availabilities in soil and utilization by both broccoli and cabbage with limited water stresses (20/30% ASMD). The nitrogen use efficiencies (NUE) in terms of partial factor productivity (PFP) and agronomic efficiencies (AEs) of broccoli and cabbage under influence of graded doses

**Table 2** Effect of simulated moisture situations and graded doses of fertilizer application on nutrient uptake by broccoli and cabbage at harvest

|                                     | Broccoli                 |                          |                          |                                     | Cabbage                  |                          |                          |
|-------------------------------------|--------------------------|--------------------------|--------------------------|-------------------------------------|--------------------------|--------------------------|--------------------------|
|                                     | N uptake (kg $ha^{-1}$ ) | P uptake (kg $ha^{-1}$ ) | K uptake (kg $ha^{-1}$ ) |                                     | N uptake (kg $ha^{-1}$ ) | P uptake (kg $ha^{-1}$ ) | K uptake (kg $ha^{-1}$ ) |
| No Stress                           | 94.05                    | 10.82                    | 73.58                    | No Stress                           | 137.97                   | 7.37                     | 131.10                   |
| 20% ASMD                            | 99.48                    | 10.15                    | 82.88                    | 30% ASMD                            | 124.47                   | 6.87                     | 127.65                   |
| 40% ASMD                            | 102.31                   | 11.40                    | 85.58                    | 50% ASMD                            | 100.78                   | 5.23                     | 104.24                   |
| 60% ASMD                            | 77.01                    | 6.51                     | 60.55                    | 70% ASMD                            | 95.22                    | 4.98                     | 79.00                    |
| <b><i>SEm</i>(<math>\pm</math>)</b> | <b>3.264</b>             | <b>1.108</b>             | <b>4.621</b>             | <b><i>SEm</i>(<math>\pm</math>)</b> | <b>3.66</b>              | <b>0.37</b>              | <b>4.50</b>              |
| <b><i>CD at 5%</i></b>              | <b>11.293</b>            | <b>NS</b>                | <b>15.991</b>            | <b><i>CD at 5%</i></b>              | <b>12.67</b>             | <b>1.29</b>              | <b>15.59</b>             |
| N0P0K0                              | 24.96                    | 2.11                     | 19.77                    | N0P0K0                              | 26.06                    | 1.39                     | 23.47                    |
| N0PSKS                              | 27.92                    | 3.78                     | 21.48                    | N0PSKS                              | 26.04                    | 2.05                     | 29.99                    |
| N1PSKS                              | 95.49                    | 10.83                    | 82.11                    | N1PSKS                              | 113.35                   | 6.03                     | 130.91                   |
| N2PSKS                              | 103.23                   | 8.00                     | 89.62                    | N2PSKS                              | 143.38                   | 7.90                     | 131.89                   |
| N3PSKS                              | 115.32                   | 12.71                    | 75.75                    | N3PSKS                              | 154.24                   | 6.12                     | 146.83                   |
| NSP0KS                              | 107.18                   | 10.66                    | 79.53                    | NSP0KS                              | 134.49                   | 7.17                     | 128.03                   |
| NSP1KS                              | 98.85                    | 13.39                    | 78.45                    | NSP1KS                              | 121.24                   | 4.64                     | 114.05                   |
| NSP2KS                              | 99.66                    | 12.35                    | 89.78                    | NSP2KS                              | 115.16                   | 5.09                     | 92.37                    |
| NSP3KS                              | 105.88                   | 14.93                    | 74.30                    | NSP3KS                              | 122.12                   | 8.74                     | 122.37                   |
| NSPSK0                              | 99.71                    | 8.90                     | 87.95                    | NSPSK0                              | 111.71                   | 5.68                     | 66.09                    |
| NSPSK1                              | 106.00                   | 9.53                     | 87.51                    | NSPSK1                              | 132.96                   | 7.69                     | 146.63                   |
| NSPSK2                              | 99.50                    | 9.74                     | 90.87                    | NSPSK2                              | 129.05                   | 7.39                     | 124.89                   |
| NSPSK3                              | 108.72                   | 8.85                     | 92.81                    | NSPSK3                              | 150.11                   | 7.52                     | 161.06                   |
| NSPSKS                              | 112.63                   | 10.27                    | 89.13                    | NSPSKS                              | 124.58                   | 8.20                     | 128.35                   |
| <b><i>SEm</i>(<math>\pm</math>)</b> | <b>3.048</b>             | <b>1.626</b>             | <b>6.094</b>             | <b><i>SEm</i>(<math>\pm</math>)</b> | <b>12.65</b>             | <b>0.93</b>              | <b>11.060</b>            |
| <b><i>CD at 5%</i></b>              | <b>8.860</b>             | <b>4.728</b>             | <b>17.714</b>            | <b><i>CD at 5%</i></b>              | <b>36.78</b>             | <b>2.71</b>              | <b>32.15</b>             |

of N fertilizer application and imposition of moisture stresses have been presented in Table 3 which is observed to reduce substantially with increasing levels of N fertilizer application while both efficiencies reduced considerably with increasing moisture stress beyond 20/30% ASMD in broccoli and cabbage.

Similar findings suggest that dry conditions substantially reduce crop nitrogen uptake, even if there is presence of mineral N in root vicinity [32]. For any crop, its critical growth stage derives significance, and if proper soil–water storage and thereafter its crop availability are ensured, efficiency of fertilizer and farm resources augment [33]. Cauliflower and broccoli have a high uptake of nitrogen, but their

**Table 3** Partial factor productivity (PFP) and agronomic efficiencies (AE) of broccoli and cabbage under graded levels of NPK fertilizer and simulated moisture stresses

| <i>Broccoli</i> |             |                  |                 |           |                  |                 |           |                  |                 |
|-----------------|-------------|------------------|-----------------|-----------|------------------|-----------------|-----------|------------------|-----------------|
|                 |             | PFP <sub>N</sub> | AE <sub>N</sub> |           | PFP <sub>P</sub> | AE <sub>P</sub> |           | PFP <sub>K</sub> | AE <sub>K</sub> |
| No stress       | <b>N1</b>   | 85.85            | 58.10           | <b>P1</b> | 446.62           | 42.03           | <b>K1</b> | 301.33           | 38.64           |
|                 | <b>N2</b>   | 84.00            | 47.28           | <b>P2</b> | 399.00           | 31.66           | <b>K2</b> | 248.79           | 29.91           |
|                 | <b>NS</b>   | 69.49            | 41.32           | <b>PS</b> | 366.40           | 31.36           | <b>KS</b> | 208.17           | 25.65           |
|                 | <b>N3</b>   | 54.38            | 37.30           | <b>P3</b> | 248.00           | 24.47           | <b>K3</b> | 185.06           | 21.32           |
|                 | <b>Mean</b> | <b>73.43</b>     | <b>46.00</b>    |           | <b>365.01</b>    | <b>32.38</b>    |           | <b>235.84</b>    | <b>28.88</b>    |
| 20%ASMD         | <b>N1</b>   | 87.62            | 60.42           | <b>P1</b> | 434.00           | 55.54           | <b>K1</b> | 256.98           | 36.28           |
|                 | <b>N2</b>   | 81.22            | 58.23           | <b>P2</b> | 407.23           | 48.23           | <b>K2</b> | 206.80           | 32.23           |
|                 | <b>NS</b>   | 75.52            | 56.43           | <b>PS</b> | 358.71           | 42.55           | <b>KS</b> | 187.16           | 28.91           |
|                 | <b>N3</b>   | 69.31            | 35.85           | <b>P3</b> | 307.77           | 33.45           | <b>K3</b> | 144.54           | 22.62           |
|                 | <b>Mean</b> | <b>78.42</b>     | <b>52.73</b>    |           | <b>376.93</b>    | <b>44.94</b>    |           | <b>198.87</b>    | <b>30.01</b>    |
| 40%ASMD         | <b>N1</b>   | 83.32            | 51.12           | <b>P1</b> | 412.37           | 32.12           | <b>K1</b> | 257.43           | 24.43           |
|                 | <b>N2</b>   | 78.67            | 47.33           | <b>P2</b> | 386.98           | 28.57           | <b>K2</b> | 219.39           | 22.32           |
|                 | <b>NS</b>   | 71.45            | 40.11           | <b>PS</b> | 339.38           | 22.12           | <b>KS</b> | 177.07           | 21.14           |
|                 | <b>N3</b>   | 62.36            | 36.35           | <b>P3</b> | 286.90           | 18.35           | <b>K3</b> | 132.47           | 19.18           |
|                 | <b>Mean</b> | <b>73.95</b>     | <b>43.73</b>    |           | <b>356.41</b>    | <b>25.29</b>    |           | <b>196.59</b>    | <b>21.77</b>    |
| 60%ASMD         | <b>N1</b>   | 100.47           | 41.42           | <b>P1</b> | 416.75           | 24.23           | <b>K1</b> | 244.94           | 29.51           |
|                 | <b>N2</b>   | 74.00            | 36.16           | <b>P2</b> | 287.14           | 20.78           | <b>K2</b> | 183.00           | 22.78           |
|                 | <b>NS</b>   | 62.04            | 30.83           | <b>PS</b> | 351.52           | 17.59           | <b>KS</b> | 183.40           | 21.98           |
|                 | <b>N3</b>   | 41.52            | 27.09           | <b>P3</b> | 205.06           | 12.31           | <b>K3</b> | 124.70           | 18.14           |
|                 | <b>Mean</b> | <b>69.51</b>     | <b>33.88</b>    |           | <b>315.12</b>    | <b>18.73</b>    |           | <b>184.01</b>    | <b>23.10</b>    |
| <i>Cabbage</i>  |             |                  |                 |           |                  |                 |           |                  |                 |
|                 |             | PFP <sub>N</sub> | AE <sub>N</sub> |           | PFP <sub>P</sub> | AE <sub>P</sub> |           | PFP <sub>K</sub> | AE <sub>K</sub> |
| No stress       | <b>N1</b>   | 280.00           | 206.40          | <b>P1</b> | 714.29           | 42.23           | <b>K1</b> | 391.32           | 39.87           |
|                 | <b>N2</b>   | 223.26           | 161.92          | <b>P2</b> | 533.43           | 39.35           | <b>K2</b> | 348.46           | 38.33           |
|                 | <b>NS</b>   | 193.02           | 140.45          | <b>PS</b> | 386.04           | 40.52           | <b>KS</b> | 225.19           | 34.58           |
|                 | <b>N3</b>   | 194.44           | 148.44          | <b>P3</b> | 344.00           | 38.33           | <b>K3</b> | 228.57           | 31.29           |
|                 | <b>Mean</b> | <b>222.68</b>    | <b>164.30</b>   |           | <b>494.44</b>    | <b>40.11</b>    |           | <b>298.39</b>    | <b>36.02</b>    |
| 30%ASMD         | <b>N1</b>   | 257.97           | 200.37          | <b>P1</b> | 600.00           | 63.23           | <b>K1</b> | 276.61           | 48.11           |
|                 | <b>N2</b>   | 240.00           | 198.86          | <b>P2</b> | 564.78           | 59.87           | <b>K2</b> | 173.06           | 45.77           |
|                 | <b>NS</b>   | 235.90           | 187.90          | <b>PS</b> | 531.74           | 51.45           | <b>KS</b> | 280.00           | 39.55           |
|                 | <b>N3</b>   | 212.32           | 141.27          | <b>P3</b> | 316.68           | 48.37           | <b>K3</b> | 190.47           | 40.32           |
|                 | <b>Mean</b> | <b>236.55</b>    | <b>182.10</b>   |           | <b>503.30</b>    | <b>55.73</b>    |           | <b>230.04</b>    | <b>43.44</b>    |
| 50%ASMD         | <b>N1</b>   | 192.00           | 135.00          | <b>P1</b> | 440.00           | 54.63           | <b>K1</b> | 308.00           | 48.55           |
|                 | <b>N2</b>   | 173.33           | 128.00          | <b>P2</b> | 389.97           | 41.11           | <b>K2</b> | 227.20           | 42.11           |

(continued)

**Table 3** (continued)

| <i>Broccoli</i> |             |                  |                 |           |                  |                 |           |                  |                 |
|-----------------|-------------|------------------|-----------------|-----------|------------------|-----------------|-----------|------------------|-----------------|
|                 |             | PFP <sub>N</sub> | AE <sub>N</sub> |           | PFP <sub>P</sub> | AE <sub>P</sub> |           | PFP <sub>K</sub> | AE <sub>K</sub> |
|                 | <b>NS</b>   | 148.57           | 120.00          | <b>PS</b> | 345.67           | 32.48           | <b>KS</b> | 173.33           | 30.03           |
|                 | <b>N3</b>   | 135.67           | 102.86          | <b>P3</b> | 224.50           | 28.63           | <b>K3</b> | 171.43           | 24.12           |
|                 | <b>Mean</b> | <b>162.39</b>    | <b>116.95</b>   |           | <b>350.04</b>    | <b>39.21</b>    |           | <b>219.99</b>    | <b>36.20</b>    |
| 70%ASMD         | <b>N1</b>   | 166.54           | 136.00          | <b>P1</b> | 445.65           | 28.75           | <b>K1</b> | 280.00           | 23.67           |
|                 | <b>N2</b>   | 162.14           | 108.27          | <b>P2</b> | 333.49           | 22.32           | <b>K2</b> | 233.06           | 21.41           |
|                 | <b>NS</b>   | 156.27           | 102.00          | <b>PS</b> | 312.53           | 18.58           | <b>KS</b> | 182.31           | 17.58           |
|                 | <b>N3</b>   | 148.00           | 92.94           | <b>P3</b> | 302.43           | 19.23           | <b>K3</b> | 171.43           | 18.23           |
|                 | <b>Mean</b> | <b>158.24</b>    | <b>92.94</b>    |           | <b>348.53</b>    | <b>22.22</b>    |           | <b>216.70</b>    | <b>20.22</b>    |

nitrogen conversion to produce is less than cabbage and Brussels sprouts [34]. Westerman and Tucker [35] suggested under moist period, mineral N of soil reduces extensively possibly either due to microbial immobilization or atmospheric loss. Better N availabilities (and utilization) at limited level of water stress followed by irrigation may be attributed to an activated mineralization by sudden water availability after a dry spell [42]. Dry period results in the death of plant roots and microbes, elevating the soil organic matter to augment immobilization and nitrification upon rewetting [36]. Clearly based on this, NUE related to Nitrogen Nutrition Index is highly impacted by shortage of moisture. Such effect was visualized in wheat by Fan and Li [13]. Gajri et al. [37] propounded the relationship between N and water to favor better yield, WUE and NUE of crops.

### 3.2 Crop Phosphorus Dynamics Under Simulated Moisture Condition

The availabilities of phosphorus and accumulation by broccoli and cabbage, subjected to simulated moisture stresses and administered with graded doses of NPK fertilizers, have been recorded in Table 2. We observed better P availabilities in soil and utilization by both broccoli and cabbage with limited water stresses (20/30% ASMD). The partial factor productivity (PFP) and agronomic efficiencies (AEs) of broccoli and cabbage under influence of graded doses of P fertilizer application and imposition of moisture stresses have been presented in Table 3 which is observed to reduce substantially with increasing levels of P fertilizer application, while both efficiencies reduced considerably and become least when subjected to moisture stress up to 70% ASMD in cabbage. Both the efficiencies in broccoli did not vary much with increasing moisture stresses and remained least when subjected to moisture stress up to 60% ASMD. Efficiencies (AE and PFP) were maximum in broccoli subjected to moisture stress up to 20% ASMD and in cabbage up to 30% ASMD.

The results reveal P supplementation in water stress can improve crop yield [38]. Similar to nitrogen, the P use efficiency (PUE) and its Nutrition Index are highly impacted by shortage of moisture. Hammond and Broadley [39] propounded water deficit and low P application can improve the PUE. P application to soil reaps the benefits of improved rooting depth and density to favor water and P uptake. This phenomenon further improves WUE and helps the plant to grow optimally even when there is limited availability of moisture [40].

### ***3.3 Crop Potassium Dynamics Under Simulated Moisture Situations***

We observed better K availabilities and utilization by both broccoli and cabbage (Table 2) with limited water stresses (20/30% ASMD). The partial factor productivity (PFP) and agronomic efficiencies (AEs) of broccoli and cabbage under influence of graded doses of K fertilizer application and imposition of moisture stresses have been presented in Table 3 and observed to reduce substantially with increasing levels of K fertilizer application, while both efficiencies reduced considerably with increasing moisture stress. Such efficiencies remained maximum when the broccoli/cabbage was subjected to moisture stresses up to 20/30% ASMD.

Foliar K application is most effective in grain filling stage although its application in other critical stages can also favor crop yield [41]. Better K availabilities (and utilization) at limited level of water stress followed by irrigation may be attributed to an activated mineralization by sudden water availability after dry period [42]. K as a growth promoter performs vital plant physiological functions and often used as an amendment to tide over water stress [43]. Like N and P, KUE and its nutrition index are severely impacted by severe shortage of water. Enhanced uptake of potash fertilizer reduces water loss through transpiration [44].

### ***3.4 Yield and Water Productivity of Broccoli and Cabbage Under Simulated Moisture Situations***

The head and curd yields of broccoli and cabbage as influenced by graded doses of NPK fertilizer application and imposition of moisture stresses have been recorded in Table 4. Increasing doses of NPK fertilizer application significantly increased yields of broccoli heads and cabbage curds. Imposition of moisture stresses up to levels of 40% ASMD in broccoli increased yield significantly, while further intense moisture stress (up to 60% ASMD) reduced the head yield. Cabbage subjected to moisture stress recorded significantly reduced yields from no stress situation. Yields of broccoli and cabbage with varying levels of fertilizer and moisture stresses remained in the range of 3.90 (no fertilizer, 60% ASMD)—21.8 (NPK-285:40:115; 40% ASMD)

**Table 4** Crop–water relations in broccoli and cabbage

| Crop–water relations in broccoli              |  |                            |  | Crop–water relations in cabbage               |  |                            |                          |
|---|--|----------------------------|--|---|--|----------------------------|--------------------------|
| Stress  | Fertilizer                                   | Yield (tha <sup>-1</sup> ) | WP (kg.m <sup>-3</sup> )                     | Stress  | Fertilizer                                   | Yield (tha <sup>-1</sup> ) | WP (kg.m <sup>-3</sup> ) |
| <b>No stress (total water use = 71.43 mm)</b> | N <sub>0</sub> P <sub>0</sub> K <sub>0</sub> | 4.16                       | 1.34   | <b>No stress (total water use = 85.71 mm)</b> | N <sub>0</sub> P <sub>0</sub> K <sub>0</sub> | 16.00                      | 4.57                     |
|   | N <sub>0</sub> P <sub>5</sub> K <sub>5</sub> | 5.55                       | 1.79   |   | N <sub>0</sub> P <sub>5</sub> K <sub>5</sub> | 18.40                      | 5.26                     |
|   | N <sub>1</sub> P <sub>5</sub> K <sub>5</sub> | 17.17                      | 5.54   |   | N <sub>1</sub> P <sub>5</sub> K <sub>5</sub> | 70.00                      | 20.00                    |
|   | N <sub>2</sub> P <sub>5</sub> K <sub>5</sub> | 17.37                      | 5.60   |   | N <sub>2</sub> P <sub>5</sub> K <sub>5</sub> | 66.98                      | 19.14                    |
|   | N <sub>3</sub> P <sub>5</sub> K <sub>5</sub> | 17.67                      | 5.70   |   | N <sub>3</sub> P <sub>5</sub> K <sub>5</sub> | 77.78                      | 22.22                    |
|   | N <sub>5</sub> P <sub>0</sub> K <sub>5</sub> | 17.39                      | 5.61   |   | N <sub>5</sub> P <sub>0</sub> K <sub>5</sub> | 66.67                      | 19.05                    |
|   | N <sub>5</sub> P <sub>1</sub> K <sub>5</sub> | 16.86                      | 5.44   |   | N <sub>5</sub> P <sub>1</sub> K <sub>5</sub> | 71.43                      | 20.41                    |
|   | N <sub>5</sub> P <sub>2</sub> K <sub>5</sub> | 17.92                      | 5.78   |   | N <sub>5</sub> P <sub>2</sub> K <sub>5</sub> | 64.68                      | 18.48                    |
|   | N <sub>5</sub> P <sub>3</sub> K <sub>5</sub> | 16.00                      | 5.16   |   | N <sub>5</sub> P <sub>3</sub> K <sub>5</sub> | 68.80                      | 19.66                    |
|   | N <sub>5</sub> P <sub>5</sub> K <sub>0</sub> | 20.50                      | 6.61   |   | N <sub>5</sub> P <sub>5</sub> K <sub>0</sub> | 60.00                      | 17.14                    |
|   | N <sub>5</sub> P <sub>5</sub> K <sub>1</sub> | 20.09                      | 6.48   |   | N <sub>5</sub> P <sub>5</sub> K <sub>1</sub> | 78.26                      | 22.36                    |
|   | N <sub>5</sub> P <sub>5</sub> K <sub>2</sub> | 17.39                      | 5.61   |   | N <sub>5</sub> P <sub>5</sub> K <sub>2</sub> | 87.11                      | 24.89                    |
|   | N <sub>5</sub> P <sub>5</sub> K <sub>3</sub> | 18.91                      | 6.10   |   | N <sub>5</sub> P <sub>5</sub> K <sub>3</sub> | 80.00                      | 22.86                    |
| N <sub>5</sub> P <sub>5</sub> K <sub>5</sub>  | 18.94  | 6.11                       | N <sub>5</sub> P <sub>5</sub> K <sub>5</sub> | 67.56   | 19.30  |                            |                          |
| <b>Mean</b>                                   | <b>16.14</b>                                 | <b>5.21</b>                |  | <b>Mean</b>                                   | <b>63.83</b>                                 | <b>18.24</b>               |                          |
| <b>20% ASMD (total water use = 57.14 mm)</b>  | N <sub>0</sub> P <sub>0</sub> K <sub>0</sub> | 5.76                       | 2.32   | <b>30% ASMD (total water use = 57.14 mm)</b>  | N <sub>0</sub> P <sub>0</sub> K <sub>0</sub> | 14.00                      | 5.96                     |
|   | N <sub>0</sub> P <sub>5</sub> K <sub>5</sub> | 5.44                       | 2.19   |   | N <sub>0</sub> P <sub>5</sub> K <sub>5</sub> | 14.40                      | 6.13                     |
|   | N <sub>1</sub> P <sub>5</sub> K <sub>5</sub> | 17.52                      | 7.07   |   | N <sub>1</sub> P <sub>5</sub> K <sub>5</sub> | 64.49                      | 27.44                    |
|   | N <sub>2</sub> P <sub>5</sub> K <sub>5</sub> | 19.06                      | 7.69   |   | N <sub>2</sub> P <sub>5</sub> K <sub>5</sub> | 70.77                      | 30.12                    |
|   | N <sub>3</sub> P <sub>5</sub> K <sub>5</sub> | 17.09                      | 6.89   |   | N <sub>3</sub> P <sub>5</sub> K <sub>5</sub> | 70.91                      | 30.17                    |
|   | N <sub>5</sub> P <sub>0</sub> K <sub>5</sub> | 20.11                      | 8.11   |   | N <sub>5</sub> P <sub>0</sub> K <sub>5</sub> | 80.00                      | 34.04                    |
|   | N <sub>5</sub> P <sub>1</sub> K <sub>5</sub> | 15.67                      | 6.32   |   | N <sub>5</sub> P <sub>1</sub> K <sub>5</sub> | 60.00                      | 25.53                    |
|   | N <sub>5</sub> P <sub>2</sub> K <sub>5</sub> | 17.36                      | 7.00   |   | N <sub>5</sub> P <sub>2</sub> K <sub>5</sub> | 58.34                      | 24.82                    |
|   | N <sub>5</sub> P <sub>3</sub> K <sub>5</sub> | 20.68                      | 8.34   |   | N <sub>5</sub> P <sub>3</sub> K <sub>5</sub> | 63.34                      | 26.95                    |
|   | N <sub>5</sub> P <sub>5</sub> K <sub>0</sub> | 17.95                      | 7.24   |   | N <sub>5</sub> P <sub>5</sub> K <sub>0</sub> | 43.26                      | 18.41                    |
|   | N <sub>5</sub> P <sub>5</sub> K <sub>1</sub> | 17.49                      | 7.05   |   | N <sub>5</sub> P <sub>5</sub> K <sub>1</sub> | 55.32                      | 23.54                    |
|   | N <sub>5</sub> P <sub>5</sub> K <sub>2</sub> | 18.61                      | 7.50   |   | N <sub>5</sub> P <sub>5</sub> K <sub>2</sub> | 34.89                      | 14.85                    |
|   | N <sub>5</sub> P <sub>5</sub> K <sub>3</sub> | 20.24                      | 8.16   |   | N <sub>5</sub> P <sub>5</sub> K <sub>3</sub> | 66.66                      | 28.37                    |
| N <sub>5</sub> P <sub>5</sub> K <sub>5</sub>  | 17.52  | 7.07                       | N <sub>5</sub> P <sub>5</sub> K <sub>5</sub> | 84.00   | 35.74  |                            |                          |
| <b>Mean</b>                                   | <b>16.46</b>                                 | <b>6.64</b>                |  | <b>Mean</b>                                   | <b>55.74</b>                                 | <b>23.72</b>               |                          |
| <b>40% ASMD (total water use = 28.57 mm)</b>  | N <sub>0</sub> P <sub>0</sub> K <sub>0</sub> | 4.48                       | 3.61   | <b>50% ASMD (total water use = 28.57 mm)</b>  | N <sub>0</sub> P <sub>0</sub> K <sub>0</sub> | 14.80                      | 12.65                    |
|   | N <sub>0</sub> P <sub>5</sub> K <sub>5</sub> | 5.55                       | 4.48   |   | N <sub>0</sub> P <sub>5</sub> K <sub>5</sub> | 16.00                      | 13.68                    |
|   | N <sub>1</sub> P <sub>5</sub> K <sub>5</sub> | 19.00                      | 15.32  |   | N <sub>1</sub> P <sub>5</sub> K <sub>5</sub> | 48.00                      | 41.03                    |
|   | N <sub>2</sub> P <sub>5</sub> K <sub>5</sub> | 19.67                      | 15.86  |   | N <sub>2</sub> P <sub>5</sub> K <sub>5</sub> | 52.00                      | 44.44                    |

(continued)

**Table 4** (continued)

| Crop–water relations in broccoli             |  |                            |                          | Crop–water relations in cabbage              |  |                            |                          |
|--|--|----------------------------|--------------------------|--|--|----------------------------|--------------------------|
| Stress                                       | Fertilizer                                   | Yield (tha <sup>-1</sup> ) | WP (kg.m <sup>-3</sup> ) | Stress                                       | Fertilizer                                   | Yield (tha <sup>-1</sup> ) | WP (kg.m <sup>-3</sup> ) |
|  | N <sub>3</sub> P <sub>5</sub> K <sub>5</sub> | 20.27                      | 16.34                    |  | N <sub>3</sub> P <sub>5</sub> K <sub>5</sub> | 70.00                      | 59.83                    |
|  | N <sub>5</sub> P <sub>0</sub> K <sub>5</sub> | 19.20                      | 15.48                    |  | N <sub>5</sub> P <sub>0</sub> K <sub>5</sub> | 36.00                      | 30.77                    |
|  | N <sub>5</sub> P <sub>1</sub> K <sub>5</sub> | 21.85                      | 17.62                    |  | N <sub>5</sub> P <sub>1</sub> K <sub>5</sub> | 44.00                      | 37.61                    |
|  | N <sub>5</sub> P <sub>2</sub> K <sub>5</sub> | 19.35                      | 15.60                    |  | N <sub>5</sub> P <sub>2</sub> K <sub>5</sub> | 36.74                      | 31.40                    |
|  | N <sub>5</sub> P <sub>3</sub> K <sub>5</sub> | 21.52                      | 17.35                    |  | N <sub>5</sub> P <sub>3</sub> K <sub>5</sub> | 44.90                      | 38.38                    |
|  | N <sub>5</sub> P <sub>5</sub> K <sub>0</sub> | 17.78                      | 14.34                    |  | N <sub>5</sub> P <sub>5</sub> K <sub>0</sub> | 56.00                      | 47.86                    |
|  | N <sub>5</sub> P <sub>5</sub> K <sub>1</sub> | 16.32                      | 13.16                    |  | N <sub>5</sub> P <sub>5</sub> K <sub>1</sub> | 61.60                      | 52.65                    |
|  | N <sub>5</sub> P <sub>5</sub> K <sub>2</sub> | 19.74                      | 15.92                    |  | N <sub>5</sub> P <sub>5</sub> K <sub>2</sub> | 44.80                      | 38.29                    |
|  | N <sub>5</sub> P <sub>5</sub> K <sub>3</sub> | 18.55                      | 14.96                    |  | N <sub>5</sub> P <sub>5</sub> K <sub>3</sub> | 60.00                      | 51.28                    |
|  | N <sub>5</sub> P <sub>5</sub> K <sub>5</sub> | 20.36                      | 16.42                    |  | N <sub>5</sub> P <sub>5</sub> K <sub>5</sub> | 52.00                      | 44.44                    |
|  | <b>Mean</b>                                  | <b>17.40</b>               | <b>14.03</b>             |  | <b>Mean</b>                                  | <b>45.49</b>               | <b>38.88</b>             |
| <b>60% ASMD (total water use = 14.29 mm)</b> | N <sub>0</sub> P <sub>0</sub> K <sub>0</sub> | 3.90                       | 6.61                     | <b>70% ASMD (total water use = 14.29 mm)</b> | N <sub>0</sub> P <sub>0</sub> K <sub>0</sub> | 16.80                      | 30.55                    |
|  | N <sub>0</sub> P <sub>5</sub> K <sub>5</sub> | 4.95                       | 8.39                     |  | N <sub>0</sub> P <sub>5</sub> K <sub>5</sub> | 18.40                      | 33.45                    |
|  | N <sub>1</sub> P <sub>5</sub> K <sub>5</sub> | 20.09                      | 34.06                    |  | N <sub>1</sub> P <sub>5</sub> K <sub>5</sub> | 41.64                      | 75.70                    |
|  | N <sub>2</sub> P <sub>5</sub> K <sub>5</sub> | 15.51                      | 26.29                    |  | N <sub>2</sub> P <sub>5</sub> K <sub>5</sub> | 59.20                      | 107.64                   |
|  | N <sub>3</sub> P <sub>5</sub> K <sub>5</sub> | 13.49                      | 22.87                    |  | N <sub>3</sub> P <sub>5</sub> K <sub>5</sub> | 59.20                      | 107.64                   |
|  | N <sub>5</sub> P <sub>0</sub> K <sub>5</sub> | 16.76                      | 28.40                    |  | N <sub>5</sub> P <sub>0</sub> K <sub>5</sub> | 54.22                      | 98.58                    |
|  | N <sub>5</sub> P <sub>1</sub> K <sub>5</sub> | 11.48                      | 19.45                    |  | N <sub>5</sub> P <sub>1</sub> K <sub>5</sub> | 56.00                      | 101.82                   |
|  | N <sub>5</sub> P <sub>2</sub> K <sub>5</sub> | 14.36                      | 24.33                    |  | N <sub>5</sub> P <sub>2</sub> K <sub>5</sub> | 60.00                      | 109.09                   |
|  | N <sub>5</sub> P <sub>3</sub> K <sub>5</sub> | 15.38                      | 26.07                    |  | N <sub>5</sub> P <sub>3</sub> K <sub>5</sub> | 60.49                      | 109.97                   |
|  | N <sub>5</sub> P <sub>5</sub> K <sub>0</sub> | 16.16                      | 27.38                    |  | N <sub>5</sub> P <sub>5</sub> K <sub>0</sub> | 56.47                      | 102.68                   |
|  | N <sub>5</sub> P <sub>5</sub> K <sub>1</sub> | 17.15                      | 29.06                    |  | N <sub>5</sub> P <sub>5</sub> K <sub>1</sub> | 52.00                      | 94.55                    |
|  | N <sub>5</sub> P <sub>5</sub> K <sub>2</sub> | 15.08                      | 25.56                    |  | N <sub>5</sub> P <sub>5</sub> K <sub>2</sub> | 58.26                      | 105.94                   |
|  | N <sub>5</sub> P <sub>5</sub> K <sub>3</sub> | 17.46                      | 29.59                    |  | N <sub>5</sub> P <sub>5</sub> K <sub>3</sub> | 60.00                      | 109.09                   |
|  | N <sub>5</sub> P <sub>5</sub> K <sub>5</sub> | 21.09                      | 35.75                    |  | N <sub>5</sub> P <sub>5</sub> K <sub>5</sub> | 54.69                      | 99.44                    |
|  | <b>Mean</b>                                  | <b>14.49</b>               | <b>24.56</b>             |  | <b>Mean</b>                                  | <b>50.53</b>               | <b>91.87</b>             |

tha<sup>-1</sup> and 14.0 (no fertilizer, 30% ASMD)—84.0 (NPK-350:175:300; 30% ASMD) tha<sup>-1</sup>. Deficit irrigation strategy, a practice that deliberately allows crops to sustain some degree of water deficit with marginal yield loss, has the potential to increase water use efficiency and save water [45]. They also observed that implementing deficit irrigation (75% ETC) could save water (16%) although a moderate decrease in yield (12%) and head size is expected.

Productivity of resources is an important issue often characterized as the ratio among its unit output and input. Water productivity (WP) can be expressed in general physical or economic term. The numerator is the sum of the yield of crops, while in

denominator the water input can be used. The observations relating to water productivities of broccoli and cabbage were recorded in Table 4. Observed values for water productivity varied widely as influenced by varying levels of NPK fertilizers and moisture stresses (from 1.34 to 35.75 kg m<sup>-3</sup> in broccoli and 4.57–109.97 kg m<sup>-3</sup> in cabbage). There are many reports that nitrogenous fertilizer enhances water productivity [46]. Moisture stress hugely affected the crop WP as evident in cotton by the study of Prieto and Angueira [47]. Another important study in this regard [48] envisioned positive relation among irrigation and nitrogen that can ultimately favor wheat yield, productivity and NUE. Higher crop water productivity is possible either by increasing production or better use efficiency of water resource. Farmers tend to improve productivity and profitability leaving aside the scope for maximizing water productivity. Thus, the time has come to take a thorough relook into the basics of irrigation science, water management and allocation of basin water resources and transform the agriculture from “maximum irrigation-maximum yield” goals to a more precise and resource-friendly “less irrigation-maximum CWP” policy [49].

### 3.5 Arsenic Uptake by the Selected Crops Under Simulated Moisture Conditions

The biggest advantage in terms of environmental safeguard that the current study can usher is the diminution of the arsenic entry from the water-soil-plant pathway to ultimately the human health continuum. The decrease in the water use of the crops broccoli and cabbage under irrigation at 20, 40, 60% and 30, 50, 70% has been elucidated in Table 1. The total arsenic content of the irrigation water of the site following Sparks et al. [50] was found to be 0.32 mg l<sup>-1</sup>. Accordingly, the lower water use mediated curtailed arsenic load of crop has been presented in Fig. 1.

Water management plays a significant role in controlling arsenic bioavailability in the soil-plant system [51]. Water-saving practices are usually associated with variations in the soil redox status, and the partial flow of oxygen promotes oxidative reduction to arsenite, the highly soluble, bioavailable and toxic form is shrunk [52, 53]. Moreover, the reduction in water application can on a simple sense reduce the

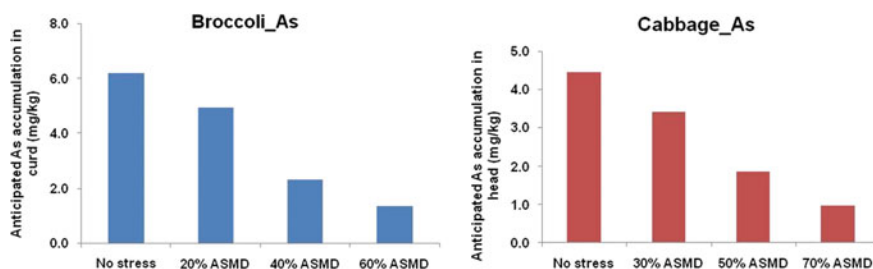


Fig. 1 Percent reduction in anticipated as accumulation in edibles by reducing water use



bulk of flow of arsenic in plant system and thus save the human population from the carcinogen to some extent.

### ***3.6 Generation of Targeted Yield Fertilizer Use Equation Through Linear and Fuzzy Regression Model***

It is known that yield of a crop is a function of several factors, which may be expressed as  $\text{Yield} = f(\text{crop, soil, climate, management})$ . The linear functional relationship between nutrient uptake and yield implicates obtaining of a definite yield. The fertilizer recommendations are usually based on response curves obtained under different soil and climatic conditions. Two different approaches were established to develop model equations for optimizing the N-P-K fertilizers rates. In the first model, a study for optimization of fertilizer doses was performed under graded doses of fertilizers to develop a targeted yield equation model-based fertilizer recommendation for judicious fertilizer application in high nutrient required crop like cabbage and broccoli. Early results established that the relationship between crop yield and the total crop nutrient uptake followed a linear relationship implying that, for obtaining a given yield, a definite quantity of nutrients must be absorbed by the plant. The multiple regression approach had been used to develop relationship between crop yields on one hand, and soil test estimates and fertilizer inputs, on the other. Various combinations of the levels of nitrogen (N), phosphorus (P) and potassium (K) to represent different levels of soil fertility from the field experiments which had been performed for both the vegetable crops to capture their optimal nutrient requirement under different moisture stress situation. These characteristics and functional relationship were then applied from the whole datasets of soil nutrients, soil moisture and plant uptakes under different irrigation-nutrient treatment combinations. The objective was to establish and compare two independent precision models, viz. common multiple linear regression (MLR) model used in many cases along with fuzzy linear models (FLR) which is not used earlier in soil or irrigation research for making a close prediction in fertilizer requirement or crop yield.

Multiple linear regression (MLR) was used with a mathematical relationship among dependent variables, viz. soil nutrient content (SN/SP/SK), fertilizer application dose (FN/FP/FK) and volumetric soil moisture content while crop yield as independent variable with some linear objective functions focusing to certain linear limitations with a view to explore the optimum solution. The main innovation with this experiment was including the agenda of considering the soil moisture as one of the inclusive factors that may influence precisely the workability of the existing targeted yield (fertilizer adjustment) multiple linear regression equation models generated through soil test crop response correlation study. In such we have simulated wide moisture conditions in experimental field by exposing our test crops broccoli and cabbage to varying moisture stresses throughout the growing season. These equations are more comprehensive and include more variability for predicting crop yield

or crop–soil-specific fertilizer application requirements for all three major plant nutrients.

We have also established the relationship of yield with soil nutrient, fertilizer nutrient and volumetric soil moisture content playing across the entire moisture strata (Table 5) advocated in the present experiment. In the newly introduced second models, all the fuzzy linear equations emerge in the form of:

$$\text{FNPK} = [Y - A_2S(\text{NPK}) + A_3M]/A_1 \quad (1)$$

where Y: yield ( $\text{tha}^{-1}$ ) and M: volumetric soil moisture content (%) and SN, SP, SK: available soil NPK ( $\text{kgha}^{-1}$ ). It can be envisaged that we have added a weighted ( $A_3/A_1$ ) value of volumetric moisture content ( $\text{m}^3.\text{m}^{-3}$ ) to get the actual fertilizer recommendation over the existing STCR recommended levels (which does not consider soil moisture parameters) in fuzzy model.

**Table 5** Multiple (Mlr) and fuzzy linear regression (Flr) functional relationship models for cabbage and broccoli

|            |     |  |
|------------|-----|--|
| Broccoli N | Mlr | $Y = (9.513 \pm 2.691) + (0.040 \pm 0.003)\text{FN} + (0.005 \pm 0.011)\text{SN} + (-0.165 \pm 0.087)\text{M}$   |
|            | Flr | $Y = (14.482 \pm 0.00) + (0.035 \pm 0.00)\text{FN} + (-0.026 \pm 0.008)\text{SN} + (-0.193 \pm 0.035)\text{M}$   |
| Broccoli P | Mlr | $Y = (17.395 \pm 4.945) + (0.054 \pm 0.030)\text{FP} + (0.249 \pm 0.497)\text{SP} + (-0.414 \pm 0.162)\text{M}$  |
|            | Flr | $Y = (10.82 \pm 5.91) + (0.018 \pm 0.00)\text{FP} + (0.299 \pm 0.312)\text{SP} + (-0.041 \pm 0.00)\text{M}$      |
| Broccoli K | Mlr | $Y = (15.015 \pm 7.96) + (0.033 \pm 0.014)\text{FK} + (0.022 \pm 0.039)\text{SK} + (-0.451 \pm 0.147)\text{M}$   |
|            | Flr | $Y = (10.429 \pm 6.046) + (0.007 \pm 0.00)\text{FK} + (0.008 \pm 0.003)\text{SK} + (0.031 \pm 0.089)\text{M}$    |
| Cabbage N  | Mlr | $Y = (19.231 \pm 3.026) + (0.125 \pm 0.137)\text{FN} + (0.060 \pm 0.052)\text{SN} + (0.467 \pm 0.086)\text{M}$   |
|            | Flr | $Y = (14.582 \pm 7.221) + (0.109 \pm 0.046)\text{FN} + (0.015 \pm 0.00)\text{SN} + (0.232 \pm 0.126)\text{M}$    |
| Cabbage P  | Mlr | $Y = (17.395 \pm 4.945) + (0.054 \pm 0.030)\text{FP} + (0.249 \pm 0.497)\text{SP} + (-0.414 \pm 0.162)\text{M}$  |
|            | Flr | $Y = (10.8293 \pm 5.91) + (0.018 \pm 0.00)\text{FP} + (0.299 \pm 0.312)\text{SP} + (-0.041 \pm 0.00)\text{M}$    |
| Cabbage K  | Mlr | $Y = (62.997 \pm 20.879) + (0.061 \pm 0.024)\text{FK} + (-0.042 \pm 0.07)\text{SK} + (-1.123 \pm 0.725)\text{M}$ |
|            | Flr | $Y = (87.708 \pm 26.586) + (0.04 \pm 0.237)\text{FK} + (-0.195 \pm 0.00)\text{SK} + (-0.470 \pm 0.00)\text{M}$   |

Y- yield ( $\text{tha}^{-1}$ ); SN, SP, SK: available soil NPK ( $\text{kgha}^{-1}$ ); FN, FP, FK: applied fertilizer NPK ( $\text{kgha}^{-1}$ ); M: volumetric soil moisture content (%)

**Table 6** Fitting of both models (Mlr and Flr) for three nutrient applications in cabbage and broccoli

|          | Average width of prediction intervals |        |            |        |           |        |
|----------|---------------------------------------|--------|------------|--------|-----------|--------|
|          | Nitrogen                              |        | Phosphorus |        | Potassium |        |
|          | Mlr                                   | Flr    | Mlr        | Flr    | Mlr       | Flr    |
| Broccoli | 12.806                                | 9.050  | 24.560     | 16.238 | 37.262    | 16.012 |
| Cabbage  | 92.690                                | 44.953 | 24.560     | 16.238 | 105.688   | 65.049 |

To compare performance of both approaches, viz. multiple linear regression (Mlr) methodology and fuzzy regression methodology (Flr), width of prediction intervals corresponding to each observed value of response variable is computed. The average width of prediction intervals was recorded (Table 6) which showed that average widths for linear regression models as compared to their fuzzy counterparts are much higher. Thus, fuzzy regression methodology is more efficient than multiple linear regression technique in reducing the vagueness of the observations and also capable of handling situations in which predictor variables are highly correlated.

Such equations, either dedicated for a precise moisture situation or playing across varying moisture situations, may be used in computing fertilizer recommendations for a targeted yield where assured irrigation facilities are not available, and fertilizer prescriptions need to be dovetailed considering the availability of irrigation.

## 4 Conclusion

The most logical protocol for formulation of fertilizer recommendation for crops uses the soil test crop response (STCR) model to arrive at targeted yield (fertilizer adjustment) equations under assured irrigation and good management practices. We thought of the possibilities if such fertilizer prescriptions model can be made flexible to situations where crops are often exposed to deficit irrigation (stresses) since a large area of our state is rain-fed or contaminated through polluted groundwater irrigation.

Planning such, we felt it is necessary to include a soil moisture parameter in the existing STCR equation which itself is a multiple linear regression model where the underlying relationship is assumed to be crisp or precise, as it gives a precise value of response for a set of values of explanatory variables. Therefore, we preferred a fuzzy linear relationship since in a realistic situation, where the underlying relationship is not a crisp function of a given form; it contains some vagueness or impreciseness.

At the end of the day, fuzzy regression methodology emerged more efficient than multiple linear regression technique in reducing the vagueness of the observations and we obtained a set of fertilizer adjustment equations that can play across varying regimes of moisture situations, empirically.

**Acknowledgements** The financial assistance of ICAR-Indian Institute of Soil Science, Bhopal-462038, Madhya Pradesh, India, and ICAR—Indian Institute of Water Management, Bhubaneswar, Odisha-751023, India, for the research execution is gratefully acknowledged by the authors.

## References

1. Truog E (1960) Fifty years of soil testing. *Trans 7th intl congr soil sci vol III, Commission IV* 7:46–53
2. Dobermann A, White PF (1998) Strategies for nutrient management in irrigated and rain fed lowland rice systems. *Nutrient Cycling Agroecosyst.* 53(1):1–18
3. Witt C, Dobermann A, Abdulrachman S, Gines HC, Guanghuo W, Nagarajan R, Satawatananon S, Son TT, Tan PS, Simbahan GC, Olk DC (1999) Internal nutrient efficiencies of irrigated lowland rice in tropical and subtropical Asia. *Field Crops Res* 63(2):113–138.
4. Ramamoorthy B, Narasimham RL, Dinesh RS (1967) Fertilizer application for specific yield targets of sonora 64 (wheat). *Indian Fmg.* 17(5):43–45
5. Ramamoorthy B, Velayutham M (1974) Soil testing for high fertilizer efficiency. *Indian Fmg.* 24(2):82–84
6. Black CA (1993) *Soil fertility evaluation and control*, Lewis Publishers, Boca Raton, 171–175
7. Sakarvadia HL, Polara KB, Davaria RL, Parmar KB, Babariya NB (2012) Soil test based fertilizer recommendation for targeted yields of garlic crop. *An Asian J Soil Sci* 7(2):378–382.
8. Khosa MK, Sekhon BS, Mavi MS, Benipal DS, Benbi DK (2012) Performance of target yield based fertilizer prescription equations in rice-wheat cropping system in Punjab. *Indian J Fertilizers* 8(2):14–18
9. Katharine S, Praveena SR, Maragatham S, Natesan R, Ravikumar V, Dey P (2013) Soil test based fertilizer prescriptions through inductive cum targeted yield model for transgenic cotton on inceptisol. *IOSR J Agricult Veterinary Sci* 6:36–44
10. Singh SR (2016) Soil test crop response: concepts and components for nutrient use efficiency enhancement. In: *Biofortification of Food Crops*. Springer, New Delhi, pp 237–246
11. Fageria NK, Moreira A, Coelho AM (2012 Sep 15) Nutrient uptake in dry bean genotypes. *Commun Soil Sci Plant Anal* 43(17):2289–2302
12. Bolton FE (1981) Optimizing the use of water and nitrogen through soil and crop management. *Plant Soil*, pp 231–247
13. Fan XL, Li YK (2001) Effect of drought stress and drought tolerance heredity on nitrogen efficiency of winter wheat. In Horst WWJ, Schenk MK, Burkert A, Claasen N, Flessa H, Frommer WB, Goldbach HE, Olf HW, Romheld W, Sattelmacher B, Schmidhalter U, Schubert S, von Wiren N, Wittenmayer L (eds), *Plant nutrition: food security and sustainability of agro-ecosystems*, American Society of Agronomy, Madison, USA, pp 62–63.
14. Fang X, Yuan J, Wang G, Zhao Z (2006 Dec 1) Fruit production of shrub, *Caragana korshinskii*, following above-ground partial shoot removal: mechanisms underlying compensation. *Plant Ecol* 187(2):213–225
15. Shaban KA, Helmy AM (2006) Response of wheat to mineral and Bio N-fertilization under saline conditions. *Zagazig J Agric Res* 33(6):1189–1205
16. Bhattacharyya K, Sengupta S (2020) Arsenic management options in soil-plant-food chain. *Proceedings-cum-abstract book national webinar* 17
17. Horticulture Statistics Division (2015) Department of agriculture, cooperation & farmers welfare, ministry of agriculture & farmers welfare, Government of India
18. Saha P, Chatterjee R, Mukhopadhyay D (2006) Effect of boron and molybdenum on yield and quality of sprouting broccoli under terai agro-ecological region of West Bengal. *Crop Res* 32(3):396–400

19. Bouyoucos GJ (1962) Hydrometer method improved for making particle size analyses of soils 1. *Agron J* 4(5):464–465
20. Walkley A, Black IA (1934) An examination of Degtjareff method for determining soil organic matter and a proposed modification of the chromic acid titration method. *Soil Sci* 37:29–37
21. Subbiah B, Asija GL (1956) Alkaline permanganate method of available nitrogen determination. *Curr Sci* 25:259
22. Olsen SR (1954) Estimation of available phosphorus in soils by extraction with sodium bicarbonate. US Department of Agriculture
23. Brown JR, Warncke D (1988) Recommended cation tests and measures of cation exchange capacity. Recommended chemical soil test procedures for the North Central Region. *Bull* 499:15–16
24. Jackson ML (1973) Soil chemical analysis, Prentice Hall of India Ltd. New Delhi 219–21
25. Cassman KG, Gines GC, Dizon MA, Samson MI, Alcantara JM (1996) Nitrogen-use efficiency in tropical lowland rice systems: contributions from indigenous and applied nitrogen. *Fields Crops Res* 47:1–12
26. Mosier AR, Syers JK, Freney JR (2004) Assessing the impacts of fertilizer use on food production and the environment. *Agriculture and the nitrogen cycle*. Scope-65. Island Press, London
27. Molden D (1997) Accounting for water use and productivity. *SWIM Paper 1*. IIMI: Colombo
28. Ramamoorthy B (1968) Project coordinator's report. In First Workshop of the STCR Project, JNKVV, Jabalpur
29. Ghosh H, Wadhwa S Application of fuzzy regression methodology in agriculture using SAS. <http://www.iasri.res.in/sscnars/socialsci/.2016>
30. Tanaka H (1987) Fuzzy data analysis by possibilistic linear models. *Fuzzy Sets Syst* 24:363–375
31. Taha HA (1997) Operations research: an introduction, 6th Edn., Prentice Hall of India, New Delhi, pp 67–109
32. Gonzalez-Dugo V, Durand JL, Gastal F, Picon-Cochard C (2005) Short-term response of the nitrogen nutrition status of tall fescue and Italian ryegrass swards under water deficit. *Australian J Agricul Res* 56:1269–1276
33. Van-Duivenbooden N, Pala M, Studer M, Biolders CL (1999) Efficient soil water use: the key to sustainable crop production in the dry areas of West Asia, and North and Sub-Saharan Africa. International Centre for Agricultural Research in the Dry Areas, Aleppo, Syria, and International Crops Research Institute for the Semi-Arid Tropics, Patancheru, India
34. Everaarts AP, De Willingen P (1999) The effect of nitrogen and method of application on yield and quality of broccoli. *Neth J Agric Sci* 47:123–133
35. Westerman RL, Tucker TC (1978 Jan) Soil fertility concepts: past, present, and future. *Future Dev Soil Sci Res* 1:171–179
36. Smolander A, Barnette L, Kitunen V, Lumme I (2005) N and C transformations in long-term N-fertilized forest soils in response to seasonal drought. *Appl Soil Ecol* 29:225–235
37. Gajri PR, Prihar SS, Arora VK (1993) Interdependence of nitrogen and irrigation effects on growth and input-use efficiencies in wheat. *Field Crop Res* 31:71–86
38. Saneoka H, Fujita K, Ogata S (1990 Jun 1) Effect of phosphorus on drought tolerance in chlorisgayanakunth and coixlacryma-jobi L. *Soil Sci Plant Nutrition* 36(2):267–274
39. Hammond JP, Martin R, Broadley PJ, White GJ, King HC, Bowen RH, Mark CM, Andrew Mead TO, William PS, Duncan JG (2009) Shoot yield drives phosphorus use efficiency in Brassica oleracea and correlates with root architecture traits. *J Exp Botany* 60(7):1953–1968.
40. Wang B, Liu W, Dang T (2011) Effect of phosphorus on crop water and nitrogen use efficiency under different precipitation year in dry land. Proceedings of international symposium on water resources and environmental protection
41. Aown M, Raza S, Saleem MF, Anjum SA, Khaliq T, Wahid MA (1 Jan 2012) Foliar application of potassium under water deficit conditions improved the growth and yield of wheat (*Triticumaestivum* L.). *J Anim Plant Sci* 22(2):431–7
42. Austin AT, Yahdjian L, Stark JM, Belnap J, Porporato A, Norton U, Ravetta DA, Schaffer SM (2004) Water pulses and biogeochemical cycles in arid and semiarid ecosystems. *Oecologia* 141:221–235

43. Cakmak I (2005) The role of potassium in alleviating detrimental effects of abiotic stresses in plants. *J Plant Nutr Soil Sci* 168:521–530
44. Lahiri AN (1980) Interaction of water stress and mineral nutrition on growth and yield. In Turner NC, Kramer PJ (eds) *Adaptation of plants to water and high temperature stress*. John, New York, pp 87–103
45. Costa M, Ortuno MF, Chaves MM (2007) Deficit irrigation as a strategy to save water: physiology and potential: application to horticulture. *J Integr Plant Biol* 49:1421–1434
46. Pandey RK, Maranville JW, Admou A (2001) Tropical wheat response to irrigation and nitrogen in a Sahelian environment. *Euro J Agron* 15:93–105
47. Prieto D, Angueira C (1999) Water stress effect on different growing stages for cotton and its influence on yield reduction. In Kirda C, Moutonnet P, Hera C, Nielsen DR (eds) *Crop yield response to deficit irrigation*. Developments in Plant and Soil Sciences. Kluwer Academic Publishers, Dordrecht vol 84, 161–179
48. Pradhan S, Chopra UK, Bandyopadhyay KK, Singh R, Jain AK, Chand I (2013) Effect of water and nitrogen management on water productivity and nitrogen use efficiency of wheat in a semi-arid environment. *Int J Agricult Food Sci Technol* 4(7):727–732
49. Zwart SW, Bastiaanssen WGM (2004) Review of crop water productivity values for irrigated wheat, rice, cotton and Maize. *Agric Water Manag* 69:115–133
50. Sparks DL, Grafe M (2006) Solid phase speciation of arsenic (Doctoral dissertation, CSIRO Publishing)
51. Takahashi Y, Minamikawa R, Hattori KH, Kurishima K, Kihou N, Yuita K (2004) Arsenic behavior in paddy fields during the cycle of flooded and non-flooded periods. *Environ Sci Technol* 38:1038–1044
52. Somenahally AC, Hollister EB, Yan W, Gentry TJ, Loeppert RH (2011) Water management impacts on arsenic speciation and iron-reducing bacteria in contrasting rice-rhizosphere compartments. *Environ Sci Technol*. <https://doi.org/10.1021/es2012403>
53. Mitra A, Chatterjee S, Moogouei R, Gupta DK (2017 Dec) Arsenic accumulation in rice and probable mitigation approaches: a review. *Agronomy* 7(4):67

# Drip Fertigation with Fertilizer Prescription Through STCR—IPNS—A Way Forward Towards Climate Change Mitigation



Santhi Rangasamy, Maragatham Subramaniam,  
Praveena Katharine Stephen, and Pradip Dey

**Abstract** Climate change worsens the serious challenges faced by the agricultural sector worldwide, more particularly in developing nations where the food production remains low, leading to poverty, weakness and food insecurity. Even as we move towards higher productivity, due emphasis has to be laid on agricultural systems which would positively reduce the emission of greenhouse gases and mitigate the environmental impact. This has remained as the long-term interest of the researchers, policy framing governments, agribusinesses and more importantly, the farming community. Cotton is the most widespread profitable non-food crop. In Tamil Nadu, urea is the main form of N fertilizer, and it also contributes for N<sub>2</sub>O emission from soils. In this context, this paper puts forth the most relevant and promising climate change mitigating agricultural technology by addressing twin issues of water scarcity and nutrient use efficiency through drip fertigation with decision on fertilizer application based on the fertilizer prescription equations (FPEs). The FPEs were derived based on the concept of Integrated Plant Nutrition System employing Soil Test Crop Response model (STCR-IPNS). The fertilizer nitrogen requirement for an yield target of 3.50 t ha<sup>-1</sup> ranged from 140 to 164 kg ha<sup>-1</sup> with fertilizer savings of 24–48 kg N ha<sup>-1</sup> when compared to general nitrogen recommendation. STCR-IPNS approach indirectly avoids wastage of fertilizer and reduces the nitrous oxide emission. This is effective as a climate change mitigation tool and also improved the crop yield and quality. The findings of this study proved the supremacy of STCR-IPNS-based fertilizer optimization for improving crop yield and quality, with limited water resource and fertilizer input without compromising climate change mitigation strategies.

---

S. Rangasamy (✉) · M. Subramaniam  
Tamil Nadu Agricultural University, Coimbatore, India

P. K. Stephen  
Karunya Institute of Technology and Sciences, Coimbatore, India

P. Dey  
ICAR-Indian Institute of Soil Science, Bhopal, India

**Keywords** Fertilizer prescription equations · Integrated plant nutrition system · Yield targets · Nitrous oxide emission · Drip fertigation

## 1 Introduction

Climate change has a pronounced effect on global food security by reducing the food production, its availability and access and also affects the food quality [1]. Agriculture is more prone to the rise in temperature, vagaries of monsoon and fluctuations in precipitation patterns. The extreme weather events leading to water scarcity results in the decline of agricultural productivity and interrupts the food delivery resulting in spikes in food prices. The increase in temperature also can cause frequent food spoilage and contamination. Climate change worsens the serious challenges faced by the agricultural sector worldwide, more particularly in developing nations where the food production remains low, leading to poverty, weakness and food insecurity.

Global surface air temperature is expected to increase the tune of 1.8–4.0 °C in the next few years resulting in severe yield reductions throughout the world [2]. One of the causative parameters of human-induced climate change is the emission of greenhouse gases (GHGs). About 10–14% of global GHG emissions is brought about by agriculture-related activities [3, 4], mostly from methane as a result of enteric fermentation, nitrous oxide, due to the application of synthetic fertilizers and carbon dioxide emitted during tillage operations [5]. As far as agriculture is concerned, the mineral fertilizers serve as a major source for the emission of greenhouse gases [6]. Escalating global warming could be considerably reduced by the reduction of methane and nitrous oxide emissions from agriculture.

Over two billion people living in severely water-stressed countries suffer water scarcity. This number would multiply in the next few decades as the population increases and the need for water grows [7]. The intensification of climate change results in frequent occurrence of unprecedented weather incidents and the variability of rainfall increases. These subsequently reflect on the food security, and the worst hit is the rainfed agriculture.

The researchers are now facing the herculean task of satisfying the demands of the exorbitantly increasing population amidst worsening climate change. Priority concern has to be given for the development of climate smart crops and improved crop and agronomic practices as these may pave the way for the researchers and farmers in mitigating the impending adversaries. Even as we move towards higher productivity, due emphasis has to be laid on agricultural systems which would positively reduce the emission of greenhouse gases and mitigate the environmental impact. This has remained as the long-term interest of the researchers, policy framing governments, agribusinesses and more importantly, the farming community.

In this context, this paper puts forth a most relevant and promising climate change mitigating agricultural technology, wherein drip fertigation is done based on soil test-based fertilizer prescription equations developed for desired yield targets of the crops under Integrated Plant Nutrition System (IPNS) adopting inductive-cum-targeted



yield model. This technology besides being effective as a climate change mitigation tool also improves the crop yield and quality. Deficit irrigation management practices have become the need of the hour in places where water resources are dwindling. Emission of nitrous oxide from agricultural fields can be minimized by reducing the quantity of nitrogenous fertilizers, improving the efficiency of these fertilizers and synchronizing the timing of fertilizer application based on the crop demand. Thereby the CO<sub>2</sub> emissions associated with the manufacture of synthetic fertilizers can also be reduced. The findings of this study proved the superiority of fertilizer prescription equations developed based on STCR-IPNS targeted yield model, in improving crop yield and quality, with limited water resource and fertilizer consumption without compromising climate change mitigation strategies.

## 2 Methodology

### 2.1 Description of the Research Soil and Site

In this study, the fertilizer prescription equations under IPNS for cotton under drip fertigation on Vertic Ustropept—mixed black calcareous soil were developed, and the validation experiments were conducted at five locations in the state of Tamil Nadu, South India, India, viz. Tamil Nadu Agricultural University, Coimbatore (location I), two farmers' holdings at Thalavaipatti, Attur Taluk, Salem district (location II and III), farmer's holding at A. Karadipatti, Pethanaickenpalayam block, Attur Taluk, Salem district (location IV) and Vadugathanpatti Pethanaickenpalayam block, Attur Taluk, Salem district (location V) (Fig. 1). Analysis on initial soil fertility revealed low available Nitrogen (190–232 kg ha<sup>-1</sup>), high available phosphorus (23.3–40 kg ha<sup>-1</sup>) and high available potassium (548–602 kg ha<sup>-1</sup>). The available micronutrient Zn was in the range of 0.96–1.32 mg kg<sup>-1</sup>, Fe was in the

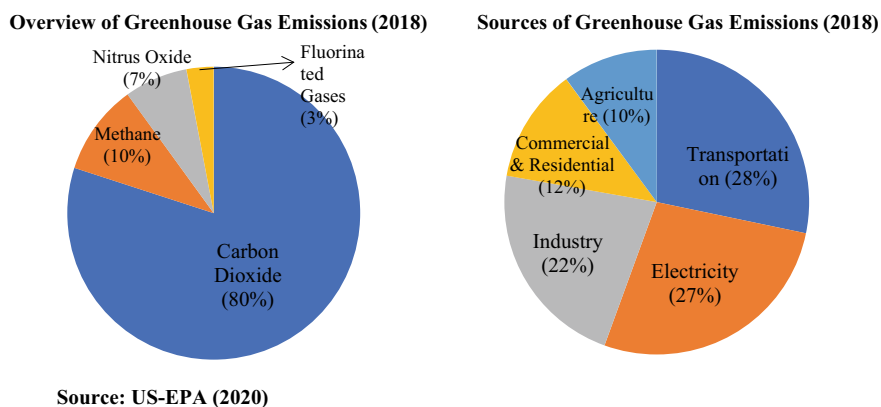


Fig. 1 Overview of greenhouse gas emissions. Source US-EPA (2020)



**Fig. 2** Field experiments on cotton at different locations of Tamil Nadu, South India

range of 3.08–4.68 mg kg<sup>-1</sup>, Cu in the range of 1.30–2.04 mg kg<sup>-1</sup> and Mn in the range of 7.64–10.70 mg kg<sup>-1</sup> of soil.

Various cotton hybrids were chosen for different locations. There were ten treatments, viz. blanket (RDF alone), blanket (RDF + FYM @ 12.5 t ha<sup>-1</sup>), STCR-NPK alone (T = 3.0, 3.5 and 4.0 t ha<sup>-1</sup>), STCR-IPNS (T = 3.0, 3.5 and 4.0 t ha<sup>-1</sup>), farmer's practice and absolute control. Based on the initial soil nutrient status of available N, P and K and the quantities of N, P<sub>2</sub>O<sub>5</sub> and K<sub>2</sub>O supplied through FYM, fertilizer doses were calculated and applied for various yield targets. STCR-NPK alone treatments received only inorganic fertilizers based on STCR equations, while STCR-IPNS treatments received FYM @ 12.5 t ha<sup>-1</sup> basally, and NPK fertilizers were applied after adjusting the nutrients supplied through FYM based on STCR-IPNS equations. At all the locations, fertilizer doses were given according to the treatments, and fertigation was scheduled from 14 days after sowing on weekly basis. All the improved agronomic operations were done periodically (Fig. 2).

## 2.2 Basic Concept—Inductive-Cum-Targeted Yield Model

The methodology adopted for the research is based on the procedure for the recommendation of fertilizers by Truog [8] and Ramamoorthy et al. [9] as “inductive-cum-targeted yield model”. This concept was adopted as a scientific tool to develop fertilizer recommendation equations. The layout design and the treatment structure followed in the research work were based on “inductive-cum-targeted yield model” [9]. The field was divided into three strips, and fertility gradient was made intentionally among the three plots by adding graded doses of fertilizers. For this purpose, a gradient experiment with fodder maize was raised prior to the test crop, cotton. Thereby the variation in the soil biology can be minimized, and similar management practices could be adopted under prevailing climatic conditions. The inductive approach and the field design were elaborated by Ramamoorthy and Velayutham [10] and are also quoted by Black [11].

At maturity, yield of various treatments was recorded, and NPK uptake values are computed. Using the data on seed cotton yield and fertilizer doses applied, certain derived parameters, viz. per cent achievement  $\{(\text{yield obtained} / \text{aimed yield target}) \times 100\}$  and response ratio (response in  $\text{kg ha}^{-1}$ /quantities of fertilizer N,  $\text{P}_2\text{O}_5$  and  $\text{K}_2\text{O}$  applied in  $\text{kg ha}^{-1}$ ) were worked out to arrive at fertilizer recommendations for desired yield targets of crops and maximum profit. In addition, benefit-cost ratio was also worked out.

### ***2.3 Essential Parameters for Deriving the Fertilizer Prescription Equations***

The basic parameters necessary for developing the fertilizer prescription equations are nutrient requirement of the crop (NR), contribution of soil nutrients towards plant uptake (Cs), contribution of fertilizer nutrients towards plant uptake (Cf) and contribution from organics, viz. farmyard manure towards plant uptake (Cfym). These were calculated using the seed cotton yield, total N, P and K uptake by the crop, initial soil available nitrogen, phosphorus and potassium and the doses of fertilizer N,  $\text{P}_2\text{O}_5$  and  $\text{K}_2\text{O}$  applied, following Ramamoorthy et al. [9].

Fertilizer prescription equations were developed using the basic parameters computed. Using the fertilizer prescription equations, doses of fertilizers at different soil nutrient levels were calculated and recommendations provided. Fertilizer recommendations can be achieved for the desired targets of seed cotton yield both under inorganics alone (NPK alone) as well as under Integrated Plant Nutrition System.

## **3 Results and Discussion**

### ***3.1 Fertilizer Prescription Equations for Cotton***

From the data obtained from the test crop experiment, the fertilizer prescription equations were derived. The fertilizer doses were calculated using these equations. These equations were developed making use of the basic parameters. The nutrients required for producing one quintal of seed cotton were calculated which were 4.43 kg of N, 2.20 kg of  $\text{P}_2\text{O}_5$  and 4.83 kg of  $\text{K}_2\text{O}$ . Seed cotton production requires higher quantities of potassium nutrient compared to nitrogen and phosphorus. The findings are similar to the nutrient requirement of beetroot as reported by Santhi et al. [13].

The soil contributed 24.65% of available N (SN), 48.95% of available P (SP) and 11.06% of available K (SK), respectively, towards plant uptake. Similarly, N,P,K contribution from fertilizer nutrients (Cf) and FYM (Cfym) was 52.01, 49.89 and 73.35 and 38.19 (ON), 16.43 (OP) and 40.35 (OK), respectively, for cotton (Table 1).

**Table 1** Fertilizer prescription equations for cotton—inorganics and IPNS [12]

| Fertilizer requirements in kg per ha for desired yield target (T) |
|---|
| <b>STCR—IPNS</b>  |
| $N = 8.51 T - 0.47$ $SN = 0.73 ON$                                |
| $P_2O_5 = 4.41 T - 2.25$ $SP = 0.75 OP$                           |
| $K_2O = 6.59 T - 0.18$ $SK = 0.66 OK$                             |

### 3.2 Fertilizer Dose Prediction for Desired Yield Targets (T) of Seed Cotton

Fertilizer doses can be predicted using the fertilizer prescription equations for predicting for specific seed cotton yield targets (T) for different levels of soil available nutrients. Sherene [14] has developed similar fertilizer prescription equations under rainfed condition for hybrid cotton [14].

The validation trials conducted confirmed the achievement of targeted yield using equations developed. Among the treatments, seed cotton yield was maximum in STCR—IPNS ( $T = 4 \text{ t ha}^{-1}$ ), ( $4.14 \text{ t ha}^{-1}$ ,  $3.95 \text{ t ha}^{-1}$ ,  $3.82 \text{ t ha}^{-1}$ ,  $3.80 \text{ t ha}^{-1}$  &  $3.92 \text{ t ha}^{-1}$  respectively for five locations) followed by STCR-NPK alone ( $T = 4 \text{ t ha}^{-1}$ ) ( $3.99 \text{ t ha}^{-1}$ ,  $3.80 \text{ t ha}^{-1}$ ,  $3.70 \text{ t ha}^{-1}$ ,  $3.64 \text{ t ha}^{-1}$  and  $3.74 \text{ t ha}^{-1}$ ).

However, STCR-inorganics alone ( $T = 3 \text{ t ha}^{-1}$ ) recorded relatively lower yields over blanket at few locations, and the response ratio and benefit-cost ratio were higher. Even among the STCR treatments, fertilization through IPNS recorded higher yield, response ratio and benefit-cost ratio (Table 2).

The percentage reduction in the consumption of inorganic nitrogen fertilizers when substituted with organic manures is given in Table 3. Nitrous oxide emissions are lower when inorganic nitrogen fertilizers are applied in combination with organic manures (IPNS). Substituting synthetic fertilizers with organic manures increases the crop yield and productivity apart from ensuring crop and environmental protection by reducing nitrous oxide emissions. In a broader sense, for any source of fertilizer, excess application than the crop requirement results in greater  $N_2O$  emissions.

Fertigation which provides a solution to the dwindling water resource also reduces nitrous oxide emission as the fertilizers are applied at the close proximity of crops ensuring greater nutrient absorption.

## 4 Summary and Conclusion

The research findings proved the supremacy of the FPEs developed for cotton under drip fertigation in terms of yield, uptake, RR and BCR. The yield increase due to STCR-IPNS ( $T = 4 \text{ t ha}^{-1}$ ) over blanket (RDF + FYM @  $12.5 \text{ t ha}^{-1}$ ) and farmer's practice were 36.45 and 42.39 per cent, respectively. Thus, fertilizer prescription equations developed adopting STCR-IPNS, i.e. application of nitrogen, phosphorus

**Table 2** Mean and range values for the five validation experiments on hybrid cotton

| Treatments                                   | Fertilizer doses (kg ha <sup>-1</sup> ) |                               |                  | Yield (t ha <sup>-1</sup> ) | % achvt | RR (kgkg <sup>-1</sup> ) | BCR  |
|--|---|-------------------------------|------------------|-----------------------------|---------|--------------------------|------|
|  | N                                       | P <sub>2</sub> O <sub>5</sub> | K <sub>2</sub> O |                             |         |                          |      |
| Blanket                                      | 120–188                                 | 60–75                         | 60–188           | 2.88                        | –       | 3.97                     | 1.95 |
| STCR-NPK alone (T = 3.0 t ha <sup>-1</sup> ) | 146–166                                 | 42–80                         | 89–99            | 2.92                        | 97.4    | 5.03                     | 2.05 |
| STCR-NPK alone (T = 3.5 t ha <sup>-1</sup> ) | 189–209                                 | 64–102                        | 122–132          | 3.34                        | 95.44   | 4.84                     | 2.25 |
| STCR-NPK alone (T = 4.0 t ha <sup>-1</sup> ) | 231–251                                 | 86–124                        | 155–165          | 3.77                        | 94.16   | 4.76                     | 2.46 |
| STCR-IPNS (T = 3.0 t ha <sup>-1</sup> )      | 101–121                                 | 38–58                         | 49–59            | 3.06                        | 102.12  | 5.49                     | 2.11 |
| STCR-IPNS (T = 3.5 t ha <sup>-1</sup> )      | 144–164                                 | 42–80                         | 82–92            | 3.48                        | 99.36   | 5.18                     | 2.34 |
| STCR-IPNS (T = 4.0 t ha <sup>-1</sup> )      | 186–206                                 | 64–102                        | 115–125          | 3.93                        | 98.06   | 5.06                     | 2.55 |
| Farmer's practice                            | 110–250                                 | 55–110                        | 60–150           | 2.76                        | –       | 3.52                     | 1.88 |
| Absolute control                             | 0                                       | 0                             | 0                | 1.37                        | –       | –                        | 1.08 |

**Table 3** Reduction in nitrogen fertilizer consumption due to the adoption of IPNS for various yield targets

| Target                 | Inorganic N fertilizer (kg ha <sup>-1</sup> ) | Inorganic N + FYM 12.5 tha <sup>-1</sup> (kg ha <sup>-1</sup> ) | Per cent reduction |
|------------------------|---|---|--------------------|
| 3.0 t ha <sup>-1</sup> | 146–166                                       | 101–121   | 27.0–30.8          |
| 3.5 t ha <sup>-1</sup> | 189–209                                       | 144–164   | 21.53–23.8         |
| 4.0 t ha <sup>-1</sup> | 231–251                                       | 186–206   | 18.0–19.5          |

and potassium fertilizers based on soil nutrient levels along with FYM @ 12.5 t ha<sup>-1</sup>, can be recommended for achieving higher yield, response ratio and BCR with cotton under drip fertigation on Vertic Ustropept soil series. Nitrous oxide emissions can be considerably reduced by adopting nutrient application based on fertilizer prescription equations wherein excess application of inorganic fertilizers is avoided.

Further adoption of Integrated Plant Nutrition System established its supremacy in terms of seed cotton yield, benefit-cost ratio and reduction in nitrous oxide emission. Fertigation which provides a solution to the dwindling water resource also

reduces nitrous oxide emission as the fertilizers are applied at the root zone preventing denitrification losses of nitrogen.

STCR-IPNS approach avoids wastage of fertilizer and thereby reduces the potential of nitrous oxide emission. This is effective as a climate change mitigation tool, besides improving the crop yield and quality. Hence, the findings of this study proved STCR-IPNS-based fertilizer optimization as the best practice for improving the crop yield and quality, with limited water resource and fertilizer input, without compromising climate change mitigation strategies.

**Acknowledgements** The authors gratefully acknowledge the ICAR—AICRP on STCR, Indian Institute of Soil Science (IISS), Bhopal, Madhya Pradesh, India and Tamil Nadu Agricultural University, Coimbatore, India, for granting funds and aiding in the implementation of the AICRP-STCR Project at TNAU, Coimbatore, India.

## References

1. USDA (2015) Brown ME, Antle JM, Backlund P, Carr ER, Easterling WE, Walsh MK, Ammann C, Attavanich W, Barrett CB, Bellemare MF, Dancheck V, Funk C, Grace K, Ingram JSI, Jiang H, Maletta H, Mata T, Murray A, Ngugi M, Ojima D, O'Neill B, Tebaldi C (2015) Climate change, global food security, and the U.S. food system. Sheet Series—MSU Extension Bulletin E3152 November, p 146
2. Anand A, Khetarpal S (2015) Impact of climate change on agricultural productivity. In *Plant Biology and Biotechnology*
3. Francesco NT, Mirella S, Simone R, Alessandro F, Nuala F, Pete S (2013) The FAOSTAT database of greenhouse gas emissions from agriculture. *Environ Res Lett* 8
4. Smith P, Martino D, Cai Z, Gwary D, Janzen H, Kumar P, McCarl B, Ogle S, O'Mara F, Rice C et al (2008) Greenhouse gas mitigation in agriculture. *Philos Trans R Soc Lond B Biol Sci* 363:789–813
5. Field CB, Barros V, Stocker TF, Qin D, Dokken DJ, Ebi KL, Mastrandrea MD, March KJ, Plattner GK, Allen SK et al (eds) (2012) *Managing the risks of extreme events and disasters to advance climate change adaptation; a special report of working groups I and II of the IPCC*, Cambridge University Press, Cambridge, UK; New York, NY, USA, p 582
6. Singh H, Northup BK, Baath GS, Gowda PP, Kakani VG (2019) Greenhouse mitigation strategies for agronomic and grazing lands of the US Southern Great Plains. In *Mitig Adapt Strateg Glob Chang*
7. <https://www.unwater.org/publications/highlights-sdg-6-synthesis-report-2018-on-water-and-sanitation-2/>
8. Truog E (1960) Fifty years of soil testing. *Trans 7th Intl Congr Soil Sci*, vol 3, Commission IV paper No.7, pp 46–53
9. Ramamoorthy B, Narasimham RK, Dinesh RS (1967) Fertilizer application for specific yield targets on Sonora 64 (wheat). In *Indian Fmg* 17, 43–45
10. Ramamoorthy B, Velayutham M (1971) Soil test crop response correlation work in India. *World soil resources report No. 41*, 96–105, FAO, Rome
11. Black CA (1993) *Soil fertility evaluation and control*. Lewis Publishers, Boca Raton, pp 171–175
12. Praveena Katharine S, Santhi R, Maragatham S, Natesan R, Ravikumar V, Pradip Dey (2013) Soil test based fertilizer prescriptions through inductive cum targeted yield model for transgenic cotton on inceptisol. *IOSR J Agricult Veterinary Sci (IOSR-JAVS)* 6(5):36–44

13. Santhi R, Bhaskaran A, Natesan R (2011) Integrated fertilizer prescription equations for beet-root through inductive cum targeted yield model on an Alfisol. *Commun Soil Sci Plant Anal* 42(16):1905–1912
14. Sherene T, Santhi R, Kavimani R, Bharathi Kumar K (2016) Integrated Fertilizer Prescriptions for Transgenic Cotton Hybrids under Rainfed Situation through Inductive cum Targeted Yield Model on Vertisol. *Commun Soil Sci Plant Anal* 47(17):1951–1960

# Effective Utilization of Water Resources Through Floating Solar Photovoltaic (FSPV) Technology: An Emerging Idea of Sustainable Development



Mehebab Alam

**Abstract** Nowadays, the availability of land has become a burning problem due to population growth. On the other hand, the penetration of renewable energy has become essential considering the environmental aspect. However, in order to meet the increasing demand of electricity, solar energy is most suitable due to ease of availability and sustainability. In this context, the water resources can be used effectively through novel floating solar photovoltaic (FSPV) technology. In this study, brief idea on the FSPV technology is highlighted. Furthermore, the techno-economic analysis of FSPV technology is outlined, and simple payback period is found 7.61 years. The benefits and challenges associated with the implementation of FSPV technology are also highlighted. The potential of generation through FSPV considering the major reservoir in India is also discussed. Finally, the possible recommendations are also provided for the implementation of the FSPV so that the water surface can be used in an effective manner.

**Keywords** Floating solar photovoltaic (FSPV) · Reservoir · Sustainability

## 1 Introduction

The hindrances to fast moving advancements and developments of civilization are the limitation of natural resources and environmental degradation. To overcome this situation and make our development “sustainable”, we need innovative ideas and upgradation in our technology. Energy is the basic necessity for growth, and development of a nation and per capita energy consumption is considered as development index across the globe. Till date, production of energy around the world is based on fossil fuels mostly which is depleting day by day. Apart from this, excessive use of fossil fuels causes environmental degradation rapidly. It is worth noting that the stock fossil fuel is limited, and thus, alternative way of power generation has drawn the attention of researchers since past few years. Over the last few decades, it is a matter

---

M. Alam (✉)

Department of Electrical Engineering, NIT Durgapur, Durgapur, West Bengal 713209, India



of high concern and every country is striving to produce energy from renewable sources to ensure sustainable development.

The solar energy is easily available, and thus, the harnessing of solar energy is the best option to meet the growing demand of electricity. The solar energy can be converted through photovoltaic (PV) modules. The Government of India (GOI) has set the target of generating 100 GW [1] solar energy by 2022. To achieve this target, various initiatives, policies, and incentive schemes have been formulated by the government [2]. However, the installation of PV modules on the ground has become a challenging issue due to land requirement. Considering the issue of land requirement and population growth, the available water surface can be utilized for installation of PV module. This technology is known as floating solar PV (FSPV) technology [3–5] which is an innovative emerging way of producing the clean energy by utilizing the water bodies like lakes, reservoirs, canals, dams, etc. This novel FSPV technology attracted the researchers as well as planners to look into deeply for possible implementation in the practical environment. The efficiency of the FSPV plant is comparatively higher than the ground-mounted PV plant due to cooling effect. Moreover, the growth of algae is also reduced due to the shading effect. Till date, a large number of FSPV plants have been installed around the globe.

In this study, a brief report on the emerging FSPV technology is outlined. The different types of FSPV along with techno-economic analysis are elaborated. The benefits, challenges as well as possible recommendations related with the FSPV plant are also discussed.

## 2 Basic Idea of FSPV

The different components [3] of FSPV plant are discussed below:

**Floating system:** It is basically a floating body (structure along with floater) which helps to float the PV module.

**Mooring system:** This helps to adjust the position along with fluctuation of water level.

**PV system:** This basically consists of PV modules, electrical junction boxes, etc.

**Cable connection:** Cables are required to transfer the power from PV panel to the grid or substation. Therefore, accurately designed cables and water proof IP67 junction boxes are required in the FSPV plants.

It is interesting to note that the structure should be capable to adjust the position along the water level. The recyclable floating materials are used. The special features of the structures are:

- The materials must be completely non-toxic, resistant to salt water and alkalis acids.
- It should withstand temperatures ranging from  $-60\text{ }^{\circ}\text{C}$  to  $80\text{ }^{\circ}\text{C}$ .
- The materials must be recyclable.
- Life time should be high, i.e. around 30 years.



**Fig. 1** Floating tracker cooling concentrator (FTCC) system, Italy

## 2.1 Types of FSPV

The different types of FSPV plants are available in literature. Some of these are discussed below:

The floating tracker cooling concentrator (FTCC) (Fig. 1) technology employs the reflectors in order to increase the efficiency during different time slot of the day. The plant is designed in such a way that is free to track the movement of the sun and utilize the cooling effect of the water surface. This system is benefitted from lower ambient temperature due to evaporation of the water. The whole system comprises of floating unit, cooling unit, tracking unit along with concentrator in order to maximize the electrical output. The single modules rating varies from 1 to 300 Wp depending on the type of modules and configuration. The installation can be classified into two categories:

- Fixed installation (main objective is to cover maximum area in this design)
- Tracking installation (key objective is to maximize the electrical output).

In submerged PV system (Fig. 2), the modules are immersed in water. In this design, the efficiency is increased approximately 20% in summer season compared to a normal weather condition.

Another FSPV concept is called SUNdy (2012), realized by Det Norske Veritas (Fig. 3). In this design, a number of PV panels connected together and hexagonal structure are formed. The panels are laminated and adhered to a flexible foam surface which provides the panel's buoyancy. A transformer is located at the centre from which the electrical power is delivered to the shore. Between each vertices and centre, walkways are present which are used for cleaning and other maintenance activities. The whole structure is like spider web design and capable to maintain the shape in spite of the wave variation.

Liquid solar array (LSA) (Fig. 4) was invented by Mr. Phil Connor, Executive Director and Chief Technology Officer of the Australian solar power company Sunergy Pvt Limited. The solar energy is focused through lens and converted into

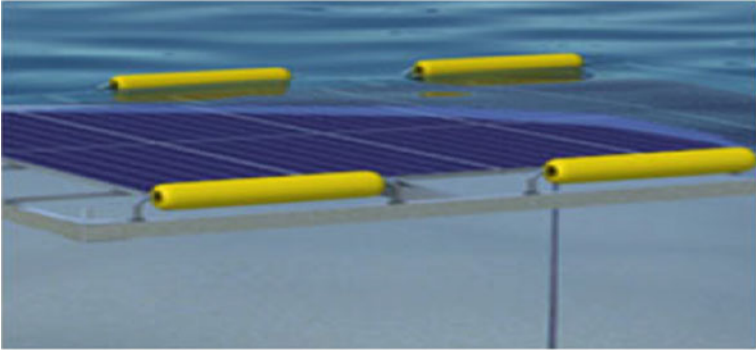


**Fig. 2** Submerged FSPV system, Australia

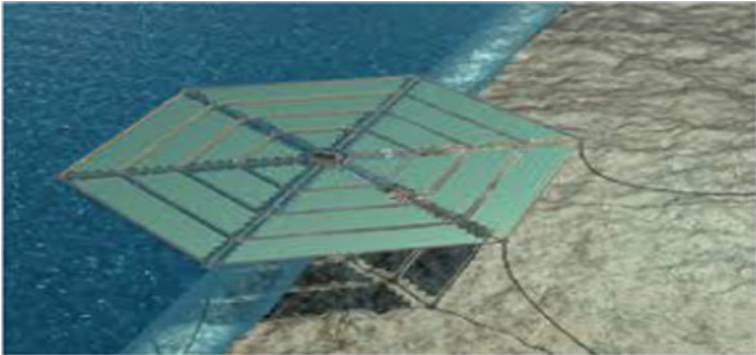


**Fig. 3** Floating hexagonal PV system design

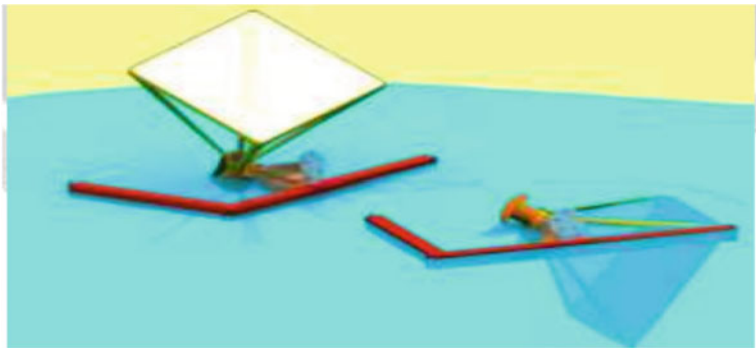


**Fig. 4** LSA operated and protected position

electricity. There is tracking mechanism which helps the lens to track the movement of the sun. A wind sensor is also connected, and this sensor helps to move the panels in accordance with the wind.

The large-scale project completed by Kyocera Corporation and Century Tokyo Leasing Corporation at Nishihira and Higashihira Ponds in Kato city. The entire project duration was only seven months, and the installed 11,250 modules are capable to generate 33,000 Mwh/year. In accordance with the Kyocera Corporation, the FSPV installation is typhoon proof (due to high-density polyethylene and array design) and yields better performance compared to the land-mounted PV installation.

### 3 Advantages and Challenges

The advantages of FSPV technologies compared to the ground-mounted PV plant are discussed below:

- PV panels are naturally cooled by water, and hence, higher efficiency is achieved [6].
- Minimal land and set-up cost;
- The LSA technology can produce the same amount of energy of a typical hydro dam by using only 10–20% of the surface area.
- For tropical monsoonal hydropower stations, during high rainfall periods, the solar power generation will be less and vice versa.
- Hydropower with FSPV combination is less dependent on water and therefore can produce reliable power than hydropower alone. During sunshine periods, the power will be generated through FSPV and there will be no water consumption.
- The systems can also improve water quality. By shading the water, the growth of algae is reduced. Therefore, water treatment and labour costs are minimized.
- The evaporation is reduced by up to 70%. A FSPV system installed on a 3-acre reservoir will lead to the saving of 4 million gallons of water per year [5].
- The implementation is easy, and installation time is comparatively low. Therefore, the cost is also low due to limited requirement of site preparation [7].
- The water is easily available for cleaning the modules [8].

Various challenges associated with FSPV technology are:

- Electrical connection at the different points needs to be done carefully. Therefore, the safety issue with the electrical connection is challenging.
- The legal restrictions are to be handled properly.
- Different regulations such as Environment Preservation Act, Protection of Wild Fauna and Flora Act, etc. are to be taken care of judiciously.
- The installation and maintenance of FSPV are affected by the different factors such as water level fluctuation, snow formation during winter season, inflow of floating matters, accessibility, etc.
- The velocity of the water should be limited up to 2 m/s.

**Table 1** Techno-economic analysis of 1 MW FSPV plant

|                                    |                            |
|------------------------------------|----------------------------|
| Total capacity of plant            | 1 MW                       |
| Capacity of each module            | 250 W                      |
| No. of modules                     | 4000                       |
| Total installation cost            | 8 Crores                   |
| Average generation hour/day        | 6 h                        |
| Total generation hrs               | 2190                       |
| Total generation in MU/day         | 0.006                      |
| Total annual generation in MU/year | 2.19                       |
| Total selling cost@ Rs 6/Kwh       | 1.314 crores               |
| Total O&M cost(20% selling cost)   | 0.2628 crores              |
| Earning per year                   | 1.0512 crores              |
| <b>Simple payback period (SPP)</b> | <b>7.61 years (approx)</b> |

SPP indicates the recovery period of investment and it is marked bold for getting better attraction

- The FSPV plant should be able to deal with water level variation, water temperature, water quality, algae growth, etc.
- The panels operate properly within certain temperature limit which is between  $-5^{\circ}\text{C}$  and  $50^{\circ}\text{C}$ .
- The FSPV plant can withstand the wind velocity up to 210 km/h.
- The performance may be affected by the moisture content [9].
- The salt content in the water may degrade the performance of FSPV plant.
- The PV panels may be degraded due to corrosion or other environmental effect [10].
- During initial year, the cost of production may be ten times than the fossil fuel-based generation [10]. However, in the long run FSPV will be beneficial.

#### 4 Techno-economic Analysis

Techno-economic analysis [4] of a typical 1 MW FSPV plant is demonstrated in Table 1. For analysis purpose, 250 W module has been chosen and electricity cost is chosen Rs. 6 per Kwh. The average generation period is considered 6 h per day.

#### 5 Government Support and FSPV Potential Study

Through Jawaharlal Nehru National Solar Mission (JNNSM), the Government of India (GOI) has set the target to install 100 GW [1] through solar energy by 2022. Plenty of solar power projects were commissioned by the previous government in last couple of years. Various bodies like Solar Energy Corporation of India (SECI),

Central Power Research Institute (CPRI), and Ministry of New and Renewable Energy (MNRE) [11] have been formulated to look into the progress of solar energy. Moreover, different incentive mechanisms and policies are formulated to promote the solar energy. It is interesting to note that 30% subsidy support from National Clean Energy Fund (NCEF) has been proposed by the GOI in order to promote the solar energy utilization. This subsidy will be disbursed in the following manner.

- After installation and commissioning of the project, 20% subsidy will be disbursed.
- After one year of operation of the plant, 5% subsidy will be given.
- After two years operation of the project, the balance 5% subsidy will be provided.

It is worth noting that 100 kWp FSPV plant was commissioned under “Make In India” initiative, at Rajiv Gandhi Combined Cycle Power Plant (RGCCPP) in Kerala’s Kayamkulam district. This FSPV project was indigenously developed by the R&D arm of NTPC which is the giant player in the Indian power sector.

It is interesting to note that a large number of reservoirs are located at different locations in India. In this context, there is a good scope of utilization of the water resources of these reservoirs through FSPV technology. Therefore, a survey has been conducted to check the potential of FSPV installation by utilizing the major reservoirs in India. If the potential of the water surface is utilized in a proper way, the power generation through sustainable means will be an added advantage in the Indian power sector.

The potential of solar energy and water saving [5] considering Indian major reservoirs is given in Table 2. The calculation is done considering 1250 million litres water saving per square Km area per year and 40 MWp potential per square Km area [5]. Here, a typical study is presented without considering the weather variability which is left as the future scope of this work.

## 6 Future Prospects and Recommendations

The population growth is increasing day by day throughout the world. At this juncture, land availability has become a crucial factor and challenging task. Therefore, FSPV project has the bright future especially in the densely populated countries like China, India, Japan, USA, Korea, etc. where the land shortage issue persists. The cost of water is very less compared to the cost of land, and therefore, the demand of FSPV is expected to increase rapidly all over the world. Moreover, the demand supply gap of electricity can be compensated through solar energy in a sustainable manner. Therefore, the GOI has also formulated different policies and incentive mechanisms to promote the solar energy. In a nutshell, the FSPV technology is an attractive and innovative way to produce the solar energy by utilizing the water resources. The few installations of FSPV plants are described in Table 3.

Two FSPV plants each having capacity 10 MW will be set up in the states of Andhra Pradesh and Kerala. Each project is expected to entail an investment of Rs.

**Table 2** Solar energy production and water saving potential in Indian major reservoirs

| Name of reservoir | Area in Sq. Km | FSPV potential (GWp) | Yearly water saving (million litres) |
|-------------------|----------------|----------------------|--------------------------------------|
| Nagarjun Sagar    | 284.9          | 19.943               | 356,125                              |
| Sriram Sagar      | 450.82         | 31.5574              | 563,525                              |
| Srisaillam        | 616.42         | 43.1494              | 770,525                              |
| Somasila          | 212.28         | 14.8596              | 265,350                              |
| Manimata Hasdeo   | 188.47         | 13.1929              | 235,587.5                            |
| Pong              | 260            | 18.2                 | 325,000                              |
| Salal             | 93.56          | 6.5492               | 116,950                              |
| Maithon           | 106.19         | 7.4333               | 132,737.5                            |
| Panchet           | 153            | 10.71                | 191,250                              |
| Tenughat          | 64.8           | 4.536                | 81,000                               |
| Krishnaraja Sagar | 129            | 9.03                 | 161,250                              |
| Tungabhadra       | 378.13         | 26.4691              | 472,662.5                            |
| Bhadra            | 117.25         | 8.2075               | 146,562.5                            |
| Linganamakki      | 316.65         | 22.1655              | 395,812.5                            |
| Malaprabha        | 129.5          | 9.065                | 161,875                              |
| Hidkal            | 78.04          | 5.4628               | 97,550                               |
| Hemavathy         | 91.62          | 6.4134               | 114,525                              |
| Supa              | 123            | 8.61                 | 153,750                              |
| Almatty           | 754.25         | 52.7975              | 942,812.5                            |
| Cheruthoni        | 59.83          | 4.1881               | 74,787.5                             |
| Gandhi Sagar      | 660            | 46.2                 | 825,000                              |
| Tawa              | 200.55         | 14.0385              | 250,687.5                            |
| Bargi             | 267.97         | 18.7579              | 334,962.5                            |
| Indira Sagar      | 913.48         | 63.9436              | 1,141,850                            |
| Koyna             | 115            | 8.05                 | 143,750                              |
| Paithan           | 398            | 27.86                | 497,500                              |
| Ujjani            | 336.5          | 23.555               | 420,625                              |
| Totladoh          | 77.71          | 5.4397               | 97,137.5                             |
| Hirakud           | 743            | 52.01                | 928,750                              |
| Rengali           | 378            | 26.46                | 472,500                              |
| Upper Kolab       | 122            | 8.54                 | 152,500                              |
| Indravati         | 110            | 7.7                  | 137,500                              |
| Ranapratap Sagar  | 198.29         | 13.8803              | 247,862.5                            |
| Mahi Bajaj        | 134            | 9.38                 | 167,500                              |
| Bisalpur          | 218.36         | 15.2852              | 272,950                              |

(continued)

**Table 2** (continued)

| Name of reservoir | Area in Sq. Km | FSPV potential (GWp) | Yearly water saving (million litres) |
|-------------------|----------------|----------------------|--------------------------------------|
| Mettur            | 153.46         | 10.7422              | 191,825                              |
| Rihand            | 468            | 32.76                | 585,000                              |
| Matatila          | 138.85         | 9.7195               | 173,562.5                            |
| Rajghat           | 2453           | 171.71               | 3,066,250                            |
| Kangsabati        | 124.32         | 8.7024               | 155,400                              |
| Total             |                | 909.05               | 16,233,187.5                         |

**Table 3** Few installation of FSPV plants

| Sl. No | Company name                | Capacity              | Location/features  |
|--------|-----------------------------|-----------------------|--|
| 1      | NHPC Ltd.                   | 50 MW                 | Kerala   |
| 2      | Vikram solar Pvt. Ltd.      | 10 kW                 | New town in West Bengal                                  |
| 3      | Kyocera TCL solar           | 13.4 MW               | Yamakura, Japan  |
| 4      | Balbina hydroelectric plant | 350 MW                | Brazil   |
| 5      | Saitama Prefecture, Japan   | 2786 panels of 255 Wp | 43%(0.81 ha) of coverage on water regulation pond, Japan |
| 6      | Hyogo prefecture, Japan     | 3392 panels of 250 Wp | World's 1st floating PV of 37%(0.91 ha) coverage         |

70 crores (\$10.7 million) and will be funded by World Bank. Both these projects will be implemented either by the corresponding state governments or SECI. The National Hydro Power Corporation (NHPC) is planning to set up 600 megawatts of FSPV plant at the hydro power project.

The government, researchers as well manufacturers should come forward to address the following issues:

- Thorough investigation is required on the effect of salt water on the PV modules and other structures.
- Improvement in the solar tracking system is utmost needed so that the tilt and azimuth angle of FSPV system can be adjusted.
- Extensive research on the flexible thin film technology for PV panels needs to be explored so that the harsh weather condition can be dealt with.
- Various factors such as maximum wind speed, water current, temperature limit, snow load, cyclone, and typhoon are to be considered during designing of the FSPV plant.
- Development of the new technology for the floating structures is also to be researched.
- The modern remote sensing and GIS-based tools may be adopted to identify the potential site for the FSPV project.



## 7 Conclusions

In this study, a comprehensive overview of the FSPV technology is discussed. The FSPV modules basically float on the water surface and the modules are naturally cooled by the water. Therefore, efficiency of the FSPV plant is comparatively higher than the conventional land-mounted PV plant. In spite of the various challenges are associated with the FSPV plant, it is an attractive and well-proven modern technology which can resolve the energy crisis utilizing the water resources. Furthermore, the techno-economic analysis of FSPV project is also highlighted to quantify the economic benefit. Undoubtedly, the FSPV technology would prove to be an innovative way as it could solve land requirement problem. The water resources can be used effectively through FSPV technology, and the huge amount of water can be saved by reducing the evaporation. This FSPV technology could be a game changer for India. Therefore, FSPV technology is an attractive option, and government should implement it in a well-planned way by considering various social, technical, and economic issues by utilizing the available water resources of India effectively. Moreover, it will help to meet the solar target and achieving the sustainability of power thus ensure sustainable development.

## References

1. Hairat MK, Ghosh S (2017) 100 GW solar power in India by 2022—a critical review. *Renew Sustain Energy Rev* 73:1041–1050
2. Chandel SS (2016) Overview of the initiatives in renewable energy sector under the national action plan on climate change in India. *Renew Sustain Energy Rev* 54:866–873
3. Krishnaveni N, Anbarasu P, Vigneshkumar D (2016) “A survey on floating solar power system”. *Int. J. Curr. Res. Mod. Educ. (IJCRME)*, ISSN (Online), 2455–5428
4. Sahu A, Yadav N, Sudhakar K (2016) Floating photovoltaic power plant: A review. *Renew Sustain Energy Rev* 66:815–824
5. Sharma AK, Kothari DP (Apr 2016) “Floating solar pv potential in large reservoirs in India”. *Int. J. Innovative Res. Sci. Technol. IJRST* 2(11) ISSN(online) 2349–6010
6. Tina GM, Rosa-Clot M, Rosa-Clot P (2011) “Electrical behavior and optimization of panels and reflector of a photovoltaic floating plant”. *Proceedings of the 26<sup>th</sup> European photovoltaic solar energy conference and exhibition (EU PVSEC’11)*, 4371–5
7. Tripathi K, Millar DL (2013) Proposing offshore photovoltaic (PV) technology to the energy mix of the Maltese islands. *Energy Convers Manag* 67:18–26
8. Choi YK, Lee NH, Kim KJ (Jul 2013) “Empirical research on the efficiency of floating PV systems compared with overland pv systems”
9. Ferrer Gisbert C et al (2013) A new photovoltaic floating cover system for water reservoirs. *Renew Energy* 60:63–70
10. Sharma P, Muni B, Sen D (2015) Design parameters of 10KW floating solar power plant. *Special Issue* 2(1):85–89
11. Ministry of New and Renewable Energy (MNRE), <https://mnre.gov.in/>

# Pumped Hydrostorage (PHS) Plant: A Scheme for Overall Efficiency Improvement by Recycling the Water



Mehebab Alam

**Abstract** The demand of the electricity is varying in nature, and this variability in the demand requires the suitable storage scheme which will meet the additional demand during peak hours. Although several energy storage schemes are available, the pumped hydrostorage (PHS) scheme is widely accepted for large-scale energy storage purpose. The PHS is operated by recycling the water through pumping mode and generating mode. In this study, the mathematical model of PHS plant is elaborated. Furthermore, the cost–benefit analysis is also highlighted considering a typical case study. The cost analysis of the already installed PHS plants in India is also discussed. In a nutshell, this study will be helpful to the researchers and planners for possible adoption of the PHS technology to improve the overall efficiency of the generation system.

**Keywords** Pumped hydrostorage (PHS) · Frequency regulation · Central electricity authority (CEA)

## 1 Introduction

The bulk energy storage schemes are growing attention day by day to meet the peak load demand. Moreover, the significant amount of renewable energy penetration into the modern grid necessitates the suitable energy storage schemes. In this context, two schemes, namely compressed air energy storage (CAES) and pumped hydrostorage (PHS), are the promising technology. However, the application of CAES is still limited due to topological restriction [1] and few installations are available worldwide. On the other hand, the PHS is comparatively matured technology and widely used [2, 3] for bulk energy storage. In India, 12 pumped storage plants are in operational condition with installed capacity of 5804 MW. Among 12 pumped storage plants, only six plants are operating in both modes, i.e., generation and pumping modes [4]. In India, 8 h pumping and 6 h generation are suggested but less pumping

---

M. Alam (✉)

Department of EE, National Institute of Technology (NIT), Durgapur, West Bengal 713209, India

hour has been noticed till 2002 [5]. A comprehensive review on PHS schemes is described in [6]. The mathematical model of PHS scheme for house building is outlined in [7]. Gradually, the increasing peak demand, the spinning reserve requirement, and renewable energy introduction into the grid singly or combined given a thrust for thinking about bulk storage option. However, the cost–benefit analysis is essential for implementation or installation of the storage plant.

In this study, an overview of PHS plant is outlined. The mathematical model of PHS plant along with cost–benefit analysis is also explained.

## 2 Overview of the PHS System

Basically, the PHS plant is used to enhance the overall efficiency of the thermal plant. During low demand period, the excess energy is used to pump the water and this is known as pumping operation mode. On the other hand, during peak demand period, the same water is used to drive the generator in order to produce the electricity and this is known as generation mode. Therefore, the water is recycled through the PHS plant by operating in pumping and generation mode.

### 2.1 Indian Grid System and Potential

The Indian grid frequency was varying from 47.8 Hz to 50.5 Hz before 2003 [8]. In this context, the sufficient power was not available for pumping operation. After 2003, the operating range was decreased to 49–50.5 Hz. Therefore, increased pumping operation was observed. Later on, the frequency band was further reduced; i.e., lower limit was changed from 49 Hz to 49.5 Hz and upper limit was changed from 50.5 Hz to 50.2 Hz. The reduction of the frequency band improves the efficiency and stability of the large interconnected grid. The change in frequency band in Indian power system is summarized in Table 1. The Indian power system has the following special features.

- There is imbalance between hydrogeneration and thermal generation

**Table 1** Operating range of frequency as per Indian grid code

| Period                                | Frequency range (Hz) |
|---------------------------------------|----------------------|
| Upto 31st March 2009                  | 49.0–50.50           |
| From 1st April 2009 upto 2nd May 2010 | 49.2–50.30           |
| From 3rd May 2010 upto 16th Feb. 2014 | 49.5–50.20           |
| With effect from 17th Feb 2014        | 49.7–50.05           |

- Shortage of peak demand
- Shortfall in spinning reserve
- Considerable gap between generation and demand.

Total of 63 sites have been identified by Central Electricity Authority (CEA) for installation of PHS plant with projected capacity 96,5000 MW [9]. Among these, 12 PHS plants have been installed so far with capacity 5804 MW. For flexible operation of the system, the hydrothermal mix should be 40:60 but it has not been achieved so far. As per National Electricity Policy, the spinning reserve should be 5% of the installed capacity but only the 60% of the requirement has been achieved so far [10].

### 3 Mathematical Model of PHS Plant

For operation of the PHS plant, two reservoirs at different heights are required. A typical diagram of PHS plant is shown in Fig. 1. In this section, brief mathematical model [7] of PHS is described.

The water will be stored at higher reservoir during pumping operation. On the other hand, during generation mode, the water will flow from upper pondage to the lower pondage through a turbine and power is generated. Therefore, stored energy  $E(J)$  can be written as

$$E = \rho Vgh \tag{1}$$

Here the density of water is represented by  $\rho$ , the volume of water at upper reservoir is represented by  $V$ ,  $g$  denotes the acceleration ( $m/s^2$ ), and  $h$  represents the difference of height between two reservoirs (m). Now, considering  $1000 \text{ kg/m}^3$  water density and  $9.81 \text{ m/s}^2$  acceleration, the stored energy  $E$  (kWh) can be expressed as.

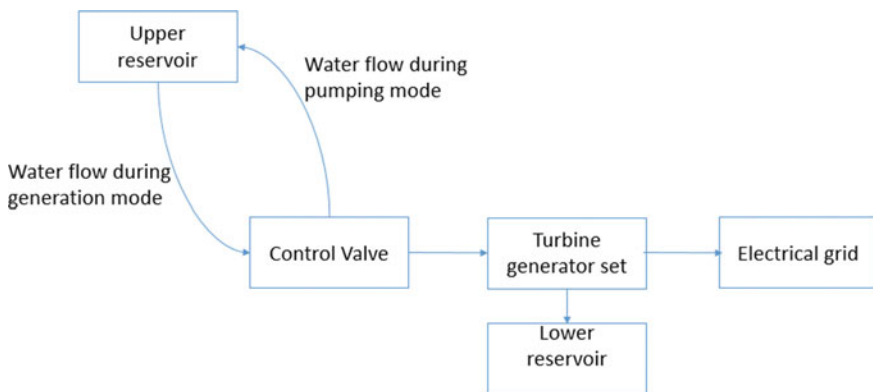


Fig. 1 Schematic layout of PHS plant

$$E \approx V h/365 \quad (2)$$

$$\text{LCOE} = \frac{\sum_{n=0}^N (C_n/(1+d)^n)}{\sum_{n=0}^N (E_{\text{out}}/(1+d)^n)} \quad (3)$$

Here  $C_n$  represents the cost in  $n$  –  $th$  year. The generated energy in  $n$  –  $th$  year is denoted by  $E_{\text{out}}$  (kWh). Further,  $d$  represents the real yearly discount rate (%) and  $N$  is the project duration in year. The total cost  $C_n$  basically consists of two components, i.e., the purchase cost of electricity at a price  $P_{\text{in}}$  and the capital cost in first year ( $C_0$ ). It is assumed that the system efficiency ( $\eta_{\text{total}}$ ) and the generated energy  $E_{\text{out}}$  (kWh) remain constant. Considering this, the levelized cost of electricity (LCOE) can be written as

$$\text{LCOE} = \frac{C_0}{E_{\text{out}} \left( \frac{(1+d)^N - 1}{d(1+d)^N} \right)} + \frac{P_{\text{in}}}{\eta_{\text{total}}} \quad (4)$$

Now we consider two assumptions; i.e., project duration  $N$  is 25 years and discount rate  $d$  is 5%. Considering these two assumptions, the LCOE will be

$$\text{LCOE} \approx \frac{C_0}{14 \times E_{\text{out}}} + \frac{P_{\text{in}}}{\eta_{\text{total}}} \quad (5)$$

From Formula (5), it is seen the dependence of LCOE on the different factors. One factor is the generated energy  $E_{\text{out}}$  which must be maximized in order to dilute the capital cost and reduce the LCOE. The other factor is the system efficiency; i.e., higher system efficiency will lead to the reduction of LCOE.

## 4 Cost–Benefit Analysis

For cost–benefit analysis, a typical 1000 MW capacity is chosen with 3 h operation per day. The cost of energy is calculated from the latest unscheduled interchange (UI) rate (Fig. 2) determined by the Central Electricity Regulatory Commission (CERC) [11]. The efficiency is chosen 75% [8]. The detailed calculation is represented in Table 2. The PHS is used to store energy during off-peak period, and this energy is fed back to the grid during peak load period. In Table 2, off-peak hour is considered at 50.05 Hz frequency and peak hour is considered at 49.9 Hz frequency. At 50.05 Hz, frequency UI rate is very less; therefore, it will be economical to store the energy instead of feeding into the grid. In view of this, cost of energy stored is calculated with Rs. 2.5/kWh which also includes the O&M cost. The cost of energy fed into the grid during 49.9 Hz frequency is taken Rs.4/kWh with reference from CERC rate.

This is a typical calculation considering full load operation of PHS. Actually, the profit may vary depending on the following factors:

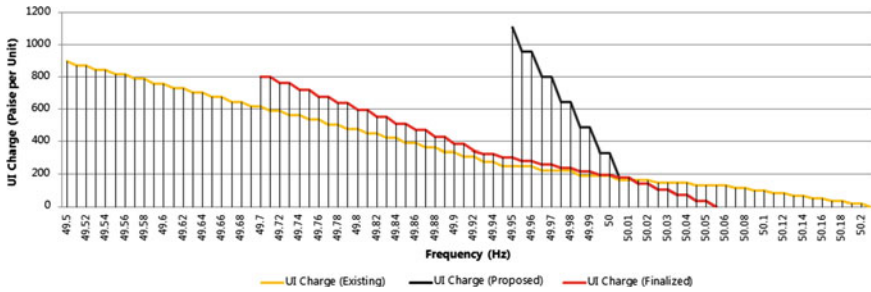


Fig. 2 CERC latest UI rate

Table 2 Cost–benefit analysis of a typical PHS plant

|  |   |
|--|---|
| Rating of PHS  | 1000 MW   |
| Hours of operation/day   | 3 h/DAY   |
| Energy stored during off-peak hour (A)@Frequency 50.05 Hz          | $1000 \times 3 \times 1000 = 3,000,000$ kWh     |
| Efficiency of the system   | 75%   |
| Energy feedback to grid during peak hours @Frequency = 49.9 Hz (B) | $A \times 0.75 = 2,250,000.00$ kWh              |
| Cost of energy stored @ Rs. 2.5/kWh(Includes O&M Cost)(C)          | $A \times 2.5 =$ RS 7,500,000                   |
| Cost of energy delivered to the grid @Rs 4/kWh(D)                  | $B \times 4 =$ RS 9,000,000                     |
| Benefit/Day (E) = D-C  | $D - C =$ RS 1,500,000 = 15 lakhs               |
| <b>Yearly benefit</b>  | <b><math>365 \times E = 54.75</math> Crores</b> |

- Frequency range at which storage and trading is done (as per CERC UI rate)
- No of hours and days of operation
- Variation of O&M costs
- Operation with full capacity or partial capacity.

## 5 Practical Indian Case Study

The capital cost of six major PHS plants is represented in Table 3 [5]. The capacity of the Srisaillam PHS plant is the highest, and Bhira PHS plant is lowest. Further, the generation, capital investment, and cost/kWh of four major plants, i.e., Kadamparai, Srisaillam, Ghatghar, Purulia PHS plant, are summarized in Table 4 [5]. It is seen from Table 4 that cost/kWh is the highest for Ghatghar PHS plant and the lowest for Kadamparai PHS plant. The generation cost and sale cost of energy from Kadamparai PHS plant are represented in Table 5 which shows that considerable amount of profit can be achieved through PHS scheme. The bulk energy is represented

**Table 3** Capital cost of major PHS plants in India

| Sl. No | Names of PHS | Installed capacity (MW) | Commissioned year | Capital cost (million) Rs. | Capital cost in 2013 |
|--------|--------------|-------------------------|-------------------|----------------------------|----------------------|
| 1      | Kadamparai   | 400                     | 1987              | 2250                       | 13,809.3             |
| 2      | Srisailam    | 900                     | 2003              | 26,200                     | 51,602.7             |
| 3      | Ghatghar     | 250                     | 2008              | 19,280                     | 23,751.2             |
| 4      | Purulia      | 900                     | 2008              | 26,388.2                   | 36,734               |
| 5      | Kadana       | 240                     | 1998              | 3425                       | 7997.1               |
| 6      | Bhira        | 150                     | 1995              | 2570                       | 6943.3               |

**Table 4** Generation cost and capital investment of major PHS plants

| Features   | Kadamparai | Srisailam | Purulia | Ghatghar |
|--|------------|-----------|---------|----------|
| Installed capacity (MW)  | 4*100      | 6*150     | 4*225   | 2*125    |
| Design energy in Million Unit (MU)                             | 797        | 1400      | 1700    | 470      |
| Year of commissioning  | 1987       | 2003      | 2008    | 2008     |
| Capital Investment on commissioning (Rs. × 10 <sup>7</sup> )   | 225        | 2620      | 2638.82 | 1578.90  |
| Capital Investment adjusted to 2013 (Rs. × 10 <sup>7</sup> )   | 1380.93    | 5160.27   | 3673.40 | 2375.12  |
| Annual Fixed Charge (20% of investment), Rs. × 10 <sup>7</sup> | 276.19     | 1032.05   | 734.68  | 475.02   |
| <i>Cost/kWh in Rs.(U)</i>                                      |            |           |         |          |
| U for 100% design energy                                       | 3.47       | 7.37      | 4.32    | 10.11    |
| U for 50% design energy  | 6.93       | 14.74     | 8.64    | 20.21    |

**Table 5** Generation and sale cost (paise/kWh) of Kadamparai PHS plant [5]

| Financial year | Generation cost | Sale cost |
|----------------|-----------------|-----------|
| 2006–2007      | 90.75           | 310.16    |
| 2007–2008      | 95.60           | 317.03    |
| 2008–2009      | 132.71          | 311.19    |
| 2009–2010      | 81.82           | 311.08    |
| 2010–2011      | 41.96           | 415.87    |
| 2011–2012      | 115.46          | 362.88    |
| 2012–2013      | 251.66          | 483.85    |

in million unit (MU) here (1 MU = 10<sup>6</sup> kWh). The designed energy refers to the maximum amount of energy that can be generated from that plant. Actual energy generation is always less than designed energy.

## 6 Future Prospects

It is worth noting that out of 12 PHS plants, 5 plants are not presently in operation with pumping mode. Therefore, they are basically operating as normal hydrogenerator. For example, due to want of tail race pool, Sardar Sarovar, Nagarjunasagar, and DVC (Panchet hill valley); these three plants are also not operating in pumping mode. Moreover, the vibration issue has made the Kadana PHS inoperational. Furthermore, due to non-availability of tail race pool, the Bhira PHS is also not operating via pumping mode. Ujjain and Paithan (12 MW) stations are operating depending on irrigation demand. In this context, it is to be noted that if efforts are being made to make all these plants to be operated in pumping mode, then the overall system efficiency will be improved.

Further, the following suggestion are recommended for better utilization of the PHS plants:

- The government should formulate flexible policy for installation and operation of the PHS plants.
- The subsidy mechanism is to be introduced as it helps to stabilize the grid
- The variable speed operation may be adopted to achieve the better performance. The variable speed technology is widely adopted throughout the world for efficiency improvement, and it has been witnessed in Kadamparai PHS plant.
- One important factor of poor performance is less pumping operation. Therefore, effort is to be made to increase the pumping operation. As the government is introducing various schemes for renewable energy integration into the grid, the pumping operating is expected to increase in near future. The improvement in performance (Fig. 3) with the pumping operation is also verified at Kadamparai PHS plant.

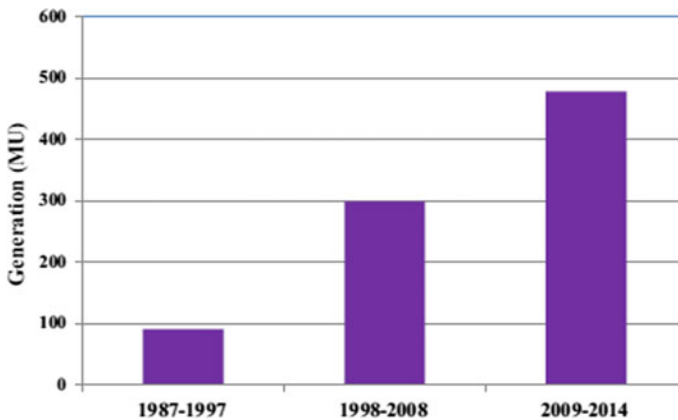


Fig. 3 Performance of Kadamparai PHS plant considering 10 year interval period [5]



It is interesting to note that nowadays the government is promoting renewable energy, and various schemes have been formulated for smooth execution of renewable energy generation. Moreover, different government bodies and ministries have been set up to look into the progress of renewable energy sectors across the country. However, the renewable energy generation pattern is quite uncertain and dependent on the weather condition. In this context, the energy generated from renewable sources can be stored during off-peak period through PHS scheme. On the other hand, the electrical energy can be produced from stored energy during peak demand of electricity. Therefore, the stability of the power grid will be achieved and system reliability will be improved.

## 7 Conclusions

It is to be noted that PHS plants are to be installed considering the geographic and topological condition of the system. In the developed countries, the cost of energy from PHS plant is fixed based on electricity trading as they have separate tariff policies. However, in India, such commercial policies have not been formulated yet. Presently, the PHS plants are operating for peak load management and improving grid reliability. The improvement in the performance of PHS plants is achieved after introduction of stringent frequency band. This case study shows that the PHS plants not only meet the peak demand but also they are economical considering the latest UI rate prescribed by CERC. Therefore, the government and policymakers must look into the matter carefully for possible implementation of the PHS plant at the potential sites in order to harness the benefit in today's competitive market.

## References

1. Safaei H, Keith DW (2014) Compressed air energy storage with waste heat export: an Alberta case study. *Energy Convers Manage* 78:114–124
2. Steffen B (2012) Prospects for pumped-hydro storage in Germany. *Energy Policy* 45:420–429
3. Ekman CK, Jensen SH (2014) Prospects for large scale electricity storage in Denmark. *Energy Convers Manage* 51:1140–1147
4. Sivakumar N, Das D, Padhy NP, Senthil ARK, Bisoyi N (2013) Status of pumped hydro-storage schemes and its future in India. *Renew Sustain Energy Revi* 19:208–213
5. Sivakumar N, Das D, Padhy NP (2014) Economic analysis of Indian pumped storage schemes. *Energy Convers Manag* 88:168–176
6. Rehman S, Al-Hadhrani LM, Alam MM (2015) Pumped hydro energy storage systems: a technological review. *Renew Sustain Energy Rev* 44:586–598
7. de Oliveira e Silva G, Hendrick P (2016) “Pumped hydro energy storage in buildings”. *Appl Energy* 179:1242–1250
8. Ibraheem NK, Sharma TP (2010) Investigation and analysis of Indian power grid after regulatory reforms and dynamic pricing. *Int J Eng Sci Technol* 2:1029–1036
9. Central Electricity Authority: Large scale grid integration of renewable energy sources—way forward (2013) [http://www.cea.nic.in/reports/powersystems/large\\_scale\\_grid\\_integ.pdf](http://www.cea.nic.in/reports/powersystems/large_scale_grid_integ.pdf)

10. Das S (2009) "Ensuring spinning reserve in generation deficient Indian power system power systems". ICPS '09 international conference, pp 1–6
11. CERC <http://www.cercind.gov.in>

# Identification of New Sites for Micro-Compost Centers: A Predictive Study for Erode Urban Region



S. Anandakumar, M. Kowsalya, K. Santhosh Kumar, M. Rama Krishnan, S. Praveenkumar, G. Mini Karthi, G. S. Rampradheep, and S. Jeeva Chithambaram

**Abstract** Municipal Solid Waste (MSW) generation gets expanded day by day due to fast urbanization and expand in population. This creates an unfavorable impact on surroundings due to the fact it pollutes nature and also acts as medium for breeding of flies. Currently, Erode District, which situated in Tamil Nadu state, India, is additionally going through this problem. The Municipality Corporation of Erode has hooked up 18 new Micro-Compost Center (MCC) in function to reduce the quantity of Municipal Solid Waste (MSW) but by taking population growth into consideration the current MCCs will not be sufficient in future, so there will be a need of new MCC. This paper aim is to establish the new sites that will be appropriate for erection of new MCC in future by integrating the geospatial data of MCC into Geographic Information System (GIS) for GIS-based analysis.

**Keywords** Municipal solid waste · Urbanization · Micro-compost center · Geographic information system

## 1 Introduction

Due to expand in population and fast urbanization the need of Municipal Solid Waste (MSW) management has been improved relatively in India [1]. In latest times, the humans had migrated from rural areas to city for employment and improved health care. This has additionally expanded the stress on present resources and contributed to more waste. The majority of waste generated is due to the fact of the sophisticated lifestyles fashion in city region. In India, extra than three fourth of MSW is contributed by way of urban area [2]. The produced MSW is hard to manage, they also act as

---

S. Anandakumar · M. Kowsalya · K. Santhosh Kumar (✉) · M. R. Krishnan · S. Praveenkumar · G. M. Karthi · G. S. Rampradheep  
Department of Civil Engineering, Kongu Engineering College, Perundurai, Erode, Tamil Nadu, India  
e-mail: [skumar.civil@kongu.edu](mailto:skumar.civil@kongu.edu)

S. J. Chithambaram  
Department of Civil Engineering, NIT Jamshedpur, Jamshedpur, Jharkhand, India

medium for breeding of flies and it also motives terrible scent which is very hard to bear [3]. The above cited problem will also be relevant to Erode city which is located in Tamil Nadu. Due to the developmental things to do in this city the per capita waste era have been multiplied from 1 to 1.3 and it is also growing each year. The Municipal Corporation of Erode is taking the critical steps to control the waste by way of gathering it and then segregating into extraordinary components for transporting and treating them in dump yard [4]. They have additionally initiated the system known as composting in 18 new Micro-Compost Center (MCC). These MCC helps a lot to decrease the volume of MSW by using incorporating worms and also creating the medium which is favorable for their increase however taking the population increase and city sprawl into account, it is growing over a length of time [5, 6]. It is additionally relevant for Erode city which ought to be viewed by using comparing the census of 2001 with 2011. Therefore, the current MCCs will be definitely insufficient in future so there will be need for new MCCs. To map existing MCC in Erode urban region and to identified site for establishing new MCC.

New sites will be chosen such that it should satisfy all the requirements of MCC. But certain type of lands should not be taken for MCCs because they have been termed as conservative lands. In order to overcome it Geographic Information System (GIS) can be used [7]. GIS primarily based evaluation of Web site determination will be useful in identifying new Web sites for MCC [8]. It is used as quantitative methods in records collection. Digitizing and buffering are used to map eligible sites reachable for finding MCCs in Erode. The designated picture of study place is extracted from Google Earth seasoned and then it is digitizing, buffered using ArcGIS 10.5 followed via overlaid is completed the use of ArcGIS 10.5 to produce the suitability map. The spatial distribution of presently existing MCCs is brought to map to get clear view of its existence [9]. To add records to quantitative techniques, qualitative methods that included interviews, questionnaires, observations and literature had been used to praise the quantitative methods. Results of the research, introduced a suitability map which showed the feasible suitable sites for New MCCs.

## ***1.1 Study Area***

The Erode urban area has been chosen as the find out about location due to the fact it comes under the list of smart cities selected in India for improvement underneath fourth phase and also quickest developing metropolis in Tamil Nadu. The district is bounded via Chamarajnar district in Karnataka to north and through Cauvery River to the East. Erode District is landlocked and is situated at between one hundred 36'N and 110 58' N latitude and between 760 49' E and 770 58' E longitude. The whole geographical area is 5,722 km<sup>2</sup>. The common temperature in Erode is 28.3 0C and about 700 mm of precipitation falls annually. The population in Erode is 2,251,744 (as per 2011 census) with 37,511 homes and about 5635 commercial building, 60 schools. In addition, there are about 20,000 floating populace in Erode town. These make contributions to the generation of 135 metric lots of strong waste every day.

## ***1.2 Software Used***

- Google earth pro.
- Arc GIs.
- ERDAS 10.

## **2 Methodology**

### **Data collection.**

### ***2.1 Primary Data***

The fundamental facts of this paper consists of getting data on the system carried out in MCC's which ought to be got by way of conducting questionnaire survey and then the geocoordinates of all facilities is recorded using Garmin GPS. The distribution of population waste generation detail of Erode District at follows,

- The total number of wards 60
- Total number of population 5,94,341.
- Ward wise high and low population W7,25,352 and W60, 6504.
- Total waste generation 1,07,020 (MT).
- %waste various from min and max value W22,165 and W17,5211.

### ***2.2 Questionnaire Survey***

Questionnaire survey is conducted in MCC to get the details about the working process in centers and also to get the coordinates of location of these centers. This questionnaire survey is answered by the staffs in charge in the centers and by the people who are working there the survey included the questions of date of interview, number of staffs working there, methodology carried out in center, space required for erecting the center, number and name of the wards for which the waste processed there in centers, capacity of center and cost involved in processing the waste. This survey helps us to identify the nature of the center and locations of existing MCC (Table 1).

**Table 1** Geographical coordinates of existing MCC'S

| S.NO | Zone | MCC Name               | Longitude | Latitude  |
|------|------|------------------------|-----------|-----------|
| 1    | 1    | BP Agraharam           | 77.713161 | 11.377447 |
| 2    |      | Vairapalayam           | 77.725266 | 11.370479 |
| 3    | 2    | Kolathupalayam         | 77.64878  | 11.356251 |
| 4    |      | VOC Park 1             | 77.719491 | 11.352912 |
| 5    |      | VOC Park 2             | 77.719491 | 11.352912 |
| 6    | 3    | Karuvil Palayam        | 11.345449 | 11.345449 |
| 7    |      | Kamaraj Nagar          | 77.686002 | 11.324769 |
| 8    |      | Therkupallam           | 77.683543 | 11.306033 |
| 9    |      | Lakshmi Garden         | 77.720706 | 11.312658 |
| 10   |      | Muthampalayam 1        | 77.706039 | 11.318598 |
| 11   |      | Muthampalayam 2        | 77.70594  | 11.318598 |
| 12   |      | Talukaa Police Station | 77.691275 | 11.299601 |
| 13   |      | Nethaji Nagar          | 77.713895 | 11.32731  |
| 14   | 4    | Kaveri Road            | 77.743783 | 11.358071 |
| 15   |      | Mohan Thottam          | 77.740343 | 11.336526 |
| 16   |      | Vendipalayam           | 77.743407 | 11.33117  |
| 17   |      | Anna Nagar             | 77.713763 | 11.31566  |
| 18   |      | Muthuswamy Colony      | 77.717487 | 11.314959 |

### 2.3 Process Carried Out in MCC

- The waste from the designated ward is accrued with the help of battery automobile and Tata Ace by using door-to-door process.
- Then the waste is transported to MCC via the above said vehicle. The employee's current in the middle will weigh the waste the use of weight balance and it is recorded in register.
- If any dry waste or any other non-degradable waste is present in the accrued waste, it is gathered into dustbin and then dumped into dump yard.
- After doing foremost procedures, the true manner starts off evolved through grinding the waste the use of Maxin India grinding machine and the grinded sparkling waste is dumped into series tank.
- Before dumping into tank, the tank is conditioned by means of use bagasse and cow dunk. • After dumping the waste into tank it is left for one week with stirring the tank for each three days.
- Then the waste is dumped into storage tank after a week earlier than that EM balls and leachate is sprinkled over it to make certain rapid rate of manure conversion and the system is persevered again for three times.
- Then the waste dumping is stopped however waste is stirred for each three days until the retention duration of 48 days after that the waste will be transformed into

manure it is then taken out and weighted and in the end given to the farmer at free of cost.

- Totally there had been 12 tanks. One tank is used for one day. 12 tanks are break up into two sets. After finishing one set of tank any other set of tank will be used.

## ***2.4 Secondary Data***

The secondary information of this paper consists of the system carried out in GIS which will be useful in figuring out the Web sites for new MCC's. In order to new Web sites for MCC preliminary steps like getting map from Google earth pro accompanied with the aid of digitizing the map and then the buffer is created to certain distance eventually extraordinary maps are overlapped to get the new Web sites.

## **3 Result and Discussion**

### ***3.1 Boundary Creation for Erode Urban Region***

The boundary map for Erode city vicinity is created to differentiate its border from other region. This will assist us to recognize the spatial details of the Erode city region more truly from other region and also help us to identify the locations that falls below the manipulate corporation. From this boundary map, we may want to genuinely see that the Erode city area as multiplied over a location of 768 km<sup>2</sup>. Figure 1 suggests the boundary map of Erode vicinity.

### ***3.2 Generation of Ward Map of Erode Region***

The Erode urban region has been divided into four zones and every zone consists of fifteen wards. These wards are digitized one at a time and then it is merged together. Each ward has one-of-a-kind populace and additionally generates the specific extent of the waste. By categorizing the district map in phrases of wards, we will be capable to recognize how an awful lot waste is generated in all wards accurately. Figure 2 suggests the Ward map of Erode city.

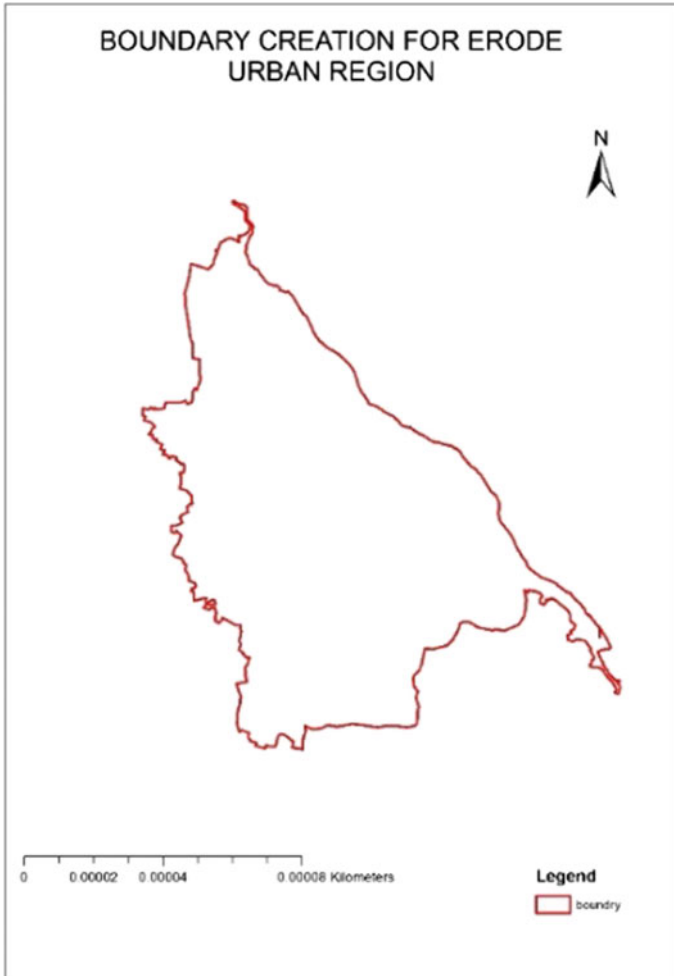


Fig. 1 Study area boundary

### 3.3 Generation of MSW Distribution Map of Erode Urban Region

With reference to the above map, the waste generated within Erode urban vicinity is dispensed alongside wards smart and the produced waste in every ward is tabulated and a map is generated. This generated map shows the density of waste produced alongside ward wise. This will helps us to detect the most effective Web site online for the MCC. Suggests the distribution of population and waste generation small print. Figure 3 suggests ward-wise waste generation.



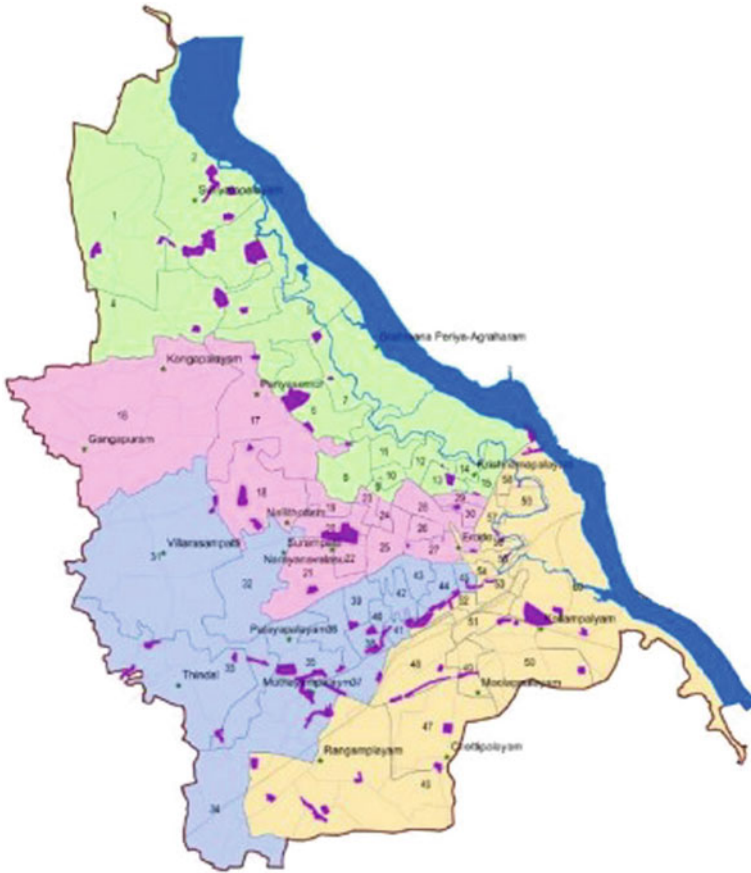


Fig. 2 Ward map

### 3.4 Location of Existing MCC

It is indispensable that we have to no longer provide extra of MCC to unique place as it might reduce the effectively of technique so there is a want of knowing the region of existing MCC. The recorded area of MCC with the aid of GPS is imported into GIS software program and pinned inside the ward map. The distribution of existing MCC is denser in south-west facet of the map, so it is very clear that there is a need for new MCC. Figure 4 suggests location of currently existing MCCs.

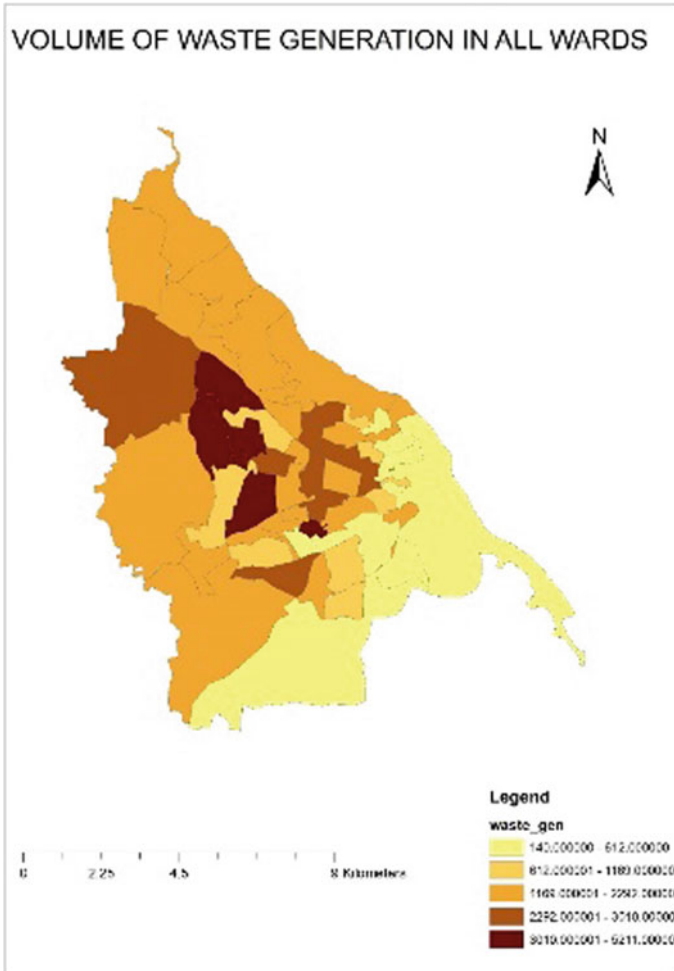


Fig. 3 Ward wise waste generation

### 3.5 Buffer Generation for Existing MCCs

After locating the existing MCC centers in Erode ward map a buffer region of radius 1 km with MCC as a center point is created around each MCC to know the area covered by all MCC, by creating the buffer zone we could see some of the buffer regions of MCCs getting overlapped as shown in Fig. 5. This shows that the waste produced in those regions are managed by both MCCs and also we could see some of the regions are not covered by any MCC so there is a need of new MCC in those region.

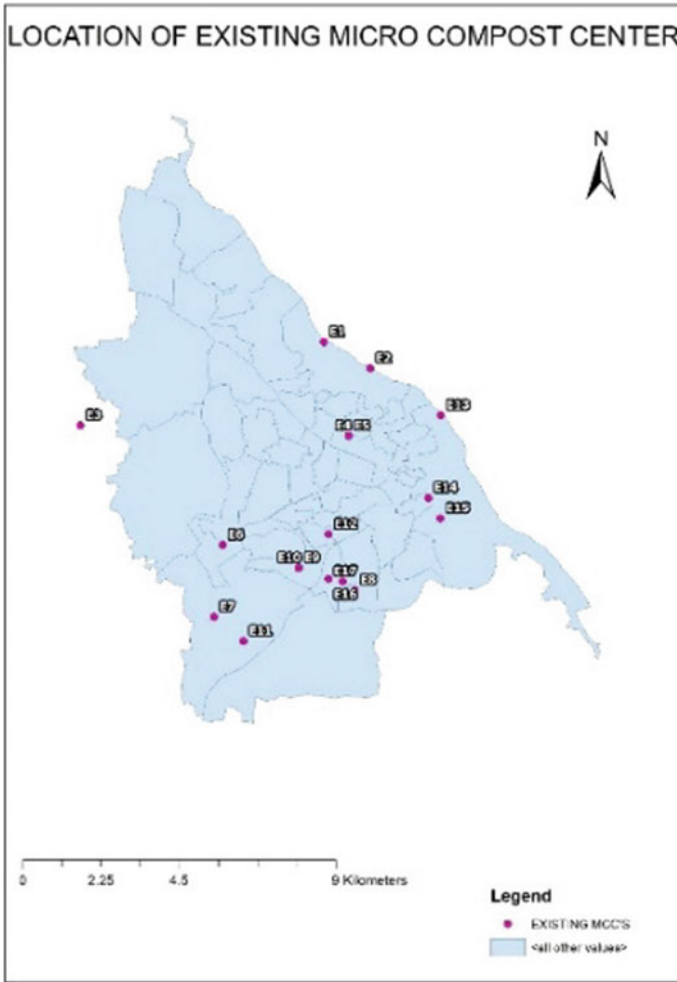


Fig. 4 Currently existing MCCs

### 3.6 Locating of New MCC

By thinking about the waste technology in all wards and location of existing MCCs, A complete of eight new MCCs is proposed to help the existing eighteen MCCs. These MCCs are provided due to the fact the waste generated in that place is extra that it cannot be handled by using nearer MCC or the nearer MCC may be away from the waste technology supply so it reasons high transportation cost. Totally nine sites are proposed for new MCC in that 6 Web sites are placed in agricultural vegetation and three Web sites are placed in urban place. The proposed new MCC's are plotted in a ward map and shown in Fig. 6.

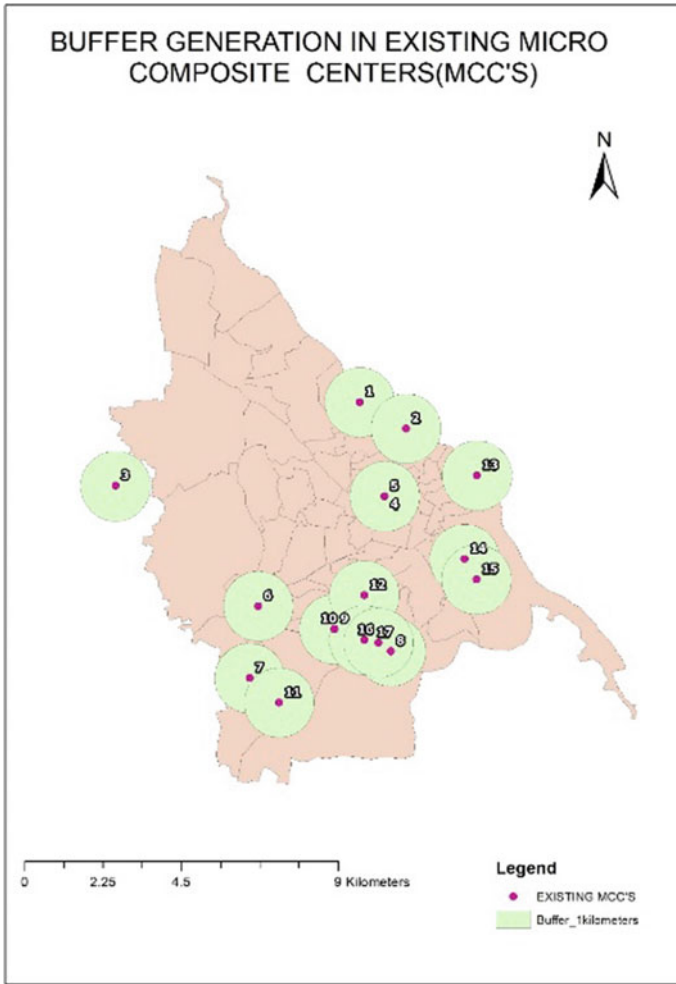


Fig. 5 Buffer generated for existing MCC

### 3.7 Location of Current and Proposed Sites for MCCs

By seeing the existing MCCs we could conclude that the current MCCs are dense in south-west region of Erode taluk and very much low in north-east region of Erode city so there is a need of establishing new MCCs there so we have chosen certain sites in those wards and numbered them as N1 to N9 these sites are chosen based on visiting sites and these sites should not interfere in residential area. like existing MCC for new MCC that we have proposed, we have created buffer regions around them in order to calculate the area covered by new MCCs. Figure 7 shows the buffer

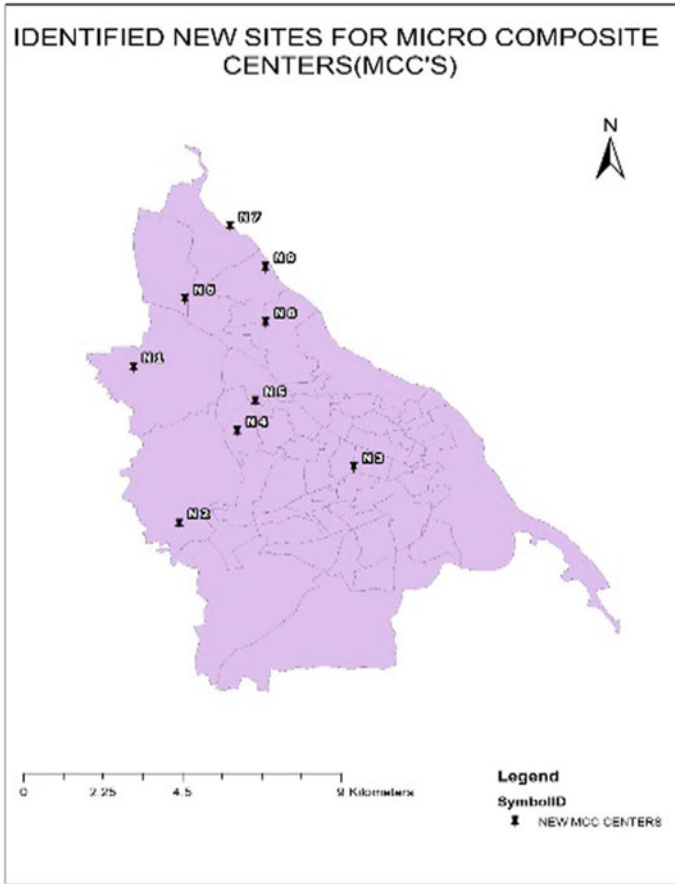


Fig. 6 Identified new MCCs

region of existing and new MCC. from this Fig. 7 we could see that the combination of old and new MCC could cover all regions of Erode taluk.

#### 4 Conclusion

This learn about objectives at offering new sites for setup of MCCs in Erode city place thru GIS-based analysis. Google Earth Pro presents the high quality updated images, for this reason being an efficient device for ERDAS and ArcGIS to pick out new sites. Analysis of main records with integration of GIS technology will be beneficial for identifying new sites. After a spatial willpower of an ultimate web page vicinity environmental monitoring allows and ensures ideal and environmentally

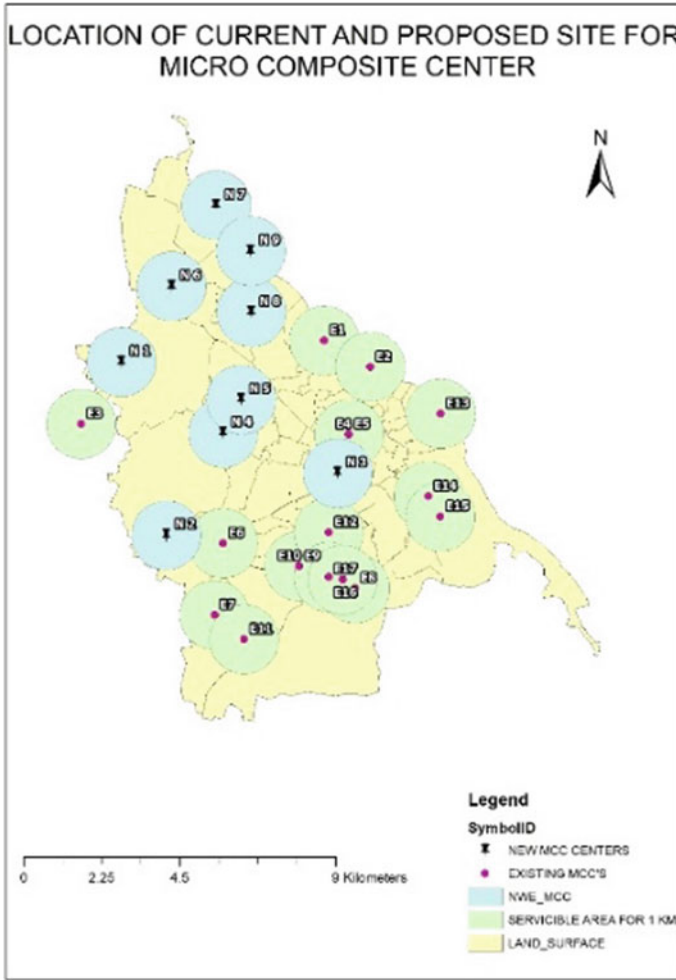


Fig. 7 Location of current and proposed MCCs for Erode urban region

sound operations at the MCCs. More significance has been given to sustainable improvement while planning to choose web page for MCC. The spatial place of present day MCC may be environmentally pleasant but by incorporating GIS and got Web sites for MCC are environmentally friendly and motives no dangerous to any human beings or animals. GIS and RS are vital environmental planning and problem-solving equipment as they had been used for trying out the suitability of the modern MCC as well as mapping the doubtlessly suitable Web sites for establishing a new MCC in Erode city. Through digitizing statistics for a range of key environmental parameters used to be obtained from Google Earth. The received data was once then converted the usage of ArcGIS from Keyhole Markup Language (KML) and it is manipulated the usage of ArcGIS10.5. Using a perfect framework of buffer distance

the parameters were buffered with their respective buffer distances then again with consideration of the relative measurement of the urban area. From the buffers, a conclusion that the current is no longer most appropriate to raise out all the manner for waste management. An overlay evaluation of all parameters produced a map of about 9 achievable sites for establishing a new MCC. Therefore the effect of the find out about has concluded that wards of 1,2,3,5,10,16,18,30,42 with a whole of 9 new MCC can be furnished to help present MCCs.

## 5 Annexure

### Micro-Compost Centre (Mcc) Questionnaire For Predicting New Sites For Mcc.

|                                   |   |
|-----------------------------------|---|
| <b>MCC name</b>                   | Kolathupalayam MCC  |
| <b>Location name</b>              | kolathupalayam main road  |
| <b>Name of the Respondent</b>     | sadam   |
| <b>Collection ward</b>            |   |
| No of Wards                       | 5   |
| Name of Wards                     | 16,17,18,19,20  |
| <b>Working days</b>               | 6 Days  |
| <b>Working hours</b>              | 10.30 am to 3.30 pm   |
| <b>Date of interview</b>          | 11/01/2020  |
| <b>No of workers</b>              |   |
| Workers for collection            | 60  |
| Workers for processing            | 4 (same Workers for collecting)   |
| <b>MCC Capacity</b>               | 2TPD (2 tonnes/day)   |
| <b>Area of MCC</b>                | 11 Cent   |
| <b>Collection process</b>         | Door to Door  |
| <b>Mode of Collection</b>         | TATA ACE  |
| <b>Kind of Waste Collection</b>   | Vegetable waste, plastic waste  |
| <b>Process carried out in MCC</b> | The waste from above said Waste is collected and weighted in MCC. Dry Waste and other non-bio-degradable waste is dumped into dustbin and thin dumped into dump yard. The workers present in site for maintain and process will first grind the waste using maxin India grinding maintain and then poured the waste into collection tank that day. Totally, there are six tanks one tank for one day. Sunday is leave. The tank is stirred of the 5 days from dumping day. The process is done for 3 weeks. One tank can hold waste for surety held every time dumping the waste, and seed balls are sported in order to boos up the decomposition process using worm |

(continued)

(continued)

|  |                    |
|--|--------------------|
| <b>MCC name</b>                            | Kolathupalayam MCC |
| <i>Quantity of waste Collected per day</i> |                    |
| <b>E-Waste</b>                             | –                  |
| <b>Recyclable waste</b>                    | 50 kg/day          |
| <b>Bio-Degradable waste</b>                | 1.8–2 tonnes/day   |
| <b>Process cost</b>                        | rs 13,200/day      |
| <b>Selling cost</b>                        | –                  |
| <b>Mode of Transportation</b>              | TATA ACE           |

## References

1. Gupta N, Yadav KK, Kumar V (2015) A review on current status of municipal solid waste management in India. *J Environ Sci* 37:206–217
2. Kawai K, Osako M, Matsui S, Dong NT (2012) Identification of junk buyers' contribution to recycling of household waste in Hanoi, Vietnam, through a physical composition analysis. *Waste Manage Res* 30(7):681–688
3. Kawai K, Osako M (2013) Advantages and disadvantages of a municipal solid waste collection service for citizens of Hanoi City Vietnam. *Waste Manag Res* 31(3):327–332
4. Ramesh N, Meenamabal T, Murugan K (2009) Quantification, characterization and leachate analysis of the municipal solid waste from Erode Municipality, Tamilnadu India. *Nat Environ Pollut Technol* 8(1):21–28
5. Sudhira HS, Ramachandra TV, Jagadish KS (2004) Urban sprawl: metrics, dynamics and modelling using GIS. *Int J Appl Earth Obs Geoinf* 5(1):29–39
6. Xiao J, Shen Y, Ge J, Tateishi R, Tang C, Liang Y, Huang Z (2006) Evaluating urban expansion and land use change in Shijiazhuang, China, by using GIS and remote sensing. *Landsc Urban Plan* 75(1–2):69–80
7. Lathrop RG Jr, Bogner JA (1998) Applying GIS and landscape ecological principles to evaluate land conservation alternatives. *Landsc Urban Plan* 41(1):27–41
8. Jerie S, Zulu S (2017) Site suitability analysis for solid waste landfill site location using geographic information systems and remote sensing: a case study of Banket Town Board Zimbabwe. *Rev Soc Sci* 2(4):19–31
9. Oh K, Jeong S (2007) Assessing the spatial distribution of urban parks using GIS. *Landsc Urban Plan* 82(1–2):25–32